SPRINGER SERIES IN COMPUTATIONAL NEUROSCIENCE

Hippocampal Microcircuits

A Computational Modeler's Resource Book

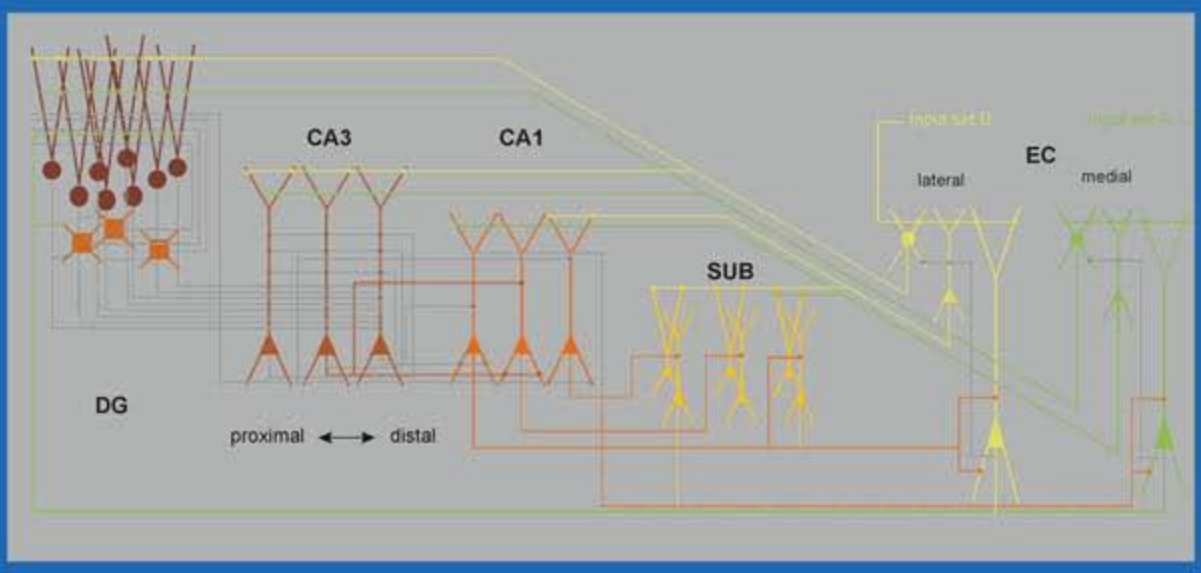

Vassilis Cutsuridis
Bruce Graham
Stuart Cobb
Imre Vida
Editors

Springer

Springer Series in Computational Neuroscience

Volume 5

For further volumes:
http://www.springer.com/series/8164

Vassilis Cutsuridis · Bruce Graham
Stuart Cobb · Imre Vida
Editors

Hippocampal Microcircuits

A Computational Modeler's Resource Book

Springer

Editors
Vassilis Cutsuridis
Department of Computing Science
and Mathematics
University of Stirling
Stirling FK9 4LA
UK
vcut@bu.edu

Bruce Graham
Department of Computing Science
and Mathematics
University of Stirling
Stirling FK9 4LA
UK
b.graham@cs.stir.ac.uk

Stuart Cobb
Neuroscience & Molecular Pharmacology
Faculty of Biomedical and Life Sciences
University of Glasgow
Glasgow G12 8QQ
UK
s.cobb@bio.gla.ac.uk

Imre Vida
Neuroscience & Molecular Pharmacology
Faculty of Biomedical and Life Sciences
University of Glasgow
Glasgow G12 8QQ
UK
i.vida@bio.gla.ac.uk

ISBN 978-1-4419-0995-4 e-ISBN 978-1-4419-0996-1
DOI 10.1007/978-1-4419-0996-1
Springer New York Dordrecht Heidelberg London

Library of Congress Control Number: 2009943440

Preface

Microcircuits are functional modules that act as elementary processing units bridging the gap between single-cell activity and large-scale network activity in the brain. Microcircuits can be found in all parts of mammalian nervous systems and involve many different neuronal types embedded within multiple feedforward and feedback loops. Synaptic connections may be excitatory and inhibitory and target-specific spatial domains of a neuron. In addition to fast signalling, neurons and their microcircuit environment are subject to neuromodulatory signals. Thus, fast synaptic transmission and neuromodulation in neuronal microcircuits combine to produce complex dynamics of neural activity and information processing at the network level.

The hippocampus has an indispensable role in spatial navigation and memory processes and is amongst the most intensively studied regions of mammalian brain. Hippocampal microcircuits exhibit a wide variety of population patterns, including oscillations at theta (4–7 Hz) and gamma frequencies (30–100 Hz), under different behavioural conditions. The complex dynamics conceivably reflects specific information processing states of the networks. Recent years have witnessed a dramatic accumulation of knowledge about the anatomical, physiological and molecular characteristics as well as the connectivity and synaptic properties of the various cell types in hippocampal microcircuits. However, much research is needed to decipher the precise function of the detailed microcircuits.

This book provides an overview of our current knowledge of hippocampal biology. Most data are presented in tabular or pictorial form so that the salient features and key parameters are readily accessible to the reader. It also provides a snapshot of the state-of-the-art approaches to investigate hippocampal microcircuits. The central aim of the volume is to provide a unique resource of data and methodology to anyone interested in developing microcircuit-level computational models of the hippocampus.

The book is divided into two thematic areas: (1) experimental background and (2) computational analysis. In the first thematic area, experimental neuroscientists describe the salient properties of the various cell types found in the hippocampus as well as their connectivity patterns and the characteristics of the different synapses. In addition, behaviour-related ensemble activity patterns of morphologically identified neurons in anaesthetized and freely moving animals provide insights on the function

of the hippocampal areas. In the second thematic area, computational neuroscientists present models of the hippocampal microcircuits at various levels of detail from single-cell to large-scale networks, developed on the basis of experimental data. Models of computation performed by single neurons, both principal cells as well as interneurons, and synapses with implemented plasticity rules are presented. Networks models of rhythm generation, spatial navigation and associative memory are discussed. Finally, a chapter is dedicated to describing simulation environments of single neurons and networks currently used by computational neuroscientists in developing their models.

Aside from offering up-to-date experimental information on the hippocampal microcircuits, our edited volume provides examples of systematic methodologies for modelling microcircuits necessary to all computational neuroscientists interested in bridging the gap between the single cell, the network and the behavioural levels. Importantly, we also identify outstanding questions and areas in need of further clarification that will guide future research in both biological and computational fields.

This volume will be an invaluable resource not only to computational neuroscientists, but also to experimental neuroscientists, electrical engineers, physicists, mathematicians and all researchers interested in microcircuits of the hippocampus. Graduate-level students and trainees in all of these fields will find this book an insightful and readily accessible source of information.

Finally, there are many people who we would like to thank for making this book possible. This includes all the contributing authors who did a great job. We would like to thank Joseph Burns, our former Springer senior editor, without whose support in the initial stages, this book would not have been possible. Last, but not least, we would like to thank Ann H. Avouris, our current Springer senior editor, and members of the production team, who were a consistent source of help and support. We dedicate this work to our families.

Stirling, UK — Vassilis Cutsuridis
Stirling, UK — Bruce P. Graham
Glasgow, UK — Stuart Cobb
Glasgow, UK — Imre Vida

Contents

Contributors

Giorgio A. Ascoli Krasnow Institute for Advanced Study George Mason University, Fairfax, VA 22030, USA, ascoli@gmu.edu

Marlene Bartos School of Medicine, Institute of Medical Sciences (IMS), University of Aberdeen, Foresterhill, Aberdeen, AB25 2ZD, UK, m.bartos@abdn.ac.uk

Guo-Qiang Bi Department of Neurobiology, University of Pittsburgh School of Medicine, Pittsburgh, PA 15213, USA, gqbi@pitt.edu

Christoph Börgers Department of Mathematics, Tufts University, Medford, MA, USA, cborgers@tufts.edu

Gastone C. Castellani Dipartimento di Fisica, Università di Bologna, Bologna 40127, Italy, gastone.castellani@unibo.it

Stuart Cobb Neuroscience & Molecular Pharmacology, Faculty of Biomedical and Life Sciences, University of Glasgow, Glasgow, G12 8QQ, UK, s.cobb@bio.gla.ac.uk

Vassilis Cutsuridis Department of Computing Science and Mathematics, University of Stirling, Stirling FK9 4LA, UK, vcut@bu.edu

Tamar Dugladze Institute of Neurophysiology, Charité – Universitätsmedizin Berlin, Berlin, Germany, tamar.dugladze@charite.de

Howard Eichenbaum Center for Memory and Brain, Boston University, Boston, MA 02215, USA, hbe@bu.edu

Péter Érdi Center for Complex Systems Studies, Kalamazoo College, Kalamazoo, Michigan 49006, USA; Department of Biophysics, KFKI Research Institute for Particle and Nuclear Physics of the Hungarian Academy of Sciences Budapest, Hungary, perdi@kzoo.edu

Erik Fransén Department of Computational Biology, School of Computer Science and Communication, Stockholm Brain Institute, Royal Institute of Technology, SE 106 91 Stockholm, Sweden, erikf@csc.kth.se

Richard C. Gerkin Department of Neurobiology, University of Pittsburgh School of Medicine; Department of Biological Sciences, Carnegie Mellon University, Pittsburgh, PA 15213, USA, rickg@cmu.edu

Padraig Gleeson Department of Neuroscience, Physiology and Pharmacology, University College London, London, UK, p.gleeson@ucl.ac.uk

Tengis Gloveli Institute of Neurophysiology, Charité – Universitätsmedizin Berlin, 10117, Berlin, Germany, tengis.gloveli@charite.de

Bruce P. Graham Department of Computing Science and Mathematics, University of Stirling, Stirling FK9 4LA, UK, b.graham@cs.stir.ac.ak

Russell Hunter Department of Computing Science and Mathematics, University of Stirling, Stirling FK9 4LA, UK, rhu@cs.stir.ac.uk

David B. Jaffe Department of Biology, The University of Texas at San Antonio, San Antonio, TX 78249, USA, david.jaffe@utsa.edu

Tamás Kiss Department of Biophysics, KFKI Research Institute for Particle and Nuclear Physics of the Hungarian Academy of Sciences Budapest, Hungary, bognor@mail.kfki.hu

Nancy Kopell Department of Mathematics and Center for BioDynamics, Boston University, Boston, MA 02215, USA, nk@math.bu.edu

Ákos Kulik Department of Anatomy and Cell Biology, University of Freiburg, Albertstraße 17, Freiburg, Germany, akos.kulik@anat.uni-freiburg.de

J. Josh Lawrence COBRE Center for Structural and Functional Neuroscience, Department of Biomedical and Pharmaceutical Sciences, University of Montana, Missoula, MT 59812, USA, lawrenjo@mail.nih.gov

Paola Malerba Center for BioDynamics and Department of Mathematics, Boston University, Boston, MA 02215, USA, malerba@bu.edu

Marco Martina Department of Physiology Northwestern, University Feinberg School of Medicine, Chicago, IL 60611, USA, m-martina@northwestern.edu

Jack Mellor MRC Centre for Synaptic Plasticity, Department of Anatomy, University of Bristol, University Walk, Bristol, BS8 1TD, UK, jack.mellor@bristol.ac.uk

Michele Migliore Institute of Biophysics, National Research Council, Palermo, Italy, michele.migliore@yale.edu

Robert J. Morgan Department of Anatomy and Neurobiology, University of California, Irvine, CA 92697-1280, USA, rjmorgan@uci.edu

Dmitri D. Pervouchine Faculty of Bioengineering and Bioinformatics, Moscow State University 1-73, GSP-2 Leninskie Gory, 119992 Moscow, Russia, dp@bioinf.msu.ru

Eleftheria-Kyriaki Pissadaki Institute of Molecular Biology and Biotechnology (IMBB), Foundation for Research and Technology-Hellas (FORTH), Heraklion, Crete, Greece, eleftheria.pissadaki@pharm.ox.ac.uk

Panayiota Poirazi Institute of Molecular Biology and Biotechnology (IMBB), Foundation for Research and Technology-Hellas (FORTH) Heraklion, Crete, Greece, poirazi@imbb.forth.gr

Jonathan E. Rubin Department of Mathematics, University of Pittsburgh, Pittsburgh, PA 15260, USA, rubin@math.pitt.edu

Fernanda Saraga Director of Clinical Research and Education, Meditech International Inc. Toronto, Ontario, Canada, fernanda.saraga@gmail.com

Jonas-Frederic Sauer Institute of Medical Sciences, University of Aberdeen, Foresterhill, Aberdeen, AB25 2ZD, UK, j.sauer@abdn.ac.uk

R. Angus Silver Department of Neuroscience, Physiology and Pharmacology, University College London, London, UK, a.silver@ucl.ac.uk

Frances Skinner Toronto Western Research Institute (TWRI), University Health Network (UHN), Toronto, ON, Canada M5T 2S8; Department of Medicine (Neurology), Department of Physiology, Institute of Biomaterials and Biomedical Engineering, University of Toronto, Canada, frances.skinner@utoronto.ca

Ivan Soltesz Department of Anatomy and Neurobiology, School of Medicine, 117 Irvine Hall, University of California, Irvine, CA 92697-1280, USA, isoltesz@uci.edu

Volker Steuber School of Computer Science, Science and Technology Research Institute, University of Hertfordshire, Hatfield, Herts AL10 9AB, UK, v.steuber@herts.ac.uk

Adriano Tort Edmond and Lily Safra International Institute of Neuroscience of Natal, Federal University of Rio Grande do Norte, Natal, RN 59066, Brazil, adrianotort@gmail.com

Katalin Tóth Centre de recherche Université Laval Robert Giffard, Quebec, QC, G1J 2G3, Canada, toth.katalin@crulrg.ulaval.ca

Balázs Ujfalussy Department of Biophysics, KFKI Research Institute for Particle and Nuclear Physics of the, Hungarian Academy of Sciences Budapest, Hungary, ubi@rmki.kfki.hu

Imre Vida Neuroscience and Molecular Pharmacology, Faculty of Biomedical and Life Sciences, University of Glasgow, Glasgow, G12 8QQ, UK, i.vida@bio.gla.ac.uk

Menno P. Witter Kavli Institute for Systems Neuroscience and Centre for the Biology of Memory, Norwegian University of Science and Technology, NO 7489 Trondheim, Norway, menno.witter@ntnu.no

Isabella Zironi Dipartimento di Fisica, Università di Bologna, Bologna 40127, Italy, zironi@biocfarm.unibo.it

Part I
Experimental Background

Stuart Cobb and Imre Vida

The hippocampus is the one of the most intensely studied structures in the brain. It has been investigated at many different levels in an attempt to understand the neurobiology of learning and memory. The accumulated knowledge of hippocampal anatomy, physiology, and function provides a rich repository of information that presents enormous opportunity to model different aspects of neuronal signaling and information processing within this structure. As a primary focus in neurobiology over many decades, studies of the hippocampus have also helped reveal elementary properties of neurons and neuronal microcircuits.

There are a number of reasons why the study of the hippocampus has been at the forefront of neurobiology research. These include the involvement of this brain structure in learning processes, spatial navigation, as well as in major disease states. Another reason is the ability to readily recognize the hippocampus as well as target it in vivo and isolate it for in vitro investigations. Finally, a major impetus for focusing basic studies of the nervous system on the hippocampus owes to its apparently simple cytoarchitecture and circuitry and thus its tractability as a cortical "model" system. While the hippocampal formation is certainly a highly organized structure and has a striking appearance at the gross level, there continues an evolution in our understanding of the constituent cells, their connectivity, their neurochemical and biophysical properties, and the emergent properties of these in terms of hippocampal-dependent behavior. The complexity of the system can appear overwhelming at first but many governing principles have emerged in terms of connectivity and the roles of different cells and circuits. Nevertheless, many of the details remain to be established and indeed significant gaps persist in our understanding of some key concepts.

In this section, experimental neuroscientists discuss the salient structural and functional properties of the hippocampus. This includes morphological, physiological, and molecular characteristics as well as the connectivity and synaptic properties

S. Cobb / I. Vida (✉)
Neuroscience & Molecular Pharmacology, Faculty of Biomedical and Life Sciences,
University of Glasgow, Glasgow G12 8QQ, UK
e-mail: s.cobb@bio.gla.ac.uk / i.vida@bio.gla.ac.uk

of the various cell types found in the hippocampus. We provide concise overviews of each aspect of hippocampal structure and function and where possible, provide quantitative descriptions of the experimental findings. While we believe this will be a valuable concise summary for all readers interested in the biology of the hippocampus, by conveying often quantitative experimental data from different levels of complexity into a coherent picture, we hope this section will provide a valuable resource for researchers embarking on modeling different aspects of this system.

In the first chapter "Connectivity of the Hippocampus", Menno Witter provides a comprehensive description of the major connectivity of the hippocampal formation. In this, he goes beyond the simplified classical models of anatomical organization to produce an updated and extended connectional scheme that incorporates important new as well as some older but hitherto overlooked details.

In the chapter "Morphology of Hippocampal Neurons", Imre Vida extends this overview to the microcircuit and single-cell levels. He provides detailed quantitative descriptions of dendritic and axonal morphology, as well as connectivity of hippocampal neuron types. While the most detailed quantitative information is available for principal cells, this chapter provides a comprehensive summary of the structural properties of the major anatomically defined classes of interneurons.

In the chapter "Physiological Properties of Hippocampal Neurons", Marco Martina provides a detailed overview of the physiological properties of the different classes of hippocampal neuron from a single cell biophysics perspective. Where possible, he provides detailed quantitative descriptions of the passive and active properties together with a discussion of the significance of these in shaping the electrical behavior of respective cell types.

In the chapter "Glutamatergic Neurotransmission in the Hippocampus", Katalin Tóth moves from individual cells to consider excitatory synaptic communication between neurons in the hippocampus. In this, she provides a detailed yet accessible overview of glutamatergic transmission at different synapses in the hippocampus including key qualitative and quantitative differences in the physiology, biophysics, and pharmacology at different synapses.

In the chapter "Fast and Slow GABAergic Transmission in Hippocampal Circuits", Marlene Bartos and colleagues provide an overview of GABAergic transmissions in hippocampal circuits. In this, they introduce a variety of different forms of GABAergic inhibition and discuss functional differences between ionotropic and metabotropic forms of GABAergic inhibition at different inhibitory synapses.

In the chapter "Synaptic Plasticity at Hippocampal Synapses – Experimental Background", Jack Mellor reviews the different forms of synaptic plasticity that are characteristic of different hippocampal synapses. Ranging from short-term frequency facilitation to more enduring forms of synaptic plasticity, he provides a succinct summary of the experimental background, highlights key literature in this area, as well as quantitative descriptions of plasticity at some major synapses.

In the chapter "Neuromodulation of Hippocampal Cells and Circuits", Stuart Cobb and Josh Lawrence introduce the concept of neuromodulation and the many

ways by which hippocampal cells and circuits can be regulated. Thereafter, they provide a detailed yet condensed summary of the main neuromodulator systems ranging from classical modulators (monoamines and acetylcholine) to neuropeptide modulators and paracrine/autocrine substances.

In the chapter “Neuronal Activity Patterns During Hippocampal Network Oscillations In Vitro”, Tengis Gloveli and colleagues describe the importance and relevance of neuronal activity patterns during hippocampal network oscillations in vitro. They provide a detailed account of the emergent electrical behaviour of hippocampal networks including the importance of intrinsic cellular and synaptic properties in their genesis and modulation.

In the chapter “Neuronal Activity Patterns in Anaesthetized Animals”, Stuart Cobb and Imre Vida extend the concept of patterned neuronal activities by describing physiological patterns of neuronal activity that occur in vivo under anesthetic conditions. Under these circumstances, it is possible to observe highly stereotyped patterns of behavior within different morphologically identified principal and interneuronal cell types when viewed with respect to ongoing EEG states. This precise sculpting of neuronal activity in the temporal domain provides important insights into the spatial and temporal processing of synaptic signals during hippocampal activity in the intact network.

In the final experimental chapter “Spatial and Behavioral Correlates of Hippocampal Neuronal Activity: A Primer for Computational Analysis”, Howard Eichenbaum describes spatial and behavioral correlates of hippocampal neuronal activity. By providing a succinct overview of the literature, he offers a framework for considering the relationship between behavior, the activity of hippocampal neurons, and how these might be modeled.

Connectivity of the Hippocampus

Menno P. Witter

Overview

More than 100 years after the first explorations of the hippocampal region by Ramon y Cajal[1] numerous detailed anatomical studies on various aspects of the region have been published. An increasingly complex picture of the intrinsic wiring has emerged over the years. During the last decade in particular, we have seen an ever-increasing number of potentially relevant connections being added to our already vast knowledge database such that by now the complexity and mere volume of the database are almost beyond comprehension. Several comprehensive reviews have been published to which the reader is referred for many of the connections not covered in this chapter or for more details on the connections described here. Recently, we published an interactive database of all known connections of principle cells in the region of the rat (Van Strien et al., 2009). All these reviews have at least two common features: they contain much valuable information, summarized such that the original publications can be recovered, and they require persistent ambition to read through them in order to obtain the relevant information one might be looking for when studying a particular experimental question.

In many other published reviews, emphasis has been on the functions of the region and most of them use a simplified diagram of the anatomical organization of the region as their reference which we will here refer to as the standard view. Here the aim is to extend this standard view, adding details that have been known for some time, but apparently have not been incorporated yet in the commonly accepted connectional scheme for the region. Use will be made of a standardized scheme of connections which hopefully will facilitate easy dissemination of these adapted connectional concepts for the region. Many of the known connections, such as all extrinsic connections of the HF and EC, will not be covered in this chapter for two reasons. First, the information is already available at a summarized (meta) level and a new summary would not assist those who are in need of anatomical details to contribute to the explanation of the functional outcome of a study. Second, this

M.P. Witter (✉)
Kavli Institute for Systems Neuroscience and Centre for the Biology of Memory, Medical-Technical Research Centre, Norwegian University of Science and Technology, Trondheim, Norway
e-mail: menno.witter@ntnu.no

V. Cutsuridis et al. (eds.), *Hippocampal Microcircuits*, Springer Series in Computational Neuroscience 5, DOI 10.1007/978-1-4419-0996-1_1,

chapter is meant to aid computational modeling of the region, and although computational power is ever increasing, there is still a limit to the amount of details than can be included into a computer model.

Microscopical Anatomy and Nomenclature

Throughout the chapter reference will be made to the hippocampal formation (HF) and the entorhinal cortex (EC) as the two main areas of interest. The HF in turn comprises three distinct sub-regions (Fig. 1): the dentate gyrus (DG), the hippocampus proper (consisting of CA3, CA2, and CA1[1]), and the subiculum (Sub). The HF is a three-layered cortex that can be easily differentiated from the EC, since that has more than three layers (see below). The deepest layer of the HF houses basal dendrites of principal cells and a mixture of afferent and efferent fibers and local circuitry – interneurons. Superficial to this polymorph layer is the cell layer, which is composed of principal cells and interneurons. On top, the most superficial layer is situated that contains the apical dendrites of the neurons and the large majority of axons that provide inputs. In the dentate gyrus these layers are, respectively, referred to as the hilus, granular (cell) layer, and molecular layer (*stratum moleculare*). In the CA region, the superficial layer is subdivided into a number of sub-layers. In the CA3, three sub-layers are distinguished: The *stratum lucidum*, representing the mossy fiber input from the DG, *stratum radiatum*, i.e., the apical dendrites of the neurons in *stratum pyramidale*, and most superficially, the *stratum lacunosum-moleculare* comprising the apical tufts of the apical dendrites. The lamination in the CA2 and the CA1 is similar to that in CA3, with the exception that the *stratum lucidum* is missing. In the Sub, the superficial layer is generally referred to as molecular layer, sometimes divided into an outer and inner portion, and the remaining two layers are referred to as the pyramidal (cell) layer (stratum pyramidale) and stratum oriens. The latter is very thin and quite often not specifically differentiated from the underlying white matter of the brain. The EC, commonly subdivided into a medial (MEC) and a lateral (LEC) part,[2] is generally described as having six layers,a molecular layer (layer I), the stellate cell layer (layer II), the superficial pyramidal cell layer (layer III), a cell-sparse lamina dissecans (layer IV),

[1] In some descriptions CA4 is differentiated in between CA3 and DG, but it has been poorly defined, resulting in using CA4 as an indication of (part of) the hilus (see below) of the DG. Therefore, here I opted not to use this term. Also, the connections of CA2 are not described here. For more details see Witter and Amaral (2004).

[2] The lateral and medial entorhinal cortex or Brodman's areas 28a and 28b, respectively, have been further subdivided by a large number of authors (for a more detailed description and comparison of different nomenclatures used in the rat and in other species the reader is referred to a number of reviews (cf. Witter et al., 1989). In the rat, and likewise in the mouse, a further division into dorsolateral (DLE), dorsal-intermediate (DIE), ventral-intermediate (VIE), caudal (CE), and medial (ME) subdivisions have been proposed (Insausti et al., 1997; van Groen et al., 2003). In monkeys, humans, and in other species in which the entorhinal cortex was described, such as cat, dog, guinea pig, and bat(Amaral et al., 1987; Witter et al., 1989; Buhl and Dann, 1991; Insausti

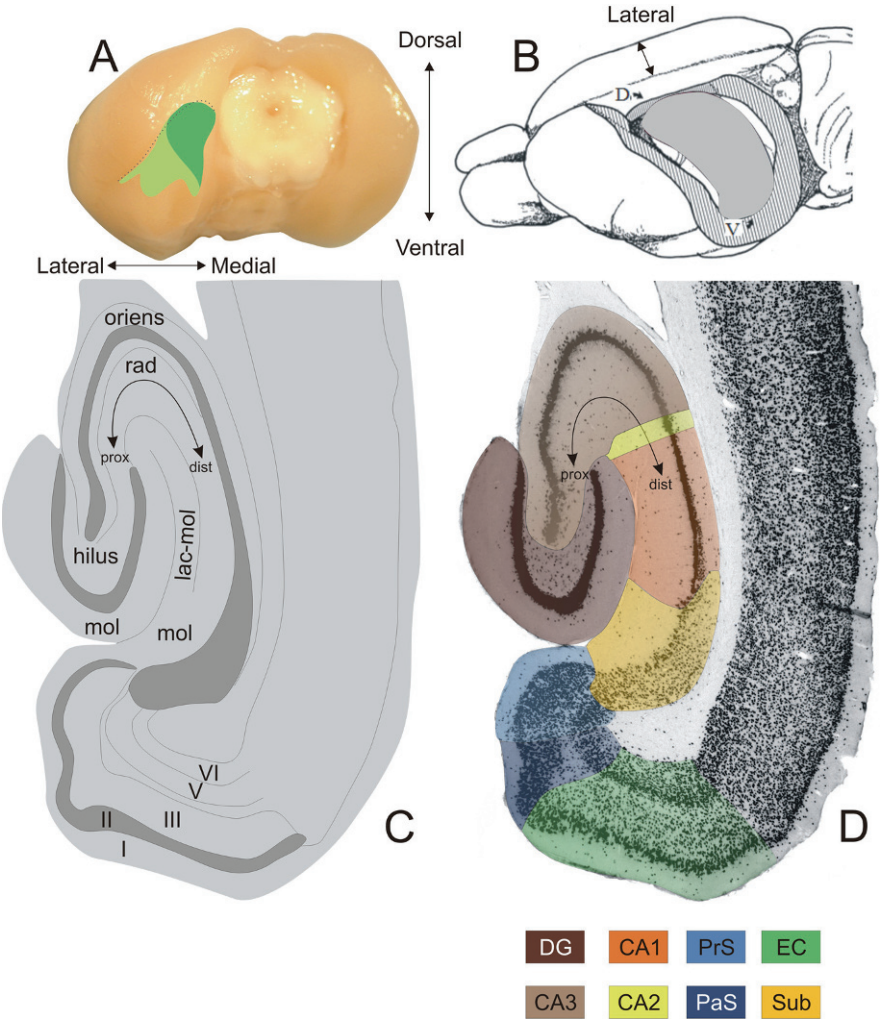

Fig. 1 Schematic representation of the position of the HF and the EC and main topological axes. **a** Posterior view of the rat brain showing the position of the LEC (*light green*) and MEC (*dark green*; modified with permission from Fyhn et al., 2004). **b** Anterolateral view of a dissected brain showing the shape and position of the HF and the longitudinal or dorsoventral axis (modified with permission from Amaral and Witter, 1998). **c** Schematic drawing of a horizontal section illustrating the main nomenclature. **d** Horizontal section stained for the neuronal marker NeuN, illustrating the main subdivisions of HF and the EC

et al., 1995; Uva et al., 2004; Woznicka et al., 2006), comparable partitioning schemes have been proposed. However, in case of most species, there is a tendency to consider the entorhinal cortex as composed of two primary components, the lateral and medial entorhinal cortex, most likely reflecting functional differences.

the deep pyramidal cell layer (layer V), and a polymorph cell layer (layer VI).[3]

In order to understand the anatomical organization it is relevant to describe the coordinate systems that define position within the HF and PHR (Fig. 1). For the HF, there are three relevant axes: the long axis; the transverse or proximodistal axis, which runs in parallel to the cell layer, starting at the DG; and the radial or superficial-to-deep axis, which is defined perpendicular to the transverse axis. In the EC, a similar superficial-to-deep axis is used in addition to mediolateral (proximodistal) and anteroposterior (rostrocaudal) axes.

The Standard Connectional View

According to the standard view (Fig. 2), neocortical projections are aimed at the parahippocampal region, eventually reaching the EC, which in turn provides the main source of input to the hippocampal formation. Within the parahippocampal region, two parallel projection streams are discerned: the perirhinal cortex (PER) projects to the LEC and the postrhinal cortex (POR) projects to the MEC. The

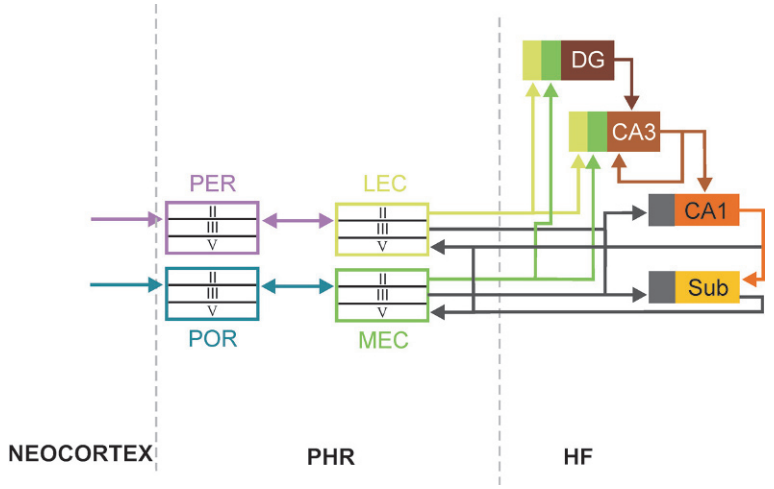

Fig. 2 The standard view of the entorhinal–hippocampal network. Two parallel cortical input streams through the PER and POR reach the LEC and MEC, respectively. Layers II and III of LEC and MEC originate the perforant pathway to all subfields of the HF. The projections from the LEC and the MEC converge onto individual neurons in the DG and the CA3. The CA1 and the Sub send return projections back to layer V of the EC, which in turn project to the PER and POR (modified with permission from Witter et al., 2000)

[3] Note that some authors have adopted a slightly different nomenclature in which the lamina dissecans is either without number or considered to be the deep part of layer III (layer IIIb), such that layer IV is used to designate the superficial part of layer V, characterized by the presence of rather large pyramidal cells that stain strongly for Nissl substance.

EC reciprocates the connections from the PER and POR. The EC is the source of the perforant pathway, which projects to all sub-regions of the hippocampal formation. Entorhinal layer II projects to the dentate gyrus and CA3, whereas layer III projects to CA1 and the Sub. The polysynaptic pathway, an extended version of the traditional tri-synaptic pathway, describes a unidirectional route that connects all sub-regions of the hippocampal formation sequentially. In short, the dentate granule cells give rise to the mossy fiber pathway which targets the CA3. The CA3 Schaffer collaterals project to CA1 and lastly CA1 projects to the Sub. Output from the hippocampal formation arises in CA1 and the Sub and is directed to the parahippocampal region, in particular to the deep layers of the EC.

In the following sections, each of the connections of the traditional view will be reviewed, detailed, and when appropriate appended, starting with the entorhinal projections to the individual subdivisions of the HF.

Entorhinal–Hippocampal Projections

The elaborate Golgi studies of Ramón y Cajal (1911) and Lorente de Nó (1933) first demonstrated that the EC is the origin of an immensely strong projection to the HF, in particular to the DG. The latter became generally known as the perforant path(way). These observations were subsequently corroborated and extended in a seemingly continuous stream of tracing studies that also drew attention to additional projections to the hippocampal fields CA1–CA3 and to the Sub. These additional "non-DG projections" of the EC were actually already described by Cajal, and he did so with remarkable detail. The perforant pathway was described and illustrated as the projection from the EC that perforated the pyramidal cell layer of the Sub, which is easily seen in, for example, a horizontal section through the central part of the rat hippocampus. In the Sub, axons subsequently travel toward DG, crossing the hippocampal fissure, or course in stratum lacunosum-moleculare of CA1, CA2, and CA3 to continue into the tip of the molecular layer of the DG. There is an additional route for entorhinal fibers to reach targets in the hippocampus, referred to as the temporo-ammonic tract. Axons in this pathway, that does not perforate the Sub, travel through stratum oriens of the Sub, CA1–CA3, and will eventually traverse the pyramidal cell layer of the CA fields at specific points and continue to stratum lacunosum-moleculare where they terminate. Note that it is possible that these axons target basal and apical dendrites of pyramidal cells as well as interneurons in strata oriens, pyramidale, and radiatum.[4]

[4] Note that the term temporo-ammonic tract is often used to refer to all of the entorhinal projections to the CA fields, but more commonly only to all fibers that reach CA1. In using the term in such a way the projections to the subiculum would yet need another term. I therefore favor the use of temporo-ammonic tract as originally meant. In the temporal portion of the hippocampus, most of the entorhinal fibers reach CA1 after perforating the subiculum (classical perforant pathway). At

EC Projections to DG and CA3

Cells in layer II of the EC give rise to projections to the DG and CA3 and this observation has been made in most if not all species studied, including humans. It is likely that both the projections to the DG and the CA3 originate as collaterals from the same neuron. Although the organization of the EC projection to the DG has been described in much more detail than the EC to CA3 projection, the latter appears to follow organization principles very similar to those that govern the projection from entorhinal layer II to the DG. Generally, two components are differentiated which have their exclusive origin in the LEC or the MEC, respectively. Projections from the LEC terminate in the outer half of the stratum moleculare of DG and the stratum lacunosum-moleculare of CA3, whereas those from the MEC terminate deep to the lateral fibers (Figs. 2, 3). In the DG, the entorhinal terminal zone occupies the outer two-thirds of the molecular layer and in CA3, the entire radial dimension of stratum lacunosum-moleculare contains entorhinal fibers.[5]

There are conflicting papers on the transverse distribution of the layer II perforant path projection. Whereas in some studies no differences were reported others reported that the lateral perforant pathway preferentially projects to the enclosed blade of the dentate gyrus, and the medial component either does not show a preference or predominantly targets the exposed blade. In CA3 no indications have been found for a further transverse organization, although it should be mentioned that the distribution of apical dendrites makes it likely that neurons in the most proximal portion of CA3 are largely devoid of entorhinal input since their dendrites do not reach into the terminal zone in CA3. In the mouse and the monkey, no transverse organization has been described in either the DG or the CA3 projection.

EC Projections to CA1 and Sub

Layer III of the EC contributes a second component to the perforant path that selectively targets CA1 and the Sub (Fig. 3). Axons originating from the LEC and the MEC show strikingly different terminal patterns, but unlike the layer II projections the difference is not along the radial axis but along the transverse axis. The projec-

---

more septal levels, however, the number of entorhinal fibers that take the alvear temporo-ammonic pathway increases. A third route taken by fibers from the entorhinal cortex involves the molecular layers of the entorhinal cortex, para- and presubiculum, continuing into the molecular layer of the subiculum. The latter route has not been given a specific name.

[5] The laminar pattern has been extensively described in the rat and available data in mice, guinea pigs, and cats indicate a similar laminar terminal differentiation between the lateral and medial components of the perforant path. In contrast, in the macaque monkey the situation is different in that irrespective of the origin in EC, at all levels of the dentate gyrus, projections have been reported to distribute throughout the extent of the outer two-thirds of the molecular layer and stratum lacunosum-moleculare in CA3. It is important though that in all species information from functionally different entorhinal domains converges onto a single population of dentate and CA3 cells.

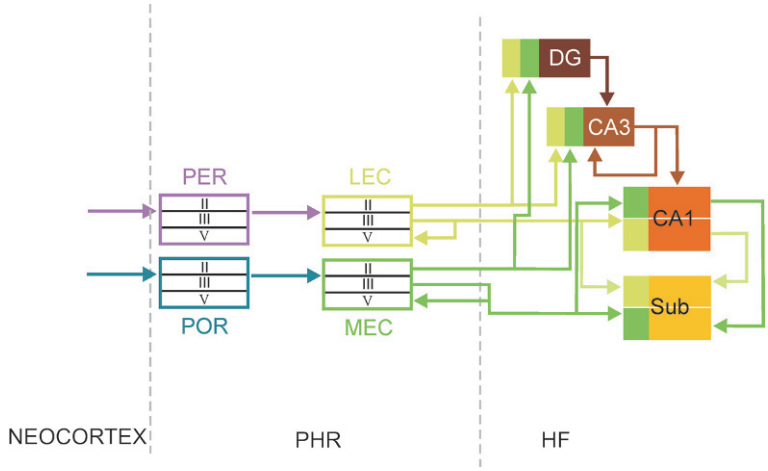

Fig. 3 The extended version of the standard view of the entorhinal–hippocampal network. Note that the differential distribution of the projections from the LEC and the MEC along the transverse axis of the CA1 and the Sub has been included, and the organization of the projections from the CA1 to the Sub and from both back to LEC and MEC is included. The longitudinal topology of neither connections is represented (modified with permission from Witter et al., 2000)

tion that arises from the LEC selectively targets neurons in the distal part of CA1 (the part closest to the Sub) and in the adjacent proximal part of the Sub. In contrast, the projection from the MEC distributes selectively to the proximal CA1 and the distal Sub (Fig. 3).[6] In their respective target domain, entorhinal fibers completely cover the radial extent of stratum lacunosum-moleculare of CA1 and the other portion of the molecular layer of the Sub.

In addition to the main innervations arising from layers II and III in the EC, a projection originating from deep layers has been described as well. In the DG, this deep layer component preferentially distributes to the inner portion of the molecular layer, the granule cell layer, as well as the sub-granular, hilar zone, where it establishes asymmetrical synapses onto granule cell dendrites as well as on their somata and onto spine-free dendrites in the sub-granular zone. The latter most likely represent dendrites of interneurons. In the other divisions of the HF, details on the distribution of this deep pathway are lacking.

Also, inputs from the PrS and PaS reach all hippocampal subfields, where they terminate throughout stratum moleculare/lacunosum-moleculare, overlapping with the inputs from the EC. The CA1 and Sub receive additional inputs from the perirhinal (PER) and postrhinal cortices (POR). The inputs from the PER and POR show a topology along the transverse axis comparable to that seen in case of the projections

[6] In rodents, the layer II components from the LEC and the MEC apparently do not overlap with respect to their respective terminal zone in the molecular layer of the DG and likely the same holds true for CA3. It has not been established whether the same holds true for the respective layer III components, i.e. whether or not they have a zone of overlap in the center part of CA1 or the Sub.

from the LEC and MEC, respectively. However, both projections have a strong preference for the extremes, such that the PER projects to the most distal part of CA1 and the most proximal part of the Sub and the projections from the POR favor the opposite extremes.

Synaptic Organization

In the rat, a majority of the terminals of the perforant path fibers (around 90%) form asymmetric synapses, and thus likely are excitatory, and no major differences have been reported between the lateral and medial components of the pathway. Fibers contact most frequently dendritic spines of dentate granule cells or of pyramidal cells in the CA fields and in the Sub. A small proportion of the presumed excitatory perforant path fibers terminate on non-spiny dendrites of presumed interneurons. In addition, a small proportion of the perforant path synapses is symmetrical, indicative of their inhibitory nature, and these likely target both interneurons and principal cells alike.

In the DG, entorhinal synapses make up at least 85% of the total synaptic population and they target mainly apical dendrites of granule cells. Interneurons that are innervated are those positive for parvalbumin, as well as those positive for somatostatin and NPY. No details have been reported for the CA3, but on the basis of quantitative analyses on reconstructed single neurons (Matsuda et al., 2004), one may assume that a large majority of the excitatory entorhinal fibers terminate on spines, i.e., indicating synapses with pyramidal cells, and only a minor percentage terminate on shafts, taken to indicate presumed contacts with interneurons. Although in the stratum lacunosum-moleculare of the CA3 inhibitory terminals make up approx 10% of the total population, it has not been established whether these all belong to local interneurons or whether part of them have an entorhinal origin. No studies to date have looked into possible interneuron targets for perforant path fibers in the CA3. In stratum lacunosum-moleculare of the CA1, about 15% of the total population of synapses are inhibitory, and the other 85% are excitatory. Unlike the situation in the DG and CA3 where most if not all of the synapses in stratum moleculare/lacunosum-moleculare are of entorhinal origin, in the CA1 the total population of excitatory terminals likely have three different origins, the EC, the thalamic midline nuclei such as nucleus reuniens, and the amygdala.[7] Regarding entorhinal inputs, over 90% is asymmetrical, i.e., excitatory terminating on spines and around 5% is excitatory terminating on shafts. Almost no symmetrical, i.e., inhibitory, entorhinal fibers have been reported in CA1. The terminals on shafts likely indicate that interneurons are among the targets and recently interneurons that reside at the interface between strata

[7] Amygdala inputs reach only the ventral two-thirds of the CA1 and the Sub. The dorsal one-third of both fields is devoid of input from the amygdala.

lacunosum-moleculare and radiatum have been identified as recipients of entorhinal input.

In the Sub, the situation in the superficial half of the molecular layer is likely to be comparable to that in stratum lacunosum-moleculare of the CA1 with the added complexity of having even more inputs distributing here, including those from the PrS, and the PER/POR. Of the entorhinal synapses, over 90% is excitatory, 80% terminates on spines, 10% on dendritic shafts, likely of interneurons, including those containing the calcium-binding protein parvalbumin, and the remaining are symmetrical terminals. The postsynaptic targets have not been identified anatomically, but electrophysiological data indicate that pyramidal cells that project back to the EC are among the targets, an observation that has not been corroborated by anatomical findings (own unpublished data).

Projections from CA1 and Subiculum to Entorhinal Cortex

Transverse and Laminar Organization

The dentate gyrus and the CA3 field of the hippocampus do not project back to the EC. Thus, the recipients of the layer II projection do not have any direct influence over the activities of the EC. It is only after the layer II and layer III projection systems are combined in CA1 and the Sub that return projections to the EC are generated. The return projections mainly terminate in the deep layers (V and VI) although a component ascends into the superficial layers (not indicated in Fig. 4). In case of the projections from the Sub, up to 93% of fibers form asymmetrical, i.e., excitatory, synapses onto dendritic spines (68%) and onto shafts (23%). A small

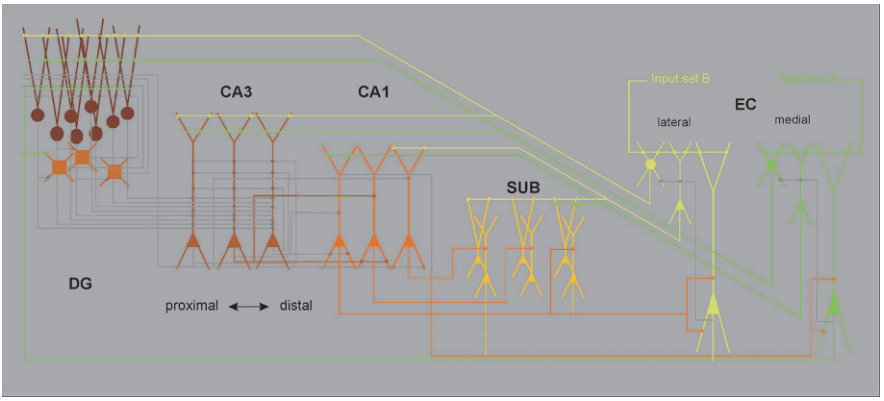

Fig. 4 Wiring diagram, illustrating the organization of the projections from layers II, III, and V of the MEC and the LEC to the various subdivisions of the HF. Note the laminar terminal distribution of the layer II component to the DG and the CA3 and the restricted transverse terminal distribution of the layer III projection to the CA1 and the Sub

proportion (7%) forms symmetrical synapses, equally onto dendritic shafts and spines. Although it is therefore likely that hippocampally processed information largely ends up on entorhinal layer V principal cells, it has not yet been established to the full extent what character these receiving neurons have, with the exception of some preliminary data indicating that at least some of the receiving neurons project to the (infralimbic) cortex. In addition, electrophysiological evidence indicate that among the target cells are neurons in layer V that project to layers II and III of the EC (see Section "*Entorhinal Associational and Commissural System*"). It is relevant to point to the fact that the projections from CA1 and the Sub to the EC show a topology along the transverse or proximo-distal axis. The projections from the proximal part of CA1 and the distal part of the Sub distribute exclusively to the MEC, whereas cells located in the distal part of CA1 and the proximal part of the Sub project mainly to the LEC. In this way the return projections thus maintain the topography displayed by the input projections from the MEC and the LEC.

Longitudinal Organization

In addition to the radial and transverse organization of the layer II and layer III projections, respectively, as described above, all connections between the EC and the HF show a striking topology along the long axis of the HF. Both the projections from and to the EC follow the same principle in that lateral and posterior parts of the EC are connected to the dorsal portion of the HF, whereas increasingly more medial and anterior parts of the EC are connected to more ventral parts of the HF (Fig. 5). It is relevant to point out that this topographical organization is indeed a gradual one such that a small portion of the EC may distribute axons over up to 25–30% of the long axis of the HF and likewise a small part of CA1 and the Sub may distribute axons to a rather extensive area of the EC.

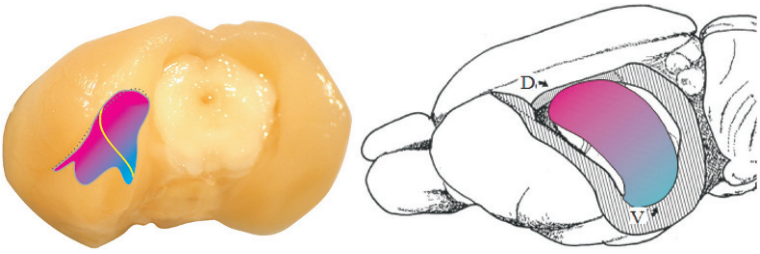

Fig. 5 Longitudinal organization of entorhinal–hippocampal connectivity. A dorsolateral-to-ventromedial gradient in the EC (*left-hand side*; magenta-to-*blue*) corresponds to a dorsal-to-ventral gradient in the HF (*right-hand side*; compare with Fig. 1). Note that the topology in the EC cuts across the MEC–LEC border indicated with the *yellow line* (*left-hand side*, modified with permission from Fyhn et al., 2004; *right-hand side*, modified with permission from Amaral and Witter, 1998)

When taking the transverse and longitudinal organization into account, the important point emerges that these return projections from CA1 and the Sub are exactly in register, i.e., they are point-to-point reciprocal, with the entorhinal inputs to these areas. This remarkable topography confirms the critical role of the EC with respect to the input to, and output from, the HF.

Entorhinal Associational and Commissural System

The EC harbors an extensive, well-developed, yet largely underestimated network of intrinsic connections (Figs. 6 and 7). There are three prevailing organizational principles that govern the overall organization. First, columnar-like projections emanate from layer V pyramidal cells distributing to the superficial layers I–III. This projection consists mainly of asymmetrical synapses (95%) which target presumed principal neurons and interneurons in almost equal proportions. Second, longitudinal connectivity prevails over transverse connectivity. The longitudinal projections that originate from a particular layer will preferentially innervate more superficial layers and they tend to be stronger from posterior (i.e., MEC) to anterior (i.e., LEC) than those that travel into the reverse direction. The transverse connections are much more restricted, and mostly confined to the layer of origin. Fairly strong homotopic commissural projections exist that terminate predominantly in layers I and II.

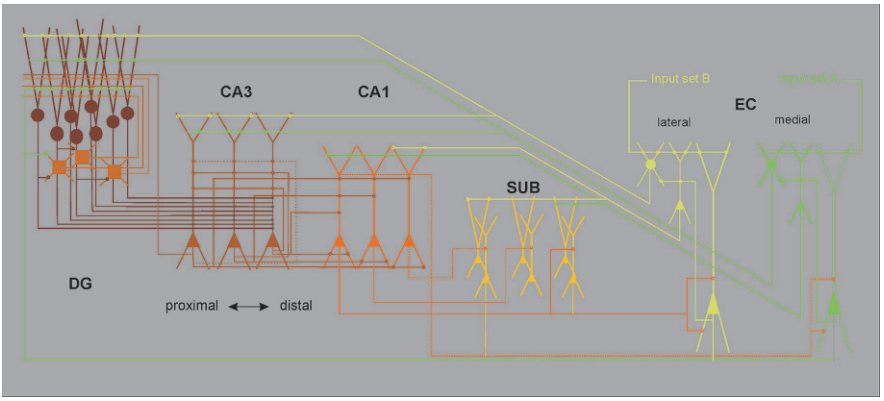

Fig. 6 Wiring diagram, extended version of Fig. 4, illustrating the organization of the intrinsic connections of the HF. Indicated are the mossy fiber projections to the hilus and to the CA3, the return projection from proximal CA3 to the DG, and the diminished contribution of proximal CA3 cells to the associate projection (*stippled line*). Also indicated are the proximo-distal organization of the CA1-to-Sub projections as well as the calbindin-positive associative connection in the CA1. Finally, the intrinsic entorhinal connections from layer V to more superficial layers are indicated. See also Fig. 7 (Note that additional associative networks in the CA1 and the Sub have not been indicated; see text for further details)

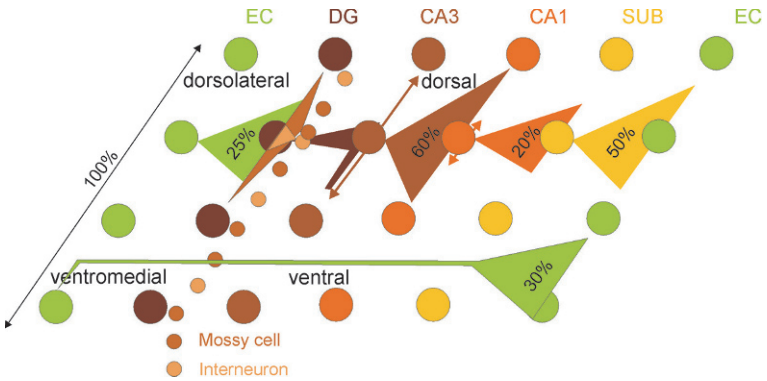

Fig. 7 Schematic representation of the longitudinal divergence of connections between and within subdivisions of the HF and the EC. The dorsoventral extent of the HF is related to the dorsolateral – to – ventromedial extent of the EC. Note the overall predominance of longitudinal connectivity in the system with the exception of the mossy fiber system from the DG to the CA3 (but note the longitudinal spread in distal CA3) as well as the alternating hilar connections arising from mossy cells and a variety of interneurons. The intrinsic network in the CA1 is also rather restricted and for the subiculum data are lacking. Note the preferential longitudinal organization of the intrinsic entorhinal system, almost lacking any transverse connectivity (see text for further details)

Connections of the Dentate Gyrus

Mossy Fiber Projections to Hilus and CA3

Dentate granule cells issue a massive projection of so-called mossy fibers to the entire transverse or proximodistal extent of CA3. Mossy fibers provide en passant presynaptic terminals that are unique with respect to size, anatomical complexity, and the fact that they are correlated with likely complex postsynaptic specializations called thorny excrescences. On their way to field CA3, these fibers contact a fairly large cell type in the hilus called mossy cells. They also give rise to many small collaterals that target a wide variety of presumed interneurons in the hilus (Fig. 6).

The projections from a single neuron or from a small group of neighboring neurons distribute axons within a fairly limited longitudinal extent that hardly ever covers more than 400–500 μm and coincides with their level of origin.There is, however, a noticeable exception, in that mossy fibers abruptly change their course from an overall transverse orientation to a longitudinal one, once they reach the distal end of CA3. The extent of the longitudinal component depends on the dorsoventral level of origin in that granule cells at dorsal levels distribute mossy fibers ventrally for about 2 mm. The more ventral the origin, the less developed the longitudinal projection such that granule cells at the ventral DG have little or no longitudinal component. The longitudinal component of the mossy fiber projection appears synaptically indifferent from the transverse component.

The anatomical organization of the mossy fiber projections along the transverse axis indicates that the influence exerted by granule cells on CA3 pyramidals depends on the position along the transverse axis of DG, since the proximal portion of CA3 is innervated preferentially by neurons in the exposed (infrapyramidal) blade, the crest, and the adjacent portion of the enclosed (suprapyramidal) blade of the DG. The distal portion of CA3 receives mossy fiber input preferentially from granule cells in the enclosed blade of DG.

Current conceptions of CA3 as having a homogeneously wired architecture are incorrect or at least incomplete. Cells at different transverse positions receive inputs from cells in the DG that in turn are different either in their connectivity or in their functionality. In addition, at the most distal end of the dorsal part of CA3, a population of CA3 pyramidal cells most likely integrates inputs from the entire dorsal tip of the DG, a feature which is absent at proximal and mid-transverse levels as well as at ventral CA3 levels.

The DG Associational and Commissural System

The mossy cells in turn give rise to axons that bilaterally innervate the inner molecular layer of the DG, thus providing a powerful excitatory input to the proximal dendrites of the dentate granule cells. Interesting feature of this associational/commissural connection is that it may innervate as much of 65% of the long axis of the DG, but the innervation is weak at the level of origin and increases in density with increasing distance from the origin. Local hilar interneurons provide an inhibitory projection to the outer portions of the molecular layer and this innervation is largely restricted to the level of origin, thus complimenting the excitatory associational system (see also Section “Neurons, Numbers, and Connections,” Fig. 7).

Connections of CA3

The CA3 to Dentate Projections

In contrast to the well-accepted view that projections within the hippocampal formation are largely if not exclusively unidirectional, implying that CA3 does not project to the DG, there is now substantial evidence to support such projections. These connections have not been described in the initial Golgi and subsequent tracing studies. However, intracellular filling consistently showed that pyramidal cells in the most proximal portion of CA3, embedded within the blades of the dentate granule cell layer issue collaterals that reach the hilar region (Fig. 6). Initially described as sparse, true at more dorsal levels of the hippocampal formation, at more ventral levels, CA3 neurons actually densely innervate the DG, not only the hilus, but numerous CA3 axon collaterals also terminate in the most inner portions of the dentate molecular layer. The increase in density of projections to the DG at ventral

levels goes hand in hand with a decreased contribution to the more traditionally known projections to CA1 (see below). Note that also GABAergic projections from CA3 to the DG have been reported.

The CA3 Associational/Commissural System

Local axon collaterals of CA3 axons make preferentially asymmetrical, thus most likely representing excitatory synapses, contacting dendrites of interneurons and importantly also spines of pyramidal cells, thus forming the strong autoassociative network considered to be the characteristic feature of the CA3 network (Fig. 6). The organization of the associational projections from CA3 to CA3 follows a few systematic principles that have been described essentially in two detailed tracing studies using either larger injections of anterogradely transported tracers or intracellular filling of individual CA3 pyramidal cells. Density and extent of local connectivity in CA3 is inversely related to the origin along the proximodistal axis. Irrespective of their dorso-ventral position, CA3 pyramidals embedded within the extent of the DG that, as described contribute to the projection to the DG, do not seem to contribute much to the intrinsic associative system. The associative fibers that do emerge from these CA3 cells are restricted both along the proximodistal axis as well as along the longitudinal (dorsoventral) axis to the level of the parent cell(s). Cells with an increasingly more distal position in CA3 tend to exhibit increased associational axonal collaterals, extending several hundred microns anterior and posterior to the cell body but restricted along the transverse axis to the region of the parent cell body. The proximodistal origin also apparently relates to the radial distribution of the axons, such that proximal neurons preferentially project to stratum radiatum, whereas axons from increasingly more distal cells distribute more to stratum oriens. To further complicate the connectional matrix, the transverse-radial relation varies along the longitudinal axis.

Single pyramidal cells in CA3 not only distribute axonal branches ipsilaterally, but also contralaterally. The detailed topography of the commissural connections has not been as thoroughly investigated as the ipsilateral connections, but it appears an image of the ipsilateral organization for both the projections to CA3 as to CA1 (see below). Also the synaptic organization of both ipsilateral and commissural projections is quite similar. Note that species differences are present with respect to whether or not the commissural connections are present and if present, how they are organized with respect to their longitudinal and radial distribution.

The CA3 to CA1 system – Schaffer Collaterals

Comparable to the situation in CA3, the postsynaptic targets in CA1 for CA3 fibers comprise both interneurons as well as pyramidal cells. CA3 projections distribute in stratum radiatum and stratum oriens of CA1, whereas almost no fibers are present in the pyramidal cell layer (Fig. 6). Almost without exception, the longitudinal extent

of the projections to CA1 is larger than that of the corresponding associative CA3 projections. Irrespective of the level of origin, projections do extent to levels both dorsal as well as ventral to the level of origin, however there is a preferential direction of the projections that relates to the transverse level of origin. Neurons with a proximal location, close to or inside the hilus preferentially project to more dorsal levels, whereas more distal origins result in a shift to more ventral levels. Irrespective of the location of the neuron of origin though, the projections exhibit differences in radial distribution along the long axis of CA1. At more dorsal levels, collaterals tend to be located deeper in stratum radiatum and in stratum oriens, whereas at progressively more ventral levels, the fibers shift towards a more superficial position in stratum radiatum and less dense innervation in stratum oriens. This pattern is thus similar to that described above for the associative CA3–CA3 projections. The transverse position of the parent CA3 neuron does relate, at and around the level of origin to two other features. First, proximal projections tend to distribute somewhat more distally in CA1, and more distal CA3 cells project with some preference to more proximal portions of CA1. Furthermore, proximally originating projections terminate more superficially in stratum radiatum, than distal projections, which distribute deeper in strata radiatum and oriens.

Connections of CA1

The CA1–CA3 Projection

No excitatory projections from CA1 have been described that systematically target neurons in CA3. All the projections that run counter to the traditional unidirectional view apparently arise from a specific group of long-range GABAergic neurons that are prominently present in CA1. These neurons also provide projections the DG, the EC, and the lateral septum.

The CA1 Associational and Commissural System

Although much weaker than in CA3, there are recurrent connections in CA1. Anterograde tracing and intracellular filling date all consistently show that pyramidal cells in CA1 issue collaterals that distribute throughout strata oriens, pyramidale, and radiatum of CA1. Of similar interest are reports on a narrow calbindin-positive bundle of fibers located at the exact border between lacunosum-moleculare and radiatum most likely emerging from calbindin-positive pyramidal cells in the distal part of CA (Fig. 6). The physiological nature and terminal distribution of any of these associational connections needs further study before any functional inferences are intelligible.

The CA1 to Subiculum Projection

Principal cells in CA1 give rise to a strong projection to the Sub, terminating on proximal distal and apical dendrites of subicular pyramidal cells, not innervating the outer half of the molecular layer. Both intracellular fills as well as tracing studies have convincingly shown that this projection shows a marked topology along the transverse axis such that a cell, or group of cells in the proximal one-third of CA1 project to the distal one-third of the Sub. Vice versa, cells in the distal CA1 will exclusively target cells in the proximal portion of the Sub, and cells in the centre of CA1 will reach cells in the centre of the Sub. Note that although a single cell will provide a set of axonal collaterals spanning about one-third of the transverse extent of the Sub, a cell with a slightly shifted position will also slightly shift its axonal pattern slightly in the opposite direction (Fig. 6).

The CA1 to Entorhinal Projection

The projection from all parts of the CA1 to the EC and the complex transverse and longitudinal topology have been dealt with already (See section projection from CA1 and subiculum to entorhinal cortex). Also the striking similarities with respect to these topologies with the reciprocal EC-to-CA1 projection have been mentioned (see also below in the next section on connections of the subiculum).

Connections of Subiculum

The Subiculum to CA1 Projection

According to at least two studies, neurons in the pyramidal cell layer of the Sub send axon collaterals into all layers of CA1. The origin of this projection includes superficial pyramidal cells and is likely to form both excitatory and inhibitory terminals on spines and dendritic shafts respectively. Although no detailed information is available on spread along the transverse or longitudinal axes, the data indicate no marked transverse topography and a restricted longitudinal spread, comparable to the CA1–CA3 projection.

The Subiculum Associational System

There are at least two types of pyramidal celltypes in the Sub that both belong to the group of projection neurons. Both types, the so-called bursters and regular spiking neurons, contribute to an extensive intrinsic innervation in the Sub. Intracellular filling of electrophysiologically identified bursting cells reveals an axonal distribution that remains within the region circumscribed by their apical dendrites. In contrast,

the regular spiking cells give rise to an axon that shows more widespread distribution along the transverse axis. Since these data have been generated in in vitro slices, it is not known whether similar differences exist with respect to a possible longitudinal spread. The longitudinal spread of the average population of neurons covers approximately 0.5–0.7 mm which is about 7% of the long axis.

The Subiculum to Entorhinal Projection

The projections from the Sub to the EC and the complex transverse and longitudinal topology have been described already (See section projection from CA1 and subiculum to entorhinal cortex). Also the striking similarities with the topological organization of the reciprocal EC-to-Sub projection have been referenced.

Neurons, Numbers, and Connections

A number of estimates are available on how many neurons there are in the different areas of the HF and the EC as well as on total dendritic length, number of synapses leading to a number of published attempts addressing questions like how many cells converge on to a single cell, and what is the level of divergence for a single cell axons. Although far from complete, in the following section an attempt is made to summarize those data in rats (Table 1). Note that possible age and strain differences as well as methodological differences are not taken into account.

Numerical estimates have indicated that the population of granule cells may carry a total number of 4.6×10^9 spines of which 77%, i.e., 3.542×10^9 would belong to entorhinal synapses. Taken the total number of entorhinal layer II cells, each of them could potentially contact 32,200 spines. If we would know how many entorhinal inputs target a single granule cell we would be able to estimate how many granule cells would be innervated by a single layer II cell in the EC, i.e., we should have a numerical estimate of the divergence of this connection. By using published estimations of the number of spines on granular cell dendrites (4,600) we could estimate that each granule cell can receive input from maximally $0.77 \times 4{,}600$ is 3,542 cells in EC or 3,542/110.000 is 3.2% of the total layer II population (based on Amaral et al., 1990). Using comparable lines of reasoning, it has been inferred that a single mossy fiber can make as many as 37 synaptic contacts with dendrites of a single CA3 pyramidal cell, a single granule cell may innervate 15 CA3 pyramidal cells, and that a single CA3 pyramidal cell may receive convergent input from 72 granule cells. A single CA3 neuron might be innervated by 6,000 other CA3 neurons, and a single CA1 cell receives input from 5,500 CA3 cells. Details on the Sub and the EC are currently lacking. A final word of caution would be in place since all these numerical estimates assume homogeneity of the network, which most likely will turn out to be a false assumption. For example, it is known that the absolute numbers as well as the percentages of the total population of principal cells and interneurons vary along the

Table 1 Quantitative data on principal neurons in the HF and the EC. Indicated are total number of neurons (# neurons), the average total dendritic length, the percentage of excitatory and inhibitory synapses that impinge on the dendrites, and the estimated total number of synapses/input (# synapses/connection)

	# Principal neurons	Dendritic length in μm	% exc & inh synapses	# Synapses/connection
DG Gcl	1.200.000	3.100		
DG hilus	50.000			
CA3	250.000	16.000	88 exc 12 inb	
CA2	12.000 cassell 1980			
CA1	390.000	12.600	95 exc 5 inh	2.000–3.000 exc EC 12.000 exc CA3
Sub	290.000			
PrS/PaS	700.000			
EC II	110.000			
LEC II	46000–59.500	Stellate 9.300 Polym 7.500 Pyr 9.800		
MEC II	36.000–66.000			
EC III	250.000			
LEC III	153.000	Pyr 11.400		
MEC III	105.000			
EC V & VI	330.000			
LEC V & VI	184.000	Pyr 7.800 Hor 8.200 Polym 10.900		
MEC V & VI	125.000	Pyr 5.200 Hor 7.800 Polym 8.300		

Sources for information: Amaral et al. (1990), Hamam et al. (2000, 2002), Lavenex and Amaral (2007), Matsuda et al. (2004), Megias et al. (2001), Merril et al. (2001), Mulder et al. (1997), Rapp and Gallagher (1996), Rapp et al. (2002), Rasmussen et al. (1996), Tahvildari and Alonso (2005), West et al. (1991).

long axis of the hippocampus. Also differences in numbers of neurons are obvious for the LEC versus the MEC (Table 1).

A complementary approach would be to look at the overall distribution of the individual connections that make up the region of interest. A single entorhinal neuron may distribute its axon along approximately 25% of the long axis of the HF. It has been estimated that in adult animals this axis extends for up to 10 mm, so a single axon targets 2.5 mm of the length of the HF. Axons from granular cells are fairly limited in their longitudinal distribution, extending for about 400 μm in CA3c-b but up to 1.5 mm in CA3a (Fig. 7). The associational projection from the hilus back into the inner molecular layer extends over 6.5 mm, exhibiting a dramatic drop in density around the level of its origin. Note that some other hilar projections, such as those originating from somatostatin positive interneurons, to the outer portions of the molecular layer fill that gap. The subsequent projection from CA3 to CA1

shows a longitudinal extent similar to that of the DG association system, whereas the autoassociative connections are slightly more restricted. The projections from a single cell in CA1 to the Sub extend up to 2 mm along the long axis forming a slab-like innervated strip. The associative connections within CA1 apparently are rather restricted along the long axis whereas currently no data are available for the associational connections in the Sub, be it that they at least extend for 400 μm. Finally the projections from CA1 and the Sub to the EC cover a narrow strip in EC that extends for at least along 60% of the longitudinal extent of either the LEC or the MEC, depending on whether the injection is in proximal or distal part of the Sub respectively.

Experimental Techniques

Most of what is known today about the pathways that connect neurons in different brain regions has been discovered by using neuroanatomical tract-tracing techniques. Tracers are molecules that are either applied extracellularly or intracellularly. In case of extracellular application, the tracer is taken up by neurons at the injection site and transported or diffused within cells. A tracer substance can be transported anterogradely (e.g., *Phaseolus vulgaris leucoagglutinin*), from the soma towards the axon terminals, retrogradely (e.g., Fast Blue), from the axon terminals towards the soma or it can be transported in both directions (e.g., *horseradish-peroxidase*). In case of intracellular application, both autofluorescent dyes (e.g., Lucifer yellow, Alexa dyes) and biotin-conjugated dyes are most often used, since they can be easily visualized for fluorescent or transmitted light microscopy (LM). All these methods can be analyzed using a variety of microscopical techniques, including to some extent electron microscopy (EM). In the latter case, one quite often combines them with lesions. Small lesions (mechanical, toxins, electrolytic) will result in local degeneration of axon terminals that show up as electron dense material in the EM.

Standard light- and confocal techniques, when applied to extracellular tracer deposits allow the visualization of distribution patterns, including laminar distribution, topologies as well as the identification of likely synaptic relationships. They are poor with respect to quantitative resolution since it is very difficult to control or estimate the number of neurons that take up and transport the tracer. A much more reliable but very time consuming method is the intracellular filling of single neurons in vivo and the subsequent complete reconstruction of its dendritic and axonal arborizations. This technique can be combined with anterograde or retrograde tracing to identify projection targets and synaptic inputs. A recently added tool is to make use of retrograde labeling with genetically modified viruses that carry the genes for certain fluorescent proteins such that infected cells express the protein throughout their dendritic and sometimes even axonal arborizations. Still the resolution is a major problem in such analyses.

Electron microscopy can be used to visualize whether a presynaptic axon contacts a post-synaptic identified neuron. This is a very accurate, but time-consuming method because only small pieces of tissue can be examined at one time. A promising development may be the use of automated systems to do serial reconstructions, at the EM level, but also at the LM level, but in all instances our limited understanding of the mechanisms underlying labeling and transport of tracers seriously hampers our aims to generate quantitative data. The only exception is the high standard of unbiased methods to count number of cells, synapses, actually any identifiable element in the nervous system, using stereological approaches. But even when applying such sophisticated methods, one has to be aware of differences between strains, effects of age, environment and gender on quantitative estimates.

The Future: Open Questions and How to Address Them

As already alluded to in the previous sections on methodology, anatomical research still lacks efficient and reliable methods to collect quantitative data. Moreover, with the increased power of resolution and our increased correlative information on how architecture may relate to or even predict function, a number of new and very interesting questions emerge. There are several open questions that ask for our attention.

Many conceptual or theoretical accounts and modeling attempts use a rather simple and generalized representation of what we know as their starting point. This no doubt results from the by now overwhelming amounts of available information. This may eventually lead to disuse of available data, such that they eventually will be forgotten. Our attempts to understand structure needs to take into account all the subtle differences in topology and densities of projections, the many parallel pathways that are so characteristic of the brain and the many different levels of integration that may occur within the different networks that constitute the HF. Many assumptions may prove false, for example the generally accepted concept that a laminar *en passent* type of innervation imply convergence onto particular cells or onto particular dendritic segments. One recent example is the reported striking difference in convergence in CA1 and the Sub; similarly organized pathways in both, but differences in convergence. In CA1, the CA3 input on the proximal apical dendrite of a CA1 pyramidal converges with the entorhinal input onto the distal part of the apical dendrite (Kajiwara et al., 2008). In contrast, in the Sub, the comparably organized inputs from CA1 and the EC apparently do not converge (Cappeart et al., 2007).

What do we know about laminar inputs to the EC, do they converge onto single cells, and do they specifically target neurons in their zone of termination? We are only at the beginning of being able to efficiently answer such questions (Canto et al., 2008). By adding the complexity of the very many specific types of interneurons, our task to describe, to model, and to understand the hippocampus is and will be a major challenge. The combination of anatomical and electrophysiological studies, with the use of promising new genetic tools and computational modeling will provide the foundation for further detailed functional studies in freely behaving

animals, which in turn form the ground work to understand the human hippocampus, both when it is healthy and when it starts to break down, as seen in many neurodegenerative diseases.

Acknowledgments The preparation of this paper has been supported by the Kavli Foundation, the Centre of Excellence scheme of the Norwegian Research Council, and a European Commission Framework 7 project (SPACEBRAIN).

Further Reading

Alonso AA (2002) Spotlight on neurons (II): Electrophysiology of the neurons in the perirhinal and entorhinal cortices and neuromodulatory changes in firing patterns. In: Witter MP, Wouterlood FG (eds) The parahippocampal region, organization and role in cognitive functions. Oxford University Press, London, pp 89–106

Amaral DG, Witter MP (1989) The three-dimensional organization of the hippocampal formation: A review of anatomical data. Neuroscience 31: 571–591

Amaral DG, Lavenex P (2007) Hippocampal neuroanatomy. In: P. Andersen et al. (eds) The hippocampus book, 1st edn. Oxford University Press, New York, pp 37–114

Amaral DG et al. (1987) The entorhinal cortex of the monkey: I. Cytoarchitectonic organization. J Comp Neurol 264: 326–355

Amaral DG, Ishizuka N, Claiborne B (1990) Neurons, numbers and the hippocampal network. Progr Brain Res 83: 1–11

Amaral DG, Scharfman HE, Lavenex P (2007) The dentate gyrus: fundamental neuroanatomical organization (dentate gyrus for dummies). Progr Br Res 163: 3–22

Blaabjerg M, Zimmer J (2007) The dentate mossy fibers: Structural organization, development and plasticity. Progr Br Res 163: 85–107

Buhl EH, Dann JF (1991) Cytoarchitecture, neuronal composition, and entorhinal afferents of the flying fox hippocampus. Hippocampus 1: 131–152

Canto CB, Wouterlood FG, Witter MP (2008) What does the anatomical organization of the entorhinal cortex tell us? Neural Plast 381243

Cappaert NLM, Wadman WJ, Witter MP (2007). Spatiotemporal analyses of interactions between entorhinal and CA1 projections to the subiculum in rat brain slices. Hippocampus 17: 909–921

Fyhn M et al. (2004) Spatial representation in the entorhinal cortex. Science 305: 1258–1264

Hamam BN, Kennedy TE, Alonso A, Amaral DG (2000) Morphological and electrophysiological characteristics of layer V neurons of the rat medial entorhinal cortex. J Comp Neurol 418: 457–472

Hamam BN, Amaral DG, Alonso A (2002) Morphological and electrophysiological characteristics of layer V neurons of the rat lateral entorhinal cortex. J Comp Neurol 451: 45–61

Insausti R et al. (1995) The human entorhinal cortex: a cytoarchitectonic analysis. J Comp Neurol 355: 171–198

Insausti R et al. (1997) Entorhinal cortex of the rat: cytoarchitectonic subdivisions and the origin and distribution of cortical efferents. Hippocampus 7:146–183

Kajiwara R, Wouterlood FG, Sah A, Boekel AJ, Baks-te Bulte LTG, Witter MP (2008) Convergence of entorhinal and CA3 inputs onto pyramidal neurons and interneurons in hippocampal area CA1. An anatomical study in the rat. Hippocampus 18: 266–280

Klausberger T, Somogyi P (2008) Neuronal diversity and temporal dynamics: The unity of hippocampal circuit operations. Science 321: 53–57

Lorente de Nó R (1933) Studies on the structure of the cerebral cortex. J für Psychologie Neurologie 45: 26–438

Matsuda S, Kobayashi Y, Ishizuka N (2004) A quantitative analysis of the laminar istribution of synaptic boutons in field CA3 of the rat hippocampus. Neurosci Res 29: 241–252
Megias M, Emri ZS, Freund TF, Gulyas AI (2001) Total number and distribution of inhibitory and excitatory synapses on hippocampal CA1 pyramidal cells. Neuroscience 102: 527–540
Merril DA, Chiba AA, Tuszynski MH (2001) Conservation of neuronal number and size in the entorhinal cortex if behaviorally characterized aged rats. J Comp Neurol 438: 445–456
Mulders WH, West MJ, Slomianka L (1997) Neuron numbers in the presubiculum, parasubiculum, and entorhinal area of the rat. J Comp Neurol 385: 83–94
Ramón Y, Cajal S (1911) Histologie du Systeme Nerveux de l'Homme et des Vertebres. Paris, Maloine
Rasmussen T, Schliemann T, Sørensen JC, Zimmer J, West MJ (1996) Memory impaired aged rats: No loss of principal hippocampal and subicular neurons. Neurobiol Ageing 17: 143–147
Rapp PR, Gallagher M (1996) Preserved neuron number in the hippocampus of aged rats with spatial learning deficits. Proc Natl Acad Sci USA 93: 9926–9930
Rapp PR, Deroche PS, Mao Y, Burwell RD (2002) Neuron number in the parahippocampal region is preserved in aged rats with spatial learning deficits. Cer Ctx 12: 1171–1179
Tahvildari B, Alonso A (2005) Morphological and electrophysiological properties of lateral entorhinal cortex layers II and III principal neurons. J Comp Neurol 491: 123–140
Uva L et al. (2004) Cytoarchitectonic characterization of the parahippocampal region of the guinea pig. J Comp Neurol 474: 289–303
van Groen T et al. (2003) The entorhinal cortex of the mouse: organization of the projection to the hippocampal formation. Hippocampus 13: 133–149
Van Strien NM. Cappeart N, Witter MP (2009) The anatomy of memory: An interactive overview of the parahippocampal-hippocampal network. Nature Rev Neurosci 10:272–282
West MJ, Slomianka L, Gundersen HJG (1991) Unbiased stereological estimation of the total number of neurons in the subdivisions of the rat hippocampus using the optical fractionator. Anat Rec 231:482–497
Wickersham IR, Finke S, Conzelmann KK, Callaway EM (2007). Retrograde neuronal tracing with a deletion-mutant rabies virus. Nat Methods 4: 47–49.
Witter MP (2006) Connections of the subiculum of the rat: Topography in relation to columnar and laminar organization. Behav Brain Res 174(2): 251–264
Witter MP (2007a) Intrinsic and extrinsic wiring of CA3; Indications for connectional heterogeneity. Learn Mem 14: 705–713
Witter MP (2007b) The Perforant path. Projections from the entorhinal cortex to the dentate gyrus. Progr Br Res 163: 43–61
Witter MP, Amaral DG (2004) Hippocampal Formation, In: Paxinos G (ed) The rat nervous system, 3rd edn. Elsevier Academic Press, San Diego, CA, pp 635–704
Witter MP, Moser EI (2006) Spatial representation and the architecture of the entorhinal cortex. Trends Neurosci 29: 671–678
Witter MP et al. (1989) Functional organization of the extrinsic and intrinsic circuitry of the parahippocampal region. Progr Neurobiol 33:161–254
Witter MP, Groenewegen HJ, Lopes da Silva FH, Lohman AHM (1989) Functional organization of the extrinsic and intrinsic circuitry of the parahippocampal region. Prog Neurobiol 33: 161–253
Witter MP et al. (2000) Cortico-hippocampal communication by way of parallel parahippocampal-subicular pathways. Hippocampus 10: 398–410
Woznicka M et al. (2006) Cytoarchitectonic organization of the entorhinal cortex of the canine brain. Brain Res Rev 52: 346–367
Wouterlood FG (2002) Spotlight on the neurons (I): Cell types, local connectivity, microcircuits, and distribution of markers. In: Witter MP, Wouterlood FG (eds) The parahippocampal region, organization and role in cognitive functions. Oxford University Press, London, pp 61–88

Morphology of Hippocampal Neurons

Imre Vida

Overview

"Form follows function" states the credo of modern architecture, defining how the shape of an object should be determined by its function. While natural objects, such as neurons, have not taken their shapes on design boards, the inquisitive observer can nevertheless gain insights about their function by studying morphological features. This teleological mindset was the main driving force behind the early neuroanatomical investigations, culminating in the work of Cajal, which formed the foundation of modern neuroscience. Neuroanatomical analysis remains an essential part of neuroscience research today and computational neuroscientists, in particular, benefit from the flow of new morphological data with increasing detail and resolution.

Nerve cells or neurons are the structural and functional units of the nervous system and come in various sizes and shapes, conceivably reflecting differences in the functional roles played by the neurons in brain circuits. On the one hand, the distribution of dendrites and axon determines the synaptic inputs and available targets to cells. On the other hand, the three-dimensional structure of neuronal processes constitutes the cable structure in which signals are integrated and processed.

Neurons in cortical areas, including the hippocampus, can be broadly divided into two major classes: principal cells and non-principal cells or interneurons. Principal cells comprise the majority (~80–90%) of the neuronal population and show largely homogeneous but area-specific morphological features. They are glutamatergic, excitatory neurons, and considered to be the workhorse of information processing. They send axon collaterals to other brain areas and therefore are also referred to as "projection neurons." Interneurons are GABAergic, inhibitory cells, and are characterized by dense local axonal arbor which enables them to control and coordinate the activity of large populations of local neurons. Although interneurons comprise only a small proportion of the neuronal population, they display a high degree of morphological heterogeneity and can be subdivided into a number of types.

I. Vida (✉)
Neuroscience & Molecular Pharmacology, Faculty of Biomedical and Life Sciences,
University of Glasgow, Glasgow G12 8QQ, UK
e-mail: i.vida@bio.gla.ac.uk

V. Cutsuridis et al. (eds.), *Hippocampal Microcircuits*, Springer Series in Computational Neuroscience 5, DOI 10.1007/978-1-4419-0996-1_2,

The diversity of the interneurons conceivably serves a division of labor in spatio-temporal control of principal cell activity.

In this chapter we will review the morphological characteristics and local connectivity of the various neuron types in the hippocampus of rodents. Although, due to the possibilities offered by genetically modified organisms, studies more commonly use mice nowadays, the majority of data available in the literature are still from the rat hippocampus.

The Data

Anatomical Structure and Nomenclature

The hippocampus is a phylogenetically ancient cortical structure ("archicortex") which evolved from the dorsomedial aspects of the cerebral hemispheres. It consists of two interlocked folds of the cortical mantel, the hippocampus proper and the dentate gyrus (DG) (Cajal, 1968; Lorente de Nó, 1934). Macroscopically the curved structure of the hippocampus bears some resemblance to the horns of a ram, hence its Latin name *cornu ammonis* (CA). Its cranial ("septal") pole is located close to the midline in the dorsal part of the hemisphere, below the *corpus callosum*, whereas its caudal ("temporal") pole extends ventrolaterally into the temporal lobes (see Fig. 1 in the chapter "Connectivity of the Hippocampus").

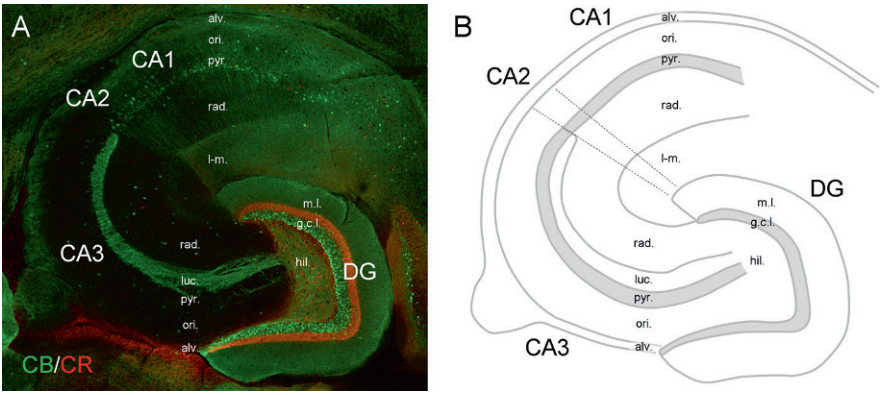

Fig. 1 Areas and layering of the hippocampus. **A** Transverse section from the mouse ventral hippocampus immunostained for the calcium-binding proteins calbindin (CB, *green*) and calretinin (CR, *red*). CB is expressed by GCs and a subset of CA1 pyramidal cells. Therefore the DG and the CA1 area show labeling of the cell bodies and a homogeneous staining of the dendritic layers. In the CA3 area, the narrow band of GC axons (the mossy fibers) is labeled in the stratum lucidum (luc.). CR immunostaining labels mossy cells in the hilus (hil.) and delineates the termination of their axon in the inner third of the molecular layer (m.l.) of the mouse hippocampus. In addition to principal cells, a subset of interneurons scattered throughout the hippocampus can be seen labeled by either CB or CR. **B** Schematic drawing of the areas and layers of the hippocampus. Abbreviations: alv. – alveus; ori. – stratum oriens; pyr. – pyramidale; rad. – radiatum; l-m. – lacunosum-moleculare; g.c.l. – granule cell layer. *Dashed lines* indicate borders between the CA areas

In cross sections, the hippocampus proper (CA areas) and the DG form two interlocked "C" shapes (Fig. 1). The hippocampus proper features pyramidal cells and can be cytoarchitectonically divided into the CA1, CA2, and CA3 areas (Lorente de Nó, 1934). Lorente de Nó further subdivided the CA1 and CA3 areas to three zones along the transverse axis: "a" (closer to the subiculum), "b," and "c" (closer to the hilus). In contrast to the CA regions, the DG comprises a homogeneous population of granule cells (GC). The interface between the DG and CA areas is called the *hilus* which contains a third population of principal cells, the mossy cells. The hilus differs from other parts of the hippocampus in that it shows no clear lamination and the ratio of principal cells and interneurons is close to 1:1. It has been a matter of some controversy whether it belongs to the hippocampus proper as a CA4 area (Lorente de Nó, 1934) or to the DG as a "polymorphic layer" (Blackstad, 1956; Amaral, 1978). Because of the tight mutual connectivity the general consensus seems to favor the latter hypothesis, the term CA4 being no longer used. Nevertheless, the hilus is often silently regarded as an area on its own right.

The hippocampus displays a strictly laminated structure (Förster et al., 2006; Fig. 1). Principal cells are tightly aligned and their somata form well-defined layers, the stratum (str.) pyramidale in the CA areas and the granule cell layer in the DG. The multiple curvatures of the hippocampus mean that the orientation of principal cells depends on their position along the septo-temporal and the transverse axes. Vertical positions are therefore referenced to the main axis of the principal neurons. The neuropil in the CA areas is subdivided into three major layers (from basal to apical direction): (1) the str. oriens, which is beneath the cell body layer; (2) the str. radiatum above the cell body layer; and (3) the str. lacunosum-moleculare. The str. oriens and radiatum are the innervation zones for the commissural/associational axons originating in the ipsi- and contralateral CA3 areas. The str. lacunosum-moleculare is the layer in which the perforant path axons from the entorhinal cortex terminate. In the CA3 area, there is an additional narrow layer, the str. lucidum, immediately above the cell body layer, which corresponds to the projection of the mossy fibers from the DG (for further details on connectivity see chapter "Connectivity of the Hippocampus"). Finally, a thin layer of white matter consisting of afferent and efferent axons, the alveus, is found below the str. oriens.

In the DG, the neuropil above the granule cell layer forms the molecular layer. Similar to the CA3 areas commissural/associational axons, originating primarily from hilar mossy cells, terminate proximally in the inner third of the molecular layer and perforant path axons innervate the middle and the outer thirds. As noted above, the area beneath the cell body layer is regarded as the polymorphic layer of the DG although GCs have no basal dendrites and only their axons extend into the region.

Principal Cells

Principal cells of the hippocampus include the pyramidal cells of the CA areas, GCs of the DG, and mossy cells of the hilus, each of which form largely homogeneous populations.

CA1 Pyramidal Cells

Pyramidal cells of the CA1 are one of the best-investigated types of neurons in the brain. These neurons are characterized by a pyramidal or ovoid soma, a large-caliber apical dendrite, and a number of small-caliber basal dendrites (Fig. 2A, B). Cell bodies of CA1 pyramidal cells are found in the cell body layer (str. pyramidale) or the adjacent region of str. oriens; however, displaced pyramidal cells have been identified in the str. radiatum (Cajal, 1968; Gulyás et al., 1998). The cell bodies have a diameter of $\sim$15 μm and a surface area of 465 $\pm$ 50 μm^2 (Megías et al., 2001). The apical dendrites (typically 1, occasionally 2) extend into the str. radiatum giving off 9 and 30 oblique side branches in this layer (Bannister and Larkman, 1995a). They end with a bifurcation in the str. radiatum and form a dendritic tuft in the str. lacunosum-moleculare. Two to eight basal dendrites emerge from the base of the cell body in the str. oriens. These dendrites bifurcate repeatedly close to the soma and the long terminal branches run toward the alveus.

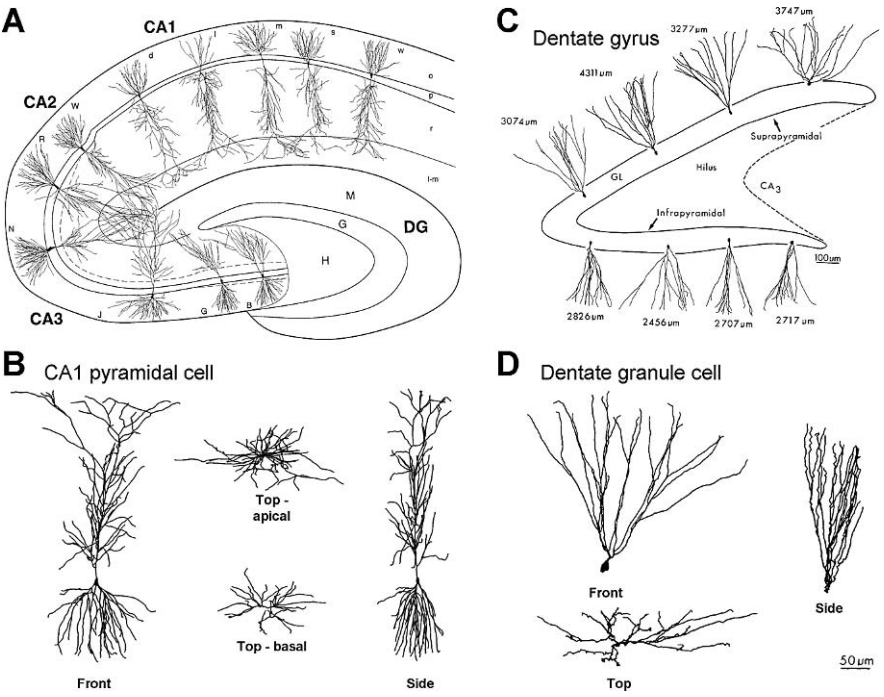

Fig. 2 Morphology of hippocampal principal cells. **A** Pyramidal cells of the CA1, CA2, and CA3 area. **B** Three-dimensional structure of a CA1 pyramidal cell illustrated from frontal, side, and top views. **C** Morphological diversity of DG GCs. Values adjacent to the cells indicate the total dendritic length. Note the difference between the upper (suprapyramidal) and lower (infrapyramidal) blades. **D** Three-dimensional structure of a GC illustrated from frontal, side, and top views (**A**, **B** from Ishizuka et al., 1995; **C**, **D** from Claiborne et al., 1990, reproduced with permission.

The total dendritic length of CA1 pyramidal cells has been reported to be in the range of 11.5 and 17.5 mm (Table 1). The considerable variability could be due to differences in the strain, sex, and age of the rats, as well as the experimental approach used in the studies (i.e., in vitro vs. in vivo labeling, correction for shrinkage). Corresponding estimates of the somatodendritic surface area are 28,860 and 36,000 μm^2, excluding dendritic spines (Bannister and Larkman, 1995b, Cannon et al., 1999; Table 1). However, dendrites of CA1 pyramidal cells are densely covered with spines and therefore they can significantly influence the calculated surface area. The total number of spines has been estimated to be over 30,000 (Bannister and Larkman, 1995b, Megías et al., 2001; see Table 2). Bannister and Larkman (1995b) calculated that spines increase the dendritic surface area by a factor of 0.89 in CA1 pyramidal cells. The distribution of spines is not homogeneous on the dendritic surface. Density is higher, with values between 1.26 and 1.43 μm^{-2} in the str. oriens and radiatum, and lower, with 0.6 μm^{-2} in the str. lacunosum-moleculare (Bannister and Larkman, 1995b). These surface density values correspond to a linear density of 7.5 μm^{-1} on the apical trunk, 2.4 – 3.2 μm^{-1} on basal and oblique dendrites, and 1.4 μm^{-1} on dendrites of the apical tuft (Bannister and Larkman, 1995b); these

Table 1 Dendritic length and somatodendritic surface area of CA1 pyramidal cells

	Dendritic length (μm)		Surface area (μm^2)	Reference/Rat strain, age
Total	13,424 ± 1,061			Ishizuka et al. (1995)
L-M	2.531 ± 571	18.8%		Sprague-Dawley, 33–57 days
Rad	6,307 ± 975	47.0%		In vitro labeling
Ori	4,586 ± 935	34.2%		
Total	16,300 ± 4,330			Pyapali et al. (1998)
Apical	11,300 ± 4,080	69.5%		Fischer 344, male, 2 months
Basal	5,070 ± 1,160	30.5%		In vitro labeling
Total	17,400 ± 3,900			Pyapali et al. (1998)
Apical	10,600 ± 2,450	60.9%		Sprague-Dawley, 2–8 months
Basal	6,890 ± 2,110	39.1%		In vivo labeling
Total	11,915 ± 1,030		28,860 ± 3,102	Bannister and Larkman (1995a, b)
L-M	2,259 ± 526	19%		Sprague-Dawley, male, 100–150 g
Rad	4,118 ± 1,203	35%		In vitro labeling
Ori/Pyr	5,538 ± 943	47%		
Total	17,400 ± 6,200		36,100 ± 17,000	Cannon et al. (1999)
				Sprague-Dawley, 2–8 months
				In vivo labeling
Total	11,549 ± 2,010			Megías et al. (2001)
L-M	2,712 ± 873	23.5%		Wistar, male, ~300 g
Rad	4,638 ± 1,022	40.2%		In vivo labeling
Ori	4,198 ± 1,056	36.3%		

Values are mean ± S.D. Surface area is given without spines.

Table 2 Laminar distribution of excitatory and inhibitory synapses on CA1 pyramidal cells

	Spines		Synapses	GABA(−) synapses		GABA(+) synapses	
Total	30,382 ± 5,214		32,351 ± 5,486	30,637 ± 5,259	(94.7%)	1,713 ± 261	(5.3%)
L-M	1,521 ± 541	(5.0%)	2,110 ± 726	1,776 ± 613	(84.2%)	334 ± 113	(15.8%)
Rad	16,878 ± 3,964	(55.6%)	17,619 ± 4,085	16,878 ± 3,964	(95.8%)	741 ± 126	(4.2%)
Ori	11,982 ± 3,164	(39.4%)	12,621 ± 3,292	11,982 ± 3,164	(94.9%)	639 ± 147	(5.1%)
Soma	N/A		92 ± 12	0	(0%)	92 ± 12	(100%)
AIS	N/A		24 ± 2	0	(0%)	24 ± 2	(100%)

Values represent estimated numbers of synapses expressed as mean ± S.D. Percentage values for the spines indicate the proportions found in the different layers; percentages after synapse numbers indicate the proportion of putative excitatory GABA-immunonegative (GABA (−)) and GABA-positive (GABA (+)) synapses. Data from Megías et al. (2001).

values are in good agreement with electron microscopic estimates of spine density (Harris et al., 1992).

Spines serve as postsynaptic targets primarily for glutamatergic terminals; therefore their high numbers indicate a massive excitatory synaptic input to these cells. In fact, in a detailed morphological study, Megías et al. (2001) showed that on average ∼30,600 terminals converge and form asymmetrical, putative excitatory synapses onto a single CA1 pyramidal cell (Table 2). Over 99% of these asymmetrical synapses are located on dendritic spines, although in the str. lacunosum-moleculare up to 17% of the synapses can be found on dendritic shafts. Somata of pyramidal cells are devoid of excitatory synapses (Fig. 3).

The number of symmetrical putative inhibitory synapses formed by GABA-immunopositive boutons is much lower. A single neuron receives ∼1,700 symmetrical synapses, which correspond to only 5.6% of the total number of synapses (Megías et al., 2001). In contrast to excitatory synapses, a large proportion (40%) of inhibitory synapses are found in the perisomatic domain, with 7% of the synapses located on the soma and the axon initial segment and 33% on proximal dendrites. In these compartments, inhibitory synapses comprise 50–100% of all synapses. In contrast, on dendrites in the str. radiatum and oriens the proportion of these synapses is only 4–5%. Interestingly, on distal apical dendrites in the str. lacunosum-moleculare the proportion increases again to 16% (Table 2). On the dendrites, almost all (>98%) inhibitory terminals form contacts with shafts. However, as an exception to this rule, in the str. lacunosum-moleculare 10–20% of the inhibitory synapses have been found on spines (Megías et al., 2001).

The axon of pyramidal cells typically originates from the base of the soma, but it may also emerge from one of the proximal basal or the apical dendrites. The main collaterals run in the alveus and are directed toward the fimbria/fornix, the subiculum, and the entorhinal cortex (see chapter "Connectivity of the Hippocampus"). Although the extent of local arborization is limited, axon collaterals are present in the str. oriens and to a lower degree in the radiatum. These collaterals provide a major excitatory input to interneurons providing feedback inhibition, in particular to somatostatin-immunopositive, O-LM interneurons (Blasco-Ibáñez and Freund, 1995; Katona et al., 1999a; Csicsvari et al., 1998; Maccaferri et al., 2000). Additionally, these collaterals also form synapses onto neighboring CA1 pyramidal cells; however, the recurrent connectivity in the CA1 area is very low at only ∼1% (Deuchars and Thomson, 1996).

CA3 Pyramidal Cells

Pyramidal cells of the CA3 area show many similarities in their morphology to CA1 pyramidal cells. There are, however, a number of notable differences. The cell bodies are larger and have a surface area approximately two to four times higher than that of CA1 pyramidal cells. The apical dendrites bifurcate closer to the str. pyramidale and often two or three apical dendrites emerge from the apical pole of the elongated soma. Finally, proximal dendrites of CA3 pyramidal cells bear large complex spines ("thorny excrescences"). These complex spines are the post-

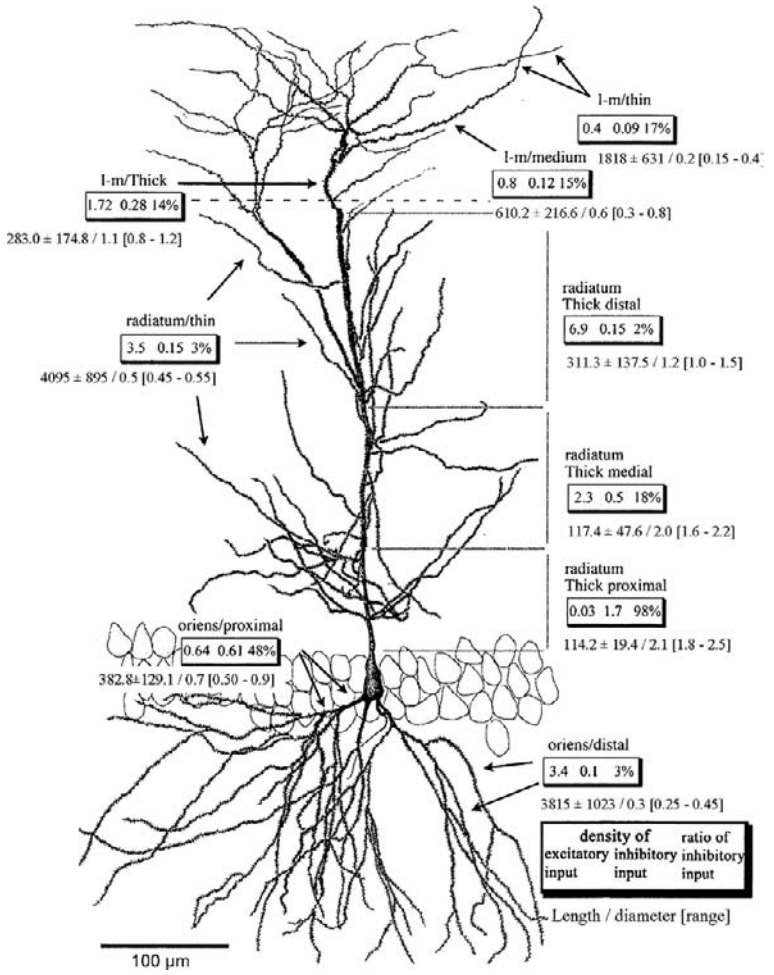

Fig. 3 Distribution of synapses on the dendrites of CA1 pyramidal cells. The drawing illustrates the subclasses of dendrites distinguished in the study by Megías et al. (2001). In the str. oriens, two types of dendritic processes were classified: first-order proximal basal dendrites with low spine density (oriens/proximal) and higher order distal dendrites with high spine density (oriens/distal). In the str. radiatum, four subclasses of dendrites were distinguished. The thick apical dendritic trunk was divided into three segments: a proximal part with no spines (radiatum/thick/proximal), a medial sparsely spiny part (radiatum/thick/medial), and a densely spiny distal part (radiatum/thick/distal). The fourth type corresponds to the thin oblique side branches (radiatum/thin). In the str. lacunosum-moleculare, three subclasses of dendrites were identified on the basis of diameter and spine density: thick dendrites possessed fewer spines (l-m/thick); intermediate sparsely spinous (l-m/medium), and more distal thin and nearly spine-free dendrites (l-m/thin). For every dendritic subclass the density of asymmetrical, putative excitatory and symmetrical, putative inhibitory synapses (*boxes*, left and middle numbers, respectively [μm^{-1}]), and the proportion of symmetrical synapses (*boxes*, right number) are shown. Values below the *boxes* indicate total length (mean ± S.D.) and diameter (mean and range in μm) (Modified from Megías et al., 2001 with permission. © Elsevier.)

synaptic targets of mossy fiber boutons (Blackstad and Kjaerheim, 1961; Claiborne et al., 1986; Chicurel and Harris, 1992).

The total dendritic length of CA3 pyramidal cells (Table 3) is comparable to that in the CA1 area. However, the cell-to-cell variability is higher, partially due to structural differences along the transverse axis of the CA3 (Ishizuka et al., 1995; Turner et al., 1995). Estimates of the somatodendritic surface without spines range between 22,033 and 50,400 μm^2 (Henze et al., 1996; Cannon et al., 1999). Spines enlarge the dendritic surface by a factor of 0.88 (based on data by Major et al., 1994, Table 3). The density (2.9 μm^{-1}) and total number (33,200) of spines are also similar to those in the CA1 area (Major et al., 1994).

Complex spines are found in small clusters on the proximal apical dendrite in the str. lucidum, corresponding to the termination zone of mossy fibers (Gonzales et al., 2001). In the CA3c, where mossy fibers form an infrapyramidal bundle, spines can also be found on the proximal basal dendrites. Due to limitations of light microscopy, the resolution of individual spines is difficult, but estimates suggest that the number of complex spines on a single CA3 pyramidal cell can be up to 41 (Gonzales et al., 2001). As each complex spine is contacted by a single mossy fiber bouton (Chicurel and Harris, 1992; Acsády et al., 1998), this number defines the convergence of GCs onto CA3 pyramidal cells. Although there is only limited information about other excitatory synaptic inputs to CA3 pyramidal cells, the distribution of dendrites and the number of spines suggest that the total number of synapses made by commissural/associational and perforant path axons is comparable to the numbers obtained in the CA1 area.

The axon of CA3 pyramidal cells emanates typically from the soma or one of the proximal dendrites. The main projection is to the ipsi- and contralateral hippocampi, forming the commissural/associational pathways to the CA3 and CA1 areas; the latter is referred to as the Schaffer collateral pathway (Ishizuka et al., 1990, Li et al., 1994). There are, however, also collaterals, mostly arising from the CA3c, which are directed to the hilus and the DG (Li et al., 1994; Scharfman, 2007). The length of the axon ipsilaterally ranges between 150 and 300 mm and may contact up to 30,000–60,000 postsynaptic neurons (Li et al., 1994). The majority of targets cells (85%) are innervated through a single synaptic contact (Sík et al., 1993; Gulyás et al., 1993b). Axons originating in the CA3a area terminate to a larger degree in the CA3 than in the CA1 area (ratio 3:1) whereas for the CA3c area the termination pattern is inverse (ratio 1:3, Li et al., 1994). Thus, local targets of a single CA3 pyramidal cell may vary between ~7,500 and 45,000 (i.e., 5–30% of the ~140,000 neurons comprising the CA3 population). Postsynaptic targets include interneurons, such as parvalbumin-containing basket cells, in proportion to their occurrence (Sík et al., 1993; Gulyás et al., 1993b).

CA2 Pyramidal Cells

CA2 pyramidal cells show morphological features in between those of the CA1 and CA3 areas. Cell bodies of these neurons are as large as those of CA3 pyramids, but the cells lack complex spines and their dendritic arborization pattern is

Table 3 Dendritic length and somatodendritic surface area of CA3 and CA2 pyramidal cells

	Dendritic length (μm)		Surface area (μm²)		Reference Rat strain, age
CA3c ($n = 4$)					
Total	11,169 ± 878[a]		59,900 ± 4,738		Major et al. (1994)
Dendrites			30,600 ± 4,700		Wistar, 18–21 days
Dendrites with spines			57,600[a]		In vitro labeling
Soma			2,300 ± 600		
Axon			22,600 ± 3,000		
CA3 ($n = 20$)					
Total	12,482 ± 2,999				Ishizuka et al. (1995)
L-M	1,983 ± 458	15.9%			Sprague-Dawley, 33–57 days
Rad	4,382 ± 975	35.1%			In vitro labeling
Luc/Pyr	471 ± 250	3.8%			
Ori	5,646 ± 1,745	45.2%			
CA3a ($n = 4$)					Turner et al. (1995)
Total	19,800 ± 2,030				Sprague-Dawley, 2–8 months
					In vivo labeling
CA3b ($n = 4$)					
Total	19,100 ± 2,330				
CA3c ($n = 4$)					
Total	10,400 ± 720				
CA3b ($n = 8$)					
Total	11,394 ± 1,735		22,033 ± 3,559		Henze et al. (1996)
Apical	6,332 ± 1,029	55.6%	12,629 ± 3,556	57.3%	Sprague-Dawley, 28–35 days
Basal	5,062 ± 1,397	44.4%	9,404 ± 4,958	42.7%	In vitro labeling
CA3 ($n = 15$)					
Total	18,100 ± 8,600		50,400 ± 24,000		Cannon et al. (1999)
					Sprague-Dawley, 2–8 months
					In vivo labeling
CA2 ($n = 14$)					
Total	15,406 ± 950				Ishizuka et al. (1995)
L-M	4,672 ± 293	30.3%			Sprague-Dawley, 33–57 days
Rad	4,799 ± 732	31.1%			In vitro labeling
Pyr	71 ± 34	0.5%			
Ori	5,865 ± 491	38.1%			

Values are given as mean ± S.D. Surface area is given without spines, unless otherwise indicated.
[a]These values was calculated using the spine numbers, densities and the assumed surface area of spines (0.83 μm²).

more similar to that of CA1 pyramids (Ishizuka et al., 1995; Mercer et al., 2007). Quantitative analysis of the dendrites of in vitro-labeled neurons indicates that CA2 pyramidal cells have the highest total dendritic length compared to CA1 and CA3 pyramidal cells in the same study (Ishizuka et al., 1995; but see Mercer et al., 2007). The difference is primarily due to the higher length of dendrites in the str. lacunosum-moleculare, whereas in the strata radiatum and oriens, values are comparable (Ishizuka et al., 1995; Table 3).

There is little information on the synaptic connectivity of these neurons. Two major excitatory inputs are the commissural/associational fibers and the perforant path with similar termination as in the CA1 and CA3 areas. Inhibitory innervation of the CA2 area strongly overlaps with both the CA1 and the CA3 areas (Mercer et al., 2007). Axons of CA2 pyramidal cells, similar to CA3 pyramids, project to the ipsi- and contralateral CA1–3 areas contributing to the commissural/associational system (Tamamaki et al., 1988; Li et al., 1994; Mercer et al., 2007). The ipsilateral length of an axon was measured to be ∼150 mm, further indicating that not only the distribution but also the number of postsynaptic targets is comparable to those of CA3 pyramids (Li et al., 1994).

DG Granule Cells

GCs are characterized by a strictly bipolar morphology: spiny dendrites originate from the upper pole of the soma and an axon emerges from the base (Fig. 2C, D; Seress and Pokorny, 1981; Claiborne et al., 1990; Schmidt-Hieber et al., 2007). The small, round, or ovoid cell bodies have a diameter of ∼10 μm and are located densely packed in the GC layer. One to four primary dendrites arise from the soma and bifurcate three to six times to form a dendritic tuft in the molecular layer. Terminal branches extend mostly to the hippocampal fissure and the tuft occupies a conical-shaped volume within the molecular layer with a wider transverse (∼300 μm) and a narrower (∼180 μm) septo-temporal extent. Dendrites show a gradual taper with diameters changing from ∼1.5 μm on proximal dendrites to 0.7 μm on distal dendrites (Schmidt-Hieber et al., 2007). The total dendritic length ranges between 2,324 and 4,582 μm, substantially shorter than for pyramidal cells (Claiborne et al., 1990; Table 4). While morphological features of these neurons are largely homogeneous, quantitative differences exist between the upper and the lower blades, as well as between superficial (near the molecular layer) and deep cells (near the hilus; Claiborne et al., 1990). Superficial neurons in the upper blade have the highest total dendritic length and the widest arbor, whereas deep neurons in the lower blade have the shortest length and the narrowest transverse extent (Table 4).

Similar to pyramidal cells, GC dendrites are densely covered with spines. The total number was calculated to be between 3,091 and 6,830 on the basis of a light microscopic estimate of spine density ($2.39 \pm 0.06\,\mu m^{-1}$; Schmidt-Hieber et al., 2007). Electron microscopic investigation obtained similar density values and indicated moderate differences between proximal ($3.36 \pm 0.35\,\mu m^{-1}$), mid-distal ($2.88 \pm 0.33\,\mu m^{-1}$), and distal ($2.02 \pm 0.28\,\mu m^{-1}$) dendritic segments (Hama et al., 1989). The differences in the density are largely explained by the decreasing

Table 4 Dendritic length and spine numbers of dentate GCs

Dendritic segments	Dendritic length (μm)	Surface (μm^2)[a]	Spine number (density [μm^{-1}])	Region	Reference Rat/Mouse strain, age
29 ± 1	3,221 ± 78			Pooled data	Claiborne et al. (1990)
31 ± 1	3,484 ± 130			Upper, superf.	Sprague-Dawley, 35–49 days
30 ± 1	3,468 ± 92			Upper, deep	In vitro labeling
28 ± 1	2,875 ± 95			Lower, superf.	
25 ± 1	2,629 ± 86			Lower, deep	
32 ± 3	2,264 ± 133	13,300 ± 900		Pooled data	Schmidt-Hieber et al. (2007) Wistar, 2–4 months In vitro labeling
24 ± 5	1,985 ± 160		2,254 ± 317 (1.14 ± 0.15)	Pooled data	Vuksic et al. (2008)
	362 ± 53		487 ± 121 (1.34 ± 0.12)	IML	Mouse, Thy1-GFP
	1,482 ± 114		1,701 ± 145 (1.14 ± 0.11)	OML	C57BL/6 background
21 ± 2	1,912 ± 90		2,272 ± 252 (1.19 ± 0.12)	Dorsal DG	male, 3–4 months
	357 ± 36		486 ± 104 (1.36 ± 0.18)	IML	
	1,475 ± 102		1,741 ± 156 (1.18 ± 0.12)	OML	
29 ± 1	2,106 ± 197		2,233 ± 473 (1.06 ± 0.18)	Ventral DG	
	369 ± 80		488 ± 143 (1.32 ± 0.16)	IML	
	1,486 ± 118		1,664 ± 143 (1.12 ± 0.11)	OML	

Values are mean ± S.E.M.

Abbreviations: upper/lower – GCs in upper/lower bade; superf./deep – superficial/deep part of the granule cell layer; IML/OML – dendrites in the inner/outer molecular layer.

[a]Surface area includes the axon and spines.

diameter and surface area of proximal to distal dendrites. In fact, the surface density of spines was comparable in the dendritic compartments with values ranging from 0.79 to 0.88 μm^{-2} (Hama et al., 1989). Spine surface contributes by a factor of 0.91–1.05 to the total surface area of the neurons (Schmidt-Hieber et al., 2007; Hama et al., 1989).

There are only limited quantitative data on the synaptic inputs to GCs. The number of excitatory synapses can be estimated on the basis of spine densities. The three main afferent systems, the commissural/associational path, the medial and the lateral perforant path, terminate in a strictly laminated fashion in the inner, middle, and outer molecular layer, respectively. The proportions of the dendrites falling into these layers are ~30, 30, and 40% (Claiborne et al., 1990; Schmidt-Hieber et al., 2007). The corresponding spine numbers on the surface of GC with a dendritic length of ~3,200 μm (Claiborne et al., 1990), calculated using the spine density estimates of Hama et al. (1989, see above), are 3,250, 2,780, and 2,600. Thus, the number of excitatory synapses onto a single GC could be as high as 8,630.

The distribution of inhibitory terminals was analyzed in a combined immunocytochemical and electron microscopic study (Halasy and Somogyi, 1993a). Results indicate that in the molecular layer ~7.5% of the synapses are GABA-immunopositive and these synapses comprise 75% of all inhibitory synapses, with the remaining 25% located in the cell body layer. Therefore, the number of inhibitory synapses onto a single granule cell can be estimated as ~860, with ~650 in the molecular layer and ~190 in the cell body layer. The compartmental distribution of the inhibitory input is broken down to 63–73% dendritic shafts and 27–37% spines in the molecular layer. In the cell body layer the majority, between 46 and 60%, are on somata, 25–28% on proximal dendritic shafts, 7–14% on spines, and 7–9% on axon initial segments (Halasy and Somogyi, 1993a).

The axons of GCs, the so-called mossy fibers, provide the major output of the DG to the CA3. The unique features of mossy fibers are the 10–18 sparsely spaced large varicosities (4–10 μm) or mossy fiber boutons that form synaptic contacts with complex spines of CA3 pyramidal in the str. lucidum and mossy cells in the hilus (Claiborne et al., 1986; Frotscher et al., 1994; Acsády et al., 1998; Rollenhagen et al., 2007). Furthermore, mossy fibers innervate a large number of inhibitory interneurons in both regions through small, en passant boutons (0.5–2 μm) and filopodial extensions emerging from the large boutons (Acsády et al., 1998).

Hilar Mossy Cells

Mossy cells share some morphological features with CA3 pyramidal cells. In particular, the presence of large complex spines on proximal dendrites and small, simple spines on distal dendrites underpins resemblance. However, major differences in their morphology, connectivity, and physiological properties demonstrate that mossy cells constitute a discrete cell population (Amaral, 1978; Buckmaster et al., 1993).

The somata of the cells are slightly larger than those of CA3 pyramidal cells and have a triangular or ovoid shape. Three to six primary dendrites arise from

the soma and bifurcate repeatedly to produce an extensive multipolar dendritic arborization confined to the hilus. Dendrites very rarely invade the granule cell layer or the molecular layer in mature rats (Amaral, 1978; Ribak et al., 1985; Buckmaster et al., 1993; Lübke et al., 1998; but see Scharfman, 1991). In vitro-labeled mossy cells from mice have a total dendritic length of 5,392 $\pm$ 313 μm (Kowalski et al., 2008). Although this value is not directly comparable to those obtained in the rat for other types of hippocampal neurons, the extent of mossy cell dendritic arbor appears to lie between GCs and pyramidal cells.

Similarly, only limited quantitative data are available on synaptic inputs to mossy cells. Proximal dendrites and the soma are covered by complex spines reflecting a high degree of convergence of GC inputs onto electrotonically proximal locations (Frotscher et al., 1991, Acsády et al., 1998). Additionally, mossy fibers make synaptic contact with distal, simple dendritic spines (Frotscher et al., 1991). Other excitatory inputs include the hilar collaterals of CA3 pyramidal cells (Scharfman, 1994, 2007) and mossy cell axons terminating mainly on distal spines. However, data from paired intracellular recordings indicate that the mutual connectivity between mossy cells is very low ($\sim$0.5%; Larimer and Strowbridge, 2008). The major source of inhibitory input is from hilar interneurons (Acsády et al., 2000; Larimer and Strowbridge, 2008).

The axon of mossy cells forms an extensive arbor in the ispi- and contralateral hippocampi (Soltesz et al., 1993; Buckmaster et al., 1996). While the extent of the dendrites is restricted along the septo-temporal axis ($<$500 μm), the axon can cover 53–61% of the hippocampus (Buckmaster et al., 1996). Thus, mossy cells provide a distributed excitatory feedback to the DG. The ipsilateral length of the axon is between 73 and 96 mm (uncorrected two-dimensional projection, Buckmaster et al., 1996). Most of the axon is in the inner molecular layer (53–56%) and the hilus (23–27%) but collaterals are also found in the granule cell layer, the middle molecular layer, the CA3, and occasionally also in the CA1 (Buckmaster et al., 1996). In the molecular layer, the axon forms synapses every $\sim$2 μm and the large majority of the postsynaptic targets are dendritic spines of GCs (Buckmaster et al., 1996). While numerically low, synaptic contacts onto interneurons have been suggested to play an important role in regulating the excitability of the DG (Ratzliff et al., 2002; Sloviter et al., 2003). In the hilus, interestingly, the density of synapses is five times lower along the axon (0.1 μm^{-1}) and the main targets are smooth dendrites of interneurons (Buckmaster et al., 1996; Larimer and Strowbridge, 2008).

GABAergic Interneurons

Morphological Classification of Interneurons

Interneurons are characterized by extensive local axonal arborization. Interneurons can thereby provide inhibitory innervation and control the activity of large sets of local neurons. In contrast to the largely uniform population of principal cells, interneurons are extremely heterogeneous with respect to not only their morphological features but also their physiological characteristics and their expression

Table 5 Passive membrane parameters of the hippocampal principal cells and interneurons in morphologically and electrophsyiologically constrained models

Cell type	R_i(Ω cm)	R_m(kΩ cm^2)	C_m(μF cm^{-2})	Surface (1,000 μm^2)	Reference
CA1 PC[a]	199	85.1	0.7	64.4	Major et al. (1993)
CA1 PC	228(198–261)	27.2(16.1–39.9)	1.43(1.02–1.86)	42.8	Golding et al. (2005)[f]
CA3 PC	270(170–340)	170(150–200)	0.75(0.69–0.81)	82.5 ± 5.2	Major et al. (1994)
CA3 PC	200/100[c]	50/1[c]	0.75	54.91	Traub et al. (1994)
GC	194 ± 24	38.0 ± 2.3	1.01 ± 0.03	13.3 ± 0.9	Schmidt-Hieber et al. (2007)
CA1 BC[a]	296 ± 75	66.2 ± 37.8	1[e]	7.9 ± 0.9	Thurbon et al. (1994)
CA3 INs[b]	189 ± 130	62 ± 34	0.92 ± 0.34	–	Chitwood et al. (1999)
DG BC	121 ± 21	6.3/30.5[d]	1.1 ± 0.1	9.8/31.2[c]	Nörenberg et al. (2008)[f]

Values are mean ± S.E.M. (or range).
Abbreviations: PC, pyramidal cell; IN, interneuron; Ri; axial resistivity; Rm, membrane resistivity; Cm, specific membrane capacitance.
[a]Recordings were obtained with sharp microelectrodes and the simulations included a shunt to reproduce the leakage around the electrode.
[b]The sample includes various interneuron types.
[c]Values indicate somatodendritic/axonal compartments separately.
[d]R_m before and after blocking Ih by ZD7288.
[e]C_m was set as a constant.
[f]Parameters of uniform models. For non-uniform models see original publications.

of neurochemical markers and transcription factors. Differences in their properties are thought to reflect the functional diversity of interneurons in the network (Table 5).

The most distinct anatomical feature of interneurons is the layer-specific distribution of the axon. Correlated light and electron microscopic studies revealed that the axon projection reflects the differential targeting of subcellular compartments (e.g., soma, proximal or distal dendrites) of the postsynaptic neurons (Han et al., 1993; Gulyás et al., 1993a; Buhl et al., 1994a). Additionally, termination of the axon often parallels afferent pathways leading to co-alignment of excitatory and inhibitory inputs.

However, not only the axon but also dendrites and cell bodies of interneurons show variability in their laminar distribution. While some interneuron types have a dendritic arbor spanning all layers, others have dendrites restricted to one or more layers. The dendritic distribution determines what inputs are available to an interneuron: whether it can be activated by one or more afferent system in a feedforward manner or by recurrent collaterals of principal cells as part of feedback inhibitory microcircuit (Fig. 4).

Thus, the precise localization of the interneurons, their dendrites and axon within the layered structure of the hippocampus determine their anatomical connectivity. In turn, input and output connections define the functions that the cells can play in the

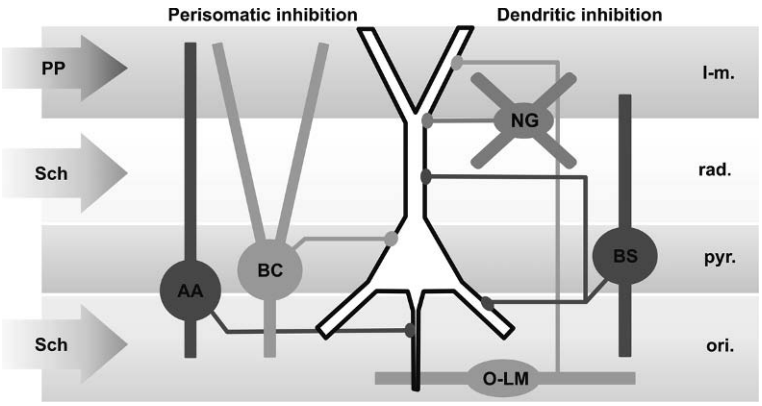

Fig. 4 Schematic representation of interneuron types of the hippocampal CA1 area. Two main classes can be distinguished on the basis of postsynaptic targets: (1) *perisomatic inhibitory interneurons* include basket cells (BC, targets: soma and proximal dendrites) and axo-axonic cells (AA, targets: axon initial segments). The axon of these interneurons terminates in and near the str. pyramidale (pyr.). (2) *Dendrite-inhibiting interneurons* include many types. Here three well-characterized types are illustrated: (i) Bistratified cells (BS) innervate the mid-distal dendrites in the str. radiatum (rad.) and oriens (ori.). (ii) Neurogliaform (NG) interneurons are found in the rad. or lacunosum-moleculare (l-m.) and inhibit the apical dendrites in the same layers. NG cells are mainly activated by the perforant path (PP) and the Schaffer collaterals (Sch) and therefore provide feedforward inhibition. (iii) O-LM interneurons are found in the orines and innervate the distal apical dendrites in the l-m. O-LM cells receive strong recurrent excitation from pyramidal cells and therefore mediate primarily feedback inhibition

circuitry. Therefore, most classification schemes have considered these anatomical features as major criteria (Freund and Buzsáki, 1996; McBain and Fisahn, 2001; Somogyi and Klausberger, 2005). Although there is still some debate regarding the terminology and identification of interneuron types (Maccaferri and Lacaille, 2003; Petilla Interneuron Nomenclature Group, 2008), two main classes of interneurons can be distinguished on the basis of postsynaptic targets: perisomatic and dendritic inhibitory cells (Fig. 4). In addition, a set of interneurons that selectively target other interneurons (interneuron-specific [IS] cells; Acsády et al., 1996a, b; Gulyás et al., 1996; Hájos et al., 1996) and interneurons with long-range projections have been identified (Jinno et al., 2007).

Perisomatic inhibitory interneurons innervate soma, proximal dendrites, and axon initial segment of principal cells. They include basket cells (BC) and axo-axonic cells (AAC). Majority of these cells have a vertically oriented dendritic tree and can mediate both feedforward and feedback inhibition.

Dendrite-inhibiting interneurons comprise several distinct types (Fig. 4) which innervate various portions of the dendritic tree of their target cells. The axon of dendrite-inhibiting interneurons is often co-aligned with afferent pathways in the dendritic layers (Han et al., 1993; Gulyás et al., 1993a; Vida et al., 1998; Vida and Frotscher, 2000). Thus, the various interneuron types can control excitatory postsynaptic responses in an input-specific manner (Miles et al., 1996; Maccaferri and Dingledine, 2002). Furthermore, the co-alignment enables mutual presynaptic interactions between glutamatergic and GABAergic axons (Vogt and Nicoll, 1999; Guetg et al., 2009; Min et al., 1999; Stafford et al., 2009). While some dendrite-inhibiting interneurons have dendrites spanning all layers and therefore can mediate feedback and feedforward inhibition, the majority of these cells have dendrites restricted to one or two layers. Interneurons in the str. oriens and the hilus, such as O-LM interneurons, receive excitation from the principal cells and mediate feedback inhibition. In contrast, interneurons in the str. radiatum and lacunosum-moleculare are activated by the Schaffer collaterals and/or the perforant path and thereby mediate feedforward inhibition.

Neurochemical Classification of Interneurons

Interneuron types differentially express a wide range of molecular markers, including calcium-binding proteins (parvalbumin, PV; calbindin, CB; and calretinin, CR), neuropeptides (somatostatin, SOM; cholecystokinin, CCK; neuropeptide Y, NPY; vasoactive intestinale peptide, VIP), and certain enzymes (NADPH-diaphorase; nitric oxide synthase, NOS). While the function of the molecules in these cells is not always fully understood, detection of the markers by immunocytochemistry, in situ hybridization, or single-cell RT-PCR has been successfully applied to identify and classify GABAergic neurons (for reviews see Freund and Buzsáki, 1996; Somogyi and Klausberger, 2005; Jinno and Kosaka, 2006; Houser, 2007; Klausberger and Somogyi, 2008). Importantly, the interneuron types defined on the basis of neurochemical identification converge well with the morphological classification, when the combinatorial expression pattern of multiple markers is considered (Table 6).

Table 6 Convergence of morphological and neurochemical classification of interneurons

	PV	CB	CR	SOM	CCK	VIP	NPY	NADPH	NOS	$GABA_A$ α1
Perisomatic inhibition										
PV–BC	++				−					++
CCK–BC	−				++	+				
AAC	++				−					
Dendritic inhibition										
BSC	++			+	−		+			++
Ivy	−						++		++	++
SCA		+			++					
PPA					+					
NG							++			
O-LM/HIPP	+	+		++			+			
MFA					++					
Interneuron-specific interneurons										
IS			++			++				

(++) indicates consistent high expression of the marker, (+) indicates low expression and/or expression in a subset, (−) indicates the consistent absence of the marker, when important for distinguishing types. For abbreviations, please see the text.

Interneurons of the CA1–3 Areas

Most interneuron types can be identified in all areas of the hippocampus on the basis of their salient anatomical properties. However, due to differences in the layering of the areas, some types may differ in certain anatomical properties, whereas a few specific types may exist only in one area. As the structure and layering of the CA1–CA3 areas are almost identical, we discuss interneuron types from these areas together. The classification and descriptions are based on results from the CA1 as this is the best study region of the hippocampus, and possibly the whole cortex. But published data from the CA3 (Gulyás et al., 1993a) and the CA2 areas (Mercer et al., 2007) confirm that the classification can be extrapolated to these regions.

Perisomatic Inhibitory Interneurons

(1) Fast-spiking parvalbumin-positive basket cells. PV–BCs form synapses with the somata and proximal dendrites of pyramidal cells as well as other interneurons (Buhl et al., 1994a; Halasy et al., 1996; Cobb et al., 1997; Pawelzik et al., 2002). At the light microscopic level, this interneuron type is characterized by an axon terminating in and near the cell body layer (Fig. 5A). In addition to PV, the cells express high levels of the alpha-1 subunit of $GABA_A$ receptors ($GABA_A$-α1; Table 6) and Kv3.1 channels. It is estimated that PV–BCs constitute ∼60% of all PV-immunoreactive cells and ∼12% of all GABAergic interneurons in the CA1 area (Kosaka et al., 1987; Baude et al., 2007).

Cell bodies of PV–BCs are located in the str. pyramidale or oriens, but a few cells have been found in the str. radiatum. The dendrites are radially orientated and span all layers (Buhl et al., 1995, 1996, Halasy et al., 1996). Work published by Gulyás et al. (1999) analyzed the distribution of dendrites and input synapses of

PV-immunoreactive neurons. Although they could not unequivocally identify the cells as BCs, their results conceivably reflect characteristics of this predominant cell type. Their quantitative data revealed that the total length of the dendrites (4,348 μm) is substantially shorter than that of pyramidal cells but their laminar distribution is similar (Table 7).

The estimated number of synapses (16,293, Table 7) is also markedly lower than for pyramidal cells but it is the highest among interneurons (Gulyás et al., 1999). The proportion of excitatory (∼93.5%) and inhibitory synapses (∼6.5%) is comparable to that for pyramidal cells. As the dendrites of BCs lack spines, both excitatory and inhibitory synapses are formed onto dendritic shafts. Inhibitory synapses show a concentration in the perisomatic domain with ∼17% of the synapses converging onto the soma, but in contrast to principal cells, the soma also receives a high number of excitatory synapses (Table 7). A large proportion of the inhibitory synapses are PV-immunopositive: ∼27.6% on the dendrites and ∼70% on the soma (Gulyás et al., 1999; Table 7). Thus, PV-containing interneurons are heavily interconnected by mutual inhibitory synapses (Sík et al., 1995; Fukuda and Kosaka, 2000; Bartos et al., 2001, 2002). In addition to the chemical synapses, PV–BCs are also coupled by electric synapses to other PV-containing interneurons (Fukuda and Kosaka, 2000, 2003; Bartos et al., 2001; Hormuzdi et al., 2001). Gap junctions are found primarily at dendritic locations with the highest density between basal dendrites at the str.

Table 7 Dendritic length and synaptic inputs of PV-containing interneurons of the CA1 area

	Dendritic length (μm)		Density of synapses			Estimated number of synapses		
			All	Exc.	Inhib.	Exc.	Inhib.	PV+
Dendrites	4,348 ± 1,125					14,825	868	240
L-M	656 ± 255	(15.0%)						
Med	214 ± 124	(4.9%)	171.34	143.44	27.89			
Thin	442 ± 208	(10.1%)	155.72	126.75	28.97			
Rad	2,369 ± 786	(54.5%)						
Thick	255 ± 165	(5.8%)	483.81	444.68	39.13			
Med	1,713 ± 635	(39.4%)	432.68	416.01	16.67			
Thin	401 ± 219	(9.2%)	145.63	133.50	12.14			
Pyr	248 ± 121	(5.7%)						
Ori	1,075 ± 535	(24.7%)						
Thick	21 ± 47	(0.4%)	612.94	568.45	44.49			
Med	686 ± 303	(15.7%)	361.08	344.95	16.13			
Thin	368 ± 243	(8.5%)	348.54	325.08	23.46			
Soma	1,006 ± 184 (surface area [μm^2])					413	177	124
AIS						0	10	0
Total						15,238	1,055	364

Values are mean ± S.E.M. Percentage values in parentheses indicate the proportion of dendrites within a layer. Density of synapses is per 100 μm. Excitatory (Exc.) and inhibitory (Inhib.) synapses were identified on the basis of postembedding immunolabeling for GABA. Data from Gulyás et al. (1999).

oriens–alveus border (Fukuda and Kosaka, 2000, 2003). This dual – chemical and electric – connectivity is thought to be important for the synchronization of the interneurons during network activity patterns, such as gamma oscillations (Bartos et al., 2001; Hormuzdi et al., 2001).

The output of BCs has been analyzed in both in vitro- and in vivo-labeled neurons. The length of the axon of in vivo-labeled BCs ranges between 40.5 and 53.5 mm and terminates in an approximately circular or ellipsoid area of the cell body layer with a diameter between 0.9 and 1.2 mm. On the basis of the bouton density of $0.226 \pm 0.039\,\mu m^{-1}$, the number of total synapses was estimated to be between 9,000 and 12,000 (Sík et al., 1995). As unitary IPSCs in pyramidal cells are mediated by multiple, 10–12 synaptic contacts (Buhl et al., 1994a), the number of postsynaptic neurons (*divergence*) is likely to be between 750 and 1,200; whereas the number of PV–BCs making synaptic contact onto a single postsynaptic pyramidal cell (*convergence*) is between 15 and 25, calculated from the total number of synaptic contacts (92–119, Megías et al., 2001; Buhl et al., 1994a) and the number of contacts formed by a single BC onto the soma (5–6, Gulyás et al., 1993a; Buhl et al., 1994a).

(2) CCK-expressing basket cells. Similar to PV–BCs, CCK–BCs form synapses with the somata and proximal dendrites of pyramidal cells as also indicated by the axonal distribution in the str. pyramidale and adjacent region of str. radiatum and oriens (Fig. 5B; Nunzi et al., 1985; Acsády et al., 1996b; Cope et al., 2002; Pawelzik et al., 2002). In addition to CCK, neurochemical markers include VIP, substance-P receptor, and vesicular glutamate transporter 3, but the cells are consistently immunonegative for PV (Table 6; Cope et al., 2002; Pawelzik et al., 2002; Mátyás et al., 2004; Somogyi et al., 2004; Klausberger et al., 2005). Terminals of these interneurons express high levels of cannabinoid CB1 receptor which plays a role in regulating the release of GABA (Katona et al., 1999b). CCK–BCs mostly show regular-spiking discharge pattern, with some exceptions showing a fast-spiking phenotype (Cope et al., 2002; Pawelzik et al., 2002).

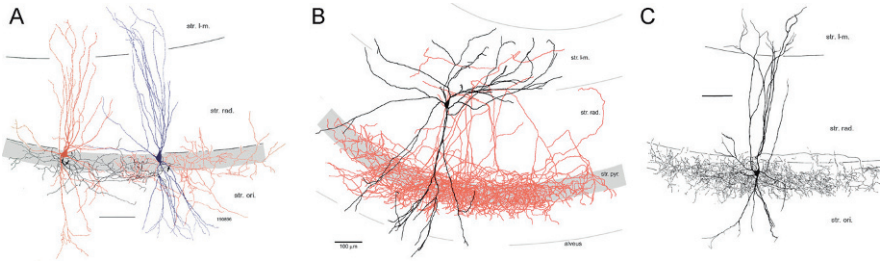

Fig. 5 Morphology of CA1 perisomatic inhibitory interneurons. **A** A synaptically coupled pair of fast-spiking BCs. The axons of both cells are found mainly in the cell body layer (shaded area, initial segments indicated by *arrows*) whereas their dendrites extend into the dendritic layers. **B** A str. radiatum BC with morphological feature of CCK–BCs. Note the dense axon (*red*) in and near the cell body layer (str. pyr.). **C** An AAC with a dense axon plexus at the border of the str. pyr. and the oriens (ori.). Scale bars – 100 μm (**A**, from Cobb et al., 1997; **B** from Vida et al., 1998; **C** from Buhl et al., 1994b, reproduced with permission. © Elsevier, Wiley-Blackwell, and the American Physiological Society.)

In contrast to PV–BCs, cell bodies of CCK–BCs can be found in all hippocampal layers. The dendrites run radially and span all layers (Cope et al., 2002; Pawelzik et al., 2002). Mátyás et al. (2004) performed a detailed quantitative analysis of the laminar distribution of dendrites and input synapses of CCK–BCs. Their analysis shows that the total dendritic length of 6,338 μm is higher than PV–BCs but markedly lower than pyramidal cells (Table 8).

Despite the larger dendritic tree, the estimated total number of afferent synaptic contacts (8,147, Table 8) is lower than for PV–BCs. This is due to the fact that the number of excitatory synapses is markedly lower. In contrast, the number of inhibitory synapses is ∼2.6-fold higher (Gulyás et al., 1999; Mátyás et al., 2004). Thus, CCK–BCs have a lower proportion of excitatory (∼64%) and a higher proportion of inhibitory synapses (∼36%) than both PV–BC and pyramidal cells. CCK–BCs are also interconnected by mutual inhibitory synapses. The number of CCK-immunopositive terminals on their surface is ∼350 (Table 8), very close to the number of mutual inhibitory synaptic contacts on PV–BCs. However, the proportion of these synapses among the inhibitory terminals is lower due to the higher overall inhibitory input (Mátyás et al., 2004). Although the PV- and CCK-interneuron networks seem largely independent, there is evidence for the existence of mutual inhibitory synapses and interactions between the two networks (Karson et al., 2009).

While immunocytochemical data at the light and electron microscopic levels demonstrate that terminals of CCK–BCs innervate soma and proximal dendrites of principal cells (Nunzi et al., 1985; Acsády et al., 1996b; Cope et al., 2002; Pawelzik et al., 2002; Klausberger et al., 2005), no quantitative data are available on the divergence or convergence of CCK–BC output.

(3) Axo-axonic cells. AACs provide GABAergic innervation to the axon initial segments of principal cells (Somogyi et al., 1983; Li et al., 1992; Gulyás

Table 8 Dendritic length and synaptic inputs of CCK–BCs of the CA1 area

		Estimated number of synapses			
	Dendritic length (μm)	All	Exc.	Inhib.	CCK+
Dendrites	6,338 ± 986	7,948 ± 1,229	5,191 ± 805	2,757 ± 430	315 ± 55
L-M	1,291 ± 456 (20.37%)	1,876		759	
Rad/L-M	647 ± 575 (10.20%)	798		258	
Rad	2,876 ± 211 (45.37%)	3,421		1,074	
Pyr	111 ± 61	3,421		1,074	
Ori	311 ± 118 (4.90%)	1,418		394	
Soma	966 ± 134 (surface area [μm^2])	193 ± 43	34 ± 14	159 ± 34	36 ± 14
AIS		6 ± 2	1 ± 1	5 ± 2	1 ± 2
Total		8,147	5,226	2,921	352

Values are mean ± S.E.M. Values in parentheses indicate percentage of dendrites in a layer. Rad/L-M denotes the broader region of the two layers which contains many horizontally running dendrites. Excitatory (Exc.) and inhibitory (Inhib.) synapses were identified on the basis of postembedding immunolabeling for GABA. Data from Mátyás et al. (2004).

et al., 1993a; Buhl et al., 1994a), placing them in a unique position to control synaptic output of the target cells. Similar to PV–BCs, the termination zone of the axon is mainly in the cell body layer, but it is slightly shifted toward the str. oriens (Fig. 5C). Many, but not all AACs can be distinguished from BCs at the light microscopic level by the presence of vertical rows of synaptic boutons (cartridges). AACs show a fast-spiking discharge pattern and contain high levels of PV but, in contrast to PV–BCs, they express low level of $GABA_A$-α1 (Katsumaru et al., 1988; Pawelzik et al., 2002). It is estimated that this type constitutes ∼15% of all PV-immunoreactive cells and ∼3% of GABAergic interneurons in the CA1 area (Baude et al., 2007).

Cell bodies of AACs are located in the str. pyramidale or oriens. The majority has vertically oriented dendrites spanning all layers. In comparison to PV–BCs, the distal apical dendrites often branch and form an extensive tuft in the str. lacunosum-moleculare (Buhl et al., 1994b; Klausberger et al., 2003) indicating a stronger perforant path input to these neurons. A few cells with horizontally oriented dendrites in str. oriens have also been reported (Ganter et al., 2004).

AACs receive input from all major afferent pathways and there is also evidence for recurrent excitatory inputs from pyramidal cells (Li et al., 1992, Buhl et al., 1994b). Regarding the quantitative distribution of input synapses, Gulyás et al. (1999) suggested that their data may apply not only to PV–BCs, but also to AACs (see Table 7). However, some disagreement remains regarding the extent of dendrites in the str. lacunosum-moleculare (see above). AACs are thought to be involved in the PV-interneuron network coupled by gap junction and also receive inhibitory synapses from this network (Fukuda and Kosaka, 2000; Baude et al., 2007). However, AACs themselves do not contribute inhibitory synapses to this network.

The output of AACs is directed exclusively to the axon initial segments of principal cells (Somogyi et al., 1983). Morphological analysis of an in vivo-labeled CA1 AAC revealed that it can innervate ∼1,200 pyramidal cells within an area of 600 by 850 μm around the cell (Li et al., 1992). However, in vitro studies indicate that the axon can have a larger extent with values up to 950 μm in the CA1 and 1, 300 μm in the CA3 area (Gulyás et al., 1993a, Buhl et al., 1994b). The in vivo data further show that the cells form 2–10 synaptic contacts on a single axon initial segment (Li et al., 1992). As the number of synaptic contacts on initial segments is ∼24 (Gulyás et al., 1999), 3–12 AACs may converge onto a single pyramidal cell.

Dendritic Inhibitory Interneurons

(4) Bistratified cells (BSC). These interneurons are characterized by an axon in the str. radiatum and oriens co-aligned with the Schaffer collaterals (Fig. 6A; Buhl et al., 1994a, 1996). BSCs show a fast-spiking discharge pattern. They express PV, the neuropeptides SOM, NPY, and high levels of the $GABA_A$-α1 (Pawelzik et al., 2002; Klausberger et al., 2004; Baude et al., 2007). This type constitutes ∼25% of all PV-immunopositive cells and ∼5% of GABAergic interneurons in the CA1 area (Baude et al., 2007).

Cell bodies of BSCs, similar to other PV-interneurons, are found primarily in the str. pyramidale or oriens. The dendrites show radial orientation and span str.

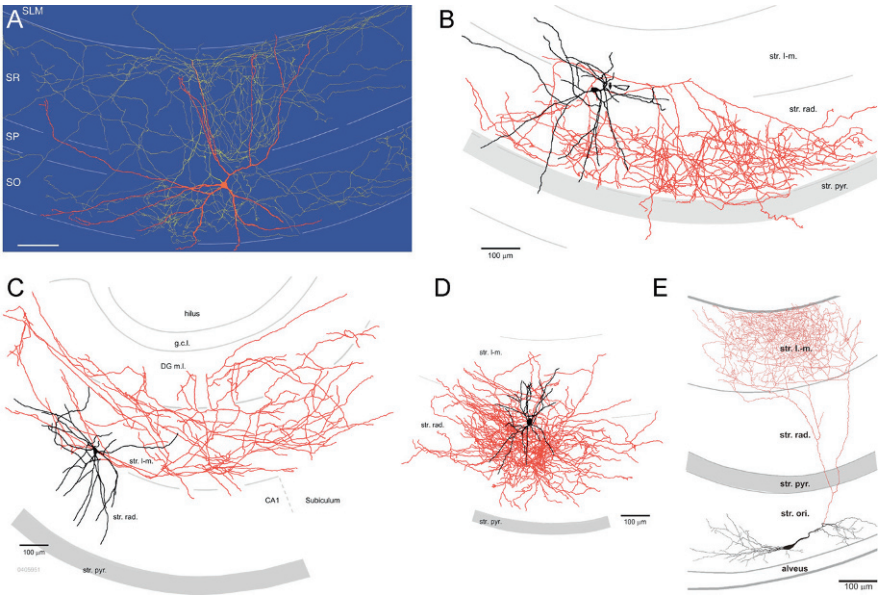

Fig. 6 Dendritic inhibitory interneuron types of the CA1 area. **A** BSC. The cell body is at the border of str. pyramidale (SP) and oriens (SO). Dendrites span the str. oriens and radiatum (SR) but do not extend into the lacunosum-moleculare (SLM). **B** SCA cell with axon (*red*) in the str. radiatum (rad.). **C** PPA interneuron. Note the axon terminating in the CA1 str. lacunosum-moleculare (l-m.), the subiculum and the DG molecular layer (m.l.). **D** NG cell with a compact dendritic and a very dense axonal arbor in the str. rad. and l-m. **E** O-LM interneurons have horizontal dendritic tree in the str. oriens and project to the distal apical dendrites of pyramidal cells in the str. l-m (**A** from Klausberger et al., 2004; **B–D** from Vida et al., 1998; **E** from Martina et al., 2000, reproduced with permission. © Nature Publishing Group, Wiley-Blackwell, and The American Association for the Advancement of Science.)

oriens and radiatum but, in contrast to other PV-interneurons, rarely invade the str. lacunosum-moleculare (Buhl et al., 1996, Halasy et al., 1996; Klausberger et al., 2004). A few cells with similar axonal arborization, but horizontal dendrites have been reported and classified as oriens-BSCs (Maccaferri et al., 2000).

Dendritic distributions and electrophysiological data indicate that the cells are activated primarily by the Schaffer collaterals and can also receive recurrent excitatory input from pyramidal cells in the str. oriens, but they generally lack perforant path input (Buhl et al., 1996). It remains unclear whether the data on the quantitative distribution of synaptic inputs described for PV-interneurons (Gulyás et al., 1999; see Table 7), apart from the lack of perforant path inputs, also apply to BSCs.

The output of BSCs targets shafts (∼76–79%) and spines (∼11–17%) of small-caliber dendrites and rarely the large-caliber main apical dendrites (∼10%) or somata (∼4%) of principal cells (Halasy et al., 1996; Klausberger et al., 2004). The proportion of interneuron targets is also low (∼3%, Klausberger et al., 2004). Nevertheless, BSCs are thought to be involved in the network of PV-interneurons connected by mutual inhibitory synapses and gap junction (Fukuda and Kosaka, 2000; Baude et al., 2007). The axon of an in vivo-labeled BSC has a total length of

78,800 μm and covers an area of 1,860 μm (septo-temporal) by 2,090 μm (medio-lateral axis). The axon of this cell has a bouton density of $0.21 \pm 0.06\,\mu m^{-1}$ and forms ~16,600 boutons. Since BSC-pyramidal cell synapses involve ~6 synaptic contacts (Buhl et al., 1994a), an individual BSC may target over 2,500 pyramidal cells.

(5) "Ivy" interneurons. Ivy interneurons can be distinguished by a very dense axonal plexus close to the soma terminating in str. oriens and radiatum (Fuentealba et al., 2008). Ivy cells are immunoreactive for NOS and NPY and express high levels of the alpha-1 subunit of $GABA_A$ receptors, but are consistently negative for PV. They show a slow-spiking discharge pattern. Ivy cells are more numerous than PV-positive perisomatic inhibitory cells (~1.4-fold higher density, Fuentealba et al., 2008) and may comprise ~20% of all GABAergic interneurons.

Cells bodies of Ivy interneurons are located in the str. pyramidale and adjacent regions of the radiatum. Dendrites extend radially into the str. oriens and radiatum but rarely reach the str. lacunosum-moleculare. Dendritic distribution and electrophysiological data indicate that these interneurons are activated by the Schaffer collaterals and receive recurrent excitatory input from pyramidal cells, but lack perforant path input, similar to BSCs (Fuentealba et al., 2008).

Postsynaptic targets of Ivy cells are primarily the shafts (81%) of basal dendrites in str. oriens and oblique dendrites in the str. radiatum (Fuentealba et al., 2008). Dendritic spines (13%) and apical dendrites of pyramidal cells (6%) are less frequently targeted. The axon profusely branches close to its point of origin and forms a dense meshwork in the str. oriens and radiatum. In comparison to BSCs labeled under similar conditions, the area covered by axon collaterals is slightly smaller (Ivy: 0.75 ± 0.12 mm [medio-lateral] by 1.31 ± 0.11 mm [rostro-caudal], Fuentealba et al., 2008; BSC: 1.15 ± 0.26 mm by 1.53 ± 0.38 mm, Klausberger et al., 2004). However, Ivy cells have a denser axonal plexus, especially in the str. oriens, and representative samples indicate a approximately two times higher total axon length (Fuentealba et al., 2008). Thus, Ivy cells could innervate larger sets of postsynaptic neurons than BSCs, but values of divergence and convergence are currently unknown.

(6) Schaffer collateral-associated (SCA) interneurons. These interneurons, similar to BSCs, are characterized by an axon in the str. radiatum and oriens co-aligned with the Schaffer collaterals (Fig. 6B; Vida et al., 1998; Cope et al., 2002). They differ, however, in their localization of the soma and dendrites, as well as neurochemical markers. The main markers are CCK and CB (Cope et al., 2002; Pawelzik et al., 2002). Similar to CCK–BCs, SCA interneurons show a regular-spiking discharge pattern.

Somata of SCA cells are found in the str. radiatum. Their dendrites run radially, mostly in the str. radiatum but can extend into the str. lacunosum-moleculare, oriens and even the alveus (Vida et al., 1998; Pawelzik et al., 2002). Although dendritic arbor and synaptic inputs of identified SCA interneurons have not been quantitatively described, Gulyás et al. (1999) provide data on CB-immunoreactive interneurons, a set of dendritic inhibitory interneurons (Gulyás and Freund, 1996) which overlap with the SCA type (Cope et al., 2002). The total dendritic length of

Table 9 Dendritic length and synaptic inputs of CB-interneurons in the CA1 area

		Estimated number of synapses		
	Dendritic length (μm)	All	Exc.	Inhib.
Dendrites	3,441 ± 938	3,585	2,498 ± 666	1,087 ± 277
L-M	130 ± 117 (3.8%)			
Rad	2,622 ± 827 (76.2%)			
Pyr	197 ± 162 (5.7%)			
Ori	492 ± 300 (14.3%)			
Soma	799 ± 140 (surface area [μm^2])	244	102 ± 10	142 ± 15
AIS		7	0	7 ± 1
Total		3,839	2,601	1,237

Values are mean ± S.E.M. Values in parentheses indicate percentage of dendrites in a layer. Excitatory (Exc.) and inhibitory (Inhib.) synapses were identified on the basis of postembedding immunolabeling for GABA. Data from Gulyás et al. (1999).

CB-interneurons is 3,441 ±938 μm with 76% localized in the str. radiatum (Table 9). The excitatory input is relatively weak (∼68%) and originates plausibly from the Schaffer collaterals, whereas the inhibitory input is strong (32%). Large part of the inhibitory input may correspond to the mutual inhibitory connections observed between CCK and SCA cells (Ali, 2007). In addition to the chemical synapses, SCA cells have been shown to be connected by gap junctions (Ali, 2007).

The axon of SCA cells terminates in the str. radiatum and to a lesser extent in the oriens. Output synapses are formed with shafts, but only rarely spines of small-caliber side branches of the pyramidal cells (∼80%) and aspiny dendritic shafts of interneurons (∼20%; Vida et al., 1998). Synaptic effects in pyramidal cells are mediated by multiple contacts (4–6, light microscopic estimates, Vida et al., 1998; Pawelzik et al., 2002). The axon of an in vitro-labeled SCA interneuron formed ∼6,000 boutons and may innervate 1,000–1,500 postsynaptic cells within a 400-μm slice.

(7) Perforant path-associated (PPA) interneurons. This cell type has an axon in the str. lacunosum-moleculare co-aligned with the perforant path (Fig. 6C; Vida et al., 1998; Pawelzik et al., 2002). Neurochemical markers of PPA cells include CCK (Pawelzik et al., 2002; Klausberger et al., 2005) and they may also express CB.

Cell bodies of PPA cells are in the str. radiatum or lacunosum-moleculare, often at the border of the two layers. Dendrites run radially in these two layers, but can also extend into the oriens/alveus (Hájos and Mody, 1997; Vida et al., 1998). The dendritic distribution suggests that the cells' input is primarily from the perforant path and Schaffer collaterals, but they may also receive feedback excitation on their distal dendrites in the oriens/alveus.

The axon terminates in the str. lacunosum-moleculare; however, collaterals often spread significantly into the subiculum and, crossing the fissure, into the DG. The postsynaptic targets are primarily principal cells, CA1 pyramidal cells (58–94%), and DG granule cells (0–26%), but also include interneurons (6–11%); the synapses

are found mostly on small-caliber dendritic shafts and to a lesser extent (5–7%) dendritic spines (Vida et al., 1998; Klausberger et al., 2005).

(8) Neurogliaform (NG) cell. This interneuron type is identified on the basis of a small, stellate dendritic arbor and an extremely dense local axon (Fig. 6D; Vida et al., 1998; Price et al., 2005). NG cells express NPY and NOS (Price et al., 2005).

The small, round cell body is located in the str. radiatum or lacunosum-moleculare. Several main dendrites emerge from the soma and branch profusely to form a dense arborization. There are no quantitative anatomical data on the input synapses. Electrophysiological recordings indicate that the cells receive excitatory input from both the perforant path and the Schaffer collaterals (Price et al., 2005). Inhibition is mediated by O-LM interneurons (Elfant et al., 2008) and other NGs cells through mutual inhibitory synapses (∼70% connectivity, Price et al., 2005). The NG cells are also extensively coupled by gap junctions (∼80% connectivity, Price et al., 2005).

The axon forms an extremely dense arbor in the str. radiatum and lacunosum-moleculare in the vicinity of the cell. An in vitro-labeled NG cell formed almost 13,000 boutons within its termination zone with less than 700-μm diameter along the transverse axis. Postsynaptic targets are mainly pyramidal cell, dendritic shafts (∼89%) but also spines (11%; Vida et al., 1998). Interestingly, unitary postsynaptic effects of NG-IPSCs are unusually slow and involve not only $GABA_A$ but also $GABA_B$ receptors (Tamás et al., 2003; Szabadics et al., 2007; Price et al., 2008).

(9) Oriens lacunosum-moleculare-projecting interneurons. O-LM interneurons, as their name indicates, are located in the str. oriens and project to the str. lacunosum-moleculare (Fig. 6E; McBain et al., 1994; Sík et al., 1995; Maccaferri et al., 2000). These interneurons are immunopositive for SOM, the metabotropic glutamate receptor mGluR1α, weakly positive for PV, and may also contain NPY (Kosaka et al., 1988; Baude et al., 1993; Klausberger et al., 2003). SOM-interneurons constitute ∼14% of all GABAergic neurons in the hippocampus (Kosaka et al., 1988), but the exact proportion of O-LM cell subset has not yet been established.

The soma of O-LM interneurons is located in the str. oriens, often at the border to the alveus. The dendritic tree has a horizontal orientation and is restricted to the str. oriens and the alveus. In contrast to other interneurons, the dendrites are densely covered with long, thin spines. Electron microscopic investigations indicate that ∼20% of the afferent synaptic contacts are inhibitory and ∼80% excitatory (Blasco-Ibáñez and Freund, 1995). Although the dendritic arbor falls in the termination zone of the Schaffer collateral pathway, degeneration studies revealed that over ∼75% of excitatory synapses originate from the pyramidal cells in the CA1 area (Blasco-Ibáñez and Freund, 1995). Thus, these interneurons primarily mediate feedback inhibition. In the CA3 area the cell bodies and dendrites of this type of interneuron are not restricted to the str. oriens, in concordance with the wider distribution of recurrent collaterals seen in this region. A smaller set of interneurons with similar axonal projection and neurochemical profile but with somata located in the str. pyramidale (P-LM cells) or radiatum (R-LM cells) and dendrites spanning str. radiatum and oriens have been identified in transgenic "GIN" mice (Oliva et al., 2000).

The axon of O-LM cells originates often from one of the major dendrites (Martina et al., 2000). Major collaterals ascend to the str. lacunosum-moleculare

and form a dense arborization in that layer. Some cells additionally form an axonal arbor, albeit much less extensive, in the str. oriens. The axon of an in vivo-labeled O-LM cell has a length of 63,436 μm occupying a relatively small termination field of 500 μm by 840 μm (medio-lateral and septo-temporal axes; Sík et al., 1995). Interestingly, in vitro-labeled O-LM interneurons in the CA3 show similar restricted axon projection in transverse slices but form multiple innervation fields along the septo-temporal axis (Gloveli et al., 2005a). Over 91% of the collaterals are found in the str. lacunosum-moleculare, only 7% in the str. oriens, and a small proportion invading the subiculum. The bouton density is $0.27 \pm 0.04\,\mu m^{-1}$ and the number of boutons was calculated to be over 16,800 (Sík et al., 1995). However, electron microscopic analysis of in vitro-labeled neurons showed that the axon can make synaptic contacts without forming varicosities, therefore it is difficult to estimate the total number of output synaptic contacts (Maccaferri et al., 2000). Postsynaptic targets of O-LM cells include dendrites of principal cells and interneurons in proportion to their occurrence (Katona et al., 1999a; Elfant et al., 2008). The synapses are found on dendritic shafts (∼70%) and to a lesser degree on spines (∼30%; Sík et al., 1995; Katona et al., 1999a; Maccaferri et al., 2000).

(10) Trilaminar (TL) interneurons. This interneuron type is characterized by an axon distributed to three adjacent layers (hence the name): the str. radiatum, pyramidale, and the oriens (Sík et al., 1995; Gloveli et al., 2005b; Ferraguti et al., 2005). TL cells express high levels of muscarinic acetylcholine receptor (M2) but other markers are unknown (Hájos et al., 1998; Ferraguti et al., 2005).

The cells show some similarities to O-LM interneurons. Their cell bodies are located in the str. oriens and the dendritic trees are restricted to the same layer. The dendrites are sparsely spiny. The cells receive synaptic input from excitatory and inhibitory terminals expressing high levels of mGluR8, indicating a strong glutamatergic modulation of the input (Ferraguti et al., 2005). The cellular origin of the synapses is unknown, but local pyramidal cells are likely to be involved in the excitatory input. A part of the inhibitory terminals shows immunoreactivity for VIP and is likely to originate from a subset of IS interneurons (Ferraguti et al., 2005).

The axon terminates in the str. radiatum, pyramidale, and oriens and extends into neighboring areas, i.e., to the subiculum from the CA1 (Ferraguti et al., 2005) or the CA1 from the CA3 (Gloveli et al., 2005b) and may also project to other brain areas as well. The total axon length of an in vivo-labeled TL cell in the CA1 area was 55,913 μm and covers an area of 2,600 μm (septo-temporal) by 2,450 μm (medio-lateral) (Sík et al., 1995). Based on bouton density ($0.28 \pm 0.05\,\mu m^{-1}$), the calculated number of boutons is 15,767. Synapses formed by TL cells are likely to involve multiple contact sites but no quantitative data are available. Postsynaptic neurons of TL cells locally include pyramidal cells and an unusually high proportion of interneurons. In the CA1, the targets are interneuron dendrites (44%), interneuron cell bodies (8%), pyramidal cell dendritic shafts (25%), and somata (23%; Ferraguti et al., 2005).

(11) Back-projection (BP) interneurons. The cell was named for its extensive axon projecting "back" to the CA3 area and the hilus from the CA1 (Sík et al., 1994, 1995). No molecular marker has been identified in BP cells, although

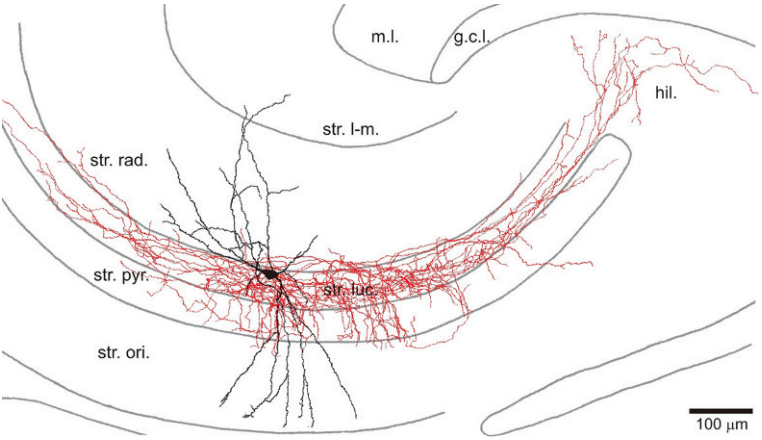

Fig. 7 MFA interneurons of the CA3 area. The axon (*red*) of this interneuron type terminates mainly in the str. lucidum (luc.), but also extends into the hilus displaying a striking association to the mossy fiber projection. The dendrites are found in the str. radiatum (rad.) and oriens (ori.) but absent from the lacunosum-moleculare (m-l.), reflecting that the cells receive excitatory input primarily from ipsi- and contralateral CA3 pyramidal cells. (Reproduced from Vida and Frotscher, 2000 with permission. © National Academy of Sciences, USA)

it has been suggested that they may correspond to a subset of NADPH-diaphorase- and NOS-immunoreactive cells (Sík et al., 1994). The somatodendritic domain of BP cells is confined to the str. oriens and shows similarities to other horizontal interneuron types of this layer (e.g., O-LM cells). The total length of axon collaterals is 20,642 μm, 59% of which is in the CA1 region and 41% project back to CA3 area innervating the str. oriens and radiatum. The synaptic connections of these cells have not been studied in detail, but they form synapses on dendrites and somata of pyramidal cells (Sík et al., 1994).

(12) Mossy fiber-associated (MFA) interneurons. This interneuron is a specific CA3 type and characterized by an axon plexus in the str. lucidum co-aligned with mossy fibers (Fig. 7; Vida and Frotscher, 2000; Losonczy et al., 2004). MFA interneurons express CCK and high levels of CB1 receptor in their synaptic terminals maintaining a very low initial release probability (Losonczy et al., 2004).

The small round or ovoid soma of MFA cells is located in or near the str. lucidum, and their dendrites extend radially into the str. radiatum and the oriens. The dendritic distribution indicates that the main sources of excitation are ipsi- and contralateral CA3 pyramidal cells (i.e., the recurrent collaterals and commissural fibers), but physiological data (Tóth and McBain, 1998) further show that the cells also receive mossy fiber input. No or minimal excitatory input arrives to these cells from the perforant path.

The axon forms a dense plexus in the str. lucidum, covering 50–100% of the transverse extent of the CA3 and fanning out into the hilus. Additionally, some collateral extend into the cell body layer. The axonal distribution is strikingly similar to that of the mossy fibers; this cell type best exemplifies the co-alignment of inhibitory interneuron axons and excitatory afferent pathway. Synaptic contacts are

located on dendritic shafts (85%), mostly large-caliber proximal dendrites, and to a lesser degree on somata (15%) in the CA3 area. Majority of the targets are pyramidal cells, although ~20% of the postsynaptic profiles belong to GABA-immunoreactive interneurons (Vida and Frotscher, 2000). The length of the axon in the in vitro-labeled neurons is 20.3 – 28.6 mm and forms ~5,000–7,000 boutons (density: 0.23 – 0.25 μm^{-1}). As the postsynaptic pyramidal cells are innervated by ~4 synaptic contact sites, a single MFA interneuron may target 1,300–1,700 neurons.

(13) Interneuron-specific interneurons. A class of interneuron specialized to innervate other interneurons has been identified by imunohistochemically staining for CR and VIP (Acsády et al., 1996a, b; Gulyás et al., 1996; Hájos et al., 1996). Three types have been distinguished on the basis of the neurochemical markers and synaptic targets (Fig. 8):

– *Type I (IS-I)* cells contain CR and target CB-positive dendrite-inhibiting interneurons. The soma of IS-I cells is in str. oriens, pyramidale, or radiatum and the dendrites span most layers.
– *Type II (IS-II)* cells express VIP and innervate mainly CCK/VIP-positive basket cells. The soma is found in str. radiatum, often at its upper border, whereas the dendrites mostly extend into the str. lacunosum-moleculare.
– *Type III (IS-III)* cells contain both CR and VIP and innervate mainly O-LM cells. The soma is located in str. pyramidale or radiatum with radial dendrites crossing most layers. These cells target mainly O-LM cells.

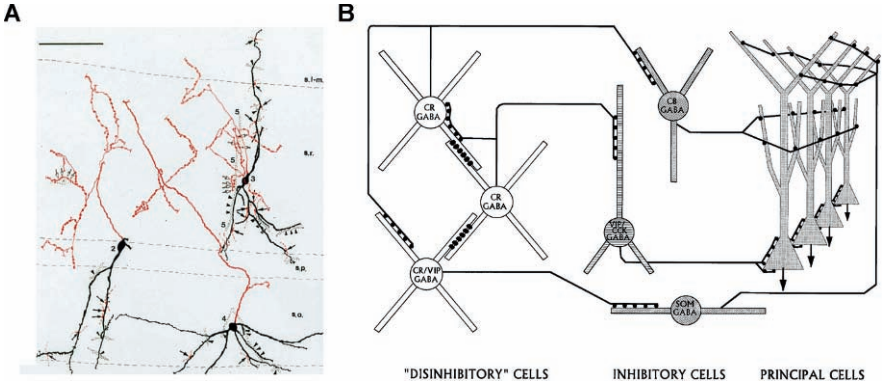

Fig. 8 IS interneurons of the hippocampus. **A** Camera lucida drawing of CR-containing interneurons of the CA1 area (cell bodies and dendrites are in black; axons are in *red*). The cells often form dendro-dendritic and axo-dendritic contacts with each other. Synaptic partners are indicated by *dotted outlines*. Arrowheads indicate locations where the dendrites ran parallel in close contact. **B** Simplified schematic representation of hippocampal microcircuits including IS interneurons ("disinhibitory cells"). IS cells are interconnected by dendro-dendritic (bars on dendrites) and axo-dendritic contacts which presumably serve their rhythmic and synchronized activity. The cells' output is directed to and controls the activity of several types of inhibitory interneurons including CCK–BCs (VIP/CCK GABA), O-LM interneurons (SOM GABA), and CB-immunoreactive dendritic inhibitory interneurons (CB GABA) (Reproduced from Gulyás et al., 1996 with permission. © Society for Neuroscience.)

Gulyás et al. (1999) provide a quantitative analysis of the dendritic arbor and synaptic inputs of CR-immonoreactive neurons. CR-interneurons also form mutual inhibitory synapses and are thought to be coupled by dendro-dendritic gap junctions (Fig. 8, Gulyás et al., 1996).

Interneurons of the DG and Hilus

The layering of the DG differs markedly from that of the CA areas. Therefore, many of the DG interneuron types show differences in their morphology to their counterparts in those areas. In the following section, we briefly review the main morphological feature and connectivity, whenever known, of the major DG interneuron types.

Perisomatic Inhibitory Interneurons

(1) Fast-spiking PV–BCs are the best investigated interneuron type of the DG (Han et al., 1993; Halasy and Somogyi, 1993b; Scharfman, 1995; Sík et al., 1997; Mott et al., 1997; Bartos et al., 2001, 2002; Doischer et al., 2008; Nörenberg et al., 2008). The somatodendritic morphology is reminiscent of pyramidal cells. The large triangular or ovoid soma is located in the granule cell layer, often at the border to the hilus. Apical dendrites extend into the molecular layer and can receive input from all major afferent pathways. Basal dendrites are found in the hilus and receive recurrent excitatory input from mossy fibers mediated by multiple, 2–4 distributed contacts (Geiger et al., 1997). The mean surface area of the apical and basal dendrites of in vitro-labeled BCs is 7,600 and $2,200\,\mu m^2$, respectively (Nörenberg et al., 2008). The main postsynaptic targets of BCs are GCs (Geiger et al., 1997; Kraushaar and Jonas, 2000; Bartos et al., 2002). Similar to the CA areas, DG PV–BCs are also extensively coupled by mutual inhibitory synapses (70–80% connectivity for closely spaced BCs) and gap junctions (~30% connectivity, Bartos et al., 2001, 2002).

(2) CCK–BCs were described in the in vivo labeling study by Sík et al. (1997), but no further data have been obtained from identified CCK–BC from the DG.

(3) AACs of DG were first described in detail by Han et al. (1993) and Buhl et al. (1994a, b). Somatodendritic morphology of AACs is largely similar to that of BCs. The output is directed exclusively to the axon initial segment of GCs. These synapses involve multiple contact sites; in case of one AAC–GC pair, eight contacts were identified and the number of AACs converging onto the same initial segment was calculated to be five (Buhl et al., 1994a).

Dendritic Inhibitory Interneurons

(4) Molecular layer perforant path-associated (MOPP) interneurons are located in the molecular layer and project to the outer two-thirds of this layer co-aligned

with the perforant path (Han et al., 1993; Halasy and Somogyi, 1993b; Sík et al., 1997). A subset of molecular layer interneurons shows a similar projection in the DG, but many of its axon collaterals cross the hilus and terminate in the CA1 area and/or the subiculum ("OML cells", Ceranik et al., 1997; Hosp et al., 2005). Many features of these interneurons correspond to those of CA1 PPA cells.

(5) Hilar perforant path-associated (HIPP) interneurons (Han et al., 1993b; Halasy and Somogyi, 1993b; Sík et al., 1997; Hosp et al., 2005) correspond to O-LM interneurons of the CA areas. Their soma and dendrites are confined to the hilus and receive recurrent excitation from the mossy fibers. Their axon terminates in the outer two-thirds of the molecular layer parallel to the perforant path. Thus, HIPP interneurons constitute the main feedback dendritic inhibitory cell types of the DG. Similar to O-LM cells, HIPP cells express SOM (Katona et al., 1999a).

(6) Hilar commissural/associational path-associated (HICAP) interneurons are characterized by an axon in the inner molecular layer, co-aligned with the commissural/associational path (Han et al., 1993b; Halasy and Somogyi, 1993b; Sík et al., 1997; Lübke et al., 1998; Hosp et al., 2005). The soma is located in the hilus, the dendrites are found both in the hilus and in the molecular layer. Therefore, HICAP cells can mediate both feedforward and feedback inhibition.

(7) Total molecular layer (TML) interneurons project to the molecular layer, covering vertically the entire layer (Mott et al., 1997; Hosp et al., 2005). The soma is located in the g.c.l. and the dendrites extend into both the hilus and the molecular layer. Therefore, TML cells can mediate inhibition to the entire dendritic tree of GCs in both feedforward and feedback manner.

Experimental Techniques

Golgi Silver Staining Method

The first experimental approach that enabled detailed analysis of the morphological features of neurons was the "black reaction" developed by Camillo Golgi in the late nineteenth century. The Golgi method results in the complete labeling of a random set of neurons. The sparse staining pattern enables the examination of the morphology of individual cells. Many neuroscientists, including Ramon y Cajal, applied this method successfully to investigate the structure and gain insights into the function of neurons in various brain areas, including the hippocampus. Although targeted labeling methods often offer clear advantages, the Golgi method can be still used to label and characterize abundant cell types (e.g., cortical principal cells). A modern version of the Golgi staining method can be observed in some transgenic lines, such as Thy1-GFP mice, in which green fluorescent protein is randomly expressed in a subset of DG GCs (Feng et al., 2000).

Immunocytochemistry

Neurons express a wide variety of molecules which can be detected and visualized using specific antibodies (Freund and Buzsáki, 1996; Somogyi and Klausberger, 2005; Jinno and Kosaka, 2006). Some of these neurochemical markers are evenly distributed in the cytoplasm (e.g., PV, CB, CR) or on the surface of the plasma membrane (mGluR1a); therefore, the immunostaining can delineate neurons in their entirety. Morphology of cell types with low density can be investigated using this method; however, the analysis is often restricted to the somatodendritic domain, as overlapping axonal arbors cannot be resolved with accuracy.

Targeted Labeling of Single Cells

Microelectrode and whole-cell patch-clamp recordings can be combined with intracellular labeling, using either fluorescent markers (including ion- and voltage-sensitive dyes) or biocytin/neurobiotin-based assay systems (Lacaille et al., 1987; Buhl et al., 1994a). While fluorescent dyes can be directly observed during recording, biocytin needs to be visualized by histological processing of the tissue after the recording session. This combined approach enables the identification and detailed morphological analysis of the recorded neurons to complement the physiological data. Intracellular staining of synaptically coupled neurons has been successfully used to establish the number and location of synaptic contacts. Furthermore, intracellular labeling can be combined with immunostaining to characterize the neurons neurochemically.

In vitro labeling in acute hippocampal slices has been extensively applied and provided much of the information on the structure and function of various hippocampal neurons obtained in the last two decades. However, in vitro labeling has obvious limitations in that the neurons are incomplete, part of the dendritic tree and the axon is removed during the slicing procedure. For this reason, in vivo labeling approaches, despite their lower efficiency and laborious nature, are often preferable.

In Vivo Labeling of Single Cells

In vivo labeling has been performed using microelectrode (Soltesz et al., 1993; Sík et al., 1994) and more recently by whole-cell patch-clamp recordings (Lee et al., 2009). These two methods provide high-resolution electrophysiological data, but inevitably lead to some degree of damage to the neurons. Alternatively, juxtacellular recordings can be performed (Klausberger et al., 2003). The physiological data, using this approach, are restricted to the discharge pattern of the neurons but high-quality anatomical data can be obtained for correlated light and electron microscopic investigations.

The Future

Neuroanatomical investigation focusing on hippocampal neurons and networks has been performed for well over a century. These investigations have identified a large number of neuron types and provided a growing body of information on their morphology and synaptic connections. However, despite the extensive research, our knowledge is still rather limited and patchy, as this chapter also reflects.

First, classification of interneurons with atypical morphological features needs further attention. Their classification is difficult while often only one or a few examples exist in the literature. The low numbers conceivably suggest low abundance; however, the recent identification of "ivy" interneurons (Fuentealba et al., 2008) indicates that there are still significant discoveries to be made. Second, detailed quantitative information about the morphological structure (Emri et al., 2001; Nörenberg et al., 2008) of many cell types is still missing; this would be required to create realistic single-cell models and investigate integrative properties of these neurons. Finally, connectivity of the various types should be systematically mapped (Li et al., 1992; Megías et al., 2001). While synaptic target profiles are mostly well established, divergence and convergence factors in the network have remained often unknown. This information is indispensable for our understanding of how microcircuits and large-scale networks are built and function under normal and pathological conditions.

To achieve these goals we need to invest, no doubt, hundreds of "man-years" of dedicated and meticulous work. However, recent and future advances in experimental techniques will offer better conditions, higher efficiency, and improved resolution to morphological analysis. Novel, high-resolution imaging techniques in combination with ion- and voltage-sensitive dyes (Rózsa et al., 2004; Homma et al., 2009) and genetically encoded markers (Oliva et al., 2000; Meyer et al., 2002; Livet et al., 2007) will facilitate correlated investigations of activity patterns and structure of hippocampal neurons and networks. Improved transsynaptic viral tools should advance mapping of functional and anatomical connectivity (Boldogköi et al., 2009). In combination with these methods, post hoc electron microscopic ultrastructural investigations remain important to confirm and extend results obtained at the light microscopic level. While in vitro recording and labeling techniques continue to dominate hippocampal research, especially in the analysis of individual synaptic connections, in vivo approaches, such as juxtacellular and whole-cell patch-clamp recordings (Klausberger et al., 2003; Lee et al., 2009), will become increasingly important not only for the physiological but also for the anatomical characterization of the neurons. Wider use of these methods will help us to create large libraries of neurons and enable us on the one hand to establish general morphological features of the various neuron types and on the other to better appreciate variability of individual cells.

Further Reading

Acsády L, Arabadzisz D, Freund TF (1996a) Correlated morphological and neurochemical features identify different subsets of vasoactive intestinal polypeptide-immunoreactive interneurons in rat hippocampus. Neuroscience 73: 299–315

Acsády L, Görcs TJ, Freund TF (1996b) Different populations of vasoactive intestinal polypeptide-immunoreactive interneurons are specialized to control pyramidal cells or interneurons in the hippocampus. Neuroscience 73: 317–34

Acsády L, Kamondi A, Sík A, Freund T, Buzsáki G (1998) GABAergic cells are the major postsynaptic targets of mossy fibers in the rat hippocampus. J Neurosci 18: 3386–403

Acsády L, Katona I, Martínez-Guijarro FJ, Buzsáki G, Freund TF (2000) Unusual target selectivity of perisomatic inhibitory cells in the hilar region of the rat hippocampus. J Neurosci 20: 6907–19

Ali AB (2007) Presynaptic Inhibition of GABAA receptor-mediated unitary IPSPs by cannabinoid receptors at synapses between CCK-positive interneurons in rat hippocampus. J Neurophysiol 98: 861–9

Amaral DG (1978) A Golgi study of cell types in the hilar region of the hippocampus in the rat. J Comp Neurol 182: 851–914

Bannister NJ, Larkman AU (1995a) Dendritic morphology of CA1 pyramidal neurones from the rat hippocampus: I. Branching patterns. J Comp Neurol 360: 150–60

Bannister NJ, Larkman AU (1995b) Dendritic morphology of CA1 pyramidal neurones from the rat hippocampus: II. Spine distributions. J Comp Neurol 360: 161–71

Bartos M, Vida I, Frotscher M, Geiger JRP, Jonas P (2001) Rapid signaling at inhibitory synapses in a dentate gyrus interneuron network. J Neurosci 21: 2687–98

Bartos M, Vida I, Frotscher M, Meyer A, Monyer H, Geiger JRP, Jonas P (2002) Fast synaptic inhibition promotes synchronized gamma oscillations in hippocampal interneuron networks. Proc Natl Acad Sci USA 99: 13222–7

Baude A, Bleasdale C, Dalezios Y, Somogyi P, Klausberger T (2007) Immunoreactivity for the $GABA_A$ receptor alpha1 subunit, somatostatin and Connexin36 distinguishes axoaxonic, basket, and bistratified interneurons of the rat hippocampus. Cereb Cortex 17: 2094–107

Baude A, Nusser Z, Roberts JD, Mulvihill E, McIlhinney RA, Somogyi P (1993) The metabotropic glutamate receptor (mGluR1 alpha) is concentrated at perisynaptic membrane of neuronal subpopulations as detected by immunogold reaction. Neuron 11: 771–87

Blackstad TW (1956) Commissural connections of the hippocampal region in the rat, with special reference to their mode of termination. J Comp Neurol 105: 417–537

Blackstad TW, Kjaerheim A (1961) Special axo-dendritic synapses in the hippocampal cortex: electron and light microscopic studies on the layer of mossy fibers. J Comp Neurol 117: 133–59

Blasco-Ibáñez JM, Freund TF (1995) Synaptic input of horizontal interneurons in stratum oriens of the hippocampal CA1 subfield: Structural basis of feed-back activation. Eur J Neurosci 7: 2170–80

Boldogköi Z, Bálint K, Awatramani GB, Balya D, Busskamp V, Viney TJ, Lagali PS, Duebel J, Pásti E, Tombácz D, Tóth JS, Takács IF, Scherf BG, Roska B (2009) Genetically timed, activity-sensor and rainbow transsynaptic viral tools. Nat Methods 6: 127–30

Buckmaster PS, Strowbridge BW, Schwartzkroin PA (1993) A comparison of rat hippocampal mossy cells and CA3c pyramidal cells. J Neurophysiol 70: 1281–99

Buckmaster PS, Wenzel HJ, Kunkel DD, Schwartzkroin PA (1996) Axon arbors and synaptic connections of hippocampal mossy cells in the rat in vivo. J Comp Neurol 366: 271–92

Buhl EH, Cobb SR, Halasy K, Somogyi P (1995) Properties of unitary IPSPs evoked by anatomically identified basket cells in the rat hippocampus. Eur J Neurosci 7: 1989–2004

Buhl EH, Halasy K, Somogyi P (1994a) Diverse sources of hippocampal unitary inhibitory postsynaptic potentials and the number of synaptic release sites. Nature 368: 823–8

Buhl EH, Han ZS, Lörinczi Z, Stezhka VV, Karnup SV, Somogyi P (1994b) Physiological properties of anatomically identified axo-axonic cells in the rat hippocampus. J Neurophysiol 71: 1289–307

Buhl EH, Szilágyi T, Halasy K, Somogyi P (1996) Physiological properties of anatomically identified basket and bistratified cells in the CA1 area of the rat hippocampus in vitro. Hippocampus 6: 294–305

Cajal SR (1968) The structure of the Ammon's horn. Charles C. Thomas, Springfield, IL

Cannon RC, Wheal HV, Turner DA (1999) Dendrites of classes of hippocampal neurons differ in structural complexity and branching patterns. J Comp Neurol 413: 619–33

Ceranik K, Bender R, Geiger JR, Monyer H, Jonas P, Frotscher M, Lübke J (1997) A novel type of GABAergic interneuron connecting the input and the output regions of the hippocampus. J Neurosci 17: 5380–94

Chicurel ME, Harris KM (1992) Three-dimensional analysis of the structure and composition of CA3 branched dendritic spines and their synaptic relationships with mossy fiber boutons in the rat hippocampus. J Comp Neurol 325(2): 169–82

Chitwood RA, Hubbard A, Jaffe DB (1999) Passive electrotonic properties of rat hippocampal CA3 interneurones. J Physiol 515: 743–56

Claiborne BJ, Amaral DG, Cowan WM (1986) A light and electron microscopic analysis of the mossy fibers of the rat dentate gyrus. J Comp Neurol 246: 435–58

Claiborne BJ, Amaral DG, Cowan WM (1990) Quantitative, three-dimensional analysis of granule cell dendrites in the rat dentate gyrus. J Comp Neurol 302: 206–19

Cobb SR, Halasy K, Vida I, Nyiri G, Tamás G, Buhl EH, Somogyi P (1997) Synaptic effects of identified interneurons innervating both interneurons and pyramidal cells in the rat hippocampus. Neuroscience 79: 629–48

Cope DW, Maccaferri G, Márton LF, Roberts JD, Cobden PM, Somogyi P (2002) Cholecystokinin-immunopositive basket and Schaffer collateral-associated interneurones target different domains of pyramidal cells in the CA1 area of the rat hippocampus. Neuroscience 109: 63–80

Csicsvari J, Hirase H, Czurkó A, Buzsáki G (1998) Reliability and state dependence of pyramidal cell-interneuron synapses in the hippocampus: An ensemble approach in the behaving rat. Neuron 21: 179–89

Deuchars J, Thomson AM (1996) CA1 pyramid-pyramid connections in rat hippocampus in vitro: dual intracellular recordings with biocytin filling. Neuroscience 74: 1009–18

Doischer D, Hosp JA, Yanagawa Y, Obata K, Jonas P, Vida I, Bartos M (2008) Postnatal differentiation of basket cells from slow to fast signaling devices. J Neurosci 28: 12956–68

Elfant D, Pál BZ, Emptage N, Capogna M (2008) Specific inhibitory synapses shift the balance from feedforward to feedback inhibition of hippocampal CA1 pyramidal cells. Eur J Neurosci 27: 104–13

Emri Z, Antal K, Gulyás AI, Megías M, Freund TF (2001) Electrotonic profile and passive propagation of synaptic potentials in three subpopulations of hippocampal CA1 interneurons. Neuroscience 104: 1013–26

Feng G, Mellor RH, Bernstein M, Keller-Peck C, Nguyen QT, Wallace M, Nerbonne JM, Lichtman JW, Sanes JR (2000) Imaging neuronal subsets in transgenic mice expressing multiple spectral variants of GFP. Neuron 28: 41–51

Ferraguti F, Klausberger T, Cobden P, Baude A, Roberts JD, Szucs P, Kinoshita A, Shigemoto R, Somogyi P, Dalezios Y (2005) Metabotropic glutamate receptor 8-expressing nerve terminals target subsets of GABAergic neurons in the hippocampus. J Neurosci 25: 10520–36

Förster E, Zhao S, Frotscher M (2006) Laminating the hippocampus. Nat Rev Neurosci 7: 259–67

Freund TF, Buzsáki G (1996) Interneurons of the hippocampus. Hippocampus 6: 347–470

Frotscher M, Seress L, Schwerdtfeger WK, Buhl E (1991) The mossy cells of the fascia dentata: a comparative study of their fine structure and synaptic connections in rodents and primates. J Comp Neurol 312: 145–63

Frotscher M, Soriano E, Misgeld U (1994) Divergence of hippocampal mossy fibers. Synapse 16: 148–60

Fuentealba P, Begum R, Capogna M, Jinno S, Márton LF, Csicsvari J, Thomson A, Somogyi P, Klausberger T (2008) Ivy cells: a population of nitric-oxide-producing, slow-spiking GABAergic neurons and their involvement in hippocampal network activity. Neuron 57: 917–29

Fukuda T, Kosaka T (2000) Gap junctions linking the dendritic network of GABAergic interneurons in the hippocampus. J Neurosci 20: 1519–28

Fukuda T, Kosaka T (2003) Ultrastructural study of gap junctions between dendrites of parvalbumin-containing GABAergic neurons in various neocortical areas of the adult rat. Neuroscience 120: 5–20

Ganter P, Szücs P, Paulsen O, Somogyi P (2004) Properties of horizontal axo-axonic cells in stratum oriens of the hippocampal CA1 area of rats in vitro. Hippocampus 14: 232–43

Geiger JR, Lübke J, Roth A, Frotscher M, Jonas P (1997) Submillisecond AMPA receptor-mediated signaling at a principal neuron-interneuron synapse. Neuron 18: 1009–23

Gloveli T, Dugladze T, Rotstein HG, Traub RD, Monyer H, Heinemann U, Whittington MA, Kopell NJ (2005a) Orthogonal arrangement of rhythm-generating microcircuits in the hippocampus. Proc Natl Acad Sci USA 102: 13295–300

Gloveli T, Dugladze T, Saha S, Monyer H, Heinemann U, Traub RD, Whittington MA, Buhl EH (2005b) Differential involvement of oriens/pyramidale interneurones in hippocampal network oscillations in vitro. J Physiol 562: 131–47

Golding NL, Mickus TJ, Katz Y, Kath WL, Spruston N (2005) Factors mediating powerful voltage attenuation along CA1 pyramidal neuron dendrites. J Physiol 568: 69–82.

Gonzales RB, DeLeon Galvan CJ, Rangel YM, Claiborne BJ (2001) Distribution of thorny excrescences on CA3 pyramidal neurons in the rat hippocampus. J Comp Neurol 430: 357–68

Guetg N, Seddik R, Vigot R, Turecek R, Gassmann M, Vogt KE, Bräuner-Osborne H, Shigemoto R, Kretz O, Frotscher M, Kulik A, Bettler B (2009) The $GABA_{B1a}$ isoform mediates heterosynaptic depression at hippocampal mossy fiber synapses. J Neurosci 29: 1414–23

Gulyás AI, Freund TF (1996) Pyramidal cell dendrites are the primary targets of calbindin D28k-immunoreactive interneurons in the hippocampus. Hippocampus 6: 525–34

Gulyás AI, Hájos N, Freund TF (1996) Interneurons containing calretinin are specialized to control other interneurons in the rat hippocampus. J Neurosci 16: 3397–411

Gulyás AI, Megías M, Emri Z, Freund TF (1999) Total number and ratio of excitatory and inhibitory synapses converging onto single interneurons of different types in the CA1 area of the rat hippocampus. J Neurosci 19: 10082–97

Gulyás AI, Miles R, Hájos N, Freund TF (1993a) Precision and variability in postsynaptic target selection of inhibitory cells in the hippocampal CA3 region. Eur J Neurosci 5: 1729–51

Gulyás AI, Miles R, Sík A, Tóth K, Tamamaki N, Freund TF (1993b) Hippocampal pyramidal cells excite inhibitory neurons through a single release site. Nature 366: 683–7

Gulyás AI, Tóth K, McBain CJ, Freund TF (1998) Stratum radiatum giant cells: a type of principal cell in the rat hippocampus. Eur J Neurosci 10: 3813–22

Hájos N, Acsády L, Freund TF (1996) Target selectivity and neurochemical characteristics of VIP-immunoreactive interneurons in the rat dentate gyrus. Eur J Neurosci 8: 1415–31

Hájos N, Mody I (1997) Synaptic communication among hippocampal interneurons: Properties of spontaneous IPSCs in morphologically identified cells. J Neurosci 17: 8427–42

Hájos N, Papp EC, Acsády L, Levey AI, Freund TF (1998) Distinct interneuron types express m2 muscarinic receptor immunoreactivity on their dendrites or axon terminals in the hippocampus. Neuroscience 82: 355–76

Halasy K, Buhl EH, Lörinczi Z, Tamás G, Somogyi P (1996) Synaptic target selectivity and input of GABAergic basket and bistratified interneurons in the CA1 area of the rat hippocampus. Hippocampus 6: 306–29

Halasy K, Somogyi P (1993a) Distribution of GABAergic synapses and their targets in the dentate gyrus of rat: a quantitative immunoelectron microscopic analysis. J Hirnforsch 34: 299–308

Halasy K, Somogyi P (1993b) Subdivisions in the multiple GABAergic innervation of granule cells in the dentate gyrus of the rat hippocampus. Eur J Neurosci 5: 411–29

Hama K, Arii T, Kosaka T (1989) Three-dimensional morphometrical study of dendritic spines of the granule cell in the rat dentate gyrus with HVEM stereo images. J Electron Microsc Tech 12: 80–7

Han ZS, Buhl EH, Lörinczi Z, Somogyi P (1993) A high degree of spatial selectivity in the axonal and dendritic domains of physiologically identified local-circuit neurons in the dentate gyrus of the rat hippocampus. Eur J Neurosci 5: 395–410

Harris KM, Jensen FE, Tsao B (1992) Three-dimensional structure of dendritic spines and synapses in rat hippocampus (CA1) at postnatal day 15 and adult ages: Implications for the maturation of synaptic physiology and long-term potentiation. J Neurosci 12: 2685–705

Henze DA, Cameron WE, Barrionuevo G (1996) Dendritic morphology and its effects on the amplitude and rise-time of synaptic signals in hippocampal CA3 pyramidal cells. J Comp Neurol 369: 331–44

Homma R, Baker BJ, Jin L, Garaschuk O, Konnerth A, Cohen LB, Bleau CX, Canepari M, Djurisic M, Zecevic D (2009) Wide-field and two-photon imaging of brain activity with voltage- and calcium-sensitive dyes. Methods Mol Biol 489: 43–79

Hormuzdi SG, Pais I, LeBeau FE, Towers SK, Rozov A, Buhl EH, Whittington MA, Monyer H (2001) Impaired electrical signaling disrupts gamma frequency oscillations in connexin 36-deficient mice. Neuron 31: 487–95

Hosp J, Vida I, Yanagawa Y, Obata K, Frotscher M, Jonas P, Bartos M (2005) Diversity of GFP-labeled GABAergic interneurons in mouse dentate gyrus and hilus. Society of Neurosci. Abstr. Program No. 272.20. Neuroscience Meeting Planner. San Diego, CA: Society for Neuroscience, 2004. Online

Houser CR (2007) Interneurons of the dentate gyrus: an overview of cell types, terminal fields and neurochemical identity. Prog Brain Res 163: 217–32

Ishizuka N, Cowan WM, Amaral DG (1995) A quantitative analysis of the dendritic organization of pyramidal cells in the rat hippocampus. J Comp Neurol 362: 17–45

Ishizuka N, Weber J, Amaral DG (1990) Organization of intrahippocampal projections originating from CA3 pyramidal cells in the rat. J Comp Neurol 295: 580–623

Jinno S, Klausberger T, Marton LF, Dalezios Y, Roberts JD, Fuentealba P, Bushong EA, Henze D, Buzsáki G, Somogyi P (2007) Neuronal diversity in GABAergic long-range projections from the hippocampus. J Neurosci 27: 8790–804

Jinno S, Kosaka T. (2006) Cellular architecture of the mouse hippocampus: A quantitative aspect of chemically defined GABAergic neurons with stereology. Neurosci Res 56: 229–45

Karson MA, Tang AH, Milner TA, Alger BE (2009) Synaptic cross talk between perisomatic-targeting interneuron classes expressing cholecystokinin and parvalbumin in hippocampus. J Neurosci 29: 4140–54

Katona I, Acsády L, Freund TF (1999a) Postsynaptic targets of somatostatin-immunoreactive interneurons in the rat hippocampus. Neuroscience 88: 37–55

Katona I, Sperlágh B, Sík A, Käfalvi A, Vizi ES, Mackie K, Freund TF (1999b) Presynaptically located CB1 cannabinoid receptors regulate GABA release from axon terminals of specific hippocampal interneurons. J Neurosci 19: 4544–58

Katsumaru H, Kosaka T, Heizmann CW, Hama K (1988) Immunocytochemical study of GABAergic neurons containing the calcium-binding protein parvalbumin in the rat hippocampus. Exp Brain Res 72: 347–62

Klausberger T, Magill PJ, Márton LF, Roberts JD, Cobden PM, Buzsáki G, Somogyi P (2003) Brain-state- and cell-type-specific firing of hippocampal interneurons in vivo. Nature 421: 844–8

Klausberger T, Márton LF, Baude A, Roberts JD, Magill PJ, Somogyi P (2004) Spike timing of dendrite-targeting bistratified cells during hippocampal network oscillations in vivo. Nat Neurosci 7: 41–7

Klausberger T, Marton LF, O'Neill J, Huck JH, Dalezios Y, Fuentealba P, Suen WY, Papp E, Kaneko T, Watanabe M, Csicsvari J, Somogyi P (2005) Complementary roles of cholecystokinin- and parvalbumin-expressing GABAergic neurons in hippocampal network oscillations. J Neurosci 25: 9782–93

Klausberger T, Somogyi P (2008) Neuronal diversity and temporal dynamics: the unity of hippocampal circuit operations. Science 321: 53–7

Kosaka T, Katsumaru H, Hama K, Wu JY, Heizmann CW (1987) GABAergic neurons containing the Ca2+-binding protein parvalbumin in the rat hippocampus and dentate gyrus. Brain Res 419: 119–30

Kosaka T, Wu JY, Benoit R (1988) GABAergic neurons containing somatostatin-like immunoreactivity in the rat hippocampus and dentate gyrus. Exp Brain Res 71: 388–98

Kowalski J, Geuting M, Drakew A, Haas C, Zhao S, Frotscher M,Vida I (2008) Altered layering of the dentate gyrus in reeler mice results in a reduced efficiency and precision of synaptic activation of hilar mossy cells. Society of Neurosci. Abstr. Program No. 437.3/J11. Neuroscience Meeting Planner. Washington, DC: Society for Neuroscience, 2008. Online

Kraushaar U, Jonas P (2000) Efficacy and stability of quantal GABA release at a hippocampal interneuron-principal neuron synapse. J Neurosci 20: 5594–607

Lacaille JC, Mueller AL, Kunkel DD, Schwartzkroin PA (1987) Local circuit interactions between oriens/alveus interneurons and CA1 pyramidal cells in hippocampal slices: electrophysiology and morphology. J Neurosci 7: 1979–93

Larimer P, Strowbridge BW (2008) Non-random local circuits in the dentate gyrus. J Neurosci 28: 12212–23

Lee AK, Epsztein J, Brecht M (2009) Head-anchored whole-cell recordings in freely moving rats. Nat Protoc 4: 385–92

Li XG, Somogyi P, Tepper JM, Buzsáki G (1992) Axonal and dendritic arborization of an intracellularly labeled chandelier cell in the CA1 region of rat hippocampus. Exp Brain Res 90: 519–25

Li XG, Somogyi P, Ylinen A, Buzsáki G (1994) The hippocampal CA3 network: an in vivo intracellular labeling study. J Comp Neurol 339: 181–208

Livet J, Weissman TA, Kang H, Draft RW, Lu J, Bennis RA, Sanes JR, Lichtman JW (2007) Transgenic strategies for combinatorial expression of fluorescent proteins in the nervous system. Nature 450: 56–62

Lorente de Nó R (1934) Studies on the structure of the cerebral cortex II: Continuation of the study of the ammonic system. J Psychol Neurol 46: 113–77

Losonczy A, Biró AA, Nusser Z (2004) Persistently active cannabinoid receptors mute a subpopulation of hippocampal interneurons. Proc Natl Acad Sci USA 101: 1362–7

Lübke J, Frotscher M, Spruston N (1998) Specialized electrophysiological properties of anatomically identified neurons in the hilar region of the rat fascia dentata. J Neurophysiol 79: 1518–34

Maccaferri G, Dingledine R (2002) Control of feedforward dendritic inhibition by NMDA receptor-dependent spike timing in hippocampal interneurons. J Neurosci 22: 5462–72

Maccaferri G, Lacaille JC (2003) Interneuron Diversity series: Hippocampal interneuron classifications – making things as simple as possible, not simpler. Trends Neurosci 26: 564–71

Maccaferri G, Roberts JD, Szucs P, Cottingham CA, Somogyi P (2000) Cell surface domain specific postsynaptic currents evoked by identified GABAergic neurones in rat hippocampus in vitro. J Physiol 524: 91–116

Major G, Evans JD, Jack JJB (1993) Solutions for transients in arbitrarily branching cables: 1. Voltage recording with a somatic shunt. Biophys J 65: 423–49

Major G, Larkman AU, Jonas P, Sakmann B, Jack JJ (1994) Detailed passive cable models of whole-cell recorded CA3 pyramidal neurons in rat hippocampal slices. J Neurosci 14: 4613–38

Martina M, Vida I, Jonas P (2000) Distal initiation and active propagation of action potentials in interneuron dendrites. Science 287: 295–300

Mátyás F, Freund TF, Gulyás AI (2004) Convergence of excitatory and inhibitory inputs onto CCK-containing basket cells in the CA1 area of the rat hippocampus. Eur J Neurosci 19: 1243–56

McBain CJ, DiChiara TJ, Kauer JA (1994) Activation of metabotropic glutamate receptors differentially affects two classes of hippocampal interneurons and potentiates excitatory synaptic transmission. J Neurosci 14: 4433–45

McBain CJ, Fisahn A (2001) Interneurons unbound. Nat Rev Neurosci 2: 11–23

Megías M, Emri Z, Freund TF, Gulyás AI (2001) Total number and distribution of inhibitory and excitatory synapses on hippocampal CA1 pyramidal cells. Neuroscience 102: 527–40

Mercer A, Trigg HL, Thomson AM (2007) Characterization of neurons in the CA2 subfield of the adult rat hippocampus. J Neurosci 27: 7329–38

Meyer AH, Katona I, Blatow M, Rozov A, Monyer H (2002) In vivo labeling of parvalbumin-positive interneurons and analysis of electrical coupling in identified neurons. J Neurosci 22: 7055–64

Miles R, Tóth K, Gulyás AI, Hájos N, Freund TF (1996) Differences between somatic and dendritic inhibition in the hippocampus. Neuron 16: 815–23

Min MY, Melyan Z, Kullmann DM (1999) Synaptically released glutamate reduces gamma-aminobutyric acid GABAergic inhibition in the hippocampus via kainite receptors. Proc Natl Acad Sci USA 96: 9932–7

Mott DD, Turner DA, Okazaki MM, Lewis DV (1997) Interneurons of the dentate-hilus border of the rat dentate gyrus: Morphological and electrophysiological heterogeneity. J Neurosci 17: 3990–4005

Nörenberg A, Bartos M, Vida I, Hu H, Jonas P (2008) Detailed cable models of fast-spiking basket cells in the dentate gyrus. Society of Neurosci. Abstr. Program No. 36.2/F2. Neuroscience Meeting Planner. Washington, DC: Society for Neuroscience, 2008. Online

Nunzi MG, Gorio A, Milan F, Freund TF, Somogyi P, Smith AD (1985) Cholecystokinin-immunoreactive cells form symmetrical synaptic contacts with pyramidal and nonpyramidal neurons in the hippocampus. J Comp Neurol 237: 485–505

Oliva AA Jr, Jiang M, Lam T, Smith KL, Swann JW (2000) Novel hippocampal interneuronal subtypes identified using transgenic mice that express green fluorescent protein in GABAergic interneurons. J Neurosci 20: 3354–68

Pawelzik H, Hughes DI, Thomson AM. Physiological and morphological diversity of immunocytochemically defined parvalbumin- and cholecystokinin-positive interneurones in CA1 of the adult rat hippocampus. J Comp Neurol 2002 443: 346–67

Petilla Interneuron Nomenclature Group, Ascoli GA, Alonso-Nanclares L, Anderson SA, Barrionuevo G, Benavides-Piccione R, Burkhalter A, Buzsáki G, Cauli B, Defelipe J, Fairén A, Feldmeyer D, Fishell G, Fregnac Y, Freund TF, Gardner D, Gardner EP, Goldberg JH, Helmstaedter M, Hestrin S, Karube F, Kisvárday ZF, Lambolez B, Lewis DA, Marin O, Markram H, Muñoz A, Packer A, Petersen CC, Rockland KS, Rossier J, Rudy B, Somogyi P, Staiger JF, Tamas G, Thomson AM, Toledo-Rodriguez M, Wang Y, West DC, Yuste R (2008) Petilla terminology: Nomenclature of features of GABAergic interneurons of the cerebral cortex. Nat Rev Neurosci 9: 557–68

Price CJ, Cauli B, Kovacs ER, Kulik A, Lambolez B, Shigemoto R, Capogna M. (2005) Neurogliaform neurons form a novel inhibitory network in the hippocampal CA1 area. J Neurosci 25: 6775–86

Price CJ, Scott R, Rusakov DA, Capogna M (2008) GABA(B) receptor modulation of feedforward inhibition through hippocampal neurogliaform cells. J Neurosci 28: 6974–82

Pyapali GK, Sík A, Penttonen M, Buzsaki G, Turner DA (1998) Dendritic properties of hippocampal CA1 pyramidal neurons in the rat: Intracellular staining in vivo and in vitro. J Comp Neurol 391: 335–52

Ratzliff AH, Santhakumar V, Howard A, Soltesz I (2002) Mossy cells in epilepsy: Rigor mortis or vigor mortis? Trends Neurosci 25: 140–4

Ribak CE, Seress L, Amaral DG (1985) The development, ultrastructure and synaptic connections of the mossy cells of the dentate gyrus. J Neurocytol 14: 835–57

Rollenhagen A, Sätzler K, Rodríguez EP, Jonas P, Frotscher M, Lübke JH (2007) Structural determinants of transmission at large hippocampal mossy fiber synapses. J Neurosci 27: 10434–44

Rózsa B, Zelles T, Vizi ES, Lendvai B (2004) Distance-dependent scaling of calcium transients evoked by backpropagating spikes and synaptic activity in dendrites of hippocampal interneurons. J Neurosci 24: 661–70

Scharfman HE (1991) Dentate hilar cells with dendrites in the molecular layer have lower thresholds for synaptic activation by perforant path than granule cells. J Neurosci 11: 1660–73

Scharfman HE (1994) Evidence from simultaneous intracellular recordings in rat hippocampal slices that area CA3 pyramidal cells innervate dentate hilar mossy cells. J Neurophysiol 72: 2167–80

Scharfman HE (1995) Electrophysiological diversity of pyramidal-shaped neurons at the granule cell layer/hilus border of the rat dentate gyrus recorded in vitro. Hippocampus 5: 287–305

Scharfman HE (2007) The CA3 "backprojection" to the dentate gyrus. Prog Brain Res 163: 627–37

Schmidt-Hieber C, Jonas P, Bischofberger J (2007) Subthreshold dendritic signal processing and coincidence detection in dentate gyrus granule cells. J Neurosci 27: 8430–41

Seress L, Pokorny J (1981) Structure of the granular layer of the rat dentate gyrus. A light microscopic and Golgi study. J Anat 133: 181–95

Sík A, Penttonen M, Buzsáki G (1997) Interneurons in the hippocampal dentate gyrus: an in vivo intracellular study. Eur J Neurosci 9: 573–88

Sík A, Penttonen M, Ylinen A, Buzsáki G (1995) Hippocampal CA1 interneurons: an in vivo intracellular labeling study. J Neurosci 15: 6651–65

Sík A, Tamamaki N, Freund TF (1993) Complete axon arborization of a single CA3 pyramidal cell in the rat hippocampus, and its relationship with postsynaptic parvalbumin-containing interneurons. Eur J Neurosci 5: 1719–28

Sík A, Ylinen A, Penttonen M, Buzsáki G (1994) Inhibitory CA1–CA3-hilar region feedback in the hippocampus. Science. 265: 1722–4

Sloviter RS, Zappone CA, Harvey BD, Bumanglag AV, Bender RA, Frotscher M (2003) "Dormant basket cell" hypothesis revisited: Relative vulnerabilities of dentate gyrus mossy cells and inhibitory interneurons after hippocampal status epilepticus in the rat. J Comp Neurol 459: 44–76

Soltesz I, Bourassa J, Deschênes M (1993) The behavior of mossy cells of the rat dentate gyrus during theta oscillations in vivo. Neuroscience 57: 555–64

Somogyi J, Baude A, Omori Y, Shimizu H, El Mestikawy S, Fukaya M, Shigemoto R, Watanabe M, Somogyi P (2004) GABAergic basket cells expressing cholecystokinin contain vesicular glutamate transporter type 3 (VGLUT3) in their synaptic terminals in hippocampus and isocortex of the rat. Eur J Neurosci 19: 552–69

Somogyi P, Klausberger T (2005) Defined types of cortical interneurone structure space and spike timing in the hippocampus. J Physiol 562: 9–26

Somogyi P, Nunzi MG, Gorio A, Smith AD (1983) A new type of specific interneuron in the monkey hippocampus forming synapses exclusively with the axon initial segments of pyramidal cells. Brain Res 259: 137–42

Stafford MM, Brown MN, Mishra P, Stanwood GD, Mathews GC (2009) Glutamate spillover augments GABA synthesis and release from axodendritic synapses in rat hippocampus. Hippocampus 2009 Mar 31. (Articles online in advance of print)

Szabadics J, Tamás G, Soltesz I (2007) Different transmitter transients underlie presynaptic cell type specificity of $GABA_{A,slow}$ and $GABA_{A,fast}$. Proc Natl Acad Sci USA 104: 14831–6

Tamamaki N, Abe K, Nojyo Y (1988) Three-dimensional analysis of the whole axonal arbors originating from single CA2 pyramidal neurons in the rat hippocampus with the aid of a computer graphic technique. Brain Res 452: 255–72

Tamás G, Lorincz A, Simon A, Szabadics J (2003) Identified sources and targets of slow inhibition in the neocortex. Science 299: 1902–5

Thurbon D, Field A, Redman S (1994) Electrotonic profiles of interneurons in stratum pyramidale of the CA1 region of rat hippocampus. J Neurophysiol 71: 1948–58

Tóth K, McBain CJ. (1998) Afferent-specific innervation of two distinct AMPA receptor subtypes on single hippocampal interneurons. Nat Neurosci 1: 572–8

Traub RD, Jefferys JG, Miles R, Whittington MA, Tóth K (1994) A branching dendritic model of a rodent CA3 pyramidal neurone. J Physiol 481: 79–95

Turner DA, Li XG, Pyapali GK, Ylinen A, Buzsáki G (1995) Morphometric and electrical properties of reconstructed hippocampal CA3 neurons recorded in vivo. J Comp Neurol 356: 580–94

Vida I, Frotscher M (2000) A hippocampal interneuron associated with the mossy fiber system. Proc Natl Acad Sci USA 97: 1275–80

Vida I, Halasy K, Szinyei C, Somogyi P, Buhl EH (1998) Unitary IPSPs evoked by interneurons at the stratum radiatum-stratum lacunosum-moleculare border in the CA1 area of the rat hippocampus in vitro. J Physiol 506: 755–73

Vogt KE, Nicoll RA (1999) Glutamate and gamma-aminobutyric acid mediate a heterosynaptic depression at mossy fiber synapses in the hippocampus. Proc Natl Acad Sci USA 96: 1118–22

Vuksic M, Del Turco D, Bas Orth C, Burbach GJ, Feng G, Müller CM, Schwarzacher SW, Deller T (2008) 3D-reconstruction and functional properties of GFP-positive and GFP-negative granule cells in the fascia dentata of the Thy1-GFP mouse. Hippocampus 18: 364–75

Physiological Properties of Hippocampal Neurons

Marco Martina

Overview

Neurons are the basic computational units of the nervous system. Information processing in the brain is critically dependent on the electrophysiological properties of individual neurons, which are determined by the presence and distribution of many functionally and pharmacologically different ion channels. The parameters that define the functional roles of individual neurons can be grouped into two major groups: on the one side are cellular morphology and topology, which dictate the connectivity of each neuron; on the other side are the different electrophysiological properties of each cell type, which are defined by the combined effects of neuronal active and passive properties and shape the integrative function of each individual cell. The type and timing of neuronal responses to synaptic inputs depend on the firing pattern of each neuron, which in turn is set by the interplay of intrinsic and synaptic electrophysiological properties. In recent years it has also become clear that within each individual neuron the electrophysiological properties are not homogeneous but vary in the various cellular compartments. In particular, it has been shown that dendrites, far from being simple cellular antennas that passively conduct synaptic inputs toward the soma and the axon, are very active structures capable of actively boosting synaptic inputs and, at least in some neurons, of generating action potentials that effectively propagate to the soma (Llinás and Sugimori, 1980; Stuart and Sakmann, 1994; Häusser et al., 1995; Spruston et al., 1995; Martina et al., 2000). Thus, the different voltage-gated ion channels expressed by each neuron and in each cellular compartment within individual neurons play a fundamental role in shaping the electrical response of individual neurons to synaptic stimulation and ultimately in dictating the role of each neuron within the hippocampal network. This chapter will focus on the properties and distribution of voltage-gated ion channels in some of the major neuronal types in the hippocampus and dentate gyrus.

M. Martina (✉)
Department of Physiology, Northwestern University Feinberg School of Medicine, Chicago, IL 60611, USA
e-mail: m-martina@northwestern.edu

V. Cutsuridis et al. (eds.), *Hippocampal Microcircuits*, Springer Series in Computational Neuroscience 5, DOI 10.1007/978-1-4419-0996-1_3,

The Data

Comprehensive models describing the function of any brain area must take account of the large differences in the electrophysiological features of individual neuronal types. Such differences mainly result from the properties of the ion channels expressed by each individual cell type. This chapter provides a brief review of the characteristics and distribution of voltage-gated ion channels in some of the main hippocampal cell types. The hippocampal formation contains two major classes of glutamatergic projection neurons (pyramidal neurons of the hippocampus and granule cells of the dentate gyrus) and many different types of GABAergic interneurons (Freund and Buzsáki, 1996; Parra et al., 1998; see also chapter "Connectivity of the Hippocampus" of this book). Hippocampal pyramidal neurons are among the most extensively studied neurons in the entire brain. Electrophysiologically, they can be grouped into two major groups, CA1 and CA3, although recent data suggest that pyramidal neurons in the subiculum may constitute a class with different electrical properties (Jung et al., 2001).

CA1 Pyramidal Neurons

The recorded resting membrane potential of CA1 pyramidal neurons varies in different preparations from −64 mV (recorded in perforated patch configuration at 32°C, Spruston and Johnston, 1992) to −84 mV, inferred from the reversal potential of voltage-gated potassium currents recorded in cell-attached configuration at 34°C (Fricker et al., 1999). These cells have typically low input resistance (27 $k\Omega \cdot cm^2$, measured in whole-cell configuration at room temperature, Taverna et al., 2005). The background conductance of CA1 pyramidal neurons is mainly mediated by inward rectifier potassium currents (Takigawa and Alzheimer, 2002), voltage-insensitive KCNK potassium currents (largely TASK3 Taverna et al., 2005), and Ih (Maccaferri et al., 1993). The voltage response of CA1 pyramidal neurons is characterized by the presence of voltage sag upon injection of hyperpolarizing current and by action potential frequency accommodation upon injection of depolarizing current. About 15% of the neurons show intrinsic bursting (defined as a ratio of <0.1 between the shortest interspike interval and the mean interspike interval; Metz et al., 2005). Spike accommodation mostly depends on the properties of the voltage-gated sodium and potassium currents expressed in these cells. Action potentials are normally initiated close to the soma and backpropagate into dendrites in an activity-dependent manner so that while action potentials early in a train propagate reliably, those occurring later may fail to actively invade the distal dendrites (Spruston et al., 1995). Sodium currents of CA1 pyramidal neurons recover from inactivation with a biexponential time course (Martina and Jonas, 1997); interestingly, longer lasting depolarizations increase both the relative contribution of the slow component and its time constant (see below). Thus, during a long depolarization, sodium channels undergo cumulative inactivation, which prevents sustained

fast firing. Additionally, sustained high-frequency firing is also hindered because most of the voltage-gated potassium current of these neurons inactivate rapidly (see below) and therefore prolonged depolarizations inactivate the potassium current and interfere with action potential repolarization.

Sodium currents. Voltage-gated sodium currents are expressed in all three functional compartments (soma, axon, dendrites, see Table 1) of pyramidal neurons. The current density appears relatively uniform in the different compartments (Colbert and Pan, 2002; Magee and Johnston, 1995a, Fig. 1), although enrichment in the axon initial segment is also compatible with the experimental data (Colbert and Pan, 2002) and would mirror observations in CA3 pyramidal neurons, where sodium channel density peaks in the axon at $\sim$50 μM from the soma (see below). The density of sodium current in CA1 pyramidal cell nucleated patches is $\sim$5 mS cm^{-2} (M. Martina, unpublished observations).

Table 1 Sodium channels of CA1 pyramidal neurons

	Soma	Dendrites	Axon
Current type	Fast/persistent (Yue et al., 2005)	Fast (Magee and Johnston, 1995)	Fast (Colbert and Pan, 2002)
Current density	+ (Magee and Johnston, 1995)	+ (Magee and Johnston, 1995)	++
Channel subunit	Nav1.1, Nav1.2 (Gong et al., 1999), Nav1.3 RNA before p30 (Felts et al., 1997)	Nav1.1, Nav1.2 (Gong et al., 1999)	Nav1.1, Nav1.2 (Gong et al., 1999)

The properties of the sodium current slightly differ between soma and dendrites. In particular, dendritic channels appear to undergo stronger cumulative inactivation during repetitive firing (Jung et al., 1997) and to have slower recovery from inactivation compared to somatic channels (Colbert et al., 1997). Recovery from inactivation in pyramidal neurons is described by a double exponential process, with the fast and slow components having time constant of $\sim$2 and $\sim$150 ms and contributing 85% and 15%, respectively, for a 30 ms-long test pulse; for 300 ms-long pulses, the values of the time constants are similar (2.6 and 351 ms, respectively), but the contribution of the slow component increases to 24% (all data were obtained at $-$120 mV holding potential and 22–24°C, Martina and Jonas, 1997). Abundant expression of two sodium channel subunits (Nav 1.1 and 1.2) has been detected in the hippocampus; type 1 channels appear to account for most of the somatodendritic staining, while type 2 staining is concentrated in the axons (Gong et al., 1999). In hippocampal pyramidal neurons, action potentials are normally initiated in the axon initial segment (Colbert and Johnston, 1996) Colbert and Pan (2002) showed that initiation at this site is probably favored by a more negative activation range of voltage-gated sodium current (sodium channel activation is shifted by $\sim$7 mV in the hyperpolarizing direction). Modulation of Na^+ channel activation is also detected in dendritic channels. Sodium channels in distal dendritic segments have more negative activation range than in proximal dendrites. The midpoint of the activation

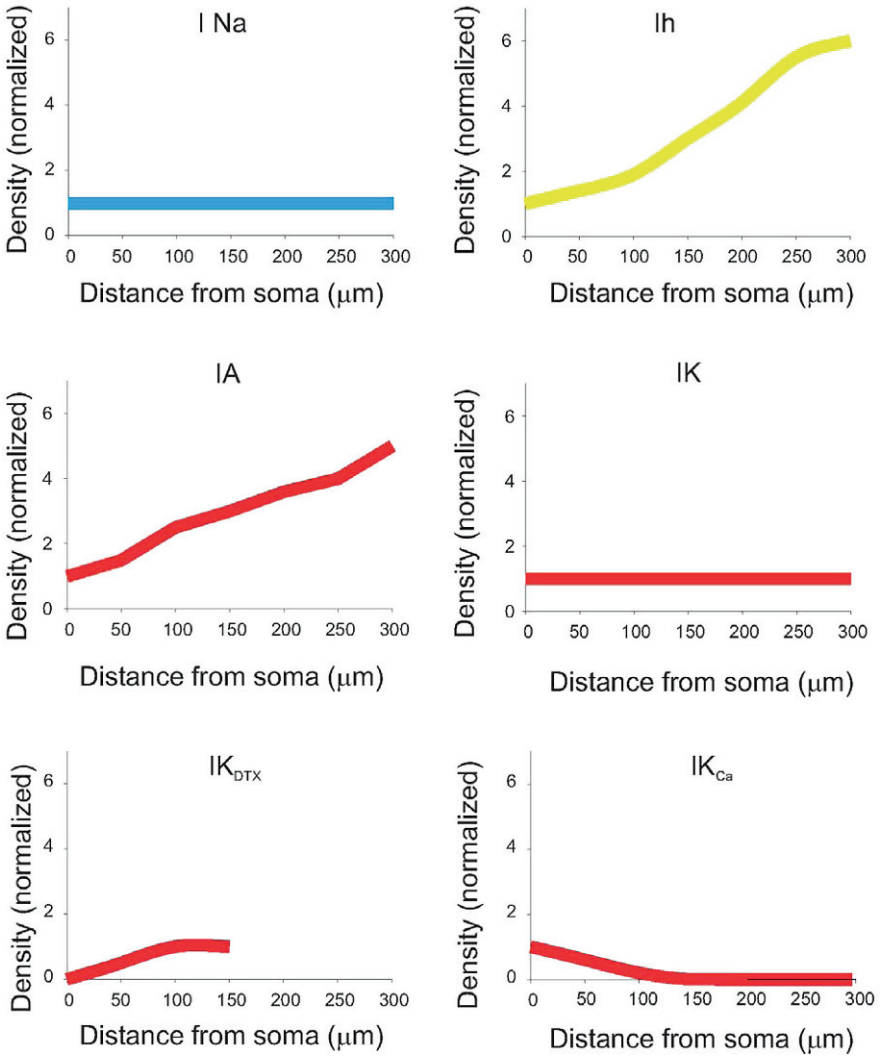

Fig. 1 Ion current density along the somatodendritic axis of CA1 pyramidal neurons. The density of each current type was normalized to its own density at the soma (except for IK_{DTX} in which it was normalized to the value in proximal dendrites). Therefore the figure only depicts the trend for each individual current, and no comparison is possible between the absolute values of the different currents

curve is ∼−12 mV for distal dendritic channels and ∼−20 mV for proximal channels (Gasparini and Magee, 2002) and this difference appears as the result of phosphorylation-dependent modulation since it is reproduced by staurosporine, a non-selective kinase inhibitor (Gasparini and Magee, 2002). Yet, in spite of the more negative activation range of sodium channels, dendritic action potential initiation is not common and requires highly synchronized (within 3 ms) activation of ∼50

synaptic inputs spread over 100 μm of the apical trunk/tuft (Gasparini et al., 2004). Moreover, the voltage threshold for dendritic action potential initiation is more positive than the somatic one (−48 ± 1 mV in the dendrites vs. –56 ± 1 mV at the soma, Gasparini et al., 2004). This apparent contradiction may be explained by the higher density of A-type potassium current in distal dendrites (Hoffman et al., 1997; Gasparini et al., 2004).

Voltage-gated potassium channels. CA1 pyramidal neurons express multiple types of voltage-gated K^+ channels (Storm, 1990; Hoffman et al., 1997; Martina et al., 1998, Table 2). Three main components can be identified on the basis of functional and molecular analysis: an A-type current (see Table 6 for the A-type current properties), most likely mediated by Kv4 channels, which contributes ∼60% of the total somatic current; a slow delayed rectifier (ID), likely attributable to Kv1

Table 2 Voltage-gated potassium channels of CA1 pyramidal neurons

	Soma	Dendrites	Axon
Current type	Potassium A-type (Storm, 1990; Martina et al., 1998)	Potassium A-type (Hoffman et al., 1997)	Potassium A-type
Current density	+	+ + +	++
Channel subunit	Kv4.2 (++), Kv4.3(++)	Kv4.2, Kv4.3	Kv1.4 (?)
Current type	Potassium fast delayed rectifier (IK)	Potassium fast delayed rectifier (IK)	Potassium fast delayed rectifier (IK)
Current density	+ (Hoffman et al., 1997)	+ (Hoffman et al., 1997)	
Channel subunit	Kv3.1, 3.2	Kv3.1, 3.2	
Current type	Potassium slow rectifier (ID)	Potassium slow rectifier (ID)	Potassium slow rectifier (ID)
Current density	+− (Martina et al., 1998)	+ (Chen and Johnston, 2004; Metz et al., 2007)	
Channel subunit	Kv1.1 (+, Wang et al., 1994, Martina et al., 1998), 1.2; Kv2.1, 2.2 (Maletic-Savatic et al., 1995; Martina et al., 1998)	Kv1.3(Metz et al., 2007); Kv1.5 (Maletic-Savatic et al., 1995); Kv2.1 (Maletic-Savatic et al., 1995; Du et al. 2000; Misonou et al., 2006)	Kv1.1; 1.2 (Wang et al. 1994)
Current type	Potassium slow rectifier (ID)	Potassium slow rectifier (ID)	Potassium slow rectifier (ID)
Ik Ca	+++	+ (Johnston et al., 2000); but not Slo1 (Misonou et al., 2006)	
M-current(KCNQ)	++ (Hu et al., 2007)	– (Chen and Johnston, 2004)	+ (Vervaeke et al., 2006)
Subunits	KCNQ2; KCNQ5 (Shah et al., 2002)	KCNQ2; KCNQ5 (Shah et al., 2002)	KCNQ2 (Devaux et al., 2004)

and Kv2 subunits, which contributes ∼27% of the total somatic current; and a fast delayed rectifier (IK) mediated by Kv3 channels that contributes ∼12% of the somatic current (Martina et al., 1998). The relative contribution of these components is different between the somatic and dendritic compartments (see Fig. 1). While the non-inactivating voltage-dependent currents (most likely mediated by Kv2 and Kv3 channels) show relatively constant density in the somatodendritic compartment, A-type current (mediated by Kv4 subunits Martina et al., 1998; Hoffman and Johnston, 1998; 2005 Kim et al., 2005) progressively increases with distance from the soma (up to fivefold, Hoffman et al., 1997). The A-type potassium current typically activates at relatively hyperpolarized membrane potentials (starting ∼−45 mV, Martina et al., 1998). Interestingly, A-type current of pyramidal neurons is highly sensitive to metabolic modulation (Hoffman and Johnston, 1998). Such modulation could play an important role in regulating synaptic plasticity, as shown by the change in the threshold for induction of long-term potentiation measured in response to pharmacological blockade of this current (Ramakers and Storm, 2002). Expression of dendrotoxin-sensitive (Kv1-mediated) potassium currents is spatially segregated in pyramidal neurons. This current is not expressed in the soma, but is expressed in proximal dendrites (Fig. 2) where it contributes to the active regulation of the action potential afterdepolarization and therefore of burst firing (Metz et al., 2007).

Calcium-dependent potassium channels. Depolarizations produced in CA1 pyramidal neurons by iontophoretically applied glutamate are followed by hyperpolarizations which are mediated by calcium-dependent potassium channels (Nicoll and Alger, 1981). Calcium-dependent, charybdotoxin-sensitive potassium channels appear to be unevenly distributed along the somatodendritic axis of CA1 neurons, with channel density decreasing with distance from the soma (Poolos and Johnston, 1999) so that the current mediated by these channels is almost completely absent at ∼150 μm from the soma (Johnston et al., 2000, see Fig. 1). This is in stark contrast to the A-type current density, which strongly increases along the dendrites, but also to the non-inactivating currents mediated by voltage-gated channels (most likely by Kv3 and Kv2 subunits), which are expressed at constant density throughout the somatodendritic compartment (Hoffman et al., 1997).

The data presented so far suggest that several different potassium channel subunits are expressed by CA1 pyramidal neurons. Indeed, in situ hybridization, immunostaining, and single-cell RT-PCR show that CA1 pyramidal neurons express many different potassium channel subunits, including Kv1.1, 1.2, 1.4, 1.5 (Maletic-Savatic, 1995; Martina et al., 1998); Kv2.1, 2.2 and Kv3.1, 3.2, 3.3 (Martina et al., 1998; Du et al., 2000); Kv4.2, 4.3 (Serôdio and Rudy, 1998; Martina et al., 1998; Rhodes et al., 2004). It is interesting that although expression of dendrotoxin-sensitive Kv1 subunits is detected in these cells, no effect of dendrotoxin, a Kv1-selective toxin (Grissmer et al., 1994), is detected on potassium currents either in nucleated patches from CA1 pyramidal neurons (Martina et al., 1998) or in focal somatic application of the toxin (Metz et al., 2007). This is consistent with reports showing that Kv1 channels are mainly expressed in presynaptic structures (Monaghan et al., 2001; Sheng et al., 1994). Whole-cell recordings, however, showed an effect of dendrotoxin on action potential initiation (Golding et al., 1999),

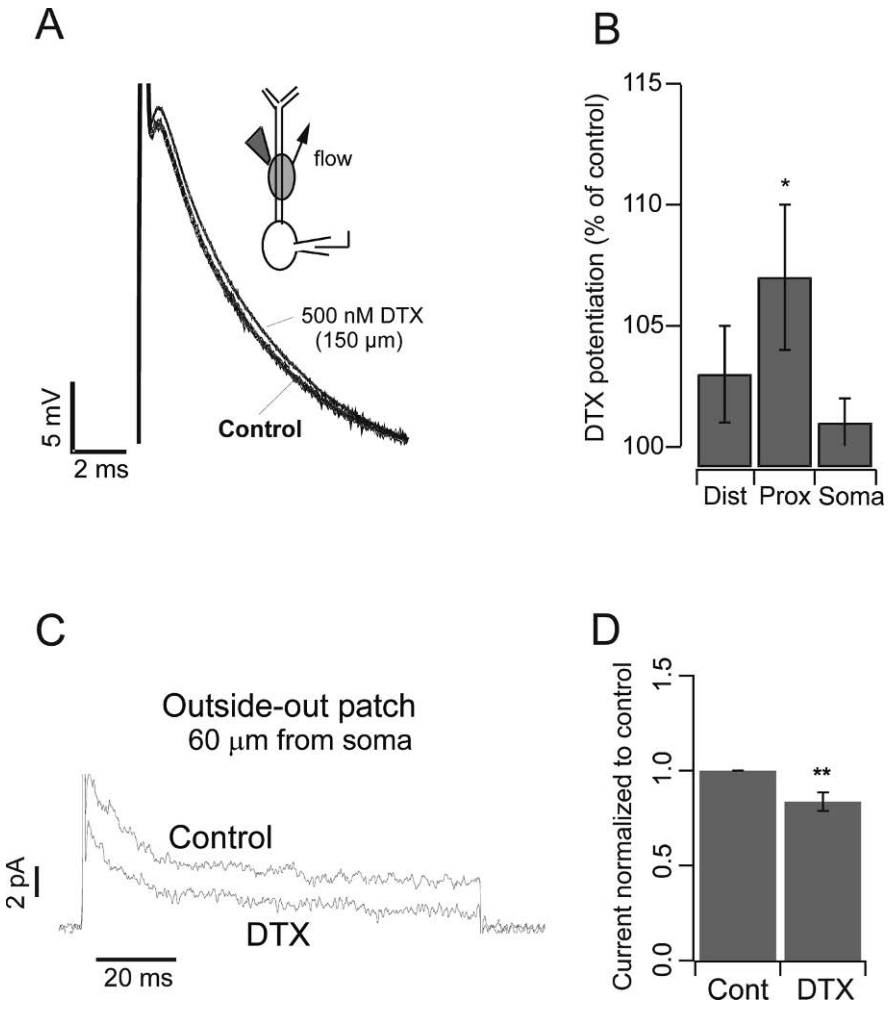

Fig. 2 Dendrotoxin-sensitive currents in dendrites of CA1 pyramidal neurons. **A**, Current clamp recording of a somatic afterdepolarization (ADP) recorded in control conditions (*thick line*) and in the presence of focal dendritic application of dendrotoxin (DTX, *thin line*). The ADP is increased by DTX. **B**, Bar chart summarizing the effects of DTX locally applied to the soma, proximal, and distal apical dendrites on the somatic ADP. **C**, Voltage-clamp outside-out dendritic recordings confirm the presence of DTX-sensitive currents in proximal apical dendrites. **D**, Bar chart summarizing the blocking effect of DTX on dendritic potassium currents (Figure modified from Metz et al., 2007.)

further suggesting axonal localization of these channels. Finally, dendritic recordings and focal drug application showed that dendrotoxin-sensitive channels are also expressed in apical dendrites, where they modulate the size of the afterdepolarization that underlies burst firing (Metz et al., 2007). These data nicely match those obtained by histological analysis that shows expression of Kv1 subunits in the

dendritic arbor of CA1 pyramidal neurons (Park et al., 2001). Thus, Kv1 subunit expression appears to be selectively absent from the soma, while present in both the axon and dendrites of CA1 pyramidal neurons.

M-current. This potassium current is mediated by members of the KCNQ family (Wang et al., 1998; Schroeder et al., 2000). M-current is expressed at very low density in the dendritic compartment of CA1 pyramidal neurons (Chen and Johnston, 2004). However, expression of KCNQ2 and KCNQ3 subunits is high in CA1 pyramidal neurons (Saganich et al., 2001), and M-type current in these neurons effectively controls burst generation (Yue and Yaari, 2004). In keeping with these observations Hu et al. (2007) have shown that M-current in CA1 pyramidal neurons is mainly localized in the perisomatic area. It has been proposed that the interaction between M-current and persistent sodium current mediates a form of theta resonance (M-resonance) in hippocampal CA1 pyramidal neurons (Hu et al., 2002).

Voltage-gated calcium channels. Both low- and high-voltage-activated calcium currents have been described in CA1 pyramidal neurons (Table 3). Calcium channels are primarily located at the soma, and their density decreases along the dendrites (Christie et al., 1995), although they are present in dendrites and in dendritic spines (Mills et al., 1994).

The high-voltage-activated current is itself mediated by multiple components. An ω-agatoxin IVA-sensitive (P-type) current contributes about 26% of the somatic high-threshold current (Mintz et al., 1992). N-type channels have also been described in the soma as well as dendrites and spines (Mills et al., 1994) although somatic expression appears more prominent. Nevertheless postsynaptic N-type current has been shown to play an important role in modulation of synaptic strength (Normann et al., 2000). CA1 pyramidal neurons also express large blocker-resistant high-voltage calcium current (R-type). In acutely dissociated cells this component (defined as the fraction of calcium current available from a holding potential of –50 mV in the presence of the combined application of ω-CgTx GVIA, ω-CgTx MVIIC, ω-AgaTx IVa, and nifedipine) contributes ∼40% of the high-voltage-activated current (Sochivko et al., 2003). Interestingly, a large fraction of the tail current activated by an action potential in nucleated patches is attributable to the R-type (Metz et al., 2005). This current appears to play an important role in the regulation of the afterdepolarization that drives burst firing in CA1 pyramidal neurons. In particular, the calcium influx mediated by this tail current appears to downregulate Kv7 potassium channels, which, if fully available, strongly attenuate the ADP (Chen and Yaari, 2008). R-type currents are present also in dendrites and dendritic spines, where, together with T-type, they are believed to provide about 50% of the calcium currents evoked by backpropagated action potentials (Hoogland and Saggau, 2004). The R-component in CA1 pyramidal neurons is partly mediated by α1E subunits (Sochivko et al., 2002), although other subunits also contribute as demonstrated by the fact that a current with the functional properties of the R-current is still present in α1E knockout mice (Wilson et al., 2000).

The classical dihydropyridine-sensitive L-type current is also present in the soma as well as in the dendrites of pyramidal neurons (Takahashi et al., 1989; Magee and Johnston, 1995; Hoogland and Saggau, 2004). A dihydropyridine-sensitive channel

Table 3 Voltage-gated calcium channels of CA1 pyramidal neurons

	Soma	Dendrites	Axon
T-type			
Density	++ (Magee and Johnston, 1995)	+ (Magee and Johnston, 1995)	
Subunits	Cav3.1; 3.2; 3.3 (McKay et al., 2006)	Cav 3.2; 3.3 (McKay et al., 2006)	Cav3.3 (McKay et al., 2006)
L-type			
Density	++ (Magee and Johnston, 1995)	++(Magee and Johnston, 1995)	
Subunits	Cav1.2(Tippens et al., 2008) +++ + (Bowden et al., 2001)	Cav1.2(Tippens et al., 2008) ++ ++ (Bowden et al., 2001)	Cav1.2(Tippens et al., 2008) ++
Subunits	Cav1.3 (Veng and Browning, 2002) ++ + (Bowden et al., 2001)	Cav1.3 (Veng and Browning, 2002) ++ ++ (Bowden et al., 2001)	Cav1.3(Veng and Browning, 2002) +−
N-type	++ (Christie et al., 1995) but NOT Cav2.2 (Chung et al., 2000)	+−(Christie et al., 1995)	
Density	++ (Magee and Johnston, 1995)	+ (Mills et al., 1994) (ω-CgTx-sensitive); − (Magee and Johnston, 1995)	
P/Q-type Density	+ (Christie et al., 1995) + (Hillman et al., 1991) ++ (Stea et al., 1994)	+− (Christie et al., 1995) + (Hillman et al., 1991)	
Subunits	Cav2.1 (Day et al., 1996) but NOT Cav2.2 (Chung et al., 2000)	+ Dendritic shaft Bloodgood and Sabatini (2007)	
T-type (CaV2.3)	+ (Metz et al., 2005) + (Wilson et al., 2000) + (Sochivko et al., 2002)	+ Dendritic spines Bloodgood and Sabatini (2007)	

appears to be open at membrane potential around resting and therefore contribute to the neuronal calcium homeostasis (Magee et al., 1996). This current is expressed in every neuronal compartment although its density appears particularly elevated in the proximal apical dendrites. Activation at negative membrane potential and sensitivity to dihydropyridine suggest that this current is mediated by the α1D subunit (Cav1.3, Xu and Lipscombe, 2001), which has been shown to be expressed throughout the somatodendritic compartment of CA1 pyramidal neurons (Veng and Browning, 2002).

Low-threshold T-type currents (in CA1 pyramidal cells these currents start activating at ∼−60 mV and reach full amplitude at ∼−20 mV; Takahashi et al., 1991) are also present in both the somatic and dendritic compartments and contribute to burst firing (Takahashi et al., 1989; Magee and Johnston, 1995; Magee and Carruth, 1999). Dendritic T-type currents are activated by subthreshold synaptic events and produce local increases in intracellular calcium, which may be important for the regulation of synaptic strength (Magee et al., 1995). It has been shown that a

selective potentiation of T-type current occurs in status epilepticus and can transform CA1 pyramidal neurons from regular firing to intrinsically low-threshold bursting cells (Su et al., 2002); it has also been proposed that the increase in T-type current density associated with status epilepticus is limited to, or more prominent, in the apical dendrites where these channels facilitate dendritic depolarization by back-propagating somatic spikes (Yaari et al., 2007).

Hyperpolarization-Activated Current (Ih)

The hyperpolarization-activated current is a depolarizing current (the reversal potential is $\sim -20\,\text{mV}$) activated by hyperpolarizations more negative than $\sim -60\,\text{mV}$ and was first described in CA1 pyramidal neurons by Maccaferri et al. (1993). This current is important for regulating firing activity as well as input resistance and its density sharply increases along the somatodendritic axis (Magee, 1998 Fig. 1, Table 4). It is worth stressing that such gradient in Ih density, although very prominent in CA1 pyramidal neurons as well as in layer 5 cortical pyramidal neurons (Stuart and Spruston, 1998), does not appear to constitute a general property of all pyramidal neurons. Bullis et al. (2007) recently described pyramidal-like principal (PLP) neurons, a novel class of hippocampal neurons with pyramidal morphology found in the stratum radiatum. Interestingly, in these neurons the Ih gradient is inverted, showing high somatic density that declines along the dendrites. This finding further supports the notion that, although general rules may regulate ion channel distribution among different neuronal classes, extrapolations should be avoided and a detailed study is required for each cell type.

Table 4 Ih of CA1 pyramidal neurons

	Soma	Dendrites
Ih	HCN	
Density	++ (Maccaferri et al., 1993)	++++ (Magee, 1998; Tsay et al., 2007)
Subunits	HCN1, HCN2	HCN1 (Tsay et al., 2007)

CA3 Pyramidal Neurons

The input resistance of CA3 pyramidal neurons is in the range 120–200 $\text{k}\Omega\,\text{cm}^2$ (Major et al., 1994). The *sodium currents* are functionally similar to those in CA1 pyramidal cells, although some differences were observed in the voltage-dependent inactivation (Steinhäuser et al., 1990). It was recently shown that in CA3 pyramidal neurons sodium channel density is maximal in the axon at 30–50 μm from the soma, which constitutes the location of first action potential generation (Meeks and Mennerick, 2007).

Similar to CA1 pyramidal neurons, the voltage-gated *potassium current* of CA3 pyramidal neurons can be classified into three main components: IA, ID, and IK. Of these, the fast activating ID and IA contribute to the repolarization of the action potential (Mitterdorfer and Bean, 2002).

A direct comparison of the potassium currents in CA1 and CA3 pyramidal neurons was performed by Klee et al. (1995). The only important difference found was a larger contribution of Ca-dependent current in CA3 cells (20% of total delayed rectifier vs. 10% in CA1). This finding fits well with the observed impact of SK channels on the frequency of intraburst action potentials in CA3 pyramidal neurons.

One potentially interesting difference is constituted by the fact that in CA3 pyramidal neurons part of the inactivating A-type current is highly 4-AP-sensitive (Bossu et al., 1996), which suggests that channels constituted either by Kv1 subunits associated to beta subunits (which confer rapid A-type inactivation to non-inactivating Kv1 channels; Rettig et al., 1994) or by Kv3.3/3.4 subunits contribute to this current. Relatively abundant expression of Kv3.3 transcript was actually reported in CA3 pyramidal layer (Weiser et al., 1994). A larger contribution of Kv3.3 subunits to the fast transient potassium current of CA3 neurons compared to the current of CA1 neurons (which is almost entirely mediated by Kv4 subunits, see above) may favor the generation of low-threshold bursts because of the more depolarized action potential values required to activate Kv3.3 channels compared to Kv4 (Baldwin et al., 1991; Fernandez et al., 2003). Another potential difference between the potassium current of CA3 and CA1 pyramidal neurons concerns the expression by CA3 cells, at least in organotypic cultures, of a current that is down-modulated by intracellular calcium and is involved in action potential repolarization as well as in the control of synaptic transmission (Saviane et al., 2003). In keeping with this observation, two of the potassium currents of CA3 pyramidal neurons, a voltage-gated current and a Ca-dependent current, are inhibited by activation of an ACPD-sensitive quisqualate receptor (Charpak et al., 1990), suggesting that the local metabolic state may have a large influence on the actual size of these currents and therefore on the input–output function of CA3 pyramidal neurons.

Similar to CA1, the *calcium current* in CA3 pyramidal neurons is the sum of multiple components (Mogul and Fox, 1991). Overall the currents are similar to those of CA1 pyramidal neurons (Thompson adn Wong, 1991). P-type contribution to the high-threshold currents, however, is smaller in CA3 neurons than in their CA1 counterparts (14% vs. 26% Mintz et al., 1992); a detailed analysis (Avery and Johnston, 1996) showed that the main difference between the currents of the two cell types is that in CA3 pyramidal neurons the low-voltage-activated current actually comprises two different components, one inactivating and nickel sensitive (typical T-type) and another sustained and partly dihydropyridine sensitive (L-type, see Xu and Lipscombe, 2001). The presence of multiple types of low-voltage-activated calcium channels may contribute to the intrinsic firing of CA3 neurons.

Dentate Gyrus Granule Neurons

Granule cells are glutamatergic projection neurons conveying information from the dentate gyrus to the CA3 area of the hippocampus. From an electrophysiological perspective these neurons are particularly interesting among central glutamatergic neurons because the large size of their axonal terminals allow patch clamp characterization of the ion channels in the boutons (Geiger and Jonas, 2000, Bischofberger et al., 2002; Engel and Jonas, 2005), thus providing a rare opportunity to compare the properties and density of ion channels in the soma and the axon terminal of an individual neuron. Granule cells have particularly negative membrane potentials (−75 mV at physiologic temperature, Lübke et al., 1998) and relative low input resistance (38 $k\Omega \cdot cm^2$, Schmidt-Hieber et al., 2007), which suggests abundant expression of background potassium channels.

Sodium current. The density of sodium current in granule cells was determined in acutely dissociated rat neurons (Ellerkmann et al., 2003); thus, these measurements offer an estimate of the density in the somatic compartment. These authors found a density of ∼33 $mS\,cm^{-2}$ (extrapolated from the reported 1,400 $pA\,pF^{-1}$, assuming a reversal potential of 30 mV, see Fig. 1 in their paper, and a specific capacitance of 0.9 $\mu F\,cm^{-2}$ (Gentet et al., 2000)), similar to that in the soma and dendrites of OLM interneurons. These authors also studied the expression profile of the different voltage-gated sodium channel subunits and found co-expression of several subunits in these neurons: in particular they demonstrated expression of Nav 1.2, 1.3, 1.5, 1.6. The current activation is strongly voltage-dependent (the slope is 5.2 mV/e-fold, Table 5); similar strong voltage dependence characterizes the fast inactivation process of the current, which is half inactivated at −48 mV and has a slope of −5.8 mV. The recovery from fast inactivation is best fit by the sum of two exponential functions: a fast component with time constant (at −80 mV) of 6.8 ms (and relative amplitude ∼90%) and a smaller slow component with time constant of 546 ms. The recovery from inactivation of somatic granule cell channels was also

Table 5 Gating properties of Na^+ channels in hippocampal neurons

	DG FS Soma (Martina and Jonas, 1997)	CA1 PC Soma (Martina and Jonas, 1997)	DGGC Soma (Ellerkmann et al., 2001, 2003)	DGGC Bouton (Engel and Jonas, 2005)
Act. $V_{1/2}$	−25.1	−23.9	−22.6 (Ellerkmann et al., 2001) −25.8 (Ellerkmann et al., 2003)	−38.4
Act slope (mv/e-fold)	11.5	11.8	5.8 (Ellerkmann et al., 2001); 5.2 (Ellerkmann et al., 2003)	8
Deact τ (−40 mV)	0.13 ms	0.2 ms		0.17 ms
Inact $V_{1/2}$	−58.3	−62.9	−56.8	−89.6
Inact slope	6.7	10.7	6.7	6.4

analyzed by Engel and Jonas (2005) in outside-out patches. Similarly to Ellerkmann et al. they found that the recovery from inactivation is best fit by a double exponential function with the fast component accounting for most of the current (relative amplitude 0.8). The time constants were, however, faster than in dissociated neurons ($\tau 1 = 4$ ms and $\tau 2$=65 ms), possibly suggesting that the recovery from inactivation is actively modulated through intracellular pathways which may be differently affected in whole-cell and excised patch recordings.

When long depolarizations are applied (10–300 s at −10 mV, at room temperature) the sodium current of dentate gyrus granule cells undergoes slow inactivation. The recovery from this inactivated state is described by a biexponential process, with fast and slow time constants ranging in 1–10 and 20–50 s, respectively (Ellerkmann et al., 2001). The importance of slow inactivation in physiologic processes remains to be explored; it is interesting, for instance, that status epilepticus deeply affects the properties of fast activation and fast inactivation of granule cells' sodium currents (half-maximal activation is shifted from −25.8 in control to −28.6 mV, and the fast inactivation half-point from −48.2 to −43.2 mV; these changes lead to a significant increase of the window current, resulting in higher neuronal excitability), but the slow inactivation appears to be unaffected (Ellerkmann et al., 2003).

The axon terminals of these neurons have been carefully studied. The gating properties of the sodium current in the mossy fiber boutons were compared to somatic component; the main difference was found in the inactivation kinetics that in the bouton is almost twofold faster than in somatic patches (Engel and Jonas, 2005). The current density in mossy fiber bouton is 49.0 mS cm^{-2} (range 9–138 mS cm^{-2}), which corresponds to an estimated channel density of 41 channels μm^{-2} in hippocampal MFBs. These density values are comparable to previous estimates in invertebrate axons (120 mS cm^{-2} in squid axons and 40 mS cm^{-2} in Myxicola axons; Hodgkin and Huxley, 1952; Goldman and Schauf, 1973). Thus, presynaptic mossy fiber terminals have axon-like properties, expressing voltage-gated Na^+ channels at very high density. Very recently, Schmidt-Hieber et al. (2008) have used dual axo-somatic recordings and computer modeling to obtain an estimate of the sodium current density in mossy fiber axons and found that axonal sodium current density of 100 mS cm^{-2} best fit the experimental data.

Potassium current. Similar to other neurons, the potassium current of granule cells is the sum of at least two components: IA (see Table 6 for the A-type current properties) and IK (Beck et al., 1992).

Contrary to pyramidal neurons, however, the fast inactivating component in granule cells is TEA sensitive and largely mediated by Kv3.4 channels (Riazanski et al., 2001). Interestingly, these authors showed that Kv3.4 expression in granule cells is spatially segregated, showing higher expression around the axon initial segment and lower expression in the somatic compartment more distal from the axon; these data suggest a role for these channels in controlling the generation of action potentials.

The heterogeneous nature of the potassium current in granule neurons is supported by the expression of multiple ion channel subunits including Kv1.1, 1.2, and 4.2 (Sheng et al., 1994; Tsaur et al., 1992), Kv4.3 (Serôdio et al., 1996); GIRK1

Table 6 Properties of inactivating voltage-gated K^+ current in hippocampal neurons

	DG FS (Martina et al., 1998)	CA1 pyramidal (Martina et al., 1998)	DG Granule (Beck et al., 1992; Riazanski et al., 2001)	MFB (Geiger et al., 2000)
Act $V_{1/2}$	−6.2	−3	−7.6 (Riazanski et al., 2001)	−26
Act slope (mV/e-fold)	5.75*	6.75*	10 (3)	5.2*
Inact $V_{1/2}$	−75.5	−77.3	−65.1 (Riazanski et al., 2001); −67 (Beck et al., 1992)	−72
Inact slope	8.5	7.4	6 (Riazanski et al., 2001); 6.3 (Beck et al., 1992)	9.6
TEA Block	No	No	Yes	Yes

* In the original papers by Martina et al. (1998) and Geiger and Jonas (2000) activation curves were fitted with a Boltzmann function raised to the fourth power. In order to allow direct comparison with data obtained fitting a simple Boltzmann component (Beck et al., 1992; Riazanski et al., 2001), the slope factors reported in the papers have been divided by 4 in this table.

and GIRK2 (Liao et al., 1996); Kv3.1 RNA expression was also detected in granule neurons, although at relatively low level (Weiser et al., 1995).

The current in the mossy fiber terminal is largely dendrotoxin-sensitive (Geiger and Jonas, 2000) in agreement with prominent expression of Kv1.2 subunits (Sheng et al., 1994). Additionally, strong expression of the Slo1 subunit (mediating the calcium-dependent large conductance potassium current, BK) has been recently demonstrated in mossy fiber boutons (Misonou et al., 2006).

Calcium Current

Voltage-gated calcium currents of granule neurons include both high- and low-voltage-activated currents (Blaxter et al., 1989; Fisher et al., 1990). About 40% of the current is blocked by dihydropyridines (and is therefore L-type), while P/Q-type and N-type current each account for about 20% of the total current (Eliot and Johnston, 1994). These data suggest that T- and R-type currents account for ∼23% of the total current. T-type current was described by Zhang et al. (1993) and contributes to the spike afterdepolarization (ADP). R-type current was estimated to contribute about half of the blocker-resistant current (Sochivko et al., 2002) and contributes to the induction of mossy fibers LTP (Dietrich et al. 2003).

Calcium currents have been carefully studied in the mossy fiber boutons (Li et al., 2007). These authors found that a single bouton contains ∼2,000 voltage-gated calcium channels. The largest current fraction (66%) is mediated by P/Q channels, while N- and R-type contribute 26% and 8% of the total current, respectively.

Dentate Gyrus Mossy Cells

Mossy cells represent the third population of glutamatergic neurons in the hippocampal formation. These large multipolar neurons of the fascia dentata (Frotscher et al., 1991; Lübke et al., 1998) are characterized by relatively slow maximum firing rate (50 Hz at 35–37°C, Lübke et al., 1998) and by the presence of a prominent membrane sag upon injection of hyperpolarizing currents. The resting membrane potential is between −60 and −62 mV at 30–37°C (Jinno et al., 2003; Lübke et al., 1998). The voltage-gated *sodium current* of mossy cells activates at potentials ≥ − 50 mV; fitting the conductance/voltage plot reveals half-activation at −31 mV(Howard et al., 2007).

The *potassium current* of these cells consist of at least three components: an A-type current, a delayed rectifier, and a third component, resistant to both 4-AP (2.5 mM) and TEA (25 mM), characterized by activation kinetics slower than the two other components (Howard et al., 2007). The kinetics and pharmacological properties strongly suggest that the A-type current is mediated by Kv4 subunits. More data are required in order to attribute the two other current components to expression of any individual channel subunit. An interesting difference in intrinsic electrophysiological properties has been reported between dorsal and ventral mossy cells. The majority of the ventral cells show intrinsic bursting, a phenotype that is never observed in dorsal mossy cells (Jinno et al., 2003). Interestingly, Ih expression is similar in bursting and non-bursting neurons; in keeping with these data, it was found that Ih in mossy cells starts activating around –65 mV, so that activation of this current is absent or minimal at resting membrane potential. Thus, in mossy cells Ih does not appear to play a role in intrinsic firing, similar to that observed in other neurons in different parts of the CNS (Atherton and Bevan, 2005; Russo et al., 2007). Bursting in these neurons appears to depend on a phenytoin-sensitive persistent sodium current that starts activating around −50 mV (Jinno et al., 2003).

Fast Spiking Interneurons

DG Basket Cells

Dentate gyrus basket cells are parvalbumin-positive fast spiking interneurons and can be considered prototypical perisomatic inhibitory interneurons (see chapter "Connectivity of the Hippocampus"). These cells can fire at extremely high frequency (>200 Hz) and have very low input resistance (10 kΩ*cm^2, Bartos et al., 2001).

Sodium currents of fast spiking interneurons (see Table 5) are characterized by their very rapid recovery from fast inactivation, which is described (at −120 mV and room temperature) by a single exponential process with a time constant of ∼2 ms. Another typical property of the sodium current of these neurons is the extremely fast deactivation (the time constant at –40 mV and ∼23°C is 0.13 ms; Martina and Jonas, 1997). These two kinetic properties constitute the main difference between the current of basket cells and that of CA1 pyramidal neurons. Whether these

differences are attributable to ion channel modulation or to expression of different subunits remains to be investigated. The sodium channel density at the soma is ~36 mS cm^{-2} and quickly declines along the dendrites with an estimated length constant of 25 μm in basal dendrites (Hu et al., 2009).

Potassium currents. Voltage-gated potassium currents of fast spiking DG interneurons (putative basket cells) were studied in detail using the nucleated patch technique and single-cell RT-PCR (Martina et al., 1998). Two aspects set the potassium current of these cells apart from that of pyramidal neurons or dentate gyrus granules: (1) the total current density is almost double than in CA1 pyramidal neurons (175 vs. 95 pS μm^{-2}) and (2) the current is, characterized by the almost complete absence of time-dependent inactivation. Functional and pharmacological dissection of the total voltage-gated current shows that, similar to the current of CA1 pyramidal cells, it is composed of three main components: a highly TEA- and 4AP-sensitive fast delayed rectifier (mediated by Kv3 subunits); a slow activating, slowly inactivating component (ID, probably mediated at least in part by Kv2 channels); and an A-type (fast activating and inactivating), TEA-resistant current (mediated by Kv4 subunits, Table 6). Contrary to pyramidal neurons, though, the A-type current only contributes ~17% of the total current, while the Kv3-like sustained current accounts for 58%. This sustained current appears ideally suited to allow effective repolarization of the fast action potential of these neurons due to extremely fast activation and deactivation kinetics (Fig. 3) and relatively positive activation potential (the activation midpoint is ~−7 mV). Contrary to the Na^+ current, the density of voltage-gated potassium current remains relatively constant in basket cell apical dendrites (length constant = 763 μm), while it decays faster in basal dendrites (length constant = 57 μm, Hu et al., 2009). Dendritic potassium channels shape the EPSP time course and allow coincidence detection in basket cell dendrites (Hu et al., 2009).

Calcium currents. Less is known about the calcium currents in basket cells; it has been recently shown that P/Q calcium channels mediate release at synapses of basket cells (Hefft and Jonas, 2005), but a comprehensive study of the calcium currents present in these cells is still missing.

It is also worth mentioning that basket cells also express connexin36, although the strength of the electrical coupling is low and appears to decline with development. In 14-day-old mice 92% of the cells tested are electrically coupled, although the coupling coefficient is low (0.029). In slices from 42-day-old mice, in contrast, only 30% of the cells are electrically coupled and the coupling coefficient is further reduced (0.012, Meyer et al., 2002).

Stratum oriens horizontal interneurons. Horizontal interneurons in the hippocampal CA1 area represent a relatively homogeneous population and are prototypical feedback interneurons (see chapter "Connectivity of the Hippocampus"). Many of these cells are somatostatin expressing OLM cells (Martina et al., 2000), which are capable of repetitive firing upon injection of depolarizing current although their maximum frequency does not reach frequencies as high as those of basket cells (Lien et al., 2003). These neurons are also functionally easily distinguishable from basket cells because they are often intrinsically firing due to presence of large Ih (Maccaferri and McBain, 1996). Ih expression also differentiates the response to

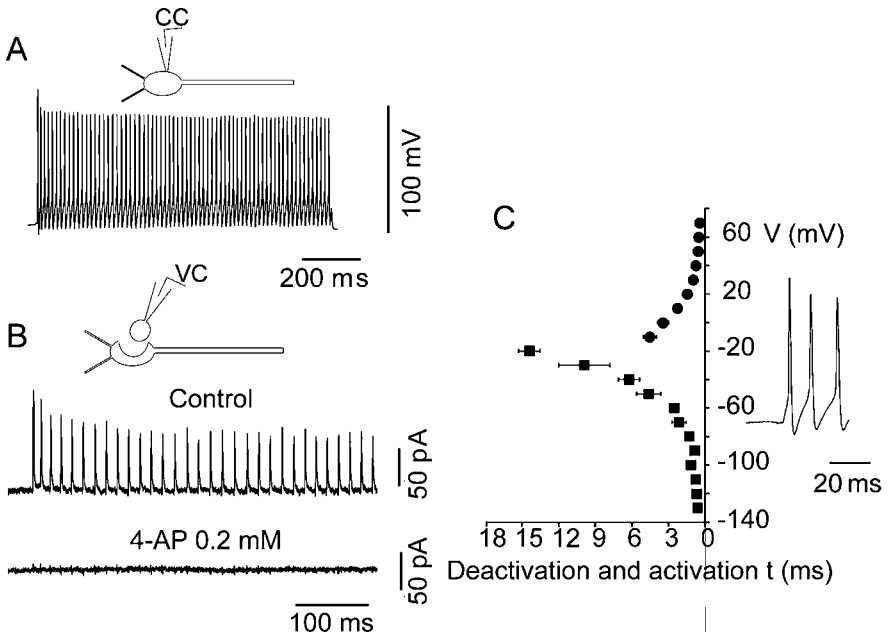

Fig. 3 Kv3 channels mediate action potential repolarization in fast spiking interneurons of the dentate gyrus. **A**, Current clamp recording of the firing response of a fast spiking interneuron to the injection of depolarizing current. **B**, The membrane potential waveform was then used as voltage stimulus to nucleated patches to study the potassium currents activated by each spike (recordings were performed after blockade of voltage-gated sodium and calcium currents). The potassium current elicited by the high-frequency action potentials was abolished by low concentration of 4-AP. **C**, Plotting the activation and deactivation time constants of the 4-AP-sensitive current vs. the voltage trajectory of the action potentials shows that asymptotic values of activation and deactivation time constants are reached at membrane potentials within the action potential range, allowing fast spike repolarization and minimum refractory period (Figure modified from Martina et al., 1998.)

hyperpolarizing current injection of these neurons from that of basket cells because the voltage response of OLM cells is characterized by a large voltage sag, which is absent in basket cells. Another interesting difference between OLM neurons and basket cells resides in the value of the input resistance, which in OLM cells is quite high ($48\,k\Omega{\cdot}cm^2$, Taverna et al., 2005), due to relatively low expression of background potassium channels (Taverna et al., 2005; Torborg et al., 2006).

Sodium currents of OLM neurons have properties similar to those of dentate gyrus basket cells; in particular the recovery from fast inactivation can be fit by a single exponential function (time constant 5 ms at -120 mV and 22–23°C, Martina et al., 2000). An interesting feature of these neurons is the capability of action potentials to undergo reliable and full-amplitude backpropagation into the dendrites. In addition, strong focal excitation may also lead to dendritic action potential initiation (Martina et al., 2000). Full-amplitude backpropagation is the consequence of high dendritic sodium current density ($\sim 25\,mS\,cm^{-2}$, calculated from data in Martina et al., 2000). Dendritic initiation may also be favored by a ~ 8 mV left shift in

voltage dependence of the activation curve (midpoint was −37.8 mV for somatic patches and −45.6 for dendritic patches). Dendritic sodium currents also contribute to boosting of excitatory synaptic inputs.

Potassium currents. Voltage-gated potassium currents are expressed at high and constant density throughout the somatodendritic compartment of OLM neurons (Martina et al., 2000). The current composition is very similar, both in functional and molecular terms, to that of dentate basket cells (Lien et al., 2002). The total current is the sum of three components: a fast delayed rectifier (57% of the total current, mediated by Kv3 channels), an A-type current (19% of the total current, mediated by Kv4 subunits), and a slow delayed rectifier (25% of the total). In these neurons the deactivation of the Kv3 component is slower than in basket cells, most likely because of the more important contribution of the Kv3.2 subunit (Lien et al., 2002). Interestingly, this deactivation velocity appears to be finely tuned to allow the maximum firing frequency in this particular cell type (Lien and Jonas, 2003). The potassium currents in OLM dendrites are very similar to the somatic ones with regard to both kinetics and sensitivity to block by broad-spectrum blockers such as TEA (Martina et al., 2000). It has also been suggested that a fraction of the TEA-sensitive current in the somatodendritic compartment of OLM cells appears to be mediated by KCNQ (M-current) channels. Although the size of this conductance is relatively small ($\sim$0.2 mS cm^{-2}, Lawrence et al., 2006), computer models suggests that this current may regulate the firing frequency of these neurons with minimal impact on the shape of the action potential (Lawrence et al., 2006).

Finally, little is known about voltage-gated *calcium channels* in these neurons. Poncer et al. (1997), however, showed that inhibitory potentials generated by interneurons in the CA3 stratum oriens are mediated by P/Q-type calcium channels.

Interneurons of the Stratum Radiatum-Lacunosum-Moleculare

Interneurons in this area can be classified into several classes. Vida et al. (1998) distinguished four classes: basket (BC), Schaffer associated (SA), perforant-path associated (PA) and neurogliaform (NC); most of these cells, however, can be classified as feedforward dendritic targeting interneurons. As it is the case in other brain areas, BC are characterized by lower input resistance (70 MΩ) and more negative resting membrane potential (−60 mV) than the other interneurons (−56 mV, 96 MΩ; −55 mV, 84 MΩ; and −58 mV, 75 MΩ for SA, PA, and NG, respectively). Although no comprehensive studies of the voltage-gated sodium currents in these cells are available, sensitivity to beta pompilidotoxin, a wasp toxin, shows that the sodium currents differ between radiatum and LM interneurons (Miyawaki et al., 2002), suggesting differential expression of individual subunits.

Contrary to basket cells of the stratum pyramidale and to OLM interneurons, which express Kv3.1b subunits at high level, interneurons in the stratum radiatum-lacunosum-moleculare only seldom express this subunit (21% vs. $\sim$90% of PV-positive basket cells; Sekirnjak et al., 1997). In agreement with this result, voltage-gated potassium currents of cultured interneurons of the stratum radiatum-lacunosum-moleculare exhibit slow activation kinetics. Although, similar to other

interneurons, the delayed rectifier current represents the sum of two components, one which is 4-AP sensitive and one which is not, the time to peak of the 4-AP-sensitive component was 4.2 ms at +45 mV (Chikwendu and McBain, 1996; by comparison, the 20–80% rise time of Kv3-like currents at 40 mV in basket cells was ∼1 ms, Martina et al., 1998). The 4-AP-insensitive component has much slower (and non voltage-dependent) activation (the time to peak at 30 mV was 46 ms, Chikwendu and McBain, 1996). It is likely that at least part of the 4-AP- and TEA-sensitive slow delayed rectifier is mediated by Kv1.1 channels, which are expressed in these cells (Rhodes et al., 1997).

Voltage-clamp recordings were performed to study calcium currents in visually identified interneurons in stratum radiatum, near the border with LM. When held at −80 mV, these cells exhibited a relatively small calcium current (0.4–1 nA in whole-cell configuration) that appeared to include at least three (L, N, and P/Q) calcium current components: the L-type component contributed ∼28% of the current, while the N-type current accounted for ∼23% of the total. The contribution of the P/Q component was more heterogeneous ranging from 0 to 30% (average ∼10%, Lambert and Wilson, 1996). It is possible that the different contributions of N-type current in different cells reflected different histological classes of interneurons; this hypothesis, however, still needs experimental confirmation.

Low-voltage-activated calcium currents were also described in interneurons acutely dissociated from CA1 lacunosum-moleculare (Fraser and MacVicar, 1991). The current size was quite small (the peak current, recorded at −30 mV, was 100 ± 7 pA, compared with ∼2 nA of TTX-sensitive sodium currents in the same neurons). This calcium current showed marked voltage-dependent inactivation, being half inactivated at −84 mV and totally inactivated at –60 mV. Less is known about dendritic calcium channels in these cells. Optical measurements, however, showed that action potential-associated calcium signals backpropagate into the dendrites of these neurons; indeed, backpropagated calcium signals progressively increase in size with distance from the soma (Rozsa et al., 2004). Whether this feature is the result of differential distribution of calcium channels or of other mechanisms (for instance a different basal calcium level) remains to be investigated. These data, however, suggest that, similar to OLM interneurons, action potentials actively backpropagate into the dendrites of CA1 SR interneurons.

Experimental Techniques

Although conventional intracellular (sharp electrode) recordings can still provide valuable information about the electrophysiological properties of neurons, most of the more recent literature (and of the data presented in this chapter) is based on patch clamp recordings. Some basic cellular properties appear quite different when compared using these two techniques. For example, resting membrane potential and input resistance measured with sharp electrodes and patch clamp techniques were directly compared in dentate gyrus basket cells (Staley et al., 1992) and the results obtained with the two techniques were quite different: with sharp-pipette

recordings the resting potential was −74 mV and the input resistance was 54 MΩ while the values obtained with patch clamp recordings were −85 mV and 228 MΩ, respectively. A potential explanation for these differences is that they are the consequence of a sub-optimal seal around the sharp electrodes that leads to some current leakage and that is not present in patch clamp recordings. Therefore, patch clamp data were preferentially used for this chapter, except when sharp electrode data were the only available. The patch clamp technique was pioneered in the late 1970s by Neher et al. (1978) and was originally developed to allow the measurement of the currents flowing through single ion channels in cellular membranes. Briefly, small tip (∼1 μM) pipettes are obtained by pulling glass capillaries, filled with saline and connected to a feedback amplifier. A tight electrical seal (in the GΩ range) is obtained between the pipette tip and the cellular membrane by applying gentle suction to the pipette. This leads to a firm attachment between the tip and the membrane, which allows several manipulations (Hamill et al., 1981) that offer invaluable tools for the study of many electrophysiological properties, varying from the cellular input resistance to the current flowing through single individual channels. The most commonly used configuration is the whole-cell configuration, in which, after obtaining the seal, continuity is obtained between the pipette and the cell interior by rupturing the cell membrane by applying brief negative pressure pulses. As a result, the pipette-cell assembly is well insulated from the bath solution. The intrapipette solution for these recordings is designed to reproduce the physiological intracellular solution (high potassium, low sodium). Whole-cell patch clamp recordings allow the accurate measurement of many basic functional properties such resting membrane potential, input resistance, action potential threshold, amplitude, and frequency. Moreover, the voltage-clamp configuration allows recording the total ionic current flowing through the entire cell at each moment. Thus, complex voltage protocols and pharmacological tools can be used to isolate the currents mediated by individual channel types.

Although extremely successful on small isolated cells, such as acutely dissociated and cultured neurons, whole-cell voltage-clamp recordings are problematic when obtained from intact neurons having complex morphologies and large axonal and dendritic trees, as is the case for most neurons in brain slices. In this case the quality of voltage clamp is dramatically limited (see Major, 1993 for a detailed discussion). Thus, data on current kinetics and voltage dependence are best obtained from excised patches, and outside-out patches in particular. This configuration is obtained by pulling the pipettes away from the cell after having achieved the whole-cell mode (Hamill et al., 1981). By doing so, the lipid membrane seals the pipette tip leaving the outer side of the cell membrane exposed to the bath, while the inner side is exposed to the intrapipette solution. This configuration allows ideal voltage control and quick solution exchange, but is not always suitable for the study of channels expressed at low density in the cell membrane because the currents are often very small. An interesting variation of this technique is the nucleated patch (Sather et al., 1992). Similar to the outside patch, the first step consists in achieving a whole-cell configuration. At this point a light suction is applied to the pipette, and the nucleus is attracted to the pipette tip. The pipette is then slowly withdrawn from

the cell to obtain an outside-out patch. Because of the presence of the nucleus, the membrane has to reseal around the nucleus itself and the result is an almost perfectly spherical outside patch comprising a large membrane area. Thus, the nucleated patch combines the possibility of precise identification of cells in a slice with the possibility to record macroscopic currents and to obtain in almost ideal voltage-clamp conditions (Martina and Jonas, 1997).

A potential pitfall common to intracellular and whole-cell patch clamp recordings is that these types of experiments lead to dialysis of the intracellular content. This fact has two main consequences: (1) it may lead to the disappearance of some currents or cell functions ("run down") due to the loss of diffusible factors into the recording pipette and (2) the intracellular ion concentrations are not the native ones but those imposed by the experimenter: this fact may become critical when examining the functional role of a conductance. A typical example is the $GABA_A$ channel, which is selective for anions and Cl^- ions in particular. Depending on the intracellular $[Cl^-]$ the $GABA_A$ conductance can be either hyperpolarizing or depolarizing. For this type of experiments, it is therefore critical to know the undisturbed cellular $[Cl^-]$. This can be obtained by establishing the electrical connection between the pipette and the cell interior not by rupturing the membrane but by inclusion in the pipette solution of a channel forming substance in the cell-attached mode (Horn and Marty, 1988). By using substances that form channels selectively permeant to cations, as gramicidin, it is possible to obtain whole-cell recordings that maintain intact the neuronal chloride gradient. The technique also prevents intracellular dialysis because of the small diameter of the pores (they are only permeant to monovalent cations).

The Future

Although the hippocampus is one of the most thoroughly studied brain areas, much work is still needed to obtain a comprehensive description of the physiological properties of hippocampal neurons. In particular, future work will have to address two important aspects: one concerns the large heterogeneity of hippocampal neurons, and interneurons in particular. Clearly, only a thorough study of each cell type will allow understanding of the fine tuning of hippocampal function; thus, detailed studies of the functional properties of anatomically identified neurons will be required for the many types of hippocampal neurons. At the same time, some technical aspects may also require further development. Patch clamp recordings have greatly improved our knowledge of the electrophysiological properties of neurons. This technique, however, is not devoid of weaknesses. Two limitations of the patch clamp technique are (1) the difficulty of obtaining data from small structures such as small dendrites, axons, and terminals, which results from the physical limitation in the size of the pipette tip as well as in the optical resolution necessary to distinguish such structures and (2) the fact that the sealing process and, even more, the formation of the whole-cell configuration may cause important changes

to the cellular cytoskeleton as well as to the composition of the intracellular milieu. Nowadays, increasing expectation is directed toward the development of low-toxic voltage-sensitive dyes, which may allow studying neuronal electrophysiology in intact cells. The signal-to-noise ratio of such dyes still represents a problem, but it is quickly improving (Baker et al., 2005). Particularly interesting is a recently developed method that allows filling neurons without the need to patch them to wash in the dye. This technique is the electrical electroporation, which has been extensively used for the delivery of DNA, RNA, and other molecules to the interior of cells. It has been shown that this technique can be effectively used to load neurons with fluorescent calcium indicators in vitro and in vivo (Nevian and Helmchen, 2007). The combined use of electroporation and voltage-sensitive dyes may allow recording from cells with intact cytoskeleton and, even more importantly, obtaining detailed functional maps of small local circuitries. Another interesting technique that allows the identification of functional connections in a brain slice is the laser-scanning photostimulation (LSPS) based on glutamate uncaging. This technique allows for rapid imaging of local synaptic circuits by recording synaptic responses from a postsynaptic neuron while stimulating small clusters of presynaptic cells with high spatial resolution (Callaway and Katz, 1993). A neuron is recorded in the whole-cell configuration and the slice bathing solution contains a molecularly caged form of glutamate. This molecule is then converted to the active form by submillisecond pulses of ultraviolet irradiation, which can be delivered selectively to small areas (of $<100\,\mu$m diameter). It has been shown that this technique is selective enough to prevent activation of axons of passage while the stimulus is potent enough to induce firing in the investigated neurons. Thus, the technique can be effectively used for mapping local circuits.

Acknowledgments The author is deeply grateful to Dr. Bruce Bean for critical reading of an earlier version of this chapter.

Further Reading

Atherton JF, Bevan MD. (2005) Ionic mechanisms underlying autonomous action potential generation in the somata and dendrites of GABAergic substantia nigra pars reticulata neurons in vitro. J Neurosci 25(36):8272–81

Avery RB, Johnston D. (1996) Multiple channel types contribute to the low-voltage-activated calcium current in hippocampal CA3 pyramidal neurons. J Neurosci 16(18):5567–82

Baker BJ, Kosmidis EK, Vucinic D, Falk CX, Cohen LB, Djurisic M, Zecevic D. (2005) Imaging brain activity with voltage- and calcium-sensitive dyes. Cell Mol Neurobiol 25(2):245–82

Baldwin TJ, Tsaur ML, Lopez GA, Jan YN, Jan LY. (1991) Characterization of a mammalian cDNA for an inactivating voltage-sensitive K+ channel. Neuron 7(3):471–83

Bartos M, Vida I, Frotscher M, Geiger JR, Jonas P. (2001) Rapid signaling at inhibitory synapses in a dentate gyrus interneuron network. J Neurosci 21(8):2687–98

Beck H, Ficker E, Heinemann U. (1992) Properties of two voltage-activated potassium currents in acutely isolated juvenile rat dentate gyrus granule cells. J Neurophysiol 68(6):2086–99

Bischofberger J, Geiger JR, Jonas P. (2002) Timing and efficacy of $Ca2^{+}$ channel activation in hippocampal mossy fiber boutons. J Neurosci 22:10593–602

Blaxter TJ, Carlen PL, Niesen C. (1989) Pharmacological and anatomical separation of calcium currents in rat dentate granule neurones in vitro. J Physiol 412:93–112

Bloodgood BL, Sabatini BL. (2007) Nonlinear regulation of unitary synaptic signals by CaV(2.3) voltage-sensitive calcium channels located in dendritic spines. Neuron 53(2):249–60

Bossu JL, Capogna M, Debanne D, McKinney RA, Gähwiler BH. (1996) Somatic voltage-gated potassium currents of rat hippocampal pyramidal cells in organotypic slice cultures. J Physiol 495:367–81

Bowden SE, Fletcher S, Loane DJ, Marrion NV. (2001) Somatic colocalization of rat SK1 and D class (Ca(v)1.2) L-type calcium channels in rat CA1 hippocampal pyramidal neurons. J Neurosci 21(20):RC175

Bullis JB, Jones TD, Poolos NP. (2007) Reversed somatodendritic I(h) gradient in a class of rat hippocampal neurons with pyramidal morphology. J Physiol 579(Pt 2):431–43. Epub 2006 Dec 21

Callaway EM, Katz LC (1993) Photostimulation using caged glutamate reveals functional circuitry in living brain slices. Proc Natl Acad Sci USA 90:7661–5

Charpak S, Gähwiler BH, Do KQ, Knöpfel T. (1990) Potassium conductances in hippocampal neurons blocked by excitatory amino-acid transmitters. Nature 347(6295):765–7

Chen X, Johnston D. (2004) Properties of single voltage-dependent K^+ channels in dendrites of CA1 pyramidal neurones of rat hippocampus. J Physiol 559:187–203

Chen S, Yaari Y. (2008) Spike $Ca2^+$ influx upmodulates the spike afterdepolarization and bursting via intracellular inhibition of KV7/M channels. J Physiol 586:1351–63

Chikwendu

A, McBain CJ. (1996) Two temporally overlapping "delayed-rectifiers" determine the voltage-dependent potassium current phenotype in cultured hippocampal interneurons. J Neurophysiol 76(3):1477–90

Christie BR, Eliot LS, Ito K, Miyakawa H, Johnston D. (1995) Different Ca2+ channels in soma and dendrites of hippocampal pyramidal neurons mediate spike-induced Ca2+ influx. J Neurophysiol 73(6):2553–7

Chung YH, Shin C, Park KH, Cha CI. (2000) Immunohistochemical study on the distribution of the voltage-gated calcium channel alpha (1B) subunit in the mature rat brain. Brain Res 866(1–2):274–80

Colbert CM, Johnston D. (1996) Axonal action-potential initiation and Na+ channel densities in the soma and axon initial segment of subicular pyramidal neurons. J Neurosci 16(21):6676–86

Colbert CM, Magee JC, Hoffman DA, Johnston D. (1997) Slow recovery from inactivation of Na+ channels underlies the activity-dependent attenuation of dendritic action potentials in hippocampal CA1 pyramidal neurons. J Neurosci 17(17):6512–21

Colbert

CM, an E. (2002) Ion channel properties underlying axonal action potential initiation in pyramidal neurons. Nat Neurosci 5(6):533–8

Day NC, Shaw PJ, McCormack AL, Craig PJ, Smith W, Beattie R, Williams TL, Ellis SB, Ince PG, Harpold MM, Lodge D, Volsen SG. (1996) Distribution of alpha 1A, alpha 1B and alpha 1E voltage-dependent calcium channel subunits in the human hippocampus and parahippocampal gyrus. Neuroscience 71(4):1013–24

Devaux JJ, Kleopa KA, Cooper EC, and Scherer SS. (2004) KCNQ2 is a nodal K^+ channel. J Neurosci 24:1236–44

Dietrich D, Kirschstein T, Kukley M, Pereverzev A, von der Brelie C, Schneider T, Beck H. (2003) Functional specialization of presynaptic Cav2.3 $Ca2^+$ channels. Neuron 39(3):483–96

Du J, Haak LL, Phillips-Tansey E, Russell JT, McBain CJ. (2000) Frequency-dependent regulation of rat hippocampal somato-dendritic excitability by the K+ channel subunit Kv2.1. J Physiol 522(Pt 1):19–31

Eliot LS, Johnston D. (1994) Multiple components of calcium current in acutely dissociated dentate gyrus granule neurons. J Neurophysiol 72(2):762–77

Ellerkmann RK, Remy S, Chen J, Sochivko D, Elger CE, Urban BW, Becker A, Beck H. (2003) Molecular and functional changes in voltage-dependent Na(+) channels following pilocarpine-induced status epilepticus in rat dentate granule cells. Neuroscience 119(2):323–33

Ellerkmann RK, Riazanski V, Elger CE, Urban BW, Beck H. (2001) Slow recovery from inactivation regulates the availability of voltage-dependent Na(+) channels in hippocampal granule cells, hilar neurons and basket cells. J Physiol 532(Pt 2):385–97

Engel D, Jonas P. (2005) Presynaptic action potential amplification by voltage-gated Na+ channels in hippocampal mossy fiber boutons. Neuron 45(3):405–17

Felts PA, Yokoyama S, Dib-Hajj S, Black JA, Waxman SG. (1997) Sodium channel alpha-subunit mRNAs I, II, III, NaG, Na6 and hNE (PN1): different expression patterns in developing rat nervous system. Brain Res Mol Brain Res 45:71–82

Fernandez FR, Morales E, Rashid AJ, Dunn RJ, Turner RW. (2003) Inactivation of Kv3.3 potassium channels in heterologous expression systems. J Biol Chem 278(42):40890–8

Fisher RE, Gray R, Johnston D. (1990) Properties and distribution of single voltage-gated calcium channels in adult hippocampal neurons. J Neurophysiol 64(1):91–104

Fraser DD, MacVicar BA. (1991) Low-threshold transient calcium current in rat hippocampal lacunosum-moleculare interneurons: kinetics and modulation by neurotransmitters. J Neurosci 11(9):2812–20

Freund TF, Buzsáki G. (1996) Interneurons of the hippocampus. Hippocampus 6(4):347–470

Fricker D, Verheugen JA, Miles R. (1999) Cell-attached measurements of the firing threshold of rat hippocampal neurones. J Physiol 517(Pt 3):791–804

Frotscher M, Seress L, Schwerdtfeger WK, Buhl E. (1991) The mossy cells of the fascia dentata: a comparative study of their fine structure and synaptic connections in rodents and primates. J Comp Neurol 312(1):145–63

Gasparini S, Magee JC. (2002) Phosphorylation-dependent differences in the activation properties of distal and proximal dendritic Na+ channels in rat CA1 hippocampal neurons. J Physiol 541(Pt 3):665–72

Gasparini S, Migliore M, Magee JC. (2004) On the initiation and propagation of dendritic spikes in CA1 pyramidal neurons. J Neurosci 24(49):11046–56

Geiger JR, Jonas P. (2000) Dynamic control of presynaptic Ca(2+) inflow by fast-inactivating K(+) channels in hippocampal mossy fiber boutons. Neuron 28:927–39

Gentet LJ, Stuart GJ, Clements JD. (2000) Direct measurement of specific membrane capacitance in neurons. Biophys J 2000 79(1):314–20

Golding NL, Jung HY, Mickus T, Spruston N. (1999) Dendritic calcium spike initiation and repolarization are controlled by distinct potassium channel subtypes in CA1 pyramidal neurons. J Neurosci 19(20):8789–98

Goldman L, Schauf CL. (1973) Quantitative description of sodium and potassium currents and computed action potentials in Myxicola giant axons. J Gen Physiol 61:361–84

Gong B, Rhodes KJ, Bekele-Arcuri Z, Trimmer JS. (1999) Type I and type II Na(+) channel alpha-subunit polypeptides exhibit distinct spatial and temporal patterning, and association with auxiliary subunits in rat brain. J Comp Neurol 412(2):342–52

Grissmer S, Nguyen AN, Aiyar J, Hanson DC, Mather RJ, Gutman GA, Karmilowicz MJ, Auperin DD, Chandy KG. (1994) Pharmacological characterization of five cloned voltage-gated K+ channels, types Kv1.1, 1.2, 1.3, 1.5, and 3.1, stably expressed in mammalian cell lines. Mol Pharmacol 45(6):1227–34

Hamill OP, Marty A, Neher E, Sakmann B, Sigworth FJ. (1981) Improved patch-clamp techniques for high-resolution current recording from cells and cell-free membrane patches. Pflugers Arch 391(2):85–100

Häusser M, Stuart G, Racca C, Sakmann B. (1995) Axonal initiation and active dendritic propagation of action potentials in substantia nigra neurons. Neuron 15:637–47

Hefft S, Jonas P. (2005) Asynchronous GABA release generates long-lasting inhibition at a hippocampal interneuron-principal neuron synapse. Nat Neurosci 8(10):1319–28. Epub 2005 Sep 11

Hillman D, Chen S, Aung TT, Cherksey B, Sugimori M, Llinás RR. (1991) Localization of P-type calcium channels in the central nervous system. Proc Natl Acad Sci USA 88(16):7076–80

Hodgkin AL, Huxley AF. (1952) A quantitative description of membrane current and its application to conduction and excitation in nerve. J Physiol 1952 117:500–44

Hoffman DA, Johnston D. (1998) Downregulation of transient K+ channels in dendrites of hippocampal CA1 pyramidal neurons by activation of PKA and PKC. J Neurosci 18(10):3521–8

Hoffman DA, Magee JC, Colbert CM, Johnston D. (1997) K+ channel regulation of signal propagation in dendrites of hippocampal pyramidal neurons. Nature 387(6636):869–75

Hoogland TM, Saggau P. (2004) Facilitation of L-type Ca2+ channels in dendritic spines by activation of beta2 adrenergic receptors. J Neurosci 24(39):8416–27

Horn R, Marty A. (1988) Muscarinic activation of ionic currents measured by a new whole-cell recording method. J Gen Physiol 92:145–59

Howard AL, Neu A, Morgan RJ, Echegoyen JC, Soltesz I. (2007) Opposing modifications in intrinsic currents and synaptic inputs in post-traumatic mossy cells: evidence for single-cell homeostasis in a hyperexcitable network. J Neurophysiol 97(3):2394–409

Hu H, Martina M, Jonas P. (2009) Dendritic mechanisms underlying rapid ynaptic activation of fast-spiking hippocampal interneurons. Science

Hu H, Vervaeke K, Storm JF. (2002) Two forms of electrical resonance at theta frequencies, generated by M-current, h-current and persistent Na+ current in rat hippocampal pyramidal cells. J Physiol 545(Pt 3):783–805

Hu H, Vervaeke K, Storm JF. (2007) M-channels (Kv7/KCNQ channels) that egulate synaptic integration, excitability, and spike pattern of CA1 pyramidal cells are located in the perisomatic egion. J Neurosci 27:1853–67

Jinno S, Ishizuka S, Kosaka T. (2003) Ionic currents underlying rhythmic bursting of ventral mossy cells in the developing mouse dentate gyrus. Eur J Neurosci 17(7):1338–54

Johnston D, Hoffman DA, Magee JC, Poolos NP, Watanabe S, Colbert CM, Migliore M. Dendritic potassium channels in hippocampal pyramidal neurons. (2000) J Physiol 525(Pt 1):75–81

Jung HY, Mickus T, Spruston N. (1997) Prolonged sodium channel inactivation contributes to dendritic action potential attenuation in hippocampal pyramidal neurons. J Neurosci 17(17): 6639–46

Jung HY, Staff NP, Spruston N. (2001) Action potential bursting in subicular pyramidal neurons is driven by a calcium tail current. J Neurosci 21(10):3312–21

Kim J, Wei DS, Hoffman DA. (2005) Kv4 potassium channel subunits control ction potential repolarization and frequency-dependent broadening in rat hippocampal CA1 pyramidal neurones. J Physiol 569:41–57

Klee R, Ficker E, Heinemann U. (1995) Comparison of voltage-dependent potassium currents in rat pyramidal neurons acutely isolated from hippocampal regions CA1 and CA3. J Neurophysiol 74(5):1982–95

Lambert NA, Wilson WA. (1996) High-threshold Ca2+ currents in rat hippocampal interneurones and their selective inhibition by activation of GABA(B) receptors. J Physiol 492(Pt 1):115–27

Lawrence JJ, Saraga F, Churchill JF, Statland JM, Travis KE, Skinner FK, McBain CJ. (2006) Somatodendritic Kv7/KCNQ/M channels control interspike interval in hippocampal interneurons. J Neurosci 26(47):12325–38

Li L, Bischofberger J, Jonas P. (2007) Differential gating and recruitment of P/Q-, N-, and R-type Ca2+ channels in hippocampal mossy fiber boutons. J Neurosci 27(49):13420–9

Liao YJ, Jan YN, Jan LY. (1996) Heteromultimerization of G-protein-gated inwardly rectifying K+ channel proteins GIRK1 and GIRK2 and their altered expression in weaver brain. J Neurosci 16(22):7137–50

Lien CC, Jonas P. (2003) Kv3 potassium conductance is necessary and kinetically optimized for high-frequency action potential generation in hippocampal interneurons. J Neurosci 23(6):2058–68

Lien CC, Martina M, Schultz JH, Ehmke H, Jonas P. (2002) Gating, modulation and subunit composition of voltage-gated K(+) channels in dendritic inhibitory interneurones of rat hippocampus. J Physiol 538(Pt 2):405–19

Llinás R, Sugimori . (1980) Electrophysiological properties of in vitro Purkinje cell dendrites in mammalian cerebellar slices. J Physiol 305:197–213

Lübke J, Frotscher M, Spruston N. (1998) Specialized electrophysiological properties of anatomically identified neurons in the hilar region of the rat fascia dentata. J Neurophysiol 79(3): 1518–34

Maccaferri G, Mangoni M, Lazzari A, DiFrancesco D. (1993) Properties of the hyperpolarization-activated current in rat hippocampal CA1 pyramidal cells. J Neurophysiol 69(6):2129–36

Maccaferri G, McBain CJ. (1996) The hyperpolarization-activated current (Ih) and its contribution to pacemaker activity in rat CA1 hippocampal stratum oriens-alveus interneurones. J Physiol 497(Pt 1):119–30

Magee JC. (1998) Dendritic hyperpolarization-activated currents modify the integrative properties of hippocampal CA1 pyramidal neurons. J Neurosci 18(19):7613–24

Magee JC, Avery RB, Christie BR, Johnston D. (1996) Dihydropyridine-sensitive, voltage-gated Ca2+ channels contribute to the resting intracellular Ca2+ concentration of hippocampal CA1 pyramidal neurons. J Neurophysiol 76:3460–70

Magee JC, Carruth M. (1999) Dendritic voltage-gated ion channels regulate the action potential firing mode of hippocampal CA1 pyramidal neurons. J Neurophysiol 82(4):1895–901

Magee JC, Christofi G, Miyakawa H, Christie B, Lasser-Ross N, Johnston D. (1995) Subthreshold synaptic activation of voltage-gated Ca2+ channels mediates a localized Ca2+ influx into the dendrites of hippocampal pyramidal neurons. J Neurophysiol 74(3):1335–42

Magee JC, Johnston D. (1995a) Characterization of single voltage-gated Na+ and Ca2+ channels in apical dendrites of rat CA1 pyramidal neurons. J Physiol 487:67–90

Magee JC, Johnston D. (1995b) Synaptic activation of voltage-gated channels in the dendrites of hippocampal pyramidal neurons. Science 268:301–4

Major G. (1993) Solutions for transients in arbitrarily branching cables: III. Voltage clamp problems. Biophys J 65:469–91

Major G, Larkman AU, Jonas P, Sakmann B, Jack JJ. (1994) Detailed passive cable models of whole-cell recorded CA3 pyramidal neurons in rat hippocampal slices. J Neurosci 14:4613–38

Maletic-Savatic M, Lenn NJ, Trimmer JS. (1995) Differential spatiotemporal expression of K+ channel polypeptides in rat hippocampal neurons developing in situ and in vitro. J Neurosci 15:3840–51

Martina M, Jonas P. (1997) Functional differences in Na+ channel gating between fast-spiking interneurones and principal neurones of rat hippocampus. J Physiol 505:593–603

Martina M, Schultz JH, Ehmke H, Monyer H, Jonas P. (1998) Functional and molecular differences between voltage-gated K+ channels of fast-spiking interneurons and pyramidal neurons of rat hippocampus. J Neurosci 18:8111–25

Martina M, Vida I, Jonas P. (2000) Distal initiation and active propagation of action potentials in interneuron dendrites. Science 287:295–300

Meeks JP, Mennerick S. (2007) Action potential initiation and propagation in CA3 pyramidal axons. J Neurophysiol 97:3460–72

Metz AE, Jarsky T, Martina M, Spruston N. (2005) R-type calcium channels contribute to afterdepolarization and bursting in hippocampal CA1 pyramidal neurons. J Neurosci 25:5763–73

Metz AE, Spruston N, Martina M. (2007) Dendritic D-type potassium currents inhibit the spike afterdepolarization in rat hippocampal CA1 pyramidal neurons. J Physiol 581:175–87

Meyer AH, Katona I, Blatow M, Rozov A, Monyer H. (2002) In vivo labeling of parvalbumin-positive interneurons and analysis of electrical coupling in identified neurons. J Neurosci 22:7055–64

Mills LR, Niesen CE, So AP, Carlen PL, Spigelman I, Jones OT. (1994) N-type Ca2+ channels are located on somata, dendrites, and a subpopulation of dendritic spines on live hippocampal pyramidal neurons. J Neurosci 14:6815–24

Mintz IM, Adams ME, Bean BP. (1992) P-type calcium channels in rat central and peripheral neurons. Neuron 9:85–95

Misonou H, Menegola M, Buchwalder L, Park EW, Meredith A, Rhodes KJ, Aldrich RW, Trimmer JS. (2006) Immunolocalization of the Ca2+-activated K+ channel Slo1 in axons and nerve terminals of mammalian brain and cultured neurons. J Comp Neurol 496:289–302

Mitterdorfer J, Bean BP. (2002) Potassium currents during the action potential of hippocampal CA3 neurons. J Neurosci 22:10106–15

Miyawaki T, Tsubokawa H, Yokota H, Oguro K, Konno K, Masuzawa T, Kawai N. (2002) Differential effects of novel wasp toxin on rat hippocampal interneurons. Neurosci Lett 328:25–8

Mogul DJ, Fox AP. (1991) Evidence for multiple types of Ca2+ channels in acutely isolated hippocampal CA3 neurones of the guinea-pig. J Physiol 433:259–81

Monaghan MM, Trimmer JS, Rhodes KJ. (2001) Experimental ocalization of Kv1 family voltage-gated K^+ channel alpha and beta subunits in rat hippocampal formation. J eurosci 21:5973–83

Neher E, Sakmann B, Steinbach JH. (1978) The extracellular patch clamp: a method for resolving currents through individual open channels in biological membranes. Pflugers Arch 375:219–28

Nevian T, Helmchen F. (2007) Calcium indicator loading of neurons using single-cell electroporation. Pflugers Arch 54:675–88

Nicoll RA, Alger BE. (1981) Synaptic excitation may activate a calcium-dependent potassium conductance in hippocampal pyramidal cells. Science 212:957–9

Normann C, Peckys D, Schulze CH, Walden J, Jonas P, Bischofberger J. (2000) Associative long-term depression in the hippocampus is dependent on postsynaptic N-type Ca2+ channels. J Neurosci 20:8290–7

Park KH, Chung YH, Shin C, Kim MJ, Lee BK, Cho SS, Cha CI. (2001) Immunohistochemical study on the distribution of the voltage-gated potassium channels in the gerbil hippocampus. Neurosci Lett 298:29–32

Parra P, Gulyás AI, Miles R. (1998) How many subtypes of inhibitory cells in the hippocampus? Neuron 20:983–93

Poncer JC, McKinney RA, Gähwiler BH, Thompson SM. (1997) Either N- or P-type calcium channels mediate GABA release at distinct hippocampal inhibitory synapses. Neuron 18: 463–72

Poolos NP, Johnston D. (1999) Calcium-activated potassium conductances contribute to action potential repolarization at the soma but not the dendrites of hippocampal CA1 pyramidal neurons. J Neurosci 19:5205–12

Ramakers GM, Storm JF. (2002) A postsynaptic transient K(+) current modulated by arachidonic acid regulates synaptic integration and threshold for LTP induction in hippocampal pyramidal cells. Proc Natl Acad Sci USA 99:10144–9

Rettig J, Heinemann SH, Wunder F, Lorra C, Parcej DN, Dolly JO, Pongs O. (1994) Inactivation properties of voltage-gated K+ channels altered by presence of beta-subunit. Nature 369: 289–94

Rhodes KJ, Carroll KI, Sung MA, Doliveira LC, Monaghan MM, Burke SL, Strassle BW, Buchwalder L, Menegola M, Cao J, An WF, Trimmer JS. (2004) KChIPs and Kv4 alpha subunits as integral components of A-type potassium channels in mammalian brain. J Neurosci 24:7903–15

Rhodes KJ, Strassle BW, Monaghan MM, Bekele-Arcuri Z, Matos MF, Trimmer JS. (1997) Association and colocalization of the Kvbeta1 and Kvbeta2 beta-subunits with Kv1 alpha-subunits in mammalian brain K+ channel complexes. J Neurosci 17:8246–58

Riazanski V, Becker A, Chen J, Sochivko D, Lie A, Wiestler OD, Elger CE, Beck H. (2001) Functional and molecular analysis of transient voltage-dependent K+ currents in rat hippocampal granule cells. J Physiol 537:391–406

Rozsa B, Zelles T, Vizi ES, Lendvai B. (2004) Distance-dependent scaling of calcium transients evoked by backpropagating spikes and synaptic activity in dendrites of hippocampal interneurons. J Neurosci 24:661–70

Russo MJ, Mugnaini E, Martina M. (2007) Intrinsic properties and mechanisms of spontaneous firing in mouse cerebellar unipolar brush cells. J Physiol 581(Pt 2):709–24

Saganich MJ, Machado E, Rudy B. (2001) Differential expression of genes encoding subthreshold-operating voltage-gated K+ channels in brain. J Neurosci 21:4609–24
Sather W, Dieudonné S, MacDonald JF, Ascher P. (1992) Activation and desensitization of N-methyl-D-aspartate receptors in nucleated outside-out patches from mouse neurones. J Physiol 450:643–72
Saviane C, Mohajerani MH, Cherubini E. (2003) An ID-like current that is downregulated by Ca2+ modulates information coding at CA3–CA3 synapses in the rat hippocampus. J Physiol 552:513–24
Schmidt-Hieber C, Jonas P, Bischofberger J. (2007) Subthreshold dendritic signal processing and coincidence detection in dentate gyrus granule cells. J Neurosci 27:8430–41
Schmidt-Hieber C, Jonas P, Bischofberger J. (2008) Action potential initiation and propagation in hippocampal mossy fibre axons. J Physiol 586:1849–57
Schroeder BC, Hechenberger M, Weinreich F, Kubisch C, Jentsch TJ. (2000) KCNQ5, a novel potassium channel broadly expressed in brain, mediates M-type currents. J Biol Chem 275:24089–95
Sekirnjak C, Martone ME, Weiser M, Deerinck T, Bueno E, Rudy B, Ellisman M. (1997) Subcellular localization of the K+ channel subunit Kv3.1b in selected rat CNS neurons. Brain Res 766:173–87
Serôdio P, Rudy B. (1998) Differential expression of Kv4 K+ channel subunits mediating subthreshold transient K+ (A-type) currents in rat brain. J Neurophysiol 79:1081–91
Serôdio P, Vega-Saenz de Miera E, Rudy B. (1996) Cloning of a ovel component of A-type K^+ channels operating at subthreshold potentials with unique expression in heart and rain. J Neurophysiol 75:2174–9
Shah M, Mistry M, Marsh SJ, Brown DA, and Delmas P. (2002) Molecular correlates of the M-current in cultured rat hippocampal neurons. J Physiol 544:29–37
Sheng M, Tsaur ML, Jan YN, Jan LY. (1994) Contrasting subcellular localization of the Kv1.2 K+ channel subunit in different neurons of rat brain. J Neurosci 14:2408–17
Sochivko D, Chen J, Becker A, Beck H. (2003) Blocker-resistant Ca2+ currents in rat CA1 hippocampal pyramidal neurons. Neuroscience 116:629–38
Sochivko D, Pereverzev A, Smyth N, Gissel C, Schneider T, Beck H. (2002) The Ca(V)2.3 Ca(2+) channel subunit contributes to R-type Ca(2+) currents in murine hippocampal and neocortical neurones. J Physiol 542:699–710
Spruston N, Johnston D. (1992) Perforated patch-clamp analysis of the passive membrane properties of three classes of hippocampal neurons. J Neurophysiol 67:508–29
Spruston N, Schiller Y, Stuart G, Sakmann B. (1995) Activity-dependent action potential invasion and calcium influx into hippocampal CA1 dendrites. Science 268:297–300
Staley KJ, Otis TS, Mody I. (1992) Membrane properties of dentate gyrus granule cells: comparison of sharp microelectrode and whole-cell recordings. J Neurophysiol 67:1346–58
Stea A, Tomlinson WJ, Soong TW, Bourinet E, Dubel SJ, Vincent SR, Snutch TP. (1994) Localization and functional properties of a rat brain alpha 1A calcium channel reflect similarities to neuronal Q- and P-type channels. Proc Natl Acad Sci USA 91:10576–80
Steinhäuser C, Tennigkeit M, Matthies H, Gündel J. (1990) Properties of the fast sodium channels in pyramidal neurones isolated from the CA1 and CA3 areas of the hippocampus of postnatal rats. Pflugers Arch 415:756–61
Storm JF. (1990) Potassium currents in hippocampal pyramidal cells. Prog Brain es 83:161–87
Stuart GJ, Sakmann B. (1994) Active propagation of somatic action potentials into neocortical pyramidal cell dendrites. Nature 367:69–72
Stuart G, Spruston N. (1998) Determinants of voltage attenuation in neocortical pyramidal neuron dendrites. J Neurosci 18:3501–10
Su H, Sochivko D, Becker A, Chen J, Jiang Y, Yaari Y, Beck H. (2002) Upregulation of a T-type Ca2+ channel causes a long-lasting modification of neuronal firing mode after status epilepticus. J Neurosci 22:3645–55

Takahashi K, Ueno S, Akaike N. (1991) Kinetic properties of T-type Ca2+ currents in isolated rat hippocampal CA1 pyramidal neurons. J Neurophysiol 65:148–55

Takahashi K, Wakamori M, Akaike N. (1989) Hippocampal CA1 pyramidal cells of rats have four voltage-dependent calcium conductances. Neurosci Lett 104:229–34

Takigawa T, Alzheimer C. (2002) Phasic and tonic attenuation of EPSPs by inward rectifier K+ channels in rat hippocampal pyramidal cells. J Physiol 539:67–75

Taverna S, Tkatch T, Metz AE, Martina M. (2005) Differential expression of TASK channels between horizontal interneurons and pyramidal cells of rat hippocampus. J Neurosci 25: 9162–70

Thompson SM, Wong RK. (1991) Development of calcium current subtypes in isolated rat hippocampal pyramidal cells. J Physiol 439:671–89

Tippens AL, Pare JF, Langwieser N, Moosmang S, Milner TA, Smith Y, Lee A. (2008) Ultrastructural evidence for pre- and postsynaptic localization of Cav1.2 L-type Ca2+ channels in the rat hippocampus. J Comp Neurol 506:569–83

Torborg CL, Berg AP, Jeffries BW, Bayliss DA, McBain CJ. (2006) TASK-like conductances are present within hippocampal CA1 stratum oriens interneuron subpopulations. J Neurosci 26:7362–7

Tsay D, Dudman JT, Siegelbaum SA. (2007) HCN1 channels constrain synaptically evoked Ca2+ spikes in distal dendrites of CA1 pyramidal neurons. Neuron 56:1076–89

Tsaur ML, Sheng M, Lowenstein DH, Jan YN, Jan LY. (1992) Differential expression of K+ channel mRNAs in the rat brain and down-regulation in the hippocampus following seizures. Neuron 8:1055–67

Veng LM, Browning MD. (2002) Regionally selective alterations in expression of the alpha (1D) subunit (Ca(v)1.3) of L-type calcium channels in the hippocampus of aged rats. Brain Res Mol Brain Res 107:120–7

Vervaeke K, Gu N, Agdestein C, Hu H, Storm JF. (2006) Kv7/KCNQ/M-channels in rat glutamatergic hippocampal axons and their role in regulation of excitability and transmitter release. J Physiol 576:235–56

Vida I, Halasy K, Szinyei C, Somogyi P, Buhl EH. (1998) Unitary IPSPs evoked by interneurons at the stratum radiatum-stratum lacunosum-moleculare border in the CA1 area of the rat hippocampus in vitro. J Physiol 506:755–73

Wang H, Kunkel DD, Schwartzkroin PA, Tempel BL. (1994) Localization of Kv1.1 and Kv1.2, two K channel proteins, to synaptic terminals, somata, and dendrites in the mouse brain. J Neurosci 14:4588–99

Wang HS, Pan Z, Shi W, Brown BS, Wymore RS, Cohen IS, Dixon JE, McKinnon D. (1998) CNQ2 and KCNQ3 potassium channel subunits: molecular correlates of the M-channel. Science 282:1890–3

Weiser M, Bueno E, Sekirnjak C, Martone ME, Baker H, Hillman D, Chen S, Thornhill W, Ellisman M, Rudy B. (1995) The potassium channel subunit KV3.1b is localized to somatic and axonal membranes of specific populations of CNS neurons. J Neurosci 15:4298–314

Weiser M, Vega-Saenz de Miera E, Kentros C, Moreno H, Franzen L, Hillman D, Baker H, Rudy B. (1994) Differential expression of Shaw-related K+ channels in the rat central nervous system. J Neurosci 14:949–72

Wilson SM, Toth PT, Oh SB, Gillard SE, Volsen S, Ren D, Philipson LH, Lee EC, Fletcher CF, Tessarollo L, Copeland NG, Jenkins NA, Miller RJ. (2000) The status of voltage-dependent calcium channels in alpha 1E knock-out mice. J Neurosci 20:8566–71

Xu W, Lipscombe D. (2001) Neuronal Ca(V)1.3alpha(1) L-type channels activate at relatively hyperpolarized membrane potentials and are incompletely inhibited by dihydropyridines. J Neurosci 21:5944–51

Yaari Y, Yue C, Su H. (2007) Recruitment of apical dendritic T-type Ca2+ channels by backpropagating spikes underlies de novo intrinsic bursting in hippocampal epileptogenesis. J Physiol 580:435–50

Yue C, Remy S, Su H, Beck H, Yaari Y. (2005) Proximal persistent Na+ channels drive spike afterdepolarizations and associated bursting in adult CA1 pyramidal cells. J Neurosci 25: 9704–20

Yue C, Yaari Y. (2004) KCNQ/M channels control spike after depolarization and burst generation in hippocampal neurons. J Neurosci 24:4614–24

Zhang L, Valiante TA, Carlen PL. (1993) Contribution of the low-threshold T-type calcium current in generating the post-spike depolarizing afterpotential in dentate granule neurons of immature rats. J Neurophysiol 70:223–31

Glutamatergic Neurotransmission in the Hippocampus

Katalin Tóth

Overview

This chapter will summarize key data about glutamatergic transmission in the hippocampus. Glutamate is the major excitatory neurotransmitter similar to other CNS regions. Biophysical properties of various receptors and channels will be described and functional relevance of these parameters discussed.

The major components of the excitatory synaptic network in the hippocampus form the so-called tri-synaptic circuit. This circuit consists of the perforant pathway input from the entorhinal cortex to the dentate gyrus; mossy fibers projecting from the dentate gyrus to the CA3 area; and the Schaffer collaterals, axons of CA3 pyramidal cells innervating the CA1 area (Fig. 1). This chapter will focus on the properties of these glutamatergic synapses, highlighting the most distinct features these inputs possess.

Glutamatergic transmission in the hippocampus is known to play a crucial role in learning and memory due to activity-dependent changes in synaptic efficacy. However, this chapter will only explore the basic properties of glutamatergic synapses, and chapter "Synaptic Plasticity at Hippocampal Synapses" will discuss synaptic plasticity in detail.

Data

Introduction

The main excitatory transmitter in the hippocampus is glutamate. Its action is mediated via two main classes of glutamate receptors: ionotropic and metabotropic receptors.

K. Tóth (✉)
Centre de recherche Université Laval Robert Giffard, Quebec, QC, Canada G1J 2G3
e-mail: toth.katalin@crulrg.ulaval.ca

V. Cutsuridis et al. (eds.), *Hippocampal Microcircuits*, Springer Series in Computational Neuroscience 5, DOI 10.1007/978-1-4419-0996-1_4,

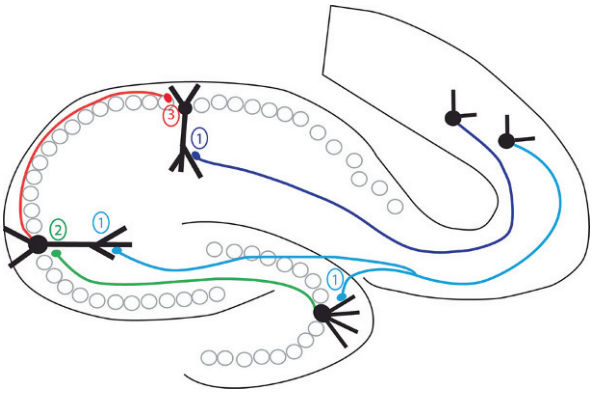

Fig. 1 Major excitatory pathways in the hippocampus. Layer II neurons in the entorhinal cortex project to the dentate gyrus and the CA3 filled via the perforant pathways (1, *blue*). Neurons in layer III of the entorhinal cortex send their axons to the CA1 subfield and the subiculum (1, *purple*). Dentate granule cells innervate the CA3 area via mossy fibers (2, *green*). Pyramidal cells of the CA3 subregion project to the CA1 area via Schaffer collaterals (3, *red*)

The ionotropic glutamate receptors are ligand-gated ion channels, they are responsible for the vast majority of fast excitatory neurotransmission in the CNS. In these receptors glutamate binding causes channel opening, with the resulting predominant Na^+ influx leading to membrane depolarization. Based on their particular pharmacology, ionotropic glutamate receptors fall into three major classes which are named after their selective agonists: AMPA (α-amino-3-hydroxy-5-methyl-4-isoxazolepropionic acid), NMDA (*N*-methyl-D-aspartate), and kainate receptors. All three receptor types form heteromeric structures consisting of four subunits.

AMPA receptors are composed of the combination of four subunits: GluR1, GluR2, GluR3, and GluR4 (or GluR A–D) (Dingledine et al. 1999). The presence or absence of the GluR2 subunit in the complex will determine several biophysical properties of the receptor. This subunit undergoes post-transcriptional RNA editing at the "Q/R site"; insertion of the edited form into AMPA receptors will result in low conductance, Ca^{2+}-impermeable channels with linear I–V relationship. In contrast, GluR2-lacking AMPA receptors have higher conductance, are Ca^{2+}-permeable, and show inwardly rectifying I–V relationships due to the block by endogenous polyamine at positive membrane potentials (Bowie and Mayer 1995, Kamboj et al. 1995, Koh et al. 1995). Principal cells in the hippocampus express high levels of GluR2, hence Ca^{2+}-impermeable AMPA receptors dominate synaptic transmission in these cells. Ca^{2+}-permeable AMPA receptors are present on some hippocampal interneurons, and during development, some fetal GluR2 subunits remain unedited.

In the hippocampus, NMDA receptors are heteromultimers of NR1 and NR2A–D subunits. NMDA receptors have very slow kinetics compared to AMPA or kainate receptors, which is explained by the slow dissociation rate of glutamate. While glutamate is bound, NMDA channels can undergo repeated opening. NMDA receptors

activation requires two agonists, glycine and glutamate. The glycine site has to be occupied first, followed by glutamate binding, when this occurs the channel can open and Na^+ and Ca^{2+} enter the cell. However, channel opening can only occur when Mg^{2+} block is removed from NMDA receptors while the membrane is depolarized, at resting membrane potentials glutamate binding does not lead to channel opening. Ca^{2+} entering the cell via NMDA receptors plays important role in synaptic plasticity.

Kainate receptors are also heteromultimers composed of the combination of GluR5,6,7 and KA1,2 subunits. KA1 and 2 subunits alone are non-functional and are retained in the endoplasmic reticulum, but can combine with GluR5–7 to form surface-localized functional receptors. GluR5 and -6 subunits undergo alternative splicing similar to the GluR2 subunit of AMPA receptors at the Q/R site. Receptors incorporating edited GluR5 and -6 subunits have linear I–V relationship, while insertion of the unedited form of GluR5 or -6 results in inward rectification due to intracellular polyamine block at depolarized membrane potentials. Receptors containing solely unedited GluR5 and -6 are also weakly permeable to Ca^{2+}. The relationship between rectification, Ca^{2+}-permeability, and subunit composition is more complex than in AMPA receptors because only a portion of GluR5 and -6 subunits are edited at the Q/R site. Recombinant kainate receptors have fast kinetics, they rapidly activate and deactivate in the submillisecond range. Interestingly these parameters are markedly different from the relatively slow kinetics of synaptically evoked kainate responses.

The metabotropic glutamate receptors contain seven transmembrane domains and their actions are mediated via G proteins. Metabotropic receptors fall into three groups based on amino acid homology, signal transduction pathway, and their pharmacological profile.

Group I metabotropic receptors are generally localized postsynaptically, coupled to the Gq signaling pathway, and their activation increases cell excitability. Group II and III receptors are localized on the presynaptic membrane and coupled to adenylyl cyclase via G proteins; in general they are involved in the control of neurotransmitter release. Presynaptically located metabotropic glutamate receptors are generally involved in plastic changes leading to modifications in synaptic strength, while glutamate binding to postsynaptic metabotropic receptors can lead to ion channel opening and closing and the generation of various intracellular messengers (Table 1).

The Perforant Pathway

The hippocampus receives its major cortical input from the entorhinal cortex via the perforant pathway. This pathway originates from layer II and III of the entorhinal cortex and provides direct inputs to all three major areas of the hippocampus. Distal dendrites of dentate granule cells receive input from the lateral entorhinal input, while the medial region of the entorhinal cortex innervates the middle third of the molecular layer (Amaral and Witter 1989). In the CA3 region entorhinal terminals

Table 1 Various glutamate receptors in the hippocampus

	Groups	Subunits	Conducting ions	Pharmacology
Ionotropic receptors	AMPA	GluR1, GluR2, GluR3, GluR4	Na^+, (Ca^{2+})	Antagonist: kyuneric acid, CNQX, GYKI53655
	NMDA	NR1, NR2A, NR2B, NR2C, NR2D, NR3A	Na^+, (Ca^{2+})	Antagonist: kyuneric acid, D-AP5, CPP
	Kainate	GluR5, GluR6, GluR7, KA1, KA2	Na^+, (Ca^{2+})	Antagonist: kyuneric acid, CNQX, LY3882884
			Signaling pathway	
Metabotropic receptors	Group I	mGluR1, mGluR5	Phospholipase C	Agonist: DHPG, 1S,3R-ACPD Antagonist: MCPG
	Group II	mGluR2, mGluR3	Adenylyl cyclase	Agonist: 1S,3R-ACPD, DCG-IV, Antagonist: MCPG, LY341496
	Group III	mGluR4, mGluR6, mGluR7, mGluR8	Adenylyl cyclase	Agonist: L-AP4, Antagonist: MSOP

are scattered throughout the stratum lacunosum-moleculare. Projection from the lateral entorhinal area innervates the superficial layers of the stratum lacunosum-moleculare, and input from the medial entorhinal area projects to the deep half of this layer (Witter 1993). Direct input to the dentate gyrus and the CA3 originates from layer II of the entorhinal cortex, in contrast distal dendrites in the CA1 area are innervated by axons from layer III.

Salient features of perforant pathway synapses:

- Distinct features of medial and lateral perforant pathway inputs
- Direct input to CA1 plays important role in feed-forward inhibition
- Input-specific subunit composition of NMDA receptors
- Complementary distribution of metabotropic receptors at the medial and lateral perforant pathway

AMPA Receptors

Stimulation of the perforant pathway from the entorhinal cortex evokes monosynaptic responses in the dentate granule cells. Both the medial and the lateral perforant

pathways use glutamate as principal transmitter, and CNQX blocks 80–90% of the synaptic events (Lambert and Jones 1989). However, the physiological and pharmacological properties of these inputs are distinct. Topographical separation of the medial and lateral pathway inputs in the dentate gyrus allows their investigation in isolation. In response to repeated stimuli lateral perforant pathway synapses exhibit marked facilitation, while medial perforant path synapses show less facilitation or even depression using a paired-pulse paradigm (McNaughton 1980). During the course of a longer train the medial perforant path input shows significant depression, while the amplitude of the synaptic events evoked with the stimulation of the lateral pathway shows minimal change (McNaughton 1980, Rush et al. 2002). Since the ratio of the EPSP to fiber response is greater in the medial pathway and the observed short-term depression converts to facilitation in lower extracellular $[Ca^{2+}]$, it is very likely that the initial release probability is lower at lateral pathway synapses than at medial perforant inputs. Discrepancy between the quanta sensed by NMDA and AMPA receptors is observed in the lateral, but not in the medial perforant path, indicating that silent synapses are present only at lateral pathway synapses. Consequently, NMDA-receptor-mediated recruitment of AMPA receptors to the active zone could play an important role in plastic changes at this synapse (Min et al. 1998). Several presynaptic receptors have different modulatory effects on these two inputs. Carbachol selectively depresses synaptic potentials evoked with the stimulation of the medial perforant pathway, indicating that acetylcholine receptors are selectively involved in the regulation of the glutamatergic responses at the medial but not at the lateral perforant pathway (Kahle and Cotman 1989). Noradrenalin has opposing effects on the long-term plasticity of medial and lateral perforant path inputs (Dahl and Sarvey 1989, Pelletier et al. 1994). Glutamatergic input from hilar mossy cells onto granule cells is potently and transiently suppressed by endocannabinoids, while both perforant path inputs are unaffected (Chiu and Castillo 2008).

Pharmacological and electrophysiological differences between lateral and medial perforant inputs terminating on CA3 pyramidal cells show similar distinct pattern even though synaptic inputs are not spatially segregated here (Berzhanskaya et al. 1998).

The dendritic arborization of certain types of inhibitory cells located in the dentate gyrus indicates that they are receiving the vast majority of their inputs from the perforant pathway (MOPP, molecular layer perforant path associated); the functional role of these cell in the modulation of hippocampal activity still needs to be determined (Han et al. 1993). In the CA3 region interneurons receiving inputs from the perforant pathway and mossy fibers were suggested to act as coincidence detectors manifesting supralinear EPSP summation (Calixto et al. 2008).

Stimulation of the direct perforant path input to the CA1 area of the hippocampus evokes a small glutamatergic current in CA1 pyramidal cells. This input is shown to have very little effect on the firing pattern of the postsynaptic cells (Colbert and Levy 1992, Empson and Heinemann 1995). However, it initiates a powerful feed-forward inhibition and is capable of regulating the probability of Schaffer collateral-evoked CA1 spikes (Empson and Heinemann 1995, Jarsky et al. 2005, Remondes and Schuman 2002) (Fig. 2).

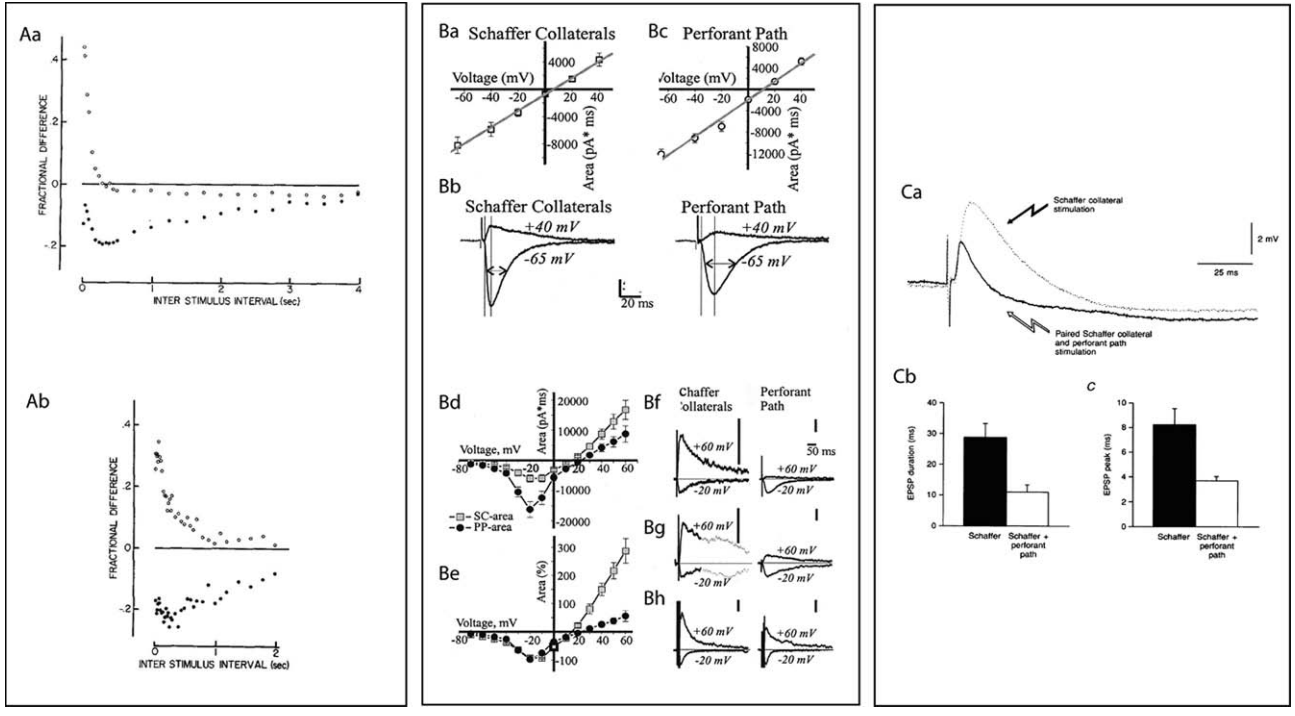

Fig. 2 Properties of the perforant path input. Different properties of short-term plasticity of the medial (*filled circles*) and lateral (*open circles*) pathway demonstrated in vivo (*Aa*) and in vitro (*Ab*). Graphs illustrating paired-pulse ratios at various inter-stimulus intervals (McNaughton 1980). Comparison of current–voltage relationship of AMPA (*Ba–Bc*) and NMDA (*Bd–Bh*) responses at Schaffer collateral and perforant path inputs (Otmakhova et al. 2002). Simultaneous activation of Schaffer collaterals and the perforant path (*Ca*) decreases both EPSP duration (*Cb*) and amplitude (*Cc*) by activating strong feed-forward inhibition (Empson and Heinemann 1995)

Properties of individual perforant pathway inputs onto granule cells and inhibitory cells were investigated using minimal stimulation. While the kinetics of synaptic inputs terminating on inhibitory and excitatory cells are similar, the amplitude of perforant pathway EPSC/Ps is significantly bigger on GABAergic basket cells. This difference could stem from larger number of active zones or higher number of AMPA receptors in synapses innervating basket cells (Sambandan and Bartos 2009) (Table 2).

Table 2 Kinetic properties of perforant pathway inputs onto granule cells and GABAergic basket cells in the dentate gyrus (Sambandan and Bartos 2009)

	Granule cells	Basket cells
EPSC		
EPSC peak amplitude (minimal stimulation)	16.77 ± 3.95 pA	44.47 ± 9.48 pA
Rise time (20–80%) (minimal stimulation)	2.4 ± 0.15 ms	1.33 ± 0.25 ms
EPSC decay time constant (minimal stimulation)	10.94 ± 1.58 ms	7.09 ± 0.90 ms
EPSP		
EPSP peak amplitude (minimal stimulation)	1.15 ± 0.24 mV	2.30 ± 0.43 mV
EPSP rise time (20–80%) (minimal stimulation)	5.31 ± 0.46 ms	2.26 ± 0.13 ms
EPSP decay time constant (minimal stimulation)	25.7 ± 1.57 ms	26.71 ± 3.60 ms

NMDA Receptors

NMDA receptors significantly contribute to the EPSP evoked by perforant pathway stimulation in dentate granule cells, CNQX blocks 80–90% of the synaptic events, and APV completely abolishes the residual component (Lambert and Jones 1989, 1990). Complete and selective deletion of the NR1 subunit in granule cells leads to impaired context discrimination in the incremental fear-conditioning paradigm, and context-modulated place cell activity in the CA3. However, both of these deficits manifested only in the initial phases of the experiments and were overcome by experience. This indicates that NMDA receptors on granule cells play an important role in the animals' ability to rapidly discriminate between similar contexts (McHugh et al. 2007). Pharmacological blockade of the NR2B-containing NMDA receptors also lead to learning difficulties and diminished activity-dependent synaptic plasticity at the medial perforant pathway–granule cell synapses (Valenzuela-Harrington et al. 2007).

In CA1 pyramidal cells perforant input forms synapses on distal dendrites in the stratum lacunosum-moleculare, NMDA/AMPA charge ratio of this input is significantly larger that those of the Schaffer collateral inputs. The properties of the NMDA component were also quite different, as the NMDA-mediated current at $+60$ mV in the perforant pathway input is six times smaller than in the Schaffer collateral input after scaling by the maximal inward current at -20 mV (Otmakhova et al. 2002). Different NMDA receptor properties could be contributed to different subunit composition of the receptors facing the two different inputs. NR2B subunit contribution to NMDA responses at Schaffer collateral inputs is larger than at perforant pathway inputs on a single CA1 pyramidal cell, indicating that NMDA receptors with distinct subunit composition are segregated in an input-specific manner along the dendritic tree (Arrigoni and Greene 2004).

Metabotropic Glutamate Receptors

In the perforant pathway terminating in the CA3 area and the dentate gyrus the localization of presynaptic mGluRs, mGluR2 and mGluR8, is complementary, mGluR2 is present at the medial and mGluR8 at the lateral perforant input (Shigemoto et al. 1997). Differential regulation of the medial and lateral perforant path by different metabotropic receptors has been demonstrated by selective Group II and Group III agonists and antagonists; indicating that Group III metabotropic receptors regulate glutamate release at the lateral perforant pathway, while Group II mGluRs serve as autoreceptors at the medial perforant path (Macek et al. 1996). Activation of presynaptic Group II mGluRs at the medial perforant pathway reduced synaptic transmission and resulted in a reduction of short-term depression (Kilbride et al. 2001). While short-term depression is not prominent at the lateral perforant input at lower frequencies, it increases with higher stimulus frequencies; L-AP4, a selective agonist of Group III mGluRs, reduced this depression (Rush et al. 2002). In the CA1 area, perforant pathway axons display both Group II and Group III mGluRs, while mGluR7a and mGluR4 are detected in active zones, mGluR2 can be found in preterminal zones (Shigemoto et al. 1997). Segregation of these mGluRs to different zones of the presynaptic terminal and their different signaling suggest that they could be involved in distinct regulatory roles (Capogna 2004). Similar pattern of mGluR distribution and regulatory function was observed on perforant path inputs terminating on CA1 interneurons located in the stratum lacunosum-moleculare (Price et al. 2005).

Mossy Fibers

Dentate granule cells send their axons to the hilus and the CA3 area of the hippocampus. Mossy fibers are unmyelinated axons arborizing in the hilar area forming a distinctive axon bundle in the stratum lucidum of the CA3 area. They form three distinct types of presynaptic terminals: complex en passant presynaptic terminals called mossy fiber expansions (Amaral and Dent 1981), filopodial extensions of large mossy boutons, and small en passant terminals (Acsády et al. 1998). Large mossy terminals innervate exclusively excitatory cells, mossy cells in the hilus and pyramidal cells in the CA3 area. In contrast, small filopodial extensions originating from the large terminals and small en passant terminals specifically terminate on GABAergic cells both in the hilus and in the CA3 (Acsády et al. 1998). Complex mossy terminals are large (4 – 10 μm) and form several (30–40) synaptic contacts (Chicurel and Harris 1992) with a single thorny excrescence on each CA3 pyramidal neuron or mossy cell. A single granule cell gives rise to 10–18 large mossy terminals (Amaral et al. 1990) innervating 11–15 CA3 pyramidal cells and 7–12 hilar mossy cells. Acsády et al. (1998) elegantly demonstrated that the number of GABAergic targets innervated via small filopodial extensions and en passant terminals is 10 times larger than the number of excitatory targets. The physiological properties of mossy fiber inputs to pyramidal cells and to interneurons are summarized in Table 3.

Table 3 Kinetic properties of mossy fiber inputs onto pyramidal cells and interneurons

		MF-P cell	MF-I cell	
Quantal parameters				
	Release probability	<0.3	>0.02–0.5	Jonas et al. (1993), Lawrence et al. (2004), Szabadics and Soltesz (2009), von Kitzing et al. (1994)
	Quantal size	~29 pA	~30 pA	Lawrence et al. (2004) but see von Jonas et al. (1993), Szabadics and Soltesz (2009)
	Release site/connection	8–35	1–2	Acsády et al. (1998), Lawrence et al. (2004), Rollenhagen et al. (2007)
	Probability of action potential generation by the first EPSC	0.28	0.1	Lawrence et al. (2004)
	Probability of action potential generation by 40 Hz train EPSC	0.76	0.22	Henze et al. (2002), Lawrence et al. (2004)
AMPA				
	Latency	2 ms	2.2 ms	Tóth et al. (2000)
	Amplitude (at −70 mV)	25–200 pA	2–100 pA	Jonas et al. (1993), Lawrence et al. (2004), Szabadics and Soltesz (2009), Tóth et al. (2000), Walker et al. (2002)
	Rise time	~1.5 ms	<1 ms	Geiger et al. (1997), Jonas et al. (1993), Lawrence et al. (2004), Tóth et al. (2000)
	Decay time const.	~10 ms	~ 2.5–4 ms	Tóth et al. (2000), Walker et al. (2002)
	Channel conductance	10 pS		Jonas et al. (1993)
NMDA				
	Rise time	20–30 ms		Spruston et al. (1995), Walker et al. (2002)
	Decay time constant (fast)	150–250 ms	58.2 CI (calcium-impermeable), 60.8 CP (calcium-permeable)	Spruston et al. (1995), Walker et al. (2002)
	Decay time constant (slow)	~1 s	525 CP, 228 CI	Spruston et al. (1995), Walker et al. (2002)
	Channel conductance	46 pS	47 pS	Spruston et al. (1995), Walker et al. (2002)

Table 3 (continued)

Kainate			
	Amplitude (at −70 mV)	5–70 pA	Castillo et al. (1997), Mulle et al. (1998), Rebola et al. (2008)
	Rise time	6.8 ms	Castillo et al. (1997)
	Decay time constant	103 ms	Castillo et al. (1997)

AMPA Receptors

Mossy Fiber–CA3 Pyramidal Cell Synapses

Investigation of the I–V relationship of mossy fiber inputs onto CA3 pyramidal cells showed that the excitatory connection between granule cells and CA3 pyramidal cells has linear I–V relationship, indicating that these receptors are Ca^{2+}-impermeable (Jonas et al. 1993, Koh et al. 1995). Inward rectification of GluR2-lacking receptors is caused by voltage-dependent block by intracellular polyamines (Bowie and Mayer 1995, Donevan and Rogawski 1995, Kamboj et al. 1995,

Salient features of mossy fiber synapses:

- Large presynaptic terminal with several release sites
- Inputs to pyramidal cells and interneurons have distinct features
- Robust short-term and frequency facilitation
- NMDA-independent LTP
- Small amplitude, slow postsynaptic kainate responses

Koh et al. 1995). Therefore, polyamine toxins, such as Philanthotoxin (PhTx), a high-affinity agonist of currents mediated by receptors lacking the GluR2 subunit, can be used to pharmacologically differentiate between Ca^{2+}-permeable and Ca^{2+}-impermeable AMPA receptors (Blaschke et al. 1993, Washburn and Dingledine 1996). Mossy fiber evoked EPSCs are insensitive to PhTx, further supporting the idea that mossy fiber input onto CA3 pyramidal cells is exclusively mediated by GluR2-containing, Ca^{2+}-impermeable AMPA receptors (Tóth et al. 2000). However, in a recent study Ho et al. (2007) have demonstrated that while AMPA receptors at mature mossy fiber synapses are Ca^{2+}-impermeable, during the first 3 weeks of postnatal development Ca^{2+}-permeable AMPA receptors contribute to mossy fiber transmission. This transient, developmentally regulated expression of Ca^{2+}-permeable AMPA receptors could play an important role in synapse maturation and various forms of synaptic plasticity.

Unitary EPSCs have fast kinetics with latency of 2.3–4.2 ms, a 20–80% rise time of 0.6–1.7 ms, a decay time constant of 6.2–9.6 ms, and a maximal peak conductance of 1 ns (Jonas et al. 1993, Tóth et al. 2000). In these studies fast kinetics

were used as criteria to ensure that evoked events are purely originating from mossy fibers, hence potential events with slower kinetics were excluded. However, Henze et al. (1997) found large presumptive mEPSCs with significantly slower kinetics; later they also postulated that these events are monoquantal (Henze et al. 2002). The major component of these events is mediated by AMPA receptors with relatively minor contribution from NMDA and kainate receptors. The amplitude of mossy fiber EPSPs can be 2 – 10 mV, and unitary EPSCs show amplitudes up to 1 nA, these values are several fold larger than synaptic events evoked with the stimulation of small glutamatergic synapses. Large unitary EPSCs are the result of highly synchronized release from multiple release sites. The number of release sites was estimated to be between 8 and 21 in the study by Lawrence et al. (2004); in the same study using variance–mean analysis the quantal amplitude of mossy fiber events was calculated to be ~30 pA. This value is quite different from earlier estimates deriving quantal parameters from amplitude histograms (8 pA) (Jonas et al. 1993, von Kitzing et al. 1994). Interestingly, in the recordings used for variance–mean analysis, in low extracellular Ca^{2+} conditions, smaller (7–12 pA) events could also be resolved. This indicates that quantal size might show high degree of variability among various release sites and potentially help to reconcile findings of these two studies. This possibility is further supported by recent morphological data finding large variability in the size of active zones within the mossy fiber terminal (from 0.07 to 0.17 μm^2) (Rollenhagen et al. 2007). The initial release probability at mossy fiber-pyramidal cell synapses is estimated to be between 0.20 and 0.28 (Lawrence et al. 2004, von Kitzing et al. 1994). However, this low release probability is increased dramatically after repeated activation of mossy fibers; frequency-dependent facilitation can lead up to 600% increase in EPSC amplitude (Salin et al. 1996, Tóth et al. 2000). Short-term facilitation can be observed at frequencies as low as 0.1 Hz. The combination of low initial probability and pronounced short-term facilitation leads to increased spike transmission following short trains. Single action potentials initiated in the dentate granule cells in vivo rarely drive their postsynaptic targets. In contrast, high-frequency trains with short interspike intervals robustly increase spike transmission probability (Henze et al. 2002). In in vitro experiments the probability that the initial EPSP in a train elicited action potentials in CA3 pyramidal cells is only 0.28; however, this value rapidly increases to 0.76 over the course of 40 Hz stimulation (Lawrence et al. 2004).

The efficacy and timing of transmitter release is largely dependent on the spatiotemporal profile of presynaptic Ca^{2+} transients. Presynaptic Ca^{2+} channels have fast activation and deactivation kinetics, with time constants in the millisecond range, gating of these channels appears to be optimized to generate maximal Ca^{2+} influx during a minimal period of time (Bischofberger et al. 2002, Geiger and Jonas 2000). Presynaptic Ca^{2+} influx is triggered by presynaptic action potentials, the duration of these action potentials is not constant, but broadens with increased presynaptic stimuli (Geiger and Jonas 2000). While the peak amplitude of Ca^{2+} current is reduced during action potential broadening, the total charge is increased, and will eventually lead to the potentiation of EPSCs (Geiger and Jonas 2000).

Mossy fibers can follow high-frequency stimuli with high precision and efficacy; this is only possible if the terminal has large enough releasable vesicle pool. Capacitance measurements indicate that sustained Ca^{2+} inflow (30 ms, 0 V) will lead to the release of ~1,400 vesicles, this corresponds to ~40 vesicles per active zone (Hallermann et al. 2003). These measurements were closely matched with data stemming from detailed electron microscopic investigation of the mossy fiber terminal (Rollenhagen et al. 2007).

Mossy Fiber–Interneuron Synapse

While principal cells express high levels of GluR2, some GABAergic inhibitory interneurons in the hippocampus have inwardly rectifying I–V relationships and are Ca^{2+}-permeable (Geiger et al. 1995, Jonas et al. 1994, Koh et al. 1995, McBain and Dingledine 1993). Mossy fibers innervate GABAergic interneurons via synapses comprised of either Ca^{2+}-permeable or Ca^{2+}-impermeable AMPA receptors (Tóth et al. 2000,Tóth and McBain 1998). The two different types of AMPA receptors differ in their plastic properties and degree by which they colocalize with NMDA receptors.

The kinetics of mossy fiber-interneuron transmission are significantly faster than the input onto pyramidal cells. The mean 10–90% rise time of EPSCs at both types of synapses were in the submillisecond range, with the time constant for decay between 1 and 4 ms (Geiger et al. 1997, Tóth et al. 2000). Geiger et al. (1997) have suggested that the kinetics at mossy fiber–interneuron synapses are fast due to the precise timing of glutamate release and the rapid deactivation of AMPA receptors.

Anatomical and physiological data equally suggest that the mossy fiber–inter- neuron synapse comprise of a small number of release sites (1–2) (Acsády et al. 1998, Lawrence et al. 2004). Variance–mean analysis indicated that the initial release probability at these synapses is significantly higher (0.1–0.5) than at pyramidal cell synapses (Lawrence et al. 2004). High initial release probability contributes to the mild facilitation or depression observed at these synapses during brief stimulus trains (Tóth et al. 2000).

The unitary quantal amplitude at this synapse was found to be 27 pA (Lawrence et al. 2004); this value was calculated using variance–mean analysis and confirmed with recorded unitary events in the presence of strontium. The average size of the EPSCs evoked in CA3 interneurons is approximately three times smaller than EPSCs recorded from pyramidal cells (88 pA vs. 20 pA) (Lawrence et al. 2004). However, the probability that an EPSC would evoke an action potential in the postsynaptic cell is not significantly different between these cells when only a single stimulus is used. After brief trains of stimulation, however, the probability of spike transmission is greater in pyramidal cell synapses, this difference could be explained by the distinct short-term plastic properties expressed by these synapses (Fig. 3).

Properties of individual contacts between mossy fiber terminals and GABAergic cells have been elegantly investigated using mossy fiber bouton to interneuron paired recordings (Szabadics and Soltesz 2009). This study demonstrate that the amplitude and transmission probability of these synaptic interactions is largely target-cell dependent. Inputs onto fast-spiking basket cells and spiny lucidum cells

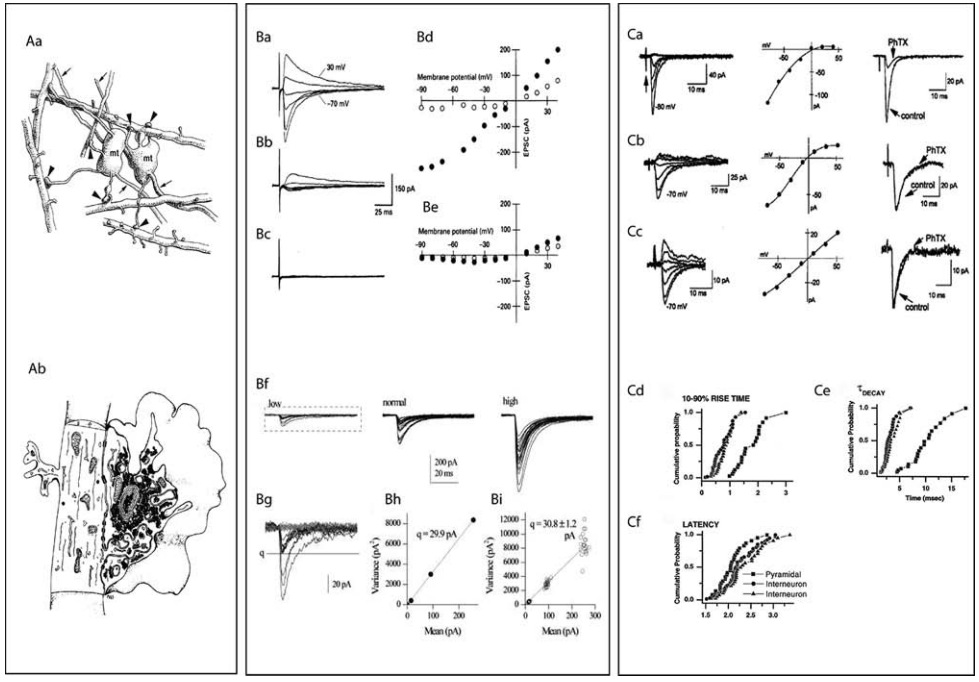

Fig. 3 Anatomical and physiological properties of mossy fiber inputs. Morphological characteristics of mossy fiber terminals, large filopodial extensions originate from the main terminal (*Aa*) (Acsády et al. 1998), boutons have several (20–30) active zones (*Ab*) (Amaral and Dent 1981). AMPA/kainate and NMDA receptor-mediated components of mossy fiber inputs (*Ba–Be*), current–voltage relationship of the peak current (*filled circles*), and the current measured 50 ms after the peak (*open circles*); *Bb* and *Be*: in the presence of CNQX; *Bc*: in the presence of CNQX and APV (Jonas et al. 1993). Variance–mean analysis is used to determine quantal parameters at the mossy fiber–CA3 pyramidal cell synapse (*Bf–Bi*) (Lawrence et al. 2004). Current–voltage relationship of mossy fiber–interneuron synapses, rectification index and philanthotoxin-sensitivity of inputs show high degree of variability (*Ca–Cc*) (Tóth and McBain 1998). Kinetic properties of mossy fiber inputs terminating on pyramidal cells and on interneurons mediated by calcium-permeable and calcium-impermeable AMPA receptors (Tóth et al. 2000)

are small in amplitude and have low transmission probabilities. In contrast, regular spiking basket cells and ivy cells receive inputs with larger amplitude and transmission probability (Szabadics and Soltesz 2009) (Table 3).

NMDA Receptors

NMDA receptors are present at mossy fiber synapses; however, mossy fiber synapses are showing lower immunostaining intensity than the Schaffer collateral inputs (Petralia et al. 1994, Takumi et al. 1999, Watanabe et al. 1998). Electrophysiological examination showed that mossy fiber synaptic inputs onto pyramidal cells are partially mediated by NMDA receptors, this component has significantly slower kinetics than those of the AMPA component (Jonas et al. 1993, Spruston et al. 1995). In a recent study, the activation of postsynaptic NMDA receptors at mossy fiber synapses was shown to influence short-term plasticity of kainate-mediated transmission (Rebola et al. 2007). NMDA receptor-mediated depression of kainate EPSC ($EPSC_{KA}$) was observed, while the AMPA component of the event was not modified, this effect was expressed postsynaptically and was homosynaptic. Unlike in the CA1 area of the hippocampus, mossy fiber LTP is independent of NMDA receptor activation. However, NMDA receptor-mediated synaptic currents at this site are potentiated by high-frequency stimuli (Kwon and Castillo 2008, Rebola et al. 2007).

At mossy fiber–interneuron synapses the distribution of different subtypes of NMDA receptors and different subtypes of AMPA receptors is highly correlated. Ca^{2+}-permeable AMPA receptors occur at synapses where NMDA receptors contain the NR2B subunit, while Ca^{2+}-impermeable AMPA receptors are associated with NR2B-lacking NMDA receptors (Lei and McBain 2002). This particular distribution pattern leads to Ca^{2+}-permeable synapses possessing smaller NMDA components with slower decay kinetics (Lei and McBain 2002) (Table 3).

Kainate Receptor

Kainate receptors are located on both the pre- and postsynaptic site at hippocampal mossy fibers. While on the postsynaptic site they generate small but prolonged depolarizations, the presynaptic receptors modulate excitatory and inhibitory synaptic transmission.

Postsynaptic Receptors

Kainate-mediated postsynaptic responses were first demonstrated at mossy fiber synapses (Castillo et al. 1997, Vignes and Collingridge 1997). Kainate-mediated component of the mossy fiber responses to a single stimuli is very small, with an amplitude $\sim$10 times smaller than the AMPA component. However, it largely increases on repetitive stimulation of the mossy fibers. Short high-frequency trains lead to several fold increase in kainate responses, but even a moderate increase in presynaptic stimuli (from 0.05 to 0.2 Hz) could almost double the amplitude of the $EPSC_{KA}$ (Castillo et al. 1997). Postsynaptic kainate responses are selectively present at mossy fiber inputs in CA3 pyramidal cells and are absent from the com-

missural/associational inputs. The mossy fiber $EPSC_{KA}$ has very slow decay kinetics with the time constant approximately 10 times slower than that of the AMPA component (~100 vs. ~10 ms); the rise time (10–90%) of the kainate response is also significantly slower than the AMPA EPSC (7 vs. 3 ms). The slow kinetics of the kainate responses could potentially indicate that these receptors are located extrasynaptically, in this case they would not be able to respond to quantal release of glutamate. This question was addressed by Cossart et al. (Cossart et al. 2002); their data indicated that kainate receptors are activated by quantal release of glutamate at mossy fiber synapses, as they were able to record pure kainate and mixed AMPA/kainate miniature responses from CA3 pyramidal cells. Frequency analysis showed that 45% of the miniature events involved kainate receptors. Morphological data indicating that kainate receptors are localized in synaptic densities (Darstein et al. 2003, Petralia et al. 1994) and the lack of effect of glutamate uptake blockers on the kinetics of kainate responses further strengthened the conclusion that the slow kinetics of $EPSC_{KA}$ are not caused by extrasynaptical localization of these receptors. Recent study by Barberis et al. (2008) rather indicates that slow decay kinetics can be explained by the intrinsic gating properties of GluR6/KA2 heteromeric receptors. In fact, studies using knockout animals suggest that kainate receptors on CA3 pyramidal cells are composed of these two subunits (GluR6 and KA2) (Contractor et al. 2003, Mulle et al. 1998).

The slow kinetics and small amplitude of kainate reposes suggest that they might play a role in frequency-dependent synaptic integration (Frerking and Ohliger-Frerking 2002). However, short-term and long-term plasticity of $EPSC_{KA}$ is attenuated compared to the AMPA component, hence endowing the AMPA component with a wider dynamic range and limiting the contribution of kainate receptors in the presence of profound increase in presynaptic strength (Ito et al. 2004) (Table 3).

Presynaptic Receptors

Endogenously applied kainate has a biphasic effect, low doses facilitate mossy fiber transmission, while higher doses depress EPSCs. Endogenous kainate released following the repetitive stimulation of mossy fibers activates presynaptic receptors and facilitates release (Contractor et al. 2001, Lauri et al. 2001, Schmitz et al. 2000). Enhancement of release via presynaptic kainate receptors was shown to contribute to the robust frequency facilitation observed in mossy fibers (Contractor et al. 2001, 2003, Lauri et al. 2001, Pinheiro et al. 2007, Schmitz et al. 2001, 2003). Presynaptic kainate receptors contributing to frequency facilitation are thought to be calcium-permeable as indicated by their sensitivity to philanthotoxin; Ca^{2+} influx through these receptors is believed to play a crucial role in frequency facilitation (Lauri et al. 2001). The apparent calcium-permeability of the receptors can only be explained by the presence of unedited forms of kainate receptor subunits; however, the mechanism by which these subunits are preferentially inserted into mossy fibers is still unknown. The subunit composition of presynaptic kainate receptors has been a matter of debate, initially the GluR5 subunit was believed to be involved in the presynaptic kainate effect (Lauri et al. 2001); however, these data obtained with pharmacological tools could not be confirmed with the genetic

ablation of the GluR5 subunit (Contractor et al. 2001) or in subsequent experiments (Breustedt and Schmitz 2004). In KA2 and Glur7 knockout animals frequency facilitation was compromised, pointing to the critical role these subunits play in the short-term plasticity (Contractor et al. 2003, Pinheiro et al. 2007) (Fig. 4).

Even though a large body of literature is dedicated to the existence and exact functional role of presynaptic kainate receptors at the mossy fibers, a recent publication by Kwon and Castillo (Neuron, 2009) questions the existence of presynaptic receptors. The authors using GluR5-specific agonist and GluR6 and GluR7 knockout animals found that presynaptic kainate receptors are not playing a significant role in short-term plasticity; they postulate that the effects generally attributed to presynaptic kainate receptors are mediated by postsynaptic receptors and the activation of recurrent CA3 network activity.

Metabotropic Glutamate Receptors

Presynaptic mossy fiber terminals contain two types of metabotropic glutamate receptors. While Group II mGluRs are equally present on synapses opposing pyramidal cells and interneurons (Kamiya et al. 1996, Tóth and McBain 2000), mGluR7 is selectively present in synapses terminating on interneurons. Group II mGluRs depress excitatory transmission at both types of synapses; interestingly mossy fiber-CA3 pyramidal cell synapses can be blocked completely with the Group II mGluR agonist DCG-IV, synaptic inputs onto interneurons are only partially depressed. mGluRs decrease the degree of frequency facilitation observed at mossy fiber–pyramidal cell and mossy fiber–interneuron synapses(Scanziani et al. 1997, Tóth et al. 2000). Group III metabotropic glutamate receptor7 (mGluR7) has low affinity for glutamate and its activation depresses glutamatergic synaptic responses (O'Connor et al. 1999). In the mossy fiber–interneuron synapses mGluR7 antagonist MSOP did not influence baseline transmission but prevented high-frequency-induced long-term depression, while application of an mGluR7 agonist led to the development of a chemical LTD at this synapse (Pelkey et al. 2005). Detailed investigation of the plastic properties of this synapse led to the discovery that mGluR7 goes through activity-dependent internalization and surface expression (Pelkey et al. 2005, 2007), contributing to state-dependent plasticity.

On the postsynaptic site, activation of Group I receptors can evoke a postsynaptic potential which is independent of the G protein function (Heuss et al. 1999), while inhibiting I_{AHP} through a G protein-coupled mechanism. Their activation also leads to Ca^{2+} release from intracellular stores, which plays a role in plastic changes (Yeckel et al. 1999).

Schaffer Collaterals

The major input of the CA1 area of the hippocampus arrives from CA3 pyramidal cells via the Schaffer collaterals. Axons of CA3 pyramidal cells heavily

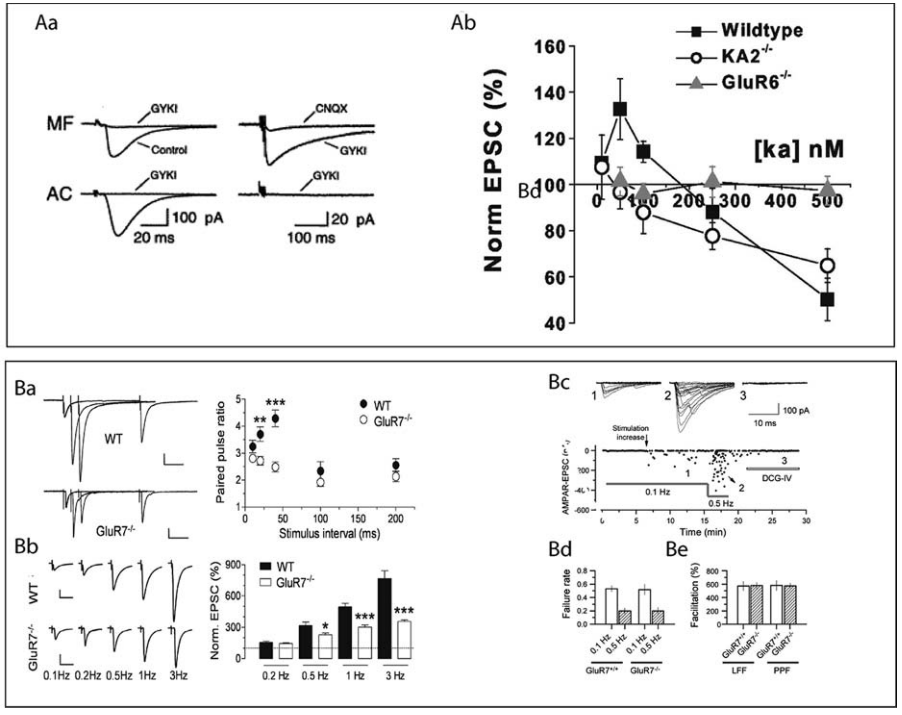

Fig. 4 Properties of kainate neurotransmission at the hippocampal mossy fibers. Kainate-mediated responses (not blocked by GYKI 53655) evoked with repetitive stimulation of the mossy fibers (MF) and are not present at associational/commissural (AC) inputs (*Aa*) (Castillo et al. 1997). Concentration-dependent, bidirectional modulation of mossy fiber EPSCs by kainate, $KA2^{-/-}$ and $GluR6^{-/-}$ mice shows altered kainate modulation (*Ab*) (Contractor et al. 2003). Controversy surrounding the role of presynaptic kainate receptors in short-term plasticity of mossy fiber inputs; AMPA receptor-mediated EPSCs from GluR7 –/– mice were shown to be less facilitated by high-frequency stimuli (*Ba, Bb*) (Pinheiro et al. 2007) and having similar properties than their wild-type counterparts (*Bc–Be*) (Kwon and Castillo 2008)

innervate both the stratum radiatum and the stratum oriens of the CA1 area; proximal postsynaptic dendrites in these layers contain relatively few spines, while distal dendrites are densely spiny, excitatory inputs terminate exclusively on dendritic spines (Megías et al. 2001). A single CA3 pyramidal cell has extensive axonal arbor and can extend to as much as two-thirds of the hippocampus and form 30,000–60,000 synapses (Li et al. 1994), while a single CA1 pyramidal cell receives approximately 30,000 excitatory synapses. The physiological properties of Schaffer-collateral inputs to pyramidal cells are summarized in Table 4.

Salient features of Schaffer collateral synapses:

- Small terminals with single release site, variable release probability
- Increased synaptic AMPA, but not NMDA conductances at distal synapses
- Silent synapses
- Kainate receptor activation depresses glutamate transmission

---

AMPA Receptors

Excitatory synaptic inputs are broadly distributed along the dendritic tree of CA1 pyramidal cells, these inputs are integrated at the level of the axon initial segment to determine the output signal of the cell. The distance between the location of the final integration of the cellular outputs and synaptic inputs shows high degree of variety. How does the distance between the soma and the synapse influence the characteristics of synaptic inputs at the level of the soma? In principle, the further the synapse is, the more and more diminished the impact on the final inputs should be due to cable filtering. Interestingly, EPSP amplitude increases with distance from the soma, this leads to proximal and distal synaptic inputs with very similar amplitudes detected at the soma (Magee and Cook 2000). Dendritic filtering is not counterbalanced by active membrane properties, these had only very minor effects on the somatic amplitude of EPSPs; it is rather overcome by the progressively increasing synaptic conductances along the dendritic tree of CA1 pyramidal cells (Magee and Cook 2000). Increased synaptic conductance in distal synapses was attributed to increased AMPA receptor number on the postsynaptic sites, while AMPA receptor subunit composition and channel modulation were indistinguishable at proximal and distal synapses (Andrasfalvy and Magee 2001). Presynaptic properties, such as release probability, paired-pulse facilitation, and the size of the readily releasable pool were also identical at these sites (Smith et al. 2003) (Fig. 5).

Excitatory synaptic potentials evoked by the stimulation of the Schaffer collaterals composed of AMPA and NMDA components; however, under certain circumstances EPSCs lack the AMPA component (Isaac et al. 2007, Kullmann 1994, Liao et al. 1995). The subpopulation of glutamatergic synapses lacking functional AMPA receptors are referred to as “silent synapses,” these synapses are not con-

Table 4 Kinetic properties of Schaffer collateral inputs terminating on proximal and distal dendrites of CA1 pyramidal cells

Quantal parameters				
	Release probability	<0.5		Enoki et al. (2009), Raastad and Lipowski (1996), Rosenmund et al. (1993)
	Quantal amplitude	~3 pA, 66–400 μV		Enoki et al. (2009), Larkman et al. (1997), Tyler et al. (2006)
AMPA receptors		soma	dendrite	
	EPSP amplitude (locally)	~0.2 mV	~0.6 mV	Larkman et al. (1997), Magee and Cook (2000)
	EPSC amplitude (locally)	~8 pA	~24 pA	Magee and Cook (2000)
	EPSC amplitude (measured at the soma)	~0.2 mV	~0.2 mV	Magee and Cook (2000)
	20–80% rise time	0.4–0.6 ms	0.4–0.6 ms	Andrasfalvy and Magee (2001)
	10–90% rise time	0.7–3.5 ms	0.7 ms	Larkman et al. (1997), Magee and Cook (2000)
	Decay time const.	~3.5 ms	~2.5 ms	Andrasfalvy (2001)
	Maximum open probability	~0.8	~0.8	Andrasfalvy and Magee (2001)
	Channel number (calculated using variance–mean analysis)	~450	~1,000	Andrasfalvy and Magee (2001)
	Latency	2–3 ms		Larkman et al. (1997)
	Single channel conductance (γ)	~8–10 pS	10 pS	Andrasfalvy and Magee (2001), Benke et al. (1998)
NMDA				
	EPSC amplitude (excised patches, 10 ms, 1 m mGlu)	~70 pA	~ 50 pA	Andrasfalvy (2001)
	20–80% rise time	~9 ms	~9 ms	Andrasfalvy and Magee (2001), Perouansky and Yaari (1993)
	Decay time constant tau 1	~250 ms	~250 ms	Andrasfalvy and Magee (2001), Perouansky and Yaari (1993)
	Decay time constant tau 2	~1.5 s	~1.5 s	Andrasfalvy and Magee (2001)
	Single channel conductance	45 ps		Spruston et al. (1995)

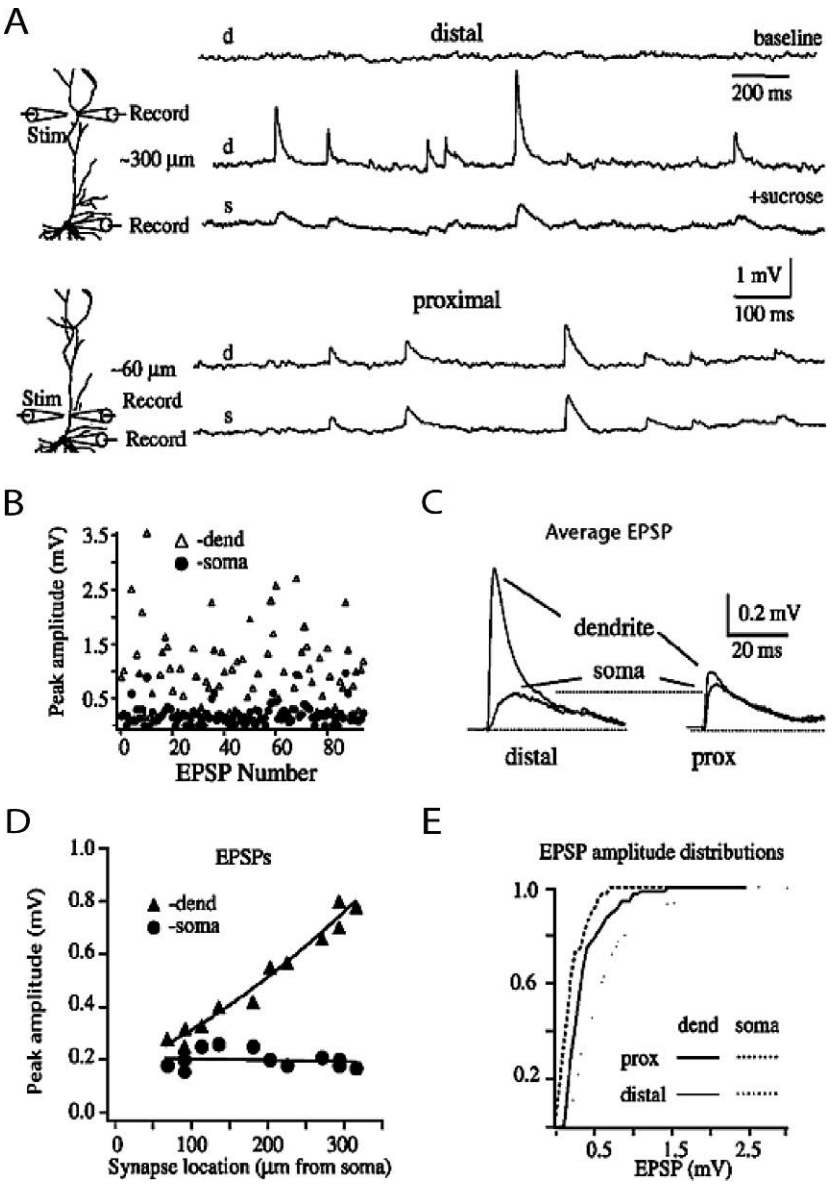

Fig. 5 The amplitude of synaptically evoked EPSP at the soma does not depend on synapse location (Magee and Cook 2000)

ducting current at resting membrane potentials. The presence of these receptors is developmentally regulated, during the first few postnatal days, almost all Schaffer collateral synapses are silent, but by the end of the third week approximately 50% of them contain functional AMPA receptors (Durand et al. 1996). Activity-

dependent modification at these synapses, such as the expression of LTP, leads to the changes which "unsilence" these synapses. How do these synapses become functional? Incorporation of AMPA receptors into silent synapse following high-frequency stimulation has been observed either though lateral diffusion (Adesnik et al. 2005) or from AMPA receptor-containing endosomes (Hayashi et al. 2000, Park et al. 2004, Shi et al. 1999). However, recent data using optical imaging suggest that AMPA receptor insertion has little influence on synaptic plasticity, the authors rather suggest that LTP is expressed on the presynaptic site in a bidirectional, graded fashion (Enoki et al. 2009).

Majority of Schaffer collateral synapses contain one active zone with several docked vesicles (Harris and Sultan 1995, Schikorski and Stevens 1997). The probability of release at various release sites arising from the same axons is highly variable (Rosenmund et al. 1993). With increased release probability more glutamate is released to the synaptic cleft; this is possible when more than one vesicle fuses with the presynaptic membrane in response to a single action potential. The probability of multivesicular release increases with release probability (Oertner et al. 2002). Multivesicular release is likely to occur at synapses with higher number of docked vesicles, which is generally observed in larger synapses (Harris and Sultan 1995) (Table 4).

NMDA Receptors

NMDA receptors are abundantly present at excitatory synapses in the CA1 region of the hippocampus, and the number of NMDA receptors in individual synapses shows very little variability (Petralia et al. 1994, Racca et al. 2000). The number of NMDA receptors activated by synaptic stimulation is small, only 1–5 NMDA channels open during synaptic transmission at low frequencies, this value is small enough to render quantal dendritic NMDA responses undetectable at the soma by physiological measurements (Nimchinsky et al. 2004). In contrast to AMPA receptors, the number of NMDA receptors expressed at synapses does not show activity-dependent changes.

Furthermore, dendritic NMDA currents do not change with distance from the soma, their kinetics and quantal parameters are very similar in proximal and distal dendrites (Andrasfalvy and Magee 2001).

NMDA receptors are activated when membrane potential depolarization removes Mg^{2+} block from the channel and when glutamate binds to the receptor. These features make NMDA receptors ideal coincidence detectors, signaling simultaneous pre- and postsynaptic activity with Ca^{2+} influx (Table 4).

Kainate Receptors

Kainate receptor activation in the CA1 region leads to the depression of glutamatergic transmission (Chittajallu et al. 1996, Frerking et al. 2001, Kamiya and Ozawa 1998, Vignes et al. 1998). Several mechanisms were suggested to explain this effect: direct action via presynaptic receptors, indirect action via somato-dendritic kainate receptors; also both ionotropic and metabotropic modes of action were

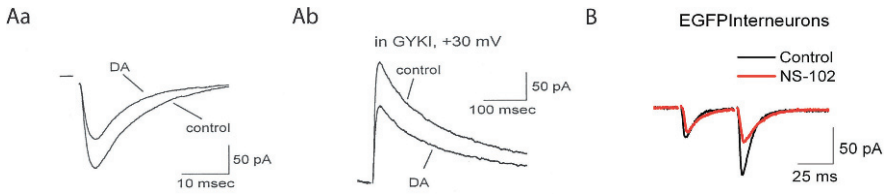

Fig. 6 Kainate responses in the CA1 area of the hippocampus. Kainate activation depresses AMPA (*Aa*) and NMDA (*Ab*) receptor-mediated events at the Schaffer collateral synapses (Frerking et al. 2001) Kainate receptor-specific antagonist reduces facilitation at inputs onto somatostatin-positive interneurons (Sun et al. 2006)

postulated. Kainate agonist depresses glutamatergic transmission via a decrease in quantal content; in agreement with this finding, little or no evidence of postsynaptic modulation was observed. Rather, the experimental data indicate that kainate receptors are directly activated on the presynaptic terminal and are coupled to G proteins (Frerking et al. 2001) (Fig. 6).

Besides the direct action on pyramidal cells, kainate receptors are also involved in the modulation of network activity via the regulation of inhibitory neurons and their synaptic inputs. Dendritic kainate receptor activation results in the increased activity of inhibitory neurons which provide increased inhibitory input onto pyramidal cells. This postsynaptic effect is mediated by GluR5 subunit-containing receptors (Cossart et al. 1998). Excitatory input onto somatostatin-containing interneurons shows unusually robust short-term facilitation; activation of presynaptic kainate receptors contribute to this effect, enabling a target cell-specific mechanism leading to the preferential activation of a subset of interneurons following repeated stimuli (Sun and Dobrunz 2006). This effect is mediated by GluR5 and GluR6 subunit-containing, calcium-permeable kainate receptors (Sun et al. 2008) (Fig. 6). Finally, GABAergic neurotransmission is also regulated by presynaptic kainate receptors. This action mostly effects inhibitory connections between interneurons and may serve to enhance interneuron–interneuron interactions (Cossart et al. 2001) (Table 4).

Metabotropic Glutamate Receptors

Metabotropic receptors have diverse effects in the CA1 area of the hippocampus, they directly excite pyramidal cells (Gereau and Conn 1995) and interneurons (McBain et al. 1994), they decrease excitatory and inhibitory synaptic transmission, and they influence long-term plasticity (Bortolotto et al. 1999, Topolnik et al. 2006). Direct excitation of pyramidal cells and interneurons is mainly mediated by Group I metabotropic receptors localized postsynaptically on the somato-dendritic membrane (Gereau and Conn 1995, McBain et al. 1994). In interneurons located in the stratum oriens/alveus, activation of mGluR1α leads to Ca^{2+} signals resulting from Ca^{2+} influx through voltage-gated channels and Ca^{2+} release from intracellular stores. Dendritic Ca^{2+} transients resulting from mGluR5 activation are solely

mediated by intracellular Ca^{2+} release. Furthermore, long-term plasticity at oriens/alveus interneurons is influenced by mGluR1- and mGluR5-specific signaling (Le Vasseur et al. 2008, Topolnik et al. 2006).

Glutamate release is suppressed by Group I and Group III metabotropic receptors at Schaffer collateral synapses (Gereau and Conn 1995), while the selective Group II receptors antagonist DCG-IV does not have influence on excitatory neurotransmission (Kamiya et al. 1996). Both Group I and Group III metabotropic receptors are localized presynaptically as evidenced by the effect observed on mEPSC frequency and paired-pulse facilitation (Gereau and Conn 1995), but the two receptors are regulating glutamatergic neurotransmission through different mechanisms. Group II metabotropic receptors are only expressed in granule cells in the adult hippocampus (Tanabe et al. 1992, 1993); however, activation of Group II mGluRs was shown to influence glutamatergic transmission, this effect is mediated by mGluR3 receptors expressed on glia cells (Winder et al. 1996).

The amplitude of GABA-mediated synaptic events is also reduced by Group I mGluR agonist; however, this effect can effectively be blocked by the pre-application of CB1 receptor antagonist indicating that mGluR1/5 receptors are not situated directly at the inhibitory presynaptic terminals (Neu et al. 2007). Group III mGluRs are known to present at GABAergic presynaptic terminals (Shigemoto et al. 1997); activation of these receptors leads to decreased inhibitory transmission among GABAergic cells. These receptors are likely to sense glutamate spillover from neighboring excitatory afferent terminals (Semyanov and Kullmann 2000).

Experimental Techniques

The key techniques used for the investigation of glutamatergic signals are intracellular recordings and patch-clamp recordings. These experimental approaches are described in detail in the chapter “Physiological Properties of Hippocampal Neurons” (Marco Martina). Synaptic inputs are evoked with either electric or osmotic stimuli. Alternatively, glutamate can be applied to the tissue in the bath or by using a more focal pressure injection. With the latter approach synapses on a specific subcellular element can selectively be activated (i.e., dendrite vs. soma). With the development of caged compounds, particular synapses can be activated at even higher spatial resolution. Activation of selected subpopulation of synapses or limited number of synapses can be challenging in in vitro slices, given the complex network connections in the tissue. Under these circumstances, paired recordings can be used to identify synaptic contacts between individual cells where both the presynaptic and the postsynaptic elements can be anatomically identified. Recordings from synaptically connected neuron pairs are harder when the pre- and postsynaptic cells are relatively far away from each other, as the probability of functional connections decreases with distance. In these cases, direct stimulation of presynaptic terminals could provide information about individual synaptic contacts. This is only possible when the presynaptic terminal is large, like the mossy fiber boutons. Currently, stimulation of small individual presynaptic terminals is not possible in in vitro slices, but

with the development of biophotonic approaches soon we might be able to achieve this goal.

The Future

Investigation of the functional role of various types of receptors is made possible by pharmacological and genetic tools; ablation of certain types of receptors allows us to determine their role in synaptic functions and network activity. Both of these techniques will eliminate sensitive receptors from every unit of the network; with the development of new genetic targeting strategies we will be able to investigate the role of certain types of receptors on specific components of the network. For example, instead of asking how calcium-permeable AMPA receptors contribute to the control of pyramidal cell firing or information integration, we can ask how calcium-permeable AMPA receptors expressed by a subset of interneurons contribute to these processes. Similarly, with the development of imaging and genetic techniques, synaptic inputs onto specific subset of cells can be studied in isolation and target cell specificity of various inputs established.

Our current knowledge about synaptic interactions is mainly based on the interaction of limited number of players in the network. Imaging techniques with high temporal and spatial resolution allow the simultaneous investigation of large population of cells. The usage of this technique in combination with modeling strategies will help to better understand the role a certain type of synapse plays at the network level in the control of input/output properties of large populations of neurons.

Further Reading

Acsády, L., Kamondi, A., Sík, A., Freund, T. and Buzsáki, G. GABAergic cells are the major postsynaptic targets of mossy fibers in the rat hippocampus. *J Neurosci* **18,** 3386–3403 (1998).

Adesnik, H., Nicoll, R. A. and England, P. M. Photoinactivation of native AMPA receptors reveals their real-time trafficking. *Neuron* **48,** 977–985 (2005).

Amaral, D. G. and Dent, J. A. Development of the mossy fibers of the dentate gyrus: I. A light and electron microscopic study of the mossy fibers and their expansions. *J Comp Neurol* **195,** 51–86 (1981).

Amaral, D. G. and Witter, M. P. The three-dimensional organization of the hippocampal formation: a review of anatomical data. *Neuroscience* **31,** 571–591 (1989).

Amaral, D. G., Ishizuka, N. and Claiborne, B. Neurons, numbers and the hippocampal network. *Prog Brain Res* **83,** 1–11 (1990).

Andrasfalvy, B. K. and Magee, J. C. Distance-dependent increase in AMPA receptor number in the dendrites of adult hippocampal CA1 pyramidal neurons. *J Neurosci* **21,** 9151–9159 (2001).

Arrigoni, E. and Greene, R. W. Schaffer collateral and perforant path inputs activate different subtypes of NMDA receptors on the same CA1 pyramidal cell. *Br J Pharmacol* **142,** 317–322 (2004).

Barberis, A., Sachidhanandam, S. and Mulle, C. GluR6/KA2 kainate receptors mediate slow-deactivating currents. *J Neurosci* **28,** 6402–6406 (2008).

Benke, T. A., Lüthi, A., Isaac, J. T. and Collingridge, G. L. Modulation of AMPA receptor unitary conductance by synaptic activity. *Nature* **393,** 793–797 (1998).

Berzhanskaya, J., Urban, N. N. and Barrionuevo, G. Electrophysiological and pharmacological characterization of the direct perforant path input to hippocampal area CA3. *J Neurophysiol* **79,** 2111–2118 (1998).

Bischofberger, J., Geiger, J. R. and Jonas, P. Timing and efficacy of Ca2+ channel activation in hippocampal mossy fiber boutons. *J Neurosci* **22,** 10593–10602 (2002).

Blaschke, M., Keller, B. U., Rivosecchi, R., Hollmann, M., et al. A single amino acid determines the subunit-specific spider toxin block of alpha-amino-3-hydroxy-5-methylisoxazole-4-propionate/kainate receptor channels. *Proc Natl Acad Sci USA* **90,** 6528–6532 (1993).

Bortolotto, Z. A., Fitzjohn, S. M. and Collingridge, G. L. Roles of metabotropic glutamate receptors in LTP and LTD in the hippocampus. *Curr Opin Neurobiol* **9,** 299–304 (1999).

Bowie, D. and Mayer, M. L. Inward rectification of both AMPA and kainate subtype glutamate receptors generated by polyamine-mediated ion channel block. *Neuron* **15,** 453–462 (1995).

Breustedt, J. and Schmitz, D. Assessing the role of GLUK5 and GLUK6 at hippocampal mossy fiber synapses. *J Neurosci* **24,** 10093–10098 (2004).

Calixto, E., Galván, E. J., Card, J. P. and Barrionuevo, G. Coincidence detection of convergent perforant path and mossy fibre inputs by CA3 interneurons. *J Physiol* **586,** 2695–2712 (2008).

Capogna, M. Distinct properties of presynaptic group II and III metabotropic glutamate receptor-mediated inhibition of perforant pathway-CA1 EPSCs. *Eur J Neurosci* **19,** 2847–2858 (2004).

Castillo, P. E., Malenka, R. C. and Nicoll, R. A. Kainate receptors mediate a slow postsynaptic current in hippocampal CA3 neurons. *Nature* **388,** 182–186 (1997).

Chicurel, M. E. and Harris, K. M. Three-dimensional analysis of the structure and composition of CA3 branched dendritic spines and their synaptic relationships with mossy fiber boutons in the rat hippocampus. *J Comp Neurol* **325,** 169–182 (1992).

Chittajallu, R., Vignes, M., Dev, K. K., Barnes, J. M., et al. Regulation of glutamate release by presynaptic kainate receptors in the hippocampus. *Nature* **379,** 78–81 (1996).

Chiu, C. Q. and Castillo, P. E. Input-specific plasticity at excitatory synapses mediated by endocannabinoids in the dentate gyrus. *Neuropharmacology* **54,** 68–78 (2008).

Colbert, C. M. and Levy, W. B. Electrophysiological and pharmacological characterization of perforant path synapses in CA1: mediation by glutamate receptors. *J Neurophysiol* **68,** 1–8 (1992).

Contractor, A., Swanson, G. and Heinemann, S. F. Kainate receptors are involved in short- and long-term plasticity at mossy fiber synapses in the hippocampus. *Neuron* **29,** 209–216 (2001).

Contractor, A., Sailer, A. W., Darstein, M., Maron, C., et al. Loss of kainate receptor-mediated heterosynaptic facilitation of mossy-fiber synapses in KA2–/– mice. *J Neurosci* **23,** 422–429 (2003).

Cossart, R., Esclapez, M., Hirsch, J. C., Bernard, C. and Ben-Ari, Y. GluR5 kainate receptor activation in interneurons increases tonic inhibition of pyramidal cells. *Nat Neurosci* **1,** 470–478 (1998).

Cossart, R., Tyzio, R., Dinocourt, C., Esclapez, M., et al. Presynaptic kainate receptors that enhance the release of GABA on CA1 hippocampal interneurons. *Neuron* **29,** 497–508 (2001).

Cossart, R., Epsztein, J., Tyzio, R., Becq, H., et al. Quantal release of glutamate generates pure kainate and mixed AMPA/kainate EPSCs in hippocampal neurons. *Neuron* **35,** 147–159 (2002).

Dahl, D. and Sarvey, J. M. Norepinephrine induces pathway-specific long-lasting potentiation and depression in the hippocampal dentate gyrus. *Proc Natl Acad Sci USA* **86,** 4776–4780 (1989).

Darstein, M., Petralia, R. S., Swanson, G. T., Wenthold, R. J. and Heinemann, S. F. Distribution of kainate receptor subunits at hippocampal mossy fiber synapses. *J Neurosci* **23,** 8013–8019 (2003).

Dingledine, R., Borges, K., Bowie, D. and Traynelis, S. F. The glutamate receptor ion channels. *Pharmacol Rev* **51,** 7–61 (1999).

Donevan, S. D. and Rogawski, M. A. Intracellular polyamines mediate inward rectification of Ca(2+)-permeable alpha-amino-3-hydroxy-5-methyl-4-isoxazolepropionic acid receptors. *Proc Natl Acad Sci USA* **92,** 9298–9302 (1995).

Durand, G. M., Kovalchuk, Y. and Konnerth, A. Long-term potentiation and functional synapse induction in developing hippocampus. *Nature* **381,** 71–75 (1996).

Empson, R. M. and Heinemann, U. Perforant path connections to area CA1 are predominantly inhibitory in the rat hippocampal-entorhinal cortex combined slice preparation. *Hippocampus* **5,** 104–107 (1995).

Empson, R. M. and Heinemann, U. The perforant path projection to hippocampal area CA1 in the rat hippocampal-entorhinal cortex combined slice. *J Physiol* **484 (Pt 3),** 707–720 (1995).

Enoki, R., Hu, Y., Hamilton, D. and Fine, A. Expression of long-term plasticity at individual synapses in the hippocampus is graded, bidirectional, and mainly presynaptic: optical quantal analysis. *Neuron* **62,** 242–253 (2009).

Frerking, M., Schmitz, D., Zhou, Q., Johansen, J. and Nicoll, R. A. Kainate receptors depress excitatory synaptic transmission at CA3–>CA1 synapses in the hippocampus via a direct presynaptic action. *J Neurosci* **21,** 2958–2966 (2001).

Frerking, M. and Ohliger-Frerking, P. AMPA receptors and kainate receptors encode different features of afferent activity. *J Neurosci* **22,** 7434–7443 (2002).

Geiger, J. R., Melcher, T., Koh, D. S., Sakmann, B., et al. Relative abundance of subunit mRNAs determines gating and Ca2+ permeability of AMPA receptors in principal neurons and interneurons in rat CNS. *Neuron* **15,** 193–204 (1995).

Geiger, J. R., Lübke, J., Roth, A., Frotscher, M. and Jonas, P. Submillisecond AMPA receptor-mediated signaling at a principal neuron-interneuron synapse. *Neuron* **18,** 1009–1023 (1997).

Geiger, J. R. and Jonas, P. Dynamic control of presynaptic Ca(2+) inflow by fast-inactivating K(+) channels in hippocampal mossy fiber boutons. *Neuron* **28,** 927–939 (2000).

Gereau, R. W. and Conn, P. J. Multiple presynaptic metabotropic glutamate receptors modulate excitatory and inhibitory synaptic transmission in hippocampal area CA1. *J Neurosci* **15,** 6879–6889 (1995).

Hallermann, S., Pawlu, C., Jonas, P. and Heckmann, M. A large pool of releasable vesicles in a cortical glutamatergic synapse. *Proc Natl Acad Sci USA* **100,** 8975–8980 (2003).

Han, Z. S., Buhl, E. H., Lörinczi, Z. and Somogyi, P. A high degree of spatial selectivity in the axonal and dendritic domains of physiologically identified local-circuit neurons in the dentate gyrus of the rat hippocampus. *Eur J Neurosci* **5,** 395–410 (1993).

Harris, K. M. and Sultan, P. Variation in the number, location and size of synaptic vesicles provides an anatomical basis for the nonuniform probability of release at hippocampal CA1 synapses. *Neuropharmacology* **34,** 1387–1395 (1995).

Hayashi, Y., Shi, S. H., Esteban, J. A., Piccini, A., et al. Driving AMPA receptors into synapses by LTP and CaMKII: requirement for GluR1 and PDZ domain interaction. *Science* **287,** 2262–2267 (2000).

Henze, D. A., Card, J. P., Barrionuevo, G. and Ben-Ari, Y. Large amplitude miniature excitatory postsynaptic currents in hippocampal CA3 pyramidal neurons are of mossy fiber origin. *J Neurophysiol* **77,** 1075–1086 (1997).

Henze, D. A., McMahon, D. B., Harris, K. M. and Barrionuevo, G. Giant miniature EPSCs at the hippocampal mossy fiber to CA3 pyramidal cell synapse are monoquantal. *J Neurophysiol* **87,** 15–29 (2002).

Henze, D. A., Wittner, L. and Buzsáki, G. Single granule cells reliably discharge targets in the hippocampal CA3 network in vivo. *Nat Neurosci* **5,** 790–795 (2002).

Heuss, C., Scanziani, M., Gähwiler, B. H. and Gerber, U. G-protein-independent signaling mediated by metabotropic glutamate receptors. *Nat Neurosci* **2,** 1070–1077 (1999).

Ho, M. T., Pelkey, K. A., Topolnik, L., Petralia, R. S., et al. Developmental expression of Ca2+-permeable AMPA receptors underlies depolarization-induced long-term depression at mossy fiber CA3 pyramid synapses. *J Neurosci* **27,** 11651–11662 (2007).

Isaac, J. T., Ashby, M. and McBain, C. J. The role of the GluR2 subunit in AMPA receptor function and synaptic plasticity. *Neuron* **54,** 859–871 (2007).

Ito, K., Contractor, A. and Swanson, G. T. Attenuated plasticity of postsynaptic kainate receptors in hippocampal CA3 pyramidal neurons. *J Neurosci* **24,** 6228–6236 (2004).

Jarsky, T., Roxin, A., Kath, W. L. and Spruston, N. Conditional dendritic spike propagation following distal synaptic activation of hippocampal CA1 pyramidal neurons. *Nat Neurosci* **8,** 1667–1676 (2005).

Jonas, P., Major, G. and Sakmann, B. Quantal components of unitary EPSCs at the mossy fibre synapse on CA3 pyramidal cells of rat hippocampus. *J Physiol* **472,** 615–663 (1993).

Jonas, P., Racca, C., Sakmann, B., Seeburg, P. H. and Monyer, H. Differences in Ca2+ permeability of AMPA-type glutamate receptor channels in neocortical neurons caused by differential GluR-B subunit expression. *Neuron* **12,** 1281–1289 (1994).

Kahle, J. S. and Cotman, C. W. Carbachol depresses synaptic responses in the medial but not the lateral perforant path. *Brain Res* **482,** 159–163 (1989).

Kamboj, S. K., Swanson, G. T. and Cull-Candy, S. G. Intracellular spermine confers rectification on rat calcium-permeable AMPA and kainate receptors. *J Physiol* **486 (Pt 2),** 297–303 (1995).

Kamiya, H., Shinozaki, H. and Yamamoto, C. Activation of metabotropic glutamate receptor type 2/3 suppresses transmission at rat hippocampal mossy fibre synapses. *J Physiol* **493 (Pt 2),** 447–455 (1996).

Kamiya, H. and Ozawa, S. Kainate receptor-mediated inhibition of presynaptic Ca2+ influx and EPSP in area CA1 of the rat hippocampus. *J Physiol* **509 (Pt 3),** 833–845 (1998).

Kilbride, J., Rush, A. M., Rowan, M. J. and Anwyl, R. Presynaptic group II mGluR inhibition of short-term depression in the medial perforant path of the dentate gyrus in vitro. *J Neurophysiol* **85,** 2509–2515 (2001).

Koh, D. S., Burnashev, N. and Jonas, P. Block of native Ca(2+)-permeable AMPA receptors in rat brain by intracellular polyamines generates double rectification. *J Physiol* **486 (Pt 2),** 305–312 (1995).

Kullmann, D. M. Amplitude fluctuations of dual-component EPSCs in hippocampal pyramidal cells: implications for long-term potentiation. *Neuron* **12,** 1111–1120 (1994).

Kwon, H. B. and Castillo, P. E. Long-term potentiation selectively expressed by NMDA receptors at hippocampal mossy fiber synapses. *Neuron* **57,** 108–120 (2008).

Kwon, H. B. and Castillo, P. E. Role of glutamate autoreceptors at hippocampal mossy fiber synapses. *Neuron* **60,** 1082–1094 (2008).

Lambert, J. D. and Jones, R. S. Activation of N-methyl-D-aspartate receptors contributes to the EPSP at perforant path synapses in the rat dentate gyrus in vitro. *Neurosci Lett* **97,** 323–328 (1989).

Lambert, J. D. and Jones, R. S. A reevaluation of excitatory amino acid-mediated synaptic transmission in rat dentate gyrus. *J Neurophysiol* **64,** 119–132 (1990).

Larkman, A. U., Jack, J. J. and Stratford, K. J. Quantal analysis of excitatory synapses in rat hippocampal CA1 in vitro during low-frequency depression. *J Physiol* **505 (Pt 2),** 457–471 (1997).

Lauri, S. E., Bortolotto, Z. A., Bleakman, D., Ornstein, P. L., et al. A critical role of a facilitatory presynaptic kainate receptor in mossy fiber LTP. *Neuron* **32,** 697–709 (2001).

Lawrence, J. J., Grinspan, Z. M. and McBain, C. J. Quantal transmission at mossy fibre targets in the CA3 region of the rat hippocampus. *J Physiol* **554,** 175–193 (2004).

Le Vasseur, M., Ran, I. and Lacaille, J. C. Selective induction of metabotropic glutamate receptor 1- and metabotropic glutamate receptor 5-dependent chemical long-term potentiation at oriens/alveus interneuron synapses of mouse hippocampus. *J Neurosci* **151,** 28–42 (2008).

Lei, S. and McBain, C. J. Distinct NMDA receptors provide differential modes of transmission at mossy fiber-interneuron synapses. *Neuron* **33,** 921–933 (2002).

Li, X. G., Somogyi, P., Ylinen, A. and Buzsáki, G. The hippocampal CA3 network: an in vivo intracellular labeling study. *J Comp Neurol* **339,** 181–208 (1994).

Liao, D., Hessler, N. A. and Malinow, R. Activation of postsynaptically silent synapses during pairing-induced LTP in CA1 region of hippocampal slice. *Nature* **375,** 400–404 (1995).

Macek, T. A., Winder, D. G., Gereau, R. W., Ladd, C. O. and Conn, P. J. Differential involvement of group II and group III mGluRs as autoreceptors at lateral and medial perforant path synapses. *J Neurophysiol* **76,** 3798–3806 (1996).

Magee, J. C. and Cook, E. P. Somatic EPSP amplitude is independent of synapse location in hippocampal pyramidal neurons. *Nat Neurosci* **3,** 895–903 (2000).

McBain, C. J. and Dingledine, R. Heterogeneity of synaptic glutamate receptors on CA3 stratum radiatum interneurones of rat hippocampus. *J Physiol* **462,** 373–392 (1993).

McBain, C. J., DiChiara, T. J. and Kauer, J. A. Activation of metabotropic glutamate receptors differentially affects two classes of hippocampal interneurons and potentiates excitatory synaptic transmission. *J Neurosci* **14,** 4433–4445 (1994).

McHugh, T. J., Jones, M. W., Quinn, J. J., Balthasar, N., et al. Dentate gyrus NMDA receptors mediate rapid pattern separation in the hippocampal network. *Science* **317,** 94–99 (2007).

McNaughton, B. L. Evidence for two physiologically distinct perforant pathways to the fascia dentata. *Brain Res* **199,** 1–19 (1980).

Megías, M., Emri, Z., Freund, T. F. and Gulyás, A. I. Total number and distribution of inhibitory and excitatory synapses on hippocampal CA1 pyramidal cells. *Neuroscience* **102,** 527–540 (2001).

Min, M. Y., Asztely, F., Kokaia, M. and Kullmann, D. M. Long-term potentiation and dual-component quantal signaling in the dentate gyrus. *Proc Natl Acad Sci USA* **95,** 4702–4707 (1998).

Mulle, C., Sailer, A., Pérez-Otaño, I., Dickinson-Anson, H., et al. Altered synaptic physiology and reduced susceptibility to kainate-induced seizures in GluR6-deficient mice. *Nature* **392,** 601–605 (1998).

Neu, A., Földy, C. and Soltesz, I. Postsynaptic origin of CB1-dependent tonic inhibition of GABA release at cholecystokinin-positive basket cell to pyramidal cell synapses in the CA1 region of the rat hippocampus. *J Physiol* **578,** 233–247 (2007).

Nimchinsky, E. A., Yasuda, R., Oertner, T. G. and Svoboda, K. The number of glutamate receptors opened by synaptic stimulation in single hippocampal spines. *J Neurosci* **24,** 2054–2064 (2004).

O'Connor, V., El Far, O., Bofill-Cardona, E., Nanoff, C., et al. Calmodulin dependence of presynaptic metabotropic glutamate receptor signaling. *Science* **286,** 1180–1184 (1999).

Oertner, T. G., Sabatini, B. L., Nimchinsky, E. A. and Svoboda, K. Facilitation at single synapses probed with optical quantal analysis. *Nat Neurosci* **5,** 657–664 (2002).

Otmakhova, N. A., Otmakhov, N. and Lisman, J. E. Pathway-specific properties of AMPA and NMDA-mediated transmission in CA1 hippocampal pyramidal cells. *J Neurosci* **22,** 1199–1207 (2002).

Park, M., Penick, E. C., Edwards, J. G., Kauer, J. A. and Ehlers, M. D. Recycling endosomes supply AMPA receptors for LTP. *Science* **305,** 1972–1975 (2004).

Pelkey, K. A., Lavezzari, G., Racca, C., Roche, K. W. and McBain, C. J. mGluR7 is a metaplastic switch controlling bidirectional plasticity of feedforward inhibition. *Neuron* **46,** 89–102 (2005).

Pelkey, K. A., Yuan, X., Lavezzari, G., Roche, K. W. and McBain, C. J. mGluR7 undergoes rapid internalization in response to activation by the allosteric agonist AMN082. *Neuropharmacology* **52,** 108–117 (2007).

Pelletier, M. R., Kirkby, R. D., Jones, S. J. and Corcoran, M. E. Pathway specificity of noradrenergic plasticity in the dentate gyrus. *Hippocampus* **4,** 181–188 (1994).

Perouansky, M. and Yaari, Y. Kinetic properties of NMDA receptor-mediated synaptic currents in rat hippocampal pyramidal cells versus interneurones. *J Physiol* **465,** 223–244 (1993).

Petralia, R. S., Wang, Y. X. and Wenthold, R. J. Histological and ultrastructural localization of the kainate receptor subunits, KA2 and GluR6/7, in the rat nervous system using selective antipeptide antibodies. *J Comp Neurol* **349,** 85–110 (1994).

Petralia, R. S., Yokotani, N. and Wenthold, R. J. Light and electron microscope distribution of the NMDA receptor subunit NMDAR1 in the rat nervous system using a selective anti-peptide antibody. *J Neurosci* **14,** 667–696 (1994).

Petralia, R. S., Wang, Y. X. and Wenthold, R. J. The NMDA receptor subunits NR2A and NR2B show histological and ultrastructural localization patterns similar to those of NR1. *J Neurosci* **14,** 6102–6120 (1994).

Pinheiro, P. S., Perrais, D., Coussen, F., Barhanin, J., et al. GluR7 is an essential subunit of presynaptic kainate autoreceptors at hippocampal mossy fiber synapses. *Proc Natl Acad Sci USA* **104,** 12181–12186 (2007).

Price, C. J., Karayannis, T., Pál, B. Z. and Capogna, M. Group II and III mGluRs-mediated presynaptic inhibition of EPSCs recorded from hippocampal interneurons of CA1 stratum lacunosum moleculare. *Neuropharmacology* **49 (Suppl 1),** 45–56 (2005).

Raastad, M. and Lipowski, R. Diversity of postsynaptic amplitude and failure probability of unitary excitatory synapses between CA3 and CA1 cells in the rat hippocampus. *Eur J Neurosci* **8,** 1265–1274 (1996).

Racca, C., Stephenson, F. A., Streit, P., Roberts, J. D. and Somogyi, P. NMDA receptor content of synapses in stratum radiatum of the hippocampal CA1 area. *J Neurosci* **20,** 2512–2522 (2000).

Rebola, N., Sachidhanandam, S., Perrais, D., Cunha, R. A. and Mulle, C. Short-term plasticity of kainate receptor-mediated EPSCs induced by NMDA receptors at hippocampal mossy fiber synapses. *J Neurosci* **27,** 3987–3993 (2007).

Rebola, N., Lujan, R., Cunha, R. A. and Mulle, C. Adenosine A2A receptors are essential for long-term potentiation of NMDA-EPSCs at hippocampal mossy fiber synapses. *Neuron* **57,** 121–134 (2008).

Remondes, M. and Schuman, E. M. Direct cortical input modulates plasticity and spiking in CA1 pyramidal neurons. *Nature* **416,** 736–740 (2002).

Rollenhagen, A., Sätzler, K., Rodríguez, E. P., Jonas, P., et al. Structural determinants of transmission at large hippocampal mossy fiber synapses. *J Neurosci* **27,** 10434–10444 (2007).

Rosenmund, C., Clements, J. D. and Westbrook, G. L. Nonuniform probability of glutamate release at a hippocampal synapse. *Science* **262,** 754–757 (1993).

Rush, A. M., Kilbride, J., Rowan, M. J. and Anwyl, R. Presynaptic group III mGluR modulation of short-term plasticity in the lateral perforant path of the dentate gyrus in vitro. *Brain Res* **952,** 38–43 (2002).

Salin, P. A., Scanziani, M., Malenka, R. C. and Nicoll, R. A. Distinct short-term plasticity at two excitatory synapses in the hippocampus. *Proc Natl Acad Sci USA* **93,** 13304–13309 (1996).

Sambandan, S. and Bartos, M. *Unpublished Observation* (2009).

Scanziani, M., Salin, P. A., Vogt, K. E., Malenka, R. C. and Nicoll, R. A. Use-dependent increases in glutamate concentration activate presynaptic metabotropic glutamate receptors. *Nature* **385,** 630–634 (1997).

Schikorski, T. and Stevens, C. F. Quantitative ultrastructural analysis of hippocampal excitatory synapses. *J Neurosci* **17,** 5858–5867 (1997).

Schmitz, D., Frerking, M. and Nicoll, R. A. Synaptic activation of presynaptic kainate receptors on hippocampal mossy fiber synapses. *Neuron* **27,** 327–338 (2000).

Schmitz, D., Mellor, J. and Nicoll, R. A. Presynaptic kainate receptor mediation of frequency facilitation at hippocampal mossy fiber synapses. *Science* **291,** 1972–1976 (2001).

Schmitz, D., Mellor, J., Breustedt, J. and Nicoll, R. A. Presynaptic kainate receptors impart an associative property to hippocampal mossy fiber long-term potentiation. *Nat Neurosci* **6,** 1058–1063 (2003).

Semyanov, A. and Kullmann, D. M. Modulation of GABAergic signaling among interneurons by metabotropic glutamate receptors. *Neuron* **25,** 663–672 (2000).

Shi, S. H., Hayashi, Y., Petralia, R. S., Zaman, S. H., et al. Rapid spine delivery and redistribution of AMPA receptors after synaptic NMDA receptor activation. *Science* **284,** 1811–1816 (1999).

Shigemoto, R., Kinoshita, A., Wada, E., Nomura, S., et al. Differential presynaptic localization of metabotropic glutamate receptor subtypes in the rat hippocampus. *J Neurosci* **17,** 7503–7522 (1997).

Smith, M. A., Ellis-Davies, G. C. and Magee, J. C. Mechanism of the distance-dependent scaling of Schaffer collateral synapses in rat CA1 pyramidal neurons. *J Physiol* **548,** 245–258 (2003).

Spruston, N., Jonas, P. and Sakmann, B. Dendritic glutamate receptor channels in rat hippocampal CA3 and CA1 pyramidal neurons. *J Physiol* **482 (Pt 2),** 325–352 (1995).

Sun, H. Y. and Dobrunz, L. E. Presynaptic kainate receptor activation is a novel mechanism for target cell-specific short-term facilitation at Schaffer collateral synapses. *J Neurosci* **26,** 10796–10807 (2006).

Sun, H. Y., Bartley, A. F. and Dobrunz, L. E. Calcium-permeable presynaptic kainate receptors involved in excitatory short-term facilitation onto somatostatin interneurons during natural stimulus patterns. *J Neurophysiol* **99 (2)**, 799–813.(2008).

Szabadics, J. and Soltesz, I. Functional specificity of mossy fiber innervation of GABAergic cells in the hippocampus. *J Neurosci* **29,** 4239–4251 (2009).

Takumi, Y., Ramírez-León, V., Laake, P., Rinvik, E. and Ottersen, O. P. Different modes of expression of AMPA and NMDA receptors in hippocampal synapses. *Nat Neurosci* **2,** 618–624 (1999).

Tanabe, Y., Masu, M., Ishii, T., Shigemoto, R. and Nakanishi, S. A family of metabotropic glutamate receptors. *Neuron* **8,** 169–179 (1992).

Tanabe, Y., Nomura, A., Masu, M., Shigemoto, R., et al. Signal transduction, pharmacological properties, and expression patterns of two rat metabotropic glutamate receptors, mGluR3 and mGluR4. *J Neurosci* **13,** 1372–1378 (1993).

Topolnik, L., Azzi, M., Morin, F., Kougioumoutzakis, A. and Lacaille, J. C. mGluR1/5 subtype-specific calcium signalling and induction of long-term potentiation in rat hippocampal oriens/alveus interneurones. *J Physiol* **575,** 115–131 (2006).

Toth, K., Suares, G., Lawrence, J. J., Philips-Tansey, E. and McBain, C. J. Differential mechanisms of transmission at three types of mossy fiber synapse. *J Neurosci* **20,** 8279–8289 (2000).

Tóth, K. and McBain, C. J. Afferent-specific innervation of two distinct AMPA receptor subtypes on single hippocampal interneurons. *Nat Neurosci* **1,** 572–578 (1998).

Tóth, K. and McBain, C. J. Target-specific expression of pre- and postsynaptic mechanisms. *J Physiol* **525 (Pt 1),** 41–51 (2000).

Tyler, W. J., Zhang, X. L., Hartman, K., Winterer, J., et al. BDNF increases release probability and the size of a rapidly recycling vesicle pool within rat hippocampal excitatory synapses. *J Physiol* **574,** 787–803 (2006).

Valenzuela-Harrington, M., Gruart, A. and Delgado-García, J. M. Contribution of NMDA receptor NR2B subunit to synaptic plasticity during associative learning in behaving rats. *Eur J Neurosci* **25,** 830–836 (2007).

Vignes, M. and Collingridge, G. L. The synaptic activation of kainate receptors. *Nature* **388,** 179–182 (1997).

Vignes, M., Clarke, V. R., Parry, M. J., Bleakman, D., et al. The GluR5 subtype of kainate receptor regulates excitatory synaptic transmission in areas CA1 and CA3 of the rat hippocampus. *Neuropharmacology* **37,** 1269–1277 (1998).

von Kitzing, E., Jonas, P. and Sakmann, B. Quantal analysis of excitatory postsynaptic currents at the hippocampal mossy fiber-CA3 pyramidal cell synapse. *Adv Second Messenger Phosphoprotein Res* **29,** 235–260 (1994).

Walker, H. C., Lawrence, J. J. and McBain, C. J. Activation of kinetically distinct synaptic conductances on inhibitory interneurons by electrotonically overlapping afferents. *Neuron* **35,** 161–171 (2002).

Washburn, M. S. and Dingledine, R. Block of alpha-amino-3-hydroxy-5-methyl-4-isoxazolepropionic acid (AMPA) receptors by polyamines and polyamine toxins. *J Pharmacol Exp Ther* **278,** 669–678 (1996).

Watanabe, M., Fukaya, M., Sakimura, K., Manabe, T., et al. Selective scarcity of NMDA receptor channel subunits in the stratum lucidum (mossy fibre-recipient layer) of the mouse hippocampal CA3 subfield. *Eur J Neurosci* **10,** 478–487 (1998).

Winder, D. G., Ritch, P. S., Gereau, R. W. and Conn, P. J. Novel glial-neuronal signalling by coactivation of metabotropic glutamate and beta-adrenergic receptors in rat hippocampus. *J Physiol* **494 (Pt 3),** 743–755 (1996).

Witter, M. P. Organization of the entorhinal-hippocampal system: a review of current anatomical data. *Hippocampus* **3 Spec No,** 33–44 (1993).

Yeckel, M. F., Kapur, A. and Johnston, D. Multiple forms of LTP in hippocampal CA3 neurons use a common postsynaptic mechanism. *Nat Neurosci* **2,** 625–633 (1999).

Fast and Slow GABAergic Transmission in Hippocampal Circuits

Marlene Bartos, Jonas-Frederic Sauer, Imre Vida, and Ákos Kulik

Overview

Cortical neuronal networks consist of excitatory glutamatergic principal cells and a heterogeneous group of GABAergic inhibitory interneurons. Interneurons are embedded in feedforward and feedback microcircuits and control key aspects of cortical network function including the timing of the activation of principal cells and the generation of network oscillations (Freund and Buzsáki, 1996; McBain and Fisahn, 2001; Klausberger and Somogyi, 2008). Although interneurons comprise only 10% of the neuronal population, they are highly diverse and can be subdivided into several types on the basis of various criteria, such as intrinsic physiological properties, neurochemical marker content, morphological features, including the laminar distribution of the axon, and finally the postsynaptic target profile of their output (Freund and Buzsáki, 1996; Avoli et al., 2006). On the basis of synaptic targets, interneurons have been classified into two major groups, perisomatic- and dendrite-targeting cells.

Transmission at perisomatic GABAergic synapses is characterized by a fast time course and large peak amplitudes (Bartos et al., 2001, 2002). Fast $GABA_A$ receptor-mediated perisomatic inhibition can precisely determine the timing and the frequency of action potential discharge in principal cells (Cobb et al., 1995; Miles et al., 1996; Pouille and Scanziani, 2001). In contrast, inhibitory signaling mediated by dendritic GABAergic contacts has a slower time course and shows a high degree of diversity (Pearce, 1993; Miles et al., 1996; Vida et al., 1998; Banks et al., 1998; Szabadics et al., 2007). The slower time course of dendritic inhibitory signals is partially due to electrotonic attenuation, when examined in somatic recordings. However, differences in the kinetics of the underlying conductance, as a consequence of differential $GABA_A$ receptor expression, are likely to contribute significantly. Dendritic inhibition plays a major role in regulating local integration of excitatory

M. Bartos (✉)
School of Medicine, Institute of Medical Sciences (IMS), University of Aberdeen, Foresterhill, Aberdeen, AB25 2ZD, Scotland, UK
e-mail: m.bartos@abdn.ac.uk

V. Cutsuridis et al. (eds.), *Hippocampal Microcircuits*, Springer Series in Computational Neuroscience 5, DOI 10.1007/978-1-4419-0996-1_5,

synaptic inputs, activation of dendritic voltage-gated conductances, and synaptic plasticity (Miles et al., 1996).

In addition to $GABA_A$ receptors, metabotropic $GABA_B$ receptors mediate a slower form of inhibition by synaptically released GABA (Solís and Nicoll, 1992; Isaacson et al., 1993; Scanziani, 2000). Activation of $GABA_B$ receptors generates a slow IPSP postsynaptically and inhibits transmitter release from axon terminals presynaptically. Finally, besides these forms of phasic inhibition, extrasynaptic GABA receptors mediate "tonic" inhibition (Nusser and Mody, 2002; Scimemi et al., 2005; Glykys et al., 2008). Tonic inhibition controls the excitability of the cell and the gain in the input–output relationship during synaptic excitation as a function of ambient GABA levels.

In this chapter, we review characteristics of $GABA_A$ receptor-mediated inhibitory transmission at perisomatic and dendritic synapses as well as $GABA_B$ receptor-mediated pre- and postsynaptic inhibition in hippocampal networks.

$GABA_A$ Receptor-Mediated Synaptic Inhibition in Hippocampal Circuits

$GABA_A$ Receptor-Mediated Perisomatic Inhibition

A major factor which determines the influence of a given interneuron on it's target cell is the location of the synapses on the surface of the target cell. Inhibitory synapses located close to the soma have a large impact on the generation of action potentials of their target neurons (Miles et al., 1996; Megías et al., 2001). These synapses therefore can precisely control timing and frequency of action potentials. Consequently, soma-near "phasic" inhibition underlies important cortical network functions such as the synchronization of neuronal activity and the generation of neuronal network oscillations (Cobb et al., 1995; Pouille and Scanziani, 2001; Mann et al., 2005; Mittmann et al., 2005; Vida et al., 2006; Doischer et al., 2008). The primary source of perisomatic inhibition are basket cells (BCs). These interneurons show characteristic physiological, pharmacological, and immunohistochemical properties (Freund and Buzsáki, 1996; Freund, 2003; see also chapter "Morphology of Hippocampal Neurons"). On the basis of the expression profile of Ca^{2+} binding proteins and neuropeptides, two types of soma-inhibiting cells have been distinguished: parvalbumin (PV)- and cholecystokinin (CCK)-expressing cells (Freund and Buzsáki, 1996; Hefft and Jonas, 2005). Another interneuron type, the so-called chandelier or axo-axonic cell (AA), innervates the axon–initial segment of principal cells (Somogyi et al., 1985; Soriano et al., 1990; Buhl et al., 1994, 1995) and therefore these interneurons are in an optimal position to control the initiation of action potentials in their postsynaptic targets. While BCs form synaptic contacts onto both pyramidal cells and other interneurons, including BCs (Bartos et al., 2001, 2002), AA cells selectively target principal cells (Buhl et al., 1994, 1995).

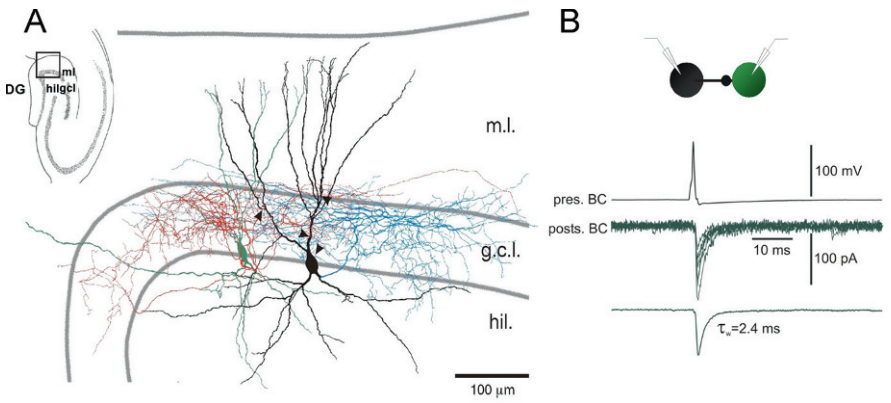

Fig. 1 Fast and reliable inhibition among soma-targeting basket cells. **A**, Camera lucida reconstruction of a pair of synaptically connected basket cells (BCs) in the dentate gyrus subfield of the hippocampus (*inset*). The somato-dendritic domain of the presynaptic BC is shown in *green*, the axon in *red*; the somato-dendritic area of the postsynaptic neuron is displayed in *black;* and the axon in *blue*. *Arrowheads* point to identified putative synaptic contacts (Bartos et al., 2001). **B**, A single postsynaptic action potential is triggered by somatic current injection into the presynaptic BC (*upper trace*), and the resulting inhibitory postsynaptic currents (IPSCs) are measured in the postsynaptic BC (*middle traces*, six individual IPSCs superimposed, and *lower trace*, average of 36 IPSCs). Note the high reliability of transmission indicated by the absence of failures and the fast time course of the IPSCs (amplitude-weighted decay time constant, τ_w: 2.4 ms). Abbreviations: DG, dentate gyrus; gcl, granule cell layer; ml, molecular layer; hil, hilus (Adapted from Bartos et al., 2001; with permission; © 2001 from the Society for Neuroscience)

PV–BCs

GABAergic transmission at PV–BC output synapses is characterized by rapid time course, large peak conductance, and high reliability of transmitter release (Kraushaar and Jonas, 2000; Bartos et al., 2001, 2002; Glickfeld and Scanziani, 2006, Glickfeld et al., 2008). Paired whole-cell patch-clamp recordings from presynaptic PV-expressing BCs and postsynaptic principal cells in acute hippocampal slices revealed that the time course of unitary $GABA_A$ receptor-mediated inhibitory postsynaptic currents (IPSCs) is extremely fast in all hippocampal areas. In the dentate gyrus granule cells (GCs), the rise times (20–80%) are in the range 0.2–0.3 ms and decay time constants are in the range 3.2–3.5 ms at near physiological temperatures (Bartos et al., 2002; Table 1).

Highly specialized pre- and postsynaptic mechanisms underlie the rapid time course of unitary IPSCs at PV–BC output synapses. Presynaptically, GABA release is initiated by a brief and precisely timed presynaptic Ca^{2+} transient. This is reflected by the highly synchronous time course of GABA release at BC–GC synapses (Hefft and Jonas, 2005). The high level of synchrony is further realized by the tight coupling of the Ca^{2+} source (P/Q – type Ca^{2+} channels) and the sensor (Bucurenciu et al., 2008). Postsynaptically, fast inhibitory signaling at PV–BC synapses is largely mediated by the $GABA_A$ receptor subunit α1 as

Table 1 Kinetic properties of perisomatic inhibition

Postsynaptic cell type	Rise time (ms)	Decay τ (ms)	Peak conductance (nS)	Failure rate (%)	Paired recording configuration	Publication
DG						
GC	0.2–0.3[a]/0.5[a,b]	3.4–6.5/20–22[b]	2.0–6.8/1.7[b,d]	6–7/1–49[b]		
	0.2 ± 0.03[a]	3.4 ± 0.4	2.0[d]	5.5 ± 4.0	PV+ BC–GC	Bartos et al. (2002)
		5.2			BC–GC	Bartos et al. (2001)
	0.26 ± 0.01[a]	6.5	6.8[d]	6.5 ± 1.0	BC–GC	Kraushaar and Jonas (2000)
	0.53 ± 0.04[a, b]	20.0 ± 1.1[b]		0.5 ± 0.3[b]	BC–GC	Hefft and Jonas (2005)
GC	0.87	20.1[b]		18.6		
	0.87 ± 0.08[b]	20.1 ± 0.8[b]		18.6 ± 6.3[b]	CCK–IN–GC	Hefft and Jonas (2005)
BC	0.3[a]	2.5	2.3[d]	5–11		
	0.3 ± 0.02[a]	2.5 ± 0.2		10.5 ± 5.5	BC–BC	Bartos et al. (2001)
	0.3 ± 0.03[a]	2.5 ± 0.4	2.29[d]	5 ± 3	PV+ BC–BC	Bartos et al. (2002)
DI cell	0.2	4.0	3.1	11		
	0.23 ± 0.04	3.95 ± 0.75	3.06	10.8 ± 6.3	BC–DI	M. Bartos unpublished
CA3						
PC	0.3[a]	3.3–4.6	5.0–5.3[d]	0–55		
	0.3 ± 0.02[a]	3.3 ± 0.1	5.27[d]	0	PV+ BC–PC	Bartos et al. (2002)
BC	0.3[a]	1.2	3.9[d]	10		
	0.25 ± 0.02[a]	1.2 ± 0.02	3.94[d]	10 ± 10	PV+ BC–BC	Bartos et al. (2002)

Table 1 (continued)

CA1						
PC	0.3[a]/0.66–0.86[c]	3.5–8.3	1.6–9.5	3–35		
	0.3 ± 0.02[a]	3.5 ± 0.5	9.53[d]	3 ± 2	PV+ BC–PC	Bartos et al. (2002)
	0.66 ± 0.06[c]	7.03 ± 1.03	2.07		Fast-spiking BC–PC	Glickfeld et al. (2008), Glickfeld and Scanziani (2006)
	0.86 ± 0.09[c]	8.3 ± 1.22	1.61		Regular spiking BC–PC	Glickfeld et al. (2008), Glickfeld and Scanziani (2006)
	0.73 ± 0.05[c]	6.8 ± 0.2	3.12[d]	35 ± 7	CCK+ BC–PC	Neu et al. (2007)
BC	0.3[a]	1.7	5.1[d]	4		
	0.27 ± 0.02[a]	1.7 ± 0.1	5.12[d]	4 ± 3	PV–GFP+ BC–BC	Bartos et al. (2002)

[a] 20–80% rise time.
[b] Recorded at room temperature ($22 \pm 2^{\circ}$C).
[c] 10–90% rise time.
[d] Calculated from peak IPSC and estimated Cl^- reversal potential.
Abbreviations: PC, pyramidal cell; PV, parvalbumin; BC, basket cell; CCK, cholecystokinin; MFA, mossy fiber-associated cell; DI cell, dendrite-inhibiting cell.

revealed by postembedding immunogold studies (Nyíri et al., 2001; Klausberger et al., 2002). Analysis of recombinant $GABA_A$ receptor subunits showed that $\alpha1\beta1\gamma2$ channels deactivate faster than $\alpha2\beta1\gamma2$ channels (Lavoie et al., 1997). Consistent with these findings, bath application of the benzodiazepine type I receptor agonist zolpidem, which has a high affinity to $GABA_A$ receptors containing the $\alpha1$ subunit (Thomson et al., 2000; Cope et al., 2005), results in a marked prolongation of the decay time constant of PV–BCs IPSCs (Thomson et al., 2000; Doischer et al., 2008).

The peak amplitude of the inhibitory conductance at PV–BC output synapses shows considerable variability across hippocampal areas (Table 1). Nevertheless, peak amplitudes are generally high (up to 9.5 nS) which can be explained by the large number of synaptic contact sites between the coupled neurons. In the CA1 area, for example, the number of contacts per unitary connection is between 10 and 12 (Buhl et al., 1995). Consistent with the high number of contact sites, the failure rate of transmission is low (Hefft and Jonas, 2005; Doischer et al., 2008; Table 1). The reliable transmission at BC output synapses is further supported by the high initial probability of transmitter release, estimated to be 0.79 in the dentate gyrus (Kraushaar and Jonas, 2000).

BC synapses display differences in kinetic properties depending on the identity of the postsynaptic target (Bartos et al., 2001, 2002; Doischer et al., 2008). In particular, the decay time constant was found to be by a factor of $\sim$2 faster in postsynaptic BCs than in principal cells. The mean value of the decay time constant at BC–BC pairs in the dentate gyrus, CA1 and CA3, are 2.5, 1.7, and 1.2 ms, respectively (Bartos et al., 2001, 2002; Table 1). These target cell-specific differences in the hippocampus (Bartos et al., 2002; Glickfeld et al., 2008) could be explained by the expression of distinct postsynaptic $GABA_A$ receptors. PV–BCs express the $GABA_A$ receptor subunit $\alpha1$ at higher levels than principal cells (Gao and Fritschy, 1994; Fritschy and Möhler, 1995; Klausberger et al., 2002). Interestingly, however, other parameters of the synapses, including the rise time, the peak amplitude of the inhibitory conductance, and the failure rate of synaptic transmission, show no differences between BC–BC and PV–BC–principal cell synapses (Bartos et al., 2001, 2002; Table 1).

Fast-spiking (FS) BCs also innervate other types of GABAergic interneurons in the dentate gyrus. Paired recordings with subsequent morphological analysis demonstrate that several types of dendrite-inhibiting interneurons DIs, for example hilar perforant pathway-associated cells (HIPP), hilar commissural–associational pathway-associated cells (HICAP), and total molecular layer cells (TML), are among the postsynaptic targets of BCs (M. Bartos, unpublished observations). Most properties of the unitary IPSCs at BC–DI synapses are similar to those at BC–BC synapses (Bartos et al., 2001; Table 2). However, the decay time constant of the unitary IPSCs is slower (3.95 ± 0.75 ms) than at BC–BC synapses (2.5 ± 0.2 ms; Table 2). This difference is conceivably due to the synapse-specific expression of postsynaptic $GABA_A$ receptor subunits such as $\alpha2$ instead of $\alpha1$ (Fritschy and Möhler, 1995). Thus, these data further underscore the target-specific differences in the properties of BC output synapses.

Table 2 Kinetic properties of dendritic inhibition

Postsynaptic cell type	Rise time (ms)	Decay τ (ms)	Peak conductance (nS)	Failure rate (%)	Paired recording configuration	Publication
DG						
GC	0.6/0.9[a]	6.1/20.1–24.0[a]	1.5/1.1[a]	32/19–65[a]		
	0.56 ± 0.13	6.1 ± 1.7	1.50	31.5 ± 8.3	DI–GC	M. Bartos unpublished
		24.0 ± 1.0[a]	1.12[a]	65 ± 5[a]	HICAP–GC	Harney and Jones (2002)
	0.87 ± 0.08[a]	20.1 ± 0.8[a]		18.6 ± 6.3[a]	CCK–GC	Hefft and Jonas (2005)
BC	0.7	5.9	0.8	41		
	0.70 ± 0.15	5.9 ± 1.7	0.84	40.5 ± 10.7	DI–BC	M. Bartos unpublished
HICAP	0.4	5.3	0.46			
	0.4 ± 0.18	5.3 ± 1.01	0.46		HICAP–HICAP	M. Bartos unpublished
DI	0.3	4.9	2.6	43		
	0.30 ± 0.09	4.86 ± 0.60	2.58	42.7 ± 12.0	DI–DI	M. Bartos unpublished

Table 2 (continued)

CA1						
PC		50	0.11[b]			
		50 ± 4.9	0.11[b]		NG–PC	Price et al. (2008)
NG		42	0.48[b]			
		42.05 ± 21.03	0.48[b]		NG–NG	Price et al. (2005)
		37.4 ± 11.86			NG- to non-NG	Price et al. (2005)
SO-IN		23	1.3	5		
		23.0 ± 5.0	1.34	5 ± 4	O-LM–IN to SL–IN	Elfant et al. (2008)
	6.2 ± 0.6	20.8 ± 1.7	0.43		O-LM–IN to PN	Maccaferri et al. (2000)
SLM–IN	10					
		10.2 ± 6.6			SLM–IN to NG	Price et al. (2005)
CA3						
MFA–IN		4.7	5.0			
	0.28 ± 0.08	4.6 ± 1.2		4.97[b]	MFA–PC1	Vida and Frotscher (2000)
	0.9 ± 0.08	4.8 ± 0.3		96–100/0.2 Hz	MFA–PC1	Losonczy et al. (2004)
				36 ± 5 /25 Hz		

[a] Recorded at room temperature (21–24°C).
[b] Calculated from peak IPSC and estimated Cl^- reversal potential.
Abbreviations: O-LM, oriens lacunosum-moleculare cell; PC, pyramidal cell; NGC, neurogliaform cell; SL, stratum lucidum; IN, interneuron; DI cell; dendrite-inhibiting cell.

Morphological analysis revealed that many BC–interneuron synapses are on proximal apical dendrites because the soma of these cells is often located below the somatic layer. The dendritic position of the synapses leads to attenuation and deceleration of the synaptic current (Johnston and Brown, 1983; Rall and Segev, 1985; Major et al., 1993). Therefore, to determine the real time course of the inhibitory conductance, rise and decay time constants of the inhibitory postsynaptic conductance were estimated using passive cable models of reconstructed BC–interneuron pairs (Bartos et al., 2001). In these simulations, the mean value for the 20–80% rise time was found to be 0.17 ± 0.04 ms and the decay time constant 1.8 ± 0.6 ms (Bartos et al., 2001). These values were by a factor of 1.8 and 1.4, respectively, faster than the experimentally obtained ones, indicating a considerable electrotonic deceleration of the evoked IPSCs for these proximally positioned dendritic synapses.

CCK–BCs

Information on kinetic properties, synaptic strength, and precision in transmitter release at CCK–BC inhibitory output synapses is limited (Table 1). Paired whole-cell patch-clamp recordings showed that unitary IPSCs at CCK–BC to Pyramidal neuron (PN) synapses in CA1 have a slow 10–90% rise time of 0.73 ± 0.05 ms and a decay time constant of 6.8 ± 0.2 ms (Neu et al., 2007), indicating that synaptic inhibition at CCK–BC output synapses might be slower than at PV–BC output synapses (Bartos et al., 2002). Furthermore, paired recordings at CCK–BC to GC synapses in the dentate gyrus revealed average unitary IPSCs with slow 20–80% rise times and decay time constants (~ 0.9 and ~ 22 ms, respectively; Table 1; Harney and Jones, 2002; Hefft and Jonas, 2005). However, these recordings have been performed at room temperature (20–22°C) and therefore cannot be directly compared with data obtained at PV–BC output synapses measured at near physiological temperatures (Bartos et al., 2002). While PV–BCs display a FS-discharge pattern, CCK–BCs have been shown to be regular-spiking (RS) (Freund, 2003). Whole-cell recordings of presynaptic RS–BCs and postsynaptic PNs in CA1 revealed unitary IPSCs with moderately fast time course with a 10–90% rise time of 0.86 ± 0.09 ms and a decay time constant of 8.3 ± 1.22 ms (Table 1; Glickfeld and Scanziani, 2006, Glickfeld et al., 2008). These values were, however, not significantly different to the ones obtained at FS–BC to PNs synapses with a 10–90% rise time of 0.66 ± 0.06 ms and a decay time constant of 7.03 ± 1.03 ms in the same experiments (Table 1; Glickfeld and Scanziani, 2006; Glickfeld et al., 2008). Although the time course of IPSCs at FS and RS output synapses are not significantly different, they seem to be mediated by different postsynaptic $GABA_A$ receptor subunits. Putative CCK/vasoactive intestinal polypeptide(VIP)-immunopositive BC synapses show several-fold lower $\alpha 1$ but higher $\alpha 2$ subunit content than PV-positive synapses (Nyíri et al., 2001; Klausberger et al., 2002). Finally, CCK interneuron to GC synapses show a higher level of transmission failures than PV–BC to GC synapses, pointing to major differences in the release probability among the two BC types (Table 1).

In addition to differences in the kinetics, strength, reliability, and transmitter release, CCK interneuron output synapses are characterized by a marked asynchrony (Maccaferri et al., 2000; Hefft and Jonas, 2005; M. Bartos, unpublished observation). The less precisely timed GABA release results in a slow rise time of unitary IPSCs observed at CCK interneuron to principal cell synapses in the dentate gyrus and CA1 (Maccaferri et al., 2000; Hefft and Jonas, 2005). The standard deviation of the first latency distribution, which can be used as a measure for synchrony of release, is significantly larger at CCK interneuron to GC than at PV–BC to GC synapses (CCK interneurons: 0.95 ± 0.3 ms versus 0.26 ± 0.06 ms). In summary, the properties of the inhibitory output differ markedly between CCK– and PV–BCs. While PV–BC output synapses are characterized by fast, strong, precisely timed transmission, CCK–BC synapses are slower, weaker, and show lower probability and asynchronous signaling.

Similar to PV–BCs, CCK–BCs do also target other interneurons including CCK–BCs. While neuroanatomical studies indicate that the mutual connectivity is comparable to that of PV–BCs, and the total inhibitory input is stronger (Mátyás et al., 2004), functionally, perisomatic inhibition appears to be weaker in CCK interneurons. Recordings from the two types in the CA1 area revealed that IPSCs evoked by minimal stimulation in the cell body layer had large peak amplitudes in PV-immunopositive cells but small peak amplitudes in CCK–BCs (Glickfeld et al., 2008). In comparison to IPSCs recorded simultaneously in pyramidal cells, the ratio of the amplitudes was close to 1 in PV – but only 0.14 ± 0.05 in CCK–BCs, pointing to a target cell-dependent difference in the strength of perisomatic inhibition (Glickfeld et al., 2008).

Chandelier or Axo-axonic (AA) Cells

In contrast to PV–BCs, information on the functional properties at AAs output synapses is scarce. Data from paired recordings in the dentate gyrus showed that these interneurons evoke fast $GABA_A$ receptor-mediated IPSPs in GCs (Buhl et al., 1994). Properties of the currents underlying the effect of AAs were examined in paired whole-cell patch-clamp recordings in the CA1 area. Results showed that unitary AA ISPCs have a large amplitude (308 ± 103 pA) and a moderately fast time course (rise time, 0.8 ± 0.1 ms; decay time constant 11.2 ± 0.9 ms; Table 1). Recordings from neocortical AA cells and synaptically coupled pyramidal cells suggested that the effect of this interneuron type is not inhibitory but excitatory (Szabadics et al., 2006). Recent results from the hippocampus, however, indicate that AA cells predominantly mediate hyperpolarization in the postsynaptic target cell population (Glickfeld et al., 2009; see further details below).

Dynamic Properties of Perisomatic Inhibition

When two action potentials are elicited in the presynaptic BC in short succession, the amplitude of the second IPSC elicited in the postsynaptic cell is smaller

than that of the first. This phenomenon is called paired-pulse depression (PPD) (kraushaar and Jonas, 2000; Bartos et al., 2001, 2002). Coefficient of variation analysis (Malinow and Tsien, 1990) suggests a presynaptic locus for PPD (Bartos et al., 2001). In fact, PPD is independent of the identity of the postsynaptic neuron: The extent of PPD of PV–BCs-evoked IPSCs was found to be similar in PV–BC and principal cells ($\sim$ 31 and $\sim$ 33%, respectively; Bartos et al., 2002). Under conditions of prolonged activity, synaptic transmission at BC–BC and BC–GC synapses shows rapid and marked initial depression but subsequently stabilizes at a lower level (Kraushaar and Jonas 2000; Bartos et al., 2001) demonstrating that GABAergic transmission is extremely stable at BC output synapses.

CCK–BC output synapses express PPD to a similar extent as PV–BCs in the dentate gyrus (Hefft and Jonas, 2005). During repetitive stimulation (10 action potentials, 50 Hz), however, the onset of depression is slower at CCK interneurons than at PV–BCs (Hefft and Jonas, 2005). Interestingly, in the CA3 and CA1 area, high-frequency trains elicited in CCK–BCs result in facilitation of IPSCs in principal cells (Losonczy et al., 2004; Földy et al., 2006; Neu et al., 2007). Release at these synapses is tightly controlled by endocannabinoids through CB1 receptors resulting in a low release probability when the cells are quiescent (Földy et al., 2006).

Dendritic $GABA_A$ Receptor-Mediated Inhibition

Dendritic inhibition is mediated by a highly heterogeneous population of interneurons. Some of these interneurons such as neurogliaform, perforant path, and Schaffer collateral-associated interneurons of the CA1 area or MOPP cells of the dentate gyrus mediate exclusively feedforward inhibition (Vida et al., 1998; Price et al., 2008; Elfant et al., 2008). Others, such as oriens lacunosum-molecular (O-LM) and HIPP interneurons, provide feedback inhibition (Han et al., 1993; Blasco-Ibáñez and Freund, 1995) and yet another group, such as CA1 bistratified cells, are involved in both types of inhibitory microcircuits. Dendritic inhibition controls excitation of cells by glutamatergic inputs, voltage-dependent activation of NMDA receptors, and synaptic plasticity (Staley and Mody, 1992; Davies et al., 1991; Mott and Lewis, 1991; Miles et al., 1996). Furthermore, dendritic inhibition modulates the activation of voltage-gated channels, the generation of slow Ca^{2+} spikes, and the backpropagation of action potentials (Miles et al., 1996; Buzsáki, 1996).

The large electrotonic distance between synapse location and the site of somatic action potential generation as well as the low-pass filtering properties of passive membranes will result in attenuation of synaptically evoked IPSCs (Johnston and Brown, 1983; Rall and Segev, 1985; Major et al., 1993; Häusser and Roth, 1997). Dendritic inhibition will thereby have a slower, "tonic" rather than fast, "phasic" inhibitory effect at the soma. Thus, in contrast to perisomatic inhibition which determines spike timing and synchronizes the activity of principal cells, dendritic inhibition may offset the input–output relation of postsynaptic target cells (Mitchell and Silver, 2003).

Information on the functional properties of GABAergic transmission of identified DIs is limited. The following section summarizes data on properties of $GABA_A$ receptor-mediated transmission at the output synapses of morphologically identified CA1 DIs available in the literature and unpublished results from the dentate gyrus (M. Bartos, unpublished observation).

Neurogliaform Cells (NGs)

NGs form a dense axonal plexus in the stratum lacunosum-moleculare of CA1 (Vida et al., 1998; Price et al., 2005, 2008). $GABA_A$ receptor-mediated inhibitory signaling at NG output synapses is characterized by slow time course and small peak amplitude (Price et al., 2005, 2008; Szabadics et al., 2007). Paired whole-cell patch-clamp recordings of presynaptic NGs and postsynaptic principal cells in acute hippocampal slice preparations at near physiological temperature (30–34°C) revealed a decay time constant of the unitary IPSCs of 50 ± 4.9 ms and an underlying peak conductance of ~ 0.48 nS (Table 2; Price et al., 2008). Similarly, paired recordings of synaptically interconnected NG cells showed slow kinetics with an average decay time constant of 42.05 ± 21.03 ms (Table 2; Price et al., 2005). NGs additionally communicate with other types of interneurons, thereby forming networks of synaptically connected GABAergic cells. Inhibition at these NG to non-NG synapses is also characterized by a long decay time constant (37.4 ± 11.86 ms; Table 2; Price et al., 2005). Thus, synaptic inhibition by NGs has a very slow time course, independent of the nature of the target cell, suggesting that this neuron type is the source of the slow dendritic inhibition observed in earlier studies (Pearce, 1993; Banks et al., 1998). The slow time course of the inhibitory conductance stems from several structural and functional characteristics, including spillover of GABA from the synapses formed by the dense axonal arbor and the properties of the GABA receptors at the postsynaptic membrane (Szabadics et al., 2007).

The dynamic properties of GABAergic transmission at NG output synapses during repetitive presynaptic activation are characterized by a marked depression (5 Hz trains of four presynaptic action potentials). The peak amplitude of the second IPSC in such a train of presynaptic activity is reduced by $\sim 40\%$ at NG to pyramidal cell synapses (Price et al., 2008) and by $\sim 25\%$ at NG–NG synapses (Price et al., 2005). Thus, GABA release at NG output synapses is strongly depressing.

Stratum Oriens Interneurons (SO-IN)

Functional synaptic communication has been identified between CA1 interneurons with their somata and dendrites in stratum oriens and postsynaptic principal cells. SO-INs are highly diverse, but one of the most abundant type is the so-called O-LM interneuron with axonal projection to the stratum lacunosum-moleculare (Maccaferri et al., 2000). Electron microscopy revealed that axon terminals of O-LM cells form symmetrical synapses with distal apical dendrites and dendritic spines of pyramidal cells and other neurons (Gulyás et al., 1993; Sik et al., 1995; Katona

et al., 1999). Unitary IPSCs originating from O-LM cells and recorded at the soma of postsynaptic principal cells at near-physiological temperature ($\sim$ 30°C) have small peak amplitudes ($\sim$ 0.43 nS) and slow time courses with a 10–90% rise time of 6.2 $\pm$ 0.6 ms and a decay time constant of 20.8 $\pm$ 1.7 ms (Table 2; Maccaferri et al., 2000). These dendritic inputs are markedly slower than perisomatic inhibitory synapses but considerably faster than "slow" dendritic inhibition mediated by NG interneurons.

Similar to O-LM to principal cell connections, $GABA_A$ receptor-mediated inhibition between presynaptic O-LM and postsynaptic SL interneurons is slow and weak with a decay time constant of 23 $\pm$ 5 ms and a peak conductance of 1.34 nS (Table 2, Elfant et al., 2008). Short-term plasticity was characterized by $\sim$40% PPD at 100 ms inter-spike intervals. Finally, paired-pulse modulation resulted always in synaptic depression independent of the type of the postsynaptic interneuron (Elfant et al., 2008). In contrast, similar activity patterns failed to influence the second IPSC in pyramidal cells (93 $\pm$ 4%; Maccaferri et al., 2000), raising the possibility of target cell-specific differences in presynaptic properties of these synapses.

Mossy Fiber-Associated Interneurons (MFA)

MFA interneurons have dense axonal arborization co-aligned with mossy fibers in the stratum lucidum of CA3 and the hilus (Vida and Frotscher, 2000). Their dendrites are located in the strata radiatum and oriens, indicating that these interneurons are innervated by associational and commissural fibers and thus primarily mediate feedback inhibition. Output synapses of MFA interneurons are found on proximal dendritic shafts and to a lesser degree on somata of pyramidal cells. IPSCs recorded at postsynaptic principal cells had fast 20–80% rise times of 0.28 $\pm$ 0.08 ms and decay time constants of 4.6 $\pm$ 1.2 ms (Vida and Frotscher, 2000; Losonczy et al., 2004; Table 2). The unitary peak conductance was high with an estimate of 5 nS. Thus, in comparison to other DIs, GABAergic transmission at MFA output synapses is characterized by fast time courses and high strength. Dynamic properties of MFA synapses are similar to CCK–BCs in that they have a low initial release probability, show a remarkable frequency dependent facilitation, and transmit with high reliability during high-frequency trains (Vida and Frotscher, 2000; Losonczy et al., 2004).

Dendritic Inhibitory Interneurons (DIs) in the Dentate Gyrus

The dense layer-specific axonal distribution of the various DI cells indicates the formation of GABAergic synapses located on the entire somato-dendritic domain of interneurons and principal cells in the dentate gyrus (Han et al., 1993; M. Bartos, unpublished data). Unitary inhibitory events elicited by the activation of DI cells recorded at the soma of GCs and interneurons are slower and weaker than perisomatic inhibition. The difference is in part due to electrotonic attenuation of the synaptic events, but properties of postsynaptic $GABA_A$ receptors are likely

to be of different subunit composition (Table 2). Paired recordings of presynaptic DIs and postsynaptic target cells at near physiological temperature (32–34°C) revealed unitary IPSCs with the following parameters: (a) the 20–80% rise times were variable with 0.3 ms for postsynaptic DIs, 0.6 ms for GCs, and 0.7 ms for BCs; (b) the average decay time constants were moderate with 4.9 ms for postsynaptic DIs, 5.9 ms for BCs, and 6.1 ms for GCs; (c) synaptic strength at DI output synapses was heterogeneous with peak conductances of 2.6 nS in postsynaptic DIs, 1.5 nS at GCs, and 0.8 nS at BCs (Table 2; M. Bartos, unpublished observations). Taking these observations together, the functional properties of GABAergic transmission at DI output synapses seem to depend on the type of the target neuron, with moderately fast and weak inhibitory signaling at DI–GC and DI–BC synapses and slightly faster and stronger inhibitory signaling at DI–DI synapses (Fig. 2).

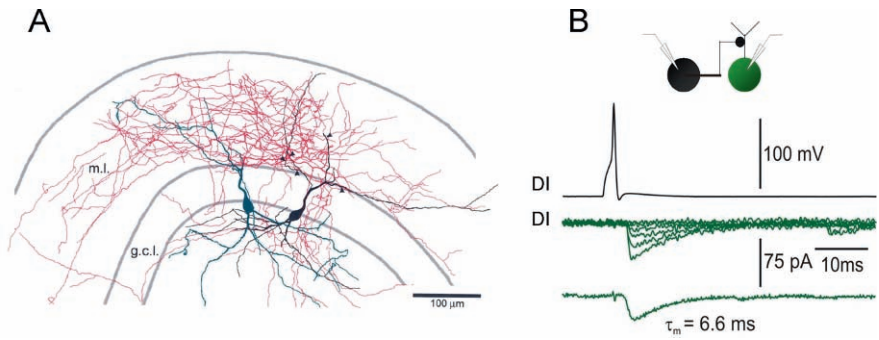

Fig. 2 Slow inhibition among dendrite-targeting interneurons. **A**, Morphological reconstructions of a pair of synaptically connected dendrite inhibiting cells (DIs). Soma and dendrites of the presynaptic cell are depicted in *green* and the axon in *red*. Note that the axon distributes in the whole molecular layer, classifying this cell as total molecular layer cell (TML). The soma and dendrites of the postsynaptic interneuron are shown in *black*. The axon of this cell was not preserved during the recording. *Arrowheads* point to synaptic contacts which have been identified using electron microscopy (data not shown). **B**, Single action potentials evoked in the presynaptic TML (*upper trace*) lead to IPSCs in the postsynaptic interneuron (*middle and lower traces*). In the middle, six traces are shown superimposed; the *lower trace* represents an average of 14 sweeps. Note that DI–DI synapses are less reliable and produce IPSCs with slower kinetic properties (20–80% rise time: 0.43 ms; τ_w: 6.6 ms) than perisomatic synapses among basket cells (see Fig. 1). Abbreviations: ml, molecular layer; gcl, granule cell layer; DI, dendrite-inhibiting interneuron (M. Bartos, unpublished observations)

Paired recordings of morphologically identified HICAP–HICAP synapses revealed kinetic properties of GABAergic transmission comparable to the data obtained at DI–DI synapses (Table 2), whereas synaptic strength of this unitary connection was much weaker with 0.46 nS (Table 2, M. Bartos, unpublished observations). However, information on release probability and number of synaptic contacts among interconnected HICAPs is not available.

Reversal Potential (E_{syn}) of Synaptically Evoked IPSCs

Several lines of evidence indicate that $GABA_A$ receptor-mediated synaptic inhibition in mature interneurons is not hyperpolarizing as previously assumed, but "shunting" (Alger and Nicoll, 1979; Andersen et al., 1980; Martina et al., 2001; Chavas and Marty, 2003; Vida et al., 2006; Sauer and Bartos, in press). Shunting inhibition is defined as an inhibitory effect which does not change the membrane potential but counteracts excitation by short circuiting the underlying currents. In this scenario, the reversal potential of synaptically evoked IPSCs (E_{syn}) is close to the resting membrane potential (V_{rest}), e.g., in the voltage range between V_{rest} and the threshold for action potential generation (Bartos et al., 2007). To determine E_{syn}, whole-cell recordings from BCs were performed in the perforated-patch configuration in the dentate gyrus of mature rats and in mature PV–EGFP-expressing mice (Vida et al., 2006; Sauer and Bartos, in press). The ionophore gramicidin is usually used for these recordings to preserve the intracellular Cl^- concentration (Kyrozis and Reichling, 1995). To determine E_{syn}, IPSCs were evoked by extracellular stimulation in the principal cell layer at varying holding potentials. Synaptically evoked IPSCs reversed on average at -52 ± 1.9 mV (Vida et al., 2006; Sauer and Bartos, in press). This value was more positive than the corresponding V_{rest} of -58.4 ± 1.4 mV, but more negative than the threshold potential (Table 3), indicating that inhibition is shunting in BCs. Similarly, perforated-patch recordings from CA3 stratum pyramidale, stratum oriens, and stratum lucidum interneurons revealed that $GABA_A$ receptor-mediated synaptic inhibition is shunting or slightly hyperpolarizing with average E_{syn} values 4–5 mV more positive than the corresponding V_{rest} (Table 3; Lamsa and Taira, 2003; Banke and McBain, 2006). These results have been further confirmed in CA1 stratum radiatum interneurons by using cell-attached recordings of $GABA_A$ receptor-mediated effects (E_{syn}: -69.1 ± 1 mV; V_{rest}: -66 ± 1 mV; Tyzio et al., 2008).

In contrast to interneurons, E_{syn} of synaptically evoked IPSCs in principal cells seems to be diverse (Table 3). Synaptic inhibition in GCs is shunting with an E_{syn} of -74 ± 7 mV, slightly more depolarized than the corresponding V_{rest} of ~ -75 mV (Table 3, Overstreet-Wadiche et al., 2005). Synaptically evoked IPSCs in CA3 PNs reverse at ~ -73 mV, which is ~ 10 mV more negative than the corresponding V_{rest} of ~ -63 mV (Table 3), reflecting hyperpolarizing inhibition in these neurons (Banke and McBain, 2006; Lamsa and Taira, 2003). In contrast, somatic cell-attached recordings from CA3 pyramidal cells reveal shunting or even depolarizing inhibition with an E_{syn} of -75.3 ± 0.9 mV and a corresponding V_{rest} of -78 ± 2 mV (Table 3, Tyzio et al., 2008). Finally, perforated-patch recordings from CA1 pyramidal cells indicate that synaptic inhibition is shunting or slightly hyperpolarizing (Table 3, Riekki et al., 2008). Differences in the excitation state of the recorded cells (Lamsa and Taira, 2003), modulations of Cl^- transporters (Woodin et al., 2003), or differences in membrane properties between neurons in different brain areas could explain the variability in the obtained E_{syn} values. Moreover, recordings from neocortical pyramidal cells indicate that inhibition may have hyperpolarizing, shunting, or depolarizing effects in different compartments of the same neuron (Gulledge and

Table 3 Reversal potential of $GABA_A$ receptor-mediated responses

Cell type	Esyn (mV)	Vrest (mV)	Gramicidin perforated–patch recording technique	Publication
DG				
GC	−72/−74–82[a]	−75[a]		
	−71.9 ± 1.9		Synaptic stimulation	Kraushaar and Jonas (2000)
	−74 ± 7[a]	75[a]	Synaptic stimulation	Overstreet-Wadiche et al. (2005)
	−81.6 ± 2.2[a]		GABA bath application	Tozuka et al. (2005)
BC	−57/−52[a]	−64/−58[a]		
	−57.2 ± 5.5	−63.5 ± 2.5	Synaptic stimulation	J. Sauer and M. Bartos, in press
	−52.3 ± 1.9[a]	−58.4 ± 1.4[a]	Synaptic stimulation	Vida et al. (2006)
CA3				
PC	−73–75	−63–78		
	−72.7 ± 0.9	−64.6 ± 0.8	Synaptic stimulation	Lamsa and Taira (2003)
	−73 ± 3.8	−62.8 ± 4.4	Synaptic stimulation	Banke and McBain (2006)
	−75.3 ± 0.9	−78 ± 2	Cell-attached GABA application[b]	Tyzio et al. (2008)
STR- and STP/STO INs	−65–69	−61–66		
	−69.1 ± 1.0	−66.0 ± 1.0	Cell-attached GABA application[b]	Tyzio et al. (2008)
	−65.3 ± 1.0	−60.5 ± 0.7	Synaptic stimulation	Lamsa and Taira (2003)
SL–INs	−78	−75		
	−78.1 ± 3.7	−75.4 ± 2.5	Synaptic stimulation	Banke and McBain (2006)
CA1				
PC	−69	−66		
	−69 ± 4	−66.0 ± 0.5	Synaptic stimulation	Riekki et al. (2008)

[a]Recorded at room temperature.
[b]GABA receptor reversal potential depicted from cell-attached recordings of individual GABA channels.
Abbreviations: GC, granule cell; BC, basket cell; PC, pyramidal cell; STR, stratum lucidum; STP, stratum pyramidale; STO, stratum oriens; SL, stratum lucidum.

Stuart, 2003; Szabadics et al., 2006). However, results of a recent study which used non-invasive field potential recordings to investigate inhibition mediated by various interneuron types, including BCs, AA, O-LM, and bistratified cells, suggest that the effects are primarily hyperpolarizing independent of the synapse location along the somato-dendritic axis of CA1 principal cells (Glickfeld et al., 2009).

In summary, synaptic $GABA_A$ receptor-mediated synaptic inhibition onto interneurons is largely shunting, independent of the nature of the recorded interneuron type or the hippocampal area. However, synaptic inhibition in principal cells is

diverse and varies from hyperpolarizing to shunting and even depolarizing inhibition depending on the cell type and the subcellular compartment.

$GABA_B$ Receptor-Mediated Post- and Presynaptic Inhibition in the Hippocampal Circuitry

Early electrophysiological and pharmacological studies demonstrated that, in addition to fast ionotropic $GABA_A$ receptors, slow-acting metabotropic $GABA_B$ receptors are also involved in mediating effects of GABA in the hippocampus. In CA1 pyramidal cells, extracellular stimulation in the stratum radiatum elicits a biphasic IPSP consisting of a fast and a slow component (Newberry and Nicoll, 1984; Dutar and Nicoll, 1988). While the fast component of the compound IPSP is blocked by the $GABA_A$ receptor antagonist bicuculline, the slow component persists under bicuculline application (Newberry and Nicoll, 1984; Dutar and Nicoll, 1988) but can be blocked by the $GABA_B$ receptor antagonist CGP35348 (Fig. 3A; Solís and Nicoll, 1992). Similarly, stimulation in dendritic layers elicits slow $GABA_B$ receptor-mediated inhibitory responses in CA3 pyramidal neurons, dentate gyrus GCs, and various types of interneurons (Thompson and Gähwiler, 1992; Otis et al., 1993; Khazipov et al., 1995; Mott et al., 1999). Results of these studies, thus, indicate an abundant postsynaptic localization of $GABA_B$ receptors in the dendrites of principal cells and interneurons.

$GABA_B$ receptors are also expressed presynaptically where they modulate release of various neurotransmitters and neuromodulators. Presynaptic receptors are commonly subdivided into autoreceptors and heteroreceptors depending on whether they control the release of GABA from the inhibitory terminals in a feedback manner (Davies et al., 1991) or act at axon terminals of other transmitter systems (e.g., glutamatergic axons; Vogt and Nicoll, 1999; Guetg et al., 2009).

Structure and Signaling Through Metabotropic $GABA_B$ Receptors

$GABA_B$ receptors belong to the family of seven transmembrane domain G protein-coupled receptors (GPCRs). Two subunits have been identified to date, the $GABA_{B1}$ and $GABA_{B2}$ proteins (Kaupmann et al., 1997, 1998; Bowery and Brown, 1997; Isomoto et al., 1998; Pfaff et al., 1999; Schwarz et al., 2000). For surface localization, efficient coupling to the physiological effectors and formation of fully functional $GABA_B$ receptors, assembly of the $GABA_{B1}$ and $GABA_{B2}$ subunits into heterodimeric complexes is required (Jones et al., 1998; Kaupmann et al., 1998; White et al., 1998; Marshall et al., 1999; Kuner et al., 1999; Calver et al., 2002; Bettler et al., 2004). In the heterodimers, the $GABA_{B1}$ protein contains the ligand-binding domain, whereas the $GABA_{B2}$ subunit binds to the G protein. Recombinant heterodimeric $GABA_{B1,2}$ receptors couple to all prominent effector systems of the native $GABA_B$ receptor, including adenylyl cyclase, phospholipase A_2, Kir3-type K^+ channels, as well as low and high voltage-activated Ca^{2+} channels (Marshall et al., 1999). Further analysis of the $GABA_B$ receptor structure revealed that the subunits exist in various spliced forms. Cloning of rat and human $GABA_{B1}$ identified

seven different splice variants, designated $GABA_{B1a-g}$, (Kaupmann et al., 1997; Isomoto et al., 1998; Schwarz et al., 2000; Wei et al., 2001). Of these isoforms, the $GABA_{B1a}$ and $GABA_{B1b}$ transcripts are the most abundant, which exhibit differences in the extracellular NH_2-terminal domain (Kaupmann et al., 1997). Although there are indications that splice variants exist for $GABA_{B2}$ ($GABA_{B2a-c}$) (Billinton et al., 2001), recent results suggest that $GABA_{B2b}$ and $GABA_{B2c}$ transcripts may represent artifacts arising during cDNA synthesis and/or PCR amplification (Bettler et al., 2004).

As GPCRs, effects of $GABA_B$ receptors are mediated by second messenger cascades regulating the activity of effector channels. Accordingly, application of pertussis toxin, an adenosyl transferase, which inactivates several types of G_i proteins, or GDPβ-S, a structural analogs of GDP, which competes with GTP for the G protein-binding site, abolishes both pre- and postsynaptic effects of $GABA_B$ receptors in hippocampal pyramidal neurons (Andrade et al., 1986; Dutar and Nicoll, 1988; Thompson and Gähwiler, 1992; Sodickson and Bean, 1996).

Postsynaptic Slow Inhibition Mediated by $GABA_B$ Receptors

Functional properties of postsynaptic $GABA_B$ receptor-mediated responses are markedly different from those of fast $GABA_A$ receptor-dependent signaling. First, $GABA_B$ IPSCs have a much slower time course (Fig. 3B). Pharmacologically isolated slow IPSCs have long onset-latency (∼12–20 ms, Otis et al., 1993; Table 4), reflecting the multiple steps involved in the activation of the receptors and their G protein-mediated coupling to the effectors. Furthermore, $GABA_B$ IPSCs have very slow rise and decay. In dentate gyrus GCs, the rise of the IPSC could be described by a fourth-order exponential with an activation time constant of ∼45 ms and the decay by a biexponential function with time constants of ∼110 and ∼516 ms (Otis et al., 1993; Fig. 3B; Table 4). Similarly slow kinetics of $GABA_B$ IPSCs have been reported in CA1 pyramidal cells (Davies et al., 1990; Ling and Benardo, 1994) and in various types of interneurons (Khazipov et al., 1995; Mott et al., 1999; Table 4).

Second, ionic mechanisms of $GABA_B$ receptor-mediated postsynaptic effects are also different from those of $GABA_A$ receptors. Slow IPSPs and baclofen-induced currents reverse close to the estimated equilibrium potential of K^+ ions (∼ −86 to −98 mV; Fig. 3C; Table 4), indicating that $GABA_B$ receptors activate a K^+-selective conductance (Gähwiler and Brown, 1985; Davies et al., 1990; Thompson and Gähwiler, 1992). Furthermore, application of Ba^{2+}, an inhibitor of inwardly rectifying K^+ (Kir) channels, abolishes these effects (Gähwiler and Brown, 1985; Thompson and Gähwiler, 1992; Sodickson and Bean, 1996). In fact, the channels mediating the $GABA_B$ responses have been identified as the G protein-coupled Kir3 channel subfamily (formerly "GIRK"). Kir3 channels comprise four subunits (Kir3.1–3.4; Dascal, 1997) and form homo- or heterotetrameric complexes (Krapivinsky et al., 1995; Inanobe et al., 1995; Kofuji et al., 1995; Spauschus

Table 4 Properties of $GABA_B$ receptor dependent IPSCs

Cell type	Onset latency (ms)	Rise[a] (ms)	Decay[b] (ms)	Peak conductance (nS)	Reversal potential (mV)	Publication
Dentate gyrus						
Granule cell						
	12–20	$\tau = 45 \pm 1$	$\tau1 = 110 \pm 7$, $\tau2 = 516 \pm 53$	1.52 ± 0.16	-98 ± 2	Otis et al. (1993)
	27 ± 3	$T_{peak} = 162 \pm 15$	$\tau1 = 133 \pm 11$, $\tau2 = 649 \pm 65$	1.31 ± 0.23	-95 ± 2	Mott et al. (1999)
Interneurons (pooled data)						
	31 ± 2	$T_{peak} = 154 \pm 6$	$\tau = 261 \pm 28$	0.75 ± 0.12	-97 ± 2	Mott et al. (1999)
BC/HICAP				1.25		
HIPP/TML				0.36		
CA1						
Pyramidal cell						
	29 ± 2	$T_{rise} = 110$	$T_{IPSC} = 723 \pm 135$		-93 ± 2	Davies et al. (1990)
	62 ± 11	$T = 74 \pm 5$	$\tau1 = 46 \pm 6$, $\tau2 = 247 \pm 32$	0.94 ± 0.28	-86 ± 2	Ling & Benardo (1994)
Interneurons						
Str. radiatum INs		$T_{rise} = 118 \pm 6$	$T_{decay} = 185 \pm 14$	0.79 ± 0.18	-94 ± 8	Khazipov et al. (1995)

[a]Values indicate either the time constant (τ) of fitted fourth-power exponential function, the peak latency (T_{peak}) or the rise time (T_{rise}) measured from onset to peak.

[b]Values indicate the time constants of mono- (τ) or biexponential ($\tau1$, $\tau2$) functions fitted to the decay, the full duration (T_{IPSC}) or the decay half-time (T_{decay}).

Abbreviations: BC, basket cell; HICAP, hilar commissural–associational pathway-associated cell; HIPP, hilar perforant pathway-associated cell; TML, total molecular layer cell.

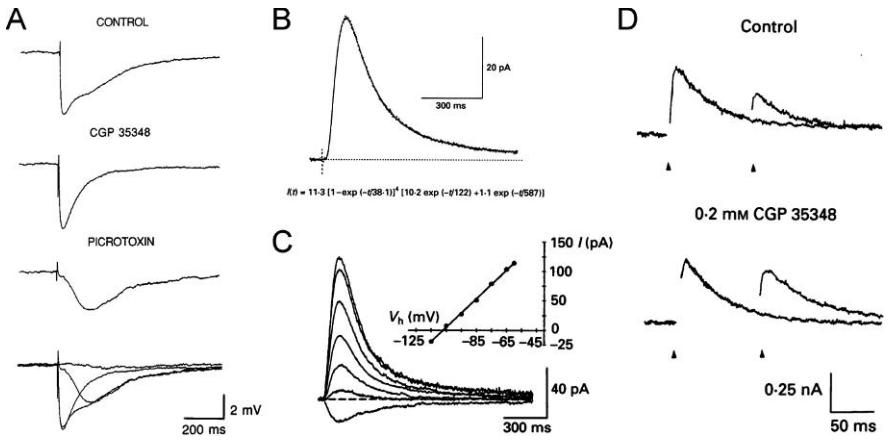

Fig. 3 $GABA_B$ receptor-mediated effects in hippocampal neurons. **A**, Pharmacological dissection of the monosynaptic IPSP reveals the fast $GABA_A$ and the slow $GABA_B$ receptor-mediated IPSP components in a CA1 pyramidal cell. Kinetics **(B)** and reversal potential **(C)** of the $GABA_B$ receptor-mediated slow IPSC in dentate gyrus granule cells. **D**, Activation of $GABA_B$ autoreceptors contribute to depression of IPSCs in response to paired stimuli (*top trace*, *arrow*). CGP 35348, a $GABA_B$ receptor antagonist relieves presynaptic inhibition and increases the amplitude of the second response (*bottom trace*, *arrow*). (**A** adapted from Solís and Nicoll, 1992; **B** and **C** adapted from Otis et al., 1993; **D** adapted from Davies and Collingridge, 1993; ©1992 by the Society for Neuroscience; ©1993 by Wiley-Blackwell)

et al., 1996; Slesinger et al., 1996; Wischmeyer et al., 1997). In the hippocampus, Kir3 channels are thought to be mainly composed of the Kir3.1 and Kir3.2 subunits (Lesage et al., 1995; Duprat et al., 1995; Leaney, 2003). The Kir3.2 subunit is an essential part of the functional channel, determining its assembly and surface localization (Inanobe et al., 1999; Ma et al., 2002). In Kir3.2 knock-out animals expression of Kir3.1 is reduced and slow inhibitory postsynaptic responses are abolished (Liao et al., 1996; Signorini et al., 1997; Lüscher et al., 1997). In good agreement with the proposed coupling of $GABA_B$ receptors and Kir3 channels, immunocytochemical investigations revealed robust colocalization of the two proteins in dendrites of CA pyramidal cells (Kulik et al., 2006).

Presynaptic Inhibition of Synaptic Transmission by $GABA_B$ Receptors

Presynaptic $GABA_B$ receptors play an important role in regulating synaptic transmission at both excitatory and inhibitory synapses. At excitatory synapses, their activation results in depression of glutamatergic synaptic responses (Lei and McBain, 2003). Evidence for presynaptic effects of GABA has been obtained at various hippocampal afferent pathways including the mossy fiber–CA3 synapse. At this synapse, it has been shown that synaptically released GABA suppresses mossy fiber responses through $GABA_B$ receptors (Vogt and Nicoll, 1999; Guetg et al., 2009).

Thus, GABA spilling over from local inhibitory synapses can regulate transmission at glutamatergic synapses by heterosynaptic inhibition (Vogt and Nicoll, 1999). As many DIs have axons co-aligned with afferent pathways (Gulyás et al., 1993; Han et al., 1993; Vida et al., 1998; Vida and Frotscher, 2000), this mechanism enables interneurons to provide input-specific presynaptic control to the main afferent systems to the hippocampal areas (Sohal and Hasselmo, 1998).

Presynaptic action of $GABA_B$ receptors is primarily dependent on G protein-mediated inhibition of the Ca^{2+} conductance. Paired recordings from calyx of Held terminals and postsynaptic neurons in the medial nucleus of the trapezoid body provided direct evidence that activation of the receptors by baclofen has no effect on presynaptic K^+ conductances, but inhibits Ca^{2+} currents in these terminals (Takahashi et al., 1998). It has been further demonstrated that the presynaptic effect of baclofen is also blocked by GDPβ-S (Takahashi et al., 1998). In the hippocampus, direct patch-clamp recordings from presynaptic elements cannot be routinely performed, with the exception of the large mossy fiber terminals on CA3 pyramidal cells (e.g. Geiger and Jonas, 2000). However, indirect evidence suggests that the main mechanisms underlying presynaptic $GABA_B$ responses involve voltage-gated Ca^{2+} channels. Presynaptic depression of EPSPs by baclofen is unaffected by Ba^{2+} in cultured hippocampal pyramidal cells (Thompson and Gähwiler, 1992) and remains also unchanged in slices from GIRK2 knock-out mice (Lüscher et al., 1997). In contrast, Ca^{2+} currents evoked in cultured pyramidal cells and interneurons are highly sensitive to baclofen (Scholz and Miller, 1991). Most compellingly, the inhibitory effects of baclofen on fast presynaptic Ca^{2+} transients and field EPSPs show similar time course in CA1 pyramidal cells (Wu and Saggau, 1995). Thus, presynaptic inhibition of excitatory transmission by $GABA_B$ receptors depends on reduction in Ca^{2+} conductance rather than activation of K^+ currents in the hippocampus. However, the involved Ca^{2+} channels types seem to differ at the various synapses. In CA1 pyramidal cells $GABA_B$-mediated presynaptic inhibition is occluded by the application of ώ-conotoxin, a selective N-type Ca^{2+} channel blocker, but not affected by ώ-agatoxin, a blocker of P/Q-type channels (Wu and Saggau, 1995). In contrast, in CA3 stratum radiatum interneurons ώ-conotoxin and ώ-agatoxin occlude presynaptic inhibitory effects of baclofen on miniature EPSCs to an equal degree (Lei and McBain, 2003).

At GABAergic synapses, activation of presynaptic $GABA_B$ receptors results in reduced inhibitory transmission. Consequently, repetitive stimulation leads to the attenuation of IPSCs ("autoinhibition," Davies et al., 1991; Mott and Lewis, 1991; Fig. 3D). This dynamic modulation of inhibitory transmission has an important function in regulating the induction of long-term potentiation (LTP) in the hippocampus (Davies et al., 1991; Mott and Lewis, 1991). The molecular mechanism of $GABA_B$ receptor-dependent presynaptic inhibition in GABAergic terminals is less well characterized. In an early study, effects of baclofen on unitary IPSPs in synaptically coupled pairs of cultured hippocampal neurons were not affected by pre-treatment with pertussis toxin (Harrison, 1990). Others have reported that pertussis toxin abolished the baclofen-induced depression of IPSPs in cultured CA3 pyramidal cells (Thompson and Gähwiler, 1992). Similarly, findings about the

ionic mechanism of presynaptic $GABA_B$ receptors remain somewhat controversial. Thompson and Gähwiler (1992) have show that extracellular Ba^{2+} reduces presynaptic depression of IPSPs by baclofen in cultured CA3 pyramidal cells, suggesting a contribution of Kir3 channels. Furthermore, baclofen decreases the frequency of both spontaneous IPSCs and Ca^{2+}-independent miniature IPSCs recorded in the presence of tetrodotoxin (Lei and McBain, 2003). Increased frequency of miniature IPSCs by elevated levels of extracellular KCl is blocked by Cd^{2+}, and the additional application of baclofen leads to a further reduction in the IPSC frequency (Lei and McBain, 2003). Thus, in GABAergic terminals the coupling of presynaptic $GABA_B$ receptors may, at least partially, utilize pertussis toxin-insensitive G proteins and affect K^+ channels or the synaptic release machinery in addition to voltage-gated Ca^{2+} channels.

Subcellular Localization of Postsynaptic $GABA_B$ Receptors

Consistent with the physiological and pharmacological data, in situ hybridization (Bischoff et al., 1999) and autoradiography (Chu et al., 1990) confirmed the abundant expression of $GABA_B$ receptor subunits in hippocampal principal cells and interneurons. Subsequent immunocytochemical studies (Fritschy et al., 1999; Sloviter et al. 1999; Margeta-Mitrovic et al., 1999; Kulik et al., 2002, 2003) further revealed the cellular and subcellular localization of $GABA_B$ receptor subunits. At the light microscopic level, the immunostaining for the $GABA_{B1}$ and $GABA_{B2}$ subunits showed very similar patterns of distribution in the hippocampus (Fig. 4A, B). In CA areas and dentate gyrus, immunoreactivity was most intense over the dendritic layers. The stratum lacunosum-moleculare of CA3 showed the strongest labeling for the proteins, whereas in CA1 the immunoreactivity for the receptor subunits was generally weak to moderate. In the dentate gyrus, the immunolabeling was weak in the hilus and moderate in the molecular layer (Kulik et al., 2003).

At the subcellular level, the immunolabeling for the two proteins was observed in postsynaptic and, to a lesser extent, presynaptic compartments of principal cells (Fig. 4C–E). Postsynaptically, the majority of the receptor subunits were localized to the extrasynaptic plasma membrane of dendritic spines and shafts of pyramidal cells and dentate GCs. Quantitative analysis further revealed an enrichment of $GABA_B$ receptors around excitatory synapses on dendritic spines, and an even distribution on dendritic shafts of pyramidal cells contacted by GABAergic axon terminals (Fig. 4F, G; Kulik et al., 2003). Interestingly, the effector Kir3 channels displayed a very similar cellular and subcellular distribution (Koyrakh et al., 2005; Kulik et al., 2006). Moreover, $GABA_B$ receptors and Kir3 channels were found to be co-clustered around excitatory synapses on dendritic spines of pyramidal cells (Fig. 4F, G;Kulik et al., 2006) indicating the functional association of these two proteins in this subcellular compartment. This enrichment of $GABA_B$ receptor–Kir3 channel complexes in dendritic spines implies their intimate involvement in the con-

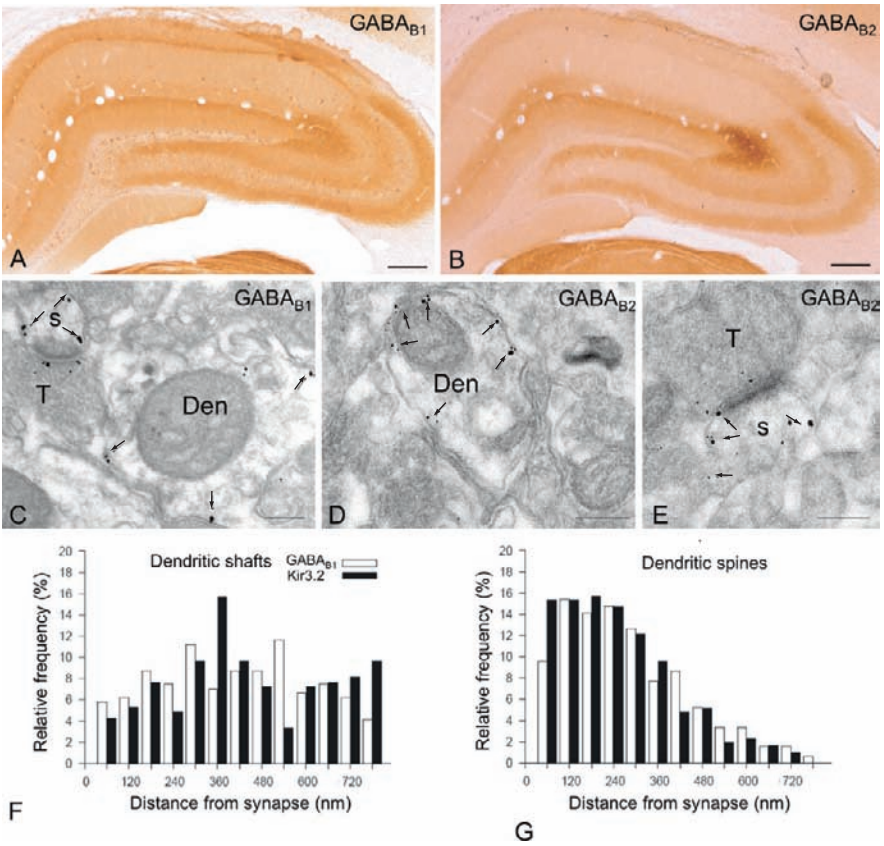

Fig. 4 Cellular and subcellular distribution of $GABA_B$ receptors in the hippocampus. **A, B**, Light micrographs show the distribution of immunoreactivity for $GABA_{B1}$ and $GABA_{B2}$ in the hippocampus. Strong labeling for the subunits was observed in dendritic layers of CA areas and dentate gyrus. Strong immunoreactivity for $GABA_{B1}$, but not for $GABA_{B2}$, was detected in somata of CA1 pyramidal cells and interneurons. **C–E**, Electron micrographs show pre-embedding immunogold labeling for the receptor subunits in pre- and postsynaptic compartments of pyramidal cells. Immunogold particles for $GABA_{B1}$ and $GABA_{B2}$ were detected on the synaptic membranes (*arrowheads* in **C** and **E**) of axon terminals (T), as well as on the extrasynaptic membranes (*arrows* in **C–E**) of dendritic spines (s) and dendritic shafts (Den) of pyramidal cells. **F, G**, Histograms illustrate the distribution of immunoparticles for $GABA_{B1}$ and Kir3.2 relative to symmetrical and asymmetrical synapses on dendrites of CA1 pyramidal cells. Note the enrichment of both molecules in the vicinity of asymmetrical, putative glutamatergic synapses on dendritic spines **(G)**, but not around symmetrical, putative inhibitory synapses on shafts **(F)**. Scale bars: **A, B**, 200 μm; **C–E**, 0.2 μm. **A**, adapted from Kulik et al., 2003; **F** and **G** adapted from Kulik et al., 2006

trol of synaptic integration and plasticity. Indeed, $GABA_B$-mediated inhibition has been shown to act as a break on NMDA receptor-mediated responses and thereby reduced synaptic plasticity (Otmakhova and Lisman, 2004). Conversely, activation of NMDA receptors results in long-term potentiation of the $GABA_B$ receptor–Kir3

channel-mediated slow IPSPs, which parallel the time course of long-term potentiation of excitatory transmission (Huang et al., 2005).

Presynaptically, the immunolabeling for $GABA_B$ receptors is substantially weaker. Nevertheless, immunoreactivity has been consistently found in both glutamatergic and, to a lesser extent, GABAergic axon terminals. The receptors subunits were mainly detected at the extrasynaptic plasma membrane and occasionally over the presynaptic membrane specialization (Kulik et al., 2003). Recent results further show that, while postsynaptic receptors are mainly composed of the $GABA_{B1b}$ and $GABA_{B2}$ subunits ($GABA_{B(1b,2)}$ receptors), terminals of excitatory afferents, including the Schaffer collaterals and the mossy fibers, preferentially contain receptors made up of $GABA_{B1a}$ and $GABA_{B2}$ subunits ($GABA_{B(1a,2)}$ receptors) (Vigot et al., 2006; Guetg et al., 2009). Interestingly, receptors with the latter subunit composition have a higher sensitivity for baclofen and can mediate heterosynaptic inhibition of glutamatergic transmission by synaptically released GABA (Guetg et al., 2009).

In addition to the labeling in principal cells, immunoreactivity for $GABA_B$ receptor subunits was also found in interneurons. Strong immunostaining for the $GABA_{B1}$ subunit, but not for the $GABA_{B2}$ subunit, is present in cell bodies of a subset of GABAergic interneurons scattered throughout the hippocampus (Fritschy et al., 1999; Sloviter et al., 1999; Kulik et al., 2003). Electron microscopic investigation demonstrated that the strong somatic immunoreactivity for $GABA_{B1}$ can be ascribed to the abundance of the protein in the endoplasmic reticulum (Kulik et al., 2003) conceivably reflecting a reserve pool of the receptor subunit. Although, the precise identity of these interneurons remains unknown, fluorescence colocalization studies showed that they include cholecystokinin-, somatostatin-, neuropeptide Y-, calbindin-, and calretinin-containing cells (Sloviter et al., 1999; Gross et al., unpublished). Ultrastructural analysis further demonstrated that immunoreactivity for both the $GABA_{B1}$ and $GABA_{B2}$ receptor proteins is present postsynaptically along the extrasynaptic plasma membrane of dendritic shafts and presynaptically on extrasynaptic and synaptic membrane surface of axon terminals in GAD-immunopositive neurons (Kulik et al., 2003).

Activation of $GABA_B$ Receptors by Spillover from Inhibitory Synapses

Conditions for the activation of $GABA_B$ receptors differ dramatically from those of $GABA_A$ receptors. Whereas $GABA_A$ receptor-mediated responses are readily observed at low-stimulus intensities and in paired recordings of synaptically coupled neurons, strong and repetitive stimulation is required to elicit $GABA_B$ receptor-mediated postsynaptic effects (Newberry and Nicoll, 1985; Isaacson et al., 1993), indicating that recruitment of a number of GABAergic neurons and the release of larger amounts of GABA is necessary to activate the receptors. It was estimated that the simultaneous activation of $\sim$ 2–20 interneurons is required to induce slow $GABA_B$ IPSPs (Scanziani, 2000).

These differences between the two receptor types appear to contradict the fact that the affinity of $GABA_B$ receptors for GABA is ~16-fold higher than that of $GABA_A$ receptors. Sodickson and Bean (1996) showed that the EC_{50} for the activation of $GABA_B$ receptor-mediated potassium conductance by GABA is much lower (1.6 mM) than for the activation of $GABA_A$ receptor-mediated chloride conductance (25 mM). However, this apparent discrepancy can be explained by the differential localization of the two types, while $GABA_A$ receptors are clustered primarily in synapses opposite to the GABA release sites (Nusser and Somogyi, 1997), $GABA_B$ receptors are preferentially localized to the extrasynaptic membrane at same distance from GABAergic synapses (Kulik et al., 2003; Fig. 5). Thus, for the activation of $GABA_B$ receptors GABA needs to escape from the inhibitory synapses and diffuse through the extracellular space ("spillover" hypothesis, Isaacson et al., 1993). In order to achieve sufficiently high concentration of GABA at the location of the receptors release from larger number of terminals is required.

An exception to this rule seems to be presented by neurogliaform interneurons. These interneurons have been reported to elicit $GABA_B$ receptors-mediated responses in synaptically coupled pyramidal cells in both the neocortex and the hippocampus (Tamás et al., 2003; Price et al., 2005). Furthermore, $GABA_B$ receptors were found to be localized in the postsynaptic membrane formed by their synapses (Price et al., 2005). Nevertheless, the dense focal axonal arborization of these interneurons suggests that volume transmission may also contribute to the observed $GABA_B$ responses. Indeed, a recent study provides evidence that GABA can spill over from synapses of neurogliaform interneurons and activate extrasynaptic $GABA_A$ and plausibly also $GABA_B$ receptors (Szabadics et al., 2007).

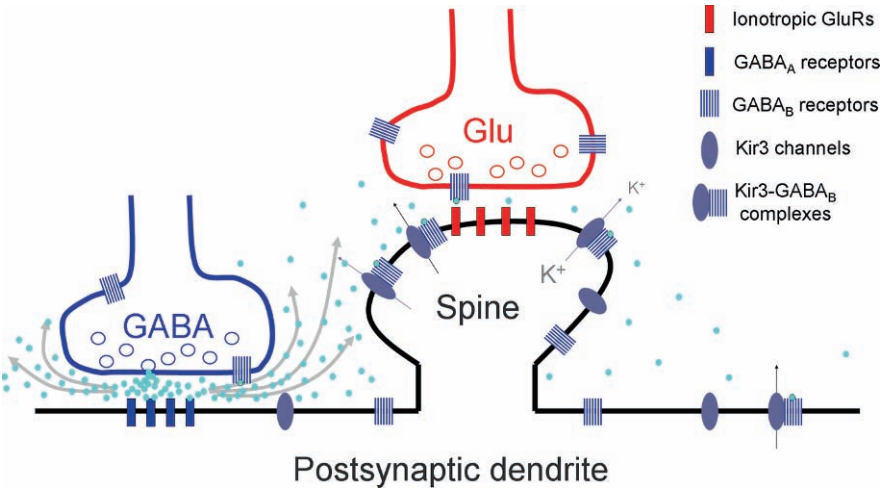

Fig. 5 Activation of the pre- and postsynaptic $GABA_B$ receptors by GABA spillover from inhibitory terminals. Abbreviations: GABA – GABAergic terminal, Glu – glutamatergic terminals, *blue circles* represent GABA molecules released from the inhibitory terminal (modified from Kulik et al., 2003); ©2003 by the Society for Neuroscience

In summary, under physiological conditions, $GABA_B$ receptor-mediated responses are evoked upon concerted activity of GABAergic interneurons. Such synchronous activity of large sets of interneurons occurs during network oscillations (see chapter "Neuronal Activity Patterns During Hippocampal Network Oscillations In Vitro") and can, indeed, lead to the activation of $GABA_B$ receptors (Scanziani, 2000). Conversely, $GABA_B$ receptor-mediated effects influence the frequency of the oscillations (Scanziani, 2000). Thus, $GABA_B$ receptors can serve an important regulatory mechanism during rhythmic oscillatory patterns in vivo.

Future Perspectives

Although our understanding on the functional and dynamic properties of soma-near $GABA_A$ receptor-mediated signaling and the underlying mechanisms increased substantially, several fundamental questions remain unanswered. What are the functional and dynamic characteristics of dendritically located GABAergic synapses? What are the pre- and postsynaptic mechanisms underlying GABAergic transmission at dendrite-targeting inhibitory synapses? How does dendritic inhibition influence local integration of excitatory afferent inputs and thereby the input–output relation of target cells? How does dendritic inhibition contribute to neuronal network function such as information processing and network synchronization? Which interneuron types express $GABA_B$ receptors and how do they contribute to signaling at the level of the individual neuron and the network?

Answering these questions is challenging and requires new experimental strategies and concepts. First, paired whole-cell patch-clamp recordings from synaptically connected interneurons in combination with light and electron microscopical analysis are required to determine synaptic properties, identity of recorded interneuron types, and the number and location of inhibitory synapses. Second, voltage-sensitive dye imaging in combination with whole-cell recordings are needed to examine dendritic integration of inhibitory and excitatory inputs. Third, in vivo whole-cell recordings from interneuron types would be useful to examine the kinetic and dynamic characteristics of synaptic inputs in dependence on the activity state of cortical circuits. Finally, a combined experimental and computational approach based on analysis of synaptic function, intrinsic morphological and physiological characteristics would be important to model integrative properties of the various interneuron types and to develop complex networks in order to identify the functional contribution of individual cell types and their synapses on information processing and network synchronization.

Further Reading

Alger BE, Nicoll RA (1979) GABA-mediated biphasic inhibitory responses in hippocampus. Nature 281:315–317.

Andersen P, Dingledine R, Gjerstad L, Langmoen IA, Laursen AM (1980) Two different responses of hippocampal pyramidal cells to application of gamma-amino butyric acid. J Physiol Lond 305:279–296.

Andrade R, Malenka RC, Nicoll RA (1986) A G protein couples serotonin and $GABA_B$ receptors to the same channels in hippocampus. Science 234:1261–1265.

Avoli M, Biagini G, de Curtis M (2006) Do interictal spikes sustain seizures and epileptogenesis? Epilepsy Curr 6:203–207.

Banke TG, McBain CJ (2006) GABAergic input onto CA3 hippocampal interneurons remains shunting throughout development. J Neurosci 26:11720–11725.

Banks MI, Li TB, Pearce RA (1998) The synaptic basis of GABAA, slow. J Neurosci 18: 1305–1317.

Bartos M, Vida I, Frotscher M, Geiger JRP, Jonas P (2001) Rapid signaling at inhibitory synapses in a dentate gyrus interneuron network. J Neurosci 21:2687–2698.

Bartos M, Vida I, Frotscher M, Meyer A, Monyer H, Geiger JRP, Jonas P (2002) Fast synaptic inhibition promotes synchronized gamma oscillations in τ hippocampal interneuron networks. Proc Natl Acad Sci USA 99:13222–13227.

Bartos M, Vida I, Jonas P (2007) Synaptic mechanisms of synchronized gamma oscillations in inhibitory interneuron networks. Nat Rev Neurosci 8:45–56.

Bettler B, Kaupmann K, Mosbacher J, Gassmann M (2004) Molecular structure and physiological functions of GABA(B) receptors. Physiol Rev 84:835–867.

Billinton A, Ige AO, Bolam JP, White JH, Marshall FH, Emson PC (2001) Advances in the molecular understanding of GABAB receptors. Trends Neurosci 24:277–282.

Bischoff S, Leonhard S, Reymann N, Schuler V, Shigemoto R, Kaupmann K, Bettler B (1999) Spatial distribution of GABA(B)R1 receptor mRNA and binding sites in the rat brain. J Comp Neurol 412:1–16.

Blasco-Ibáñez JM, Freund TF (1995) Synaptic input of horizontal interneurons in stratum oriens of the hippocampal CA1 subfield: structural basis of feed-back activation. Eur J Neurosci 7:2170–2180.

Bowery NG, Brown DA (1997) The cloning of GABA(B) receptors. Nature 386:223–224.

Bucurenciu I, Kulik A, Schwaller B, Frotscher M, Jonas P (2008) Nanodomain coupling between Ca^{2+} channels and Ca^{2+} sensors promotes fast and efficient transmitter release at a cortical GABAergic synapse. Neuron 57:536–545.

Buhl EH, Halasy K, Somogyi P (1994) Diverse sources of hippocampal unitary inhibitory postsynaptic potentials and the number of synaptic release sites. Nature 368:823–828.

Buhl EH, Cobb SR, Halasy K, Somogyi P (1995) Properties of unitary IPSPs evoked by anatomically identified basket cells in the rat hippocampus. Eur J Neurosci 7:1989–2004.

Buzsáki G (1996) The hippocampo-neocortical dialogue. Cereb Cortex 6:81–92.

Calver AR, Davies CH, Pangalos M (2002) GABA(B) receptors: From monogamy to promiscuity. Neurosignals 11:299–314.

Chavas J, Marty A (2003) Coexistence of excitatory and inhibitory GABA synapses in the cerebellar interneuron network. J Neurosci 23:2019–2031.

Chu DCM, Albin RL, Young AB, Penney JB (1990) Distribution and kinetics of $GABA_B$ binding sites in rat central nervous system: A quantitative autoradiographic study. Neuroscience 34:341–357.

Cobb SR, Buhl EH, Halasy K, Paulsen O, Somogyi P (1995) Synchronization of neuronal activity in hippocampus by individual GABAergic interneurons. Nature 378:75–78.

Cope DW, Halbsguth C, Karayannis T, Wulff P, Ferraguti F, Hoeger H, Leppä E, Linden AM, Oberto A, Ogris W, Korpi ER, Sieghart W, Somogyi P, Wisden W, Capogna M (2005) Loss of zolpidem efficacy in the hippocampus of mice with the $GABA_A$ receptor gamma2 F77I point mutation. Eur J Neurosci 21:3002–3016.

Dascal N (1997) Signalling via the G protein-activated K^+ channels. Cell Signal 9:551–573.

Davies CH, Collingridge GL. (1993) The physiological regulation of synaptic inhibition by GABAB autoreceptors in rat hippocampus. J Physiol 1993 Dec;472:245–65.

Davies CH, Davies SN, Collingridge GL (1990) Paired-pulse depression of monosynaptic GABA-mediated inhibitory postsynaptic responses in rat hippocampus. J Physiol Lond 424:513–531.
Davies CH, Starkey SJ, Pozza MF, Collingridge GL (1991) GABA autoreceptors regulate the induction of LTP. Nature 349:609–611.
Doischer D, Hosp JA, Yanagawa Y, Obata K, Jonas P, Vida I, Bartos M (2008) Postnatal differentiation of basket cells from slow to fast signaling devices. J Neurosci 28:12956–12968.
Duprat F, Lesage F, Guillemare E, Fink M, Hugnot J-P, Bigay J, Lazdunski M, Romey G, Barhanin J (1995) Heterologous multimeric assembly is essential for K^+ channel activity of neuronal and cardiac G-protein-activated inward rectifiers. Biochem Biophys Res Commun 212:657–663.
Dutar P, Nicoll RA (1988) Pre- and postsynaptic $GABA_B$ receptors in the hippocampus have different pharmacological properties. Neuron 1:585–591.
Elfant D, Pál BZ, Emptage N, Capogna M (2008) Specific inhibitory synapses shift the balance from feedforward to feedback inhibition of hippocampal CA1 pyramidal cells. Eur J Neurosci 27:104–113.
Földy C, Neu A, Jones MV, Soltesz I (2006) Presynaptic, activity-dependent modulation of cannabinoid type 1 receptor-mediated inhibition of GABA release. J Neurosci 26:1465–1469.
Freund TF (2003) Interneuron diversity series: Rhythm and mood in perisomatic inhibition. Trends Neurosci 26:489–495.
Freund TF, Buzsáki G (1996) Interneurons of the hippocampus. Hippocampus 6:347–470.
Fritschy J-M, Möhler H (1995) $GABA_A$-receptor heterogeneity in the adult rat brain: differential regional and cellular distribution of seven major subunits. J Comp Neurol 359:154–194.
Fritschy JM, Meskenaite V, Weinmann O, Honer M, Benke D, Möhler H (1999) $GABA_B$-receptor splice variants GB1a and GB1b in rat brain: Developmental regulation, cellular distribution and extrasynaptic localization. Eur J Neurosci 11:761–768.
Gähwiler BH, Brown DA (1985) $GABA_B$-receptor-activated K^+ current in voltage-clamped CA3 pyramidal cells in hippocampal cultures. Proc Natl Acad Sci USA 82:1558–1562.
Gao B, Fritschy JM (1994) Selective allocation of $GABA_A$ receptors containing the alpha 1 subunit to neurochemically distinct subpopulations rat hippocampal interneurons. Eur J Neurosci 6:837–853.
Geiger JR, Jonas P (2000) Dynamic control of presynaptic Ca^{2+} inflow by fast-activating K^+ channels in hippocampal mossy fiber boutons. Neuron 28:927–939.
Glickfeld LL, Scanziani M (2006) Distinct timing in the activity of cannabinoid-sensitive and cannabinoid-insensitive basket cells. Nat Neurosci 9:807–815.
Glickfeld LL, Atallah BV, Scanziani M (2008) Complementary modulation of somatic inhibition by opioids and cannabinoids. J Neurosci 28:1824–1832.
Glickfeld LL, Roberts JD, Somogyi P, Scanziani M (2009) Interneurons hyperpolarize pyramidal cells along their entire somatodendritic axis. Nat Neurosci 12:21–23.
Glykys J, Mann EO, Mody I (2008) Which GABA(A) receptor subunits are necessary for tonic inhibition in the hippocampus? J Neurosci 6:1421–1426.
Guetg N, Seddik R, Vigot R, Turecek R, Gassmann M, Vogt KE, Bräuner-Osborne H, Shigemoto R, Kretz O, Frotscher M, Kulik A, Bettler B (2009) The $GABA_{B1a}$ isoform mediates heterosynaptic depression at hippocampal mossy fiber synapses. J Neurosci 29:1414–1423.
Gulledge AT, Stuart GJ (2003) Excitatory actions of GABA in the cortex. Neuron 37:299–309.
Gulyás AI, Miles R, Hájos N, Freund TF (1993) Precision and variability in postsynaptic target selection of inhibitory cells in the hippocampal CA3 region. Eur J Neurosci 5:1729–1751.
Häusser M, Roth A (1997) Estimating the time course of the excitatory synaptic conductance in neocortical pyramidal cells using a novel voltage jump method. J Neurosci 17: 7606–7625.
Han Z, Buhl E, Lörinczi Z, Somogyi P (1993) A high degree of spatial selectivity in the axonal and dendritic domains of physiologically identified local-circuit neurons in the dentate gyrus of the rat hippocampus. Euro J Neurosci 5:396–410.
Harney SC, Jones MV (2002) Pre- and postsynaptic properties of somatic and dendritic inhibition in dentate gyrus. Neuropharmacology 43:584–594.
Harrison NL (1990) On the presynaptic action of baclofen at inhibitory synapses between cultured rat hippocampal neurones. J Physiol Lond 422:433–446.

Hefft S, Jonas P (2005) Asynchronous GABA release generates long-lasting inhibition at a hippocampal interneuron-principal neuron synapse. Nat Neurosci 8:1319–1328.

Huang CS, Shi S-H, Ule J, Ruggiu M, Barker LA, Darnell RB, Jan YN, Jan LY (2005) Common molecular pathways mediate long-term potentiation of synaptic excitation and slow synaptic inhibition. Cell 123:105–118.

Inanobe A, Ito H, Ito M, Hosoya Y, Kurachi Y (1995) Immunological and physical characterization of the brain G protein-gated muscarinic potassium channel. Biochem Biophys Res Commun 217:1238–1244.

Inanobe A, Yoshimoto Y, Horio Y, Morishige K-I, Hibino H, Matsumoto S, Tokunaga Y, Maeda T, Hata Y, Takai Y, Kurachi Y (1999) Characterization of G-protein-gated K^+ channels composed of Kir3.2 subunits in dopaminergic neurons of the substantia nigra. J Neurosci 19:1006–1013.

Isaacson JS, Solís JM, Nicoll RA (1993) Local and diffuse synaptic actions of GABA in the hippocampus. Neuron 10:165–175.

Isomoto S, Kaibara M, Sakurai-Yamashita Y, Nagayama Y, Uezono Y, Yano K, Taniyama K (1998) Cloning and tissue distribution of novel splice variants of the rat $GABA_B$ receptor. Biochem Biophys Res Commun 253:10–15.

Johnston D, Brown TH (1983) Interpretation of voltage-clamp measurements in hippocampal neurons. J Neurophysiol 50:464–486.

Jones KA, Borowsky B, Tamm JA, Craig DA, Durkin MM, Dai M, Yao WJ, Johnson M, Gunwaldsen C, Huang LY, Tang C, Shen Q, Salon JA, Morse K, Laz T, Smith KE, Nagarathnam D, Noble SA, Branchek TA, Gerald C (1998) GABA(B) receptors function as a heteromeric assembly of the subunits GABA(B)R1 and GABA(B)R2. Nature 396:674–679.

Katona I, Acsády L, Freund TF (1999) Postsynaptic targets of somatostatin-immunoreactive interneurons in the rat hippocampus. Neuroscience 88:37–55.

Kaupmann K, Huggel K, Heid J, Flor PJ, Bischoff S, Mickel SJ, McMaster G, Angst C, Bittiger H, Froestl W, Bettler B (1997) Expression cloning of GABA(B) receptors uncovers similarity to metabotropic glutamate receptors. Nature 386:239–246.

Kaupmann K, Malitschek B, Schuler V, Heid J, Froestl W, Beck P, Mosbacher J, Bischoff S, Kulik A, Shigemoto R, Karschin A, Bettler B (1998) GABA(B)-receptor subtypes assemble into functional heteromeric complexes. Nature 396:683–687.

Khazipov R, Congar P, Ben-Ari Y (1995) Hippocampal CA1 lacunosum-moleculare interneurons: Modulation of monosynaptic GABAergic IPSCs by presynaptic $GABA_B$ receptors. J Neurophysiol 74:2126–2137.

Klausberger T, Somogyi P (2008) Neuronal diversity and temporal dynamics: The unity of hippocampal circuit operations. Science.321:53–57.

Klausberger T, David J, Roberts B, Somogyi P (2002). Cell type- and input-specific differences in the number and subtypes of synaptic $GABA_A$ receptors in the hippocampus. J Neurosci 22:2513–2521.

Kofuji P, Davidson N, Lester HA (1995) Evidence that neuronal G-protein-gated inwardly rectifying K^+ channels are activated by G beta gamma subunits and function as heteromultimers. Proc Natl Acad Sci USA 92:6542–6546.

Koyrakh L, Luján R, Colón J, Karschin C, Kurachi Y, Karschin A, Wickman K (2005) Molecular and cellular diversity of neuronal G-protein-gated potassium channels. J Neurosci 25:11468–11478.

Krapivinsky G, Gordon EA, Wickman K, Velimirović B, Krapivinsky L, Clapham DE (1995) The G-protein-gated atrial K^+ channel IKACh is a heteromultimer of two inwardly rectifying K(+)-channel proteins. Nature 374:135–141.

Kraushaar U, Jonas P (2000) Efficacy and stability of quantal GABA release at a hippocampal interneuron-principal neuron synapse. J Neurosci 20:5594–5607.

Kulik A, Nakadate K, Nyíri G, Notomi T, Malitschek B, Bettler B, Shigemoto R (2002) Distinct localization of GABA(B) receptors relative to synaptic sites in the rat cerebellum and ventrobasal thalamus. Eur J Neurosci 15:291–307.

Kulik A, Vida I, Luján R, Haas CA, López-Bendito G, Shigemoto R, Frotscher M (2003) Subcellular localization of metabotropic $GABA_B$ receptor subunits $GABA_{B1a/b}$ and $GABA_{B2}$ in the rat hippocampus. J Neurosci 23:11026–11035.

Kulik A, Vida I, Fukazawa Y, Guetg N, Kasugai Y, Marker CL, Rigato F, Bettler B, Wickman K, Frotscher M, Shigemoto R (2006) Compartment-dependent colocalization of Kir3.2-containing K^+ channels and $GABA_B$ receptors in hippocampal pyramidal cells. J Neurosci 26:4289–4297.

Kuner R, Köhr G, Grünewald S, Eisenhardt G, Bach A, Kornau HC (1999) Role of heteromer formation in $GABA_B$ receptor function. Science 283:74–77.

Kyrozis A, Reichling DB (1995) Perforated-patch recording with gramicidin avoids artifactual changes in intracellular chloride concentration. J Neurosci Methods 57:27–35.

Lamsa K, Taira T (2003) Use-dependent shift from inhibitory to excitatory $GABA_A$ receptor action in SP-O interneurons in the rat hippocampal CA3 area. J Neurophysiol 90:1983–1995.

Lavoie AM, Tingey JJ, Harrison NL, Pritchett DB, Twyman RE (1997) Activation and deactivation rates of recombinant $GABA_A$ receptor channels are dependent on alpha-subunit isoform. Biophys J 73:2518–2526.

Leaney JL (2003) Contribution of Kir3.1, Kir3.2A and Kir3.2C subunits to native G protein-gated inwardly rectifying potassium currents in cultured hippocampal neurons. Eur J Neurosci 18:2110–2118.

Lei S, McBain CJ (2003) GABA B receptor modulation of excitatory and inhibitory synaptic transmission onto rat CA3 hippocampal interneurons. J Physiol Lond 546:439–453.

Lesage F, Guillemare E, Fink M, Duprat F, Heurteaux C, Fosset M, Roemy G, Barhanin J, Lazdunski M (1995) Molecular properties of neuronal G-protein-activated inwardly rectifying K^+ channels. J Biol Chem 270:28660–28667.

Liao YJ, Jan YN, Jan LY (1996) Heteromultimerization of G-protein-gated inwardly rectifying K^+ channel proteins GIRK1 and GIRK2 and their altered expression in *weaver* brain. J Neurosci 16:7137–7150.

Ling DS, Benardo LS (1994) Properties of isolated $GABA_B$-mediated inhibitory postsynaptic currents in hippocampal pyramidal cells. Neuroscience 63:937–944.

Losonczy A, Biró AA, Nusser Z (2004) Persistently active cannabinoid receptors mute a subpopulation of hippocampal interneurons. Proc Natl Acad Sci USA 101:1362–1367.

Lüscher C, Jan LY, Stoffel M, Malenka RC, Nicoll RA (1997) G protein-coupled inwardly rectifying K^+ channels (GIRKs) mediate postsynaptic but not presynaptic transmitter actions in hippocampal neurons. Neuron 19:687–695.

Ma D, Zerrangue N, Raab-Graham K, Fried SR, Jan YN, Jan LY (2002) Diverse trafficking patterns due to multiple traffic motifs in G protein-activated inwardly rectifying potassium channels from brain and heart. Neuron 33:715–729.

Maccaferri G, Roberts JD, Szucs P, Cottingham CA, Somogyi P (2000) Cell surface domain specific postsynaptic currents evoked by identified GABAergic neurones in rat hippocampus in vitro. J Physiol Lond 524:91–116.

Major G, Evans JD, Jack JJB (1993) Solutions for transients in arbitrarily branching cables: II. Voltage clamp theory. Biophys J 65:450–468.

Malinow R, Tsien RW (1990) Presynaptic enhancement shown by whole-cell recordings of long-term potentiation in hippocampal slices. Nature 346:177–180.

Mann EO, Suckling JM, Hajos N, Greenfield SA, Paulsen O (2005) Perisomatic feedback inhibition underlies cholinergically induced fast network oscillations in the rat hippocampus in vitro. Neuron 45:105–117.

Margeta-Mitrovic M, Mitrovic I, Riley RC, Jan LY, Basbaum AI (1999) Immunohistochemical localization of GABA(B) receptors in the rat central nervous system. J Comp Neurol 405: 299–321.

Marshall FH, White J, Main M, Green A, Wise A (1999) GABA(B) receptors function as heterodimers. Biochem Soc Trans 27:530–535.

Martina M, Royer S, Paré D (2001) Cell-type-specific GABA responses and chloride homeostasis in the cortex and amygdala. J Neurophysiol 86:2887–2895.

Mátyás F, Freund TF, Gulyás AI (2004) Immunocytochemically defined interneuron populations in the hippocampus of mouse strains used in transgenic technology. Hippocampus.14:460–481.
McBain CJ, Fisahn A (2001) Interneurons unbound. Nat Rev Neurosci 2:11–23.
Megías M, Emri Z, Freund TF, Gulyás AI (2001) Total number and distribution of inhibitory and excitatory synapses on hippocampal CA1 pyramidal cells. Neuroscience 102:527–540.
Miles R, Tóth K, Gulyás AI, Hájos N, Freund TF (1996) Differences between somatic and dendritic inhibition in the hippocampus. Neuron 16:815–823.
Mitchell SJ, Silver RA (2003) Shunting inhibition modulates neuronal gain during synaptic excitation. Neuron 38:433–445.
Mittmann W, Koch U, Häusser M (2005) Feed-forward inhibition shapes the spike output of cerebellar Purkinje cells. J Physiol Lond 563:369–378.
Mott DD, Lewis DV (1991) Facilitation of the induction of long-term potentiation by $GABA_B$ receptors. Science 252:1718–1720.
Mott DD, Li Q, Okazaki MM, Turner DA, Lewis DV (1999) $GABA_B$-receptor-mediated currents in interneurons of the dentate-hilus border. J Neurophysiol 82:1438–1450.
Neu A, Földy C, Soltesz I (2007) Postsynaptic origin of CB1-dependent tonic inhibition of GABA release at cholecystokinin-positive basket cell to pyramidal cell synapses in the CA1 region of the rat hippocampus. J Physiol Lond 578:233–247.
Newberry NR, Nicoll RA (1984) Direct hyperpolarizing action of baclofen on hippocampal pyramidal cells. Nature 308:450–452.
Newberry NR, Nicoll RA (1985) Comparison of the action of baclofen with γ–aminobutyric acid on rat hippocampal pyramidal cells in vitro. J Physiol Lond 360:161–185.
Nusser Z, Somogyi P (1997) Compartmentalised distribution of $GABA_A$ and glutamate receptors in relation to transmitter release sites on the surface of cerebellar neurones. Prog Brain Res 114:109–127.
Nusser Z, Mody I (2002) Selective modulation of tonic and phasic inhibitions in dentate gyrus granule cells. J Neurophysiol 87:2624–2628.
Nyíri G, Freund TF, Somogyi P (2001) Input-dependent synaptic targeting of alpha(2)-subunit-containing GABA(A) receptors in synapses of hippocampal pyramidal cells of the rat. Eur J Neurosci 13:428–442.
Otis TS, De Koninck Y, Mody I (1993) Characterization of synaptically elicited $GABA_B$ responses using patch-clamp recordings in rat hippocampal slices. J Physiol Lond 463:391–407.
Otmakhova NA, Lisman JE (2004) Contribution of I_h and $GABA_B$ to synaptically induced afterhyperpolarizations in CA1: A brake on the NMDA response. J Neurophysiol 92:2027–2039.
Overstreet-Wadiche L, Bromberg DA, Bensen AL, Westbrook GL (2005) GABAergic signaling to newborn neurons in dentate gyrus. J Neurophysiol 94:4528–4532.
Pearce RA (1993) Physiological evidence for two distinct GABAA responses in rat hippocampus. Neuron 10:189–200.
Pfaff T, Malitschek B, Kaupmann K, Prézeau L, Pin JP, Bettler B, Karschin A (1999) Alternative splicing generates a novel isoform of the rat metabotropic GABA(B)R1 receptor. Eur J Neurosci 11:2874–2882.
Pouille F, Scanziani M (2001) Enforcement of temporal fidelity in pyramidal cells by somatic feed-forward inhibition. Science 293:1159–1163.
Price CJ, Cauli B, Kovacs ER, Kulik A, Lambolez B, Shigemoto R, Capogna M (2005) Neurogliaform neurons form a novel inhibitory network in the hippocampal CA1 area. J Neurosci 25:6775–6786.
Price CJ, Scott R, Rusakov DA, Capogna M (2008) GABA(B) receptor modulation of feedforward inhibition through hippocampal neurogliaform cells. J Neurosci 28:6974–6982.
Rall W, Segev I (1985) Space-clamp problems when voltage clamping branched neurons with intracellular microelectrodes. In: Smith Jr TG, Lecar H, Redman SJ, Gage P (eds) Voltage and patch clamping with microelectrodes, pp 191–215. American Physiological Society, Bethesda, MD.
Riekki R, Pavlov I, Tornberg J, Lauri SE, Airaksinen MS, Taira T (2008) Altered synaptic dynamics and hippocampal excitability but normal long-term plasticity in mice lacking

hyperpolarizing GABA A receptor-mediated inhibition in CA1 pyramidal neurons. J Neurophysiol 99:3075–3089.
Sauer J-F, Bartos M (2010) Recruitment of early postnatal PV^+ hippocampal interneurons by GABAergic excitation. J Neurosci, in press.
Scanziani M (2000) GABA spillover activates postsynaptic $GABA_B$ receptors to control rhythmic hippocampal activity. Neuron 25:673–681.
Scholz KP, Miller RJ (1991) $GABA_B$ receptor-mediated inhibition of Ca^{2+} currents and synaptic transmission in cultured rat hippocampal neurones. J Physiol Lond 444:669–686.
Schwarz DA, Barry G, Eliasof SD, Petroski RE, Conlon PJ, Maki RA (2000) Characterization of γ-aminobutyric acid receptor GABAB(1e), a GABAB(1) splice variant encoding a truncated receptor. J Biol Chem 275:32174–32181.
Scimemi A, Semyanov A, Sperk G, Kullmann DM, Walker MC. (2005) Multiple and plastic receptors mediate tonic GABAA receptor currents in the hippocampus. J Neurosci 25:10016–24.
Signorini S, Liao YJ, Duncan SA, Jan LY, Stoffel M (1997) Normal cerebellar development but susceptibility to seizures in mice lacking G protein-coupled, inwardly rectifying K^+ channel GIRK2. Proc Natl Acad Sci USA 94:923–927.
Sik A, Penttonen M, Ylinen A, Buzsáki G (1995) Hippocampal CA1 interneurons: An in vivo intracellular labeling study. J Neurosci 15:6651–6665.
Slesinger PA, Patil N, Liao J, Jan YN, Jan LY, Cox DR (1996) Functional effects of the mouse *weaver* mutation on G protein-gated inwardly rectifying K^+ channels. Neuron 16:321–331.
Sloviter RS, Ali-Akbarian L, Elliott RC, Bowery BJ, Bowery NG (1999) Localization of GABA(B) (R1) receptors in the rat hippocampus by immunocytochemistry and high resolution autoradiography, with specific reference to its localization in identified hippocampal interneuron subpopulations. Neuropharmacology 38:1707–1721.
Sodickson DL, Bean BP (1996) $GABA_B$ receptor-activated inwardly rectifying potassium current in dissociated hippocampal CA3 neurons. J Neurosci 16:6374–6385.
Sohal VS, Hasselmo ME (1998) GABA(B) modulation improves sequence disambiguation in computational models of hippocampal region CA3. Hippocampus 8:171–193.
Solís JM, Nicoll RA (1992) Pharmacological characterization of $GABA_B$-mediated responses in the CA1 region of the rat hippocampal slice. J Neurosci 12:3466–3472.
Somogyi P, Freund TF, Hodgson AJ, Somogyi J, Beroukas D, Chubb IW (1985) Identified axo-axonic cells are immunoreactive for GABA in the hippocampus and visual cortex of cat. Brain Res 332:143–149.
Soriano E, Nitsch R, Frotscher M (1990) Axo-axonic chandelier cells in the rat fascia dentata: Golgi-electron microscopy and immunocytochemical studies. J Comp Neurol 293:1–25.
Spauschus A, Lentes KU, Wischmeyer E, Dissmann E, Karschin C, Karschin A (1996) A G-protein-activated inwardly rectifying K^+ channel (GIRK4) from human hippocampus associates with other GIRK channels. J Neurosci 16:930–938.
Staley KJ, Mody I (1992) Shunting of excitatory input to dentate gyrus granule cells by a depolarizing GABAA receptor-mediated postsynaptic conductance. J Neurophysiol 68:197–212.
Szabadics J, Varga C, Molnár G, Oláh S, Barzó P, Tamás G (2006) Excitatory effect of GABAergic axo-axonic cells in cortical microcircuits. Science 311:233–235.
Szabadics J, Tamás G, Soltesz I (2007) Different transmitter transients underlie presynaptic cell type specificity of $GABA_A$,slow and $GABA_A$,fast. Proc Natl Acad Sci USA 104:14831–14836.
Tamás G, Lorincz A, Simon A, Szabadics J (2003) Identified sources and targets of slow inhibition in the neocortex. Science 299:1902–1905.
Takahashi T, Kajikawa Y, Tsujimoto T (1998) G-protein coupled modulation of presynaptic calcium currents and transmitter release by a $GABA_B$ receptor. J Neurosci 18:3138–3146.
Thompson SM, Gähwiler BH (1992) Comparison of the actions of baclofen at pre- and postsynaptic receptors in the rat hippocampus in vitro. J Physiol Lond 451:329–345.
Thomson AM, Bannister AP, Hughes DI, Pawelzik H (2000) Differential sensitivity to zolpidem of IPSPs activated by morphologically identified CA1 interneurons in slices of rat hippocampus. Eur J Neurosci 12:425–436.

Tozuka Y, Fukuda S, Namba T, Seki T, Hisatsune T (2005) GABAergic excitation promotes neuronal differentiation in adult hippocampal progenitor cells. Neuron 6:803–815.

Tyzio R, Minlebaev M, Rheims S, Ivanov A, Jorquera I, Holmes GL, Zilberter Y, Ben-Ari Y, Khazipov R (2008) Postnatal changes in somatic γ-aminobutyric acid signalling in the rat hippocampus. Eur J Neurosci 27:2515–2528.

Vida I, Frotscher M (2000) A hippocampal interneuron associated with the mossy fiber system. Proc Natl Acad Sci USA 97:1275–1280.

Vida I, Halasy K, Szinyei C, Somogyi P, Buhl EH (1998) Unitary IPSPs evoked by interneurons at the stratum radiatum-stratum lacunosum-moleculare border in the CA1 area of the rat hippocampus in vitro. J Physiol 506:755–773.

Vida I, Bartos M, Jonas P (2006) Shunting inhibition improves robustness of gamma oscillations in hippocampal interneuron networks by homogenizing firing rates. Neuron 49:107–117.

Vigot R, Barbieri S, Bräuner-Osborne H, Turecek R, Shigemoto R, Zhang YP, Luján R, Jacobson LH, Biermann B, Fritschy JM, Vacher CM, Müller M, Sansig G, Guetg N, Cryan JF, Kaupmann K, Gassmann M, Oertner TG, Bettler B (2006) Differential compartmentalization and distinct functions of $GABA_B$ receptor variants. Neuron 50:589–601.

Vogt KE, Nicoll RA (1999) Glutamate and γ-aminobutyric acid mediate a heterosynaptic depression at mossy fiber synapses in the hippocampus. Proc Natl Acad Sci USA 96:1118–1122.

White JH, Wise A, Main MJ, Green A, Fraser NJ, Disney GH, Barnes AA, Emson P, Foord SM, Marshall FH (1998) Heterodimerization is required for the formation of a functional GABA(B) receptor. Nature 396:679–682.

Wei K, Jia Z, Wang YT, Yang J, Liu CC, Snead OC III (2001) Cloning and characterization of a novel variant of rat GABA-BR1 with a truncated C-terminus. Brain Res 89:103–110.

Wischmeyer E, Döring F, Wischmeyer E, Spauschus A, Thomzig A, Veh R, Karschin A (1997) Subunit interactions in the assembly of neuronal Kir3.0 inwardly rectifying K^+ channels. Mol Cell Neurosci 9:194–206.

Woodin MA, Ganguly K, Poo MM (2003) Coincident pre- and postsynaptic activity modifies GABAergic synapses by postsynaptic changes in Cl^- transporter activity. Neuron 39:807–820.

Wu LG, Saggau P (1995) $GABA_B$ receptor-mediated presynaptic inhibition in guinea-pig hippocampus is caused by reduction of presynaptic Ca^{2+} influx. J Physiol Lond 485:649–657.

Synaptic Plasticity at Hippocampal Synapses

Jack Mellor

Overview

This chapter will discuss what is currently known about synaptic plasticity at glutamatergic synapses in the hippocampus. Hippocampal synaptic plasticity is potentially a vast topic with many thousands of research papers published in the field. However, this chapter will not discuss the detailed molecular mechanisms underlying synaptic plasticity and instead will concentrate on the precise activity patterns required to induce synaptic plasticity. This includes the contribution of presynaptic and postsynaptic spiking and the importance of subthreshold postsynaptic depolarisation. Also, this chapter will attempt to relate various induction protocols to known in vivo patterns of neuronal activity.

All glutamatergic synapses in the hippocampus are plastic and can undergo activity-dependent bidirectional persistent changes in synaptic strength known as long-term potentiation (LTP) and long-term depression (LTD). This is important since a neuronal network cannot be functional if synaptic strength can only ever change in one direction. Therefore, distinct activity patterns need to be sensed by the synapse to initiate either LTP or LTD. The original description of a general principle for synaptic plasticity stated that coincident firing of inputs onto a neuron or coincident firing of the presynaptic and postsynaptic neurons would strengthen synaptic connections (Hebb, 1949). This theory is broadly correct for associative or Hebbian LTP and has been modified to include a description of LTD induction by uncorrelated firing patterns (Bienenstock et al., 1982). However, it does not apply to non-associative or non-Hebbian synaptic plasticity which requires activity in only one neuron (see below). In addition, these theories do not incorporate the role of homeostatic or heterosynaptic plasticity (see below).

All synapses in the hippocampus also undergo transient changes in synaptic strength known as short-term potentiation (STP) and short-term depression (STD).

J. Mellor (✉)
MRC Centre for Synaptic Plasticity, Department of Anatomy,
University of Bristol, University Walk, Bristol BS8 1TD, UK
e-mail: jack.mellor@bristol.ac.uk

V. Cutsuridis et al. (eds.), *Hippocampal Microcircuits*, Springer Series in Computational Neuroscience 5, DOI 10.1007/978-1-4419-0996-1_6,

The timescale for STP and STD is generally less than a second. Although short-term changes in synaptic strength are clearly important for the processing of information in the hippocampus, it is not clear that they play a major role in learning and memory.

For the purposes of this book, the key questions are the following:

(i) What patterns of activity are required to induce LTP and LTD?
(ii) How do these relate to patterns of activity found in vivo?
(iii) What are the functional consequences of long-term synaptic plasticity?

The answers to these questions will need to be incorporated into any model for how the hippocampus functions as a centre for learning within the brain.

The Data

The Different Forms of Hippocampal Synaptic Plasticity

Short-term synaptic plasticity is found at all synapses in the hippocampus and is believed to result from a combination of presynaptic vesicle depletion and presynaptic Ca^{2+} accumulation (Zucker and Regehr, 2002). In general, synapses with a high initial probability of release will exhibit STD and those with a low initial probability of release STP. The majority of GABAergic synapses exhibit STD whereas glutamatergic synapses exhibit either STP or STD. Short-term synaptic plasticity can be measured by giving pairs of synaptic stimuli separated by a short interval ($\sim$100 ms) to determine if the second stimulus results in a larger (STP) or smaller (STD) response. Some examples are shown in Fig. 1.

Perhaps the most interesting example of short-term synaptic plasticity occurs at mossy fibre synapses between dentate gyrus granule cells and CA3 pyramidal cells. At these synapses, the initial probability of release is extremely low allowing the synapses to undergo massive facilitation in the probability of release and therefore strength of transmission, in some cases up to 1,000%. This facilitation can be activated in milliseconds and lasts for several seconds.

LTP and LTD can also be found at both GABAergic and glutamatergic synapses in the hippocampus. In general, LTP is induced by short, high-frequency stimulation whereas LTD is induced by prolonged low-frequency stimulation (Fig. 1). In both cases the key mediator of long-term synaptic change is Ca^{2+}. LTP and LTD can be induced at all the major excitatory synapses within the hippocampus but have varying properties (Fig. 2).

Ca^{2+} as a Trigger for the Induction of LTP and LTD

It is widely accepted that the critical trigger for the induction of associative synaptic plasticity is a rise in intracellular Ca^{2+} concentrations within the postsynaptic

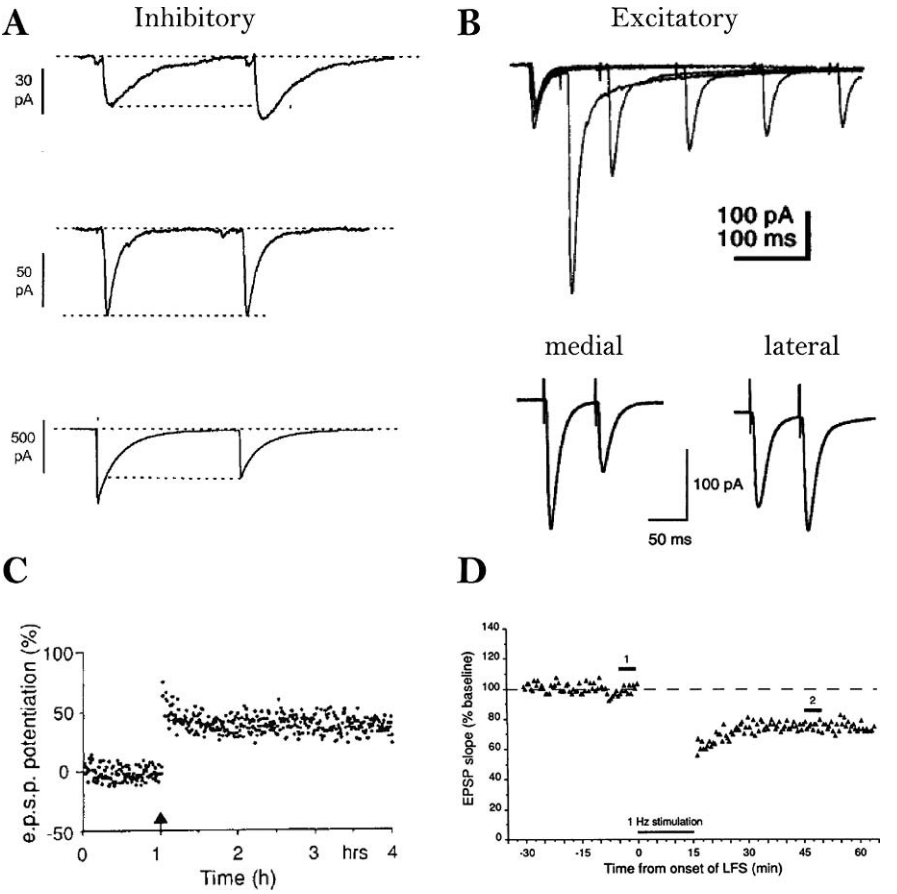

Fig. 1 Examples of synaptic plasticity. (**a**) Three examples of short-term plasticity at inhibitory synapses measured with pairs of stimuli given 100 ms apart (reproduced with permission from Maccaferri et al., 2000, Fig. 15a–c, p. 112, Copyright 2000 Physiological society). (**b**) *Top* shows STP measured with pairs of stimuli at varying intervals at the mossy fibre synapse (reproduced with permission from Salin et al., 1996, Fig. 1a, p. 33305, Copyright 1996 National Academy of Sciences). *Bottom* shows STD or STP in the dentate gyrus measured with pairs of stimuli given to the medial or lateral perforant path (reproduced with permission from Asztely et al., 2000, Fig. 2a–b, p. 665, Copyright 2000 Wiley-Blackwell Publishing). (**c**) Example of LTP experiment performed at the perforant path synapse in the dentate gyrus in vivo plotting the evoked EPSP amplitude with time. The *arrow* represents stimulation at 250 Hz for 200 ms (reproduced with permission from Bliss and Collingridge, 1993, Fig. 1b, p. 2, Copyright 1993 Nature Publishing Group). (**d**) Example of LTD experiment where LTD is induced by 900 stimuli at 1 Hz (reproduced with permission from Dudek and Bear, 1992, Fig. 1a, p. 4364, Copyright 1992 National Academy of Sciences)

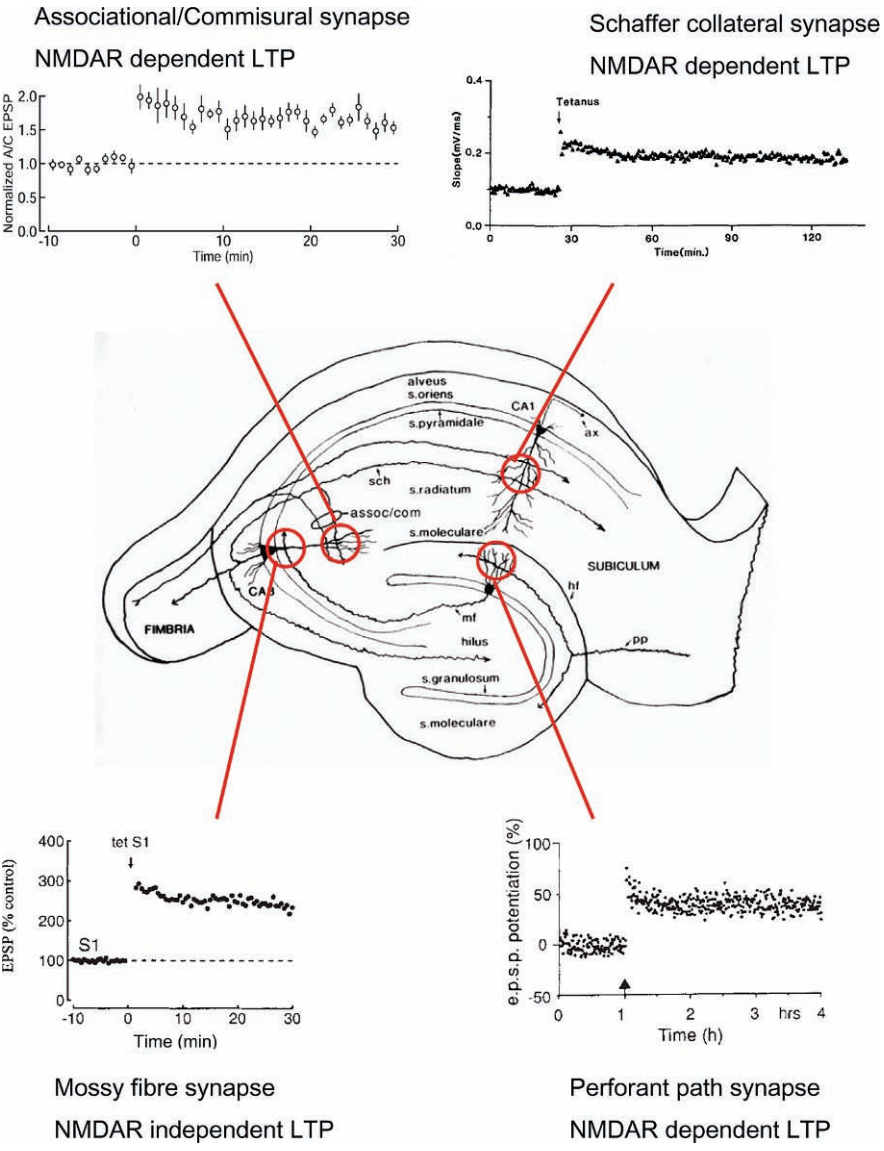

Fig. 2 Examples of four different forms of LTP at the major excitatory synapses in the hippocampus. (*Top-left*) Reproduced with permission from Kobayashi and Poo, 2004, Fig. 7, p. 450, Copyright 2004 Elsevier Inc. (*Top-right*) Reproduced with permission from Nicoll et al., 1988, Fig. 2a, p. 2, Copyright 1988 Elsevier Inc. (*Bottom-right*) Reproduced with permission from Bliss and Collingridge, 1993, Fig. 1b, p. 2, Copyright 1993, Nature Publishing Company. (*Bottom-left*) Reproduced with permission from Weisskopf et al., 1993, Fig. 4a, p. 4, Copyright 1993, Nature Publishing Company

dendrite (Lisman, 1989). For many years, the magnitude and duration of the Ca^{2+} increase was thought to determine the direction of plasticity (Bear et al., 1987; Hansel et al., 1996). As a general rule, it was proposed that short, large-magnitude increases in intracellular Ca^{2+} concentration lead to synaptic potentiation whereas prolonged, small-magnitude increases lead to synaptic depression (Cho et al., 2001; Cormier et al., 2001; Gall et al., 2005; Hansel et al., 1997; Ismailov et al., 2004) (Fig. 3).

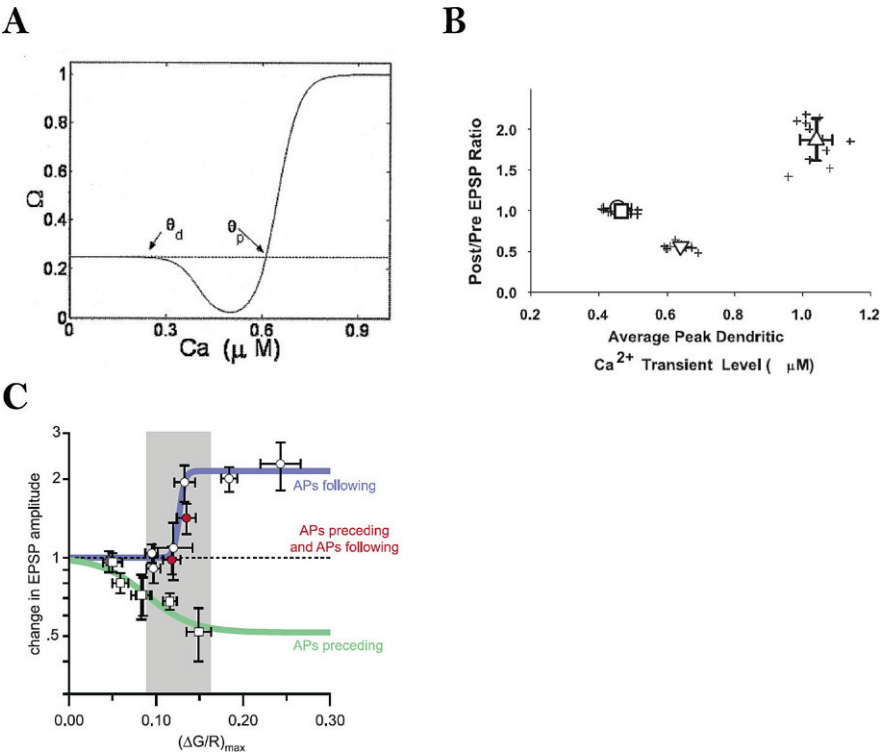

Fig. 3 Calcium concentration determines the direction of plasticity. (**a**) Theoretical relationship between dendritic calcium concentration and direction of synaptic plasticity (Ω) as originally proposed in the Bienenstock–Cooper–Munro (BCM) model (1982) and subsequently modified (reproduced with permission from Shouval and Kalantzis, 2005, Fig. 1a, p. 1070, Copyright 2005, American Physiological Society). Dendritic calcium concentrations below a value θ_d cause no change in synaptic strength. Between values θ_d and θ_p, LTD is induced and above θ_p LTP is induced (reproduced with permission from Shouval and Kalantzis, 2005, Fig. 1a, p. 1070, Copyright 2005, American Physiological Society). (**b**) Experimentally determined relationship between $[Ca^{2+}]$ and synaptic plasticity in cortical slices during pairing of presynaptic and postsynaptic activity (reproduced with permission from Ismailov et al., 2004, Fig. 10b, p. 9857, Copyright 2004, Society for Neuroscience). (**c**) Experimentally determined relationship between $[Ca^{2+}]$ and synaptic plasticity in cortical slices during pairing of presynaptic and postsynaptic spikes separated according to the spike timing (reproduced with permission from Nevian and Sakmann, 2006, Fig. 8, p. 11009, Copyright 2006, Society for Neuroscience)

Thus, sustained dendritic concentrations of Ca^{2+} between approximately 300 and 600 nM induce LTD and shorter duration concentrations above 600 nM induce LTP. However, recent evidence has questioned this simple model and proposed rules that depend on the timing (Nevian and Sakmann, 2006), source (Karmarkar and Buonomano, 2002; Nevian and Sakmann, 2006) and microdomain (Keller et al., 2008) of the Ca^{2+} concentration increase. It is important to point out that the majority of these data come from experiments performed on cortical synapses.

Non-associative synaptic plasticity (see below) also requires a Ca^{2+} signal but in this case in the presynaptic terminal. Again it is believed that prolonged small-magnitude increases in Ca^{2+} ($\sim$100–200 nM) result in LTD whereas short, large-magnitude increases in Ca^{2+} ($\sim$500–1000 nM) result in LTP (Castillo et al., 1994; Kobayashi et al., 1999; Regehr and Tank, 1991).

NMDA Receptors Are Coincidence Detectors

The increase in intracellular Ca^{2+} can arise from a number of sources including voltage-dependent Ca^{2+} channels and intracellular Ca^{2+} stores, but the most important source for associative synaptic plasticity is through *N*-methyl-D-aspartate receptors (NMDARs). These glutamate-gated ion channels are permeable to K^+, Na^+ and Ca^{2+} but at the resting membrane potential their pore is blocked by Mg^{2+}. Depolarisation of the membrane potential removes the Mg^{2+} block which confers a voltage dependence on the NMDAR (Fig. 4). This makes this receptor ideally placed to detect coincident activity in presynaptic and postsynaptic neurons since to open it requires both the release of glutamate from the presynaptic terminal as well as postsynaptic depolarisation. Activation of NMDARs allows Ca^{2+} to flow into the postsynaptic cell and the resultant rise in intracellular Ca^{2+} concentration initiates signalling pathways for LTP or LTD expression.

Since NMDARs control the induction of synaptic plasticity, the timecourse of NMDAR activation is thought to be critical for determining the window for plasticity induction by coincident presynaptic and postsynaptic activity. NMDARs bind glutamate with a high affinity ($EC_{50} \sim 2\,\mu M$) (Patneau and Mayer, 1990) and remain bound long after glutamate has been cleared from the synaptic cleft (time constant of decay $\sim$ 100 ms) (Jahr and Stevens, 1990; McBain and Mayer, 1994; Silver et al., 1992). The precise decay kinetics are dependent on the NMDAR subunit complement that can be developmentally regulated and can range from 100 ms to 5 s (Monyer et al., 1994). Typical NMDAR-mediated currents are longlasting in comparison to AMPARs (Fig. 4), and this produces a long time window during which presynaptic and postsynaptic spikes may be considered coincident for the purposes of NMDAR activation. However, depolarisation becomes increasingly less effective at removing the Mg^{2+} block and activating NMDARs the longer the interval after glutamate binding (Kampa et al., 2004).

Other receptors and mechanisms have also been proposed to act as coincidence detectors either on their own or in combination with NMDARs. Synaptic activation

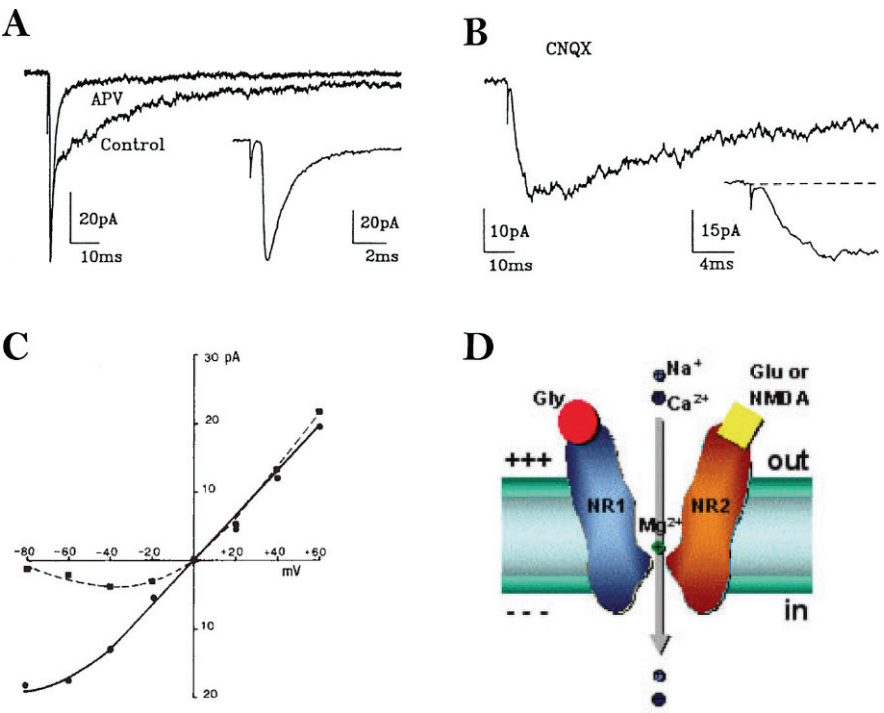

Fig. 4 Characteristics of NMDA receptors. (**a**) Excitatory postsynaptic currents (EPSCs) recorded from a cerebellar granule cell in the absence of Mg^{2+} before and during application of the NMDA receptor antagonist APV. Inset: rapid AMPAR-mediated component of the EPSC at a faster time scale. Reproduced with permission from Silver et al., 1992, Fig. 1a, p. 2, Copyright 1992, Nature Publishing Company. (**b**) NMDAR-mediated EPSCs recorded in isolation, following block of AMPARs by CNQX. Note prolonged decay and slow rise time (inset) compared with AMPAR EPSCs (reproduced with permission from Silver et al., 1992, Fig. 1b, p. 2, Copyright 1992, Nature Publishing Company). (**c**) Voltage dependence of NMDA receptor-mediated currents in 0 mM Mg^{2+} (*solid line*) and 0.5 mM Mg^{2+} (*dashed line*). The current–voltage relationship is approximately linear in the absence of Mg^{2+} but currents are reduced at negative potentials in the presence of Mg^{2+} (reproduced with permission from Nowak et al., 1984, Fig. 1a, p. 2, Copyright 1984, Nature Publishing Company). (**d**) Depiction of the NMDAR illustrating the requirement for glutamate (Glu) and glycine (Gly) binding and the removal of the Mg^{2+} block for channel opening

of metabotropic glutamate receptors (mGluRs) has been shown to induce LTD or to modulate the induction of LTP at a number of synapses (Bashir et al., 1993; Kemp et al., 2000; Malenka and Bear, 2004), and it is clear that there is interaction between the signalling pathways initiated by mGluR and NMDAR activation (Kemp et al., 2000). It has been proposed that the coincident activation of mGluRs and postsynaptic voltage-activated calcium channels is sufficient for the induction of LTD and can override the induction of LTP (Nevian and Sakmann, 2006). At hippocampal synapses, postsynaptic calcium transients produced by synaptic stimulation and postsynaptic action potentials arise from multiple sources including NMDARs and voltage-activated calcium channels (Bloodgood and Sabatini, 2007).

Hebbian Synaptic Plasticity

NMDAR-dependent LTP and LTD are often termed associative or Hebbian synaptic plasticity because they require coincident activity in the presynaptic and postsynaptic neurons. Postsynaptic depolarisation can come from a variety of sources including back-propagating action potentials, local dendritic spikes and activation of nearby synapses that are subthreshold for spike initiation.

All of the synaptic connections between glutamatergic neurons in the hippocampus exhibit associative long-term synaptic plasticity with one exception (see next section) but the best studied and characterised in vitro are the Schaffer collateral synapses between CA3 and CA1 pyramidal cells. Compared to these synapses, relatively little is known about the properties of synaptic plasticity at other hippocampal synapses but it is generally assumed that similar rules apply (with a few variations). The other synapses include (i) the perforant path synapses between entorhinal cortex pyramidal cells and dentate gyrus granule cells, CA3 pyramidal cells or CA1 pyramidal cells; (ii) the recurrent collateral synapses between CA3 pyramidal cells and other CA3 pyramidal cells; and (iii) the synapses between CA1 and subicular pyramidal cells (Fig. 2). No significant differences in synaptic plasticity induction have been found between Schaffer collateral synapses and CA3 recurrent collateral synapses. Perforant path synapses onto CA3 or CA1 pyramidal cells do show different induction properties largely because back-propagating action potentials do not reach these synapses due to their extreme distance from the soma (Golding et al., 2002). This means that the postsynaptic depolarisation required to activate NMDARs must come from other sources such as other synapses and/or dendritic Ca^{2+} spikes (Golding et al., 2002). Perforant path synapses onto dentate gyrus granule cells are divided into the medial and lateral synapses corresponding to inputs from layer IV and layer V pyramidal cells of the entorhinal cortex, respectively. These two pathways have similar rules for synaptic plasticity induction but the lateral pathway has a higher threshold for LTP induction. Pairing of presynaptic stimulation with postsynaptic depolarisation requires a higher rate of stimulation for the lateral pathway (1–4 Hz) compared to the medial pathway (0.5 Hz) (Colino and Malenka, 1993).

Activity at spatially distant synapses can also alter the threshold for LTP or LTD induction. The original description of this effect is found at the medial and lateral perforant path synapses in the dentate gyrus where activity in one pathway lowers the threshold for the induction of plasticity in the other (Levy and Steward, 1979; McNaughton et al., 1978). Since then the mossy fibre synapse in CA3 has been shown to transform subthreshold activity at CA3 associational/commissural synapses into suprathreshold activity for LTP induction (Kobayashi and Poo, 2004) (but not vice versa), and a similar effect is seen in CA1 where perforant path synapses influence Schaffer collateral LTP (Dudman et al., 2007).

Non-Hebbian Synaptic Plasticity

Mossy fibre synapses connecting dentate gyrus granule cells with CA3 pyramidal cells are the only instance of glutamatergic synapses exhibiting non-Hebbian synaptic plasticity in the hippocampus. LTP at mossy fibre synapses is induced by a high-frequency train of action potentials in the presynaptic granule cells that cause Ca^{2+} influx into the presynaptic terminals (Harris and Cotman, 1986; Zalutsky and Nicoll, 1990). Conversely, LTD at these synapses is induced by low-frequency presynaptic stimulation (Kobayashi et al., 1996; Tzounopoulos et al., 1998). Although this model has no requirement for postsynaptic activity, some researchers have argued for a postsynaptic role (Contractor et al., 2002; Yeckel et al., 1999 but see Mellor and Nicoll, 2001). In addition, there are also Hebbian forms of synaptic plasticity present at these synapses. Short bursts of high-frequency stimulation (24 stimuli at 25 Hz) can potentiate NMDAR-mediated synaptic transmission (Kwon and Castillo, 2008; Rebola et al., 2008), and low-frequency stimulation (0.33 Hz) paired with postsynaptic depolarisation can depress AMPAR-mediated synaptic transmission (Lei et al., 2003).

Non-Hebbian synaptic plasticity will clearly have a very different function to Hebbian synaptic plasticity since it is non-associative and requires only firing in a single neuron. If a granule cell fires a high-frequency burst of action potentials above a threshold (approximately 12 action potentials at 25 Hz; Schmitz et al., 2003) then LTP will be induced. The threshold for LTD is not precisely characterised but generally 900 stimuli at 1 Hz is sufficient (Kobayashi et al., 1996).

Homeostatic Synaptic Regulation, Metaplasticity and Heterosynaptic Plasticity

Synaptic regulation that is not synapse specific and therefore not induced by the activation of individual synapses is known as homeostatic synaptic plasticity. By increasing or decreasing the strength of all the synapses on its dendrites, a neuron can regulate its overall excitability and keep its response to synaptic activity within an efficient and dynamic range. Mechanisms exist to globally decrease the strength of synaptic connections if the postsynaptic neuron experiences hyperactivity and conversely can increase global synaptic strength in conditions of low neuronal activity (Burrone et al., 2002; O'Brien et al., 1998; Turrigiano et al., 1998). These mechanisms occur over a period of days and can lead to twofold increases or decreases in the density of synapses. Homeostatic synaptic regulation thus allows a neuron to normalise its inputs in a range that allows an optimal signal-to-noise ratio (Miller, 1996) and ensures network stability (Golowasch et al., 1999). However, since most experiments on homeostatic synaptic plasticity use cells in dissociated culture, with induction protocols that last for hours or days, and furthermore do not record the activity that occurs during that period it is hard to specify the precise conditions that are required to induce this plasticity and relate them to in

vivo situations. Homeostatic synaptic regulation also predicts that LTP of specific synapses will result in synaptic depression at other synapses on the neuron and vice versa (Miller, 1996), otherwise known as heterosynaptic plasticity.

LTP induction at specific synapses on a single cell can induce heterosynaptic LTD at other synapses (Abraham et al., 1994; Doyere et al., 1997; Levy and Steward, 1979). This has been found between the medial and lateral perforant pathways in the dentate gyrus and between Schaffer collateral pathways in CA1 (Daw et al., 2000). In these instances, an LTP of 50% in one synaptic pathway can induce a 20% LTD in the other pathway. This could be an important mechanism to increase synaptic signal-to-noise ratio and it occurs over the same time frame as LTP or LTD. However, heterosynaptic LTD is not consistently observed so it is hard to predict what stimuli will reliably induce it.

The ability of prior activity to modify the threshold for subsequent synaptic plasticity induction is termed metaplasticity and has been shown for Schaffer collateral synapses in CA1 and perforant path synapses in the dentate gyrus. Metaplasticity can occur through NMDAR or mGluR-mediated mechanisms. Prior NMDAR activation increases the threshold for LTP induction (Huang et al., 1992) and decreases the threshold for LTD induction (Christie and Abraham, 1992) but, conversely, prior mGluR activation decreases the LTP threshold in CA1 (Cohen and Abraham, 1996) although it increases the threshold in the dentate gyrus (Gisabella et al., 2003). It is not known how these two opposing mechanisms interact but a general rule along similar lines to homeostatic plasticity would indicate that prior LTP induction enhances the subsequent probability of LTD induction and vice versa. The inconsistency of metaplastic effects once again makes it hard to predict the precise patterns of stimuli that will reliably induce it in vivo.

Role of Inhibition in the Induction of LTP

Inhibitory inputs onto the postsynaptic neuron decrease the degree of depolarisation and therefore limit the activation of NMDARs and the induction of associative synaptic plasticity. The timecourse of synaptic $GABA_A$ receptor responses is very similar to synaptic NMDAR responses and therefore effectively counteracts NMDAR activation. This predicts that pharmacological blockade of $GABA_A$ receptors lowers the threshold for LTP induction and this is indeed the case (Meredith et al., 2003; Wigstrom and Gustafsson, 1983). The situation with $GABA_B$ receptor activation is somewhat more complex since $GABA_B$ receptors have both presynaptic and postsynaptic effects. Presynaptically, they inhibit release of GABA from inhibitory terminals at both feedforward and feedback interneurons. The suppression of GABA release then facilitates LTP induction at glutamatergic synapses (Davies et al., 1991). Postsynaptically, however, $GABA_B$ receptors on excitatory neurons suppress the induction of LTP by hyperpolarising the dendrite and reducing NMDAR activity. For these reasons, many synaptic plasticity experiments have been performed with pharmacological blockade of $GABA_A$ and/or $GABA_B$ receptors.

During the theta rhythm cycle, hippocampal interneurons fire in specific phases providing a powerful inhibitory drive (see Chapter 8 by Glovelli and Chapter 2 by Vida) that is believed to prevent the induction of LTP. During the theta rhythm, LTP can only be induced at the peak of the cycle and the same induction protocol induces LTD in the trough (Huerta and Lisman, 1993, 1995). Similarly, theta burst stimulation protocols to induce LTP or LTD are thought to be effective because $GABA_B$ receptor-mediated inhibition of GABA release is maximal ~200 ms after the initial GABA release (Davies et al., 1991).

Plasticity of Inhibition

Inhibitory inputs can also undergo plasticity either at the glutamatergic synapses onto interneurons (Lamsa et al., 2005) or at GABAergic synapses (Chevaleyre and Castillo, 2003; Woodin et al., 2003).

At glutamatergic synapses, the induction of LTP or LTD requires a rise in postsynaptic Ca^{2+} through either NMDARs or Ca^{2+} permeable AMPARs (Laezza et al., 1999; Lamsa et al., 2005; Lei and McBain, 2002). These involve different postsynaptic activity patterns since NMDARs require postsynaptic depolarisation whereas Ca^{2+} permeable AMPARs are blocked at depolarised potentials (Lamsa et al., 2007). High-frequency presynaptic stimulation induces LTD at mossy fibre inputs onto CA3 interneurons and LTP at mossy fibre inputs onto dentate gyrus interneurons (Alle et al., 2001; Laezza et al., 1999; Maccaferri et al., 1998). It also induces LTP and LTD at feedforward and feedback interneurons in CA1 (Lamsa et al., 2005, 2007; McMahon and Kauer, 1997) where the feedforward interneuron synapses exhibit NMDAR-dependent LTP and the feedback synapses Ca^{2+} permeable AMPAR-dependent LTP (Lamsa et al., 2005, 2007).

At GABAergic synapses, LTD is induced by a rise in intracellular Ca^{2+} in either the postsynaptic interneuron (Woodin et al., 2003) or a nearby CA1 pyramidal cell (Chevaleyre and Castillo, 2003). LTP is also induced by high-frequency stimulation (Caillard et al., 1999; Shew et al., 2000).

Synaptic $GABA_B$ receptors have also recently been shown to undergo synaptic plasticity. Potentiation of synaptic $GABA_B$ receptors was seen after pairing 3-Hz stimulation with postsynaptic depolarisation (Huang et al., 2005).

Induction of LTP and LTD by Artificial Induction Protocols

The proposed scheme whereby short, large-magnitude increases in intracellular Ca^{2+} concentration lead to synaptic potentiation whereas prolonged, small-magnitude increases lead to synaptic depression (Bienenstock et al., 1982) has been reinforced by the use of short high-frequency presynaptic stimulation to induce LTP and long low-frequency presynaptic stimulation to induce LTD. Typical frequencies used to induce LTP sit in the range 10–250 Hz and contain 20–100 stimuli with trains of stimuli often given multiple times. For LTD induction, frequencies range

from 1 to 3 Hz and the number of stimuli is generally much greater at 100–900 stimuli (Dudek and Bear, 1993; Dunwiddie and Lynch, 1978). However, LTD is only easily induced, and therefore almost exclusively studied, in immature preparations. In adult preparations, LTD is difficult to induce reliably whereas LTP is readily induced.

An alternative method to activate NMDARs by correlating presynaptic glutamate release with postsynaptic depolarisation uses intracellular recordings to depolarise the postsynaptic neuron whilst stimulating presynaptic release (Isaac et al., 1995). Using this technique, presynaptic stimulation frequency is kept similar for LTP or LTD induction, but the degree of depolarisation is greater for LTP induction. Typically this is −10 to 0 mV for LTP and −40 to −30 mV for LTD (Daw et al., 2000; Isaac et al., 1995). Again, this reinforces the idea that more NMDAR activation is required for LTP induction resulting in higher intracellular Ca^{2+} concentrations. The number of stimuli given is again generally greater for LTD induction.

Induction of LTP and LTD by Theta Burst Stimulation

In the hippocampus, states during which learning is thought to occur are characterised by pronounced population activity at the theta frequency (5–10 Hz). The principal glutamatergic neurons of the hippocampus fire action potentials in bursts on the peak of every theta cycle and are largely silent during the rest of the cycle. This is thought to be due to activity in the interneuron population that inhibits glutamatergic neuron firing during other phases of the cycle. This observation led to the development of theta burst stimulation (TBS) protocols for synaptic plasticity induction (Larson et al., 1986; Rose and Dunwiddie, 1986) (Fig. 5). The progressive increase in synaptic strength after TBS is in contrast to the generally stable or decreasing synaptic strength caused by artificial LTP induction protocols such as high-frequency stimulation or pairing (see Fig. 2). TBS induces LTP when presynaptic and postsynaptic entities are stimulated in synchrony but induces LTD when presynaptic and postsynaptic entities are non-coincident (Huerta and Lisman, 1995). Therefore, if presynaptic bursts of activity occur at the peak of the theta cycle then LTP will be induced but if they occur in the trough then LTD results (Huerta and Lisman, 1995).

Spike Timing-Dependent Synaptic Plasticity

Another method of activating NMDARs is to directly pair presynaptic and postsynaptic action potentials so they coincide at the synapse. In this way, the presynaptic action potential causes release of glutamate and the postsynaptic action potential back-propagates along the dendrite to depolarise the spine. This method induces LTP in both cortical and hippocampal slices (Magee and Johnston, 1997; Markram et al., 1997). In the cortical slice it was also shown that the temporal precision of the presynaptic and postsynaptic action potentials was critical. If the presynaptic action

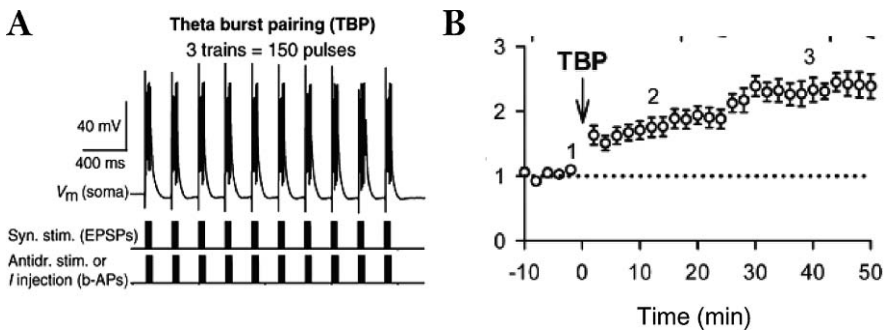

Fig. 5 Induction of LTP by theta burst stimulation. (**a**) Theta burst stimulation (TBS) protocol showing the pattern of presynaptic and postsynaptic stimulation used to induce LTP. The *upper trace* illustrates the cellular response to a train of TBS. *Lower traces* represent the stimulation given to the presynaptic axons (*upper*) and postsynaptic cell to induce back-propagating action potentials (b-APs, *lower*) (reproduced with permission from Frick et al., 2004, Fig. 1a, p. 2, Copyright 2004, Nature Publishing Company). (**b**) TBS induces LTP (reproduced with permission from Yang et al., 2008, Fig. 1a, p. 11389, Copyright 2008 National Academy of Sciences)

potential occurred before the postsynaptic action potential then LTP was induced, but LTD was induced if the timings were reversed (Markram et al., 1997). This temporal specificity has been termed spike timing-dependent plasticity (STDP) and was subsequently demonstrated in hippocampal dissociated cultures (Bi and Poo, 1998), slice cultures (Debanne et al., 1998) and acute slices (Nishiyama et al., 2000). However, recently doubt has been raised over the precise protocols required to induce bidirectional plasticity using STDP (Buchanan and Mellor, 2007; Wittenberg and Wang, 2006). Figure 6 illustrates the experimental evidence to date for STDP relationships at hippocampal synapses.

There is a marked variability in the relationships deduced from the experiments and this highlights the need for caution when using such data to model synaptic plasticity in the hippocampus. It is becoming clear that multiple postsynaptic spikes, or bursts, are required to induce STDP in the hippocampus (Fig. 6d) (Buchanan and Mellor, 2007; Pike et al., 1999; Wittenberg and Wang, 2006). The temporal requirements for burst firing have yet to be fully elucidated and it remains to be seen how this affects synaptic plasticity induced by naturally occurring spike patterns. In contrast, the evidence from cortical slice experiments consistently indicates a strong temporal dependence on the direction of plasticity (Froemke et al., 2006; Nevian and Sakmann, 2006; Sjostrom and Nelson, 2002; Sjostrom et al., 2001) that varies slightly between synapses (Letzkus et al., 2006; Sjostrom and Hausser, 2006) and can be altered by neuromodulators (Seol et al., 2007; Sjostrom et al., 2003). The temporal specificity of STDP in the cortex is also affected by multiple postsynaptic spikes, and in the cortex the requirements for postsynaptic burst firing are better characterised than in the hippocampus (Froemke et al., 2006; Nevian and Sakmann, 2006).

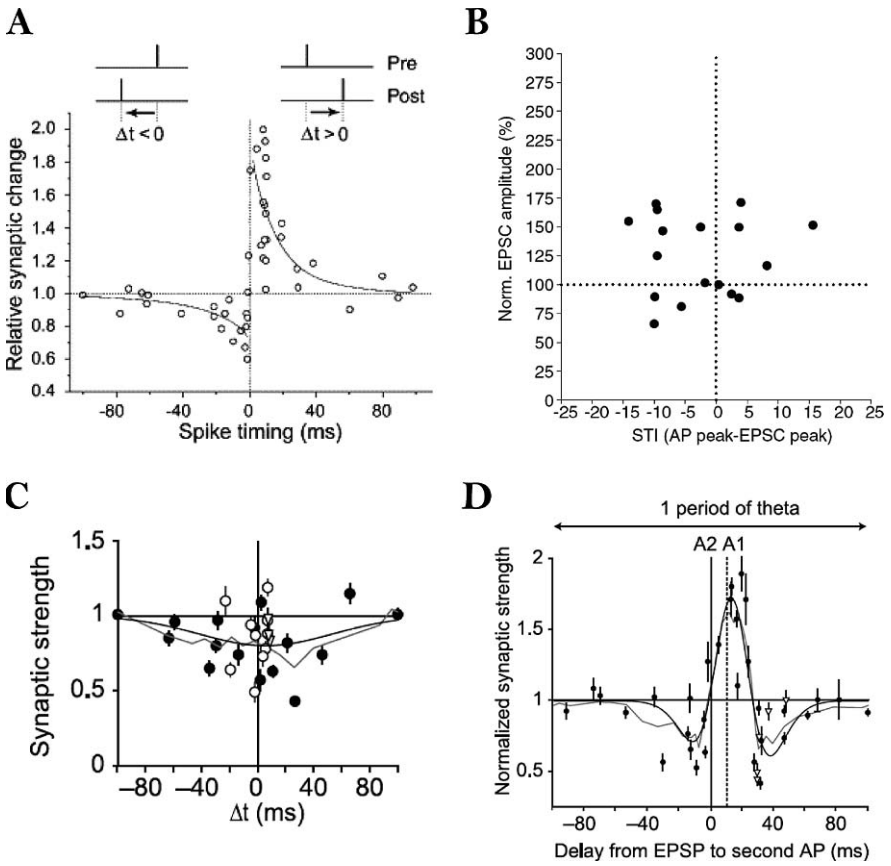

Fig. 6 Relationships between relative spike timing of pre- and postsynaptic spikes in a pair and the synaptic plasticity induced from different studies. (**a**) Reproduced with permission from Bi and Poo, 1998, Fig. 7, p. 10470, Copyright 1998 Society for Neuroscience. (**b**) Reproduced with permission from Buchanan and Mellor, 2007, Fig. 5c, p. 437, Copyright 2007 Physiological Society. (**c**) *Open circles* indicate pairings delivered at frequencies from 0.1 to 0.5 Hz, filled circles at 5 Hz. Reproduced with permission from Wittenberg and Wang, 2006, Fig. 1d, p. 6612, Copyright 2006 Society for Neuroscience. (**d**) The STDP relationship shown in **c** changes when two postsynaptic stimuli are given for each presynaptic and postsynaptic pairing. *Dashed line* indicates the time of the first postsynaptic action potential in most experiments. Reproduced with permission from Wittenberg and Wang, 2006, Fig. 3e, p. 6614, Copyright 2006 Society for Neuroscience

Induction of LTP and LTD by Natural Stimulus Patterns

Surprisingly few studies have attempted to induce long-term synaptic plasticity using naturally occurring patterns of activity recorded from cells in vivo. This is possibly because it is difficult to know precisely what activity is present in both the presynaptic and postsynaptic cells. In the visual cortex, spike patterns from individual cells responding to overlapping visual receptive fields induce STDP when

replayed into synaptically coupled cells in a cortical slice (Froemke and Dan, 2002). In the hippocampus, place cell firing patterns have been used to induce LTP by stimulating a population of Schaffer collateral axons and recording the change in fEPSP (Dobrunz and Stevens, 1999). More recently, it has been shown that spike patterns from pairs of place cells with overlapping place fields induce LTP when replayed into synaptically coupled pyramidal cells in a hippocampal slice (Isaac et al., 2009). These experiments are perhaps most relevant to this chapter since they demonstrate the patterns of activity that induce synaptic plasticity in the hippocampus in vivo.

Functional Significance of Synaptic Plasticity

Synaptic plasticity increases or decreases the amplitude and initial slope of the EPSP or IPSP leading to changes in the ability of a specific synaptic input to influence the spike output of the postsynaptic neuron (Bliss and Lomo, 1973). For excitatory synapses, this changes the probability that an individual synaptic input will cause the postsynaptic neuron to fire an action potential and the latency of postsynaptic spike firing. However, the probability of postsynaptic firing never equals 1 for a single presynaptic stimulus and only at the very powerful mossy fibre synapses in CA3 does it approach 1 if multiple EPSPs from a single input summate temporally (Henze et al., 2002;). In this case, increasing the presynaptic firing frequency increases the probability of inducing a postsynaptic action potential ($\sim$0.1 at 10 Hz rising to $\sim$0.8 at 100 Hz). However, it is not clear if mossy fibre LTP will change the probability of inducing a postsynaptic action potential since it reduces the pronounced short-term facilitation exhibited at this synapse (Gundlfinger et al., 2007). For all other excitatory synapses, postsynaptic action potentials are dependent on the temporal and spatial summation of other synaptic inputs to the neuron. The majority of data addressing the effects of synaptic plasticity on the probability of a postsynaptic action potential use bulk stimulation of presynaptic axons that necessarily diminishes the ability to make conclusions about the effects of synapse-specific plasticity. This is because the recording of single synaptic inputs requires the recording of synaptically coupled pairs of neurons that is technically very difficult in the hippocampus. Technical advances to achieve single synaptic recording are discussed in the final section of this chapter. Data regarding the summation of synaptic inputs can be found in other chapters.

Experimental Techniques

The study of synaptic plasticity has largely been performed by electrophysiological recording of synaptic strength. In the hippocampus this can be done in a variety of hippocampal preparations listed below together with a description of their strengths and weaknesses (Table 1).

Table 1 Hippocampal preparations used for the study of synaptic plasticity

System	Uses	Limitations
Dissociated culture	Easy to isolate the presynaptic and postsynaptic cells and therefore to perform paired intracellular recordings. This has enabled the study of synaptic plasticity at unitary connections between neurons	Synapses and networks have regrown in culture and exhibit very different properties to those found in the intact hippocampus. For example connections between pairs of neurons have many more synapses and LTP is hard to induce by conventional high-frequency activity
Acute slices	Retains many of the network connections found in vivo. Easy to make intra cellular or extra-cellular recordings	Many connections from other brain areas are cut. The slicing procedure introduces acute trauma to the tissue that alters synaptic properties. Very hard to make paired recordings
Cultured slices	Retains many of the network connections found in vivo. Easy to make intracellular recordings. Connectivity between neurons is high thus enabling paired recordings	Many connections from other brain areas are cut. The slicing procedure introduces acute trauma to the tissue that alters synaptic properties. New synaptic connections that are not found in vivo are formed during culture
In vivo	Most physiological systems	Technically challenging especially intracellular recordings that are difficult to maintain for extended periods. Easier to perform experiments on anaesthetised animals but this reduces the physiological relevance. Technology not currently available to make paired recordings

There are also a number of different recording techniques both electrophysiological and non-electrophysiological that can be used to measure synaptic strength (Table 2). Whilst the non-electrophysiological techniques do not directly measure the electrical input from a synapse, in the majority of cases they have been shown to be positively correlated with electrophysiological measurements. Here, three types of imaging technique are assessed. Ca^{2+} imaging can be used at presynaptic or postsynaptic sites using intracellular loading of Ca^{2+} indicators. Voltage imaging can also be used at presynaptic or postsynaptic sites by intracellular loading of membrane voltage indicators. Morphological imaging of presynaptic terminals or postsynaptic spines uses intracellular fluorescent markers such as GFP or actin bound GFP.

Table 2 Techniques used to measure synaptic strength

Technique	Strengths	Weaknesses
Field recording	The laminar structure of the hippocampus lends itself to extra-cellular field recording. Recordings are stable for long periods (several hours in vitro, and several days in vivo). Non-invasive	Large populations of synapses are recorded so difficult to assign synapse specificity. No control of postsynaptic neuronal activity
Whole-cell recording	Control over postsynaptic somatic membrane potential. Paired recordings from two synaptically coupled neurons are possible	Invasive. Endogenous intracellular constituents are progressively washed out of the cell during recordings leading to loss of LTP
Perforated patch recording	Control over postsynaptic somatic membrane potential. Non-invasive intracellular recording	Perforation takes time to stabilise access resistance (up to 1 h)
Ca^{2+} imaging	Measures the critical trigger for the induction of synaptic plasticity. Pinpoints the spatial location of the synapses stimulated. Activity at single synapses can be monitored	Ca^{2+} indicators buffer rises in intracellular Ca^{2+}. Ca^{2+} rises are not linearly related to the amplitude of synaptic transmission. Images lose sensitivity and resolution in deep tissue
Membrane potential imaging	Measures the spatial location of fast membrane voltage changes. Combines the strengths of both electrophysiology and imaging. Non-invasive	Low sensitivity restricts imaging to relatively large voltage changes. Images lose sensitivity and resolution in deep tissue
Morphological imaging	Pinpoints the spatial location of stimulated synapses. Non-invasive	Morphological changes are not linearly related to the amplitude of synaptic transmission. Images lose sensitivity and resolution in deep tissue

The Future

It is increasingly apparent that the rules that apply to the induction of synaptic plasticity in vivo are not necessarily the same as those found in in vitro preparations. Furthermore, it is also clear that the patterns of activity that might induce synaptic plasticity in vivo are not the same as those used to induce plasticity in vitro.

The reasons for the discrepancies are unclear but an obvious possibility is that the in vitro approaches are too reductionist and need to incorporate more data. For

example, better information on the interaction between different synaptic pathways would be useful both in terms of the type of activity patterns involved and the mechanisms underlying any interaction. Furthermore, better data about how network activity affects the induction of synaptic plasticity and the interaction between glutamatergic and GABAergic systems are required.

To bridge the gap between the in vivo and in vitro situations and to generate more realistic models for the changes that occur in the hippocampal network as a result of synaptic plasticity, more data are needed on how plasticity is induced by natural patterns of activity. It is remarkable that so many models and hypotheses have been put forward for the role of synaptic plasticity in vivo without evidence to show either that synaptic plasticity is induced or what patterns of activity are required. This lack of data could be overcome by advances in a number of methodologies (Neves et al., 2008).

Historically, the measurement of synaptic plasticity has necessitated a trade-off between the ease of data acquisition and the physiological relevance of the system and technique. Thus, recordings in dissociated culture are easier than slices which are easier than recordings in vivo but the proximity of the experimental system to the situation in a behaving animal goes in the opposite direction. Progress is being made towards achieving intracellular recordings from neurons in vivo but so far this has largely been from superficial cortical layers. However, intracellular recordings have been attained from hippocampal neurons in vivo (e.g. Harvery et al., 2009; Henze et al., 2002; Lee et al., 2006) and it is hoped that these technologies will become increasingly more widespread.

It is also possible that the advances being made in brain imaging may supersede conventional electrophysiological techniques for in vivo recording. The ability to image synapse strength by morphological, voltage or calcium imaging may prove to be easier in vivo than intracellular electrophysiological recording. In particular, voltage-sensitive dyes offer the promise of measuring fast voltage changes at high spatial resolution combining the best aspects of electrophysiology and imaging techniques. However, current methods do not provide enough resolution or sensitivity and it is hoped that these drawbacks may be overcome in the near future.

The recent demonstration of a method using genetic techniques to insert ligand-activated or light-activated ion channels into the membrane of neurons could be used in this context. In particular, the ability to stimulate specific single neurons within the brain using light would remove some of the technical difficulties of recording single synaptic connections in vivo. However, recording the strength of individual synapses would still be technically challenging. In addition, the light-activated channels currently in use induce action potentials that are significantly different to those initiated by synaptic activity or current injection.

An alternative approach involves recording the activity of individual neurons in vivo during learning tasks and then using this spike activity information to replay the activity seen in vivo into a synapse in an in vitro slice preparation. Surprisingly, to date this approach has not been adopted by many researchers (Dobrunz and Stevens, 1999; Isaac et al. 2009) but it has the potential to provide a wealth of data on the activity patterns required to induce synaptic plasticity and the behavioural conditions under which they occur.

Advances are also being made in determining the role of synaptic plasticity at specific synapses in hippocampal-dependent learning and memory by using genetic approaches. In the past, the role of synaptic plasticity has been inferred by blocking plasticity with intra-hippocampal infusion of pharmacological agents that block LTP (Morris et al., 1986; Pastalkova et al., 2006). Recently, new technologies to genetically target synaptic plasticity at specific synapses at specific times have been developed. These have employed deletion of the NR1 subunit of NMDARs from either granule cells, CA3 pyramidal cells or CA1 pyramidal cells and reveal the contribution made by NMDAR-dependent synaptic plasticity in each cell type (McHugh et al., 1996, 2007; Nakazawa et al., 2002).

Ultimately, it is hoped that individual synapses will be recorded from the hippocampi of unanaesthetised animals before, during and after performance in learning tasks. This would enable researchers to visualise the contribution of synaptic plasticity at single synapses to learning and memory (Neves et al., 2008).

Acknowledgments The author would like to thank Tim Bliss for critical reading and comments.

Further Reading

Abraham, W.C., Christie, B.R., Logan, B., Lawlor, P., and Dragunow, M. (1994). Immediate early gene expression associated with the persistence of heterosynaptic long-term depression in the hippocampus. Proc Natl Acad Sci U S A *91*, 10049–10053.

Alle, H., Jonas, P., and Geiger, J.R. (2001). PTP and LTP at a hippocampal mossy fiber-interneuron synapse. Proc Natl Acad Sci U S A *98*, 14708–14713.

Asztely, F., Kokaia, M., Olofsdotter, K., Ortegren, U., and Lindvall, O. (2000). Afferent-specific modulation of short-term synaptic plasticity by neurotrophins in dentate gyrus. Eur J Neurosci *12*, 662–669.

Bashir, Z.I., Bortolotto, Z.A., Davies, C.H., Berretta, N., Irving, A.J., Seal, A.J., Henley, J.M., Jane, D.E., Watkins, J.C., and Collingridge, G.L. (1993). Induction of LTP in the hippocampus needs synaptic activation of glutamate metabotropic receptors. Nature *363*, 347–350.

Bear, M.F., Cooper, L.N., and Ebner, F.F. (1987). A Physiological-basis for a theory of synapse modification. Science *237*, 42–48.

Bi, G.Q., and Poo, M.M. (1998). Synaptic modifications in cultured hippocampal neurons: dependence on spike timing, synaptic strength, and postsynaptic cell type. J Neurosci *18*, 10464–10472.

Bienenstock, E.L., Cooper, L.N., and Munro, P.W. (1982). Theory for the development of neuron selectivity – orientation specificity and binocular interaction in visual-cortex. J Neurosci *2*, 32–48.

Bliss, T.V., and Collingridge, G.L. (1993). A synaptic model of memory: long-term potentiation in the hippocampus. Nature *361*, 31–39.

Bliss, T.V., and Lomo, T. (1973). Long-lasting potentiation of synaptic transmission in the dentate area of the anaesthetized rabbit following stimulation of the perforant path. J Physiol *232*, 331–356.

Bloodgood, B.L., and Sabatini, B.L. (2007). Nonlinear regulation of unitary synaptic signals by CaV(2.3) voltage-sensitive calcium channels located in dendritic spines. Neuron *53*, 249–260.

Buchanan, K.A., and Mellor, J.R. (2007). The development of synaptic plasticity induction rules and the requirement for postsynaptic spikes in rat hippocampal CA1 pyramidal neurones. J Physiol (Lond) *585*, 429–445.

Burrone, J., O'Byrne, M., and Murthy, V.N. (2002). Multiple forms of synaptic plasticity triggered by selective suppression of activity in individual neurons. Nature *420*, 414–418.

Caillard, O., Ben-Ari, Y., and Gaiarsa, J.L. (1999). Long-term potentiation of GABAergic synaptic transmission in neonatal rat hippocampus. J Physiol *518*(Pt 1), 109–119.

Castillo, P.E., Weisskopf, M.G., and Nicoll, R.A. (1994). The role of Ca2+ channels in hippocampal mossy fiber synaptic transmission and long-term potentiation. Neuron *12*, 261–269.

Chevaleyre, V., and Castillo, P.E. (2003). Heterosynaptic LTD of hippocampal GABAergic synapses: a novel role of endocannabinoids in regulating excitability (vol 38, pg 461, 2003). Neuron *38*, 997–997.

Cho, K., Aggleton, J.P., Brown, M.W., and Bashir, Z.I. (2001). An experimental test of the role of postsynaptic calcium levels in determining synaptic strength using perirhinal cortex of rat. J Physiol-London *532*, 459–466.

Christie, B.R., and Abraham, W.C. (1992). Priming of associative long-term depression in the dentate gyrus by theta frequency synaptic activity. Neuron *9*, 79–84.

Cohen, A.S., and Abraham, W.C. (1996). Facilitation of long-term potentiation by prior activation of metabotropic glutamate receptors. J Neurophysiol *76*, 953–962.

Colino, A., and Malenka, R.C. (1993). Mechanisms underlying induction of long-term potentiation in rat medial and lateral perforant paths in vitro. J Neurophysiol *69*, 1150–1159.

Contractor, A., Rogers, C., Maron, C., Henkemeyer, M., Swanson, G.T., and Heinemann, S.F. (2002). Trans-synaptic Eph receptor-ephrin signaling in hippocampal mossy fiber LTP. Science *296*, 1864–1869.

Cormier, R.J., Greenwood, A.C., and Connor, J.A. (2001). Bidirectional synaptic plasticity correlated with the magnitude of dendritic calcium transients above a threshold. J Neurophysiol *85*, 399–406.

Davies, C.H., Starkey, S.J., Pozza, M.F., and Collingridge, G.L. (1991). GABA autoreceptors regulate the induction of LTP. Nature *349*, 609–611.

Daw, M.I., Chittajallu, R., Bortolotto, Z.A., Dev, K.K., Duprat, F., Henley, J.M., Collingridge, G.L., and Isaac, J.T.R. (2000). PDZ proteins interacting with C-terminal GluR2/3 are involved in a PKC-dependent regulation of AMPA receptors at hippocampal synapses. Neuron *28*, 873–886.

Debanne, D., Gahwiler, B.H., and Thompson, S.M. (1998). Long-term synaptic plasticity between pairs of individual CA3 pyramidal cells in rat hippocampal slice cultures. J Physiol-London *507*, 237–247.

Dobrunz, L.E., and Stevens, C.F. (1999). Response of hippocampal synapses to natural stimulation patterns. Neuron *22*, 157–166.

Doyere, V., Srebro, B., and Laroche, S. (1997). Heterosynaptic LTD and depotentiation in the medial perforant path of the dentate gyrus in the freely moving rat. J Neurophysiol *77*, 571–578.

Dudek, S.M., and Bear, M.F. (1992). Homosynaptic long-term depression in area CA1 of hippocampus and effects of N-methyl-D-aspartate receptor blockade. Proc Natl Acad Sci U S A *89*, 4363–4367.

Dudek, S.M., and Bear, M.F. (1993). Bidirectional long-term modification of synaptic effectiveness in the adult and immature hippocampus. J Neurosci *13*, 2910–2918.

Dudman, J.T., Tsay, D., and Siegelbaum, S.A. (2007). A role for synaptic inputs at distal dendrites: instructive signals for hippocampal long-term plasticity. Neuron *56*, 866–879.

Dunwiddie, T., and Lynch, G. (1978). Long-term potentiation and depression of synaptic responses in the rat hippocampus: localization and frequency dependency. J Physiol *276*, 353–367.

Frick, A., Magee, J., and Johnston, D. (2004). LTP is accompanied by an enhanced local excitability of pyramidal neuron dendrites. Nat Neurosci *7*, 126–135.

Froemke, R.C., and Dan, Y. (2002). Spike-timing-dependent synaptic modification induced by natural spike trains. Nature *416*, 433–438.

Froemke, R.C., Tsay, I.A., Raad, M., Long, J.D., and Dan, Y. (2006). Contribution of individual spikes in burst-induced long-term synaptic modification. J Neurophysiol *95*, 1620–1629.

Gall, D., Prestori, F., Sola, E., D'Errico, A., Roussel, C., Forti, L., Rossi, P., and D'Angelo, E. (2005). Intracellular calcium regulation by burst discharge determines bidirectional long-term synaptic plasticity at the cerebellum input stage. J Neurosci *25*, 4813–4822.

Gisabella, B., Rowan, M.J., and Anwyl, R. (2003). Mechanisms underlying the inhibition of long-term potentiation by preconditioning stimulation in the hippocampus in vitro. Neuroscience *121*, 297–305.

Golding, N.L., Staff, N.P., and Spruston, N. (2002). Dendritic spikes as a mechanism for cooperative long-term potentiation. Nature *418*, 326–331.

Golowasch, J., Casey, M., Abbott, L.F., and Marder, E. (1999). Network stability from activity-dependent regulation of neuronal conductances. Neural Comput *11*, 1079–1096.

Gundlfinger, A., Leibold, C., Gebert, K., Moisel, M., Schmitz, D., and Kempter, R. (2007). Differential modulation of short-term synaptic dynamics by long-term potentiation at mouse hippocampal mossy fibre synapses. J Physiol *585*, 853–865.

Hansel, C., Artola, A., and Singer, W. (1996). Different threshold levels of postsynaptic [Ca2+]i have to be reached to induce LTP and LTD in neocortical pyramidal cells. J Physiol Paris *90*, 317–319.

Hansel, C., Artola, A., and Singer, W. (1997). Relation between dendritic Ca2+ levels and the polarity of synaptic long-term modifications in rat visual cortex neurons. Eur J Neurosci *9*, 2309–2322.

Harris, E.W., and Cotman, C.W. (1986). Long-term potentiation of guinea pig mossy fiber responses is not blocked by N-methyl D-aspartate antagonists. Neuroscience Letters *70*, 132–137.

Harvey, C.D., Collman, F., Dombeck, D.A., and Tank, D.W. (2009). Intracellular dynamics of hippocampal place cells during virtual navigation. Nature *461*, 941–946.

Hebb, D. (1949). The organisation of behaviour. New York: Wiley.

Henze, D.A., Wittner, L., and Buzsaki, G. (2002). Single granule cells reliably discharge targets in the hippocampal CA3 network in vivo. Nat Neurosci *5*, 790–795.

Huang, C.S., Shi, S.H., Ule, J., Ruggiu, M., Barker, L.A., Darnell, R.B., Jan, Y.N., and Jan, L.Y. (2005). Common molecular pathways mediate long-term potentiation of synaptic excitation and slow synaptic inhibition. Cell *123*, 105–118.

Huang, Y.Y., Colino, A., Selig, D.K., and Malenka, R.C. (1992). The influence of prior synaptic activity on the induction of long-term potentiation. Science *255*, 730–733.

Huerta, P.T., and Lisman, J.E. (1993). Heightened synaptic plasticity of hippocampal ca1 neurons during a cholinergically induced rhythmic state. Nature *364*, 723–725.

Huerta, P.T., and Lisman, J.E. (1995). Bidirectional synaptic plasticity induced by a single burst during cholinergic theta-oscillation in ca1 in-vitro. Neuron *15*, 1053–1063.

Isaac, J.T., Nicoll, R.A., and Malenka, R.C. (1995). Evidence for silent synapses: implications for the expression of LTP. Neuron *15*, 427–434.

Isaac, J.T., Bucahanan, K.A., Muller, R.U. and Mellor, J.R. (2009). Hippocampal place cell firing patterns can induce long-term synaptic plasticity in vitro. J Neurosci *29*, 6840–6850.

Ismailov, I., Kalikulov, D., Inoue, T., and Friedlander, M.J. (2004). The kinetic profile of intracellular calcium predicts long-term potentiation and long-term depression. J Neurosc *24*, 9847–9861.

Jahr, C.E., and Stevens, C.F. (1990). A quantitative description of NMDA receptor-channel kinetic behavior. J Neurosci *10*, 1830–1837.

Kampa, B.M., Clements, J., Jonas, P., and Stuart, G.J. (2004). Kinetics of Mg2+ unblock of NMDA receptors: implications for spike-timing dependent synaptic plasticity. J Physiol *556*, 337–345.

Karmarkar, U.R., and Buonomano, D.V. (2002). A model of spike-timing dependent plasticity: one or two coincidence detectors? J Neurophysiol *88*, 507–513.

Keller, D.X., Franks, K.M., Bartol, T.M., Jr., and Sejnowski, T.J. (2008). Calmodulin activation by calcium transients in the postsynaptic density of dendritic spines. PLoS ONE *3*, e2045.

Kemp, N., McQueen, J., Faulkes, S., and Bashir, Z.I. (2000). Different forms of LTD in the CA1 region of the hippocampus: role of age and stimulus protocol. Eur J Neurosci *12*, 360–366.

Kobayashi, K., Manabe, T., and Takahashi, T. (1996). Presynaptic long-term depression at the hippocampal mossy fiber-CA3 synapse. Science *273*, 648–650.

Kobayashi, K., Manabe, T., and Takahashi, T. (1999). Calcium-dependent mechanisms involved in presynaptic long-term depression at the hippocampal mossy fibre-CA3 synapse. Eur J Neurosci *11*, 1633–1638.

Kobayashi, K., and Poo, M.M. (2004). Spike train timing-dependent associative modification of hippocampal CA3 recurrent synapses by mossy fibers. Neuron *41*, 445–454.

Kwon, H.B., and Castillo, P.E. (2008). Long-term potentiation selectively expressed by NMDA receptors at hippocampal mossy fiber synapses. Neuron *57*, 108–120.

Laezza, F., Doherty, J.J., and Dingledine, R. (1999). Long-term depression in hippocampal interneurons: joint requirement for pre- and postsynaptic events. Science *285*, 1411–1414.

Lamsa, K., Heeroma, J.H., and Kullmann, D.M. (2005). Hebbian LTP in feed-forward inhibitory interneurons and the temporal fidelity of input discrimination. Nat Neurosci *8*, 916–924.

Lamsa, K.P., Heeroma, J.H., Somogyi, P., Rusakov, D.A., and Kullmann, D.M. (2007). Anti-Hebbian long-term potentiation in the hippocampal feedback inhibitory circuit. Science *315*, 1262–1266.

Larson, J., Wong, D., and Lynch, G. (1986). Patterned stimulation at the theta-frequency is optimal for the induction of hippocampal long-term potentiation. Brain Res *368*, 347–350.

Lee, A.K., Manns, I.D., Sakmann, B., and Brecht, M. (2006). Whole-cell recordings in freely moving rats. Neuron *51*, 399–407.

Lei, S., and McBain, C.J. (2002). Distinct NMDA receptors provide differential modes of transmission at mossy fiber-interneuron synapses. Neuron *33*, 921–933.

Lei, S., Pelkey, K.A., Topolnik, L., Congar, P., Lacaille, J.C., and McBain, C.J. (2003). Depolarization-induced long-term depression at hippocampal mossy fiber-CA3 pyramidal neuron synapses. J Neurosci *23*, 9786–9795.

Letzkus, J.J., Kampa, B.M., and Stuart, G.J. (2006). Learning rules for spike timing-dependent plasticity depend on dendritic synapse location. J Neurosci *26*, 10420–10429.

Levy, W.B., and Steward, O. (1979). Synapses as associative memory elements in the hippocampal formation. Brain Res *175*, 233–245.

Lisman, J. (1989). A mechanism for the hebb and the anti-hebb processes underlying learning and memory. P Natl Acad Sci U S A *86*, 9574–9578.

Maccaferri, G., Roberts, J.D., Szucs, P., Cottingham, C.A., and Somogyi, P. (2000). Cell surface domain specific postsynaptic currents evoked by identified GABAergic neurones in rat hippocampus in vitro. J Physiol *524*(Pt 1), 91–116.

Maccaferri, G., Toth, K., and McBain, C.J. (1998). Target-specific expression of presynaptic mossy fiber plasticity. Science *279*, 1368–1370.

Magee, J.C., and Johnston, D. (1997). A synaptically controlled, associative signal for Hebbian plasticity in hippocampal neurons. Science *275*, 209–213.

Malenka, R.C., and Bear, M.F. (2004). LTP and LTD: An embarrassment of riches. Neuron *44*, 5–21.

Markram, H., Lubke, J., Frotscher, M., and Sakmann, B. (1997). Regulation of synaptic efficacy by coincidence of postsynaptic APs and EPSPs. Science *275*, 213–215.

McBain, C.J., and Mayer, M.L. (1994). N-methyl-D-aspartic acid receptor structure and function. Physiol Rev *74*, 723–760.

McHugh, T.J., Blum, K.I., Tsien, J.Z., Tonegawa, S., and Wilson, M.A. (1996). Impaired hippocampal representation of space in CA1-specific NMDAR1 knockout mice. Cell *87*, 1339–1349.

McHugh, T.J., Jones, M.W., Quinn, J.J., Balthasar, N., Coppari, R., Elmquist, J.K., Lowell, B.B., Fanselow, M.S., Wilson, M.A., and Tonegawa, S. (2007). Dentate gyrus NMDA receptors mediate rapid pattern separation in the hippocampal network. Science *317*, 94–99.

McMahon, L.L., and Kauer, J.A. (1997). Hippocampal interneurons express a novel form of synaptic plasticity. Neuron *18*, 295–305.

McNaughton, B.L., Douglas, R.M., and Goddard, G.V. (1978). Synaptic enhancement in fascia dentata: cooperativity among coactive afferents. Brain Res *157*, 277–293.

Mellor, J., and Nicoll, R.A. (2001). Hippocampal mossy fiber LTP is independent of postsynaptic calcium. Nat Neurosci *4*, 125–126.

Meredith, R.M., Floyer-Lea, A.M., and Paulsen, O. (2003). Maturation of long-term potentiation induction rules in rodent hippocampus: role of GABAergic inhibition. J Neurosci *23*, 11142–11146.

Miller, K.D. (1996). Synaptic economics: competition and cooperation in synaptic plasticity. Neuron *17*, 371–374.

Monyer, H., Burnashev, N., Laurie, D.J., Sakmann, B., and Seeburg, P.H. (1994). Developmental and regional expression in the rat brain and functional properties of four NMDA receptors. Neuron *12*, 529–540.

Morris, R.G.M., Anderson, E., Lynch, G.S., and Baudry, M. (1986). Selective impairment of learning and blockade of long-term potentiation by an N-Methyl-D-aspartate receptor antagonist, Ap5. Nature *319*, 774–776.

Nakazawa, K., Quirk, M.C., Chitwood, R.A., Watanabe, M., Yeckel, M.F., Sun, L.D., Kato, A., Carr, C.A., Johnston, D., Wilson, M.A., and Tonegawa, S. (2002). Requirement for hippocampal CA3 NMDA receptors in associative memory recall. Science *297*, 211–218.

Neves, G., Cooke, S.F., and Bliss, T.V. (2008). Synaptic plasticity, memory and the hippocampus: a neural network approach to causality. Nat Rev Neurosci *9*, 65–75.

Nevian, T., and Sakmann, B. (2006). Spine Ca2+ signaling in spike-timing-dependent plasticity. J Neurosci *26*, 11001–11013.

Nicoll, R.A., Kauer, J.A., and Malenka, R.C. (1988). The current excitement in long-term potentiation. Neuron *1*, 97–103.

Nishiyama, M., Hong, K., Mikoshiba, K., Poo, M., and Kato, K. (2000). Calcium stores regulate the polarity and input specificity of synaptic modification. Nature *408*, 584–588.

Nowak, L., Bregestovski, P., Ascher, P., Herbet, A., and Prochiantz, A. (1984). Magnesium gates glutamate-activated channels in mouse central neurons. Nature *307*, 462–465.

O'Brien, R.J., Kamboj, S., Ehlers, M.D., Rosen, K.R., Fischbach, G.D., and Huganir, R.L. (1998). Activity-dependent modulation of synaptic AMPA receptor accumulation. Neuron *21*, 1067–1078.

Pastalkova, E., Serrano, P., Pinkhasova, D., Wallace, E., Fenton, A.A., and Sacktor, T.C. (2006). Storage of spatial information by the maintenance mechanism of LTP. Science *313*, 1141–1144.

Patneau, D.K., and Mayer, M.L. (1990). Structure-activity relationships for amino acid transmitter candidates acting at N-methyl-D-aspartate and quisqualate receptors. J Neurosci *10*, 2385–2399.

Pike, F.G., Meredith, R.M., Olding, A.W.A., and Paulsen, O. (1999). Postsynaptic bursting is essential for 'Hebbian' induction of associative long-term potentiation at excitatory synapses in rat hippocampus. J Physiol-London *518*, 571–576.

Rebola, N., Lujan, R., Cunha, R.A., and Mulle, C. (2008). Adenosine A2A receptors are essential for long-term potentiation of NMDA-EPSCs at hippocampal mossy fiber synapses. Neuron *57*, 121–134.

Regehr, W.G., and Tank, D.W. (1991). The maintenance of LTP at hippocampal mossy fiber synapses is independent of sustained presynaptic calcium. Neuron *7*, 451–459.

Rose, G.M., and Dunwiddie, T.V. (1986). Induction of hippocampal long-term potentiation using physiologically patterned stimulation. Neurosci Lett *69*, 244–248.

Salin, P.A., Scanziani, M., Malenka, R.C., and Nicoll, R.A. (1996). Distinct short-term plasticity at two excitatory synapses in the hippocampus. P Natl Acad Sci U S A *93*, 13304–13309.

Schmitz, D., Mellor, J., Breustedt, J., and Nicoll, R.A. (2003). Presynaptic kainate receptors impart an associative property to hippocampal mossy fiber long-term potentiation. Nat Neurosci *6*, 1058–1063.

Seol, G.H., Ziburkus, J., Huang, S., Song, L., Kim, I.T., Takamiya, K., Huganir, R.L., Lee, H.K., and Kirkwood, A. (2007). Neuromodulators control the polarity of spike-timing-dependent synaptic plasticity. Neuron *55*, 919–929.

Shew, T., Yip, S., and Sastry, B.R. (2000). Mechanisms involved in tetanus-induced potentiation of fast IPSCs in rat hippocampal CA1 neurons. J Neurophysiol *83*, 3388–3401.
Shouval, H.Z., and Kalantzis, G. (2005). Stochastic properties of synaptic transmission affect the shape of spike time-dependent plasticity curves. J Neurophysiol *93*, 1069–1073.
Silver, R.A., Traynelis, S.F., and Cull-Candy, S.G. (1992). Rapid-time-course miniature and evoked excitatory currents at cerebellar synapses in situ. Nature *355*, 163–166.
Sjostrom, P.J., and Hausser, M. (2006). A cooperative switch determines the sign of synaptic plasticity in distal dendrites of neocortical pyramidal neurons. Neuron *51*, 227–238.
Sjostrom, P.J., and Nelson, S.B. (2002). Spike timing, calcium signals and synaptic plasticity. Curr Opin Neurobiol *12*, 305–314.
Sjostrom, P.J., Turrigiano, G.G., and Nelson, S.B. (2001). Rate, timing, and cooperativity jointly determine cortical synaptic plasticity. Neuron *32*, 1149–1164.
Sjostrom, P.J., Turrigiano, G.G., and Nelson, S.B. (2003). Neocortical LTD via coincident activation of presynaptic NMDA and cannabinoid receptors. Neuron *39*, 641–654.
Turrigiano, G.G., Leslie, K.R., Desai, N.S., Rutherford, L.C., and Nelson, S.B. (1998). Activity-dependent scaling of quantal amplitude in neocortical neurons. Nature *391*, 892–896.
Tzounopoulos, T., Janz, R., Südhof, T.C., Nicoll, R.A., and Malenka, R.C. (1998). A role for cAMP in long-term depression at hippocampal mossy fiber synapses. Neuron *21*, 837–845.
Weisskopf, M.G., Zalutsky, R.A., and Nicoll, R.A. (1993). The opioid peptide dynorphin mediates heterosynaptic depression of hippocampal mossy fibre synapses and modulates long-term potentiation. Nature *365*, 188.
Wigstrom, H., and Gustafsson, B. (1983). Facilitated induction of hippocampal long-lasting potentiation during blockade of inhibition. Nature *301*, 603–604.
Wittenberg, G.M., and Wang, S.S.H. (2006). Malleability of spike-timing-dependent plasticity at the CA3-CA1 synapse. J Neurosci *26*, 6610–6617.
Woodin, M.A., Ganguly, K., and Poo, M.M. (2003). Coincident pre- and postsynaptic activity modifies GABAergic synapses by postsynaptic changes in Cl-transporter activity. Neuron *39*, 807–820.
Yang, Y., Wang, X.B., Frerking, M., and Zhou, Q. (2008). Delivery of AMPA receptors to perisynaptic sites precedes the full expression of long-term potentiation. Proc Natl Acad Sci U S A *105*, 11388–11393.
Yeckel, M.F., Kapur, A., and Johnston, D. (1999). Multiple forms of LTP in hippocampal CA3 neurons use a common postsynaptic mechanism. Nat Neurosci *2*, 625–633.
Zalutsky, R.A., and Nicoll, R.A. (1990). Comparison of two forms of long-term potentiation in single hippocampal neurons. Science *248*, 1619–1624.
Zucker, R.S., and Regehr, W.G. (2002). Short-term synaptic plasticity. Annu Rev Physiol *64*, 355–405.

Neuromodulation of Hippocampal Cells and Circuits

Stuart Cobb and J. Josh Lawrence

Overview

Neuromodulation is the process by which the properties of neurons and synapses are altered by neuroactive substances termed neuromodulators. The distinction between neuromodulation and classical neurotransmission can be fuzzy but in general neuromodulation is more diffuse, less targeted, and acts over a longer time course than classical fast neurotransmission. Often the same neurochemical may have rapid neurotransmitter-like effects followed by more sustained modulator-like actions. What makes neuromodulation an important consideration is that it appears to be a fundamental process in modifying all aspects of neural network functioning and information processing. Neural networks are not hard-wired, but plastic, and the neuromodulation of its components yields distinct activity patterns that are associated with behavioral state, allowing the same neural circuit to have added computational power. These components include the modification of neuronal excitability, integrative properties of neurons, synaptic transmission, and synaptic plasticity. Neuromodulators often have more than one cellular or synaptic consequence. Moreover, not all cellular or synaptic targets of neuromodulation produce the same effects. Due to the supreme control of the user over parameter space, computational modeling is a powerful tool for gaining insight into how cellular and synaptic targets of neuromodulation alter the functional output of neuronal populations and the processing of synaptic signals within networks. Beyond the acute effects of neuromodulation on cellular and synaptic excitability are longer term changes in gene expression and neuronal architecture that are essential in regulating developmental processes and structural plasticity. This chapter circumscribes the acute cellular and synaptic effects of neuromodulation on targets within the hippocampal formation.

S. Cobb / J.J. Lawrence (✉)
Neuroscience and Molecular Pharmacology, Faculty of Biomedical and Life Sciences, University of Glasgow, Glasgow, G12 8QQ, UK / COBRE Center for Structural and Functional Neuroscience, Department of Biomedical and Pharmaceutical Sciences, University of Montana, Missoula, MT 59812, USA
e-mail: s.cobb@bio.gla.ac.uk/lawrenjo@mail.nih.gov

V. Cutsuridis et al. (eds.), *Hippocampal Microcircuits*, Springer Series in Computational Neuroscience 5, DOI 10.1007/978-1-4419-0996-1_7,

The Data

Introduction

The hippocampus experiences a multitude of neuromodulatory substances, the release of which is often associated with particular external factors or dependent upon particular behavioral states. This chapter summarizes some of the primary neuromodulators including those that arise from sources extrinsic to the hippocampus (mainly subcortical nuclei) as well as those originating from cells intrinsic to the hippocampal formation. There may be important functional distinctions between intrinsic and extrinsic forms of neuromodulation (Katz and Frost, 1996) with the most obvious being that extrinsic neuromodulation is usually independent of ongoing activity within the circuits being modulated, whereas cells or synapses undergoing intrinsic modulation often do so as a result of ongoing activity within those same circuits. As discussed in earlier chapters, glutamate and GABA have multiple modes of action. In addition to ligand-gated ion channels for rapid transmission, slower, often intrinsic neuromodulatory actions are also produced through metabotropic signaling. Many of the "classical" neuromodulators presented here act in a similar manner and generally provide extrinsic neuromodulation as their sources of input derived predominantly from subcortical nuclei. Although some modulators, such as acetylcholine and serotonin, appear to possess machinery for fast, point-to-point transmission, "volume transmission," in which release of transmitter at non-synaptic varicosities diffuses to high-affinity metabotropic receptors, appears to be a major mode of transmission. It is possible, due to differences in the proximity of neuromodulatory release sites and postsynaptic composition of receptors, that specific cellular targets may employ point-to-point, volume, or both modes of transmission. Therefore, it is important to develop a more thorough understanding of how specific neuromodulatory afferents interact with their cellular targets.

In contrast to classical neuromodulators, many hippocampal neuropeptides are released from local hippocampal circuits to provide rich sources of intrinsic modulation. Other modulators including endocannabinoids and nitric oxide have an even more localized autocrine/paracrine modulatory action and mediate exclusively intrinsic modulation. In some cases, extrinsic neuromodulation induces secondary effects mediated by intrinsic modulation, as demonstrated by the ability of muscarinic receptor activation to induce release of endocannabinoids. However, whether the modulation is driven by extrinsic or intrinsic sources, the loci of action is an essential factor and can include modification of (1) the properties of presynaptic neurotransmitter release, (2) the modification of postsynaptic responsiveness/receptor signaling, and/or (3) the modulation of the postsynaptic intrinsic electrical and biochemical properties or gene regulation. Understanding the overall actions of a neuromodulator is thus especially challenging. The most significant obstacle is that neuromodulators do not simply excite or inhibit neurons in the classical sense. Rather, they usually signal through intracellular messenger cascades to modulate not one but a range of effectors. This may include the gating of ion channels that orchestrate the response to classical neurotransmitters. That is, they change

the way neurons respond to signals arising from other neurons whether that be due to altered intrinsic properties of the receptive neuron, to altered postsynaptic responsiveness, or as a result of altered properties of the presynaptic neuron such as action potential patterns or release probability. As a consequence, what an experimenter sees following manipulation of neurotransmitter/modulator mechanisms depends upon how the cell or system is investigated. As pointed out by Surmeier (2007) – different questions produce different answers!

Modulation of Intrinsic Properties

Neuromodulators can regulate a diverse range of ion channels and other effectors that modify the active and passive properties of hippocampal neurons. The excitability of cells can be altered in three different ways. Neuromodulation can alter the resting membrane potential, in the form of depolarization or hyperpolarization. This action has two consequences. First, it will bring the cell closer to or farther away from the threshold for action potential initiation. This makes a given excitatory synaptic input more or less effective. Second, alteration in the resting membrane potential may be associated with a different set of cellular conductances, which themselves could influence the properties of the cell. Neuromodulation also can alter the passive properties of the cell, including the cell input resistance and membrane time constant. This is done through neuromodulation of the conductances involved at a given resting potential, such as leak conductances or steady state conductance. This changes the integrative and filtering properties of the neuron. For example, an increase in the membrane time constant will broaden the excitatory postsynaptic potential so that fewer EPSPs are required to summate to action potential threshold. Increasing input resistance and membrane time constant also alters the RC filtering characteristics of the cell, thereby impacting the ability of the cell to follow frequency-specific input. Finally, active conductances also undergo neuromodulation. Depending on the kinetics of activation of the conductances modulated, the action potential waveform, various afterhyperpolarizing potentials, and/or action potential discharge patterns are altered by neuromodulation. Some of these effects are summarized in Table 1 and described under the individual neuromodulator headings.

Different neuromodulatory substances often converge onto common effectors to produce similar actions. For example, activation of metabotropic GABA receptors, adenosine receptors, and serotonin receptors in CA1 pyramidal cells all increase a common potassium conductance (Nicoll et al., 1990), thereby providing several mechanisms for reducing cellular excitability. However, while some generalizations may be made, the situation often is far more complex. As seen in the earlier chapters, different hippocampal neurons are endowed with different channels and neurotransmitter receptors. For any given modulatory substance in any given cell, the exact channels modulated will depend upon the presence and spatial localization of particular subtype(s) of receptors, together with the presence and spatial localization of coupled ion channels and other effectors. Intracellular signaling is another major determinant of the response and despite their ubiquity, recent studies suggest that

their actions can be very specific and targeted to specific loci or subcellular compartments within a cell (Shigemoto et al., 1996; Kulik et al., 2006). Moreover, if release of calcium from internal stores is involved, the response will also depend on the history of action potential activity, since intracellular calcium stores can be depleted unless replenished through activation of voltage-gated calcium channels. It is through calcium imaging and the introduction of molecular sensors for cyclic-AMP and other transduction processes that we are beginning to learn how modulation can be restricted to localized microdomains or compartments.

Table 1 Summary of key neuromodulator actions

Modulator	Pyramidal cells Postsynaptic Presynaptic	Interneurons Postsynaptic Presynaptic
Acetylcholine	Depolarization, ↓ adaptation ↑ I_h, I_{CAT}; ↓ I_M, I_{AHP}, I_{Kleak} (m) ↓ glutamate release (m), ↑(n)	Depolarization or hyperpolarization (m / n) ↓ GABA release (m), ↑ (n)
Norepinephrine	↓ sAHP; ↓ adaptation (β)	↓ K conductance (α); ↑ *I*h (β)
Dopamine	Hyperpolarization, ↓ adaptation, ↓ AHP, ↓ Ca^{++} activated *I*k ↓ glutamate release (most pathways), ↑ transmitter release (mossy fibers)	ND ↓ GABA release (D_3)
Serotonin	Hyperpolarization, ↓adaptation ↓I_h (5HT1A); ↑I_h, ↓I_{AHP} ($5HT_7$, $5HT_4$) ↓ glutamate release, ↓ induction of LTP	$5HT_2$ is excitatory ↑ GABA release ($5HT_{2+3}$)
Histamine	Depolarization (dominant, H_2) or hyperpolarization (H_1) ↓ glutamate release, direction action on NMDA receptors	Depolarization (H_2) ↓Kv3.2 ND
Adenosine	Hyperpolarization (A_1, A_{2A}), ↑gK ↓ glutamate release, ↓ induction of LTP	ND Little effect
ATP	Fast inward current (P2X), ↑gK Contribute to fast EPSP/C (P2X), regulate LTP/LTD	ND ND
Endocananninoids	Modest depolarization, ↓I_M ↓ glutamate release, DSE	Little effect ↓ GABA release, DSI
Nitric oxide	None ↑ LTP	None May contribute to DSI
Neuropeptides	See table 7	

Arrows indicate direction of change. Normal text and grey highlighted text represent postsynaptic and presynaptic actions respectively (for more detail and other actions see text below). Parenthesis show receptor subtypes where known. Abbreviations: ND, not determined; I_{AHP}, afterhyperpolarization current; I_{CAT}, cation current; I_h, hyperpolarization-activated current; I_M, M current

Modulation of Excitatory Synaptic Transmission

The laminar structure of the hippocampal formation lends itself to the study of excitatory pathways. It has long been observed that a wide range of neuromodulatory substances can affect glutamatergic neurotransmission. While many modulators

have general actions across very many synapses such as the suppressant actions of adenosine, others appear to have very precise synapse-specific actions. One of the best examples of synapse-specific effects is the suppression of transmission by activation of group II mGluRs at the mossy fiber-to-CA3 pyramidal cell synapse but not at Schaffer collateral synapses onto the same neuron (McBain, 2008) (see Chapter "Physiological Properties of Hippocampal Neurons"). This example, as well as others, has made the concept of a generic glutamatergic synapse essentially obsolete. Several other examples of synapse-specific neuromodulation at different hippocampal glutamatergic synapses are illustrated in this chapter.

Modulation of Inhibitory Synaptic Transmission

As described in earlier chapters, GABAergic cells and circuits show great diversity in terms of their neurochemistry, morphology, connectivity, and expression of neurotransmitter receptors. Similarly, the neuromodulation of GABAergic circuits appear to be complex and poorly understood. This stems in part from issues that arise from attempting to classify GABAergic interneurons into defined subtypes (Maccaferri and Lacaille, 2003; Ascoli et al., 2008; Klausberger and Somogyi, 2008). However, it is also complicated by the findings that application of the same neuromodulator to what are considered anatomically discrete cell types, can often give rise to variable and unpredictable responses even when considering a simple question such as whether a modulator is excitatory or inhibitory (Parra et al., 1998; Widmer et al., 2006). From this muddle, some patterns are starting to emerge and we are just beginning to understand principles by which neurochemically and functionally distinct interneuron subtypes are differentially recruited, suppressed, or modified in a coordinated manner to orchestrate the flow of information in hippocampal circuits (Madison and McQuiston, 2006; Lawrence, 2008). As has been shown in neocortex (Kawaguchi, 1997; Xiang et al., 1998; Porter et al., 1999; Bacci et al., 2005), one important factor is the neurochemical identity of the hippocampal interneuron subtype (Glickfeld and Scanziani, 2006; Lawrence et al., 2006a; Freund and Katona, 2007; Cea del Rio et al., 2008; Glickfeld et al., 2008; Lawrence, 2008). Understanding exactly how neuromodulation alters the cellular and synaptic properties of neurochemically distinct target cells to modulate the frequency and magnitude of network oscillations remains a major challenge in the years ahead.

"Classical" Modulators

Many of the classical modulators have an established role in mediating synaptic transmission/neuromodulation and indeed their discovery as such significantly predates the discovery of glutamate and GABA as neurotransmitter substances. Despite this however, our knowledge of the precise action of classical modulators on hippocampal cells and circuits is rather disjointed and incomplete. It is with

acetylcholine that most progress toward a systematic understanding of its multitude of actions has been achieved and we therefore start with a detailed account of the current state of knowledge with this system. Thereafter, we provide an overview of other classical neuromodulators, highlighting their key features as well as the significant gaps in our current knowledge.

Acetylcholine

Acetylcholine (ACh) is a key neuromodulator that plays a key role in arousal (Jones, 2004), attention (Sarter et al., 2005), and learning (Hasselmo, 2006). Cholinergically induced oscillatory activity in the hippocampus correlates with these behavioral states (Lee et al., 1994), but the precise neuronal and synaptic targets of cholinergic neuromodulation that give rise to these oscillations remain incomplete.

Structural Organization of Cholinergic Afferents

The medial septum/diagonal band of Broca (MS-DBB) provides the major source of cholinergic innervation to the hippocampus (Swanson et al., 1987; Woolf, 1991; Dutar et al., 1995; Lucas-Meunier et al., 2003) and presents a direct synaptic input to both principal neurons and interneurons (Frotscher and Leranth, 1985; Leranth and Frotscher, 1987; Deller et al., 1999). MS-DBB cholinergic neurons are rhythmically active during waking and quiescent during sleep (Lee et al., 2005). Cholinergic axons ramify extensively throughout all regions of the hippocampal formation and in all layers (Leranth and Frotscher, 1987). At the ultrastructural level, a significant proportion of cholinergic boutons are not associated with distinct postsynaptic specializations (Vizi and Kiss, 1998). These observations support two forms of cholinergic transmission: precise synaptic transmission, involving highly localized ACh transients onto low-affinity nAChRs, and volume-mediated cholinergic transmission, where ACh is released into the extracellular space, diffusing to high-affinity receptors at some distance from the synaptic terminal (Vizi and Kiss, 1998). In addition to the extrinsic cholinergic input, the hippocampus receives an intrinsic source of ACh from a numerically sparse population of cholinergic interneurons (Frotscher et al., 1986; Frotscher et al., 2000).

One important consideration is whether particular cholinergic septo-hippocampal fibers preferentially target particular cell types. Given that nAChRs cluster under cholinergic terminals (Zago et al., 2006), it is possible that a high expression level of postsynaptic nAChRs may indicate a higher level of cholinergic terminal contacts relative to interneuron subtypes associated with lower nAChR expression. In the dentate gyrus, cholinergic afferents appear to exhibit some target selectivity, preferentially innervating NPY+ neurons over PV+ neurons (Dougherty and Milner, 1999). Moreover, using vesicular acetylcholine transporter (vAChT) labeling in combination with anterograde labeling of basal forebrain afferents, Jones and colleagues recently found cholinergic terminals more closely apposed

to CB+ cells than to PV+ cells (Henny and Jones, 2008). These observations are consistent with the demonstration of fast α7 receptor-mediated synaptic responses in SR interneurons (Alkondon et al., 1998; Frazier et al., 1998a; Chang and Fischbach, 2006), a population of interneurons more likely to be CB+ or CCK+ than PV+. Finally, there is growing evidence that cholinergic afferents may target precise spatial locations relative to other afferents. The overlap of cholinergic and GABAergic terminal specializations (Zago et al., 2006; Henny and Jones, 2008) and recently demonstrated crosstalk between nAChRs and $GABA_A$ receptors (Wanaverbecq et al., 2007; Zhang and Berg, 2007) suggest that GABAergic synapses may be targets of cholinergic afferents.

Do cholinergic interneurons intrinsic to the hippocampus target particular cell types? Recently, with the use of a transgenic mouse that expressed GFP in ChAT-positive neurons, Monyer and colleagues recorded from intrinsic cholinergic cells in neocortex (von Engelhardt et al., 2007). Although evoked nicotinic EPSPs onto postsynaptic targets were not observed, a moderate enhancement in spontaneous glutamatergic transmission was detected, suggesting that ACh release from these neurons may spill over to presynaptic nicotinic receptors located on glutamatergic boutons (von Engelhardt et al., 2007). Given evidence that this class of interneuron possesses a high density of nAChRs (Porter et al., 1999), one possible role of these cells is to amplify cortical or hippocampal ACh release through a feed-forward, excitatory cholinergic circuit (Tricoire and Cea-Del Rio, 2007).

Acetylcholine Receptors

To complement its rich cholinergic input, hippocampal neurons express a broad range of acetylcholine receptors (Buckley et al., 1988; Levey et al., 1995). Cholinergic neuromodulation has complex effects on both glutamatergic and GABAergic neurons in the hippocampus, which occur by the binding of ACh to ionotropic nicotinic receptors (nAChR) and muscarinic receptors (mAChRs) at presynaptic and postsynaptic locations (Cobb and Davies, 2005; Giocomo and Hasselmo, 2007) (Figure 1). Many of the effects are mediated through metabotropic muscarinic acetylcholine receptors (mAChRs, M1-5). Early studies suggested M1 and M3 receptor proteins being mainly expressed in principal neurons and M2 and M4 receptors predominantly expressed on interneurons (Levey et al., 1995). Within glutamatergic circuits of the hippocampal formation there is extreme variability in mAChR-immunoreactivity between subfields and laminae (Rouse et al., 1999). The termination zones of the perforant path differentially express presynaptic M2, M3, and M4 receptors.

The septo-hippocampal pathway is also thought to activate nicotinic acetylcholine receptors (nAChRs). The exact expression of nAChR subunits with respect to the afferent cholinergic input is not fully established, but binding studies suggest that populations of interneurons that are suspected to receive direct septo-hippocampal innervation bind the nAChR ligand α-bungarotoxin (Freedman et al., 1993). Immunocytochemical studies have demonstrated the α7 AChR subunit to

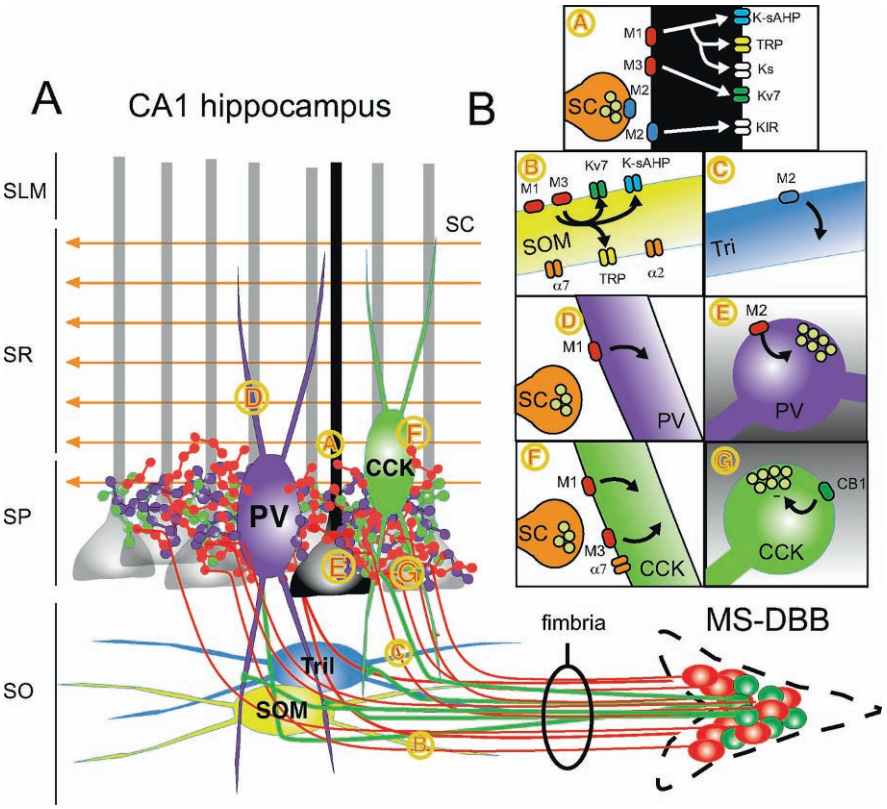

Fig. 1 The medial septal-diagonal band of Broca (MS-DBB) projection to defined cellular and synaptic targets of the CA1 hippocampus. (**a**) The MS-DBB is composed of cholinergic (*red*) and GABAergic (*green*) neurons that project via the fimbria to hippocampal regions. Cholinergic projection fibers (*red*) pass through stratum oriens (SO), where the somatostatin (SOM)-positive oriens-lacunosum moleculare (O-LM) neurons (*yellow*) and trilaminar (*blue*) interneurons are located and arborize in a dense network within stratum pyramidale (SP) with CA1 pyramidal cells (*black*), CCK BCs, and PV BCs (cholinergic terminals in stratum oriens and stratum radiatum (SR) omitted for clarity). MS-DBB GABAergic neurons (**a**, *green cells*) are thought to innervate exclusively hippocampal interneurons. Areas of interest, denoted by *circled numbers* in **a**, are expanded in **b**. Known cellular and synaptic targets, denoted by *circled numbers*, are shown. These are (**a**) the dendrites of pyramidal cells, acting at M1, M2, and M3 mAChRs and presynaptic terminals of Schaffer collaterals (*orange*) acting at M2 mAChRs (**b**) somatodendritic regions of O-LM cells acting at M1 mAChRs, M3 mAChRs, α7 nAChRs, and non-α7 nAChRs, (**c**) somatodendritic regions of trilaminar interneurons acting at M2 mAChRs, (**d**) somatodendritic regions of PV BCs acting at M1 mAChRs, (**e**) presynaptic terminals of PV BCs acting on M2 mAChRs, (**f**) Somatodendritic regions of CCK BCs acting on M1 and M3 mAChRS and α7 nAChRs, and (**g**) presynaptic terminals of CCK BCs acting indirectly through presynaptic CB1 mAChRs

be highly expressed across multiple cell types and multiple cellular and synaptic compartments, including somata, dendrites, spines, axon fibers, glutamatergic axon terminals, and GABAergic axon terminals (Fabian-Fine et al., 2001).

Action of Acetylcholine on Intrinsic Properties

Pyramidal Cells

Acetylcholine has been known for many years to excite hippocampal pyramidal cells (Dodd et al., 1981; Cole and Nicoll, 1983; Cobb and Davies, 2005) and the ionic basis of such effects have now been elucidated in some detail. Through mAChRs, ACh is known to modulate a large number of conductances and second messenger cascades in pyramidal neurons. These include Kv7/KCNQ/I_M potassium channels; I_{AHP}, the slow Ca^{2+}-activated K^+ current responsible for the slowing of action potential discharges; I_{leak}, the voltage-dependent leak current responsible in large part for the resting membrane potential (Halliwell and Adams, 1982; Madison et al., 1987; Halliwell, 1990) and an inwardly rectifying potassium conductance (Seeger and Alzheimer, 2001). mAChR activation also potentiates two mixed cation currents (I_h, the hyperpolarization-activated nonspecific cation current; I_{cat}, Ca^{2+}-dependent nonspecific cation current) (Brown and Adams, 1980; Halliwell and Adams, 1982; Colino and Halliwell, 1993) as well as modulating a voltage-dependent Ca^{2+} current (Toselli et al., 1989). The action of exogenously applied acetylcholine on hippocampal pyramidal cells is that of a pronounced membrane potential depolarization and increase in cell membrane resistance (Cole and Nicoll, 1984a, b; Fraser and MacVicar, 1996). Recently, using puff application of mAChR agonists, carbachol application to soma/proximal dendritic regions of principal cells induces a transient hyperpolarization caused by mAChR-induced release of calcium from internal stores, which then activates Ca^{2+}-dependent SK channels (Gulledge and Kawaguchi, 2007). Using electrical stimulation of cholinergic afferents, Power and Sah demonstrated that synaptic activation of mAChRs leads to propagating calcium signals within the somatodendritic axis of pyramidal cells (Power and Sah, 2002). Despite difficulties in interpreting nAChR pharmacology from early studies using cultured hippocampal neurons, in acute native tissues, pharmacological activation of nAChRs is generally reported to produce either no or a barely detectable level of response in principal cells (Reece and Schwartzkroin, 1991; Frazier et al., 1998a, b; McQuiston and Madison, 1999a; Frazier et al., 2003). There are some reports that nAChRs are detected postsynaptically in principal cells (Hefft et al., 1999), where they facilitate the induction of LTP (Ge and Dani, 2005) through enhanced cellular excitability (Szabo et al., 2008). However, with the hippocampal circuit intact, the effect may be minor, since bath application of nicotine reduces the excitability of pyramidal cells, through tonic GABAergic inhibition (Jia et al., 2009).

Interneurons

In the majority but not all GABAergic interneurons, pharmacological activation of mAChRs results in a similar membrane depolarization to that seen in pyramidal cells but with a less prominent change in cell input resistance (Parra et al., 1998; McQuiston and Madison, 1999b, c; Lawrence et al., 2006a), confirming earlier studies (Benardo and Prince, 1982a, b, c; Reece and Schwartzkroin, 1991). GABAergic interneurons represent a highly heterogenous population of neurons with respect to their connectivity and neurochemistry (Freund and Buzsaki, 1996; Klausberger

and Somogyi, 2008), and there is wide variation in their response to activation of mAChRs compared to that seen in the relatively homogeneous population of principal neurons (Parra et al., 1998; McQuiston and Madison, 1999c; Widmer et al., 2006). In contrast to the slow sustained mAChR-mediated modulation of both pyramidal cells and interneurons, activation of nAChRs produces a more transient response. Similar to neocortical interneurons (Xiang et al., 1998; Porter et al., 1999; Couey et al., 2007; Gulledge et al., 2007), there is evidence for cell type specificity in postsynaptic expression of nAChRs in hippocampal interneurons.

O-LM cells: One cell type that exhibits a highly reproducible response to mAChR activation is O-LM cells (Maccaferri and Lacaille, 2003; Lawrence et al., 2006a), similar to neocortical Martinotti cells, another somatostatin-positive interneuron subtype (Kawaguchi, 1997; Fanselow et al., 2008). When induced to fire in the presence of mAChR agonists, O-LM cells exhibit an acceleration in firing frequency that is accompanied by a prominent suprathreshold afterdepolarization (ADP) (Lawrence et al., 2006a). The ADP, mediated by M1/M3 mAChR activation, is associated with the activation of a nonselective cationic current (I_{cat}) and the inhibition of both M (I_M) and slow afterhyperpolarization K^+ (I_{AHP}) currents. Importantly, the mAChR-induced ADP was not generated in SO interneurons shown to be morphologically distinct from O-LM cells, demonstrating a strong dependence of mAChR responsiveness on interneuron subtype (Lawrence et al., 2006a). mAChR modulation of O-LM cells enhances their intrinsic oscillatory properties to theta-specific input (Lawrence et al., 2006b), which is mimicked by inhibition of M-current in O-LM multicompartmental models (Lawrence et al., 2006c; Lawrence, 2008). In stratum oriens (SO), a mixed fast α7-mediated and slow non-α7 nAChR-mediated response is consistently observed in oriens-lacunosum moleculare (O-LM) cells (McQuiston and Madison, 1999a; Buhler and Dunwiddie, 2001). Recently, α2 nAChR subunits have been identified on stratum oriens cells, the activation of which contributes to nAChR-mediated inhibition of principal cells (Jia et al., 2009).

M2 mAChR-positive trilaminar cells: There also appears to be a population of GABAergic interneurons that is instead hyperpolarized in response to mAChR activation. The neurochemical identity of ADP-lacking SO interneurons is less clear, but likely comprises M2-expressing trilaminar cells (Hajos et al., 1998; Ferraguti et al., 2005) and horizontally oriented PV+ BCs (Maccaferri, 2005; Lawrence et al., 2006a). Recent immunocytochemical studies showing that mGluR1a+ and M2+ SO interneurons are distinct cell types (Ferraguti et al., 2005), likely corresponding to O-LM and trilaminar cells, strengthen the evidence that SO interneuron subtypes possess a different complement of postsynaptic mAChRs. The most likely consequence of M2 mAChR activation in these cells is a reduction in input resistance and cellular excitability (Lawrence et al., 2006a), possibly mediated through inward rectifier potassium channels (McQuiston and Madison, 1999c; Seeger and Alzheimer, 2001).

Parvalbumin-positive basket cells: Fast-spiking basket cells, usually corresponding to PV+ BCs, neither express high levels of nAChRs nor respond to mAChR activation with strong depolarization in neocortex (Kawaguchi, 1997; Xiang et al., 1998; Gulledge et al., 2007) or hippocampus (McQuiston and Madison, 1999a;

Buhler and Dunwiddie, 2001). With the use of GFP mice, hippocampal PV+ BCs have recently been studied as a homogenous interneuron subtype (Lawrence and McBain, 2007; Cea del Rio et al., 2008; Lawrence et al., 2008). In response to bath application of 10 μM muscarine, PV BCs depolarize, increase in firing frequency, and exhibit a loss of an afterhyperpolarization, all of which do not occur in M1 KO mice (Cea del Rio et al., 2008; Lawrence et al., 2008). This depolarizing response profile is consistent with that observed previously in a subset of morphologically defined basket cells (McQuiston and Madison, 1999c; Widmer et al., 2006). Interneurons that are insensitive to nAChR activation are encountered predominantly in stratum pyramidale (SP) (McQuiston and Madison, 1999a) and tend to be fast spiking, a hallmark feature of PV+ BCs (Buhler and Dunwiddie, 2001).

CCK-positive basket cells: Cholinergic neuromodulation of CCK BCs has recently been investigated with the use of a GAD65 GFP transgenic mouse line (Cea del Rio et al., 2008) in which GFP is expressed in non-PV^+ cells (Lopez-Bendito et al., 2004). CCK BCs show characteristics of cholinergic neuromodulation different than PV BCs. First, a prominent mAChR-induced ADP is observed in these cells (McQuiston and Madison, 1999b; Madison and McQuiston, 2006; Cea del Rio et al., 2008), which is slower in time course than that seen in O-LM cells and is sometimes briefly interrupted by a mAChR-insensitive fast afterhyperpolarization that occurs after the offset of a suprathreshold current step. Hyperpolarization followed by depolarization is often observed, consistent with biphasic response profiles of a subset of basket cells reported previously (McQuiston and Madison, 1999c; Widmer et al., 2006). One interesting feature of CCK BCs is that M3 mAChRs appear to control mAChR-induced changes in firing, but both M1 and M3 mAChRs control the emergence of the mAChR-induced ADP (Cea del Rio et al., 2008; Lawrence et al., 2008). Therefore, the expression of M3 mAChRs and its coupling to mAChR-sensitive conductances in CCK BCs distinguishes it from PV BCs. CCK is highly co-localized with α7 nAChRs at mRNA (Morales et al., 2007) and protein levels (Freedman et al., 1993). In this context, it is interesting that SR interneurons, which are enriched in CCK content, exhibit only fast α7 nAChR-mediated responses (McQuiston and Madison, 1999a), differentiating these cells from both O-LM and fast-spiking (PV+ BC) populations.

Other interneuron subtypes: CCK-positive Schaffer collateral-associated interneurons are similar in their response to mAChR-induced neuromodulation (Lawrence et al., 2008), also exhibiting a mAChR-induced ADP. Although neurochemically not as well-defined as other cell types (Freund and Buzsaki, 1996; Bowser and Khakh, 2004), interneurons located at the radiatum/lacunosum moleculare border are depolarized by mAChR activation and exhibit intrinsic subthreshold membrane potential oscillations (Chapman and Lacaille, 1999). Both pharmacological activation (Reece and Schwartzkroin, 1991; Jones and Yakel, 1997; McQuiston and Madison, 1999a) and synaptic activation (Frazier et al., 1998a) have shown these interneurons to exhibit a functional nAChR-mediated response. This typically takes the form of a brief depolarization or inward current which tends to desensitize rapidly. The kinetics and pharmacology of the response vary, but fast depolarization by α7 subunit-containing nAChRs is the predominant response seen in

interneurons. A further interneuron population displays a slow membrane potential oscillatory response to mAChR activation, while another group appears completely unresponsive to mAChR activation with respect to changes on membrane potential/conductance (Parra et al., 1998; McQuiston and Madison, 1999c). The specific cell types associated with oscillatory and non-responsive cell types are not clear.

Clearly, the activities of the cholinergic septo-hippocampal afferents are going to excite the hippocampal network generally and differentially gate inhibitory circuits through both nAChR- and mAChR-mediated mechanisms. This has been proposed to result in switches in inhibition between perisomatic- and pathway-specific dendritic domains (Gulyas et al., 1999). A major challenge for the future is in understanding how different patterns of cholinergic afferent input can differentially recruit different receptor populations and cell types. There is evidence in the literature to suggest that a single stimulation of cholinergic fibers is effective at evoking nAChR-mediated postsynaptic potentials in interneurons, but is relatively inefficient at evoking mAChR-mediated membrane potential depolarizations. In contrast, trains of stimuli delivered at 10–20 Hz, within the range at which most putative septal cholinergic cells discharge (Brazhnik and Fox, 1999; Lee et al., 2005), result in a robust mAChR-mediated synaptic response while at the same time depressing nAChR-mediated responses (Morton and Davies, 1997). During more sustained ACh release, it is also possible that mAChR activation induces postsynaptic depression of nAChR responses (Shen et al., 2009).

Action of Acetylcholine on Defined Excitatory Synapses

Presynaptic Muscarinic Receptors on Defined Excitatory Synapses

ACh depresses Schaffer-collateral (SC) afferents onto CA1 pyramidal cells through a presynaptic mechanism involving mAChR activation (Valentino and Dingledine, 1981) and presynaptic N-type calcium channels (Qian and Saggau, 1997). The nAChR antagonist hexamethonium does not block the action of ACh, suggesting that nAChRs are absent from presynaptic SC afferents (Valentino and Dingledine, 1981). mAChR activation also inhibits glutamatergic transmission of CA3 collateral glutamatergic transmission (Vogt and Regehr, 2001; Kremin and Hasselmo, 2007). The mAChRs involved in presynaptic inhibition of SCs are most likely M2 mAChRs (Seeger et al., 2004) but possibly include M4 mAChRs (Sanchez et al., 2009). While acetylcholine generally suppresses glutamatergic neurotransmission at most excitatory synapses tested (Valentino and Dingledine, 1981), mAChR modulation has a greater effect at SC synapses than on perforant path synapses in both CA1 (Hasselmo and Schnell, 1994) and CA3 (Kremin and Hasselmo, 2007). Similarly, in the dentate gyrus, cholinergic suppression of transmitter release differs between medial and lateral pathway (Kahle and Cotman, 1989). mAChRs are not present at mossy fiber (MF) glutamatergic synapses, but bath application of muscarine enhances GABA release from local interneurons, which then inhibits MF transmission indirectly through activation of $GABA_B$ receptors (Vogt and Regehr, 2001). This same indirect effect on presynaptic $GABA_B$ receptors, however, is not present at SC synapses (Kremin et al., 2006). This differential

effect of cholinergic neuromodulation on aspects of glutamatergic circuitry has been suggested to amplify the impact of sensory input arriving at hippocampus, whereby mAChR activation shifts the weight of glutamatergic input in favor of external (entorhinal cortical) influences over internal (intrahippocampal pathways) activity such as recall upon cholinergic modulation (Giocomo and Hasselmo, 2007). This synaptic "heightening" of sensory awareness has interesting implications for the behavioral manifestation of attention (Sarter et al., 2005; Giocomo and Hasselmo, 2007).

Concomitant with acute mAChR-induced presynaptic inhibition of glutamate release discussed above, the action of ACh can induce synaptic plasticity at SC synapses, including long-term potentiation (Auerbach and Segal, 1994, 1996; Shinoe et al., 2005; Fernandez de Sevilla et al., 2008) and, usually at higher concentrations of cholinergic agonist, long-term depression (Auerbach and Segal, 1996; Scheiderer et al., 2006, 2008). Release of ACh by stimulation of the medial septum reproduces this effect (Fernandez de Sevilla et al., 2008; Habib and Dringenberg, 2009). The underlying mechanisms appear to be an enhancement in the NMDA receptor component of the excitatory postsynaptic event (Markram and Segal, 1990a, b). More recently, Fernandez de Sivilla and colleagues have discovered a postsynaptic mechanism involving enhanced surface trafficking of AMPA receptors (Fernandez de Sevilla et al., 2008). Presumably through a convergence underlying synaptic, intrinsic, and network mechanisms, LTP is preferentially induced at synapses firing on the positive phase of the θ rhythm during cholinergically induced theta oscillations in the hippocampus in vitro and in vivo (Pavlides et al., 1988; Huerta and Lisman, 1993; Holscher et al., 1997; Hyman et al., 2003).

Presynaptic Nicotinic Receptors on Hippocampal Glutamatergic Terminals

Nicotine application increases the frequency of miniature glutamatergic EPSCs in tissue culture (Radcliffe and Dani, 1998), raising the possibility that presynaptic nAChRs exist. Several lines of evidence support the presence of nAChRs on CA3 mossy fiber terminals, where calcium influx through α7 nAChRs induces concerted release of multiple quanta (Gray et al., 1996; Sharma and Vijayaraghavan, 2003; Sharma et al., 2008). Nicotine selectively depresses perforant path but not SC glutamatergic transmission in CA3 (Giocomo and Hasselmo, 2005), but this effect is accounted for by an indirect effect on inhibitory interneurons (Giocomo and Hasselmo, 2005), possibly related to tonic activation of O-LM interneurons by nicotine (Jia et al., 2009).

Action of Acetylcholine on Defined Inhibitory Synapses

As demonstrated by the early work of Pitler and Alger (1992b), as well as other laboratories (Behrends and ten Bruggencate, 1993), the actions of ACh on GABAergic interneurons not only include direct excitation but also presynaptic inhibition. Pharmacological activation of mAChRs directly increases the frequency and

amplitude of spontaneous IPSCs while at the same time depressing monosynaptically evoked IPSCs and reducing the frequency of miniature IPSCs (Pitler and Alger, 1992b; Behrends and ten Bruggencate, 1993). In a landmark study demonstrating the differential expression of mAChRs on hippocampal interneurons, Hajos et al. found that M2 receptors (M2Rs) were expressed on the presynaptic axon terminals of PV+ basket cells (Hajos et al., 1998). Consistent with M2-mediated inhibition of GABAergic transmission evoked in the pyramidal cell layer (Seeger et al., 2004), mAChR activation reduces GABA release from PV+ BC terminals (Lawrence and McBain, 2007). Whether mAChRs might be present at PV-negative terminals still remains an open question. Interestingly, Soltesz and colleagues recently demonstrated that mAChR activation inhibits GABA release from identified CCK+ BCs (Neu et al., 2007). Here, mAChR modulation was indirect (Fukudome et al., 2004), occurring via postsynaptic release of endocannabinoids (see endocannabinoid section below) from pyramidal cells and subsequent activation of presynaptic CB1 receptors (Lawrence, 2007; Neu et al., 2007) (Fig. 2). Therefore, mAChR-induced modulation of GABA transmission from PV+ BCs likely involves direct activation of presynaptic M2 receptors, while mAChR-induced modulation of GABA transmission from CCK+ BCs is indirect, involving endocannabinoid signaling (Freund and Katona, 2007). Finally, in addition to mAChR-mediated presynaptic inhibition of GABA release, calcium permeable nAChRs also regulate GABAergic inhibition through postsynaptic intracellular signaling

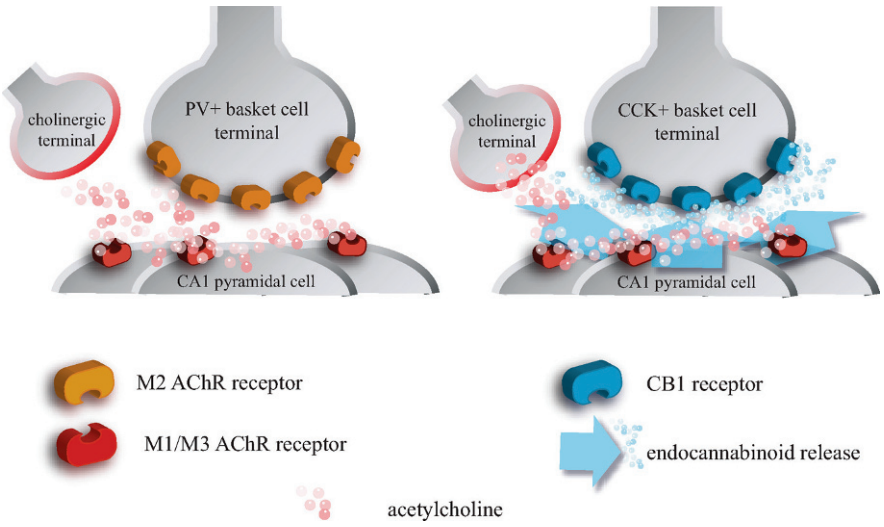

Fig. 2 Cholinergic modulation of GABA release from PV and CCK BC terminals through direct and indirect mechanisms. There is evidence that mAChRs can regulate GABA release through both direct and indirect mechanisms (Fukudome et al., 2004; Freund and Katona, 2007). The direct mechanism involves binding of ACh to presynaptic M2 mAChRs (Lawrence and McBain, 2007). The indirect mechanism involves postsynaptic M1/M3 mAChR activation and release of endocannabinoids onto CB1 receptor-expressing terminals of CCK+ BCs (Neu et al., 2007)

pathways (Wanaverbecq et al., 2007; Zhang and Berg, 2007). Therefore, cholinergic neuromodulation can alter the efficacy of GABAergic transmission through both presynaptic and postsynaptic mechanisms.

Presynaptic Modulation of ACh Release

M2 receptors additionally occur at septo-hippocampal cholinergic terminals where they are thought to have an auto-regulatory role (Rouse et al., 1999). Other studies have shown more directly that while acetylcholine auto-feedback can regulate, the activation of a range of other transmitters can suppress evoked cholinergic responses including A1 adenosine receptors (Morton and Davies, 1997), opiate receptors (Kearns et al., 2001), and $GABA_B$ receptors (Morton et al., 2001).

Dopamine

Dopamine is considered to play an important role in hippocampal-dependent learning by enhancing the saliency of relevant stimuli and is released into the hippocampus when animals are exposed to a novel environment (Ihalainen et al., 1999; Lisman and Grace, 2005; Muzzio et al., 2009). Lesions of the dopaminergic system impair learning and memory (Gasbarri et al., 1996; El-Ghundi et al., 1999) and dysfunction of the dopamine system have been implicated in neurological disease (Seeman and Van Tol, 1994). However, at the cellular and network levels, the action of dopamine is rather poorly defined with most information coming from pharmacological studies investigating the respective dopamine receptor subtypes.

Structural Organization of Dopaminergic Afferents

The hippocampal formation receives a prominent dopaminergic projection from A9 (substantia nigra) and A10 (ventral tegmental area) cell groups (Scatton et al., 1980; Swanson et al., 1987). The ventral tegmental area projects heavily to the subiculum and CA1, and to a lesser extent to the CA3 and dentate gyrus (Gasbarri et al., 1994; Gasbarri et al., 1997). There is often a mismatch between the expression patterns of particular dopamine receptors and the innervation pattern (Goldsmith and Joyce, 1994). This has led some authors to hypothesize that it is the distribution of the receptors and not of dopaminergic fibers that determines the neuronal systems influenced by dopaminergic afferent activation.

Dopamine Receptors

All five dopamine receptors are expressed in the hippocampus with D1/5 and D2-4 receptors being positively and negatively coupled to adenylyl cyclase, respectively. The expression pattern of dopamine receptors at the level of single cells remains relatively poorly defined, but dopamine receptors have been shown to display both

presynaptic and postsynaptic localization (Bergson et al., 1995) and to be expressed both in principal cells and interneuronal populations (Mrzljak et al., 1996).

Action of Dopamine on Intrinsic Properties

Dopamine has been reported to produce a range of actions, which are largely attributed to the activation of D1-like (D1/5) and D2-like (D2-4) receptors, respectively (Table 2). In principal neurons, dopamine produces a pronounced hyperpolarization and an elevation of action potential threshold (Benardo and Prince, 1982d) coupled with a suppression of the I_{AHP} and inhibition of spike-frequency adaptation (Malenka and Nicoll, 1986; Pedarzani and Storm, 1995). This is mainly attributed to suppression of the activation of Ca^{2+}-sensitive potassium channels (Benardo and Prince, 1982d, e; Bernardi et al., 1984; Stanzione et al., 1984). To date, although some analogous cell types have been investigated in neocortex (Towers and Hestrin, 2008) and prefrontal cortex (Gorelova et al., 2002), very little information exists on the effects of dopamine on intrinsic membrane properties of defined hippocampal interneuron subtypes.

Action of Dopamine on Defined Excitatory Synapses

The actions of dopamine on excitatory synaptic transmission are generally suppressant in nature (Hsu, 1996). However, in parallel with other modulators, certain excitatory pathways are more profoundly affected than others. For instance, dopamine together with noradrenaline and serotonin, produce a strong (30–50%) acute suppression of the perforant path input to CA1 pyramidal cells in comparison to no or very minimal change in Schaffer-collateral input to the same cells (Otmakhova and Lisman, 2000). This is consistent with the stratum lacunosum moleculare having an especially high concentration of dopamine receptors. The action of dopamine is thought to involve both D1 (Noriyama et al., 2006) and possibly D2 (Otmakhova and Lisman, 1999) type receptors and be mediated through presynaptic suppression of glutamate release. A similar acute suppressant action is reported in the subiculum (Behr et al., 2000). Conversely, in area CA3, dopamine produces a pronounced synaptic potentiation of the mossy fiber inputs but no effect on associational/commissural synapses onto CA3 pyramidal cells (Kobayashi and Suzuki, 2007).

Another important feature is the temporal aspects of dopaminergic modulation. Many reports describe a biphasic action whereby an initial acute action (e.g., suppression) of synaptic transmission is followed by a long-lasting enhancement of the evoked synaptic response (Gribkoff and Ashe, 1984). In this context, dopamine is considered an important modulator of synaptic plasticity whereby it enhances long-term potentiation (Frey et al., 1993; Huang and Kandel, 1995; Otmakhova and Lisman, 1996; Thompson et al., 2005) and inhibits depotentiation (Otmakhova and Lisman, 1998). During exposure to a novel environment, the threshold for LTP is reduced transiently (absent in animals exploring a familiar environment) and this facilitation is suggested to be dependent upon dopamine acting via D1/5 receptors

(Li et al., 2003). In agreement with this observation, D1 receptor knockout mice display deficits in hippocampal-dependent spatial learning (El-Ghundi et al., 1999). Moreover, amphetamine, which induces release of endogenous dopamine, enhances hippocampal-dependent memory tasks (Packard et al., 1994).

There appear to be several mechanisms by which dopamine may induce synaptic plasticity. These include increased surface expression of AMPA receptors through both direct phosphorylation of the AMPA receptors as well as through the stimulation of local dendritic protein synthesis (Yang, 2000; Wolf et al., 2003; Smith et al., 2005; Gao et al., 2006). Also, dopamine may enhance NMDA receptor expression (Yang, 2000). Interestingly, depending on the NR2A/NR2B subunit composition, synaptic NMDA receptor-mediated currents are differentially modulated by D1/D5 dopamine agonists (Varela et al., 2009). Shaffer collaterals, which contain abundant NR2B NMDA receptor subunits, are potentiated by D1/D5 receptor activation whereas, NR2A-rich perforant path synapses are depressed (Varela et al., 2009). Dopamine may gate synaptic transmission and plasticity in a frequency-specific and synapse-specific manner, which includes modulation of excitatory synapses onto hippocampal interneurons (Ito and Schuman, 2007).

Action of Dopamine on Inhibitory Synapses

Detailed understanding of action of dopamine on hippocampal interneurons and GABAergic synaptic transmission is extremely sparse though some analogous systematic studies have been conducted in neocortex and prefrontal cortex (Gorelova et al., 2002; Gao and Goldman-Rakic, 2003; Gao et al., 2003; Gonzalez-Burgos et al., 2005; Kroner et al., 2007; Towers and Hestrin, 2008). It has been reported recently that D3 receptors can modulate GABAergic transmission in area CA1, suppressing evoked IPSCs in stratum radiatum but not in stratum oriens (Hammad and Wagner, 2006). This laminar-specific action has been reported to be due to dopamine (via D3 receptors) modulating $GABA_A$ receptor endocytosis and has been postulated to be significant in terms of postsynaptic means of modulating inhibitory synaptic transmission (Swant et al., 2008). More indirect evidence suggests that dopamine may also modulate feed-forward inhibition of the perforant path input to the dentate gyrus and hippocampal area CA1 through D4 receptor signaling (Romo-Parra et al., 2005).

Further indirect evidence for dopamine-regulating inhibitory networks comes from the finding that dopamine depresses cholinergically generated gamma band oscillatory activity in hippocampus (Weiss et al., 2003; Wojtowicz et al., 2009), an emergent property of oscillatory activity that is increasingly appreciated to involve fast-spiking parvalbumin-positive interneurons (Bartos et al., 2007; Sohal et al., 2009). However, dopamine enhances stimulus-evoked gamma oscillations (Wojtowicz et al., 2009), which may be consistent with the notion that dopamine increases neuronal synchrony (Muzzio et al., 2009) mediated by its depolarizing (Towers and Hestrin, 2008) action on fast-spiking, parvalbumin-positive basket cells (Bartos et al., 2007; Sohal et al., 2009). The action of dopamine on precise types of hippocampal interneurons and circuits remain to be systematically investigated.

Table 2 Summary of D1-like and D2-like receptors

Receptor family	D1-like	D2-like
Expression in hippocampus	Widespread	Widespread
Signaling	G_s	G_i
Gross effect	Hyperpolarization, ↑ AP threshold, ↓AHP ↓ accommodation	
	↓ Perforant path signaling, ↑ mossy fiber signaling	↓ Perforant path signaling

Norepinephrine

Norepinephrine is a major monoamine neuromodulator and its actions in the hippocampus appear complex and sometimes paradoxical. Through multiple actions on intrinsic excitability and synaptic transmission, norepinephrine is considered to be important in learning and memory processes (Gibbs and Summers, 2002; Murchison et al., 2004).

Structural Organization of Central Adrenergic Afferents

The hippocampus receives strong noradrenergic input from the locus coeruleus, terminating heavily in the polymorph layer of the dentate gyrus, stratum lucidum of area CA3, and stratum lacunosum-moleculare in area CA1 (Loy et al., 1980; Swanson et al., 1987; Oleskevich et al., 1989). The total NE bouton density varies across hippocampal regions but is estimated to be about twice as high as in cortex (Oleskevich et al., 1989). In the dentate gyrus it has been estimated that two thirds of NA boutons form synaptic specializations with the remainder forming no specialized synaptic profiles and presumably mediating volume transmission (Milner and Bacon, 1989b). GABAergic interneurons are often the targets of NA boutons forming synaptic specializations (Milner and Bacon, 1989a).

Noradrenergic Receptors

Norepinephrine acts on a range of adrenoceptors with alpha and beta classes being widely expressed on both dendritic and axonal elements (Nicholas et al., 1996; Harley, 2007). α1d receptor appears to be the predominant α receptor in all areas with the exception of the hilus where α1a appears to be the dominant subtype (Day et al., 1997). α2a appears to be located mainly presynaptically (Milner et al., 1998), but like many other subtypes shows dramatic changes in expression level during development. β adrenoceptors show laminar-specific differences and are mainly expressed postsynaptically on both principal cells and interneurons (Milner et al., 2000). Recent studies on neurochemically defined interneuron subtypes indicate that the expression of both α (Hillman et al., 2005) and β(Cox et al., 2008) adrenoceptor subunits is cell type specific. However, they can also be found on presynaptic profiles. In terms of signaling, all adrenoceptors are G protein-coupled receptors with

α1 being coupled to G_q, α2 being coupled to G_i, and the β family receptors being coupled to G_s (Nicholas et al., 1996; Harley, 2007).

Action of Norepinephrine on Intrinsic Properties

Norepinephrine is reported to produce a wide and sometimes contradictory range of effects in principal cells. These include hyperpolarization and reduced excitability in some cells to depolarization (Madison and Nicoll, 1986), reduction of afterhyperpolarizing potentials, and loss of action potential accommodation in cells of the same class (see Table 3). Pharmacological studies suggest that these inhibitory versus excitatory actions may, in part, be due to a differential recruitment of α versus β subclass of adrenoceptors (Bijak, 1989; Harley, 2007). Studies investigating hilar neurons suggest that the dominant response in putative GABAergic cells is depolarization and loss of a slow afterhyperpolarization. In contrast, the dominant response in putative mossy cells was a loss of spike-frequency adaptation (Bijak and Misgeld, 1995).

Table 3 Primary actions of norepinephrine on hippocampal neurons

Cell type	Cellular effects	Ion channels effects
Pyramidal	Hyperpolarization, ↑ increased input resistance	↓ A-type current (α receptors)
	or	
	Depolarization, ↓ input resistance, ↓ AHP, ↓ spike-frequency adaptation	↓ Ca^{2+}-activated K^+/I_{AHP} (β1 receptors)
	or	
	Hyperpolarization followed by depolarization	Both above (α and β1)
Granule	As above	As above Activation of L-type current (via β receptor) leading to ↓ gK^+

The underlying ion mechanisms for the change in intrinsic properties are thought to be a reduction in a Ca^{2+}-activated K conductance leading to an inhibition of the slow afterhyperpolarization and a reduction in spike-frequency adaptation (Madison and Nicoll, 1982; Haas and Rose, 1987; Lacaille and Schwartzkroin, 1988; Pedarzani and Storm, 1996). In dentate gyrus granule cells, β1 receptors are also reported to enhance the voltage-dependent Ca^{2+} currents (Gray and Johnston, 1987).

In addition to its action on principal neurons, noradrenaline is also known to excite hippocampal interneurons (Bergles et al., 1996; Papay et al., 2006; Hillman et al., 2009). The effect is due to an α1 receptor-mediated decrease in potassium conductance though a small β receptor component is also sometimes apparent, especially in interneurons displaying a pronounced time-dependent inward rectification (see Chapter "Physiological Properties of Hippocampal Neurons"). Though not tested systematically, noradrenaline appears to produce these potent

depolarizing actions across multiple classes of interneurons including basket cells located outside the pyramidal cell layer (Bergles et al., 1996) and interneurons located in stratum oriens (Bergles et al., 1996; Papay et al., 2006). Norepinephrine and the beta-adrenergic receptor agonist isoprenaline increase spontaneous firing in O-LM cells through a mechanism consistent with a shift in the activation curve for the hyperpolarization-activated cationic conductance I_h (Maccaferri and McBain, 1996). A smaller subpopulation of hippocampal interneurons exists that exhibits hyperpolarization or reduced excitability to noradrenaline application (Parra et al., 1998), although the neurochemical identity of these cells is not clear.

Action of Norepinephrine on Excitatory Synapses

Norepinephrine has a general suppressant action on hippocampal excitatory pathways. The perforant path input to CA1 is profoundly suppressed by noradrenaline (∼55%) (Otmakhova et al., 2005), whereas the CA3-to-CA1 Schaffer-collateral pathway is more weakly (10–15%) suppressed (Otmakhova and Lisman, 2000). Studies in acute tissues provide evidence for α2 receptor-mediated postsynaptic mechanisms (Otmakhova et al., 2005). However, detailed studies in culture systems provide evidence for a presynaptic mode of inhibition of excitatory transmission via α1 (Scanziani et al., 1993) and α2 receptors (Boehm, 1999).

Action of Norepinephrine on Inhibitory Synapses

Information on the regulation of inhibitory synaptic transmission by noradrenaline is relatively sparse. Intracellular studies have shown noradrenaline to produce a marked (∼50%) suppression of evoked inhibitory synaptic potentials recorded in CA1 pyramidal cells (Madison and Nicoll, 1988a). However, subsequent studies have suggested this effect to be independent of a direct action of noradrenaline on interneuron soma or axon terminals and instead be due to depressed excitatory input to the interneurons (Doze et al., 1991). Noradrenaline, like other transmitters, is also reported to facilitate depolarization-induced suppression of inhibition (Martin et al., 2001) (see cannabinoids below). Finally, NE may also influence hippocampal network behavior through the modulation of electrical coupling of GABAergic circuits in stratum lacunosum-moleculare (Zsiros and Maccaferri, 2008).

Serotonin

Serotonin is an important modulator of hippocampal-dependent behaviors and cognitive performance (Richter-Levin and Segal, 1996). In general terms, serotonin has been implicated in the regulation of mood, anger, and aggression. Cells providing serotonergic input show an interesting dichotomy with one population of cells displaying state-dependent fluctuations in activity across the sleep–wake cycle, while another population is tightly regulated to the hippocampal theta rhythm (Kocsis et al., 2006). These findings suggest that ascending serotonergic projections may

be an important regulator of dynamic (fast) information processing in addition to being a mediator of slow state-dependent transitions.

Structural Organization of Serotonergic Afferents

The serotonergic projection of the hippocampus originates in the dorsal raphe nucleus and ramifies extensively throughout the hippocampal formation but is particularly abundant within the subgranular layer of the dentate gyrus and high in the molecular layers of areas CA3 and CA1 (see Swanson et al., 1987). Serotonergic afferents exhibit target specificity, avoiding parvalbumin-positive interneurons and preferentially innervating calbindin-positive interneurons (Freund et al., 1990; Gulyas et al., 1999).

Serotonin Receptors

There are multiple serotonin receptor subtypes expressed in the hippocampus and these have been linked to an array of neurophysiological responses (reviewed by Andrade, 1998; Barnes and Sharp, 1999). The localization of receptors is not fully established but it is evident that receptor subtypes differ markedly in their expression patterns within individual cells as well as between cell types (Table 4). For instance, in CA1 pyramidal cells 5HT1a and 5HT4 receptors mediate principal postsynaptic actions whereas 5HT1b receptors, considered to be expressed at presynaptic terminals, regulate neurotransmitter release. 5HT3 receptors are preferentially expressed on hippocampal interneurons (Chameau and van Hooft, 2006).

Action of Serotonin on Intrinsic Properties

The primary recorded actions of serotonin on hippocampal principal (mainly CA1 but also subicular) cells are membrane hyperpolarization and a decrease ($\sim$30%) in cell input resistance (Jahnsen, 1980; Segal, 1980; Behr et al., 1997). This is mediated mainly through activation of a Ca^{2+}-dependent potassium channel (Andrade et al., 1986; Andrade and Nicoll, 1987; Colino and Halliwell, 1987). However, a suppression of a secondary slow Ca^{2+}-dependent potassium current leads to a concomitant reduction in action potential accommodation. Serotonin also produces a delayed but longer lasting suppression of I_M resulting in a secondary depolarization response. In various systems, serotonin inhibits voltage-gated calcium currents. Through $4HT_4$ receptors, serotonin also reduces afterhyperpolarization potentials through a reported reduction in Ca^{2+}-induced Ca^{2+} release (Torres et al., 1996). Finally, serotonin is also known to regulate I_h with the increase or decrease in current-associated alteration in activation curve depending on the subtypes of serotonin receptors recruited (Bickmeyer et al., 2002).

In interneurons in stratum radiatum (McMahon and Kauer, 1997; Sudweeks et al., 2002) and dentate basket cells (Kawa, 1994), both most likely to be CCK+ interneurons (Ferezou et al., 2002), serotonin exerts a strong fast excitation though 5HT3 receptor channels. The fast inward currents (-15 to -600 pA) are present in

Table 4 Summary of serotonin receptors in the hippocampus

Receptor family	5HT1	5HT2	5HT3	5HT4	5HT5	5HT6	5HT7
Expression in hippocampus	5HT1a,b,f widespread; 5HT1c strong in CA3	Widespread	Strong in SLM and interneurons	Widespread, dendritic, and axonal (mf)	5HT5a widespread, 5HT5B restricted to CA1	Widespread	Strongest in CA3
Signalling	G_i	$G_{q/11}$	Cation channel	G_s	G_i	G_s	G_s
Gross effect	Hyperpolarization, secondary depolarization, ↓accommodation, ↓EPSPs		Fast depolarization of SR interneurons and DG basket cells; strong negative slope conductance, effect very dependent upon MP	↓AHP	?	?	Increased I_h
References	Pompeiano et al. (1994), Wright et al. (1995)	Clemett et al. (2000)	Tecott et al. (1993)	Vilaro et al. (2005)	Matthes et al. (1993)	Ruat et al. (1993), Ward et al. (1995)	Gustafson et al. (1996), Bonaventure et al. (2002)

most dendritic layer interneurons though the range of specific cell types remain to be identified. In a minority of cells, an additional slower inward current, presumably mediated by metabotropic serotonin receptors, has been reported (McMahon and Kauer, 1997).

Action of Serotonin on Excitatory Synapses

Serotonin is known to regulate neurotransmission at a wide range of synapses in the brain (Fink and Gothert, 2007). Within hippocampal excitatory networks, serotonin suppresses perforant path inputs to area CA1 (by ∼40%), but has little effect at the Schaffer-collateral input to area CA1 at low concentrations (Schmitz et al., 1995; Levkovitz and Segal, 1997; Otmakhova and Lisman, 2000). This lack on modulation of Schaffer collateral-to-CA1 transmission agrees with earlier findings (Segal, 1980), although other authors report a modest suppression (∼14%) that appears to be mediated via 5HT1a receptors (Pugliese et al., 1998). Differences in sensitivity to serotonergic modulation are also evident between areas CA1 and CA3 (Matsumoto et al., 2002). The activity of serotonin at other synapses in the hippocampal formation and the relative contribution of respective serotonin receptor subtypes remains poorly characterized (Otmakhova et al., 2005).

Serotonin is also an important modulator of synaptic plasticity where it typically inhibits the induction of LTP (Corradetti et al., 1992; Shakesby et al., 2002; Kojima et al., 2003) through mechanisms involving 5HT1A receptors. However, antagonist studies have shown that 5HT2 and 5HT3 receptors also contribute to suppression of LTP (Staubli and Xu, 1995; Wang and Arvanov, 1998). With respect to the latter, the 5HT3 receptor-mediated suppression of mossy fiber-CA3 LTP by serotonin may be due to indirect actions through enhanced GABAergic inhibition (Maeda et al., 1994). Unlike other receptors, 5HT4 receptors are reported to enhance transmission (Matsumoto et al., 2002).

Action of Serotonin on Inhibitory Synapses

The actions of serotonin on inhibitory synaptic transmission have been studied in a number of brain regions but data on hippocampal inhibitory synaptic transmission are relatively sparse. The limited reports to date suggest that serotonin facilitates GABAergic transmission (Ropert and Guy, 1991; Katsurabayashi et al., 2003; Dorostkar and Boehm, 2007) through a calcium influx mechanism via 5HT3 receptors (Turner et al., 2004). 5HT2 (Shen and Andrade, 1998) receptors have also been reported to contribute a facilitation effect, whereas 5HT1A receptors inhibit GABA release (Katsurabayashi et al., 2003) but probably not from CCK basket cells (Neu et al., 2007). While the exact ion channels mediating serotonin actions on hippocampal GABAergic transmission remain to be established, studies in entorhinal cortex have shown the inhibition of TASK-3 type potassium channels to be important in the serotonin-mediated enhancement of GABAergic signaling (Deng and Lei, 2008).

Histamine

Histaminergic neurons comprise a small cluster of cells in the tuberomammillary nucleus, which project to most brain areas, including the hippocampus. The activity of histaminergic neurons innervating the hippocampus is modulated across the sleep–wake cycle, and the histamine system is considered to be important in a number of central nervous system functions ranging from arousal to stress-related events (Brown et al., 2001).

Structural Organization of Histaminergic Afferents

All histaminergic neurons originate in the tuberomammillary nucleus of the hypothalamus (Haas and Panula, 2003; Haas et al., 2008). The input to the hippocampal formation terminates in all areas but are particularly pronounced in the subiculum and dentate gyrus and sparser in hippocampal areas CA1 and CA3 (Barbin et al., 1976; Inagaki et al., 1988; Panula et al., 1989). Like other aminergic modulators, histaminergic axons form varicosities with very few synaptic specializations consistent with a volume transmission mode of action (Takagi et al., 1986). Whether histaminergic afferents exhibit target specificity has not been systematically examined in the hippocampus.

Histamine Receptors

All three histamine receptors are found at high density throughout the hippocampal formation (Martinez-Mir et al., 1990). H1 and H2 receptors are strongly expressed in all areas (Bouthenet et al., 1988; Vizuete et al., 1997) and are predominantly postsynaptic while H3 receptors are most prominent in the subiculum and dentate gyrus (Pollard et al., 1993; Pillot et al., 2002) and are thought to be exclusively located at presynaptic terminals. In terms of signaling, the three histamine receptors couple to separate G proteins. H1 receptors couple through G_q to directly increase the leak potassium channel and also via phospholipase C to trigger calcium release from intracellular stores. Through protein kinase C, H1 receptor activation is also reported to alter the Mg^{2+} block of NMDA receptors. Other actions attributed to the activation of H1 receptors include alterations in nitric oxide signaling and the modulation of expression of various proteins including gap junctions (review by Brown et al., 2001). In contrast, H2 receptors couple through G_s to reduce a Ca^{2+}-activated potassium conductance (Greene and Haas, 1990) and shift the activation threshold for I_h (see Brown et al., 2001). H3 receptors couple through G_i to result in an inhibition of high-threshold voltage-gated Ca^{2+} channels and resultant suppression of transmitter release (Brown and Haas, 1999). Finally, histamine is also reported to directly modulate signaling through NMDA receptors in a process distinct from classical histamine receptors (Bekkers, 1993; Vorobjev et al., 1993). It has been concluded that this action is due to affinity for a polyamine site though the relevance of this during physiological conditions is equivocal (see Brown et al., 2001).

Action of Histamine on Intrinsic Properties

Histamine is a powerful modulator of excitability (Fig. 3) with the dominant action being excitation (depolarization) mediated via H2 receptors in both pyramidal cells (Haas and Konnerth, 1983; Haas and Greene, 1986; Selbach et al., 1997; Yanovsky and Haas, 1998) and granule cells (Greene and Haas, 1990). Selective activation of H1 receptors can however result in hyperpolarization (Selbach et al., 1997). The dominant depolarizing action is caused by enhancing I_h and through reducing the calcium-activated potassium conductance responsible for the slow after-hyperpolarization and action potential accommodation (Haas and Konnerth, 1983; Pedarzani and Storm, 1993, 1995; Brown et al., 2001). Intracellular studies show histamine to promote burst discharge patterns in CA3 pyramidal cells (Yanovsky and Haas, 1998). Histamine is also reported to regulate interneuronal excitability as indicated by the dramatic increase in spontaneous inhibitory synaptic potentials in both the dentate gyrus and hippocampus (Haas and Greene, 1986; Greene and Haas, 1990). Direct recordings from putative O-LM interneurons confirm an enhanced firing activity in response to histamine (Brown et al., 2001). In more detailed studies, H2 receptor activation has been shown to regulate Kv3.2 channels (~40% reduction in current) in fast-spiking interneurons including parvalbumin and somatostatin-immunopositive cells (Atzori et al., 2000).

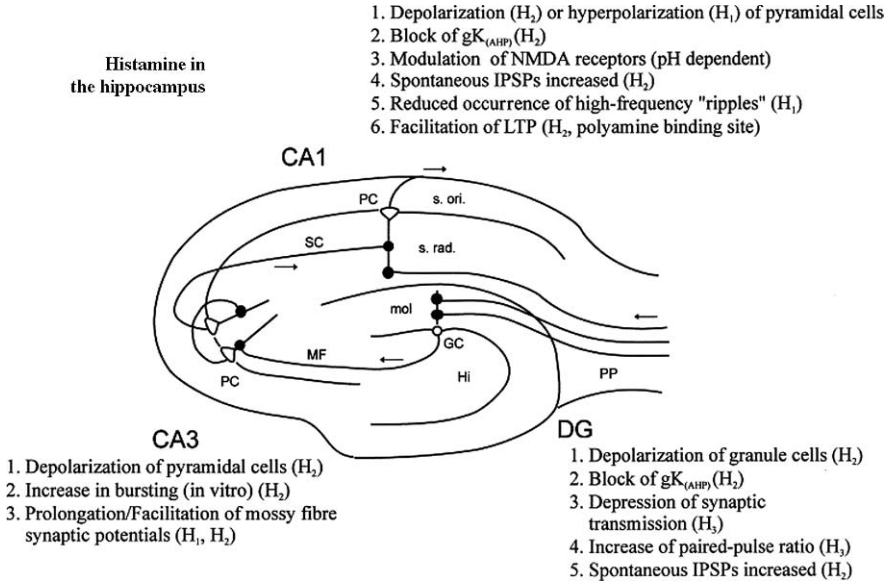

Fig. 3 Primary actions of histamine in the hippocampal formation. From Brown et al. (2001) (with permission)

Action of Histamine on Excitatory Synapses

Histamine depresses EPSPs from perforant path stimulation of the dentate gyrus in vivo (Chang et al., 1998). The action of histamine on evoked synaptic responses

at the Schaffer collateral-to-CA1 pyramidal cell synapse is an enhanced population spike (Segal, 1981; Yanovsky and Haas, 1998) but modest reduction (∼10%) in the excitatory synaptic potential (Brown et al., 1995). These data are consistent with histamine suppressing transmitter release but with the enhanced postsynaptic excitability dominating the response. Histamine is also known to potentiate NMDA-mediated synaptic transmission and enhance LTP through direction actions on the NMDA receptor (Bekkers, 1993; Brown et al., 1995).

Action of Histamine on Inhibitory Synapses

Early studies using paired-pulse stimulation provided evidence that histamine may modulate inhibitory, synaptic transmission in the hippocampus (Springfield and Geller, 1988). However, a detailed understanding of how histamine modulates GABAergic transmission remains to be established.

Purines

Production and Release of Purine Transmitters

Adenosine, adenosine triphosphate (ATP), and other purine nucleotides (UTP, UDP, etc.) are not only important cellular metabolites but also released as modulatory substances in the central nervous system where they display a range of actions. ATP not only is often stored with other transmitters including GABA and glutamate but can also be released independently. It has been suggested that in the hippocampus, ATP is stored and released from distinct pools of vesicles independent of GABA and glutamate (Pankratov et al., 2006). ATP may be transmitted through gap junctions and other channels. It may also be the source of adenosine, especially when released from astrocytes (Pascual et al., 2005). In contrast to ATP, the release of adenosine is more enigmatic. It is not stored in vesicles and in general the level of adenosine rises with increasing neuronal activity as well as in disease conditions such as seizures and hypoxia. Despite not being released by exocytosis, adenosine is nevertheless a powerful homeostatic modulator of neuronal excitability and synaptic transmission (Dunwiddie and Masino, 2001; Fredholm et al., 2005).

Purine Receptors

Separate receptors exist for adenosine (P1 receptors) and ATP (P2 receptors). The latter is broadly divided into ion channel receptors (P2X) and metabotropic receptors (P2Y). Overall, the purine receptors are widely expressed and mediate a number of actions as summarized in Table 5.

Action on Intrinsic Properties

Adenosine causes a hyperpolarization of all hippocampal neurons (Thompson et al., 1992) that has been attributed to the activation of inwardly rectifying K^+ (GIRK)

Table 5 Summary of purine receptors' signaling and primary actions

Receptor family	Adenosine ($A_{1,2A,2B,3}$)	P2X ($P2X_{1-7}$)	P2Y ($P2Y_{1,2,4-6,8-14}$)
Expression in hippocampus	A1, widespread A2, widespread A3, presynaptic	Widespread	Widespread
Signaling	A_1, $G_{i/o}$; $A_{2A/B,}$ G_s; A_3, $G_{i/o}$	Cation channels (subunits confer biophysics, some have very high Ca^{2+} permeability)	$P2Y_{1,2,4,6,14}$ $G_{q/11}$ $P2Y_{4,12,13}$ G_i $P2Y_{11}$ $G_{Q/11}$ and G_s
Gross effect	A_1, A_{2A} hyperpolarization, suppression of synaptic transmission A2B A3	Depolarization, can contribute to evoked EPSPs	Poorly defined.
Comments			
References	Dunwiddie and Masino (2001)	Pankratov et al. (1998), Abbracchio et al. (2009)	Abbracchio et al. (2009)

channels (Dunwiddie and Masino, 2001). The postsynaptic actions of ATP are mediated through both P2X and P2Y receptors as well as indirectly via P1 receptors when metabolized to adenosine. P2X receptors mediate a fast inward current that is reported to contribute to the EPSC recorded upon afferent fiber (e.g., Schaffer-collateral) stimulation (Pankratov et al., 1998). It is proposed that ATP is co-released with glutamate at associational fibers but not mossy fiber synapses (Mori et al., 2001). The cationic current associated with P2X-mediated signaling is generally modest (typically 50–100 pA). However, it has often a significant calcium component which can in turn give rise to activation of calcium-dependent potassium conductances (Illes et al., 1996). Little is known about the action of P2Y receptors in regulating hippocampal primary neurons. Studies in cultured hippocampal neurons report the activation of an outwardly rectifying K^+ current (Ikeuchi et al., 1996) or inhibition of the M-current (Filippov et al., 2006). In contrast to principal cells, hippocampal interneurons in stratum radiatum, identified as calbindin-positive and calretinin-positive interneurons, are excited by ATP (Bowser and Khakh, 2004). This depolarization is associated with a reduction of potassium conductances and activation of non-selective cationic conductances mediated by P2Y1 receptor activation (Bowser and Khakh, 2004; Kawamura et al., 2004).

Action Purines on Excitatory Synapses

The primary action of adenosine is to profoundly (up to ~75–100%) suppress glutamatergic transmission at all hippocampal synapses tested (Dunwiddie and

Hoffer, 1980; Thompson et al., 1992). This may be mediated by multiple mechanisms but principal amongst these is a profound suppression of terminal calcium currents by A1 receptors (Fredholm and Dunwiddie, 1988; Wu and Saggau, 1997). The exact role of A2A receptors in regulating transmission is unclear but it may counteract the suppression of glutamatergic transmission by A1 receptors (Lopes et al., 2002) and even facilitate the release of other transmitters in the hippocampus, notably acetylcholine (Cunha et al., 1994). In line with the suppressant action, adenosine is also reported to depress the induction of LTP at a range of synapses (Alzheimer et al., 1991). However, the situation is complex in that low-frequency plasticity induction paradigms are more sensitive to adenosine than higher frequency patters which appear to overcome the effect of adenosine (Mitchell et al., 1993).

As mentioned above, ATP appears to act as a classical neurotransmitter by mediating fast excitatory synaptic reposes through P2X receptors. However, it may also modulate excitatory synaptic transmission and plasticity although the precise mechanistic detail remains unclear (Inoue et al., 1999; Pankratov et al., 2009). Despite this, it has been shown that ATP can induce LTP and LTD in it own right depending on the level of Ca^{2+} influx associated with the ATP current (Yamazaki et al., 2003). ATP can also regulate plasticity induced by classical induction methods (Pankratov et al., 2002). P2X channel-mediated modulation may show some selectivity between different synapses in the hippocampus. For instance, presynaptic P2X2 channels are reported to facilitate excitatory synapses onto stratum radiatum interneurons in area CA1 but not CA1 pyramidal neurons (Khakh et al., 2003; Khakh, 2009). Very little is known concerning the possible role of P2Y receptors in regulating synaptic transmission and plasticity.

Action of Purines on Inhibitory Synapses

The actions of adenosine on GABAergic signaling are poorly defined. Early studies suggested that adenosine could suppress GABA release in cortical tissues (Hollins and Stone, 1980). However, similar experiments in hippocampal slices failed to find an effect of adenosine on GABA release (Burke and Nadler, 1988) while more recent electrophysiological studies using cultured neurons have failed to show a suppressant action of adenosine despite a pronounced action of evoked glutamatergic responses (Yoon and Rothman, 1991). The actions of ATP via P2X and P2Y classes of receptor on GABAergic signaling remain to be defined.

Paracrine/Autocrine Modulators

Endocannabinoids

Production and Release of Endocannabinoids

Cannabinoids are a group of related lipid-derived modulators that regulate hippocampal circuits through activation of specific cannabinoid receptors (Kano et al., 2009). Some endocannabinoids such as anandamide can also signal through TRPV1

receptors and thus also mediate endovanilloid actions. Anandamide and other major cannabinoids including 2-AG (2-arachidonoyl glycerol) are not stored but synthesized and released tonically on demand in response to neuronal and synaptic activity (Stella et al., 1997). The primary action of endocannabinoids is to mediate retrograde signaling and in particular induce various forms of presynaptic inhibition. Common forms of endocannabinoid-mediated short-term depression are driven by postsynaptic depolarization, Ca^{2+} influx through NMDA receptors, or via muscarinic acetylcholine receptor activation (Kano et al., 2009). However, the most significant trigger for endocannabinoids release and subsequent suppression of synaptic transmission is activation of metabotropic glutamate receptors (Varma et al., 2001).

Endocannabinoid Receptors

The two major forms of cannabinoid receptor (CB1 and CB2) are both metabotropic receptors with the CB1 being the archetypal "brain" form, while the CB2 is mainly restricted to immune cells including microglia (Table 6). Other cannabinoid receptors may exist and there is still debate on whether the orphan receptor GPR55 might be a target for cannabinoid modulators. CB1 receptors are highly abundant but most strongly expressed in GABAergic interneurons. Hippocampal pyramidal cells and dentate granule cells are lightly immunopositive for CB1 receptors but are surrounded by a dense plexus of CB1 positive GABAergic terminals (Tsou et al., 1998). However, low but significant levels of CB1 mRNA are expressed in principal cells suggesting low levels of CB1 signaling in these cells (Marsicano and Lutz, 1999). Within the GABAergic cell population, it appears that CB1 receptors are preferentially expressed in the terminals of perisomatically terminating basket cells. The two main classes of basket cells are parvalbumin and CCK-expressing cells and it is striking that over 95% of CCK positive cells express CB1 which contrasts with parvalbumin cells for which only ~5% of cells are CB1 immunoreactive (Katona et al., 1999). Recent studies suggest that CB1 receptors are also expressed at glutamatergic terminals (Katona et al., 2006).

Action of Endocannabinoids on Intrinsic Properties

Most of the actions of endocannabinoids are attributed to their influence on synaptic transmission (see Figure 4). Studies addressing the actions of endocannabinoids on hippocampal neuronal excitability are very limited (Kirby et al., 2000), but the primary postsynaptic action of endocannabinoid appears to be a modest increased excitability that is mediated through a reduction (~45%) in the M-type K^+ current (Schweitzer, 2000). More detailed studies in somatosensory cortex suggest that low-threshold spiking-type interneurons can exhibit a long-lasting form of action potential suppression whereby activity-dependent release of endocannabinoids causes an autocrine-like enhancement of potassium conductances (Bacci et al., 2004). Whether similar mechanisms occur in hippocampal circuits remains to be established.

Table 6 Summary of cannabinoid signaling in the hippocampus

Receptor	CB1	CB2	GPR55
Expression in hippocampus	Strongly expressed in interneurons (especially CCK basket cells)	Highly expressed in non-neuronal cell types (e.g., microglia), weak neuronal expression	Widely expressed
Signalling	Gi and others, ↑A-type K^+, ↓N and P/Q Ca^{2+}, ↓M and D type K^+	Gi and others	Gα13 and others
Gross effect	Decrease GABA release (main effect) and other transmitters, metabolic actions	None reported	Not defined in hippocampus
References	Pagotto et al. (2006), Kano et al. (2009)	Onaivi et al. (2006)	Ryberg et al. (2007), Lauckner et al. (2008), Henstridge et al. (2009)

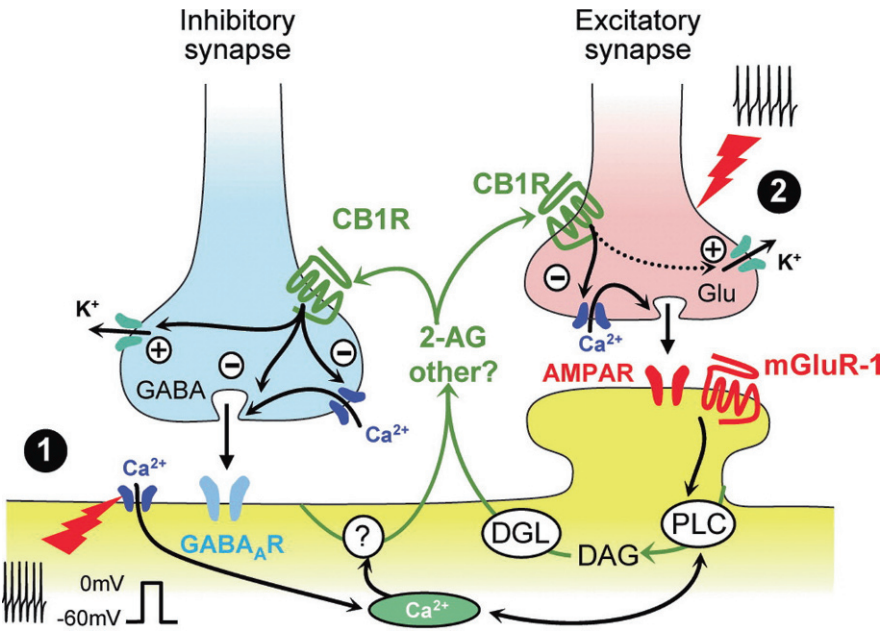

Fig. 4 Summary of cannabinoid crosstalk at excitatory and inhibitory synapses. From Chevaleyre et al. (2006) (with permission)

Action of Endocannabinoids on Excitatory Synapses

Pharmacological activation of CB1 receptors has been shown to cause a profound (~86%) suppression of EPSCs in cultured neurons (Shen et al., 1996) and this effect is consistent with a presynaptic reduction in glutamate release. In terms of functional control of synaptic transmission, endocannabinoids have been shown to act as a retrograde messenger at glutamatergic synapses to produce a suppression glutamate release (Ohno-shosaku et al., 2002). This is an activity-dependent depolarization-induced suppression of excitatory transmission (DSE) and is analogous to the more rigorously characterized suppression seen at inhibitory synapses (below). However, the CB1-mediated suppression of excitatory and inhibitory transmission differs in certain respects. First, a more pronounced depolarization (~10 s) is necessary to induce DSE than to cause suppression at inhibitory synapses (Ohno-shosaku et al., 2002). Second, the excitatory terminals themselves are less sensitive to cannabinoid receptor activation (Ohno-shosaku et al., 2002).

Action of Endocannabinoids on Inhibitory Synapses

Early reports by Pitler and Alger first described a phenomenon known as depolarization-induced suppression of inhibition (DSI) in CA1 pyramidal cells (Pitler and Alger, 1992a). This phenomenon has subsequently been demonstrated in CA3 pyramidal cells, dentate granule cells, mossy cells, CCK-positive interneurons (Kano et al., 2009) as well as other brain areas, notably the cerebellum. DSI is a transient but profound suppression of inhibition (spontaneous or evoked inhibitory postsynaptic events) that follows activity (e.g., depolarization and action potentials) in the postsynaptic cell. Studies in brain slices and cultured hippocampal neurons later confirmed that postsynaptic depolarization and resultant increase in intracellular free Ca^{2+} cause a transient suppression of IPSCs and that this suppression was due to retrograde cannabinoid signaling-mediated reduction of GABA release (Ohno-Shosaku et al., 2001; Wilson and Nicoll, 2001). It is now widely accepted that retrograde signaling by cannabinoid receptors is an important process in the dynamic regulation of GABAergic transmission. However, there is considerable evidence that cannabinoid signaling is not ubiquitous but preferentially regulates specific interneuronal connections. For instance, the output of major classes of basket cells is proposed to be differentially sensitive to cannabinoid regulation, with the parvalbumin-containing basket cells being insensitive to CB1 receptor activation, whereas GABA released from CCK-containing population are exquisitely sensitive (Glickfeld and Scanziani, 2006; Freund and Katona, 2007). However, the nature of the suppression of release is complex, with evidence for both presynaptic and postsynaptic loci of action (Foldy et al., 2006; Neu et al., 2007).

The actions of endocannabinoids on inhibitory synapses highlight the need to view neuromodulation as a complex network phenomenon. In addition to classical DSI, cannabinoids are known to mediate activity-dependent, long-lasting, heterosynaptic LTD at GABAergic synapses. This mechanism is initially triggered by the synaptic release of glutamate and activation of group 1 metabotropic

receptors on CA1 pyramidal cells. In turn, release of endocannabinoids is triggered, which then initiates a long-lasting depression of GABA release (Chevaleyre and Castillo, 2003) with the ultimate effect being a long-lasting increase in pyramidal cell excitability.

Nitric Oxide

Production and Release of Nitric Oxide

Nitric oxide is synthesized de novo by a series of enzymes known as nitric oxide synthases (NOS). All three forms of nitric oxide synthases are expressed in the hippocampus. Original studies suggested pyramidal cells to express high levels of the endothelial form of NOS whereas the neuronal form of the protein was restricted to diffuse populations of interneurons (Dinerman et al., 1994). However, more recent evidence has shown principal cells and selected interneurons to express the neuronal form with the endothelial form being restricted to vascular endothelium (Blackshaw et al., 2003). As nitric oxide is not stored and is a highly membrane permeable molecule, the wide distribution of the enzymes in dendrites, soma and axon is likely to reflect the nature of its dispersal and suggested primary role as a retrograde transmitter. The prototypical activator of nitric oxide synthase is postsynaptic Ca^{2+} entry via the NMDA receptor leading to Ca^{2+}/calmodulin interaction and nitric oxide production (Garthwaite, 2008). Nitric oxide may be released from presynaptic nerves by action potential-dependent activation of voltage-gated Ca^{2+} channels. Reports also suggest that calcium permeable AMPA receptors are an important regulator of NO production (Frade et al., 2008). Once produced, nitric oxide gas is itself is highly soluble, rapidly diffusible, highly membrane permeant but also highly labile.

Nitric Oxide Effectors

Nitric oxide acts through the regulation of soluble guanylyl cyclase. Within the context of neurons, guanylyl cyclase (the nitric oxide "receptor") occurs in various isoforms and is often associated with the postsynaptic density in both principal cells and interneurons (Szabadits et al., 2007). However, other forms of the receptor may be transported to the membrane by signals including cannabinoids (Jones et al., 2008). The resultant production of cGMP regulates a range of cyclic nucleotide-gated channels as well as regulating multiple effectors through activation of PKG.

Action of Nitric Oxide on Intrinsic Properties

Despite abundant literature on the role of nitric oxide in regulating synaptic transmission, the action of nitric oxide on intrinsic postsynaptic properties of hippocampal neurons remains to be described.

Action of Nitric Oxide on Excitatory Synapses

There exists a significant body of evidence suggesting that certain forms of hippocampal LTP are dependent upon the action of nitric oxide as a diffusible retrograde messenger (Schuman and Madison,1991, 1994; Garthwaite and Boulton, 1995; Feil and Kleppisch, 2008). Blockade of nitric oxide signaling prevents LTP, whereas application of nitric oxide donors promotes the development of LTP (Schuman and Madison, 1991; Arancio et al., 1996). However, the significance of nitric oxide in regulating synaptic plasticity seems to vary between species and between synapses. For instance, in areas CA1, nitric oxide-mediated/regulated LTP is more prominent at apical dendrites than at synapses targeting basal dendrites (Haley et al., 1996; Son et al., 1996). In terms of the action of nitric oxide on basal synaptic transmission, there is evidence to suggest that nitric oxide may also produce an enhancement of glutamatergic transmission distinct from the enduring forms of potentiation such as LTP (Bon and Garthwaite, 2001). However, studies have shown that nitric oxide may also transiently suppress glutamatergic transmission (Boulton et al., 1994). This may in part be mediated through triggering the release of adenosine (Arrigoni and Rosenberg, 2006).

Action of Nitric Oxide on Inhibitory Synapses

While morphological studies suggest that hippocampal GABAergic synapses are endowed with the molecular machinery for nitric oxide signaling, functional studies to assess the significance of nitric oxide in regulating inhibitory transmission is rather limited (Szabadits et al., 2007). However, recent evidence suggests that nitric oxide signaling may be an important mediator in depolarization-induced suppression of inhibition (Makara et al., 2007).

Neuropeptides

Production and Release of Neuropeptides

The hippocampal formation is modulated by a diverse array of neuroactive peptides. Some of these are released from neurons intrinsic to the hippocampus (mainly interneurons but also principal cells), whereas others are supplied by inputs from diverse brain regions (Baraban and Tallent, 2004). In general, neuropeptides are synthesized and stored for action potential-dependent release. The levels of neuropeptides and their receptors are often dynamically regulated, especially in association with plasticity processes and disease states. The neuropeptides represent a major category of modulator and a detailed description of their expression, signaling, and actions at different hippocampal cells and circuits is beyond the scope of this chapter. While some actions of peptide modulators are rather ubiquitous, other effects can be highly cell type or synapse specific. Table 7 summarizes some of the major peptide systems and their primary effects and actions in the hippocampus.

Table 7 Summary of neuropeptide transmitter actions in hippocampus

Neuropeptide	Expression	Receptors	Signaling	Modulation of intrinsic properties	Modulation of synaptic transmission	References
NPY	Various interneurons (bistratified cells), small amounts in principal cells. Strongest in dentate gyrus. NB. Important species differences in expression between human and rodent brain	Y_{1-5} Y1 mainly postsynaptic on principal cell dendrites in areas CA1 and CA3; Y2 postsynaptic on principal cells (DG) and on presynaptic mossy terminals	Y1 Y2	↓ N-type Ca^{2+} currents (Y1 and Y2) but little overt postsynaptic action	↓ glutamatergic transmission (Y2), ↓ LTP induction; ↓ IPSC frequency	Haas et al. (1987), Klapstein and Colmers (1993), McQuiston et al. (1996), Whittaker et al. (1999), Sperk et al. (2007)
Substance P	Various interneurons and granule cells as well as extrinsic projections (e.g., supramammillary)	NK_{1-3}	Most actions mediated by NK1	Depolarization on pyramidal cells and interneurons	↓EPSP (~30%) and IPSP amplitude in pyramidal cells, ↑IPSPs between interneurons	Davies and Kohler (1985), Dreifuss and Raggenbass (1986), Borhegyi and Leranth (1997), Kouznetsova and Nistri (1998)
CCK	Various interneurons (basket, Schaffer-associated, PP-associated), released mainly as CCK8	Mainly CCK_B	CCK_B	Depolarization, ↓ K_{leak}, ↓ Ca^{2+}-activated K^+ currents; increase tonic inhibition through depolarization of interneurons	↓glutamatergic transmission (Schaffer collateral), ↑ or ↓ GABAergic transmission depending on interneuronal class	Dodd and Kelly, (1979), MacVicar et al. (1987), Boden and Hill (1988), Bohme et al. (1988), Miller et al. (1997), Shinohara and Kawasaki (1997), Foldy et al. (2007), Karson et al. (2008)

Table 7 (continued)

Neuropeptide	Expression	Receptors	Signaling	Modulation of intrinsic properties	Modulation of synaptic transmission	References
Opioids	Widely distributed	μ, δ, κ	various	Hyperpolarization of interneurons, mixed action on principal cells	↓glutamatergic transmission, ↓ LTP, ↓GABAergic transmission	Zieglgansberger et al. (1979), Madison and Nicoll (1988b), Wagner et al. (1993), Weisskopf et al. (1993), Moore et al. (1994), Glickfeld et al. (2008)
CGRP	Widely distributed but important species differences, some (CA2) pyramidal cells and strongly expressed in specific interneurons; hilar mossy cells and CA3c pyramidal cells			ND	ND	Sakurai and Kosaka (2007), Freund et al. (1997)
Leptin	Synthesized in adipocytes and transported into brain, local biosynthesis	Ob-$R_{a–f}$	Cytokine receptor, JAK2	Hyperpolarization, ↑ BK channel activity		Mercer et al. (1996), Harvey (2007)
Somatostatin	Various interneurons (e.g., bistratified, OLM cells)	$SST_{1–5}$	↓N-type Ca^2+ currents, ↑ M-current, ↑ K_{leak}	Hyperpolarization of pyramidal cells	↓glutamatergic transmission, suppress PP-GC LTP,	Pittman and Siggins (1981), Moore et al. (1988), Schweitzer et al. (1990), Tallent and Siggins (1997), Baratta et al. (2002), Qiu et al. (2008), Tallent and Qiu (2008)

Table 7 (continued)

Neuropeptide	Expression	Receptors	Signaling	Modulation of intrinsic properties	Modulation of synaptic transmission	References
VIP	Various interneurons (basket cells, interneuron targeting cells)	$VPAC_1$ and $VPAC_2$	Various inc. I_{SAHP}	Depolarization of pyramidal cells	Enhance GABAergic and glutamatergic transmission (may be indirect)	Haas and Gahwiler (1992), Haug and Storm (2000), Cunha-Reis et al. (2004), Cunha-Reis et al. (2005)
Oxytocin	Produced in hypothalamo-neurohypophyseal cells as well as neurons terminating throughout CA1, CA3, and DG	OXTR	Multiple	No direct effect on pyramidal cells, depolarize subset of interneurons (important species differences)	Suppress PP-DG LTP; alter chloride transporter expression to regulate polarity of inhibition	Zaninetti and Raggenbass (2000), Raggenbass (2001), Dubrovsky et al. (2002), Tyzio et al. (2006)
Vasopressin	As above	AVPR1A, AVPR1B are major brain forms		Depolarize subset of interneurons	Conflicting reports showing ↑ and ↓ LTP	Muhlethaler et al. (1984), Chen et al. (1993), Hallbeck et al. (1999), Dubrovsky et al. (2002)
Cortistatin	Hippocampal interneurons, partially co-localized with somatostatin-positive cells	SST_{1-5}		$\uparrow I_h$	↓LTP	de Lecea and Sutcliffe (1996), de Lecea et al. (1997), Schweitzer et al. (2003), Tallent et al. (2005)

Table 7 (continued)

Neuropeptide	Expression	Receptors	Signaling	Modulation of intrinsic properties	Modulation of synaptic transmission	References
Bombesin (neuromedin B and gastrin-releasing peptide)	Widely expressed	BB1 and BB2		Depolarize subset of interneurons (BB2)	ND	Dreifuss and Raggenbass (1986), Battey and Wada (1991), Lee et al. (1999)
TRH	Widespread expression of hormone mRNA and receptors	TRHR	IP3 and PKC pathways	Hyperpolarization, regulation of various K^+ channels in CA1 pyramidal cells	↓PP-GC LTP, ↑Mossy fiber-CA3 LTP, ↓IPSPs	Manaker et al. (1985), Ishihara et al. (1992), Ebihara and Akaike (1993), Stocca and Nistri (1996), Deng et al. (2006)

Abbreviation: ND, not determined.

Action of Neuropeptides on Intrinsic Properties

Miscellaneous Neuromodulators

This chapter has aimed to provide a primer to the concept of neuromodulation by reviewing some of the major neuromodulator systems. However, it should be noted that there are likely to be very many other systems that may be significant regulators of hippocampal cells and circuits. Most of these are activators of metabotropic receptors. Examples here would include sphingolipids (Kajimoto et al., 2007), neurosteroids (Belelli and Lambert, 2005), and various orphan and recently deorphanized receptors. Moreover, it is possible that other forms of neuromodulation may be brought about by less orthodox forms of signaling such as the proteolytic cleavage of protease-activated receptors (Gingrich et al., 2000; Bushell et al., 2006). In addition to metabotropic receptor signaling, there are many additional modulators that act through direct orthosteric modulation of channels and receptors. One of the best characterized forms of such modulation is neurosteroids which are widely distributed and which produce an orthosteric modulation of the $GABA_A$ receptor. While they do not overtly affect postsynaptic excitability, they exert a powerful potentiation of GABAergic transmission within hippocampal circuits (Belelli and Lambert, 2005).

Experimental Techniques

Most of the functional data concerning the action of neuromodulators on cellular and synaptic properties are obtained from electrophysiological experiments conducted in vitro either in brain slice experiments or using hippocampal neuronal cultures as described in earlier chapters. Classically this has been extracellular, intracellular (sharp), and more recently patch clamp recordings. Clearly in vitro hippocampal preparations enable detailed scrutiny of the action of neuromodulators on active, passive intrinsic properties as well as synaptic transmission. They also permit detailed pharmacological investigation as drugs can be applied directly to the cells at a precise concentration. In contrast, the majority of in vivo recordings (multiunit recording or evoked field potentials) provide less mechanistic cellular/synaptic information, and pharmacological studies are limited by the difficulty in directing drugs to the site of action at a known concentration. Studies in vivo are typically limited to detecting changes in action potential discharge rate when specific drugs/modulators are applied. However, in vivo studies are often valuable in determining the endogenous action of neuromodulators within the context of behavioral states. Moreover, in vivo recording can be used to relate the activity of neuromodulator sources (e.g., a specific subcortical nuclei) with activity within hippocampal circuits. Recently, the introduction of the juxtacellular recording technique (Pinault, 1996) has permitted the labeling of recorded neurons so that it is possible to relate the activity and modulation of recorded cells with their morphological characteristics and connectivity (Klausberger et al., 2003). Moreover, patch clamp

recording from neurons in vivo (Ferster and Jagadeesh, 1992; Jagadeesh et al., 1992) has undergone recent technical advances so that it is now not only possible to record from fine structures such as presynaptic boutons (Rancz et al., 2007) but also to visualize and target individual neurons in vivo (Kitamura et al., 2008). Finally, the introduction of optical (Deisseroth et al., 2006; Zhang et al., 2007) and genetic (Miyoshi and Fishell, 2006; Gong et al., 2007) techniques to selectively excite or silence specific cells and circuits have already begun to address precise roles of specific cell types in behaviorally relevant network activity (Sohal et al., 2009). Aided by computational modeling, such correlated physiological, pharmacological, transgenic, and morphological studies will be essential for the future understanding of how hippocampal cells and circuits are modulated at the whole organism level.

The Future

As has been apparent from the content this chapter, compared with previous chapters, the field of hippocampal neuromodulation is still at a nascent stage, with many unresolved questions remaining for the years ahead. Even for the most well characterized classical modulators there are still many unresolved questions, particularly in the context of how neuromodulators couple to specific channels across discrete neuronal subtypes. The cellular and synaptic specificity of many neuromodulators demands molecular tools for systematic targeting of discrete afferents and cells. Using existing combined electrophysiological, pharmacological, and anatomical techniques, some progress is being made in this direction (Lawrence, 2008). However, such careful studies require great effort and it is likely that a number of existing and emerging technologies will be useful in moving the field forward. The availability of genetic manipulation and transgenic animals is already proving very useful, especially in defining the importance of specific receptor subtypes where specific pharmacological tools do not yet exist. The increasing use of Cre-loxP systems whereby specific modulator systems can be modified in a cell type-specific manner shows great potential over conventional pharmacological or global knockout strategies in resolving the precise functions of neuromodulators in specific cell types (Gong et al., 2007). At the level of individual cell types, we are still far from gaining detailed knowledge of the repertoire of neuromodulator receptors expressed and localized in cell types. Some progress is being made in this direction using techniques such as single cell RT-PCR (Monyer and Markram, 2004; Toledo-Rodriguez and Markram, 2007) in which it is possible to fully characterize the expression profile of receptors in neurochemically defined cell types (Hillman et al., 2005; Lawrence et al., 2008), but these techniques will ultimately prove to be limiting unless additional molecular tools are developed that enable the visualization and spatial localization of neuromodulatory receptors with respect to cellular and synaptic domains (Triller and Choquet, 2008).

While the current chapter has focused on individual neuromodulator systems and receptors essentially in isolation, it is important to be mindful that a single

neuromodulator can often induce secondary effects that are mediated through different neuromodulators. For example, mAChR activation can induce endocannabinoid release, resulting in CB1-dependent presynaptic depression of GABAergic transmission (Kim et al., 2002; Fukudome et al., 2004; Neu et al., 2007). An additional complication is that multiple neuromodulators may be present in the in vivo milieu in any given point in time; substantial crosstalk across multiple neuromodulatory systems is probably a common occurrence. Behavioral states, rather than discrete neuromodulatory systems turning on and off, are probably comprised of alterations of many different neuromodulatory systems that occur across a broad range of activity levels. At the level of the postsynaptic cell, the dimerization and oligomerization of different G protein-coupled receptors (Milligan, 2007) and neuromodulatory channels (van Hooft et al., 1998) might create novel interactions between different neuromodulators. These interactions and their modulation in hippocampal cells and circuits remain to be fully explored.

Finally, the synaptic and cellular architecture places important spatial constraints on the physiological functions of neuromodulators. Experiments in which receptors are activated exogenously might yield very different results from studies in which endogenous transmitter is released in a naturalistic fashion from endogenous sources within spatially restricted microdomains. An understanding of the physiological significance of neuromodulation will be greatly assisted by the stimulation of subcortical modulator centers in vivo, brain slice preparations in which neuromodulatory pathways are preserved (Widmer et al., 2006; Manseau et al., 2008), and new molecular or transgenic approaches to optically stimulate neuromodulatory centers (Deisseroth et al., 2006; Zhang et al., 2007). It is only by adopting a range of these approaches that it will be possible to fully understand the action of neuromodulators on hippocampal circuitry.

Further Reading

Abbracchio MP, Burnstock G, Verkhratsky A, Zimmermann H (2009) Purinergic signalling in the nervous system: an overview. Trends Neurosci 32:19–29.

Alkondon M, Pereira EF, Albuquerque EX (1998) Alpha-bungarotoxin- and methyllycaconitine-sensitive nicotinic receptors mediate fast synaptic transmission in interneurons of rat hippocampal slices. Brain Res 810:257–263.

Alzheimer C, Rohrenbeck J, ten Bruggencate G (1991) Adenosine depresses induction of LTP at the mossy fiber-CA3 synapse in vitro. Brain Res 543:163–165.

Andrade R (1998) Regulation of membrane excitability in the central nervous system by serotonin receptor subtypes. Ann N Y Acad Sci 861:190–203.

Andrade R, Nicoll RA (1987) Pharmacologically distinct actions of serotonin on single pyramidal neurones of the rat hippocampus recorded in vitro. J Physiol 394:99–124.

Andrade R, Malenka RC, Nicoll RA (1986) A G protein couples serotonin and GABAB receptors to the same channels in hippocampus. Science 234:1261–1265.

Arancio O, Kiebler M, Lee CJ, Lev-Ram V, Tsien RY, Kandel ER, Hawkins RD (1996) Nitric oxide acts directly in the presynaptic neuron to produce long-term potentiation in cultured hippocampal neurons. Cell 87:1025–1035.

Arrigoni E, Rosenberg PA (2006) Nitric oxide-induced adenosine inhibition of hippocampal synaptic transmission depends on adenosine kinase inhibition and is cyclic GMP independent. Eur J Neurosci 24:2471–2480.
Ascoli GA et al. (2008) Petilla terminology: nomenclature of features of GABAergic interneurons of the cerebral cortex. Nat Rev Neurosci 9:557–568.
Atzori M, Lau D, Tansey EP, Chow A, Ozaita A, Rudy B, McBain CJ (2000) H2 histamine receptor-phosphorylation of Kv3.2 modulates interneuron fast spiking. Nat Neurosci 3: 791–798.
Auerbach JM, Segal M (1994) A novel cholinergic induction of long-term potentiation in rat hippocampus. J Neurophysiol 72:2034–2040.
Auerbach JM, Segal M (1996) Muscarinic receptors mediating depression and long-term potentiation in rat hippocampus. J Physiol 492(Pt 2):479–493.
Bacci A, Huguenard JR, Prince DA (2004) Long-lasting self-inhibition of neocortical interneurons mediated by endocannabinoids. Nature 431:312–316.
Bacci A, Huguenard JR, Prince DA (2005) Modulation of neocortical interneurons: extrinsic influences and exercises in self-control. Trends Neurosci 28:602–610.
Baraban SC, Tallent MK (2004) Interneuron diversity series: interneuronal neuropeptides – endogenous regulators of neuronal excitability. Trends Neurosci 27:135–142.
Baratta MV, Lamp T, Tallent MK (2002) Somatostatin depresses long-term potentiation and Ca2+ signaling in mouse dentate gyrus. J Neurophysiol 88:3078–3086.
Barbin G, Garbarg M, Schwartz JC, Storm-Mathisen J (1976) Histamine synthesizing afferents to the hippocampal region. J Neurochem 26:259–263.
Barnes NM, Sharp T (1999) A review of central 5-HT receptors and their function. Neuropharmacology 38:1083–1152.
Bartos M, Vida I, Jonas P (2007) Synaptic mechanisms of synchronized gamma oscillations in inhibitory interneuron networks. Nat Rev Neurosci 8:45–56.
Battey J, Wada E (1991) Two distinct receptor subtypes for mammalian bombesin-like peptides. Trends Neurosci 14:524–528.
Behr J, Gloveli T, Schmitz D, Heinemann U (2000) Dopamine depresses excitatory synaptic transmission onto rat subicular neurons via presynaptic D1-like dopamine receptors. J Neurophysiol 84:112–119.
Behr J, Empson RM, Schmitz D, Gloveli T, Heinemann U (1997) Effects of serotonin on synaptic and intrinsic properties of rat subicular neurons in vitro. Brain Res 773:217–222.
Behrends JC, ten Bruggencate G (1993) Cholinergic modulation of synaptic inhibition in the guinea pig hippocampus in vitro: excitation of GABAergic interneurons and inhibition of GABA-release. J Neurophysiol 69:626–629.
Bekkers JM (1993) Enhancement by histamine of NMDA-mediated synaptic transmission in the hippocampus. Science 261:104–106.
Belelli D, Lambert JJ (2005) Neurosteroids: endogenous regulators of the GABA(A) receptor. Nat Rev Neurosci 6:565–575.
Benardo LS, Prince DA (1982a) Cholinergic pharmacology of mammalian hippocampal pyramidal cells. Neuroscience 7:1703–1712.
Benardo LS, Prince DA (1982b) Ionic mechanisms of cholinergic excitation in mammalian hippocampal pyramidal cells. Brain Res 249:333–344.
Benardo LS, Prince DA (1982c) Cholinergic excitation of mammalian hippocampal pyramidal cells. Brain Res 249:315–331.
Benardo LS, Prince DA (1982d) Dopamine action on hippocampal pyramidal cells. J Neurosci 2:415–423.
Benardo LS, Prince DA (1982e) Dopamine modulates a Ca^{2+}-activated potassium conductance in mammalian hippocampal pyramidal cells. Nature 297:76–79.
Bergles DE, Doze VA, Madison DV, Smith SJ (1996) Excitatory actions of norepinephrine on multiple classes of hippocampal CA1 interneurons. J Neurosci 16:572–585.

Bergson C, Mrzljak L, Smiley JF, Pappy M, Levenson R, Goldman-Rakic PS (1995) Regional, cellular, and subcellular variations in the distribution of D1 and D5 dopamine receptors in primate brain. J Neurosci 15:7821–7836.

Bernardi G, Calabresi P, Mercuri N, Stanzione P (1984) Effect of dopamine on the threshold of the voltage-dependent ionic channels in the rat brain. Ann Ist Super Sanita 20:1–4.

Bickmeyer U, Heine M, Manzke T, Richter DW (2002) Differential modulation of I(h) by 5-HT receptors in mouse CA1 hippocampal neurons. Eur J Neurosci 16:209–218.

Bijak M (1989) Antidepressant drugs potentiate the alpha 1-adrenoceptor effect in hippocampal slices. Eur J Pharmacol 166:183–191.

Bijak M, Misgeld U (1995) Adrenergic modulation of hilar neuron activity and granule cell inhibition in the guinea-pig hippocampal slice. Neuroscience 67:541–550.

Blackshaw S, Eliasson MJ, Sawa A, Watkins CC, Krug D, Gupta A, Arai T, Ferrante RJ, Snyder SH (2003) Species, strain and developmental variations in hippocampal neuronal and endothelial nitric oxide synthase clarify discrepancies in nitric oxide-dependent synaptic plasticity. Neuroscience 119:979–990.

Boden PR, Hill RG (1988) Effects of cholecystokinin and pentagastrin on rat hippocampal neurones maintained in vitro. Neuropeptides 12:95–103.

Boehm S (1999) Presynaptic alpha2-adrenoceptors control excitatory, but not inhibitory, transmission at rat hippocampal synapses. J Physiol 519(Pt 2):439–449.

Bohme GA, Stutzmann JM, Blanchard JC (1988) Excitatory effects of cholecystokinin in rat hippocampus: pharmacological response compatible with 'central'- or B-type CCK receptors. Brain Res 451:309–318.

Bon CL, Garthwaite J (2001) Exogenous nitric oxide causes potentiation of hippocampal synaptic transmission during low-frequency stimulation via the endogenous nitric oxide-cGMP pathway. Eur J Neurosci 14:585–594.

Bonaventure P, Nepomuceno D, Kwok A, Chai W, Langlois X, Hen R, Stark K, Carruthers N, Lovenberg TW (2002) Reconsideration of 5-hydroxytryptamine (5-HT)(7) receptor distribution using [(3)H]5-carboxamidotryptamine and [(3)H]8-hydroxy-2-(di-n-propylamino)tetraline: analysis in brain of 5-HT(1A) knockout and 5-HT(1A/1B) double-knockout mice. J Pharmacol Exp Ther 302:240–248.

Borhegyi Z, Leranth C (1997) Substance P innervation of the rat hippocampal formation. J Comp Neurol 384:41–58.

Boulton CL, Irving AJ, Southam E, Potier B, Garthwaite J, Collingridge GL (1994) The nitric oxide – cyclic GMP pathway and synaptic depression in rat hippocampal slices. Eur J Neurosci 6:1528–1535.

Bouthenet ML, Ruat M, Sales N, Garbarg M, Schwartz JC (1988) A detailed mapping of histamine H1-receptors in guinea-pig central nervous system established by autoradiography with [125I]iodobolpyramine. Neuroscience 26:553–600.

Bowser DN, Khakh BS (2004) ATP excites interneurons and astrocytes to increase synaptic inhibition in neuronal networks. J Neurosci 24:8606–8620.

Brazhnik ES, Fox SE (1999) Action potentials and relations to the theta rhythm of medial septal neurons in vivo. Exp Brain Res 127:244–258.

Brown DA, Adams PR (1980) Muscarinic suppression of a novel voltage-sensitive K+ current in a vertebrate neurone. Nature 283:673–676.

Brown RE, Haas HL (1999) On the mechanism of histaminergic inhibition of glutamate release in the rat dentate gyrus. J Physiol 515(Pt 3):777–786.

Brown RE, Stevens DR, Haas HL (2001) The physiology of brain histamine. Prog Neurobiol 63:637–672.

Brown RE, Fedorov NB, Haas HL, Reymann KG (1995) Histaminergic modulation of synaptic plasticity in area CA1 of rat hippocampal slices. Neuropharmacology 34:181–190.

Buckley NJ, Bonner TI, Brann MR (1988) Localization of a family of muscarinic receptor mRNAs in rat brain. J Neurosci 8:4646–4652.

Buhler AV, Dunwiddie TV (2001) Regulation of the activity of hippocampal stratum oriens interneurons by alpha7 nicotinic acetylcholine receptors. Neuroscience 106:55–67.
Burke SP, Nadler JV (1988) Regulation of glutamate and aspartate release from slices of the hippocampal CA1 area: effects of adenosine and baclofen. J Neurochem 51:1541–1551.
Bushell TJ, Plevin R, Cobb S, Irving AJ (2006) Characterization of proteinase-activated receptor 2 signalling and expression in rat hippocampal neurons and astrocytes. Neuropharmacology 50:714–725.
Cea del Rio CA, Erdelyi F, Szabo G, Mcbain CJ, Lawrence JJ (2008) Neurochemical identity governs cholinergic phenotype across hippocampal basket cell networks. Society for Neuroscience Abstracts Online 532.12.
Chameau P, van Hooft JA (2006) Serotonin 5-HT(3) receptors in the central nervous system. Cell Tissue Res 326:573–581.
Chang M, Saito H, Abe K (1998) Histamine H3 receptor-mediated inhibition of excitatory synaptic transmission in the rat dentate gyrus in vivo. Jpn J Pharmacol 77:251–255.
Chang Q, Fischbach GD (2006) An acute effect of neuregulin 1 beta to suppress alpha 7-containing nicotinic acetylcholine receptors in hippocampal interneurons. J Neurosci 26:11295–11303.
Chapman CA, Lacaille JC (1999) Cholinergic induction of theta-frequency oscillations in hippocampal inhibitory interneurons and pacing of pyramidal cell firing. J Neurosci 19: 8637–8645.
Chen C, Diaz Brinton RD, Shors TJ, Thompson RF (1993) Vasopressin induction of long-lasting potentiation of synaptic transmission in the dentate gyrus. Hippocampus 3:193–203.
Chevaleyre V, Castillo PE (2003) Heterosynaptic LTD of hippocampal GABAergic synapses: a novel role of endocannabinoids in regulating excitability. Neuron 38:461–472.
Chevaleyre V, Takahashi KA, Castillo PE (2006) Endocannabinoid-mediated synaptic plasticity in the CNS. Annu Rev Neurosci 29:37–76.
Clemett DA, Punhani T, Duxon MS, Blackburn TP, Fone KC (2000) Immunohistochemical localisation of the 5-HT2C receptor protein in the rat CNS. Neuropharmacology 39:123–132.
Cobb SR, Davies CH (2005) Cholinergic modulation of hippocampal cells and circuits. J Physiol 562:81–88.
Cole AE, Nicoll RA (1983) Acetylcholine mediates a slow synaptic potential in hippocampal pyramidal cells. Science 221:1299–1301.
Cole AE, Nicoll RA (1984a) Characterization of a slow cholinergic post-synaptic potential recorded in vitro from rat hippocampal pyramidal cells. J Physiol 352:173–188.
Cole AE, Nicoll RA (1984b) The pharmacology of cholinergic excitatory responses in hippocampal pyramidal cells. Brain Res 305:283–290.
Colino A, Halliwell JV (1987) Differential modulation of three separate K-conductances in hippocampal CA1 neurons by serotonin. Nature 328:73–77.
Colino A, Halliwell JV (1993) Carbachol potentiates Q current and activates a calcium-dependent non-specific conductance in rat hippocampus in vitro. Eur J Neurosci 5:1198–1209.
Corradetti R, Ballerini L, Pugliese AM, Pepeu G (1992) Serotonin blocks the long-term potentiation induced by primed burst stimulation in the CA1 region of rat hippocampal slices. Neuroscience 46:511–518.
Couey JJ, Meredith RM, Spijker S, Poorthuis RB, Smit AB, Brussaard AB, Mansvelder HD (2007) Distributed network actions by nicotine increase the threshold for spike-timing-dependent plasticity in prefrontal cortex. Neuron 54:73–87.
Cox DJ, Racca C, LeBeau FE (2008) Beta-adrenergic receptors are differentially expressed in distinct interneuron subtypes in the rat hippocampus. J Comp Neurol 509:551–565.
Cunha RA, Milusheva E, Vizi ES, Ribeiro JA, Sebastiao AM (1994) Excitatory and inhibitory effects of A1 and A2A adenosine receptor activation on the electrically evoked [3H]acetylcholine release from different areas of the rat hippocampus. J Neurochem 63: 207–214.
Cunha-Reis D, Ribeiro JA, Sebastiao AM (2005) VIP enhances synaptic transmission to hippocampal CA1 pyramidal cells through activation of both VPAC1 and VPAC2 receptors. Brain Res 1049:52–60.

Cunha-Reis D, Sebastiao AM, Wirkner K, Illes P, Ribeiro JA (2004) VIP enhances both pre- and postsynaptic GABAergic transmission to hippocampal interneurones leading to increased excitatory synaptic transmission to CA1 pyramidal cells. Br J Pharmacol 143:733–744.

Davies S, Kohler C (1985) The substance P innervation of the rat hippocampal region. Anat Embryol (Berl) 173:45–52.

Day HE, Campeau S, Watson Jr SJ, Akil H (1997) Distribution of alpha 1a-, alpha 1b- and alpha 1d-adrenergic receptor mRNA in the rat brain and spinal cord. J Chem Neuroanat 13:115–139.

de Lecea L, Sutcliffe JG (1996) Peptides, sleep and cortistatin. Mol Psychiatry 1:349–351.

de Lecea L, del Rio JA, Criado JR, Alcantara S, Morales M, Danielson PE, Henriksen SJ, Soriano E, Sutcliffe JG (1997) Cortistatin is expressed in a distinct subset of cortical interneurons. J Neurosci 17:5868–5880.

Deisseroth K, Feng G, Majewska AK, Miesenbock G, Ting A, Schnitzer MJ (2006) Next-generation optical technologies for illuminating genetically targeted brain circuits. J Neurosci 26:10380–10386.

Deller T, Katona I, Cozzari C, Frotscher M, Freund TF (1999) Cholinergic innervation of mossy cells in the rat fascia dentata. Hippocampus 9:314–320.

Deng PY, Lei S (2008) Serotonin increases GABA release in rat entorhinal cortex by inhibiting interneuron TASK-3 K+ channels. Mol Cell Neurosci 39:273–284.

Deng PY, Porter JE, Shin HS, Lei S (2006) Thyrotropin-releasing hormone increases GABA release in rat hippocampus. J Physiol 577:497–511.

Dinerman JL, Dawson TM, Schell MJ, Snowman A, Snyder SH (1994) Endothelial nitric oxide synthase localized to hippocampal pyramidal cells: implications for synaptic plasticity. Proc Natl Acad Sci U S A 91:4214–4218.

Dodd J, Kelly JS (1979) Excitation of CA1 pyramidal neurones of the hippocampus by the tetra- and octapeptide C-terminal fragments of cholecystokinin [proceedings]. J Physiol 295: 61P–62P.

Dodd J, Dingledine R, Kelly JS (1981) The excitatory action of acetylcholine on hippocampal neurones of the guinea pig and rat maintained in vitro. Brain Res 207:109–127.

Dorostkar MM, Boehm S (2007) Opposite effects of presynaptic 5-HT3 receptor activation on spontaneous and action potential-evoked GABA release at hippocampal synapses. J Neurochem 100:395–405.

Dougherty KD, Milner TA (1999) Cholinergic septal afferent terminals preferentially contact neuropeptide Y-containing interneurons compared to parvalbumin-containing interneurons in the rat dentate gyrus. J Neurosci 19:10140–10152.

Doze VA, Cohen GA, Madison DV (1991) Synaptic localization of adrenergic disinhibition in the rat hippocampus. Neuron 6:889–900.

Dreifuss JJ, Raggenbass M (1986) Tachykinins and bombesin excite non-pyramidal neurones in rat hippocampus. J Physiol 379:417–428.

Dubrovsky B, Harris J, Gijsbers K, Tatarinov A (2002) Oxytocin induces long-term depression on the rat dentate gyrus: possible ATPase and ectoprotein kinase mediation. Brain Res Bull 58:141–147.

Dunwiddie TV, Hoffer BJ (1980) Adenine nucleotides and synaptic transmission in the in vitro rat hippocampus. Br J Pharmacol 69:59–68.

Dunwiddie TV, Masino SA (2001) The role and regulation of adenosine in the central nervous system. Annu Rev Neurosci 24:31–55.

Dutar P, Bassant MH, Senut MC, Lamour Y (1995) The septohippocampal pathway: structure and function of a central cholinergic system. Physiol Rev 75:393–427.

Ebihara S, Akaike N (1993) Potassium currents operated by thyrotrophin-releasing hormone in dissociated CA1 pyramidal neurones of rat hippocampus. J Physiol 472:689–710.

El-Ghundi M, Fletcher PJ, Drago J, Sibley DR, O'Dowd BF, George SR (1999) Spatial learning deficit in dopamine D(1) receptor knockout mice. Eur J Pharmacol 383:95–106.

Fabian-Fine R, Skehel P, Errington ML, Davies HA, Sher E, Stewart MG, Fine A (2001) Ultrastructural distribution of the alpha7 nicotinic acetylcholine receptor subunit in rat hippocampus. J Neurosci 21:7993–8003.

Fanselow EE, Richardson KA, Connors BW (2008) Selective, state-dependent activation of somatostatin-expressing inhibitory interneurons in mouse neocortex. J Neurophysiol 100:2640–2652.
Feil R, Kleppisch T (2008) NO/cGMP-dependent modulation of synaptic transmission. Handb Exp Pharmacol 184:529–560.
Ferezou I, Cauli B, Hill EL, Rossier J, Hamel E, Lambolez B (2002) 5-HT3 receptors mediate serotonergic fast synaptic excitation of neocortical vasoactive intestinal peptide/cholecystokinin interneurons. J Neurosci 22:7389–7397.
Fernandez de Sevilla D, Nunez A, Borde M, Malinow R, Buno W (2008) Cholinergic-mediated IP3-receptor activation induces long-lasting synaptic enhancement in CA1 pyramidal neurons. J Neurosci 28:1469–1478.
Ferraguti F, Klausberger T, Cobden P, Baude A, Roberts JD, Szucs P, Kinoshita A, Shigemoto R, Somogyi P, Dalezios Y (2005) Metabotropic glutamate receptor 8-expressing nerve terminals target subsets of GABAergic neurons in the hippocampus. J Neurosci 25:10520–10536.
Ferster D, Jagadeesh B (1992) EPSP-IPSP interactions in cat visual cortex studied with in vivo whole-cell patch recording. J Neurosci 12:1262–1274.
Filippov AK, Choi RC, Simon J, Barnard EA, Brown DA (2006) Activation of P2Y1 nucleotide receptors induces inhibition of the M-type K+ current in rat hippocampal pyramidal neurons. J Neurosci 26:9340–9348.
Fink KB, Gothert M (2007) 5-HT receptor regulation of neurotransmitter release. Pharmacol Rev 59:360–417.
Foldy C, Neu A, Jones MV, Soltesz I (2006) Presynaptic, activity-dependent modulation of cannabinoid type 1 receptor-mediated inhibition of GABA release. J Neurosci 26:1465–1469.
Foldy C, Lee SY, Szabadics J, Neu A, Soltesz I (2007) Cell type-specific gating of perisomatic inhibition by cholecystokinin. Nat Neurosci 10:1128–1130.
Frade JG, Barbosa RM, Laranjinha J (2008) Stimulation of NMDA and AMPA glutamate receptors elicits distinct concentration dynamics of nitric oxide in rat hippocampal slices. Hippocampus 19:603–611.
Fraser DD, MacVicar BA (1996) Cholinergic-dependent plateau potential in hippocampal CA1 pyramidal neurons. J Neurosci 16:4113–4128.
Frazier CJ, Strowbridge BW, Papke RL (2003) Nicotinic receptors on local circuit neurons in dentate gyrus: a potential role in regulation of granule cell excitability. J Neurophysiol 89: 3018–3028.
Frazier CJ, Buhler AV, Weiner JL, Dunwiddie TV (1998a) Synaptic potentials mediated via alpha-bungarotoxin-sensitive nicotinic acetylcholine receptors in rat hippocampal interneurons. J Neurosci 18:8228–8235.
Frazier CJ, Rollins YD, Breese CR, Leonard S, Freedman R, Dunwiddie TV (1998b) Acetylcholine activates an alpha-bungarotoxin-sensitive nicotinic current in rat hippocampal interneurons, but not pyramidal cells. J Neurosci 18:1187–1195.
Fredholm BB, Dunwiddie TV (1988) How does adenosine inhibit transmitter release? Trends Pharmacol Sci 9:130–134.
Fredholm BB, Chen JF, Cunha RA, Svenningsson P, Vaugeois JM (2005) Adenosine and brain function. Int Rev Neurobiol 63:191–270.
Freedman R, Wetmore C, Stromberg I, Leonard S, Olson L (1993) Alpha-bungarotoxin binding to hippocampal interneurons: immunocytochemical characterization and effects on growth factor expression. J Neurosci 13:1965–1975.
Freund TF, Buzsaki G (1996) Interneurons of the hippocampus. Hippocampus 6:347–470.
Freund TF, Katona I (2007) Perisomatic inhibition. Neuron 56:33–42.
Freund TF, Gulyas AI, Acsady L, Gorcs T, Toth K (1990) Serotonergic control of the hippocampus via local inhibitory interneurons. Proc Natl Acad Sci U S A 87:8501–8505.
Freund TF, Hajos N, Acsady L, Gorcs TJ, Katona I (1997) Mossy cells of the rat dentate gyrus are immunoreactive for calcitonin gene-related peptide (CGRP). Eur J Neurosci 9:1815–1830.

Frey U, Huang YY, Kandel ER (1993) Effects of cAMP simulate a late stage of LTP in hippocampal CA1 neurons. Science 260:1661–1664.

Frotscher M, Leranth C (1985) Cholinergic innervation of the rat hippocampus as revealed by choline acetyltransferase immunocytochemistry: a combined light and electron microscopic study. J Comp Neurol 239:237–246.

Frotscher M, Schlander M, Leranth C (1986) Cholinergic neurons in the hippocampus. A combined light- and electron-microscopic immunocytochemical study in the rat. Cell Tissue Res 246:293–301.

Frotscher M, Vida I, Bender R (2000) Evidence for the existence of non-GABAergic, cholinergic interneurons in the rodent hippocampus. Neuroscience 96:27–31.

Fukudome Y, Ohno-Shosaku T, Matsui M, Omori Y, Fukaya M, Tsubokawa H, Taketo MM, Watanabe M, Manabe T, Kano M (2004) Two distinct classes of muscarinic action on hippocampal inhibitory synapses: M2-mediated direct suppression and M1/M3-mediated indirect suppression through endocannabinoid signalling. Eur J Neurosci 19:2682–2692.

Gao C, Sun X, Wolf ME (2006) Activation of D1 dopamine receptors increases surface expression of AMPA receptors and facilitates their synaptic incorporation in cultured hippocampal neurons. J Neurochem 98:1664–1677.

Gao WJ, Goldman-Rakic PS (2003) Selective modulation of excitatory and inhibitory microcircuits by dopamine. Proc Natl Acad Sci U S A 100:2836–2841.

Gao WJ, Wang Y, Goldman-Rakic PS (2003) Dopamine modulation of perisomatic and peridendritic inhibition in prefrontal cortex. J Neurosci 23:1622–1630.

Garthwaite J (2008) Concepts of neural nitric oxide-mediated transmission. Eur J Neurosci 27:2783–2802.

Garthwaite J, Boulton CL (1995) Nitric oxide signaling in the central nervous system. Annu Rev Physiol 57:683–706.

Gasbarri A, Sulli A, Packard MG (1997) The dopaminergic mesencephalic projections to the hippocampal formation in the rat. Prog Neuropsychopharmacol Biol Psychiatry 21:1–22.

Gasbarri A, Packard MG, Campana E, Pacitti C (1994) Anterograde and retrograde tracing of projections from the ventral tegmental area to the hippocampal formation in the rat. Brain Res Bull 33:445–452.

Gasbarri A, Sulli A, Innocenzi R, Pacitti C, Brioni JD (1996) Spatial memory impairment induced by lesion of the mesohippocampal dopaminergic system in the rat. Neuroscience 74: 1037–1044.

Ge S, Dani JA (2005) Nicotinic acetylcholine receptors at glutamate synapses facilitate long-term depression or potentiation. J Neurosci 25:6084–6091.

Gibbs ME, Summers RJ (2002) Role of adrenoceptor subtypes in memory consolidation. Prog Neurobiol 67:345–391.

Gingrich MB, Junge CE, Lyuboslavsky P, Traynelis SF (2000) Potentiation of NMDA receptor function by the serine protease thrombin. J Neurosci 20:4582–4595.

Giocomo LM, Hasselmo ME (2005) Nicotinic modulation of glutamatergic synaptic transmission in region CA3 of the hippocampus. Eur J Neurosci 22:1349–1356.

Giocomo LM, Hasselmo ME (2007) Neuromodulation by glutamate and acetylcholine can change circuit dynamics by regulating the relative influence of afferent input and excitatory feedback. Mol Neurobiol 36:184–200.

Glickfeld LL, Scanziani M (2006) Distinct timing in the activity of cannabinoid-sensitive and cannabinoid-insensitive basket cells. Nat Neurosci 9:807–815.

Glickfeld LL, Atallah BV, Scanziani M (2008) Complementary modulation of somatic inhibition by opioids and cannabinoids. J Neurosci 28:1824–1832.

Goldsmith SK, Joyce JN (1994) Dopamine D2 receptor expression in hippocampus and parahippocampal cortex of rat, cat, and human in relation to tyrosine hydroxylase-immunoreactive fibers. Hippocampus 4:354–373.

Gong S, Doughty M, Harbaugh CR, Cummins A, Hatten ME, Heintz N, Gerfen CR (2007) Targeting Cre recombinase to specific neuron populations with bacterial artificial chromosome constructs. J Neurosci 27:9817–9823.
Gonzalez-Burgos G, Kroener S, Seamans JK, Lewis DA, Barrionuevo G (2005) Dopaminergic modulation of short-term synaptic plasticity in fast-spiking interneurons of primate dorsolateral prefrontal cortex. J Neurophysiol 94:4168–4177.
Gorelova N, Seamans JK, Yang CR (2002) Mechanisms of dopamine activation of fast-spiking interneurons that exert inhibition in rat prefrontal cortex. J Neurophysiol 88:3150–3166.
Gray R, Johnston D (1987) Noradrenaline and beta-adrenoceptor agonists increase activity of voltage-dependent calcium channels in hippocampal neurons. Nature 327:620–622.
Gray R, Rajan AS, Radcliffe KA, Yakehiro M, Dani JA (1996) Hippocampal synaptic transmission enhanced by low concentrations of nicotine. Nature 383:713–716.
Greene RW, Haas HL (1990) Effects of histamine on dentate granule cells in vitro. Neuroscience 34:299–303.
Gribkoff VK, Ashe JH (1984) Modulation by dopamine of population responses and cell membrane properties of hippocampal CA1 neurons in vitro. Brain Res 292:327–338.
Gulledge AT, Kawaguchi Y (2007) Phasic cholinergic signaling in the hippocampus: functional homology with the neocortex? Hippocampus 17:327–332.
Gulledge AT, Park SB, Kawaguchi Y, Stuart GJ (2007) Heterogeneity of phasic cholinergic signaling in neocortical neurons. J Neurophysiol 97:2215–2229.
Gulyas AI, Acsady L, Freund TF (1999) Structural basis of the cholinergic and serotonergic modulation of GABAergic neurons in the hippocampus. Neurochem Int 34:359–372.
Gustafson EL, Durkin MM, Bard JA, Zgombick J, Branchek TA (1996) A receptor autoradiographic and in situ hybridization analysis of the distribution of the 5-ht7 receptor in rat brain. Br J Pharmacol 117:657–666.
Haas H, Panula P (2003) The role of histamine and the tuberomamillary nucleus in the nervous system. Nat Rev Neurosci 4:121–130.
Haas HL, Konnerth A (1983) Histamine and noradrenaline decrease calcium-activated potassium conductance in hippocampal pyramidal cells. Nature 302:432–434.
Haas HL, Greene RW (1986) Effects of histamine on hippocampal pyramidal cells of the rat in vitro. Exp Brain Res 62:123–130.
Haas HL, Rose GM (1987) Noradrenaline blocks potassium conductance in rat dentate granule cells in vitro. Neurosci Lett 78:171–174.
Haas HL, Gahwiler BH (1992) Vasoactive intestinal polypeptide modulates neuronal excitability in hippocampal slices of the rat. Neuroscience 47:273–277.
Haas HL, Sergeeva OA, Selbach O (2008) Histamine in the nervous system. Physiol Rev 88: 1183–1241.
Haas HL, Hermann A, Greene RW, Chan-Palay V (1987) Action and location of neuropeptide tyrosine (Y) on hippocampal neurons of the rat in slice preparations. J Comp Neurol 257: 208–215.
Habib D, Dringenberg HC (2009) Alternating low frequency stimulation of medial septal and commissural fibers induces NMDA-dependent, long-lasting potentiation of hippocampal synapses in urethane-anesthetized rats. Hippocampus 19:299–307.
Hajos N, Papp EC, Acsady L, Levey AI, Freund TF (1998) Distinct interneuron types express m2 muscarinic receptor immunoreactivity on their dendrites or axon terminals in the hippocampus. Neuroscience 82:355–376.
Haley JE, Schaible E, Pavlidis P, Murdock A, Madison DV (1996) Basal and apical synapses of CA1 pyramidal cells employ different LTP induction mechanisms. Learn Mem 3:289–295.
Hallbeck M, Hermanson O, Blomqvist A (1999) Distribution of preprovasopressin mRNA in the rat central nervous system. J Comp Neurol 411:181–200.
Halliwell JV (1990) Physiological mechanisms of cholinergic action in the hippocampus. Prog Brain Res 84:255–272.

Halliwell JV, Adams PR (1982) Voltage-clamp analysis of muscarinic excitation in hippocampal neurons. Brain Res 250:71–92.
Hammad H, Wagner JJ (2006) Dopamine-mediated disinhibition in the CA1 region of rat hippocampus via D3 receptor activation. J Pharmacol Exp Ther 316:113–120.
Harley CW (2007) Norepinephrine and the dentate gyrus. Prog Brain Res 163:299–318.
Harvey J (2007) Leptin: a diverse regulator of neuronal function. J Neurochem 100:307–313.
Hasselmo ME (2006) The role of acetylcholine in learning and memory. Curr Opin Neurobiol 16:710–715.
Hasselmo ME, Schnell E (1994) Laminar selectivity of the cholinergic suppression of synaptic transmission in rat hippocampal region CA1: computational modeling and brain slice physiology. J Neurosci 14:3898–3914.
Haug T, Storm JF (2000) Protein kinase A mediates the modulation of the slow Ca(2+)-dependent K(+) current, I(sAHP), by the neuropeptides CRF, VIP, and CGRP in hippocampal pyramidal neurons. J Neurophysiol 83:2071–2079.
Hefft S, Hulo S, Bertrand D, Muller D (1999) Synaptic transmission at nicotinic acetylcholine receptors in rat hippocampal organotypic cultures and slices. J Physiol 515(Pt 3):769–776.
Henny P, Jones BE (2008) Projections from basal forebrain to prefrontal cortex comprise cholinergic, GABAergic and glutamatergic inputs to pyramidal cells or interneurons. Eur J Neurosci 27:654–670.
Henstridge CM, Balenga NA, Ford LA, Ross RA, Waldhoer M, Irving AJ (2009) The GPR55 ligand L-alpha-lysophosphatidylinositol promotes RhoA-dependent Ca2+ signaling and NFAT activation. Faseb J 23:183–193.
Hillman KL, Lei S, Doze VA, Porter JE (2009) Alpha-1A adrenergic receptor activation increases inhibitory tone in CA1 hippocampus. Epilepsy Res 84:97–109.
Hillman KL, Knudson CA, Carr PA, Doze VA, Porter JE (2005) Adrenergic receptor characterization of CA1 hippocampal neurons using real time single cell RT-PCR. Brain Res Mol Brain Res 139:267–276.
Hollins C, Stone TW (1980) Adenosine inhibition of gamma-aminobutyric acid release from slices of rat cerebral cortex. Br J Pharmacol 69:107–112.
Holscher C, Anwyl R, Rowan MJ (1997) Stimulation on the positive phase of hippocampal theta rhythm induces long-term potentiation that can Be depotentiated by stimulation on the negative phase in area CA1 in vivo. J Neurosci 17:6470–6477.
Hsu KS (1996) Characterization of dopamine receptors mediating inhibition of excitatory synaptic transmission in the rat hippocampal slice. J Neurophysiol 76:1887–1895.
Huang YY, Kandel ER (1995) D1/D5 receptor agonists induce a protein synthesis-dependent late potentiation in the CA1 region of the hippocampus. Proc Natl Acad Sci U S A 92:2446–2450.
Huerta PT, Lisman JE (1993) Heightened synaptic plasticity of hippocampal CA1 neurons during a cholinergically induced rhythmic state. Nature 364:723–725.
Hyman JM, Wyble BP, Goyal V, Rossi CA, Hasselmo ME (2003) Stimulation in hippocampal region CA1 in behaving rats yields long-term potentiation when delivered to the peak of theta and long-term depression when delivered to the trough. J Neurosci 23:11725–11731.
Ihalainen JA, Riekkinen P, Jr., Feenstra MG (1999) Comparison of dopamine and noradrenaline release in mouse prefrontal cortex, striatum and hippocampus using microdialysis. Neurosci Lett 277:71–74.
Ikeuchi Y, Nishizaki T, Okada Y (1996) Repetitive applications of ATP potentiate potassium current by Ca2+/calmodulin kinase in cultured rat hippocampal neurons. Neurosci Lett 203: 115–118.
Illes P, Nieber K, Norenberg W (1996) Electrophysiological effects of ATP on brain neurones. J Auton Pharmacol 16:407–411.
Inagaki N, Yamatodani A, Ando-Yamamoto M, Tohyama M, Watanabe T, Wada H (1988) Organization of histaminergic fibers in the rat brain. J Comp Neurol 273:283–300.
Inoue K, Koizumi S, Ueno S, Kita A, Tsuda M (1999) The functions of ATP receptors in the synaptic transmission in the hippocampus. Prog Brain Res 120:193–206.

Ishihara K, Katsuki H, Sugimura M, Satoh M (1992) YM-14673, a new thyrotropin-releasing hormone analog, augments long-term potentiation in the mossy fiber-CA3 system of guinea pig hippocampal slices. J Pharmacobiodyn 15:75–78.
Ito HT, Schuman EM (2007) Frequency-dependent gating of synaptic transmission and plasticity by dopamine. Front Neural Circuits 1:1.
Jagadeesh B, Gray CM, Ferster D (1992) Visually evoked oscillations of membrane potential in cells of cat visual cortex. Science 257:552–554.
Jahnsen H (1980) The action of 5-hydroxytryptamine on neuronal membranes and synaptic transmission in area CA1 of the hippocampus in vitro. Brain Res 197:83–94.
Jia Y, Yamazaki Y, Nakauchi S, Sumikawa K (2009) Alpha2 nicotine receptors function as a molecular switch to continuously excite a subset of interneurons in rat hippocampal circuits. Eur J Neurosci 29:1588–1603.
Jones BE (2004) Activity, modulation and role of basal forebrain cholinergic neurons innervating the cerebral cortex. Prog Brain Res 145:157–169.
Jones JD, Carney ST, Vrana KE, Norford DC, Howlett AC (2008) Cannabinoid receptor-mediated translocation of NO-sensitive guanylyl cyclase and production of cyclic GMP in neuronal cells. Neuropharmacology 54:23–30.
Jones S, Yakel JL (1997) Functional nicotinic ACh receptors on interneurones in the rat hippocampus. J Physiol 504(Pt 3):603–610.
Kahle JS, Cotman CW (1989) Carbachol depresses synaptic responses in the medial but not the lateral perforant path. Brain Res 482:159–163.
Kajimoto T, Okada T, Yu H, Goparaju SK, Jahangeer S, Nakamura S (2007) Involvement of sphingosine-1-phosphate in glutamate secretion in hippocampal neurons. Mol Cell Biol 27:3429–3440.
Kano M, Ohno-Shosaku T, Hashimotodani Y, Uchigashima M, Watanabe M (2009) Endocannabinoid-mediated control of synaptic transmission. Physiol Rev 89:309–380.
Karson MA, Whittington KC, Alger BE (2008) Cholecystokinin inhibits endocannabinoid-sensitive hippocampal IPSPs and stimulates others. Neuropharmacology 54:117–128.
Katona I, Sperlagh B, Sik A, Kafalvi A, Vizi ES, Mackie K, Freund TF (1999) Presynaptically located CB1 cannabinoid receptors regulate GABA release from axon terminals of specific hippocampal interneurons. J Neurosci 19:4544–4558.
Katona I, Urban GM, Wallace M, Ledent C, Jung KM, Piomelli D, Mackie K, Freund TF (2006) Molecular composition of the endocannabinoid system at glutamatergic synapses. J Neurosci 26:5628–5637.
Katsurabayashi S, Kubota H, Tokutomi N, Akaike N (2003) A distinct distribution of functional presynaptic 5-HT receptor subtypes on GABAergic nerve terminals projecting to single hippocampal CA1 pyramidal neurons. Neuropharmacology 44:1022–1030.
Katz PS, Frost WN (1996) Intrinsic neuromodulation: altering neuronal circuits from within. Trends Neurosci 19:54–61.
Kawa K (1994) Distribution and functional properties of 5-HT3 receptors in the rat hippocampal dentate gyrus: a patch-clamp study. J Neurophysiol 71:1935–1947.
Kawaguchi Y (1997) Selective cholinergic modulation of cortical GABAergic cell subtypes. J Neurophysiol 78:1743–1747.
Kawamura M, Gachet C, Inoue K, Kato F (2004) Direct excitation of inhibitory interneurons by extracellular ATP mediated by P2Y1 receptors in the hippocampal slice. J Neurosci 24: 10835–10845.
Kearns IR, Morton RA, Bulters DO, Davies CH (2001) Opioid receptor regulation of muscarinic acetylcholine receptor-mediated synaptic responses in the hippocampus. Neuropharmacology 41:565–573.
Khakh BS (2009) ATP-gated P2X receptors on excitatory nerve terminals onto interneurons initiate a form of asynchronous glutamate release. Neuropharmacology 56:216–222.
Khakh BS, Gittermann D, Cockayne DA, Jones A (2003) ATP modulation of excitatory synapses onto interneurons. J Neurosci 23:7426–7437.

Kim J, Isokawa M, Ledent C, Alger BE (2002) Activation of muscarinic acetylcholine receptors enhances the release of endogenous cannabinoids in the hippocampus. J Neurosci 22: 10182–10191.

Kirby MT, Hampson RE, Deadwyler SA (2000) Cannabinoid receptor activation in CA1 pyramidal cells in adult rat hippocampus. Brain Res 863:120–131.

Kitamura K, Judkewitz B, Kano M, Denk W, Hausser M (2008) Targeted patch-clamp recordings and single-cell electroporation of unlabeled neurons in vivo. Nat Methods 5:61–67.

Klapstein GJ, Colmers WF (1993) On the sites of presynaptic inhibition by neuropeptide Y in rat hippocampus in vitro. Hippocampus 3:103–111.

Klausberger T, Somogyi P (2008) Neuronal diversity and temporal dynamics: the unity of hippocampal circuit operations. Science 321:53–57.

Klausberger T, Magill PJ, Marton LF, Roberts JD, Cobden PM, Buzsaki G, Somogyi P (2003) Brain-state- and cell-type-specific firing of hippocampal interneurons in vivo. Nature 421: 844–848.

Kobayashi K, Suzuki H (2007) Dopamine selectively potentiates hippocampal mossy fiber to CA3 synaptic transmission. Neuropharmacology 52:552–561.

Kocsis B, Varga V, Dahan L, Sik A (2006) Serotonergic neuron diversity: identification of raphe neurons with discharges time-locked to the hippocampal theta rhythm. Proc Natl Acad Sci U S A 103:1059–1064.

Kojima T, Matsumoto M, Togashi H, Tachibana K, Kemmotsu O, Yoshioka M (2003) Fluvoxamine suppresses the long-term potentiation in the hippocampal CA1 field of anesthetized rats: an effect mediated via 5-HT1A receptors. Brain Res 959:165–168.

Kouznetsova M, Nistri A (1998) Modulation by substance P of synaptic transmission in the mouse hippocampal slice. Eur J Neurosci 10:3076–3084.

Kremin T, Hasselmo ME (2007) Cholinergic suppression of glutamatergic synaptic transmission in hippocampal region CA3 exhibits laminar selectivity: implication for hippocampal network dynamics. Neuroscience 149:760–767.

Kremin T, Gerber D, Giocomo LM, Huang SY, Tonegawa S, Hasselmo ME (2006) Muscarinic suppression in stratum radiatum of CA1 shows dependence on presynaptic M1 receptors and is not dependent on effects at GABA(B) receptors. Neurobiol Learn Mem 85:153–163.

Kroner S, Krimer LS, Lewis DA, Barrionuevo G (2007) Dopamine increases inhibition in the monkey dorsolateral prefrontal cortex through cell type-specific modulation of interneurons. Cereb Cortex 17:1020–1032.

Kulik A, Vida I, Fukazawa Y, Guetg N, Kasugai Y, Marker CL, Rigato F, Bettler B, Wickman K, Frotscher M, Shigemoto R (2006) Compartment-dependent colocalization of Kir3.2-containing K+ channels and GABAB receptors in hippocampal pyramidal cells. J Neurosci 26: 4289–4297.

Lacaille JC, Schwartzkroin PA (1988) Intracellular responses of rat hippocampal granule cells in vitro to discrete applications of norepinephrine. Neurosci Lett 89:176–181.

Lauckner JE, Jensen JB, Chen HY, Lu HC, Hille B, Mackie K (2008) GPR55 is a cannabinoid receptor that increases intracellular calcium and inhibits M current. Proc Natl Acad Sci U S A 105:2699–2704.

Lawrence JJ (2007) Homosynaptic and heterosynaptic modes of endocannabinoid action at hippocampal CCK+ basket cell synapses. J Physiol 578:3–4.

Lawrence JJ (2008) Cholinergic control of GABA release: emerging parallels between neocortex and hippocampus. Trends Neurosci 31:317–327.

Lawrence JJ, Mcbain CJ (2007) Pre- and postsynaptic cholinergic neuromodulation of parvalbumin positive (PV+) CA1 basket cells. Society for Neuroscience Abstracts Online 144.13.

Lawrence JJ, Statland JM, Grinspan ZM, McBain CJ (2006a) Cell type-specific dependence of muscarinic signalling in mouse hippocampal stratum oriens interneurones. J Physiol 570: 595–610.

Lawrence JJ, Grinspan ZM, Statland JM, McBain CJ (2006b) Muscarinic receptor activation tunes mouse stratum oriens interneurones to amplify spike reliability. J Physiol 571:555–562.

Lawrence JJ, Saraga F, Churchill JF, Statland JM, Travis KE, Skinner FK, McBain CJ (2006c) Somatodendritic Kv7/KCNQ/M channels control interspike interval in hippocampal interneurons. J Neurosci 26:12325–12338.
Lawrence JJ, Tricoire L, Cea del Rio CA, Cauli B, Erdelyi F, Szabo G, Mcbain CJ (2008) Hippocampal interneuron subtypes are associated with distinct muscarinic receptor mRNA expression profiles. Society for Neuroscience Abstracts Online 532.11.
Lee K, Dixon AK, Gonzalez I, Stevens EB, McNulty S, Oles R, Richardson PJ, Pinnock RD, Singh L (1999) Bombesin-like peptides depolarize rat hippocampal interneurones through interaction with subtype 2 bombesin receptors. J Physiol 518(Pt 3):791–802.
Lee MG, Hassani OK, Alonso A, Jones BE (2005) Cholinergic basal forebrain neurons burst with theta during waking and paradoxical sleep. J Neurosci 25:4365–4369.
Lee MG, Chrobak JJ, Sik A, Wiley RG, Buzsaki G (1994) Hippocampal theta activity following selective lesion of the septal cholinergic system. Neuroscience 62:1033–1047.
Leranth C, Frotscher M (1987) Cholinergic innervation of hippocampal GAD- and somatostatin-immunoreactive commissural neurons. J Comp Neurol 261:33–47.
Levey AI, Edmunds SM, Koliatsos V, Wiley RG, Heilman CJ (1995) Expression of m1-m4 muscarinic acetylcholine receptor proteins in rat hippocampus and regulation by cholinergic innervation. J Neurosci 15:4077–4092.
Levkovitz Y, Segal M (1997) Serotonin 5-HT1A receptors modulate hippocampal reactivity to afferent stimulation. J Neurosci 17:5591–5598.
Li S, Cullen WK, Anwyl R, Rowan MJ (2003) Dopamine-dependent facilitation of LTP induction in hippocampal CA1 by exposure to spatial novelty. Nat Neurosci 6:526–531.
Lisman JE, Grace AA (2005) The hippocampal-VTA loop: controlling the entry of information into long-term memory. Neuron 46:703–713.
Lopes LV, Cunha RA, Kull B, Fredholm BB, Ribeiro JA (2002) Adenosine A(2A) receptor facilitation of hippocampal synaptic transmission is dependent on tonic A(1) receptor inhibition. Neuroscience 112:319–329.
Lopez-Bendito G, Sturgess K, Erdelyi F, Szabo G, Molnar Z, Paulsen O (2004) Preferential origin and layer destination of GAD65-GFP cortical interneurons. Cereb Cortex 14:1122–1133.
Loy R, Koziell DA, Lindsey JD, Moore RY (1980) Noradrenergic innervation of the adult rat hippocampal formation. J Comp Neurol 189:699–710.
Lucas-Meunier E, Fossier P, Baux G, Amar M (2003) Cholinergic modulation of the cortical neuronal network. Pflugers Arch 446:17–29.
Maccaferri G (2005) Stratum oriens horizontal interneurone diversity and hippocampal network dynamics. J Physiol 562:73–80.
Maccaferri G, McBain CJ (1996) The hyperpolarization-activated current (Ih) and its contribution to pacemaker activity in rat CA1 hippocampal stratum oriens-alveus interneurones. J Physiol 497(Pt 1):119–130.
Maccaferri G, Lacaille JC (2003) Interneuron Diversity series: hippocampal interneuron classifications – making things as simple as possible, not simpler. Trends Neurosci 26:564–571.
MacVicar BA, Kerrin JP, Davison JS (1987) Inhibition of synaptic transmission in the hippocampus by cholecystokinin (CCK) and its antagonism by a CCK analog (CCK27-33). Brain Res 406:130–135.
Madison DV, Nicoll RA (1982) Noradrenaline blocks accommodation of pyramidal cell discharge in the hippocampus. Nature 299:636–638.
Madison DV, Nicoll RA (1986) Actions of noradrenaline recorded intracellularly in rat hippocampal CA1 pyramidal neurones, in vitro. J Physiol 372:221–244.
Madison DV, Nicoll RA (1988a) Norepinephrine decreases synaptic inhibition in the rat hippocampus. Brain Res 442:131–138.
Madison DV, Nicoll RA (1988b) Enkephalin hyperpolarizes interneurones in the rat hippocampus. J Physiol 398:123–130.
Madison DV, McQuiston AR (2006) Toward a unified hypothesis of interneuronal modulation. J Physiol 570:435.

Madison DV, Lancaster B, Nicoll RA (1987) Voltage clamp analysis of cholinergic action in the hippocampus. J Neurosci 7:733–741.
Maeda T, Kaneko S, Satoh M (1994) Inhibitory influence via 5-HT3 receptors on the induction of LTP in mossy fiber-CA3 system of guinea-pig hippocampal slices. Neurosci Res 18:277–282.
Makara JK, Katona I, Nyiri G, Nemeth B, Ledent C, Watanabe M, de Vente J, Freund TF, Hajos N (2007) Involvement of nitric oxide in depolarization-induced suppression of inhibition in hippocampal pyramidal cells during activation of cholinergic receptors. J Neurosci 27: 10211–10222.
Malenka RC, Nicoll RA (1986) Dopamine decreases the calcium-activated afterhyperpolarization in hippocampal CA1 pyramidal cells. Brain Res 379:210–215.
Manaker S, Winokur A, Rostene WH, Rainbow TC (1985) Autoradiographic localization of thyrotropin-releasing hormone receptors in the rat central nervous system. J Neurosci 5: 167–174.
Manseau F, Goutagny R, Danik M, Williams S (2008) The hippocamposeptal pathway generates rhythmic firing of GABAergic neurons in the medial septum and diagonal bands: an investigation using a complete septohippocampal preparation in vitro. J Neurosci 28:4096–4107.
Markram H, Segal M (1990a) Long-lasting facilitation of excitatory postsynaptic potentials in the rat hippocampus by acetylcholine. J Physiol 427:381–393.
Markram H, Segal M (1990b) Acetylcholine potentiates responses to N-methyl-D-aspartate in the rat hippocampus. Neurosci Lett 113:62–65.
Marsicano G, Lutz B (1999) Expression of the cannabinoid receptor CB1 in distinct neuronal subpopulations in the adult mouse forebrain. Eur J Neurosci 11:4213–4225.
Martin LA, Wei DS, Alger BE (2001) Heterogeneous susceptibility of GABA(A) receptor-mediated IPSCs to depolarization-induced suppression of inhibition in rat hippocampus. J Physiol 532:685–700.
Martinez-Mir MI, Pollard H, Moreau J, Arrang JM, Ruat M, Traiffort E, Schwartz JC, Palacios JM (1990) Three histamine receptors (H1, H2 and H3) visualized in the brain of human and non-human primates. Brain Res 526:322–327.
Matsumoto M, Kojima T, Togashi H, Mori K, Ohashi S, Ueno K, Yoshioka M (2002) Differential characteristics of endogenous serotonin-mediated synaptic transmission in the hippocampal CA1 and CA3 fields of anaesthetized rats. Naunyn Schmiedebergs Arch Pharmacol 366: 570–577.
Matthes H, Boschert U, Amlaiky N, Grailhe R, Plassat JL, Muscatelli F, Mattei MG, Hen R (1993) Mouse 5-hydroxytryptamine5A and 5-hydroxytryptamine5B receptors define a new family of serotonin receptors: cloning, functional expression, and chromosomal localization. Mol Pharmacol 43:313–319.
McBain CJ (2008) Differential mechanisms of transmission and plasticity at mossy fiber synapses. Prog Brain Res 169:225–240.
McMahon LL, Kauer JA (1997) Hippocampal interneurons are excited via serotonin-gated ion channels. J Neurophysiol 78:2493–2502.
McQuiston AR, Madison DV (1999a) Nicotinic receptor activation excites distinct subtypes of interneurons in the rat hippocampus. J Neurosci 19:2887–2896.
McQuiston AR, Madison DV (1999b) Muscarinic receptor activity induces an afterdepolarization in a subpopulation of hippocampal CA1 interneurons. J Neurosci 19:5703–5710.
McQuiston AR, Madison DV (1999c) Muscarinic receptor activity has multiple effects on the resting membrane potentials of CA1 hippocampal interneurons. J Neurosci 19:5693–5702.
McQuiston AR, Petrozzino JJ, Connor JA, Colmers WF (1996) Neuropeptide Y1 receptors inhibit N-type calcium currents and reduce transient calcium increases in rat dentate granule cells. J Neurosci 16:1422–1429.
Mercer JG, Hoggard N, Williams LM, Lawrence CB, Hannah LT, Trayhurn P (1996) Localization of leptin receptor mRNA and the long form splice variant (Ob-Rb) in mouse hypothalamus and adjacent brain regions by in situ hybridization. FEBS Lett 387:113–116.

Miller KK, Hoffer A, Svoboda KR, Lupica CR (1997) Cholecystokinin increases GABA release by inhibiting a resting K+ conductance in hippocampal interneurons. J Neurosci 17:4994–5003.
Milligan G (2007) G protein-coupled receptor dimerisation: molecular basis and relevance to function. Biochim Biophys Acta 1768:825–835.
Milner TA, Bacon CE (1989a) GABAergic neurons in the rat hippocampal formation: ultrastructure and synaptic relationships with catecholaminergic terminals. J Neurosci 9:3410–3427.
Milner TA, Bacon CE (1989b) Ultrastructural localization of tyrosine hydroxylase-like immunoreactivity in the rat hippocampal formation. J Comp Neurol 281:479–495.
Milner TA, Shah P, Pierce JP (2000) Beta-adrenergic receptors primarily are located on the dendrites of granule cells and interneurons but also are found on astrocytes and a few presynaptic profiles in the rat dentate gyrus. Synapse 36:178–193.
Milner TA, Lee A, Aicher SA, Rosin DL (1998) Hippocampal alpha2a-adrenergic receptors are located predominantly presynaptically but are also found postsynaptically and in selective astrocytes. J Comp Neurol 395:310–327.
Mitchell JB, Miller K, Dunwiddie TV (1993) Adenosine-induced suppression of synaptic responses and the initiation and expression of long-term potentiation in the CA1 region of the hippocampus. Hippocampus 3:77–86.
Miyoshi G, Fishell G (2006) Directing neuron-specific transgene expression in the mouse CNS. Curr Opin Neurobiol 16:577–584.
Monyer H, Markram H (2004) Interneuron Diversity series: molecular and genetic tools to study GABAergic interneuron diversity and function. Trends Neurosci 27:90–97.
Moore SD, Madamba SG, Joels M, Siggins GR (1988) Somatostatin augments the M-current in hippocampal neurons. Science 239:278–280.
Moore SD, Madamba SG, Schweitzer P, Siggins GR (1994) Voltage-dependent effects of opioid peptides on hippocampal CA3 pyramidal neurons in vitro. J Neurosci 14:809–820.
Morales M, Hein K, Vogel Z (2007) Hippocampal interneurons co-express transcripts encoding the alpha7 nicotinic receptor subunit and the cannabinoid receptor 1. Neuroscience 152:70–81.
Mori M, Heuss C, Gahwiler BH, Gerber U (2001) Fast synaptic transmission mediated by P2X receptors in CA3 pyramidal cells of rat hippocampal slice cultures. J Physiol 535:115–123.
Morton RA, Davies CH (1997) Regulation of muscarinic acetylcholine receptor-mediated synaptic responses by adenosine receptors in the rat hippocampus. J Physiol 502(Pt 1):75–90.
Morton RA, Manuel NA, Bulters DO, Cobb SR, Davies CH (2001) Regulation of muscarinic acetylcholine receptor-mediated synaptic responses by GABA(B) receptors in the rat hippocampus. J Physiol 535:757–766.
Mrzljak L, Bergson C, Pappy M, Huff R, Levenson R, Goldman-Rakic PS (1996) Localization of dopamine D4 receptors in GABAergic neurons of the primate brain. Nature 381:245–248.
Muhlethaler M, Charpak S, Dreifuss JJ (1984) Contrasting effects of neurohypophysial peptides on pyramidal and non-pyramidal neurones in the rat hippocampus. Brain Res 308:97–107.
Murchison CF, Zhang XY, Zhang WP, Ouyang M, Lee A, Thomas SA (2004) A distinct role for norepinephrine in memory retrieval. Cell 117:131–143.
Muzzio IA, Kentros C, Kandel E (2009) What is remembered? Role of attention on the encoding and retrieval of hippocampal representations. J Physiol 587:2837–2854.
Neu A, Foldy C, Soltesz I (2007) Postsynaptic origin of CB1-dependent tonic inhibition of GABA release at cholecystokinin-positive basket cell to pyramidal cell synapses in the CA1 region of the rat hippocampus. J Physiol 578:233–247.
Nicholas AP, Hokfelt T, Pieribone VA (1996) The distribution and significance of CNS adrenoceptors examined with in situ hybridization. Trends Pharmacol Sci 17:245–255.
Nicoll RA, Malenka RC, Kauer JA (1990) Functional comparison of neurotransmitter receptor subtypes in mammalian central nervous system. Physiol Rev 70:513–565.
Noriyama Y, Ogawa Y, Yoshino H, Yamashita M, Kishimoto T (2006) Dopamine profoundly suppresses excitatory transmission in neonatal rat hippocampus via phosphatidylinositol-linked D1-like receptor. Neuroscience 138:475–485.

Ohno-Shosaku T, Maejima T, Kano M (2001) Endogenous cannabinoids mediate retrograde signals from depolarized postsynaptic neurons to presynaptic terminals. Neuron 29:729–738.
Ohno-Shosaku T, Tsubokawa H, Mizushima I, Yoneda N, Zimmer A, Kano M (2002) Presynaptic cannabinoid sensitivity is a major determinant of depolarization-induced retrograde suppression at hippocampal synapses. J Neurosci 22:3864–3872.
Oleskevich S, Descarries L, Lacaille JC (1989) Quantified distribution of the noradrenaline innervation in the hippocampus of adult rat. J Neurosci 9:3803–3815.
Onaivi ES, Ishiguro H, Gong JP, Patel S, Perchuk A, Meozzi PA, Myers L, Mora Z, Tagliaferro P, Gardner E, Brusco A, Akinshola BE, Liu QR, Hope B, Iwasaki S, Arinami T, Teasenfitz L, Uhl GR (2006) Discovery of the presence and functional expression of cannabinoid CB2 receptors in brain. Ann N Y Acad Sci 1074:514–536.
Otmakhova NA, Lisman JE (1996) D1/D5 dopamine receptor activation increases the magnitude of early long-term potentiation at CA1 hippocampal synapses. J Neurosci 16:7478–7486.
Otmakhova NA, Lisman JE (1998) D1/D5 dopamine receptors inhibit depotentiation at CA1 synapses via cAMP-dependent mechanism. J Neurosci 18:1270–1279.
Otmakhova NA, Lisman JE (1999) Dopamine selectively inhibits the direct cortical pathway to the CA1 hippocampal region. J Neurosci 19:1437–1445.
Otmakhova NA, Lisman JE (2000) Dopamine, serotonin, and noradrenaline strongly inhibit the direct perforant path-CA1 synaptic input, but have little effect on the Schaffer collateral input. Ann N Y Acad Sci 911:462–464.
Otmakhova NA, Lewey J, Asrican B, Lisman JE (2005) Inhibition of perforant path input to the CA1 region by serotonin and noradrenaline. J Neurophysiol 94:1413–1422.
Packard MG, Cahill L, McGaugh JL (1994) Amygdala modulation of hippocampal-dependent and caudate nucleus-dependent memory processes. Proc Natl Acad Sci U S A 91:8477–8481.
Pagotto U, Marsicano G, Cota D, Lutz B, Pasquali R (2006) The emerging role of the endocannabinoid system in endocrine regulation and energy balance. Endocr Rev 27:73–100.
Pankratov Y, Castro E, Miras-Portugal MT, Krishtal O (1998) A purinergic component of the excitatory postsynaptic current mediated by P2X receptors in the CA1 neurons of the rat hippocampus. Eur J Neurosci 10:3898–3902.
Pankratov Y, Lalo U, Verkhratsky A, North RA (2006) Vesicular release of ATP at central synapses. Pflugers Arch 452:589–597.
Pankratov Y, Lalo U, Krishtal OA, Verkhratsky A (2009) P2X receptors and synaptic plasticity. Neuroscience 158:137–148.
Pankratov YV, Lalo UV, Krishtal OA (2002) Role for P2X receptors in long-term potentiation. J Neurosci 22:8363–8369.
Panula P, Pirvola U, Auvinen S, Airaksinen MS (1989) Histamine-immunoreactive nerve fibers in the rat brain. Neuroscience 28:585–610.
Papay R, Gaivin R, Jha A, McCune DF, McGrath JC, Rodrigo MC, Simpson PC, Doze VA, Perez DM (2006) Localization of the mouse alpha1A-adrenergic receptor (AR) in the brain: alpha1AAR is expressed in neurons, GABAergic interneurons, and NG2 oligodendrocyte progenitors. J Comp Neurol 497:209–222.
Parra P, Gulyas AI, Miles R (1998) How many subtypes of inhibitory cells in the hippocampus? Neuron 20:983–993.
Pascual O, Casper KB, Kubera C, Zhang J, Revilla-Sanchez R, Sul JY, Takano H, Moss SJ, McCarthy K, Haydon PG (2005) Astrocytic purinergic signaling coordinates synaptic networks. Science 310:113–116.
Pavlides C, Greenstein YJ, Grudman M, Winson J (1988) Long-term potentiation in the dentate gyrus is induced preferentially on the positive phase of theta-rhythm. Brain Res 439:383–387.
Pedarzani P, Storm JF (1993) PKA mediates the effects of monoamine transmitters on the K+ current underlying the slow spike frequency adaptation in hippocampal neurons. Neuron 11: 1023–1035.
Pedarzani P, Storm JF (1995) Dopamine modulates the slow $Ca^{(2+)}$-activated K^+ current IAHP via cyclic AMP-dependent protein kinase in hippocampal neurons. J Neurophysiol 74:2749–2753.

Pedarzani P, Storm JF (1996) Interaction between alpha- and beta-adrenergic receptor agonists modulating the slow $Ca^{(2+)}$-activated K+ current IAHP in hippocampal neurons. Eur J Neurosci 8:2098–2110.

Pillot C, Heron A, Cochois V, Tardivel-Lacombe J, Ligneau X, Schwartz JC, Arrang JM (2002) A detailed mapping of the histamine H(3) receptor and its gene transcripts in rat brain. Neuroscience 114:173–193.

Pinault D (1996) A novel single-cell staining procedure performed in vivo under electrophysiological control: morpho-functional features of juxtacellularly labeled thalamic cells and other central neurons with biocytin or Neurobiotin. J Neurosci Methods 65:113–136.

Pitler TA, Alger BE (1992a) Postsynaptic spike firing reduces synaptic GABAA responses in hippocampal pyramidal cells. J Neurosci 12:4122–4132.

Pitler TA, Alger BE (1992b) Cholinergic excitation of GABAergic interneurons in the rat hippocampal slice. J Physiol 450:127–142.

Pittman QJ, Siggins GR (1981) Somatostatin hyperpolarizes hippocampal pyramidal cells in vitro. Brain Res 221:402–408.

Pollard H, Moreau J, Arrang JM, Schwartz JC (1993) A detailed autoradiographic mapping of histamine H3 receptors in rat brain areas. Neuroscience 52:169–189.

Pompeiano M, Palacios JM, Mengod G (1994) Distribution of the serotonin 5-HT2 receptor family mRNAs: comparison between 5-HT2A and 5-HT2C receptors. Brain Res Mol Brain Res 23:163–178.

Porter JT, Cauli B, Tsuzuki K, Lambolez B, Rossier J, Audinat E (1999) Selective excitation of subtypes of neocortical interneurons by nicotinic receptors. J Neurosci 19:5228–5235.

Power JM, Sah P (2002) Nuclear calcium signaling evoked by cholinergic stimulation in hippocampal CA1 pyramidal neurons. J Neurosci 22:3454–3462.

Pugliese AM, Passani MB, Corradetti R (1998) Effect of the selective 5-HT1A receptor antagonist WAY 100635 on the inhibition of e.p.s.ps produced by 5-HT in the CA1 region of rat hippocampal slices. Br J Pharmacol 124:93–100.

Qian J, Saggau P (1997) Presynaptic inhibition of synaptic transmission in the rat hippocampus by activation of muscarinic receptors: involvement of presynaptic calcium influx. Br J Pharmacol 122:511–519.

Qiu C, Zeyda T, Johnson B, Hochgeschwender U, de Lecea L, Tallent MK (2008) Somatostatin receptor subtype 4 couples to the M-current to regulate seizures. J Neurosci 28:3567–3576.

Radcliffe KA, Dani JA (1998) Nicotinic stimulation produces multiple forms of increased glutamatergic synaptic transmission. J Neurosci 18:7075–7083.

Raggenbass M (2001) Vasopressin- and oxytocin-induced activity in the central nervous system: electrophysiological studies using in-vitro systems. Prog Neurobiol 64:307–326.

Rancz EA, Ishikawa T, Duguid I, Chadderton P, Mahon S, Hausser M (2007) High-fidelity transmission of sensory information by single cerebellar mossy fiber boutons. Nature 450: 1245–1248.

Reece LJ, Schwartzkroin PA (1991) Effects of cholinergic agonists on two non-pyramidal cell types in rat hippocampal slices. Brain Res 566:115–126.

Richter-Levin G, Segal M (1996) Serotonin, aging and cognitive functions of the hippocampus. Rev Neurosci 7:103–113.

Romo-Parra H, Aceves J, Gutierrez R (2005) Tonic modulation of inhibition by dopamine D4 receptors in the rat hippocampus. Hippocampus 15:254–259.

Ropert N, Guy N (1991) Serotonin facilitates GABAergic transmission in the CA1 region of rat hippocampus in vitro. J Physiol 441:121–136.

Rouse ST, Marino MJ, Potter LT, Conn PJ, Levey AI (1999) Muscarinic receptor subtypes involved in hippocampal circuits. Life Sci 64:501–509.

Ruat M, Traiffort E, Arrang JM, Tardivel-Lacombe J, Diaz J, Leurs R, Schwartz JC (1993) A novel rat serotonin (5-HT6) receptor: molecular cloning, localization and stimulation of cAMP accumulation. Biochem Biophys Res Commun 193:268–276.

Ryberg E, Larsson N, Sjogren S, Hjorth S, Hermansson NO, Leonova J, Elebring T, Nilsson K, Drmota T, Greasley PJ (2007) The orphan receptor GPR55 is a novel cannabinoid receptor. Br J Pharmacol 152:1092–1101.

Sakurai O, Kosaka T (2007) Nonprincipal neurons and CA2 pyramidal cells, but not mossy cells are immunoreactive for calcitonin gene-related peptide in the mouse hippocampus. Brain Res 1186:129–143.

Sanchez G, Alvares Lde O, Oberholzer MV, Genro B, Quillfeldt J, da Costa JC, Cervenansky C, Jerusalinsky D, Kornisiuk E (2009) M4 muscarinic receptors are involved in modulation of neurotransmission at synapses of Schaffer collaterals on CA1 hippocampal neurons in rats. J Neurosci Res 87:691–700.

Sarter M, Hasselmo ME, Bruno JP, Givens B (2005) Unraveling the attentional functions of cortical cholinergic inputs: interactions between signal-driven and cognitive modulation of signal detection. Brain research 48:98–111.

Scanziani M, Gahwiler BH, Thompson SM (1993) Presynaptic inhibition of excitatory synaptic transmission mediated by alpha adrenergic receptors in area CA3 of the rat hippocampus in vitro. J Neurosci 13:5393–5401.

Scatton B, Simon H, Le Moal M, Bischoff S (1980) Origin of dopaminergic innervation of the rat hippocampal formation. Neurosci Lett 18:125–131.

Scheiderer CL, Smith CC, McCutchen E, McCoy PA, Thacker EE, Kolasa K, Dobrunz LE, McMahon LL (2008) Coactivation of M(1) muscarinic and alpha1 adrenergic receptors stimulates extracellular signal-regulated protein kinase and induces long-term depression at CA3-CA1 synapses in rat hippocampus. J Neurosci 28:5350–5358.

Scheiderer CL, McCutchen E, Thacker EE, Kolasa K, Ward MK, Parsons D, Harrell LE, Dobrunz LE, McMahon LL (2006) Sympathetic sprouting drives hippocampal cholinergic reinnervation that prevents loss of a muscarinic receptor-dependent long-term depression at CA3-CA1 synapses. J Neurosci 26:3745–3756.

Schmitz D, Empson RM, Heinemann U (1995) Serotonin and 8-OH-DPAT reduce excitatory transmission in rat hippocampal area CA1 via reduction in presumed presynaptic Ca^{2+} entry. Brain Res 701:249–254.

Schuman EM, Madison DV (1991) A requirement for the intercellular messenger nitric oxide in long-term potentiation. Science 254:1503–1506.

Schuman EM, Madison DV (1994) Nitric oxide and synaptic function. Annu Rev Neurosci 17: 153–183.

Schweitzer P (2000) Cannabinoids decrease the K(+) M-current in hippocampal CA1 neurons. J Neurosci 20:51–58.

Schweitzer P, Madamba S, Siggins GR (1990) Arachidonic acid metabolites as mediators of somatostatin-induced increase of neuronal M-current. Nature 346:464–467.

Schweitzer P, Madamba SG, Siggins GR (2003) The sleep-modulating peptide cortistatin augments the h-current in hippocampal neurons. J Neurosci 23:10884–10891.

Seeger T, Alzheimer C (2001) Muscarinic activation of inwardly rectifying K(+) conductance reduces EPSPs in rat hippocampal CA1 pyramidal cells. J Physiol 535:383–396.

Seeger T, Fedorova I, Zheng F, Miyakawa T, Koustova E, Gomeza J, Basile AS, Alzheimer C, Wess J (2004) M2 muscarinic acetylcholine receptor knock-out mice show deficits in behavioral flexibility, working memory, and hippocampal plasticity. J Neurosci 24:10117–10127.

Seeman P, Van Tol HH (1994) Dopamine receptor pharmacology. Trends Pharmacol Sci 15: 264–270.

Segal M (1980) The action of serotonin in the rat hippocampal slice preparation. J Physiol 303:423–439.

Segal M (1981) Histamine modulates reactivity of hippocampal CA3 neurons to afferent stimulation in vitro. Brain Res 213:443–448.

Selbach O, Brown RE, Haas HL (1997) Long-term increase of hippocampal excitability by histamine and cyclic AMP. Neuropharmacology 36:1539–1548.

Shakesby AC, Anwyl R, Rowan MJ (2002) Overcoming the effects of stress on synaptic plasticity in the intact hippocampus: rapid actions of serotonergic and antidepressant agents. J Neurosci 22:3638–3644.

Sharma G, Vijayaraghavan S (2003) Modulation of presynaptic store calcium induces release of glutamate and postsynaptic firing. Neuron 38:929–939.

Sharma G, Grybko M, Vijayaraghavan S (2008) Action potential-independent and nicotinic receptor-mediated concerted release of multiple quanta at hippocampal CA3-mossy fiber synapses. J Neurosci 28:2563–2575.

Shen JX, Tu B, Yakel JL (2009) Inhibition of alpha7-containing nicotinic ACh receptors by muscarinic M1 ACh receptors in rat hippocampal CA1 interneurones in slices. J Physiol 587: 1033–1042.

Shen M, Piser TM, Seybold VS, Thayer SA (1996) Cannabinoid receptor agonists inhibit glutamatergic synaptic transmission in rat hippocampal cultures. J Neurosci 16:4322–4334.

Shen RY, Andrade R (1998) 5-Hydroxytryptamine2 receptor facilitates GABAergic neurotransmission in rat hippocampus. J Pharmacol Exp Ther 285:805–812.

Shigemoto R, Kulik A, Roberts JD, Ohishi H, Nusser Z, Kaneko T, Somogyi P (1996) Target-cell-specific concentration of a metabotropic glutamate receptor in the presynaptic active zone. Nature 381:523–525.

Shinoe T, Matsui M, Taketo MM, Manabe T (2005) Modulation of synaptic plasticity by physiological activation of M1 muscarinic acetylcholine receptors in the mouse hippocampus. J Neurosci 25:11194–11200.

Shinohara S, Kawasaki K (1997) Electrophysiological changes in rat hippocampal pyramidal neurons produced by cholecystokinin octapeptide. Neuroscience 78:1005–1016.

Smith WB, Starck SR, Roberts RW, Schuman EM (2005) Dopaminergic stimulation of local protein synthesis enhances surface expression of GluR1 and synaptic transmission in hippocampal neurons. Neuron 45:765–779.

Sohal VS, Zhang F, Yizhar O, Deisseroth K (2009) Parvalbumin neurons and gamma rhythms enhance cortical circuit performance. Nature 459:698–702.

Son H, Hawkins RD, Martin K, Kiebler M, Huang PL, Fishman MC, Kandel ER (1996) Long-term potentiation is reduced in mice that are doubly mutant in endothelial and neuronal nitric oxide synthase. Cell 87:1015–1023.

Sperk G, Hamilton T, Colmers WF (2007) Neuropeptide Y in the dentate gyrus. Prog Brain Res 163:285–297.

Springfield SA, Geller HM (1988) Histamine modulates local inhibition in the rat hippocampal slice. Cell Mol Neurobiol 8:431–445.

Stanzione P, Calabresi P, Mercuri N, Bernardi G (1984) Dopamine modulates CA1 hippocampal neurons by elevating the threshold for spike generation: an in vitro study. Neuroscience 13:1105–1116.

Staubli U, Xu FB (1995) Effects of 5-HT3 receptor antagonism on hippocampal theta rhythm, memory, and LTP induction in the freely moving rat. J Neurosci 15:2445–2452.

Stella N, Schweitzer P, Piomelli D (1997) A second endogenous cannabinoid that modulates long-term potentiation. Nature 388:773–778.

Stocca G, Nistri A (1996) The neuropeptide thyrotropin-releasing hormone modulates GABAergic synaptic transmission on pyramidal neurones of the rat hippocampal slice. Peptides 17: 1197–1202.

Sudweeks SN, Hooft JA, Yakel JL (2002) Serotonin 5-HT(3) receptors in rat CA1 hippocampal interneurons: functional and molecular characterization. J Physiol 544:715–726.

Surmeier DJ (2007) Dopamine and working memory mechanisms in prefrontal cortex. J Physiol 581:885.

Swanson LW, Köhler C, Björklund A (1987) The limbic region, I: the septohippocampal system. In: Handbook of Chemical Neuroanatomy, Integrated Systems of the CNS (Björklund A, Hökfelt T, Swanson LW, eds.), pp 125–277. Amsterdam: Elsevier.

Swant J, Stramiello M, Wagner JJ (2008) Postsynaptic dopamine D3 receptor modulation of evoked IPSCs via GABA(A) receptor endocytosis in rat hippocampus. Hippocampus 18:492–502.

Szabadits E, Cserep C, Ludanyi A, Katona I, Gracia-Llanes J, Freund TF, Nyiri G (2007) Hippocampal GABAergic synapses possess the molecular machinery for retrograde nitric oxide signaling. J Neurosci 27:8101–8111.

Szabo SI, Zelles T, Vizi ES, Lendvai B (2008) The effect of nicotine on spiking activity and Ca2+ dynamics of dendritic spines in rat CA1 pyramidal neurons. Hippocampus 18:376–385.

Takagi H, Morishima Y, Matsuyama T, Hayashi H, Watanabe T, Wada H (1986) Histaminergic axons in the neostriatum and cerebral cortex of the rat: a correlated light and electron microscopic immunocytochemical study using histidine decarboxylase as a marker. Brain Res 364:114–123.

Tallent MK, Siggins GR (1997) Somatostatin depresses excitatory but not inhibitory neurotransmission in rat CA1 hippocampus. J Neurophysiol 78:3008–3018.

Tallent MK, Qiu C (2008) Somatostatin: an endogenous antiepileptic. Mol Cell Endocrinol 286:96–103.

Tallent MK, Fabre V, Qiu C, Calbet M, Lamp T, Baratta MV, Suzuki C, Levy CL, Siggins GR, Henriksen SJ, Criado JR, Roberts A, de Lecea L (2005) Cortistatin overexpression in transgenic mice produces deficits in synaptic plasticity and learning. Mol Cell Neurosci 30:465–475.

Tecott LH, Maricq AV, Julius D (1993) Nervous system distribution of the serotonin 5-HT3 receptor mRNA. Proc Natl Acad Sci U S A 90:1430–1434.

Thompson AM, Swant J, Wagner JJ (2005) Cocaine-induced modulation of long-term potentiation in the CA1 region of rat hippocampus. Neuropharmacology 49:185–194.

Thompson SM, Haas HL, Gahwiler BH (1992) Comparison of the actions of adenosine at pre- and postsynaptic receptors in the rat hippocampus in vitro. J Physiol 451:347–363.

Toledo-Rodriguez M, Markram H (2007) Single-cell RT-PCR, a technique to decipher the electrical, anatomical, and genetic determinants of neuronal diversity. Methods Mol Biol 403: 123–139.

Torres GE, Arfken CL, Andrade R (1996) 5-Hydroxytryptamine4 receptors reduce afterhyperpolarization in hippocampus by inhibiting calcium-induced calcium release. Mol Pharmacol 50:1316–1322.

Toselli M, Lang J, Costa T, Lux HD (1989) Direct modulation of voltage-dependent calcium channels by muscarinic activation of a pertussis toxin-sensitive G-protein in hippocampal neurons. Pflugers Arch 415:255–261.

Towers SK, Hestrin S (2008) D1-like dopamine receptor activation modulates GABAergic inhibition but not electrical coupling between neocortical fast-spiking interneurons. J Neurosci 28:2633–2641.

Tricoire L, Cea-Del Rio CA (2007) Illuminating cholinergic microcircuits in the neocortex. J Neurosci 27:12119–12120.

Triller A, Choquet D (2008) New concepts in synaptic biology derived from single-molecule imaging. Neuron 59:359–374.

Tsou K, Brown S, Sanudo-Pena MC, Mackie K, Walker JM (1998) Immunohistochemical distribution of cannabinoid CB1 receptors in the rat central nervous system. Neuroscience 83:393–411.

Turner TJ, Mokler DJ, Luebke JI (2004) Calcium influx through presynaptic 5-HT3 receptors facilitates GABA release in the hippocampus: in vitro slice and synaptosome studies. Neuroscience 129:703–718.

Tyzio R, Cossart R, Khalilov I, Minlebaev M, Hubner CA, Represa A, Ben-Ari Y, Khazipov R (2006) Maternal oxytocin triggers a transient inhibitory switch in GABA signaling in the fetal brain during delivery. Science 314:1788–1792.

Valentino RJ, Dingledine R (1981) Presynaptic inhibitory effect of acetylcholine in the hippocampus. J Neurosci 1:784–792.

van Hooft JA, Spier AD, Yakel JL, Lummis SC, Vijverberg HP (1998) Promiscuous coassembly of serotonin 5-HT3 and nicotinic alpha4 receptor subunits into Ca(2+)-permeable ion channels. Proc Natl Acad Sci U S A 95:11456–11461.

Varela JA, Hirsch SJ, Chapman D, Leverich LS, Greene RW (2009) D1/D5 modulation of synaptic NMDA receptor currents. J Neurosci 29:3109–3119.

Varma N, Carlson GC, Ledent C, Alger BE (2001) Metabotropic glutamate receptors drive the endocannabinoid system in hippocampus. J Neurosci 21:RC188.
Vilaro MT, Cortes R, Mengod G (2005) Serotonin 5-HT4 receptors and their mRNAs in rat and guinea pig brain: distribution and effects of neurotoxic lesions. J Comp Neurol 484:418–439.
Vizi ES, Kiss JP (1998) Neurochemistry and pharmacology of the major hippocampal transmitter systems: synaptic and nonsynaptic interactions. Hippocampus 8:566–607.
Vizuete ML, Traiffort E, Bouthenet ML, Ruat M, Souil E, Tardivel-Lacombe J, Schwartz JC (1997) Detailed mapping of the histamine H2 receptor and its gene transcripts in guinea-pig brain. Neuroscience 80:321–343.
Vogt KE, Regehr WG (2001) Cholinergic modulation of excitatory synaptic transmission in the CA3 area of the hippocampus. J Neurosci 21:75–83.
von Engelhardt J, Eliava M, Meyer AH, Rozov A, Monyer H (2007) Functional characterization of intrinsic cholinergic interneurons in the cortex. J Neurosci 27:5633–5642.
Vorobjev VS, Sharonova IN, Walsh IB, Haas HL (1993) Histamine potentiates *N*-methyl-D-aspartate responses in acutely isolated hippocampal neurons. Neuron 11:837–844.
Wagner JJ, Terman GW, Chavkin C (1993) Endogenous dynorphins inhibit excitatory neurotransmission and block LTP induction in the hippocampus. Nature 363:451–454.
Wanaverbecq N, Semyanov A, Pavlov I, Walker MC, Kullmann DM (2007) Cholinergic axons modulate GABAergic signaling among hippocampal interneurons via postsynaptic alpha 7 nicotinic receptors. J Neurosci 27:5683–5693.
Wang RY, Arvanov VL (1998) M100907, a highly selective 5-HT2A receptor antagonist and a potential atypical antipsychotic drug, facilitates induction of long-term potentiation in area CA1 of the rat hippocampal slice. Brain Res 779:309–313.
Ward RP, Hamblin MW, Lachowicz JE, Hoffman BJ, Sibley DR, Dorsa DM (1995) Localization of serotonin subtype 6 receptor messenger RNA in the rat brain by in situ hybridization histochemistry. Neuroscience 64:1105–1111.
Weiss T, Veh RW, Heinemann U (2003) Dopamine depresses cholinergic oscillatory network activity in rat hippocampus. Eur J Neurosci 18:2573–2580.
Weisskopf MG, Zalutsky RA, Nicoll RA (1993) The opioid peptide dynorphin mediates heterosynaptic depression of hippocampal mossy fiber synapses and modulates long-term potentiation. Nature 365:188.
Whittaker E, Vereker E, Lynch MA (1999) Neuropeptide Y inhibits glutamate release and long-term potentiation in rat dentate gyrus. Brain Res 827:229–233.
Widmer H, Ferrigan L, Davies CH, Cobb SR (2006) Evoked slow muscarinic acetylcholinergic synaptic potentials in rat hippocampal interneurons. Hippocampus 16:617–628.
Wilson RI, Nicoll RA (2001) Endogenous cannabinoids mediate retrograde signalling at hippocampal synapses. Nature 410:588–592.
Wojtowicz AM, van den Boom L, Chakrabarty A, Maggio N, Haq RU, Behrens CJ, Heinemann U (2009) Monoamines block kainate- and carbachol-induced gamma-oscillations but augment stimulus-induced gamma-oscillations in rat hippocampus in vitro. Hippocampus 19:273–288.
Wolf ME, Mangiavacchi S, Sun X (2003) Mechanisms by which dopamine receptors may influence synaptic plasticity. Ann N Y Acad Sci 1003:241–249.
Woolf NJ (1991) Cholinergic systems in mammalian brain and spinal cord. Prog Neurobiol 37:475–524.
Wright DE, Seroogy KB, Lundgren KH, Davis BM, Jennes L (1995) Comparative localization of serotonin1A, 1C, and 2 receptor subtype mRNAs in rat brain. J Comp Neurol 351:357–373.
Wu LG, Saggau P (1997) Presynaptic inhibition of elicited neurotransmitter release. Trends Neurosci 20:204–212.
Xiang Z, Huguenard JR, Prince DA (1998) Cholinergic switching within neocortical inhibitory networks. Science 281:985–988.
Yamazaki Y, Kaneko K, Fujii S, Kato H, Ito K (2003) Long-term potentiation and long-term depression induced by local application of ATP to hippocampal CA1 neurons of the guinea pig. Hippocampus 13:81–92.

Yang SN (2000) Sustained enhancement of AMPA receptor- and NMDA receptor-mediated currents induced by dopamine D1/D5 receptor activation in the hippocampus: an essential role of postsynaptic Ca2+. Hippocampus 10:57–63.

Yanovsky Y, Haas HL (1998) Histamine increases the bursting activity of pyramidal cells in the CA3 region of mouse hippocampus. Neurosci Lett 240:110–112.

Yoon KW, Rothman SM (1991) Adenosine inhibits excitatory but not inhibitory synaptic transmission in the hippocampus. J Neurosci 11:1375–1380.

Zago WM, Massey KA, Berg DK (2006) Nicotinic activity stabilizes convergence of nicotinic and GABAergic synapses on filopodia of hippocampal interneurons. Mol Cell Neurosci 31: 549–559.

Zaninetti M, Raggenbass M (2000) Oxytocin receptor agonists enhance inhibitory synaptic transmission in the rat hippocampus by activating interneurons in stratum pyramidale. Eur J Neurosci 12:3975–3984.

Zhang F, Wang LP, Brauner M, Liewald JF, Kay K, Watzke N, Wood PG, Bamberg E, Nagel G, Gottschalk A, Deisseroth K (2007) Multimodal fast optical interrogation of neural circuitry. Nature 446:633–639.

Zhang J, Berg DK (2007) Reversible inhibition of GABAA receptors by alpha7-containing nicotinic receptors on the vertebrate postsynaptic neurons. J Physiol 579:753–763.

Zieglgansberger W, French ED, Siggins GR, Bloom FE (1979) Opioid peptides may excite hippocampal pyramidal neurons by inhibiting adjacent inhibitory interneurons. Science 205: 415–417.

Zsiros V, Maccaferri G (2008) Noradrenergic modulation of electrical coupling in GABAergic networks of the hippocampus. J Neurosci 28:1804–1815.

Neuronal Activity Patterns During Hippocampal Network Oscillations In Vitro

Tengis Gloveli, Nancy Kopell, and Tamar Dugladze

Overview

Neurons form transient, functionally specialized assemblies by coordinating their activity within networks. Assembly activity is important for coding and information processing in the brain; oscillations are assumed to entrain and provide temporal structure to this. Recent work from different laboratories has uncovered cell type-specific activity patterns during network oscillations, indicating that the cells may differentially contribute to the generation of oscillation and thereby the coordination of cell assemblies. The purpose of this chapter is to summarize recent findings from these works in in vitro preparations highlighting the importance of different neuronal activity patterns of hippocampal principal cells and different subtypes of interneurons. Special attention will be paid to the role of the firing properties of hippocampal interneurons on the network oscillatory activity at the theta and gamma frequency range. Models based on these ideas are found in "Gamma and Theta Rhythms in Biophysical Models of Hippocampal Circuits" by Kopell et al., this book.

In Vitro Models of Network Oscillations

Hippocampal Population Activity Patterns In Vivo and In Vitro

Hippocampal networks show rhythmic oscillations in various frequency ranges in a behavior-dependent manner (Singer, 1999; Buzsaki and Draguhn, 2004). In the freely moving rat, three types of hippocampal oscillatory activities have been observed (Leung et al., 1982). Theta (5–10 Hz) and gamma (30–100 Hz) frequency rhythms are observed in the rat during exploration and rapid eye movement sleep (Fig. 1A). The frequency range of both rhythms is described differently in different

T. Gloveli (✉)
Institute of Neurophysiology, Charité – Universitätsmedizin Berlin, 10117 Berlin, Germany
e-mail: tengis.gloveli@charite.de

V. Cutsuridis et al. (eds.), *Hippocampal Microcircuits*, Springer Series in Computational Neuroscience 5, DOI 10.1007/978-1-4419-0996-1_8,

studies. These two rhythms often coexist but can also occur separately (Fig. 1A, for review see Whittington and Traub, 2003). Gamma and theta rhythms also occur throughout the neocortex in vivo and have been proposed to constitute a fundamental mechanism underlying cognitive tasks such as feature recognition, associative learning, and content-sensitive and context-sensitive processing of sensory information. In addition, intermittent population bursts, sharp wave-associated field ripples (100–300 Hz), are present in the CA3–CA1–subiculum–entorhinal cortex axis during awake immobility, consummatory behaviors, and slow-wave sleep (Fig. 1B, Vanderwolf, 1969; Buzsaki et al., 1983; Bland, 1986; Chrobak and Buzsaki, 1996, Csicsvari et al., 1999).

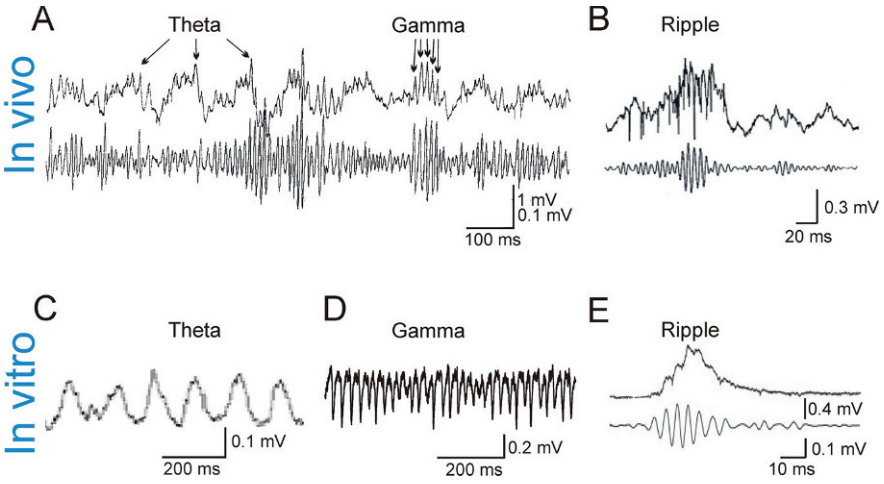

Fig. 1 Hippocampal network oscillations in vivo **A**, **B** and in vitro **C**–**E**. **A** Theta-related and gamma-related modulation of the field in the dentate gyrus (hilar region) during exploratory waking. **B** Sharp wave-associated field ripples in CA1 area during slow-wave sleep. *Upper traces*, wide band recording, *lower traces*, band bath (40–150 Hz, **A**; 150–250 Hz, **B**) filtered gamma and ripple activity. **C** Metabotropic glutamate receptor activation under conditions of reduced AMPA receptor activation generates in CA1 area theta population activity. **D** Kainate receptor activation induces network oscillations at the gamma frequency range in CA3 area. **E** Spontaneously occurring sharp wave-associated ripple oscillation in CA1 area in vitro. *Upper trace*, wide band recording, *lower trace*, ripple band-pass (140–320 Hz) filtered activity. Panels are adapted from **A**, Bragin et al. (1995); **B**, Csicsvari et al. (1999); **C**, Gillies et al. (2002); **D**, Gloveli et al. (2005b); **E**, Both et al. (2008)

Various in vitro models have been developed to gain insight into the cellular and synaptic mechanisms of theta, gamma, and ripple oscillations (Fig. 1C–E). In vitro models of network oscillations, such as the carbachol (Fisahn et al., 1998; Buhl et al., 1998), the kainate (Buhl et al., 1998), the metabotropic glutamate receptor activation (Gillies et al., 2002), and the tetanically induced (Whittington et al., 1997) gamma activity models, reproduce salient features of oscillatory activity in slice preparations maintained in “interface” slice chamber. To determine activity

pattern of individual neurons, sharp microelectrode or blind whole-cell patch-clamp recordings have been obtained from principal cells or putative interneurons. In addition, an in vivo model, the juxtacellular recording technique, was developed to conjointly record action potential series from single neurons and the extracellular field potential during different forms of network activity in anesthetized animals (Pinault, 1996; Klausberger et al., 2003, 2004). These in vitro and in vivo methods have some clear advantages in studying network activity. However, the sparse distribution of interneurons makes them unlikely targets for these blind approaches. Therefore, these investigations are very inefficient in mapping neuronal activity patterns. Whole-cell patch-clamp recordings using infrared differential contrast videomicroscopy (Dodt and Zieglgänsberger, 1994) have greatly facilitated selection and recordings from interneuron. However, this approach has been hampered by the difficulty of generating population activity in the submerged-type slice chambers. Recently, technical modification of the pharmacological paradigms, brief pressure ejection of kainate (Gloveli et al., 2005a, b) or bath application of carbachol (Hájos et al., 2004), permitted the reproduction of the network oscillatory activity in submerged slices. Using these approaches, it was possible to record from visually identified pyramidal cells and interneurons during gamma and theta frequency network oscillation in vitro.

Cell Types Involved in Rhythms

Morphological properties discriminate hippocampal pyramidal cells (PCs) from inhibitory interneurons. In addition, further distinctions exist within both PCs and interneurons. It is reasonable to postulate that hippocampal neurons with different structural features are also likely to have different functions in the network.

Pyramidal cells. Despite the morphological similarities (pyramid-shaped somata, apical and basal dendritic trees), PCs in CA1 and CA3 areas display some important differences such as the existence of excitatory recurrent collaterals. The latter is considered to be the hallmark of the CA3 but not the CA1 area. The pyramidal cells of the CA3 area themselves are not homogeneous. Whereas most axon collaterals of the CA3a and CA3b neurons give rise to extensive recurrent collaterals that are confined to the CA3 region, pyramidal cells in CA3c subregion are mostly projection cells, with most of their axon collaterals terminating in the CA1 region (Li et al., 1994; Wittner et al., 2007). It was hypothesized (Csicsvari et al., 2003) that intrahippocampal gamma oscillations emerge in the recurrent collateral-rich CA3a,b subregions; their activity recruits CA3c subregion, which, in turn, entrains CA1 cells.

Interneuron types. In contrast to glutamatergic principal cells, GABAergic interneurons of the hippocampus exhibit substantial diversity. In the CA1 area, for instance, at least 21 classes of interneurons were described (for review see Klausberger and Somogyi, 2008 [see “Morphology of Hippocampal Neurons” by Vida, this book]). In contrast to principal cells, the vast majority of interneurons have

locally restricted axons and lack spines. Interneurons can be broadly classified into several classes on the basis of different criteria, such as action potential firing properties, somato-dendritic architecture and axonal ramification pattern, neurochemical content, voltage- and ligand-gated conductances as well as plastic changes in excitatory synaptic transmission (for reviews see Freund and Buzsáki, 1996; McBain and Fisahn, 2001; Whittington and Traub, 2003). Functionally, at least three main GABAergic cell types coexist in hippocampal networks: perisomatic inhibitory neurons, dendritic inhibitory interneurons, and GABAergic cells specifically innervating other inhibitory interneurons (Miles et al., 1996). The most striking morpho–functional dichotomy in the population of cortical interneurons is the targeting of the dendritic versus the perisomatic domain of principal cells. Dendritic inhibition is likely to control the efficacy and plasticity of excitatory synaptic inputs of principal cells, whereas perisomatic inhibition is ideally suited to control output, synchronizing the action potential firing of large groups of principal cells (Freund and Buzsáki, 1996). Further distinctions exist within the same class of interneurons. Thus, different types *of perisomatic targeting* parvalbumin (PV)-expressing interneurons innervate distinct subcellular domains of principal cells. Axo-axonic cells (AACs) innervate exclusively the axon initial segment of PCs; in contrast, basket cells (BCs) innervate the somata and proximal apical dendrites. In addition, two distinct populations of basket cells – PV-expressing and cholecystokinin (CCK)-expressing interneurons – could be defined on the basis of their neurochemical content (see "Morphology of Hippocampal Neurons" by Vida, this book). Dendrite-targeting interneurons could also be subdivided into the distal (such as oriens lacunosum-moleculare, O-LM, and radiatum lacunosum-moleculare – R-LM cells) and proximal (such as trilaminar, bistratified, and radiatum cells) dendrite-targeting cells. Interneurons belonging to distinct classes defined by their axonal target domain on the pyramidal cell have clearly different intrinsic, synaptic, and firing properties.

As an example, Fig. 2 illustrates the morphology and the physiological properties of two types of interneurons: non-fast spiking distal dendrite-targeting O-LM cells, which present one of the best studied interneuron classes in the hippocampus, and fast-spiking proximal dendrite-targeting trilaminar cells. These cells differ in their morphology, neurochemical marker contents, and intrinsic membrane properties (see Fig. 2A, B). Clear differences were also detected in spontaneous EPSC properties between these two subtypes of interneurons – with slower kinetics in O-LM than those in trilaminar interneurons (Fig. 2B). Furthermore, while the excitatory input displayed a late-persistent firing in O-LM cells, fast-spiking trilaminar interneurons displayed an onset-transient firing in response to stimulation of CA1 axons in the alveus (Fig. 2B; Pouille and Scanziani, 2004).

These differences in morphological and electrophysiological properties of interneurons indicate that they are likely to have specific roles in the network. In fact, analysis of their spike timing during the oscillations suggests that a division of labor exist among interneuron subtypes involved in hippocampal network oscillations (see Sections "Firing Patterns in Gamma Oscillations" and "Firing Patterns in Theta Oscillations").

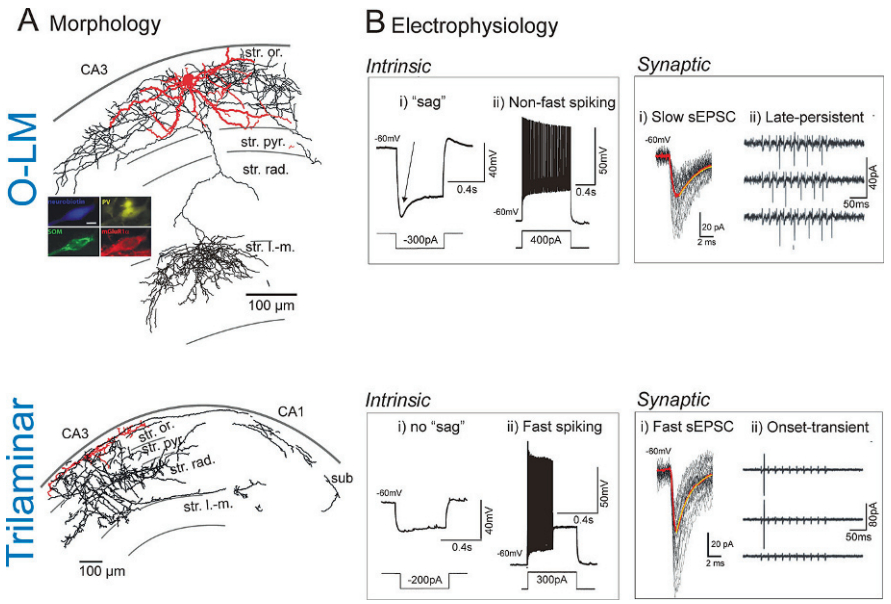

Fig. 2 Properties of distal (O-LM) and proximal (trilaminar) dendrite-targeting interneurons. **A** Morphology of O-LM and trilaminar cells. Somata and dendrites are drawn in *red*, axons are in *black*. The somata of O-LM cells are located in stratum oriens and have mainly horizontally running dendrites. The main axon of these cells crosses strata pyramidale and radiatum and branches in stratum lacunosum-moleculare. O-LM cells innervate the distal dendrites of pyramidal cells which are co-aligned with the entorhinal input (Sik et al., 1995; Maccaferri et al., 2000). **A** inset, O-LM cells are immunopositive for the metabotropic glutamate receptor (mGluR1α) and the neuropeptide somatostatin (SOM, Tukker et al., 2007) and express low levels of calcium binding protein PV (Maccaferri et al., 2000; Klausberger et al., 2003). The trilaminar cells have similar horizontally distributed dendrites in stratum oriens, but are clearly different from O-LM cells in respect of axonal arborization (Sik et al., 1995). Sub – subiculum; str. or. – stratum oriens; str. pyr. – stratum pyramidale; str. rad. – stratum radiatum; str. l-m. – stratum lacunosum-moleculare. **B** *Intrinsic*, intrinsic membrane (*i*) and firing properties (*ii*) of O-LM and trilaminar cells during hyperpolarizing and depolarizing current injection. O-LM cells demonstrate clear "sag" potential and non-fast spiking pattern in marked contrast to trilaminar cells showing no "sag" and fast-spiking character upon hyperpolarizing and depolarizing pulses. **B** *Synaptic* (*i*), spontaneous EPSC (sEPSC) in O-LM and trailaminar interneurons. Forty individual traces are *black* and superimposed averaged currents are *red*. **B** *Synaptic* (*ii*), cell-attached responses from an O-LM and trilaminar cells. Current deflections indicate action potential firing in response to the stimulation of CA1 axons in the alveus. Panels **A** and **B**, *Intrinsic* (*i, ii*) and *Synaptic* (*i*) are from Gloveli et al. (2005a); panel **B** *Synaptic* (*ii*) is from Pouille and Scanziani (2004); inset **A**, (O-LM) is from Tukker et al. (2007)

Gamma Oscillations

Two forms of local network gamma frequency oscillations can be induced in vitro in hippocampal slices (Table 1). Transient forms of gamma frequency oscillations (lasting for a few seconds or minutes) can be evoked in vitro by titanic stimulation (Whittington et al., 1997) or through pressure ejection of glutamate

Table 1 Properties of in vitro models of theta and gamma oscillations

Oscillation type	Activated by	Blocked by	Region	Mean freq. (rec. temp.)	Main references
Persistent θ	mGlutR	NMDAR, $GABA_AR$	CA1	7 Hz (35°C)	Gillies et al. (2002)
	mAChR	NMDAR, $GABA_AR$	CA1	9 Hz (35°C)	Gillies et al. (2002)
	mGlutR, mAChR	AMPAR	CA3	8 Hz (33°C)	Cobb et al. (2000) Konopacki et al. (1992)
	KAR, long. slice	N.T.	CA3	8 Hz (29°C)	Gloveli et al. (2005b)
Transient θ	Puff KA, long. slice	$GABA_AR$	CA3	8 Hz (29°C)	Gloveli et al. (2005b)
Persistent γ	KAR	$GABA_AR$	CA3	35 Hz (35°C) 37 Hz (34°C)	Fisahn et al. (2004) Gloveli et al. (2005b)
	mAChR	AMPAR, $GABA_AR$	CA3	32 Hz (30°C)	Pálhalmi et al. (2004)
			CA3	39 Hz (34°C)	Fisahn et al. (1998) Hájos et al. (2004)
	mGluR	AMPAR, $GABA_AR$	CA3	41 Hz (30°C)	Pálhalmi et al. (2004)
Transient γ	Puff Glut.	$GABA_AR$	CA1/DG	42/64 Hz (36°C)	Pöschel et al. (2002)
	Puff KA	$GABA_AR$	CA3	33 Hz (29°C)	Gloveli et al. (2005a)
	Puff K^+	$GABA_AR$	DG	67 Hz (34°C)	Towers et al. (2002)
		AMPAR, $GABA_AR$	CA1	63 Hz (34°C)	LeBeau et al. (2002)

Abbreviations: R, receptor; m, metabotropic; KAR, kainate R; long., longitudinal; Puff, pressure jection; N.T., not tested.

(Pöschel et al., 2002), high molarities of kainate (Gloveli et al., 2005a, b) or potassium (LeBeau et al., 2002; Towers et al., 2002) (Table 1).

Another model of gamma frequency oscillations is known as "persistent gamma" (lasting for hours). This kind of oscillation can be induced in the hippocampal CA3 area in vitro by bath application of agonists of muscarinic acetylcholine (mAChR) (Fisahn et al., 1998; Fellous and Sejnowski, 2000; Shimono et al., 2000; Fisahn et al., 2002) and kainite receptors (KAR) (Fisahn et al., 2004; Gloveli et al., 2005a, b) (Table 1). mAChR agonist (carbachol)-induced and kainate-induced fast network oscillations provide a useful model to explore the mechanisms underlying physiological gamma frequency oscillations for the following reasons. The hippocampus receives a dense cholinergic projection from the medial septum/diagonal band of Broca, which plays an important role in the generation of hippocampal network activity (Leung, 1985). In addition, kainate receptors are expressed by both principal cells and interneurons of the hippocampus (Cossart et al., 1998; Frerking et al., 1998; for review see Lerma, 2003). Moreover, these oscillations in vitro share many of the features of intrahippocampal gamma oscillations in vivo, including the

firing of pyramidal neurons at low frequencies (<5 Hz) phase-locked to the oscillation, and the generation of oscillations in CA3 then propagating to CA1 (Fisahn et al., 1998; Gloveli et al., 2005a). Finally, both in vivo and in vitro cholinergically induced oscillations have similar current source density profiles, and the gamma phase relationship between pyramidal cells and perisomatic innervating interneurons is comparable (Csicsvari et al., 2003; Mann et al., 2005; Oren et al., 2006).

Both persistent and transient gamma oscillations can be evoked in different hippocampal areas, including CA3, CA1, and DG (Table 1, Towers et al., 2002; Pöschel et al., 2002; Gloveli et al., 2005a). However, there are regional differences in frequency and power of the oscillations, suggesting the existence of different rhythm-generating networks in the hippocampus. In line with this suggestion, both persistent and transient forms of kainate-induced gamma oscillations demonstrate faster gamma frequency oscillations in isolated CA1 area than those in CA3 area (N. Maziashvili and T. Gloveli, unpublished observation, Middleton et al., 2008). However, gamma oscillations in the same area (CA3 area) induced by different pharmacological drugs (carbachol and DHPG) also show significant differences in their properties (the peak frequencies, maximal power, and spectral width, Table 1, Pálhalmi et al., 2004), suggesting involvement of different network mechanisms, such as the recruitment of distinct types of interneurons. In addition, the gamma oscillations evoked under different conditions differ in their dependence on excitation and inhibition (Table 1). Thus, one form of transient oscillations, "Interneuronal network gamma" (ING) (Whittington et al., 1995), are based on mutual inhibition between the interneurons (for computational models see Wang and Buzsáki, 1996; White et al., 1998; Vida et al., 2006) whereas "pyramidal-interneuronal network gamma" (PING) (Whittington et al., 1997) is based on reciprocal interneuron–pyramidal cell interaction (see "Gamma and Theta Rhythms in Biophysical Models of Hippocampal Circuits" by Kopell et al., this book). It seems likely that all of these forms are relevant in vivo, possibly reflecting region and state dependence of mechanisms underlying hippocampal gamma oscillations.

Firing Patterns in Gamma Oscillations

A key requirement for the generation of network oscillations is rhythmic and synchronized activity of large sets of neurons. An important step in understanding the role of hippocampal neurons in network oscillations is to examine their spike patterns during these oscillations.

Principal cells. Analysis of firing properties of electrophysiologically and morphologically identified pyramidal cells in CA3 area has recently been performed in vitro for KAR (Gloveli et al., 2005a, b) and mAChR (Fisahn et al., 1998; Hájos et al., 2004) agonist-induced gamma frequency oscillations. Both KAR and mAChR activation (by kainate and carbachol, respectively) revealed low-frequency, <5 Hz, firing of pyramidal cells (Table 2, Fisahn et al., 1998; Hájos et al., 2004; Gloveli et al., 2005a). These results are in agreement with in vivo observations demonstrating similar low-frequency firing of PCs (Csicsvari et al., 2003). Moreover,

PC firing is phase-locked to the field oscillations (Table 2). In carbachol-induced gamma oscillations, PCs fired action potentials around the negative peak of the field recorded in the pyramidal cell layer (Fig. 3a, d, Hájos et al., 2004). Both in vivo and in vitro observations suggest that during gamma frequency oscillations, PCs of CA3 area drive local interneurons in a feedback manner (Fisahn et al., 1998; Csicsvari et al., 2003; Pálhalmi et al., 2004; Hájos et al., 2004). If PC–interneuron interactions generate gamma oscillations, the firing of PCs should precede interneuron discharge so that PC can recruit interneuron activity in the next gamma cycle (Oren et al., 2006). Consistent with this suggestion, interneuron responses were indeed preceded by PC firing (Fig. 3d, Hájos et al., 2004).

Table 2 Firing properties of some hippocampal neurons during gamma frequency oscillations in vitro

Neuron type	Activated by	Mean firing frequency (Hz)	Spikes/gamma cycle	Angle of spikes relative to the field	Main references
Pyramidal	KAR	3.5 ± 0.6	0.18 ± 0.05	N.T.	Gloveli et al. (2005a)
	mAChR	2.82 ± 0.7	0.09 ± 0.02	58.1 ± 5.3^0	Hájos et al. (2004)
					Fisahn et al. (1998)
O-LM	KAR	8.3 ± 2.1	0.26 ± 0.04	N.T.	Gloveli et al. (2005a)
	mAChR	12.9 ± 1.8	0.4 ± 0.07	88.1 ± 6.1^0	Hájos et al. (2004)
Trilaminar	KAR	32.1 ± 2.8	1.82 ± 0.07	N.T.	Gloveli et al. (2005a)
	mAChR	18.2 ± 2.7	0.6 ± 0.09	96.8 ± 2.2^0	Hájos et al. (2004)
Bistratified	KAR	35.0 ± 2.5	1.04 ± 0.08	N.T.	Gloveli et al. (2005a)
Basket	KAR	33.6 ± 2.6	1.28 ± 0.06	N.T.	Gloveli et al. (2005a)
	mAChR	18.1 ± 2.7	0.62 ± 0.09	93 ± 2.1^0	Hájos et al. (2004)
R-LM	mAChR	13.2 ± 3.9	N.T.		Hájos et al. (2004)
Radiatum	mAChR	2.3 ± 0.6	0.07 ± 0.02	128.4 ± 12.4^0	Hájos et al. (2004)

Abbreviations: O-LM, oriens lacunosum-moleculare; R-LM, radiatum lacunosum-moleculare; N.T., not tested.

During in vitro gamma frequency oscillations induced by kainate, the interneurons receive a high-frequency barrage of compound EPSPs, modulated at gamma frequency, which are temporally correlated with extracellular population activity (Gloveli et al., 2005a). Since the slice is deafferented, it is likely that the action potential-dependent excitatory events are mediated by local excitatory input from neighboring pyramidal neurons. Given the relatively low PC somatic spike rate with

respect to the frequency of EPSPs invading interneurons, the question remains as to how PCs generate these rhythmic burst of events and reliably discharge interneurons. Interneurons may receive a rhythmic barrage of gamma frequency EPSPs for the following reasons. First, in the active network, multiple pyramidal cells are likely to fire on any given oscillatory cycle. Due to the convergence of numerous pyramidal cell axons onto a single postsynaptic interneuron it follows that each interneuron is also likely to receive multiple unitary excitatory inputs on each successive gamma wave. Second, there are suggestions that activity in pyramidal cell axons may orthodromically excite interneurons, without pyramidal cell somata necessarily firing (Traub et al., 2003). Computational models of carbachol (Traub et al., 2000) and kainate-induced gamma oscillations (Fisahn et al., 2004) emphasize the importance of ectopic axonal action potentials for the generation of hippocampal gamma oscillations. The coexistence of phasic, high-frequency oscillations in principal cell axon populations and field potential gamma frequency oscillations was demonstrated in kainate model (Traub et al., 2003).

Interneuron types. During gamma frequency oscillation in vivo and in vitro, the different classes of interneurons fire action potentials at different times and inhibit distinct subcellular domains of PCs (Fig. 2–4). During pharmacologically induced gamma frequency oscillations in vitro, perisomatic-targeting *PV-expressing basket* cells generate a predominantly gamma frequency output (Fig. 3B, Gloveli et al., 2005a; Hájos et al., 2004). Moreover, the firing of perisomatic basket cells is tightly coupled to the oscillation (Fig. 3B, D). The anatomical and physiological properties make these neurons ideally suited for generating local gamma rhythms. In contrast, spiking of other PV-expressing perisomatic-targeting interneurons, *axo-axonic* cells, was found to be only moderately coupled to the field gamma in anesthetized animals (Tukker et al., 2007).

There are no in vitro data available on the activity of *CCK-expressing basket* cells. In vivo results indicate that, in contrast to PV-expressing BCs, these interneurons fire earlier than pyramidal cells and out of phase with PV-expressing interneurons during the gamma oscillations in anesthetized animals (Tukker et al., 2007). Therefore, CCK-expressing basket cells are likely to interfere with gamma synchronicity (Freund and Katona, 2007; Galarreta et al., 2008).

While PV-expressing perisomatic inhibitory interneurons are thought to play a major role in gamma oscillations (Hájos et al., 2004; Gloveli et al., 2005a), other classes of fast-spiking interneurons, such as bistratified and trilaminar cells, may also be important for this rhythm (Gloveli et al., 2005a). *Bistratified* cells were so named because the axonal arbor is found in two strata: oriens and radiatum (Buhl et al., 1994). In addition to pyramidal cells they also innervate interneurons including basket cells (Halasy et al., 1996). During the gamma oscillations in vitro bistratified cells discharge at high frequency, phase-locked to the field gamma (Gloveli et al., 2005a; Hájos et al., 2004; Tukker et al., 2007). Therefore, they are also likely to be involved in the generation of the gamma oscillatory activity. Interestingly, the most prominent interneuronal output seen during pharmacologically induced gamma oscillations in vitro was associated with *trilaminar* interneurons (Gloveli et al., 2005a; Hájos et al., 2004). These fast-spiking cells project to three layers

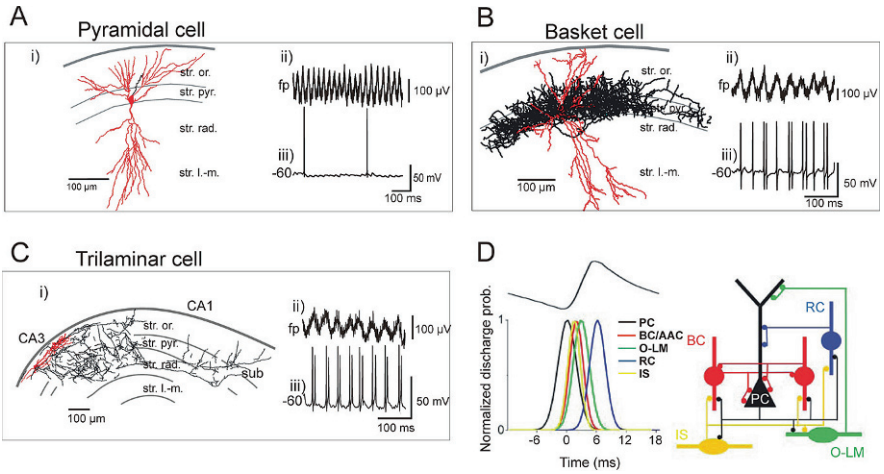

Fig. 3 Morphological and firing properties of hippocampal neurons during pharmacologically induced gamma oscillations. Reconstructions of representative biocytin-filled pyramidal (**A***i*), PV-positive basket (**B***i*), and trilaminar (**C***i*) cells. The soma and dendrites are drawn in *red*, whereas the axons are in *black*. CA3, CA3 area; str. or., stratum oriens; str. pyr., stratum pyramidale; str. rad., stratum radiatum; str. l.-m., stratum lacunosum-moleculare. During kainate-induced field oscillatory activity (**A***ii*; **B***ii*) pyramidal cells fire sporadically (**A***iii*), whereas basket cells discharged with single spikes interrupted by irregularly occurring doublets of action potentials, phase-locked to the field gamma activity (**B***iii*). Trilaminar cells produced spike doublets (**C***iii*) on every gamma cycle (**C***ii*). (**D,** *left*) Time sequence of firing of different neuron types during carbachol-induced oscillatory cycle (*top trace*). Pyramidal cells fired at the negative peak of the oscillation followed by the interneurons. Gaussian functions were fitted to the spike time distribution for each type of neuron, and the average mean and SD were used to represent each cell class as a Gaussian function. (**D,** *right*) Schematic diagram of the connectivity among phase-coupled neuron types in the CA3 hippocampal circuitry taking part in the gamma oscillation. Panel **A***ii*–**C,** adapted from Gloveli et al. (2005a); **D,** adapted from Hájos et al. (2004)

of CA3 area, the strata oriens, pyramidale, and radiatum. Additionally, axon collaterals of trilaminar cells were seen projecting to area CA1 and into the subiculum, and possibly to other brain areas as well (Somogyi and Klausberger, 2005). These cells generated highly regular, short latency spike doublets (Fig. 3C, Gloveli et al., 2005a). Their axonal arborization indicates that these interneurons innervate somatic and dendritic compartments of pyramidal cells, locally as well as in distant regions. Thus, via these cells, gamma rhythms generated locally in area CA3 could be efficiently transmitted to distal sites "downstream" in the hippocampal processing pathway.

Interneurons located in the stratum *radiatum* (with both the dendrites and axonal arborization localized in the stratum radiatum) have the lowest firing rate among all dendrite-targeting interneurons with weak coupling to the gamma oscillations in vitro (Table 2, Hájos et al., 2004). Although *R-LM* cells (with dendritic tree in stratum radiatum and axon restricted to stratum lacunosum-moleculare) fire at higher frequency than other radiatum cells, they also do not show significant phase-related firing (Hájos et al., 2004).

Theta Oscillations

A prominent network pattern in the hippocampus of all mammals studied to date, including humans (Arnolds et al., 1980; Tesche and Karhu, 2000), is a slow oscillation in the theta frequency band (5–10 Hz). Theta oscillations are most consistently present during various types of locomotor activities (Vanderwolf, 1969) and rapid eye movement (REM) sleep (Jouvet, 1969). In general, theta waves are absent in the immobile animal (Bland, 1986; for review see Buzsáki, 2002). To explain the generation of these oscillations, various external pacemakers have been proposed (for review see Buzsáki, 2002). One classical hypothesis is that cholinergic excitation from the septum and the diagonal band of Broca activates inhibitory interneurons, which in turn induce rhythmic IPSPs on the soma of pyramidal cells (Petsche et al., 1962). Alternatively, the entorhinal cortex may entrain hippocampal areas at theta frequency. In rodents, hippocampal theta activity has maximal power in the CA1 region and the synaptic currents underlying these oscillations are mainly generated by the entorhinal input (for review see Buzsáki, 2002). However, recent in vitro experimental data and computational analysis indicate that theta activity can be generated intrinsically in the CA1 (Gillies et al., 2002; Rotstein et al., 2005) and CA3 (Gloveli et al., 2005b) areas of the hippocampus. In fact, Cobb et al. (1995) demonstrated that individual GABAergic interneurons can effectively phase subthreshold membrane potential oscillations and spontaneous firing in pyramidal cells at theta frequencies. Alternating inhibition and post-inhibitory "rebound" activation underlies the entrainment of pyramidal cells (Cobb et al., 1995). Intrinsic GABAergic mechanisms are thus sufficient to generate theta activity in cortical networks.

Various in vitro models of the theta oscillatory activity have been developed based on either mAChR (Konopacki et al., 1992; Fisahn et al., 1998), metabotropic glutamatergic-receptor (mGluR) (Gillies et al., 2002) or kainate receptor activation (Gloveli et al., 2005a, b). Coactivation of mGluRs and metabotropic cholinergic receptors has also been reported to generate robust theta frequency oscillations in the hippocampus in vitro (Cobb et al., 2000).

Metabotropic GluR activation generates prominent, inhibition-based, atropine-resistant theta population oscillations under conditions of reduced AMPA receptor activation in the hippocampal CA1 area (Gillies et al., 2002). This field oscillation was independent of muscarinic cholinergic receptor drive, but strongly dependent on NMDA receptor and $GABA_A$ receptor activity (Table 1, Gillies et al., 2002). The mechanism of generation of theta frequency population activity in this model appeared to involve intrinsic theta frequency membrane potential oscillations in a subset of stratum oriens interneurons. The blockade of AMPA receptors was a critical requirement of the experimental conditions needed to see this population theta activity. Many of the properties of theta frequency oscillations in this reduced model match those seen in area CA1 in vivo (Gillies et al., 2002). In particular, the resulting population theta rhythm resembled atropine-resistant theta oscillations recorded in vivo (Buzsáki et al., 1986) and may be generated by a subset of stratum oriens interneurons displaying intrinsic membrane potential oscillations at theta frequency

(Gillies et al., 2002). In addition, the coherent theta oscillations may come from the interaction of other GABAergic interneurons with the O-LM cells (see "Gamma and Theta Rhythms in Biophysical Models of Hippocampal Circuits" by Kopell et al., this book).

In the CA3 area, theta oscillations can be induced by application of kainate. A necessary prerequisite to ensure precisely synchronized theta activity was specific orientation of the slices: theta frequency population activity was detected predominantly in longitudinal hippocampal slice preparation (Gloveli et al., 2005b). These data demonstrate that theta activity can be generated intrinsically both in the CA1 and in the CA3 areas of the hippocampus. While there are several differences between these models a common feature is their dependence on GABAergic inhibition (Table 1).

Firing Patterns in Theta Oscillations

Principal cells. In a model of atropine-resistant theta oscillations following mGluR activation, with AMPA receptor activation blocked, pyramidal cell somatic firing was seen in only few cells recorded, but could be elicited with injection of tonic depolarizing current (0.1–0.2 nA). In these conditions, pyramidal cells fired one spike per field theta (~7 Hz) cycle during the trough of the field oscillation (Gillies et al., 2002). Consistent with this finding, pyramidal neurons in the CA1 region showed subthreshold resonance and firing preference at theta frequencies (range 2–7 Hz) (Pike et al., 2000).

Interneuron types. Ample evidence supports the critical involvement of hippocampal interneurons in theta oscillations. The best documented is the involvement of stratum oriens distal dendrite-targeting *O-LM* interneurons (Fig. 2, Fig. 4A) in generation of theta rhythm. This cell type was found to participate in hippocampal theta activity both in vivo (Buzsáki, 2002; Klausberger et al., 2003) and in vitro (Pike et al., 2000; Gillies et al., 2002; Hájos et al., 2004; Gloveli et al., 2005a, b). In particular, involvement of O-LM cells was investigated in vitro in kainate and mAChR-mediated network oscillatory activity. In kainate-induced oscillations O-LM cells fired at the theta frequency range during both theta and gamma population activity (Fig. 4B, Gloveli et al., 2005b). O-LM cells show prominent membrane potential oscillations in the theta frequency range (Maccaferri and McBain, 1996). In contrast, hippocampal fast-spiking cells preferentially resonate in the gamma range (Pike et al., 2000). Furthermore, O-LM cells have longer membrane time constants than the gamma-preferring interneurons and a considerably longer afterhyperpolarization (AHP). Changes in AHP profiles in interneurons have been shown to have dramatic effects on firing patterns (e.g., see Savić et al., 2001). Thus O-LM cells and gamma-preferring interneurons discharge at different frequencies and participate preferentially in theta or gamma activity, respectively (Gloveli et al., 2005a). The theta frequency discharge of O-LM interneurons (Fig. 4B, C, Gloveli et al., 2005b) will provide a robust theta frequency rhythmic inhibitory output to the apical dendrites of PCs.

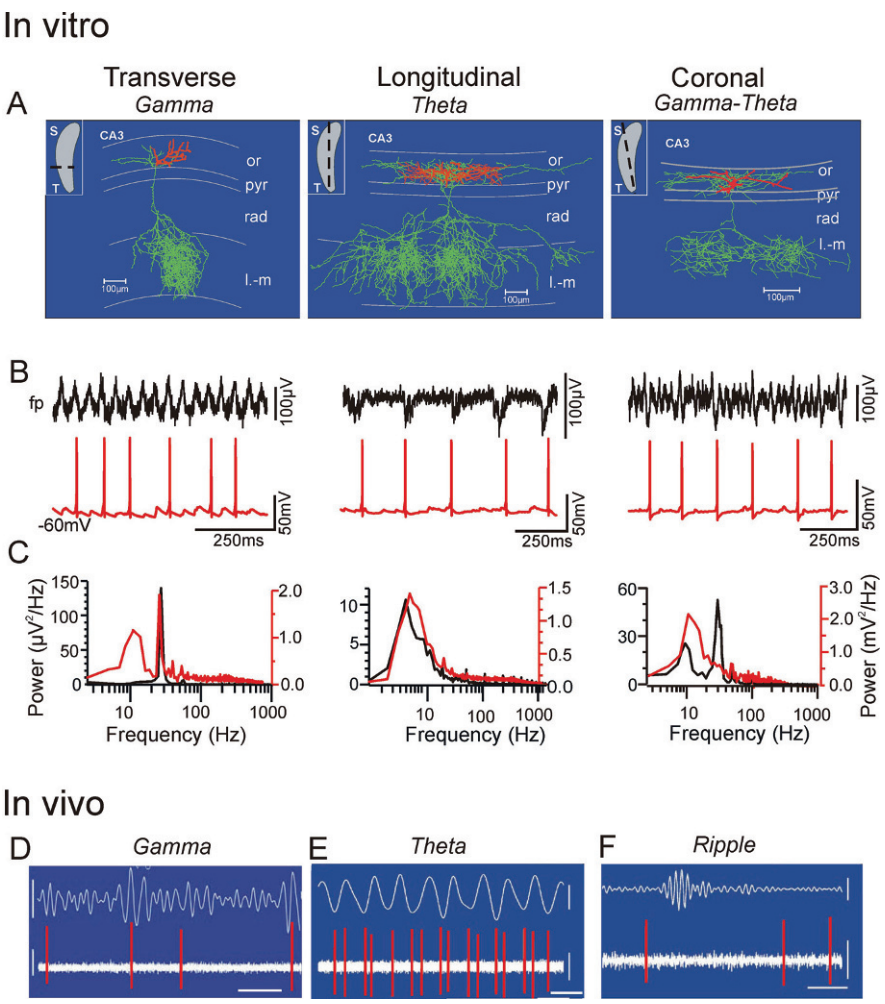

Fig. 4 Morphological and firing properties of O-LM interneurons. **A** Neurolucida reconstruction of biocytin-filled O-LM cell in area CA3 from transverse, longitudinal, and coronal slices. The soma and dendrites are drawn in *red*, whereas the axon is in *green*. Note different axonal ramification pattern in stratum lacunosum-moleculare in different slice preparations. Hippocampal layers are depicted schematically. CA3, CA3 area; str. or., stratum oriens; str. pyr., stratum pyramidale; str. rad., stratum radiatum; str. l.-m., stratum lacunosum-moleculare. **B** Typical example of extracellular field potential (fp) and concomitant current clamp (−60 mV) recordings in an O-LM cell after induction of oscillatory activity with kainate in different slices. **C** Corresponding power spectra (60-s epoch) from field (*black*) and current clamp (*red*) recordings. **D–F** O–LM firing in vivo is specifically associated with different types of brain state and network activity. Filtered extracellular network oscillations (*top*) and extracellularly recorded action potentials (*bottom*). Note that the O-LM cell firing is not phase-coupled to gamma cycle, but fired rhythmically on the trough of theta oscillations and was silent during sharp-wave-associated ripples. Calibrations: **D** 0.1 mV (*upper trace*); 0.2 mV (*lower trace*) and 0.1 s; **E**, **F**, 0.3 mV (*lower traces*), 0.2 mV (*upper theta trace*), 0.05 mV (*upper sharp-wave-ripple trace*) and 300 ms (theta), 50 ms (sharp-wave-ripple). Adapted: Panels **A–C** from Gloveli et al. (2005b), Dugladze et al. (2007), Tort et al. (2007); Panel **D** from Tukker et al. (2007); Panels **E** and **F** from Klausberger et al. (2003)

In addition to distal dendrite inhibiting O-LM cells, the dendrite domains of principal cells are innervated by other types of interneurons, whose involvement in the hippocampal oscillations has not been addressed in vitro. This includes, for example, recently described interneuron type in CA1 area in anesthetized animal, *Ivy* cells, expressing neuropeptide Y (NPY), and the neuronal nitric oxide (NO). The soma of these cells is located in stratum pyramidale and axonal collaterals innervate two strata: oriens and radiatum. Ivy cells discharged at low frequency during theta as well as gamma and ripple oscillations in anesthetized animals (Fuentealba et al., 2008). Another GABAergic interneuron type, *neurogliaform* cells that share some similarity with Ivy cells, such as dense axonal fields, low-frequency discharge, and slow synaptic transmission (Vida et al., 1998; Price et al., 2005; Szabadics et al., 2007), are located in stratum lacunosum-moleculare and innervate the apical dendrite tuft of CA1 pyramidal cells co-aligned with the entorhinal input (Price et al., 2005). This cell type provides both fast $GABA_A$ receptor-mediated and slow $GABA_B$ receptor-mediated (Price et al., 2005; Szabadics et al., 2007) inhibition and therefore represents a potential candidate to be involved in both theta and gamma frequency oscillations. However, there is very little information about the activity pattern of this interneuron type and their role in network oscillations.

Nested Theta and Gamma Oscillations

Theta and gamma oscillations often occur simultaneously and show interaction. Amplitude of gamma oscillations is modulated with the phase of the theta rhythm. In addition, the frequencies of the two oscillations are also correlated, providing additional evidence of their interrelated function (Bragin et al., 1995). The coordinated nature of the two rhythms, and the observation that gamma power is stronger during theta-associated behavior (Leung et al., 1982; Bragin et al., 1995), implies that the neuronal generators of the two rhythms interact (and may be also overlap). This nested activity pattern is hypothesized to play a critical role in memory encoding and retrieval (Lisman and Idiart, 1995; Lisman, 2005).

Recently, combined anatomical and physiological studies have provided evidence that in vitro gamma and theta rhythms are supported by neuronal circuits arranged orthogonally along the transverse and longitudinal axes, respectively (Table 1, Gloveli et al., 2005b). In hippocampal coronal slice preparation with intermediate orientations (between the transverse and longitudinal axis), both theta and gamma population rhythms were manifest (Fig. 4B, C, Gloveli et al., 2005b). The reason for that is a differential preservation of rhythm-generating microcircuits in transverse, longitudinal, and coronal slice preparation. Analysis of the three-dimensional axonal arborization patterns of different hippocampal CA3 interneurons recorded in transverse slices show that PV-expressing perisomatic-targeting interneurons, along with trilaminar and bistratified cells, show a clear tendency to arborize widely within the transverse plane (Gloveli et al., 2005a, b). In contrast,

distal dendrite-targeting O-LM cells arborized most extensively in the longitudinal plane forming two or three clusters in this direction (see Fig. 4A, Gloveli et al., 2005b). In longitudinal slices, the preservation of these projections facilitated the generation of theta rhythms (Fig. 4B, C) with robust coherence over large distances (Gloveli et al., 2005b; Tort et al., 2007). Thus, orthogonal arrangement of rhythm-generating microcircuits alongside the longitudinal and transverse axis, and distinct firing patterns of certain classes of interneurons during the theta and gamma frequency oscillations (Gloveli et al., 2005b; Tort et al., 2007), enables the hippocampus to produce different (solely or combined) population activity (for related simulation see "Gamma and Theta Rhythms in Biophysical Models of Hippocampal Circuits" by Kopell et al., this book).

Sharp-Waves Ripple Activity

The high-frequency oscillations termed ripples (100–300 Hz) are typically associated with sharp-wave activity (Buzsaki et al., 1992; Wilson and McNaughton, 1994; O'Neill et al., 2006). The hippocampal sharp-wave-ripple (SPW-R) complex is thought to play an important role in synaptic plasticity and the transfer of new memory trace from the hippocampus to the neocortex (Buzsáki, 1989).

The mechanisms of these fast oscillatory patterns in the hippocampus and neocortex are not fully understood (Buzsaki et al., 1992; Ylinen et al., 1995; Draguhn et al., 1998). Both in vivo and in vitro studies suggest that SWP-Rs arise in the recurrent collateral system of the CA3 area (similar to gamma oscillations), propagate toward CA1, and leave the hippocampal formation via the subiculum and the EC (Chrobak and Buzsaki, 1996; Csicsvari et al., 2000; Maier et al., 2003; Both et al., 2008). During this state, the hippocampus seems to be less controlled by input from the EC; rather, it generates output signals itself (Chrobak and Buzsaki, 1996).

SPW-R complex can be induced in vitro by electrical stimulation, pharmacologically, or can occur spontaneously with properties similar to the events seen in vivo (Maier et al., 2003; Nimmrich et al., 2005; Behrens et al., 2005). Several local network mechanisms underlying these patterns have been identified within CA1, including strong inhibition of non-participating pyramidal cells during SPW-R (Ylinen et al., 1995; Maier et al., 2003) and electrical coupling of CA1 pyramidal cells (Draguhn et al., 1998; Schmitz et al., 2001; Nimmrich et al., 2005). Concomitant extracellular and intracellular recordings of SPW-R complexes show that pyramidal cells display EPSP-IPSP sequences, IPSP-EPSP sequences, and prominent IPSPs, but never isolated EPSPs (Behrens et al., 2005). These results suggest that inhibitory inputs are strong during the development of ripple complexes. Consistent with this finding, fast-spiking basket and bistratified interneurons strongly increase their firing rate during ripple oscillations in vivo (Ylinen et al., 1995; Klausberger et al., 2004). Another fast-spiking cell type, axo-axonic interneurons fire before the ripple episode but are silenced during and after it (Klausberger

et al., 2003). In contrast, non-fast-spiking O-LM cell firing is suppressed during ripples (Klausberger et al., 2003). Gap junctions also seem to be important for ripples, since the blockade of gap junctions with carbenoxolone attenuated ripple occurrence (Behrens et al., 2005; LeBeau et al., 2003). Interestingly, SPW-R can be induced with stimulation protocols known to induce LTP, a model of learning and memory, suggesting that this pattern is associated with changes in functional connectivity (Behrens et al., 2005).

Cellular and Synaptic Mechanisms Involved in Oscillations

Intrinsic properties. The voltage-gated ion channels strongly contribute to *pyramidal cell* excitability. These channels influence intrinsic properties of the neuron, such as the action potential threshold, spike AHP and afterdepolarization (ADP), and action potential firing mode. Na^+ and A-type K^+ channels are expressed in both CA1 and CA3 PCs whereas hyperpolarization-activated cation channels (HCN channels) are expressed in CA1 PCs, but are almost absent from CA3 PCs (for review see Spruston, 2008). The HCN channels in PCs have important influences also on synaptic integration. Deactivation of these channels reduces EPSP duration and results in a slight hyperpolarization following EPSPs (Magee, 1999). Conversely, activation of HCN channels reduces IPSP duration and produces a slight depolarization following the IPSP (Williams and Stuart, 2003, for review see Spruston, 2008). This interaction of HCN channels and synaptic conductances may represent elementary mechanisms for rhythmogenesis at the cellular and subcellular levels.

Another feature relevant for the firing pattern of pyramidal cells in the hippocampus is their ability to generate subthreshold membrane potential oscillations (MPOs) in the theta frequency range and their resonance properties (Leung and Yu, 1998; Pike et al., 2000). These properties of hippocampal pyramidal cells are likely to contribute to theta activity (Leung and Yu, 1998). In hippocampal pyramidal cells the electrical resonance at theta frequencies is generated by M-current, h-current, and persistent Na^+ current (Hu et al., 2002).

How the different firing patterns of certain *GABAergic interneurons* are generated remains largely unknown. Intrinsic membrane properties of these cells may be important for hippocampal network oscillations. For instance, O-LM cells have a longer membrane time constant and a considerably longer (5-fold to 10-fold slower) AHP than the gamma-preferring interneurons (Gloveli et al., 2005a), restricting their firing to low, theta frequencies (see Savić et al., 2001). In addition, O-LM cells show prominent slow subthreshold membrane potential oscillations and the resonance properties in the theta frequency range (Maccaferri and McBain, 1996; Pike et al., 2000).

Hyperpolarization-activated cationic currents (I_h) and I_A currents which have been detected in hippocampal interneurons may influence not only the intrinsic and firing properties but also their synchronization. I_h currents are activated at voltages close to rest (Gu et al., 2005). Different subunit composition (HCN1–4) that is

co-expressed in hippocampal GABAergic interneurons (Notomi and Shigemoto, 2004) influences not only the kinetics but also the voltage dependency of I_h activation (see Chen et al., 2002). Besides O-LM and other types of non-fast-spiking interneurons, I_h channels are expressed in the somato-dendritic region, axon, and presynaptic elements of fast-spiking basket cell in the hippocampus (Aponte et al., 2006). In contrast, hippocampal lacunosum-moleculare and radiatum interneurons display subthreshold MPOs generated by an interplay of Na^+ and 4-AP-sensitive A-type K^+ currents, independent of I_h currents and muscarine-sensitive K^+ currents, I_M (Bourdeau et al., 2007).

Synaptic properties. The properties of excitatory events discriminate hippocampal principal cells from inhibitory neurons (Miles, 1990; Jonas et al., 1993; Geiger et al., 1997; Toth et al., 2000). It appears that excitatory synapses onto interneurons not only tend to have a larger number of AMPA receptors (Nusser et al., 1998), thereby increasing the quantal amplitude, but the postsynaptic receptors also appear to have a different molecular composition (Geiger et al., 1995), which, in turn, endows them with faster kinetics (Geiger et al., 1997). Further discrimination in the properties of excitatory input was found between different interneuron types. Different classes of hippocampal interneurons with distinct axonal ramification patterns and efferent target profiles show clear differences in both amplitude and kinetics of EPSCs/Ps during gamma frequency network oscillations (Gloveli et al., 2005a). For instance, the amplitudes of excitatory drive are considerably larger in fast-spiking BCs and trilaminar cells than in O-LM cells (Fig. 2B), suggesting that the intensity of synaptic drive may play a role in generating their different outputs (Gloveli et al., 2005a).

Similar to the kinetics of excitatory postsynaptic currents at PC–BC, unitary inhibitory postsynaptic currents at BC–BC synapses demonstrated very fast kinetics (Bartos et al., 2001, 2002). In addition to IPSCs with fast kinetic properties ($GABA_{A,fast}$) mediated by perisomatic synapses, IPSCs with slowly rising and decaying kinetic ($GABA_{A,slow}$) mediated by dendritic synapses were also detected in CA1 area (Banks et al., 2000). Interplay of CA1 interneurons, mediating $GABA_{A,slow}$ and $GABA_{A,fast}$, may contribute to theta and gamma rhythms occurring separately or as a nested gamma/theta rhythm (Banks et al., 2000).

Thus, different intrinsic membrane properties together with different kinetics of excitatory and inhibitory inputs govern the specific roles of hippocampal cells in shaping distinct network oscillatory activity.

Neuromodulatory Control of In Vitro Oscillations

Sources of neuromodulators in the brain are the four aminergic systems: the dopaminergic, histaminergic, serotonergic, and noradrenergic systems. All four of the associated modulators (dopamine, histamine, serotonin, and noradrenalin) are released from small groups of neurons, which have projection patterns to most of the brain, including the hippocampus. Effects of these neuromodulators have been tested in vitro on theta and gamma oscillatory activity.

The hippocampus receives dopaminergic input from the ventral tegmental area. Activation of D1-like *dopamine* receptors strongly depresses cholinergic gamma oscillations in area CA3 of rat hippocampus, and this effect is most likely mediated via impairment of interneurons involved in generation and maintenance of the carbachol-induced network rhythm (Weiss et al., 2003).

Histamine 3 (H3) receptors seem likely to play an important role in regulation of hippocampal theta oscillation. Systemic administration of the H3 receptor antagonists (ciproxifan and thioperamide) enhances the power of spontaneous theta in anesthetized rats. Since H3 receptors are located at axon terminals of histamine-containing neurons and function as autoreceptors (Arrang et al., 1983), their blockade could enhance histamine release and subsequently promote hippocampal theta oscillation. Regulation of hippocampal theta oscillations by H3 receptors may represent one of the probable mechanisms involved in histamine-induced modulation of higher brain functions, such as attention and learning (Hajós et al., 2008).

Serotonergic neurons of the midbrain raphe have been implicated in the control of affective and cognitive functions and in modulating the neural activities of networks across the sleep–wake cycle. The midbrain raphe nuclei form a strong serotonergic projection to the hippocampus. Recent in vivo findings suggest that a subpopulation of raphe neurons discharged action potentials that were phase-locked to the hippocampal theta rhythm (Kocsis et al., 2006). Hippocampal PCs and interneurons show different expression of metabotropic 5-HT receptor subtypes, such as 5-HT_{1A}, 5-HT_{1B}, 5-HT_2 (Ropert and Guy, 1991; Schmitz et al., 1995; Shen and Andrade, 1998), which may result in a differential modulation of intrinsic and synaptic properties of these cells in response to serotonin (for review see Schmitz et al., 1998). Serotonin input may influence the hippocampal network also via ionotropic 5-HT_3 receptors, which are expressed by several classes of GABAergic interneurons (Tecott et al., 1993; Ropert and Guy, 1991; Morales et al., 1998). These cells include CCK-containing basket cells, an interneuron type that has been proposed to hamper the gamma rhythm (see Section "Firing Patterns in Gamma Oscillations", Freund and Katona, 2007; Galarreta et al., 2008), as well as calbindin-containing and calretinin-containing GABAergic cells (Morales and Bloom, 1997). In contrast, serotonergic fibers do not contact the PV-containing GABAergic basket cells, which are responsible for some gamma frequency oscillations (see Section "Firing Patterns in Gamma Oscillations"). Therefore, the rhythmic serotonergic input may modulate, but not drive, hippocampal network oscillations at gamma frequency range.

The brain *noradrenergic* (NE) neurons, located in the pontine nucleus of locus coeruleus (LC), are presumed to play a role in regulation of the circadian sleep–wake cycle and alertness (Aston-Jones and Cohen, 2005). Several experimental findings suggest involvement of these neuromodulators on the hippocampal network activity. Local injection of glutamate in the LC results in multiple actions on the hippocampus, which include an increase in theta rhythm (Brown et al., 2005). Activation of LC–NE neurons by local application of a cholinergic agonist (bethanechol) induces theta oscillation of MS/DB neurons and theta-wave oscillation of hippocampal EEG in anesthetized rats (Berridge and Foote, 1991). Furthermore, the selective NE

reuptake inhibitor reboxetine modulates hippocampal theta activity in a state-dependent manner, i.e., can either increase or decrease theta amplitude depending on the behavioral state of the animal (Kocsis et al., 2007).

Pharmacological agents which are used with in vitro models of oscillation, such as KAR, mGluR, and mAChR agonist, also have a direct modulatory effect on hippocampal neurons in a manner that is remarkably cell specific. Various types of interneurons express *KARs* (Cossart et al., 1998, 2002; Frerking et al., 1998; Mulle et al., 2000; Lerma, 2003). Kinetics of KA-mediated EPSCs is slower than that of AMPAR (Frerking et al., 1998; Cossart et al., 2002), which could enable these two receptor types to generate oscillations with different dominating frequencies (Frerking and Ohliger-Frerking, 2002). Consistent with this, O-LM interneurons, which receive a large input mediated by KARs (Cossart et al., 2002), show post-synaptic KAR-mediated action potential firing at 10 Hz during theta stimulations, in contrast to perisomatic, bistratified, or septum/back-projecting cells (Goldin et al., 2007). Activation of *mGluRs* in the hippocampus has a range of effects (Anwyl, 1999) which include decreases in I_{M} and I_{AHP} currents. Therefore, activation of these receptors increases the excitability of hippocampal cells. mGluR subtypes are differentially expressed in specific hippocampal interneurons resulting in their different responsiveness to agonists. Thus, O-LM cells express a large number of group I mGluRs and are very sensitive to agonists, in marked contrast to other stratum oriens interneurons, including basket cells that express only a small number of this receptor subtype and are less sensitive (van Hooft et al., 2000). Also *mAChR* agonists may act on different GABAergic inhibitory interneurons that possess the muscarinic receptors (Pitler and Alger, 1992). Activation of these receptors may increase the excitability of interneuronal activity. In particular, muscarinic receptor agonist-carbachol blocks several potassium conductances, including I_{AHP} and I_{M} in a concentration-dependent manner (Madison et al., 1987). This depolarizes the pyramidal cells, unmasking subthreshold membrane potential oscillations in the theta frequency range (Leung and Yim, 1986; Fellous and Sejnowski, 2000). In addition, muscarinic receptor activation consistently enhanced firing frequency and produced large, sustained ADPs of O-LM but not other stratum oriens interneurons (Lawrence et al., 2006).

In summary, the effects of state-dependent activation of different neuromodulators can be markedly different on hippocampal network activity and depend on the expression and distribution of receptors across the cellular components of the network.

Oscillations in Disease

Schizophrenia

A number of studies have shown changes in gamma frequency EEG activity in schizophrenia. Reduced gamma activity was found in stimulus-dependent responses

in the auditory and visual cortices of schizophrenic patients (for review see Kehrer et al., 2008), and there is also evidence for a change in neuronal synchrony during high-frequency oscillations (Spencer et al., 2004). Interestingly, the amounts of RNA and immunoreactivity for PV are reduced in postmortem tissue from the frontal cortex and the hippocampus, pointing to a reduction in perisomatic inhibitory interneuron population (Zhang and Reynolds, 2002). The loss of these interneurons could directly explain the observed changes in gamma oscillations (Lewis et al., 2005; Vierling-Claassen et al., 2008). Although most clinical studies have found reductions in gamma band activity in schizophrenics (e.g., Slewa-Younan et al., 2001), there appears to be a symptom-specific pattern in the alterations in gamma activity indicating that increases in amplitude and power are associated with positive symptoms, particularly hallucinations and reality distortions, whereas negative symptoms, such as psychomotoric deficits, are linked to decreased gamma activity (Baldeweg et al., 1998; Bucci et al., 2007). Similar to clinical observations, in in vitro NMDA-hypofunction models of schizophrenia, both increased (Kehrer et al., 2007; Pinault, 2008) and decreased gamma activities (Cunningham et al., 2006) have been demonstrated (for review see Kehrer et al., 2008; Roopun et al., 2008).

Alterations of cortical interneurons in schizophrenia, especially parvalbumin and somatostatin-containing interneurons, are well documented. These alterations are likely to have significant effects on the network oscillatory activity and therefore on cognitive processes (Gonzalez-Burgos and Lewis, 2008; Morris et al., 2008). The axo-axonic subclass of GABAergic interneurons containing the calcium binding protein parvalbumin has attracted the most scrutiny in studies of schizophrenia (Behrens et al., 2007; Sakai et al., 2008; Wang et al., 2008). Although the altered network activities were recently reported in vivo and in vitro (see e.g., Cunningham et al., 2006; Behrens et al., 2007; Braun et al., 2007; Gonzalez-Burgos and Lewis, 2008; Spencer, 2008), further investigation needs to be undertaken to address possible model-specific and region-specific alterations in the gamma network oscillatory activity in different animal models of schizophrenia. Establishing the contingencies of increased versus decreased gamma band activity is of high importance since aberrant network oscillatory activity may underlie the cognitive decline observed in schizophrenic patients and offer vital clues to the relationship between positive and negative symptoms in schizophrenia at a network level (Cho et al., 2006; Bucci et al., 2007; Ford et al., 2007).

Mesial Temporal Lobe Epilepsy (mTLE)

Epileptic seizures are less frequent in conditions during which theta frequency occurs (e.g., wakefulness or REM sleep, Montplaisir et al., 1987) and thus the theta rhythm appears to indicate a hippocampal functional state in which generation of seizures is hindered (Colom et al., 2006).

In epileptic mice, the power of low-frequency theta oscillations has been reported to be reduced (Arabadzisz et al., 2005; Dugladze et al., 2007). Apart from

suppression of the theta oscillatory activity, as a potential anticonvulsant factor (Colom et al., 2006), a strong enhancement of the gamma activity (Dugladze et al., 2007) may underlie emergence of epileptiform activity. Observations in humans support this scenario: spatially localized increase in the power of gamma frequency oscillations has been observed preceding seizures in human TLE patients (Fisher et al., 1992). In addition, gamma oscillatory activity and increases in firing rate of the interneuronal network have been suggested as mechanisms of seizure occurrence in patients with drug-resistant TLE (Bragin et al., 2007). Consistent with this suggestion, intracellular recordings in kainate model of mTLE reveal an increased firing frequency of both pyramidal cells and dendrite-inhibiting interneurons in the ventral hippocampal CA3 area of epileptic mice (Dugladze et al., 2007). The involvement of the perisomatic targeting interneurons remains, however, to be investigated.

The epileptic tissue may also generate a specific rhythm, transient high-frequency oscillations (HFOs) in the 200–500 Hz frequency band known as fast ripple (Bragin et al., 1999). In fact, fast ripples may represent a specific marker for the area of the brain in which seizures begin (Bragin et al., 2002). The frequency of these oscillations is about twice as fast as the maximum rate at which most neurons in the hippocampus can fire action potentials. This fact raises the question of how these oscillations are generated. Analysis of the firing properties of hippocampal neurons during HFOs in vitro low-Mg^{2+} model of epileptiform activity showed that the pyramidal cells fired at the rising phase of the highest frequency portion of the field oscillation. In addition, distal dendrite-targeting interneurons (R-LM cells) fired at the start of the epileptiform bursts (on average 140 Hz) but stopped firing before its end (Spampanato and Mody, 2007). However, neither the principal cells nor the distal dendrite-targeting interneurons (R-LM and O-LM cell) fired action potentials at high frequencies (200–600 Hz) seen in the field oscillations (Spampanato and Mody, 2007). Another study (Foffani et al., 2007) suggested that these synchronous population oscillations could be generated as a consequence of the out-of-phase activities of two independent oscillators, each operating at half the frequency of the ensemble. In line with this suggestion, it was found that hippocampal pyramidal cells fired short bursts of action potentials at frequencies up to 300 Hz (Kandel and Spencer, 1961) and some interneurons could sustain frequencies of 400 Hz (Foffani et al., 2007).

Thus, numerous studies suggest that alterations in inhibition-based network oscillations may underlie the pathophysiology in schizophrenia and mTLE, which are associated with impaired information processes.

Perspectives

The spatiotemporal patterns of activity during network oscillations would ideally be explored in vivo (Bragin et al., 1995; Penttonen et al., 1998; Csicsvari et al., 2003; Buzsáki et al., 2003). However, it is reasonable to use relevant in vitro models to test hypotheses for the basic mechanisms involved. The replication of an endogenous

brain pattern in vitro allows for the investigation of a number of important cellular and synaptic mechanisms that are difficult or even impossible to explore in vivo. In addition, using transgenic, fluorescent EGFP-expressing mice under the control of different gene promoters (Oliva et al., 2000; Meyer et al., 2002) enables the identification and selection of different interneurons in the acute slice preparation. The firing properties of single cells in the active network and the contribution of excitation and inhibition to the generation of network oscillatory activity can be systematically examined in different models of in vitro oscillations (Table 1), which may reflect region and state dependence of mechanisms underlying network oscillations in vivo. Although there are some differences between the data obtained from in vitro and in vivo observations, these observations show substantial homology. The development of new transgenic methods for activating, inactivating, and labeling neurons and synapses (Marek and Davis, 2003; Polleux, 2005) will certainly facilitate progress in this area. Furthermore, several recently developed methods in vitro may help to overcome the limitations in vivo. These include the following: simultaneous patch-clamp recording from several cells in a brain slice (Miles and Poncer, 1996; Markram et al., 1997); recording of sufficiently large numbers of cells at once using optical methods; stimulation/suppression of different cellular compartments using uncaging of different substances or optically activated channels (Callaway, 2002; Boyden et al., 2005; Deisseroth et al., 2006; Zhang et al., 2007).

Further Reading

Anwyl R (1999) Metabotropic glutamate receptors: electrophysiological properties and role in plasticity. Brain Res Rev 29:83–120.

Aponte Y, Lien CC, Reisinger E, Jonas P (2006) Hyperpolarization-activated cation channels in fast-spiking interneurons of rat hippocampus. J Physiol 574:229–243.

Arabadzisz D, Antal K, Parpan F, Emri Z, Fritschy JM (2005) Epileptogenesis and chronic seizures in a mouse model of temporal lobe epilepsy are associated with distinct EEG patterns and selective neurochemical alterations in the contralateral hippocampus. Exp Neurol 194:76–90.

Arnolds DE, Lopes da Silva FH, Aitink JW, Kamp A, Boeijinga, P (1980) The spectral properties of hippocampal EEG related to behaviour in man. Electroencephalogr Clin Neurophysiol 50: 324–328.

Arrang JM, Garbarg M, Schwartz JC (1983) Auto-inhibition of brain histamine release mediated by a novel class (H3) of histamine receptor. Nature (Lond) 302:832–837.

Aston-Jones G, Cohen JD (2005) An integrative theory of locus coeruleus-norepinephrine function: adaptive gain and optimal performance. Annu Rev Neurosci 28:403–450.

Baldeweg T, Spence S, Hirsch SR, Gruzelier J (1998) Gamma-band electroencephalographic oscillations in a patient with somatic hallucinations. Lancet 352:620–621.

Banks MI, White JA, Pearce RA (2000) Interactions between distinct GABA(A) circuits in hippocampus. Neuron 25:449–457.

Bartos M, Vida I, Frotscher M, Geiger JR, Jonas P (2001) Rapid signaling at inhibitory synapses in a dentate gyrus interneuron network. J Neurosci 21:2687–2698.

Bartos M, Vida I, Frotscher M, Meyer A, Monyer H, Geiger JR, Jonas P (2002) Fast synaptic inhibition promotes synchronized gamma oscillations in hippocampal interneuron networks. Proc Natl Acad Sci USA 99:13222–13227.

Behrens CJ, van den Boom LP, de Hoz L, Friedman A, Heinemann U (2005) Induction of sharp wave-ripple complexes in vitro and reorganization of hippocampal networks. Nat Neurosci 8:1560–1567.

Behrens MM, Ali SS, Dao DN, Lucero J, Shekhtman G, Quick KL, Dugan LL (2007) Ketamine-induced loss of phenotype of fast-spiking interneurons is mediated by NADPH-oxidase. Science 318:1645–1647.

Berridge CW, Foote SL (1991) Effects of locus coeruleus activation on electroencephalographic activity in neocortex and hippocampus. J Neurosci 11:3135–3145.

Bland BH (1986) Physiology and pharmacology of hippocampal formation theta rhythms. Prog Neurobiol 26:1–54.

Both M, Bähner F, von Bohlen und Halbach O, Draguhn A (2008) Propagation of specific network patterns through the mouse hippocampus. Hippocampus 18:899–908.

Bourdeau ML, Morin F, Laurent CE, Azzi M, Lacaille JC (2007) Kv4.3-mediated A-type K+ currents underlie rhythmic activity in hippocampal interneurons. J Neurosci 27: 1942–1953.

Boyden ES, Zhang F, Bamberg E, Nagel G, Deisseroth K (2005) Millisecond-timescale, genetically targeted optical control of neural activity. Nat Neurosci 8:1263–1268.

Bragin A, Jandó G, Nádasdy Z, Hetke J, Wise K, Buzsáki G (1995) Gamma (40–100 Hz) oscillation in the hippocampus of the behaving rat. J Neurosci 15:47–60.

Bragin A, Engel J Jr, Wilson CL, Fried I, Buzsáki G (1999) High-frequency oscillations in human brain. Hippocampus 9:137–142.

Bragin A, Mody I, Wilson CL, Engel J Jr (2002) Local generation of fast ripples in epileptic brain. J Neurosci 22:2012–2021.

Bragin A, Claeys P, Vonck K, Van Roost D, Wilson C, Boon P, Engel J Jr (2007) Analysis of initial slow waves (ISWs) at the seizure onset in patients with drug resistant temporal lobe epilepsy. Epilepsia 48:1883–1894.

Braun I, Genius J, Grunze H, Bender A, Möller HJ, Rujescu D (2007) Alterations of hippocampal and prefrontal GABAergic interneurons in an animal model of psychosis induced by NMDA receptor antagonism. Schizophr Res 97:254–263.

Brown RA, Walling SG, Milway JS, Harley CW (2005) Locus coeruleus activation suppresses feedforward interneurons and reduces β-γ electroencephalogram frequencies while it enhances theta frequencies in rat dentate gyrus. J Neurosci 25:1985–1991.

Bucci P, Mucci A, Merlotti E, Volpe U, Galderisi S (2007) Induced gamma activity and event-related coherence in schizophrenia. Clin EEG Neurosci 38:96–104.

Buhl EH, Halasy K, Somogyi P (1994) Diverse sources of hippocampal unitary inhibitory postsynaptic potentials and the number of synaptic release sites. Nature 368:823–828.

Buhl EH, Tamás G, Fisahn A (1998) Cholinergic activation and tonic excitation induce persistent gamma oscillations in mouse somatosensory cortex in vitro. J Physiol 513:117–126

Buzsáki, G (1989) Two-stage model of memory trace formation: a role for "noisy" brain states. Neuroscience 31:3551–3570.

Buzsáki G (2002) Theta oscillations in the hippocampus. Neuron 33:325–340.

Buzsáki G, Buhl DL, Harris KD, Csicsvari J, Czéh B, Morozov A (2003) Hippocampal network patterns of activity in the mouse. Neuroscience 116:201–211.

Buzsáki G, Czopf J, Kondakor J, Kellenyi L (1986) Laminar distribution of hippocampal rhythmic slow activity (RSA) in the behaving rat; current source density analysis, effects of urethane and atropine. Brain Res 365:125–137.

Buzsaki G, Draguhn A (2004) Neuronal oscillations in cortical networks. Science 304:1926–1929.

Buzsaki G, Horvath Z, Urioste R, Hetke J, Wise K (1992) High-frequency network oscillation in the hippocampus. Science 256:1025–1027.

Buzsaki G, Leung LW, Vanderwolf CH (1983) Cellular bases of hippocampal EEG in the behaving rat. Brain Res 287:139–171.

Callaway EM (2002) Cell type specificity of local cortical connections. J Neurocytol 31:231–237.

Chen K, Aradi I, Santhakumar V, Soltesz I (2002) H-channels in epilepsy: new targets for seizure control? Trends Pharmacol Sci 23:552–557.

Cho RY, Konecky RO, Carter CS (2006) Impairments in frontal cortical gamma synchrony and cognitive control in schizophrenia. Proc Natl Acad Sci USA 103:19878–19883.

Chrobak JJ, Buzsaki G (1996) High-frequency oscillations in the output networks of the hippocampal-entorhinal axis of the freely behaving rat. J Neurosci 16:3056–3066.
Cobb SR, Buhl EH, Halasy K, Paulsen O, Somogyi P (1995) Synchronisation of neuronal activity in hippocampus by individual GABAergic interneurons. Nature 378:75–78.
Cobb SR, Butlers DO, Davies CH (2000) Coincident activation of mGluRs and MAChRs imposes theta frequency patterning on synchronised network activity in the hippocampal CA3 region. Neuropharmacology 23:1933–1942.
Colom LV, Garcia-Hernandez A, Castaneda MT, Perez-Cordova MG, Garrido-Sanabria ER (2006) Septo-hippocampal networks in chronically epileptic rats: potential antiepileptic effects of theta rhythm generation. J Neurophysiol 95:3645–3653.
Cossart R, Esclapez M, Hirsch JC, Bernard C, Ben-Ari Y (1998) GluR5 kainate receptor activation in interneurons increases tonic inhibition of pyramidal cells. Nature Neurosci 1: 470–478.
Cossart R, Epsztein J, Tyzio R, Becq H, Hirsch J, Ben-Ari Y, Crépel V (2002) Quantal release of glutamate generates pure kainate and mixed AMPA/kainate EPSCs in hippocampal neurons. Neuron 35:147–159
Csicsvari J, Hirase H, Czurko' A, Mamiya A, Buzsa'ki G (1999) Oscillatory coupling of hippocampal pyramidal cells and interneurons in the behaving rat. J Neurosci 19:274–287.
Csicsvari J, Hirase H, Mamiya A, Buzsaki G (2000) Ensemble patterns of hippocampal CA3-CA1 neurons during sharp wave-associated population events. Neuron 28:585–594.
Csicsvari J, Jamieson B, Wise KD, Buzsáki G (2003) Mechanisms of gamma oscillations in the hippocampus of the behaving rat. Neuron 37:311–322.
Cunningham MO, Hunt J, Middleton S, LeBeau FE, Gillies MJ, Davies CH, Maycox PR, Whittington MA, Racca C (2006) Region-specific reduction in entorhinal gamma oscillations and parvalbumin-immunoreactive neurons in animal models of psychiatric illness. J Neurosci 26:2767–2776.
Deisseroth K, Feng G, Majewska AK, Miesenböck G, Ting A, Schnitzer MJ (2006) Next-generation optical technologies for illuminating genetically targeted brain circuits. J Neurosci 26:10380–10386.
Dodt HU, Zieglgänsberger W (1994) Infrared videomicroscopy: a new look at neuronal structure and function. Trends Neurosci 17:453–458.
Draguhn A, Traub RD, Schmitz D, Jefferys JG (1998) Electrical coupling underlies high-frequency oscillations in the hippocampus in vitro. Nature 394:189–192.
Dugladze T, Vida I, Tort AB, Gross A, Otahal J, Heinemann U, Kopell NJ, Gloveli T (2007) Impaired hippocampal rhythmogenesis in a mouse model of mesial temporal lobe epilepsy. Proc Natl Acad Sci USA 104:17530–17535.
Fellous JM, Sejnowski TJ (2000) Cholinergic induction of oscillations in the hippocampal slice in the slow bands (0.5–2 Hz), theta (5–12 Hz), and gamma (35–70 Hz). Hippocampus 10: 187–197.
Fisahn A, Pike FG, Buhl EH, Paulsen O (1998) Cholinergic induction of network oscillations at 40 Hz in the hippocampus in vitro. Nature 394:186–189.
Fisahn A, Yamada M, Duttaroy A, Gan JW, Deng CX, McBain CJ, Wess J (2002) Muscarinic induction of hippocampal gamma oscillations requires coupling of the M1 receptor to two mixed cation currents. Neuron 33:615–624.
Fisahn A, Contractor A, Traub RD, Buhl EH, Heinemann SF, McBain CJ (2004) Distinct roles for the kainate receptor subunits GluR5 and GluR6 in kainate-induced hippocampal gamma oscillations. J Neurosci 24:9658–9668.
Fisher RS, Webber WR, Lesser RP, Arroyo S, Uematsu S (1992) High-frequency EEG activity at the start of seizures. J Clin Neurophysiol 9:441–448.
Ford JM, Krystal JH, Mathalon DH (2007) Neural synchrony in schizophrenia: from networks to new treatments. Schizophr Bull 33:848–852.
Frerking M, Malenka RC, Nicoll RA (1998) Synaptic activation of kainate receptors on hippocampal interneurons. Nat Neurosci 1:479–486.

Frerking M, Ohliger-Frerking P (2002) AMPA receptors and kainate receptors encode different features of afferent activity. J Neurosci 22:7434–7443.
Freund TF, Buzsáki G (1996) Interneurons of the hippocampus. Hippocampus 6:347–470.
Freund TF, Katona I (2007) Perisomatic inhibition. Neuron 56:33–42.
Foffani G, Uzcategui YG, Gal B, Menendez de la Prida L (2007) Reduced spike-timing reliability correlates with the emergence of fast ripples in the rat epileptic hippocampus. Neuron 55: 930–941.
Fuentealba P, Begum R, Capogna M, Jinno S, Márton LF, Csicsvari J, Thomson A, Somogyi P, Klausberger T (2008) Ivy cells: a population of nitric-oxide-producing, slow-spiking GABAergic neurons and their involvement in hippocampal network activity. Neuron 57:917–929.
Galarreta M, Erdélyi F, Szabó G, Hestrin S (2008) Cannabinoid sensitivity and synaptic properties of 2 GABAergic networks in the neocortex. Cereb Cortex 18:2296–22305.
Geiger JR, Melcher T, Koh DS, Sakmann B, Seeburg PH, Jonas P, Monyer H (1995) Relative abundance of subunit mRNAs determines gating and Ca2+ permeability of AMPA receptors in principal neurons and interneurons in rat CNS. Neuron 15:193–204.
Geiger JR, Lübke J, Roth A, Frotscher M, Jonas P (1997) Submillisecond AMPA receptor-mediated signaling at a principal neuron-interneuron synapse. Neuron 18:1009–1023.
Gillies MJ, Traub RD, LeBeau FE, Davies CH, Gloveli T, Buhl EH, Whittington MA (2002) A model of atropine-resistant theta oscillations in rat hippocampal area CA1. J Physiol (Lond) 543:779–793.
Gloveli T, Dugladze T, Saha S, Monyer H, Heinemann U, Traub RD, Whittington MA, Buhl EH (2005a) Differential involvement of oriens/pyramidale interneurones in hippocampal network oscillations in vitro. J Physiol 562:131–147
Gloveli T, Dugladze T, Rotstein HG, Traub RD, Monyer H, Heinemann U, Whittington MA, Kopell NJ (2005b) Orthogonal arrangement of rhythm-generating microcircuits in the hippocampus. Proc Natl Acad Sci USA 102:13295–13300.
Goldin M, Epsztein J, Jorquera I, Represa A, Ben-Ari Y, Crépel V, Cossart R (2007) Synaptic kainate receptors tune oriens-lacunosum moleculare interneurons to operate at theta frequency. J Neurosci 27:9560–9572.
Gonzalez-Burgos G, Lewis DA (2008) GABA Neurons and the mechanisms of network oscillations: implications for understanding cortical dysfunction in schizophrenia. Schizophr Bull 34:944–961.
Gu N, Vervaeke K, Hu H, Storm JF (2005) Kv7/KCNQ/M and HCN/h, but not KCa2/SK channels, contribute to the somatic medium after-hyperpolarization and excitability control in CA1 hippocampal pyramidal cells. J Physiol 566:689–715.
Hájos N, Pálhalmi J, Mann EO, Németh B, Paulsen O, Freund TF (2004) Spike timing of distinct types of GABAergic interneuron during hippocampal gamma oscillations in vitro. J Neurosci 24:9127–9137.
Hajós M, Siok CJ, Hoffmann WE, Li S, Kocsis B (2008) Modulation of hippocampal theta oscillation by histamine H3 receptors. J Pharmacol Exp Ther 324:391–398.
Halasy K, Buhl EH, Lörinczi Z, Tamás G, Somogyi P (1996) Synaptic target selectivity and input of GABAergic basket and bistratified interneurons in the CA1 area of the rat hippocampus. Hippocampus 6:306–329.
Hu H, Vervaeke K, Storm JF (2002) Two forms of electrical resonance at theta frequencies, generated by M-current, h-current and persistent Na+ current in rat hippocampal pyramidal cells. J Physiol 545:783–805.
Jonas P, Major G, Sakmann B (1993) Quantal components of unitary EPSCs at the mossy fibre synapse on CA3 pyramidal cells of rat hippocampus. J Physiol 472:615–663.
Jouvet M (1969) Biogenic amines and the states of sleep. Science 163:32–41.
Kandel ER, Spencer WA (1961) Electrophysiology of hippocampal neurons. II. After-potentials and repetitive firing. J Neurophysiol 24:243–259.
Kehrer C, Dugladze T, Maziashvili N, Wójtowicz A, Schmitz D, Heinemann U, Gloveli T (2007) Increased inhibitory input to CA1 pyramidal cells alters hippocampal gamma frequency oscillations in the MK-801 model of acute psychosis. Neurobiol Dis 25:545–552.

Kehrer C, Maziashvili N, Dugladze T, Gloveli T (2008) Altered excitatory-inhibitory balance in the NMDA-hypofunction model of schizophrenia. Front Mol Neurosci 1:6.
Klausberger T, Somogyi P (2008) Neuronal diversity and temporal dynamics: the unity of hippocampal circuit operations. Science 321:53–57.
Klausberger T, Magill PJ, Márton LF, Roberts JD, Cobden PM, Buzsáki G, Somogyi P (2003) Brain-state- and cell-type-specific firing of hippocampal interneurons in vivo. Nature 421: 844–848.
Klausberger T, Márton LF, Baude A, Roberts JD, Magill PJ, Somogyi P (2004) Spike timing of dendrite-targeting bistratified cells during hippocampal network oscillations in vivo. Nat Neurosci 7:41–47.
Kocsis B, Varga V, Dahan L, Sik A (2006) Serotonergic neuron diversity: identification of raphe neurons with discharges time-locked to the hippocampal theta rhythm. Proc Natl Acad Sci USA 103:1059–1064.
Kocsis B, Li S, Hajos M (2007) Behavior-dependent modulation of hippocampal EEG activity by the selective norepinephrine reuptake inhibitor reboxetine in rats. Hippocampus 17:627–633.
Konopacki J, Gołebiewski H, Eckersdorf B (1992) Carbachol-induced rhythmic slow activity (theta) in cat hippocampal formation slices. Brain Res 578:13–16.
Lawrence JJ, Statland JM, Grinspan ZM, McBain CJ (2006) Cell type-specific dependence of muscarinic signalling in mouse hippocampal stratum oriens interneurones. J Physiol 570: 595–610
LeBeau FEN, Towers SK, Traub RD, Whittington MA, Buhl EH (2002) Fast network oscillations induced by potassium transients in the rat hippocampus in vitro. J Physiol (Lond) 542:167–179.
LeBeau FE, Traub RD, Monyer H, Whittington MA, Buhl EH (2003) The role of electrical signaling via gap junctions in the generation of fast network oscillations. Brain Res Bull 62:3–13.
Lerma J (2003) Roles and rules of kainate receptors in synaptic transmission. Nat Rev Neurosci 4:481–495.
Leung LW (1985) Spectral analysis of hippocampal EEG in the freely moving rat effects of centrally active drugs and relations to evoked potentials. Electroencephalogr Clin Neurophysiol 60:65–77.
Leung LS, Yim CY (1986) Intracellular records of theta rhythm in hippocampal CA1 cells of the rat. Brain Res 367:323–327.
Leung LS, Yu HW (1998) Theta-frequency resonance in hippocampal CA1 neurons in vitro demonstrated by sinusoidal current injection. J Neurophysiol 79:1592–1596.
Leung LS, Lopes da Silva F, Wadman WJ (1982) Spectral characteristics of the hippocampal EEG in the freely moving rat. Clin Neurophysiol 54:203–219.
Lewis DA, Hashimoto T, Volk DW (2005) Cortical inhibitory neurons and schizophrenia. Nat Rev Neurosci 6:312–324.
Li XG, Somogyi P, Ylinen A, Buzsáki G (1994) The hippocampal CA3 network: an in vivo intracellular labeling study. J Comp Neurol 339:181–208.
Lisman JE (2005) The theta/gamma discrete phase code occurring during the hippocampal phase precession may be a more general brain coding scheme. Hippocampus 15:913–922.
Lisman JE, Idiart MAP (1995) Storage of 7+– 2 short term memories in oscillatory subcycles. Science 267:1512–1515.
Maccaferri G, McBain CJ (1996) The hyperpolarization-activated current (Ih) and its contribution to pacemaker activity in rat CA1 hippocampal stratum oriens-alveus interneurones. J Physiol 497:119–130.
Maccaferri G, Roberts JD, Szucs P, Cottingham CA, Somogyi P (2000) Cell surface domain specific postsynaptic currents evoked by identified GABAergic neurones in rat hippocampus in vitro. J Physiol 524:91–116.
Madison DV, Lancaster B, Nicoll RA (1987) Voltage clamp analysis of cholinergic action in the hippocampus. J Neurosci 7:733–741.
Magee JC (1999) Dendritic hyperpolarization-activated currents modify the integrative properties of hippocampal CA1 pyramidal neurons. J Neurosci 18:7613–7624.

Maier N, Nimmrich V, Draguhn A (2003) Cellular and network mechanisms underlying spontaneous sharp wave-ripple complexes in mouse hippocampal slices. J Physiol 550:873–887.
Mann EO, Suckling JM, Hajos N, Greenfield SA, Paulsen O (2005) Perisomatic feedback inhibition underlies cholinergically induced fast network oscillations in the rat hippocampus in vitro. Neuron 45:105–117.
Marek KW, Davis GW (2003) Controlling the active properties of excitable cells. Curr Opin Neurobiol 13:607–611.
Markram H, Lubke J, Frotscher M, Roth A, Sakmann B (1997) Physiology and anatomy of synaptic connections between thick tufted pyramidal neurones in the developing rat neocortex. J Physiol 500:409–440.
McBain CJ, Fisahn A (2001) Interneurons unbound. Nat Rev Neurosci 2:11–23.
Meyer AH, Katona I, Blatow M, Rozov A, Monyer H (2002) In vivo labeling of parvalbumin-positive interneurons and analysis of electrical coupling in identified neurons. J Neurosci 22:7055–7064.
Middleton S, Jalics J, Kispersky T, Lebeau FE, Roopun AK, Kopell NJ, Whittington MA, Cunningham MO (2008) NMDA receptor-dependent switching between different gamma rhythm-generating microcircuits in entorhinal cortex. Proc Natl Acad Sci USA 105:18572–18577.
Miles R (1990) Synaptic excitation of inhibitory cells by single CA3 hippocampal pyramidal cells of the guinea-pig in vitro. J Physiol 428:61–77.
Miles R, Poncer JC (1996) Paired recordings from neurones. Curr Opin Neurobiol 6:387–394.
Miles R, Tóth K, Gulyás AI, Hájos N, Freund TF (1996) Differences between somatic and dendritic inhibition in the hippocampus. Neuron 16:815–823.
Montplaisir J, Laverdiere M, Saint-Hilaire JM, Rouleau I (1987) Nocturnal sleep recording in partial epilepsy: a study with depth electrodes, J Clin Neurophysiol 4:383–388.
Morales M, Bloom FE (1997) The 5-HT3 receptor is present in different subpopulations of GABAergic neurons in the rat telencephalon. J Neurosci 17:3157–3167.
Morales M, Battenberg E, Bloom F (1998) Distribution of neurons expressing immunoreactivity for the 5HT3 receptor subtype in the rat brain and spinal cord. J Comp Neurol 402: 385–401.
Morris HM, Hashimoto T, Lewis DA (2008) Alterations in somatostatin mRNA expression in the dorsolateral prefrontal cortex of subjects with schizophrenia or schizoaffective disorder. Cereb Cortex 18:1575–1587.
Mulle C, Sailer A, Swanson GT, Brana C, O'Gorman S, Bettler B, Heinemann SF (2000) Subunit composition of kainate receptors in hippocampal interneurons. Neuron 28:475–484.
Nimmrich V, Maier N, Schmitz D, Draguhn A (2005) Induced sharp wave-ripple complexes in the absence of synaptic inhibition in mouse hippocampal slices. J Physiol 563:663–670.
Notomi T, Shigemoto R (2004) Immunohistochemical localization of Ih channel subunits, HCN1-4, in the rat brain. J Comp Neurol 471:241–276.
Nusser Z, Lujan R, Laube G, Roberts JD, Molnar E, Somogyi P (1998) Cell type and pathway dependence of synaptic AMPA receptor number and variability in the hippocampus. Neuron 21:545–559.
Oliva AA Jr, Jiang M, Lam T, Smith KL, Swann JW (2000) Novel hippocampal interneuronal subtypes identified using transgenic mice that express green fluorescent protein in GABAergic interneurons. J Neurosci 20:3354–3368.
O'Neill J, Senior T, Csicsvari J (2006) Place-selective firing of CA1 pyramidal cells during sharp wave/ripple network patterns in exploratory behavior. Neuron 49:143–155.
Oren I, Mann EO, Paulsen O, Hajos N (2006) Synaptic currents in anatomically identified CA3 neurons during hippocampal gamma oscillations in vitro. J Neurosci 26:9923–9934.
Pálhalmi J, Paulsen O, Freund TF, Hájos N (2004) Distinct properties of carbachol- and DHPG-induced network oscillations in hippocampal slices. Neuropharmacology 47:381–289.
Penttonen M, Kamondi A, Acsády L, Buzsáki G (1998) Gamma frequency oscillation in the hippocampus of the rat: intracellular analysis in vivo. Eur J Neurosci 10:718–728.

Petsche H, Stumpf C, Gogolák G (1962) The significance of the rabbit's septum as a relay station between midbrain and the hippocampus: I. The control of hippocampus arousal activity by the septum cells. Electroencephalogr Clin Neurophysiol 14:202–211.
Pike FG, Goddard RS, Suckling JM, Ganter P, Kasthuri N, Paulsen O (2000) Distinct frequency preferences of different types of rat hippocampal neurones in response to oscillatory input currents. J Physiol 529:205–213.
Pinault D (1996) A novel single-cell staining procedure performed in vivo under electrophysiological control: morpho-functional features of juxtacellularly labeled thalamic cells and other central neurons with biocytin or neurobiotin. J Neurosci Methods 65:113–136.
Pinault D (2008) N-methyl d-aspartate receptor antagonists ketamine and MK-801 induce wake-related aberrant gamma oscillations in the rat neocortex. Biol Psychiatry 63:730–735.
Pitler TA, Alger BE (1992) Cholinergic excitation of GABAergic interneurons in the rat hippocampal slice. J Physiol 450:127–142.
Polleux F (2005) Genetic mechanisms specifying cortical connectivity: let's make some projections together. Neuron 46:395–400.
Pöschel B, Draguhn A, Heinemann U (2002) Glutamate-induced gamma oscillations in the dentate gyrus of rat hippocampal slices. Brain Res 938:22–28.
Pouille F, Scanziani M (2004) Routing of spike series by dynamic circuits in the hippocampus. Nature 429:717–723.
Price CJ, Cauli B, Kovacs ER, Kulik A, Lambolez B, Shigemoto R, Capogna M (2005) Neurogliaform neurons form a novel inhibitory network in the hippocampal CA1 area. J Neurosci 25:6775–6786.
Roopun AK, Cunningham MO, Racca C, Alter K, Traub RD, Whittington MA (2008) Region-specific changes in gamma and beta2 rhythms in NMDA receptor dysfunction models of schizophrenia. Schizophr Bull 34:962–973.
Ropert N, Guy N (1991) Serotonin facilitates GABAergic transmission in the CA1 region of rat hippocampus in vitro. J Physiol (Lond) 441:121–136.
Rotstein HG, Pervouchine DD, Acker CD, Gillies MJ, White JA, Buhl EH, Whittington MA, Kopell N (2005) Slow and fast inhibition and an H-current interact to create a theta rhythm in a model of CA1 interneuron network. J Neurophysiol 94:1509–1518.
Sakai T, Oshima A, Nozaki Y, Ida I, Haga C, Akiyama H, Nakazato Y, Mikuni M (2008) Changes in density of calcium-binding-protein-immunoreactive GABAergic neurons in prefrontal cortex in schizophrenia and bipolar disorder. Neuropathology 28:143–150.
Savić N, Pedarzani P, Sciancalepore M (2001) Medium afterhyperpolarization and firing pattern modulation in interneurons of stratum radiatum in the CA3 hippocampal region. J Neurophysiol 85:1986–1997.
Schmitz D, Empson RM, Heinemann U (1995) Serotonin reduces inhibition via 5-HT1A receptors in area CA1 of rat hippocampal slices in vitro. J Neurosci 15:7217–7225.
Schmitz D, Gloveli T, Empson RM, Heinemann U (1998) Comparison of the effects of serotonin in the hippocampus and the entorhinal cortex. Mol Neurobiol 17:59–72.
Schmitz D, Schuchmann S, Fisahn A, Draguhn A, Buhl EH, Petrasch-Parwez E, Dermietzel R, Heinemann U, Traub RD (2001) Axo-axonal coupling. A novel mechanism for ultrafast neuronal communication. Neuron 31:831–840.
Shen RY, Andrade R (1998) 5-Hydroxytryptamine2 receptor facilitates GABAergic neurotransmission in rat hippocampus. J Pharmacol Exp Ther 285:805–12.
Shimono K, Brucher F, Granger R, Lynch G, Taketani M (2000) Origins and distribution of cholinergically induced beta rhythms in hippocampal slices. J Neurosci 20:8462–8473.
Sik A, Penttonen M, Ylinen A, Buzsáki G (1995) Hippocampal CA1 interneurons: an in vivo intracellular labeling study. J Neurosci 15:6651–6665.
Singer W (1999) Neuronal synchrony: a versatile code for the definition of relations? Neuron 24:49–65.
Slewa-Younan S, Gordon E, Williams L, Haig AR, Goldberg E (2001) Sex differences, gamma activity and schizophrenia. Int J Neurosci 107:131–144.

Somogyi P, Klausberger T (2005) Defined types of cortical interneurone structure space and spike timing in the hippocampus. J Physiol (Lond) 562:9–26.
Spampanato J, Mody I (2007) Spike timing of lacunosum-moleculare targeting interneurons and CA3 pyramidal cells during high-frequency network oscillations in vitro. J Neurophysiol 98:96–104.
Spencer KM, Nestor PG, Perlmutter R, Niznikiewicz MA, Klump MC, Frumin M, Shenton ME, McCarley RW (2004) Neural synchrony indexes disordered perception and cognition in schizophrenia. Proc Natl Acad Sci USA 101:17288–17293.
Spencer KM (2008) Visual gamma oscillations in schizophrenia: implications for understanding neural circuitry abnormalities. Clin EEG Neurosci 39:65–68.
Spruston N (2008) Pyramidal neurons: dendritic structure and synaptic integration. Nat Rev Neurosci 9:206–221.
Szabadics J, Tamas G, Soltesz I (2007) Different transmitter transients underlie presynaptic cell type specificity of GABAA, slow and GABAA, fast. Proc Natl Acad Sci USA 104: 14831–14836.
Tecott LH, Maricq AV, Julius D (1993) Nervous system distribution of the serotonin 5-HT3 receptor mRNA. Proc Natl Acad Sci USA 90:1430–1434.
Tesche CD, Karhu J (2000) Theta oscillations index human hippocampal activation during a working memory task. Proc Natl Acad Sci USA 97:919–924.
Tort AB, Rotstein HG, Dugladze T, Gloveli T, Kopell NJ (2007) On the formation of gamma-coherent cell assemblies by oriens lacunosum-moleculare interneurons in the hippocampus. Proc Natl Acad Sci USA 104:13490–13495.
Toth K, Suares G, Lawrence JJ, Philips-Tansey E, McBain CJ (2000) Differential mechanisms of transmission at three types of mossy fiber synapse. J Neurosci 20:8279–8289.
Towers SK, LeBeau FE, Gloveli T, Traub RD, Whittington MA, Buhl EH (2002) Fast network oscillations in the rat dentate gyrus in vitro. J Neurophysiol 87:1165–1168.
Traub RD, Bibbig A, Fisahn A, LeBeau FE, Whittington MA, Buhl EH (2000) A model of gamma-frequency network oscillations induced in the rat CA3 region by carbachol in vitro. Eur J Neurosci 12:4093–4106.
Traub RD, Cunningham MO, Gloveli T, LeBeau FE, Bibbig A, Buhl EH, Whittington MA (2003) GABA-enhanced collective behavior in neuronal axons underlies persistent gamma-frequency oscillations. Proc Natl Acad Sci USA 100:11047–11052.
Tukker JJ, Fuentealba P, Hartwich K, Somogyi P, Klausberger T (2007) Cell type-specific tuning of hippocampal interneuron firing during gamma oscillations in vivo. J Neurosci 27:8184–8189.
van Hooft JA, Giuffrida R, Blatow M, Monyer H (2000) Differential expression of group I metabotropic glutamate receptors in functionally distinct hippocampal interneurons. J Neurosci 20:3544–3551.
Vanderwolf CH (1969) Hippocampal electrical activity and voluntary movement in the rat. Electroencephalogr Clin Neurophysiol 26:407–418.
Vida I, Halasy K, Szinyei C, Somogyi P, Buhl EH (1998) Unitary IPSPs evoked by interneurons at the stratum radiatum-stratum lacunosum-moleculare border in the CA1 area of the rat hippocampus in vitro. J Physiol 506:755–773.
Vida I, Bartos M, Jonas P (2006) Shunting inhibition improves robustness of gamma oscillations in hippocampal interneuron networks by homogenizing firing rates. Neuron 49:107–117.
Vierling-Claassen D, Siekmeier P, Stufflebeam S, Kopell N (2008) Modeling GABA alterations in schizophrenia: a link between impaired inhibition and altered gamma and beta range auditory entrainment. J Neurophysiol 99:2656–2671.
Wang X-J, Buzsáki G (1996) Gamma oscillation by synaptic inhibition in a hippocampal interneuronal network model. J Neurosci 16:6402–6413.
Wang CZ, Yang SF, Xia Y, Johnson KM (2008) Postnatal phencyclidine administration selectively reduces adult cortical parvalbumin-containing interneurons. Neuropsychopharmacology 33:2442–2455.
Weiss T, Veh RW, Heinemann U (2003) Dopamine depresses cholinergic oscillatory network activity in rat hippocampus. Eur J Neurosci 18:2573–2580.

White JA, Chow CC, Ritt J, Soto-Treviño C, Kopell N (1998) Synchronization and oscillatory dynamics in heterogeneous, mutually inhibited neurons. J Comput Neurosci 5:5–16.

Whittington MA, Traub RD (2003) Interneuron diversity series: inhibitory interneurons and network oscillations in vitro. Trends Neurosci 26:676–682.

Whittington MA, Stanford IM, Colling SB, Jefferys JG, Traub RD (1997) Spatiotemporal patterns of gamma frequency oscillations tetanically induced in the rat hippocampal slice. J Physiol 502:591–607.

Whittington MA, Traub RD, Jefferys JGR (1995) Synchronized oscillations in interneuron networks driven by metabotropic glutamate receptor activation. Nature 373:612–615.

Williams SR, Stuart GJ (2003) Voltage- and site-dependent control of the somatic impact of dendritic IPSPs. J Neurosci 23:7358–7367.

Wilson MA, McNaughton BL (1994) Reactivation of hippocampal ensemble memories during sleep. Science 265:676–679.

Wittner L, Henze DA, Záborszky L, Buzsáki G (2007) Three-dimensional reconstruction of the axon arbor of a CA3 pyramidal cell recorded and filled in vivo. Brain Struct Funct 212:75–83.

Ylinen A, Bragin A, Nadasdy Z, Jando G, Szabo I, Sik A, Buzsaki G (1995) Sharp wave-associated high-frequency oscillation (200 Hz) in the intact hippocampus: network and intracellular mechanisms. J Neurosci 15:30–46.

Zhang ZJ, Reynolds GP (2002) A selective decrease in the relative density of parvalbumin-immunoreactive neurons in the hippocampus in schizophrenia. Schizophr Res 55:1–10.

Zhang F, Wang LP, Brauner M, Liewald JF, Kay K, Watzke N, Wood PG, Bamberg E, Nagel G, Gottschalk A, Deisseroth K (2007) Multimodal fast optical interrogation of neural circuitry. Nature 446:633–639.

Neuronal Activity Patterns in Anaesthetized Animals

Stuart Cobb and Imre Vida

Overview

A major goal in hippocampal computational biology is to understand how neuronal circuits encode, process, store and retrieve information. To achieve this goal we must identify the activity of single neurons involved in specific neural processes within the context of the surrounding network. A major aspect of this question is how the activity of the neurons and the network is orchestrated by the many types of interneurons embedded in feedforward and feedback inhibitory microcircuits. To gain experimental insights into such dynamical processes it would be ideal to monitor the synaptic inputs, outputs and discharge pattern of anatomically defined single cells and to correlate these activities with a detailed knowledge of how the cells are incorporated into the surrounding hippocampal network, the coordinated activity of other cells in that network and ultimately the resultant behavioural consequences. Of course, only limited aspects of this are achievable within a single experimental study and therefore a reductionist approach is a necessity. Cellular resolution studies are a practical and powerful method to investigate the activity of individual cells ("units") during behaviourally relevant situations in freely moving animals using extracellular recording techniques. However, in the absence of morphological data, robust identification of the recorded neuron is not possible and the nature of the cell (e.g. classification of cell type) remains speculative. In contrast, in vivo studies in which the morphological features of cells under investigation are pertinent require intracellular or juxtacellular recordings performed in immobilized/anaesthetized animals for improved stability of the recording. While anaesthesia clearly prevents the simultaneous acquisition of overt behavioural data, it nevertheless provides a stable substrate in which to study the activity and characteristics of anatomically defined hippocampal neurons in an intact, albeit suppressed, hippocampal network. This approach has been especially effective in characterizing

S. Cobb / I. Vida (✉)
Neuroscience and Molecular Pharmacology, Faculty of Biomedical and Life Sciences, University of Glasgow, Glasgow G12 8QQ, UK
e-mail: s.cobb@bio.gla.ac.uk/i.vida@bio.gla.ac.uk

V. Cutsuridis et al. (eds.), *Hippocampal Microcircuits*, Springer Series in Computational Neuroscience 5, DOI 10.1007/978-1-4419-0996-1_9,

discharge patterns of morphologically and neurochemically identified principal cells and interneurons during ensemble activities, in particular, during synchronized oscillatory brain states.

The Data

Introduction

Anaesthesia is essential to sedate and immobilize animals for stereotaxic implantation of hippocampal recording electrodes. Wire or silicone microelectrodes enable the removal of the animal from the stereotaxic apparatus and the monitoring of extracellular activity in freely moving animals to powerful effect (see chapter "Spatial and Behavioral Correlates of Hippocampal Neuronal Activity: A Primer for Computational Analysis"). While the recording of hippocampal unit activity is a long established and valuable approach (O'Keefe and Dostrovsky, 1971), it nevertheless provides only a time-stamp of action potentials occurring in anatomically unidentified cells. It is therefore unsuitable to monitor intrinsic electrical properties and subthreshold membrane potential signals or to reveal the morphology, neurochemistry or connectivity of the cells being recorded. These data are essential to gain a complete understanding of how hippocampal circuits operate in the real world and thus considerable effort has been directed towards applying intracellular techniques to intact in vivo hippocampus. However, invasive single cell techniques involving sharp microelectrodes have typically been unstable and result in relatively brief recordings. For this reason, most recordings have been restricted to animals maintained under anaesthesia. This chapter describes some of the key findings from such studies including insights into intracellular correlates of patterned oscillatory activities as well as morphological features and morphology-activity correlates that have been discovered using in vivo approaches in anaesthetized animals.

The hippocampus is a highly laminated brain area with both the extrinsic afferent fibres inputting the structure and the intrinsic local and intra-areal connectivity intrinsic to the hippocampus forming highly precise laminar termination domains (the strata; see chapters "Connectivity of the Hippocampus" and "Morphology of Hippocampal Neurons"). Consequently, principal cells are themselves orientated in a laminar fashion and send out dendrites to sample these laminar-specific afferent excitatory inputs. Thus, excitatory afferents arising from different sources are distributed on the surface for principal cells so that the different inputs (e.g. local recurrent collaterals or intra-hippocampal inputs versus entorhinal and thalamic inputs) are segregated in space. As described in the earlier chapters, the various GABAergic interneuron types target the surface of principal cells in a similar and indeed co-aligned domain-specific manner (see chapter "Morphology of Hippocampal Neurons").

Many cellular studies have aimed at unravelling this cellular complexity and in particular how inhibition targeted to sub-domains of principal cells may differentially influence the integration of signals in hippocampal neurons (Buhl et al., 1994; Cobb et al., 1995; Miles et al., 1996; Hájos et al., 2004; Gloveli et al., 2005). From this body of experimental data, derived from in vitro preparations, it is apparent that the precise timing of GABAergic inhibition is crucial for such effects and therefore addressing the question of how discrete species of GABAergic inhibitory neuron behave within the intact brain and during ongoing network activity has been an important goal.

Early Studies and Characterization of Physiological Properties In Vivo

Early cellular studies conducted in vivo were instrumental in first characterizing the basic intrinsic electrophysiological features of hippocampal neurons "in situ" including action potential properties and discharge patterns (Kandel and Spencer, 1961; Kandel et al., 1961), intrinsic conductances (Fujita, 1975) and responsiveness to afferent synaptic stimulation and neuromodulation (chapter "Neuromodulation of Hippocampal Cells and Circuits"). While these studies provided a valuable initial insight into the basic electrical characteristics of hippocampal neurons, the advent of in vitro methods and in particular the introduction of the hippocampal slice preparation (Andersen and Langmoen, 1980) led to more refined single cell biophysical characterization being conducted under in vitro conditions where the cells were more accessible to electrophysiological and pharmacological intervention and from where recordings were typically more controlled and stable. However, a limited number of more recent studies have described the salient membrane and active properties of identified CA1 principal neurons under anaesthesia conditions in vivo (Henze and Buzsáki, 2001). These studies have revealed a surprising large variation in certain parameters such as the threshold for action potential generation (5.7 ± 1.7 mV). Further studies have characterized the basic properties of other principal cells including CA3 pyramidal cells and dentate mossy cells under in vivo conditions (Henze and Buzsáki, 2007). These data provide an interesting comparison to the same parameters recorded in reduced in vitro preparations (see, e.g., chapters "Physiological Properties of Hippocampal Neurons" and "Neuronal Activity Patterns During Hippocampal Network Oscillations In Vitro"). It is important to note that while in vivo cellular recordings are typically not as detailed as equivalent studies conducted in brain slices, they are nevertheless more physiological in certain respects. For instance, the extracellular milieu is natural and not a wholly artificial mixture of salts as occurs with in vitro studies. Second, the cells are typically intact and lack severed processes as is invariably the case in brain slice systems. Third, it is possible to investigate interaction between brain regions through afferent fibre stimulation.

Morphological Findings In Vivo

The past two decades have seen an astonishing increase in the number of discrete cell types identified in the hippocampus. Much of this knowledge has come as a result of more detailed scrutiny of intracellularly labelled cells. In fact, it is today commonplace to combine in vitro patch-clamp recording with intracellular labelling by markers such as biocytin in order to characterize the morphological features of cells under investigation and to correlate their physiology with their morphology, neurochemistry and connectivity. This has been invaluable in the brain slice preparation whereby such labelling approaches have revealed an astonishing complexity and diversity of interneurons based upon their dendritic architecture and highly targeted axonal arborization patterns (chapter "Morphology of Hippocampal Neurons"). Such studies in brain slices are powerful at revealing very local microcircuitry which remains, for the most part, intact within the confines of the hippocampal slice. However, it is only by labelling cells in vivo that one gets a true appreciation of the three-dimensional extent by which dendritic and axonal processes ramify within the hippocampus. Moreover, in vivo experiments uniquely reveal the long-range, inter-regional hippocampal connectivity as well as connectivity with reciprocal brain regions.

Using a intracellular labelling approaches in anaesthetized animals has led to discoveries of fundamental features of hippocampal circuits including the demonstration that GABAergic cells are a major recipient of the mossy fibre pathway (Acsády et al., 1998) and revealing unprecedented and unexpectedly long-range cross-regional inhibition of area CA1–CA3 and the dentate gyrus (Sik et al., 1994) as well as between the hippocampus and the medial septal nucleus and retrohippocampal areas (Jinno et al., 2007). In vivo reconstructions of interneurons have confirmed patterns of axon target selectivity towards different perisomatic domains of principal cells (Sik et al., 1995, 1997). Injection of single cells in anaesthetized animals has also been invaluable in providing robust quantitative morphological measurements of dendritic architecture (coupled with electrical properties) (Li et al., 1992, 1994; Turner et al., 1995) as well as providing key data for calculating convergence and divergence estimates for connections between interneurons and pyramidal cells (Li et al., 1994; Sik et al., 1995) (chapter "Morphology of Hippocampal Neurons").

Neural Activity Patterns In Vivo

The abundance and homogeneity of the principal cell population make it practicable to monitor their activity within the intact brain with some certainty using classical unit recordings techniques. This focus on principal cells, as exemplified in the next chapter, has been instrumental in revealing aspects of neuronal coding in the hippocampus. In contrast, however, assessing interneuronal activity in the intact hippocampal network is considerably more demanding in that classical unit recording

can only discriminate certain interneurons, especially fast-spiking cells, from principal cells but is unable to resolve much beyond this broad separation (Fig. 1). Indeed, discriminating activity patterns within the myriad of interneuronal subtypes is not feasible without some form of additional cellular labelling technique. Much of the classical literature has taken a "lumper/splitter" approach by broadly describing two primary cell types in terms of in vivo firing signature – complex (principal) cells and theta (fast spiking, putatively GABAergic neurons that are especially active during theta rhythms EEG). Refinements of these descriptive classifications of neural activity patterns seen in unidentified (in terms of morphology) cells have included theta-off cells, single-peak cells, biphasic cells and sharp-wave-independent cells and anti sharp-wave cells (Csicsvari et al., 1999). However, it is now widely accepted that hippocampal circuits have evolved a vast array of different anatomically and connectionally discrete subtypes and that these different cells types are likely to perform an equally diverse array of functional roles within the hippocampal circuitry. A major challenge has therefore been to attempt to characterize the activity of different cell types in the intact hippocampus and to relate these activities to the position in which the particular cell or cell class is embedded within the hippocampal network.

As seen in earlier chapters, GABAergic interneurons occur as specialized types that provide GABAergic inhibition throughout hippocampal circuits in a segmented but sometimes overlapping inhibitory input across the entire dendrite-soma-axonal extent of the principal cells. Why do so many subtypes of inhibitory interneuron exist? Why is it not possible for a single subtype of GABAergic cell with highly

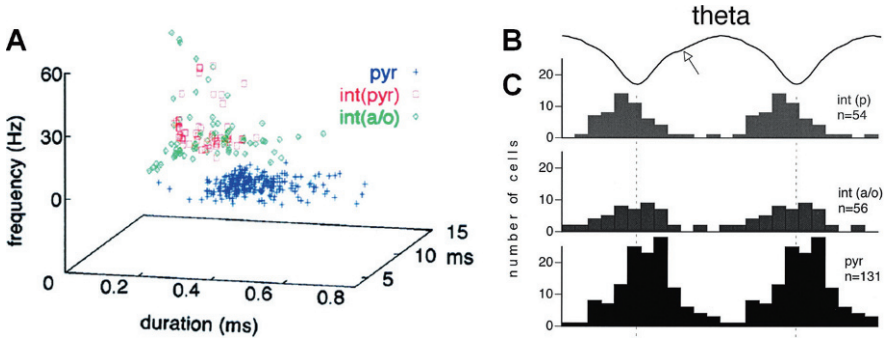

Fig. 1 Activity pattern of principal cells and interneurons during theta oscillations in the behaving animal. **A** Physiological identification of pyramidal cells (*blue symbols*) and interneurons (*red and green symbols*) on the basis of parameters of the extracellularly recorded unit activity. The parameters plotted are spike duration (*x* axis, "duration"), first momentum of the autocorrelogram (*y* axis, "periodicity") and the mean discharge frequency of the units (*z* axis, "frequency"). Note the clear separation of pyramidal cells and the overlapping clusters of interneurons recorded in the stratum pyramidale [int(pyr)] and the oriens/alveus [int(a/o)]. **B** Average waveform of theta oscillation recorded in the stratum pyramidale. **C** Preferred phase distribution of the individual cells belonging to the three neuron classes relative to the locally recorded theta waves (dashed vertical lines indicate the negative peak) (Reproduced from Csicsvari et al., 1999 with permission)

diffuse and divergent output and mediating a blanket form of inhibition sufficient to mediate the function of inhibition within GABAergic circuits? The answer to this question appears to lie in the spatio-temporal pattern of inhibition (Buzsáki and Chrobak, 1995; Klausberger and Somogyi, 2008). In fact, the GABAergic interneurons regulate when and where information can flow in the structure of neurons and neuronal networks. Through the compartmentalized inhibitory input, the various interneuron types may selectively control excitatory inputs, synaptic integration or the output of their postsynaptic neurons. Furthermore, the various interneuron types act at different times, in different temporal patterns. That is, the requirement for precise timing of glutamatergic signalling in encoding, coincidence detection and synaptic plasticity is matched by temporally precise activity of GABAergic inputs onto the dendrites, soma, or axon initial segment of postsynaptic neurons. To provide this dynamic temporal control of inhibition, it is hypothesized that GABAergic interneurons have evolved their diversity in electrical properties, sources of efferent inputs and targeting of axonal outputs. The best evidence for this comes from studies investigating the activity patterns of GABAergic interneurons during network oscillatory states. Whilst significant progress has been made from in vitro investigations (see chapter "Neuronal Activity Patterns During Hippocampal Network Oscillations In Vitro"), dramatic and compelling evidence comes from a detailed analysis of neuronal activity patterns in anaesthetized animals in which network oscillations and their cellular and anatomical correlates have been scrutinized in detail.

Oscillatory Activity Patterns in the Hippocampus

The hippocampus displays a range of oscillatory states including theta, gamma and high-frequency ripples. Theta oscillations or rhythmic slow activity in rodents (4–12 Hz) are considered to represent the "online state" of hippocampal (and related structures) processing. Often nested with higher frequency gamma oscillations (30–90 Hz), theta oscillations are especially pronounced during information acquisition such as occurs during exploration, spatial navigation, various memory tasks as well as during rapid-eye-movement sleep in both rodents and humans. Conversely, sharp wave-associated ripples (~100–200 Hz) are considered to represent the "offline" mode of hippocampal activity, whereby previous experiences are replayed or consolidated and occur during consummatory behaviour when the animal is at rest or in slow-wave sleep (Foster and Wilson, 2006). The underlying cellular and network basis for such activities and their importance in hippocampal information processing is today a major preoccupation in hippocampal neurobiology.

Early studies conducted using single-cell recordings revealed a remarkable intracellular correlation between theta frequency membrane depolarization and spike discharge patterns of hippocampal pyramidal cells during in vivo theta rhythm (Fujita and Sato, 1964). This work was extended over the years to investigate the intracellular correlates of network activities for different neuronal subtypes during different

oscillatory states but with a particular focus on theta oscillations as this is most overt and readily measured hippocampal EEG signature (Buzsáki and Eidelberg, 1983; Soltesz et al., 1993; Soltesz and Deschênes, 1993; Ylinen et al., 1995). By altering the intracellular concentration of Cl^- ions in the recording microelectrode and hence changing the reversal potential of $GABA_A$ receptor-mediated conductance in the recorded neurons, Soltész and colleagues (Soltesz and Deschênes, 1993) were able to demonstrate a role of phasic GABAergic inhibition in the generation of theta activity but also faster oscillatory network patterns. Hippocampal oscillations are indicative of highly coordinated neuronal activity within hippocampal circuits. However, indirect evidence from single unit recording studies have suggested that GABAergic interneurons display diverse role in this control as evidenced by their diverse firing patterns during network oscillations (Csicsvari et al., 1999). Using juxtacellular recording techniques which enable the recording of action potentials in single cells combined with anatomical identification and classification of cell types, Klausberger and colleagues (Klausberger et al., 2003, 2004, 2005; Tukker et al., 2007; reviewed in Klausberger and Somogyi, 2008) have performed an elegant series of detailed studies in anaesthetized animals to reveal strong associations between interneuron morphology and the timing of their activity with respect to different oscillatory cycles.

Network oscillations represent the coordinated activity of neuronal populations within hippocampal circuits and this makes an ideal and indeed necessary reference by which to map the activity of individual cells within that network. Using this approach, Klausberger and colleagues have shown convincingly that interneurons targeting different domains of the principal cell surface do indeed fire action potentials during different oscillatory states at distinct times/phases within any individual oscillatory cycle (Fig. 2). Moreover, the characteristic and temporally distinct activation of interneurons innervating functionally distinct domains of principal cells highlights an important mechanism by which interneurons orchestrate the temporal dynamics of hippocampal inhibition and consequently the activity of hippocampal circuits during different brain states.

Theta Oscillations

Theta oscillations, which under non-anaesthesia conditions would be associated with exploratory activity and information acquisition, occur under anaesthesia upon elevated arousal either spontaneously or following tactile stimulation. During these oscillations pyramidal cells are relatively inactive but when they fire they preferentially do so close to the trough of the theta cycle recorded in the cell body layer (Fig. 2, Table 1; Csicsvari et al., 1999; Klausberger et al., 2003). In contrast to principal cells, many interneuron types are highly active and show a strong modulation during theta activity, but the different types discharge at different phases of the cycle. Two major activity patterns can be identified: perisomatic-inhibitory

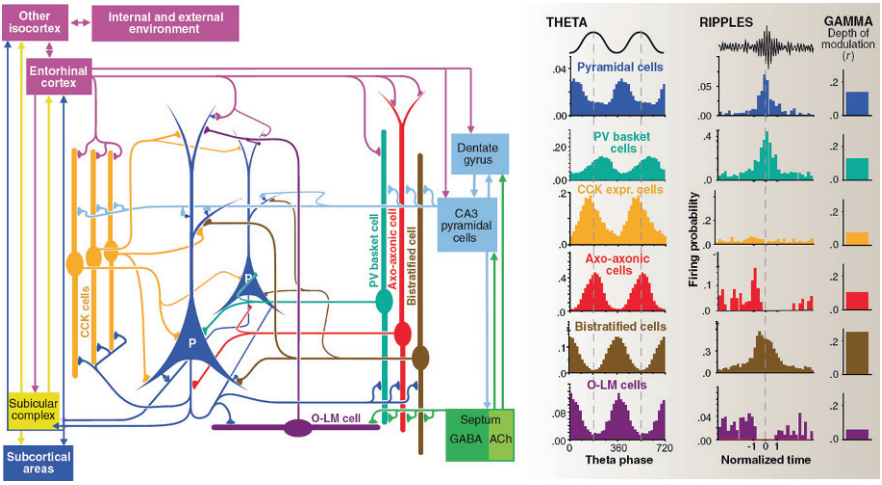

Fig. 2 Primary connectivity of pyramidal cells and five major classes of interneuron in area CA1 and corresponding firing histograms showing their preferred spike timing with respect to locally recorded theta, gamma and fast ripple oscillatory states. Note that defined interneurons targeting different aspects of the somato-dendritic surface are differentially recruited during different oscillatory states and are preferentially activity at distinct phases of the respective oscillatory cycles, thus compartmentalizing inhibition in space and time. Abbreviations: P, pyramidal cell; PV, parvalbumin; CCK, colecystokinin, O–LM and three classes of CCK-expressing interneurons; ACh, acetylcholine (From Klausberger and Somogyi, 2008, with permission)

cells (basket and axo-axonic cells) fire typically on the opposite phase of the theta cycle, whereas dendritic inhibitory neurons (O–LM and bistratified) fire mostly on the same phase as pyramidal cells.

PV-positive axo-axonic cells are active at the peak of the extracellular theta oscillations with ∼180° phase difference to pyramidal cells (Klausberger et al., 2003). PV-positive basket cells discharge later in the cycle, approximately one-quarter of a cycle (at ∼270°, Table 1, Klausberger et al., 2003) in advance of principal cells. CCK-containing basket cells, in contrast, fire slightly earlier in the cycle (at ∼155°, Table 1, Klausberger et al., 2005). Thus, the perisomatic domain of principal cells receives a high level of inhibitory input during this half of the theta cycle. This inhibitory input is conceivably very important in preventing discharge of pyramidal cells during this period. Furthermore, rebound excitation may be instrumental in bringing the cells close to threshold once inhibition by basket cells decays (Cobb et al., 1995). The strong phase modulation of these interneurons reflects the rhythmic input from the excitatory afferents as well as extrinsic (sepothippocampal) and intrinsic (O–LM and bistratified interneurons) inhibitory influences but it remains unknown how the phase differences between these interneurons types emerge.

As mentioned above, dendritically terminating O–LM, bistratified and ivy interneurons become also more active during theta oscillations and fire close to the maximum of pyramidal cell discharge (Table 1, Klausberger et al., 2004; Fuentealba

Table 1 The modulation of interneuronal subtypes during theta, gamma and sharp wave-associated ripples in anaesthetized animals. Phase measurement is in relation to trough of cycle = 0°

Cell type	Theta modulation (phase)	Gamma modulation (phase)	Ripple modulation
Pyramidal cells	Moderate ($20 \pm 65°$)	Moderate or weak (early)	Moderate, centred on ripple
PV basket cells	Strong ($271 \pm 68°$)	Moderate or weak	Moderate, centred on ripple
CCK basket	Strong ($155 \pm 81°$)	Moderate or weak (early)	Weakly modulated
Axo-axonic cells	Strong ($185 \pm 55°$)	Moderate or weak	Moderate, increased activity prior to ripple but then silent followed by "rebound" activity
OLM	Strong ($19 \pm 57°$)	None or weak	Strong, silent during peak of ripple
Bistratified	Strong ($1 \pm 60°$)	Strong	Strong, centred on ripple
Ivy	Strong ($30 \pm 63°$)	Sparse activity but strongly modulated ($11 \pm 68°$)	Largely silent
Long-range projections	Strong modulation of SOM negative retrohippocampal projecting cells	None or weak	↑ Firing

Based on Klausberger et al. (2003, 2004, 2005), Jinno et al. (2007), Tukker et al. (2007), Fuentealba et al. (2008).

et al., 2008). Similarly, long-range double-projection neurons fire at the same phase, albeit with a lower frequency, and provide inhibition locally to the dendrites of pyramidal cells (Jinno et al., 2007). Therefore, pyramidal cell activity is associated with a concurrent period of coherent dendritic inhibition. The functional relevance of this may be the suppression of weak inputs and thereby enhancing signal-to-noise ratio. Activity of long-range projection neurons most probably also plays a role in the coordination of theta activity in the hippocampus, septum and retrohippocampal structures (Jinno et al., 2007). The discharge and phase modulation of these interneurons is mainly driven by excitatory inputs, but while interneurons in the stratum oriens, such as O–LM cells, are activated primarily by the feedback excitation from local CA1 pyramidal cells, bistratified cell discharge most likely depends on input from the Schaffer collaterals, i.e. from CA3 pyramidal cells.

In summary, over the period of the theta cycle, not only are pyramidal cells tuned to fire at a particular phase of the cycle but inhibition will fluctuate across different functional domains of the cell surface as discrete interneuronal populations are actively recruited in a stereotyped and coordinated pattern of network activity. The functional consequences of such orchestration remain to be tested experimentally but modelling studies suggest an important role in memory encoding and recall within the CA1 microcircuits (Cutsuridis et al., 2009).

Gamma Oscillations

Gamma activity occurs often during theta oscillations ("nested theta-gamma activity") and shows strong modulation during the theta cycle: gamma activity has large amplitude on the peak and small amplitude during the trough. Pyramidal cell discharge probability shows a reverse theta modulation (i.e. silent at the peak and discharge at the trough) but the cells also show phase-locked activity to gamma activity and fire preferentially at the trough of the gamma cycles (Bragin et al., 1995; Csicsvari et al., 2003; Tukker et al., 2007). Many interneurons fire at high frequency and show modulation during gamma activity. However, as with theta activity, the different types are active at distinct phases of the oscillatory cycle (Tukker et al., 2007; Table 1 and Fig. 2).

PV-positive basket and axo-axonic cells are active when gamma activity is strong at the theta peak. Although their gamma modulation is relatively weak, they fire mostly at the trough or the ascending phase of the gamma cycle, together with or shortly after pyramidal cells. These interneurons, therefore, most likely provide an important contribution to the generation of the strong gamma activity observed during the theta cycle.

CCK-positive interneurons also display high activity when gamma activity is strong at the theta peak. Within the gamma cycle, though, these interneurons fire slightly earlier than PV-positive interneurons, at the gamma trough (Tukker et al., 2007). Thus, inhibition mediated by CCK-containing cells is strongest when pyramidal cell discharge probability reaches its maximum during gamma oscillations, suggesting that inhibition by these interneurons may serve to threshold principal cell activity rather than participate directly in the generation of the oscillations.

Somewhat surprisingly, dendrite-inhibiting bistratified cells show the strongest gamma phase-modulated activity among interneuron classes investigated so far. This is especially interesting because bistratified cells fire preferentially when gamma activity is the weakest at the theta trough. Within the gamma cycle, bistratified interneurons discharge at the trough or the ascending phase and thereby provide phasic inhibition which may act to entrain pyramidal cell activity (most other cell types being inactive during this period).

O–LM and certain GABAergic projection cells show only a very weak gamma-modulated activity and likely do not contribute to gamma synchronization (Tukker et al., 2007). Ivy cells with their relatively slow action potential kinetics are sparsely active during gamma episodes but when active, are nevertheless phase modulated to the gamma cycle, firing at the trough of the extracellular field oscillation (Fuentealba et al., 2008).

Sharp Wave-Associated Ripples

Different from theta-gamma activity, sharp wave-associated high-frequency ripple oscillations occur during consummatory behavioural and are believed to play a role in memory consolidation. During sharp wave-associated ripple episodes

PV-expressing basket cells and bistratified cells discharge at high frequency (Fig. 2; Klausberger et al., 2003, 2004). Basket cells fire in the middle of ripple episode when the amplitude of ripple oscillations is the highest. Bistratified cells in contrast increase their firing rate already shortly before the episode starts and continue to fire at high frequency through the whole ripple episode. Interestingly, PV-expressing axo-axonic cells also increase their firing frequency transiently at the beginning of the ripples, but become silent from the peak of the ripple episode. The rapid phasic $GABA_A$-receptor-mediated inhibition provided by these interneurons, in particular by BCs, is thought to be essential in structuring the high-frequency activity of the population.

In contrast to the highly stereotyped activity of PV-expressing interneurons, CCK-positive interneurons, both basket cell and dendritic inhibitory cells, discharge at low frequencies and show a variable activity pattern during ripple episodes (Klausberger et al., 2003). The difference between these two families of interneurons may indicate that PV-positive interneurons provide a reliable global clock signal to the entire network whereas the variability of CCK basket cell activity may suggest a dynamic role. These interneurons may be recruited in the formation of transient and local cell assemblies.

Interestingly, long-range double-projection neurons are one of the most active intereneuron types during ripple episodes (Jinno et al., 2007). The high activity is likely to be driven by the strong recurrent excitatory input from local pyramidal cells. As a major output of these cells is directed to the medial septum, their activity conceivably leads to the suppression of septal GABAergic and cholinergic neurons and prevents the generation of theta oscillations (Jinno et al., 2007). In contrast, O–LM cells, which also receive a strong recurrent excitatory input from pyramidal cells (Blasco-Ibanez and Freund, 1995), are surprisingly suppressed during ripple activity. A possible explanation for this difference could be that release probability at pyramidal cell-O–LM synapses might be very low and O–LM cells may receive strong inhibition from interneuron-specific interneurons. The importance of the silencing of O–LM cells during ripple activity is unknown, but the reduction in slow inhibition to the apical dendrites may play a role in enabling the high-frequency activity of both PV-expressing interneurons and principal cells, thereby promoting or even initiating the ripple episode. Loss of inhibition to the dendrites may also facilitate synaptic plasticity.

While the firing patterns described above were, for technical reasons, all obtained under anaesthesia, the characteristic and stereotyped patterns of firing activity were nevertheless similar to patterns of activity seen in unidentified interneurons in the behaving animal (Csicsvari et al., 1999), suggesting that the patterns observed were not an artefact of the anaesthetic upon the hippocampal circuits.

In summary, an accumulating body of evidence indicates that morphologically and presumably, functionally distinct, interneurons are differentially active in a finely orchestrated temporal pattern of activity within the intact hippocampal network. The resultant temporal sculpting of inhibition is hypothesized to have a profound yet specific impact of the dynamical processing of hippocampal circuits. If, as appears to be the case, converging forms of inhibition across the surface

of pyramidal cells has to be segregated in time, this would explain why a single GABAergic input or cell type would inadequate to provide the necessary spatial and temporal segregation. In addition, it would help explain the extraordinary diversity that has developed within the GABAergic interneuron population and the critical necessity to understand this system in much greater detail.

Experimental Techniques

The relative advantages and disadvantages of the various recording configurations have been described earlier in this and in other chapters. When considering interneuronal activity it is essential to identify the specific cell type being investigated and this invariably involves labelling of the cell with a marker (e.g. biocytin, neurobiotin) and subsequent *post hoc* processing. Two major approaches were applied previously: sharp microelectrode and juxtacellular recording techniques. Microelectrode recordings provide intracellular electrophysiological data in combination with intracellular labelling of single neurons but the impalement may result in substantial damage to the neurons and an electric shunt reducing the quality of the recording. The juxtacellular technique (Pinault, 1996) is an extracellular recording method; therefore it is less damaging to the neurons. The microelectrode is positioned close to a neuron to pick up its discharge (as "unit activity") superimposed on the local field potential. Labelling of the cell is performed by iontophoretic application of the dye through the recording pipette. With both methods, there is of course a potential to label neighbouring cells through leakage of the neurobiotin or through gap-junction-mediated transfer. As with any invasive technique, there is the potential for the recording electrode to influence the activity of the cell being recorded through damage or mechanical manipulation. In addition to labelling the recorded cell, it is also highly desirable to label the cell with various markers for interneuronal subtypes by using immunocytochemical staining as this can greatly facilitate the further categorization of the cells being considered. However, combining these approaches is not trivial and it is common to develop incomplete data sets where one or more of these variables are missing.

Apart from the recording and identification issues, in vivo recording presents a number of specific variables and considerations. For instance, the anaesthetic agent and the depth of anaesthesia is an important determinant in terms of the oscillatory network states generated and whether such activities are spontaneous and require stimulating as in the case of theta oscillations following foot-pinch (Klausberger et al., 2003). Indeed, different anaesthetics may have differential effects throughout the hippocampal network and on different synapses. For instance two anaesthetics commonly used in studies of this type are ketamine and urethane which affect glutamatergic transmission (NMDA receptors) and GABAergic transmission ($GABA_A$ receptors), respectively. Another variable is the species and strain of experimental animal used. For instance, Wistar rats have been shown to develop ultra-slow hippocampal oscillations which are not apparent in Sprague–Dawley rats of the same age and sex (Penttonen et al., 1999).

The Future

One of the major limitations of recording extracellular signals is the inability to obtain intracellular data such as membrane potential levels and synaptic potentials at a single-cell resolution. In vivo whole cell patch-clamp recordings in anaesthetized animals and more recently in freely moving animals (Furue et al., 2007) may have tremendous future benefit by providing good quality, high-resolution intracellular data on action potential kinetics as well as subthreshold electrical activities. Furthermore, such recordings will enable the stimulation, suppression or other interference with ongoing activity of single neurons. Patch-clamp studies may also enable more rapid and reliable labelling of neurons as well as stability of recording. Until recently, such recordings from the hippocampus have remained a major technical challenge due to the inaccessibility of the hippocampus behind the overlying neocortex. However, recent progress in this area is beginning to open up possibilities for such detailed single-cell in vivo experiments in hippocampal areas (Lee et al., 2006, 2009).

The recent development of in vivo *optical* imaging techniques has enabled monitoring of the structure and activity of neurons in vivo (Hillman, 2007). While most studies have focussed on superficial cortical areas, the combined application with fibre optic technology means it is now possible to monitor deeper brain structures such as the hippocampus.

Finally, as indicated in other chapters, great strides are also being made in the use of genetic approaches to dissect the functional properties of defined neural circuits. The cell-type specific expression of sensors for free calcium, membrane potential and intracellular signalling will not only be valuable for investigating the activity of single neurons and neuronal populations but such approaches can also be used to perturb specific cells and circuits so that their roles within the intact hippocampal network can be assessed in vivo (Luo et al., 2008).

Further Reading

Acsády L, Kamondi A, Sik A, Freund T, Buzsáki G (1998) GABAergic cells are the major postsynaptic targets of mossy fibers in the rat hippocampus. J Neurosci 18:3386–3403.

Andersen P, Langmoen IA (1980) Intracellular studies on transmitter effects on neurones in isolated brain slices. Q Rev Biophys 13:1–18.

Blasco-Ibanez JM, Freund TF (1995) Synaptic input of horizontal interneurons in stratum oriens of the hippocampal CA1 subfield: structural basis of feed-back activation. Eur J Neurosci 7: 2170–2180.

Bragin A, Jando G, Nadasdy Z, Hetke J, Wise K, Buzsáki G (1995) Gamma (40–100 Hz) oscillation in the hippocampus of the behaving rat. J Neurosci 15:47–60.

Buhl EH, Halasy K, Somogyi P (1994) Diverse sources of hippocampal unitary inhibitory postsynaptic potentials and the number of synaptic release sites. Nature 368:823–828.

Buzsáki G, Eidelberg E (1983) Phase relations of hippocampal projection cells and interneurons to theta activity in the anesthetized rat. Brain Res 266:334–339.

Buzsáki G, Chrobak JJ (1995) Temporal structure in spatially organized neuronal ensembles: a role for interneuronal networks. Curr Opin Neurobiol 5:504–10.

Cobb SR, Buhl EH, Halasy K, Paulsen O, Somogyi P (1995) Synchronization of neuronal activity in hippocampus by individual GABAergic interneurons. Nature 378:75–78.
Csicsvari J, Jamieson B, Wise KD, Buzsáki G (2003) Mechanisms of gamma oscillations in the hippocampus of the behaving rat. Neuron 37:311–322.
Csicsvari J, Hirase H, Czurko A, Mamiya A, Buzsáki G (1999) Oscillatory coupling of hippocampal pyramidal cells and interneurons in the behaving Rat. J Neurosci 19:274–287.
Cutsuridis V, Cobb S, Graham BP (2009) Encoding and retrieval in a model of the hippocampal CA1 microcircuit. Hippocampus.
Foster DJ, Wilson MA (2006) Reverse replay of behavioural sequences in hippocampal place cells during the awake state. Nature 440:680–683.
Fuentealba P, Begum R, Capogna M, Jinno S, Marton LF, Csicsvari J, Thomson A, Somogyi P, Klausberger T (2008) Ivy cells: a population of nitric-oxide-producing, slow-spiking GABAergic neurons and their involvement in hippocampal network activity. Neuron 57:917–929.
Fujita Y (1975) Two types of depolarizing after-potentials in hippocampal pyramidal cells of rabbits. Brain Res 94:435–446.
Fujita Y, Sato T (1964) Intracellular records from hippocampal pyramidal cells in rabbit during theta rhythm activity. J Neurophysiol 27:1012–1025.
Furue H, Katafuchi T, Yoshimura M (2007) In vivo patch-clamp technique. In: Walz W (ed) Neuromethods: Patch-clamp analysis, 2nd edn., pp 229–251, Humana Press, Totowa.
Gloveli T, Dugladze T, Saha S, Monyer H, Heinemann U, Traub RD, Whittington MA, Buhl EH (2005) Differential involvement of oriens/pyramidale interneurons in hippocampal network oscillations in vitro. J Physiol 562:131–147.
Hájos N, Pálhalmi J, Mann EO, Németh B, Paulsen O, Freund TF (2004) Spike timing of distinct types of GABAergic interneuron during hippocampal gamma oscillations in vitro. J Neurosci 24:9127–9137.
Henze DA, Buzsáki G (2001) Action potential threshold of hippocampal pyramidal cells in vivo is increased by recent spiking activity. Neuroscience 105:121–130.
Henze DA, Buzsáki G (2007) Hilar mossy cells: functional identification and activity in vivo. Prog Brain Res 163:199–216.
Hillman EM (2007) Optical brain imaging in vivo: Techniques and applications from animal to man. J Biomed Opt 12:051402.
Jinno S, Klausberger T, Marton LF, Dalezios Y, Roberts JD, Fuentealba P, Bushong EA, Henze D, Buzsáki G, Somogyi P (2007) Neuronal diversity in GABAergic long-range projections from the hippocampus. J Neurosci 27:8790–8804.
Kandel ER, Spencer WA (1961) Electrophysiology of hippocampal neurons. II. After-potentials and repetitive firing. J Neurophysiol 24:243–259.
Kandel ER, Spencer WA, Brinley FJ, Jr. (1961) Electrophysiology of hippocampal neurons. I. Sequential invasion and synaptic organization. J Neurophysiol 24:225–242.
Klausberger T, Somogyi P (2008) Neuronal diversity and temporal dynamics: The unity of hippocampal circuit operations. Science 321:53–57.
Klausberger T, Magill PJ, Marton LF, Roberts JD, Cobden PM, Buzsáki G, Somogyi P (2003) Brain-state- and cell-type-specific firing of hippocampal interneurons in vivo. Nature 421: 844–848.
Klausberger T, Marton LF, Baude A, Roberts JD, Magill PJ, Somogyi P (2004) Spike timing of dendrite-targeting bistratified cells during hippocampal network oscillations in vivo. Nat Neurosci 7:41–47.
Klausberger T, Marton LF, O'Neill J, Huck JH, Dalezios Y, Fuentealba P, Suen WY, Papp E, Kaneko T, Watanabe M, Csicsvari J, Somogyi P (2005) Complementary roles of cholecystokinin- and parvalbumin-expressing GABAergic neurons in hippocampal network oscillations. J Neurosci 25:9782–9793.
Lee AK, Epsztein J, Brecht M (2009) Head-anchored whole-cell recordings in freely moving rats. Nat Protoc 4:385–392.

Lee AK, Manns ID, Sakmann B, Brecht M (2006) Whole-cell recordings in freely moving rats. Neuron 51:399–407.

Li XG, Somogyi P, Tepper JM, Buzsáki G (1992) Axonal and dendritic arborization of an intracellularly labeled chandelier cell in the CA1 region of rat hippocampus. Exp Brain Res 90: 519–525.

Li XG, Somogyi P, Ylinen A, Buzsáki G (1994) The hippocampal CA3 network: An in vivo intracellular labeling study. J Comp Neurol 339:181–208.

Luo L, Callaway EM, Svoboda K (2008) Genetic dissection of neural circuits. Neuron 57:634–660.

Miles R, Tóth K, Gulyás AI, Hájos N, Freund TF (1996) Differences between somatic and dendritic inhibition in the hippocampus. Neuron 16:815–823.

O'Keefe J, Dostrovsky J (1971) The hippocampus as a spatial map. Preliminary evidence from unit activity in the freely-moving rat. Brain Res 34:171–175.

Penttonen M, Nurminen N, Miettinen R, Sirvio J, Henze DA, Csicsvari J, Buzsaki G (1999) Ultra-slow oscillation (0.025 Hz) triggers hippocampal after discharges in Wistar rats. Neuroscience 94:735–743.

Pinault D (1996) A novel single-cell staining procedure performed in vivo under electrophysiological control: Morpho-functional features of juxtacellularly labeled thalamic cells and other central neurons with biocytin or Neurobiotin. J Neurosci Methods 65:113–136.

Sik A, Penttonen M, Buzsáki G (1997) Interneurons in the hippocampal dentate gyrus: an in vivo intracellular study. Eur J Neurosci 9:573–588.

Sik A, Penttonen M, Ylinen A, Buzsáki G (1995) Hippocampal CA1 interneurons: An in vivo intracellular labeling study. J Neurosci 15:6651–6665.

Sik A, Ylinen A, Penttonen M, Buzsáki G (1994) Inhibitory CA1-CA3-hilar region feedback in the hippocampus. Science 265:1722–1724.

Soltesz I, Deschênes M (1993) Low- and high-frequency membrane potential oscillations during theta activity in CA1 and CA3 pyramidal neurons of the rat hippocampus under ketamine-xylazine anesthesia. J Neurophysiol 70:97–116.

Soltesz I, Bourassa J, Deschênes M (1993) The behavior of mossy cells of the rat dentate gyrus during theta oscillations in vivo. Neuroscience 57:555–564.

Tukker JJ, Fuentealba P, Hartwich K, Somogyi P, Klausberger T (2007) Cell type-specific tuning of hippocampal interneuron firing during gamma oscillations in vivo. J Neurosci 27:8184–8189.

Turner DA, Li XG, Pyapali GK, Ylinen A, Buzsáki G (1995) Morphometric and electrical properties of reconstructed hippocampal CA3 neurons recorded in vivo. J Comp Neurol 356:580–594.

Ylinen A, Soltesz I, Bragin A, Penttonen M, Sik A, Buzsáki G (1995) Intracellular correlates of hippocampal theta rhythm in identified pyramidal cells, granule cells, and basket cells. Hippocampus 5:78–90.

Spatial and Behavioral Correlates of Hippocampal Neuronal Activity: A Primer for Computational Analysis

Howard Eichenbaum

Overview

Hippocampal neurons are extraordinarily interesting to observe in action. As animals perform a variety of natural or learned behaviors, hippocampal principal cells of areas CA1 and CA3, which otherwise are characterized by very low baseline firing rates, suddenly fire at rapid rates related to the current location of the animal, its ongoing behavior, specific salient stimuli, or some combination of these factors and the context of the behavioral situation. Unlike in many brain areas where specific sensory or behavioral correlates of neuronal activity are difficult to observe, in the hippocampus it sometimes seems there are as many behavioral correlates as experimental paradigms in which they might be observed. The challenge is not to find correlates of neural activity in the hippocampus – it is to make sense of the broad range of sensory- and behavior-related firing properties observed.

Here I will provide an overview of the literature on spatial and behavioral correlates of hippocampal neural activity. This is a large literature, so this review will not be comprehensive. Rather, my aim is to sketch the breadth of the correlates observed and to provide a framework for thinking about these properties and how they might be modeled. More detailed analyses and large lists of citations to the primary experimental literature are available in recent reviews (Eichenbaum et al., 1999; Eichenbaum, 2004; Leutgeb et al., 2005b; McNaughton et al., 2007).

I will begin with a summary of the anatomy of the medial temporal lobe system in which the hippocampus is a central component. In all biological systems, function follows form and the hippocampus is no exception. Understanding the functional properties of hippocampal neuronal activity should be helped considerably by an appreciation of the information contained in neural activity observed in areas that send inputs to the principal neurons of hippocampus. In this section I will argue that the hippocampus is a convergence site for highly processed information about space (the so-called where, or dorsal stream of the cerebral cortex) and about objects (the

H. Eichenbaum (✉)
Center for Memory and Brain, Boston University, Boston, MA 02215, USA
e-mail: hbe@bu.edu

V. Cutsuridis et al. (eds.), *Hippocampal Microcircuits*, Springer Series in Computational Neuroscience 5, DOI 10.1007/978-1-4419-0996-1_10,

"what" or ventral stream). From this perspective, the unsurprising outcome is that major correlates of hippocampal neural activity reflect both these kinds of information.

This will be followed by a discussion of the spatial coding features of hippocampal neural activity. These are the easiest to observe and the most commonly studied properties of hippocampal neural activity. While many hippocampal neurons fire associated with the current location of an animal, it should not be assumed the hippocampus provides a map of space, nor that the function of the hippocampus is navigation. The distinctions between place coding, map building, and navigation will be highlighted.

Then I will consider the nonspatial firing properties of hippocampal neurons. It will be argued that hippocampal neurons do not reflect simple sensory perceptions or behavioral actions, but rather that sensory and behavioral events are also a major component of the information encoded by hippocampal neuronal activity.

A consensual general view is that the hippocampus does not so much encode the specific details of events (or places) but rather encodes a sufficient "gist" of events to generate some sort of index that points to where the details can be found in the cortical areas that provide the detailed inputs to the hippocampus and receive its outputs. Furthermore, it is believed that the hippocampus must also represent information about the spatial and temporal context in which events occurred, in order to select event representations that should be regenerated in the cortex to support remembering. Therefore I will also consider evidence that hippocampal neurons encode contextual information about where events occurred and about the order in which they happened.

These considerations then will be combined in a framework I have offered called the "memory space" hypothesis of hippocampal neuronal representations. According to this view, hippocampal neurons encode events as associations among stimuli and places; they represent episodes as sequences of events; and hippocampal ensembles represent networks of memories as linked events and episodes. Such a framework matches the functional role of the hippocampus in memory as described by a convergence of cognitive and neuroscience approaches.

The Data

Input/Output Circuitry and the Information Contained in Inputs to the Hippocampus

The hippocampus receives inputs from widespread areas of the neocortex and olfactory cortex that are relayed via the parahippocampal region, a set of highly interconnected cortical areas immediately surrounding the hippocampus (see Chapter "Connectivity of the Hippocampus"; also Manns and Eichenbaum, 2006). The purpose of this section is not to provide details on the anatomical circuitry of these inputs, but rather to emphasize the information they contain. Sensory information that enters

the primary cortical areas subsequently passes through multiple secondary and tertiary stages of unimodal sensory processing, ultimately arriving in the parietal, retrosplenial, and temporal association areas. Similarly, motor and emotional information that are processed in early level cortical and subcortical areas pass into association areas of the prefrontal and limbic cortex. This large set of association areas provide the inputs to the parahippocampal region.

The cortical inputs to the parahippocampal region demonstrate a systematic organization, but one that is unlike the punctate topographies that characterize the primary sensory and motor thalamocortical pathways (Suzuki and Amaral, 1994; Burwell, 2000; Manns and Eichenbaum, 2006; Fig. 1). Association areas that process unimodal sensory information about qualities of objects, e.g., superior temporal and inferotemporal cortex, are sent primarily to one component of the parahippocampal region called the perirhinal cortex. By contrast, association areas that process polymodal spatial information, e.g., parietal and retrosplenial cortex, are sent primarily to another component of the parahippocampal region called the parahippocampal cortex in monkeys and the postrhinal cortex in rats. One view of this segregation of inputs is that information from the well-known "what" (ventral) stream of visual processing, as well as its counterparts in other sensory modalities, arrives in the perirhinal cortex, whereas information from the "where" (dorsal) stream arrives in the parahippocampal cortex (Eichenbaum et al., 2007). There are connections

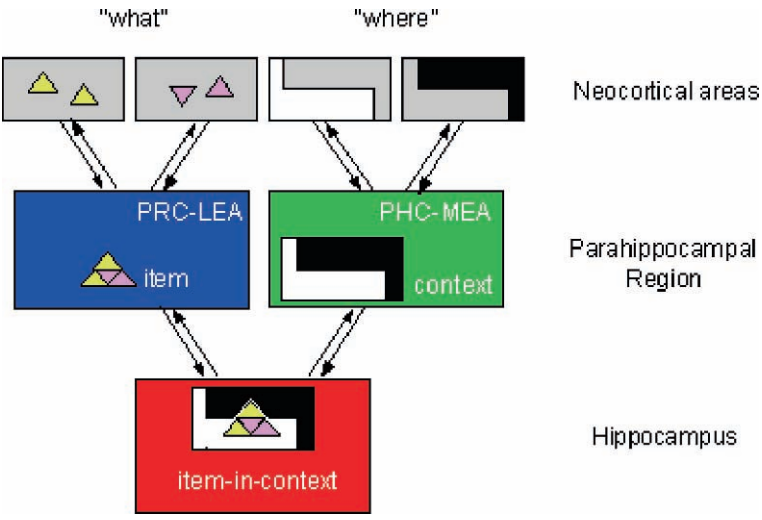

Fig. 1 Functional organization of the hippocampal memory system. Neocortical input regarding the object features ("what") converges in the perirhinal cortex (PRC) and lateral entorhinal area (LEA), whereas details about the location ("where") of objects converges in the parahippocampal cortex (PHC) and medial entorhinal area (MEA). These streams converge in the hippocampus which represents items in the context in which they were experienced. Reverse projections follow the same pathways back to the parahippocampal and neocortical regions. Back projections to the PHC-MEA may support recall or context, whereas back projections to the PHC-LEA may support recall of item associations. From Eichenbaum et al., 2007

between the perirhinal cortex and the parahippocampal cortex, but the "what" and "where" streams of processing remain largely segregated as they reach the parahippocampal region. Subsequently, the perirhinal and parahippocampal cortical areas project to the entorhinal cortex, and in doing so, maintain the segregation of "what" and "where" inputs to these areas. The lateral entorhinal area receives more cortical projections from the perirhinal cortex, whereas the medial entorhinal area receives more cortical projections from the parahippocampal cortex. There are also some connections between the perirhinal and parahippocampal cortices and between the lateral and medial entorhinal areas, but the "what" and "where" information mainly converge at the next stage, within the hippocampus.

The response properties of neurons in the parahippocampal region follow the functional differentiation suggested by the anatomy. Neurons in the perirhinal cortex of monkeys and rats respond to specific object stimuli, such as complex visual patterns and odors (Suzuki and Eichenbaum, 2000; Eichenbaum, 2000). In addition, many cells in the perirhinal cortex and lateral entorhinal area have selective responses to specific memory cues that are sustained through memory delays as animals perform short-term and working memory tasks. Also, many neurons in these areas show suppressed or enhanced responses to stimuli that are repeated, such as during the test phase of a short-term or working memory task (Brown and Xiang, 1998). These findings are consistent with observations from functional imaging studies showing diminished activation to specific verbal or pictorial stimuli in the perirhinal cortex of humans (see Eichenbaum et al., 2007). These combined findings have led to the view that perirhinal cortex, perhaps along with the lateral entorhinal area, can support a sense of familiarity with specific stimuli, even in the absence of a contribution of the hippocampus (Eichenbaum et al., 1994; Brown and Aggleton, 2001; Eichenbaum et al., 2007).

Neurons in parahippocampal cortex and medial entorhinal area, the regions that receive inputs from the "where" neocortical stream, respond to the spatial arrangement of stimuli (Wan et al., 1999; Fyhn et al., 2004; Hargreaves et al., 2005). Most prominently, neurons in the medial entorhinal area fire when an animal is in multiple places in the environment organized as a regular array environmental locations (the so-called grid cells). Cells located more dorsally in the medial entorhinal area activate associated with more punctate locations within the grid, whereas cells located more ventrally fire associated with larger areas within the grid. Like hippocampal neurons (see below), grid cell activity can also reflect an animal's orientation and speed of movement, as well as contextual features (Sargolini et al., 2006; Lipton et al., 2007). Notably, the closely associated parahippocampal cortex of humans is activated when subjects view spatial scenes or objects that generate associations with particular spatial contexts (Epstein and Kanwisher; 1998; Bar and Aminoff, 2003). The combined observations from all these studies suggest a functional organization in which nonspatial object representation occurs in the perirhinal-lateral entorhinal "what" stream, spatial, and perhaps other aspects of context are represented in the parahippocampal-medial entorhinal "where" stream, and that one critical role of the hippocampus is to associate objects with the context in which they were experienced (Eichenbaum et al., 2007).

Spatial Firing Patterns of Hippocampal Neurons

Nearly all of our information on hippocampal neuronal firing patterns comes from data on CA1 and CA3 pyramidal cells in the dorsal hippocampus of rats and to a lesser extent, in mice, monkeys, and humans. There also exists substantial data on interneurons in the dorsal hippocampus – the firing patterns of these neurons corresponds closely to the theta rhythm such that interneurons tend to burst at high rates locked to theta phase.

The most striking and prevalent pattern of firing in hippocampal pyramidal cells involves selective activation when a rat is in a particular location in its environment (see Muller, 1996; Eichenbaum et al., 1999, for a more detailed reviews). These so-called place cells are typically observed by monitoring extracellularly recorded action potentials from principal cells in CA1 and CA3 of freely behaving rats. As the animal explores or merely traverses a large environment, one can readily observe dramatic increases in a place cell's firing rate when the rat arrives at a particular location, called the "place field" (Fig. 2). From a baseline of less than 1 spikes/s, the firing rate can exceed 100 Hz, although during some passes through the place field, the cell may not fire at all. Typically a large fraction of cells (40–75%) have place fields in any environment, although the low baseline firing rates may result in many cells without place fields going undetected. Place fields vary in size from

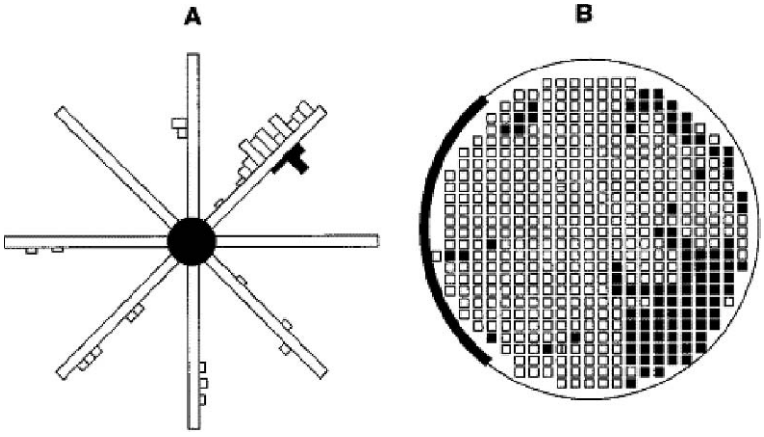

Fig. 2 Schematic overhead views of two types of apparatus and examples of location specific activity of hippocampal place cells. **a**. Eight arm radial maze where the rat can obtain a food reward the first time it reaches the end of each arm. The figure includes bar graphs on either side of the maze arms showing firing rates of a place cell associated with inward (*white bars*) and outward (*black bars*) movements on each arm. This cell fires primarily as the animal moves inward on the NE arm. From McNaughton et al., 1991. **b**. Cylinder, with the location of the cue card indicated by a thickened part of the *circle*, in which rats continuously forage for food dropped at random locations on the floor. The firing pattern of a place cell is indicated by open pixels at loci associated with low firing rates and filled pixels at loci associated with high firing rates. From Muller et al., 1987

a few centimeters to half the size of an environment and are dispersed throughout the environment, although they may be concentrated at areas of particular salience (e.g., Hollup et al., 2001)

A major issue is what cues are driving the responses of place cells. Early studies showed that spatially specific activity can be dissociated from potential confounding influences of particular behaviors that might occur at different locations. For example, Olton and colleagues (1978) observed hippocampal cellular activity in rats performing the same inward and outward traversals on all arms of a radial maze and found that many hippocampal cells fired only when the rat was on a particular arm (Fig. 2a). Muller et al. (1987) equalized behavior throughout an environment by observing hippocampal cellular activity in rats foraging in random walks for food pellets randomly dispersed in a circular open field (Fig. 2b) and found location specific activity evident in many of the events when behaviors and movement patterns were randomized.

Other studies have focused on the environmental cues that could drive spatially specific activity. Summarizing the early studies, O'Keefe (1979) defined place cells as neurons whose activity is not dependent on any particular stimulus, but rather reflects the presence and topography of multiple environmental cues. Whereas these early studies suggested that many place cells meet this criterion, more recent studies indicate that place cells are driven by relatively few relatively proximal cues. O'Keefe and Burgess (1996) showed that the shape and locus of most place fields within a simple rectangular chamber are determined by the dimensions of, and spatial relations between, only a few nearby walls of the environment. Several other recent studies have shown that place cells can encode subsets of the spatial cues and that these representations are not bound to other spatial representations in the same environment. Shapiro, Tanila, and colleagues (Shapiro et al., 1997; Tanila et al., 1997a, b, c) examined the responses of hippocampal cells to systematic manipulations of a large set of spatial cues. Different place cells encoded individual proximal and distant stimuli, combinations of proximal or distant stimuli, or relations between proximal and distant cues. The place fields of some cells were fully controlled by as little as a single cue within a very complex environment and most cells were controlled by different subsets of the controlled cues.

Gothard and colleagues (1996a, b) found that when a particularly salient cue or enclosure within an open field is moved repeatedly and randomly, the spatial firing patterns of some cells become tied to that cue. When rats were trained to shuttle between a mobile starting box and a goal location defined by landmarks in an open field, some cells fired relative to the static environmental cues, but others fired relative to a landmark-defined goal site, or in relation to the start box. When rats were trained to shuttle between a movable start-end box and goal site on a linear track, the anchor of the spatial representation of many cells switched between these two cues, depending on which was closer. Under these conditions the majority of the activated hippocampal cells did not exhibit location-specific activity that was associated with fixed environmental cues. Instead, their activity could be characterized as "spatial" only to the extent that they fired at specific distances from a particular stimulus or goal.

In addition, these and other studies have shown that place cells are not linked together to form a cohesive map of the environment. Tanila et al. (1997b) found that ensembles of simultaneously recorded place cells changed their firing patterns independently when distinct subsets of the cues at the same time, indicating that the spatial representation was not cohesive. In several cases where two cells had overlapping place fields associated with one configuration of the cues, each cell responded differently when the same cues were rearranged. This finding shows that each cell was controlled by a different subset of the cues at the same time and that their differential encodings are not due to shifts between two different spatial "reference frames" used by all cells at different times (Gothard et al., 1996b). Skaggs and McNaughton (1998) confirmed this finding by recording from a large number of place cells simultaneously in rats foraging randomly in two identical enclosures, between which they could move freely. Each hippocampal ensemble contained cells that had similar place fields and others that had distinct spatial firing patterns between the two enclosures. In this situation, some cells encoded the physical cues, whereas the activity of others at the same time reflected the knowledge that the two environments were distinct.

Combining the findings from all these studies, one can conclude that place fields reflect a collection of independent representations, each one encoding the place the animal occupies defined by a subset of cues. Spatial representations are not bound as coordinates within a systematic framework for the global topology, indicating that hippocampal spatial codings are not organized as elements of a Cartesian "map." Rather, place cells seem to encode places where important events or stimuli occur.

Nonspatial Firing Properties of Hippocampal Neurons

According to O'Keefe (1979) true place cells fire whenever an animal is in the place field, regardless of its orientation or ongoing behavior. However, few hippocampal neurons meet this criterion because nearly all of them alter their activity associated with the animal's direction and behavior in most behavioral situations. Perhaps the only situation where large numbers of true place cells are observed is when animals forage by random walk through an environment (Fig. 2b), where behavior is held constant and the meaning of movement directions is homogenious. In virtually any situation where movement directions are meaningfully different (e.g., in and out of a maze arm) or behaviors are differentiated throughout the environment, other factors dramatically influence spatial firing patterns, and in some situations where space is particularly irrelevant, some hippocampal neuronal activity can be closely linked to nonspatial stimuli and behaviors.

In many situations, spatially specific activity is influenced by meaningfully distinct movement directions. For example, in the radial maze task, where animals regularly run outward on each maze arm to obtain a reward then return to the central platform to initiate the next choice (Fig. 2a), outward and inward arm movements reflect meaningfully distinct behavioral episodes that occur repetitively.

Correspondingly, hippocampal neurons reflect the relevant "directional structure" imposed by this protocol, and almost all place cells fire only during outward or inward journeys. Similarly, place cells are activated selectively during distinct approach or return episodes and from variable goal and start locations in open fields and linear tracks. Markus et al. (1995) directly compared the directionality of place cells under different task demands and found that place cells that were nondirectional when rats foraged randomly in an open field were directional when they systematically visited a small number of reward locations. Taken together, these findings emphasize that place cells exhibit movement-related firing patterns whenever particular movements are associated with meaningfully different events.

Other studies have demonstrated firing patterns of hippocampal neurons directly related to nonspatial stimulus, cognitive, and behavioral events. In rats and rabbits performing different classical conditioning tasks, a large fraction of hippocampal neurons fire strongly associated with the learned significance of stimuli and with learned responses. Hippocampal cells begin to fire early in training, prior to the appearance of the conditioned responses, and the responses of individual cells can be related to the timing of stimuli and conditioned responses. A large fraction of hippocampal neurons are also activated in animals performing a variety of instrumental learning tasks that involve discriminations among olfactory, visual, or auditory stimuli, and delayed matching and nonmatching to sample tasks that test recognition memory (see Eichenbaum et al., 1999). Different neurons are activated during virtually every moment of task performance, including during approach and stimulus sampling behaviors, discriminative responses, and consummatory behaviors (Fig. 3).

Several recent studies suggest that some hippocampal neurons fire associated with specific stimulus, spatial, and action combinations, and their significance, and these findings show a remarkable range of information and combinations of information encoded by hippocampal neural activity. For example, Wirth et al. (2003) described hippocampal cells that change their responses to stimuli as animals learn to make a particular spatially directed behavioral response to those stimuli. Moita et al. (2003) recently reported that place cells begin to fire to tone stimuli associated with shock when a rat occupies the cell's place field. Leutgeb et al. (2005b) characterized hippocampal neurons as responding with changed firing rates when the rat occupied different small chambers within a constant large environment, but the same cells qualitatively changed firing patterns when the global environmental cues were altered. They suggested that specific events within an overall environment are encoded by a rate code within an overall consistent spatial representation. Rivard et al. (2004) described a class of place cells that fire when a rat is in proximity to a large object that occupies different positions in the environment (and even in multiple environments), as well as place cells whose activity is not influenced by the object, and yet others that fire only when the object is in a particular location. Similarly, Wood et al. (1999) described hippocampal neurons that fired associated with odorous stimuli, the location where they appeared in the environment as the animal explored them, or combinations of the odor and location (Fig. 3). In addition, the activity of some cells reflects the relevant cognitive demands of

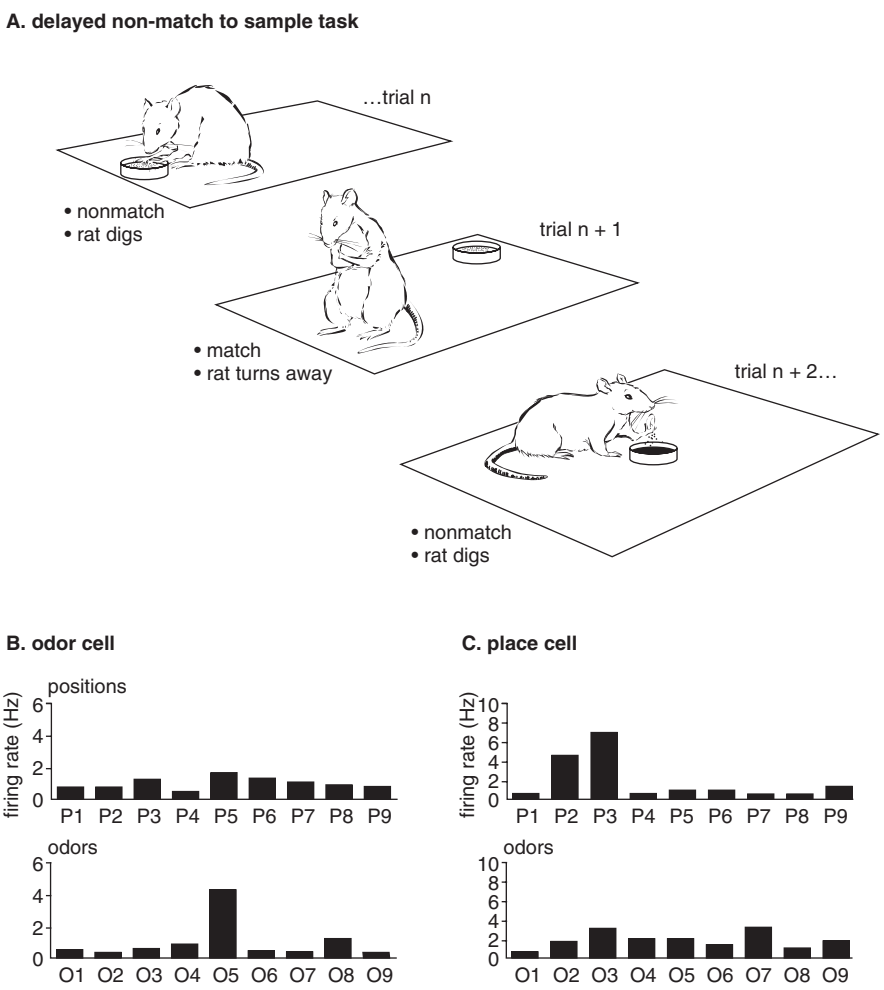

Fig. 3 Hippocampal neuronal firing patterns in rats performing an odor-delayed nonmatch to sample task (Wood et al., 1999) **a**. On each trial the rat is presented with one of nine odors at any of nine randomly selected locations. To obtain a buried reward, the rat must identify whether the odor is the same as (matches, trial n + 1) or differs from (nonmatches, trial n + 2) the odor presented on the previous trial. **Panels B** & **C** show the average firing rates of two cells associated with all the places and all the odors. **b**. This cell fires selectively when the rat samples odor 5 and this cell does not fire differentially depending on where the trial was performed. **c**. This cell fires selectively when the rat performs the trial at adjacent positions 2 & 3 and fires similarly associated with all the odors

the task, for example, the match or nonmatch relationship between stimuli when a judgment between these is required. These firing patterns could also reflect reward expectancies associated with particular stimulus contingencies (Hok et al., 2007), also observed when rats discover a new goal location (Fyhn et al., 2002).

The nonspatial firing patterns of hippocampal neurons are as robust as spatial firing patterns, whenever the neural activity can be closely time-locked to critical sensory or behavioral events and the prevalence of spatial and nonspatial firing patterns is also comparable in studies where the incidence of both types of coding was evaluated (e.g., Wood et al., 1999). This combination of findings indicates that hippocampal neurons represent a broad variety of objects, places, and object-location conjunctions as well as actions taken toward those objects and their significance.

In addition, it is notable that hippocampal neurons represent sequences of events that compose entire behavioral episodes. As animals perform virtually all behavioral tasks a series of hippocampal cells are sequentially active, consistent with the view that the hippocampus automatically encodes the flow of events in experience (Eichenbaum et al., 1999, 2004). In addition, when rats traverse routes through space the firing patterns of individual neurons are dependent on which neurons fired before and after, further suggesting sequence coding (Ferbinteanu and Shapiro, 2003). Finally, sequences of spatial firing patterns produced during specific experiences are "replayed" during subsequent sleep, consistent with the binding of sequences of firing patterns (e.g., Louie and Wilson, 2001).

Finally, both the spatial and nonspatial firing patterns of hippocampal neurons are as easily observed in behavioral tasks that do not depend upon the integrity of the hippocampus as they are in situations where the hippocampus is necessary for performance. For example, place cells are as readily observed in rats during random foraging or other spatial tasks without a memory demand, as they are in animals performing a hippocampal-dependent radial maze task. Similarly, nonspatial firing patterns were as robust and as prevalent in hippocampal cells recorded from animals performing classical conditioning or odor discrimination tasks where performance is not disrupted by hippocampal damage as in variants of the same task where hippocampal damage affects performance. Thus both nonspatial and spatial representations by hippocampal neurons are "automatic" in the sense that they arise regardless of whether task performance depends on hippocampal function.

Context

One view of hippocampal function is that the hippocampus represents the context in which specific events occur. What is meant by "context" is not clear, and whether its domain includes spatial and temporal, as well as other aspects of the situation in which events occur, is also not clear. The data suggest that all aspects of the background context in which specific events occur and when places are occupied can dramatically affect hippocampal neural activity. For example, the spatial firing patterns, and the extent to which firing is dependent on spatial orientation, are dramatically different when a rat forages randomly or produces repeated paths as it traverses an environment (Markus et al., 1995). Notably, as in most experiments, some cells fire similarly in the two situational contexts, whereas others change dramatically – showing that the hippocampus represents both the commonalities and differences in the two contextually defined situations.

Seemingly subtle changes in environmental cues can also produce dramatic changes in the spatial firing patterns of hippocampal neurons. For example, changes in the background color or background odor of an environment can dramatically change the spatial firing patterns of individual hippocampal neurons (Anderson and Jeffery, 2003). As in other studies, in this experiment some cells did not change for each contextual shift, whereas others did. What cues and the extent of situational change that causes alterations in firing patterns is not clear, but several recent studies have examined the dynamics of firing pattern changes when cues are gradually altered. For example, when the shape of an environment is gradually altered (Wills et al., 2005), or critical cues are gradually changed (Rotenberg and Muller, 1997), most place cells do not alter their firing patterns initially, but at some level of change, dramatically alter their firing patterns. This sudden switch of firing patterns when a threshold of cue alteration is passed suggests an attractor state dynamic (not unlike that of many other brain areas) in which the contextual representation switches from pattern completion to pattern separation. Area CA3 demonstrates a particularly sharp discrimination gradient in making this switch (Leutgeb et al., 2004; Lee et al., 2004). It appears that hippocampal cell assemblies can rapidly switch between spatial representations as animals perform different tasks in the same environment (Fenton et al., 1998; Jackson and Redish, 2007).

Several other recent studies have focused on changes in context defined by the behavioral demands of a task. In some of the most productive of these studies, animals traverse multiple overlapping paths such that the common places compose part of different overlapping routes. For example, in several of these studies, rats alternate left and right turn routes through a T maze, where traversal of the stem of the maze is common to both paths (Fig. 4). In this and similar tasks, many hippocampal neurons have distinct firing patterns, even when the rat traverses the common stem depending on whether the rat is performing a left-turn or right-turn trial (Wood et al., 2000; Frank et al., 2000; Ferbinteanu and Shapiro, 2003; Ainge et al., 2007; Bower et al., 2005; Lee et al., 2006; Griffin et al., 2007). Importantly, some cells fire similarly as the rat performs both routes, indicating the hippocampus represents both the distinct paths and the common elements among them. A recent extension on these findings showed that when the alternation task is separated into distinct sample and choice phases, most hippocampal neurons have different spatial firing patterns on the distinct trial phases, and within that, some cells also differentiate the two routes within each phase (Griffin et al., 2007). These data show that different contextual conditions within a complex task are represented distinctly and are linked through representations of their common features by hippocampal neurons.

Additional recent data have shown global shifts in hippocampal firing patterns during the course of events over time, suggesting a representation of temporal context. In one study, as rats performed the T-maze alternation task for 100+ trials, ensembles of simultaneously recorded place fields gradually shifted forward along the maze (Lee et al., 2006). The gradually shifting of the overall spatial representation provided information that could distinguish between sequential trials along the same left-turn or right-turn paths.

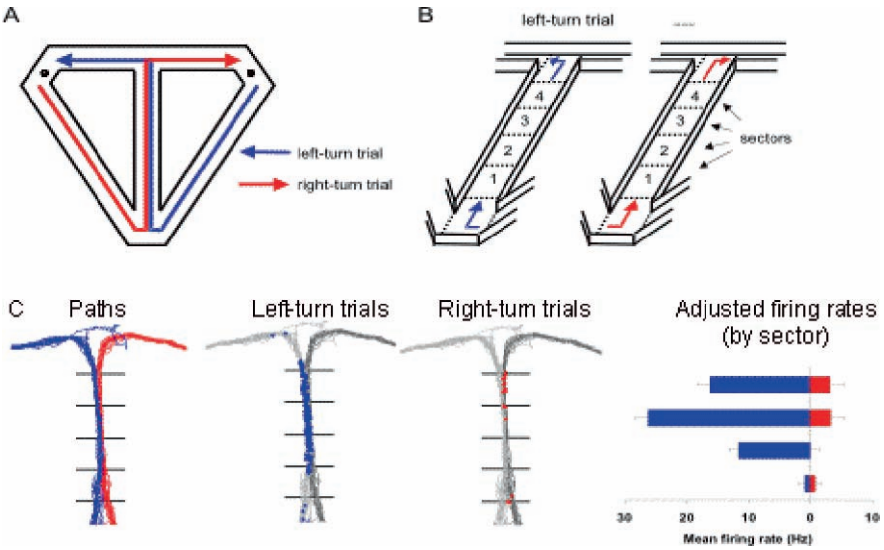

Fig. 4 Hippocampal neuronal activity as rats perform a delayed alternation task. **a**. Schematic view of the modified T-maze. Rats performed a continuous alternation task in which they traversed the central stem of the apparatus on each trial and then alternated between left and right turns at the T-junction. Reinforcement for correct alternations was provided at water ports (small *circles*) on the end of each choice arm. The rat returned to the base of the stem via connecting arms and then traversed the central stem again on the next trial. For analysis of neural firing patterns, left-turn (*blue arrow*) and right-turn (*red arrow*) trials were distinguished. Only trials that involved correct responses were included in the analyses. **b**. Schematic of the stem of the T-maze indicating divisions of the central portion of the stem into the four sectors used in the data analyses (see below) **c**. Example of a hippocampal cell that was active when the rat is traversing the central stem of the maze. This cell fired almost exclusively during left-turn trials. The paths taken by the animal are plotted in the left panel (*blue*: left-turn trial; *red*: right-turn trial). In the *middle* panels, the location of the rat when individual spikes occurred is indicated separately for left-turn trials (*blue* dots on *light grey* path) and right-turn trials (*red* dots on *dark grey* path). In the *right* panel, the mean firing rate of the cell for each sector (see **b** above) is shown separately for left-turn trials (*blue*) and right-turn trials (*red*)

In another study, rats were trained to alternate between two ends of a chamber where they sampled a sequence of odors, then were presented with two of the odors in the sequence and asked to judge their order (Fig. 5; Manns et al., 2007). In order to examine whether the firing patterns of hippocampal neurons differentiated the two spatial contexts in which odors were sampled and the temporal context in which odors were sampled within and between trials, small ensembles of hippocampal neurons were recorded around the time of odor sampling on each stimulus presentation in the sequence. The similarity of firing patterns of hippocampal ensembles was measured as the distance between *n*-dimensional population vectors wherein each dimension was the firing rate of each cell around the odor-sampling period. Hippocampal neuronal ensembles differentiated the two sampling locations and gradually changed between odor-sampling events, both within the stimulus sequence

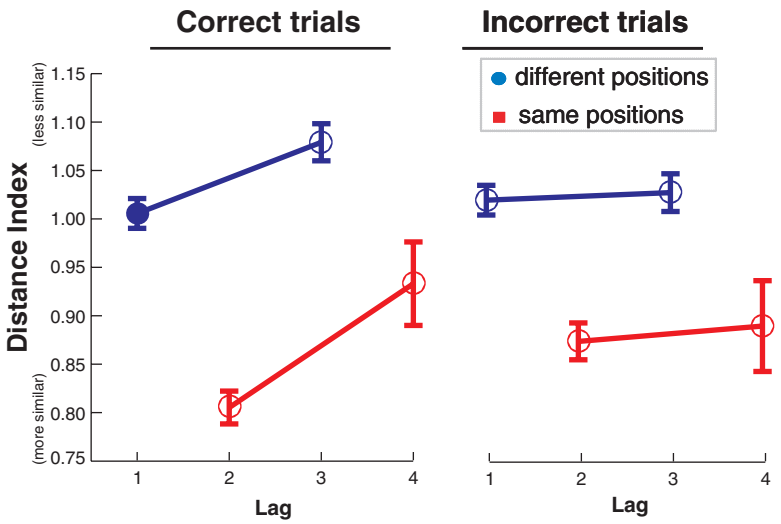

Fig. 5 Representation of temporal context supports memory for the order of a sequence of odors. This graph shows the similarity of ensemble responses according to temporal lag between odors encountered during the sample phase. Results from odors encountered in the same position (*red*) are plotted separately from odors encountered in different positions (*blue*). In addition, results from trials that were subsequently performed correctly are plotted separately from incorrect trials. A lower Distance Index corresponds to greater similarity of the population firing rates. Note steeper slopes of the lines, indicating greater change in the temporal context signal, on correct trials. From Manns and Eichenbaum, 2007

that composed each trial and across trials within a session. Moreover, the appearance of a substantial change in the contextual representation within trials predicted subsequent success in the judgment about the order of odors, whereas errors were marked by a lack of this temporal context signal. These data strongly suggest that hippocampal neural activity represents a combination of the spatial and temporal context of events both within specific experiences and across experiences over prolonged periods.

Summing Up: The Memory Space Hypothesis

What theoretical framework could capture the broad range of behavioral-related firing patterns of hippocampal neurons – and explain the role of these representations in hippocampal-dependent memory? Some have focused on the place cell phenomenon, and its variants observed in areas that are outside of and connected with the hippocampus: head direction cells and grid cells. Combinations of these behavioral firing properties have been used to formulate schemes by which the hippocampus is used in navigation and path integration (e.g., McNaughton et al., 2007). Such narrow formulations fall short of matching the range of memory that relies on

hippocampal processing (Eichenbaum et al., 2007; Squire et al., 2004). On the other hand, memory for routes does provide a good example of the kind of memory that depends on the hippocampus. When we remember a spatially extended episode, one recalls a starting point, a series of landmarks and turns in the path one takes, turns examined with thoughts of where they would have led but then rejected, prospects of choices made, and finally what one discovered at the end of the route. Expanding on the example of spatial memories, we employ similar recollective processing to remember the twisting plot of a complex action thriller, the relationships and interactions among characters in a soap opera, and the scientific history and relationships among our own colleagues.

All of these examples highlight three central features in association prominent in the firing properties of hippocampal neurons and hippocampal-dependent memory. First, specific items, persons, and events are represented in the spatial and temporal context in which they occur. This is why spatial representations are both always prominent and strongly dependent on the objects and actions associated with locations. Second, representations of events are bound in sequences that compose distinct episodes. Such time-binding explains the dependence of hippocampal representations on past and future events and supports the ability to remember the order of events in experiences. Third, event and episode representations are linked by common features of experience. These "nodal" events are reflected in the firing patterns of hippocampal neurons that are activated for a particular stimulus experienced in many different locations (Fig. 3b; Wood et al., 1999) or object features common to many stimuli (Hampson et al., 2004) or particular people presented in different scenarios (e.g., "Bill Clinton cells"; Kreiman et al., 2000). These nodal representations support our capacity to weave experiences into networks of memories. Remembering routes through the environment, action thrillers, soap operas, and collegial organizations are exceptionally vivid examples of each of these features of memory, and they reflect the fundamental features of declarative memory. The mission of modeling hippocampal function, in the view of this experimentalist, is to explain the mechanisms and structures of the hippocampal memory space and how it interacts with cortical areas to encode and generate the details of declarative memories.

Experimental Techniques

The state-of-the-art method for recording the extracellular spike activity of hippocampal neurons involves the tetrode array, a set of independently driven electrodes, each composed of four twisted 12–13 μm insulated wires gold plated at the exposed surface that is in contact with the brain tissue. Electrodes are connected to a head stage that typically includes a unity gain preamplifier for each wire used to decrease the impedance of the signal to be passed on. Signals are fed through a multiwire cable, often using a commutator to prevent cable twisting, to an A/D converter as the interface to a computer workstation, which digitizes the spike waveforms at high speed (e.g., 30 kHz).

The close spacing of the four individual wires within each tetrode makes it likely that multiple wires will record the activity of a neuron whose cell body or axon is in proximity with the electrode tips. Each channel is likely to differ slightly in distance or area of contact with the neuron resulting in slightly differing waveforms of the action potential from each wire within a tetrode. Furthermore, when a tetrode is driven into a densely packed cell layer, such as found in the pyramidal cell layers of CA1 and CA3, wires are likely to record from several different cells, each characterized by a unique profile of action potential waveforms among the four wires within a tetrode. To isolate individual neurons, software programs compare the amplitude, width, and other parameters of spikes across wires within the tetrode, yielding distinct scatter plots of spike waveform clusters associated with different neurons for each parameter compared (Fig. 6). Each tetrode typically records the activity of up to approximately 6–8 isolatable cells, and tetrode arrays often have as many as 12–14 closely spaced electrodes, providing a realistic capability of simultaneous recording of 50–100+ neurons (Wilson and McNaughton, 1993). Tetrodes perform well in recording from pyramidal cells, and less well in recording interneurons, presumably because of their smaller cell body size, and success is rare in recording action potentials from dentate granule cells. Tetrodes are also suitable for recording extracellular local field potentials.

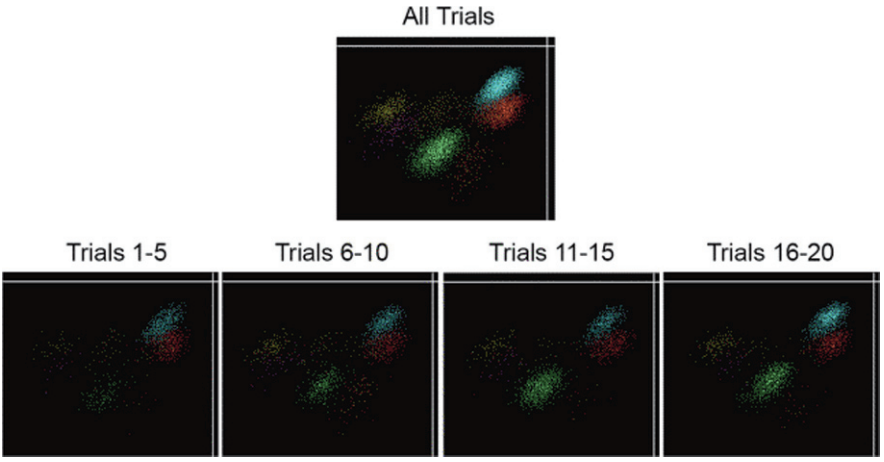

Fig. 6 Example data from one tetrode showing similar projections of spike waveform clusters across quartiles of a recording session in the test of memory for the order of a series of odors. Individual points correspond to neuronal spikes and are colored to represent the different neurons recorded on this tetrode. The *Y* axis shows the amplitude of each spike as it was recorded on one wire of the tetrode, and the *X* axis shows the amplitude of another wire from the same tetrode. The clusters are similar in each of the session quartiles, indicating that no tetrode movement occurred over the long recording session. From Manns and Eichenbaum, 2007

Once cells are isolated, spike trains are saved as lists of the time of arrival of spikes along with the onset times of behavioral parameters including task relevant stimuli and behaviors. In many experiments, the position of the animal's head is

also recorded at regular intervals (e.g., 30–60/s) by placing one or more lamps on the head stage and using a camera system to isolate the location if the lamps with the environment in an X–Y coordinate system. The firing rates of individual neurons are typically related to the onset or period of specific events by peri-event histograms (PETHs), and neuronal activity is usually considered related to a stimulus or event if the firing rate is reliably changed just after event onset compared to a baseline period before event onset, as tested with standard parametric statistical methods. Sometimes the selectivity of firing associated with different stimuli or events is characterized by comparing firing rates during specified event periods, and testing for reliable differences between multiple repetitions of each different stimulus or event.

Spatial firing patterns are typically assessed by dividing the environment into a two-dimensional array of location pixels of 1–3 cm^2. Firing rate for each pixel is calculated as the number of spikes per second occupancy in the pixel. Often firing rates are smoothed by a weighted average of a target pixel and all surrounding pixels. Place fields are usually defined as a set of adjacent pixels that meet a firing rate criterion, e.g., above 1 Hz, 2 SD above the overall average firing rate. Similarity or difference in spatial firing patterns between conditions is typically measured by correlating activity among pixels in a pair of firing rate maps.

A major problem in comparing sensory-behavioral and spatial firing patterns of hippocampal neurons involves technical requirements for collecting data for each type of analysis. To collect multiple samples of recordings during well-controlled behavioral events, which is required to assess the statistical reliability sensory-behavioral correlates, one needs to have several repetitions of each discrete event. By contrast, to collect spatial firing patterns independent of behavior, one needs to have the animal occupy all locations in the environment many times in constant or randomly changing behavioral patterns. These demands for data collection in behavioral and spatial characterizations are mutually exclusive and make it impossible to simultaneously determine sensory-behavioral and spatial correlates of activity.

Some of the best examples where both kinds of information have been obtained come from studies where the environment is “linearized”, that is, the animal moves along a narrow track that restricts its movements to one dimension and all locations are automatically occupied as the animal moves along a linear, rectangular, or circular track, and when specific behaviors or stimuli occur at particular locations that can be changed in some way relevant to the task under study. The continuous T-maze alternation task (Fig. 4a) is a particularly successful and productive example of such a protocol. Animals move throughout the maze every other trial, alternating left-turn and right-turn routes that overlap in the maze stem, and firing patterns associated with past or future locations and accuracy of decisions can readily be determined. Several variants on this task have provided opportunities to study many aspects of memory, movement, and decision processes.

The Future

The near future will surely bring continued investigation of potential differences in the spatial- and behavior-related firing patterns of neurons in different subfields and

along the dorsal–ventral axis of the hippocampus as well as in the structures that send inputs into and receive the outputs of neurons in the hippocampus. Progress in providing sufficient information for constructing models of the functional microcircuitry of the hippocampus surely depends on characterizations of the major cell types in all the hippocampal subfields and areas to which they are connected. In addition, we have only begun to scratch the surface of characterizing the time series of firing patterns, particularly in relation to local rhythmic activity that can be recorded along with spikes.

Another dilemma that has to be resolved is how to combine the prevalence and ease of recording spatial firing patterns with the need to relate firing patterns to the kinds of learning and memory that are dependent on hippocampal function. Because it is so difficult to align electrodes to record from large numbers of neurons simultaneously, many of the best recording studies have maximized recording yield by minimizing the concurrent demands of the behavioral task. In many of these studies, the behavior is trivialized to asking the rat to merely find food scattered in the environment. Experimenters assume that learning occurs when this behavior is executed under conditions of novel environmental stimuli, but the protocol lacks any metric or evidence that learning has actually occurred or when it occurred. This strategy severely limits the extent and precision to which firing patterns can be linked to memory processes. Ultimately, methods must be found to maximize the recording yield while incorporating sufficient behavioral content to allow meaningful interpretation of the observed firing patterns.

Another challenge for the longer range future will be to isolate where within the hippocampus particular sensory, behavioral, or spatial firing patterns arise. Because subfields and components of the hippocampal region are highly interconnected, it can be expected that firing patterns that reflect a specific aspect of memory processing will be projected to several other closely connected areas. In order to localize the origins of particular firing patterns, new advances will be required to record from specific hippocampal subfields while the activity in other subfields is silenced, and preferably the silencing can be reversible so that activity patterns can be compared in intact versus disconnected conditions.

The long-range future of recording behavior-related firing patterns in the hippocampus is bright, despite the above-described challenges. Activity patterns of hippocampal neurons provide a crucial bridge between cellular plasticity phenomena, local and global circuitry, overt behavior and cognition. This bridge will be required to show how intracellular processes and microcircuit connectivity leads to functional activity of the information processing units that generate behavior.

Further Reading

Ainge JA, Tamosiunaite M, Woergoetter F, & Dudchencko PA (2007) Hippocampal CA1 place cells encode intended destination on a maze with multiple choice points. J Neurosci 27: 9769–9779.

Anderson MI, & Jeffery KJ (2003) Heterogeneous modulation of place cell firing by changes in context. J Neurosci 23: 8827–8835.

Bar M, & Aminoff E (2003) Cortical analysis of visual context. Neuron 38: 347–358.

Best PJ, White AW, & Minai A (2001) Spatial processing in the brain: The activity of hippocampal place cells. Annu Rev Neurosci 24: 459–486.
Bower MR, Euston DR, & McNaughton BL (2005) Sequential-context dependent hippocampal activity is not necessary to learn sequences with repeated elements. J Neurosci 15: 1313–1323.
Brown MW, & Xiang JZ (1998) Recognition memory: Neuronal substrates of the judgment of prior occurrence. Prog Neurobiol 55: 149–189.
Brown MW, & Aggleton JP (2001) Recognition memory: What are the roles of the perirhinal cortex and hippocampus? Nat Rev Neurosci 2: 51–61.
Burwell RD (2000) The parahippocampal region: Corticocortical connectivity. Ann NY Acad Sci 911: 25–42.
Eichenbaum H, Otto T, & Cohen NJ (1994) Two functional components of the hippocampal memory system. Brain Behav Sci 17: 449–518.
Eichenbaum H, Dudchencko P, Wood E, Shapiro M, & Tanila H (1999) The Hippocampus memory, and place cells: Is it spatial memory or a memory space? Neuron 23: 209–226.
Eichenbaum H (2000) A cortical-hippocampal system for declarative memory. Nat Rev Neurosci 1: 41–50.
Eichenbaum H (2004) Hippocampus: Cognitive processes and neural representations that underlie declarative memory. Neuron 44: 109–120.
Eichenbaum H, Yonelinas AR, & Ranganath C (2007) The medial temporal lobe and recognition memory. Annu Rev Neurosci 20: 123–152.
Ekstrom AD, Kahana MJ, Caplan JB, Fields TA, Isham EA, Newman EL, et al. (2003) Cellular networks underlying human spatial navigation. Nature 425: 184–187.
Epstein R, & Kanwisher N (1998) A cortical representation of the local visual environment. Nature 392: 598–601.
Fenton AA, Wsierska M, Kaminsky Y, & Bures J (1998) Both here and there: Simultaneous expression of autonomous spatial memories in rats. PNAS USA, 95: 11493–11498.
Ferbinteanu J, & Shapiro ML (2003) Prospective and retrospective memory coding in the hippocampus. Neuron 40: 1227–1239.
Frank L, Brown EN, & Wilson M (2000) Trajectory encoding in the hippocampus and entorhinal cortex. Neuron 27: 169–178.
Fyhn M, Molden S, Hollup, Moser M-B, & Moser EI (2002) Hippocampal neurons responding to first-time dislocation of a target object. Neuron 35: 555–566.
Fyhn M, Molden S, Witter MP, Moser EI, & Moser M-B (2004) Spatial representation in the entorhinal cortex. Science 305: 1258–1264.
Gothard KM, Skaggs WE, Moore KM, & McNaughton BL (1996a) Binding of hippocampal CA1 neural activity to multiple reference frames in a landmark-based navigation task. J Neurosci 16: 823–835.
Gothard KM, Skaggs W, & McNaughton BL (1996b) Dynamics of mismatch correction in the hippocampal ensemble code for space: Interaction between path integration and environmental cues. J Neurosci 16: 8027–8040.
Griffin AL, Eichenbaum H, & Hasselmo ME (2007) Spatial representations of hippocampal CA1 neurons are modulated by behavioral context in a hippocampus-dependent memory task. J Neurosci 27: 2416–2423.
Hampson RE, Pons TP, Stanford TR, & Deadwyler SA (2004) Categorization in the monkey hippocampus: A possible mechanism for encoding information into memory. PNAS USA 101: 3184–3189.
Hargreaves EL, Rao G, Lee I, & Knierim JJ (2005) Major dissociation between medial and lateral entorhinal input to dorsal hippocampus. Science 5729: 1792–1794.
Hok V, Lenck-Santini P-P, Roux S, Save E, Muller RU, & Poucet B (2007) Goal-related activity in hippocampal place cells. J Neurosci 27: 472–482.
Hollup SA, Molden S, Donnett JG, Moser M-B, & Moser EI (2001) Accumulation of hippocampal place fields at the goal location in an annular watermaze task. J Neurosci 21: 1635–1644.

Jackson J, & Redish AD (2007) Network dynamics of hippocampal cell assemblies resemble multiple spatial maps within single trials. Hippocampus 17(12): 1209–1229.

Kreiman G, Koch C, & Fried I (2000) Category-specific visual responses of single neurons in the human medial temporal lobe. Nat Neurosci 3: 946–953.

Lee I, Yoganarasimha D, Rao G, & Knierim JJ (2004) Comparison of population coherence of place cells in hippocampal subfields CA1 and CA3. Nature 430: 456–459.

Lee I, Griffin AL, Zilli EA, Eichenbaum H, & Hasselmo M (2006) Gradual translocation of spatial correlates of neuronal firing in the hippocampus toward prospective reward locations. Neuron 51: 539–650.

Leutgeb S, Leutgeb JK, Treves A, Moser M-B, & Moser EI (2004) Distinct ensemble codes in hippocampal areas CA3 and CA1. Science 305: 1295–1298.

Leutgeb S, Leutgeb JK, Barnes CA, Moser EI, McNaughton BL, & Moser M-B (2005a) Independent codes for spatial and episodic memory in hippocampal neuronal ensembles. Science 309: 619–623.

Leutgeb S, Leutgeb JK, Moser M-B, & Moser EI (2005b) Place cells, spatial maps, and the population code for memory. Curr Opin Neurobiol 15: 1–9.

Lipton PA, White J, & Eichenbaum H (2007) Disambiguation of overlapping experiences by neurons the medial entorhinal cortex. J Neurosci 27: 5787–5795.

Louie K, & Wilson MA (2001) Temporally structured replay of awake hippocampal ensemble activity during rapid eye movement sleep. Neuron 29: 145–156.

Manns JR, & Eichenbaum H (2006) Evolution of the hippocampus. In J.H. Kaas, (Ed.), Evolution of nervous systems. Vol 3. (pp. 465–490) Oxford, UK: Academic Press.

Manns JR, Howard M, & Eichenbaum H (2007) Gradual changes in hippocampal activity support remembering the order of events. Neuron 56: 530–540.

McNaughton BL, Chen L, & Markus EJ (1991) "Dead reckoning", landmark learning, and the sense of direction: A neurophysiological and computational hypothesis. J Cog Neuro 3: 190–202.

McNaughton BL, Battaglia FP, Jensen O, Moser EI, & Moser M-B (2007) Path integration and the neural basis of the 'cognitive map'. Nat Rev Neurosci 7: 663–678.

Markus EJ, Qin Y-L, Leonard B, Skaggs WE, McNaughton BL, & Barnes CA (1995) Interactions between location and task affect the spatial and directional firing of hippocampal neurons. J Neurosci 15: 7079–7094.

Moita MA, Rosis S, Zhou Y, LeDoux JE, & Blair HT (2003) Hippocampal place cells acquire location-specific responses to the conditioned stimulus during auditory fear conditioning. Neuron 37: 485–497.

Muller RU, Kubie JL, & Ranck JB Jr. (1987) Spatial firing patterns of hippocampal complex spike cells in a fixed environment. J Neurosci 7: 1935–1950.

Muller RU (1996) A quarter of a century of place cells. Neuron 17: 813–822.

O'Keefe JA (1979) A review of hippocampal place cells. Prog Neurobiol 13: 419–439.

O'Keefe J, & Burgess N (1996) Geometric determinants of the place fields of hippocampal neurons. Nature 381: 425–428.

Olton DS, Branch M, & Best PJ (1978) Spatial correlates hippocampal unit activity. Exp Neuro 58: 387–409.

Rivard B, Li Y, Lenck-Santini P-P, Poucet B, & Muller RU (2004) Representation of objects in space by two classes of hippocampal pyramidal cells. J Gen Physiol 124: 9–25.

Rotenberg A, & Muller RU (1997) Variable place-cell coupling to a continuously viewed stimulus: evidence that the hippocampus acts as a perceptual system. Philos Trans R Soc Lond B 352: 1505–1513.

Sargolini F, Fyhn M, Hafting T, McNaughton BL, Witter MP, Moser M-B, Moser EI (2006) Conjunctive representation of position, direction, and velocity in entorhinal cortex. Science 312: 758–762.

Shapiro ML, Tanila H, & Eichenbaum H (1997) Cues that hippocampal place cells encode: Dynamic and hierarchical representation of local and distal stimuli. Hippocampus 7: 624–642.

Skaggs WE, & McNaughton BL (1998) Spatial firing properties of hippocampal CA1 populations in an environment containing two visually identical regions. J Neurosci 18: 8455–8466.
Squire LR, Stark CE, & Clark RE (2004) The medial temporal lobe. Annu Rev Neurosci 27: 279–306.
Suzuki WA, & Amaral DG (1994) Perirhinal and parahippocampal cortices of the macaque monkey: Cortical afferents. J Comp Neuro 350: 497–533.
Suzuki W, & Eichenbaum H (2000) The neurophysiology of memory. Ann NY Acad Sci 911: 175–191.
Tanila H, Shapiro M, Gallagher M, & Eichenbaum H (1997a) Brain aging: Impaired coding of novel environmental cues. J Neurosci 17: 5167–5174.
Tanila H, Shapiro ML, & Eichenbaum H (1997b) Discordance of spatial representation in ensembles of hippocampal place cells. Hippocampus 7: 613–623.
Tanila H, Sipila P, Shapiro M, & Eichenbaum H (1997c) Brain aging: Changes in the nature of information coding by the hippocampus. J Neurosci 17: 5155–5166.
Wan H, Aggleton JP, & Brown MW (1999) Different contributions of the hippocampus and perirhinal cortex to recognition memory. J Neurosci 19: 1142–1148.
Wiener SI, Paul CA, & Eichenbaum H (1989) Spatial and behavioral correlates of hippocampal neuronal activity. J Neurosci 9: 2737–2763.
Wills TJ, Lever C, Cacucci F, Burgess N, & O'Keefe J (2005) Attractor dynamics in the hippocampal representation of the local environment. Science 308: 873–876.
Wilson M, & McNaughton BL (1993) Dynamics of the hippocampal ensemble code for space. Science 261: 1055–1058.
Wirth S, Yanike M, Frank LM, Smith AC, Brown EN, & Suzuki WA (2003) Single neurons in the monkey hippocampus and learning of new associations. Science 300: 1578–1581.
Wood E, Dudchenko PA, & Eichenbaum H (1999) The global record of memory in hippocampal neuronal activity. Nature 397: 613–616.
Wood E, Dudchenko P, Robitsek JR, & Eichenbaum H (2000) Hippocampal neurons encode information about different types of memory episodes occurring in the same location. Neuron 27: 623–633.

Part II
Computational Analysis

Vassilis Cutsuridis and Bruce P. Graham

In the Experimental Background section, leading experimental neuroscientists discussed the morphological, physiological, and molecular characteristics as well as the connectivity and synaptic properties of the various cell types found in the hippocampus. Behavior-related ensemble activity patterns of morphologically identified neurons in anesthetized and freely moving animals provided insights into the functions of the hippocampal areas. However, this accumulation of knowledge about the neural components (e.g., genes, molecules, synapses, dendrites, single neurons, and networks) does not in itself provide conclusive insight into the computations performed in different hippocampal areas. Mathematical and computational modeling and analysis play an instrumental role in exploring these computations. They allow the synthesis of experimental data from different levels of complexity into a coherent picture of the system under study.

In this section, leading computational neuroscientists present models of the hippocampus at various levels of detail (molecular, synaptic, single cell, and network). These models make use of the knowledge presented in the Experimental Background section to discuss the overall global function of hippocampal microcircuits (areas CA1, CA3, dentate gyrus, and entorhinal cortex). Detailed models of single neuron (principal and interneuronal) computation and their synaptic plasticity rules are presented. Network models of associative memory, rhythm generation, and spatial navigation are then discussed. Finally, a chapter is dedicated to describing computer simulation environments of single neurons and networks currently used by computational neuroscientists in developing their models.

In chapter "The Making of a Detailed CA1 Pyramidal Neuron Model", Pissadaki and Poirazzi analyze the creation process of a detailed CA1 pyramidal neuron previously published in Poirazi et al. (*Neuron 37*, 977–987, 2003), and try to provide guidelines and justifications about the development and use of similar models. They describe the different validation experiments performed to constrain the model as well as its application for studying dendritic integration. They analyze the strengths

V. Cutsuridis (✉)
Department of Computing Science and Mathematics, University of Stirling,
Stirling FK9 4LA, UK,
e-mail: vcut@bu.edu

and limitations of the specific model and talk about similar modeling approaches for studying primarily issues regarding dendritic integration properties in CA1 pyramidal neurons. They conclude by discussing the "optimal" level of abstraction needed in order to understand different aspects of neuronal physiology and characterize the functional properties of CA1 pyramidal neurons.

In chapter "CA3 Cells: Detailed and Simplified Pyramidal Cell Models", Migliore, Ascoli, and Jaffe discuss the development of a detailed CA3 pyramidal neuron. They start from a set of experimental recordings and a basic set of ion channels uniformly distributed on a realistic morphology. They use a step-by-step procedure to show how all the different firing patterns exhibited by these neurons can be modeled using the properties of each channel as a tool to implement specific features of the experimental traces. Their realistic model, and its reduced single-compartment version, demonstrate how the interaction between a relatively small number of ionic currents can take into account the large range of firing properties observed in these neurons, from weakly adapting to delayed and bursting. Their results suggest specific, experimentally testable predictions on the relative contributions of the various channels to each firing pattern.

In chapter "Entorhinal Cortex Cells", Fransén presents two models of entorhinal cortex (EC) function. The first model is concerned with the cellular mechanisms giving rise to theta rhythmicity, which is central to grid field generation and memory processing. Its focus is on the stellate cell in layer II and specifically on how the ion channel I_h contributes to the cellular properties. The second model is concerned with the cellular mechanisms giving rise to sustained neuronal activity in relation to working memory. The involvement of calcium-dependent cationic currents in the generation of depolarizing plateau potentials in pyramidal cells of layers II and V is studied.

In chapter "Single Neuron Models: Interneurons", Skinner and Saraga present a step-by-step process of developing detailed models of two interneuron types – perisomatic-inhibitory fast-spiking basket cells and dendritic-inhibitory O-LM cells – from the perspective of their intrinsic properties. There are several ways in which different intrinsic properties could produce similar neuronal outputs (homeostasis). Skinner and Saraga argue that if we are to understand how the specific, intrinsic properties of interneuron subtypes contribute to hippocampal output, it is important to build detailed, single cell mathematical models of them.

In chapter "Gamma and Theta Rhythms in Biophysical Models of Hippocampal Circuits", Kopell, Börgers, Pervouchine, Malerba, and Tort focus on the main rhythms displayed by the hippocampus, the gamma (30–90 Hz), and theta (4–12 Hz) rhythms. One theme in their chapter is the interaction of gamma and theta rhythms. A second theme is the use of mathematical tools to get a deeper understanding of the dynamics of rhythmic networks. They apply these ideas mainly to the question of how networks can produce a theta rhythm from cells that do not naturally synchronize. A final theme is the use of model networks to understand how dynamics contributes to function. Using simple biophysical cell models, they concentrate on modeling in vitro experiments, but with an eye toward possible in vivo implications. All cell models have a single compartment only. They aim not so much at reproducing dynamics in great detail, but at clarifying the essential mechanisms

underlying the production of the rhythms and their interactions. In particular, they attempt to highlight the dynamical as well as physiological mechanisms associated with rhythms, and to begin to classify them by mechanisms, not just frequencies.

In chapter "Associative Memory Models of Hippocampal Areas CA1 and CA3", Graham, Cutsuridis, and Hunter present two models of associative memory function in areas CA3 and CA1 of the hippocampus. It has long been postulated that the recurrent connections between CA3 pyramidal cells enable this network to function as an autoassociative memory through Hebbian strengthening of these connections. Similarly, the feedforward connections from CA3 PCs onto CA1 pyramidal cells may form an heteroassociative memory. Here models of both networks, incorporating simple, but biophysically reasonable models of pyramidal cells and inhibitory interneurons are used to explore memory recall performance when patterns previously have been stored using Hebbian learning. The focus is on the role of inhibitory interneurons in setting appropriate firing thresholds in the pyramidal cells.

In chapter "Microcircuit Model of the Dentate Gyrus in Epilepsy", Morgan and Soltesz provide a comprehensive description of a large-scale dentate gyrus network model, which has evolved from an initial implementation with approximately 500 model cells to a network with over 50,000 multicompartmental model neurons. They discuss the experimental data underlying the model parameters and the rationale for the assumptions made in the model. They then discuss how the model was applied to a problem that is critical for understanding the structure–function relationships of hippocampal microcircuits and highlight the importance of accurate network topology in data-driven models. Finally, they speculate on potentially useful additions to the dentate model and future questions that could be addressed.

In chapter "Multi-Level Models", Érdi, Kiss, and Ujfalussy present a framework for combining models from different levels of abstraction, which allows different levels of neural organization to be integrated. They then apply this framework to an integrated hippocampal model to show how hippocampus is involved in spatial representation and navigation. Finally, they argue that multi-scale models seem to be indispensable tools to offer new computational approaches to neurological and psychiatric disorders including the search for new therapeutic strategies and also in designing new devices capable of computation, navigation, etc. based on our knowledge about neural mechanisms.

In chapter "Biophysics-Based Models of LTP/LTD", Castellani and Zironi describe an interesting and perhaps new type of approach to modeling the biochemical cycle of synaptic plasticity, underpinning learning and memory, in terms of stochastic differential equations. They show that this mathematical formalism is more adherent to the biological reality, because the concentration of involved synaptic molecular receptors is low and their production is a noisy process. An interesting consequence of this formalization is the possibility to have a constructive role of noise, which can serve to stabilize memory properties. Using this mathematical formalism they describe some of the main experimental results recently carried out to study learning and memory mechanisms at a molecular level.

In chapter "A Phenomenological Calcium-Based Model of STDP", Gerkin, Bi, and Rubin present a more phenomenological model of synaptic plasticity. They detail a calcium time course detection model of long-term plasticity at a CA1

synapse that is capable of reproducing the results of spike-timing-dependent plasticity experiments in hippocampal cultured neurons.

In the final chapter "Computer Simulation Environments" Gleeson, Silver, and Steuber give a brief overview of simulation tools and resources available to researchers wishing to create computational models of hippocampal function. They outline first a number of software applications, which provide a range of functionality for simulating networks of neurons with varying levels of biophysical detail. They then present some ongoing initiatives designed to facilitate the development of models in a transparent and portable way across different environments. Next, they describe some of the publicly accessible databases which can be used as resources for computational models. Finally, they provide an outlook for the field, highlighting some of the current issues facing biophysically detailed modeling, and point out some of the key initiatives and sources of information for future modeling efforts.

The Making of a Detailed CA1 Pyramidal Neuron Model

Panayiota Poirazi and Eleftheria-Kyriaki Pissadaki

Introduction

The CA1 region of the hippocampal formation plays a key role in numerous learning and memory processes including working memory (Lee and Kesner, 2002, 2003, 2004; Lee et al., 2005) acquisition and retrieval of contextual fear conditioning (Lee and Kesner, 2004), temporal pattern completion (Hoang and Kesner, 2008), temporal processing of information (Hunsaker et al., 2008), spatial and object novelty detection (Hunsaker et al., 2007; Vago and Kesner, 2008) and several others. However, despite its functional significance, the exact ways in which neurons in the CA1 region contribute to all these memory processes remain elusive. According to a number of modelling studies, the function of the CA1 region is to compare information from its two primary inputs: (a) the Schaffer collateral afferents that relay processed cortical information from layer II of the entorhinal cortex via the trisynaptic loop and (b) the temporoammonic pathway which carries direct sensory information from layer III of the EC (Hjorth-Simonsen and Jeune, 1972; Steward and Scoville, 1976; Witter et al., 1988). Since CA1 is the primary output of the hippocampus, information about the outcome of this comparison would then be propagated through the subiculum, to the deeper layers of EC and the parahippocampal areas. It has been suggested that by comparing their intra- and extra-hippocampal converging inputs CA1 neurons may be able to detect novelty (Vinogradova, 2001) or mismatch from expectations (Hasselmo and Schnell, 1994), and/or activate retrieval mechanisms (Lee and Kesner, 2002). Specifically, Rolls and Treves (1994) suggested that during retrieval, the CA1 performs a comparison between the processed input arriving from the Schaffer collaterals and the information-rich input coming directly from the EC. Likewise, O'Reilly and McClelland (1994) view CA1 as a "translator" between the CA3 representation and the direct input from EC. It has also been suggested that the CA1 may be involved in directing the movement from one pattern to the next in a stored sequence of events (Treves, 2004).

P. Poirazi (✉)
Institute of Molecular Biology and Biotechnology (IMBB), Foundation for Research and Technology-Hellas (FORTH), Heraklion, Crete, Greece
e-mail: poirazi@imbb.forth.gr

V. Cutsuridis et al. (eds.), *Hippocampal Microcircuits*, Springer Series in Computational Neuroscience 5, DOI 10.1007/978-1-4419-0996-1_11,

Since the CA1 region plays a key role in numerous memory processes, it is of vital importance to understand the functional properties of its fundamental processing units – namely the CA1 pyramidal neurons. Despite the amount of work devoted to investigating the biophysical and functional properties of CA1 cells over the last few decades (Andersen et al., 1980; Johnston et al., 2000, 2003; Kesner et al., 2004; Johnston and Amaral, 2005; Rolls and Kesner, 2006; Spruston, 2008) when it comes to dendritic and synaptic integration properties experimental techniques often fail to answer some of the most fundamental questions: How do single neurons combine hundreds of incoming inputs across their highly elaborated dendritic structures, in real time, and what are the rules that underlie synaptic integration? This inability stems from the fact that dendrites are often less than 1–2 μm in diameter, and thus very hard to visualize, more so to precisely stimulate in vivo. Recent advancements have allowed for the first time to characterize the electrophysiological properties of thin dendrites in layer V somatosensory neurons (Nevian et al., 2007), while state-of-the-art imaging techniques enable the tracking of molecules (Raab-Graham et al., 2006; Kim et al., 2007) and the observation of growth/retraction of spines in vivo (Trachtenberg et al., 2002; Holtmaat et al., 2005, 2008). Yet, none of these techniques can track synaptic activation and neuronal firing in vivo, in real time, throughout an entire cell.

Models on the other hand, if detailed enough, can be used to simulate the in vivo situation and hopefully shed some light on how information is processed within an individual pyramidal neuron. The availability of a large body of experimental data regarding the anatomical and physiological properties of CA1 pyramidal neurons facilitates the development of detailed models that incorporate information regarding passive and active properties along their soma-dendritic axis (for a nice review see Migliore and Shepherd, 2002). Since dendritic properties significantly affect the computational role of these neurons (Koch and Segev, 2000; Poirazi et al., 2003b; London and Hausser, 2005; Gasparini and Magee, 2006; Losonczy and Magee, 2006; Johnston and Narayanan, 2008; Losonczy et al., 2008), it is critical to develop models that take into account all available observations. In this chapter, we will take you through the steps and hurdles of building realistic CA1 pyramidal neuron models, capable of reproducing numerous experimental recordings under different conditions. We will first describe such a model in detail and then discuss the advantages and limitations of using realistic biophysical models to elucidate neuronal function.

Building the Model

The model described here was developed within the NEURON simulation environment (Hines and Carnevale, 1997) and is available for download from the ModelDB database at http://senselab.med.yale.edu/modeldb/showmodel.asp?model=20212. The cell morphology is the reconstructed CA1 pyramidal neuron “n123” (shown in Fig. 1) and it is available for public download at www.neuromorpho.org,

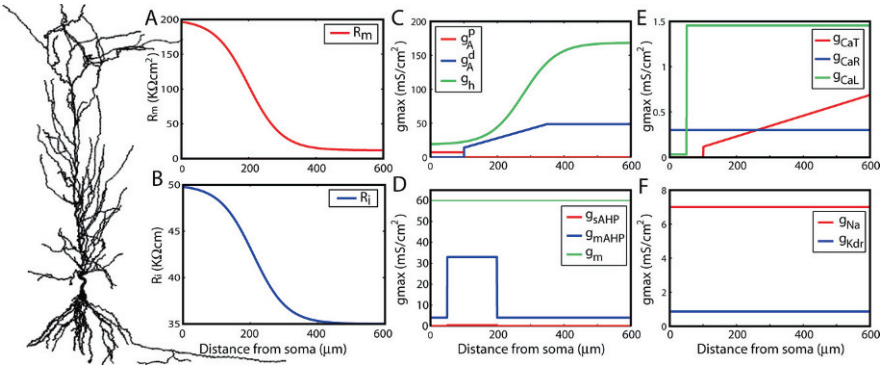

Fig. 1 Mechanism distributions along the apical trunk of the model cell. (**a**) Membrane resistance (R_m, **a**) and axial resistance (R_i, **b**) attenuate according to sigmoidal functions. (**c, d**) Channel conductance distributions along the apical trunk for the A- and h-type channels (**c**), the sAHP, mAHP and m-type channels (**d**), the CaR, CaL and CaT Ca^{++} channels (**e**) and the Na^{+} and delayed rectifier channels (**f**)

(Cannon et al., 1998; Ascoli, 2006). Since this morphology did not include an axon, we created one consisting of 10 dendrite-like sections connected in series. The total length of the axon is 721 μm averaging 0.9 μm in diameter. We did not model nodes of Ranvier or myelination. The entire model consists of 183 compartments and includes a variety of active and passive membrane mechanisms known to be present in CA1 pyramidal cells.

In order to construct a realistic model, we had to develop new mathematical descriptions and/or adjust the internal parameters of 17 types of ion channels – most of them distributed non-uniformly along the soma-dendritic axis – and 4 types of synaptic conductances. These include a leak current (I_{leak}), two kinds of Hodgkin–Huxley-type sodium and potassium currents (somatic/axonic $I^{\text{sa}}{}_{\text{Na}}$ and $I^{\text{sa}}{}_{\text{K-DR}}$, dendritic $I^{\text{d}}{}_{\text{Na}}$ and $I^{\text{d}}{}_{\text{K-DR}}$), two types of A-type (proximal and distal) and one type of m-type potassium currents ($I^{\text{p}}{}_{A}$, $I^{\text{d}}{}_{A}$, I_m), a mixed conductance hyperpolarization-activated h-current (I_{h}), three types of voltage-dependent calcium currents, namely a LVA T-type current (I_{CaT}), two HVA R-type currents (somatic: $I^{\text{s}}{}_{\text{CaR}}$, dendritic: $I^{\text{d}}{}_{\text{CaR}}$) and two HVA L-type currents (somatic: $I^{\text{s}}{}_{\text{CaL}}$, dendritic: $I^{\text{d}}{}_{\text{CaL}}$), two types of Ca^{++}-dependent potassium currents (a slow AHP current: I_{sAHP} and a medium AHP current: I_{mAHP}), a persistent sodium current (I_{Nap}) and four types of synaptic currents, namely AMPA, NMDA, GABA_{A} and GABA_{B}. Conductance values for the various mechanisms in different compartments of the model are listed in Table 1 (if constant). The distribution of conductances which change as a function of distance along the apical trunk is shown in Fig. 1.

Parameter constraints for these mechanisms arose from two main sources: (1) data from studies primarily concerned with individual channel properties, including activation and inactivation curves, time constants, location-dependent channel densities, etc., and (2) data from studies primarily concerned with dendritic physiology and synaptic integration, including responses to current, voltage and/or synaptic

Table 1 Distribution of active and passive parameters in the model cell

Conductances (mS/cm^2)	Soma	Axon	Basal dendrites	Apical trunk	Oblique side branches		
					$D^a < 300$	$D > 300$	$D > 350$
Na^{sa}	7	100	0	0	0	0	0
K^{sa}_{dr}	1.4	20	0	0	0	0	0
Na^{d}	0	0	7	7	7	7	7
K^{d}_{dr}	0	0	0.867	0.867	0.867	0.867	0.867
$Leak = 1/R_m$ (1/K Ωcm^2)	5e-3	5e-3	5e-3	Fig. 1	6.94e-3	6.94e-3	6.94e-3
A_{prox}	7.5	0	12	Fig. 1	0	0	0
A_{dist}	0	0	0	Fig. 1	27.285	67.4	67.4
H	18.72	0	18.72	Fig. 1	30.5	30.5	30.5
CaT	0.05	0	0	Fig. 1	0.179	0.179	0.179
CaR^{s}	3	0	0	0	0	0	0
CaR^{d}	0	0	0	Fig. 1	0.03	0.39	0.39
CaL^{s}	0.316	0	0	0	0	0	0
CaL^{d}	7	0	0	Fig. 1	1.455	20.37	21.82
sAHP	0.5	0	0	Fig. 1	0.5	2.5	2.5
mAHP	90.75	0	0	Fig. 1	18.5	18.5	18.5
M	60	30	0	Fig. 1	60	60	60
Nap	0	0	0	0	0.00028	0.00028	0.00056
Calcium pump	Yes	No	No	Yes	Yes	Yes	Yes
Passive properties							
R_m (K Ωcm^2)	200	200	200	Fig. 1	Fig. 1	Fig. 1	Fig. 1
R_i (K Ωcm)	50	50	50	Fig. 1	50	50	50
C_m(μF/cm^2)	1	1	1	1	1	1	1

[a] D is the perpendicular distance from the cell body.

stimuli under control and different channel blockade conditions. In some cases, NEURON channel models developed by others were used with little or no modification, as detailed in the Appendix.

Passive biophysical parameters of the model are as follows: R_m and R_i are sigmoidally changing along the apical trunk (see Fig. 1), $C_m = 1\,\mu\text{F/cm}^2$, the temperature used in all experiments is 34°C and the reversal potentials are set to $E_{\text{Na}} = 50\,\text{mV}$, $E_{\text{K}} = -80\,\text{mV}$, $E_h = -10\,\text{mV}$, $E_{\text{Ca}} = 140\,\text{mV}$. The reversal potential for the passive model conductance, E_{leak}, is calculated so that the membrane potential at rest is equal to $-70\,\text{mV}$ everywhere.

The AMPA and NMDA conductance values are estimated such that a single pulse depolarization delivered at any location along the apical tree will give rise to a 5 mV local EPSP. Therefore, the AMPA and NMDA conductances vary with location, but the ratio between the two is constant within a dendritic subregion. In the trunk and soma, the NMDA/AMPA ratio is 0.6, while in oblique dendrites the ratio is 2.5. These values were set in order to match the effects of NMDA channel

blockade reported by Cash and Yuste (1999), as shown in Figs. 4 and 5 of Poirazi et al. (2003a).

The $GABA_A$ and $GABA_B$ kinetic model implementation followed (Destexhe et al., 1994; Contreras et al., 1997). We use a uniform distribution of both $GABA_A$ and $GABA_B$ receptors along the entire model, where each compartment activated by a single high-frequency stimulus delivered at a group of synapses receives one $GABA_A$ and one $GABA_B$ inhibitory input. The $GABA_A$ conductance is set to 100%; the local AMPA conductance value and $GABA_B$ conductance are set equal to 60% of the $GABA_A$ value.

No additional manipulations were made to account for spines in this model.

The Experimental Data to be Modelled

Our main interest when building this model was to study dendritic integration properties and characterize the input/output function of an individual CA1 pyramidal neuron under realistic stimulus conditions. This is quite an ambitious goal since the data regarding channel densities and distributions in thin dendrites of CA1 pyramidal neurons are scant. On the other hand an impressive amount of studies have characterized the properties of the main apical dendrite, somatic and axonal compartments of these neurons and/or recorded their responses under different conditions (Magee and Johnston, 1995; Avery and Johnston, 1997; Hoffman et al., 1997; Golding and Spruston, 1998; Magee, 1998; Stuart and Spruston, 1998; Golding et al., 1999; Migliore et al., 1999; Golding et al., 2001; Wei et al., 2001; Golding et al., 2005) just to name a few. This information was used to constrain as well as fine tune the model parameters so that numerous experimental recordings could be reproduced by the final model. In spite of the complexity of the model as a whole, we were able to achieve good fits to a variety of experimental data, covering a broad range of phenomena. Parameter tuning in this model was done exclusively by hand. We chose to take this painstaking approach because in our experience, basic knowledge about the effects of various ionic mechanisms on voltage and current waveforms could be used as an effective guide for determining which parameters needed to be adjusted and how in order to achieve a desired behaviour. Moreover, alternative approaches such as automated parameter tuning (Keren et al., 2005; Achard and De Schutter, 2006) require the use of numerous input/output electrophysiological waveforms for comparing the model responses, which are not easily available. Following is a presentation of the validation studies we performed to ensure the soundness of our model along with a discussion of the primary mechanisms involved in generating the respective model behaviour.

Effect of I_h on Input Resistance and Steady-State Voltage Propagation

The h-current, a hyperpolarization-activated mixed cation current, is responsible for the pronounced rectifying sag in response to a hyperpolarizing current pulse

(Magee, 1998). The spatial distribution of I_h in CA1 pyramidal neurons is highly nonuniform, with a 7-fold increase in channel density from the soma to the distal apical trunk. Though the apical trunk is of much smaller diameter than the soma, the huge resting conductance provided by the h-channels in the apical tree contributes to a lower input resistance measured distally than at the cell body and leads to an asymmetry in the distance-dependent attenuation of steady-state voltage signals – favouring voltage signals travelling inward from a dendritic stimulus to a recording electrode in the cell body (Magee, 1998).

To fit these empirical data, the I_h mechanism in the model cell was distributed in a sigmoidally increasing manner from the soma to the main apical trunk (as described in the Appendix) so that the maximal channel conductance increased along the main apical trunk reaching a value seven times larger than the somatic at 350 μm. To test the accuracy of the model in replicating these data we used constant hyperpolarizing current injections either at the soma or 325 μm away in the main apical trunk and recorded at both sites simultaneously (Fig. 2). We found voltage traces similar to those reported by Magee (1998), including (1) a pronounced depolarizing voltage sag, eliminated by blockade of I_h (dashed traces), (2) lower input resistance in the trunk compared to the cell body (averaging $50 \pm 3\,M\Omega$ distally vs. $62 \pm 4\,M\Omega$ at the soma) and (3) asymmetric steady-state voltage attenuation favouring voltage signals propagating from the dendritic injection site to the cell body. Differences include a smaller decay for signals travelling to the soma and a higher dendritic input resistance in the model neuron (also see Poirazi et al., 2003a).

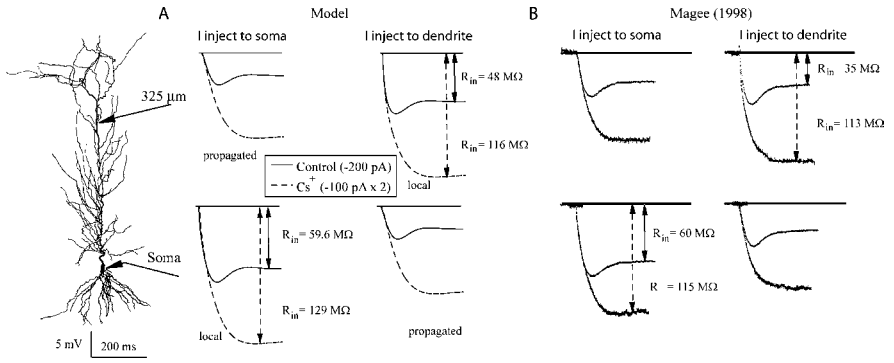

Fig. 2 Contribution of I_h to input resistance and steady-state voltage propagation. (**a**) Following the methods of Magee (1998), a steady current was injected at either a somatic or a dendritic electrode and voltages were recorded at both locations. Responses are shown for somatic (*left* column) and dendritic (*right* column) current injections under control conditions (−200 pA, *solid curves*) and with bath application of 3 mM Cs^+ (−100 pA, *dashed curves*) which we assumed blocked 80% of I_h (see Channel Blockers). Cs^+ traces were doubled in height in both **a** and **b** to allow more direct comparison of input resistances. R_{in} values are indicated in upper *right* and lower *left* panels, corresponding to measurements made at the site of current injection. Soma diameter was 8.6 μm, and dendritic diameter at recording site was 2.1 μm. (**b**) Traces for same experiment, adapted with permission from Magee (1998)

Properties of Backpropagating and Dendritically Initiated Action Potentials

A number of studies have examined the properties of backpropagating action potentials (BPAPs) in the apical trunk (Stuart et al., 1997), including their tendency to attenuate with distance from the soma, and as a function of distance, their tendency to attenuate in the time course of a spike train. The distance-dependent attenuation in CA1 pyramidal cells has been attributed to the 6-fold increase in the density of I_A in the apical trunk, a fast inactivating K^+ current that opposes transient depolarizations (Hoffman et al., 1997). The time-dependent attenuation, which is increasingly evident at greater distances from the cell body, has been attributed to slow inactivation of the Na^+ channel itself (Jung et al., 1997).

To account for the slow inactivation of the Na^+ channel, we used a model mechanism that contains an additional, slowly inactivating state variable as described in the Appendix. We tested our model cell using a constant depolarizing current injection at the soma while recording simultaneously at the soma and two locations in the apical trunk. We observed a pattern of distance and time-dependent attenuation of BPAPs (Fig. 3a) similar to that reported by Spruston et al. (1995) (Fig. 3b). One difference is the height of the first BPAP in the distal dendrite: high in the data of Spruston et al. (1995) and low in our traces. However, a subsequent study by Golding et al. (2001) found that CA1 pyramidal cells fall into two categories: those for which the first BPAP propagates at nearly full height into the distal dendrites and those for which the first spike is reduced to a small spikelet by around 300 μm from the cell body. Thus, both types of responses are "normal."

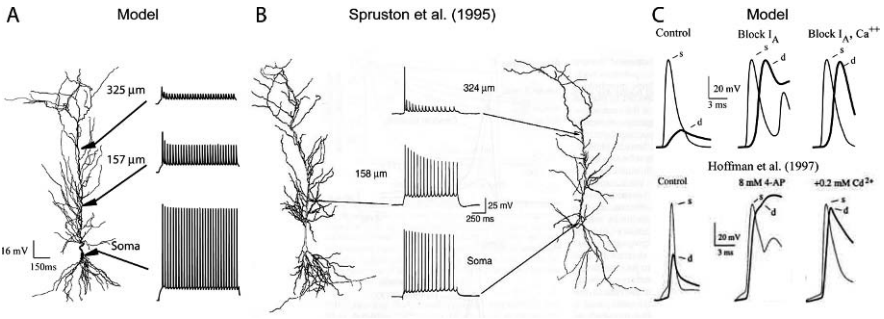

Fig. 3 Properties of action potentials in the soma and apical trunk. (**a**) Backpropagating action potentials elicited by steady somatic current injection (220 pA, 700 ms) show typical pattern of distance and time-dependent attenuation of spike height; results from Spruston et al. (1995) are reproduced with permission in **b** for comparison. (**c**) Initial somatic and dendritic spikes are shown in response to somatic current injection (300 pA, 50 ms) in control conditions (*left*), with block of I_A (*middle*), and with block of Ca^{++} currents (*right*). Results are comparable to those of Hoffman et al. (1997), reproduced with permission

We repeated the same experiment after blocking I_A throughout the cell and found that the initial BPAP now reached full height at the dendritic recording electrode as was also observed by Hoffman et al. (1997) (Fig. 3c). Given that the cell is much more excitable in this condition than normal, the dendritic response in both data

and model shows a failure to repolarize, as if the voltage were dominated by an unopposed dendritic Ca^{++} current. When calcium currents were 75% blocked to mimic bath application of 200 mM Cd^{++}, the dendritic spike, though broader than in control conditions, was more fully repolarized.

Differences between our model and the data of Hoffman et al. (1997) include generally broader spikes in the model in both the soma and dendrites, somewhat less Ca^{++} excitability in the model cell after complete block of I_A, and a somewhat greater suppression of Ca^{++}-channel-dependent excitability after 75% block of calcium channels.

Properties of Dendritically Initiated Ca^{++} Spikes

The distal apical dendrites of CA1 pyramidal neurons have the ability to generate Ca^{++} spikes in response to direct dendritic stimulation, but not when activated by BPAPs initiated at the cell body (Amitai et al., 1993) unless, e.g. coupled with local synaptic events (Larkum et al., 1999). Golding et al. (1999) found that the increased concentrations of Ca^{++}-dependent potassium currents near the cell body were primarily responsible for the active suppression of calcium spiking near the soma. To replicate these findings we had to incorporate a fast-activating, slowly-inactivating voltage-dependent Ca^{++}-channel (CaL^d) together with an R-type Ca^{++} channel (CaR^d) in large amounts primarily in the distal apical dendrites of the model cell (see Table 1). The parameters of the CaL^d mechanism were tuned to qualitatively match the shape of dendritically induced Ca^{++} spikes. Due to lack of experimental data regarding the kinetics and conductance values of these channels, we had to manually tune these parameters in order to achieve the best fit between the model traces and the recordings of Golding et al. (1999). The role of the CaR^d mechanism in these experiments was to mimic the slow experimental increase in the repolarization potential of dendritic spike trains, which was associated with an incremental attenuation of spike amplitude (shown in Fig. 4c). A much smaller increase in the repolarization potential is observed in somatic spike trains (Fig. 4a, light traces) and this was modelled using a slower version of the R-type mechanism in the somatic section of the model (CaR^s). To achieve the large repolarization of the membrane following the occurrence of a calcium spike (Fig. 4c), a dendritic calcium pump/buffering mechanism in conjunction with the calcium-activated mAHP and sAHP mechanisms was also needed. Their kinetics, conductances and distribution properties were finely tuned, within acceptable published values, to reproduce the above-mentioned experimental data (see Appendix for details).

Following these modifications/extensions the model was capable of eliciting realistic calcium spikes in the apical tree in response to a direct dendritic current injection (Fig. 4). The response of the cell to a 480 pA current injection at a distance of 212 μm is shown in Fig. 4b. Model responses recorded in the apical trunk at a distance of 157 μm and the cell body were similar to respective experimental traces from Golding et al. (1999) shown in Fig. 4a. The characteristic pattern of large

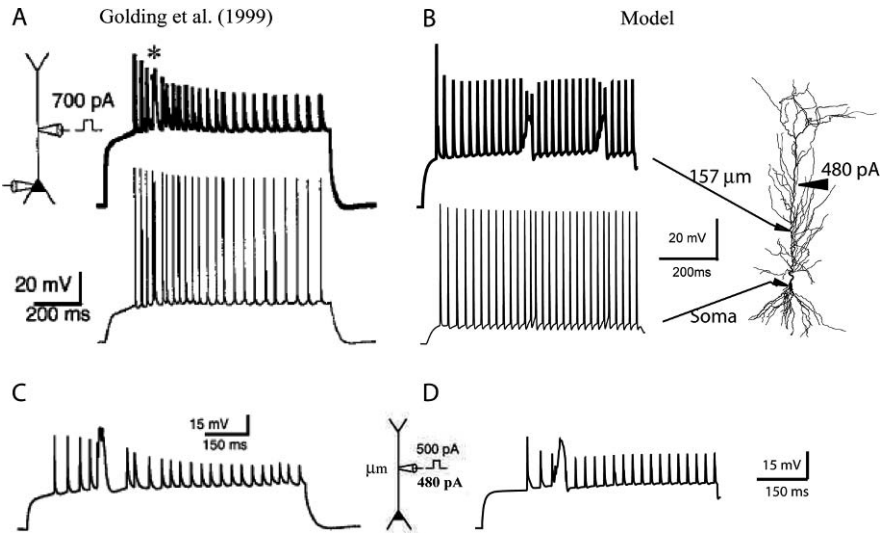

Fig. 4 Properties of dendritic Ca^{++} spikes. (**a**) Current injection on the distal apical trunk (220 µm) elicits dendritic Ca^{++} spikes which do not propagate to the cell body. Data are reproduced from Golding et al. (1999). Similar dendritic current injection in the model cell (480 pA, 212 µm, 700 ms) leads to triggering of calcium spikes, which are large in the distal apical tree but seen at the cell body only as brief accelerations in spike rate. Model responses are very similar to the experimental data shown in **a**. (**c, d**) Comparison of a calcium spike elicited by dendritic current injection in the model (**d**) compared to the data of Golding et al. (1999) (**c**), reproduced with permission

amplitude slow spikes interrupting the regular train of fast spikes, with an initial onset delay of 200 ms or more, is also very similar in the model traces (Fig. 4d) to that reported by Golding et al. (1999) under comparable stimulus conditions (Fig. 4c).

Differences between model and experimental data regarding calcium spikes include a smaller and faster decay in spike height in our dendritic traces in response to dendritic current injection, than the experimental traces, due to a difference of unknown origin in the dynamics of the two cells. The membrane repolarization after the occurrence of a calcium spike in the model is also not as slow or smooth as in the experimental data. Overall, however, the model captures several major trends regarding the complex physiology of calcium spiking including spike shape and size as a function of location, time and injection site.

Modelling Synaptic Integration in CA1 Pyramidal Cells

In a study by Cash and Yuste (1999), the authors used single pulse stimuli delivered at different locations along the apical dendrites to investigate the rules for synaptic integration in CA1 pyramidal cells. The authors found that summation was sublinear when two stimuli were delivered to different locations along the apical trunk

and this effect was even more pronounced for larger combined responses (Fig. 5a). Using pharmacological blockers for NMDA channels, Na^+ channels, Ca^{++} channels and A-type K^+ channels, the authors found that the nonlinear suppression of combined responses was due primarily to voltage-dependent rectification by I_A, which is present in high concentrations in the apical tree of these neurons (Fig. 5b). To test the validity of our model cell, we repeated the same experiments and contrasted model with experimental findings. Single pulse stimulation was delivered at two sets of synapses, separately and together, to two randomly drawn sections of the apical trunk in the model neuron, as described in Poirazi et al. (2003a). We found that model responses under both control and blockade conditions were very similar to the reported experimental data shown in Fig. 5. One difference is that our model neuron did not yield as large subthreshold combined responses as the cells reported in Cash and Yuste (1999), topping out at 14 mV rather than 20 mV. A possible explanation for this difference is that Na^+ currents appear to play a greater role in the apical trunk of our model cell than in the cells reported by Cash and Yuste (1999). An excess of Na^+ channel activity in the model is suggested by the slightly taller control column and slightly shorter Na^+-block column in Fig. 5d vs. 5b and could explain our inability to generate very large (e.g. >15 mV) depolarizations at the soma without triggering a somatic spike. Nevertheless, over the range of data acquired, model responses were closely matched to the experimental data.

A similar match between model and experimental data regarding the integration properties of apical oblique branches was also found (see Fig. 2 of Poirazi et al., 2003a). Overall, summation of EPSP peaks within the apical trunk as well as the thin branches of the model cell, and its dependence on NMDA, Na^+, A-type K^+ and Ca^{++} currents, was consistent with the experimental data of Cash and Yuste (1999).

Summary: Results of Validation Studies

The validation studies shown in Figs. 2, 3, 4, and 5 were necessary in order to ensure that the model provides reasonable fits to a large variety of in vitro data bearing on the biophysical and integrative properties of hippocampal CA1 pyramidal cells. Specifically, the model was shown to exhibit (1) several I_h-dependent effects, including a realistic sag current, reasonable values for input resistance in the soma and dendrites and the characteristic pattern of asymmetric voltage attenuation travelling to and from the cell body through the apical trunk, (2) a realistic pattern of distance and time-dependent attenuation in trains of backpropagating action potentials, with appropriate dependence on I_A and (3) the elicitation of delayed-onset Ca^{++} spikes from a distal but not proximal stimulating electrode. In addition, the model reproduces two different patterns of synaptic summation seen in different parts of the apical tree as reported by Cash and Yuste (1999), including the effects of pharmacological blockers.

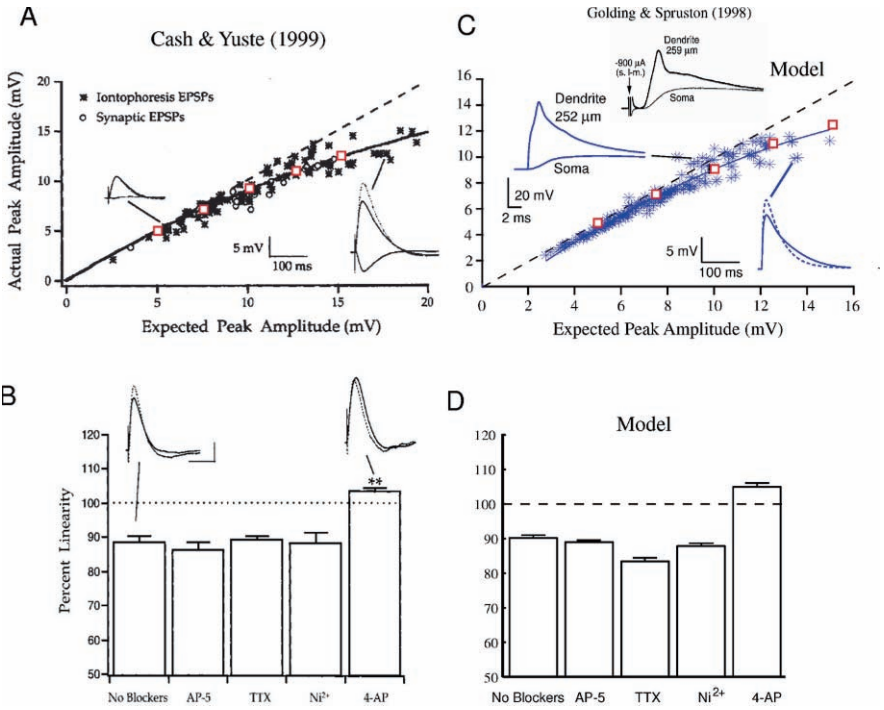

Fig. 5 Summation of EPSP peaks in apical trunk. (**a**) Excitation was delivered to two trunk locations beyond 100 microns first individually and then synchronously. Peak of the combined EPSP (*y*-axis) was plotted against expected response, given by sum of individual somatic EPSP peaks (*x*-axis). Data reproduced with permission from Cash and Yuste (1999) shows sublinear summation in apical trunk. Inset shows expected (*dotted*) vs. actual (*solid*) traces for two cases. Open *squares* were added to facilitate comparison to model responses in **c**. (**b**) Blockade of NMDA (AP-5), Na^{+} (TTX) or Ca^{++} (Ni^{++}) currents shows relatively small effect on sublinearity in the somatic response, while blockade of I_A (4-AP) leads to large upswing in percent linearity. (**c**) Model responses to be compared with data in **a**. Inset shows isolated dendritic spike accounting for superlinearity in a cluster of cases in the 10 mV range. A comparable trace is reproduced from Golding and Spruston (1998). (**d**) Effects of channel blockade in model cell are similar to experimental data shown in **b**. Reproduced with permission from Poirazi et al. (2003a)

Investigating Dendritic Integration in the CA1 Pyramidal Model Cell

It is now well established that dendrites of CA1 pyramidal cells contain a large variety of voltage-dependent mechanisms, distributed non-uniformly throughout the dendritic tree, which heavily influence the cells integrative behaviour (Magee, 1998; Johnston et al., 1999; Hausser et al., 2000; Johnston et al., 2000; Reyes, 2001; Johnston et al., 2003; Magee and Johnston, 2005; Spruston, 2008). There is also evidence that elemental synaptic conductances may vary systematically as a function of dendritic location (Magee and Cook, 2000; Otmakhova et al., 2002), while dendritic

K^+ conductances can modify the excitability properties of apical dendrites in an activity-dependent manner, revealing a new plasticity mechanism that takes place at the level of a small branch (Losonczy et al., 2008). Many questions remain, however, regarding the contributions of these highly nonlinear membrane mechanisms to synaptic integration.

The classical view of a single pyramidal cell is that of a virtual "point neuron" whereby voltage-dependent dendritic currents and scaling of synaptic conductances exist to transform the morphologically elaborated and biophysically complex cell into a thresholded summing unit. According to this view, dendritic nonlinearities may exist to (1) make the cell more linear, by counteracting the classical synaptic nonlinearity that arises from the summation of conductances (Bernander et al., 1994; Cash and Yuste, 1999), and in conjunction with synaptic scaling, they could (2) make the cell more functionally compact, by counteracting the distance-dependent attenuation of synaptic responses that arise from the cable properties of dendrites (Cauller and Connors, 1994; De Schutter and Bower, 1994; Magee and Cook, 2000). Both ideas emphasize the coupling of individual synapses to the cell body, and the uniformity and linearity thereof.

A second view, and one that continuously gains support in the experimental and modelling areas alike, entails that dendrites exist to create a number of independent functional compartments within which various kinds of nonlinear computations can be performed (Shepherd and Brayton, 1987; Mel, 1992a, b, 1993; Ariav et al., 2003; Chklovskii et al., 2004; Gasparini et al., 2004; London and Hausser, 2005; Gasparini and Magee, 2006; Losonczy and Magee, 2006; Losonczy et al., 2008).

To investigate these two hypotheses, we used our validated model neuron to characterize the dendritic and somatic input/output functions of CA1 pyramidal neurons under realistic stimulus conditions. First, we studied the responses of our model cell when two sets of synapses were stimulated separately or concurrently using two different stimulus formats (single shock vs. 50 Hz trains) and two different spatial arrangements (within vs. between-branch inputs) (Poirazi et al., 2003a). Our main goal in these experiments was to assess how well the linear vs. nonlinear models of synaptic integration account for the arithmetic of summation in CA1 pyramidal cells. We found that individual apical oblique dendrites of CA1 pyramidal neurons act as independent computational units that combine inputs using a sigmoidal activation function and that different branch outputs are linearly combined at the cell body. Both of these predictions were verified experimentally in a layer V pyramidal neuron (Polsky et al., 2004) while a recent experimental study (Losonczy and Magee, 2006) confirmed that radial oblique dendrites of CA1 pyramidal neurons function as single integrative compartments. As shown in Fig. 6, layer V neocortical neurons summate linearly between-branch excitatory postsynaptic potentials (EPSPs) but implement a sigmoidal activation function for within-branch EPSPs (Fig. 6b), similar to the model predictions (Fig. 6a). Similarly, radial oblique dendrites of CA1 pyramidal neurons combine synaptic inputs in a sigmoidal-like way (Fig. 6c), as predicted by our model neuron (Fig. 6a, red traces). In other words, thin dendritic branches seem capable of combining incoming signals according to a thresholding non-linearity, much like a typical "point neuron."

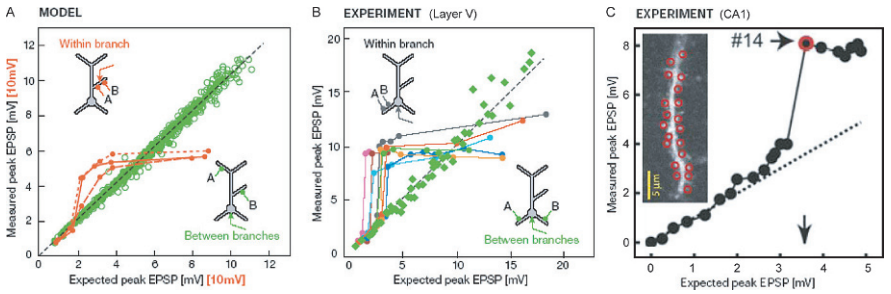

Fig. 6 Nonlinear dendritic computations in pyramidal neurons. (**a**) Summation of paired, single-pulse inputs in the apical dendrites of our CA1 pyramidal model cell. Simulations predict a sigmoidal modulation of combined excitatory postsynaptic potentials (EPSPs) *within* a branch (*red* symbols) and a linear summation of EPSPs *between* branches (*green* symbols). *Red* curves correspond to within-branch data for dendrites at 92 µm (*short dashes*), 232 µm (*solid*) and 301 µm (*long dashes*) from the soma. Due to differences in local vs. somatic responses, axis values for the red curves are scaled up by 10. (**b**) Experimental verification of predicted summation rules in basal dendrites of a layer V pyramidal neuron. Single-pulse stimulation of synapses in different branches results in linear summation at the cell body (*green squares*). When γ-amino butyric acid (GABA)ergic inhibition is blocked, the summation of within-branch EPSPs is modulated by a sigmoidal nonlinearity (all other *symbols*). Reproduced with permission from Polsky et al. (2004). (**c**) Sequential single-pulse stimulation of individual spines within radial oblique dendrites of CA1 pyramidal neurons using multisite two photon glutamate uncaging. The summation of somatic EPSPs generate in response to individual vs. combined stimulation of increasing number of synapses is highly nonlinear and closely resembles the model predictions shown in **a** (*red* traces). Reproduced with permission from Losonczy and Magee (2006)

If apical oblique dendrites are individually thresholded in CA1, layer V and most likely other classes of pyramidal neurons, the question that naturally arises is what advantage does this feature offer to the mammalian brain? The effects on memory capacity of such neurons were explored previously in less detailed neuron models (Mel et al., 1998; Mel, 1999; Archie and Mel, 2000; Poirazi and Mel, 2001). To investigate the benefits of having compartmentalized, non-linear subunits we presented our model neuron with a large number of high-frequency input patterns varying in their spatio-temporal characteristics and recorded the model responses (Poirazi et al., 2003b). We found that the average firing rate of our detailed model cell in response to hundreds of different input patterns was accurately predicted by a two-layer neural network abstraction where individual oblique dendrites provided the "hidden" nodes and the soma acted as the output layer (Fig. 7). These findings suggested that the integrative properties of a highly complex, realistic model of a CA1 pyramidal neuron containing more than 20 different membrane mechanisms could be described by a simple mathematical equation. Such a simplification is of great importance for future modelling efforts that try to understand the functionalities of large-scale neuronal networks, since it allows the development of network models where each node (neuron) is modelled as a simplified two-layer neural network instead of a full-blown compartmental cell.

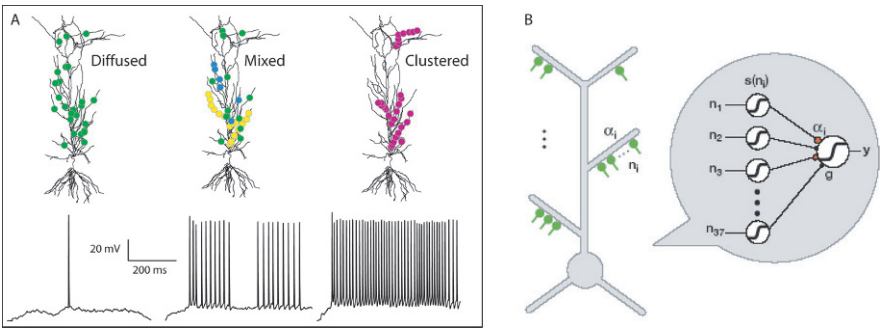

Fig. 7 Modelling the model. (**a**) Somatic model responses to high-frequency synaptic stimulation (lasting 600 ms) shown for three cases with 40 excitatory synapses distributed across the apical tree. In a fully dispersed case (*left* column), all 40 synapses were randomly assigned to the 37 terminal branches. In a fully concentrated case (*right* column), synapses were placed eight to a branch on five randomly chosen branches. Mixed cases consisted of randomized assignments of 1, 2, 4, 6 or 8 synapses to varying numbers of terminal branches. *Middle* column shows a case with 2 groups each of 2 (*blue*) and 6 (*yellow*), plus 24 randomly dispersed synapses (*green*). Excitatory synapses were distributed at equally spaced intervals on each branch. A fixed set of 11 inhibitory synapses was used in all runs including 5 at the cell body and 6 inhibitory synapses at ~60 μm intervals along the main trunk. In runs containing more than 40 excitatory synapses, an additional $GABA_A$ conductance (equal to the AMPA conductance value) and a $GABA_B$ conductance (equal to 60% of the AMPA conductance value) were placed in the middle of each distal apical tip more than 350 μm from the cell body (6 tips). Figure was adapted with permission from Poirazi et al. (2003b). (**b**) Schematic representation of a pyramidal neuron as a two-layer neural network. Radial oblique dendrites provide the first layer of the network, each performing individually thresholded computations as shown in **a** and **b**. The outputs of this layer feed into the cell body, which constitutes the second layer of the network model. Model responses shown in **a** were fit by the abstract model shown in **b**, where n_i were the number of excitatory inputs to each branch and α_i was the branch coefficient. Reproduced with permission from Sidiropoulou et al. (2006)

Discussion

Model Advantages and Usability

The primary goal of this chapter was to convey the logic behind the development of a detailed compartmental model of a CA1 pyramidal neuron. Towards this goal, we argued about the need and feasibility of building such a model, we elaborated on the strenuous efforts required for constraining and validating the model and presented some of the most interesting predictions that our model has generated.

The main strength of our model lies in its ability to closely mimic the physiology of CA1 pyramidal neurons. It can replicate the largest number of in vitro experiments regarding the electrophysiological and integrative properties of these neurons (Spruston et al., 1995; Hoffman et al., 1997; Magee, 1998; Cash and Yuste, 1999; Golding et al., 1999) than any other currently available compartmental model of any pyramidal neuron.

However, replicating what is already known should not be the primary goal of such a realistic model. It is simply a way for ensuring the soundness of the model and an absolutely essential step when dealing with hundreds of model parameters. The more condition-dependent responses the model can generate, the larger are the constraints on the parameter space. And despite a common belief that compartmental models can be "tuned" to replicate almost anything and should thus be interpreted with caution, in our experience it proved to be extremely difficult to find a single set of parameters which lie within physiological limits and reproduce *all* the above-mentioned validation experiments without compromising the model's robustness.

Beyond its ability to match electrophysiological responses under numerous different conditions, one of the strongest advantages of our model lies in its predictive power. The thresholded nonlinear computations supported by individual dendrites in CA1 pyramidal neurons that were predicted by our model in Poirazi et al. (2003a, b) have also been verified experimentally in neocortical (Polsky et al., 2004) and CA1 pyramidal cells (Losonczy and Magee, 2006). The second prediction that CA1 pyramidal neurons essentially operate like two-layer neural networks, although it has yet to be shown experimentally primarily due to limitations in experimental techniques, it has stirred up quite an amount of fruitful discussion in the Neuroscience community and has led to several theories regarding the computational power of single cells (Chklovskii et al., 2004; London and Hausser, 2005; Laurent and Borst, 2007; Spruston, 2008).

Model Extensions and Limitations

Due to the ongoing accumulation of data regarding the complex physiology of CA1 pyramidal neurons, our model has undergone a series of extensions and refinements over the last few years.

To account for the reduced spike afterhyperpolarization at the cell body (Metz et al., 2007) and the restriction of calcium spikes to the dendrites of CA1 pyramidal neurons (Golding et al., 1999), the model has been furnished with a D-type K^+ channel. The addition of a fast afterhyperpolarization current (fAHP) based on the models of Borg-Graham (1998) and Shao et al. (1999) was also needed to replicate the sharp membrane repolarization after each of the first 2–3 action potentials in a spike train. An additional L-type Ca^{++} channel which exhibits delayed facilitation (Zuhlke et al., 2000) coupled with a refined sAHP mechanism was distributed along the soma and proximal dendrites of the model in clusters, as suggested by the experimental data of Marrion and Tavalin (1998) and Bowden et al. (2001). This version of the model was used as a basis for the development of "aged" (Markaki et al., 2005) and "stressed" CA1 pyramidal neuron models (Sidiropoulou et al., 2007; Liebmann et al., 2008) and generated a number of interesting predictions regarding the role of specific Ca^{++} subunits in regulating aging-induced as well as stress-induced changes in the excitability of these cells.

Small changes in the kinetics and conductance values of the original AMPA and NMDA receptors were also needed to replicate the tight temporal synchronization requirements for supralinear integration of synaptic events in radial oblique dendrites of CA1 pyramidal neurons (Losonczy and Magee, 2006). With these modifications, the model predicted a key role of NMDA receptors in widening the above-mentioned window when synapses were activated with double pulses (Gomez González et al., 2009).

According to the experimental data of Dvorak-Carbone and Schuman (1999), the distal dendrites of CA1 pyramidal neurons contain $GABA_B$ receptors which exhibit short-term depression of activity in response to multiple high-frequency events. Moreover, when activated by entorhinal inputs, these receptors have been suggested to play an important role in gating intra-hippocampal signals arriving via the Schaffer collateral pathway. To replicate these findings, a desensitizing $GABA_B$ mechanism was incorporated into the model (Pissadaki and Poirazi, 2007) and the distribution of all synaptic mechanisms was tailored to match the anatomical data of Megias et al. (2001). A very interesting prediction made by this model entails that a single CA1 neuron is able to map spatio-temporal information about incoming signals through the Temporoammonic and Schaffer collateral pathways into its response pattern (Pissadaki et al., 2009).

In all versions of our model, validation experiments like the ones described here were performed to ensure that the model replicates as many as possible of the CA1 pyramidal neuron firing properties. The various predictions generated by the model at different stages of refinement will hopefully inspire new experiments which will further enhance our understanding of how CA1 pyramidal neurons process, transmit and store information.

While the above-mentioned modifications have significantly improved the realism of our model, a number of improvements are still possible. Dendritic spines could be explicitly modelled, an important change if issues relating to synaptic plasticity were to be addressed in future work. Spines were not included as they can add significantly to the computational burden – depending on the number of compartments per spine and whether modelling of Ca^{++} machinery is included – and results of previous studies suggest that synaptic integration on the spatial scale of entire dendritic branches is not very sensitive to the presence or absence of dendritic spines. Spike shape in the soma and main apical trunk could also be improved through further tailoring of the various conductances involved. Spikes in the present model do not exhibit the smooth scoop-like repolarizations to the extent that is seen in typical slice recordings from CA1 pyramidal cells (Hoffman et al., 1997). Tailoring of spike shape is an arduous process, however, and we do not anticipate a significant change in model behaviour as relates to synaptic integration. Another shortcoming of the model is the simplified channel composition of the basal dendrites, which were not directly stimulated in any of the above-mentioned experiments. However, this deficit could be remedied through a relatively straightforward "technology transfer" from the apical to the basal tree, subject to additional constraints from studies of basal dendritic physiology. The results of earlier modelling studies involving basal dendrites lead us to believe a similar form of synaptic

integration may apply there as well (Mel, 1993; Mel et al., 1998; Archie and Mel, 2000).

Questions Addressed by Similar Models

A larger number of interesting predictions regarding the contribution of morphological and/or biophysical properties of CA1 pyramidal neurons in the integrative properties of these cells have been generated by computational studies utilizing detailed compartmental models. For example, in a morphologically realistic, four-conductance model, dendritic spike initiation in response to Perforant Path (PP) stimulation, confined in the distal tuft, could be forwarded to the soma by activation of the Schaffer collateral (SC) pathway (Jarsky et al., 2005). This prediction is very similar to the experimental findings of Larkum et al. (2004) whereby dendritic Ca^{2+} conductances in the distal tuft of a layer V cortical neuron model, unable to initiate an AP at the soma, could be amplified by coincident backpropagating APs.

The studies of Migliore (2003) and Migliore et al. (2004) using compartmental models with similar biophysical properties as the one in Jarsky et al. (2005) suggested that the h-current could be involved in setting the temporal window for input summation around sub-threshold levels, thus enabling coincidence detection and minimizing the effectiveness of unsynchronized signals arriving from the PP and SC pathways. However, according to experimental evidence in the mouse frontal cortex, other dendritic K^+ conductances could either support or counteract the predicted effect of I_h on temporal summation (Day et al., 2005) and more studies are needed to fully characterize its role in CA1 pyramidal neurons.

The effects of morphology and biophysical mechanisms on the back- and forward propagation of action potentials in CA1 pyramidal neurons were investigated in a number of compartmental modelling studies (Golding et al., 2001, Migliore et al., 2005, Watanabe et al., 2002). An interesting finding regarding the thin apical dendrites of CA1 pyramidal neurons was shown by Migliore et al. (2005) who used 27 reconstructed three-dimensional morphologies and different distributions of the A-type ionic mechanism (K_A) in a model containing only four conductances. The model predicted a major role for the local K_A distribution in modulating action potential backpropagation, while forward propagation of dendritically induced spikes was mainly affected by local morphological properties. In both cases, signal processing in any given oblique was effectively independent of the rest of the neuron, in accordance with previous modelling studies (Poirazi et al., 2003a) as well as experimental findings in layer V neocortical neurons (Polsky et al., 2004).

The Need for Simplification

Detailed compartmental models such as the one presented here are especially powerful for characterizing the contributions of biophysical and morphological parameters in synaptic integration and the cell's ability to perform various kinds of

neuronal computations (Koch and Segev, 2000; Poirazi et al., 2003a; London and Hausser, 2005; Sidiropoulou et al., 2006). However, what seems to be their major advantage, i.e. morphological and biophysical realism, can also be their most important drawback. Optimizing the large parameter space of these models requires laborious efforts while assigning causality to the emergent neuronal functions becomes a very demanding task. Incorporating detailed compartmental models in network simulations comprising of hundreds or thousands of single cells can also be prohibitive due to their computational power requirements. On the other hand, investigating several aspects of single neuron functionality, for instance their ability to perform logical operations (Koch et al., 1983; Koch, 1999) or discriminate among different input patterns (Softky, 1994; Koch and Segev, 2000; Graham, 2001; Katz et al., 2007), does not require the use of such detailed models. With that in mind, a modeller's goal should be the development of models which are complex enough to capture key functionalities of single cells and simple enough to allow the simulation of large-scale neural computations (Koch, 1999).

A reduced compartmental model, e.g. one with simplified morphology and/or biophysical mechanism composition, often compensates for the above-mentioned limitations, albeit the range of its potential applications also decreases significantly (Herz et al., 2006). Actually, most of the compartmental modelling studies already use simplified models of CA1 pyramidal neurons, including only a small subset of the known biophysical mechanisms present in these cells while maintaining the cell's elaborated geometry (Golding et al., 2001; Graham, 2001; Poolos et al., 2002; Watanabe et al., 2002; Migliore, 2003; Gasparini et al., 2004; Migliore et al., 2004; Golding et al., 2005; Jarsky et al., 2005; Migliore et al., 2005; Li and Ascoli, 2006). A nice example of a morphologically simplified model comes from Golomb et al. (2006), where a conductance-based, one-compartment model of a CA1 pyramidal neuron incorporating five ionic mechanisms was used to study the contributions of persistent sodium and M-type K^+ channels in modulating bursting activity in these cells.

Integrate and fire models represent the next level of abstraction and their advantages and disadvantages are discussed elsewhere (Burkitt, 2006a,b; Gerstner and Kistler, 2002). Last but not least, mathematical abstractions can also describe certain functions of CA1 pyramidal neurons, such as their ability to perform logical operations (Koch and Segev, 2000). A nice example comes from our own work (Poirazi et al., 2003b) where we showed that the detailed compartmental model presented here can be reduced to a very simple mathematical equation describing a conventional two-layer, feed-forward neural network.

Concluding Remarks

Since Ramon y Cajal revealed the web-like structure of the brain and defined the neuron as its fundamental unit, the efforts of many neuroscientists, experimentalists and theoreticians alike concentrated on assigning function to this "independent"

entity. Over the last few decades, compartmental models like the ones presented here have contributed greatly to these endeavours.

The making of a detailed compartmental model neuron is not a trivial task. It requires artful integration of anatomical, physiological and molecular data with mathematical formalisms and sophisticated computational algorithms. The model presented here is a good example of such coordinated efforts: based on the strong mathematical background of multi-compartmental cable theory set forth by Wilfrid Rall (1964), it incorporates a plethora of experimental data regarding the complex physiology of CA1 pyramidal neurons, rendering the simulated cell a pluripotent tool for investigating neuronal functionalities. Combined with an increasing amount of in vivo data regarding the properties of these cells, such models are likely to open up new avenues for linking computational properties to behaviour, a major challenge for both modelling and experimental studies of the future. The degree of complexity in the models, which defines both their realism and computational burden, can always be tailored to the question at hand: whether simplified or multicompartmental, members of a network or a microcircuit, CA1 pyramidal neuron models should be built according to the issues they are meant to tackle. With the right level of abstraction, compartmental models can provide some of the missing pieces in the mosaic of neural function.

Acknowledgments We would like to thank Bruce Graham and members of our lab for their useful comments on the manuscript. This work was supported by the EMBO Young investigator Programme, a Marie Curie Fellowship of the European Commission (PIOF-GA-2008-219622) and the National Science Foundation (NSF 0515357).

Appendix: The Model

Densities, kinetic properties and distributions of the mechanisms included in our model are based on published empirical data as detailed below.

Nonuniform R_m

The efficacy of signal transduction within a neuron depends heavily on the membrane properties and internal resistivity of the dendritic arbour. Stuart and Sprusston (1998) showed that while intracellular resistivity of layer V pyramidal neurons is low ($R_i \approx 65$–$100\,\Omega$cm), voltage attenuation is substantial in these cells due to nonuniformity of the membrane resistance. The authors found that resting conductances in the distal dendrites have significant higher concentrations than in the proximal and somatic regions (up to a ratio of 36). Furthermore, they suggested that R_m follows a sigmoidally decreasing distribution from the soma to the distal trunk of pyramidal neurons. We implement a similar nonuniformity in our model, where the membrane resistance ($R_m = \frac{1}{g_{\text{leak}}}$) decreases sigmoidally from the soma to the apical trunk:

$$R_m(x) = R_{m_{\text{soma}}} + \frac{(R_{m_{\text{end}}} - R_{m_{\text{soma}}})}{\left(1 + e^{\frac{d_{\text{half}} - d_x}{\text{steep}}}\right)}$$

where $R_{m_{\text{soma}}} = 200\,\text{K}\Omega\text{cm}^2$, $R_{m_{\text{end}}} = 12\,\text{K}\Omega\text{cm}^2$, $d_{\text{half}} = 200\,\mu\text{m}$, steep $= 50\,\mu\text{m}$, and d_x represents the perpendicular distance of a point x from the cell body.

Nonuniform R_i

Based on these findings (Stuart and Spruston, 1998), and in order to replicate experimental data regarding signal attenuation, the axial model resistance also decreases sigmoidally from the soma to the apical trunk:

$$R_i(x) = R_{i_{\text{soma}}} + \frac{(R_{i_{\text{end}}} - R_{i_{\text{soma}}})}{\left(1 + e^{\frac{d_{\text{half}} - d_x}{\text{steep}}}\right)}$$

where $R_{i_{\text{soma}}} = 50\,\Omega\text{cm}$, $R_{i_{\text{end}}} = 35\,\Omega\text{cm}$, $d_{\text{half}} = 210\,\mu\text{m}$, steep $= 50\,\mu\text{m}$.

The axial resistance in all apical oblique and basal dendrites is set to the somatic value, i.e. $R_i = 50\,\Omega\text{cm}$.

Ionic Currents

Our model cell contains a large variety of active currents which are expressed by the generic form:

$$I_i = \overline{g} \cdot m^M \cdot h^N \cdot (V - E_i)$$

where $\overline{g}_i$ is the maximal conductance of current I_i and E_i is its reversal potential. The current activates according to M activation gates represented by the gating variable m. It inactivates with N inactivation gates represented by the variable h. h and m obey to first-order kinetic equations.

Voltage-Dependent Sodium Current $\mathbf{I_{Na}}$ and Delayed Rectifier $\mathbf{I_{K\text{-}DR}}$

The model kinetics for the Hodgkin-Huxley-like currents I_{Na} and $I_{\text{K-DR}}$ are adapted originally from Bernander et al. (1991). The sodium current is described by the equation:

$$I_{\text{Na}} = \overline{g}_{\text{Na}} \cdot m^2 \cdot h \cdot s \cdot (V - E_{\text{Na}})$$

where an additional variable "s" is introduced to account for dendritic location-dependent slow attenuation of the sodium current (Jung et al., 1997; Migliore

et al., 1999). We use this parameter to vary the amount of attenuation along the apical trunk as a function of distance from the cell body such that proximal sections show little attenuation and distal sections show comparably more (with the exception of distal obliques which show very little signal attenuation). Activation and inactivation kinetics for I_{Na} are given by

$$m_{t+dt} = m_t + (1 + e^{\frac{dt}{\tau_m}}) \cdot (m_{\inf} - m_t)$$
$$h_{t+dt} = h_t + (1 - e^{\frac{dt}{\tau_h}}) \cdot (h_{\inf} - h_t)$$
$$s_{t+dt} = s_t + (1 + e^{\frac{dt}{\tau_\sigma}}) \cdot (s_{\inf} - s_t)$$

with $dt = 0.1$ ms and corresponding steady-state equations:

$$m_{\inf} = \frac{1}{1 + e^{(-\frac{V+40}{3})}}, h_{\inf} = \frac{1}{1 + e^{(\frac{V+45}{3})}}, s_{\inf} = \frac{1 + \mathrm{Na}_{\mathrm{att}} \cdot e^{(\frac{V+60}{2})}}{1 + e^{(\frac{V+60}{2})}}$$

and time constants $\tau_m = 0.05$ ms, $\tau_h = 0.5$ ms and

$$\tau_\sigma = \frac{0.00333(\mathrm{ms}) \cdot e^{0.0024(1/\mathrm{mV}) \cdot (V+60) \cdot Q(\deg \mathrm{C})}}{1 + e^{0.0012(1/\mathrm{mV}) \cdot (V+60) \cdot Q(\deg \mathrm{C})}}$$

The function $Q(^\circ\mathrm{C})$ is given by

$$Q(\deg \mathrm{C}) = \frac{F}{R \cdot (T + \deg \mathrm{C})}$$

where $R = 8.315\,\mathrm{J/deg\,C}$, $F = 9.648 \times 10^4\,\mathrm{C}$, $T = 273.16$ in degrees Kelvin and deg C is the temperature in degrees Celsius. The $\mathrm{Na}_{\mathrm{att}}$ variable represents the degree of sodium current attenuation and varies linearly from soma to distal trunk ($\mathrm{Na}_{\mathrm{att}}\ \varepsilon[0 \rightarrow 1]$: maximum $\rightarrow$ zero attenuation).

Similarly, channel kinetics for the delayed rectifier current are given by

$$I_{\text{K-DR}} = \overline{g}_{\text{K-DR}} \cdot m^2 \cdot (V - E_K)$$
$$m_{t+dt} = m_t + (1 - e^{-\frac{dt}{2.2}}) \cdot (m_{\inf} - m_t)$$
$$m_{\inf} = \frac{1}{1 + e^{(-\frac{V+42}{2})}}$$

The sodium and delayed rectifier channel properties are slightly different in the soma, axis and dendritic arbour. To fit experimental data regarding the backpropagation of spike trains, soma and axon compartments have a lower threshold for Na^+ spike initiation (≈ -57 mV) than dendritic ones (≈ -50 mV). Thus, the $m_{\inf}$ and $h_{\inf}$ somatic/axonic HH channel kinetics as well as the time constants for both $I_{\mathrm{Na}}^{\mathrm{sa}}$ and $I_{\text{K-DR}}^{\mathrm{sa}}$ are modified as follows. For the sodium,

$$m_{\text{inf}}^{\text{sa}} = \frac{1}{1+e^{(\frac{V+44}{3})}}, h_{\text{inf}}^{\text{sa}} = \frac{1}{1+e^{(\frac{V+49}{3.5})}},$$

while for the potassium delayed rectifier

$$m_{\text{inf}}^{sa} = \frac{1}{1+e^{(-\frac{V+46.3}{3})}}$$

The somatic time constant for somatic/axonic Na^+ channel activation is kept the same $\tau_m = 0.05$ ms while for inactivation is set to $\tau_h = 1$ ms. The τ value for the delayed rectifier channel activation is set to $\tau_m = 3.5$ ms. In all of the following equations, τ values are given in ms while in functions with V as an input, the symbol V is in mV.

Fast Inactivating Potassium Current I_A

A-type potassium channels are known to be distributed in high densities in the dendrites of CA1 pyramidal neurons while channel kinetics are different between proximal and distal populations. Furthermore, the density of these channels was found to increase by more than a factor of 6 from the soma to 350 μm in the apical trunk (Hoffman et al., 1997; Migliore et al., 1999). Based on these findings, a linear increase in I_A channel conductance was implemented along the apical trunk, with different channel kinetics for proximal ($I_{A_{\text{prox}}}$) vs. ($I_{A_{\text{dist}}}$) distal compartments, as per Hoffman et al. (1997). Kinetic equations for both channels are given by

$$\begin{aligned} I_A &= \overline{g}_A \cdot m \cdot h \cdot (V - E_K) \\ m_{t+dt} &= m_t + \left(1 - e^{-\frac{dt}{\tau_m}}\right) \cdot \left(\frac{1}{1+\alpha_m(V)} - m_t\right) \\ h_{t+dt} &= h_t + \left(1 - e^{-\frac{dt}{\tau_h}}\right) \cdot \left(\frac{1}{1+\alpha_h(V)} - h_t\right) \end{aligned}$$

with $\alpha(V)$, $\beta(V)$ equations and time constants (in ms) for the proximal I_A given by

$$\begin{aligned} \alpha_m(V) &= e^{(10^{-3}\cdot\zeta(V)\cdot(V-11)\cdot Q(\deg \text{C}))} \\ \beta_m(V) &= e^{(0.00055\cdot\zeta(V)\cdot(V-11)\cdot Q(\deg \text{C}))} \\ \alpha_h(V) &= e^{(0.003\cdot(V+56)\cdot Q(\deg \text{C}))} \\ \beta_h(V) &= \alpha_h(V) \\ \tau_m &= \max\left(\frac{\beta_m(V)}{0.05(1/\text{ms})\cdot qt(\deg \text{C})\cdot(1+\alpha_m(V))}, 0.1\right) \\ \tau_h &= \max(0.26(\text{ms/mV})\cdot(V+50), 2) \end{aligned}$$

The functions $\zeta(V)$ and $qt(\deg \text{C})$ are

$$\zeta(V) = -1.5 - \frac{1}{1 + e^{(V+40)/5}}(1/\text{mV}),\ qt(\text{deg C}) = 5^{\frac{(\text{deg C}-24)(\text{C}^\circ)}{10(\text{C}^\circ)}}$$

For distal channels, the equations $\alpha(V)$ and $\beta(V)$ are given by

$$\alpha_m(V) = e^{(10^{-3}\cdot\zeta(V)\cdot(V+1)\cdot Q(\text{deg C}))},\ \beta_{\text{m}}(V) = e^{(0.00039\cdot\zeta(V)\cdot(V+1)\cdot Q(\text{deg C}))}$$
$$\alpha_h(V) = e^{(0.003\cdot(V+56)\cdot Q(\text{deg C}))},\ \beta_{\text{h}}(V) = \alpha_h(V)$$
$$\tau_m = \max\left(\frac{\beta_m(V)}{0.1\cdot qt(\text{deg C})\cdot(1+\alpha_m(V))}, 0.1\right)$$
$$\tau_h = \max(0.26(\text{ms/mV})\cdot(V+50), 2)$$

where $\zeta(V)$ is expressed as

$$\zeta(V) = -1.8 - \frac{1}{1 + e^{(V+40)/5}}(1/\text{mV})$$

The maximal conductance values for both channel types vary as a function of distance from the cell body according to the following equations:

$$\overline{g}_{A_{\text{prox}}(x)} = \begin{cases} g_{A_{\text{soma}}} & \text{if } d_x \le 100\,\mu\text{m} \\ 0 & \text{if } d_x > 100\,\mu\text{m} \end{cases}$$

$$\overline{g}_{A_{\text{dist}}(x)} = \begin{cases} 0 & \text{if } d_x \le 100\,\mu\text{m} \\ \overline{g}_{A_{\text{init}}}\cdot\overline{g}_{A_{\text{factor}}}\cdot\frac{d_x}{350\,\mu\text{m}} & \text{if } 100 < d_x \le 350\,\mu\text{m} \\ \overline{g}_{A_{\text{init}}}\cdot\overline{g}_{A_{\text{factor}}} & \text{if } d_x > 350\,\mu\text{m} \end{cases}$$

where the somatic conductance $\overline{g}_{A_{\text{soma}}} = 7.5\,\text{mS/cm}^2$, the initial conductance value $\overline{g}_{A_{\text{init}}} = 7.488\,\text{mS/cm}^2$ and the maximum dendritic factor $g_{A_{\text{factor}}} = 6.5$. The above trunk distribution results in more than 5-fold increase in the A-current conductance at 300 μm, similar to the experimental value reported by Hoffman et al. (1997).

Hyperpolarization Activated Current I_h

The hyperpolarization-activated h-current is known to be differentially distributed along the dendritic arbour of CA1 neurons with increasing channel density from the soma to the distal trunk sections (Magee, 1998). The elevated dendritic conductance has been shown to have a location-dependent impact in the basic membrane properties and the propagation of voltage traces (Magee, 1998). In order to fit these empirical data, the I_{h} mechanism in our model cell is distributed in a sigmoidally increasing manner from the soma to the main apical trunk:

$$\overline{g}_h(x) = \overline{g}_{h_{\text{soma}}} + \frac{\overline{g}_{h_{\text{end}}} - \overline{g}_{h_{\text{soma}}}}{(1.0 + \exp((d_{\text{half}} - d_x)/\text{steep}))}$$

where

$$\overline{g}_{h_{\text{soma}}} = 18.72\,\text{mS/cm}^2,\ g_{h_{\text{end}}} = 9 \cdot \overline{g}_{h_{\text{soma}}},\ d_{\text{half}} = 280\,\mu\text{m},\ \text{steep} = 50\,\mu\text{m}.$$

This implementation results in a 7-fold increase in I_{h} conductance at 350 μm as per Magee (1998).

The kinetic equations for h-type channels are given by

$$I_h = \overline{g}_h \cdot m \cdot (V - E_h)$$

$$\frac{dm}{dt} = \frac{1 - \left(\frac{1}{1 + e^{-(V+90)/8.5}}\right) - m}{\tau}$$

$$\tau = \begin{cases} 1 & \text{if } V > -30\,\text{mV} \\ \frac{2}{(e^{-((V+145)/17.5)} + e^{((V+16.8)/16.5)})} + 10 & \text{otherwise} \end{cases}$$

where $E_h = -10\,\text{mV}$ is the h-current reversal potential.

Voltage-Dependent Calcium Currents

Calcium channel kinetic equations and density distributions are adapted from Magee and Johnston (1995) and were modified to account for distally evoked Ca^{2+} spikes.

LVA (T-type) Ca^{++} Channel

The kinetics are given by

$$I_{\text{CaT}} = \overline{g}_{\text{CaT}} \cdot m^2 \cdot h \frac{0.001\,\text{mM}}{0.001\,\text{mM} + \text{Ca}_{\text{in}}} \cdot ghk(V, \text{Ca}_{\text{in}}, \text{Ca}_{\text{out}})$$

$$ghk(V, \text{Ca}_{\text{in}}, \text{Ca}_{\text{out}}) = -x \cdot \left(1 - \frac{\text{Ca}_{\text{in}}}{\text{Ca}_{\text{out}}} \cdot e^{\frac{V}{x}}\right) \cdot f\left(\frac{V}{x}\right)$$

$$x = \frac{0.0853 \cdot (T + \deg \text{C})}{2},\ f(z) = \begin{cases} 1 - \frac{z}{2} & \text{if abs(z)} < 10^{-4} \\ \frac{z}{e^z - 1} & \text{otherwise} \end{cases}$$

$$m_{t+dt} = m_t + (1 + e^{-\frac{dt}{\tau_m}}) \cdot \left(\frac{\alpha_m(V)}{\alpha_m(V) + \beta_m(V)} - m_t\right)$$

$$h_{t+dt} = h_t + (1 - e^{-\frac{dt}{\tau_h}}) \cdot \left(\frac{\alpha_h(V)}{\alpha_h(V) + \beta_h(V)} - h_t\right)$$

$$\alpha_m(V) = -0.196 \cdot \frac{(V - 19.88)}{e^{-(V-19.88)/10} - 1},\ \beta_m(V) = 0.046 \cdot e^{-(V/22.73)}$$

$$\alpha_h(V) = 0.00016 \cdot e^{-(V+57)/19},\ \beta_h(V) = \frac{1}{e^{-(V-15)/10} + 1}$$

$$\tau_m = \frac{1}{\alpha_m(V) + \beta_m(V)},\ \tau_h = \frac{1}{0.68 \cdot (\alpha_h(V) + \beta_h(V))}$$

where Ca_{in} and Ca_{out} are the internal and external calcium concentrations.

LVA (T-type), Ca^{2+} channels are distributed along the main trunk, starting from the proximal dendrites to the distal tuft, with linearly increasing conductance as shown by

$$\overline{g}_{\mathrm{CaT}}(x) = \begin{cases} 0 & \text{if } d_x < 100\,\mu\mathrm{m} \\ \overline{g}_{\mathrm{CaT_{int}}} \cdot \overline{g}_{\mathrm{CaT_{factor}}} \cdot \frac{d_x}{350\,\mu\mathrm{m}} & \text{if } d_x \geq 100\,\mu\mathrm{m} \end{cases}$$

where $\overline{g}_{\mathrm{CaT_{int}}} = 0.1\,\mathrm{mS/cm^2}$ and $\overline{g}_{\mathrm{CaT_{factor}}} = 4$. LVA (T-type), Ca^{2+} channels are also inserted at the soma with a conductance value of $g_{\mathrm{CaT_{factor}}} = 0.05\,\mathrm{mS/cm^2}$.

HVAm (R-type) Ca^{++} Channels

The dendritic HVAm (R-type) Ca^{2+} channels are distributed in a uniform way along the apical trunk, with a small conductance value of $\overline{g}^{d}_{\mathrm{CaR}} = 0.3\,\mathrm{mS/cm^2}$. The corresponding somatic conductance is 10 times higher than the apical trunk value, $\overline{g}^{s}_{\mathrm{CaR}} = 3\,\mathrm{mS/cm^2}$. Channel kinetics are given by the equations

$$\begin{aligned} I_{\mathrm{CaR}} &= \overline{g}_{\mathrm{CaR}} \cdot m^3 \cdot h \cdot (V - E_{\mathrm{Ca}}) \\ m_{t+dt} &= m_t + (1 + e^{-\frac{dt}{\tau_m}}) \cdot (\alpha(V) - m_t) \\ h_{t+dt} &= h_t + (1 - e^{\frac{dt}{\tau_h}}) \cdot (\beta(V) - h_t) \end{aligned}$$

The difference between somatic and dendritic CaR currents lies in the $\alpha(V)$, $\beta(V)$ and τ parameter values. For the somatic current, $\tau_m = 100\,\mathrm{ms}$ and $\tau_h = 5\,\mathrm{ms}$ while for the dendritic current $\tau_m = 50\,\mathrm{ms}$ and $\tau_h = 5\,\mathrm{ms}$. The $\alpha(V)$ and $\beta(V)$ equations for dendritic CaR channels are

The $\alpha(V)$ and the $\beta(V)$ equations for the dendritic CaR channels are

$$\alpha(V) = \frac{1}{1 + e^{-(V+48.5)/3}},\ \beta(V) = \frac{1}{1 + e^{(V+53)}}$$

While for the somatic CaR channels

$$\alpha(V) = \frac{1}{1 + e^{-(V+60)/3}},\ \beta(V) = \frac{1}{1 + e^{(V+62)}}$$

HVA (L-type) Ca^{++} Channels

Most of the kinetic equations for somatic HVA (L-type) channels are the same as the equations for T-type channels. Equations that are different between the two mechanisms are given by

$$I^s_{\mathrm{CaL}} = \overline{g}^s_{\mathrm{CaL}} \cdot m \cdot \frac{0.001\,\mathrm{mM}}{0.001\,\mathrm{mM} + \mathrm{Ca_{in}}} \cdot ghk(V, \mathrm{Ca_{in}}, \mathrm{Ca_{out}})$$
$$\alpha_m(V) = -0.055 \cdot \frac{(V + 27.01)}{e^{-(V+27.01)/3.8} - 1}, \beta_m(V) = 0.94 \cdot e^{-(V+63.01)/17}$$
$$\tau_m = \frac{1}{5 \cdot (\alpha_m(V) + \beta_m(V))}$$

where $\overline{g}^s_{\mathrm{CaL}} = 7\,\mathrm{mS/cm^2}$.

Dendritic L-type calcium channels have different kinetics:

$$I^d_{\mathrm{CaL}} = \overline{g}^d_{\mathrm{CaL}} \cdot m^3 \cdot h \cdot (V - E_{\mathrm{Ca}})$$
$$\alpha(V) = \frac{1}{1 + e^{-(V+37)}}, \beta(V) = \frac{1}{1 + e^{(V+41)/0.5}}$$

Time constants are equal to $\tau_m = 3.6\,\mathrm{ms}$ and $\tau_h = 29\,\mathrm{ms}$.

The dendritic HVA (L-type) channels are distributed in a nonuniform way along the apical trunk:

$$\overline{g}^d_{\mathrm{CaL}}(x) = \begin{cases} 0.1 \cdot \overline{g}_{\mathrm{CaL_{int}}} & \text{if } d_x < 50\,\mu\mathrm{m} \\ 4.6 \cdot \overline{g}_{\mathrm{CaL_{init}}} & \text{if } d_x \geq 50\,\mu\mathrm{m} \end{cases}$$

where $\overline{g}_{\mathrm{CaL_{init}}} = 0.316\,\mathrm{mS/cm^2}$ and the corresponding somatic conductance is equal to $\overline{g}_{\mathrm{CaL_{init}}} = 7\,\mathrm{mS/cm^2}$. No Ca^{2+} channels were inserted in the axon or the basal dendrites of this model.

Calcium Pumping/Buffering

A calcium pump/buffering mechanism is also inserted at the cell body and along the apical trunk. The mechanism is taken from Destexhe et al. (1994) and was modified to replicate the sharp Ca^{2+} spike repolarization observed in Golding et al. (1999). The factor for Ca^{2+} entry was changed from $f_e = 10,000$ to $f_e = 10,000/18$ and the rate of calcium removal was made seven times faster. The kinetic equations are given by

$$\text{drive\_channel} = \begin{cases} -f_e \cdot \frac{I_{\mathrm{Ca}}}{0.2 \cdot \mathrm{FARADAY}} & \text{if drive\_channel} > 0\,\mathrm{mM/ms} \\ 0 & \text{otherwise} \end{cases}$$
$$\frac{d\mathrm{Ca}}{dt} = \text{drive\_channel} + \frac{(10^{-4}(\mathrm{mM}) - \mathrm{Ca})}{7 \cdot 200(\mathrm{ms})}.$$

Calcium-Dependent Potassium Current I_{sAHP}

Empirical data suggest that the excitatory effects of calcium channels in the soma and proximal trunk regions are counteracted by Ca^{2+}-activated potassium channels (Sah and Bekkers, 1996). Thus, Ca^{2+}-dependent slow and medium AHP potassium channels (along with a calcium pump/buffering mechanism) are distributed in a higher conductance along these regions:

$$\overline{g}_{\mathrm{sAHP}}(x) = \begin{cases} 5 \cdot \overline{g}_{\mathrm{sAHP_{init}}} & \text{if } 50 < d_x < 200\,\mu\mathrm{m} \\ 0.5 \cdot \overline{g}_{\mathrm{sAHP_{init}}} & \text{otherwise} \end{cases}$$

$$\overline{g}_{\mathrm{mAHP}}(x) = \begin{cases} 2 \cdot \overline{g}_{\mathrm{mAHP_{init}}} & \text{if } 50 < d_x < 200\,\mu\mathrm{m} \\ 0.25 \cdot \overline{g}_{\mathrm{mAHP_{init}}} & \text{otherwise} \end{cases}$$

where $\overline{g}_{\mathrm{sAHP_{init}}} = 0.1\,\mathrm{mS/cm^2}$ and $\overline{g}_{\mathrm{mAHP_{init}}} = 16.5\,\mathrm{mS/cm^2}$. The somatic values for these two channels are equal to $\overline{g}_{\mathrm{sAHP_{init}}} = 0.5\,\mathrm{mS/cm^2}$ and $\overline{g}_{\mathrm{mAHP_{init}}} = 90.75\,\mathrm{mS/cm^2}$.

The channel kinetics for I_{sAHP} are taken with no modifications from Destexhe et al. (1994) and the kinetics equations are given by

$$I_{\mathrm{sAHP}} = \overline{g}_{\mathrm{sAHP}} \cdot m^3 \cdot (V - E_K)$$

$$\frac{dm}{dt} = \frac{\frac{\mathrm{Cac}}{(1+\mathrm{Cac})} - m}{\tau}$$

$$\tau = \max\left(\frac{1}{0.003(1/\mathrm{ms}) \cdot (1 + \mathrm{Cac}) \cdot 3^{(\deg \mathrm{C}-22)/10}}, 0.5\right)$$

where $\mathrm{Cac} = (\mathrm{Ca_{in}}/0.025(\mathrm{mM}))^2$

Calcium-Dependent Potassium Current I_{mAHP}

The medium AHP current I_{mAHP} taken from Moczydlowski and Latorre (1983) is given by

$$I_{\mathrm{mAHP}} = \overline{g}_{\mathrm{mAHP}} \cdot m \cdot (V - E_K)$$

$$m_{t+dt} = m_t + (1 + e^{-\frac{dt}{\tau_m}}) \cdot \left(\frac{\alpha_m(V)}{\tau_m} - m_t\right)$$

$$\alpha_m(V) = \frac{0.48(1/\mathrm{ms})}{1 + \frac{0.18(\mathrm{mM})}{\mathrm{Ca_{in}}} \cdot e^{(-1.68 \cdot V \cdot Q(\deg \mathrm{C}))}}$$

$$\beta_m(V) = \frac{0.28(1/\mathrm{ms})}{1 + \frac{\mathrm{Ca_{in}}}{0.011(\mathrm{mM}) \cdot e^{(-2 \cdot V \cdot Q(\deg \mathrm{C}))}}}$$

$$\tau_m = \frac{1}{\alpha_m(V) + \beta_m(V)}$$

Slowly Inactivating Potassium Current I_m

A slowly activating voltage-dependent potassium current I_m is inserted along the apical trunk and cell body with a fixed conductance value $\overline{g}_{km} = 60\,\mathrm{mS/cm^2}$ with the exception of oblique side branches, where $\overline{g}_{km} = 120\,\mathrm{mS/cm^2}$. The channel is given by the equations:

$$I_m = 10^{-4} \cdot T_{adj}(\deg \mathrm{C}) \cdot \overline{g}_m \cdot m \cdot (V - E_K)$$

$$T_{\mathrm{adj}}(\deg \mathrm{C}) = 2.3^{(\deg \mathrm{C}-23)/10}$$

$$m_{t+dt} = m_t + \left(1 - e^{-\frac{dt \cdot T_{\mathrm{adj}}(\deg \mathrm{C})}{\tau}}\right) \cdot \left(\frac{\alpha(V)}{(\alpha(V) + \beta(V)} - m_t\right)$$

$$\alpha(V) = 10^{-3} \cdot \frac{(V + 30)}{(1 - e^{-(V+30)/9})}$$

$$\beta(V) = -10^{-3} \cdot \frac{(V + 30)}{(1 - e^{(V+30)/9})}$$

$$\tau = \frac{1}{\alpha(V) + \beta(V)}$$

Persistent Sodium Current I_{Nap}

Finally, a persistent sodium channel is inserted in the distal apical tuft. The channel is described by the equations:

$$I_{\mathrm{Nap}} = \overline{g}_{\mathrm{Nap}} \cdot m^3 \cdot (V - E_{\mathrm{Na}})$$

$$m = \frac{1}{(1 + e^{-(V+50.4)/4.5})}$$

Synaptic Mechanisms

In addition to the above channel mechanisms, AMPA, NMDA, GABA_A and GABA_B synaptic mechanisms are implemented in the model. These were taken from Destexhe et al. (1997) without modification.

The AMPA Mechanism

$$I = g_{\max} \cdot R \cdot (V - E_{\mathrm{rev}})$$

$$R = R_{\mathrm{inf}} + (R_0 - R_{\mathrm{inf}}) \cdot e^{(-\frac{t - t_{\mathrm{last}}}{\tau_R})}$$

where R represents the fraction of open channels, R_{inf} the open channels in steady state and t_{last} the last time of neurotransmitter release.

$$R_{\text{inf}} = (C_{\max} \cdot \alpha)/(C_{\max} \cdot \alpha + \beta)$$
$$\tau_R = \frac{1}{\alpha \cdot C_{\max} + \beta}$$

The parameter $C_{\max}$ is the maximum transmitter concentration, $C_{\max} = 1\,\text{mM}$, α represents the forward binding rate, $\alpha = 10\text{ms}^{-1}\text{mM}^{-1}$ and β is the backward unbinding rate, $\beta = 0.5\,\text{ms}^{-1}$.

The NMDA Mechanism

$$I = g \cdot (V - E_{\text{rev}})$$
$$g = \frac{g_{\max} \cdot R}{(1 + \text{eta} \cdot \text{Mg} \cdot e^{-\gamma \cdot V})}$$
$$R = R_{\text{inf}} + (R_0 - R_{\text{inf}}) \cdot e^{(-\frac{t - t_{\text{last}}}{\tau_R})}$$

where eta $= 0.33/\text{mM}$, Mg $= 1\,\text{mM}$ and $\gamma = 0.06/\text{mV}$.

The GABA$_A$ Mechanism

$$I = g_{\max} \cdot R \cdot (V - E_{\text{rev}})$$
$$R = R_{\text{inf}} + (R_0 - R_{\text{inf}}) \cdot e^{(-\frac{t - t_{\text{last}}}{\tau_R})}$$
$$R_{\text{inf}} = C_{\max} \cdot \alpha/(C_{\max} \cdot \alpha + \beta)$$
$$\tau_R = \frac{1}{\alpha \cdot C_{\max} + \beta}$$

The forward and binding rates are $\alpha = 5\,\text{ms}^{-1}\text{mM}^{-1}$, $\beta = 0.18\,\text{ms}^{-1}$ and $C_{\max} = 1\,\text{mM}$.

The GABA$_B$ Mechanism

$$I = \frac{g_{\max} \cdot G^n}{G^n + KD}(V - E_{\text{rev}})$$
$$\frac{dR}{dt} = K_1 \cdot T \cdot (1 - R) - K_2 \cdot R$$
$$\frac{dG}{dt} = K_3 \cdot R - K_4 \cdot G$$

where R is the activated receptors, T the transmitter binding to the receptor and G the activated G-protein. Parameter n represents the activated G-protein that binds to a potassium channel. Parameter K_1 equals to $K_1 = 0.09\,\text{ms}^{-1}\text{mM}^{-1}$ and corresponds to the forward binding rate to receptor. Parameter K_2 equals to $K_2 = 0.00129\,\text{ms}^{-1}$ and corresponds to the backward unbinding rate of the receptor. $K_3 = 0.18\,\text{ms}^{-1}$ and stands for the rate of G-protein production whereas $K_4 = 0.034\,\text{ms}^{-1}$ is the rate of G-protein decay. The dissociation constant of potassium current is $KD = 100$ and the number of binding sites of G-protein potassium equals to $n = 4$.

Channel Distributions in Apical Oblique Dendrites

Due to the lack of empirical data bearing on the densities and distribution of conductances within oblique side branches, most channel properties in our model are set to be identical for all branches extending from the main apical trunk, after an initial section. Membrane properties for oblique sections within 50 μm from the trunk follow the respective trunk values while most conductance values beyond the first 50 μm are set equal to the values in a selected trunk section located at 157 μm from the cell body. Specifically, conductance values are distributed as follows:

$$\overline{g}_{\text{all}}(x) = \begin{cases} \overline{g}_{\text{all}_{\text{trunk}}} & \text{if } d(x, \text{trunk}) \leq 50\,\mu\text{m} \\ \overline{g}_{\text{all}_{\text{hold}}} & \text{if } d_x < 300\,\mu\text{m and } d(x, \text{trunk}) > 50\,\mu\text{m} \end{cases}$$

where $\overline{g}_{\text{all}}$ includes conductance values for I_A ($\overline{g}_{\text{Aprox}_{\text{hold}}} = 0$, $g_{\text{Adist}_{\text{hold}}} = 27.285\,\text{ms/cm}^2$) for $I_h(g_{\text{h}_{\text{hold}}} = 30.5\,\text{mS/cm}^2)$, $\overline{g}_{\text{leak}}(g_{\text{leak}_{\text{hold}}} = 6.94 \times 10^{-6}\,1/\Omega\text{cm}^2)$, $I^d_{\text{CaR}}(g^d_{\text{CaR}_{\text{hold}}} = 0.03\,\text{mS/cm}^2)$, $I^{\text{d}}_{\text{CaL}}(g^d_{\text{CaL}_{\text{hold}}} = 1.455\,\text{mS/cm}^2)$, $I_{\text{CaT}}(g_{\text{CaT}_{\text{hold}}} = 0.179\,\text{mS/cm}^2)$, $I_{\text{sAHP}}(g_{\text{sAHP}_{\text{hold}}} = 0.5\,\text{mS/cm}^2)$, $I_{\text{mAHP}}(\overline{g}_{\text{mAHP}_{\text{hold}}} = 18.5\,\text{mS/cm}^2)$, $I_m(g_{\text{Km}_{\text{hold}}} = 60\,\text{mS/cm}^2)$, and $I_{\text{pNa}}(g_{\text{pNa}_{\text{trunk}}} = 5.6 \times 10^{-5}\,\text{mS/cm}^2$, $g_{\text{pNa}_{\text{hold}}} = 0.00028\,\text{ms/cm}^2)$ inserted only in the oblique dendrites. The Na^+ spike attenuation variable Na_{att} also follows the above rules. The parameter $\overline{g}_{\text{all}_{\text{trunk}}}$ refers to the respective trunk values for all conductances within each oblique, while $\overline{g}_{\text{all}_{\text{hold}}}$ denotes the selected conductance values taken from the trunk section at 157 μm. The function $d(x$,trunk) measures the path distance from any point x in the oblique to the connection side with the trunk.

For oblique dendrites located beyond 300 μm (vertical distance from soma), channel conductances are modified as follows to account for distally evoked Ca^{++} spikes:

$$\begin{aligned} \overline{g}_{A_{\text{dist}}}(x) &= 2.47 \cdot \overline{g}_{\text{Adist}_{\text{hold}}} && \text{if } d_x > 300\,\mu\text{m} \\ \overline{g}^d_{\text{CaR}}(x) &= 13 \cdot g_{\text{CaR}^d_{\text{hold}}} && \text{if } d_x > 300\,\mu\text{m} \end{aligned}$$

$$\begin{aligned} \overline{g}_{\text{sAHP}}(x) &= 5 \cdot \overline{g}_{\text{sAHP}_{\text{init}}} && \text{if } d_x > 300\,\mu\text{m} \\ g^d_{\text{K-DR}}(x) &= 1.07 g^d_{\text{K-DR}_{\text{hold}}} && \text{if } d_x > 300\,\mu\text{m} \\ \overline{g}_{\text{pNa}}(x) &= 2 \cdot \overline{g}_{\text{pNa}_{\text{hold}}} && \text{if } d_x > 350\,\mu\text{m} \\ \text{Na}_{\text{att}}(x) &= 0.95 && \text{if } d_x > 350\,\mu\text{m} \end{aligned}$$

$$\overline{g}^d_{\text{CaL}}(x) = \begin{cases} 14 \cdot g_{\text{CaL}^d_{\text{hold}}} & \text{if } 300 < d_x \leq 350\,\mu\text{m} \\ 15 \cdot g_{\text{CaL}^d_{\text{hold}}} & \text{if } d_x > 350\,\mu\text{m} \end{cases}$$

To account for the activity-dependent attenuation of sodium channel conductance in CA1 cells, we vary the amount of attenuation along the apical trunk of our model

as a function of distance from the cell body such that proximal sections show little attenuation and distal sections show comparably more. We implement a linear decay from proximal to distal dendrites with an exception in the distal oblique dendrites where the sodium channel attenuation is very small ($\mathrm{Na}_{\mathrm{att}} = 0.95$ for $d_x > 300\,\mu\mathrm{m}$).

The basal dendrites of our model contain significantly fewer membrane mechanisms since the focus of the current work is to study synaptic integration in apical oblique dendrites. To define basal conductance values in addition to the HH mechanisms, we select (hold) the conductance values at an apical trunk section located at $50\,\mu\mathrm{m}$ and use the following equations:

$$\overline{g}_{A_{\mathrm{dist}}}(x) = 1.6 \cdot \overline{g}_{A_{\mathrm{dist}_{\mathrm{hold}}}}$$
$$\overline{g}_{A_{\mathrm{prox}}}(x) = 1.6 \cdot \overline{g}_{A_{\mathrm{prox}_{\mathrm{hold}}}}$$
$$R_m(x) = R_{m_{\mathrm{hold}}}$$
$$\overline{g}_h(x) = \overline{g}_{h_{\mathrm{soma}}}$$

Further Reading

Achard, P., and De Schutter, E. (2006). Complex parameter landscape for a complex neuron model. PLoS Comput Biol. *2*, e94.

Amitai, Y., Friedman, A., Connors, B., and Gutnick, M. (1993). Regenerative electrical activity in apical dendrites of pyramidal cells in neocortex. Cerebral Cortex *3*, 26–28.

Andersen, P., Silfvenius, H., Sundberg, S.H., Sveen, O. (1980). A comparison of distal and proximal dendritic synapses on CA1 pyramids on guinea pig hippocampal slices in vitro. J Physiol *307*, 273–299.

Archie, K.A., and Mel, B.W. (2000). A model for intradendritic computation of binocular disparity. Nat Neurosci *3*, 54–63.

Ariav, G., Polsky, A., and Schiller, J. (2003). Submillisecond precision of the input-output transformation function mediated by fast sodium dendritic spikes in basal dendrites of CA1 pyramidal neurons. J Neurosci *23*, 7750–7758.

Ascoli, G.A. (2006). Mobilizing the base of neuroscience data: the case of neuronal morphologies. Nat Rev Neurosci *7*, 318–324.

Avery, R.B., and Johnston, D. (1997). Ca2+ channel antagonist U-92032 inhibits both T-type Ca2+ channels and Na+ channels in hippocampal CA1 pyramidal neurons. J Neurophysiol *77*, 1023–1028.

Bernander, O., Douglas, R.J., Martin, K.A., and Koch, C. (1991). Synaptic background activity influences spatiotemporal integration in single pyramidal cells. Proc Natl Acad Sci USA *88*, 11569–11573.

Bernander, O., Koch, C., and Douglas, R.J. (1994). Amplification and linearization of distal synaptic input to cortical pyramidal cells. J Neurophysiol *72*, 2743–2753.

Borg-Graham, L. (1998). Interpretations of data and mechanisms for hippocampal pyramidal cell models. In Cerebral Cortex (New York: Kluwer Academic/Plenum Publishers), pp. 19–138.

Bowden, S.E., Fletcher, S., Loane, D.J., and Marrion, N.V. (2001). Somatic colocalization of rat SK1 and D class (Ca(v)1.2) L-type calcium channels in rat CA1 hippocampal pyramidal neurons. J Neurosci *21*, RC175.

Burkitt, N. (2006). A Review of the Integrate-and-fire Neuron Model: I. Homogeneous Synaptic Input. Biol Cybern *95*(1), 1–19.

Burkitt, N. (2006). A review of the integrate-and-fire neuron model: II. Inhomogeneous synaptic input and network properties. Biol Cybern *95*(1), 97–112.

Cajal, S.R.Y. (1995). Histology of the Nervous System (New York: Oxford).

Cannon, R.C., Turner, D.A., Pyapali, G.K., and Wheal, H.V. (1998). An on-line archive of reconstructed hippocampal neurons. J Neurosci Methods *84*, 49–54.

Cash, S., and Yuste, R. (1999). Linear summation of excitatory inputs by CA1 pyramidal neurons. Neuron *22*, 383–394.

Cauller, L.J., and Connors, B.W. (1994). Synaptic physiology of horizontal afferents to layer I in slices of rat SI neocortex. J Neurosci *14*, 751–762.

Chklovskii, D.B., Mel, B.W., and Svoboda, K. (2004). Cortical rewiring and information storage. Nature *431*, 782–788.

Contreras, D., Destexhe, A., and Steriade, M. (1997). Intracellular and computational characterization of the intracortical inhibitory control of synchronized thalamic inputs in vivo. J Neurophysiol *78*, 335–350.

Day, M., Carr, D.B., Ulrich, S., Ilijic, E., Tkatch, T., and Surmeier, D.J. (2005). Dendritic excitability of mouse frontal cortex pyramidal neurons is shaped by the interaction among HCN, Kir2, and Kleak channels. J Neurosci *25*, 8776–8787.

De Schutter, E., and Bower, J.M. (1994). Simulated responses of cerebellar Purkinje cells are independent of the dendritic location of granule cell synaptic inputs. Proc Natl Acad Sci USA *91*, 4736–4740.

Destexhe, A., Mainen, Z.F., and Sejnowski, T.J. (1994). Synthesis of models for excitable membranes, synaptic transmission and neuromodulation using a common kinetic formalism. J Comput Neurosci *1*, 195–230.

Destexhe, A., Mainen, Z.F., and Sejnowski, T.J. (1997). Kinetic models of synaptic transmission. In Methods in Neuronal Modeling, C. Koch, and I. Segev, eds. (Cambridge, MA: MIT Press).

Dvorak-Carbone, H., and Schuman, E.M. (1999). Patterned activity in stratum lacunosum moleculare inhibits CA1 pyramidal neuron firing. J Neurophysiol *82*, 3213–3222.

Gasparini, S., and Magee, J.C. (2006). State-dependent dendritic computation in hippocampal CA1 pyramidal neurons. J Neurosci *26*, 2088–2100.

Gasparini, S., Migliore, M., and Magee, J.C. (2004). On the initiation and propagation of dendritic spikes in CA1 pyramidal neurons. J Neurosci *24*, 11046–11056.

Gerstner, W., and Kistler, W. (2002). *Spiking Neurons Models: Single Neurons, Populations, Plasticity*. Cambridge, UK: Cambridge University Press.

Golding, N.L., Jung, H.Y., Mickus, T., and Spruston, N. (1999). Dendritic calcium spike initiation and repolarization are controlled by distinct potassium channel subtypes in CA1 pyramidal neurons. J Neurosci *19*, 8789–8798.

Golding, N.L., Kath, W.L., and Spruston, N. (2001). Dichotomy of action-potential backpropagation in CA1 pyramidal neuron dendrites. J Neurophysiol *86*, 2998–3010.

Golding, N.L., Mickus, T.J., Katz, Y., Kath, W.L., and Spruston, N. (2005). Factors mediating powerful voltage attenuation along CA1 pyramidal neuron dendrites. J Physiol *568*, 69–82.

Golding, N.L., and Spruston, N. (1998). Dendritic sodium spikes are variable triggers of axonal action potentials in hippocampal CA1 pyramidal neurons. Neuron *21*, 1189–1200.

Golomb, D., Yue, C., and Yaari, Y. (2006). Contribution of persistent Na+ current and M-type K+ current to somatic bursting in CA1 pyramidal cells: combined experimental and modeling study. pp. 1912–1926.

Gomez González, J.F., Mel, B.W., and Poirazi, P. (2009). Distinguishing linear vs. nonlinear integration in CA1 radial oblique dendrites: it's about time. submitted.

Graham, B.P. (2001). Pattern recognition in a compartmental model of a CA1 pyramidal neuron. Network *12*, 473–492.

Hasselmo, M., and Schnell, E. (1994). Laminar selectivity of the cholinergic suppression of synaptic transmission in rat hippocampal region CA1: computational modeling and brain slice physiology. J Neurosci *14*, 3898–3914.

Hausser, M., Spruston, N., and Stuart, G.J. (2000). Diversity and dynamics of dendritic signaling. Science *290*, 739–744.

Herz, A.V.M., Gollisch, T., Machens, C.K., and Jaeger, D. (2006). Modeling single-neuron dynamics and computations: a balance of detail and abstraction. Science *314* (5796), 80–85.

Hines, M.L., and Carnevale, N.T. (1997). The NEURON simulation environment. Neural Comput *9*, 1179–1209.

Hjorth-Simonsen, A., and Jeune, B. (1972) Origin and termination of the hippocampal perforant path in the rat studied by silver impregnation. J Comp Neurol *144*, 215–232.

Hoang, L., Kesner, R.P. (2008). Dorsal hippocampus, CA3, and CA1 lesions disrupt temporal sequence completion. Behav Neurosci *122*, 9–15.

Hoffman, D.A., Magee, J.C., Colbert, C.M., and Johnston, D. (1997). K+ channel regulation of signal propagation in dendrites of hippocampal pyramidal neurons. Nature *387*, 869–875.

Holtmaat, A., De Paola, V., Wilbrecht, L., and Knott, G.W. (2008). Imaging of experience-dependent structural plasticity in the mouse neocortex in vivo. Behav Brain Res *192*, 20–25.

Holtmaat, A.J., Trachtenberg, J.T., Wilbrecht, L., Shepherd, G.M., Zhang, X., Knott, G.W., and Svoboda, K. (2005). Transient and persistent dendritic spines in the neocortex in vivo. Neuron *45*, 279–291.

Hunsaker, M., Lee, B., and Kesner, R.P. (2008). Evaluating the temporal context of episodic memory: the role of CA3 and CA1. Behav Brain Res. *188*, 310–315.

Hunsaker, M., Mooy, G.G., Swift, J.S., Kesner, R.P. (2007). Dissociations of the medial and lateral perforant path projections into dorsal DG, CA3, and CA1 for spatial and nonspatial (visual object) information processing. Behav Neurosci *121*, 742–750.

Jarsky, T., Roxin, A., Kath, W.L., and Spruston, N. (2005). Conditional dendritic spike propagation following distal synaptic activation of hippocampal CA1 pyramidal neurons. Nat Neurosci *8*, 1667–1676.

Johnston, D., and Amaral, D. (2005). Hippocampus. In The Synaptic Organization of the Brain, G. Shepherd, ed. (New York: Oxford University Press), pp. 455–498.

Johnston, D., Christie, B.R., Frick, A., Gray, R., Hoffman, D.A., Schexnayder, L.K., Watanabe, S., and Yuan, L.L. (2003). Active dendrites, potassium channels and synaptic plasticity. Philos Trans R Soc Lond B Biol Sci *358*, 667–674.

Johnston, D., Hoffman, D.A., Colbert, C.M., and Magee, J.C. (1999). Regulation of back-propagating action potentials in hippocampal neurons. Curr Opin Neurobiol *9*, 288–292.

Johnston, D., Hoffman, D.A., Magee, J.C., Poolos, N.P., Watanabe, S., Colbert, C.M., and Migliore, M. (2000). Dendritic potassium channels in hippocampal pyramidal neurons. J Physiol *525 Pt 1*, 75–81.

Johnston, D., and Narayanan, R. (2008). Active dendrites: colorful wings of the mysterious butterflies. Trends Neurosci *31*, 309–316.

Jung, H.Y., Mickus, T., and Spruston, N. (1997). Prolonged sodium channel inactivation contributes to dendritic action potential attenuation in hippocampal pyramidal neurons. J Neurosci *17*, 6639–6646.

Katz, Y., Kath, W.L., Spruston, N., and Hasselmo, M.E. (2007). Coincidence detection of place and temporal context in a network model of spiking hippocampal neurons. PLoS Comput Biol *3*, e234.

Keren, N., Peled, N., and Korngreeen, A. (2005). Constraining compartmental models using multiple voltage recordings and genetic algorithms. J Neurophysiol *94*, 3730–3742.

Kesner, R.P., Lee, I., and Gilbert, P. (2004). A behavioral assessment of hippocampal function based on a subregional analysis. Rev Neurosci *15*, 333–351.

Kim, J., Jung, S.-C., Clemens, A.M., Petralia, R.S., and Hoffman, D.A. (2007). Regulation of dendritic excitability by activity-dependent trafficking of the A-type K+ channel subunit Kv4.2 in hippocampal neurons. Neuron *54*, 933–947.

Koch, C. (1999). Biophysics of Computation: Information Processing in Single Neurons (New York: Oxford University Press).

Koch, C., Poggio, T., and Torre, V. (1983). Nonlinear interactions in a dendritic tree: localization, timing, and role in information processing. Proc Natl Acad Sci USA *80*, 2799–2802.

Koch, C., and Segev, I. (2000). The role of single neurons in information processing. Nat Neurosci *3 Suppl*, 1171–1177.

Larkum, M.E., Senn, W., and Luscher, H.R. (2004). Top-down dendritic input increases the gain of layer 5 pyramidal neurons. Cereb Cortex *14*, 1059–1070.

Larkum, M.E., Zhu, J.J., and Sakmann, B. (1999). A new cellular mechanism for coupling inputs arriving at different cortical layers. Nature *398*, 338–341.

Laurent, G., and Borst, A. (2007). Short stories about small brains: linking biophysics to computation. In Dendrites, G.J. Stuart et al., ed. (New York: Oxford University Press), pp. 441–464.

Lee, I., Jerman, TS, Kesner, RP. (2005). Disruption of delayed memory for a sequence of spatial locations following CA1- or CA3-lesions of the dorsal hippocampus. Neurobiol Learn Mem. *84*, 138–147.

Lee, I., and Kesner, R.P. (2002). Differential contribution of NMDA receptors in hippocampal subregions to spatial working memory. Nat Neurosci *5*, 162–168.

Lee, I., and Kesner, R.P. (2003). Differential roles of dorsal hippocampal subregions in spatial working memory with short versus intermediate delay. Behav Neurosci *117*, 1044–1053.

Lee, I., and Kesner, R.P. (2004). Differential contributions of dorsal hippocampal subregions to memory acquisition and retrieval in contextual fear-conditioning. Hippocampus *14*, 301–310.

Li, X., and Ascoli, G.A. (2006). Computational simulation of the input-output relationship in hippocampal pyramidal cells. J Comput Neurosci *21*, 191–209.

Liebmann, L., Karst, H., Sidiropoulou, K., van Gemert, N., Meijer, O.C., Poirazi, P., and Joels, M. (2008). Differential effects of corticosterone on the slow afterhyperpolarization in the basolateral amygdala and CA1 region: possible role of calcium channel subunits. J Neurophysiol *99*, 958–968.

London, M., and Hausser, M. (2005). Dendritic computation. Annu Rev Neurosci *28*, 503–532.

Losonczy, A., and Magee, J.C. (2006). Integrative properties of radial oblique dendrites in hippocampal CA1 pyramidal neurons. Neuron *50*, 291–307.

Losonczy, A., Makara, J.K., and Magee, J.C. (2008). Compartmentalized dendritic plasticity and input feature storage in neurons. Nature *452*, 436–441.

Maccaferri, G., McBain, C.J. (1995). Passive propagation of LTD to stratum oriens-alveus inhibitory neurons modulates the temporoammonic input to the hippocampal CA1 region. *15(1)*, 137–145.

Magee, J., Hoffman, D., Colbert, C., and Johnston, D. (1998). Electrical and calcium signaling in dendrites of hippocampal pyramidal neurons. Annu Rev Physiol *60*, 327–346.

Magee, J.C. (1998). Dendritic hyperpolarization-activated currents modify the integrative properties of hippocampal CA1 pyramidal neurons. J Neurosci *18*, 7613–7624.

Magee, J.C., and Cook, E.P. (2000). Somatic EPSP amplitude is independent of synapse location in hippocampal pyramidal neurons. Nat Neurosci *3*, 895–903.

Magee, J.C., and Johnston, D. (1995). Synaptic activation of voltage-gated channels in the dendrites of hippocampal pyramidal neurons. Science *268*, 301–304.

Magee, J.C., and Johnston, D. (2005). Plasticity of dendritic function. Curr Opin Neurobiol *15*, 334–342.

Markaki, M., Orphanoudakis, S., and Poirazi, P. (2005). Modelling reduced excitability in aged CA1 neurons as a calcium-dependent process. Neurocomputing *65–66*, 305–314.

Marrion, N.V., and Tavalin, S.J. (1998). Selective activation of Ca2+-activated K+ channels by co-localized Ca2+ channels in hippocampal neurons. Nature *395*, 900–905.

Megias, M., Emri, Z., Freund, T.F., Gulyas, A.I. (2001). Total number and distribution of inhibitory and excitatory synapses on hippocampal CA1 pyramidal cells. Neuroscience *102*, 527–540.

Mel, B.W. (1992a). NMDA-Based pattern discrimination in a modeled cortical neuron. Neural Comput *4*, 502–516.

Mel, B.W. (1992b). The clusteron: toward a simple abstraction for a complex neuron. In Advances in Neural Information Processing Systems, J. Moody, S. Hanson, and R. Lippman, eds. (San Mateo, CA: Morgan Kaufmann), pp. 35–42.

Mel, B.W. (1993). Synaptic integration in an excitable dendritic tree. J Neurophysiol *70*, 1086–1101.

Mel, B.W. (1999). Computational neuroscience. Think positive to find parts. Nature *401*, 759–760.

Mel, B.W., Ruderman, D.L., and Archie, K.A. (1998). Translation-invariant orientation tuning in visual "complex" cells could derive from intradendritic computations. J Neurosci *18*, 4325–4334.

Metz, A.E., Spruston, N., and Martina, M. (2007). Dendritic D-type potassium currents inhibit the spike afterdepolarization in rat hippocampal CA1 pyramidal neurons. J Physiol *581*, 175–187.

Migliore, M. (2003). On the integration of subthreshold inputs from Perforant Path and Schaffer Collaterals in hippocampal CA1 pyramidal neurons. J Comput Neurosci *14*, 185–192.

Migliore, M., Ferrante, M., and Ascoli, G.A. (2005). Signal propagation in oblique dendrites of CA1 pyramidal cells. J Neurophysiol *94*, 4145–4155.

Migliore, M., Hoffman, D.A., Magee, J.C., and Johnston, D. (1999). Role of an A-type K+ conductance in the back-propagation of action potentials in the dendrites of hippocampal pyramidal neurons. J Comput Neurosci *7*, 5–15.

Migliore, M., Messineo, L., and Ferrante, M. (2004). Dendritic Ih selectively blocks temporal summation of unsynchronized sistal inputs in CA1 pyramidal neurons. J Comput Neurosci *16*, 5–13.

Migliore, M., and Shepherd, G.M. (2002). Emerging rules for the distributions of active dendritic conductances. Nat Rev Neurosci *3*, 362–370.

Moczydlowski, E., and Latorre, R. (1983). Gating kinetics of Ca2+-activated K+ channels from rat muscle incorporated into planar lipid bilayers. Evidence for two voltage-dependent Ca2+ binding reactions. J Gen Physiol *82*, 511–542.

Nevian, T., Larkum, M.E., Polsky, A., and Schiller, J. (2007). Properties of basal dendrites of layer 5 pyramidal neurons: a direct patch-clamp recording study. Nat Neurosci *10*, 206–214.

O'Reilly, R., McClelland, J.L. (1994). Hippocampal conjunctive encoding, storage, and recall: avoiding a trade-off. Hippocampus *4*, 661–682.

Otmakhova, N.A., Otmakhov, N., and Lisman, J.E. (2002). Pathway-specific properties of AMPA and NMDA-mediated transmission in CA1 hippocampal pyramidal cells. J Neurosci *22*, 1199–1207.

Pissadaki, E.K., and Poirazi, P. (2007). Modulation of excitability in CA1 pyramidal neurons via the interplay of entorhinal cortex and CA3 inputs. Neurocomputing *70*, 1735–1740.

Pissadaki, E.K., Sidiropoulou K., Reczko M., and Poirazi, P. Encoding of spatio-temporal input characteristics by a single CA1 pyramidal neuron model. (submitted).

Poirazi, P., Brannon, T., and Mel, B.W. (2003a). Arithmetic of subthreshold synaptic summation in a model CA1 pyramidal cell. Neuron *37*, 977–987.

Poirazi, P., Brannon, T., and Mel, B.W. (2003b). Pyramidal neuron as two-layer neural network. Neuron *37*, 989–999.

Poirazi, P., and Mel, B.W. (2001). Impact of active dendrites and structural plasticity on the memory capacity of neural tissue. Neuron *29*, 779–796.

Polsky, A., Mel, B.W., and Schiller, J. (2004). Computational subunits in thin dendrites of pyramidal cells. Nat Neurosci *7*, 621–627.

Poolos, N.P., Migliore, M., and Johnston, D. (2002). Pharmacological upregulation of h-channels reduces the excitability of pyramidal neuron dendrites. Nat Neurosci *5*, 767–774.

Raab-Graham, K., Haddick, P.C., Jan, Y.N., and Jan, L.Y. (2006). Activity- and mTOR-dependent suppression of Kv1.1 channel mRNA translation in dendrites. Science *314*, 144–148.

Rall, W. (1964). Theoretical significance of dendritic trees for neuronal input-output relations. In Neural Theory and Modeling, R.F. Reiss, ed. (Stanford University Press).

Reyes, A. (2001). Influence of dendritic conductances on the input-output properties of neurons. Annu Rev Neurosci *24*, 653–675.

Rolls, E., and Treves, A. (1994). Neural networks in the brain involved in memory and recall. Prog Brain Res *102*, 335–341.

Rolls, E.T., and Kesner, R.P. (2006). A computational theory of hippocampal function, and empirical tests of the theory. Prog Neurobiol *79*, 1–48.

Sah, P., and Bekkers, J.M. (1996). Apical dendritic location of slow afterhyperpolarization current in hippocampal pyramidal neurons: implications for the integration of long-term potentiation. J Neurosci *16*, 4537–4542.

Shao, L.R., Halvorsrud, R., Borg-Graham, L., and Storm, J.F. (1999). The role of BK-type Ca2+-dependent K+ channels in spike broadening during repetitive firing in rat hippocampal pyramidal cells. J Physiol *521 Pt 1*, 135–146.

Shepherd, G.M., and Brayton, R.K. (1987). Logic operations are properties of computer-simulated interactions between excitable dendritic spines. Neuroscience *21*, 151–165.

Sidiropoulou, K., Joels, M., and Poirazi, P. (2007). Modeling stress-induced adaptations in Ca2+ dynamics. Neurocomputing *70*, 1640–1644.

Sidiropoulou, K., Pissadaki, E.K., and Poirazi, P. (2006). Inside the brain of a neuron. EMBO Rep *7*, 886–892.

Softky, W. (1994). Sub-millisecond coincidence detection in active dendritic trees. Neuroscience *58*, 13–41.

Spruston, N. (2008). Pyramidal neurons: dendritic structure and synaptic integration. Nat Rev Neurosci *9*, 206–221.

Spruston, N., Schiller, Y., Stuart, G., and Sakmann, B. (1995). Activity-dependent action potential invasion and calcium influx into hippocampal CA1 dendrites. Science *268*, 297–300.

Steward, O., and Scoville, S.A. (1976). Cells of origin of entorhinal cortical afferents to the hippocampus and fascia dentata of the rat. J Comp Neurol *169*, 343–370.

Stuart, G., and Spruston, N. (1998). Determinants of voltage attenuation in neocortical pyramidal neuron dendrites. J Neurosci *18*, 3501–3510.

Stuart, G., Spruston, N., Sakmann, B., and Hausser, M. (1997). Action potential initiation and backpropagation in neurons of the mammalian CNS. Trends Neurosci *20*, 125–131.

Trachtenberg, J.T., Chen, B.E., Knott, G.W., Feng, G., Sanes, J.R., Welker, E., and Svoboda, K. (2002). Long-term in vivo imaging of experience-dependent synaptic plasticity in adult cortex. Nature *420*, 788–794.

Treves, A. (2004). Computational constraints between retrieving the past and predicting the future, and the CA3–CA1 differentiation. Hippocampus *14*, 539–556.

Vago, D., and Kesner, R.P. (2008). Disruption of the direct perforant path input to the CA1 subregion of the dorsal hippocampus interferes with spatial working memory and novelty detection. Behav Brain Res *189*, 273–283.

Vinogradova, O. (2001). Hippocampus as comparator: role of the two input and two output systems of the hippocampus in selection and registration of information. Hippocampus *11*, 578–598.

Watanabe, S., Hoffman, D.A., Migliore, M., and Johnston, D. (2002). Dendritic K+ channels contribute to spike-timing dependent long-term potentiation in hippocampal pyramidal neurons. Proc Natl Acad Sci USA *99*, 8366–8371.

Wei, D.S., Mei, Y.A., Bagal, A., Kao, J.P., Thompson, S.M., Tang, C.M. (2001). Compartmentalized and binary behavior of terminal dendrites in hippocampal pyramidal neurons. Science *293*, 2272–2275.

Witter, M.P., Griffioen, A.W., Jorritsma-Byham, B., and Krijnen, J.L. (1988). Entorhinal projections to the hippocampal CA1 region in the rat: an underestimated pathway. Neurosci Lett *85*, 193–198.

Zuhlke, R.D., Pitt, G.S., Tsien, R.W., and Reuter, H. (2000). Ca2+-sensitive inactivation and facilitation of L-type Ca2+ channels both depend on specific amino acid residues in a consensus calmodulin-binding motif in the(alpha)1C subunit. J Biol Chem *275*, 21121–21129.

CA3 Cells: Detailed and Simplified Pyramidal Cell Models

Michele Migliore, Giorgio A. Ascoli, and David B. Jaffe

Overview

From rodents to humans, the hippocampus has been implicated in a variety of cognitive functions, including spatial navigation, memory storage, and recall (Hölscher, 2003). The classic anatomical representation of the hippocampal circuitry is organized around the synaptic loop from the entorhinal cortex to the dentate gyrus, to area CA3, to CA1, to the subicular complex, and back to the entorhinal cortex. In this pathway, area CA3 constitutes a pivotal crossroad of synaptic convergence and integration. In particular, the principal neurons of this region, CA3 pyramidal cells, receive monosynaptic excitatory inputs from the entorhinal stellate cells (via the perforant pathway), dentate granule cells (mossy fibers), and from other CA3 pyramidal cells (recurrent collaterals). These afferents pathways are laminated, with mossy fibers synapsing on the most proximal apical dendrites, recurrent collaterals on basal trees and medial apical dendrites, and perforant pathway on the distal apical branches. In order to understand the computational function of the hippocampus, it is important to relate its structure and activity at the cellular level. The electrophysiological repertoire of CA3 pyramidal cells includes single spiking and bursting, spanning a broad range of firing frequencies (∼1–200 Hz). This activity is mediated in part by a number of voltage-gated channels, each with specific properties and dendritic distributions.

Due to their unique anatomical and physiological properties, CA3 pyramidal cells play a central role in most theories of hippocampal function. The extensive network of recurrent collaterals, for example, has inspired proposals that CA3pcs form an autoassociative network, capable of pattern completion (Treves, 1995), path integration (Samsonovich and McNaughton, 1997), and trace conditioning (Rodriguez and Levy, 2001). Likewise, the layered arrangement of mossy fibers and perforant pathway afferent has stimulated theories of supervised learning (Lisman, 1999) and memory retrieval (O'Reilly and McClelland, 1994) in CA3 pyramidal cells,

M. Migliore (✉)
Institute of Biophysics, National Research Council, Palermo, Italy
e-mail: michele.migliore@cnr.it

V. Cutsuridis et al. (eds.), *Hippocampal Microcircuits*, Springer Series in Computational Neuroscience 5, DOI 10.1007/978-1-4419-0996-1_12,

as well as place field emergence (Kali and Dayan, 2000). The observation that CA3 pyramidal cells alternate high-frequency "sharp waves" with theta-modulated activity has led to influential "two-stage" theories of mnemonic processes (Buzsaki, 1989) with several variants (Hasselmo et al., 2002). Recent experimental evidence also demonstrated the central involvement of CA3 pyramidal cells in spatial memory acquisition (Nakazawa et al., 2003) and recall (Nakazawa et al., 2002).

Yet most basic elements of the computational role of CA3 pyramidal cells within the hippocampal circuit are still obscure. In particular, the specific contribution of mossy fiber, recurrent collateral, and perforant pathway excitation to CA3 pyramidal cell discharge is largely unknown. On the basis of relative synaptic strength, number of synapses, and relative firing frequency of the three afferent pathways, for example, mossy fiber may be more suitable to discriminate among stimuli (Urban et al., 2001) than to play the role of "detonator" assumed by some of the above theories. Nevertheless, the experimental and computational evidence on this matter is too sparse to definitely support either view (see, e.g., Henze et al., 2002). Similarly, the distribution and sparseness of synaptic inputs are important variables in the theory of information processing in CA3 pyramidal cells (Treves and Rolls, 1994), yet no experimentally validated computational model has related such variables to the resulting firing patterns of these neurons in vivo.

There is now abundant evidence that specific sets of active channels are present on the dendrites of hippocampal principal cells (Johnston et al., 1996). The dendritic distributions of these channels may define the computational role of a given cell type within its functional neural circuit (Migliore and Shepherd, 2002). Most electrophysiological investigations on the hippocampus in the last decade have mainly focused on CA1 pyramidal cells. The reason for this bias is mainly technical: due to their location and shape, CA1 pyramidal cells are more amenable to electrophysiological studies than CA3 pyramidal cells. As a result, while the properties and distribution of voltage-gated channels have been characterized fairly well in CA1 neurons, very little is known for CA3 pyramidal cells. This situation has led data-driven computational models to emphasize CA1 neurons, while the theory-driven models of CA3 have drifted away from empirical observations. In fact, the composition and distribution of dendritic channels of CA3 pyramidal cells are likely to be different from CA1, given the distinct morphologies, passive properties, and firing behaviors of these neurons. In turn, we expect that CA3 pyramidal cells will have different patterns of dendritic electrogenesis from CA1 and unique characteristics with respect to synaptic integration.

The general passive properties of CA3 pyramidal cells have been the subject of seminal investigations (Spruston and Johnston, 1992; Major et al., 1994). However, these studies used very young animals without specifying the location (CA3a–c) of the neurons. CA3 pyramidal cell morphology varies considerably between sublayers (Ishizuka et al., 1995) and with the age of the animal (Pyapali and Turner, 1996), and the passive and active properties are likely to vary as well (Jaffe and Carnevale, 1999). Because of the dramatic potential effect of morphological differences on CA3 pyramidal cell firing (Krichmar et al., 2002), we characterized the properties of these neurons in specified central location (CA3b) and animal model.

The Model

The Experimental Traces to be Modeled

We are interested in modeling the different firing types experimentally observed at physiological temperatures in pyramidal neurons of the CA3b area to suggest a physiological explanation in terms of the mechanism underlying each firing type and their possible interplay. The widely assumed view for hippocampal pyramidal neurons of the CA3 area, supported by several experimental findings (most of which dating back to the late 1980s), is that the primary firing mode of CA3 pyramidal neurons is bursting, elicited by a minimal somatic stimulation. However, we have previously found (Hemond et al., 2008) that neurons in this area behave in a very different way, much more flexible from a computational point of view. Here we will consider four different firing patterns experimentally observed in these neurons, represented by the typical experimental traces (from different cells) plotted in Fig. 1. All of them were generated by the same stimulation protocol (a 400 ms constant somatic current injection). The first (and admittedly the simplest one) is the classical train of action potentials (APs) showing a weak adaptation (Fig. 1a). The next one (Fig. 1b) shows an unexpected property for CA3 neurons, a delayed first spike. Next (Fig. 1c) is a strongly adapting pattern and, finally, a burst (Fig. 1d).

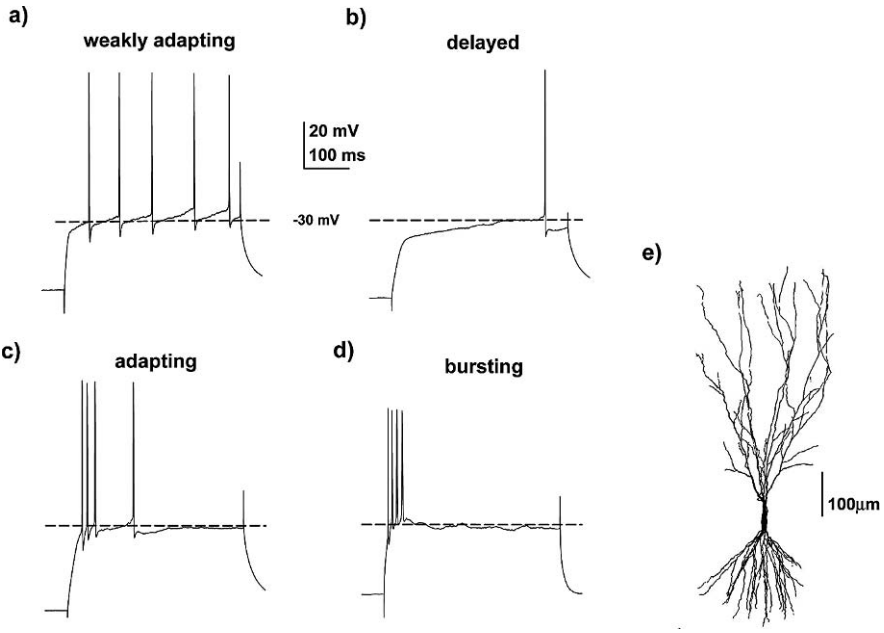

Fig. 1 Typical experimental traces from different CA3b neurons showing the various firing types observed in these cells (**a–d**), and the 3D reconstruction used in most simulations (**e**). The traces were those used as reference to implement the model. Details on the experimental methods are given in Hemond et al. (2008). *Dotted lines* are drawn at −30 mV

For the purposes of this chapter, we have decided to use a step-by-step approach, in the attempt to highlight what we think are fundamental considerations in trying to model a set of experimental traces. For this particular case (pyramidal neurons of the hippocampal CA3 area) as modelers we are at the same time in the best and the worst position to attempt a realistic modeling of a number of different firing properties. In fact, practically all the basic information that we would need to implement a "good" model is missing. There is practically not enough detailed information on the channels that are expressed in these neurons, and/or their kinetic, and/or their dendritic distribution. This is usually a bad start for a realistic model but, at the same time, we are left with many possible choices to explore, several experiments to suggest, and predictions to make.

Whenever we would like to model a set of experimental data, we must decide the level of details we intend to reach during the implementation process. In our case, each trace is a single suprathreshold current clamp experiment, and the different firing examples are from different cells. Under these conditions, as general rule of thumb, we avoided any quantitative fit, for a very simple reason: perfect fits require perfect experiments, currently a kind of an impossible condition to achieve in most cases, especially for current clamps eliciting a train of APs. There are simply too many experimental variables that cannot be controlled during the recordings. Even the simplest repetition of a stimulation protocol on the same cell will not result in overlapping traces, invalidating all the efforts of a quantitative fit. We will then focus on the more general properties that characterize the different traces in Fig. 1, such as the interspike intervals and, for the reasons explained below, the spike's amplitude. With our model, we expect to be able to show which conductance underlies each firing pattern and why.

The Set of Conductances

All simulations were implemented using the NEURON v6.2 simulation environment (Hines and Carnevale, 1997). In some cases, simulations were carried out using the *ParallelContext* class of NEURON on a 5120-processor IBM Linux cluster under MPI (CINECA consortium, Bologna). The model files, based on a previously published model, are available for public download under the ModelDB section of the Senselab database (http://senselab.med.yale.edu, accession number 101629).

In all simulations carried out to implement a realistic model we used the cell depicted in Fig. 1e. Its 3D morphology (together with many others) is available for public download (www.neuromorpho.org, Ascoli, 2006, cell1zr). This is a typical CA3 pyramidal neuron, with several main apical dendrites stemming out from (or very close to) the soma, many second-order and third-order bifurcations, and thin dendrites. One of the very first decisions in implementing a realistic model is related to the passive properties to use in the simulations. In our case, we are confronted with traces from different cells, in a population that has been found (Hemond et al., 2008) to have passive membrane properties that span a large range

of values, with membrane time constants in the 30–120 ms range, input resistance (R_N) between 20 and 200 MΩ, and resting membrane potential between −70 and −53 mV (with average at −60 mV). Under these conditions, even assuming that charging curves with small subthreshold stimulation are available for all the cells we intend to model, we think that the same representative values should be used in all cases. In fact, the large variability observed in the experiments, independently from the various firing modes, suggests that there is no point in using specific passive properties for each case. We then decided to use −60 mV as resting potential (the average value) and (unless noted otherwise) 30 KΩ/cm^2 for the membrane-specific resistance, with a membrane capacitance of 1.4 μF/cm^2 (which implicitly takes into account spines and dendrites missed from the reconstruction). This results in a membrane time constant of $\tau_m = 42$ ms. To test for the effects of larger τ_m, we have occasionally tested the results using a larger specific membrane resistance (50 KΩ/cm^2 instead of 30 KΩ/cm^2).

In order to have some success in modeling the different traces that we have chosen (Fig. 1), we need some "tools," i.e., a set of membrane conductances that are most likely involved with the various firing properties. The main conductances, as in virtually any pyramidal neuron, are *Na*, K_{DR}, and K_A. These are responsible for spike generation and repolarization. There are no experimental data for the kinetic of these channels in CA3b neurons at physiological temperature, so we started from the kinetic used to model a number of experimental findings on CA1 pyramidal neurons (e.g., Migliore et al., 1999; Watanabe et al., 2002; Poolos et al., 2002). The voltage dependence of their activation, inactivation, and time constants are shown in Fig. 2a. We can immediately see a problem: in all experimental traces the action potentials are elicited at full amplitude (∼90 mV) when the membrane potential reaches around −30 mV. This occurs under both low (such as in Fig. 1b) and high (such in Fig. 1d) somatic current injections. If we use CA1 channels, e.g., trying to model the weakly adapting case in Fig. 1a, we can adjust the peak conductances in such a way to obtain a good qualitative agreement for the spike amplitude and the first few interspike intervals (as in Fig. 2b). However, these channels have been implemented to reproduce APs in CA1 neurons, which are elicited at around −55 mV. For CA3b neurons, the experimental traces imply that the *Na* current must be substantially de-inactivated, and ready to activate, around −30 mV. This is a condition impossible to achieve with *Na* channels for CA1 neurons (Fig. 2a) that at −30 mV are almost completely inactivated: there is no way to elicit an action potential from this level of membrane depolarization. An easy solution is to shift toward a more depolarized potential the *Na* (and consequently K_A and K_{DR}) conductance. By trial and error we found that with a +24 mV shift we were able to reproduce the higher spike threshold (Fig. 2c), and the spike height and duration (Fig. 2d) of CA3b neurons. Here is a first, experimentally testable prediction of the model: at least the *Na*, K_A, and K_{DR} conductances should be shifted to the right, with respect to those expressed in CA1 neurons. If it turns out that this is not the case, then another mechanism must be found to explain such a high spike threshold in these neurons.

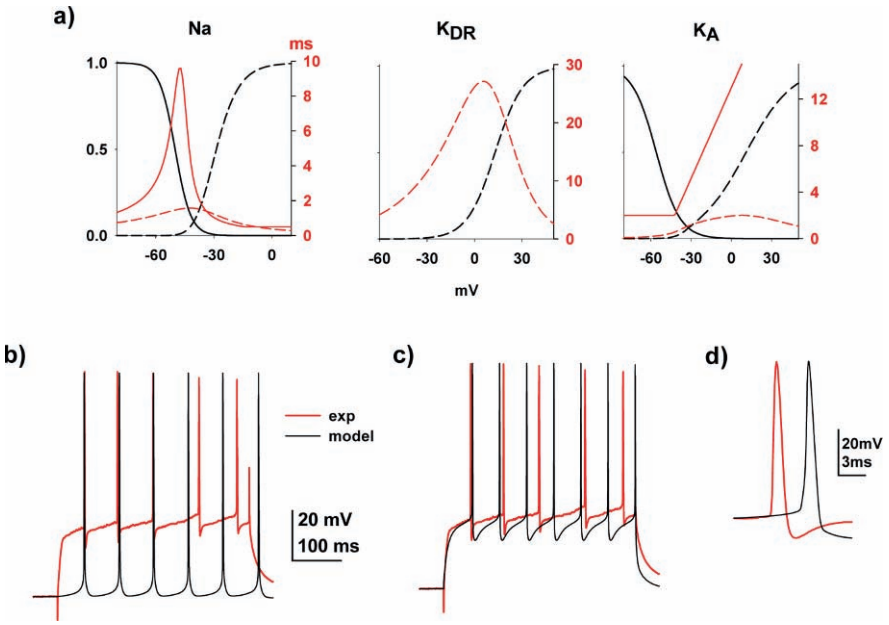

Fig. 2 Channel kinetic for *Na*, K_{DR} and K_A conductances from CA1 neurons. (**a**) **G**ate variables for activation (*black dashed lines*), inactivation (*black solid traces*), and their time constant (*red lines*) for *Na*, K_{DR}, and K_A conductances used to model a number of different experimental findings on CA1 neurons at physiological temperature; the time constant for *Na* activation is plotted with a 10× factor; (**b**) CA1 channels can reproduce the spike height and interspike intervals, but not the high rheobase observed in CA3b neurons; (**c**) (*red*) experimental trace; (*black*) model using a + 24 mV shift for Na, K_{DR}, and K_A; (**d**) expanded view of the first action potential of the traces in (**c**). The peak conductances for all cases are reported in Table 1

Model Justification

We are now ready to attack the other problems posed by the experimental traces. In order to do that we, of course, need more "tools." In addition to *Na*, K_A, and K_{DR}, we need conductances that would be able to generate adaptation, bursting, and delayed firing.

One of the simplest adaptation mechanisms is the K_M conductance (Fig. 3a, top right). We used the same kinetic (with the +24 mV shift) used to model experimental findings in CA1 neurons (Shah et al., 2008). It is relatively slow at physiological temperatures and it would be substantially open around −30 mV. It can thus be used to model long-lasting adapting properties.

Next, of course, are the *Ca* channels. These are virtually everywhere in every principal neuron. We can not possibly include all of the *Ca* channels studied so far in hippocampal neurons. We decided to use three different types of *Ca* channels, covering the three main properties of these channels: transient (Ca_T), long-lasting (Ca_L), and neither of those (Ca_N). Their kinetics, and the resulting current under a

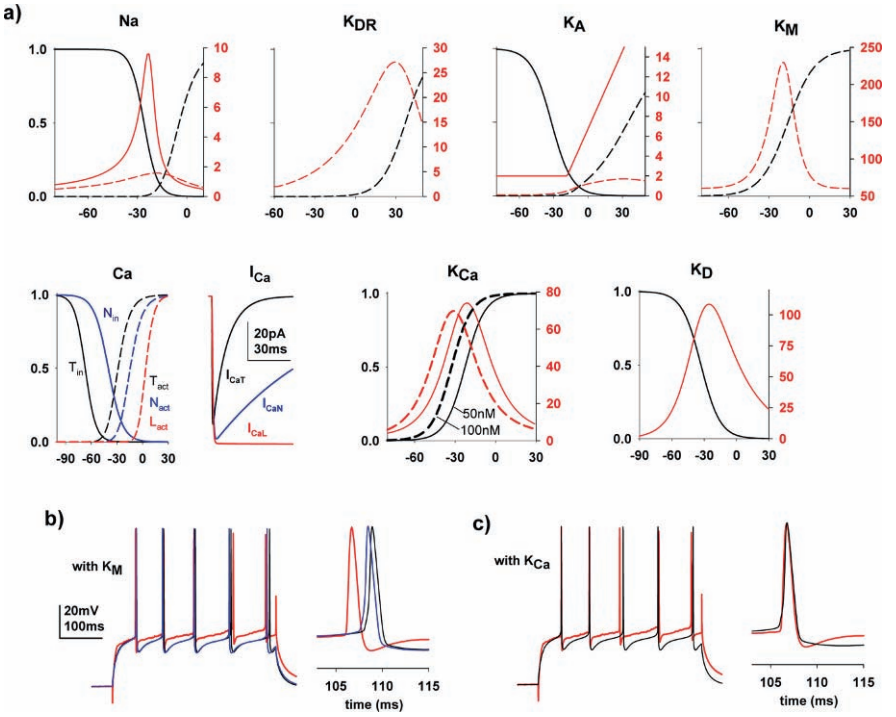

Fig. 3 Conductances used to model all the experimental traces in Fig. 1; (**a**) gate variables and time constants (line type and color as in Fig. 2, except for *Ca* and K_{Ca}) for each conductance used in the model. For clarity, time constants for *Ca* channels were omitted, and an additional panel showing the time course of the different *Ca* currents (Ca_T, Ca_N, and Ca_L) under voltage clamp to +20 mV (from −80 mV) has been included; activation of the *Ca*-dependent *K* conductance, K_{Ca}, is shown at two $[Ca]_i$ concentrations. (**b**) Model of a weakly adapting CA3b neuron using only K_M as adaptation mechanism; the traces on the right show an expanded view of the first spike in the experimental and model traces. (*red*) experimental trace; (*black*) model; (*blue*) model using a higher membrane time constant; (**c**) Model of a weakly adapting CA3b neuron using only K_{Ca} as adaptation mechanism; the traces on the right show an expanded view of the first spike in the experimental and model traces

voltage clamp, are shown in Fig. 3a (*Ca* and I_{Ca}). Given the very sparse information on properties, distribution, and relative density of these channels in CA3b neurons, we will just use the same peak conductance for all types in all cases (Table 1). In fact, for the traces we intend to model, we are not in the position to appreciate the different contributions of the different channels in the various cases. The same applies to the intracellular Ca dynamics, for which we decided to use a simple extrusion mechanism with a 100 ms time constant.

The presence of *Ca* channels in the model implies the use of another very popular mechanism of adaptation, i.e., *Ca*-dependent K^+ conductances. There are different kinds of these conductances. In this case we used the one responsible for the fast hyperpolarization. Its kinetic and *Ca*-dependence is shown in Fig. 3a (K_{Ca}).

Table 1 Peak conductances (S/cm^2) and current injection used to model the experimental traces

	g_{Na}	$g_{K\text{-}DR}$	g_{KA}	g_{KM}	g_{Ca}	g_{KCa}	g_{KD}	I_{inj}(nA)
Figure 2b (no shift)	0.024	0.00144	0.0161	0	0	0	0	0.008
Figure 2c (shift)	0.035	0.012	0.055	0	0	0	0	0.76
Figure 3b (with K_M)	0.035	0.012	0.055	0.00058 0.0007	5e-5	0	0	0.76 0.69
Figure 3c (with K_{Ca})	0.035	0.012	0.055	0	5e-5	2.1e-6	0	0.76
Figure 4b	0.045	0.012	0.055	0	5e-5	2.1e-6	0.001	0.778 0.835
Figure 4c	0.045	0.012	0.055	0	5e-5	7e-6	0.001	0.809 0.850
Figure 4d	0.045	0.012	0.055	0.0025	5e-5	0	0.001	0.848 0.868
Figure 5b	0.035	0.012	0.055	0.00058	5e-5	0	0	0.85
Figure 5c	0.035	0.0035	0.025	0.0061	5e-5	0	0	0.614
Figure 5d	0.035	0.0035	0.025	0	5e-5	1.65e-5	0	0.6
Figure 5e	0.035	0.0035	0.025	0.0025	5e-5	1.07e-5	0	0.61
Figure 6b	0.035	0.012	0.055	0.0	5e-5	2.1e-6	0	1.58
Figure 6c	0.025	0.012	0.055	0.0	5e-5	2.1e-6	0	1.58
Figure 6d	0.025	0.012	0.055	0.0	5e-5	8e-5	0	1.58
Figure 6e	0.025	0.012	0.055	0.01	5e-5	4.1e-5	0	1.58 1.15

Finally, we need a "tool" to implement the delayed firing. In fact, we need a specific mechanism that would be active around -30 mV, slowly inactivating beyond that. Again, there are no experimental indications on its kinetic in these neurons, so we just implemented a generic K^+ conductance with these properties, since delayed firing is a property typically dependent on what is termed K_D current. Its activation and time constant are plotted in Fig. 3a (K_D).

Weak Adaptation

We are now ready to model the first of our traces, from a weakly adapting cell (Fig. 1a). In our set of conductances, we have two mechanisms for adaptation, K_M (alone) and K_{Ca} (paired with *Ca* channels). We then started from the configuration that we used to model the first spike time, the spike height, and the spike duration (but not the adapting phase, Fig. 2c). Using just the K_M peak conductance as a free parameter, we were easily able to reproduce quantitatively weak adaptation firing (Fig. 3b, black). This is a good condition to test the possible differences between cells with different τ_m. What do we expect in this case? The increase in the membrane resistance from 30 to 50 KΩ/cm^2 will increase not only the membrane time constant (from 42 to 70 ms) but also the input resistance of the cell from 90 to 130 MΩ (within the experimental range). The neuron now will appear to be more

excitable. Thus, in order to get the five spikes observed in the experimental trace during the 400 ms of current injection, we should expect a lower current and/or a higher K_M, to compensate for the increased excitability. The results confirmed our hypothesis: with a higher τ_m we needed a lower input (-10%) and a higher K_M ($+17\%$) to model the same firing behavior (Fig. 3b, blue), without affecting the spike shape (Fig. 3b, right), which depends more on K_A and K_{DR}.

Delayed Firing

Next, we considered the delayed firing (Fig. 1b). There are experimental indication for a K_D involvement, so we just added our K_D conductance to the soma (since its distribution is unknown), a minimal modification to the weakly adapting model of Fig. 3b, c. In this case we have two experimental traces to use as reference, plotted in Fig. 4a. They are from the same cell under two different current injections. By including a somatic K_D in the model of Fig. 3c (which uses K_{Ca} as adaptation mechanism) we were readily able to model the delayed firing under low-current injection (Fig. 4b, left). However, if we use a higher current, to reproduce the first spike time (Fig. 4b, right), we elicit too many spikes. There is a reason for this effect. By including K_D we had to use a higher current to reach the spike threshold, to compensate for the additional shunting effect produced by a K^+ current. As K_D inactivates, only the K_{Ca} is left to modulate the interspike frequency, and its actual density (which was used to model a weakly adapting firing) is too low for this case. In fact, its increase (Fig. 4c) resulted in a much better qualitative agreement with the experiments. The same good agreement can be obtained by increasing K_M instead, as shown in Fig. 4d. This suggests a prediction that should be relatively easy to test experimentally: in addition to K_D, cells showing a delayed firing should have a larger K_{Ca} or K_M, with respect to those showing weakly adapting behavior.

Strong Adaptation

The typical experimental trace that we used as reference to model strong adaptation is shown in Fig. 5a. As usual we started from one of the configurations used to model the weakly adapting cell, in this case using K_M (Fig. 5b). After adjusting the current injection to obtain the first spike coincident with the one in the experimental trace, we can immediately spot a few problems: the spike frequency is too high (Fig. 5b, left), the first interspike interval is too long, and the spikes are lower and with a shorter duration, with respect to the experiment (Fig. 5, right). This gives us an indication of what we should change in our model. In order to increase the spike amplitude, at first one can be tempted to increase the *Na* conductance. This, however, will cause an additional activation of K_A and K_{DR}, during the AP upstroke, reducing even more the spike duration. The right move is instead to reduce K_A and K_{DR}, in such a way to reduce their effect on the spike shape (mostly caused by K_A)

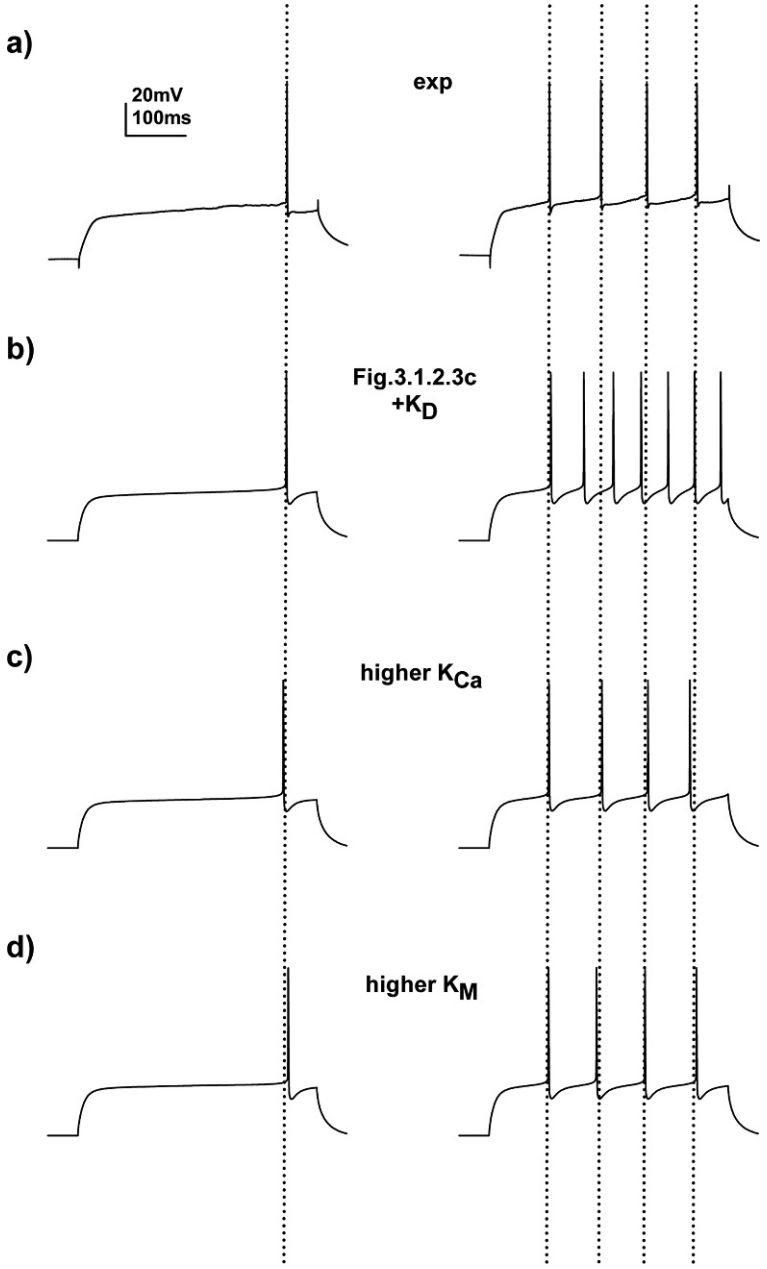

Fig. 4 Modeling CA3b pyramidal neurons showing delayed firing. (**a**) Experimental traces from the same cell under two somatic 400 ms current injections; (**b**) model results for low- and high-current injections with the set of conductances used for Fig. 3 plus K_D; (**c**) increasing K_{Ca} results in a much better agreement with the experiments; (**d**) using K_M, instead of K_{Ca}, to increase the interspike intervals, also results in a very good agreement with the experiments. *Vertical dotted lines* mark the spike times in the experimental traces

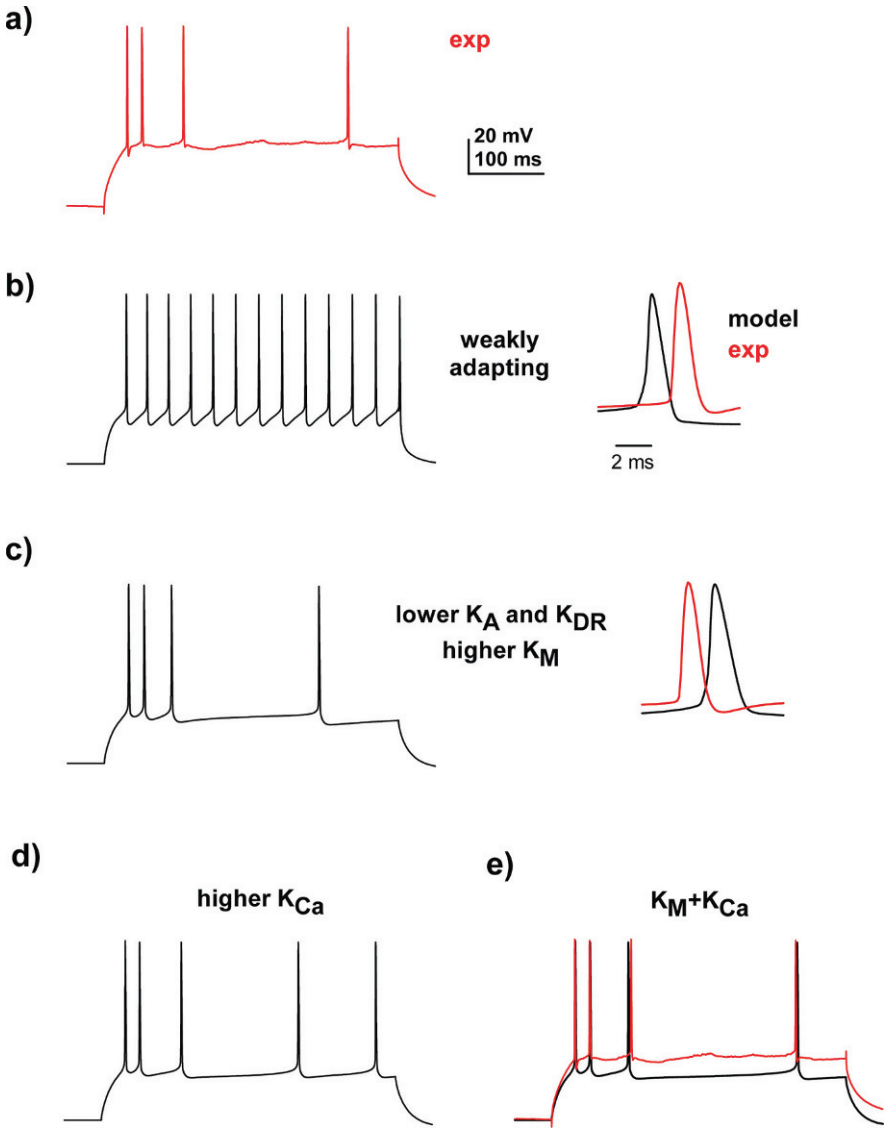

Fig. 5 Modeling CA3b pyramidal neurons showing strong adaptation. (**a**) Typical experimental trace; (**b**) model results using the same stimulation protocol as in the experiment (400 ms somatic current injection) and peak conductances used to model weakly adapting cells with K_M (Fig. 3b); traces on the right are an expanded view of the first spike in the experiment (*red*) and the model (*black*); (**c**) Modeling result using a lower peak conductances for K_{DR} and K_A, and a higher value for K_M; traces on the right are an expanded view of the first spike in the experiment (*red*) and the model (*black*); (**d**) modeling result using a lower peak conductances for K_{DR} and K_A, and a higher value for K_{Ca}; (**e**) using both K_M and K_{Ca} to model the strong adaptation results in very good agreement between model (*black*) and experiment (*red*) . The peak conductances used in all cases are listed in Table 1

and on the first ISI (mostly caused by K_{DR}). The other obvious change is to increase K_M, to increase adaptation, as shown in Fig. 5c. The result is now much better, although we still see a relatively minor, but significant, problem. Because of the kinetic characteristics of K_M, we can not obtain a good reproduction of this kind of experimental traces. On the one hand, if K_M is too high the cell would stop firing after the first few spikes, since it activates slowly and will remain substantially open at around -30 mV. On the other hand, if K_M is too low, we cannot obtain the long ISI. We need a mechanism that would activate faster at the beginning of the current injection, with a relatively lower later effect. It is easy to see that the K_{Ca} (modulated by $[Ca]_i$) has just these properties: the first few spikes, with short ISIs, produce a significant *Ca* entry, amplifying the effect of this current, and increasing the ISIs. Longer ISIs, in turn, reduce $[Ca]_i$ and consequently the K_{Ca} effect. This process can be observed in the simulation of Fig. 5d, where a higher K_{Ca} (but a low K_M) was used to model the experimental trace. The first two ISIs are now in very good agreement with the experiment, whereas the latter two are somewhat at odd with the experiment, and indirectly reflect the properties of the *Ca* extrusion mechanism (which has a 100 ms time constant). A combination of K_{Ca} and K_M will result in a very good agreement with the experiment, as shown in Fig. 5e.

Bursting

Finally, we considered a typical bursting cell, where a strong current injection elicited a few (3–5) APs at high frequency within the first 100 ms from the beginning of the stimulus, and (usually) no more spikes (rarely one) until the end of the stimulus (Fig. 6, see Hemond et al., 2008). With respect to the previous traces, here we have spikes with lower amplitude, much higher interspike frequency, and a depolarizing envelope during the firing period. As usual, to assess where we are with the model, we start from the configuration used for the weakly adapting cell and adjust the current injection to match the first spike time. The first 150 ms of such a simulation is shown in Fig. 6b. From this result, we can draw several useful hints on how to proceed. First of all, a lower *Na* conductance should be used to reduce the spikes amplitude. In principle, to reduce the spikes amplitude we can alternatively increase K_A (as, for example, in the apical dendrites of CA1 neurons), but this would also reduce the spike duration, in contrast with the experimental finding that these cells have the same spike duration independently from their firing behavior (Hemond et al., 2008). Reducing the *Na* conductance (Fig. 6c) produced a depolarizing envelope. However, the lower peak APs amplitude also reduced the activation of the K^+ conductances (K_A and K_{DR}) and results in a saturating trace caused by the progressive inactivation of the *Na* conductance. We need to include a mechanism that would be able to stop the depolarizing envelope after a few spikes: K_{Ca} (Fig. 6d). However, as we have discussed for the strong adaptation case, the K_{Ca} will reduce its effect later in the trace, because of the intracellular Calcium dynamics. Adding K_M will complete the picture, and a burst is obtained (Fig. 6e, left).

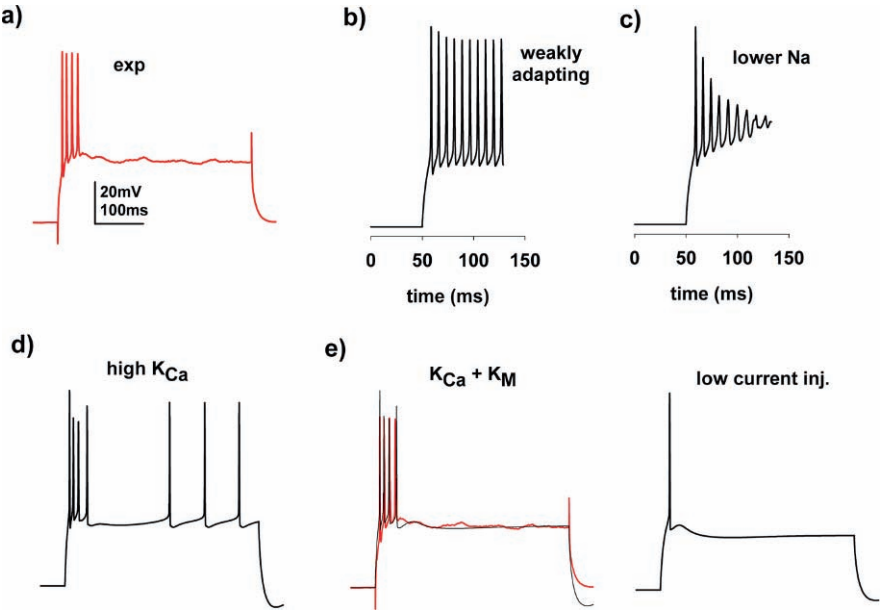

Fig. 6 Modeling CA3b burst firing. (**a**) Typical experimental trace; (**b**) model results using the same stimulation protocol as in the experiment (400 ms somatic current injection) and peak conductances used to model weakly adapting cells with K_{Ca} (Fig. 3c); for clarity, only the first 150 ms of simulation are plotted; (**c**) a lower Na conductance results in saturation of the membrane potential; (**d**) using a higher K_{Ca} there is an initial burst, but with several late spikes that are in contrast with experiments; (**e**) adding also K_M a good agreement with the experiments can be achieved; the trace on the *right* was obtained with a lower somatic current injection

One more experimental finding remains to be tested, i.e., the single spike elicited by a bursting cell under a low-current injection (Hemond et al., 2008). This is also reproduced by the model (Fig. 6e, right).

Simplified Model

Although the results using the realistic morphology gave precise indications on the mechanisms underlying the different firing properties observed in the experiments, possible questions still remain. In fact, no matter how convincing is the explanation for the relative contribution of the conductances suggested by the simulations in the various cases, the validity and robustness of the model (especially in the absence of specific experimental findings) can still be questioned. For example: How really important is the presence of K_D in delayed firing cells? Is there a most likely mechanism used for adaptation (between K_M and K_{Ca}) or it does not matter? How important is to have a low K_{DR} or K_A in bursting cells? What role is played by the cell morphology in bursting?

In order to explore these questions, we analyzed in more detail the results obtained in a previous paper (Hemond et al., 2008) using a brute force approach.

The morphology was reduced to a single compartment with passive membrane properties similar to those used here for the full model ($C_{\mathrm{m}} = 1.41\,\mu\mathrm{F/cm}^2$, $R_{\mathrm{m}} = 25,000\,\Omega\mathrm{cm}^2$) and including all of the conductances described here with identical kinetics (Fig. 3a). It should be noted that using a single compartment we eliminated, by default, the possible coupling between dendritic and somatic currents as burst-promoting mechanism (Pinsky and Rinzel, 1994). This would imply that the bursting observed in our CA3b neurons does not depend on the segregation of dendritic and somatic currents but on the relative interaction between inward and outward currents.

Simulations were run on a parallel computer system using all possible combinations of conductances with densities varying from 0, 0.25, 0.5, 1, 2, and 4 times values used for the bursting model and a range of input currents (0.01–0.3 nA in steps of 0.02 nA, for 400 ms) for a total of 20,995,200 configurations. Among the many different rules that could be devised to automatically classify each configuration in one of the four typical firing types (Fig. 1), we decided to use the following criteria:

- "bursting": four spikes within the first 80 ms of stimulation;
- "adapting": six to eight spikes, first ISI < 100 ms, no subsequent ISI < 20 ms, ratio of any two consecutive ISIs < 0.8, and the ratio of the sixth-ISI/first-ISI > 3;
- "non-adapting": five to eight spikes, the last spike occurring > 200 ms after the start of the current step, and a ratio of any two consecutive ISIs in the range 0.9–1.1;
- "delayed": up to three spikes generated by the current pulse and the first spike latency > 200 ms.

Additional rules were used to eliminate configurations resulting in a failure to fire or trapped in an inactivated state at the end of the current step. Only 91,914 configurations (0.4%) remained after applying these criteria. Of these remaining configurations, 94% exhibited a burst-firing pattern, 2% adapting, 3 % non-adapting, and 1% a delayed firing pattern. The high percentage of bursting configuration could be expected, since the reference values for the peak conductances were those used to obtain a burst in the full model (Hemond et al., 2008). This distribution thus should not be considered as representative of the CA3b population but, rather, as a striking evidence of how robust is the model. In spite of an eightfold span in the peak conductances, the great majority of configurations were still bursting.

A more detailed analysis of the configurations reveals the possible relations between the different conductances in the different firing patterns. In Fig. 7, we show the results for the delayed, strong adapting, and bursting cases. The first interesting suggestion is that delayed firing (as observed in CA3b neurons) cannot be obtained without K_D (Fig. 7a). Almost 40% of the configurations produced delayed firing with K_D alone, although additional conductances such as K_M and K_{Ca} could also be involved. In this latter case, however, the model predicts a quite larger first spike latency (the first spike in the traces "$+K_M$" and "*both*" shown in Fig. 7a, right, would occur at a later time using a longer current injection).

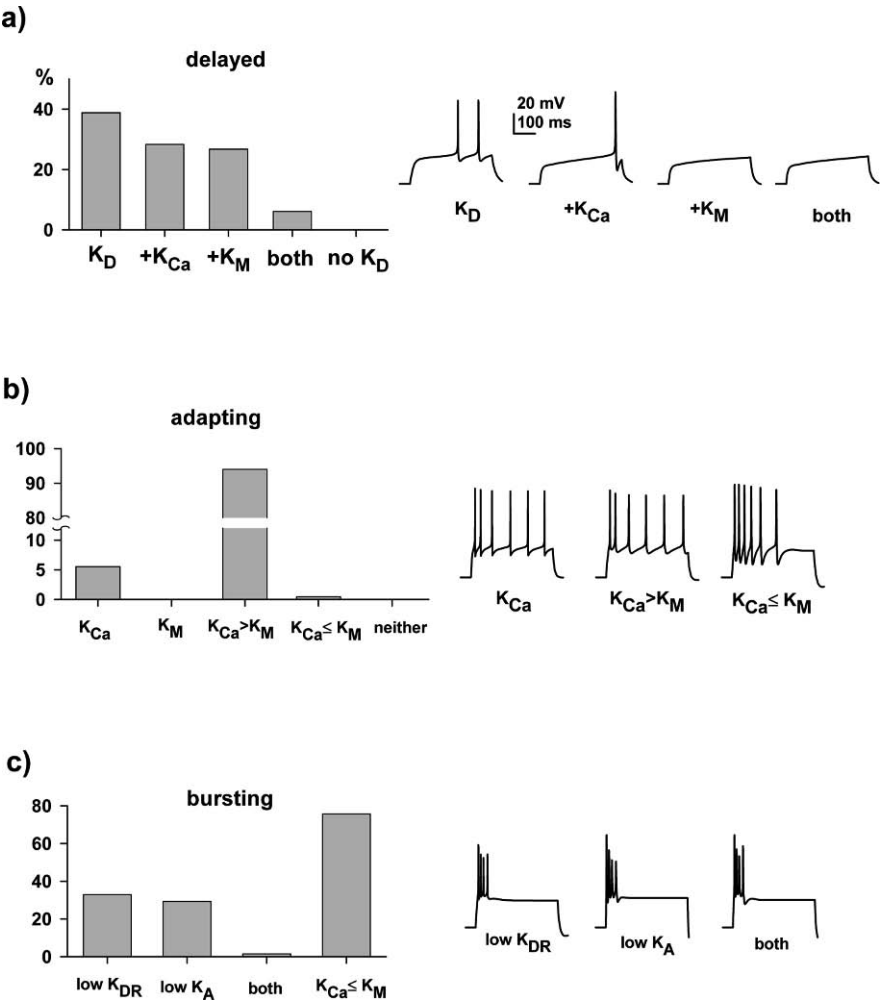

Fig. 7 The results using a simplified a single compartment confirm the findings using the realistic model. (**a**) Configurations (% of the total) showing delayed firing obtained with different combinations of conductances (*left*), and a typical sample trace for each case (*right*); (**b–c**) as in (a) but for adapting and bursing firing, respectively

For adapting configurations (Fig. 7b) the model suggested that in most cases the main mechanism was the K_{Ca}, either alone ($\sim$5%) or in combination with a lower K_M (in $\sim$90% of the cases). Configurations with a higher K_M (very few in our analysis because of our criteria) were those cases in which the cell stopped firing after a few spikes. Note that the third ISI in the "K_{Ca}" trace (Fig. 7b) is larger than the following ISIs, a characteristic that we already noted in modeling the adapting trace with the full model. It confirms the full model's suggestion to also have K_M in cells showing strongly adapting patterns.

Finally, bursting cases (Fig. 7c) confirmed our hypothesis of a lower K_A or K_{DR} in those cells with bursting behavior. In the simplified model, almost 60% of the configurations had either one of these conductances lower than 20% of the maximum value used in the simulations. The presence of a K_M larger than K_{Ca} in most cases ($\sim$75%) confirmed its role in ending the train of APs, also suggested by the simulation using a full morphology.

The Future

The goal of creating a model of any so-called "integrate and fire" neuron aims to understand how the cell responds to both the spatial and temporal combinations of excitatory and inhibitory inputs (Stuart et al., 1999). Central to this question is a knowledge of the combinatorial "rules" by which the *intrinsic* non-linear properties of the dendrites, soma, and spike-generating zone contribute to the neuron's output (Hausser and Mel, 2003). Data regarding non-linear mechanisms in the dendrites of CA3 pyramidal neurons still remain minimal at best mostly due to methodological considerations; unlike CA1 or neocortical pyramidal neurons – but like many other central neurons – one cannot make direct electrical recordings from CA3 pyramidal neuron dendrites distal to the soma using conventional visually assisted techniques (Stuart et al., 1993). CA3 cells "suffer" from having rapidly tapering dendritic trees and a conical arbor that, in a slice of tissue, generally travel at an angle against the focal plane so that they cannot be readily observed using differential interference contrast optics. Although new approaches for patching thin dendrites are being refined and applied to small processes (Nevian et al., 2007), other indirect methods must be employed to probe the properties of the dendrites relative to the soma and spike-generating zone (presumably the axon).

We do know that the dendrites of CA3 pyramidal neurons are not passive; voltage-gated channels, such as Ca_V, and K_V, as well as I_h, are all expressed in the dendrites (Elliott et al., 1995; Hell et al., 1993; Santoro et al., 2004; Varga et al., 2000; Park et al., 2001). Voltage-gated Na^+ channels most likely are expressed in the dendrites as well, albeit at lower densities than at the soma, discussed below. Unlike their CA1 counterparts, much of the basic quantitative parameters required to model the dendrites of CA3 pyramidal neurons are still needed, specifically, the relative spatial density, distribution, and properties of their intrinsic non-linear mechanisms. Given the technical limitations of these cells, mentioned above, a combined experimental and modeling approach where more traditional and conventional techniques can be used to generate constraints for the free parameters of the model. Therefore, to further constrain the model the following three experimental domains can not only provide important functional information regarding these cells but also serve as constraints for the model.

The first domain focuses in the subthreshold voltage range and asks how do particular voltage-gated channels shape postsynaptic potentials. We already know that the presence of certain types of voltage-gated Na^+, Ca^{2+}, and K^+ channels shape

distal apical synaptic inputs (Urban and Barrionuevo, 1998; Urban et al., 1998). This is important for constraining the model as it is evidence that these channels are functionally active in the dendrites. This is further supported by the observation that at the soma the subthreshold membrane response looks apparently linear for most cells (Hemond et al., 2008). This apparent contradiction only makes sense when one is reminded that voltage attenuates with distance from the soma; the voltage signal from the soma never reaches the activation range for the channels in the distal dendrite. Thus, taken together these experiments locate the channels in the distal dendrites. However, they do not tell us whether their density is higher or their properties are different than those at the soma. A non-linear mechanism shaping postsynaptic potentials may occur within dendritic spines and may also play a role in shaping synaptic signals. Interactions between non-NMDA receptor, voltage-gated Ca^{2+} influx, and Ca^{2+}-dependent K^+ channels affect EPSPs in CA1 pyramidal neuron dendrites and may occur in CA3 pyramidal neurons as well (Bloodgood and Sabatini, 2008).

A second experimental domain to constrain the model is with regard to the antidromic, back-propagation of action potentials. From early imaging experiments we know that action potentials back-propagate into the dendrites of CA3 pyramidal neurons (Muller and Connor, 1992), as in other types of neurons (Stuart et al., 1999). Antidromic spike invasion into the dendrites communicate to synapses that the cell has fired allowing for coincidence detection between cell firing and synaptic activation and may be vital for spike-timing-dependent forms of synaptic plasticity, especially for the recurrent/associational synaptic contacts between CA3 pyramidal neurons (Johnston and Amaral, 1997). That said, it is highly likely that CA3 dendrites are weakly excitable; spike threshold is lowest at a perisomatic location, most likely the initial node of the axon (Stuart et al., 1997), where Na^+ channel density is highest (Jarnot and Corbett, 2006; Krzemien et al., 2000; Westenbroek et al., 1989) and/or activation threshold is lower (Colbert and Pan, 2002). This further constrains the model; the density and properties of Na^+ and K^+ channels must allow for spike backpropagation but with a threshold higher than at the soma or axon. But how does a spike's amplitude vary both in space and in time across the dendritic tree? This is particularly important if spike amplitude is variable and can be modulated by synaptic input or neuromodulators (Johnston et al., 1999, 2000; Migliore et al., 1999). Again, this is a difficult question to address in the absence of direct experimental measurement. Surprisingly, more traditional approaches such as current–source density analysis and wide-field fluorescence imaging methods have not been applied to the study of CA3 pyramidal neuron dendrites and may therefore be the most immediate approaches to providing indirect avenues into this question.

Finally, a third area or domain for constraining the CA3 model concerns whether the dendrites are capable of displaying electrogenesis; regenerative events that are restricted or compartmentalized in some way to the dendrite (Hausser and Mel, 2003; Stuart et al., 1997). As a result, one can view a neuron as a series of hierarchical processing units from the dendrites to the soma to the axonal spike-generating zone (Poirazi et al., 2003). Both dendritic Na^+ and $Ca2^+$ spikes, as

well as NMDA-receptor mediated spikes, are potential non-linear mechanisms for establishing dendrites as individual processing units (Golding et al., 1999; Golding and Spruston, 1998; Larkum et al., 1999; Polsky et al., 2004; Wei et al., 2001). Experiments designed to elicit and characterize such events would put significant constraints on the location and properties of the ion channels responsible for their generation.

Appendix: Model Equations

$$\mathbf{I_{Na}} = g_{\mathrm{Na}} \cdot m^3 \cdot h \cdot (v{-}50), \quad \frac{dm}{dt} = (m_\infty - m)/\tau_m,$$

$$\frac{dh}{dt} = (h_\infty - h)/\tau_h$$

$$m_\infty = \frac{\alpha_m}{\alpha_m + \beta_m} \qquad \tau_m = \frac{2.14}{\alpha_m + \beta_m}$$

$$h_\infty = \frac{1}{1 + \exp((v+26)/4)} \qquad \tau_h = \frac{2.14}{\alpha_h + \beta_h}$$

$$\alpha_m = \frac{0.4 \cdot (v+6)}{1 - \exp(-(v+6)/7.2)} \quad \beta_m = -\frac{0.124 \cdot (v+6)}{1 - \exp((v+6)/7.2)}$$

$$\alpha_h = \frac{0.03 \cdot (v+21)}{1 - \exp(-(v+21)/1.5)} \quad \beta_h = -\frac{0.01 \cdot (v+21)}{1 - \exp((v+21)/1.5)}$$

$$\mathbf{I_{K\text{-}DR}} = g_{\text{K-DR}} \cdot n \cdot (v+90), \quad \frac{dn}{dt} = (n_\infty - n)/\tau_n$$

$$n_\infty = \frac{1}{1 + \exp(-0.12 \cdot (v-37))} \quad \tau_n = \frac{50 \cdot \exp(-0.08 \cdot (v-37))}{1 + \exp(-0.12 \cdot (v-37))}$$

$$\mathbf{I_{KA}} = g_{\mathrm{KA}} \cdot n \cdot l \cdot (v+90), \quad \frac{dn}{dt} = (n_\infty - n)/\tau_n \quad \frac{dl}{dt} = (l_\infty - l)/\tau_l$$

$$n_\infty = \frac{1}{1 + \exp(0.038 \cdot z \cdot (v-35))} \qquad \tau_n = \frac{3.4 \cdot \exp(0.021 \cdot z \cdot (v-35))}{1 + \exp(0.038 \cdot z \cdot (v-35))}$$

$$z = -1.5 - \frac{1}{1 + \exp((v+16)/5)}$$

$$l_\infty = \frac{1}{1 + \exp(0.12 \cdot (v+32))} \qquad \tau_l = 0.26 \cdot (v+26)$$

$$\mathbf{I_{KM}} = g_{\mathrm{KM}} \cdot m \cdot (v+90), \quad \frac{dm}{dt} = (m_\infty - m)/\tau_m$$

$$m_\infty = \frac{1}{1 + \exp(-0.1 \cdot (v+16))} \qquad \tau_m = 60 + \frac{333 \cdot \exp(-0.106 \cdot (v+18))}{1 + \exp(-0.265 \cdot (v+18))}$$

$$\mathbf{I_{KD}} = g_{\mathrm{KD}} \cdot n \cdot (v+90), \quad \frac{dn}{dt} = (n_\infty - n)/\tau_n$$

$$n_\infty = \frac{1}{1 + \exp(0.12 \cdot (v+33))} \qquad \tau_n = \frac{200 \cdot \exp(-0.082 \cdot (v+33))}{1 + \exp(0.12 \cdot (v+33))}$$

$$\mathbf{I_{KCa}} = g_{KCa} \cdot n \cdot (v + 90), \qquad \frac{dn}{dt} = (n_\infty - n)/\tau_n$$

$$n_\infty = \frac{\alpha}{\alpha + \beta} \qquad \tau_n = \frac{1}{\alpha + \beta}$$

$$\alpha = \frac{0.28 \cdot [Ca]_i}{[Ca]_i + 0.48 \cdot 10^3 \cdot \exp(-63.27 \cdot v)},$$

$$\beta = \frac{0.48}{1 + [Ca]_i / 0.13 \cdot 10^{-6} \cdot \exp(-75.32 \cdot v)}$$

Ca pump

$$\frac{d\,[Ca]_i}{dt} = (I_{Ca0} - I_{Ca})/d/F/2 \cdot 10^4 + (50 \cdot 10^{-6} - [Ca]_i)/100$$

d = diameter; F = Faraday's constant; I_{Ca0} = Ca current at rest; $[Ca]$ in mM.

$$\mathbf{I_{CaT}} = g_{Ca} \cdot m^2 \cdot h \cdot ghk(v, [Ca]_i, [Ca]_o)$$

$$\frac{dm}{dt} = (m_\infty - m)/\tau_m; \quad \frac{dh}{dt} = (h_\infty - h)/\tau_h; \quad ghk = \frac{v \cdot (1 - \frac{[Ca]_i}{[Ca]_o} \cdot \exp(v/13.14))}{1 - \exp(v/13.14)}$$

$$m_\infty = \frac{0.2 \cdot (-\mathrm{v} + 19.26)/(\exp((-\mathrm{v} + 19.26)/10) - 1)}{0.2 \cdot (-\mathrm{v} + 19.26)/(\exp((-\mathrm{v} + 19.26)/10) - 1) + 0.009 \cdot \exp(-\mathrm{v}/22.03)}$$

$$\tau_m = \frac{5 \cdot \exp(0.0076 \cdot (\mathrm{v} + 28))}{1 + \exp(0.076 \cdot (v + 28))}$$

$$h_\infty = \frac{10^{-6} \cdot \exp(-\mathrm{v}/16.26)}{10^{-6} \cdot \exp(-\mathrm{v}/16.26) + 1/(\exp((-\mathrm{v} + 29.79)/10) + 1)}$$

$$\tau_h = \frac{13.3 \cdot \exp(0.079 \cdot (\mathrm{v} + 75))}{1 + \exp(0.1323 \cdot (v + 75))}$$

$$\mathbf{I_{CaN}} = g_{Ca} \cdot m^2 \cdot h \cdot h2([Ca]_i) \cdot ghk(v, [Ca]_i, [Ca]_o)$$

$$\frac{dm}{dt} = (m_\infty - m)/\tau_m; \quad \frac{dh}{dt} = (h_\infty - h)/\tau_h; \quad ghk = \frac{v \cdot (1 - \frac{[Ca]_i}{[Ca]_o} \cdot \exp(v/13.14))}{1 - \exp(v/13.14)}$$

$$m_\infty = \frac{0.2 \cdot (-\mathrm{v} + 19.88)/(\exp((-\mathrm{v} + 19.88)/10) - 1)}{0.2 \cdot (-\mathrm{v} + 19.88)/(\exp((-\mathrm{v} + 19.88)/10) - 1) + 0.046 \cdot \exp(-\mathrm{v}/20.73)}$$

$$\tau_m = \frac{6.7 \cdot \exp(0.0076 \cdot (\mathrm{v} + 14))}{1 + \exp(0.076 \cdot (v + 14))}$$

$$h_\infty = \frac{1.6 \cdot 10^{-4} \cdot \exp(-\mathrm{v}/48.4)}{1.6 \cdot 10^{-4} \cdot \exp(-\mathrm{v}/48.4) + 1/(\exp((-\mathrm{v} + 39)/10) + 1)}$$

$$\tau_h = 80$$

$$h2 = \frac{0.001}{0.001 + [Ca]_i}$$

$$\mathbf{I_{CaL}} = \mathrm{g_{Ca}} \cdot m^2 \cdot h2([Ca]_i) \cdot ghk(v, [Ca]_i, [Ca]_o)$$

$$\frac{dm}{dt} = (m_\infty - m)/\tau_m; \quad ghk = \frac{v \cdot (1 - \frac{[Ca]_i}{[Ca]_o} \cdot \exp(v/13.14))}{1 - \exp(v/13.14)}$$

$$m_\infty = \frac{15.69 \cdot (-\mathrm{v} + 81.5)/(\exp((-\mathrm{v} + 81.5)/10) - 1)}{15.69 \cdot (-\mathrm{v} + 81.5)/(\exp((-\mathrm{v} + 81.5)/10) - 1) + 0.29 \cdot \exp(-\mathrm{v}/10.86)}$$

$$\tau_m = \frac{2 \cdot \exp(0.0076 \cdot (\mathrm{v} - 4))}{1 + \exp(0.076 \cdot (v - 4))}$$

$$h2 = \frac{0.001}{0.001 + [Ca]_i}$$

Further Reading

Ascoli GA (2006) Mobilizing the base of neuroscience data: the case of neuronal morphologies. Nat. Rev. Neurosci. 7:318–24.

Bloodgood BL, Sabatini BL (2008) Regulation of synaptic signalling by postsynaptic, non-glutamate receptor ion channels. J. Physiol. 586:1475–80.

Buzsaki G (1989) Two-stage model of memory trace formation: a role for "noisy" brain states. Neuroscience 31:551–70.

Colbert CM, Pan E (2002) Ion channel properties underlying axonal action potential initiation in pyramidal neurons. Nat. Neurosci. 5:533–8.

Elliott EM, Malouf AT, Catterall WA (1995) Role of calcium channel subtypes in calcium transients in hippocampal CA3 neurons. J. Neurosci. 15:6433–44.

Golding NL, Jung HY, Mickus T, Spruston N (1999) Dendritic calcium spike initiation and repolarization are controlled by distinct potassium channel subtypes in CA1 pyramidal neurons. J. Neurosci. 19:8789–98.

Golding NL, Spruston N (1998) Dendritic sodium spikes are variable triggers of axonal action potentials in hippocampal CA1 pyramidal neurons. Neuron 21:1189–200.

Hasselmo ME, Bodelon C, Wyble BP (2002) A proposed function for hippocampal theta rhythm: separate phases of encoding and retrieval enhance reversal of prior learning. Neural Comput. 14:793–817.

Hausser M, Mel B (2003) Dendrites: bug or feature? Curr. Opin. Neurobiol. 13:372–83.

Hell JW, Westenbroek RE, Warner C, Ahlijanian MK, Prystay W, Gilbert MM, Snutch TP, Catterall WA (1993) Identification and differential subcellular localization of the neuronal class C and class D L-type calcium channel alpha 1 subunits. J. Cell Biol. 123:949–62.

Hemond P, Epstein D, Boley A, Migliore M, Ascoli GA, Jaffe DB (2008) Distinct classes of pyramidal cells exhibit mutually exclusive firing patterns in hippocampal area CA3b. Hippocampus 18:411–424.

Henze DA, Wittner L, Buzsaki G (2002) Single granule cells reliably discharge targets in the hippocampal CA3 network in vivo. Nat. Neurosci. 5:790–5.

Hines ML, Carnevale NT (1997) The NEURON simulation environment. Neural Comput. 9: 1179–209.

Ishizuka N, Cowan WM, Amaral DG (1995) A quantitative analysis of the dendritic organization of pyramidal cells in the rat hippocampus. J. Comp. Neurol. 362:17–45.

Hölscher C (2003) Time, space and hippocampal functions. Rev. Neurosci. 14:253–84.

Jaffe DB, Carnevale NT (1999) Passive normalization of synaptic integration influenced by dendritic architecture. J. Neurophysiol. 82:3268–85.

Jarnot M, Corbett AM (2006) Immunolocalization of NaV1.2 channel subtypes in rat and cat brain and spinal cord with high affinity antibodies. Brain Res. 1107:1–12.

Johnston D, Amaral D (1997) Hippocampus. In: Shepherd GM, editor. The synaptic organization of the brain. New York: Oxford University.
Johnston D, Hoffman DA, Colbert CM, Magee JC (1999) Regulation of back-propagating action potentials in hippocampal neurons. Curr. Opin. Neurobiol. 9:288–92.
Johnston D, Hoffman DA, Magee JC, Poolos NP, Watanabe S, Colbert CM, Migliore M (2000) Dendritic potassium channels in hippocampal pyramidal neurons. J. Physiol. 525 Pt 1:75–81.
Johnston D, Magee JC, Colbert CM, Cristie BR (1996) Active properties of neuronal dendrites. Annu. Rev. Neurosci. 19:165–86.
Kali S, Dayan P (2000) The involvement of recurrent connections in area CA3 in establishing the properties of place fields: a model. J. Neurosci. 20:7463–77.
Krichmar JL, Nasuto SJ, Scorcioni R, Washington SD, Ascoli GA (2002) Effects of dendritic morphology on CA3 pyramidal cell electrophysiology: a simulation study. Brain Res. 941: 11–28.
Krzemien DM, Schaller KL, Levinson SR, Caldwell JH (2000) Immunolocalization of sodium channel isoform NaCh6 in the nervous system. J. Comp. Neurol. 420:70–83.
Larkum ME, Zhu JJ, Sakmann B (1999) A new cellular mechanism for coupling inputs arriving at different cortical layers. Nature 398:338–41.
Lisman JE (1999) Relating hippocampal circuitry to function: recall of memory sequences by reciprocal dentate-CA3 interactions. Neuron 22:233–42.
Major G, Larkman AU, Jonas P, Sakmann B, Jack JJ (1994) Detailed passive cable models of whole-cell recorded CA3 pyramidal neurons in rat hippocampal slices. J. Neurosci. 14: 4613–38.
Migliore M, Hoffman DA, Magee JC, Johnston D (1999) Role of an A-type K+ conductance in the back-propagation of action potentials in the dendrites of hippocampal pyramidal neurons. J. Comput. Neurosci. 7:5–15.
Migliore M, Shepherd GM (2002) Emerging rules for the distributions of active dendritic conductances. Nat. Rev. Neurosci. 3:362–370.
Muller W, Connor JA (1992) Ca2+ signalling in postsynaptic dendrites and spines of mammalian neurons in brain slice. J. Physiol. Paris 86:57–66.
Nakazawa K, Quirk MC, Chitwood RA, Watanabe M, Yeckel MF, Sun LD, Kato A, Carr CA, Johnston D, Wilson MA, Tonegawa S (2002) Requirement for hippocampal CA3 NMDA receptors in associative memory recall. Science. 297:211–8.
Nakazawa K, Sun LD, Quirk MC, Rondi-Reig L, Wilson MA, Tonegawa S (2003) Hippocampal CA3 NMDA receptors are crucial for memory acquisition of one-time experience. Neuron 38:305–15.
Nevian T, Larkum ME, Polsky A, Schiller J (2007) Properties of basal dendrites of layer 5 pyramidal neurons: a direct patch-clamp recording study. Nat. Neurosci. 10:206–14.
O'Reilly RC, McClelland JL (1994) Hippocampal conjunctive encoding, storage, and recall: avoiding a trade-off. Hippocampus 4:661–82.
Park KH, Chung YH, Shin C, Kim MJ, Lee BK, Cho SS, Cha CI (2001) Immunohistochemical study on the distribution of the voltage-gated potassium channels in the gerbil hippocampus. Neurosci. Lett. 298:29–32.
Pinsky PF, Rinzel J (1994) Intrinsic and network rhythmogenesis in a reduced Traub model for CA3 neurons. J. Comput. Neurosci. 1:39–60.
Poirazi P, Brannon T, Mel BW (2003) Pyramidal neuron as two-layer neural network. Neuron 37:989–99.
Polsky A, Mel BW, Schiller J (2004) Computational subunits in thin dendrites of pyramidal cells. Nat. Neurosci. 7:621–7.
Poolos NP, Migliore M, Johnston D (2002) Pharmacological upregulation of h-channels selectively reduces the excitability of pyramidal neuron dendrites, Nat. Neurosci. 5: 767–774.
Pyapali GK, Turner DA (1996) Increased dendritic extent in hippocampal CA1 neurons from aged F344 rats. Neurobiol. Aging 17:601–11.
Rodriguez P, Levy WB (2001) A model of hippocampal activity in trace conditioning: where's the trace? Behav. Neurosci. 115:1224–38.

Samsonovich A, McNaughton BL (1997) Path integration and cognitive mapping in a continuous attractor neural network model. J. Neurosci. 17:5900–20.
Santoro B, Wainger BJ, Siegelbaum SA (2004) Regulation of HCN channel surface expression by a novel C-terminal protein-protein interaction. J. Neurosci. 24:10750–62.
Shah MM, Migliore M, Valencia I, Cooper EC, Brown DA (2008) Functional significance of axonal Kv7 channels in hippocampal pyramidal neurons. Proc. Nat. Acad. Sci. USA 105:7869–74.
Spruston N, Johnston D (1992) Perforated patch-clamp analysis of the passive membrane properties of three classes of hippocampal neurons. J. Neurophysiol. 67:508–29.
Stuart GJ, Dodt HU, Sakmann B (1993) Patch-clamp recordings from the soma and dendrites of neurons in brain slices using infrared video microscopy. Pflugers Arch. 423:511–8.
Stuart G, Spruston N, Hausser M (1999) Dendrites. New York: Oxford University Press.
Stuart G, Spruston N, Sakmann B, Hausser M (1997) Action potential initiation and backpropagation in neurons of the mammalian CNS. Trends Neurosci. 20:125–31.
Treves A (1995) Quantitative estimate of the information relayed by the Schaffer collaterals. J. Comput. Neurosci. 2:259–72.
Treves A, Rolls ET (1994) Computational analysis of the role of the hippocampus in memory. Hippocampus 4:374–91.
Urban NN, Barrionuevo G (1998) Active summation of excitatory postsynaptic potentials in hippocampal CA3 pyramidal neurons. Proc. Natl. Acad. Sci. USA 95:11450–5.
Urban NN, Henze DA, Barrionuevo G (1998) Amplification of perforant-path EPSPs in CA3 pyramidal cells by LVA calcium and sodium channels. J. Neurophysiol. 80:1558–61.
Urban NN, Henze DA, Barrionuevo G (2001) Revisiting the role of the hippocampal mossy fiber synapse. Hippocampus 11:408–17.
Varga AW, Anderson AE, Adams JP, Vogel H, Sweatt JD (2000) Input-specific immunolocalization of differentially phosphorylated Kv4.2 in the mouse brain. Learn. Mem. 7:321–32.
Watanabe S, Hoffman DA, Migliore M, Johnston D (2002) Dendritic K^+ channels contribute to spike-timing dependent long-term potentiation in hippocampal pyramidal neurons. Proc. Natl. Acad. Sci. USA 99:8366–8371.
Wei DS, Mei YA, Bagal A, Kao JP, Thompson SM, Tang CM (2001) Compartmentalized and binary behavior of terminal dendrites in hippocampal pyramidal neurons. Science 293:2272–5.
Westenbroek RE, Merrick DK, Catterall WA (1989) Differential subcellular localization of the RI and RII Na+ channel subtypes in central neurons. Neuron 3:695–704.

Entorhinal Cortex Cells

Erik Fransén

Entorhinal cortex (EC) has recently gained increased interest following the findings of grid cells (Fyhn et al., 2004; Hafting et al., 2005). It has also recently been shown that place cells, intensely studied in the hippocampus, exist upstream of hippocampus in superficial layers of entorhinal cortex (Fyhn et al., 2004). In the light of these findings, mechanisms generating the gradient in rhythmicity of entorhinal grid cells have received large interest (Giocomo et al., 2007). In previous work we have studied the ionic mechanisms behind the subthreshold membrane potential oscillations found in layer II stellate cells experimentally (Klink and Alonso, 1993, Dickson et al., 2000) and using modeling (Dickson et al., 2000; Fransén et al., 2004). Moreover, the entorhinal cortex has also been shown to be specifically involved in the representation of novel items in working memory experiments in humans (Stern et al., 2001; Schön et al., 2004, 2005) and rodents (McGaughy et al., 2005). Behavioural neurophysiological investigations have shown that principal cells in the EC show spiking activities correlated with the different phases (including the delay and choice periods) of delayed matching tasks (Young et al., 1997; Suzuki et al., 1997). In modeling studies of layer II (Fransén et al., 2002) and layer V (Fransén et al., 2006) pyramidal cells, we have investigated the potential mechanism of persistent activity established during muscarinic modulation of cells in EC layer II (Alonso and Klink, 1993) and layer V (Egorov et al., 2002; Fransén et al., 2006), respectively. Interestingly, working memory processing also depends on theta oscillations (Bunce et al., 2004; Kay, 2005, Lee et al., 2005). For instance, a significant enhancement in theta band energy was found during the delay period of a visual working memory task (Lee et al., 2005). Importantly, they also observed a correlation between single neuron activities with theta phase as measured by local field potentials. Thus, despite the apparent differences between working memory activity and grid field activity, they may share common functional components in theta rhythmicity and neuronal components such as depolarizing slow cationic currents.

E. Fransén (✉)
Department of Computational Biology, School of Computer Science and Communication; Stockholm Brain Institute, Royal Institute of Technology, SE–106 91, Stockholm, Sweden
e-mail: erikf@csc.kth.se

V. Cutsuridis et al. (eds.), *Hippocampal Microcircuits*, Springer Series in Computational Neuroscience 5, DOI 10.1007/978-1-4419-0996-1_13,

Entorhinal cortex (EC) has a unique role as it is positioned as a "gateway" between neocortical association areas and the hippocampal system. Anatomically, the superficial layers of EC receive the input from neocortex and provide the main input via the perforant path to the dentate gyrus of the hippocampal formation. The deeper layers receive input mainly from hippocampus field CA1 and the subiculum and provide the output back to the neocortical areas. The deeper layers also project to the more superficial layers, creating a loop through the entorhinal–hippocampal system. Sensory, motor, and associational information is thereby assumed to be processed in EC and hippocampus before being stored permanently in neocortex.

In this chapter, we will describe our modeling of several cell types found in EC. For the superficial layer II we describe the major excitatory cell types, the stellate cell and the pyramidal-like cell. For the deep layer V, we describe the pyramidal cell which was the first neuron to be found to have the graded persistent activities later also found in pyramidal cells of perirhinal cortex, lateral amygdala, and prefrontal cortex. We will give two examples from our modeling of EC function. One will be concerned with the generation of theta rhythmicity which is central to grid field generation and memory processing and the other with generation of sustained neuronal activity in relation to working memory. In the first example, the focus will be on the stellate cell in layer II and specifically how the ion channel I_h contributes to the cellular properties. In the second example, the involvement of calcium-dependent cationic currents in the generation of depolarizing plateau potentials in pyramidal cells of layers II and V is studied.

Models of Layer II Stellate Cells and Pyramidal Neurons of Layers II and V

Stellate cell Model

The properties of stellate cells were developed in work on the mechanisms of subthreshold membrane potential oscillations (Dickson et al., 2000; Fransén et al., 1998, 2001). Electrotonically, it is composed of seven compartments. One compartment represents the soma, one compartment represents the initial segment, three compartments connected in succession represent the primary, secondary, and tertiary segments of a single principal dendrite, and two connected compartments represent all remaining dendrites lumped together and thereby constitute the main "load" on the soma. The lengths and cross sections of the three principal dendrite compartments were adjusted to give the dendrite a length constant of 2 (sealed-end condition). The compartment profiles are found in Table 1. Motivations behind the compartmental structure are further elaborated in Section "Model Justification".

Passive Properties

Simulations of the passive membrane properties of the cell utilized the standard equivalent circuit representation for each compartment (Bower and Beeman, 1995).

Table 1 Compartment profile for the stellate cell. IS = initial segment compartment, dendr. = principal dendrite compartment

Compartment	Length (μm)	Diameter (μm)
soma	20	15
IS	50	2.2
dendr. (×3)	100	1.9
lump (×2)	200	5.5

The passive parameters are as follows: $R_M = 5.0\,\Omega m^2$, $R_A = 1.0\,\Omega m$, $C_M = 0.01\,F/m^2$. The value of the membrane reversal potential E_m depends on contributions from leakage Na^+ and leakage Cl^- currents (the K^+ leak current is explicitly represented as a separate current). One may also view synaptic background activation with slow kinetics, e.g., NMDA and $GABA_B$, as part of the leakage current. Note that as the K^+ current is represented separately, its conductance should be added to the value of R_M given above when comparing to other data.

Active Properties of Stellate Cells

The stellate cell model includes the following currents described in Appendix A (with the appropriate subsection in parentheses): the Na^+ and K^+ currents responsible for fast action potentials (described in sections "Na" and "K_{dr}"), a "persistent"-type Na current (NaP), a high-threshold Ca^{2+} current (Ca_L), a fast calcium- and voltage-dependent K^+ current (K_C), a calcium-dependent K^+ current (K_{AHP}(LIIS)), a potassium leak current (K(leak)), a non-specific calcium-activated cationic current (NCM), and a hyperpolarization-activated non-specific cation current I_h (h). The channel models used Hodgkin–Huxley representations of intrinsic currents. Equations describing the currents can be found in Appendix A and the respective conductances are found in Table 2. As the h-channel holds such a central position in the model, it is described below.

Table 2 Conductance profile of the stellate cell. Prox. = proximal compartment, med. = medial compartment, dist. = distal compartment, dendr. = principal dendritic compartment, lump = lumped dendritic compartment

Current	IS (S/m^2)	Soma (S/m^2)	Prox.+med. dendr. (S/m^2)	Prox. lump (S/m^2)	Dist. dendr. (S/m^2)	Dist. lump (S/m^2)
gNa	150	38	38	38	19	19
gNaP	0.0	1.25	1.25	1.25	1.25	1.25
$g$$Ca_L$	0.0	1.0	1.0	1.0	1.0	1.0
$g$$K_{dr}$	215	107	107	107	54	54
$g$$K_C$	0.0	13400	0.0	0.0	0.0	0.0
$g$$K_{AHP}$	0.0	0.1	0.1	0.1	0.1	0.1
gK(leak)	0.9	0.9	0.9	0.9	0.9	0.9
gh(fast)	0.0	2.5	2.5	2.5	2.5	2.5
gh(slow)	0.0	1.2	1.2	1.2	1.2	1.2
gNCM	0.0	280	0.0	0.0	0.0	0.0
$\phi_{Ca(K_C)pool}$	0.0	61.34×10^{12}	97.37×10^{12}	16.73×10^{12}	21.91×10^{12}	3.76×10^{12}
$\phi_{Ca(K_{AHP})pool}$	0.0	61.34×10^{12}	97.37×10^{12}	16.73×10^{12}	21.91×10^{12}	3.76×10^{12}

The simulations included a conductance-based noise source. This represents potential effects of channel noise (White et al., 1998) or synaptic noise in actual neural function. The noise was generated from a Poisson process and was placed on the proximal lumped dendritic compartment.

h-channel Model

The hyperpolarization-activated non-specific cation current I_h was modeled according to previous work (Fransén et al., 2004; Dickson et al., 2000). The maximal conductance was adjusted to comply with voltage clamp data as well as current clamp data on the "sag" produced by I_h (Dickson et al., 2000).

$$\tau_m(\text{fast})(V) = \frac{0.00051}{exp((V - 0.0017)/0.010) + exp(-(V + 0.34)/0.052)}$$

$$m_{\text{inf(fast)}}(V) = \frac{1}{(1 + exp((V + 0.0742)/0.00978))^{1.36}}$$

$$\text{gate exponent} = 1$$

$$\tau_m(\text{slow})(V) = \frac{0.0056}{exp((V - 0.017)/0.014) + exp(-(V + 0.26)/0.043)}$$

$$m_{\text{inf(slow)}}(V) = \frac{1}{(1 + exp((V + 0.00283)/0.0159))^{58.5}}$$

$$\text{gate exponent} = 1$$

The model shows, due to the properties of I_h membrane sag, a membrane potential overshoot following a current injection pulse and due to this rebound spiking following a hyperpolarizing current pulse. The model could also reproduce the characteristic subthreshold membrane potential oscillations of the stellate cell both in terms of the voltage interval in which they appear, and in terms of oscillation amplitude and frequency within this interval. Moreover, we showed how the fast component of I_h is the main contributor to the oscillations and that it is involved in the medium afterhyperpolarization produced by the neuron. Further, the model also displays the sequence of firing patterns displayed by the stellate cells when subjected to a depolarizing current ramp. This includes first single spikes, then clusters of spikes (doublets, then triplets), and finally tonic firing. In this regard, we show that the slow component of I_h is involved in the clustering phenomena, see Fig. 1. The figure shows how the slow component, but not the fast component of I_h could be involved in the spike clustering property of stellate cells.

Layer II Pyramidal Neuron

The properties of layer II pyramidal cells were simulated with biophysical models containing multiple compartments, with an emphasis on the calcium-sensitive

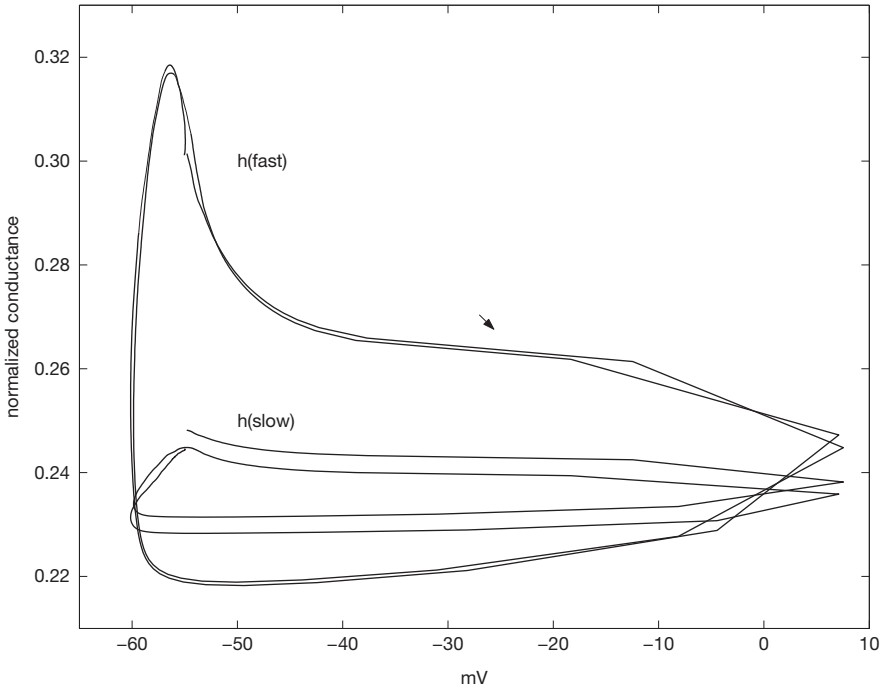

Fig. 1 Fast (larger orbit) and the slow component's normalized conductances (smaller orbit) are plotted versus membrane potential (–60–10 mV). As shown in the larger orbit, the two cycles are almost superimposed, indicating that the fast component does not change significantly between the two spikes, i.e., it does not contribute to making a difference between the first and the second spike. The slow component, in contrast, decreases (shifts downward) between the two spikes. The reduction of the slow component is 6.4 times larger than the reduction of the fast component, indicating that reduction in the depolarization caused by deactivation of the slow component of the current may contribute to the clustering

non-specific cation current I_{NCM}. The pyramidal cell is composed of six compartments, one representing the soma, three the apical dendrite, one a basal dendrite, and one compartment representing all but one basal dendrite lumped together, to constitute the main "load" to the soma. The proximal of the apical compartments, the basal dendrite, and the lump compartment are all connected to the soma. The lengths and cross sections of the three apical dendrite compartments were adjusted to give the dendrite a length constant of 2 (sealed-end condition). The compartment profiles are found in Table 3. Simulations with just a soma compartment and its conductances showed that dendritic compartments were not necessary for obtaining robust spiking activity during delay periods in the cell. However, these dendritic compartments were important for matching a range of features in the data including spike shape, afterhyperpolarization shape, and spike frequency accommodation, as well as providing a more realistic attenuation of excitatory synaptic input.

Table 3 Compartment profile for the pyramidal cell. api. = apical dendrite compartment, bas. = basal dendrite compartment

Compartment	Length (μm)	Diameter (μm)
soma	20	15
api. (×3)	100	1.9
bas. (×1)	100	1.9
lump (×1)	200	5.5

Passive Properties

Simulations of the passive membrane properties of the cell utilized the same properties described for the stellate cell in the previous section.

Active Properties of Pyramidal Cells

The simulations included multiple currents underlying the active properties of the membrane, including both currents sensitive to changes in membrane potential and currents sensitive to intracellular calcium concentration. Equations describing the currents can be found in Appendix A and the respective conductances are found in Table 4. The neuron has the same ionic currents as the stellate cell with the following exceptions: we added a non-inactivating muscarinic K^+ current (K_M), it did not contain the hyperpolarization-activated cationic current h, and we developed the model of the CAN current, in this neuron denoted NCM, according to our new data.

Table 4 Conductance profile of the pyramidal cell. Maximal conductances g and calcium conversion factor ϕ for each compartment. For some of the currents, the density was assumed to be uniform. For the others the general profile, with a higher conductance at the soma, and gradually lower conductances for more distal dendritic compartments, was adopted from Traub et al., (1991). The criteria selected to adjust the conductances do not give a unique solution (Traub et al., 1991; Deschutter and Bower, 1994). Prox. = proximal compartment, med. = medial compartment, dist. = distal compartment, api. = apical dendritic compartment, bas. = basal compartment, lump = lumped dendritic compartment

Current	Soma S/m^2	Prox.+med. api. + bas. S/m^2	lump S/m^2	Dist. api. S/m^2
gNa	0	60	60	30
gNaIS	250	0	0	0
gNaP	2.0	0	0	0
$g\mathrm{Ca_L}$	1.5	1.5	1.5	1.5
$g\mathrm{K_{dr}}$	0	25	25	12
$g\mathrm{K_{dr}IS}$	25	0	0	0
$g\mathrm{K_C}$	1960	1960	1960	1960
$g\mathrm{K_{AHP}}$	0.5	0.5	0.5	0.5
$g\mathrm{K_M}$	35	0	0	0
gK(leak)	1.0	1.0	1.0	1.0
gNCM	26	0	0	0
$\phi_{\mathrm{Ca(K_C)pool}}$	61.34×10^{12}	38.85×10^{12}	16.73×10^{12}	38.85×10^{12}
$\phi_{\mathrm{Ca(K_{AHP})pool}}$	61.34×10^{12}	38.85×10^{12}	16.73×10^{12}	38.85×10^{12}
$\phi_{\mathrm{Ca(NCM)pool}}$	61.34×10^{12}	0	0	0

The compartment where spikes are initiated, the soma, has Na and K currents with faster kinetics (Na(soma) and K(soma)), based on previous work (Traub et al., 1994). In the experimental preparation there are indications of a T-type Ca-current (Bruehl and Wadman, 1999), but as these simulations resulted in relatively depolarized membrane potentials, this current was not included. Experimental studies using a calcium chelator suggested that the C-type potasssium current might play a substantial role in action potential repolarization. The conductance of K_{dr} is therefore relatively low and for K_C relatively high. The K_{AHP} current is stronger in pyramidals than in stellate cells, and the K_M current is not present in stellate cells. As a consequence of the difference in conductance amplitudes, spike frequency adaptation is stronger in pyramidals than in stellate cells. Moreover, the stellate cells included a hyperpolarization-activated non-specific cation current I_h not included in the pyramidal cell models.

The simulations included a conductance-based noise source. This represents potential effects of channel noise (White et al., 1998) or synaptic noise in actual neural function. The noise was generated from a Poisson process and was placed on the proximal lumped dendritic compartment.

The key ionic current of the pyramidal neuron, a non-specific Ca^{2+}-dependent cationic current (NCM), was modeled according to the calcium-dependent K^+ current by Traub et al. (1991). For the associated calcium, we used 1D diffusion models of the intracellular calcium (Traub et al., 1991). Diffusion and subdivision into calcium pools affecting the different calcium-sensitive ion channels are described in Appendix B.

NCM

The non-specific Ca^{2+}-dependent cationic current was modeled using a framework similar to the calcium-dependent K^+ current found in previous work (Traub et al., 1991). Time constants for the I_{NCM} were derived by replicating experimental data (Klink and Alonso, 1997a, b). Note that this experimental data were fitted by modifying the total kinetics of both the calcium diffusion and the I_{NCM} current to replicate experimental traces.

$$\alpha_m([Ca^{2+}]) = \min(0.02 \times [Ca^{2+}], 10)$$
$$\beta_m = 1.0$$
$$\text{gate exponent} = 1$$

In the model, we focused on the Ca-sensitive component of I(NCM). Later evidence suggests that I(NCM) also has a calcium-insensitive component, but this was not explicitly modeled in our simulations. The resting potential of our simulations, before any input has been presented, corresponds to a resting state with cholinergic modulation which could include conductance contributions due to the calcium-insensitive component. The maximal conductance of I_{NCM} was adjusted to produce spiking frequencies similar to those observed during delay activity and

during match enhancement in recordings of single units in awake rats performing a delayed non-match to sample task (Young et al., 1997).

Layer II Synaptic Model

Synaptic contacts on stellate and pyramidal cell types were of either a mixed AMPA/kainate and NMDA type, or of a mixed $GABA_A$ and $GABA_B$ type (originating from an interneuron model described in Fransén et al., 2002). Equations describing the currents can be found below and the respective parameters are found in Table 5.

Table 5 Synaptic parameters

Compartment	E_{rev} V	τ_r s	τ_d s
AMPA	0	0.002	0.002
NMDA	0	0.08	0.00067
$GABA_A$	–0.070	0.001	0.007
$GABA_B$	–0.085	0.03	0.09

Synaptic conductances between neurons were modeled with an alpha function (Bower and Beeman, 1995):

$$g_{syn} = \frac{A * g_{max}}{\tau_d - \tau_r} * (e^{-t/\tau_d} - e^{-t/\tau_r})$$

g_{max} is the peak synaptic conductance, τ_r is the rising time constant, τ_d is the decaying time constant. A is a scaling constant set to yield a maximum conductance of g_{max}.

For the NMDA current the conductance was multiplied with the magnesium block conductance described in previous work (Zador et al., 1990):

$$g_{Mg} = \frac{1}{1 + 0.018e^{-60V}}$$

Before determining the synaptic conductance values, the relative proportions of the various components were fixed according to the following experimental data: The NMDA component had the same PSP height as AMPA at −72 mV (Alonso et al., 1990). $GABA_A$ was 70% of $GABA_B$ at −66 mV (Gloveli et al., 1999). In several networks, $GABA_B$ had approximately the same PSP height as NMDA at −55 mV, (Alonso, personal communication).

The synaptic conductances were adjusted so that firing rates would resemble those observed in recordings of entorhinal units from rats performing a delayed non-match to sample task (Young et al., 1997) for the various parts of an experiment, i.e., sample, delay, test. Note that firing rates were matched to firing rates observed in rats, but for phenomena of match as well as non-match enhancement and non-

match suppression the relative changes in firing rates were adjusted to match those observed in monkeys (Suzuki et al., 1997).

Layer V Pyramidal Neuron

Graded firing rates were simulated in a compartmental biophysical model of an entorhinal cortex layer V principal neuron. This model was based on the pyramidal cell of layer II (Fransén et al., 2002) and had the same compartmental structure. To address the distinct properties of EC layer V neurons (Hamam et al., 2000), modifications in terms of ion channels included were made. The following modifications were made: (a) addition of a transient potassium current K_A, modeled according to Traub et al. (1991); (b) replacing the non-specific muscarinic-activated calcium-sensitive current I_{NCM} with an I_{CAN} current described below. Conductances for channels are listed in Table 6. Calcium diffusion was modeled as in the layer II pyramidal neuron and can be found in Appendix C. The CAN current was, as in Fransén et al., (2002) modeled according to Traub et al. (1991); and (c) addition of a biochemical pathway connecting I_{CAN} to spike-related Ca^{2+} influx, as described briefly below.

Table 6 Conductance profile of the layer V pyramidal neuron model. Maximal conductances g and calcium conversion factor ϕ for each compartment. For some of the currents, the density was assumed to be uniform. For the others the general profile, with a higher conductance at the soma, and gradually lower conductances for more distal dendritic compartments, was adopted from Traub et al., (1991). The criteria selected to adjust the conductances do not give a unique solution (Traub et al., 1991). Prox. = proximal compartment, med. = medial compartment, dist. = distal compartment, api. = apical dendritic compartment, bas. = basal compartment, lump = lumped dendritic compartment

Current	Soma (S/m^2)	Prox.+med. api. + bas. (S/m^2)	lump (S/m^2)	Dist. api. (S/m^2)
gNa	0	60	60	30
gNaIS	250	0	0	0
gNaP	2.0	0	0	0
$g$$Ca_L$	1.5	1.5	1.5	1.5
$g$$K_{dr}$	0	25	25	12
$g$$K_{dr}$IS	25	0	0	0
$g$$K_C$	1960	1960	1960	1960
$g$$K_{AHP}$	0.5	0.5	0.5	0.5
$g$$K_M$	35	0	0	0
$g$$K_A$	5.0	0	0	0
gK(leak)	1.0	1.0	1.0	1.0
gCAN	39	0	0	0
$\phi_{Ca(K_C)pool}$	61.34×10^{12}	38.85×10^{12}	16.73×10^{12}	38.85×10^{12}
$\phi_{Ca(K_{AHP})pool}$	61.34×10^{12}	38.85×10^{12}	16.73×10^{12}	38.85×10^{12}
$\phi_{Ca(CAN)pool}$	61.34×10^{12}	0	0	0
$\phi_{Ca(PD)pool}$	61.34×10^{12}	0	0	0

Biochemical Pathway

Experiments indicated involvement of intracellular calcium from high-threshold calcium channels and activation of a cationic current (Egorov et al., 2002). The full signaling mechanism from intracellular calcium to cationic current is still unknown. This section describes the proposed biochemical pathways added to give the graded properties of firing.

The influx of calcium through the high-threshold calcium channel Ca_L changes intracellular calcium concentration $[Ca]_{PD}$ which is regulated through pumping and buffering processes modeled according to Traub et al. (1991) and McCormick and Huguenard (1992). $[Ca]_{PD}$ has a linear rise of Ca^{2+} proportional to the Ca_L current and a time constant. The time constant of cytosolic Ca^{2+} for entorhinal layer II stellate cells and layer III pyramidal cells is on the order of 5 s (Gloveli et al., 1999), comparable to Ca^{2+} diffusion simulations of a cell of comparable size (Yamada et al., 1989), where a time constant of around 5 s was found for the core volume. However, to represent Ca^{2+} in a volume closer to the membrane, we used a shorter time constant of 250 ms, in agreement with Yamada et al. (1989). Thus, the slow kinetics of our system is not primarily determined by the time constant of the Ca^{2+} concentration. Instead, it arises from the regulation of I_{CAN} by the intracellular calcium $[Ca]_{CAN}$ as well as by the channel kinetics of I_{CAN} itself, symbolized by the Hodgkin–Huxley-type gates between open (O) and closed (C) state. $[Ca]_{PD}$ affects two pathways:

(1) High calcium pathway – P. When the calcium concentration $[Ca]_{PD}$ crosses a transition point, it can increase I_{CAN} current via production of a compound X increasing the concentration [X]. The product X controls the balance between hypothetical kinases and phosphatases which in turn controls the balance between a phosphorylated state (H) and an unphosphorylated state (L) of the I_{CAN} channel. An increase in [X] causes a fine grain increase in the number of channels I_{CAN} in a high-conductance state, thereby causing a graded increase in firing frequency. This pathway operates only when $[Ca]_{PD}$ is above the transition point $[Ca]_{ThP} = 20$. The flux of X production was modeled according to

$$\phi_P = d_P \times ([Ca]_{PD} - [Ca]_{ThP}) \text{ for } [Ca]_{PD} \geq [Ca]_{ThP}$$
$$\phi_P = 0 \text{ otherwise}$$
$$d_P = 0.00015, [X] \leq 100$$

(2) Low calcium pathway – D. When the calcium concentration $[Ca]_{PD}$ falls below a transition point, it can decrease I_{CAN} current via breakdown of compound X and reduction in concentration [X], $[X] \geq 0$. This pathway operates only when $[Ca]_{PD}$ is below a transition point $[Ca]_{ThD} = 5$. The flux of X removal was modeled according to

$$\phi_D = d_D \times ([Ca]_{PD} - [Ca]_{ThD}) \text{ for } [Ca]_{PD} < [Ca]_{ThD}$$
$$\phi_D = 0 \text{ otherwise}$$
$$d_D = 0.00005 \text{ and } [Ca]_{ThD} < [Ca]_{ThP}$$

A decrease in [X] causes a decrease in the number of individual I_{CAN} channels in a high-conductance state, and thereby causes a graded decrease in firing frequency. Importantly, in the interval of $[Ca]_{PD}$ between $[Ca]_{ThD}$ and $[Ca]_{ThP}$ there is no change in [X]. This allows the graded levels to remain stable despite small variations (or brief large amplitude changes) in membrane potential and/or variations in intracellular calcium concentration. Therefore, the graded levels only change when there are large-scale changes in $[Ca]_{PD}$ passing either transition point.

As noted above, the concentration [X] regulates the conductance of I_{CAN}. This was implemented in the model by changing the effective CAN channel current dependent on the level of [X]. This describes the transition between the channel state producing a low charge transfer to the state producing a high charge transfer and is meant to encompass processes such as changes in single channel conductance or channel open time. Any single channel is assumed to be in either in its high- or low-conductance state. The total conductance of the ion channel $G_{tot} = g_L \times N_L + g_H \times N_H$. When N_x are large numbers, transitions appear graded (Lisman and Goldring, 1988).

The low- and high-conductance state dynamics $z = z([X])$ are modeled similarly to the calcium-dependent K current in Traub et al., (1991). The sensitivity to compound X is described by

$$\alpha_z([X]) = \min(0.015 \times [X], 1.5)$$
$$\beta_z = 1.0$$
$$\text{gate exponent} = 1$$

z, which is normalized between 0 and 1, is the degree of phosphorylation where 0 represents all CAN channels in the low state and 1 represents the case where the maximal possible number of CAN channels are in the high state.

The conductance of I_{CAN} depends on $[Ca]_{CAN}$ as described in Fransén et al. (2002). The CAN current's open and closed gating $y = y([Ca]_{CAN})$ was similarly described by

$$\alpha_m([Ca^{2+}]) = \min(0.006 \times [Ca^{2+}], 3.0)$$
$$\beta_m = 1.0$$
$$\text{gate exponent} = 1$$

The additional conductivity of the high-conductance state compared to the low-conductance state (i.e., the net increase) was added to the maximal conductance of I_{CAN} of the low-conductance state associated with its calcium sensitivity: $G_{tot} = y \times (G_{CAN} + G_{mod} \times z)$, where $G_{mod} = 3.7 \times 10^{-8}$ is the scaling constant for the modification z; G_{CAN} is the maximal conductance of the low state; and G_{tot} is the maximal conductance of I_{CAN} at the current level of [X] and $[Ca^{2+}]$.

The pathway model components should not be studied in isolation, they only have a meaning as a whole and do not necessarily by themselves correspond to specific parts of the biochemical pathway. The order of the components does likewise not necessarily correspond to any order in the real system. The gating was modeled according to a first-order scheme (like an equilibrium reaction or like the gating of a H–H channel). We have used a linear model for I_{CAN} as we presently cannot separate the kinetics of the different components in the pathway due to insufficient experimental data. An alternative could have been a second-order scheme of an enzyme-type reaction for the modification of I_{CAN}, yielding a hyperbolic system. With regard to localization of functional components on the soma or dendrites, we have used a somatic localization for the model and results presented. Simulations using a dendritic localization (data not shown) produced similar results.

Figure 2 shows a simulation investigating the properties of the neuron and particularly its capability to generate stable levels. The figure shows how the model replicates several of the observed characteristics of graded firing. The model also produces some characteristics that were not intentionally put into the model, like the transient decays toward a stable graded level following a current injection pulse.

Model Justification

In this chapter, we have described modeling of several neuron types found in EC, in particular the pyramidal neurons found in layers II and V. These two models share many features which they also share with pyramidal neurons found in other regions, e.g., hippocampus CA1 and neocortex. Following the principle of Occam's razor, similar features call for similar (identical) models. It is also worth noting that we along these lines did not include ion channels if we could not see a direct influence of them on the function studied. One such example is the calcium T-type channel of the pyramidal neuron of layer II which was not included as it would be essentially closed at the potentials under study. However, the pyramidal neuron models do have differences reflecting particular experimental findings by us and others. The layer II model has the calcium-activated cation current NCM which displays calcium activation and deactivation. The layer V neuron also has a cation current, but for this neuron we also included a model biochemical pathway to reflect the activation leading to graded persistent firing plateaus. In our current research, we are studying the pyramidal neurons found in layer III. These also have distinct properties from the others. For this lamina, we have data from both lateral and medial EC. Whereas the neuron found in the medial subdivision shares properties of medial layer V neurons in terms of capacity to show graded persistent plateaus, the neuron found in lateral EC is different. This neuron displays so-called on and off plateaus which are turned on and turned off by depolarizing input (Tahvildari et al., 2007). In this case, we are studying both ionic currents and dendritic locations of these as possible explanations for the phenomena observed.

In many cases, an experimental observation can be explained by several different models. In the case of the firing properties of the layer V pyramidal neuron we had

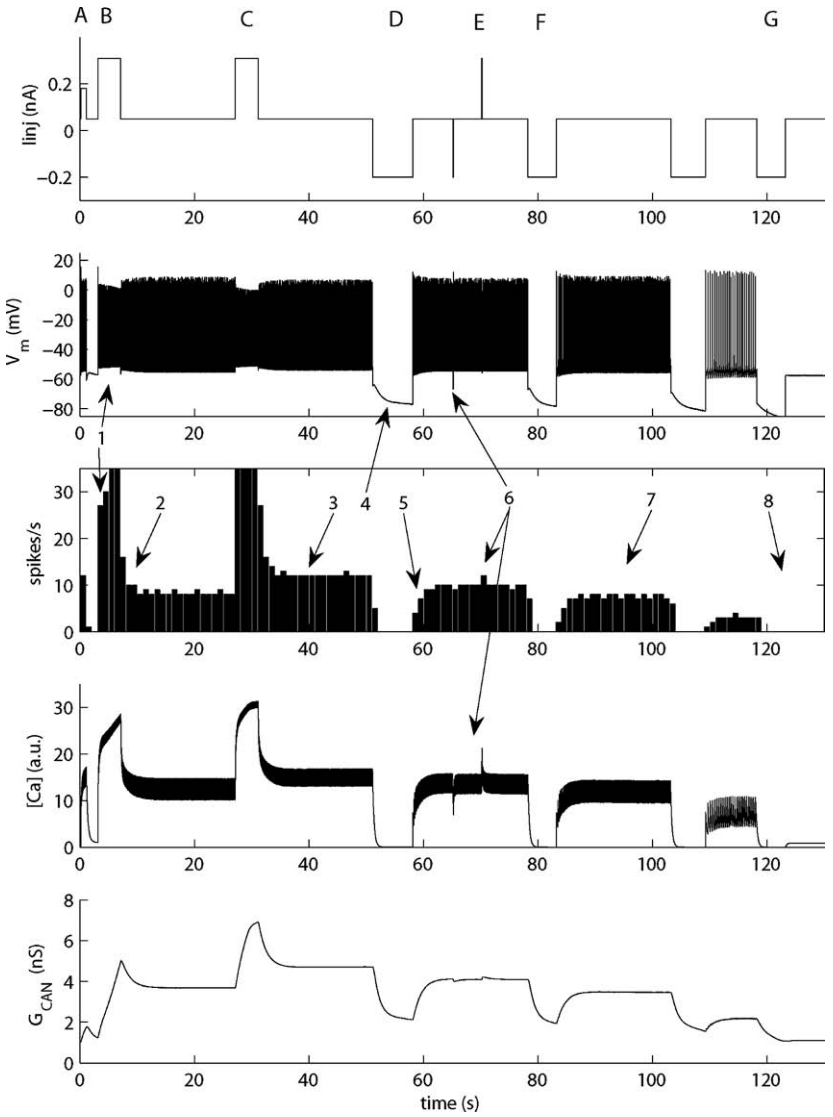

Fig. 2 Simulation of graded spiking. In the figure we plot from top: the current injection Inj (nA), soma membrane potential V_m (mV), spike histogram (bin width 1 s), calcium concentration (arbitrary units), and cationic current conductance G_{CAN} (nS). Starting from left, at (**A**) the neuron responds to a weak current injection (0–2 s) with spiking during injection alone. Next (**B**), a larger magnitude depolarization (at time 3–7 s) causes a firing increase followed by transient decay to a stable firing frequency. This stable firing persists until another depolarizing injection (**C**) at time 27–31 s. Firing increases during injection and decays to a higher graded level. At 51–58 s (**D**), a hyperpolarizing injection prevents firing during injection, but after injection the firing rate transiently increases to a lower graded level. Very brief distractor injections (**E**) (hyperpolarizing at 65 s and depolarizing at 70 s) do not alter this frequency. At 78 and 101 s (**F**), more hyperpolarizing injections shift the stable state to subsequent lower frequencies, and at 118 s (**G**), a final hyperpolarizing current injection terminates the stable firing

studied (Egorov et al., 2002), a line attractor hypothesis had been proposed. Several models were presented along these lines. In our continued analysis we experimentally tested assumptions behind some of these models and did not find support of these. In the modeling work, the strategy was to extend the analysis of experimental data to identify more characteristics of the phenomenon. These additional characteristics could then be used to compare and evaluate different models and to construct new models. Thus, by deriving a more precise characterization of the phenomenon at hand, models can be evaluated and the additional information can be used when developing new models.

The compartmental structure of the layer II stellate cell model was not based on anatomical reconstruction as that was not available at the time of the study. Rather it is a functional compartmentalization addressing the basic electrophysiological features, input resistance, length constant, and membrane time constant in conjunction with known gross anatomical data such as number of principal dendrites, diameter, and length of dendrites. A common strategy is to collapse the dendrites using Rall's rule and potentially obtain a single equivalent cylinder. This provides the correct load to the soma, but does not offer the proper attenuation of synaptic inputs. By collapsing all but one of the dendrites into a load cylinder, and keeping one of the dendrites intact, a compromise was achieved that limited the model complexity (number of compartments) while providing proper soma load and synaptic attenuation. We would like to stress that this is an example of a functional model. It does not aim at providing information about anatomical location but only on electrophysiological functional compartments. Furthermore, during our modeling work we noticed that it was hard to replicate the spike shape and fast AHP. That led us to add an initial segment compartment as had been done for the same reason by Ekeberg and colleagues (Ekeberg et al., 1991). This separates the spike generating compartment from the large load of the dendritic tree. By providing the initial segment compartment with relatively high conductances of Na- and K_{dr} currents, spikes are initiated in the initial segment. The soma can thereby be given a lower density, which in turn gives a more adequate amplitude of the backpropagating action potential.

To test the stability of graded firing of the layer V pyramidal cell model, we made a number of tests regarding ion channel density. Densities of the CAN, K_{AHP}, Ca_L, and Na_P currents were varied 20% with no effect on stability or the graded nature of activity. Further, we blocked the potassium A-type current with no effect, also consistent with experiments. Finally, we added an h current to the model as 60–70% of the layer V pyramidal cells have intermediate levels of (a third to half of that of the stellate cells in layer II). Even at the highest levels of where the sag comprises a third of the initial hyperpolarizing amplitude, stability of graded activity was unaffected. Thus, consistent with experimental findings, presence or absence does not affect stable graded activity. To test the parameter sensitivity of graded firing of the model, we made two additional models by changing parameters of the CAN channel, the K_{AHP} channel, and the calcium concentration of the signaling network. One model was constructed as to produce small range of 3–10 Hz and the other a larger range of 2–26 Hz for the graded plateaus. Both models were extensively evaluated. This showed that stable graded firing did not depend on one specific set of parameters.

To further test the properties of the signaling network and specifically the noise sensitivity of the neutral region and the location of the transition points, the properties of the neutral region between the transition points were modified. The interval was subdivided into three parts, a central part remaining at zero, with a nonzero part on either side representing influences of noise, thus a lower part starting at the lower transition point extending into the neutral region set at a constant small negative value, and an upper part ending at the upper transition point set at a small positive value. The upper part could extend up to a third of the width of the neutral region and the lower part up to a sixth without interfering with stable graded activity. Beyond these ranges slow drifts appeared. Such slow drifts for plateaus at the ends of the interval are consistent with occasional experimental findings (Egorov, unpublished observations). Thus, it is important to note that the model does not break down if transition points are moved into the region defined by the calcium level of the stable plateaus, the uppermost or lowermost levels may become unstable, but the center levels will remain stable. Finally, experimental observations (Egorov et al., 2002, Egorov, unpublished observations, Tahvildari, unpublished observations) show that the graded activity is stable also during synaptic activation resulting in irregular firing of the cell. We tested our model by adding synaptic noise from an AMPA-type synapse located at the compartment where the cationic channel and its signaling network are located, the soma. Graded activity was stable also at noise levels increasing the standard deviation of the ISI 90-fold leading to fluctuations in spike counts within 500 ms bins.

Commonly sensitivity analysis is performed to address parameter sensitivity around a working point. In some cases it may be of interest to study the behavior of the model in an interval of parameter values. This can be relevant when a parameter is known to vary, when different experiments give different values or values only for special cases, or when the values are unknown. In the stellate cell model, the time constant for activation of the fast and slow component of I_h could not be experimentally measured above -40 mV. Blocking experiments suggested an involvement in spike shape and clustering. We therefore investigated several scenarios. For instance, we compared the two cases of a rapid decrease of time constant above -40 mV to that of a leveling off toward a value close to that at -40 mV. Simulations with the latter were more consistent with data, implying that I_h remains open during and contributes to the spike. We also studied this in regard to clustering, see Fig. 3. The figure shows classification of firing pattern depending on the value of the K_{AHP} current and of the fate (approaching zero or staying finite) of the slow time constant of I_h.

The Future

Execution of behavioral functions like working memory or exploration of the environment resulting in grid field activity rely on coordinated activity of networks at multiple locations in the medial temporal lobe. The integrity and mechanism of function of these networks, however, not only depend on network properties, but may also depend on characteristics of the neurons building up the networks. We

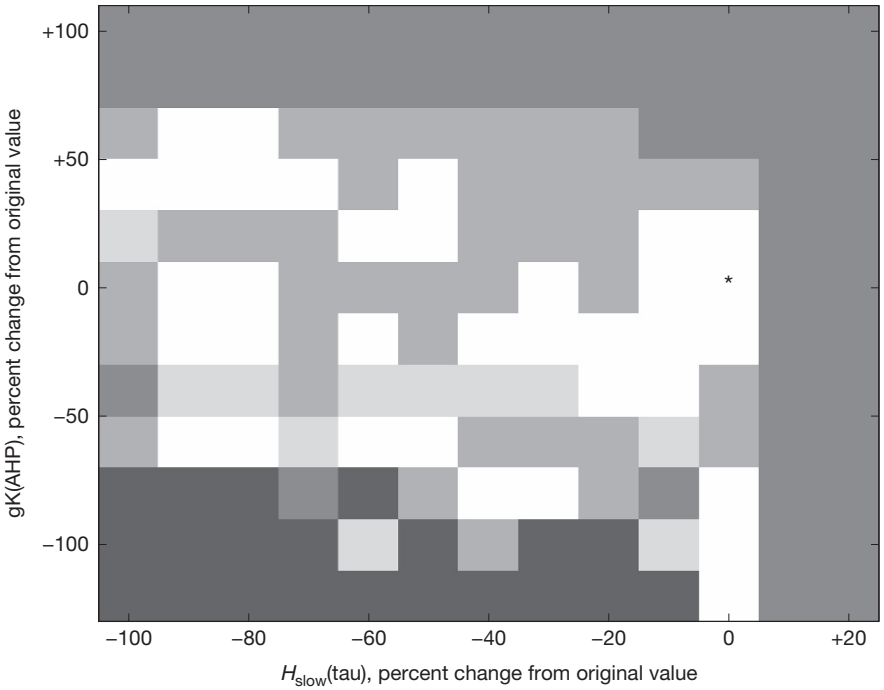

Fig. 3 To investigate the role of the slow component further, together with the role of the K_{AHP} current, a variation in conductance of IK(AHP) and variation in time constant of the slow component of I_h was conducted. The original value of IK(AHP) and the slow component of I_h is indicated by an asterisk (*). These two components enclose a region of robust clustering. Note that every point corresponds to a full run with a linearly increased current ramp. The firing was then classified according to the following: *black*: only tonic firing, *dark gray*: only single spikes with oscillations between as well as tonic firing, *medium gray*: doublets and single spikes and tonic firing, *light gray*: triplets and single spikes and tonic firing, *white*: doublets, triplets, single spiking, and tonic firing. The value for IK(AHP) is percentage change from original value (–100 means IK(AHP) 0, 100 means a doubling of IK(AHP)). The value for I_h slow time constant was varied by fixing the peak of the curve and compressing or expanding the curve along the time constant axis, with the multiplicative factor (in percentage change from original value) indicated. This means that –100 corresponds to a constant value at the peak 390 ms, –50 corresponds to the tails of the curve only reaching halfway down to the control value. (For increases, i.e., values above 0, a lower limit of 1 ms was used.)

have modeled the ionic bases of several observed characteristics of EC neurons. For both stellate cells and pyramidal cells we discuss how cationic currents might be involved and relate their kinetics and pharmacology to behavioral and cellular experimental results. Behavioral data have provided information on cellular firing patterns in relation to the different phases during an experiment. Pharmacological studies give information on ion channels or receptors involved. Slice data have provided information on soma membrane potential as well as ionic profiles of neurons studied, and thus provided increased spatial and temporal resolution. We selected a level of detail where effects of ion channels of different types and spatial locations

could be studied. This provided a stronger relationship to data from slices, but a weaker one to the behavioral level. Recent experimental techniques, however, will diminish this gap. By, for instance, transfecting selected neuron types with genes coding for hyperpolarizing ion channels, neurons can be functionally turned on or off in behavioral studies depending on whether the gene transcription is turned on or off. Moreover, with the use of fluorescent proteins, "in vivo" studies of network function will add new data that to a large degree is lacking today. The gap between the molecular and behavioral levels is thereby bridged at a precision in terms of spatial location, neuron or ionic-type specificity which classical pharmacology or lesion experiments could not provide. On the technical side of modeling, model development will increasingly be performed using more systematic approaches, including parameter estimation using automized optimization tools. Tests of models will include not only sensitivity analysis for a select number of parameters, but will use techniques to assess parameter influence over the time course of a simulation. The issue of observability will become increasingly important, prompting for model reduction techniques to be used during model construction. This will lead to models with a larger range of applicability and hopefully to models with a higher structural content.

Appendix A Ionic Currents

Voltage-dependent conductances were modeled using a Hodgkin–Huxley type of kinetic model. The following reversal potentials were used: Na^+ +55 mV, K^+ –75 mV, Ca^{2+} +80 mV, I_h–20 mV, and for I_{NCM} 0 mV.

Na, K_{dr}

The Na^+ current responsible for fast action potentials had kinetics taken from a model of hippocampal pyramidal cells (Traub et al., 1991, 1994). The pyramidal cell has Na and K currents with faster kinetics (described in a separate section below and labeled Na(soma) and K_{dr}(soma)) on the compartment where spikes are initiated (Traub et al., 1994). Both the Na and the K currents were shifted +5 mV from the Traub model to get the spiking threshold more positive, around −50 mV. The spatial distribution and maximal conductance of all currents on the different compartments are found in Tables 2, 4, and 6. The maximal conductances were adjusted to match experimental data (Alonso and Klink, 1993) on the action potential rate of depolarization (Na^+) and rate of repolarization (K^+) as well as spike threshold, amplitude, and duration of action potentials. The currents used the following equations:

Na

$$\alpha_m(V) = \frac{320 \times 10^3 (0.0131 - V)}{\exp((0.0131 - V)/0.004) - 1}$$

$$\beta_m(V) = \frac{280 \times 10^3 (V - 0.0401)}{\exp((V - 0.0401)/0.005) - 1}$$

gate exponent $= 2$

$$\alpha_{\mathrm{h}}(V) = 128 \exp((0.017 - V)/0.018)$$

$$\beta_{\mathrm{h}}(V) = \frac{4 \times 10^3}{1 + \exp((0.040 - V)/0.005)}$$

gate exponent $= 1$

Na(soma)

$$\alpha_{\mathrm{m}}(V) = \frac{800 \times 10^3 (0.0172 - V)}{\exp((0.0172 - V)/0.004) - 1}$$

$$\beta_{\mathrm{m}}(V) = \frac{700 \times 10^3 (V - 0.0422)}{\exp((V - 0.0422)/0.005) - 1}$$

gate exponent $= 3$

$$\alpha_{\mathrm{h}}(V) = 320 \exp((0.042 - V)/0.018)$$

$$\beta_{\mathrm{h}}(V) = \frac{10 \times 10^3}{1 + \exp((0.042 - V)/0.005)}$$

gate exponent $= 1$

$\mathrm{K_{dr}}$

$$\alpha_{\mathrm{m}}(V) = \frac{16 \times 10^3 (0.0351 - V)}{\exp((0.0351 - V)/0.005) - 1}$$

$$\beta_{\mathrm{m}}(V) = 250 \exp((0.020 - V)/0.040)$$

gate exponent $= 2$

$\mathrm{K_{dr}}$(soma)

$$\alpha_{\mathrm{m}}(V) = \frac{30 \times 10^3 (0.0172 - V)}{\exp((0.0172 - V)/0.005) - 1}$$

$$\beta_{\mathrm{m}}(V) = 450 \exp((0.012 - V)/0.040)$$

gate exponent $= 4$

NaP

The "persistent-type" slowly inactivating Na^+ current was modeled according to experimental data Magistretti et al., (1999) for the steady-state activation and inactivation and kinetics of inactivation, and for the reversal potential, and according to McCormick and Huguenard, (1992) for the kinetics of activation and the exponents of the activation rates m, h. The maximal conductance was adjusted to the conductance of I_{h} to allow subthreshold oscillations to develop.

$$\tau_{\mathrm{m}}(V) = \frac{1}{\alpha_{\mathrm{m}} + \beta_{\mathrm{m}}}, \text{ where } \alpha_{\mathrm{m}}(V) = \frac{0.091 \times 10^6 (V + 0.038)}{1 - \exp(-(V + 0.038)/0.005)}$$

$$\text{and } \beta_{\mathrm{m}}(V) = \frac{-0.062 \times 10^6 (V + 0.038)}{1 - \exp((V + 0.038)/0.005)}$$

$$m_{\mathrm{inf}}(V) = \frac{1}{1 + \exp(-(V + 0.0487)/0.0044)}$$

gate exponent = 1

$$\tau_{\mathrm{h}}(V) = \frac{1}{\alpha_{\mathrm{h}} + \beta_{\mathrm{h}}}, \text{ where } \alpha_{\mathrm{h}}(V) = \frac{-2.88V - 0.0491}{1 - \exp((V - 0.0491)/0.00463)}$$

$$\text{and } \beta_{\mathrm{h}}(V) = \frac{6.94V + 0.447}{1 - \exp(-(V + 0.447)/0.00263)}$$

$$h_{\mathrm{inf}}(V) = \frac{1}{1 + \exp((V + 0.0488)/0.00998)}$$

gate exponent = 1

$\mathbf{Ca_L}$

The high-threshold Ca^{2+} current was modeled according to previous models (Traub et al., 1994). The maximal conductance was set to the same value as in previous work (Traub et al., 1994).

$$\alpha_{\mathrm{m}}(V) = \frac{1.6 \times 10^3}{1 + \exp(-72(V - 0.065))}$$

$$\beta_{\mathrm{m}}(V) = \frac{20 \times 10^3 (V - 0.0511)}{\exp((V - 0.0511)/0.005) - 1}$$

gate exponent = 2

$\mathbf{K_C}$

The fast calcium- and voltage-dependent K^+ current was modeled according to previous work (Traub et al., 1991). The maximal conductance was adjusted to match the fAHP depth and Ca-dependent spike repolarization rate (Alonso and Klink, 1993).

$$V \leq 0.050$$

$$\alpha_{\mathrm{m}}(V) = \frac{\exp(53.872V - 0.66835)}{0.018975}$$

$$\beta_{\mathrm{m}}(V) = 2000(\exp((0.0065 - V)/0.027)) - \alpha_{\mathrm{m}}$$

$$V > 0.050$$

$$\alpha_{\mathrm{m}}(V) = 2000(\exp((0.0065 - V)/0.027))$$

$$\beta_{\mathrm{m}}(V) = 0$$

gate exponent = 1

K_A

The transient potassium current K_A was modeled according to previous models (Traub et al., 1991).

$$\alpha_h(V) = \frac{0.02(13.1 - V)}{\exp(\frac{13.1-V}{10}) - 1}$$
$$\beta_h(V) = \frac{0.0175(V - 40.1)}{\exp(\frac{V-40.1}{10}) - 1}$$
$$\text{gate exponent} = 1$$
$$\alpha_m(V) = 0.0016 \exp(\frac{-13 - V}{18})$$
$$\beta_m(V) = \frac{0.05}{1 + \exp(\frac{10.1-V}{5})}$$
$$\text{gate exponent} = 1$$

K_{AHP} (LIIP)

The calcium-dependent K^+ (afterhyperpolarization) current was modeled according to previous models (Traub et al., 1991), with the slope set at 30 and the saturation set at 30 (arbitrary units). The maximal conductance was adjusted to match the sAHP depth in experimental data (Alonso and Klink, 1993).

$$\alpha_m([Ca^{2+}]) = \min(30[Ca^{2+}], 30)$$
$$\beta_m = 1.0$$
$$\text{gate exponent} = 1$$

K_{AHP} (LIIS)

The maximal conductance was adjusted to match the sAHP depth in experimental data (Alonso and Klink, 1993).

$$\alpha_m([Ca^{2+}]) = \min(6[Ca^{2+}], 30)$$
$$\beta_m = 1.0$$
$$\text{gate exponent} = 1$$

K_{AHP}(LVP)

The maximal conductance was adjusted to match the sAHP depth in experimental data (Egorov, unpublished observations).

$$\alpha_m([Ca^{2+}]) = \min(0.2 \times [Ca^{2+}], 3.0) \text{ for } [Ca^{2+}] \leq 15$$
$$\alpha_m([Ca^{2+}]) = \min(3.0 + 0.8 \times ([Ca^{2+}] - 15), 15) \text{ for } [Ca^{2+}] > 15$$
$$\beta_m = 1.0$$
$$\text{gate exponent} = 1$$

K_M

The slowly activated voltage-dependent K^+ current was modeled according to Bhalla and Bower, (1993). The maximal conductance was adjusted to match the length of the suprathreshold plateau following a spike in the presence of Ca block (Klink and Alonso, 1993).

$$\tau_m(V) = \frac{1}{3.3 \exp((V + 0.035)/0.040) + exp(-(V + 0.035)/0.020)}$$
$$m_{inf}(V) = \frac{1}{1 + \exp(-(V + 0.035)/0.005)}$$
$$\text{gate exponent} = 1$$

K(leak)

The K(leak) conductance was considered to be linear and uniformly distributed with a reversal potential $E_{rev} = -0.075$ V.

Appendix B Layer II Pyramidal Cell Ca^{2+} Buffering

The Ca^{2+} diffusion and buffering were modeled according to previous techniques (Traub et al., 1991; McCormick and Huguenard, 1992). To take into account the differences in distances and diffusion constants for the calcium influencing each of the different currents, the calcium kinetics was modeled separately for each case, consistent with separate calcium compartments and reaction pathways within the cell. In addition, until calcium-clamp data exist on the individual currents, it is not possible to separate the kinetics of the calcium concentration from the kinetics of the channel itself. Therefore, the models of the concentration and of the individual currents should be seen as a unit.

Following the convention used in Traub et al., (1991), the calcium concentration has arbitrary units. Because the calcium concentration is converted to an effect on rate parameters of the calcium-sensitive channel, the absolute concentration of calcium can be arbitrary, though we have tried to keep the magnitude in a range similar to millimolar to enable comparisons. For the calcium related to the calcium-dependent K^+ current the diffusion rate constant of 0.1 s was set to give a spike frequency adaptation rate according to Alonso and Klink (1993). The minimal $[Ca^{2+}]_i$ was set to 5.0×10^{-3}.

For the fast calcium- and voltage-dependent K^+ current, K_C, the calcium values were 0.5 ms and 5.0×10^{-6}, respectively, and the related values for the non-specific Ca^{2+}-dependent cationic current were 1.333 s and 1.0×10^{-5}, respectively. This was determined by tuning the channel to replicate data obtained during blockade of calcium influx in Klink and Alonso (1993). The changes in concentration of calcium used for K_{AHP} above were too slow to effectively represent K_C, so different dynamics were necessary. Similarly, the slower changes in NCM relative to K_{AHP} required use of the slower calcium dynamics for NCM described above. Further, the conversion factor, ϕ, from charge density to concentration for each component and compartment is found in Tables 2, 4, and 6. Because this conversion factor converts channel current to calcium concentration, valence is implicitly addressed by using current.

Appendix C Layer V Pyramidal Cell Ca^{2+} Buffering

As in Fransén et al. (2002), the Ca^{2+} diffusion and buffering were modeled according to previous techniques (Traub et al., 1991; McCormick and Huguenard, 1992).

For the calcium related to the calcium-dependent K^+ current the diffusion decay time constant of 0.1 s was set to give a spike frequency adaptation rate according to Alonso and Klink (1993). The minimal $[Ca^{2+}]_i$ was set to 5.0×10^{-3}. For the fast calcium- and voltage-dependent K^+ current, K_C, the calcium concentration values were 0.5 ms for the diffusion decay time constant and 5.0×10^{-6} for the minimal $[Ca^{2+}]_i$, respectively. The changes in concentration of calcium used for K_{AHP} above were too slow to effectively represent K_C, so different dynamics were necessary. All values above were taken from Fransén et al. (2002). Further, the conversion factor, ϕ, from charge density to concentration for each component and compartment is found in Tables 2, 4, and 6. Because this conversion factor converts channel current to calcium concentration, valence is implicitly addressed by using current. The related values for the non-specific Ca^{2+}-dependent cationic current were 0.2 s and 10.0, respectively. This was determined by tuning the channel to replicate current clamp data (Alonso, unpublished observations). For the calcium affecting the P and D processes, the calcium concentration values were 0.25 s and 5.0×10^{-5}, respectively.

Membrane potential and calcium level are not independent factors due to the interaction between voltage-dependent calcium channels and calcium-dependent channels, e.g., K and CAN currents producing currents affecting the potential. Any change will thus be a change in 3D space of I, V_m,$[Ca^{2+}]$.

Further Reading

Alonso, A., & Klink, R. (1993). Differential electroresponsiveness of stellate and pyramidal-like cells of medial entorhinal cortex layer II. J Neurophysiol, 70, 128–143.

Bunce, J. G., Sabolek, H. R., & Chrobak, J. J. (2004). Intraseptal infusion of the cholinergic agonist carbachol impairs delayed-non-match-to-sample radial arm maze performance in the rat. Hippocampus, 14, 450–459.

Dickson, C., Magistretti, J., Shalinsky, M. H., Fransén, E., Hasselmo, M., & Alonso, A. (2000). Properties and role of Ih in the pacing of subthreshold oscillations in entorhinal cortex layer II neurons. J Neurophysiol, 83, 2562–2579.

Egorov, A. V., Hamam, B. N., Fransén, E., Hasselmo, M. E., & Alonso, A. A. (2002). Graded persistent activity in entorhinal cortex neurons. Nature, 420, 173–178.

Ekeberg, Ö., Wallén, P., Lansner, A., Tråvén, H., Brodin, L., & Grillner, S. (1991). A computer based model for realistic simulations of neural networks. I. The single neuron and synaptic interaction. Biol Cybern, 65, 81–90.

Fransén, E., Alonso, A. A., Dickson, C. T., Magistretti, J., & Hasselmo, M. E. (2004). Ionic mechanisms in the generation of subthreshold oscillations and action potential clustering in entorhinal layer II stellate neurons. Hippocampus, 14, 368–384.

Fransén, E., Alonso, A. A., & Hasselmo, M. E. (2002). Simulations of the role of the muscarinic-activated calcium-sensitive non-specific cation current INCM in entorhinal neuronal activity during delayed matching tasks. J Neurosci, 22, 1081–1097.

Fransén, E., Tahvildari, B., Egorov, A. V., Hasselmo, M. E., & Alonso, A. A. (2006). Mechanism of graded persistent cellular activity of entorhinal cortex layer V neurons. Neuron, 49, 735–746.

Fyhn, M., Molden, S., Witter, M., Moser, E., & Moser, M.-B. (2004). Spatial representation in the entorhinal cortex. Science, 305, 1258–1264.

Giocomo, L. M., Zilli, E. A., Fransén, E., & Hasselmo, M. E. (2007, Mar 23). Temporal frequency of subthreshold oscillations scales with entorhinal grid cell field spacing. Science, 315(5819), 1719–1722.

Gloveli, T., Egorov, A. V., Schmitz, D., Heinemann, U., & Mller, W. (1999, Oct). Carbachol-induced changes in excitability and [Ca2+]i signalling in projection cells of medial entorhinal cortex layers II and III. Eur J Neurosci, 11(10), 3626–3636.

Hafting, T., Fyhn, M., Molden, S., Moser, M. B., & Moser, E. I. (2005, Aug 11). Microstructure of a spatial map in the entorhinal cortex. Nature, 436(7052), 801–806.

Hamam, B. N., Kennedy, T. E., Alonso, A., & Amaral, D. G. (2000, Mar 20) Morphological and electrophysiological characteristics of layer V neurons of the rat medial entorhinal cortex. J Comp Neurol, 418(4), 457–472.

Kay, L. M. (2005). Theta oscillations and sensorimotor performance. Proc Natl Acad Sci USA, 102, 3863–3868.

Klink, R., & Alonso, A. (1993, Jul). Ionic mechanisms for the subthreshold oscillations and differential electroresponsiveness of medial entorhinal cortex layer II neurons. J Neurophysiol, 70(1), 144–57.

Klink, R., & Alonso, A. (1997). Morphological characteristics of layer II projection neurons in the rat medial entorhinal cortex. Hippocampus, 7(5), 571–583.

Lee, H., Simpson, G. V., Logothetis, N. K., & Rainer, G. (2005). Phase locking of single neuron activity to theta oscillations during working memory in monkey extrastriate visual cortex. Neuron, 45, 147–156.

Lisman, J. E., & Goldring, M. A. (1988, Jul). Feasibility of long-term storage of graded information by the Ca2+/calmodulin-dependent protein kinase molecules of the postsynaptic density. Proc Natl Acad Sci USA, 85(14), 5320–5324.

McCormick, D. A., & Huguenard, J. R. (1992, Oct). A model of the electrophysiological properties of thalamocortical relay neurons. J Neurophysiol, 68(4), 1384–1400.

McGaughy, J., Koene, R. A., Eichenbaum, H., & Hasselmo, M. E. (2005, Nov 2). Cholinergic deafferentation of the entorhinal cortex in rats impairs encoding of novel but not familiar stimuli in a delayed nonmatch-to-sample task. J Neurosci, 25(44), 10273–10281.

Schön, K., Atri, A., Hasselmo, M. E., Tricarico, M. D., LoPresti, M. L., & Stern, C. E. (2005). Scopolamine reduces persistent activity related to long-term encoding in the parahippocampal gyrus during delayed matching in humans. J Neurosci, 25, 9112–9123.

Schön, K., Hasselmo, M. E., Lopresti, M. L., Tricarico, M. D., & Stern, C. E. (2004). Persistence of parahippocampal representation in the absence of stimulus input enhances long-term encoding: A functional magnetic resonance imaging study of subsequent memory after a delayed match-to-sample task. J Neurosci, 24, 11088–11097.

Stern, C. E., Sherman, S. J., Kirchhoff, B. A., & Hasselmo, M. E. (2001). Medial temporal and prefrontal contributions to working memory tasks with novel and familiar stimuli. Hippocampus, 11(4), 337–346.

Suzuki, W. A., Miller, E. K., & Desimone R. (1997, Aug). Object and place memory in the macaque entorhinal cortex. J Neurophysiol, 78(2), 1062–1081.

Tahvildari, B., Fransén, E., Alonso, A. A., & Hasselmo, M. E. (2007). Switching between "On" and "Off" states of persistent activity in lateral entorhinal layer III neurons. Hippocampus, 17(4), 257–263.

Traub, R. D., Wong, R. K., Miles, R., & Michelson, H. (1991 Aug). A model of a CA3 hippocampal pyramidal neuron incorporating voltage-clamp data on intrinsic conductances. J Neurophysiol, 66(2), 635–650.

Yamada, W., Koch, C., & Adams, P. (1989). Multiple channels and calcium dynamics. In: C. Koch and I. Segev, Editors, Methods in Neuronal Modeling. From Synapses to Networks, MIT Press, Cambridge, MA, pp. 97–134.

Young, B. J., Otto, T., Fox, G. D., & Eichenbaum, H. (1997, Jul 1). Memory representation within the parahippocampal region. J Neurosci, 17(13), 5183–5195.

Zador, A., Koch, C., & Brown, T. H. (1990 Sep). Biophysical model of a Hebbian synapse. Proc Natl Acad Sci USA, 87(17), 6718–6722.

Single Neuron Models: Interneurons

Frances Skinner and Fernanda Saraga

Overview

Interneurons are recognized to be critical controllers of brain rhythms and activities in normal and pathological states (Buzsáki 2006; Buzsáki and Chrobak 1995; Mann and Paulsen 2007). As such, we need to understand the intrinsic and synaptic network dynamics of interneurons. For example, it is clear that plasticity (Perez et al. 2001) and place cell coding (Maurer et al. 2006; Wilent and Nitz 2007) specifically involve interneurons and that interneurons are specific targets of neuromodulation (Glickfeld and Scanziani 2006; Lawrence et al. 2006b).

The diversity of interneurons in terms of morphology, calcium-binding proteins, neurochemical marker content, axonal targets, and firing properties has been appreciated for over a decade (e.g., Buhl et al. 1994; Gulyás et al. 1993; Han et al. 1993), and their complex contributions have been laid down in several reviews (McBain and Fisahn 2001; Somogyi and Klausberger 2005, also see chapter "Morphology of Hippocampal Neurons"). Moreover, this diversity likely has functional relevance as different interneuron subtypes fire at particular phases of in vivo theta and gamma rhythms – for example, Klausberger et al. (2003) and Tukker et al. (2007), suggesting distinct and specific contributions to behavior-dependent patterning of neuronal population activities.

The research questions that are typically addressed with interneuron models focus on how their intrinsic details and synaptic properties affect and give rise to population rhythms in hippocampus. In this chapter we concentrate on single interneuronal models from the perspective of their intrinsic properties. There are several ways in which different intrinsic properties could produce similar neuronal outputs. Thus, if we are to understand how the specific, intrinsic properties of interneuron subtypes contribute to hippocampal output, it is important to build detailed, single cell mathematical models of them. By detailed models we mean

F. Skinner (✉)
Toronto Western Research Institute (TWRI), University Health Network (UHN), Toronto, ON, Canada M5T 2S8; Department of Medicine (Neurology), Department of Physiology, Institute of Biomaterials and Biomedical Engineering, University of Toronto, Canada
e-mail: frances.skinner@utoronto.ca

V. Cutsuridis et al. (eds.), *Hippocampal Microcircuits*, Springer Series in Computational Neuroscience 5, DOI 10.1007/978-1-4419-0996-1_14,

those in which there is a morphological representation and voltage-gated ion channel properties appropriate to the cell type in the model. Subsequent reduction and analyses of these models could then be considered in different contexts to obtain a deep and thorough understanding of their dynamic outputs (e.g., as was done for ghostbursting in electric fish pyramidal cells, reviewed in Laing (2004)). Indeed, analysis of the nonlinear dynamics of neuronal models has shown that it is possible to capture a wide range of firing properties using models with only a few parameters and variables (Izhikevich 2007).

Passive Multi-compartment Models

A morphological representation translates into a multi-compartment model with an appropriate electrical "backbone" onto which voltage-gated channels can be added. Such passive multi-compartment models of hippocampal interneurons have been used to reconstruct synaptic signals at distal sites that are technically difficult to access. In this way, an understanding of the contribution of distal inputs can be obtained. For example, Geiger et al. (1997) and Bartos et al. (2001) built detailed passive models of basket cells in dentate gyrus to be able to infer non-somatic synaptic conductance characteristics as measured in the soma. In another example, Chitwood et al. (1999) built CA3 interneuron models based on inhibitory cells located in different strata and used them to show that despite differences in dendritic synaptic locations, the amplitude of postsynaptic potentials did not vary much. Multi-compartment models of three CA1 interneuron subpopulations (calbindin-, calretinin-, and parvalbumin-containing cells) were built and their morphotonic and branching patterns examined (Emri et al. 2001). Differences between the three subpopulations were found – for example, parvalbumin-containing cells characteristically had a large number of primary dendrites, short morphotonic lengths, and little variation in morphotonic distance of dendrite ends within a cell. The authors thus suggest that the effectiveness of evoked synaptic potentials varies between the different subpopulations.

Biophysically and Morphologically Detailed Interneuron Models

For technical recording and identification reasons, mainly two types of interneurons have been investigated experimentally and modeled extensively. They are (i) the fast-spiking, basket cell type which target perisomatic regions of pyramidal cells (e.g., see Freund 2003) and (ii) those with cell bodies in the stratum oriens that have horizontal dendrites and which target more distal regions of the pyramidal trees in the stratum lacunosum/moleculare, O-LM interneurons (Maccaferri 2005), in a feedback fashion. These two types can be considered representative examples of the perisomatic inhibitory and the dendritic inhibitory interneuron classes. *In this chapter we present a step-by-step description of how models based on these two*

different interneurons were built. We provide the rationale and details behind the choices made at each step.

Basket Cell Models

The first detailed interneuron model was built by Traub and Miles in 1995. It is a 51-compartment model representing a stratum pyramidale (SP) CA3 interneuron (putative basket cell) and was built to investigate the physiologically powerful connection between pyramidal neurons and SP inhibitory neurons in the CA3 region in evoking a spike. Use of the model indicated that active, voltage-gated channels needed to be present in the dendrites for a spike to be evoked. This prediction of voltage-gated channels being present in the dendrites of interneurons has since been shown to be the case for O-LM and basket cells (Maccaferri et al. 2004; Martina et al. 2000). In 1996, Wang and Buzsáki (WB) built a single compartment basket cell model neuron in which the kinetics and maximal conductances allowed the model to display spiking characteristics of hippocampal and neocortical fast-spiking interneurons. Due to its less complicated single compartment representation, this model is often used in network modeling.

Basket cells are known to participate in several hippocampal rhythms (such as gamma activity) and are interconnected not only with inhibitory synapses, but also with gap junctions located on their dendrites (Fukuda and Kosaka 2000). Thus to understand the contribution of basket cells in hippocampal functioning, it is necessary to have detailed models to gain insight on issues such as dendritic gap junction coupling, which necessarily depend on the intrinsic properties of the single cell. *In the next section, we describe a detailed basket cell model that we built to be able to explore dendritic gap junction coupling (Saraga and Skinner 2004; Saraga et al. 2006).* The WB model is used as a basis for the model's intrinsic current representations and, similar to Traub and Miles, active dendrites are included since voltage-gated channels are known to be present in the dendrites of basket cells. However, unlike Traub and Miles, the model's morphology is quantitatively based on a hippocampal basket cell. Theory was used in a reduced version of the model to predict how network output is affected by the active dendrites in the single cell model representation.

O-LM Cell Models

The importance of particular intrinsic properties in oriens interneuron models was shown in our earlier work where we investigated how the combined effect of electrical and inhibitory coupling could produce synchronized bursting as observed experimentally, given particular intrinsic properties (Skinner et al. 1999). This led us to explore a 12-compartment oriens interneuron model representation with dendritic voltage-gated channels (Saraga and Skinner 2002). With actual morphology and biophysical details of some of the voltage-gated channels in the dendrites (Martina et al. 2000), we proceeded to build a full multi-compartment model of an oriens-lacunosum/moleculare (O-LM) cell (Saraga et al. 2003). The focus of the 2003

model version was to examine how the dendritic conductances might be distributed. The models were used to show the dependence of forward-propagating and back-propagating spikes on synaptic input strength and location.

With direct access to morphological and passive properties and a well-defined question, we have now built more realistic O-LM models (Lawrence et al. 2006a). The 2006 models have more extensive morphology and axonal representation and build on the ion currents used in the 2003 model. These more realistic models were used to explore M-current density and distribution. *These O-LM model cells represent the most complete interneuron models to date and are described in the next section.*

The Models and Model Justification

We present a step-by-step description of the model development in three parts: (i) reconstruction of 3-D morphology, (ii) passive properties, and (iii) active properties. These parts need to be considered in the building of any multi-compartment model. Detailed methodological descriptions are given in De Schutter 2001: chapter 6 by D. Jaeger for morphology reconstruction, and chapter 8 by G. Major for passive properties. Also see chapters "Morphology of Hippocampal Neurons" and "Physiological Properties of Hippocampal Neurons" for morphology, physiology, and some practical aspects of relevant techniques.

Morphology reconstruction involves creating a multi-compartment representation of the neuron using various software (see details below). The passive parameters of a cell include the membrane capacitance, C_{m}, the membrane resistivity (inverse of leak conductance), R_{m}, and the cytoplasmic or axial resistivity, R_{a}. Estimating the passive properties of the model essentially involves matching experimental data and model simulations to transient responses (see more details in Segev et al. 1998). See below for the active properties.

Mathematical Model Description

The general structure of the model equations are summarized here and the specific kinetic equations are discussed for the two models below. The discrete version of the cable equation, an approximation to the original partial differential cable equation, describes the evolution of membrane voltage in each model compartment k, V_k:

$$C_m \frac{\mathrm{d}V_k}{\mathrm{d}t} = \sum_{\substack{n \\ n \neq k}} \gamma_{n,k}(V_n - V_k) - I_{\mathrm{ionic},k} \tag{1}$$

The sum is taken over all compartments n that are connected to compartment k. $\gamma_{n,k}$ is the internal conductance between respective compartments, and whose inverse is the axial resistivity, R_{a}. $I_{\text{ionic},k}$ is the transmembrane ionic current for compartment k. Inward currents, which depolarize the membrane, are by convention, negative. For the sake of simplicity, the compartment subscript k will be dropped from now on. The term I_{ionic} encompasses various ionic currents which are discussed in more detail for each particular model. The individual ionic current, I_{ionic}, follows an ohmic relationship:

$$I_{\text{ionic}} = g_{\text{ionic}} x (V - E_{\text{ionic}}) \tag{2}$$

where g_{ionic} is the maximal conductance of the particular ion channel and E_{ionic} is the ionic reversal potential given by the Nernst equation for the particular ionic species. x is an activation or an inactivation variable (or a combination of variables depending on the particular current being modeled, and which can be raised to a non-unity power for a better fit to the data) that determines the fraction of open channels at a given time. These variables follow first-order kinetics:

$$\frac{\mathrm{d}x}{\mathrm{d}t} = \alpha_x (1 - x) - \beta_x x \tag{3}$$

where α_x and β_x are voltage-dependent rate constants. Using a voltage-dependent time constant, τ_x, and a steady-state value, x_∞, the differential equation can be rewritten as:

$$\frac{\mathrm{d}x}{\mathrm{d}t} = \frac{x_\infty - x}{\tau_x} \tag{4}$$

where

$$\tau_x = \frac{1}{\alpha_x + \beta_x} \qquad \text{and} \quad x_\infty = \frac{\alpha_x}{\alpha_x + \beta_x} \tag{5}$$

These types of equations are used to describe a variety of different voltage-gated ion channels. This method of describing the gating and kinetics of ion channels is a conductance-based formalism (Skinner 2006) based on Hodgkin and Huxley's work. Experimentally, the steady-state activation variable can be measured using the voltage-clamp protocol and fit to a Boltzmann function:

$$x_\infty = \frac{1}{1 + \exp(-(V - V_{1/2})/k)} \tag{6}$$

Basket Cell Interneuron Model

Morphology

A 372-compartment model (1 somatic compartment and 371 dendritic compartments) was built using NEURON (Hines and Carnevale 1997; http://www.neuron.yale.edu). It is based on a traced hippocampal basket cell morphology taken from Gulyás et al. (1999) and http://www.koki.hu/~gulyas/ca1cells and has a surface area of $18,069\,\mu m^2$. For the basket cell model in Saraga et al. (2006) and Saraga and Skinner (2004), a parvalbumin (PV)-positive interneuron morphology was chosen due to known gap junction connections between these interneurons (Fukuda and Kosaka 2000). A detailed geometry of the dendritic tree including diameters and branching structure of the PV interneuron (.swc format) was imported to the shareware program CVAPP (www.compneuro.org/CDROM/docs/cvapp.html), which enabled us to test electrical connectivity between soma and all processes and change the morphology into a file format readable by NEURON. Since the morphology file omitted a detailed reconstruction of the soma, we added a somatic cylindrical compartment ourselves, based on the average surface area measured in PV basket cell somata by Gulyás et al. (1999) ($\sim 1,000\,\mu m^2$) (Saraga and Skinner 2004; Saraga et al. 2006).

Passive Properties

Although direct measurements of these parameters have not been performed in basket cells specifically, studies have arrived at estimates for hippocampal neurons in the following ranges; C_m : 0.5–1.5 $\mu F/cm^2$, R_m : 7–100 $k\Omega cm^2$, R_a: 50–484 Ωcm (Major 1993; Spruston et al.1994; Thurbon et al. 1994). Values for these three parameters were chosen in order to match the input resistance ($R_{in} = 245\,M\Omega$)) and membrane time constant ($\tau_m = 30$ ms) measured in basket cells (Morin et al. 1996; van Hooft et al. 2000). Parameter values are given in Appendix Table 1.

Active Properties

Since voltage-clamp data were not specifically available for hippocampal basket cell currents, we used the kinetic equations of ion channels described in Wang and Buzsáki (1996) for a fast-spiking hippocampal interneuron. These equations were modified by Wang and Buzsáki (1996) from the original Hodgkin and Huxley (1952) equations in order to match electrophysiological properties such as a brief after-hyperpolarization potential and current–frequency relationship as measured in hippocampal interneurons (Lacaille and Williams 1990; McCormick et al. 1985; Zhang and McBain 1995a). The sum of the intrinsic membrane terms that, in each compartment, contribute to I_{ionic} can be written as follows:

$$I_{ionic} = g_{Na} m^3 h (V - E_{Na}) + g_{K(DR)} n^4 (V - E_K) + g_L (V - E_L) \qquad (7)$$

The somatic compartment contains the traditional Hodgkin–Huxley (HH) sodium (I_{Na}) and delayed rectifier potassium ($I_{K(DR)}$) currents and a leak current (I_L). Conductance values for these currents were modified from Martina and Jonas (1997) and Martina et al. (1998) where they were measured in dentate gyrus basket cells. Collectively, these values in the multi-compartment model were hand-tuned to match electrophysiological properties measured in hippocampal basket cells (Morin et al. 1996; van Hooft et al. 2000) for the situation with passive dendrites.

For some simulations, the dendrites were considered passive (i.e., they only contained I_L), whereas other simulations included active dendrites (i.e., they contained I_{Na}, $I_{K(DR)}$, and I_L). Although basket cells are known to contain active dendrites (Maccaferri et al. 2004), the exact densities and distributions are not known. Therefore, when considering active dendrites, we used a percentage of the sodium and potassium maximal conductances at the same density throughout the dendritic tree while the leak current and other passive properties were kept the same. Parameter values are given in Appendix Table 2, and kinetic equations in Appendix Table 3.

In Fig. 1 from Saraga et al. (2006) we show a schematic of the basket cell multicompartment model (Fig. 1A) with its firing pattern when the dendrites are passive (Fig. 1B). Electrotonic profiles of the model cell both to and from the soma are shown in Fig. 1C, D respectively. Model details have been uploaded to ModelDB and can be accessed via http://senselab.med.yale.edu/ModelDb/ShowModel.asp?model=114047.

O-LM Cell Interneuron Model

Morphology

In a subset of O-LM cells in which electrophysiological recordings were obtained, slices were fixed in 4% paraformaldehyde (>24 h) in 0.1 M phosphate buffer. Slices were immersed in PBS and resectioned into 70 μm sections on a freezing microtome. Biocytin staining was revealed using an avidin-biotin-peroxidase reaction (ABC Standard Kit; Vector Laboratories, Burlingame, CA). Slices were mounted on gelatin-coated glass slides, dehydrated, and coverslipped with Permount. Two O-LM interneuron morphologies were reconstructed using 20× (air), 40× (oil-immersion), and 100× (oil-immersion) objectives on a Leica DMRB bright-field light microscope and Neurolucida software (MicroBrightField, Colchester, VT, USA), which records the visually determined diameters and three-dimensional coordinates of all neuronal processes. The three different magnifications were used in order to visualize how traced sections fit into one interneuron morphology (lowest magnification), to trace the dendrites (middle magnification), and to trace the small axonal diameters (highest magnification). Full somatic, dendritic, and axonal reconstructions were created for two cells. Vector coordinate files of the two O-LM cells were imported from Neurolucida to the program CVAPP (see above) to test for connectivity between compartments. The reconstructions were then imported

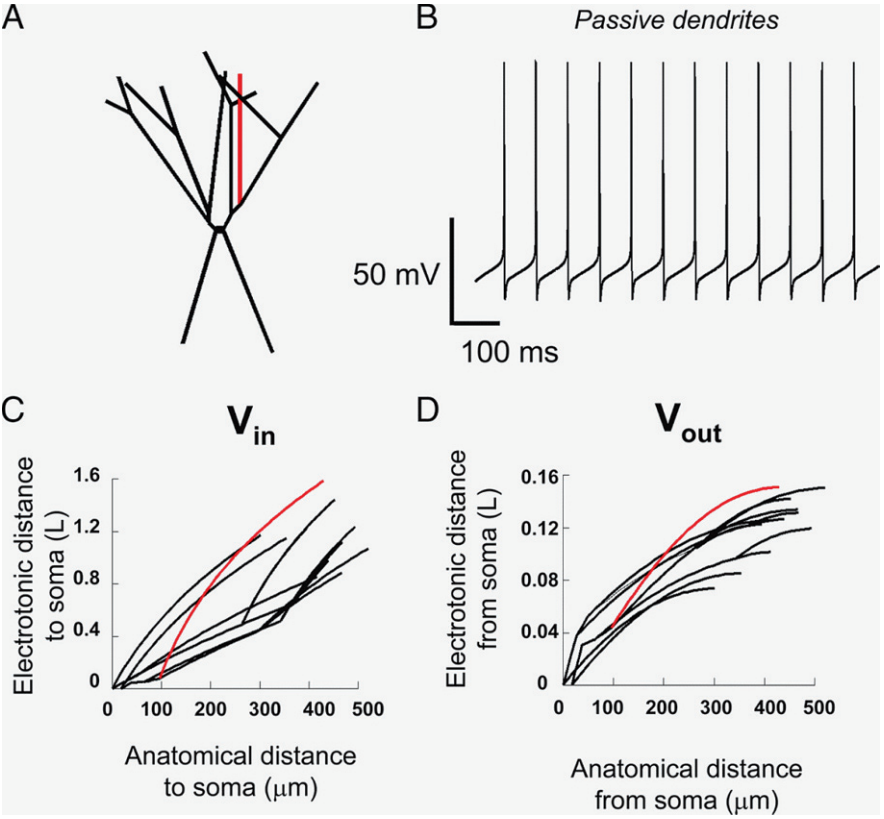

Fig. 1 Multi-compartment model of a hippocampal CA1 basket cell interneuron and properties. **A**: schematic of basket cell morphology taken from Gulyás et al. (1999). Computational model built using NEURON consists of 372 compartments. **B**: spontaneous firing of the model interneuron at 12.7 Hz when the dendrites are kept passive. **C** and **D**: plots of electrotonic distances to (V_{in}) and from (V_{out}) the soma for the basket cell with passive dendrites, where electrotonic distance is defined as the logarithm of voltage attenuation (Used with permission from Saraga et al. 2006, Fig. 1)

into NEURON. Although O-LM interneurons have a characteristic morphological orientation, with horizontal dendrites in stratum oriens and an axon that traverses vertically through the layers to arborize in stratum lacunosum-moleculare, variability in the extent of the dendritic field among O-LM interneurons was observed experimentally. Thus, similar simulations on two O-LM interneurons, one with a larger dendritic field, Cell 1, and one with a smaller dendritic field, Cell 2, were used to address the issue of morphological variability (Lawrence et al. 2006a).

Little is known about the passive properties, ion channel content, and distribution in axons of any neuron. Sodium channel kinetics and densities have been examined in axon initial segments of cortical neurons (Colbert and Pan 2002) and recently in mossy fiber end terminals or boutons (Engel and Jonas 2005; Kole

et al. 2008; Schmidt-Hieber et al. 2008), but little else is known about the remainder of the axonal arborization. In particular, nothing is known about the channel content or kinetics of axons for interneurons.

The axonal surface area made up a large fraction of the total surface area of the O-LM cells. The axonal morphology was reduced at the point in which it entered the lacunosum/moleculare region of the hippocampus which means that axon collaterals were removed leaving only the primary axon. Although this approximation would introduce some errors, the long and thin primary axon isolates the distal axonal arborization from the somatodendritic compartment electrotonically, minimizing any introduced error. Also, using the reduced primary axon helps limit the error produced by choosing arbitrary parameters for such a large surface area of membrane. Passive properties and ion channels for the reduced axon are described below.

The number of compartments determines the spatial resolution of the model. If the number of compartments is too low, simulation results will be inaccurate. If the number is too high, the simulation time may be extended unnecessarily. To check for optimal spatial resolution, the original number of compartments was multiplied by 3 (to keep the original node in place), and simulations were repeated with increasing compartments until the difference between the simulations was negligible. For the reduced axon reconstructed morphologies used here, the total number of compartments is 1,785 for Cell 1 and 1,154 for Cell 2.

Passive Properties

Two leak currents were incorporated into the models. The first is a standard leak current, I_{L}, which primarily represents a chloride current (Hodgkin and Huxley 1952; Maduke et al. 2000) and the second is a potassium leak channel, I_{KL}, which has the reversal potential set by potassium ions at -95 mV. There is growing evidence that many different neurons contain a potassium leak channel (Talley et al. 2003). Simulations of a membrane test were performed and values for passive properties including R_{a}, g_{L}, E_{L}, and g_{KL} were optimized uniformly throughout the somatic, dendritic, and axonal tree of the full (unreduced axonal arborization) morphology models using the run fitter module in NEURON. The membrane test is a voltage-clamp protocol in which the cell is held at -60 mV, dropped to -65 mV for 1 s, and then returned to -60 mV. The passive properties for each model interneuron were optimized to the average membrane test performed on that particular cell. The membrane capacitance, C_{m}, was fixed at 0.9 μF/cm^2 as measured in neuronal membranes (Gentet et al. 2000).

After the axonal morphology was reduced, as described above, the passive properties were re-optimized in the reduced axon segments while keeping the passive properties fixed to the previously determined values in the soma and dendrite sections. This provided a correction for reducing the surface area.

Input resistance was measured experimentally from each cell using the membrane test described above. Using Ohm's law, *voltage* $=$ *current* $\times$ *resistance* ($V = IR$), the steady-state current difference before and after the voltage step in the membrane test was used in combination with the known voltage difference to

calculate the input resistance of each cell. The experimentally measured values for input resistance were 349 MΩ for Cell 1 and 506 MΩ for Cell 2. With the optimized passive properties, as described above, the model neurons had an input resistance of 318 MΩ for Cell 1 and 524 MΩ for Cell 2.

The membrane time constant of a neuron is defined as the time at which the voltage has decayed to $1/e$ of its original value in response to a hyperpolarizing tonic current step. This was not measured experimentally for these particular cells since only voltage-clamp recordings were performed. Membrane time constants measured for O-LM interneurons range in value from 33 to 66 ms (Gloveli et al. 2005; *personal communication with Dr. J. Lawrence*). For the model interneurons, the membrane time constants were 49 ms for Cell 1 and 45 ms for Cell 2 which falls within the experimental range.

Active Properties

Only channels known to be found in this interneuron, as determined from the literature and experiment, were incorporated. The ionic currents include the traditional Hodgkin–Huxley sodium current, I_{Na}, two (fast and slow) delayed rectifier potassium currents, $I_{\mathrm{K\text{-}DRf}}$ and $I_{\mathrm{K\text{-}DRs}}$, the transient potassium current, I_{A}, the L-type calcium current, I_{CaL}, the T-type calcium current, I_{CaT}, the calcium-activated potassium current, I_{AHP}, the hyperpolarization-activated cation current, I_{h}, and the muscarinic potassium current, I_{M}. The sum of the intrinsic membrane terms that, in each compartment, contribute to I_{ionic} can be written as follows:

$$\begin{aligned} I_{\mathrm{ionic}} = & g_{\mathrm{Na}} m^3 h (V - E_{\mathrm{Na}}) + g_{\mathrm{K\text{-}DRf}} np (V - E_{\mathrm{K}}) + g_{\mathrm{K\text{-}DRs}} np (V - E_{\mathrm{K}}) \\ & + g_{\mathrm{KA}} ab (V - E_{\mathrm{K}}) + g_{\mathrm{h}} r (V - E_{\mathrm{h}}) + g_{\mathrm{M}} d (V - E_{\mathrm{K}}) \\ & + g_{\mathrm{CaL}} f^2 l ([\mathrm{Ca}^{2+}]_i) \Gamma (V, [\mathrm{Ca}^{2+}]_i, [\mathrm{Ca}^{2+}]_o) \\ & + g_{\mathrm{CaT}} u^2 w \Gamma (V, [\mathrm{Ca}^{2+}]_i, [\mathrm{Ca}^{2+}]_o) \\ & + g_{\mathrm{AHP}} s (v, [\mathrm{Ca}^{2+}]_i) (V - E_{\mathrm{K}}) + g_{\mathrm{KL}} (V - E_{\mathrm{K}}) + g_{\mathrm{L}} (V - E_{\mathrm{L}}) \end{aligned} \quad (8)$$

Conductance values, distributions, and reversal potentials are listed in Appendix Table 2. Equations governing the kinetics of the channels are provided in Appendix Table 4. The details of where the dynamics of each channel were obtained are provided below.

Sodium Current, I_{Na}

Using patch-clamp recordings in the soma and up to $\sim 100\,\mu\mathrm{m}$ from the soma along the dendrite, Martina et al. (2000) measured the kinetics and conductances of sodium and potassium channels in hippocampal oriens/alveus interneurons. They found that the dendrites of these interneurons contain a density of channels comparable to that measured in the soma. The dendritic sodium channel steady-state activation curve was found to be slightly more hyperpolarized than the somatic steady-state activation curve. The conductance values were taken from Martina

et al. (2000) and resulted in spontaneous action potentials without injected current. The kinetics for this channel were taken from our previously developed model (Saraga et al. 2003). The sodium current density and kinetics measured in the soma was used for the soma of our model interneuron, while the dendritically measured sodium current density and kinetics measured up to $\sim$100 μm from the soma was used uniformly throughout the model's dendritic tree (Martina et al. 2000).

Delayed Rectifier Potassium Currents, $I_{\text{K-DRf}}$, $I_{\text{K-DRs}}$

Kinetics for the fast, $I_{\text{K-DRf}}$, and slow, $I_{\text{K-DRs}}$, delayed rectifier potassium currents were obtained from Lien et al. (2002). Nucleated patch recordings, in voltage-clamp mode, were performed on oriens/alveus interneurons. Fast and slow delayed rectifier channels were shown to have different sensitivities to tetraethylammonium (TEA) and 4-aminopyridine (4-AP), which allowed for the separation of currents. The kinetics for the channels were incorporated into computational kinetic models freely available on the ModelDB web site (http://senselab.med.yale.edu/senselab/modeldb/).

Lien et al. (2002) did not measure channel conductance or density but they did measure the relative percentage each current contributed to the total outward current for a particular voltage-clamp protocol. The fast delayed rectifier, $I_{\text{K-DRf}}$, was found to be $57 \pm 5\%$ and the slow delayed rectifier, $I_{\text{K-DRs}}$, was found to be $25 \pm 6\%$ of the total outward current. The remainder of the outward current was attributed to the transient potassium current, I_{A}. These percentages were used to determine the relative conductance density of each channel in the models. Literature values for the fast delayed rectifier channel densities range from 6.6 pS/μm^2 in nucleated patches from layer 5 neocortical neurons (Korngreen and Sakmann 2000) to 27.7 ± 3 pS/μm^2 in nucleated patches from hippocampal oriens interneurons (Lien and Jonas 2003) to $\sim$320 pS/μm^2 in outside-out patches from oriens interneurons (Martina et al. 2000). This 50-fold range of densities stems from the many factors including cell type, recording type, experimental solutions, electrode resistances, and estimation of patch area. The lower density values in the 6–27 pS/μm^2 range are considered more realistic (*personal communication with Dr. P. Jonas*). These lower density values are also more consistent with the high input resistances measured in hippocampal interneurons, suggesting lower ion channel densities. These densities were distributed uniformly throughout the model's soma and dendritic tree.

Transient Potassium Current, I_{A}

Kinetics for the transient potassium channel, I_{A}, were also obtained from Lien et al. (2002). The kinetics for this channel were obtained by isolating the current using a subtraction protocol from control with a combination of TEA and 4-AP. The transient potassium channel was found to contribute to $19 \pm 2\%$ of the outward current, as measured from the peak of the outward current. This percentage allowed an estimation of the conductance density relative to the delayed rectifier channels. The density for I_{A} was kept constant in the soma and dendrites of the model interneuron.

Hyperpolarization-Activated Cation Current, I_h

The nonspecific cation channel current, I_h, was taken from the previously developed model (Saraga et al. 2003). The conductance value, g_h, was adjusted in order to obtain a "sag" voltage trace, upon hyperpolarization of the model interneuron, consistent with experimental recordings. The steady-state activation curve for this channel was taken from voltage-clamp data performed on oriens interneurons by Maccaferri and McBain (1996). The voltage-dependent activation time constant was modified from one described for CA1 pyramidal neurons by Warman et al. (1994) in order to match voltage-clamp data from oriens interneurons by Maccaferri and McBain (1996).

Although it is known that in hippocampal pyramidal neurons, I_h is distributed in both the soma and dendrites (Magee 1998), the somatodendritic distribution of I_h is not known for interneurons. We therefore compared both somatic only and somatic-dendritic distributions of I_h in our model neurons. The density of h-channels was adjusted in the two cases so as to produce the same "sag" when a hyperpolarizing step current of 100 pA was applied to the soma (soma only, 5.00×10^{-5} S/cm^2; somatodendritic, 1.56×10^{-6} S/cm^2). Neither the spontaneous frequency (2.6 vs. 2.3 Hz) nor the response of the cell to 100 pA of tonic depolarizing current injected into the soma (9.4 vs. 9.2 Hz) differed substantially between soma only and somatodendritic conditions, respectively. Because results were very similar for both distributions of I_h, all subsequent simulations were performed with only somatic I_h.

Calcium Currents, I_{CaL}, I_{CaT}

Calcium channels have not been extensively studied in any interneuron subtype although there is some evidence that oriens interneurons contain both T-type and L-type calcium channels (*personal communication with Dr. L. Topolnik*). Zhang and McBain (1995a) also showed that with application of TTX, a sodium channel blocker, a prominent calcium spike could be elicited with a sustained depolarizing current from a hyperpolarized resting voltage.

Previously developed kinetic models from Migliore et al. (1995) were used to represent the T-type and L-type calcium channels, where they were constructed for a CA3 pyramidal cell model. The driving force equation, $\Gamma(V, [Ca^{2+}]_i, [Ca^{2+}]_o)$, is of the Goldman–Hodgkin–Katz form and depends on voltage, V, intracellular calcium, $[Ca^{2+}]_i$, and extracellular calcium, $[Ca^{2+}]_o$, for both I_{CaL} and I_{CaT}:

$$\Gamma(V, [Ca^{2+}]_i, [Ca^{2+}]_o) = \\ -161.3\left(1 - \frac{[Ca^{2+}]_i}{[Ca^{2+}]_o}\exp\left(\frac{V}{12.7}\right)\right)\left(\frac{12.7}{\exp\left(\frac{V}{12.7}\right) - 1}\right) \quad (9)$$

where $[Ca^{2+}]_i = 5 \times 10^{-5}$ mM and $[Ca^{2+}]_o = 2$ mM.

Simulations were performed with the conductance values of the sodium channels in the soma, dendrites, and axon set to zero to mimic the effect of TTX.

A hyperpolarizing current was injected into the soma of each cell to hold the membrane voltage at a resting voltage of −80 mV. A depolarizing step current of 100 pA was then injected into the soma for 500 ms in order to elicit a calcium spike. The maximal conductances of the T-type and L-type calcium channels were adjusted in order to qualitatively match the shape, amplitude, and delay of the calcium spike from Zhang and McBain (1995a).

Since the T-type calcium channel is a low-threshold activated channel, adjustments in the conductance of this channel determined whether a calcium spike was initiated. Changes in the L-type channel conductance had no effect on the initiation of the calcium spike, but did have an effect on the spike repolarization plateau. The T-type and L-type calcium channel conductances were set to 50 and 10,000 pS/μm^2, respectively, in the dendrites, which best matched experimentally recorded calcium spikes from oriens interneurons (Zhang and McBain 1995a).

Since calcium channels have not as yet been characterized in terms of kinetics and densities in hippocampal interneurons, we kept the kinetics constant from previous models (see above) and explored a range of somatic-dendritic distributions and densities. Including calcium channels in the soma of our model interneuron dominated the waveform of the action potential and resulted in a hyperexcitable cell. We therefore chose to include the calcium channel, I_{CaL} and I_{CaT}, as well as the potassium activated calcium channel described below, $I_{\mathrm{K(Ca)}}$, only in the dendrites in order to match the calcium spikes described above as well as the current-frequency relationship measured experimentally (Lawrence et al. 2006a).

Calcium Dynamics

Calcium dynamics were defined by a simple first-order kinetics equation taken from Destexhe et al. (1998). Calcium current across the membrane in each compartment is assumed to elevate intracellular calcium, $[\mathrm{Ca}^{2+}]_i$, in a thin cylindrical shell. Calcium concentration is used as a signal for gating the calcium-dependent potassium channel, I_{AHP}. $[\mathrm{Ca}^{2+}]_i$ decays exponentially with a fixed time constant. In each compartment,

$$\frac{\mathrm{d}\left[\mathrm{Ca}^{2+}\right]_i}{\mathrm{d}t} = -BI_{\mathrm{Ca}} + \frac{\left[\mathrm{Ca}^{2+}\right]_\infty - \left[\mathrm{Ca}^{2+}\right]_i}{\tau} \tag{10}$$

where τ is set to 200 ms, I_{Ca} includes both I_{CaL} and I_{CaT} and $[\mathrm{Ca}^{2+}]_\infty$ is the steady-state calcium concentration which is set to 1×10^{-4} mM. $B = -10,000/2 \times F \times d$ is time independent but depends on the radial depth from the membrane, $d = 0.1\,\mu$m, which defines the shell of calcium ions in each compartment and Faraday's constant, $F = 96,480$ coulombs.

Calcium-Activated Potassium Current, I_{AHP}

Although there is evidence for an apamin-sensitive calcium-activated potassium channel in oriens interneurons (Zhang and McBain 1995b), kinetics and conductance

values for this channel are not available. Therefore, a calcium-activated potassium channel kinetic model was taken from the Migliore et al. (1995) CA3 pyramidal cell model. The conductance for this channel was adjusted along with the calcium currents in order to generate the calcium spike described above.

Muscarinic Potassium Current, I_M

A kinetic model for the M-current was built using voltage-clamp experiments from O-LM interneurons. The steady-state activation curve for the M-current was obtained by performing a whole-cell pre-pulse voltage-clamp protocol in control and with the application of linopirdine, an I_M blocker. The resulting curve was fit to a Boltzmann equation of the form given in Eq. (6). The voltage-dependent M-current time constant was obtained by adjusting the time constant form given in Eq. (5) to match voltage-clamp experimental data. In particular, the slow relaxation time constant of deactivation from -30 to -50 mV data was matched in the model.

Four different I_M distributions were explored in Lawrence et al. (2006a). These were soma only, soma and all dendrites, soma and primary dendrites, and axon only in both Cell 1 and Cell 2. Primary dendrites are defined as the dendrites of branch order one, namely the length of dendrite from the soma before it branches. To compensate for the lack of space clamp in extended structures, $V_{1/2}$ and k values were adjusted so that the steady-state activation curve obtained from simulations would match the experimentally measured curves (see Saraga 2006 for further details).

The pre-pulse voltage-clamp protocol was performed using the model cells with the kinetic models for I_M developed above. To determine the conductance density, the experimentally determined measurement that I_M was ~20% of the total outward current, as measured at the soma, was used as a constraint for all four distributions of I_M. This resulted in a range of I_M densities of 0.12–0.75 pS/μm^2 for the soma and all dendrites case, to 280–1,200 pS/μm^2 for the axon only case (see Table 1 in Lawrence et al. 2006a). An independent estimate of the I_M density was obtained using experimental measurements of the capacitance transient, which can be used to determine the approximate surface area that is sampled by the somatic recording electrode. In stepping from -60 to -65 mV under whole-cell voltage-clamp conditions, the capacitance transient was generated in the same cells that were modeled (Cell 1, 38.0 pF; Cell 2, 32.4 pF). Assuming a specific membrane capacitance of 0.9 μF/cm^2 and E_K of -95 mV, the density required to generate 20% of the outward current (~1 nA) for Cell 1 is obtained as follows:

$$\text{surface area} = 38.0\,\text{pF}/0.009\,\text{pF}/\mu\text{m}^2 = 4,222\,\mu\text{m}^2 \tag{11}$$

$$\text{conductance} = 1\,\text{nA}/121.2\,\text{mV} = 8.25\,\text{nS} \tag{12}$$

$$\text{density} = 8.25\,\text{nS}/4,222\,\mu\text{m}^2 = 1.95\,\text{pS}/\mu\text{m}^2 \tag{13}$$

A similar calculation for Cell 2 yields a density of 2.29 pS/μm^2. These density values lie between those predicted for I_M distributed somatodendritically and I_M distributed in the soma and primary dendrites only (Lawrence et al. 2006a), thus predicting I_M's distribution profile. This calculated distribution also corresponds

with the immunocytochemical localization of Kv7.2 and 7.3 subunits to the soma and dendrites found experimentally (Lawrence et al. 2006a).

In Fig. 2 from Lawrence et al. (2006a) we show multi-compartment models of O-LM Cell 1with red regions containing I_M, with insets showing I_M for a family of voltage steps. Model details have been uploaded to ModelDB and can be accessed via: http://senselab.med.yale.edu/modeldb/ShowModel.asp?model=102288.

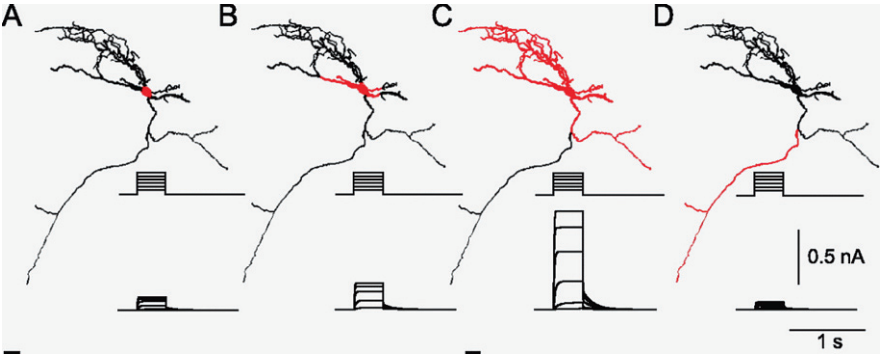

Fig. 2 Somatodendritic localization of Kv7 channels best reproduced I_M-mediated outward currents. **A–D**, In a multi-compartment O-LM interneuron model, I_M was localized to soma only (**A**), soma and primary dendrites (**B**), soma and all dendrites (**C**), or axon only (**D**). Compartmental regions lacking (*black*) and containing (*red*) I_M are indicated. *Insets*, I_M-mediated outward currents generated by a family of 400 ms somatic voltage step commands from −60 to +35 mV in −15 mV increments. A fixed g_M of 0.75 pS/μm^2 was used in all simulations (Used with permission from Lawrence et al. 2006a, Fig. 8 **A–D**)

The Future

We have focused on models of two interneuron types – perisomatic inhibitory fast-spiking basket cells and dendritic inhibitory O-LM cells. The model morphology and passive properties were specific for the particular interneuron type. However, while the O-LM model incorporated voltage-clamp data for many of the different ion channel types specific for O-LM cells, the basket cell model did not. Instead, an exploration of the density of sodium and potassium channels in the dendrites relative to the soma was done to examine their influence on electrical coupling at dendritic sites. Various intrinsic properties that account for estimated spike attenuation characteristics have now been incorporated and how they affect synchronous output in electrically coupled networks has been examined (Zahid and Skinner 2009). Voltage-clamp data of ion channels in basket cells are needed along with their incorporation into multi-compartment models. Detailed basket cell models are currently under development (*personal communication: Anja Noerenberg, Marlene Bartos, Imre Vida, and Peter Jonas*).

Calcium channels are important contributors to a neuron's spiking properties and its ability to express synaptic plasticity. While these channels have been extensively

studied in hippocampal pyramidal neurons, much less is known about specific calcium channels in different interneuron subtypes. Although the existence of calcium currents in interneurons is known (Parra et al. 1998; Zhang and McBain 1995a), specific kinetics, distributions, and densities are not. Calcium imaging studies have shown the importance and specificity of dendritic calcium processing in different interneuron types (Goldberg et al. 2003, 2004; Rozsa et al. 2004). A detailed study of calcium currents in basket and O-LM cell types would benefit the models and allow further understanding of the functional role of these interneurons in hippocampal networks.

Distribution of Ion Channels

To understand the functional contribution of the single cell, the distribution and density of different ion channels are of critical importance as they shape and dictate the action potential and synaptic potential generation and propagation. This is where multi-compartment models are most helpful in understanding single cell contributions. Firing frequencies, the ability to evoke a spike, and spike timing relative to synaptic input at particular locations will all affect the temporal contributions that are known to be specific to different interneuron subtypes (Klausberger et al. 2003).

In our original O-LM model (Saraga et al. 2003) we investigated seven possible dendritic channel combinations and found two cases that were able to produce appropriate electrophysiological responses. With these cases we showed that back-propagating spikes occurred with distal synaptic input. This suggests that O-LM cells can regulate the amount of input coming from the entorhinal cortex via the direct path, which dominates during theta/gamma rhythms (Buzsáki 2002). That LTP can be induced in these cells (Perez et al. 2001; Pelletier and Lacaille 2008) suggests critical functional roles for O-LM cells and in which back-propagating spikes may be important contributors. We also found that either forward-propagating or back-propagating spikes could occur for less distal synaptic inputs depending on synaptic strength. Although O-LM cells derive most of their input from CA1 pyramidal collaterals (i.e., being feedback inhibitors), CA3 input is also likely to be present (Li et al. 1994). Thus, depending on the relative CA1 and CA3 synaptic input locations and strengths on O-LM dendrites, forward-propagating or back-propagating spikes could result. It has been previously suggested that O-LM cells provide a switch mechanism for dominance of either direct (EC input) or indirect (via DG-CA3) afferent pathways to the CA1 area (Blasco-Ibáñez and Freund 1995; Maccaferri and McBain 1995). Therefore, stronger synapses and forward-propagating spikes in O-LM cells would enhance their inhibitory effect on CA1 pyramidal cells and so decrease the incoming effect from the direct EC pathway that dominates during theta/gamma rhythms. Back-propagating spikes and LTP in O-LM cells would enhance subsequent activation of O-LM cells. In this way, these forward-propagating and back-propagating spikes affect hippocampal functioning by controlling the dominance of direct or indirect pathways.

In light of the above, an experimental investigation of spike propagation using dual somatic and dendritic recordings would be interesting to explore. The location and strength of input needed for forward-propagating and/or back-propagating spikes to occur along with information on the synaptic input locations from CA1 and CA3 neurons would be desirable. Such information could support the importance of forward-propagating and/or back-propagating spikes, as determined by the distribution of ion currents in the dendrites, in the switching mechanism. An exploration of spike propagation in the more detailed models described in this chapter should also be done to obtain more specific predictions of location and strengths of synaptic inputs for forward-propagating and back-propagating spikes.

It has been found that O-LM cell axons can emerge from somatic or dendritic compartments (Lawrence et al. 2006a; Martina et al. 2000). In our original 2003 O-LM model (Saraga et al. 2003) we made predictions of axonal sodium and potassium channel densities based on current clamp recordings measuring propagation speed performed on axon-bearing and axon-lacking dendrites in these interneurons (Martina et al. 2000). A narrow range of possible densities was needed to match experimental recordings. However, the axon used in the earlier model was not directly obtained from experimental data and was structurally limited. The more detailed 2006 O-LM models (Lawrence et al. 2006a) have extensive axonal structures and the spike ordering on axon-bearing and axon-lacking dendrites and propagation speeds observed in Martina et al. (2000) should be fully explored in them. It would be useful to have more dendritic recordings in O-LM cells to constrain axonal parameters for which no information is currently available.

With multiple dendritic recordings one could measure propagation speeds at less distal sites and use them to estimate more distal channel densities by adjusting those parameter values in the model to match measured speeds. Given that it is very difficult to obtain distal recordings, obtaining less distal dendritic recordings to use with the multi-compartment model to predict distal channel densities would be helpful.

The O-LM multi-compartment model was used to help determine the somatodendritic location of M-channels (Lawrence et al. 2006a). However, with the availability of voltage-clamp recording of M-channels in the dendrites one could take advantage of theoretical and algorithmic approaches (Cox 2008; Schaefer et al. 2003) to more accurately predict the kinetics and conductances of these channels in the non-space clamped structure.

Reductions and Robustness

An important reason to construct detailed multi-compartment models is to allow reduced models to be developed. These reduced models could then be linked to the biology (via the detailed model) as could insights obtained from mathematical analyses of the reduced models. In this way, the contribution of single cell dynamics with its repertoire of intrinsic properties could be appreciated when the reduced models are incorporated into network architectures. Reductions have been done for

pyramidal cell models of electric fish (Laing 2004) and Traub's CA3 pyramidal cell model (Pinsky and Rinzel 1994). A phenomenological reduction of our 2003 O-LM model to a single compartment was done and used to investigate gamma/theta rhythms in microcircuits (Gloveli et al. 2005; Tort et al. 2007) since the characteristics of the O-LM cell played a critical role in the proposed circuit mechanism. We created a reduced three-compartment model of the basket cell model described herein to allow us to apply weakly coupled oscillator theory and predict network dynamics of the coupled system (Saraga et al. 2006).

In addition to incorporating voltage-clamp data as it become available, the robustness of models could be formally explored. In particular, the sensitivity of the model output could be explored using recently developed tools that allow one to assess the firing sensitivity to active dendritic parameters (Weaver and Wearne 2008).

The Need for Computational Models of Interneurons

Although this chapter has focused on models of two types of interneurons, it is clear that more interneuron types exist with potentially specialized roles (see chapter "Morphology of Hippocampal Neurons" and Somogyi and Klausberger 2005 review). For example, bistratified cells, which mainly innervate the small dendritic shafts of pyramidal cells, show a stronger gamma activity modulation (relative to basket and O-LM cells), thus suggesting a role for dendritic processing in gamma rhythms (Tukker et al. 2007). More recently, a single compartment model of a hippocampal interneuron that is located on the border between the lacunosum-moleculare and radiatum hippocampal layers has been developed using voltage-clamp data (Morin et al. 2007; Haufler 2008). This interneuron type likely contributes to theta rhythms because it expresses subthreshold oscillations at theta frequency in the absence of synaptic input (Chapman and Lacaille 1999).

With ever increasing experimental data and insight it may not be too early to consider building models of different types of basket cells such as parvalbumin-containing and cholechokinin-containing basket cells which have different firing properties and proposed functional roles (Baude et al. 2007; Freund and Katona 2007). There are also different subtypes of oriens interneurons (Maccaferri 2005) with a morphologically similar class of oriens interneurons which have horizontally oriented dendrites and an axonal arborization which extends vertically through the hippocampal layers and projects to the septum (Gulyás et al. 2003; Tóth and Freund 1992). These different classes of oriens interneurons may have different ion channels, kinetics, and densities. Preliminary model explorations along these lines might be worth considering.

In conclusion, the necessity for specificity in considering different types of interneurons is clear and the functional relevance of the different types has been shown by their distinct firing properties during different brain rhythms. Computational models which incorporate these differences are needed to address and understand how interneurons contribute to hippocampal functioning.

Appendix

Table 1 Passive properties of interneuron models

Reference	Number of compartments in model	Input resistance R_{in}(MΩ)	Axial resistivity R_a(Ωcm)	Membrane time constant τ_m (ms)	Membrane capacitance C_m(μF/cm^2)
Saraga et al. (2006) Saraga and Skinner (2004)	372	245	200	30	0.8
Lawrence et al. (2006a)	Cell 1:1,785	318	300	49	0.9
	Cell 2:1,184	524	300	45	0.9

Table 2 Active properties of interneuron models

Reference	Currents	Maximal conductance densities in soma (mS/cm^2)	Maximal conductance densities in dendrites (mS/cm^2)	Maximal conductance densities in axon (mS/cm^2)	Reversal potentials (mV)
Saraga et al. (2006)	I_{Na}	184	0 − 184[a]		$E_{Na} = 55$
	I_K	140	0 − 140[a]	–	$E_K = -90$
Saraga and Skinner (2004)	I_L	0.025	0.025		$E_L = -60$
	Cell 1:				
	I_{Na}	10.7	11.7	11.7,	$E_{Na} = 50$
	$I_{K\text{-}DRf}$	0.6	0.6	0.6	$E_K = -95$
	$I_{K\text{-}DRs}$	0.23	0.23	0.23	$E_h = -32.9$
	I_A	0.25	0.25	0	$E_L = -66.2$
	I_h	0.05	0	0	
	I_{CaL}	0	1000	0	
	I_{CaT}	0	5	0	
	I_{AHP}	0	0.01	0	
Lawrence et al. (2006a)	I_M	0.075–0.64[a]	0.075–0.3[a]	0–120[a]	
	$I_{K,L}$	0.032	0.032	0.018	
	I_L	0.011	0.011	0.062	
	Cell 2:				
	I_{Na}	10.7	11.7	11.7,	$E_{Na} = 50$
	$I_{K\text{-}DRf}$	0.6	0.6	0.6	$E_K = -95$
	$I_{K\text{-}DRs}$	0.23	0.23	0.23	$E_h = -32.9$
	I_A	0.25	0.25	0	$E_L = -59.4$
	I_h	0.05	0	0	
	I_{CaL}	0	1,000	0	
	I_{CaT}	0	5	0	
	I_{AHP}	0	0.01	0	
	I_M	0.012–0.57[a]	0.012–0.26[a]	0–28[a]	
	$I_{K,L}$	0.032	0.032	0.011	
	I_L	0.013	0.013	0.043	

[a]Indicates that a range of current densities were explored

Table 3 Forward and backward rate functions for Saraga et al. (2006) basket cell model

Conductance type	Forward rate function (α)	Backward rate function (β)
g_{Na} activation (m)	$\frac{-0.1(V+35)}{\exp(-(V+35)/10)-1}$	$4\exp(-(V+60)/18)$
g_{Na} inactivation (h)	$0.07\exp(-(V+58)/20)$	$\frac{1}{\exp(-(V+28)/10)+1}$
$g_{K(DR)}$ activation (n)	$\frac{-0.01(V+34)}{\exp(-(V+34)/10)-1}$	$0.125\exp(-(V+44)/80)$

Table 4 Forward and backward rate functions for Lawrence et al. (2006a) O-LM cell model

Conductance type	Forward rate function (α)	Backward rate function (β)
$g_{Na,soma}$ activation (m)	$\frac{-0.1(V+38)}{\exp(-(V+38)/10)-1}$	$4\exp(-(V+65)/18)$
$g_{Na,dend}$ activation (m)	$\frac{-0.1(V+45)}{\exp(-(V+45)/10)-1}$	$4\exp(-(V+70)/18)$
g_{Na} inactivation (h)	$0.07\exp(-(V+63)/20)$	$\frac{1}{1+\exp[-(V+33)/10]}$
g_{CaL} activation (f)	$\frac{15.69(-(V-81.5))}{\exp(-(V-81.5)/10)-1}$	$0.29\exp(-V/10.86)$
g_{CaT} activation (u)	$\frac{0.2(-(V-19.26))}{\exp(-(V-19.26)/10)-1}$	$0.009\exp(-V/22.03)$
g_{CaT} inactivation (w)	$1\times10^{-6}\exp(-V/16.26)$	$\frac{1}{\exp(-(V-29.79)/10)+1}$
$g_{K(Ca)}$ activation (s)	$\frac{0.28\,\text{mM}[Ca^{2+}]_i}{[Ca^{2+}]_i+4.8\times10^{-4}\exp(-65.64)}$	$\frac{0.48\,\text{mM}}{1+[Ca^{2+}]_i/1.36\times10^{-7}\exp(-78.14V)}$
Conductance type	Steady-state activation/inactivation	Time constant (ms)
g_M activation (d)	$\frac{1}{1+\exp(-(V+27)/7)}$	$\frac{1}{0.003/\exp(-(V+63)/15)+0.003/\exp((V+63)/15)}$
$g_{K\text{-}DRf}$ activation (n)	$\frac{1}{1+\exp(-(V+36.2)/16.1)}$	$\frac{27.8\exp((V+33)/14.1)}{1+\exp((V+33)/10)}$
$g_{K\text{-}DRf}$ inactivation (p)	$\frac{0.92}{1+\exp((V+40.6)/7.8)}+0.08$	1,000
$g_{K\text{-}DRs}$ activation (n)	$\frac{1}{1+\exp(-(V+41.9)/23.1)}$	$\frac{66.7\exp((V+25)/13.3)}{1+\exp((V+25)/6.7)}$
$g_{K\text{-}DRs}$ inactivation (p)	$\frac{0.93}{1+\exp((V+52.2)/15.2)}+0.07$	1,000
g_{KA} activation (a)	$\frac{1}{1+\exp(-(V+41.4)/26.6)}$	0.5
g_{KA} inactivation (b)	$\frac{1}{1+\exp((V+78.5)/6)}$	$0.17(V+105)$
g_h activation (r)	$\frac{1}{1+\exp((V+84)/10.2)}$	$\frac{1}{\exp(-17.9-0.116V)+\exp(-1.84+0.09V)}+100$
g_{CaL} inactivation (l)	$\frac{0.001\,\text{mM}}{0.001\,\text{mM}+[Ca^{2+}]_i}$	

Further Reading

Bartos M, Vida I, Frotscher M, Geiger JR, and Jonas P. Rapid signaling at inhibitory synapses in a dentate gyrus interneuron network. *J Neurosci* 21: 2687–2698, 2001.

Baude A, Bleasdale C, Dalezios Y, Somogyi P, and Klausberger T. Immunoreactivity for the GABAA receptor alpha1 subunit, somatostatin and Connexin36 distinguishes axoaxonic, basket, and bistratified interneurons of the rat hippocampus. *Cereb Cortex* 17: 2094–2107, 2007.

Blasco-Ibáñez JM and Freund TF. Synaptic input of horizontal interneurons in stratum oriens of the hippocampal CA1 subfield: structural basis of feed-back activation. *Eur J Neurosci* 7: 2170–2180, 1995.

Buhl EH, Halasy K, and Somogyi P. Diverse sources of hippocampal unitary inhibitory postsynaptic potentials and the number of synaptic release sites. *Nature* 368: 823–828, 1994.

Buzsáki G. *Rhythms of the Brain*. New York: Oxford University Press, 2006.

Buzsáki G. Theta oscillations in the hippocampus. *Neuron* 33: 325–340, 2002.

Buzsáki G and Chrobak JJ. Temporal structure in spatially organized neuronal ensembles: a role for interneuronal networks. *Curr Opin Neurobiol* 5: 504–510, 1995.

Chapman CA and Lacaille JC. Intrinsic theta-frequency membrane potential oscillations in hippocampal CA1 interneurons of stratum lacunosum-moleculare. *J Neurophysiol* 81: 1296–1307, 1999.

Chitwood RA, Hubbard A, and Jaffe DB. Passive electrotonic properties of rat hippocampal CA3 interneurones. *J Physiol* 515 (Pt 3): 743–756, 1999.

Colbert CM and Pan E. Ion channel properties underlying axonal action potential initiation in pyramidal neurons. *Nat Neurosci* 5: 533–538, 2002.

Cox SJ. Direct correction of non-space-clamped currents via Cole's theorem. *J Neurosci Methods* 169: 366–373, 2008.

De Schutter E. *Computational Neuroscience: Realistic Modeling for Experimentalists*. FL: CRC Press, 2001.

Destexhe A, Neubig M, Ulrich D, and Huguenard J. Dendritic low-threshold calcium currents in thalamic relay cells. *J Neurosci* 18: 3574–3588, 1998.

Emri Z, Antal K, Gulyás AI, Megias M, and Freund TF. Electrotonic profile and passive propagation of synaptic potentials in three subpopulations of hippocampal CA1 interneurons. *Neuroscience* 104: 1013–1026, 2001.

Engel D and Jonas P. Presynaptic action potential amplification by voltage-gated Na+ channels in hippocampal mossy fiber boutons. *Neuron* 45: 405–417, 2005.

Freund TF. Interneuron diversity series: rhythm and mood in perisomatic inhibition. *Trends Neurosci* 26: 489–495, 2003.

Freund TF and Katona I. Perisomatic inhibition. *Neuron* 56: 33–42, 2007.

Fukuda T and Kosaka T. Gap junctions linking the dendritic network of GABAergic interneurons in the hippocampus. *J Neurosci* 20: 1519–1528, 2000.

Geiger JR, Lubke J, Roth A, Frotscher M, and Jonas P. Submillisecond AMPA receptor-mediated signaling at a principal neuron-interneuron synapse. *Neuron* 18: 1009–1023, 1997.

Gentet LJ, Stuart GJ, and Clements JD. Direct measurement of specific membrane capacitance in neurons. *Biophys J* 79: 314–320, 2000.

Glickfeld LL and Scanziani M. Distinct timing in the activity of cannabinoid-sensitive and cannabinoid-insensitive basket cells. *Nat Neurosci* 9: 807–815, 2006.

Gloveli T, Dugladze T, Rotstein HG, Traub RD, Monyer H, Heinemann U, Whittington MA, and Kopell NJ. Orthogonal arrangement of rhythm-generating microcircuits in the hippocampus. *Proc Natl Acad Sci U S A* 102: 13295–13300, 2005.

Goldberg JH, Yuste R, and Tamas G. Ca2+ imaging of mouse neocortical interneurone dendrites: contribution of Ca2+-permeable AMPA and NMDA receptors to subthreshold Ca2+dynamics. *J Physiol* 551: 67–78, 2003.

Goldberg JH, Lacefield CO, and Yuste R. Global dendritic calcium spikes in mouse layer 5 low threshold spiking interneurones: implications for control of pyramidal cell bursting. *J Physiol* 558: 465–478, 2004.

Gulyás AI, Miles R, Sik A, Toth K, Tamamaki N, and Freund TF. Hippocampal pyramidal cells excite inhibitory neurons through a single release site. *Nature* 366: 683–687, 1993.

Gulyás AI, Hajos N, Katona I, and Freund TF. Interneurons are the local targets of hippocampal inhibitory cells which project to the medial septum. *Eur J Neurosci* 17: 1861–1872, 2003.

Gulyás AI, Megias M, Emri Z, and Freund TF. Total number and ratio of excitatory and inhibitory synapses converging onto single interneurons of different types in the CA1 area of the rat hippocampus. *J Neurosci* 19: 10082–10097, 1999.

Han ZS, Buhl EH, Lorinczi Z, and Somogyi P. A high degree of spatial selectivity in the axonal and dendritic domains of physiologically identified local-circuit neurons in the dentate gyrus of the rat hippocampus. *Eur J Neurosci* 5: 395–410, 1993.

Haufler D. Characterizing the potassium current contribution to sub-threshold membrane potential fluctuations. *MSc Thesis*, University of Toronto 2008.

Hines ML and Carnevale NT. The NEURON simulation environment. *Neural Comput* 9: 1179–1209, 1997.

Hodgkin AL and Huxley AF. A quantitative description of membrane current and its application to conduction and excitation in nerve. *J Physiol* 117: 500–544, 1952.

Izhikevich EM. *Dynamical Systems in Neuroscience: The Geometry of Excitability and Bursting.* Cambridge, MA: MIT Press, 2007.

Klausberger T, Magill PJ, Marton LF, Roberts JD, Cobden PM, Buzsáki G, and Somogyi P. Brain-state- and cell-type-specific firing of hippocampal interneurons in vivo. *Nature* 421: 844–848, 2003.

Kole MH, Ilschner SU, Kampa BM, Williams SR, Ruben PC, and Stuart GJ. Action potential generation requires a high sodium channel density in the axon initial segment. *Nat Neurosci* 11: 178–186, 2008.

Korngreen A and Sakmann B. Voltage-gated K+ channels in layer 5 neocortical pyramidal neurones from young rats: subtypes and gradients. *J Physiol* 525 Pt 3: 621–639, 2000.

Lacaille JC and Williams S. Membrane properties of interneurons in stratum oriens-alveus of the CA1 region of rat hippocampus in vitro. *Neuroscience* 36: 349–359, 1990.

Laing C. Ghostbursting in sensory cells of electric fish. *Nonlinear Studies* 11: 469–480, 2004.

Lawrence JJ, Saraga F, Churchill JF, Statland JM, Travis KE, Skinner FK, and McBain CJ. Somatodendritic Kv7/KCNQ/M channels control interspike interval in hippocampal interneurons. *J Neurosci* 26: 12325–12338, 2006a.

Lawrence JJ, Statland JM, Grinspan ZM, and McBain CJ. Cell type-specific dependence of muscarinic signalling in mouse hippocampal stratum oriens interneurones. *J Physiol* 570: 595–610, 2006b.

Li XG, Somogyi P, Ylinen A, and Buzsáki G. The hippocampal CA3 network: an in vivo intracellular labeling study. *J Comp Neurol* 339: 181–208, 1994.

Lien CC and Jonas P. Kv3 potassium conductance is necessary and kinetically optimized for high-frequency action potential generation in hippocampal interneurons. *J Neurosci* 23: 2058–2068, 2003.

Lien CC, Martina M, Schultz JH, Ehmke H, and Jonas P. Gating, modulation and subunit composition of voltage-gated K(+) channels in dendritic inhibitory interneurones of rat hippocampus. *J Physiol* 538: 405–419, 2002.

Maccaferri G. Stratum oriens horizontal interneurone diversity and hippocampal network dynamics. *J Physiol* 562: 73–80, 2005.

Maccaferri G, Bartos M, Lawrence JJ, LeBeau FEN, Martina M, and Tóth K. Interneuron diversity and hippocampal network dynamics. Program No. 246. *Society for Neuroscience Abstract*, 2004.

Maccaferri G and McBain CJ. The hyperpolarization-activated current (Ih) and its contribution to pacemaker activity in rat CA1 hippocampal stratum oriens-alveus interneurones. *J Physiol* 497 (Pt 1): 119–130, 1996.

Maccaferri G and McBain CJ. Passive propagation of LTD to stratum oriens-alveus inhibitory neurons modulates the temporoammonic input to the hippocampal CA1 region. *Neuron* 15: 137–145, 1995.

Maduke M, Miller C, and Mindell JA. A decade of CLC chloride channels: structure, mechanism, and many unsettled questions. *Annu Rev Biophys Biomol Struct* 29: 411–438, 2000.

Magee JC. Dendritic hyperpolarization-activated currents modify the integrative properties of hippocampal CA1 pyramidal neurons. *J Neurosci* 18: 7613–7624, 1998.

Major G. Solutions for transients in arbitrarily branching cables: III. Voltage clamp problems. *Biophys J* 65: 469–491, 1993.

Mann EO and Paulsen O. Role of GABAergic inhibition in hippocampal network oscillations. *Trends Neurosci* 30: 343–349, 2007.

Martina M and Jonas P. Functional differences in Na+ channel gating between fast-spiking interneurones and principal neurones of rat hippocampus. *J Physiol* 505 (Pt 3): 593–603, 1997.

Martina M, Schultz JH, Ehmke H, Monyer H, and Jonas P. Functional and molecular differences between voltage-gated K+ channels of fast-spiking interneurons and pyramidal neurons of rat hippocampus. *J Neurosci* 18: 8111–8125, 1998.

Martina M, Vida I, and Jonas P. Distal initiation and active propagation of action potentials in interneuron dendrites. *Science* 287: 295–300, 2000.

Maurer AP, Cowen SL, Burke SN, Barnes CA, and McNaughton BL. Phase precession in hippocampal interneurons showing strong functional coupling to individual pyramidal cells. *J Neurosci* 26: 13485–13492, 2006.

McBain CJ and Fisahn A. Interneurons unbound. *Nat Rev Neurosci* 2: 11–23, 2001.

McCormick DA, Connors BW, Lighthall JW, and Prince DA. Comparative electrophysiology of pyramidal and sparsely spiny stellate neurons of the neocortex. *J Neurophysiol* 54: 782–806, 1985.

Migliore M, Cook EP, Jaffe DB, Turner DA, and Johnston D. Computer simulations of morphologically reconstructed CA3 hippocampal neurons. *J Neurophysiol* 73: 1157–1168, 1995.

Morin F, Beaulieu C, and Lacaille JC. Membrane properties and synaptic currents evoked in CA1 interneuron subtypes in rat hippocampal slices. *J Neurophysiol* 76: 1–16, 1996.

Morin F, Haufler D, Skinner FK, and Lacaille J-C. Cell-type specific expression of voltage-gated K+ currents underlies intrinsic membrane potential oscillations in hippocampal CA1 interneurons. Program No. 587.6. *Society for Neuroscience*, 2007.

Parra P, Gulyás AI, and Miles R. How many subtypes of inhibitory cells in the hippocampus? *Neuron* 20: 983–993, 1998.

Pelletier JG and Lacaille JC. Long-term synaptic plasticity in hippocampal feedback inhibitory networks. *Prog Brain Res* 169: 241–250, 2008.

Perez Y, Morin F, and Lacaille JC. A hebbian form of long-term potentiation dependent on mGluR1a in hippocampal inhibitory interneurons. *Proc Natl Acad Sci U S A* 98: 9401–9406, 2001.

Pinsky PF and Rinzel J. Intrinsic and network rhythmogenesis in a reduced Traub model for CA3 neurons. *J Comput Neurosci* 1: 39–60, 1994.

Rozsa B, Zelles T, Vizi ES, and Lendvai B. Distance-dependent scaling of calcium transients evoked by backpropagating spikes and synaptic activity in dendrites of hippocampal interneurons. *J Neurosci* 24: 661–670, 2004.

Saraga F. Use of compartmental models to predict physiological properties of hippocampal inhibitory neurons. *PhD Thesis*, University of Toronto 2006.

Saraga F, Ng L, and Skinner FK. Distal gap junctions and active dendrites can tune network dynamics. *J Neurophysiol* 95: 1669–1682, 2006.

Saraga F and Skinner FK. Dynamics and diversity in interneurons: a model exploration with slowly inactivating potassium currents. *Neuroscience* 113: 193–203, 2002.

Saraga F and Skinner FK. Location, location, location (and density) of gap junctions in multicompartment models. *Neurocomputing* 58–60: 713–719, 2004.

Saraga F, Wu CP, Zhang L, and Skinner FK. Active dendrites and spike propagation in multicompartment models of oriens-lacunosum/moleculare hippocampal interneurons. *J Physiol* 552: 673–689, 2003.

Schaefer AT, Helmstaedter M, Sakmann B, and Korngreen A. Correction of conductance measurements in non-space-clamped structures: 1. Voltage-gated K+ channels. *Biophys J* 84: 3508–3528, 2003.

Schmidt-Hieber C, Jonas P, and Bischofberger J. Action potential initiation and propagation in hippocampal mossy fibre axons. *J Physiol* 586: 1849–1857, 2008.

Segev I, Burke RE, and Hines ML. Compartmental models of complex neurons. In: *Methods in Neuronal Modeling: From Ions to Networks* (2nd ed.), edited by Koch C and Segev I, Cambridge: MIT Press, 1998, pp. 93–136.

Skinner FK. Conductance-based models. *Scholarpedia* 1(11): 1408, 2006.

Skinner FK, Zhang L, Velazquez JL, and Carlen PL. Bursting in inhibitory interneuronal networks: a role for gap-junctional coupling. *J Neurophysiol* 81: 1274–1283, 1999.

Somogyi P and Klausberger T. Defined types of cortical interneurone structure space and spike timing in the hippocampus. *J Physiol* 562: 9–26, 2005.

Spruston N, Jaffe DB, and Johnston D. Dendritic attenuation of synaptic potentials and currents: the role of passive membrane properties. *Trends Neurosci* 17: 161–166, 1994.

Talley EM, Sirois JE, Lei Q, and Bayliss DA. Two-pore-Domain (KCNK) potassium channels: dynamic roles in neuronal function. *Neuroscientist* 9: 46–56, 2003.

Thurbon D, Field A, and Redman S. Electrotonic profiles of interneurons in stratum pyramidale of the CA1 region of rat hippocampus. *J Neurophysiol* 71: 1948–1958, 1994.

Tort AB, Rotstein HG, Dugladze T, Gloveli T, and Kopell NJ. On the formation of gamma-coherent cell assemblies by oriens lacunosum-moleculare interneurons in the hippocampus. *Proc Natl Acad Sci U S A* 104: 13490–13495, 2007.

Tóth K and Freund TF. Calbindin D28k-containing nonpyramidal cells in the rat hippocampus: their immunoreactivity for GABA and projection to the medial septum. *Neuroscience* 49: 793–805, 1992.

Traub RD and Miles R. Pyramidal cell-to-inhibitory cell spike transduction explicable by active dendritic conductances in inhibitory cell. *J Comput Neurosci* 2: 291–298, 1995.

Tukker JJ, Fuentealba P, Hartwich K, Somogyi P, and Klausberger T. Cell type-specific tuning of hippocampal interneuron firing during gamma oscillations in vivo. *J Neurosci* 27: 8184–8189, 2007.

van Hooft JA, Giuffrida R, Blatow M, and Monyer H. Differential expression of group I metabotropic glutamate receptors in functionally distinct hippocampal interneurons. *J Neurosci* 20: 3544–3551, 2000.

Wang XJ and Buzsáki G. Gamma oscillation by synaptic inhibition in a hippocampal interneuronal network model. *J Neurosci* 16: 6402–6413, 1996.

Warman EN, Durand DM, and Yuen GL. Reconstruction of hippocampal CA1 pyramidal cell electrophysiology by computer simulation. *J Neurophysiol* 71: 2033–2045, 1994.

Weaver CM and Wearne SL. Neuronal firing sensitivity to morphologic and active membrane parameters. *PLoS Comput Biol* 4: e11, 2008.

Wilent WB and Nitz DA. Discrete place fields of hippocampal formation interneurons. *J Neurophysiol* 97: 4152–4161, 2007.

Zahid T and Skinner FK. Predicting synchronous and asynchronous network groupings of hippocampal interneurons coupled with dendritic gap junctions. *Brain Res* 1262:115–129, 2009.

Zhang L and McBain CJ. Potassium conductances underlying repolarization and after-hyperpolarization in rat CA1 hippocampal interneurones. *J Physiol* 488 (Pt 3): 661–672, 1995a.

Zhang L and McBain CJ. Voltage-gated potassium currents in stratum oriens-alveus inhibitory neurones of the rat CA1 hippocampus. *J Physiol* 488 (Pt 3): 647–660, 1995b.

Gamma and Theta Rhythms in Biophysical Models of Hippocampal Circuits

N. Kopell, C. Börgers, D. Pervouchine, P. Malerba, and A. Tort

Introduction

The neural circuits of the hippocampus are extremely complex, with many classes of interneurons whose contributions to network dynamics and function are still unknown. Nevertheless, reduced models can provide insight into aspects of the dynamics and associated function. In this chapter, we discuss models at a variety of levels of complexity, all simple enough to probe the reasons for the behavior of the model. The chapter focuses on the main rhythms displayed by the hippocampus, the gamma (30–90 Hz) and theta (4–12 Hz) rhythms. We concentrate on modeling in vitro experiments, but with an eye toward possible in vivo implications.

Models of gamma and theta rhythms range from very detailed, biophysically realistic descriptions to abstract caricatures. At the most detailed levels, the cells are described by Hodgkin–Huxley-type equations, with many different cell types and large numbers of ionic currents and compartments (Traub et al., 2004). We use simpler biophysical models; all cells have a single compartment only, and the interneurons are restricted to two types: fast-spiking (FS) basket cells and oriens lacunosum-moleculare (O-LM) cells. Unlike Traub et al. (2004), we aim not so much at reproducing dynamics in great detail, but at clarifying the essential mechanisms underlying the production of the rhythms and their interactions (Kopell, 2005). In particular, we wish to highlight the dynamical as well as physiological mechanisms associated with rhythms, and to begin to classify them by mechanisms, not just frequencies.

One theme in this chapter is the interaction of gamma and theta rhythms. To understand this interaction, it is necessary to describe the mechanisms of the gamma and theta rhythms separately before putting them together. A second theme is the use of mathematical tools to get a deeper understanding of the dynamics of rhythmic networks. We apply these ideas mainly to the question of how networks can produce

N. Kopell (✉)
Department of Mathematics and Center for BioDynamics, Boston University, Boston, MA 02215, USA
e-mail: nk@math.bu.edu

V. Cutsuridis et al. (eds.), *Hippocampal Microcircuits*, Springer Series in Computational Neuroscience 5, DOI 10.1007/978-1-4419-0996-1_15,

a theta rhythm from cells that do not naturally synchronize. A final theme is the use of model networks to understand how dynamics contributes to function.

To maintain coherence, we use the same models for our interneurons and pyramidal cells in all sections of the chapter. Similarly, we use the same models for synapses in each section. These models are closely related, but not identical, to other models previously published (Acker et al., 2003; Pervouchine et al., 2006; Gloveli et al., 2005b; Börgers et al., 2005; Börgers and Kopell, 2003, 2005, 2008). Different versions of the same rhythms are produced by the same general model, but with different parameter sets. All the equations and parameters employed throughout this chapter are given in the appendices. Several different codes were used to generate the simulation results in this chapter; all codes, with manuals for their use, are included on the disk.

Gamma Rhythms, in Various Guises

The circumstances under which the gamma rhythm is observed both in vivo and in vitro are described in chapter "Neuronal Activity Patterns During Hippocampal Network Oscillation In Vitro" (see also Whittington et al., 2000). As we will discuss below, we believe that the gamma rhythm is important for the creation, modulation, and protection of cell assemblies. How that happens depends on the mechanisms associated with the formation of this rhythm, and so we focus below on these mechanisms.

The name "gamma rhythm" has been used to denote rhythms in a very large range of frequencies, from 20 Hz to over 100 Hz. We use here a more limited definition: we define the gamma rhythm to be neural dynamics in which the population of basket cells (and/or other FS interneurons) fires rhythmically on a time scale dependent on the decay time of inhibitory postsynaptic potentials (Whittington et al., 2000). In practice, that restricts the gamma range to approximately 30–90 Hz. The high-frequency rhythms seen in neocortex (Canolty et al., 2006) and hippocampus and striatum (Tort et al., 2008) are not considered gamma in this mechanistically based nomenclature.

The gamma rhythm is found in many structures of the brain, including the cerebral cortex and the entorhinal cortex (EC). Though there are some differences between gamma rhythms in different parts of the brain (Cunningham et al., 2004), the models we discuss do not make use of specific properties of hippocampal neurons. The gamma rhythm is treated in the models discussed below as an interaction of pyramidal cells and FS cells (or sometimes just as an interaction among FS cells). We treat both the FS cells and the pyramidal cells as single compartments with minimal currents: the spiking Na^+ and K^+ currents, leak, and the synaptic $GABA_A$ and AMPA currents. The gamma rhythms discussed here are believed to be formed near the somata of the pyramidal cells (Buhl et al., 1995), justifying a one-compartment model of those cells.

An essential feature of the gamma models discussed here is that the decay time of the $GABA_A$ current is the longest time scale in the system; in particular, it is longer

than the membrane time "constant" of either of the cell types involved. The latter hypothesis seems counter-factual at first: the membrane time constant is often taken to be about 10 ms or more (see Whittington et al., 1996), while the unitary IPSC decay time constant has been measured in some contexts to be less than 2 ms (Bartos et al., 2001, 2002). The central point is that the above measurements were not taken in the context of ongoing gamma oscillations, in which the decay time has been measured to be about 8–12 ms. It is not known if the unitary IPSCs are longer in the context of an oscillating network. It may also be that other interneurons play a role in the gamma oscillations, and that they have longer IPSCs. Finally, when the network is producing a gamma rhythm, the basket cell interneurons are highly correlated, but may not be exactly synchronous, and hence produce population IPSCs that take longer to decay. Since there are far fewer cells in the model networks than in real brain networks, each model synapse represents a large number of real synapses. For these reasons, we have chosen to use parameters derived directly from the gamma oscillations rather than the technically more accurate measurements (Bartos et al., 2001, 2002) from situations that are less relevant to the data we model.

The issue of the membrane time is more subtle. This "constant" actually changes dynamically, along with the currents expressed at any moment: the larger the sum of the intrinsic and synaptic currents, the smaller the instantaneous membrane time. With an inhibitory decay time in the above range, and the maximal inhibitory conductance an order of magnitude larger than the resting conductance (Whittington et al., 1996), the effective membrane time is small for at least half the gamma cycle. With instantaneous membrane times short enough for a long enough period, voltages "equilibrate" to the instantaneous inhibitory current, rendering the neurons' history irrelevant for their future behavior. This was spelled out in Börgers and Kopell (2005) for a reduced model, and we find the same behavior in our physiological models. The lack of history dependence turns out to be central for some of the functional implications of the gamma rhythms (e.g. see section "PING and Cell Assemblies). The exact choice of the membrane time is not critical, provided it is not too long relative to the inhibitory decay time. In the work by Bartos et al. on models of gamma oscillations in networks of GABAergic interneurons, the inhibitory time constant is very short, but the maximal inhibitory conductance is chosen to be two orders of magnitude larger than the resting conductance; this is quite different from our parameter regime and may lead to different conclusions.

Real pyramidal cells have a multitude of other currents (Traub et al., 2005). However, we hypothesize that the other currents are not important for some kinds of gamma rhythms (see PING below); for other kinds, they modulate the properties, but are not critical for the existence of the rhythms. Some of the other currents, such as the hyperpolarization-activated h-current, are inactive at the high voltage ranges associated with gamma. During spiking, others may be swamped by the size of the spiking currents. The high frequency of the gamma rhythm may not allow currents with slow kinetics to change much during the interspike interval. Thus, though the kinetics of pyramidal cells can be very complex, especially in the dendritic integration, the aspects that are important to the gamma rhythm can be captured in models as simple as integrate-and-fire.

The rhythms that occur in the gamma frequency range are not all the same mechanistically, either in vivo or in vitro. In vitro, rhythms in the 30–50 Hz range can be produced in the hippocampus in at least three qualitatively different ways: Interneuronal network gamma (ING), pyramidal-interneuronal network gamma (PING), and persistent gamma (see chapter "Neuronal Activity Patterns During Hippocampal Network Oscillation In Vitro" for details). These are distinguished less by their different frequencies than by the sets of neurons that are involved. In ING, the effects of the AMPA synapses are blocked, so that only inhibitory cells are involved, and these fire at or near the population frequency. In PING, both excitatory and inhibitory cells are involved, with both classes of cells firing at or near the population frequency. In vitro PING is a short-lived phenomenon induced by tetanic stimulation. Persistent gamma, produced pharmacologically, lasts for hours; in this version of the gamma rhythm, FS cells fire at close to population frequency, while the pyramidal cells fire at much lower rates (see chapter "Neuronal Activity Patterns During Hippocampal Network Oscillation In Vitro"). In all three of these forms of gamma, the population frequency depends on the decay time of $GABA_A$-receptor mediated synapses. Since the ING rhythm plays no role in our discussion of the interaction of gamma and theta rhythms, we will not say much more about it; see Kopell and Ermentrout (2004) for references. The code for simulating gamma rhythms that we include with this chapter is capable of producing all three kinds of gamma. We give the parameter values associated with PING and persistent gamma in Appendix 2.

PING

The PING rhythm has been modeled in a variety of ways, from the very detailed (Traub et al., 1997) to the very simple (Ermentrout and Kopell, 1998). In discussing model pyramidal and FS cells, we will use the abbreviations E- and I-cells (for excitatory and inhibitory). A cycle of the PING rhythm begins with a surge in spiking of the E-cells, which triggers a surge in spiking of the I-cells. The resulting pulse of inhibitory input to the E-cells brings them closer to synchrony. When inhibition wears off, the E-cells resume spiking, and the cycle repeats. The period of the rhythm depends primarily on the decay time constant of the $GABA_A$ synapses, less on the strengths of those synapses and the excitability of the E-cells (Börgers and Kopell, 2005, Eq. (3.15)). A key step in the analysis of the PING mechanism is to explain why and when a common inhibitory input pulse has a synchronizing effect on a population of neurons. The effect of the inhibition is to create, transiently, a stable fixed point. All trajectories move toward this fixed point, thereby getting close to each other. The synchronization can be interpreted as the effect of an attracting river (Diener, 1985a,b) in a phase space that includes the decaying strength of inhibition as a dependent variable (Börgers and Kopell, 2005).

Assuming E-cells of type I (Ermentrout, 1996), the PING mechanism works if the following conditions hold (Börgers and Kopell, 2003):

(1) The E-cells receive external input that would drive them, in the absence of any synaptic input, at or above gamma frequency.

(2) The E→I synapses are so strong and have so short a rise time that a surge in spiking of the E-cells quickly triggers a surge in spiking of the I-cells.
(3) The I-cells spike only in response to the E-cells.
(4) The I→E synapses are strong enough that a population spike of the I-cells approximately synchronizes the E-cells.

The analysis of the PING mechanism becomes more complicated if there is noise and/or heterogeneity in the network. It has been shown (Golomb and Hansel, 2000; Börgers and Kopell, 2003) that the formation of a coherent gamma rhythm depends on the number of connections to a given E- or I-cell from the opposite population, independent of the size of the network; thus, the connections can be arbitrarily sparse. The analysis of Börgers and Kopell (2003) shows that the I-cells are typically synchronized more tightly than the E-cells. Further analysis also shows that, while ING is vulnerable to heterogeneity (Wang and Buzsáki, 1996; White et al., 1998a), PING is more robust. (ING becomes robust if gap junctions are added to the network; see Kopell and Ermentrout, 2004 and Traub et al., 2001). However, PING can be destroyed by too much noise, especially when the excitability of the E- and I-cells is low, and so the frequency of the network is also low. For frequencies above of about 90 Hz, the rhythm is often quite sensitive to heterogeneity. Hence the PING mechanism operates best in the 30–90 Hz regime (Börgers and Kopell, 2005).

The analysis of PING rhythms enables one to understand how modulation of the network, which changes network parameters, can lead to loss of rhythmicity. In particular, the PING mechanism breaks down when the drive to the I-cells becomes too large relative to the drive to the E-cells. In a simple 2-cell network, the I-cell fires without being prompted by the E-cell, leading to "phase walk-through." In larger networks of E- and I-cells, the rhythmicity is typically lost in a different manner: the I-cells become incoherent, which reduces, or even suppresses, the firing of the E-cells (Börgers and Kopell, 2005). For examples of parameter values for which this happens, see the paragraph on Fig. 1a in Appendix 2.

PING and Cell Assemblies

It has often been suggested that gamma rhythms are associated with the formation of "cell assemblies" (Singer and Gray, 1995). A cell assembly is a group of cells that are temporarily synchronous. Although synchrony can promote synaptic plasticity (Hebb, 1949), we will not assume that the cells are connected to one another. The suggestion is that temporary synchrony tags the neurons belonging to the assembly as working together and potentiates their down-stream effects.

When this hypothesis was first proposed, the gamma rhythm was thought to be relevant to binding partly because this frequency band had notably stronger power in situations in which such binding was seen to be important, such as early sensory processing (Gray, 1999). However, it was not clear what it was about this frequency band that should associate it with the creation of cell assemblies. A deeper understanding of the PING rhythm enables us to see why gamma and cell assemblies might indeed be related. The most relevant work is Olufsen et al. (2003). That paper considered an E/I network producing PING as described above, with the E-cells

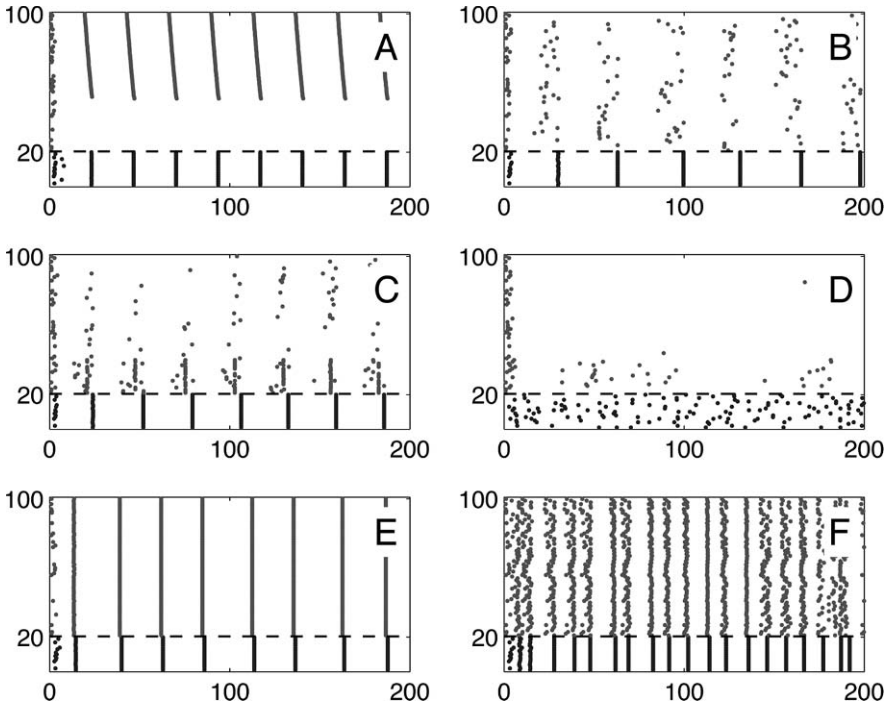

Fig. 1 Spike rastergrams of model E/I networks. Cells 1–20 (below the *dashed line*) are the I-cells, and cells 21–100 (above the *dashed line*) are the E-cells. (**a**) PING with heterogeneous input to the E-cells; strongly driven E-cells participate on every cycle, while weakly driven ones are suppressed altogether. (**b**) Weak PING driven by stochastic input to the E-cells. (**c**) Strong PING rhythm on a weak PING background. (**d**) Asynchronous activity of the I-cells at the same frequency as in panel **C** suppresses the E-cells. (**e**) E/I network entrained by sharp input pulses at gamma frequency; a strong but less coherent distractor was present as well, but its influence is not visible. (**f**) Without I→E synapses, the less coherent distractor prevents entrainment. All parameter values are given in Appendix 2

given a range of applied current, producing a range of natural frequencies for the individual cells. During PING, the E-cells with the highest drive fire with phases very close to one another, while the other E-cells are suppressed for the duration of the input. Thus, the cells that fire form a cell assembly; see also Fig. 1a of this chapter.

The dynamical reason for this behavior is found in the timing of the E- and (here, homogeneous) I-cells: when enough of the E-cells fire to cause the I-cells to fire, the resulting inhibition suppresses the rest of the E-cells. The fraction of cells firing depends on the kinetics and strength of the synapses and also on how the input is distributed across the E-cells. This fraction can be modulated by non-oscillatory inhibition, perhaps for instance from CCK-expressing cells (Tukker et al., 2007). The key point is that the same E-cells that fire on one gamma cycle fire again on the next, as long as the input to the cells remains the same. For this to happen, it

is critical that the decay time of inhibition is the longest time scale in the system. When this is true, by the time inhibition has worn off in a given gamma cycle, there is no cellular memory of which cells have spiked; thus, the same cells spike on each cycle, forming the cell assembly. If other currents with longer time scales (e.g., the M-current) are added, the cell assembly no longer forms. Instead, all the E-cells participate, at different times and at different frequencies (Olufsen et al., 2003).

Persistent Gamma

There is another kind of gamma in which the E-cells fire much less frequently than the population. This rhythm, known as "persistent gamma" or "weak gamma," is formed in hippocampal slices by the addition of kainate and/or carbachol; for details, see chapter "Neuronal Activity Patterns During Hippocampal Network Oscillation In Vitro". It is intrinsically more complex than ING and PING, since the firing of the E-cells seems stochastic. Indeed, the most detailed models of persistent gamma (Traub et al., 2000) require the existence of axo-axonal gap junctions among the pyramidal cells (Hamzei-Sichani et al., 2007). The axo-axonal connections give rise to very high-frequency ($>$ 100 Hz) oscillations (VFOs) (Traub et al., 2000; Lewis and Rinzel, 2000, 2001; Munro, 2008), which are modulated by gamma frequency rhythms induced by the chemical synapses.

It might seem that the behavior of the resulting model cannot be captured by a less complicated model without the axonal plexus. However, it was shown by Börgers et al. (2005) that the noisy and low-frequency participation of the E-cells can be captured in a network of one-compartment E- and I-cells, without any axo-axonal interactions. This was done by replacing the noisy input to the E-cells generated within the axonal plexus by externally imposed noisy drive. We consider the gamma rhythm produced by this reduced network to have the same mechanism for the creation of the dynamics of the E/I interaction, but leaving out the details of how the network creates the necessary noise; see Fig. 1b for a rastergram of persistent gamma. We refer to this kind of rhythm as a "weak PING rhythm." For clarity, we sometimes also call the standard, deterministically driven PING "strong PING."

Local excitatory drive can generate a local PING rhythm on a background of persistent gamma (Börgers et al., 2005). The resulting acceleration of the inhibitory population leads to a reduction in activity of the non-assembly cells; see Fig. 1c. In order to form the cell assembly, it can in fact be critical that there be a background gamma: if this gamma is removed, for instance, by adding too much noise, weakening the I$\rightarrow$E synapses too much, or giving extra drive to the I-cells, the same input to a subset of E-cells may not produce a cell assembly (Fig. 1d).

Gamma Rhythm and Protection Against "Distractors"

Synchrony does not require oscillations; a single common inhibitory input pulse, for instance, can produce it (Börgers and Kopell, 2003). However, the gamma rhythm is well-adapted biophysically to support the construction and use of cell assemblies

for several reasons. One such reason was discussed in Börgers and Kopell (2008) in the context of attention; although the assemblies were thought of as neocortical, similar issues pertain to the hippocampus, where cell assemblies have been recorded and analyzed (Harris et al., 2003). In Börgers and Kopell (2008), we considered a simple target network of one E- and one I-cell. The cells were coupled synaptically as in PING, but the target network did not fire in the absence of external input. The network received two rhythmic input trains at gamma frequency, a tightly coherent ("spiky") one and a less coherent (more "sinusoidal") one, both affecting the E- and the I-cell. The less coherent input train was faster or slower than the more coherent one, so that its effects on the target network could be distinguished, but both input frequencies were always in the gamma range.

Simulations showed, not surprisingly, that a single input entrained the target network. The more surprising result is that, in the presence of both input trains, the target network responded to the more coherent one, ignoring the less coherent one almost entirely, even when both input trains had the same temporal averages. The presence of the more coherent input made the less coherent input essentially invisible; see Börgers and Kopell (2008), and also Fig. 1e.

Further simulations and analysis showed that this effect depends on local inhibition within the target network; see Fig. 1f, in which the local inhibitory coupling has been removed, and the effect has disappeared. Inhibition greatly raises the leakiness of the target neurons; the more coherent input pulses can break through in spite of this leakiness, whereas the less coherent ones cannot (Börgers and Kopell, 2008). Once the coherent pulses entrain the target network, there is also a timing effect stabilizing the entrainment: the coherent pulses arrive at times when inhibition is weak, whereas the less coherent ones usually arrive at times when inhibition is stronger. The mechanism can work only at or above gamma frequency. At frequencies below the gamma range, there are substantial windows of low inhibition during which even the less coherent input can substantially affect the target network.

The Many Forms of Gamma, In Vitro and In Vivo

The relationship between in vitro and in vivo gamma rhythms is still not understood, though they are thought to be similar (Senior et al., 2008). Our current hypothesis is that the PING rhythm is associated with the formation of cell assemblies during active processing, and that the persistent rhythm is analogous to a background gamma rhythm associated with vigilance. Differences in frequencies may not point to differences between in vitro and in vivo mechanisms, since there is more background input in the in vivo structures. However, within in vitro varieties (as in CA3 or in CA1) the different frequencies may turn out to be salient. There are also differences in the gamma rhythms seen in vivo in a variety of structures. Recent work from the Graybiel lab (Tort et al., 2008) shows that different bands of gamma (30–60 Hz and 60–90 Hz) in the hippocampus are modulated differently by the theta rhythm, suggesting that they are mechanistically different. Work in the olfactory system (Kay, 2003) also suggests multiple gammas, a lower frequency one

associated with background attention, and a higher frequency one associated with active processing.

The distinctions between PING and persistent gamma do not adequately account for additional subtle differences seen even in vitro. For example, there are structure-dependent differences in gamma frequency, with CA3 in vitro persistent gamma slower than that of CA1 (Middleton et al., 2008). In the EC, there are two distinct gammas formed in vitro, associated with different kinds of interneurons; the slower one (in the 30 Hz range) is formed from an interaction of pyramidal cell with a class of interneurons named "goblet cells" (Middleton et al., 2008). It also remains to understand how other currents, not necessary for the existence of gamma rhythms, can nonetheless modulate them if they are present in high enough amounts. An example is the M-currents in the E-cells, which can affect the rate of firing of gamma or even make it disappear (Börgers et al., 2005; Olufsen et al., 2003). These subtleties may have important in vivo implications (Middleton et al., 2008).

Theta Rhythms

Unlike the gamma rhythm, which is governed (at least in its simplest forms) primarily by the decay time of inhibition, the theta rhythm seems to depend on the kinetics of intrinsic currents that determine the theta frequency or give rise to resonance at that frequency. Cells with intrinsic currents that may play a role in setting the theta frequency include the stellate cells of the EC and the O-LM cells in the hippocampus. For more information on the physiology and pharmacology of these and related cells, please see chapters "Neuronal Activity Patterns During Hippocampal Network Oscillation In Vitro" and "Single Neuron Models: Interneurons".

Models of the Theta Rhythm in a Single Cell

The first physiological models of the theta rhythm were developed to describe the behavior of stellate cells of the EC (White et al., 1998b; Dickson et al., 2000; Acker et al., 2003). In these models, the time scale of the theta oscillation in an individual stellate cell comes from the interaction of a persistent Na^+ current with either a slow K^+ current (such as an M-current) or an h-current.

One outcome of modeling of the EC theta oscillations has been the suggestion that a geometric structure in the trajectories known as a "canard structure" is responsible for the theta period in subthreshold oscillations (Rotstein et al., 2006). The canard structure is related to the so-called canard phenomenon in which low amplitude oscillations blow up into large ones as some parameter is changed (Rotstein et al., 2006), which can occur when there are multiple time scales. In the canard structure, some trajectories follow repelling (unstable) manifolds for a significant amount of time, and that geometry determines the period of the oscillations for trajectories that stay close to oscillations for one or more cycles. In such a case, even when the oscillation has small amplitude, linearization around a fixed point does not

yield the period. This structure appears to affect resonance to theta-frequency input (Rotstein et al., unpublished observations).

A more detailed, multi-compartment model of an O-LM cell was created by Saraga et al., using the interaction of an h-current with an A-current, but no persistent Na^+ current (Saraga et al., 2003). The same group has more recently (Lawrence et al., 2006) incorporated the M-current into the model (chapter "Single Neuron Models: Interneurons"), and is currently modeling the R-LM cell (Chapman and Lacaille, 1999), making prominent use of the A-current. The different combinations of inward and outward currents have been shown to lead to some subtle differences in cellular dynamics (Acker et al., 2003). However, it is still not well understood how different combinations of currents lead to a propensity to produce subthreshold theta oscillations (Rotstein et al., 2006; Dickson et al., 2000) or respond in a resonant manner to inputs that have a theta-rich frequency distribution (Haas and White, 2002).

For the figures in this section, we will focus on a single-compartment version of the Saraga et al. model, which includes an h-current with a single time scale, and an A-current. The equations and all relevant parameters are in Appendix 1. We will refer to these model cells as O-cells. To put this model in context, we also describe related models below.

Synchronization Properties of Stellate Cells and O-LM Cells

The fact that single cells produce a given frequency does not imply that coupling those cells by their natural neurotransmitters will lead to a coherent rhythm. Previous modeling work on stellate cells and dynamic clamp experiments on stellate and O-LM cells illustrate this. Model stellate cells, coupled by AMPA synapses, do synchronize (Acker et al., 2003; Netoff et al., 2005a). This is counter to the results found earlier that simpler models of cells (integrate and fire or voltage-gated conductance with only spiking currents and leak) tend to synchronize with mutual inhibition, and not synchronize with excitation (van Vreeswijk et al., 1994; Gerstner et al., 1996). However, the addition of slower currents can change the synchronization properties. This is particularly true of the h-current and the M-current, both of which oppose applied currents (h-currents are inward currents that turn on with hyperpolarization, and M-currents are outward currents that turn on with depolarization) (Crook et al., 1998; Acker et al., 2003; Ermentrout et al., 2001). In addition to models cited above, this idea was tested by Netoff et al. (2005a), using the dynamic clamp method (Dorval et al., 2001; Sharp et al., 1993) on hybrid networks consisting of one stellate cell or O-LM cell, and one in silico (stellate) model of such a cell. The dynamic clamp could produce either excitation or inhibition in the hybrid network, and the results were compatible with the earlier modeling results: both stellate cell pairs and O-LM cell pairs can synchronize with excitation, but not with inhibition. Since the O-LM cells are inhibitory, this implies that a network of O-LM cells alone cannot produce a coherent theta rhythm. The results also suggested that, in spite of some differences in intrinsic currents between O-LM and stellate cells,

their synchronization properties are similar. Simulation of pairs of (reduced Saraga model) O-cells show that they also do not synchronize with inhibition (Pervouchine, unpublished).

There are various mathematical tools that are used to relate biophysical properties of cells to whether or not a pair of such cells can synchronize with a particular kind of synapse. More generally, the methods help decide and explain how a pair of cells phase-locks via the synaptic connection, and with what phase relationship (Kopell and Ermentrout, 2002). One such technique, emphasized in some of the examples mentioned above, involves "spike-time response curves" (STRCs) or, equivalently, "phase response curves" (PRCs) (Acker et al., 2003; Oprisan et al., 2004; Gutkin et al., 2005). In that methodology, one measures, from an experiment or in a numerical simulation (Galán et al., 2005; Netoff et al., 2005b), how much an input to a periodic cell changes the time of the next spike as a function of the time of the input (Fig. 2a). This change can be measured in time units (in STRCs) or in phase units (in PRCs), where phase usually represents the time normalized to the unperturbed, free-running period of the cell.

From the STRC, one can compute a "spike-time difference map" (STDM). The latter takes the time Δ in a given cycle between the spikes of the two cells and gives the time $\overline{\Delta} = \Delta + F(\Delta)$ between those spikes in the next cycle (Fig. 2b). Fixed points of that map (or, equivalently, zeroes of F) correspond to phase locking, and the slope of the map at the fixed point determines if the locking is stable to perturbations: stable phase locking occurs if and only if the slope of F is between -2 and zero. A fixed point with zero spike-time difference corresponds to synchrony; there is often another fixed point that (in a case of identical cells with symmetric coupling) corresponds to antiphase. If a fixed point is stable, its domain of stability (i.e., the set of initial phase lags which will lead to that fixed point) is the interval on either side of the fixed point up to the next fixed point; the sign of $F(\Delta)$ indicates whether the time lag between spikes will increase ($F(\Delta) > 0$) or decrease ($F(\Delta) < 0$) on the next cycle. An analog of STDM, which operates with phase instead of time, is called "phase transition map" (PTM). Note that the properties of locking regimes can be easily seen from STDM or PTM graphs, while the direct dynamic simulations convey information of a different sort, one that is more detailed but not as straightforward for the stability analysis.

The STRC and STDM connect physiological properties of the cells and synapses to the dynamical properties of the network of these cells, thus allowing one to understand how changes in some currents or time scales affect the network. For weak coupling, this theory is equivalent to the standard weak coupling theory (see Kopell and Ermentrout, 2002). But the theory can work for significantly larger coupling as well, and produces different answers. However, there are significant restrictions on the use of such methods: the major one is that the effect of the input of each cell on the other is assumed to happen within the current cycle, so that there is no further memory from one cycle to another. This can be relaxed to two cycles (Oprisan et al., 2004) and can deal with multiple inputs to the target (Netoff et al., 2005a). Another is that, in the most straightforward applications, the method applies to only two cells; this contrasts with weak coupling methods, in which an arbitrary number of cells can

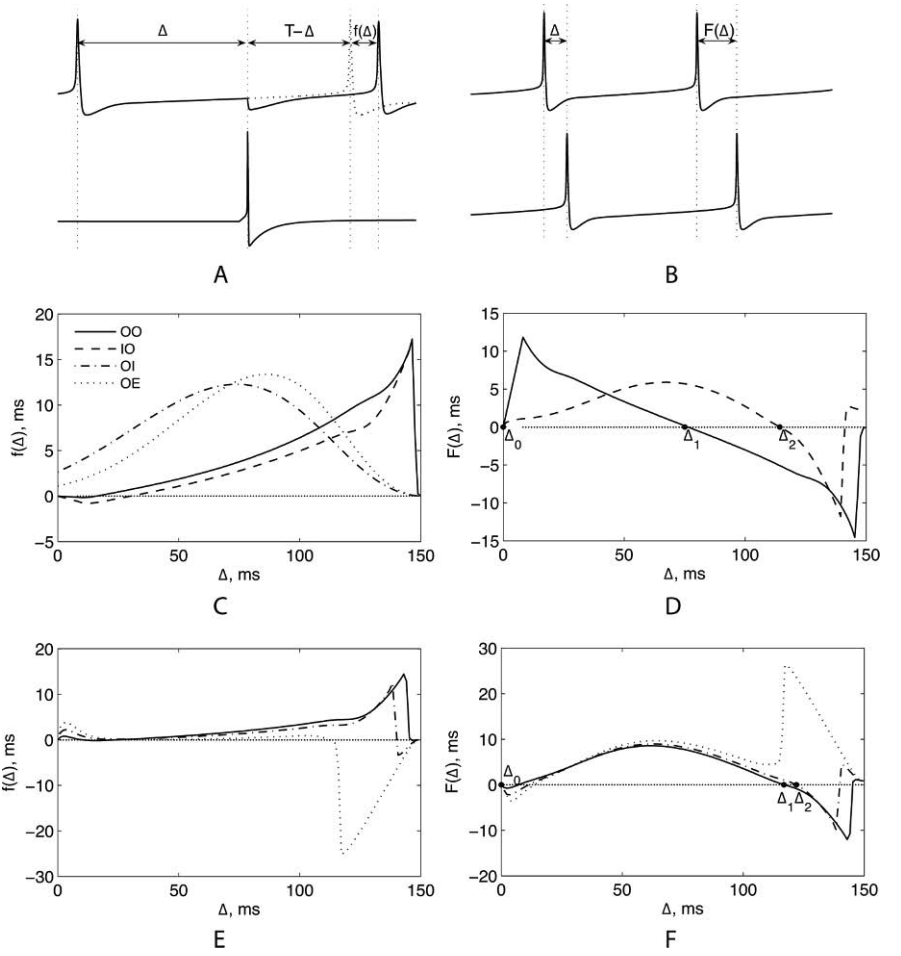

Fig. 2 (**a**) Construction of STRCs: Δ is the time of the perturbation; T is the unperturbed interspike interval; $f(\Delta)$ is the difference between the perturbed interspike interval and T. (**b**) Construction of STDMs: Δ and $F(\Delta)$ are time differences between spikes in two consecutive cycles. (**c**) STRCs for: an O-LM cell receiving input from another O-LM cell (*solid*); an O-LM cell receiving input from an I-cell (*dashed*); an I-cell receiving input from an O-LM cell (*dot-dashed*); an E-cell receiving input from an O-LM cell (*dotted*). Time units are normalized to the unperturbed period of 150 ms. (**d**) STDMs for: the network of mutually coupled O-LM cells (*solid*); the network of mutually coupled O-LM and I-cells (*dashed*). (**e**) STRCs for an O-LM cell receiving combined inhibitory and excitatory input from PING. The amount of inhibition is fixed, while excitation is used at three different levels: weak (*solid*), moderate (*dot-dashed*), and strong (*dotted*). (**f**) STDMs for the network of mutually coupled O-LM cell and E-I cell module (PING). *Line strokes* correspond to different levels of excitation, as in part **e**. All parameters for these simulations are given in Appendix 3

be combined in a network. The weak coupling hypothesis essentially assumes that all inputs to a cell are additive in their effects, an assumption that breaks down for non-linear coupling that is not infinitesimal. The method also assumes that the order of the cell spikes remains the same over different cycles.

Some of these constraints (notably, ones on time scales) are violated in our use of these methods. The 1-D reduction inherently involves a certain degree of inaccuracy since it neglects the dynamics of slow variables. While these effects are not noticeable for many simple Hodgkin–Huxley type of models, they can and do affect the Saraga O-LM cell model, which contains slow currents such as h-current or A-current. Nevertheless, the methods worked well for understanding synchronization of pairs of O-cells or stellate cells in the presence of inhibition or excitation, for reasons that may depend on further structure in the equations: we modeled how the resulting STRCs would change depending on the initial conditions of the slow variables and found that the dependence did not change the qualitative behavior, only the amplitude of STRCs. Although this could be broken by sufficiently large changes in the initial conditions of slow variables, we chose the initial values of gating variables close to those on the limit cycle, and the perturbations used to construct STRCs keep those slow variables within the range in which the quantitative behavior was not affected.

We now show how these ideas apply to a pair of mutually coupled O-cells. If we denote spike times of these cells by t_1 and t_2, where $t_1 < t_2$, then on the next cycle the respective spike times will be $\bar{t}_1 = t_1 + T_O + f_{OO}(t_2 - t_1)$ and $\bar{t}_2 = t_2 + T_O + f_{OO}(\bar{t}_1 - t_2)$, where T_O is the period of a free-running O-cell, and $f_{OO}(\Delta)$ is the O-to-O STRC (Fig. 2c, solid line). The time difference between the two O-cells in the next cycle will be $\overline{\Delta} = \bar{t}_2 - \bar{t}_1 = \Delta + F_{OO}(\Delta)$, where $\Delta = t_2 - t_1$ and $F_{OO}(\Delta) = f_{OO}(T_O + f_{OO}(\Delta) - \Delta) - f_{OO}(\Delta)$. This function has two intercepts, one corresponding to synchronous, and another corresponding to antiphase oscillations (Fig. 2d, solid line). Standard theory of 1-D maps predicts that the synchrony (Δ_0) is unstable, while the antiphase locking regime (Δ_1) is stable, with domain of stability the entire period (this was confirmed in simulations). Thus, the O-cells do not synchronize with inhibition to produce the theta rhythm. Similar analyses made with other models of O-LM cells (Pervouchine et al., 2006) show qualitatively similar behavior.

Theta Rhythms in Hippocampal Networks

I-O Networks

In spite of the fact that the (model) O-LM cells do not synchronize with standard $GABA_A$ inhibition, it is possible to have a theta rhythm in a network that is wholly inhibitory: Gillies et al. (2002) produced an atropine-sensitive theta rhythm in a CA1 slice in which glutamatergic synapses were blocked. In that experimental model, presumably there were multiple interneurons involved, in addition to the O-LM cells. Rotstein et al. (2005) produced a model of coherent theta in a network of

O-LM and basket (I) cells. Both types of cells were modeled as single compartment; and since the previous dynamic clamp work had suggested that the O-LM cells and EC stellate cells are biophysically similar in their synchronization properties, the 1-compartment models of the stellate cells were used. The frequency of the model cells was determined by the choice of the applied current (but see Goldin et al., 2007). The simplest such network model consisted of two Acker et al. models of the O-LM cell and one I-cell, with the former cells uncoupled, and the I-cell mutually coupled to each of the other two cells.

An essential hypothesis for this model is that I-cells, representing fast-firing interneurons (presumably parvalbumin-positive basket cells) do indeed receive inhibition from theta-producing cells such as the O-LM cells and vice versa. This has not been demonstrated anatomically or with paired cell recordings. However, in vitro, it has been seen that the O-LM cells display IPSPs with kinetics comparable to those of the FS cell, and basket cells display long IPSPs associated with the O-LM cells (Rotstein et al., 2005). There is also evidence that somatostatin-immunoreactive O-LM cells innervate distal apical dendrites of parvalbumin-positive basked and/or axo-axonic interneurons (Katona et al., 1999, Fig. 7).

Analysis of how this synchronization works does not fit the standard uses of STRC and STDM, since the network has three cells. Nevertheless, it is possible to extend the analysis to this case. This was done in Pervouchine et al., (2006) for the Acker et al. model of the O-LM cell. The analysis done below illustrates the same results for the reduced Saraga et al. model (O-cells). Equations for O- and I-cells are in Appendix 1. The I-cells are as in previous sections.

A first step shows that, if the I-cells have weak enough drive to fire intrinsically in the theta-frequency range, each O-cell can phase-lock to the I-cell, at a phase such that the spike of the I-cell occurs relatively late in the O-cell cycle. This happens because the decay time of the inhibition induced by the O-LM cell is several times larger (20 ms) than that of the inhibition induced by basket cells (9 ms). Indeed, STRCs measuring the effects of the O- and the I-cell spikes on each other (Fig. 2c, dashed and dot-dashed lines) result in a STDM[1] that predicts stable non-synchronous oscillations (Δ_2 in Fig. 2d, dashed line).

The next step shows that, in the three cell network, the O-cells synchronize with each other because each synchronizes to the I-cell at the same phase. More specifically, if Δ is the time difference between spikes of the two O-cell and the I-cell spikes τ ms after the last of the two O-cells has spiked, then the time difference between the O-cells on the next cycle is $\overline{\Delta} = \Delta + F_{OO}(\Delta)$, where $F_{OO}(\Delta) = f_{IO}(\tau) - f_{IO}(\tau + \Delta)$ and $f_{IO}(\Delta)$ is the STRC function that models an input to the O-cell from an I-cell (Fig. 2c, dashed line). The synchronous solution is stable if $-2 < F'_{OO}(0) < 0$, i.e., if $0 < f'_{IO}(\tau) < 2$ (note that the derivative is with

[1] The derivation of STDM for the O-I network is very similar to that for the O-O network and yields $F_{OI}(\Delta) = f_{OI}(T + f_{IO}(\Delta) - \Delta) - f_{OI}(\Delta)$, where $f_{IO}(\Delta)$ and $f_{OI}(\Delta)$ are I-to-O and O-to-I STRCs shown in Fig. 2c (dashed and dot-dashed lines, respectively), and T is the unperturbed period of O- and I-cells.

respect to Δ). The latter condition holds for a relatively large range of values of τ, as shown by the dashed line in Fig. 2c.

We have shown that the entire O-I-O network can be regarded as a perturbation of an O-I network, in which the O-cells synchronize, provided that the I-cell does not spike shortly after one of the O-cells. In experimental observations and in the analysis done for the Acker et al. model (Pervouchine et al., 2006), this does not happen unless the decay time of the O-cells is set to be much longer than that of the I-cells. For the Saraga et al. model, the decay time of the O-cell inhibition does not have to be as long (Fig. 2c). The crucial distinction between the two models is that the Saraga et al. model has an A-current, which counterbalances the h-current and reduces the advance produced early in the cycle by the h-current in the Acker et al. model.

E-I-O Networks

There are several possible parameter regimes, producing theta frequency with different mechanisms. The central distinction is whether the O-cell fires as a result of excitation from the E-cell, or is held back by the inhibition from the I-cell (note that O-cells can also fire by post-inhibitory rebound, but this is more typical for the Acker et al. model rather than for the reduced Saraga model). Similar to what was described for O-I-O networks, a two-cell reduction is also possible for E-I-O networks, provided that the E-cell and the I-cell produce an oscillation of roughly the same frequency as does the O-cell. The dynamics are similar to PING, but at a lower frequency. (Without a model O-LM cell, this can lead to instability in the presence of noise; see Börgers and Kopell, 2005). The analysis of network dynamics then addresses the question of synchrony between the O-cell and either the E- or I-cells (the latter two cells spike almost synchronously and thus are referred to as an EI-module).

The combined effect of E- and I-cell spikes onto the O-cell can be regarded as a pulse that has both excitatory and inhibitory components. For simplicity, we change the excitatory conductance while keeping the amount of inhibition fixed; this results in a family of STRCs (depending on the excitatory conductance) from the EI-module to the O-cell, where the time of the perturbation is the time of the E-cell spike. (See Fig. 2e, where the different lines represent different strengths of the excitatory conductance). In turn, the O-cell spike impacts both E- and I-cells; here we use the assumption that the inhibitory feedback from the O-cell to the I-cell is negligible compared to the excitation, i.e., the E-to-I conductance is sufficient to make the I-cell fire independently of other inputs. The construction of the STDM is very similar to that in the O-O and O-I networks; the difference is only in the STRCs used.[2] The two functions needed to construct the STDM in this case are the O-to-E STRC (Fig. 2c, dotted line) and the EI-to-O STRC (Fig. 2e).

---

[2] In this case, the STRC is $F_{OE}(\Delta) = f_{OE}(T + f_{\mathrm{EI},O}(\Delta) - \Delta) - f_{OE}(\Delta)$, where $f_{OE}(\Delta)$ is the dotted line in Fig. 2c, and $f_{\mathrm{EI},O}(\Delta)$ is one of the functions shown in Fig. 2e.

The E-I-O network can oscillate in distinct modes (Fig. 2f). In the excitation-dominated regime (dotted line), the O-cell fires as a result of E-cell firing, in which case the zero phase lag between O- and E-cells (Δ_0) is the only fixed point, i.e., E, I, and O are roughly synchronous. In the inhibition-dominated regime (solid line), the O-cell phase-locks to the I-cell at a non-zero phase (Δ_1), as was observed in the O-I-O network, while the synchronous phase locking (Δ_0) has a tiny domain of stability. There is also a variety of intermediate regimes (dot-dashed line). In these regimes, additional (unstable) fixed points change the stability domains of Δ_0 and Δ_1, thus providing a continuous transition between the two dominant regimes.

The distinction between "inhibition-dominated" and "excitation-dominated" versions of theta sheds light on the relationship to a theta rhythm model of Orban et al. (2006). Our inhibition-dominated model is based on Gillies et al.'s in vitro work, in which the AMPA receptors are blocked. This differs in some critical ways from the model of Orban et al., which also has pyramidal cells and two classes of inhibitory cells, basket cells, and O-LM cells. Unlike the models of this section, the Orban et al. model relies on the h-current in the pyramidal cells to promote rebound excitation; the firing of the pyramidal cells is critical for the creation of the model theta oscillation. Our "excitation-dominated" mechanism is also different from the Orban et al. model. In ours, the pyramidal cell is now crucial to the phases of the different kinds of cells, with the I- and O-cells roughly synchronous, but the theta frequency still comes from the properties of O-cells, not the h-current of the pyramidal cells. We also note that, in large-scale excitation-dominated models with the gamma rhythm nested in the theta rhythm (see section "Nested Gamma and Theta Rhythms"), the I-cells fire more often in parts of the theta cycle in which the O-cells are quiet, and hence in vivo measurements would indicate that I- and O-LM cells fire (statistically) at different times.

Nested Gamma and Theta Rhythms

As mentioned above and also reviewed elsewhere (chapter "Neuronal Activity Patterns During Hippocampal Network Oscillation In Vitro"), several in vitro pharmacological models have shown that the microcircuits of the hippocampus are able to generate theta and gamma rhythms locally (i.e., independently of an external pacemaker). It is also known that the co-existence of theta and gamma seen in vivo can be reproduced by certain protocols in vitro (Fisahn et al., 1998; Gillies et al., 2002; Gloveli et al., 2005b; Dugladze et al., 2007); i.e., there exists an intra-hippocampal mechanism for the coupling of gamma and theta rhythms. As in the sections above, many of the computational models built to date, including those reviewed here, were based on important in vitro results.

Inhibitory Networks

Both experiments and simulations show that a nested gamma and theta rhythm can occur in purely inhibitory networks (Gillies et al., 2002; Rotstein et al., 2005; Serenevy, 2007). The same network that produces a theta rhythm with a coherent set

of O-cells can also produce a nested gamma rhythm inside the theta, provided that the I-cells have enough drive and that there are I-I synapses. This was shown for the Acker et al. model of O-LM cells in Rotstein et al. (2005). Figure 3a shows an example for the reduced Saraga et al. model (O-cells). In this situation, the mutual coupling of the model O-LM and I-cells is critical; a common input from the I-cells to the model O-LM cells, without O-I feedback, is not enough to synchronize the latter. Although each model O-LM cell adjusts its phase to the I-cell input, if the latter is much faster, the model O-LM cells skip I-cell cycles; the lack of synchronization is due to the fact that the different model O-LM cells skip different cycles. With mutual feedback between the I-cell and O-LM model cells (both models), the O-cells synchronize, with the I-cells forming a nested gamma (Fig. 3a).

If the synapses are strong, the standard STRC methods do not work well to explain this situation, even in a network of only one I- and one O-cell. The essential difficulty is that the inhibition from each successive spike of the I-cell in the O-cell network encounters a different set of O-cell conductances, since the currents in those cells are fairly long lasting. For both O-LM cell models, there are also large parameter regimes in which the number of I-spikes per O-cycle is erratic (P. Malerba, unpublished data). Simulations suggest that the erratic behavior may be related to trajectories passing nearby canards in the O-LM model equations.

A nested theta/gamma rhythm in a purely inhibitory network was also investigated numerically in White et al. (2000). In that set of simulations, there were again two kinds of interneurons, one with long IPSPs, and one with short ones. In contrast to the Rotstein et al. paper, the O-LM cell model had only spiking currents, no I_h, and there was a lot of heterogeneity in the drive to the cells. The network displayed gamma nested in theta, but not in a robust manner. The theta power went up with forcing at a theta frequency, and this was more effective, unintuitively, when the forcing was phase-dispersed. It is not fully understood how this resynchronization works. An analysis of a closely related system was given by Serenevy (2007) for a single population of weakly driven interneurons. The synchronization was most effective when the weak periodic drive was close in frequency to the effective frequency of the network of interneurons. The analysis showed that the phase dispersion of the input changes that effective frequency by changing the number of interneurons that participate in the rhythm, recruiting more or suppressing more (see also Bathellier et al., 2008).

Since the gamma/theta behavior can be obtained with no intrinsic currents besides those needed for spiking, this raises the question of what role the special currents (I_A, I_h, maybe $I_{Na,P}$) play in these rhythms. For theta in a single cell, these currents are believed to be important for subthreshold oscillations (Dickson et al., 2000), and also for resonance (Hu et al., 2002; Haas and White, 2002). But it is less clear what roles these currents play in oscillatory regimes in which the O-LM cells spike. However, we note that the gamma/theta nesting in the White et al. (2000) model is not very robust without adding periodic input, and we conjecture that the time scales associated with the h-current and A-current are important in making these interactions more robust, probably by shaping the input resistance.

In fact, the result presented in Fig. 3a could not be achieved if the h- and A-currents were removed from the O-cell (after appropriate compensation of the drive current; data not shown), pointing to an important role of these currents for the coherence of the theta rhythm at the population level.

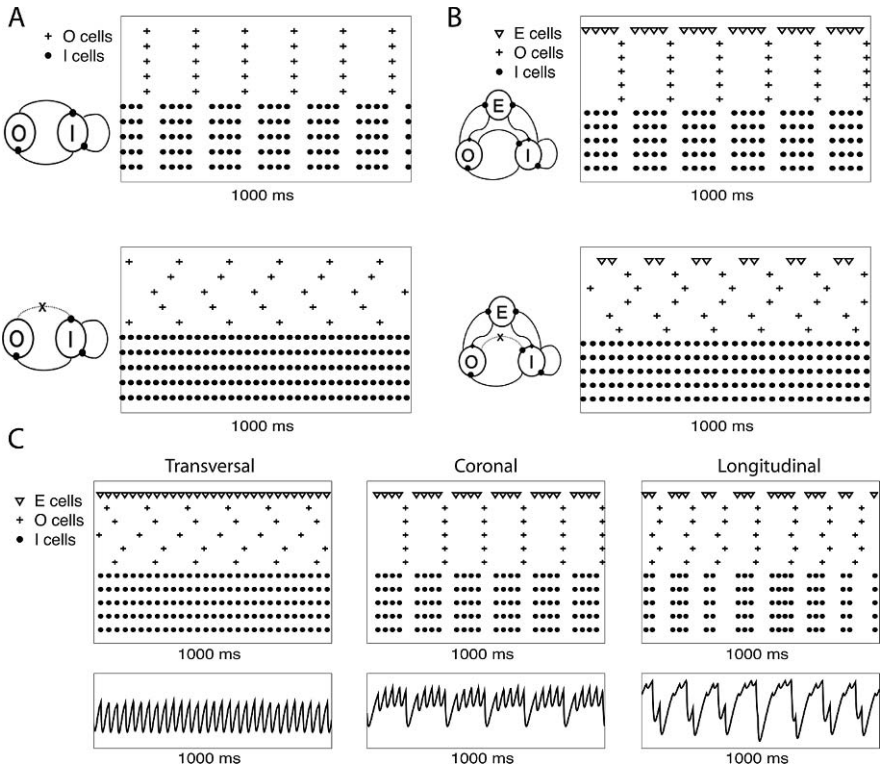

Fig. 3 Nested gamma and theta rhythms in simple hippocampal network models. (**a**) Pure inhibitory networks composed of I- and O-cells are able to generate coherent theta and gamma rhythms when the different cell types are mutually connected. Shown are the spike rastergrams for a network composed of 5 O- and 5 I-cells. The *bottom panel* shows a representative rastergram in the absence of O-I connections. In this case, although each individual O-cell spikes at theta frequency, the population of O-cells do not exhibit a coherent rhythm. Adding these connections, however, creates a coherent theta rhythm at the population level (*top panel*). (**b**) Theta and gamma rhythms in excitatory/inhibitory networks. Adding an E-cell to the network changes the type of gamma generation from ING to PING, i.e., the I-cells spike after the E-cell excitation. As shown for pure inhibitory networks, notice that a coherent theta rhythm is still dependent on the existence of O-I connections. (**c**) E-I-O network models of three hippocampal slice orientations. From transversal to longitudinal slices, O-cell connections (to all outputs) get stronger while I-cell connections get weaker, mimicking the orthogonal ramification property between these two interneurons (Gloveli et al., 2005b). The result is that the model LFP exhibits mostly gamma, mixed gamma/theta, or mostly theta oscillations in transversal, coronal, and longitudinal slices, respectively, as observed experimentally (Gloveli et al., 2005b). All parameter values are given in Appendix 4

Excitatory/Inhibitory Networks

In vivo, the networks producing the nested gamma/theta contain pyramidal cells as well as interneurons. Networks of pyramidal cells (E-cells), basket cells (I-cells), and O-LM cells (O-cells) were first studied in the context of in vitro work by Gloveli et al. on gamma and theta in CA3 (Gloveli et al., 2005b). In CA3, slices that are cut transversely and placed in an ACSF that contains kainate produce robust gamma rhythms (see chapter "Neuronal Activity Patterns During Hippocampal Network Oscillation In Vitro" for more details). If the slices are longitudinal, the same ACSF produces dynamics whose spectral content is mainly in the theta range; for a coronal slice, whose slice angle is in between, the spectral content has peaks in both the gamma and theta frequencies. The question addressed by the modeling is how different angles of the slice produce outputs with different frequency content.

The major difference between the three situations is in what part of the circuitry is preserved in the slices. The O-LM cells have long axons that project more in the longitudinal direction than in the transversal one (Gloveli et al., 2005b; Tort et al., 2007). Which connections are preserved in the transversal slice is not well understood: earlier studies suggested a lamellar organization of the hippocampus, in which the pyramidal cells would exert a greater influence in the transversal direction (Andersen et al., 1969, 2000), but this view has been challenged by other studies (Amaral and Witter, 1989; Wittner et al., 2007). More recently, however, it was shown that the gamma-producing basket cells do project more in the transverse direction (Gloveli et al., 2005b, see also Gloveli et al., 2005a). Thus, the longitudinal slice preserves more of the O-LM circuitry, and the transversal slice preserves more of the pyramidal-basket cell recurrent circuitry. We considered constructing a 3-D (or at least a 2-D) model in which that anatomy was explicitly modeled. Instead, we produced a more reduced description in which there was no explicit anatomy, but the preservation of more of the circuitry is modeled as a larger effect of those classes of cells. The O-LM cells are modeled by a 1-compartment reduction of the Saraga et al. model (O-cell), and the E- and I-cells are also modeled as in the previous sections; the one E-cell in the network is made to represent all the cells that are involved in a given cell population, while multiple I- and O-cells are used to explore issues of synchronization. We also employ a non-spiking E-cell as a caricature of a local field potential (LFP). This cell receives exactly the same synaptic inputs as the active E-cell in the network, but it is made silent by the absence of drive currents. The model LFP thus reflects subthreshold voltage changes in the E-cell population.

We first observe that such networks composed of E-I-O cells are able to produce nested gamma and theta oscillations (Fig. 3b). As in the case of pure inhibitory networks, O-I connections are required for a higher coherence of the theta rhythm by the O-cell population (Fig. 3b), and, likewise, removing I-O connections greatly reduces theta coherence (not shown). Next we study the effects of changing the strength of synaptic connections inside this network (Fig. 3c). The longitudinal slice is represented in this model by large O-I and O-E and lower I-O, I-I, and I-E conductances. The transverse slice has lower O-I and O-E and larger I-O, I-I, and I-E conductances, and the coronal slice has parameters in between. The results from these

simulations show behavior closely matching the experimental results: in the model transverse slice, the O-cells produce theta rhythms, not necessarily synchronized (given the low O-I synaptic conductance), and the E- and I-cells produce a PING rhythm. Given the strong I-E connections and the lack of coherence among O-cells, the model LFP exhibits mostly a gamma rhythm, as seen in the experiments. In the model longitudinal slice, the O-cells produce strong inhibition at theta frequency to both E- and I-cells. This is reflected in the model LFP, which shows mostly theta oscillations. The gamma rhythm is strongly reduced in the longitudinal slice model because of the large gap between the I-spikes (promoted by the long inhibition from the O-cells), together with a low I-E connection strength. In the coronal slice, where both interneurons present important influences over the E-cell population, the model LFP exhibits a clear nesting of the gamma and theta rhythm. Notice further that the gamma envelope (i.e., the amplitude of the gamma oscillation) is governed by the theta dynamics, which also matches experimental observations.

These observations have been reproduced in a more complex model in which there are many O- and I-cells, and the E-cell has five compartments, with the O-cell projecting to the distal dendrites, as in the actual anatomy (Tort et al., 2007). They also hold in models in which there are a large number of E-cells, and each E-cell fires at a low rate, while the population frequency is higher (e.g., persistent gamma for the transverse slice) (Tort et al., 2007).

We note that the present model differs from our previous modeling study of these phenomena (see Gloveli et al., 2005b). In our previous study, we also changed the strength of excitatory connections between the distinct slice angles. The main difference between the simulation results can be seen when comparing the longitudinal slice models: in Gloveli et al. (2005b) the low excitatory connections and strong inhibition by the O-cells impose a theta frequency for spikes in both the E- and I-cells, contrary to the present model. Whether there is such a difference in the frequency of spikes of basket and pyramidal cells between longitudinal and transversal slices remains to be studied experimentally; the two models make different predictions in this regard.

The simulation results give insight into recent in vivo work by the Monyer group in which the $GABA_A$ receptors were knocked out in cells that are parvalbumin-positive (PV+), which include the fast-spiking basket cells (I-cells). Thus, in terms of the current model, the O-I and I-I connections are gone, but the O-cells and all the connections to them are preserved. The experiments showed that the gamma oscillation is preserved, but the theta oscillation is much reduced, as is the theta modulation of the gamma amplitude and frequency (Wulff et al., 2009). Indeed the latter is reduced beyond what is expected by the reduction of the theta amplitude (Wulff et al., 2009).

These results can be reproduced in the above networks (see the modeling study done in Wulff et al., 2009). In the larger E/I/O model with one E-cell, both the O-I and I-O connections are important for the production of a coherent theta oscillation. When the O-I connection is removed, the O-cells lose their coherence, as in the O/I model described above for the completely inhibitory theta rhythm. The theta power is reduced by the lack of coherence, and the theta modulation of gamma is reduced

further because the O-cells are no longer able to convey their theta rhythmicity to the I-cells, the cell type most critical for the gamma oscillation.

We note that the synapses from pyramidal cells to O-LM cells have been shown to be plastic, especially during the times that the O-LM cells are hyperpolarized (Oren et al., 2009). Thus, the parameter regimes may be subject to plastic changes.

Gamma/Theta and Cell Assemblies

Since gamma rhythms are associated with cell assemblies, and the O-LM cells extend across much of the longitudinal direction of the hippocampus, a natural question is whether the O-LM cells can help to coordinate the cells assemblies that the gamma rhythm helps to create. This question was addressed in Tort et al. (2007). The model used was a collection of modules with many E-, I-, and O-cells, each module a representation of a transversal slice. Each module has many O-, I-, and E-cells. The E-cells were multi-compartmental. This is important, since the O-LM cells project to the distal apical dendrites and the I-cells project more proximally, an anatomical arrangement that could potentially affect any coordination via the O-LM cells. The O-cells were connected to E-cells within a module and also, with a weaker synaptic strength, to E-cells of other modules. The full network had different anatomies, from nearest neighbor to multiple neighbors to all–all connections of modules, with or without conduction delays between modules. To test for the ability of the O-LM cells alone to create this coordination, we omitted any long excitatory connections. Indeed, we think of the connections from the O-cells to E-cells as hard wired, while the mutually excitatory connections can be formed plastically when the cells are part of a cell assembly; thus, the connectivity may change with experience.

The simulations showed that the O-LM cells alone can coordinate cell assemblies, and that the same theta rhythm can coordinate different cell assemblies with different frequencies in the gamma range (Tort et al., 2007; see also Fig. 4). Also, cell assemblies can be formed with only some of the E-cells in a participating module, depending on their level of excitation. As both O- and I-cells were phasically excited by the E-cells, gamma and theta frequencies move together as the drive to the pyramidal cells is changed, with a gamma/theta-frequency ratio roughly constant (Tort et al., 2007). The constancy of this ratio was shown in our models to be related to the dynamics of the excitation-dominated regime (see section "E-I-O Networks").

The coordination of cell assemblies promoted by the O-cells was robust to changes in the conduction delays between modules compatible with the anatomy, and a little conduction delay actually provided tighter synchrony than none. The main drive to the E-cells in this model was considered to be derived from EC excitation and was therefore applied to the distal apical dendritic compartment. Interestingly, having the O-E synapse exactly at the same distal location as the E-cell drive led to higher robustness of the findings than an anatomical configuration having a perisomatic location of the O-E synapses. Also, the distal location of the drive to the E-cells makes the formation of inter-module gamma assemblies (promoted

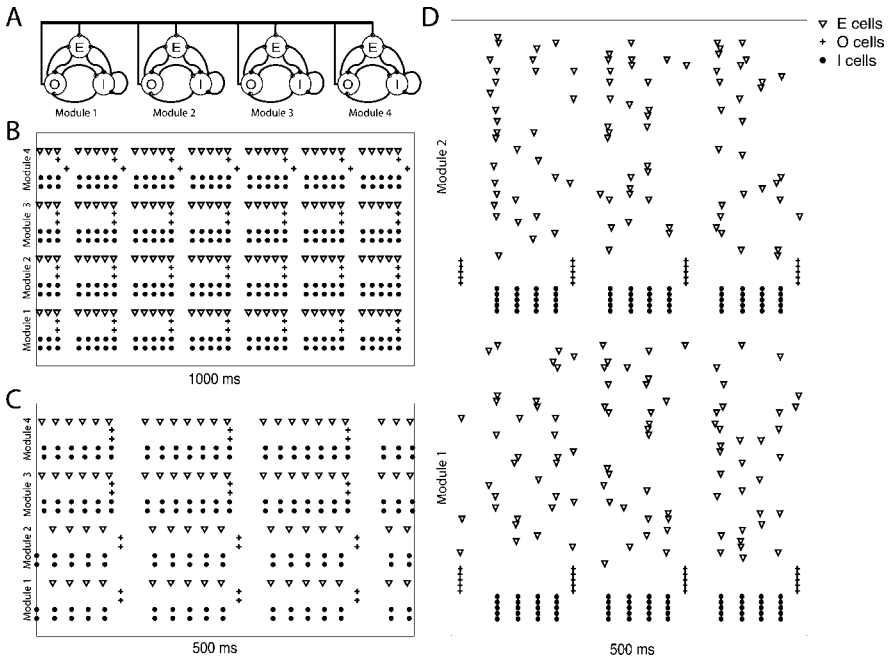

Fig. 4 O-LM cells can promote the formation of multiple gamma cell assemblies. (**a**) Multiple modules network scheme. Each module is composed of E-, I-, and O-cells (connected as in Fig. 3b *top*). Connections among modules are made only through O-E synapses, which is made to represent the larger axonal ramifications in the longitudinal direction of the hippocampus presented by the O-LM cells (Gloveli et al., 2005b; Tort et al., 2007). (**b**) Spike rastergram of a network composed of four modules (each module in the network is composed of 1 E-, 2 O-, and 2 I-cells), showing that O-LM cells are able to promote gamma synchrony among modules. (**c**) Same network as above, but with subsets of two modules excited with different E-cell drive levels. Note the formation of two gamma assemblies of distinct frequencies. (**d**) Spike rastergram of a network composed of two modules, with 40 E-, 5 O-, and 5 I-cells each. The network parameters are set so that each module exhibits weak PING (i.e., each E-cell spikes randomly and sparsely, below the gamma frequency, but the E-cell population still exhibits gamma; see also Fig. 1b). The O-LM cells are also able to promote gamma synchrony among modules under this regime. All parameter values for these simulations are given in Appendix 4

by the O-cells) more robust to distinct levels of excitation among E-cells. This robustness is related to the A-current, which is higher at the pyramidal cell dendrites and flattens the spiking frequency vs. applied drive (F–I) curve. The flatter F–I curve allows more coordination for the same amount of drive heterogeneity when compared to the somatic location of the drive currents. The modeling suggests that this circuit is well organized to coordinate and form gamma cell assemblies from EC inputs.

Although the use of a multi-compartmental model in the previous study provided insights about the functional architecture of this microcircuit and its multiple participating currents, in Fig. 4 we show that the formation of gamma assemblies

promoted by O-cells is robust enough to hold with simpler models of pyramidal cells; for instance, all the results in this figure were obtained by using the same E-, I-, and O-cell models as in the other sections of this chapter.

Conclusions and Future Directions

The model networks described here are very simple approximations of the actual biological systems. Nevertheless, we believe that their analysis constitutes an important attempt to gain further knowledge about the possible biophysical mechanisms underlying hippocampal oscillations as well as about their potential functions. The aim is to capture what is essential to produce the rhythms and their interactions.

There are many future directions for the work presented above. The current work considers the formation of gamma and theta rhythms, their interactions, and their roles in the formation and coordination of cell assemblies. Challenging questions that can build upon the current work include how the multiple inputs from the EC, the septal nucleus, and other structures can be integrated within CA3 and CA1 to produce associations of memories occuring simultaneously and in sequences (Dragoi and Buzsáki, 2006; Senior et al., 2008; Pastalkova et al., 2008; Itskov et al., 2008). It is likely that other kinds of interneurons known to fire at different phases in the theta rhythm (Klausberger et al., 2003) will be important for such extensions. We believe that an understanding of how the physiology and anatomy of the cells and circuits give rise to the rhythms of the hippocampus provides central clues to how the hippocampus makes use of these dynamics in learning and recall.

Appendix 1: Neuronal and Synaptic Models

Pyramidal cells: We use the pyramidal cell model of Olufsen et al. (2003):

$$C\frac{dV}{dt} = g_{\mathrm{Na}} m_\infty(V)^3 h(V_{\mathrm{Na}} - V) + g_{\mathrm{K}} n^4 (V_{\mathrm{K}} - V) + g_L(V_L - V) + I \quad (1)$$

$$\frac{dh}{dt} = \frac{h_\infty(V) - h}{\tau_h(V)} \quad (2)$$

$$\frac{dn}{dt} = \frac{n_\infty(V) - n}{\tau_n(V)} \quad (3)$$

with

$$x_\infty(V) = \frac{\alpha_x(V)}{\alpha_x(V) + \beta_x(V)} \quad \text{for } x = m, h, \text{ or } n \quad (4)$$

$$\tau_x(V) = \frac{1}{\alpha_x(V) + \beta_x(V)} \quad \text{for } x = h \text{ or } n \quad (5)$$

$$\alpha_m(V) = \frac{0.32(V + 54)}{1 - \exp(-(V + 54)/4)}$$

$$\beta_m(V) = \frac{0.28(V+27)}{\exp((V+27)/5)-1}$$

$$\alpha_h(V) = 0.128\ \exp(-(V+50)/18)$$

$$\beta_h(V) = \frac{4}{1+\exp(-(V+27)/5)}$$

$$\alpha_n(V) = \frac{0.032(V+52)}{1-\exp(-(V+52)/5)}$$

$$\beta_n(V) = 0.5\ \exp(-(V+57)/40)$$

In Eqs. (1), (2), and (3), the letters C, V, t and τ, g, and I denote capacitance density, voltage, time, conductance density, and current density, respectively. The units that we use for these quantities are μF/cm^2, mV, ms, mS/cm^2, and μA/cm^2. For brevity, units will usually be omitted from here on. The parameter values of the model are $C = 1$, $g_{\mathrm{Na}} = 100$, $g_{\mathrm{K}} = 80$, $g_{\mathrm{L}} = 0.1$, $V_{\mathrm{Na}} = 50$, $V_{\mathrm{K}} = -100$, and $V_{\mathrm{L}} = -67$.

This model is a variation on one proposed by Ermentrout and Kopell (1998); the difference is that in Ermentrout and Kopell (1998), the gating variable h was taken to be a function of n. The model of Ermentrout and Kopell (1998), in turn, is a reduction of a model due to Traub and Miles (1991).

Fast-spiking interneurons: For fast-spiking interneurons, we use the Wang and Buzsáki (1996) model. Equations (1), (2), (3), and (4) are as in the pyramidal cell model. Equation (5) is replaced by

$$\tau_x(V) = \frac{0.2}{\alpha_x(V)+\beta_x(V)} \text{ for } x = h \text{ or } n \tag{5}$$

The rate functions α_x and β_x, $x = m, h$, and n, are defined as follows:

$$\alpha_m(V) = \frac{0.1(V+35)}{1-\exp(-(V+35)/10)}$$

$$\beta_m(V) = 4\ \exp(-(V+60)/18)$$

$$\alpha_h(V) = 0.07\ \exp(-(V+58)/20)$$

$$\beta_h(V) = \frac{1}{\exp(-0.1(V+28))+1}$$

$$\alpha_n(V) = \frac{0.01(V+34)}{1-\exp(-0.1(V+34))}$$

$$\beta_n(V) = 0.125\ \exp(-(V+44)/80)$$

The parameter values, using the same units as for the pyramidal cells, are $C = 1$, $g_{\mathrm{Na}} = 35$, $g_{\mathrm{K}} = 9$, $g_{\mathrm{L}} = 0.1$, $V_{\mathrm{Na}} = 55$, $V_{\mathrm{K}} = -90$, and $V_{\mathrm{L}} = -65$.

O-LM interneurons: For the oriens lacunosum-moleculare interneurons, we use the model described in Tort et al. (2007), which is a reduction of the multicompartmental model described in Saraga et al. (2003). The current-balance equation is given by

$$\begin{aligned} C\frac{dV}{dt} &= g_{\mathrm{Na}} m^3 h(V_{\mathrm{Na}} - V) + g_{\mathrm{K}} n^4 (V_K - V) + g_A ab(V_A - V) \\ &\quad + g_h r(V_h - V) + g_L(V_L - V) + I \end{aligned} \tag{6}$$

with

$$\frac{dx}{dt} = \frac{x_\infty(V) - x}{\tau_x(V)} \text{ for } x = m, h, n, a, b, r \tag{7}$$

For $x = m, n, h$, the functions $x_\infty(V)$ and $\tau_x(V)$ are the same as in (4) and (5), and the rate functions α_x and β_x are defined as follows:

$$\alpha_m(V) = \frac{-0.1(V + 38)}{\exp(-(V + 38)/10) - 1}$$

$$\beta_m(V) = 4\ \exp(-(V + 65)/18)$$

$$\alpha_h(V) = 0.07\ \exp(-(V + 63)/20)$$

$$\beta_h(V) = \frac{1}{1 + \exp(-(V + 33)/10)}$$

$$\alpha_n(V) = \frac{0.018(V - 25)}{1 - \exp(-(V - 25)/25)}$$

$$\beta_n(V) = \frac{0.0036(V - 35)}{\exp((V - 35)/12) - 1}$$

For $x = a, b, r$, we provide the functions $x_\infty(V)$ and $\tau_x(V)$ below:

$$a_\infty(V) = \frac{1}{1 + \exp(-(V + 14)/16.6)}$$

$$\tau_a(V) = 5$$

$$b_\infty(V) = \frac{1}{1 + \exp((V + 71)/7.3)}$$

$$\tau_b(V) = \frac{1}{\frac{0.000009}{\exp((V-26)/18.5)} + \frac{0.014}{0.2+\exp(-(V+70)/11)}}$$

$$r_\infty(V) = \frac{1}{1+\exp((V+84)/10.2)}$$

$$\tau_r(V) = \frac{1}{\exp(-14.59-0.086V)+\exp(-1.87+0.0701V)}$$

The parameter values are $C = 1.3$, $g_L = 0.05$, $g_{\mathrm{Na}} = 30$, $g_{\mathrm{K}} = 23$, $g_A = 16$, $g_h = 12$, $V_{\mathrm{Na}} = 90$, $V_{\mathrm{K}} = -100$, $V_A = -90$, $V_h = -32.9$, $V_L = -70$.

Synaptic model: We adopt the synaptic model of Ermentrout and Kopell (1998).[3] Each synapse is characterized by a synaptic gating variable s associated with the presynaptic neuron, with $0 \leq s \leq 1$. This variable obeys

$$\frac{ds}{dt} = \rho(V)\frac{1-s}{\tau_R} - \frac{s}{\tau_D}$$

where ρ denotes a smoothed Heaviside function:

$$\rho(V) = \frac{1+\tanh(V/4)}{2}$$

and τ_R and τ_D are the rise and decay time constants, respectively. To model the synaptic input from neuron i to neuron j, we add to the right-hand side of the equation governing the membrane potential V_j of neuron j a term of the form

$$g_{ij}s_i(t)(V_{\mathrm{rev}} - V_j)$$

where g_{ij} denotes the maximal conductance associated with the synapse, s_i denotes the gating variable associated with neuron i, and V_{rev} denotes the synaptic reversal potential. For AMPA receptor-mediated synapses, we use $\tau_R = 0.1$, $\tau_D = 3$, and $V_{\mathrm{rev}} = 0$; for $\mathrm{GABA_A}$ receptor-mediated synapses, $\tau_R = 0.3$, $\tau_D = 9$, and $V_{\mathrm{rev}} = -80$, if the synapse originates from a basket cell, and $\tau_R = 0.2$, $\tau_D = 20$, and $V_{\mathrm{rev}} = -80$, if it originates from an O-LM cell.

[3] The models presented in section "Nested Gamma and Theta Rhythms" use the NEURON built-in function *Exp2Syn()* for modeling the synaptic gating variable s, which takes as parameters the rise and decay time constants. This is a double exponential function that is close to, but not identical with, the function s described here.

Appendix 2: Parameter Values in Section "Gamma Rhythms, in Various Guises"

Here we specify the parameter values used in the simulations of Fig. 1, and briefly discuss how variations in these values would affect the results. We have also included with the code the six parameter files which produce the panels of Fig. 1.

Notation: We denote by N_{E} and N_{I} the numbers of E- and I-cells, respectively. We take the maximal conductance of the synaptic connection from the ith I-cell to the jth E-cell to be

$$X_{\mathrm{IE},ij}\,\frac{\hat{g}_{\mathrm{IE}}}{p_{\mathrm{IE}}N_{\mathrm{I}}}$$

with $\hat{g}_{\mathrm{IE}} \geq 0$, $0 < p_{\mathrm{IE}} \leq 1$, and

$$X_{\mathrm{IE},ij} = \begin{cases} 1 \text{ with probability } p_{\mathrm{IE}}, \\ 0 \text{ with probability } 1 - p_{\mathrm{IE}} \end{cases}$$

where $p_{\mathrm{IE}}N_{\mathrm{I}}$ is the expected number of I-cells from which an E-cell receives synaptic input, and $\hat{g}_{\mathrm{IE}}$ is the expected value of the maximal total inhibitory conductance affecting an E-cell. Similar formulas are used for the E→I, I→I, and E→E synapses. The random variables $X_{\mathrm{IE},ij}$, $X_{\mathrm{EI},ij}$, $X_{\mathrm{II},ij}$, and $X_{\mathrm{EE},ij}$ are assumed to be independent.

The external drive has deterministic and stochastic components. The deterministic drive ("I" in Eq. (1) of Appendix 1) is $I_{\mathrm{E},i}$ for the ith E-cell and $I_{\mathrm{I},i}$ for the ith I-cell. The stochastic component of the drive to a cell is modeled by an additional term on the right-hand side of Eq. (1), of the form $-s_{\mathrm{stoch}}(t)\, g_{\mathrm{stoch}}\, V$. The gating variable s_{stoch} decays exponentially with time constant $\tau_{D,\mathrm{stoch}}$ during each time step. At the end of each time step, s_{stoch} jumps up to 1 with probability $\Delta t\, f_{\mathrm{stoch}}/1000$. This simulates the arrival of external synaptic input pulses. The mean frequency with which input pulses arrive is f_{stoch}. Even though we measure time in ms, we measure frequencies in Hz $= \mathrm{s}^{-1}$; this unit, like the others, will usually be omitted from here on. Different cells in the network receive independent stochastic input streams. We use subscripts E and I to label the values of g_{stoch}, f_{stoch}, and $\tau_{D,\mathrm{stoch}}$ for the E- and I-cells, respectively; for instance, the value of g_{stoch} for the E-cells is $g_{\mathrm{stoch,E}}$.

Numerics: The simulations shown in Fig. 1 were carried out using the midpoint method with $\Delta t = 0.02$. Results obtained with smaller values of Δt were not significantly different.

Parameter values common to all panels of Fig. 1: $N_{\mathrm{E}} = 80$ and $N_{\mathrm{I}} = 20$. Since we scale the excitatory and inhibitory synaptic conductances by N_{E} and N_{I}, respectively, the network size does not affect the results much. Connectivity is all-to-all: $p_{\mathrm{EE}} = p_{\mathrm{EI}} = p_{\mathrm{IE}} = p_{\mathrm{II}} = 1$. Plots similar to those of Fig. 1 are also obtained with sparse, random connectivity, provided that each I-cell receives input from sufficiently many E-cells, and vice versa (Börgers and Kopell, 2003; Golomb and

Hansel, 2000). The synaptic rise and decay time constants and reversal potentials are as specified in Appendix 1. Variations in the rise time constants, and in the decay time constant $\tau_{D,\mathrm{E}}$ of excitation can have effects similar to those of variations in synaptic strengths (see below). The decay time constant $\tau_{D,\mathrm{I}}$ of inhibition is a crucial factor in determining the frequency of the rhythms of panels A through C: the oscillation period depends on it linearly. The reversal potential of the excitatory synapses, $V_{\mathrm{rev,E}} = 0$, does not much affect the simulations of Fig. 1. However, if the reversal potential of inhibitory synapses, $V_{\mathrm{rev,I}} = -80$, is raised (for instance, to -65, modeling inhibition that is shunting rather than hyperpolarizing), gamma frequency rhythms are obtained only if the external drive to the E-cells is lowered, or the I→E synapses strengthened. There are no E→E synapses in Fig. 1: $\hat{g}_{\mathrm{EE}} = 0$. Such synapses can raise the number of E-cells participating in each population spike volley; for instance, with $\hat{g}_{\mathrm{EE}} = 0.5$, no E-cells would be suppressed in Fig. 1a, and the weak PING rhythm of Fig. 1b would turn into strong PING.

Specific parameter values for the six panels:

Panel A: (strong PING) $\hat{g}_{\mathrm{EI}} = 0.5$, $\hat{g}_{\mathrm{IE}} = 1.5$, $\hat{g}_{\mathrm{II}} = 0.5$, $I_{\mathrm{E},i} = 2.5 + 2i/N_{\mathrm{E}}$ for the ith E-cell (cell number $20+i$ in Fig. 1), $g_{\mathrm{stoch,E}} = 0$, $I_{\mathrm{I},i} = 0$, $g_{\mathrm{stoch,I}} = 0$. All parameters can be varied considerably without losing the PING rhythm. When $\hat{g}_{\mathrm{EI}}$ is raised, the spiking of the E-cells triggers the response of the I-cells more promptly; as a result, more E-cells are suppressed. In agreement with analysis (Börgers and Kopell, 2003), the population period T depends logarithmically on $\hat{g}_{\mathrm{IE}}$ ($T = 23.4$, 29.4, 35.4 for $\hat{g}_{\mathrm{IE}} = 1.5$, 3, 6), and linearly on $\tau_{D,\mathrm{I}}$ ($T = 23.4$, 29.1, 34.6 for $\tau_{D,\mathrm{I}} = 9$, 12, 15). The external drive I_{E} must be strong enough to drive the E-cells at an *intrinsic frequency* (the frequency that would be obtained in the absence of any synaptic connections) in or above the gamma range (Börgers and Kopell, 2003). In Fig. 1a, the intrinsic frequencies of the E-cells vary between 80 Hz ($I_{\mathrm{E}} = 2.5$) and 120 Hz ($I_{\mathrm{E}} = 4.5$). Strong drive to the I-cells abolishes the rhythm. Under idealized circumstances, there is a sharp threshold value of I_{I} above which the rhythm is lost (Börgers and Kopell, 2005). In a more realistic network, the threshold is not sharp, but the transition can be fairly rapid (Börgers et al., 2008). For instance, there is a PING rhythm very similar to that in Fig. 1a if $I_{\mathrm{I},i} = 1.5 + i/N_{\mathrm{I}}$, but for $I_{\mathrm{I},i} = 2.0 + i/N_{\mathrm{I}}$, the I-cells spike largely asynchronously, and the E-cells are suppressed. The PING rhythm can be protected against the effects of external drive to the I-cells by raising $\hat{g}_{\mathrm{II}}$ (Börgers and Kopell, 2005).

Panel B: (weak PING) Much of the external drive to the E-cells is stochastic in Fig. 1b: $I_{\mathrm{E},i} = 1.25$, $g_{\mathrm{stoch,E}} = 0.1$, $f_{\mathrm{stoch,E}} = 20$, $\tau_{D,\mathrm{stoch,E}} = 3$ (the decay time constant of AMPA receptor-mediated synapses), all other parameters as for Fig. 1a. The properties of weak PING rhythms and their parameter dependence require further study. However, as one would expect, the frequency is a decreasing function of $\tau_{D,\mathrm{I}}$ and $\hat{g}_{\mathrm{IE}}$. It is an increasing function of $f_{\mathrm{stoch,E}}$,

though the dependence is surprisingly weak. (See Figs. 4 and 6 of Reinker et al. (2006) for a similar observation.)

Panel C: (strong PING on a weak PING background) $I_{\mathrm{E},i} = 3.25$ for the first 20 E-cells (cells 21 through 40 in Fig. 1), all other parameters as in panel B.

Panel D: (asynchronous I-cells suppress E-cells) All synaptic inputs to the I-cells are removed here ($\hat{g}_{\mathrm{EI}} = \hat{g}_{\mathrm{II}} = 0$), replaced by strong, brief stochastic input pulses, forcing the I-cells to spike stochastically at approximately 38 Hz (the frequency of the I-cells in panel C): $g_{\mathrm{stoch,I}} = 0.5$, $f_{\mathrm{stoch,I}} = 38$, $\tau_{D,\mathrm{stoch,I}} = 1$. All other parameters are as in panel C.

Panel E: (entrainment by a 40-Hz sequence of tight input pulses, in the presence of a competing 56-Hz sequence of broader pulses) All parameters as in panel A, except $I_{\mathrm{E},i} = 4\ \sin^8(40\pi t/1{,}000) + 4\ \sin^2(56\pi t/1{,}000)$.

Panel F: All parameters as in panel E, except $\hat{g}_{\mathrm{IE}} = 0$.

Appendix 3: Parameter Values in Section "Theta Rhythms"

Below we describe the protocol used to construct spike-time response curves (STRCs) and spike-time difference maps (STDMs). We also specify the parameter values used in Fig. 2.

The dynamical models of cells and synapses are given in Appendix 1. To construct a phase response curve, two cells (referred to as presynaptic cell and postsynaptic cell, respectively) were connected by a synapse. The synaptic conductance is denoted by g_{XY}, where X is the presynaptic and Y is the postsynaptic cell. The period of each postsynaptic cell was set to approximately 150 ms by using the corresponding value of the DC current ($I_{\mathrm{app}} = 0.137$ for pyramidal cells, $I_{\mathrm{app}} = 0.185$ for fast-spiking interneurons, and $I_{\mathrm{app}} = -4.70$ for O-LM interneurons). Presynaptic cells were set not to spike using appropriate DC currents. The postsynaptic cell was run for three full periods to make the values of gating variables close to those on the limit cycle. At that, the dynamical models of pyramidal cells and fast-spiking interneurons approach their limit cycles well enough regardless of initial conditions. The initial values of gating variables for the Saraga O-LM cell model, which contains slow currents such as h-current and A-current, were as follows: $V = -75.61$, $m = 0.0122$, $n = 0.07561$, $h = 0.9152$, $r = 0.06123$, $a = 0.0229$, $b = 0.2843$.

At time t, the presynaptic cell was given a short (3 ms) DC current pulse to trigger exactly one spike, and the effect of this spike on the spike time of the postsynaptic cell was measured (we define the time of the spike as the midpoint between the two time points at which the membrane potential crosses the +10 mV threshold). Denote by t_0 and t_2 the spike times of the postsynaptic cell in two consecutive periods and

assume that the presynaptic cell spikes at time t_1 ($t_0 < t_1 < t_2$). Note that the presynaptic cell spikes shortly after, but not at the same time as the DC pulse arrives, i.e., $t_1 > t$. We define the spike-time response function as $f(\Delta) = t_2 - t_0 - T$, where $\Delta = t_1 - t_0$ and $T = 150$ ms. This procedure was repeated for different values of t with the time increment of 1 ms and yielded the values of $f(\Delta)$ on a uniform grid of Δ ($0 < \Delta < T$). Additionally, we define $f(0) = f(T) = 0$.

The synaptic conductances used in Fig. 2c were $g_{OO} = 0.09$, $g_{IO} = 0.30$, $g_{OI} = 0.002$, and $g_{OE} = 0.002$. Spike time difference maps in Fig. 2d were constructed as explained in section "Theta Rhythms" using linear interpolation of STRCs shown in Fig. 2c. To construct PING-to-O STRCs (Fig. 2e), we created a PING network by connecting one pyramidal cell (E) and one fast-spiking interneuron (I); the synaptic conductances were $g_{\mathrm{IE}} = 0.4$, $g_{\mathrm{EI}} = 0.2$, and $g_{\mathrm{II}} = 0.3$, where g_{II} is an autapse. At that, a short DC current pulse to the E-cell triggered exactly one spike and, through synaptic excitation, exactly one spike of the I-cell. The effect of the combined excitatory and inhibitory inputs to the O-cell was measured by the function $f_{\mathrm{EI},O}(\Delta)$ shown in Fig. 2e. The PING module was connected to an O-cell by using $g_{IO} = 0.2$ and three levels of excitatory conductance: $g_{EO} = 0.04$, $g_{EO} = 0.08$, and $g_{EO} = 0.14$ (solid, dot-dashed, and dotted traces in Fig. 2e). STDMs in Fig. 2f were constructed by using the corresponding STRCs from Figs. 2c and 2e.

Appendix 4: Parameter Values in Section "Nested Gamma and Theta Rhythms"

Here we specify the parameter values used in the simulations of Figs. 3 and 4. All these simulations were performed using the software NEURON (Hines and Carnevale, 1997), which is available for free download.[4]

Notation: We denote by N_{E}, N_{I}, and N_O the numbers of E-, I-, and O-cells inside a module, respectively. The maximal conductance of the synaptic connection from the cell type X to cell type Y is given by[5]

$$G_{XY} = \frac{\hat{g}_{XY}}{N_X}, \qquad X, Y = O, I, E.$$

We denote by I_X the drive current to cell type X ($X = O, I, E$). Below we report the values employed for $\hat{g}_{XY}$ and I_X in each figure, panel by panel. Any parameter not explicitly specified has value equal to zero.

[4] http://www.neuron.yale.edu/neuron/ and http://neuron.duke.edu/

[5] Note that the normalization is only made for the number of cells within one module, and, in particular, it does not take into consideration the number of modules in the network.

Figure 3:

Panel A: Top panel: $\hat{g}_{\mathrm{II}} = 0.1$, $\hat{g}_{OI} = 0.2$, $\hat{g}_{IO} = 0.5$, $I_{\mathrm{I}} = 1$, $I_O = -3$. In the bottom panel, $\hat{g}_{OI}$ was set to zero.

Panel B: Top panel: $\hat{g}_{\mathrm{II}} = 0.1$, $\hat{g}_{OI} = 0.2$, $\hat{g}_{IO} = 0.5$, $\hat{g}_{\mathrm{IE}} = 0.1$, $\hat{g}_{OE} = 0.15$, $\hat{g}_{\mathrm{EI}} = 0.05$, $\hat{g}_{EO} = 0.01$, $I_{\mathrm{E}} = 0.8$, $I_{\mathrm{I}} = 0.8$, $I_O = -3$. In the bottom panel, $\hat{g}_{OI}$ was set to zero.

Panel C: Left panel: $\hat{g}_{\mathrm{II}} = 0.13$, $\hat{g}_{OI} = 0.03$, $\hat{g}_{IO} = 0.7$, $\hat{g}_{\mathrm{IE}} = 0.15$, $\hat{g}_{OE} = 0.03$, $\hat{g}_{\mathrm{EI}} = 0.05$, $\hat{g}_{EO} = 0.01$, $I_{\mathrm{E}} = 0.8$, $I_{\mathrm{I}} = 0.8$, $I_O = -3$. Middle panel: $\hat{g}_{\mathrm{II}} = 0.1$, $\hat{g}_{OI} = 0.15$, $\hat{g}_{IO} = 0.5$, $\hat{g}_{\mathrm{IE}} = 0.08$, $\hat{g}_{OE} = 0.15$, $\hat{g}_{\mathrm{EI}} = 0.05$, $\hat{g}_{EO} = 0.01$, $I_{\mathrm{E}} = 0.8$, $I_{\mathrm{I}} = 0.8$, $I_O = -3$. Right panel: $\hat{g}_{\mathrm{II}} = 0.05$, $\hat{g}_{OI} = 0.3$, $\hat{g}_{IO} = 0.2$, $\hat{g}_{\mathrm{IE}} = 0.02$, $\hat{g}_{OE} = 0.3$, $\hat{g}_{\mathrm{EI}} = 0.05$, $\hat{g}_{EO} = 0.01$, $I_{\mathrm{E}} = 0.8$, $I_{\mathrm{I}} = 0.8$, $I_O = -3$.

Figure 4:

Panel B: $\hat{g}_{\mathrm{II}} = 0.1$, $\hat{g}_{OI} = 0.2$, $\hat{g}_{IO} = 0.5$, $\hat{g}_{\mathrm{IE}} = 0.1$, $\hat{g}_{OE} = 0.1$, $\hat{g}_{\mathrm{EI}} = 0.1$, $\hat{g}_{EO} = 0.01$, $I_{\mathrm{E}} = 1.3$ (all modules), $I_{\mathrm{I}} = 0.8$, $I_O = -1$. We set $\hat{g}_{OE} = 0.08$ among modules, with a 3-ms conduction delay among modules.

Panel C: Same parameters as in Panel B, except that Modules 1 and 2 had $I_{\mathrm{E}} = 1.4$, whereas $I_{\mathrm{E}} = 2$ in Modules 3 and 4.

Panel D: $\hat{g}_{\mathrm{II}} = 0.1$, $\hat{g}_{OI} = 0.2$, $\hat{g}_{IO} = 0.5$, $\hat{g}_{\mathrm{IE}} = 0.1$, $\hat{g}_{OE} = 0.6$, $\hat{g}_{\mathrm{EI}} = 0.2$, $\hat{g}_{EO} = 0.05$, $I_{\mathrm{E}} = 0.5 + W$ (all modules), where W is a white noise process with Var $= 0.02$, $I_{\mathrm{I}} = 1$, $I_O = -2$. We set $\hat{g}_{OE} = 0.06$ among modules, with a 3-ms conduction delay among modules.

Further Reading

Acker, C. D., Kopell, N., and White, J. A. 2003. Synchronization of strongly coupled excitatory neurons: relating network behavior to biophysics. J Comput Neurosci, 15, 71–90.

Amaral, D. G., and Witter, M. P. 1989. The three-dimensional organization of the hippocampal formation: a review of anatomical data. Neuroscience, 31(3), 571–591.

Andersen, P., Bliss, T. V., Lomo, T., Olsen, L. I., and Skrede, K. K. 1969. Lamellar organization of hippocampal excitatory pathways. Acta Physiol Scand, 76(1), 4A–5A.

Andersen, P., Soleng, A. F., and Raastad, M. 2000. The hippocampal lamella hypothesis revisited. Brain Res, 886(1–2), 165–171.

Bartos, M., Vida, I., Frotscher, M., Geiger, J. R., and Jonas, P. 2001. Rapid signaling at inhibitory synapses in a dentate gyrus interneuron network. J Neurosci, 21(8), 2687–98.

Bartos, M., Vida, I., Frotscher, M., Meyer, A., Monyer, H., Geiger, J. P. R., and Jonas, P. 2002. Fast synaptic inhibition promotes synchronized gamma oscillations in hippocampal interneuron networks. Proc Natl Acad Sci USA, 99(20), 13222–13227.

Bathellier, B., Carleton, A., and Gerstner, W. 2008. Gamma oscillations in a nonlinear regime: a minimal model approach using heterogeneous integrate-and-fire networks. Neural Comp, 20(12), 2973–3002.

Börgers, C., and Kopell, N. 2003. Synchronization in networks of excitatory and inhibitory neurons with sparse, random connectivity. Neural Comp, 15(3), 509–539.

Börgers, C., and Kopell, N. 2005. Effects of noisy drive on rhythms in networks of excitatory and inhibitory neurons. Neural Comp, 17(3), 557–608.

Börgers, C., and Kopell, N. 2008. Gamma oscillations and stimulus selection. Neural Comp, 20, 383–414.

Börgers, C., Epstein, S., and Kopell, N. 2005. Background gamma rhythmicity and attention in cortical local circuits: a computational study. Proc Natl Acad Sci USA, 102(19), 7002–7007.

Börgers, C., Epstein, S., and Kopell, N. 2008. Gamma oscillations mediate stimulus competition and attentional selection in a cortical network model. Proc Natl Acad Sci USA, 105(46), 18023–8.

Buhl, E. H., Cobb, S. R., Halasy, K., and Somogyi, P. 1995. Properties of unitary IPSPs evoked by anatomically identified basket cells in the rat hippocampus. Eur J Neurosci, 7(9), 1989–2004.

Canolty, R. T., Edwards, E., Dalal, S. S., Soltani, M., Nagarajan, S. S., Kirsch, H. E., Berger, M. S., Barbaro, N. M., and Knight, R. T. 2006. High gamma power is phase-locked to theta oscillations in human neocortex. Science, 313, 1626–1628.

Chapman, C. A., and Lacaille, J. C. 1999. Cholinergic induction of theta-frequency oscillations in hippocampal inhibitory interneurons and pacing of pyramidal cell firing. J Neurosci, 19, 8637–8645.

Crook, S. M., Ermentrout, G. B., and Bower, J. M. 1998. Spike frequency adaptation affects the synchronization properties of networks of cortical oscillators. Neural Comp, 10(4), 837–854.

Cunningham, M. O., Whittington, M. A., Bibbig, A., Roopun, A., LeBeau, F. E. N., Vogt, A., Monyer, H., Buhl, E. H., and Traub, R. D. 2004. A role for fast rhythmic bursting neurons in cortical gamma oscillations in vitro. Proc Natl Acad Sci USA, 101(18), 7152–7157.

Dickson, C. T., Magistretti, J., Shalinsky, M. H., Fransen, E., Hasselmo, M. E., and Alonso, A. 2000. Properties and role of I(h) in the pacing of subthreshold oscillations in entorhinal cortex layer II neurons. J Neurophysiol, 83(5), 2562–2579.

Diener, F. 1985a. Propriétés asymptotiques des fleuves. C R Acad Sci Paris, 302, 55–58.

Diener, M. 1985b. Détermination et existence des fleuves en dimension 2. C R Acad Sci Paris, 301, 899–902.

Dorval, A. D., Christini, D. J., and White, J. A. 2001. Real-time linux dynamic clamp: a fast and flexible way to construct virtual ion channels in living cells. Ann Biomed Eng, 29(10), 897–907.

Dragoi, G., and Buzsáki, G. 2006. Temporal encoding of place sequences by hippocampal cell assemblies. Neuron, 50, 145–157.

Dugladze, T., Vida, I., Tort, A. B., Gross, A., Otahal, J., Heinemann, U., Kopell, N. J., and Gloveli, T. 2007. Impaired hippocampal rhythmogenesis in a mouse model of mesial temporal lobe epilepsy. Proc Natl Acad Sci USA, 104(44), 17530–17535.

Ermentrout, G. B. 1996. Type I membranes, phase resetting curves, and synchrony. Neural Comp, 8, 879–1001.

Ermentrout, G. B., and Kopell, N. 1998. Fine structure of neural spiking and synchronization in the presence of conduction delay. Proc Natl Acad Sci USA, 95, 1259–1264.

Ermentrout, B., Pascal, M., and Gutkin, B. 2001. The effects of spike frequency adaptation and negative feedback on the synchronization of neural oscillators. Neural Comp, 13, 1285–1310.

Fisahn, A., Pike, F. G., Buhl, E. H., and Paulsen, O. 1998. Cholinergic induction of network oscillations at 40 Hz in the hippocampus in vitro. Nature, 394(6689), 186–189.

Galán, R. F., Ermentrout, G. B., and Urban, N. N. 2005. Efficient estimation of phase-resetting curves in real neurons and its significance for neural-network modeling. Phys Rev Lett, 94(15), 158101.

Gerstner, W., van Hemmen, J. L., and Cowen, J. 1996. What matters in neuronal locking? Neural Comp, 8, 1653–1676.

Gillies, M. J., Traub, R. D., LeBeau, F. E. N., Davies, C. H., Gloveli, T., Buhl, E. H., and Whittington, M. A. 2002. A model of atropine-resistant theta oscillations in rat hippocampal area CA1. J Physiol, 543(Pt 3), 779–793.

Gloveli, T., Dugladze, T., Saha, S., Monyer, H., Heinemann, U., Traub, R. D., Whittington, M. A., and Buhl, E. H. 2005a. Differential involvement of oriens/pyramidale interneurones in hippocampal network oscillations in vitro. J Physiol, 562(Pt 1), 131–147.

Gloveli, T., Dugladze, T., Rotstein, H. G., Traub, R. D., Monyer, H., Heinemann, U., Whittington, M. A., and Kopell, N. J. 2005b. Orthogonal arrangement of rhythm-generating microcircuits in the hippocampus. Proc Natl Acad Sci USA, 102(37), 13295–13300.

Goldin, M., Epsztein, J., Jorquera, I., Represa, A., Ben-Ari, Y., Crépel, V., and Cossart, R. 2007. Synaptic kainate receptors tune oriens-lacunosum moleculare interneurons to operate at theta frequency. J Neurosci, 27(36), 9560–9572.

Golomb, D., and Hansel, D. 2000. The number of synaptic inputs and the synchrony of large sparse neuronal networks. Neural Comp, 12, 1095–1139.

Gray, C. M. 1999. The temporal correlation hypothesis of visual feature integration: still alive and well. Neuron, 24(1), 31–47.

Gutkin, B. S., Ermentrout, G. B., and Reyes, A. D. 2005. Phase-response curves give the responses of neurons to transient inputs. J Neurophysiol, 94, 1623–1635.

Haas, J. S., and White, J. A. 2002. Frequency selectivity of layer II stellate cells in the medial entorhinal cortex. J Neurophysiol, 88(5), 2422–2429.

Hamzei-Sichani, F., Kamasawa, N., Janssen, W. G. M., Yasumura, T., Davidson, K. G. V., Hof, P. R., Wearne, S. L., Stewart, M. G., Young, S. R., Whittington, M. A., Rash, J. E., and Traub, R. D. 2007. Gap junctions on hippocampal mossy fiber axons demonstrated by thin-section electron microscopy and freeze-fracture replica immunogold labeling. Proc Natl Acad Sci USA, 104(30), 12548–12553.

Harris, K. D., Csicsvari, J., Hirase, H., Dragoi, G., and Buzsaki, G. 2003. Organization of cell assemblies in the hippocampus. Nature, 424(6948), 552–556.

Hebb, D. O. 1949. The Organization of Behavior: A Neuropsychological Theory. New York: Wiley.

Hines, M. L., and Carnevale, N. T. 1997. The NEURON simulation environment. Neural Comp, 9(6), 1179–1209.

Hu, H., Vervaeke, K., and Storm, J. F. 2002. Two forms of electrical resonance at theta frequencies, generated by M-current, h-current and persistent Na+ current in rat hippocampal pyramidal cells. J Physiol, 545(Pt 3), 783–805.

Itskov, V., Pastalkova, E., Mizuseki, K., Buzsaki, G., and Harris, K. D. 2008. Theta-mediated dynamics of spatial information in hippocampus. J Neurosci, 28, 5959–5964.

Katona, I., Acsády, L., and Freund, T. F. 1999. Postsynaptic targets of somatostain-immunoreactive interneurons in the rat hippocampus. Neuroscience 88(1), 37–55.

Kay, L. M. 2003. Two species of gamma oscillations in the olfactory bulb: dependence on behavioral state and synaptic interactions. J Integr Neurosci, 2(1), 31–44.

Klausberger, T., Magill, P. J., Márton, L. F., Roberts, J. D. B., Cobden, P. M., Buzsáki, G., and Somogyi, P. 2003. Brain-state- and cell-type-specific firing of hippocampal interneurons in vivo. Nature, 421, 844–848.

Kopell, N., and Ermentrout, G. B. 2002. Mechanisms of phase-locking and frequency control in pairs of coupled neural oscillators. In Handbook on Dynamical Systems: Toward Applications. Ed. B. Fiedler, Vol. 2, Elsevier, Amsterdam, 3–54.

Kopell, N., and Ermentrout, B. 2004. Chemical and electrical synapses perform complementary roles in the synchronization of interneuronal networks. Proc Natl Acad Sci USA, 101(43), 15482–15487.

Kopell, N. 2005. Does it have to be this complicated? Focus on "Single-column thalamocortical network model exhibiting gamma oscillations, spindles, and epileptogenic bursts". J Neurophysiol, 93(4), 1829–1830.

Lawrence, J. J., Saraga, F., Churchill, J. F., Statland, J. M., Travis, K. E., Skinner, F. K., and McBain, C. J. 2006. Somatodendritic Kv7/KCNQ/M channels control interspike interval in hippocampal interneurons. J Neurosci, 26(47), 12325–12338.

Lewis, T. J., and Rinzel, J. 2000. Self-organized synchronous oscillations in a network of excitable cells coupled by gap junctions. Network Comput Neural Syst, 11, 299–320.

Lewis, T. J., and Rinzel, J. 2001. Topological target patterns and population oscillations in a network with random gap junctional coupling. Neurocomputing, 763–768.

Middleton, S., Jalics, J., Kispersky, T., Lebeau, F. E. N., Roopun, A. K., Kopell, N. J., Whittington, M. A., and Cunningham, M. O. 2008. NMDA receptor-dependent switching

between different gamma rhythm-generating microcircuits in entorhinal cortex. Proc Natl Acad Sci USA, 105(47), 18572–18577.

Munro, E. C. 2008. The axonal plexus: a description of the behavior of a network of axons connected by gap junctions. Ph.D. thesis, Tufts University.

Netoff, T. I., Acker, C. D., Bettencourt, J. C., and White, J. A. 2005a. Beyond two-cell networks: experimental measurement of neuronal responses to multiple synaptic inputs. J Comput Neurosci, 18(3), 287–295.

Netoff, T. I., Banks, M. I., Dorval, A. D., Acker, C. D., Haas, J. S., Kopell, N., and White, J. A. 2005b. Synchronization in hybrid neuronal networks of the hippocampal formation. J Neurophysiol, 93(3), 1197–1208.

Olufsen, M., Whittington, M., Camperi, M., and Kopell, N. 2003. New functions for the gamma rhythm: population tuning and preprocessing for the beta rhythm. J Comput Neurosci, 14, 33–54.

Oprisan, S. A., Prinz, A. A., and Canavier, C. C. 2004. Phase resetting and phase locking in hybrid circuits of one model and one biological neuron. Biophys J, 87, 2283–2298.

Orban, G., Kiss, T., and Erdi, P. 2006. Intrinsic and synaptic mechanisms determining the timing of neuron population activity during hippocampal theta oscillation. J Neurophysiol, 96(6), 2889–2904.

Oren, I., Nissen, W., Kullmann, D. M., Somogyi, P., and Lamsa, K. P. 2009. Role of ionotropic glutamate receptors in long-term potentiation in rat hippocampal CA1 oriens-lacunosum moleculare interneurons. J Neurosci, 29(4), 939–950.

Pastalkova, E., Itskov, V., Amarasingham, A., and Buzsáki, G. 2008. Internally generated cell assembly sequences in the rat hippocampus. Science, 321, 1322–1327.

Pervouchine, D. D., Netoff, T. I., Rotstein, H. G., White, J. A., Cunningham, M. O., Whittington, M. A., and Kopell, N. J. 2006. Low-dimensional maps encoding dynamics in entorhinal cortex and hippocampus. Neural Comp, 18(11), 2617–2650.

Reinker, S., Li, Y.-X., and Kuske, R. 2006. Noise-induced coherence and network oscillations in a reduced bursting model. Bull Math Biol, 68(6), 1401–1427.

Rotstein, H. G., Pervouchine, D. D., Acker, C. D., Gillies, M. J., White, J. A., Buhl, E. H., Whittington, M. A., and Kopell, N. 2005. Slow and fast inhibition and an H-current interact to create a theta rhythm in a model of CA1 interneuron network. J Neurophysiol, 94(2), 1509–1518.

Rotstein, H. G., Oppermann, T., White, J. A., and Kopell, N. 2006. The dynamic structure underlying subthreshold oscillatory activity and the onset of spikes in a model of medial entorhinal cortex stellate cells. J Comput Neurosci, 21(3), 271–292.

Saraga, F., Wu, C. P., Zhang, L., and Skinner, F. K. 2003. Active dendrites and spike propagation in multi-compartment models of oriens-lacunosum/moleculare hippocampal interneurons. J Physiol, 552(3), 502–509.

Senior, T. J., Huxter, J. R., Allen, K., O'Neill, J., and Csicsvari, J. 2008. Gamma oscillatory firing reveals distinct populations of pyramidal cells in the CA1 region of the hippocampus. J Neurosci, 28(9), 2274–2286.

Serenevy, A. 2007. Dynamic mechanisms in networks of interneurons with periodic drives. Ph.D. thesis, Boston University.

Sharp, A. A., O'Neil, M. B., Abbott, L. F., and Marder, E. 1993. Dynamic clamp: computer-generated conductances in real neurons. J Neurophysiol, 69(3), 992–995.

Singer, W., and Gray, C. M. 1995. Visual feature integration and the temporal correlation hypothesis. Annu Rev Neurosci, 18, 555–586.

Tort, A. B. L., Rotstein, H. G., Dugladze, T., Gloveli, T., and Kopell, N. J. 2007. On the formation of gamma-coherent cell assemblies by oriens lacunosum-moleculare interneurons in the hippocampus. Proc Natl Acad Sci USA, 104(33), 13490–13495.

Tort, A. B. L., Kramer, M. A., Thorn, C., Gibson, D. J., Kubota, Y., Graybiel, A. M., and Kopell, N. 2008. Dynamic cross-frequency couplings of local field potential oscillations in rat striatum and hippocampus during performance of a T-maze task. Proc Natl Acad Sci USA, 105(51), 20517–20522.

Traub, R. D., and Miles, R. 1991. Neuronal Networks of the Hippocampus. Cambridge, UK: Cambridge University Press.

Traub, R. D., Jefferys, J. G. R., and Whittington, M. 1997. Simulation of gamma rhythms in networks of interneurons and pyramidal cells. J Comput Neurosci, 4, 141–150.

Traub, R. D., Bibbig, A., Fisahn, A., LeBeau, F. E. N., Whittington, M. A., and Buhl, E. H. 2000. A model of gamma-frequency network oscillations induced in the rat CA3 region by carbachol in vitro. Eur J Neurosci, 12, 4093–4106.

Traub, R. D., Kopell, N., Bibbig, A., Buhl, E. H., Lebeau, F. E. N., and Whittington, M. A. 2001. Gap junctions between interneuron dendrites can enhance long-range synchrony of gamma oscillations. J Neurosci, 21, 9478–9486.

Traub, R. D., Bibbig, A., LeBeau, F. E. N., Buhl, E. H., and Whittington, M. A. 2004. Cellular mechanisms of neuronal population oscillations in the hippocampus in vitro. Annu Rev Neurosci, 27, 247–278.

Traub, R. D., Contreras, D., Cunningham, M. O., Murray, H., LeBeau, F. E. N., Roopun, A., Bibbig, A., Wilent, W. B., Higley, M. J., and Whittington, M. A. 2005. Single-column thalamocortical network model exhibiting gamma oscillations, sleep spindles, and epileptogenic bursts. J Neurophysiol, 93(4), 2194–2232.

Tukker, J., Fuentealba, P., Hartwich, K., Somogyi, P., and Klausberger, T. 2007. Cell type-specific tuning of hippocampal interneuron firing during gamma oscillations in vivo. J Neurosci, 27(31), 8184–8189.

van Vreeswijk, C., Abbott, L. F., and Ermentrout, G. B. 1994. When inhibition not excitation synchronizes neural firing. J Comput Neurosci, 1, 313–322.

Wang, X.-J., and Buzsáki, G. 1996. Gamma oscillation by synaptic inhibition in a hippocampal interneuronal network model. J Neurosci, 16, 6402–6413.

White, J., Chow, C., Ritt, J., Soto-Trevino, C., and Kopell, N. 1998a. Synchronization and oscillatory dynamics in heterogeneous, mutually inhibited neurons. J Comput Neurosci, 5, 5–16.

White, J. A., Klink, R., Alonso, A., and Kay, A. R. 1998b. Noise from voltage-gated ion channels may influence neuronal dynamics in the entorhinal cortex. J Neurophysiol, 80, 262–269.

White, J. A., Banks, M. I., Pearce, R. A., and Kopell, N. J. 2000. Networks of interneurons with fast and slow gamma-aminobutyric acid type A (GABAA) kinetics provide substrate for mixed gammatheta rhythm. Proc Natl Acad Sci USA, 97(14), 8128–8133.

Whittington, M. A., Jefferys, J. G., and Traub, R. D. 1996. Effects of intravenous anaesthetic agents on fast inhibitory oscillations in the rat hippocampus in vitro. Br J Pharmacol, 118(8), 1977–1986.

Whittington, M. A., Traub, R. D., Kopell, N., Ermentrout, B., and Buhl, E. H. 2000. Inhibitionbased rhythms: experimental and mathematical observations on network dynamics. Int J Psychophysiol, 38, 315–336.

Wittner, L., Henze, D. A., Zaborszky, L., and Buzsaki, G. 2007. Three-dimensional reconstruction of the axon arbor of a CA3 pyramidal cell recorded and filled in vivo. Brain Struct Funct, 212(1), 75–83.

Wulff, P., Ponomarenko, A. A., Bartos, M., Korotkova, T. M., Fuchs, E. C., Bähner, F., Both, M., Tort, A. B. L., Kopell, N., Wisden, W., and Monyer, H. 2009. Hippocampal theta rhythm and its coupling with gamma oscillations require fast inhibition onto parvalbumin-positive interneurons. Proc Natl Acad Sci USA, 106(9), 3561–3566.

Associative Memory Models of Hippocampal Areas CA1 and CA3

Bruce P. Graham, Vassilis Cutsuridis, and Russell Hunter

Overview

The hippocampal regions CA3 and CA1 have long been proposed to be auto- and heteroassociative memories, respectively (Marr, 1971; McNaughton and Morris, 1987; Treves and Rolls, 1994), for the storage of declarative information. An autoassociative memory is formed when a set of neurons are recurrently connected by modifiable synapses, whereas a heteroassociative memory is formed through modifiable connections from an input layer of neurons to an output layer. Associative memory storage simply requires a Hebbian strengthening of connections between neurons that are coactive (Amit, 1989; Hopfield, 1982; Willshaw et al., 1969). Recall proceeds from a cue activity pattern across neurons that is a partial or noisy version of a previously stored pattern. A suitable firing threshold on each neuron that receives input from already active neurons ensures that neural activity evolves towards the stored pattern. This may happen with only one or two updates of each neuron's activity. Accurate recall is obtainable provided not too many patterns have been stored, otherwise recall is poor, or even impossible.

Network models of spiking neurons can be used to explore the dynamics of storage and recall in such memory networks. Here we introduce a recurrent network model based on hippocampal area CA3 and a feedforward network model for area CA1. Cells are simplified compartmental models with complex ion channel dynamics. In addition to pyramidal cells, one or more types of interneuron are present. We investigate, in particular, the roles of these interneurons in setting the appropriate threshold for memory recall.

B.P. Graham (✉)
Department of Computing Science and Mathematics, University of Stirling, Stirling FK9 4LA, UK
e-mail: b.graham@cs.stir.ac.ak

V. Cutsuridis et al. (eds.), *Hippocampal Microcircuits*, Springer Series in Computational Neuroscience 5, DOI 10.1007/978-1-4419-0996-1_16,

Associative Memory and the Hippocampus

Pyramidal cells within CA3 form sufficient recurrent connections between themselves that they can putatively operate as an associative memory network (de Almeida et al., 2007; Treves and Rolls, 1994). Patterns of pyramidal cell (PC) activity may largely be determined by mossy fibre inputs from the dentate gyrus (Fig. 1). Such patterns are stored autoassociatively by Hebbian modification of recurrent connections between CA3 PCs (Treves and Rolls, 1994). Patterns of CA1 PC activity may be determined by direct afferent input from the entorhinal cortex (Fig. 1). Temporal correspondence between these patterns and patterns of activity in CA3 PCs results in their heteroassociation in CA1 by modification of CA3 Schaffer collateral synapses onto active CA1 PCs (Hasselmo et al., 2002a).

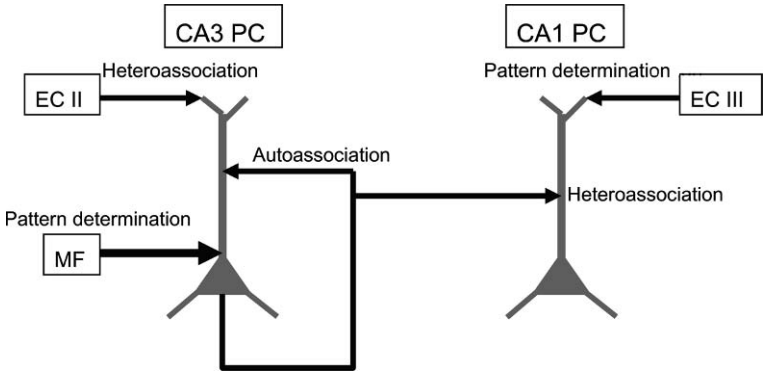

Fig. 1 Associative memory in the hippocampus. Mossy fibre (MF) inputs from the dentate gyrus create pyramidal cell (PC) activity in CA3 that is stored autoassociatively by Hebbian modification of recurrent collateral synapses between coactive PCs. Patterns of activity in layer II of entorhinal cortex (EC II) may be heteroassociated with these CA3 patterns. At the same time, CA1 PCs receiving input both from layer III of entorhinal cortex and from CA3 PCs form a heterassociation with the active CA3 PCs through Hebbian modification of the Schaffer collateral synapses

Gamma frequency rhythms (30–100 Hz) are assumed to constitute a basic clock cycle such that patterns of activity for storage and recall correspond to PCs that are active in a particular gamma cycle (Axmacher et al., 2006; Buzsaki and Chrobak, 1995; Lisman and Idiart, 1995). The slower theta rhythm (4–10 Hz) is assumed to modulate episodes of storage of new information and recall of old information in its half cycles (Hasselmo et al., 2002a, b). During exploration an animal is likely to encounter both familiar and novel situations. Storage of new episodes with minimal interference from already encoded episodes takes place most efficiently if storage and recall are temporally separated in the encoding neural networks (Wallenstein and Hasselmo, 1997). Waxing and waning of GABA-mediated inhibition from the medial septum lead alternately to disinhibition and inhibition of PCs during a theta cycle, corresponding to ideal conditions for pattern recall and pattern storage, respectively. In the results to follow, we only consider the

recall phase. Results on modelling both storage and recall in CA1 can be found in Cutsuridis et al. (2007, 2008a, 2009a) and Cutsuridis and Wennekers (2009). Other models consider storage and recall in CA3 (Kunec et al., 2005; Wallenstein and Hasselmo, 1997).

Hebbian Pattern Storage and Recall

Rather than considering the biological requirements for pattern storage via induction of long-term potentiation (LTP), patterns are stored in our networks by generating a weight matrix using a Hebbian learning rule (the reader is referred to Cutsuridis and colleagues (2008a, 2009a, 2009) for an example of using a spike timing-dependent plasticity rule to store patterns). These weights are then used to set the conductance strengths of AMPA synapses between PCs. Patterns are specified as binary vectors, which represent the activity (1) or silence (0) of each PC. A clipped Hebbian rule is used to generate a binary weight matrix, where an entry of 1 at index (i,j) indicates that the PCs i and j, where i connects onto j, were both active in the same pattern during storage. An example weight matrix that results from the storage of two patterns in an autoassociative memory (or, equivalently, a heteroassociative memory in which the input and output patterns are identical) is illustrated in Fig. 2a.

In an artificial neural network implementation with binary computing units, recall of a previously stored pattern proceeds by multiplying a cue pattern (full, partial or noisy version of a stored pattern) with the weight matrix to give the weighted sum

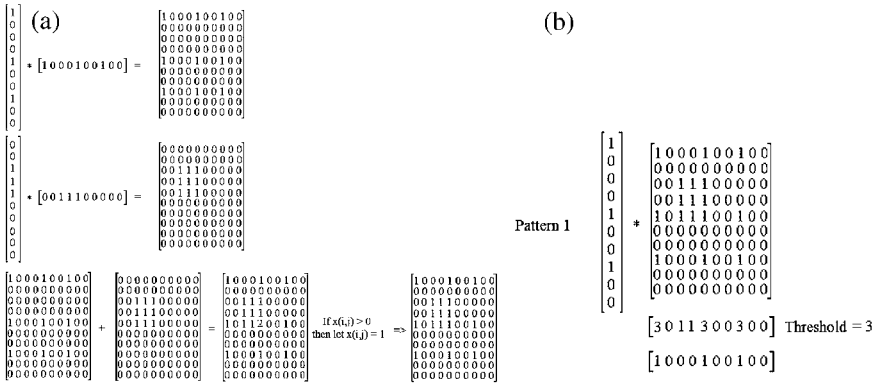

Fig. 2 (**a**) Weight matrix from the autoassociative storage of two patterns via clipped Hebbian learning. The individual weight matrices from the individual storage of the patterns are simply obtained as the outer product of the pattern with itself. The combined weight matrix is obtained by summing the individual matrices and then clipping entries to be 0 or 1. (**b**) Pattern recall strategy. The cue pattern is multiplied with the weight matrix to give a vector of weighted input sums. This vector is thresholded to give the recalled binary vector. With the noiseless cue illustrated here, a suitable threshold is simply the number of active units in the cue pattern

of the inputs to each cell in the network. Recall then involves thresholding these weighted sums to create an output pattern that contains 1 s for all those cells that are receiving the highest input sums. This output pattern will equal the stored cue pattern if recall is error-free. To give an example, we use the weight matrix in which the two patterns shown in Fig. 2a have been stored. The first of these patterns is used as the recall cue. The input column vector (cue pattern 1) is multiplied with the weight matrix to give the output row vector which is the weighted input sums to each of the 10 cells in the network (Fig. 2b). This vector is [3 0 1 1 3 0 0 3 0 0]. It is easily seen that the highest sums (3) are all to the cells that belong to the stored cue pattern. Some other cells get a lower input of 1, since the two stored patterns overlap with each other. Recall proceeds by applying an activity threshold, and in this case a threshold of 3 is appropriate. The final output activity vector is determined by making active (vector entry 1) all those cells whose input sum is greater than or equal to the threshold (3), else the vector entry is 0. The new output vector after the threshold setting is applied is [1 0 0 0 1 0 0 1 0 0], which is identical to the input vector. Therefore the pattern has been successfully recalled.

More challenging scenarios are when a noisy or partial cue is applied to the network, or when the network is only partially connected (that is, not all neurons are connected to all other neurons, which is typical in biological neural nets). Then the appropriate threshold on the input sums is not so easily chosen. One rule is to chose a threshold that will guarantee the expected number of cells are active in the output pattern (this does not, however, guarantee that they are the correct cells!)

In the scenario of spiking neurons, this thresholding process involves the intrinsic action potential generation threshold of a neuron and its modulation by such factors as inhibition. Weighted input sums are now the summation of EPSPs of differing amplitude generated by action potentials from active input neurons arriving at roughly the same time at different excitatory synapses. If the summed EPSPs, which may be inhibited, cause the membrane potential of the axon initial segment to reach threshold, then the cell fires an action potential and is deemed to be active.

The models that follow explore this process in detail for partially connected autoassociative and heteroassociative networks of spiking neurons.

The Models

Autoassociative Memory in CA3

The principal excitatory cells of the CA3 region are pyramidal cells. These cells are driven by inputs from the dentate gyrus and entorhinal cortex, and may have sufficient recurrent connectivity to act as an autoassociative memory (de Almeida et al., 2007; Treves and Rolls, 1994). We construct a recurrent neural network model consisting of a large number of pyramidal cells (PCs) and a smaller number

of inhibitory neurons (putative basket cells). Connectivity between PCs is determined by a connectivity matrix derived from storing patterns using Hebbian learning as described above. Inhibitory connectivity is tuned to achieve accurate recall of a stored pattern when a few of the PCs belonging to a particular stored pattern are given tonic stimulation to make them active and thus act as a recall cue. This model is an extension of the Sommer and Wennekers work (2000, 2001) in which now a number of explicit, spiking interneurons provide the inhibition (Hunter et al., 2008a, b, 2009).

The CA3 Network

The network contains 100 pyramidal cells (PCs), whose interconnectivity is determined by a random pattern of physical connections plus the setting of connection weights as determined by Hebbian learning of stored activity patterns. To represent our learnt binary weights, all AMPA synapses are given the same maximum conductance value. A fully connected PC network involves an individual PC connecting to every other PC, but not to itself, giving n^2–n physical connections, where n is the number of PCs in the network. Full connectivity is not biologically realistic, but serves as a control case for examining the effects of missing connections on memory performance. In CA3, recurrent connections between PCs are numerous, but still sparse, with a single PC receiving connections on average from around 10% of other PCs (Ishizuka et al., 1990; Li et al., 1994). In the model network, partial connectivity is achieved by random deletion of possible connections, without any topographical considerations of relative PC spatial positions. This is a reasonable first approximation to connectivity within a subpart of CA3 (de Almeida et al., 2007; Ishizuka et al., 1990; Li et al., 1994).

Individual PCs are modelled using the tried-and-tested two-compartment model of Pinsky and Rinzel (1994). This model is sufficient to reproduce regular spiking and bursting behaviour in these cells, and to provide a spatial separation of inputs to the dendrites from inputs to the soma.

The somatic compartment contains fast sodium and delayed-rectifier potassium currents. The dendritic compartment contains a calcium current and two (fast and slow) calcium-activated potassium currents. The two compartments are joined by a coupling conductance. Slow calcium spikes and their termination by the calcium-activated potassium currents can generate burst firing in this cell model. Inhibition in the network is provided by fast-spiking basket cells (BCs). A small compartmental model is used that is derived from experimental data on such cells in the dentate gyrus (Santhakumar et al., 2005). Full details of both cell models are given in Appendix 1.

The network model of Sommer and Wennekers (2000, 2001) used “pseudo-inhibition”, in which each PC also provided an inhibitory connection onto all other PCs, so that each PC received inhibition in proportion to the amount of PC activity. Explicit interneurons were not modelled. Here, explicit inhibitory circuitry is included in two configurations (Hunter et al., 2009):

1. A single inhibitory interneuron (basket cell - BC) is driven by all pyramidal cells and feeds back inhibition to all PCs equally (Fig. 3a).
2. The network contains 100 BCs, each of which is driven by a single PC, but all of which feedback inhibition to all PCs (Fig. 3b).

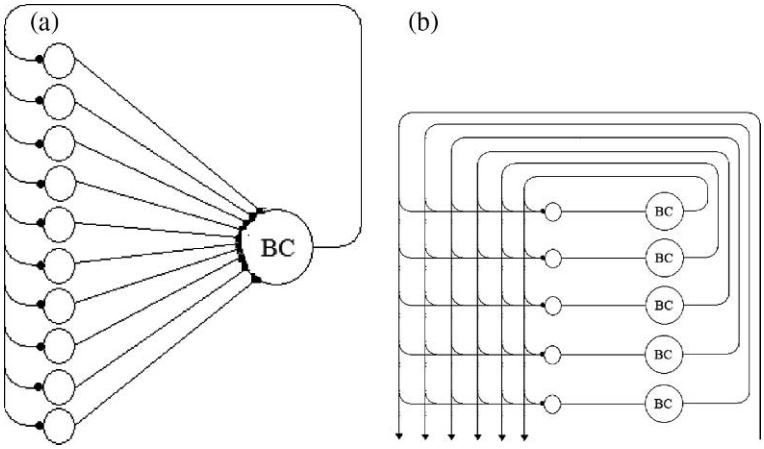

Fig. 3 Two network configurations with explicit inhibitory basket cells (BC) that act to modify PC firing thresholds. (**a**) One inhibitory interneuron that is driven equally by all PCs and feeds back inhibition to all PCs. (**b**) One interneuron (BC) for each PC, with each BC being driven by a single PC, but feeding back inhibition to all PCs

The first configuration provides inhibition that is relatively constant, provided that sufficient PCs are active to cause the BC to spike. The BC spiking rate is only a moderate function of PC activity. In the second configuration, the amount of inhibition projected to each PC is a strong function of the current PC activity level across the network. This should be closest to the "pseudo-inhibition" of Sommer and Wennekers (2000, 2001). The purpose of these configurations is to determine whether it is necessary for inhibition to accurately reflect PC activity levels for accurate pattern recall.

Pattern Recall in CA3

To test recall in these networks, 50 random patterns, each consisting of 10 active PCs, were stored in the network using the Hebbian learning procedure described above. Then 5 PCs from a given pattern were stimulated using a constant current injection to cause them to fire and act as a recall cue. Network activity was monitored over a period of time to see if the remaining PCs of the stored pattern, or other PCs became active through the recurrent connections from the cued PCs.

With no inhibition in the network, most PCs become activated and so it cannot be said that the stored pattern is recalled. However, as illustrated in Fig. 4, a suitable level of inhibition results in reasonably accurate recall of the stored pattern. In Fig. 4a the network contains the "pseudo-inhibition" of Sommer and Wennekers

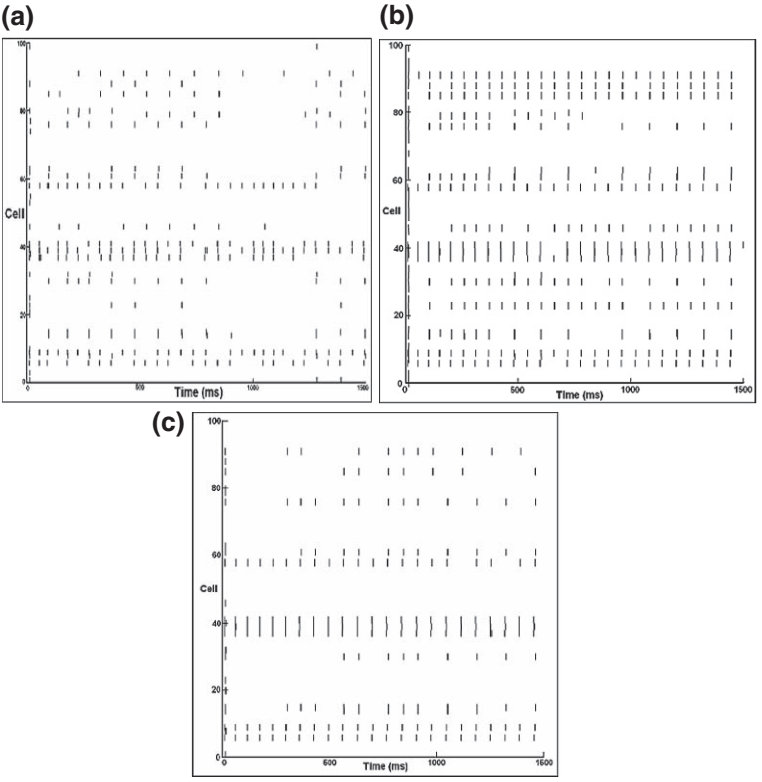

Fig. 4 Raster plots of pyramidal cell activity during recall over 1,500 ms in a partially connected (10%) net. (**a**) Pseudo-inhibition, (**b**) 1 BC, (**c**) 100 BCs

(2000, 2001). Now most active cells either belong to the cue or to the stored pattern. This is a partially connected network, which introduces noise into the recall procedure and results in occasional spurious firings of non-pattern PCs. Recall activity proceeds at around 20 Hz, at the low end of the gamma frequency range. Figure 4b, c illustrates recall with networks that include explicit interneurons. Recall dynamics and quality are very similar to the "pseudo-inhibition" case, irrespective as to whether there is a single inhibitory interneuron, or whether there is 100 INs. Thus it seems that recall is rather robust to the precise level of inhibition and whether or not it is in proportion to the PC activity level (which is relatively constant in these examples).

Heteroassociative Memory in CA1

In this section we describe a more detailed model, this time of the CA1 microcircuitry (Fig. 5). The principal excitatory cells of the CA1 region also are pyramidal cells. These cells are driven by excitatory inputs from layer III of the entorhinal cortex and the CA3 Schaffer collaterals and an inhibitory input from

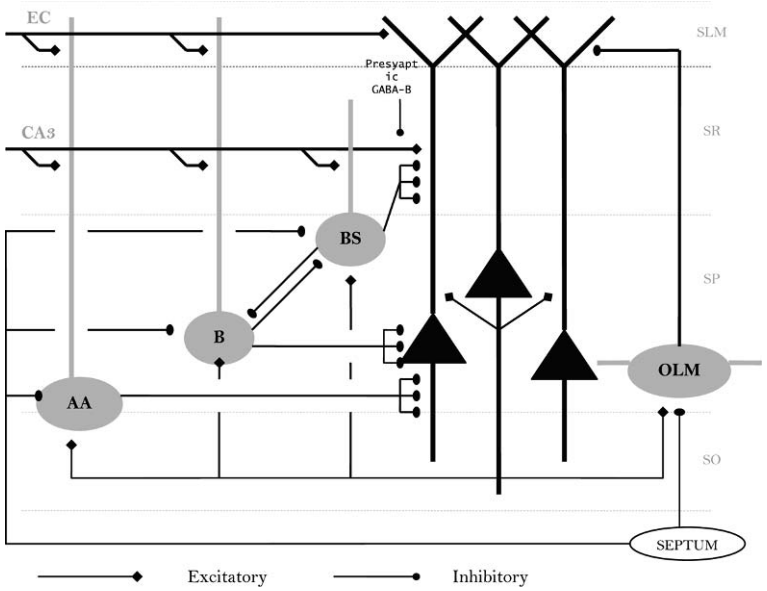

Fig. 5 Hippocampal CA1 microcircuit showing major cell types and their connectivity. *Black filled triangles*: pyramidal cells. *Grey filled circles*: CA1 inhibitory interneurons. EC: entorhinal cortex input; CA3: CA3 Schaffer collateral input; AA: axo-axonic cell; B: basket cell; BS: bistratified cell; OLM: oriens lacunosum-moleculare cell; SLM: stratum lacunosum-moleculare; SR: stratum radiatum; SP: stratum pyramidale; SO: stratum oriens. *Open circles*: Septal GABA inhibition. (Reproduced with permission from Cutsuridis et al. (2009a), Fig. 1, Copyright Wiley-Blackwell.)

the medial septum. Recurrent connectivity between pyramidal cells is negligible in CA1 (less than 1%). We construct a feedforward neural network model consisting of pyramidal cells and four types of inhibitory interneurons: basket cells, axo-axonic cells, bistratified cells and oriens lacunosum-moleculare cells. As with the CA3 model, a connectivity matrix is derived by storing patterns using Hebbian learning, as described above. This matrix is used to specify connectivity from CA3 PCs onto CA1 PCs, forming an excitatory feedforward network. Inhibitory connectivity is tuned to achieve accurate recall of stored patterns when CA3 PCs belonging to a particular stored pattern are active and thus act as a recall cue. Preliminary versions of this model has been published previously in Cutsuridis et al. (2007, 2008a), in Graham and Cutsuridis (2009) and in its complete form in Cutsuridis et al. (2009a) and Cutsuridis and Wennekers (2009).

The CA1 Network

The network contains 100 pyramidal cells (PC), 2 basket cells (BC), 1 bistratified cell (BSC), 1 axo-axonic cell (AAC) and 1 oriens lacunosum-moleculare (OLM) cell (see Fig. 5). All cell morphologies included a soma, apical and basal dendrites and a portion of axon. The dimensions of the somatic, axonic and dendritic

compartments of the model cells are presented in Table 3. The biophysical properties of each cell were adapted from cell types reported in the literature (Poirazi et al., 2003a, b; Saraga et al., 2003; Santhakumar et al., 2005). The complete mathematical formalism of the model is described in Appendix 2. The parameters of all passive and active ionic conductances used in the model are listed in Tables 4, 5, and 6. The synaptic waveform parameters are given in Table 7 and synaptic conductances are listed in Table 8.

Synaptic properties: In the model, AMPA, NMDA, GABA-A and GABA-B synapses are considered. GABA-A is present in all strata, whereas GABA-B is present in medium and distal SR and SLM dendrites. AMPA synapses are present in strata LM (EC connections) and radiatum (CA3 connections), whereas NMDA are present only in stratum radiatum (CA3 connections).

Model inputs: Inputs to the CA1 model come from the medial septum (MS), entorhinal cortex (EC) and CA3 Schaffer collaterals. The EC input is modelled as the firing of 20 entorhinal cortical cells at an average gamma frequency of 40 Hz (spike trains only modelled and not the explicit cells), and the CA3 input is modelled with the same gamma frequency spiking of 20 out of 100 CA3 pyramidal cells (see Appendix 2 for details). PCs, BCs, AACs, BSCs received CA3 input in their medial SR dendrites, whereas PCs, BCs and AACs received also the EC layer III input in their apical LM dendrites. EC inputs preceded CA3 inputs by 9 ms on average, in accord with experimental data showing that the conduction latency of the EC-layer III input to CA1 LM dendrites is less than 9 ms (ranging between 5 and 8 ms), whereas the conduction latency of EC-layer II input to CA1 radiatum dendrites via the di/tri-synaptic path is greater than 9 ms (ranging between 12 and 18 ms) (Leung et al., 1995; Soleng et al., 2003). MS input, which is modelled as the rhythmic firing of 10 septal cells (see Appendix 2 for details), provides GABA-A inhibition to all INs in the model (strongest to BC and AAC; Freund and Antal, 1988). MS input is phasic at theta rhythm and is on for 125 ms during the retrieval phase.

Presynaptic GABA-B inhibition: It has been shown that the strengths of the synaptic inputs from the EC perforant path and the CA3 Schaffer collaterals wax and wane according to the extracellular theta rhythm and 180° out of phase from each other (Brankack et al., 1993; Wyble et al., 2000). These cyclical theta changes are likely due to the presynaptic GABA-B inhibition to CA3 Schaffer collateral input to CA1 PCs' synapses, which is active during the storage cycle and inactive during recall (Molyneaux and Hasselmo, 2002). This is modelled simply as a reductive scaling during storage of the CA3-AMPA synaptic conductance, so that the effective conductance g' is

$$g' = g_s \cdot g \tag{1}$$

where g_s is the scaling factor (set to 0.4 in the presented simulations). During recall, g' is simply equal to g (the AMPA conductance determined by the connectivity weight matrix).

Pattern Recall in CA1

Hasselmo and colleagues (2002a, b) have hypothesized that the hippocampal theta rhythm (4–7 Hz) contributes to memory formation by separating storage and recall into different functional subcycles. Recent experimental evidence has shown that different types of inhibitory interneurons fire at different phases of the theta rhythm (Klausberger et al., 2003, 2004; Somogyi and Klausberger, 2005; Klausberger and Somogyi, 2008). Here, we demonstrate how the recall performance of previously stored patterns is affected by the presence/absence of various types of inhibitory interneurons, which fire at different phases of the simulated theta rhythm (Paulsen and Moser, 1998). A larger set of recall performance and memory capacity results can be found in Cutsuridis et al. (2009a).

As detailed previously, a set of patterns are stored by generating a weight matrix based on a clipped Hebbian learning rule, and using the weight matrix to prespecify the CA3 to CA1 PC connection weights. To test recall of a previously stored pattern, the associated input pattern is applied as a cue in the form of spiking of active CA3 inputs (those belonging to the pattern) distributed within a gamma frequency time window. The entire cue pattern is repeated at gamma frequency (40 Hz). At the same time, 20 EC inputs also fire randomly distributed within a 25 ms gamma window, but with mean activity preceding the CA3 activity by 9 ms. The CA3 spiking drives the CA1 PCs plus the B, AA and BS interneurons. The EC input also drives the B and AA interneurons.

To test pure recall by the CA3 input cue, the EC input is disconnected from the CA1 PCs and no learning takes place at CA3 synapses on CA1 PCs. The CA3 synapses are suppressed during the "storage" phase of theta. Pattern recall only occurs during the "recall" half-cycle. Typical firing patterns of the different cell types across theta cycles are illustrated in Fig. 6.

The recall of the first pattern in a set of five is shown in Fig. 7. Figure 7a shows a raster plot of the spiking of the septal (top 10 rows), EC (next 20 rows) and CA3 (bottom 100 rows) inputs. The remaining subplots show raster plots of CA1 PC activity for different configurations of network inhibition. Figure 7b shows CA1 activity with all inhibitory pathways present. The CA1 PCs are active two or three times during a theta recall cycle, with their spiking activity being a very close match to the stored pattern. Only occasional spurious firings are seen (see recall events at 900, 1,350 and 1,850 ms). Seven recall cycles are shown, following an initialization period of 200 ms.

To test the influence of the inhibitory pathways on recall, different pathways are selectively removed. Bistratified cell inhibition to the medial SR PC dendrites is hypothesized to mediate thresholding of PC firing during recall. Removal of BC and AAC inhibition does not spoil recall quality (Fig. 7c), as they both fire 180° out of phase with respect to the bistratified cells (Klausberger and Somogyi, 2008). Removal of all inhibitory pathways leads to gamma frequency firing of virtually all PCs during recall cycles and the CA3 cued pattern during storage cycles (Fig. 7d). In this latter case, without BC and AAC inhibition, the suppressed CA3 input in a storage cycle is still strong enough to fire the pattern cells, but not the non-pattern cells.

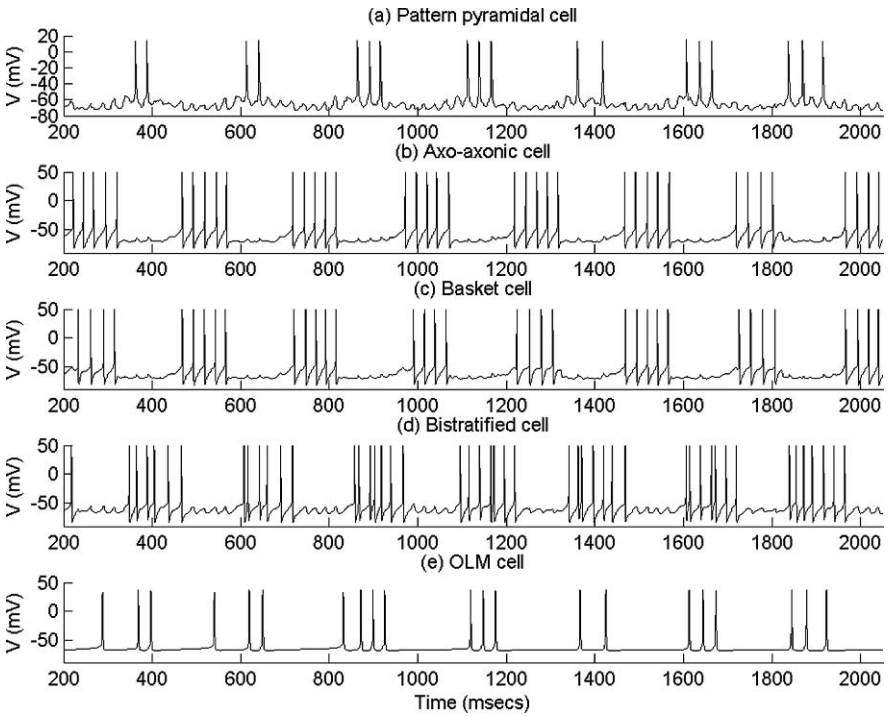

Fig. 6 Voltage traces in an example of a PC belonging to the pattern, and each type of inhibitory interneuron, for the recall episodes in the full network shown in Fig. 7b. (Reproduced with permission from Cutsuridis et al. (2009a), Fig. 10, Copyright Wiley-Blackwell.)

What happens to recall when the EC input is present in CA1 PCs? The EC input corresponding to the cued pattern could potentially aid recall. With such EC input, the pattern is now nearly perfectly recalled on each gamma cycle during a recall theta half-cycle, with occasional spurious firings (Cutsuridis et al., 2009a). OLM inhibition is hypothesized to remove interference from spurious EC input during recall. If the EC input is taken to be due to a different pattern from that of the CA3 input cue, i.e. CA1 PCs receiving the EC input may or may not belong to the cued pattern, then recall is disrupted by the spurious EC input, but this disruption is significantly worse if the OLM inhibition is absent (Cutsuridis et al., 2009a).

Justification

The hypothesis of associative memory function in the subsystems of the hippocampus cannot yet be tested by direct experiments. It is technically not possible to instantiate specific patterns of neural activity for either storage or subsequent recall. That such a process does take place is based on the suitability of the network architecture and evidence from tissue slice experiments of the Hebbian induction

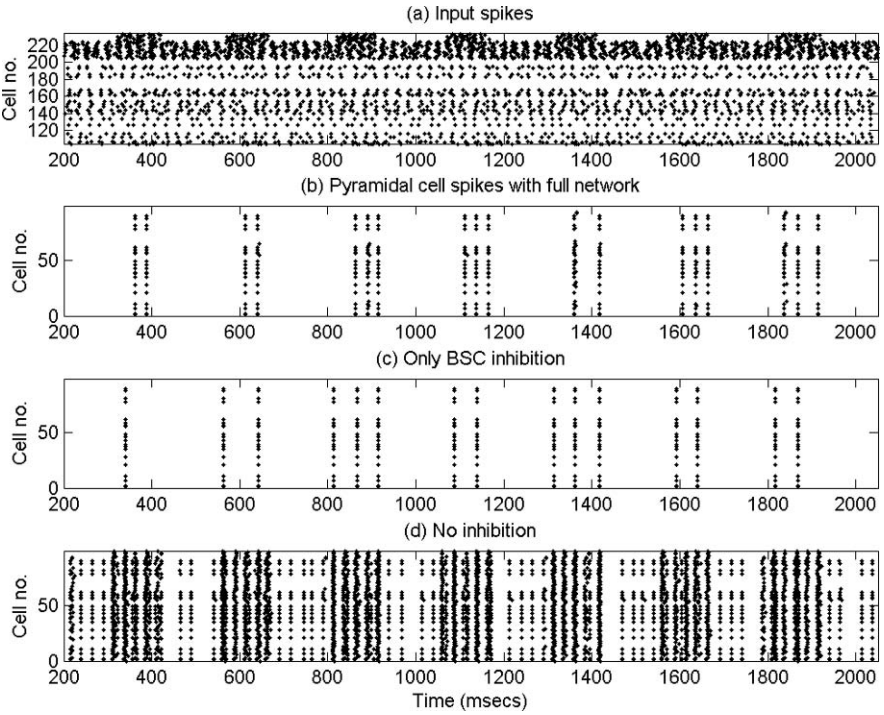

Fig. 7 Example of pattern recall in CA1. The CA3 input is cueing the first pattern in a stored set of five. EC input is present to drive the inhibitory interneurons, but is disconnected from the CA1 PCs, so that recall is purely due to the CA3 input cue. Seven 125 ms recall half-cycles are shown, starting at 300 ms (interspersed with 125 ms storage half-cycles, but STDP is turned off) (**a**) Raster plot showing the septal (*top* 10), EC (*next* 20) and CA3 input (*bottom* 100) spikes. (**b**) Raster plot showing CA1 PC activity – virtually the only active cells are those belonging to the stored pattern. (**c**) BC and AAC inhibition removed, so that recall is mediated only by BSC inhibition. (**d**) BSC and OLM inhibition also removed. (Reproduced with permission from Cutsuridis et al. (2009a), Fig. 9a, b and 11c, d, Copyright Wiley-Blackwell.)

of long-lasting changes in synaptic strength at the relevant connections (Bliss et al., 2007; Mellor, this volume). Behavioural experiments in mammals, including humans, implicate the hippocampus in the intermediate-term storage of episodic memories (see Eichenbaum, this volume). Thus we must rely on computational models to assess the recall and storage abilities of the neural subnetworks of the hippocampus. The models presented here are devised to address the specific issue of whether network inhibition provides suitable control of pyramidal cell activity to allow the successful recall of previously stored patterns. They build upon a variety of models that include different levels of biological realism in exploring associative memory function in the hippocampus (Kunec et al., 2005; Levy, 1996; Menschik and Finkel, 1998; Sommer and Wennekers, 2001; Wallenstein and Hasselmo, 1997). The advance from previous models is to test explicitly the roles during pattern recall

of defined populations of inhibitory interneurons that make specific spatial contacts onto pyramidal cells.

These network models are based upon identified cell types and their known connectivity. Cells of a particular type make connections to other cells at specific spatial locations on the receiving cell, according to the pre- and post-synaptic cell types. Connection probabilities are assumed to be uniform throughout a network, so that there are no spatial gradients in connectivity. Though we refer to these models as being of areas CA3 and CA1, it is better to consider them as models of subsets of these areas. Inter- and intra-areal connectivity does vary along the transverse and longitudinal axes of the hippocampus (Amaral and Witter, 1989; Amaral and Lavenex, 2007; Ishizuka et al., 1990; Li et al., 1994). Sufficient recurrent connectivity for autoassociative memory function may be restricted to subregion CA3a (de Almeida et al., 2007).

All cell models are derived from previously published models of the representative cell types. In turn, these published models are based on known anatomical and electrophysiological data. As detailed in the earlier chapters in the Computational Analysis section of this book, development of such models has reached a considerable degree of sophistication, but any given model still cannot be considered to be the complete and final model of a particular cell type. Simple, but multicompartmental cell anatomies are used here, which allow suitable spatial distributions of ion channels and segregation of synaptic inputs, while minimizing the computational load. The network behaviour studied here is rather robust to the precise details of the individual cell models.

With our autoassociative memory model of area CA3 we have tested whether feedback inhibition during recall needs to accurately reflect pyramidal cell (PC) activity (Hunter et al., 2009). A given basket cell (BC) is driven by many, but not all pyramidal cells in the surrounding network. The firing rate of a BC will be a function of the neural activity level in a sample of pyramidal cells. Thus neural activity across the population of BCs should be proportional to activity in the PC population. However, BCs are known to synchronize their firing through mutual inhibition and gap junction connections (Bartos et al., 2007). This leads to the possibility that the BC network acts more like a single, powerful BC that is activated by the entire population of PCs. In this case the main indicator of the level of PC activity would be the BC firing rate, which may be only moderately modulated by changes in PC activity. Here we tested the two extreme cases of a network with only a single BC driven by all PCs and a network with the same number of BCs as PCs, with each BC being driven by a single PC. The reality is somewhere between these extremes. In any case, the models demonstrate that recurrent inhibition is sufficient to effectively threshold PCs for accurate pattern recall and to maintain fairly constant PC activity levels. The consequence of this is that only a relatively constant level of inhibition is required, which can be provided by either network configuration. Thus the pattern recall process is rather robust to the precise connectivity of the feedback inhibitory network.

The heteroassociative memory model of CA1 is more detailed, containing four types of inhibitory interneuron (axo-axonic, basket, bistratified and oriens

lacunosum-moleculare cells) that form specific feedforward and feedback inhibitory circuits with spatially separated contacts onto PCs (Cutsuridis et al., 2009a). We have used this model to test the hypothesis that storage and recall of patterns can be temporally separated into successive theta rhythm half-cycles (Hasselmo et al., 2002a, b). In vivo recordings have determined that the different classes of interneuron are most active during distinct phases of theta (Klausberger et al., 2003, 2004; Somogyi and Klausberger, 2005; Klausberger and Somogyi, 2008). In particular, bistratified and O-LM cells are most active during the putative recall half-cycle, whereas basket and axo-axonic cells are most active during storage half-cycles. Thus we hypothesize that PC activity during recall is thresholded by inhibition to the proximal dendrites as provided by bistratified cells, rather than by perisomatic inhibition from basket cells. The model results clearly indicate that bistratified cell inhibition can indeed provide appropriate thresholding. In addition, feedback inhibition from O-LM cells can reduce interference to pattern recall from spurious entorhinal cortical inputs to PC distal dendrites. In further work (Cutsuridis et al., 2009a), we have shown that BC and AAC activity, combined with BSC and O-LM inactivity, during a storage half-cycle can effectively block PC output from the soma, while allowing sufficient dendritic excitability due to EC inputs to drive the activity-dependent changes in synaptic strength required for pattern storage. In summary, our model demonstrates that the phasic responses of different classes of inhibitory interneuron seen with in vivo recordings are compatible with the hypothesis that pattern storage and recall occur in separate theta half-cycles. Different IN pathways mediate control of PC activity thresholding and synaptic plasticity (Paulsen and Moser, 1998).

The Future

All aspects of the models we have presented are subject to refinement on the basis of current and future experimental data. This includes cell characteristics, cell types, network connectivity and synaptic strengths and their modification. Fine details of cellular anatomy and ion channel distributions may impact upon signal integration in cells and subsequent cell output. Computational modelling has been vital for examining signal integration in dendrites (Cook and Johnston, 1997; Graham, 2001; Kali and Freund, 2005; Migliore et al., 2005; Poirazi et al., 2003a, b). For example, the oblique dendrites of pyramidal cells may perform local, nonlinear processing of their inputs before integration in the apical trunk on the way to the soma (Poirazi et al., 2003a, b). Backpropagation of action potentials into obliques, which may be required for synaptic plasticity, is strongly influenced by local active membrane properties (Migliore et al., 2005). Further structure in the anatomy of our PC models would be required to capture these aspects, at the cost of computational expense. Nonetheless, these details will likely impact upon memory capacity and recall quality (Graham, 2001).

It is already well known that the inhibitory interneurons within CA3 and CA1 are incredibly diverse, with at least 16 different classes that can be identified

on morphological, electrophysiological and pharmacological grounds (Freund and Buzsaki, 1996; Maccafferi and Lacaille, 2003; Somogyi and Klausberger, 2005). Our CA1 model includes only four classes of inhibitory interneuron. It is clearly a major challenge to develop models that enable the definition and exploration of the function of these many different types of interneuron within the operating neural network. They are likely to provide further fine control of signal integration and synaptic plasticity in pyramidal cells, and may be variously active in different behavioural states of an animal (Axmacher et al., 2006; Klausberger and Somogyi, 2008). With our CA3 network model we are exploring the ability of particular architectures of inhibitory network to improve recall quality in partially connected networks of PCs (Hunter et al., 2008a, b, 2009).

An obvious extension to the models presented here is to explore pattern storage through the use of a suitable learning rule that captures the properties of long-term potentiation (LTP) and depression (LTD) at the pyramidal cell synapses. Here we have generated long-term synaptic strengths using a simple Hebbian learning rule, and these strengths are imposed upon the network when it is instantiated. A rule that could modify synaptic strengths on the basis of ongoing neural activity would allow the exploration of the dynamics of both storage and recall in the same network. An initial exploration in this direction shows that a spike-timing-dependent plasticity (STDP) rule based on the amplitude of postsynaptic voltage transients can be used to store patterns in these memory networks, and that such a pattern can subsequently be successfully recalled (Cutsuridis et al., 2009a). Inclusion of such learning rules within these network models also allows for the investigation of how learning can be modified by intrinsic cell properties and by the timing of inhibitory inputs directed to dendritic locations adjacent to the modifiable synapse (Cutsuridis et al., 2008b, 2009b, c; Paulsen and Moser, 1998; Sjostrom et al., 2008).

Other pathways in these networks are also modifiable, particularly the entorhinal input to the distal dendrites of CA1 PCs (Remondes and Schuman, 2002). Such modifiability could be included in the models via an STDP rule at these synapses. However, an hypothesis as to what information is being learnt, or stored, in this way is required. As discussed below, it seems likely that EC input also plays a significant role in determining CA1 output, which may be underpinned by the heteroassociation of patterns of EC activity with CA1 activity. The strength of inhibition is also modifiable through changes in the strength of excitatory synapses onto inhibitory interneurons. Learning rules at these synapses may be quite different, for example, anti-Hebbian (Lamsa et al., 2007). Network dynamics, and consequent storage and recall of patterns, are also affected by short-term changes in synaptic strength, on time scales of milliseconds to seconds (Sun et al., 2005).

Finally, our models look at information storage and retrieval in isolated hippocampal areas. They do not address the larger questions of information representation, recoding and flow through the hippocampus as a whole (Treves and Rolls, 1994). An assumption of our CA1 model is that EC input is largely responsible for instantiating a pattern of CA1 activity to be associated with a concurrent pattern of CA3 activity through modification of the Schaffer collateral synapses from CA3 PCs onto CA1 PCs. However, CA1 can still maintain sensory coding,

in so-called place cells, without the presence of CA3 (Brun et al., 2002), leading to the view that the direct EC input to CA1 is a major determinant of CA1 output, which may be modulated by the inputs via CA3 (Guzowski et al., 2004; Knierim et al., 2006). In this case the EC input may still contribute to pattern association between CA3 and CA1, but is at the same time determining CA1 spiking activity for output from the hippocampus. Given that EC inputs arrive at the distal apical dendrites of CA1 PCs, it is unclear how much effect they can have on PC spiking. Modelling studies indicate that dendritic spiking, driven by sodium or calcium currents, is crucial to the efficacy of EC inputs in generating output spiking (Kali and Freund, 2005). Since dendritic spiking may also contribute to synaptic plasticity (Golding et al., 2002), this allows for the possible dual role of EC input. There is also a significant inhibitory input to the PC apical dendrites associated with the EC input, the timing of which has significant effects on the efficacy and plasticity of CA3 inputs (Pissadaki and Poirazi, 2007; Remondes and Schuman, 2002).

In summary, computational neural network models of biophysically realistic neurons are invaluable in studying information processing, such as associative memory storage and retrieval, in hippocampal circuits. They are built upon available experimental data and allow the exploration of issues that currently are beyond the scope of experiments with real neural tissue.

Appendix 1: CA3 Cell Models

CA3 Pyramidal Cell Model

The model pyramidal cell is the two-compartment minimal model proposed by Pinsky and Rinzel (1994), that reproduces the essential spiking characteristics, including bursting behaviour, of CA3 pyramidal cells. The current balance equations for the two compartments (soma: s and dendrite: d) are

$$C_{\mathrm{m}}\frac{dV_{\mathrm{s}}}{dt} = -I_{\mathrm{leak}}(V_{\mathrm{s}}) - I_{\mathrm{Na}}(V_{\mathrm{s}}) - I_{\text{K-DR}}(V_{\mathrm{s}}) + \frac{g_{\mathrm{c}}}{p}(V_{\mathrm{d}} - V_{\mathrm{s}}) + \frac{I_S}{p}$$

$$C_{\mathrm{m}}\frac{dV_{\mathrm{d}}}{dt} = -I_{\mathrm{leak}}(V_{\mathrm{d}}) - I_{\mathrm{Ca}}(V_{\mathrm{d}}) - I_{\text{K-AHP}}(V_{\mathrm{d}}, \mathrm{Ca}) - I_{\text{K-C}}(V_{\mathrm{d}}, \mathrm{Ca}) - \frac{I_{\mathrm{syn}}}{(1-p)} + \frac{g_{\mathrm{c}}}{(1-p)}(V_{\mathrm{s}} - V_{\mathrm{d}}) + \frac{I_{\mathrm{d}}}{(1-p)}$$

The two compartments are connected by a coupling conductance, g_{c}, and have relative surface areas specified by p.

The active ionic currents in the soma are

I_{Na} – inward sodium current
$I_{\text{K-DR}}$ – outward delayed-rectifier potassium current

In the dendrite the active currents are

I_{Ca} – inward current and is carried by calcium and its activation, s, is fast.
$I_{\text{K-C}}$ – calcium-activated potassium current and is proportional to a fast activation variable, c, times a saturating function, $\chi(\text{Ca})$.
$I_{\text{K-AHP}}$ – has a slow activation variable q which is calcium dependent.

There is also a synaptic current, I_{syn}, which is a constant injected current.
The active ionic currents are given by the following equations:

$$\begin{aligned}
I_{\text{leak}}(V_{\text{s}}) &= \overline{g}_{\text{L}}(V_{\text{s}} - V_{\text{L}}) \\
I_{\text{leak}}(V_{\text{d}}) &= \overline{g}_{\text{L}}(V_{\text{d}} - V_{\text{L}}) \\
I_{\text{Na}}(V_{\text{s}}) &= \overline{g}_{\text{Na}} m_{\infty}^2(V_{\text{s}}) h(V_{\text{s}} - V_{\text{Na}}) \\
I_{\text{K-DR}}(V_{\text{s}}) &= \overline{g}_{\text{K-DR}} n(V_{\text{s}} - V_{\text{K}}) \\
I_{\text{Ca}}(V_{\text{d}}) &= \overline{g}_{\text{Ca}} s^2(V_{\text{d}} - V_{\text{Ca}}) \\
I_{\text{K-C}}(V_{\text{d}}, \text{Ca}) &= \overline{g}_{\text{K-C}} c\chi(\text{Ca})(V_{\text{d}} - V_{\text{K}}) \\
I_{\text{K-AHP}}(V_{\text{d}}, \text{Ca}) &= \overline{g}_{\text{K-AHP}} q(V_{\text{d}} - V_{\text{K}})
\end{aligned}$$

The kinetic equation for each of the gating variables h, n, s, c and q takes the form

$$\frac{dy}{dt} = \frac{(y_{\infty}(U) - y)}{\tau_y(U)}$$

The argument U equals V_{s} when $y = h, n$; V_{d} when $y = s, c$; and Ca when $y = q$. The steady state and time constant for each gating variable are derived from functions α_y, β_y, where $y_{\infty} = \alpha_y/(\alpha_y + \beta_y)$ and $\tau_y = 1/(\alpha_y + \beta_y)$. These functions for each gating variable are

$$\begin{aligned}
\alpha_{\text{m}} &= \frac{0.32(13.1 - V_{\text{s}})}{\exp((13.1 - V_{\text{s}})/4) - 1} \\
\beta_{\text{m}} &= \frac{0.28(V_{\text{s}} - 40.1)}{\exp((V_{\text{s}} - 40.1)/5) - 1} \\
\alpha_{\text{n}} &= \frac{0.016(35.1 - V_{\text{s}})}{\exp((35.1 - V_{\text{s}})/5) - 1} \\
\beta_{\text{n}} &= 0.25\ \exp(0.5 - 0.025 V_{\text{s}}) \\
\alpha_{\text{h}} &= 0.128\ \exp((17 - V_{\text{s}})/18) \\
\beta_{\text{h}} &= \frac{4}{1 + \exp((40 - V_{\text{s}})/5)} \\
\alpha_{\text{s}} &= \frac{1.6}{1 + \exp(-0.072(V_{\text{d}} - 65))}
\end{aligned}$$

$$\beta_s = \frac{0.02(V_d - 51.1)}{\exp((Vd - 51.1)/5) - 1}$$

$$\alpha_c = \frac{\exp((V_d - 10)/11) - \exp((V_d - 6.5)/27)}{18.975} \text{ for } V_d \leq 50$$

$$\alpha_c = 2\ \exp((6.5 - V_d)/27) \text{ for } V_d > 50$$

$$\beta_c = 2\ \exp((6.5 - V_d)/27) - \alpha_c \text{ for } V_d \leq 50$$

$$\beta_c = 0 \text{ for } V_d > 50$$

$$\alpha_q = \min((0.00002)\mathrm{Ca}, 0.01)$$

$$\beta_q = 0.001$$

The sodium current activates instantaneously ($m \equiv m_\infty(V_s)$).

These equations are supplemented by an equation for Ca^{2+} handling in the dendritic compartment,

$$\frac{d\mathrm{Ca}}{dt} = -0.13 I_{\mathrm{Ca}} - 0.075\mathrm{Ca}$$

All other parameter values for these equations are listed in Table 1.

Table 1 Parameter values CA3 pyramidal cell model

Mechanism	CA3 pyramidal cell
Leak conductance ($\overline{g}_L$) (mS/cm^2)	0.1
Sodium ($\overline{g}_{\mathrm{Na}}$) (mS/cm^2)	30
Delayed rectifier K^+ ($\overline{g}_{\mathrm{K\text{-}DR}}$) (mS/cm^2)	15
Calcium ($\overline{g}_{\mathrm{Ca}}$) (mS/cm^2)	10
Ca-activated potassium ($\overline{g}_{K-C}$) (mS/cm^2)	15
Potassium afterhyperpolarization ($\overline{g}_{\mathrm{K\text{-}AHP}}$) (mS/cm^2)	0.8
$\overline{g}_{\mathrm{NMDA}}$ (mS/cm^2)	0.0
$\overline{g}_{\mathrm{AMPA}}$ (mS/cm^2)	0.0
V_{Na} (mV)	120
V_{Ca} (mV)	140
V_{K} (mV)	−15
V_{L} (mV)	0
V_{Syn} (mV)	60
I_s (μA/cm^2)	−0.5
I_d (μA/cm^2)	0.0
g_c (mS/cm^2)	2.1
$p(\mathrm{area_d}/\mathrm{area_s})$	0.5
C_m (μF/cm^2)	3

Basket Cell Model

The basket cell (BC) is a five-compartment cell (Santhakumar et al., 2005) comprised of a soma (length = 20 μm, diameter = 4 μm), two apical dendritic compartments (length = 75 μm, diameter reduces outwards from the cell body through

sub-compartments 1–4) and two basal dendritic compartments (length = 50 μm, diameter reduces outwards from the cell body through sub-compartments 1–4). The reduction in diameter simulates the increase in resistance of the outer regions of the dendrite where a current injection of a larger value would be required to activate the cell's firing properties in the soma. Details of the active membrane properties are given below in Appendix 2, in the specification for the basket cell used in the CA1 model.

AMPA and GABA Synapse Models

Excitatory AMPA synapses onto PCs and BCs have a conductance with instantaneous rise time and an exponential decay with time constant 0.1 ms, a current reversal potential of 5 mV and a synaptic delay of 0.33 ms. The GABA-A synapses from the BCs onto the PCs have a conductance with a dual exponential waveform with rise time of 1 ms and decay time of 7 ms, a current reversal potential of −75 mV and a synaptic delay of 2 ms. The maximum conductance for each synaptic pathway for the different network configurations is given in Table 2.

Table 2 Maximum synaptic conductances (μS) in CA3 models

Model	PC-PC AMPA	PC-BC AMPA	GABA-A
Pseudo inhibition	0.0154	–	0.00017
1 basket cell	0.014	0.05	0.01
100 basket cells	0.014	0.18	0.003

Appendix 2: CA1 Cell Models

Pyramidal Cell Model

The geometry of the pyramidal cell, and for the other cell models for CA1, is given in Table 3. The active properties of the PC are derived from the model of Poirazi (see the on-line supplement to Poirazi et al., 2003a, b and Pissadaki and Poirazi, this volume). The somatic (s), axonic (a) and radiatum (rad), lacunosum-moleculare (LM) and oriens (ori) dendritic compartments of pyramidal cells obey the following current balance equations:

$$C\frac{dV_s}{dt} = -I_L - I_{Na} - I_{K-DR} - I_A - I_M - I_h - I_{sAHP} - I_{mAHP} - I_{CaL} - I_{CaT} - I_{CaR} - I_{buff} - I_{syn}$$

$$C\frac{dV_a}{dt} = -I_L - I_{Na} - I_{K-DR} - I_M - I_{syn}$$

Table 3 Structure of CA1 model cells

Dimensions	Pyramidal cell	Axo-axonic cell	Basket cell	Bistratified cell	OLM cell
Soma					
Diameter (μm)	10	10	10	10	10
Length (μm)	10	20	20	20	20
Total number of compartments (soma + dendritic compartments)	15	17	17	13	4
Dendritic compartments and dimensions (diameter × length, μm^2)					
Basal dendrite					3 × 250
Axon	1 × 150				1.5 × 150
Thick proximal SR dendrite	4 × 100				
Thick medium SR dendrite	3 × 100				
Thick distal SR dendrite	2 × 200				
Proximal SO dendrite	2 × 100				
Distal SO dendrite	1.5 × 200				
Thick SLM dendrite	2 × 100				
Medium SLM dendrite	1.5 × 100				
Thin SLM dendrite	1 × 50				
Thick SR dendrite		4 × 100	4 × 100	4 × 100	
Medium SR dendrite		3 × 100	3 × 100	3 × 100	
Thin SR dendrite		2 × 200	2 × 200	2 × 200	
Medium SLM dendrite		1.5 × 100	1.5 × 100		
Thin SLM dendrite		1 × 100	1 × 100		
Thick SO dendrite		2 × 100	2 × 100	2 × 100	
Medium SO dendrite		1.5 × 100	1.5 × 100	1.5 × 100	
Thin SO dendrite		1 × 100	1 × 100	1 × 100	

$$C\frac{dV_{\mathrm{rad,ori}}}{dt} = -I_{\mathrm{L}} - I_{\mathrm{Na}} - I_{\mathrm{K-DR}} - I_{\mathrm{A}} - I_{\mathrm{M}} - I_{\mathrm{h}} - I_{\mathrm{sAHP}} - I_{\mathrm{mAHP}} - I_{\mathrm{CaL}} - I_{\mathrm{CaT}} - I_{\mathrm{CaR}} - I_{\mathrm{buff}} - I_{\mathrm{syn}}$$

$$C\frac{dV_{\mathrm{LM}}}{dt} = -I_{\mathrm{L}} - I_{\mathrm{Na}} - I_{\mathrm{K-DR}} - I_{\mathrm{A}} - I_{\mathrm{syn}}$$

where I_{L} is the leak current, I_{Na} is the fast sodium current, $I_{\mathrm{K-DR}}$ is the delayed rectifier potassium current, I_{A} is the A-type K^+ current, I_{M} is the M-type K^+ current, I_{h} is a hyperpolarizing h-type current, I_{CaL}, I_{CaT} and I_{CaR} are the L-, T- and R-type Ca^{2+} currents, respectively, I_{sAHP} and I_{mAHP} are slow and medium Ca^{2+}-activated K^+ currents, I_{buff} is a calcium pump/buffering mechanism and I_{syn} is the synaptic

current. The conductance and reversal potential values for all ionic currents are listed in Table 4.

The sodium current is described by

$$I_{\mathrm{Na}} = \overline{g}_{\mathrm{Na}} \cdot m^2 \cdot h \cdot s \cdot (V - E_{\mathrm{Na}})$$

where an additional variable "s" is introduced to account for dendritic location-dependent slow attenuation of the sodium current.

Activation and inactivation kinetics for $\mathrm{I_{Na}}$ are given by

$$\begin{aligned} m_{t+dt} &= m_t + \left(1 + \exp -\frac{dt}{\tau_{\mathrm{m}}}\right) \cdot (m_{\mathrm{inf}} - m_t), \\ m_{\mathrm{inf}} &= \frac{1}{1 + \exp\left(-\frac{V+40}{3}\right)} \\ h_{t+dt} &= h_t + \left(1 - \exp\left(-\frac{dt}{\tau_{\mathrm{h}}}\right)\right) \cdot (h_{\mathrm{inf}} - h_t) \end{aligned}$$

$$\begin{aligned} h_{\mathrm{inf}} &= \frac{1}{1 + e\left(\frac{V+45}{3}\right)} \\ s_{t+dt} &= s_t + \left(1 + \exp\left(-\frac{dt}{\tau_\sigma}\right)\right) \cdot (s_{\mathrm{inf}} - s_t), \\ s_{\mathrm{inf}} &= \frac{1 + \mathrm{Na_{att}} \cdot \exp\left(\frac{V+60}{2}\right)}{1 + \exp\left(\frac{V+60}{2}\right)} \end{aligned}$$

with $dt = 0.1$ ms and time constants $\tau_{\mathrm{m}} = 0.05$ ms, $\tau_{\mathrm{h}} = 0.5$ ms, and

$$\tau_\sigma = \frac{0.00333(\mathrm{ms}) \cdot e^{0.0024(1/\mathrm{mV}) \cdot (V+60) \cdot Q(^\circ\mathrm{C})}}{1 + e^{0.0012(1/\mathrm{mV}) \cdot (V+60) \cdot Q(^\circ\mathrm{C})}}$$

The function $Q(^\circ\mathrm{C})$ is given by

$$Q(^\circ\mathrm{C}) = \frac{F}{R \cdot (T + ^\circ\mathrm{C})}$$

where $R = 8.315\,\mathrm{J}/^\circ\mathrm{C}$, $F = 9.648 \times 10^4$ Coul, $T = 273.16$ in Kelvin and $^\circ$C is the temperature in degrees Celsius. The $\mathrm{Na_{att}}$ variable represents the degree of sodium current attenuation and varies linearly from soma to distal trunk ($\mathrm{Na_{att}}\,\varepsilon[0 \rightarrow 1]$: maximum $\rightarrow$ zero attenuation).

The delayed rectifier current is given by

Table 4 Passive parameters and active ionic conductances of channels for all compartments of pyramidal model cells

Mechanism	Soma	Axon	OriProx	OriDist	RadProx	RadMed	RadDist	LM
C_m ($\mu F/cm^2$)	1	1	1	1	1	1	1	1
R_m (Ωcm^2)	20,000	20,000	20,000	20,000	20,000	20,000	20,000	20,000
R_a (Ωcm)	150	150	150	150	150	150	150	150
Leak conductance (S/cm^2)	0.0002	0.000005	0.000005	0.000005	0.000005	0.000005	0.000005	0.000005
Sodium conductance (S/cm^2)	0.007	0.1	0.007	0.007	0.007	0.007	0.007	0.007
Delayed rectifier K^+ conductance (S/cm^2)	0.0014	0.02	0.000868	0.000868	0.000868	0.000868	0.000868	0.000868
Proximal A-type K^+ conductance (S/cm^2)	0.0075	–	0.0075	0.0075	0.015	0	0	–
Distal A-type K^+ conductance (S/cm^2)	–	–	0	0	0	0.03	0.045	0.049
M-type K^+ conductance (S/cm^2)	0.06	0.03	0.06	0.06	0.06	0.06	0.06	–
I_h conductance (S/cm^2)	0.00005	–	0.00005	0.0001	0.0001	0.0002	0.00035	–
$V_{half,h}$ (mV)	−73	–	−81	−81	−82	−81	−81	–

Table 4 (continued)

Mechanism	Soma	Axon	OriProx	OriDist	RadProx	RadMed	RadDist	LM
L-type Ca^{2+} conductance (S/cm^2)	0.0007	–	0.000031635	0.000031635	0.000031635	0.0031635	0.0031635	–
T-type Ca^{2+} conductance (S/cm^2)	0.00005	–	0.0001	0.0001	0.0001	0.0001	0.0001	–
R-type Ca^{2+} conductance (S/cm^2)	0.0003	–	0.00003	0.00003	0.00003	0.00003	0.00003	–
Ca^{2+}-dependent sAHP K^+ conductance (S/cm^2)	0.0005	–	0.0005	0.0005	0.0005	0.0005	0.0005	–
Ca^{2+}-dependent mAHP K^+ conductance (S/cm^2)	0.09075	–	0.033	0.033	0.033	0.033	0.0041	–
E_L (mV)	−70	−70	−70	−70	−70	−70	−70	−70
E_{Na} (mV)	50	50	50	50	50	50	50	50
E_h, (mV)	−10	–	−10	−10	−10	−10	−10	−10
E_{Ca}, (mV)	140	–	140	140	140	140	140	–
E_K (mV)	−80	−80	−80	−80	−80	−80	−80	−80

$$I_{\mathrm{K-DR}} = \overline{g}_{\mathrm{K-DR}} \cdot m^2 \cdot (V - E_{\mathrm{K}})$$
$$m_{t+dt} = m_t + \left(1 - \exp\left(-\frac{dt}{2.2}\right)\right) \cdot (m_{\mathrm{inf}} - m_t),$$
$$m_{\mathrm{inf}} = \frac{1}{1 + \exp\left(-\frac{V+42}{2}\right)}$$

The sodium and delayed rectifier channel properties are slightly different in the soma, axon and dendritic arbor. To fit experimental data regarding the backpropagation of spike trains, soma and axon compartments have a lower threshold for Na^+ spike initiation (≈ -57 mV) than dendritic ones (≈ -50 mV). Thus, the m_{inf} and h_{inf} somatic/axonic HH channel kinetics as well as the time constants for both $I_{\mathrm{Na}}^{\mathrm{sa}}$ and $I_{\mathrm{K-DR}}^{\mathrm{sa}}$ are modified as follows. For the sodium

$$m_{\mathrm{inf}}^{\mathrm{sa}} = \frac{1}{1 + \exp\left(-\frac{V+44}{3}\right)},$$
$$h_{\mathrm{inf}}^{\mathrm{sa}} = \frac{1}{1 + \exp\left(\frac{V+49}{3.5}\right)}$$

while for the potassium delayed rectifier

$$m_{\mathrm{inf}}^{\mathrm{sa}} = \frac{1}{1 + \exp\left(-\frac{V+46.3}{3}\right)}$$

The somatic time constant for somatic/axonic Na^+ channel activation is kept the same $\tau_{\mathrm{m}} = 0.05$ ms while for inactivation is set to $\tau_{\mathrm{h}} = 1$ ms. The τ value for the delayed rectifier channel activation is set to $\tau_{\mathrm{m}} = 3.5$ ms. In all of the following equations, τ values are given in ms.

The fast inactivating A-type K^+ current is described by

$$I_{\acute{\mathrm{A}}} = \overline{g}_{\mathrm{A}} \cdot n_{\mathrm{A}} \cdot l \cdot (V - E_{\mathrm{K}})$$
$$n_{\mathrm{A}}(t+1) = n_{\mathrm{A}}(t) + (n_{A_\infty} - n_{\mathrm{A}}(t)) \cdot (1 - e^{-dt/\tau_{\mathrm{n}}})$$

where $\tau_{\mathrm{n}} = 0.2$ ms

$$n_{\mathrm{A}_\infty} = \frac{\alpha_{\mathrm{n_A}}}{\alpha_{\mathrm{n_A}} + \beta_{\mathrm{n_A}}}$$
$$\alpha_{\mathrm{n_A}} = \frac{-0.01(V+21.3)}{e^{-(V+21.3)/35} - 1}, \qquad \beta_{\mathrm{n_A}} = \frac{0.01(V+21.3)}{e^{(V+21.3)/35} - 1}$$
$$l(t+1) = l(t) + (l_\infty - l(t)) \cdot (1 - e^{-dt/\tau_{\mathrm{l}}})$$
$$l_\infty = \frac{\alpha_{\mathrm{l}}}{\alpha_{\mathrm{l}} + \beta_{\mathrm{l}}}$$
$$\alpha_{\mathrm{l}} = \frac{-0.01(V+58)}{e^{(V+58)/8.2} - 1}, \qquad \beta_{\mathrm{l}} = \frac{0.01(V+58)}{e^{-(V+58)/8.2} - 1}$$

where $\tau_l = 5 + 2.6(V + 20)/10$, if $V > 20\,\text{mV}$ and $\tau_l = 5$, elsewhere.

The hyperpolarizing h-current is given by

$$I_h = g_h \cdot tt \cdot (V - E_h)$$
$$\frac{dtt}{dt} = \frac{tt_\infty - tt}{\tau_{tt}}$$
$$tt_\infty = \frac{1}{1 + e^{-(V - V_{halft})/k_l}}, \qquad \tau_{tt} = \frac{e^{0.0378 \cdot \varsigma \cdot gmt \cdot (V - V_{halft})}}{qtl \cdot q10^{(T-33)/10} \cdot a0t \cdot (1 + a_{tt})}$$
$$a_{tt} = e^{0.00378 \cdot \varsigma \cdot (V - V_{halft})}$$

where ζ, gmt, $q10$ and qtl are 2.2, 0.4, 4.5 and 1, respectively, $a0t$ is 0.0111 1/ms, $V_{halft} = -75\,\text{mV}$ and $k_l = -8$.

The slowly activating voltage-dependent potassium current, I_M, is given by the equations:

$$I_m = 10^{-4} \cdot T_{adj}(^\circ\text{C}) \cdot \overline{g}_m \cdot m \cdot (V - E_K)$$
$$T_{adj}(^\circ\text{C}) = 2.3^{(^\circ\text{C}-23)/10}$$
$$m_{t+dt} = m_t + \left(1 - e\left(-\frac{dt \cdot T_{adj}(^\circ\text{C})}{\tau}\right)\right) \cdot \left(\frac{\alpha(V)}{(\alpha(V) + \beta(V)} - m_t\right)$$
$$\alpha(V) = 10^{-3} \cdot \frac{(V + 30)}{(1 - e^{-(V+30)/9})}$$
$$\beta(V) = -10^{-3} \cdot \frac{(V + 30)}{(1 - e^{(V+30)/9})}$$
$$\tau = \frac{1}{\alpha(V) + \beta(V)}$$

The slow afterhyperpolarizing current, I_{sAHP}, is given by

$$I_{sAHP} = \overline{g}_{sAHP} \cdot m^3 \cdot (V - E_K)$$
$$\frac{dm}{dt} = \frac{\frac{\text{Cac}}{(1+\text{Cac})} - m}{\tau}$$
$$\tau = \max\left(\frac{1}{0.003(1/\text{ms}) \cdot (1 + \text{Cac}) \cdot 3^{(^\circ\text{C}-22)/10}}, 0.5\right)$$

where $\text{Cac} = (\text{Ca}_{in}/0.025(\text{mM}))^2$.

The medium afterhyperpolarizing current, I_{mAHP}, is given by

$$
\begin{aligned}
I_{\mathrm{mAHP}} &= \overline{g}_{\mathrm{mAHP}} \cdot m \cdot (V - E_{\mathrm{K}}) \\
m_{t+dt} &= m_t + \left(1 + \exp\left(-\frac{dt}{\tau_{\mathrm{m}}}\right)\right) \cdot \left(\frac{\alpha_{\mathrm{m}}(V)}{\tau_{\mathrm{m}}} - m_t\right) \\
\alpha_{\mathrm{m}}(V) &= \frac{0.48(1/\mathrm{ms})}{1 + \frac{0.18(\mathrm{mM})}{\mathrm{Ca_{in}}} \cdot e^{(-1.68 \cdot V \cdot Q(^{\circ}\mathrm{C}))}} \\
\beta_{\mathrm{m}}(V) &= \frac{0.28(1/\mathrm{ms})}{1 + \frac{\mathrm{Ca_{in}}}{0.011(\mathrm{mM}) \cdot e^{(-2 \cdot V \cdot Q(^{\circ}\mathrm{C}))}}} \\
\tau_{\mathrm{m}} &= \frac{1}{\alpha_{\mathrm{m}}(V) + \beta_{\mathrm{m}}(V)}
\end{aligned}
$$

The somatic high-voltage-activated (HVA) L-type Ca^{2+} current is given by

$$
\begin{aligned}
I^s_{\mathrm{CaL}} &= \overline{g}^s_{\mathrm{CaL}} \cdot m \cdot \frac{0.001\,\mathrm{mM}}{0.001\,\mathrm{mM} + \mathrm{Ca_{in}}} \cdot ghk(V, \mathrm{Ca_{in}}, \mathrm{Ca_{out}}) \\
\alpha_{\mathrm{m}}(V) &= -0.055 \cdot \frac{(V + 27.01)}{e^{-(V+27.01)/3.8} - 1} \\
\beta_{\mathrm{m}}(V) &= 0.94 \cdot e^{-(V+63.01)/17} \\
\tau_{\mathrm{m}} &= \frac{1}{5(\alpha_{\mathrm{m}}(V) + \beta_{\mathrm{m}}(V))}
\end{aligned}
$$

whereas the dendritic L-type calcium channels have different kinetics:

$$
\begin{aligned}
I^d_{\mathrm{CaL}} &= \overline{g}^d_{\mathrm{CaL}} \cdot m^3 \cdot h \cdot (V - E_{\mathrm{Ca}}) \\
\alpha(V) &= \frac{1}{1 + e^{-(V+37)}}, \beta(V) = \frac{1}{1 + e^{(V+41)/0.5}}
\end{aligned}
$$

Their time constants are equal to $\tau_{\mathrm{m}} = 3.6\,\mathrm{ms}$ and $\tau_{\mathrm{h}} = 29\,\mathrm{ms}$.
The low-voltage-activated (LVA) T-type Ca^{2+} channel kinetics are given by

$$
\begin{aligned}
I_{\mathrm{CaT}} &= \overline{g}_{\mathrm{CaT}} \cdot m^2 \cdot h \frac{0.001\,\mathrm{mM}}{0.001\,\mathrm{mM} + \mathrm{Ca_{in}}} \cdot ghk(V, \mathrm{Ca_{in}}, \mathrm{Ca_{out}}) \\
ghk(V, \mathrm{Ca_{in}}, \mathrm{Ca_{out}}) &= -x \cdot (1 - \tfrac{\mathrm{Ca_{in}}}{\mathrm{Ca_{out}}} \cdot e^{V/x}) \cdot f(V/x) \\
x &= \frac{0.0853 \cdot (T + ^{\circ}\mathrm{C})}{2}, \; f(z) = \begin{cases} 1 - \frac{z}{2} & \text{if abs(z)} < 10^{-4} \\ \frac{z}{e^z - 1} & \text{otherwise} \end{cases}
\end{aligned}
$$

$$m_{t+dt} = m_t + (1 + e^{-dt/\tau_m}) \cdot \left(\frac{\alpha_{m(V)}}{\alpha_m(V) + \beta_m(V)} - m_t \right)$$
$$h_{t+dt} = h_t + (1 - e^{-dt/\tau_h}) \cdot \left(\frac{\alpha_h(V)}{\alpha_h(V) + \beta_h(V)} - h_t \right)$$
$$\alpha_m(V) = -0.196 \cdot \frac{(V - 19.88)}{e^{-(V-19.88)/10} - 1}, \beta_m(V) = 0.046 \cdot e^{-(V/22.73)}$$
$$\alpha_h(V) = 0.00016 \cdot e^{-(V+57)/19}, \beta_h(V) = \frac{1}{e^{-(V-15)/10} + 1}$$
$$\tau_m = \frac{1}{\alpha_m(V) + \beta_m(V)}, \tau_h = \frac{1}{0.68 \cdot (\alpha_h(V) + \beta_h(V)}$$

where Ca_{in} and Ca_{out} are the internal and external calcium concentrations. The HVA R-type Ca^{2+} current is described by

$$I_{CaR} = \overline{g}_{CaR} \cdot m^3 \cdot h \cdot (V - E_{Ca})$$
$$m_{t+dt} = m_t + (1 + e^{-dt/\tau_m}) \cdot (\alpha(V) - m_t)$$
$$h_{t+dt} = h_t + (1 - e^{-dt/\tau_h}) \cdot (\beta(V) - h_t)$$

The difference between somatic and dendritic CaR currents lies in the $\alpha(V)$, $\beta(V)$ and τ parameter values. For the somatic current, $\tau_m = 100\,\text{ms}$ and $\tau_h = 5\,\text{ms}$ while for the dendritic current $\tau_m = 50\,\text{ms}$ and $\tau_h = 5\,\text{ms}$. The $\alpha(V)$ and $\beta(V)$ equations for dendritic CaR channels are

$$\alpha(V) = \frac{1}{1 + e^{-(V+48.5)/3}}, \beta(V) = \frac{1}{1 + e^{(V+53)}}$$

while for the somatic CaR channels

$$\alpha(V) = \frac{1}{1 + e^{-(V+60)/3}}, \beta(V) = \frac{1}{1 + e^{(V+62)}}$$

Finally, a calcium pump/buffering mechanism is inserted at the cell body and along the apical and basal trunk. The kinetic equations are given by (where $f_e = 10,000/18$)

$$\text{drive\_channel} = \begin{cases} -f_e \cdot \frac{I_{Ca}}{0.2 \cdot F} & \text{if drive\_channel} > 0\,\text{mM/ms} \\ 0 & \text{otherwise} \end{cases}$$
$$\frac{d\text{Ca}}{dt} = \text{drive\_channel} + \frac{(10^{-4}(\text{mM}) - \text{Ca})}{7 \cdot 200\,(\text{ms})}$$

Axo-axonic, Basket and Bistratified Cell Models

Active properties of these cells are derived from the interneuron model of Santhakumar et al. (2005). All compartments obey the following current balance equation:

$$C_m \frac{dV}{dt} = I_{\text{ext}} - I_{\text{L}} - I_{\text{Na}} - I_{\text{K-DR,fast}} - I_{\text{A}} - I_{\text{CaL}} - I_{\text{CaN}} - I_{\text{AHP}} - I_{\text{C}} - I_{\text{syn}}$$

where C_m is the membrane capacitance, V is the membrane potential, I_{L} is the leak current, I_{Na} is the sodium current, $I_{\text{K-DR,fast}}$ is the fast delayed rectifier K^+ current, I_{A} is the A-type K^+ current, I_{CaL} is the L-type Ca^{2+} current, I_{CaN} is the N-type Ca^{2+} current, I_{AHP} is the Ca^{2+}-dependent K^+ (SK) current, I_{C} is the Ca^{2+} and voltage-dependent K^+ (BK) current and I_{syn} is the synaptic current. The conductance and reversal potential values of all ionic currents are listed in Table 5.

Table 5 Passive parameters and active ionic conductances of channels for all compartments of axo-axonic, basket and bistratified model cells

Mechanism	Axo-axonic cell	Basket cell	Bistratified cell
C_m (μF/cm^2)	1.4	1.4	1.4
R_a (Ωcm)	100	100	100
Leak conductance (S/cm^2)	0.00018	0.00018	0.00018
Sodium (S/cm^2)	0.15	0.2	0.3
Delayed rectifier K^+ (S/cm^2)	0.013	0.013	0.013
A-type K^+ (S/cm^2)	0.00015	0.00015	0.00015
L-type Ca^{2+} (S/cm^2)	0.005	0.005	0.005
N-type Ca^{2+} (S/cm^2)	0.0008	0.0008	0.0008
Ca^{2+}-dependent K^+ (S/cm^2)	0.000002	0.000002	0.000002
Ca^{2+}- and voltage-dependent K^+ (S/cm^2)	0.0002	0.0002	0.0002
Time constant for decay of intracellular Ca^{2+} (ms)	10	10	10
Steady-state intracellular Ca^{2+} concentration (μM)	$5.e^{-6}$	$5.e^{-6}$	$5.e^{-6}$
E_{Na} (mV)	55	55	55
E_{K} (mV)	-90	-90	-90
E_{Ca} (mV)	130	130	130
E_{L} (mV)	-60	-60	-60
$[Ca^{2+}]_0$ (μM)	2	2	2

The sodium current and its kinetics are described by

$$I_{\text{Na}} = g_{\text{Na}} m^3 h (V - E_{\text{Na}})$$
$$\frac{dm}{dt} = \alpha_{\text{m}}(1 - m) - \beta_{\text{m}} m,\ \alpha_{\text{m}} = \frac{-0.3(V - 25)}{(1 - e^{(V-25)/-5})},\ \beta_{\text{m}} = \frac{0.3(V - 53)}{(1 - e^{(V-53)/5})}$$
$$\frac{dh}{dt} = \alpha_{\text{h}}(1 - h) - \beta_{\text{h}} h,\ \alpha_{\text{h}} = \frac{0.23}{e^{(V-3)/20}},\ \beta_{\text{h}} = \frac{3.33}{(1 + e^{(V-55.5)/-10})}$$

The fast delayed rectifier K^+ current, $I_{\text{K-DR,fast}}$, is given by

$$I_{\mathrm{K-DR,fast}} = g_{\mathrm{K-DR,fast}} n_{\mathrm{f}}^4 (V - E_{\mathrm{K}})$$
$$\frac{dn_{\mathrm{f}}}{dt} = \alpha_{\mathrm{n_f}}(1 - n_{\mathrm{f}}) - \beta_{\mathrm{n_f}} n_{\mathrm{f}}$$
$$\alpha_{\mathrm{n_f}} = \frac{-0.07(V - 47)}{(1 - e^{(V-47)/-6})}$$
$$\beta_{\mathrm{n_f}} = 0.264\, e^{(V-22)/4}$$

The N-type Ca^{2+} current, I_{CaN}, is given by

$$I_{\mathrm{CaN}} = g_{\mathrm{CaN}} c^2 d (V - E_{\mathrm{Ca}})$$
$$\frac{dc}{dt} = \alpha_{\mathrm{c}}(1 - c) - \beta_{\mathrm{c}} c,\ \alpha_{\mathrm{c}} = \frac{0.19(19.88 - V)}{(e^{(19.88-V)/10} - 1)},\ \beta_{\mathrm{c}} = 0.046 e^{-V/20.73}$$
$$\frac{dd}{dt} = \alpha_{\mathrm{d}}(1 - d) - \beta_{\mathrm{d}} d,\ \alpha_{\mathrm{d}} = 1.6 \cdot 10^{-4} e^{-V/48.4},\ \beta_{\mathrm{d}} = \frac{1}{(1 + e^{(39-V)/10})}$$

The Ca^{2+}-dependent K^+ (SK) current, I_{AHP}, is described by

$$I_{\mathrm{AHP}} = g_{\mathrm{AHP}} q^2 (V - E_{\mathrm{K}})$$
$$\frac{dq}{dt} = \alpha_{\mathrm{q}}(1 - q) - \beta_{\mathrm{q}} q$$

$$\alpha_{\mathrm{q}} = \frac{0.00246}{e^{(12 \cdot \log_{10}([\mathrm{Ca}^{2+}]) + 28.48)/-4.5}},\ \beta_{\mathrm{q}} = \frac{0.006}{e^{(12 \cdot \log_{10}([\mathrm{Ca}^{2+}]) + 60.4)/35}}$$

$$\frac{d[\mathrm{Ca}^{2+}]_{\mathrm{i}}}{dt} = B \sum_{T,N,L} I_{\mathrm{Ca}} - \frac{[\mathrm{Ca}^{2+}]_{\mathrm{i}} - [\mathrm{Ca}^{2+}]_0}{\tau}$$

where $B = 5.2 \cdot 10^{-6}/Ad$ in units of mol/(C m^3) for a shell of surface area A and thickness d (0.2 μm), and $\tau = 10$ ms was the calcium removal rate. $[\mathrm{Ca}^{2+}]_0 = 5$ μM was the resting calcium concentration.

The Ca^{2+} and voltage-dependent K^+ (BK) current, I_{c}, is

$$I_{\mathrm{C}} = g_{\mathrm{c}} o (v - E_{\mathrm{K}})$$

where o is the activation variable (Migliore et al. J. Neurophysiol. 73:1157–1168, 1995). The A-type K^+ current, I_A, is described by

$$I_{\mathrm{A}} = g_{\mathrm{A}} ab(V - E_{\mathrm{k}})$$

$$\frac{da}{dt} = \alpha_{\mathrm{a}}(1 - a) - \beta_{\mathrm{a}} a$$

$$\alpha_{\mathrm{a}} = \frac{0.02(13.1 - V)}{e^{13.1 - V/10} - 1},\ \beta_{\mathrm{a}} = \frac{0.0175(V - 40.1)}{e^{V - 40.1/10} - 1}$$

$$\frac{db}{dt} = \alpha_{\mathrm{b}}(1 - b) - \beta_{\mathrm{b}} b$$

$$\alpha_{\mathrm{b}} = 0.0016\, e^{-13 - V/18},\ \beta_{\mathrm{b}} = \frac{0.05}{1 + e^{10.1 - V/5}}$$

The L-type Ca^{2+} current, I_{CaL}, is described by

$$I_{\mathrm{CaL}} = g_{\mathrm{CaL}} \cdot s_{\infty}^{2} \cdot V \cdot \frac{1 - \frac{[\mathrm{Ca}^{2+}]_{\mathrm{i}}}{[\mathrm{Ca}^{2+}]_{0}} e^{2\mathrm{FV/kT}}}{1 - e^{2\mathrm{FV/kT}}}$$

where g_{CaL} is the maximal conductance, s_{∞} is the steady-state activation variable, F is Faraday's constant, T is the temperature, k is Boltzmann's constant, $[\mathrm{Ca}^{2+}]_0$ is the equilibrium calcium concentration and $[\mathrm{Ca}^{2+}]_{\mathrm{i}}$ is described above. The activation variable, s_{∞}, is then

$$s_{\infty} = \frac{\alpha_{\mathrm{s}}}{\alpha_{\mathrm{s}} + \beta_{\mathrm{s}}},\ \alpha_{\mathrm{s}} = \frac{15.69(-V + 81.5)}{e^{-V + 81.5/10} - 1},\ \beta_{\mathrm{s}} = 0.29 \cdot e^{-V/10.86}$$

OLM Cell Model

Active properties are derived from the model of Saraga et al. (2003). The somatic (s), axonic (a) and dendritic (d) compartments of each OLM cell obeyed the following current balance equations:

$$C_m \frac{dV_{\mathrm{s}}}{dt} = I_{\mathrm{ext}} - I_{\mathrm{L}} - I_{\mathrm{Na,s}} - I_{\mathrm{K,s}} - I_{\mathrm{A}} - I_{\mathrm{h}} - I_{\mathrm{syn}}$$

$$C_m \frac{dV_{\mathrm{d}}}{dt} = I_{\mathrm{ext}} - I_{\mathrm{L}} - I_{\mathrm{Na,d}} - I_{\mathrm{K,d}} - I_{\mathrm{A}} - I_{\mathrm{syn}}$$

$$C_m \frac{dV_{\mathrm{a}}}{dt} = I_{\mathrm{ext}} - I_{\mathrm{L}} - I_{\mathrm{Na,d}} - I_{\mathrm{K,d}}$$

The conductance and reversal potential values per compartment are listed in Table 6.

Table 6 Passive parameters and active ionic conductances of channels for all compartments of OLM model cells

	Compartment		
Mechanism	Soma	Dendrite	Axon
C_m ($\mu F/cm^2$)	1.3	1.3	1.3
R_a (Ωcm)	150	150	150
Leak conductance (S/cm^2)	0.00005	0.00005	0.00005
E_L (mV)	–70	–70	–70
Sodium (S/cm^2)	0.0107	0.0234	0.01712
E_{Na} (mV)	90	90	90
Delayed rectifier K^+ (S/cm^2)	0.0319	0.046	0.05104
E_K (mV)	–100	–100	–100
A-type K^+ (S/cm^2)	0.0165	0.004	–
E_A (mV)	–100	–100	–100
I_h (S/cm^2)	0.0005	–	–
E_h (mV)	–32.9	–32.9	–32.9

Table 7 Synaptic parameters

Mechanisms	AMPA	NMDA	GABA-A	GABA-B
Rise (ms)	0.5	2.3	1	35
Fall (ms)	3	100	8	100
Reversal potential (mV)	0	0	–75	–75

Table 8 Synaptic conductance parameters (in μS). Text in parenthesis signifies the type of post-synaptic receptor

		Postsynaptic							
		EC	CA3	Septum	Pyr	AAC	BC	BSC	OLM
Presynaptic	EC				0.001 (AMPA)	0.00015 (AMPA)	0.00015 (AMPA)	0.00015 (AMPA)	
	CA3				0.0005 (NMDA)	0.00015 (AMPA)	0.00015 (AMPA)	0.00015 (AMPA)	
	Septum					0.02 (GABA-A)	0.02 (GABA-A)		
	Pyr				0.001 (AMPA)	0.0005 (AMPA)	0.0005 (AMPA)	0.0005 (AMPA)	0.0005 (AMPA)
	AAC				0.04 (GABA-A)				
	BC				0.02 (GABA-A)	0.001 (GABA-A)		0.02 (GABA-A)	
	BSC				0.002 (GABA-A) 0.0004 (GABA-B)		0.01 (GABA-A)		
	OLM				0.04 (GABA-A) 0.0004 (GABA-B)		0.01 (GABA-A)		

The sodium current is described by

$$I_{\mathrm{Na}} = g_{\mathrm{Na}} m^3 h (V - E_{\mathrm{Na}})$$
$$\frac{dm}{dt} = \alpha_{\mathrm{m}}(1 - m) - \beta_{\mathrm{m}} m$$
$$\frac{dh}{dt} = \alpha_{\mathrm{h}}(1 - h) - \beta_{\mathrm{h}} h$$

where m and h are the activation and inactivation variables, respectively. The forward and backward rate constants are described by

$$\alpha_{\mathrm{m,soma/axon}} = \frac{-0.1(V + 38)}{\exp\left(\frac{-(V+38)}{10}\right) - 1},\ \beta_{\mathrm{m,soma/axon}} = 4\ \exp\left(\frac{-(V + 63)}{18}\right)$$
$$\alpha_{\mathrm{h,soma/axon}} = 0.07\ \exp\left(\frac{-(V + 63)}{20}\right),\ \beta_{\mathrm{h,soma/axon}} = \frac{1}{1 + \exp\left(\frac{-(V+33)}{10}\right)}$$
$$\alpha_{\mathrm{m,dend}} = \frac{-0.1(V + 45)}{\exp\left(\frac{-(V+45)}{10}\right) - 1},\ \beta_{\mathrm{m,dend}} = 4\ \exp\left(\frac{-(V + 70)}{18}\right)$$
$$\alpha_{\mathrm{h,dend}} = 0.07\ \exp\left(\frac{-(V + 70)}{20}\right),\ \beta_{\mathrm{h,dend}} = \frac{1}{1 + \exp\left(\frac{-(V+40)}{10}\right)}$$

The potassium current, I_{K}, is described by

$$I_{\mathrm{K}} = g_{\mathrm{K}} n^4 (V - E_{\mathrm{K}})$$
$$\frac{dn}{dt} = \alpha_{\mathrm{n}}(1 - n) - \beta_{\mathrm{n}} n$$

where n is the activation variable for this channel. The forward and backward constants are described by

$$\alpha_{\mathrm{n,soma/axon}} = \frac{-0.018(V - 25)}{\exp\left(\frac{-(V-25)}{25}\right) - 1},\ \beta_{\mathrm{n,soma/axon}} = \frac{0.0036(V - 35)}{\exp\left(\frac{V-35}{12}\right) - 1}$$
$$\alpha_{\mathrm{n,dend}} = \frac{-0.018(V - 20)}{\exp\left(\frac{-(V-20)}{21}\right) - 1},\ \beta_{\mathrm{n,soma/axon}} = \frac{0.0036(V - 30)}{\exp\left(\frac{V-30}{12}\right) - 1}$$

The transient potassium current, I_A, is described by

$$I_A = g_A ab(V - E_k)$$
$$\frac{da}{dt} = \frac{(a_\infty - a)}{\tau_a},\ a_\infty = \frac{1}{\left(1 + \exp\left(\frac{-(V+14)}{16.6}\right)\right)},\ \tau_a = 5\,\text{ms} \quad \frac{db}{dt} = \frac{(b_\infty - b)}{\tau_b}$$
$$b_\infty = \frac{1}{\left(1 + \exp\left(\frac{-(V+71)}{7.3}\right)\right)},\ \tau_b = \frac{1}{\alpha_b - \beta_b}$$

where a and b are the activation and inactivation variables, respectively. The rate constants are given by

$$\alpha_b = \frac{0.000009}{\exp\left(\frac{V-26}{18.5}\right)},\ \beta_b = \frac{0.014}{0.2 + \exp\left(\frac{-(V+70)}{11}\right)}$$

The non-specific cation channel, I_h, is described by

$$I_h = g_h r(V - E_r)$$
$$\frac{dr}{dt} = \frac{(r_\infty - r)}{\tau_r}$$

where r is the activation variable for this channel. The steady-state activation curve and time constant are given by

$$r_\infty = \frac{1}{\left(1 + \exp\left(\frac{V+84}{10.2}\right)\right)},\ \tau_r = \frac{1}{\exp(-17.9 - 0.116V) + \exp(-1.84 + 0.09V)} + 100$$

Network Input Spike Trains

Septal cells: Septal cell output was modelled as bursts of action potentials using a presynaptic spike generator. A spike train consisted of bursts of action potentials at a mean frequency of 50 Hz for a half-theta cycle (125 ms; corresponding to a recall period) followed by a half-theta cycle of silence. Due to 40% noise in the interspike intervals, the 10 spike trains in the septal population were asynchronous.

Entorhinal cells (EC): EC cells were also modelled as noisy spike trains, using a presynaptic spike generator. A spike train consisted of spikes at an average gamma frequency of 40 Hz, but with individual spike times Gaussian-distributed around the regular ISI of 25 ms, with a standard deviation of 0.2. The population of EC inputs fired asynchronously.

CA3 pyramidal cells: CA3 pyramidal cells were modelled as spike trains of the same form and with the same characteristics (mean frequency and noise level) as the EC cells. Onset of CA3 firing was delayed by 9 ms relative to the EC trains to model the respective conduction delays of direct and trisynaptic loop inputs to CA1.

Further Reading

de Almeida, L., Idiart, M., and Lisman, J.E. (2007). Memory retrieval time and memory capacity of the CA3 network: role of gamma frequency oscillations. *Learning & Memory*, 14: 795–806.

Amaral, D. and Lavenex, P. (2007). Hippocampal neuroanatomy. In: *The Hippocampus Book* (eds. P. Andersen, R. Morris, D. Amaral, T. Bliss, and J. O'Keefe), Oxford: Oxford University Press, pp. 37–114.

Amaral, D. and Witter, M. (1989). The three-dimensional organization of the hippocampal formation: a review of anatomical data. *Neuroscience*, 31:571–591.

Amit, D. J. (1989). *Modeling Brain Function: The World of Attractor Neural Networks*. Cambridge: Cambridge University Press.

Axmacher, N., Mormann, F., Fernandez, G., Elger, C., and Fell, J. (2006). Memory formation by neuronal synchronization. *Brain Research Reviews*, 52:170–182.

Bartos, M., Vida, I., and Jonas, P. (2007). Synaptic mechanisms of synchronized gamma oscillations in inhibitory interneuron networks. *Nature Reviews Neuroscience*, 8:45–56.

Bliss, T., Collingridge, G., and Morris, R. (2007). Synaptic plasticity in the hippocampus. In: *The Hippocampus Book* (eds. P. Andersen, R. Morris, D. Amaral, T. Bliss, and J. O'Keefe), Oxford: Oxford University Press, chapter 10, pp. 343–474.

Brankack, J., Stewart, M., and Fox S. (1993). Current source density analysis of the hippocampal theta rhythm: associated sustained potentials and candidate synaptic generators. *Brain Research*, 615:310–327.

Brun, V.H., Otnass, M.K., Molden, S., Steffenach, H.A., Witter, M.P., Moser, M.B., and Moser, E.I. (2002). Place cells and place recognition maintained by direct entorhinal-hippocampal circuitry. *Science*, 296:2243–2246.

Buzsaki, G. and Chrobak, J. (1995). Temporal structure in spatially organized neuronal ensembles: a role for interneuronal networks. *Current Opinion in Neurobiology*, 5:504–510.

Cook, E.P. and Johnston, D. (1997). Active dendrites reduce location-dependent variability of synaptic input trains. *Journal of Neurophysiology*, 78:2116–2128.

Cutsuridis, V., Cobb, S., and Graham, B.P. (2008a). Encoding and retrieval in a CA1 microcircuit model of the hippocampus. In: *ICANN 2008*, LNCS 5164 (eds. V. Kurkova, R. Neruda, and J. Koutnik), Springer-Verlag Berlin Heidelberg, pp. 238–247.

Cutsuridis, V., Cobb, S., and Graham, B.P. (2008b). A Ca^{2+} dynamics model of the STDP symmetry-to-asymmetry transition in the CA1 pyramidal cell of the hippocampus. In: *ICANN 2008*, LNCS 5164 (eds. V. Kurkova, R. Neruda, and J. Koutnik), Springer-Verlag Berlin Heidelberg, pp. 627–635.

Cutsuridis, V., Cobb, S., and Graham B.P. (2009a). Encoding and retrieval in a model of the hippocampal CA1 microcircuit. *Hippocampus, DOI 10.1002/hipo.20661*, in press

Cutsuridis, V., Cobb, S., and Graham, B.P. (2009b). Modelling the STDP symmetry-to-asymmetry transition in the presence of GABAergic inhibition. *Neural Network World*, 19:471–481.

Cutsuridis, V., Cobb, S., and Graham, B.P. (2009c). How bursts shape the STDP curve in the presence/absence of GABA inhibition. In: *Artificial Neural Networks – ICANN 2009*, LNCS 5768, Springer Berlin Heidelberg, pp. 229–238.

Cutsuridis, V., Hunter, R., Cobb, S., and Graham B. P. (2007). Storage and recall in the CA1 microcircuit of the hippocampus: a biophysical model. *BMC Neuroscience* 8(Suppl 2): P33

Cutsuridis, V. and Wennekers, T (2009). Hippocampus, microcircuits and associative memory. *Neural Networks, Special issue: Neural Models of Cortical Microcircuits*, 22:1120–1128.

Freund, T. and Antal, M. (1988). GABA-containing neurons in the septum control inhibitory interneurons in the hippocampus. *Hippocampus*, 336:170–173.

Freund, T. and Buzsaki, G. (1996). Interneurons of the hippocampus. *Hippocampus*, 6:347–470.

Golding, N.L., Staff, N.P., and Spruston, N. (2002). Dendritic spikes as a mechanism for cooperative long-term potentiation. *Nature*, 418:326–331.

Graham, B.P. (2001). Pattern recognition in a compartmental model of a CA1 pyramidal cell. *Network: Computation in Neural Systems*, 12:473–492.

Graham, B.P. and Cutsuridis, V. (2009). Dynamical Information Processing in the CA1 Microcircuit of the Hippocampus. In: *Computational Modeling in Behavioral Neuroscience: Closing the Gap Between Neurophysiology and Behavior*. (eds. D. Heinke and E. Mavritasaki), pp. 1–20, London: Psychology Press, Taylor and Francis Group.

Guzowski, J.F., Knierim, J.J., and Moser, E.I. (2004). Ensemble dynamics of hippocampal regions CA3 and CA1. *Neuron*, 44:581–584.

Hasselmo, M., Bodelon, C., and Wyble, B. (2002a). A proposed function for hippocampal theta rhythm: separate phases of encoding and retrieval enhance reversal of prior learning. *Neural Computation*, 14:793–817.

Hasselmo, M., Hay, J., Ilyn, M., and Gorchetchnikov, A. (2002b). Neuromodulation, theta rhythm and rat spatial navigation. *Neural Networks*, 15:689–707.

Hopfield, J. (1982). Neural networks and physical systems with emergent collective computational abilities. *Proceedings of the National Academy of Science*, 79:2554–2558.

Hunter, R., Cobb, S., and Graham, B.P. (2008a). Improving recall in an associative neural network of spiking neurons. *Dynamic Brain - from Neural Spikes to Behaviors*, LNCS Vol. 5286, Springer, Berlin/Heidelberg, pp. 137–141.

Hunter, R., Cobb, S., and Graham, B.P. (2008b). Improving associative memory in a network of spiking neurons. *Artificial Neural Networks – ICANN 2008*, LNCS Vol. 5164, Springer, Berlin/Heidelberg, pp. 636–645.

Hunter, R., Cobb, S., and Graham, B.P. (2009). Improving associative memory in a network of spiking neurons. *Neural Network World*, 19:447–470.

Ishizuka, N., Weber, J., and Amaral, D. (1990). Organization of intrahippocampal projections originating from CA3 pyramidal cells in the rat. *Journal of Comparative Neurology*, 295:580–623.

Kali, S. and Freund, T.F. (2005). Distinct properties of two major excitatory inputs to hippocampal pyramidal cells: a computational study. *European Journal of Neuroscience*, 22:2027–2048.

Klausberger, T., Magill, P., Maki, G., Marton, L., Roberts, J., Cobden, P., Buzsaki, G., and Somogyi, P. (2003). Brain-state-and cell-type-specific firing of hippocampal interneurons in vivo. *Nature*, 421:844–848.

Klausberger, T., Marton, L., Baude, A., Roberts, J., Magill, P., and Somogyi, P. (2004). Spike timing of dendrite-targeting bistratified cells during hippocampal network oscillations in vivo. *Nature Neuroscience*, 7:41–47.

Klausberger, T., and Somogyi, P. (2008). Neuronal diversity and temporal dynamics: the unity of hippocampal circuit operations. *Science*, 321(5885):53–57.

Knierim, J.J., Lee, I., and Hargreaves, E.L.. (2006). Hippocampal place cells: parallel input streams, subregional processing, and implications for episodic memory. *Hippocampus*, 16:755–764.

Kunec, S., Hasselmo, M., and Kopell, N. (2005). Encoding and retrieval in the CA3 region of the hippocampus: a model of theta-phase separation. *Journal of Neurophysiology*, 94:70–82.

Lamsa, K., Heeroma, J., Somogyi, P., Rusakov, D., and Kullmann, D. (2007). Anti-Hebbian long-term potentiation in the hippocampal feedback circuit. *Science*, 315:1262–1266.

Leung, L., Roth, L., and Canning, K. (1995). Entorhinal inputs to hippocampal CA1 and dentate gyrus in the rat: a current-source-density study. *Journal of Neurophysiology*, 73: 2392–2403.

Levy, W.B. (1996). A sequence predicting CA3 is a flexible associator that learns and uses context to solve hippocampal-like tasks. *Hippocampus*, 6:579–590.

Li, X.G., Somogyi, P., Ylinen, A., and Buzaki, G. (1994). The hippocampal CA3 network: An in vivo intracellular labeling study. *Journal of Comparative Neurology*, 339:181–208.

Lisman, J. and Idiart, M. (1995). Storage of 7+-2 short-term memories in oscillatory subcycles. *Science*, 267:1512–1514.

Maccaferri, G. and Lacaille, J.-C. (2003). Hippocampal interneuron classifications -making things as simple as possible, not simpler. *Trends in Neuroscience*, 26:564–571.

Marr, D. (1971). A simple theory of archicortex. *Philosophical Transactions of the Royal Society of London. Series B, Biological Sciences*, 262(841): 23–81.

McNaughton, B.L. and Morris, R.G.M. (1987). Hippocampal synaptic enhancement and information storage within a distributed memory system. *TINS*, 10(10): 408–415.

Menschik E.D. and Finkel L.H. (1998). Neuromodulatory control of hippocampal function: towards a model of Alzheimer's disease. *Artificial Intelligence in Medicine*, 13: 99–121.

Migliore, M., Ferrante, M., and Ascoli, G.A. (2005). Signal propagation in oblique dendrites of CA1 pyramidal cells. *Journal of Neurophysiology*, 94:4145–4155.

Molyneaux, B.J. and Hasselmo ME. (2002). $GABA_B$ presynaptic inhibition has an in vivo time constant sufficiently rapid to allow modulation at theta frequency. *Journal of Neurophysiology*, 87:1196–1205.

Paulsen, O. and Moser, E. (1998). A model of hippocampal memory encoding and retrieval: GABAergic control of synaptic plasticity. *Trends in Neuroscience*, 21:273–279.

Pinsky, P. and Rinzel, J. (1994). Intrinsic and network rhythmogenesis in a reduced Traub model for CA2 neurons. *Journal of Computational Neuroscience*, 1:39–60.

Pissadaki, E. and Poirazi, P. (2007). Modulation of excitability in CA1 pyramidal neurons via the interplay of entorhinal cortex and CA3 inputs. *Neurocomputing*, 70:1735–1740.

Poirazi, P., Brannon, T., and Mel, B. (2003a). Arithmetic of subthreshold synaptic summation in a model CA1 pyramidal cell. *Neuron*, 37:977–987.

Poirazi, P., Brannon, T., and Mel, B. (2003b). Pyramidal neuron as a two-layer neural network. *Neuron*, 37:989–999.

Remondes, M. and Schuman, E. (2002). Direct cortical input modulates plasticity and spiking in CA1 pyramidal neurons. *Nature*, 416:736–740.

Santhakumar, V., Aradi, I., and Soltetz, I. (2005). Role of mossy fiber sprouting and mossy cell loss in hyperexcitability: a network model of the dentate gyrus incorporating cell types axonal typography. *Journal of Neurophysiology*, 93:437–453.

Saraga, F., Wu, C., Zhang, L., and Skinner, F. (2003). Active dendrites and spike propagation in multicompartmental models of oriens-lacunosum/moleculare hippocampal interneurons. *Journal of Physiology*, 552:673–689.

Sjostrom, P.J., Rancz, E.A., Roth, A., and Hausser, M. (2008). Dendritic excitability and synaptic plasticity. *Physiological Reviews*, 88:769–840.

Soleng, A.F., Raastad, M., and Andersen P. (2003). Conduction latency along CA3 hippocampal axons from rat. *Hippocampus*, 13:953–961.

Sommer, F. and Wennekers, T. (2000). Modelling studies on the computational function of fast temporal structure in cortical circuit activity. *Journal of Physiology (Paris)*, 94:473–488.

Sommer, F. and Wennekers, T. (2001). Associative memory in networks of spiking neurons. *Neural Networks*, 14:825–834.

Somogyi, P. and Klausberger, T. (2005). Defined types of cortical interneurone structure space and spike timing in the hippocampus. *Journal of Physiology*, 562.1:9–26.

Sun, H., Lyons, S., and Dobrunz, L. (2005). Mechanisms of target-cell specific short-term plasticity at Schaffer collateral synapses onto interneurones versus pyramidal cells in juvenile rats. *Journal of Physiology*, 568:815–840.

Treves, A. and Rolls, E. (1994). Computational analysis of the role of the hippocampus in memory. *Hippocampus*, 4:374–391.

Wallenstein, G. and Hasselmo, M. (1997). GABAergic modulation of hippocampal population activity: sequence learning, place field development, and the phase precession effect. *Journal of Neurophysiology*, 78:393–408.

Willshaw, D., Buneman, O., and Longuet-Higgins, H. (1969). Non-holographic associative memory. *Nature*, 222:960–962.

Wyble B.P., Linster C., and Hasselmo ME. (2000). Size of CA1-evoked synaptic potentials is related to theta rhythm phase in rat hippocampus. *Journal of Neurophysiology*, 83(4): 2138–44.

Microcircuit Model of the Dentate Gyrus in Epilepsy

Robert J. Morgan and Ivan Soltesz

Introduction

The dentate gyrus in the mammalian brain is an extremely complex structure containing millions of cells (over 1 million in the rat and many more in primates) of numerous types connected together by billions of synapses. Despite this complexity, the dentate is a highly ordered structure and decades of research have led to a deep understanding of the anatomical and physiological properties of the cells contained therein. Since the dentate is thought to serve as a gate for activity propagation throughout the limbic system (Heinemann et al. 1992; Lothman et al. 1992), understanding of its structure and components is important for developing therapeutic interventions for treating neurological disorders such as epilepsy. Epilepsy and the process by which a normal brain becomes epileptic (epileptogenesis) are complex themselves, however, and result in myriad changes to the dentate gyrus on both molecular and cellular levels. For this reason it is quite difficult to understand the functional implications of specific alterations within the dentate circuitry using traditional methods such as animal models or culture systems. On the other hand, computational models are ideally suited to the task of dissociating the effects of one change from others since it is possible to model only the change of interest. A main drawback of computational modeling is that in order to be confident that what is modeled is an accurate reflection of reality, the model must be sufficiently detailed to reproduce a control situation derived from experimental data. This is especially true for the dentate gyrus as some of the most interesting alterations during epileptogenesis are structural changes that occur on a very large scale and affect the activity and propagation of activity throughout the entire network. Fortunately, the massive amount of experimental data that has been collected about the dentate has facilitated the creation of a large-scale, biophysically realistic computational model that is an excellent tool for studying numerous questions related to how microcircuit changes

R.J. Morgan (✉)
Department of Anatomy and Neurobiology, University of California, Irvine, CA, USA
e-mail: rjmorgan@uci.edu

V. Cutsuridis et al. (eds.), *Hippocampal Microcircuits*, Springer Series in Computational Neuroscience 5, DOI 10.1007/978-1-4419-0996-1_17,

during epileptogenesis affect network activity and propagation of seizures throughout the hippocampus.

In this chapter, we will provide a comprehensive description of a large-scale dentate network model which has evolved from an initial implementation with approximately 500 model cells (Santhakumar et al. 2005) to a network with over 50,000 multicompartmental model neurons (Dyhrfjeld-Johnsen et al. 2007; Morgan and Soltesz 2008). Additionally, we will discuss the experimental data underlying the model parameters and the rationale for the assumptions made in the model. We will then discuss how the model was applied to a problem that is critical for understanding the structure–function relationships of hippocampal microcircuits and highlight the importance of accurate network topology in data-driven models. Finally, we will speculate on potentially useful additions to the dentate model and future questions that could be addressed.

Details of Network Construction

This section will describe the parameters of the dentate gyrus network, including both experimental and model data for comparison (experimental data is derived predominantly from rat, and the model therefore simulates the rat dentate gyrus). The majority of data in this section will be presented in tables in order to provide the reader with a quick and concise way to access a large volume of information.

Construction of a dentate gyrus model requires a number of considerations such as cell types, cell numbers, synaptic connectivity, cellular physiological parameters. These factors can be grouped into two major components which can then be combined to form a complete model. The first component is the connection matrix, which describes as precisely and realistically as possible, the connectivity of each of the cell types in the dentate gyrus. The second component is the model cells themselves, with all of their various properties. This section will present the following in order:

1. Unscaled dentate gyrus connection matrix derived from experimental data
2. Structure of the model cells
3. Passive parameters and channel conductances in the model cells
4. Physiological properties of the cells
5. Scaled model connection matrix with synaptic parameters of model cells

The comprehensive connection matrix of the rat dentate gyrus was constructed from many sources of experimental data, and they are referenced in the appropriate boxes in Table 1. This table contains the eight well-defined cellular subtypes found within the dentate gyrus, their numbers, and their cell type-specific connectivities (for example, from the third row, second column in Table 1: a single basket cell (BC) innervates about 1,250 granule cells (GCs); mean and ranges are indicated). Justifications for the numbers of each cell type as well as the numbers of connections can be found in the following section. While this connection matrix is

Table 1 Connection matrix of the biological dentate gyrus derived from experimental data

	Granule cells	**Mossy cells**	**Basket cells**	**Axo-axonic cells**	**MOPP Cells**	**HIPP cells**	**HICAP cells**	**IS cells**
Granule cells	**X**	**9.5**	**15**	**3**	**X**	**110**	**40**	**20**
(**1,000,000**)	X	7–12	10–20	1–5	X	100–120	30–50	10–30
Ref. [1–5]	Ref. [6]	Ref. [7]	Ref. [6–9]	Ref. [6, 7, 9]	Ref. [6]	Ref. [4, 10, 11]	Ref. [4, 7, 10, 11]	Ref. [7]
Mossy cells	**32,500**	**350**	**7.5**	**7.5**	**5**	**600**	**200**	**X**
(**30,000**)	30,000–35,000	200–500	5–10	5–10	5	600	200	X
Ref. [11]	Ref. [4, 11–13]	Ref. [12, 13]	Ref. [13]	Ref. [13]	Ref. [14]	Ref. [12, 13]	Ref. [12, 13]	Ref. [15]
Basket cells	**1,250**	**75**	**35**	**X**	**X**	**0.5**	**X**	**X**
(**10,000**)	1,000–1,500	50–100	20–50	X	X	0–1	X	X
Ref. [16, 17]	Ref. [4, 16–19]	Ref. [11, 16, 17, 19]	Ref. [16, 17, 20, 21]	Ref. [18]	Ref. [18]	Ref. [18]	Ref. [18]	Ref. [10, 20]
Axo-axonic cells	**3,000**	**150**	**X**	**X**	**X**	**X**	**X**	**X**
(**2,000**)	2,000–4,000	100–200	X	X	X	X	X	X
Ref. [4, 22]	Ref. [4, 18, 22]	Ref. [4, 5, 11, 14, 23]	Ref. [5, 18]	Ref. [5, 18]	Ref. [5, 18]	Ref. [5, 18]	Ref. [5, 18]	Ref. [5, 18, 19]
MOPP cells	**7,500**	**X**	**40**	**1.5**	**7.5**	**X**	**7.5**	**X**
(**4,000**)	5,000–10,000	X	30–50	1–2	5–10	X	5–10	X
Ref. [11, 14]	Ref. [14]	Ref. [14, 24]	Ref. [14, 25]	Ref. [14, 26]	Ref. [14, 25]	Ref. [14, 20, 25]	Ref. [14, 25]	Ref. [14, 15]

Table 1 (continued)

	Granule cells	Mossy cells	Basket cells	Axo-axonic cells	MOPP Cells	HIPP cells	HICAP cells	IS cells
HIPP cells	**1,550**	**35**	**450**	**30**	**15**	**X**	**15**	**X**
(**12,000**)	1,500–1,600	20–50	400–500	20–40	10–20	X	10–20	X
Ref. [11]	Ref. [4, 11, 20]	Ref. [4, 11, 12, 27, 28]	Ref. [4, 11, 20]	Ref. [20, 25]	Ref. [25]	Ref. [14, 20, 25]	Ref. [25]	Ref. [15, 20]
HICAP cells	**700**	**35**	**175**	**X**	**15**	**50**	**50**	**X**
(**3,000**)	700	30–40	150–200	X	10–20	50	50	X
Ref. [5, 29, 30]	Ref. [4, 11, 20]	Ref. [20]	Ref. [4, 11, 20]	Ref. [20]	Ref. [14, 20]	Ref. [20]	Ref. [20]	
IS cells	**X**	**X**	**7.5**	**X**	**X**	**7.5**	**7.5**	**450**
(**3,000**)	X	X	5–10	X	X	5–10	5–10	100–800
Ref. [15, 29, 30]	Ref. [15]	Ref. [15]	Ref. [15, 19]	Ref. [15]	Ref. [19]	Ref. [19]	Ref. [15]	

Cell numbers and connectivity values were estimated from published data for granule cells, mossy cells, basket cells, axo-axonic cells, molecular layer interneurons with axons in perforant-path termination zone (MOPP), hilar interneurons with axons in perforant-path termination zone (HIPP), hilar interneurons with axons in the commissural/associational pathway termination zone (HICAP), and interneuron-selective cells (IS). Connectivity is given as the number of connections to a postsynaptic population (*row 1*) from a single presynaptic neuron (*column 1*). The average number of connections is given in bold. References given correspond to: [1]Gaarskjaer (1978); [2]Boss et al. (1985); [3]West (1990); [4]Patton and McNaughton (1995); [5]Freund and Buzsáki (1996); [6]Buckmaster and Dudek (1999); [7]Acsady et al. (1998); [8]Geiger et al. (1997); [9]Blasco-Ibanez et al. (2000); [10]Gulyas et al. (1992); [11]Buckmaster and Jongen-Relo (1999); [12]Buckmaster et al. (1996); [13]Wenzel et al. (1997); [14]Han et al. (1993); [15]Gulyas et al. (1996); [16]Babb et al. (1988); [17]Woodson et al. (1989); [18]Halasy and Somogyi (1993); [19]Acsady et al. (2000); [20]Sik et al. (1997); [21]Bartos et al. (2001); [22]Li et al. (1992); [23]Ribak et al. (1985); [24]Frotscher et al. (1991); [25]Katona et al. (1999); [26]Soriano et al. (1990); [27]Claiborne et al. (1990); [28]Buckmaster et al. (2002a); [29]Nomura et al. (1997a); [30]Nomura et al. (1997b). Used with permission from Dyhrfjeld-Johnsen et al. (2007).

extremely useful for creating a structural graph of the dentate gyrus (as was done in Dyhrfjeld-Johnsen et al. 2007), and in the future may also be used to create a complete functional model of the dentate, current computing power and experimental data are insufficient to incorporate all of the cell types and cell numbers that are present in vivo into a model containing physiologically realistic cells. Instead, the functional dentate gyrus model is a 1:20 scale model containing four multicompartmental neuronal types: excitatory granule cells and mossy cells, and inhibitory basket cells (BCs) and hilar perforant-path associated (HIPP) cells. The properties of these models cells are depicted in Tables 2, 3, and 4.

Table 2 gives the structural properties of the four cell types implemented in the functional dentate model. Corresponding schematics of these cell types are seen in the top panels of Fig. 1a–d. The passive properties and somatic conductances of these cell types are shown in Table 3, and the physiological properties of the cells are displayed in Table 4. The combination of these two sets of parameters results in biophysically realistic model cells that reproduce the firing properties of cells recorded in vivo. Example traces for each cell type in response to depolarizing and hyperpolarizing pulses are shown in the middle and bottom panels of Fig. 1a–d, respectively.

While Tables 2, 3, and 4 provide a great deal of detail about the single-cell models used to construct the *in silico* dentate gyrus, they do not provide any information about how the cells should be connected together. Using the information in Table 1 as a starting point and accounting for the computational power available to run simulations, a new connection matrix was constructed for the four cell types making up the functional model network. This matrix, along with synaptic parameters for each of the cell type-specific connections, is given in Table 5. Additionally, a schematic diagram illustrating the cell type-specific connectivity of the model is shown in Fig. 2. Note that the dashed line in Fig. 2 that connects the GC to itself represents sprouted GC axon (mossy fiber) connections that do not exist in the healthy dentate gyrus. Rather these connections form as a result of pathological alterations during epileptogenesis, and the number of GC-to-GC connections that exist in the dentate network is a function of the degree of injury to the dentate. This is why GC-to-GC connections are indicated as "Variable" in Table 5. The specific topology of these connections has been shown to play a major role in determining seizure susceptibility in the injured dentate circuit (Morgan and Soltesz 2008) and will be discussed in a later section.

Justification and Explanation of Model Parameters

Cell Types

The following are some of the important factors that determine the cell type:

1. Nature of the neurotransmitter released
2. Location in the laminar structure of the dentate gyrus

Table 2 Structure of model cells

Dimensions	Granule cell	Mossy cell	Basket cell	HIPP cell
Soma				
Diameter, μm	16.8	20	15	10
Length, μm	16.8	20	20	20
Number of dendrites	2	4	4 (2 apical and 2 basal)	4 (2 short and 2 long)
Number of compartments in each dendrite	4	4	4	3
Total number of compartments (soma + dendritic compartments)	9	17	17	13
Dendritic compartments and dimensions			Apical dendrites:	Short dendrites:
Diameter × length, μm	Dendrite in the granule cell layer: 3 × 50	Prox. dendrite: 5.78 × 50	Prox. dendrite: 4 × 75	Prox. dendrite: 3 × 50
	Mid 1 dendrite: 4 × 50	Mid 1 dendrite: 3 × 75	Mid dendrite: 2 × 50	
	Prox. dendrite: 3 × 150	Mid 2 dendrite: 25 × 50	Mid 2 dendrite: 2 × 75	Distal dendrite: 1 × 50
	Mid dendrite: 3 × 150	Distal dendrite: 1 × 50	Distal dendrite: 1 × 75	
	Distal dendrite: 3 × 150			Long dendrites:
			Basal dendrites:	Prox. dendrite: 3 × 75
			Prox. dendrite: 4 × 50	Mid dendrite: 2 × 75
			Mid 1 dendrite: 3 × 50	Distal dendrite: 1 × 75
			Mid 2 dendrite: 2 × 50	
			Distal dendrite: 1 × 50	
References	Aradi and Holmes (1999)	Based on morphological data in Buckmaster et al. (1993)	Based on morphological data in Bartos et al. (2001); Geiger et al. (1997)	Based on morphological data in Buckmaster et al. (2002a); Freund and Buzsáki (1996)

Used with permission from Santhakumar et al. (2005).

Table 3 Passive parameters and maximum conductance of the channels in model cell somata

Mechanism	Source	Granule cell	Mossy cell	Basket cell	HIPP cell
C_m, $\mu F/cm^2$		1	0.6	1.4	1.1
R_a, Ωcm		210	100	100	100
Leak conductance (S/cm^2)	Aradi and Holmes (1999)	0.00004	0.000011	0.00018	0.000036
Sodium (S/cm^2)	Aradi and Soltesz, (2002)	0.12	0.12	0.12	0.2
Delayed rectifier K (Slow) (S/cm^2)	Aradi and Holmes, (1999)	0.006	X	X	X
Delayed rectifier K (Fast) (S/cm^2)	Aradi and Soltesz, (2002)	0.016	0.0005	0.013	0.006
A-type K (S/cm^2)	Aradi and Soltesz, (2002)	0.012	0.00001	0.00015	0.0008
I_h(S/cm^2)	Chen et al. (2001)	X	0.000005	X	0.000015
L-type Calcium (S/cm^2)	Migliore et al. (1995)	0.005	0.0006	0.005	0.0015
N-type Calcium (S/cm^2)	Aradi and Holmes, (1999)	0.002	0.00008	0.0008	X
T-type Calcium (S/cm^2)	Aradi and Holmes, (1999)	0.000037	X	X	X
Ca-dependent K (SK) (S/cm^2)	Aradi and Holmes, (1999)	0.001	0.016	0.000002	0.003
Ca and voltage-dependent K (BK) (S/cm^2)	Migliore et al. (1995)	0.0006	0.0165	0.0002	0.003
Time constant for decay of intracellular Ca (ms)	Aradi and Soltesz, (2002)	10	10	10	10
Steady-state intracellular Ca concentration (mol)	Aradi and Soltesz, (2002)	5×10^{-6}	5×10^{-6}	5×10^{-6}	5×10^{-6}

Used with permission from Santhakumar et al., J Neurophysiol. 2005 Jan;93(1):437–53.

3. Morphological features such as shape of the soma, dendritic arbor, and axonal distribution pattern
4. Presence of specific markers such as calcium binding proteins and neuropeptides

Table 4 Physiological properties of individual cell types

Physiological property	Granule cell		Mossy cell		Basket cell		HIPP cell	
	Model	Biological	Model	Biological	Model	Biological	Model	Biological
RMP (mV)	−70.4	−75 ± 2	−60	−59.7 ± 4.9	−60	−56 to −66	−70	−65 ± 6
R_{in} (MΩ)	183	107–228	210	199 ± 19	64.7	56 ± 9	350	371 ± 47
T_{memb} (ms)	30	31 ± 2	54	24 to 52	8	9–11	17.6	16.9 ± 1.8
AP amp. (mV)	80	86.6 ± 0.7	88	89.8 ± 1.1	78	74 mV	90	83
AP threshold (mV)	−48.70	−49 ± 0.8	−52	−47.33 ± 1.45	−49	−40.5 ± 2.5 (< −52)	−50	−50
Fast AHP (mV)	−7.91	−22.5 to −3.4	−12.2	−15.5	−23.39	−24.9 to −14.9	−18.5	−20 to −7
Spike frequency adaptation	0.31	0.3	0.86	0.8	0.97	.98	0.8	0.82 ± 0.42
Sag ratio	1	0.97 ± 0.01	0.97	0.81 ± 0.02	1	0.9 to 1	0.83	0.78–0.86
Source of biological cell parameters	Lubke et al. (1998); Santhakumar et al. (2000); Staley et al. (1992)		Lubke et al. (1998); Ratzliff et al. (2004); and Santhakumar et al. (2000)		Bartos et al. (2001); Geiger et al. (1997); Harney and Jones (2002); Lubke et al. (1998) and Mott (1997)		Lubke et al. (1998) and Mott (1997)	

Used with permission from Santhakumar et al. (2005).

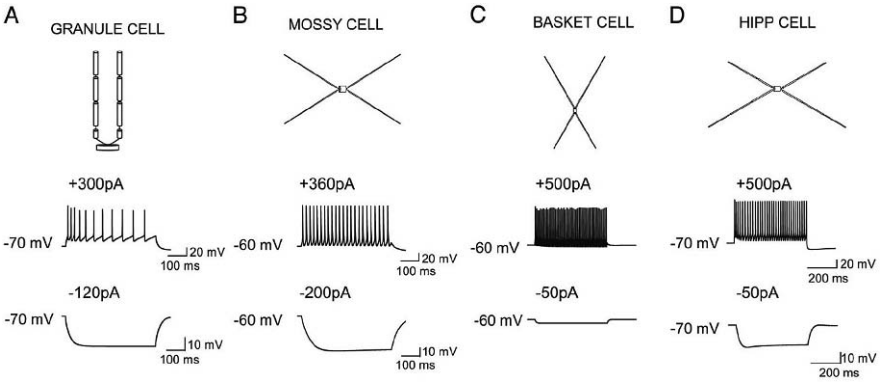

Fig. 1 Structure and intrinsic excitability of model cells. **a**. Schematic representation of the structure (*top*) of the granule cell model and membrane voltage traces of the granule cell in response to 300-pA (*middle*) and 120-pA (*bottom*) current injections. **b**. Illustration of the structure of the model mossy cell (*top*) and the membrane voltage responses to 360-pA (*middle*) and 200-pA (*bottom*) current injections. **c**. The structure of the model basket cell (*top*) and responses to 500 pA (*middle*) and 50 pA (*bottom*) current injections. **d**. Structure (*top*) and responses to 500 pA (*middle*) and 50 pA (*bottom*) of the model hilar perforant-path associated cells (HIPP cells). Used with permission from Santhakumar et al. (2005)

(For detailed description of cell type discrimination see Freund and Buzsáki (1996).) According to the four criteria established above, two excitatory cell types (GCs and MCs) and at least six distinct inhibitory interneurons can be identified in the dentate gyrus (Table 1). Identifying which cell types are appropriate to include in the dentate model is somewhat more complicated than simply identifying the cell types, however. This dilemma occurs because, despite a wealth of information about the dentate gyrus and its cellular composition, there is much information that remains unknown, particularly for the rarer interneuron subtypes. The rationale for including or excluding various cell types from the model based on the available data follows.

Both excitatory cell types (GCs and MCs) are well defined and have a vast amount of electrophysiological data available for the construction of single-cell models. However, the wealth of information available for the interneurons is substantially more limited for many cell types. Additionally, the role of interneurons in the network must be considered with regard to the question being asked. For example, in a model network (such as the one discussed later) that is pursuing the question of the role of topology of sprouted mossy fibers on dentate excitability following injury (Morgan and Soltesz 2008), several factors must be considered. First, the injury to the dentate results in both mossy fiber sprouting and hilar cell loss (including both MCs and inhibitory interneurons). Thus it is critical that the network contains both excitatory cell types plus some form of inhibition. Inhibition can operate in two principal modes. One mode is feed-forward inhibition, where an interneuron is activated by the same afferent input as the excitatory neuron that it contacts. The BC is the primary source of feed-forward inhibition in the dentate gurus (Freund and Buzsáki 1996). The second mode is feedback inhibition, where

Table 5 Functional model network network parameters

From	To -->	GC	MC	BC	HC
Perforant path	Synapse weight (nS)	20	5	10	n/a
	Rise/decay/delay (ms)	1.5/5.5/3	1.5/5.5/3	2/6.3/3	n/a
Granule cells	Convergence	Variable	78.05	370.95	2,266.64
(50,000)	Divergence	Variable	2.34	3.71	27.19
	Synapse weight (nS)	1.00	0.20	0.94	0.10
	Rise/decay/delay (ms)	1.5/5.5/0.8	0.5/6.2/1.5	0.3/0.6/0.8	0.3/0.6/1.5
Mossy cells	Convergence	243.62	87.23	5.59	375.53
(1,500)	Divergence	8,120.82	87.23	1.86	150.21
	Synapse weight (nS)	0.30	0.50	0.30	0.20
	Rise/decay/delay (ms)	1.5/5.5/3	0.45/2.2/2	0.9/3.6/3	0.9/3.6/3
Basket cells	Convergence	3.11	6.31	8.98	n/a
(500)	Divergence	313.22	18.93	8.98	n/a
	Synapse weight (nS)	1.60	1.50	7.60	n/a
	Rise/decay/delay (ms)	0.26/5.5/0.85	0.3/3.3/1.5	0.16/1.8/0.8	n/a
HIPP cells	Convergence	4.82	3.76	140.13	n/a
(600)	Divergence	401.86	9.39	116.77	n/a
	Synapse weight (nS)	0.50	1.00	0.50	n/a
	Rise/decay/delay (ms)	0.5/6/1.6	0.5/6/1	0.4/5.8/1.6	n/a

Used with permission from Dyhrfjeld-Johnsen et al. (2007).

interneurons are activated by excitatory cells which they subsequently inhibit. The BCs and HIPP cells are the two key feedback inhibitory cells in the dentate (Freund and Buzsáki 1996; Buckmaster et al. 2002a). Another important aspect of inhibition is the location of synaptic contact between interneuron and principal cell. Perisomatic inhibition by BCs is considered crucial in maintaining limited GC activity in response to afferent input (limiting the propagation of afferent activity is important for the gating function of the dentate gyrus). The HIPP cells, on the other hand, synapse on the dendritic region near the afferent inputs, and they are likely to modulate integration of dendritic inputs. The loss of this dendritic inhibition with an essentially intact or increased somatic inhibition has been proposed to be particularly relevant to epileptogenesis (Cossart et al. 2001). Furthermore, BCs are resistant to cell death whereas HIPP cells are extremely vulnerable in epileptic tissue (Buckmaster et al. 2002a). These features make the basket and HIPP cells essential constituents of the dentate model.

The remaining four interneurons also possess unique features of inhibition. The molecular layer perforant-path associated (MOPP) cells operate by providing GCs with feed-forward dendritic inhibition (Halasy and Somogyi 1993). The hilar cells with axonal projections to the commissural-associational pathway (HICAP cells) synapse on the proximal dendrites of GCs, near where MC axons terminate and provide feedback inhibition (Freund and Buzsáki 1996). The axo-axonic cells provide GABAergic input at the axon initial segments of GCs and MCs and potentially play powerful roles in modifying spike initiation (Freund and Buzsáki 1996;

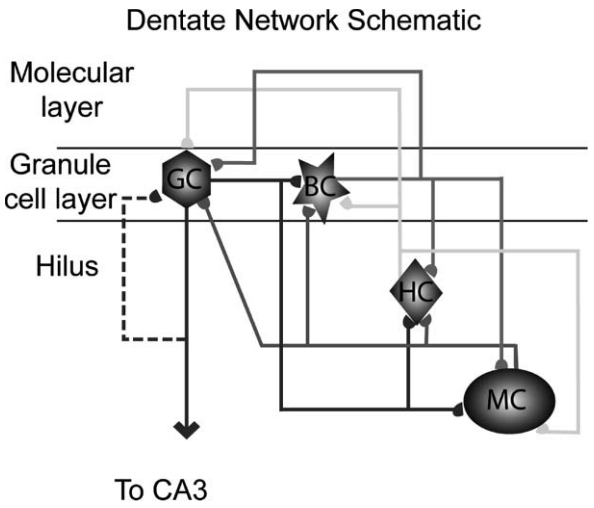

Fig. 2 Schematic of the dentate gyrus model showing the four cell types implemented, the layers in which they reside, and their cell type-specific connectivity. Cell types from left to right: excitatory granule cells (GC, *hexagon*), inhibitory somatically projecting basket cells (BC, *star*), inhibitory dendritically projecting hilar interneurons with axonal projections to the perforant path (HIPP cells, HC, *diamond*), and excitatory mossy cells (MC, *oval*). Dashed line: recurrent GC connections from sprouted mossy fibers following dentate injury. Used with permission from Morgan and Soltesz (2008)

Howard et al. 2005). The interneuron-selective (IS) cells connect exclusively to other interneurons and form a well connected network that could modulate excitability and synchrony of the network.

Unfortunately, detailed physiological data for the development of realistic models of MOPP, HICAP, axo-axonic, and IS cells are not readily available. Therefore, the model of the dentate gyrus presented here contains only basket and HIPP cells as the inhibitory interneurons in the network. Note that the exclusion of other known inhibitory cell types makes it essential to perform control simulations to examine whether augmenting inhibition (in an effort to compensate for excluded cell types) influences the overall outcome of the network simulations. These simulations, among many others aimed at testing the model's robustness, were performed and are thoroughly explained in Dyhrfjeld-Johnsen et al. (2007).

Cell Numbers

Cell numbers can be determined by identifying the cellular layers of the dentate gyrus and then counting the total number of cells in each layer. Then, it is possible to estimate subtype numbers based on the percentage of neurons that express specific markers (Buckmaster et al. 1996; Nomura et al. 1997a, b; Buckmaster et al. 2002a). There are three cell layers in the dentate gyrus: the molecular layer, GC layer, and

hilus (Fig. 2). The GCs are the primary projection cells of the dentate gyrus. These are small, densely packed cells, typically located in the GC layer of the dentate gyrus. The number of GCs in the rat dentate gyrus is approximately 1,000,000 (Gaarskjaer 1978; Boss et al. 1985; West 1990; Patton and McNaughton 1995; Freund and Buzsáki 1996). The other major excitatory cell type, the MC, is located in the hilus and does not express the GABA synthetic enzyme GAD. Buckmaster and Jongen-Relo (1999) estimated the number of GAD-mRNA negative neurons in the dentate hilus (presumed MCs) to be approximately 30,000. The GABAergic interneurons are located in all three layers of the dentate gyrus. These include the BCs, parvalbumin-positive (PV) axo-axonic cells (whose axon terminals project exclusively to the axon initial segment of excitatory cells), somatostatin-positive HIPP cells (Freund and Buzsáki 1996; Katona et al. 1999), nitric oxide synthase-positive HICAP cells (Freund and Buzsáki 1996), and aspiny and calretinin-positive hilar IS cells (Gulyas et al. 1996). The number of GABAergic cell types along the GC-hilar border and in the hilus can be determined based on published histochemical data (Buckmaster et al. 1996; Nomura et al. 1997a, b; Buckmaster et al. 2002a). In the molecular layer, there are approximately 10,000 GAD-mRNA positive interneurons, comprised of approximately 2,000 axo-axonic cells (AACs) (Patton and McNaughton 1995) and 4,000 MOPP cells (Han et al. 1993). The remaining 4,000 cells were excluded from the dentate model, as they are the molecular layer interneurons that project primarily outside of the dentate gyrus such as the outer molecular layer interneurons projecting to the subiculum. Because the HIPP cells are thought to be identical to the somatostatin-positive interneurons in the dentate hilus (Freund and Buzsáki 1996; Katona et al. 1999) and because Buckmaster and Jongen-Relo (1999) estimated that there were 12,000 somatostatin-positive neurons in the hilus, 12,000 HIPP cells were included in the dentate network. HICAP cells are thought to be NOS-positive (Freund and Buzsáki 1996), and because roughly 50% of the nearly 7,000 NOS-positive cells in the hilus are single labeled (i.e., not somatostatin/neuropeptide-Y or calretinin-positive; Nomura et al. 1997a, b), the number of HICAP cells was estimated to be 3,000. The hilus contains about 6,500 calretinin-positive cells (Nomura et al. 1997a, b), roughly 30% of which are somatostatin-positive (presumably spiny calretinin-positive cells), and some calretinin-positive cells overlap with the NOS-positive cells (Nomura et al. 1997a, b). IS cells are aspiny and calretinin-positive (Gulyas et al. 1996), and, assuming that maximally 50% of the calretinin-positive cells are aspiny, we estimated the number of IS cells to be 3,000.

Multicompartmental Single-Cell Models

The single-cell models, as described in Tables 2, 3, and 4, were constructed based on morphological data from the literature (Buckmaster et al. 1993; Freund and Buzsáki 1996; Geiger et al. 1997; Bartos et al. 2001; Buckmaster et al. 2002a). Their intrinsic properties were also modeled based on experimental data, and specific justifications for the passive parameters, ionic conductances, and physiological

properties are described in the following sections. Additionally, the equations used for the single-cell ion channel models are given.

Passive Parameters and Ionic Conductances

The intrinsic properties of the cell types were modeled based on data derived from experiments (Staley et al. 1992; Lubke et al. 1998) that were conducted in the presence of blockers of synaptic activity. The passive membrane parameters and source and densities of active conductances in the somatic compartment of the model cells are listed in Table 3. For GCs, the somato-dendritic distribution of active conductances was adapted from Aradi and Holmes (1999). In all other cell types, the active conductances, with the exception of sodium and fast delayed rectifier potassium channels, were distributed uniformly in all compartments. Sodium and fast delayed rectifier potassium conductances were present only in the soma and proximal dendritic compartments. Additionally, because GCs (Desmond and Levy 1985) and MCs (Amaral 1978) are rich in dendritic spines, the membrane area contribution of dendritic spines was accounted for as in Rall et al. (1992). For GCs, correction for the membrane contribution of spines was performed by decreasing membrane resistivity (increasing leak conductance to $63\,\mu S/cm^2$) and increasing the capacitance to $1.6\,\mu F/cm^2$ (Aradi and Holmes 1999). In the case of MCs (which share several structural and functional properties with CA3 pyramidal cells; Buckmaster et al. 1993), spine density estimates from CA3 cells (Hama et al. 1994) were used to estimate the spine contribution to membrane area. This compensation resulted in an increase of the dendritic leak conductance and capacitance in the MC model.

Physiological Properties

The physiological properties of the model cells were tuned such that the parameters listed in Table 4 were consistent with the data derived from biological cells. The sources for the biological parameters of the various cells are given in Table 4. As is evident from the table, the model cells were accurate replicas of their biological counterparts.

Single-Cell Ion Channel Model Equations

Fast Sodium Current

$$
\begin{aligned}
&I_{\mathrm{Na}} = G_{\mathrm{Na}}(V,t)\cdot(V - E_{\mathrm{Na}}), \quad E_{\mathrm{Na}} = 45\,\mathrm{mV}\\
&G_{\mathrm{Na}}(V,t) = g_{\mathrm{Na}}^{\max}\cdot m^3(V,t)\cdot h(V,t)\\
&\quad \alpha_{\mathrm{m}}(V) = -0.3(V-25)/(e^{(V-25)/-5}-1)
\end{aligned}
$$

$$\beta_{\mathrm{m}}(V) = 0.3(V - 53)/(e^{(V-53)/5} - 1)$$
$$\alpha_{\mathrm{h}}(V) = 0.23/e^{(V-3)/20}$$
$$\beta_{\mathrm{h}}(V) = 3.33/(e^{(V-55.5)/-10} + 1)$$

Fast and Slow Delayed Rectifier Potassium Currents

$$I_{\text{fK-DR}} = G_{\text{fK-DR}}(V,t) \cdot (V - EK), \quad E_{\mathrm{K}} = -85\,\mathrm{mV}$$
$$G_{\text{fK-DR}}(V,t) = g^{\max}_{\text{fK-DR}} \cdot n_f^4(V,t)$$
$$\alpha_{\mathrm{nf}}(V) = -0.07(V - 47)/(e^{(V-47)/-6} - 1)$$
$$\beta_{\mathrm{nf}}(V) = 0.264/e^{(V-22)/40}$$
$$I_{\text{sK-DR}} = G_{\text{sK-DR}}(V,t) \cdot (V - EK), \quad E_{\mathrm{K}} = -85\,\mathrm{mV}$$
$$G_{\text{sK-DR}}(V,t) = g^{\max}_{\text{sK-DR}} \cdot n_s^4(V,t)$$
$$\alpha_{\mathrm{ns}}(V) = -0.028(V - 35)/(e^{(V-35)/-6} - 1)$$
$$\beta_{\mathrm{ns}}(V) = 0.1056/e^{(V-10)/40}$$

A-Type Potassium Current

$$I_{\mathrm{KA}} = G_{\mathrm{KA}}(V,t) \cdot (V - EK), \quad E_{\mathrm{K}} = -85\,\mathrm{mV}$$
$$G_{\mathrm{KA}}(V,t) = g^{\max}_{\mathrm{KA}} \cdot k(V,t) \cdot l(V,t)$$
$$\alpha_{\mathrm{k}}(V) = -0.05(V + 25)/(e^{(V+25)/-15} - 1)$$
$$\beta_{\mathrm{k}}(V) = 0.1(V + 15)/(e^{(V+15)/8} - 1)$$
$$\alpha_{\mathrm{l}}(V) = 0.00015/e^{(V+13)/15}$$
$$\beta_{\mathrm{l}}(V) = 0.06/(e^{(V+68)/-12} + 1)$$

Calcium Channels (T, N, and L-Type)

$$I_{\mathrm{TCa}} = G_{\mathrm{TCa}}(V,t) \cdot (V - E_{\mathrm{Ca}})$$
$$G_{\mathrm{TCa}}(V,t) = g^{\max}_{\mathrm{TCa}} \cdot a^2(V,t) \cdot b(V,t)$$
$$\alpha_{\mathrm{a}}(V) = 0.2(19.26 - V)/(e^{(19.26-V)/10} - 1)$$
$$\beta_{\mathrm{a}}(V) = 0.009e^{-V/22.03}$$
$$\alpha_{\mathrm{b}}(V) = 10^{-6}e^{-V/16.26}$$
$$\beta_{\mathrm{b}}(V) = 1/(e^{(29.79-V)/10} + 1)$$
$$I_{\mathrm{NCa}} = G_{\mathrm{NCa}}(V,t) \cdot (V - E_{\mathrm{Ca}})$$
$$G_{\mathrm{NCa}}(V,t) = g^{\max}_{\mathrm{NCa}} \cdot c^2(V,t) \cdot d(V,t)$$

$$\alpha_c(V) = 0.19(19.88 - V)/(e^{(19.98-V)/10} - 1)$$
$$\beta_c(V) = 0.046e^{-V/20.73}$$
$$\alpha_d(V) = 1.6 \cdot 10^{-4} e^{-V/48.4}$$
$$\beta_d(V) = 1/(e^{(39-V)/10} + 1)$$
$$I_{LCa} = G_{LCa}(V, t) \cdot (V - E_{Ca})$$
$$G_{LCa}(V, t) = g_{LCa}^{max} \cdot e^2(V, t)$$
$$\alpha_e(V) = 15.69(81.5 - V)/(e^{(81.5-V)/10} - 1)$$
$$\beta_e(V) = 0.29e^{-V/10.86}$$

Calcium-Dependent Potassium Channels (Big K and Small K)

$$I_C = G_{BK}(V, [Ca^{2+}], t) \cdot (V - E_K), \quad E_K = -85\,\text{mV}$$
$$G_{BK}(V, [Ca^{2+}], t) = g_{BK}^{max} \cdot r(V, t) \cdot s^2([Ca^{2+}])$$
$$\alpha_r(V) = 7.5$$
$$\beta_r(V) = 0.11/e^{(V-35)/14.9}$$
$$s_\infty = 1/(1 + 4/[Ca^{2+}])$$
$$\tau_s = 10$$

$$I_{AHP} = G_{SK}([Ca^{2+}]) \cdot (V - E_K), \quad E_K = -85\,\text{mV}$$
$$G_{SK}([Ca^{2+}]) = g_{SK}^{max} \cdot q^2([Ca^{2+}])$$
$$\alpha_q([Ca^{2+}]) = 0.00246/e^{(12 \cdot \log_{10}([Ca^{2+}]) + 28.48/-4.5}$$
$$\beta_q([Ca^{2+}]) = 0.006/e^{(12 \cdot \log_{10}([Ca^{2+}]) + 60.4/35}$$

Hyperpolarization-Activated Current

$$I_h = G_h(V, t) \cdot (V - E_h)$$
$$G_h = g_h^{max} \cdot c^2(V, t)$$
$$c(V) = 1/(1 + e^{(V-V50)/10}), \quad V_{50soma} = -81\,\text{mV};\ V_{50distaldend} = -91\,\text{mV}$$
$$\tau_{fast}(V) = 14.9 + 14.1/(1 + e^{-(V+95.2)/0.5})$$
$$\tau_{slow}(V) = 80 + 172.7/(1 + e^{-(V+59.3)/-0.83})$$

Additional details on single-cell ion channel models can be found in Aradi and Holmes (1999) and Chen et al. (2001).

Network Parameters

Network Scaling

The size of the model network is a critical issue both for biological realism and computational feasibility. For a network that is implemented with the goal to study the effects of network topology on excitability (as this one was), preserving the structure of the biological network as much as possible is extremely important. On the other hand, obtaining meaningful results in a reasonable timeframe is also a priority. This balance can only be reached by scaling the dentate gyrus network to a size in which simulations can be run on an hours-to-days timescale (approximate runtime of the described model ranged from 12 to 24 h per simulation on a Tyan Thunder 2.0 GHz dual Opteron server with 32 GB RAM) while allowing biologically realistic cell type-specific connectivity (as described below) to be implemented between neurons. The dentate network model was therefore created as a 1:20 scale model of the biological dentate. Cell numbers and other network parameters are detailed in Table 5. Cell type-specific connectivity numbers were determined as described below and subsequently scaled down by a factor of 20 for use in the model. The number of connections was then increased by a factor of 5 in order to prevent cells in the network from becoming disconnected. Synaptic weights were scaled down appropriately to compensate for the increased connectivity.

Cell Type-Specific Connectivity

Over many years a vast amount of high quality data about the connectivity of the dentate gyrus has been collected, and from this data arose the cell type-specific connectivity matrix for the dentate gyrus (Table 1). Each value presented in the table was determined by a detailed survey of the anatomical literature and was based on an assumption of uniform bouton density along the axon of the presynaptic cell. This assumption is in agreement with the in vivo data of Sik et al. (1997), and it is extremely useful in modeling because it greatly simplifies the estimation of connectivity from anatomical data on axonal length and synapse density per unit length of axon. The rationale behind the connectivity of each of the cell types is given in the following eight sections. Finally, the spatial constraints of the model and the role of axonal arbors in shaping cell type-specific connectivity is explained in Spatial Constraints and Axonal Distributions.

Granule Cells

Mossy fibers (GC axons) in the healthy rat dentate gyrus are primarily restricted to the hilus (97%), with few collaterals (3%) in the GC layer (Buckmaster and Dudek 1999). In addition to MCs (Acsady et al. 1998), mossy fibers have also been shown to contact BCs (Buckmaster and Schwartzkroin 1994; Geiger et al. 1997) and PV interneurons (Blasco-Ibanez et al. 2000). With a total of 400–500 synaptic

contacts made by a single mossy fiber (Acsady et al. 1998), the 3% of each axon located in the GC layer (Buckmaster and Dudek 1999) is estimated to contact 15 BCs and 3 axo-axonic cells. In the hilus, a single GC forms large, complex mossy fiber boutons that innervate 7–12 MCs (Acsady et al. 1998), while an estimated 100–150 mossy fiber terminals target hilar interneurons with approximately one synapse per postsynaptic interneuron (Acsady et al. 1998). Gulyas et al. (1992) estimated that a single spiny calretinin-positive cell (presumed HIPP cell) is contacted by about 9,000 GCs. With 12,000 HIPP cells and 1,000,000 GCs, each GC can be estimated to contact about 110 HIPP cells and 40 HICAP cells. Additionally, in agreement with the presence of mossy fiber terminals on aspiny calretinin-positive interneurons (Acsady et al. 1998), 15 mossy fibers are expected to synapse onto IS cells. Since mossy fibers avoid the molecular layer (Buckmaster and Dudek 1999) in the healthy dentate gyrus, it is assumed that they do not contact MOPP cells. However, in animal models of temporal lobe epilepsy, sprouted mossy fibers have been shown to contact up to 500 postsynaptic GCs (Buckmaster et al. 2002b).

Mossy Cells

A single filled MC axon has been reported to make 35,000 synapses in the inner molecular layer (Buckmaster et al. 1996; Wenzel et al. 1997). Assuming a single synapse per postsynaptic cell, a single MC is estimated to contact 30,000–35,000 GCs. Of the 2,700 synapses made by a single MC axon in the hilus, about 40% target GABA-negative neurons (Wenzel et al. 1997). As each MC is estimated to make 1–5 synaptic contacts on a single postsynaptic MC (Buckmaster et al. 1996), it is estimated that each MC contacts about 350 other MCs. (This is likely to be a generous estimate since it is based on the assumption that all GAD negative somata in the hilus represent MCs.) The remaining 60% of the hilar MC axons target GABA-positive cells (Buckmaster et al. 1996; Wenzel et al. 1997), with no reports demonstrating MC synapses onto IS cells. Assuming that there is no preferential target selectivity between HIPP and HICAP cells and that each postsynaptic hilar interneuron receives two synaptic contacts from a single MC axon (Buckmaster et al. 1996), each MC is estimated to contact 600 HIPP and 200 HICAP cells. There is very low MC to interneuron connectivity in the inner molecular layer (Wenzel et al. 1997); MCs could contact 5–10 basket and axo-axonic cells and approximately 5 MOPP cells with somata in the inner molecular layer (Han et al. 1993).

Basket Cells

In the CA3 region of the rat hippocampus, each principal cell is contacted by about 200 BCs (Halasy and Somogyi 1993), but a GC in the dentate could be contacted by as few as 30 BCs. Assuming that each of the 1,000,000 GCs is contacted by 115 BCs each making 1–20 synaptic connections (Halasy and Somogyi 1993; Acsady et al. 2000), it can be estimated that each BC contacts about 1,250 GCs. MCs receive 10–15 BC synapses (Acsady et al. 2000), resulting in an estimate of 75 BC to MC synapses per BC. Approximately 1% of the 11,000 synapses made by

a single BC axon in the GC layer are onto other BCs (Sik et al. 1997), with 3–7 synapses per postsynaptic cell (Bartos et al. 2001). Consequently, each BC in the dentate gyrus contacts approximately 35 other BCs. Since hilar and molecular layer interneurons are not a major target of BCs (Halasy and Somogyi 1993), a single BC may contact 0–1 HIPP cells. Similarly, the BC synapses onto axo-axonic cells, HICAP, and MOPP cells are assumed to be negligible. As PV cells preferentially contact other PV cells in the hilus (Acsady et al. 2000), we assume that BCs do not contact calretinin-positive IS cells (Gulyas et al. 1992).

Axo-Axonic Cells

Most synapses made by axo-axonic cell axons are thought to target GC axon initial segments (Halasy and Somogyi 1993). However, a small fraction of axon collaterals also descend into the superficial and deep hilus (Han et al. 1993; Freund and Buzsáki 1996). In neocortex, an axo-axonic cell makes 4–10 synapses on the axon intial segment of a postsynaptic cell (Li et al. 1992). With 22,000,000 estimated axon initial segment synapses in the GC layer (Halasy and Somogyi 1993) and 4 synapses per postsynaptic cell (based on the data from the neocortex from Li et al. 1992), each of the 2,000 axo-axonic cells are estimated to target about 3,000 GCs. MCs receive axo-axonic cell input (Ribak et al. 1985), and with the comparatively small fraction of axons from axo-axonic cells in the hilus (Han et al. 1993; Freund and Buzsáki 1996), it can be estimated that axo-axonic cells target a number of MCs equal to about 5% of their GC targets, which results in approximately 150 MCs. Since axo-axonic cells primarily target the axon initial segment of non-GABAergic cells (Halasy and Somogyi 1993; Freund and Buzsáki 1996), it may be assumed that these cells do not project to interneurons.

HIPP Cells

HIPP cells have been estimated to contact about 1,600 GCs and 450 BCs with 1–5 synapses per postsynaptic cell (Sik et al. 1997). MCs can have one dendrite in the molecular layer (Buckmaster et al. 1996) which can be targeted by HIPP cell axons, whereas GCs have two primary dendrites (Claiborne et al. 1990; Lubke et al. 1998). Since the MC to GC ratio is approximately 1:30, the MC dendrites constitute only about 1/60 of the targets for HIPP cells. Increasing this fraction to about 1/45 to account for the presence of a few HIPP cell contacts on MCs in the hilus (Buckmaster et al. 2002a) results in an estimate that each HIPP cell contacts about 35 MCs. HIPP cell axonal divergence onto HICAP and MOPP cells in the molecular layer can be assumed to be similar to that of somatostatin-positive cells in CA1 (Katona et al. 1999) and estimated to be 15 connections onto each population. The HIPP cell axonal divergence to axo-axonic cells is estimated to be between the divergence to basket and HICAP cells; therefore the HIPP cell axon likely contacts 30 axo-axonic cells.

MOPP Cells

MOPP cells target an estimated 7,500 GCs in the rat dentate gyrus. While MOPP cell axons project in the horizontal axis to a similar extent as HIPP cells, they show considerably less collateralization (Han et al. 1993), resulting in an estimate of half as many synapses onto MOPP and HICAP cells as HIPP cells make. As MOPP cell axons are restricted to the molecular layer (Han et al. 1993) and do not target the basal dendrites of BCs, they are assumed to contact less than 1/10 the number of BCs targeted by HIPP cells. Likewise, MOPP cells with axons restricted to the outer and middle molecular layers (Han et al. 1993) would not target the hilar dendrites of axo-axonic cells (Soriano et al. 1990) or the axo-axonic cells with somata and proximal dendrites in the hilus (Han et al. 1993). It is estimated that MOPP cells only contact 1–2 axo-axonic cells. As the MOPP cell axonal arbors in the molecular layer (Han et al. 1993) do not overlap with major parts of the dendritic arborizations of MCs (Frotscher et al. 1991), HIPP cells (Han et al. 1993; Sik et al. 1997; Katona et al. 1999), or IS cells (Gulyas et al. 1996), the connectivity to these cells is negligible.

HICAP Cells

Sik et al. (1997) estimated that the septo-temporal extent and bouton density of HICAP cell axons is similar to that of the HIPP cell axons, whereas the estimated axonal length of HICAP cells is approximately half of the HIPP cell axonal length. Thus, it is estimated that HICAP cells contact about half the number of GCs contacted by HIPP cells. However, since HICAP cells have an additional 3% of axon collaterals in the hilus (Sik et al. 1997), their number of postsynaptic MCs can be assumed to be the same as that of the HIPP cells. HICAP cells are assumed to contact less than half the number of BCs targeted by HIPP cells (∼175) and a negligible number of axo-axonic cells. With a total of 26,000 synapses from a single HICAP cell axon (Sik et al. 1997), approximately 700 synapses should be present in the hilus. Assuming 2–5 synapses per postsynaptic cell, each HICAP cell could contact 100–300 hilar cells. Each HICAP cell is assumed to target 50 HIPP and HICAP cells, which, along with 35 synapses on MCs, is in the estimated range. Although the total axonal length of HICAP cells is only about half of that of HIPP cells, the number of MOPP cells targeted is assumed to be the same (∼10–20), as the HICAP cell axons primarily project to the inner molecular layer where both cell bodies and proximal dendrites of MOPP cells are located (Han et al. 1993).

IS Cells

IS cells contact an estimated 100–800 other IS cells and 5–10 (presumably CCK positive) BCs (Gulyas et al. 1996). Acsady et al. (2000) suggested that CCK cells would include both BC and HICAP morphologies and that IS cells also project to somatostatin-positive HIPP cells. These data result in an estimate that IS cells project to 5–10 HICAP cells and HIPP cells.

Spatial Constraints and Axonal Distributions

The dentate gyrus was represented as a 6 mm strip (corresponding to the approximate septo-temporal extent of the rat dentate gyrus; West et al. 1978) subdivided into 60-μm bins. Cells were distributed evenly among these bins. In addition to the cell type-specific connection probabilities derived from the average number of projections from the pre- to the postsynaptic neuronal class in the literature (i.e., according to the connectivity matrix shown in Table 5), the probability of connections from one particular cell A to another cell B was also dependent on the extent of the axonal arbor of cell A and the relative distance between cells A and B. Therefore the cell type-specific connection probability was modified by a factor obtained by the normalized Gaussian fits to the experimentally determined axonal distributions of the presynaptic cells (Fig. 3) and the relative positions of the pre- and postsynaptic neurons within the dentate strip. Within these cell type-specific constraints, connections were made probabilistically on a neuron to neuron basis with a uniform synapse density along the axon (in agreement with the in vivo data in Sik et al. (1997)), treating multiple synapses between two cells as a single link and excluding autapses.

Receptor Types and Synapses

Building a model of a dentate network with thousands of biophysically realistic multicompartmental model cells is only a meaningful venture if those cells have a way to talk to one another. They can do so via synaptic contacts, but the precise synaptic mechanisms to be included in the model must be determined, and again what to include depends on the particular goal of the model. For the dentate model with the previously-mentioned goal of determining the role of mossy fiber topology in promoting excitability after injury, the minimal requirement is to incorporate ionotropic glutamatergic AMPA synapses (for excitatory transmission) and $GABA_A$ synapses (for inhibitory transmission). Experiments from both normal and epileptic animals are constantly ongoing, and as the data become available it will be possible to add other receptors such as NMDA and metabotropic receptors. Each addition to the network must be carefully considered, however, as greater complexity necessarily increases the load on the computational resources. Since the basic circuit effects of mossy fiber sprouting and cell loss post-injury can be simulated by including AMPA and $GABA_A$ synapses, these were the only synaptic subtypes included in the dentate model.

Postsynaptic conductances were represented as a sum of two exponentials (Bartos et al. 2001). The peak conductance (g_{max}), rise and decay time constants, and synaptic delays for each network connection were estimated from experimental data (Kneisler and Dingledine 1995; Geiger et al. 1997; Bartos et al. 2001; Santhakumar et al. 2005) and are given in Table 5.

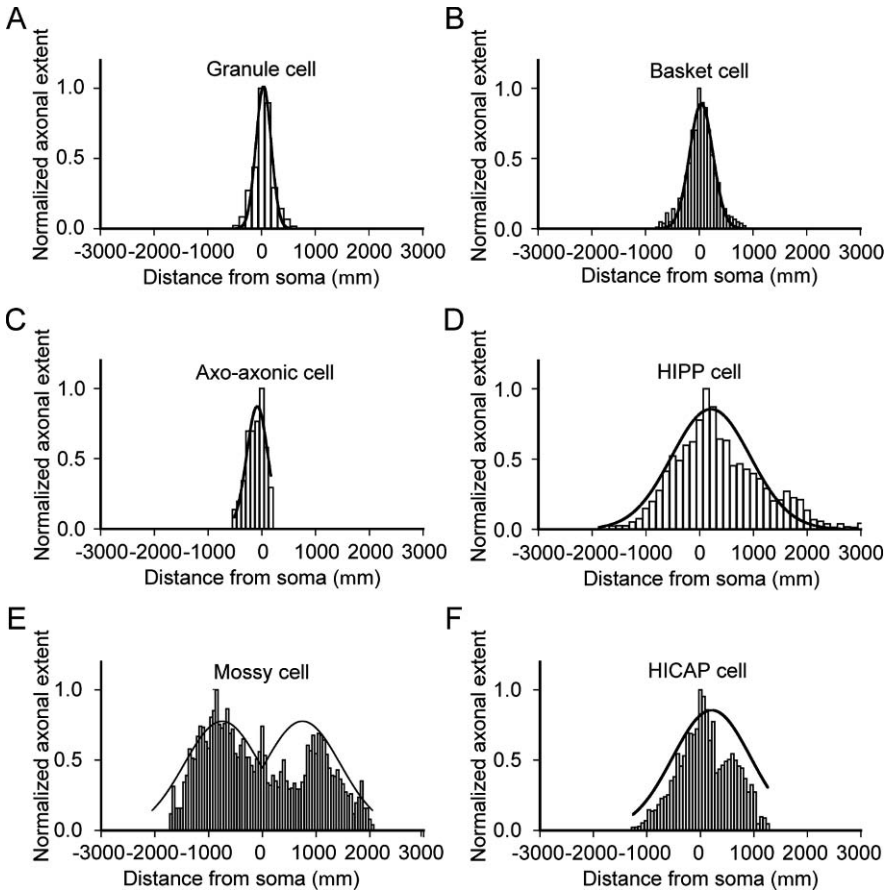

Fig. 3 Gaussian fits to experimentally determined distributions of axonal branch length used in construction of the structural and functional models of the dentate gyrus. **a**. Plot shows the averaged axonal distribution of 13 granule cells (Buckmaster and Dudek 1999) and the corresponding Gaussian fit. **b**. Fit to the septo-temporal distribution of axonal lengths of a filled and reconstructed basket cell (Sik et al. 1997). **c**. Fit to the axonal distribution of a CA1 axo-axonic cell (Li et al. 1992). **d**. Gaussian fit to the averaged axonal distributions of three HIPP cells from gerbil (Buckmaster et al. 2002a). **e**. Fit to averaged axonal distributions of three mossy cells illustrates the characteristic bimodal pattern of distribution (Buckmaster et al. 1996). **f**. Histogram of the axonal lengths of a HICAP cell along the long axis of the dentate gyrus (Sik et al. 1997) and the Gaussian fit to the distribution. All distributions were based on axonal reconstruction of cells filled in vivo. In all plots, the septal end of the dentate gyrus is on the *left* (indicated by negative coordinates) and the soma is located at zero. Used with permission from Dyhrfjeld-Johnsen et al. (2007)

Network Topology

The shape of the network and the way in which connections are made depend strongly on the size of the network. For instance, a network of approximately 50 or 500 cells (Lytton et al. 1998; Santhakumar et al. 2005, respectively) may require

a ring structure to avoid edge effects (i.e., cells on the edge of a network have as few as half as many presynaptic and postsynaptic targets compared to cells in the middle). The network presented here, however, (Dyhrfjeld-Johnsen et al. 2007, Morgan and Soltesz 2008), is large enough that it was set up as a linear strip, more similar to the actual topology of the biological dentate. Similarly, small networks may require non-topographic connectivity. That is, the postsynaptic targets of each cell are selected at random from the pool of potential target neurons while maintaining the cell type-specific divergence and convergence. Larger networks can incorporate the spatial rules discussed above in section "Spatial constraints and axonal distributions" where the connectivity is derived from the axonal distributions and cell type-specific connectivity probabilities established from the literature.

Network topology is an extremely important consideration even on a much finer scale microcircuit level. Indeed, nonrandom connectivity patterns within the recurrent mossy fiber circuit after dentate injury have been shown to play major roles in influencing network excitability (Morgan and Soltesz 2008). The presence of even a small number of highly interconnected GCs that serve as "hubs" can promote seizure-like activity propagation in the dentate. It is therefore very important to carefully consider the potential biological topologies of the network being constructed and, if the particular question the model is designed to answer is thought to be independent of topology, to perform adequate controls to ensure model robustness in the face of topological alterations. The role of network topology in promoting excitability in the dentate microcircuit will be more fully discussed in a later section.

Network Stimulation

The final consideration that must be discussed is the way in which the network is stimulated. The dentate network described in this chapter contains four cell types of which only the MCs have been programmed to have spontaneous activity (and this is a variable parameter which can be turned off by the modeler if desired). Thus, if the network is allowed to run with no afferent stimulus, it will simply sit in a quiescent state with very few neurons firing. This is not entirely uncharacteristic of the dentate gyrus, as it is presumed to be a gate that can filter activity and prevent aberrant propagation throughout the hippocampus, but it is not terribly informative to watch a network do nothing. Additionally, the GCs (among others) in the dentate gyrus are known to receive input from the perforant path (the path that projects from the entorhinal cortex to the hippocampal formation), and this input is quite strong. For this model, the perforant-path input was located on both dendrites of all GCs and the apical dendrites of all BCs. Since 15% of MCs have also been shown to receive direct perforant-path input (Scharfman 1991; Buckmaster et al. 1992), this percentage of MCs also received input. Mass stimulation of the perforant path was simulated by activating a maximum peak AMPA conductance in cells postsynaptic to the stimulation (Santhakumar et al. 2000). The strength of the perforant-path input is shown in Table 5 (note the very large synaptic weight for perforant-path input compared to the small weights for cell-to-cell synapses). In the biological network and in physiological studies it is unlikely that the entire network is activated

simultaneously. Therefore, this network employed a focal stimulation in which a single lamella of the dentate (equivalent to 10% of the dentate strip) was stimulated via the perforant-path input. Other methods of stimulation are also possible, such as providing uncorrelated activation (perforant-path inputs with Poisson distributed interspike intervals; see Dyhrfjeld-Johnsen et al. (2007)) to each GC, BC, and 15% of the MCs. Additional methods for initiation of network activity can be devised as necessary.

Simulated Dentate Injury

Since one of the main purposes of this model was to determine the role of injury-induced structural alterations on network excitability, there had to be a way to simulate the injury. The two primary injury-induced structural alterations in the dentate are the formation of previously nonexistent GC-to-GC connections via mossy fiber sprouting, and the loss of a percentage of MCs and hilar interneurons (the HIPP cells). Mossy fiber sprouting was simulated by first determining the maximum number of new GC-to-GC connections that have been reported in the literature (approximately 275 new connections per GC following pilocarpine-induced status epilepticus in rats (Buckmaster et al. 2002b)), and then scaling this value appropriately (as described for the connectivity above) and implementing the desired percentage of the maximum for moderate injuries. Likewise, hilar interneuron and MC loss were implemented by removing a different percentage of cells at different levels of injury. The model results showed that increasing levels of injury changed both the structure and function of the dentate gyrus, with functional activity closely paralleling the structural alterations. As the dentate network became more highly clustered and interconnected via mossy fiber sprouting, activity increased. However, when nearly all the MCs died, eliminating the primary source of long range connections in the network, the network was no longer as capable of propagating signals over long distances and overall activity and synchrony decreased (Fig. 4, combination of mossy fiber sprouting and cell loss is collectively referred to as "sclerosis" – note that as sclerosis progresses to 80%, there is an increase in network activity followed by a decrease at 100%). The interested reader should refer to Dyhrfjeld-Johnsen et al. (2007) for a more thorough analysis of the topological determinants of epileptogenesis revealed by this model.

Tests for Robustness

As mentioned throughout this chapter, it is important to ensure that the model is robust both in its control state and in its final predictions or in findings to alterations in variables from which the main question should be independent. In a model of this size and complexity, these tests for robustness are particularly important. Therefore, numerous simulations were carried out, and detailed analysis of the various con-

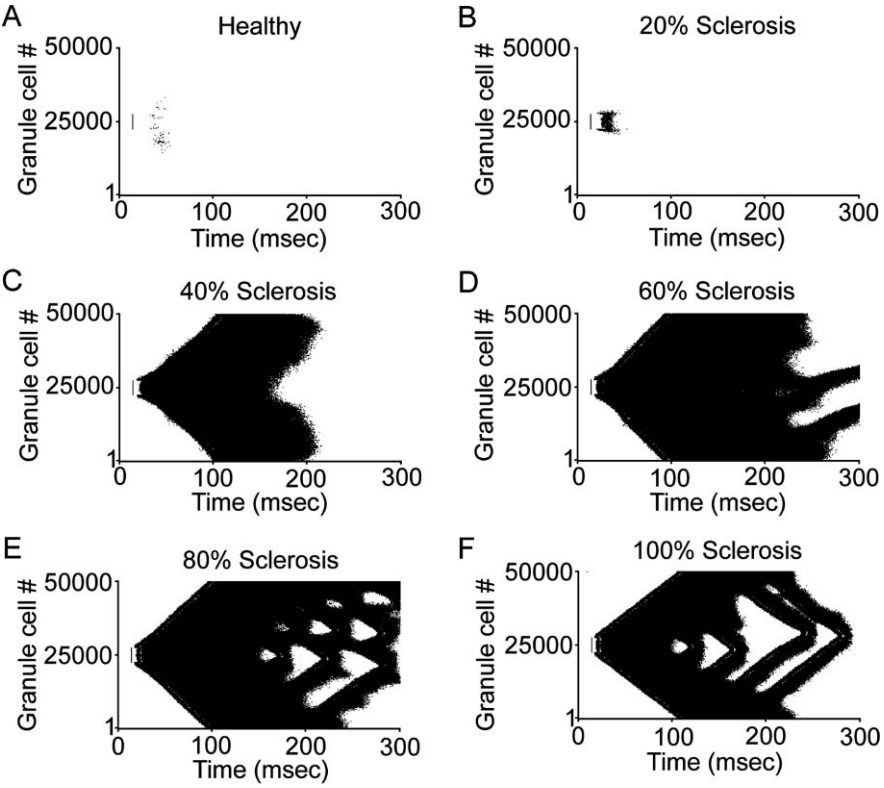

Fig. 4 Effects of the injury-induced topological changes on granule cell activity in functional model networks. **a–f**. Raster plots of the first 300 ms of granule cell action potential firing in the functional model network (Granule cells #1–#50,000, plotted on the y-axis) at increasing degrees of sclerosis. Network activity was initiated by a single stimulation of the perforant-path input to granule cells #22,500 to #27,499 and to 10 mossy cells and 50 basket cells (distributed in the same area as the stimulated granule cells) at t = 5 ms (as in Santhakumar et al. 2005). Note that the most pronounced hyperactivity was observed at submaximal (80%) sclerosis with a decrease in overall activity at 100% sclerosis. Used with permission from Dyhrfjeld-Johnsen et al. (2007)

ditions present in the simulations can be found in Dyhrfjeld-Johnsen et al. (2007). Briefly, the simulations included the following:

1. Variations in cell numbers
2. Variations in connectivity estimates
3. Inhomogeneous distribution of neuron densities along the septo-temporal axis
4. Inhomogeneity in connectivity along the transverse axis
5. Altered neuronal distributions at the septal and temporal poles (the anatomical boundaries of the dentate gyrus)
6. Offset degrees of mossy fiber sprouting and cell loss (after simulated injury)
7. Implementation of a bilateral model of the dentate gyrus including commissural projections and over 100,000 multicompartmental cells

8. Double inhibitory conductance values
9. Variable axonal delays
10. Spontaneous instead of evoked perforant-path stimulation

Using the Dentate Model to Understand the Importance of Hippocampal Microcircuit Topology

The modeling results discussed briefly in section "Simulated Dentate Injury" showed that after dentate injury, the newly formed connections between GCs are instrumental in creating a hyperexcitable dentate network. However, GC-to-GC connectivity is quite sparse; indeed, GCs in the biological dentate only connect to approximately 275 other GCs out of 100,000 potential targets (Buckmaster et al. 2002b). This means that the probability of two GCs connecting, even at maximal levels of sprouting, is only approximately 0.55%, and the probability of random formation of a three-neuron "recurrent" circuit where cell A connects to B which connects to C and back to A is miniscule at 4.16×10^{-6}%. Therefore, the specific patterns of GC-to-GC connections that define the microcircuit structure are likely to play a critical role in affecting network excitability.

The recurrent activity within the GC network may arise from the formation of nonrandom patterns of connectivity that can substantially increase the probability of hyperexcitability and seizures. Other research with this model (such as that described in section "Simulated Dentate Injury") implemented mossy fiber sprouting using random connectivity with the only constraint being the Gaussian distribution of the GC axonal arbors. However, numerous studies have indicated that connectivity in a wide variety of neural systems exhibits highly nonrandom characteristics. For example, the nervous system of the *C. elegans* worm has local connectivity patterns (network motifs) that are over- or underrepresented compared to what would be present in a random network (Milo et al. 2002; Reigl et al. 2004; Sporns and Kotter 2004). These connectivity patterns have dynamical properties that could influence their abundance, closely tying structure to function (Prill et al. 2005). Nonrandom connectivity features such as power-law distributions of connectivity (scale-free topology; Watts and Strogatz 1998; Barabasi and Albert 1999; Dyhrfjeld-Johnsen et al. 2007) and nonrandom distributions of connection strengths (Song et al. 2005) have been discovered in mammalian cortices as well. Additionally, it has been shown that connection probabilities can demonstrate fine-scale specificity that is dependent both upon neuronal type and the presence or absence of other connections in the network (Yoshimura and Callaway 2005).

Morgan and Soltesz (2008) therefore used this model to examine the role of several biologically plausible GC microcircuits on dentate excitability after a moderate insult (resulting in 50% of maximal mossy fiber sprouting and 50% loss of MCs and hilar interneurons). They discovered that a small percentage of highly interconnected GCs serving as network "hubs" can greatly augment hyperexcitability in the model (Fig. 5a, diamonds represent hub cells). This change in hyperexcitability

was mediated only by a change in the topology of GC-to-GC connections in the network (i.e., only the GC-to-GC connections were reconnected such that 5% of all GCs had approximately 5 times as many connections as the average GC; Fig. 5a), as no other network connections were altered and the total number of connections in the dentate network remained constant at all times. Figure 5b displays network activity from this model network incorporating 50% of the maximum mossy fiber sprouting and 50% of MC and hilar interneuron loss when GC-to-GC connections were made randomly. Figure 5c shows activity of the network in which 5% of GCs were vastly more interconnected than the average GC, creating network hubs (Fig. 5a – it was necessary for hubs to have both enhanced incoming as well as outgoing connectivity in order to effectively increase network excitability; refer to Fig. 4d in Morgan and Soltesz (2008)). Figure 5d shows traces from both an average GC and a hub cell, demonstrating the powerful impact that topological changes in hippocampal microcircuits can exert on cellular activity. Inclusion of hub cells massively enhanced excitability of the dentate network without changing the total excitatory drive of the network, demonstrating the importance that hub cells can play seizures.

Computational models are most effectively utilized when they either confirm experimental findings or provide predictions that can be tested experimentally. Therefore, the finding that hub cells can promote hyperexcitability in the dentate means little unless there is biological evidence for the model's prediction. Indeed, there are cells in the dentate gyrus that have a very long basal dendrite which receives many times more incoming excitatory synaptic connections than average GCs (Spigelman et al. 1998). However, these cells with basal dendrites had previously been shown only to have increased incoming connectivity, and the model predicted that hubs need both increased incoming and outgoing connectivity. Until recently, there were no data suggesting whether GCs with basal dendrites form either more numerous or stronger outgoing connections. In agreement with the model, though, a study of post-status epilepticus GCs recently revealed a previously unseen increase in axonal protrusions (often within the GC layer) among newborn cells that likely corresponds to an increased number of outgoing connections onto other GCs (Walter et al. 2007). Additionally, over 40% of post-SE newborn GCs retain a basal dendrite in addition to nearly 10% of mature post-status epilepticus (SE) GCs (Walter et al. 2007), thereby resulting in the probable existence of GCs with both increased axonal protrusions *and* a basal dendrite (i.e., satisfying the model's requirement for both enhanced incoming as well as outgoing connectivity). While more experimental work is necessary to fully characterize the outgoing connectivity of GCs with basal dendrites, our results combined with the described experimental work strongly support the likelihood that neuronal hubs play a hitherto unrecognized, major role in promoting hyperexcitability and seizures.

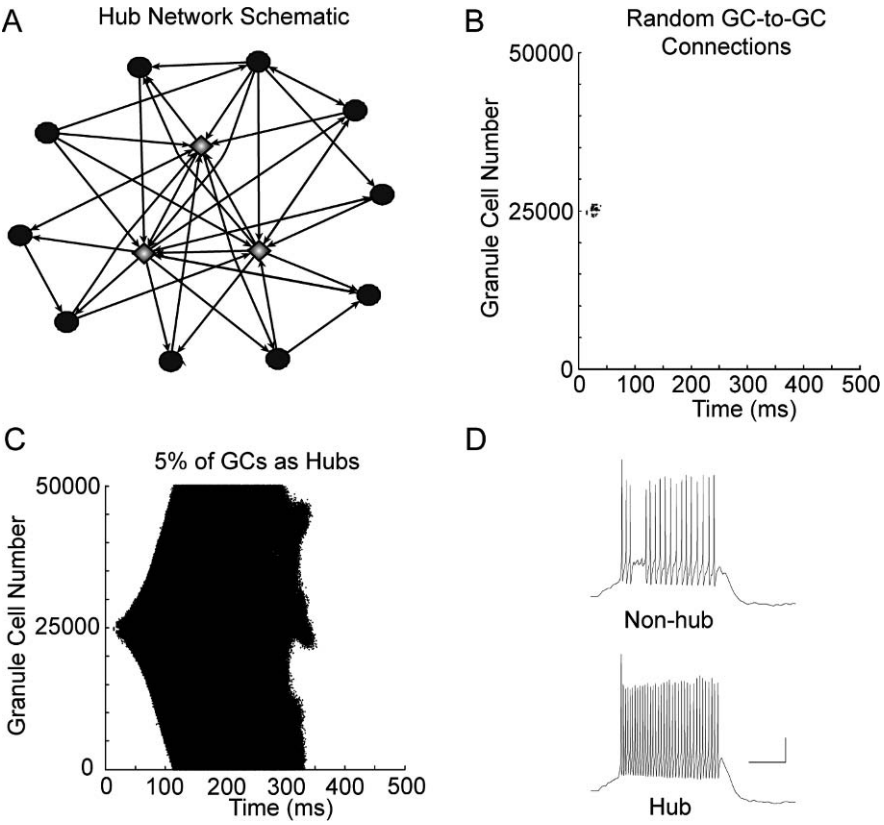

Fig. 5 Granule cell hubs can promote hyperexcitability in the dentate gyrus. **a**. Schematic of a hub network. Average granule cells (*black circles*) have relatively few connections compared to the highly interconnected hubs (*grey diamonds*). **b**. Raster plot of granule cell activity in response to simulated perforant-path stimulation of 1,000 granule cells, 1 mossy cell, and 5 basket cells, in the network in which sprouted mossy fibers connected randomly onto other granule cells. Note that this network was implemented at 50% mossy fiber sprouting and 50% mossy cell and hilar interneuron loss. **c**. Raster plot of granule cell activity in response to the same stimulation as in (**b**), but in the network in which 5% of granule cells participated in many more connections than the average granule cell. (scale: 20 mV and 100 ms). **d**. Representative traces of a non-hub (*top*) and hub (*bottom*) granule cell (scale: 20 mV and 100 ms). Used with permission from Morgan and Soltesz (2008)

Future Directions for the Dentate Model

Both computational power and our knowledge of the inner workings of the dentate gyrus are expanding rapidly. For computational modelers interested in the dentate, this is an ideal situation. While no model can ever fully capture the complete reality of the biological system it attempts to model, it is only by increasing our knowledge of the biology that we can become more confident in models' abilities to make accurate predictions. Likewise, it is by increasing the complexity and detail of models

that we can learn more about what to look for in biological systems. Thus, modelers must look for numerous ways in which to improve a large-scale model like the one discussed in this chapter in order to increase its realism and predictive utility, some of which have been mentioned previously. Most obviously, the size of the model can be expanded to approach the number of cells in the biological dentate. This expansion would allow the most realistic connectivity, without the need for scaling factors or somewhat arbitrary compensations to synaptic weights and connection numbers. Additionally, it would pave the way for construction of bilateral models of the dentate. While this has already been done for the current model, more biological data is required to better implement the commissural connectivity and more computational power is necessary to handle the doubling of the model's size. Further additions to the model that are currently in progress are the inclusion of the omitted interneurons. Specifically, model MOPP cells are nearly completed and will be included in the model soon. Numerous other model expansions have not yet begun but could increase the biological realism of the model as well as present new and interesting questions. These include the addition of short-term and long-term plasticity mechanisms (and the requisite inclusion of NMDA synaptic elements), gap junctions, and realistic dendritic arbors like the axonal distributions in Fig. 3. Finally, the dentate model can be combined with other detailed models of entorhinal cortex, CA1, CA3, and the subiculum to create a truly realistic hippocampal circuit.

Highly detailed, large-scale models of hippocampal microcircuits will someday make it possible to cheaply and efficiently test new therapeutic agents for neurological disorders such as epilepsy, determine the effects of selective surgical lesions on hippocampal function, and provide new insights into the interplay between hippocampus and other brain regions in pathological states (Soltesz and Staley 2008). As computational resources expand and new biological data is discovered, computational modeling will only become more useful as a tool to tie all of our newfound knowledge together and create order from complexity.

Acknowledgments This work was funded by NIH grant NS35915 to IS and UCI MSTP to RM.

Further Reading

Acsady L, Kamondi A, Sik A, Freund T, Buzsaki G (1998) GABAergic cells are the major postsynaptic targets of mossy fibers in the rat hippocampus. J Neurosci 18, 3386–3403.

Acsady L, Katona I, Martinez-Guijarro FJ, Buzsaki G, Freund TF (2000) Unusual target selectivity of perisomatic inhibitory cells in the hilar region of the rat hippocampus. J Neurosci 20, 6907–6919.

Amaral DG (1978) A Golgi study of cell types in the hilar region of the hippocampus in the rat. J Comp Neurol 182, 851–914.

Aradi I and Holmes WR (1999) Role of multiple calcium and calcium-dependent conductances in regulation of hippocampal dentate granule cell excitability. J Comput Neurosci 6, 215–235.

Barabasi AL and Albert R (1999) Emergence of scaling in random networks. Science 286, 509–512.

Bartos M, Vida I, Frotscher M, Geiger JRP, Jonas P (2001) Rapid signaling at inhibitory synapses in a dentate gyrus interneuron network. J Neurosci 21, 2687–2698.

Blasco-Ibanez JM, Martinez-Guijarro FJ, Freund TF (2000) Recurrent mossy fibers preferentially innervate parvalbumin-immunoreactive interneurons in the granule cell layer of the rat dentate gyrus. Neuroreport 11, 3219–3225.

Boss BD, Peterson GM, Cowan WM (1985) On the number of neurons in the dentate gyrus of the rat. Brain Res 338, 144–150.

Buckmaster PS and Dudek FE (1999) In vivo intracellular analysis of granule cell axon reorganization in epileptic rats. J Neurophysiol 81, 712–721.

Buckmaster PS and Jongen-Relo AL (1999) Highly specific neuron loss preserves lateral inhibitory circuits in the dentate gyrus of kainate-induced epileptic rats. J Neurosci 19, 9519–9529.

Buckmaster PS and Schwartzkroin PA (1994) Hippocampal mossy cell function: a speculative view. Hippocampus 4, 393–402.

Buckmaster PS, Strowbridge BW, Kunkel DD, Schmiege DL, Schwartzkroin PA (1992) Mossy cell axonal projections to the dentate gyrus molecular layer in the rat hippocampal slice. Hippocampus 2, 349–362.

Buckmaster PS, Strowbridge BW, Schwartzkroin PA (1993) A comparison of rat hippocampal mossy cells and CA3c pyramidal cells. J Neurophysiol 70, 1281–1299.

Buckmaster PS, Wenzel HJ, Kunkel DD, Schwartzkroin PA (1996) Axon arbors and synaptic connections of hippocampal mossy cells in the rat in vivo. J Comp Neurol 366, 270–292.

Buckmaster PS, Yamawaki R, Zhang GF (2002a) Axon arbors and synaptic connections of a vulnerable population of interneurons in the dentate gyrus in vivo. J Comp Neurol 445, 360–373.

Buckmaster PS, Zhang GF, Yamawaki R (2002b) Axon sprouting in a model of temporal lobe epilepsy creates a predominantly excitatory feedback circuit. J Neurosci 22, 6650–6658.

Chen K, Aradi I, Thon N, Eghbal-Ahmadi M, Baram TZ, Soltesz I (2001) Persistently modified h-channels after complex febrile seizures convert the seizure-induced enhancement of inhibition to hyperexcitability. Nat Med 7, 331–337.

Claiborne BJ, Amaral DG, Cowan WM (1990) Quantitative, three-dimensional analysis of granule cell dendrites in the rat dentate gyrus. J Comp Neurol 302, 206–219.

Cossart R, Dinocourt C, Hirsch JC, Merchan-Perez A, De Felipe J, Ben-Ari Y, Esclapez M, Bernard C (2001) Dendritic but not somatic GABAergic inhibition is decreased in experimental epilepsy. Nat Neurosci 4, 52–62.

Desmond NL and Levy WB (1985) Granule cell dendritic spine density in the rat hippocampus varies with spine shape and location. Neurosci Lett 54, 219–224.

Dyhrfjeld-Johnsen J, Santhakumar V, Morgan RJ, Huerta R, Tsimring L, Soltesz I (2007) Topological determinants of epileptogenesis in large-scale structural and functional models of the dentate gyrus derived from experimental data. J Neurophysiol 97, 1566–1587.

Freund TF and Buzsaki G (1996) Interneurons of the hippocampus. Hippocampus 6, 347–470.

Frotscher M, Seress L, Schwerdtfeger WK, Buhl E (1991) The mossy cells of the fascia dentata: a comparative study of their fine structure and synaptic connections in rodents and primates. J Comp Neurol 312, 145–163.

Gaarskjaer FB (1978) Organization of mossy fiber system of rat studied in extended Hippocampi .1. Terminal area related to number of granule and pyramidal cells. J Comp Neurol 178, 49–71.

Geiger JRP, Lubke J, Roth A, Frotscher M, Jonas P (1997) Submillisecond AMPA receptor-mediated signaling at a principal neuron-interneuron synapse. Neuron 18, 1009–1023.

Gulyas AI, Hajos N, Freund TF (1996) Interneurons containing calretinin are specialized to control other interneurons in the rat hippocampus. J Neurosci 16, 3397–3411.

Gulyas AI, Miettinen R, Jacobowitz DM, Freund TF (1992) Calretinin is present in nonpyramidal cells of the rat hippocampus. 1. A new type of neuron specifically associated with the mossy fiber system. Neuroscience 48, 1–27.

Halasy K and Somogyi P (1993) Subdivisions in the multiple GABAergic innervation of granule cells in the dentate gyrus of the rat hippocampus. Eur J Neurosci 5, 411–429.

Hama K, Arii T, Kosaka T (1994) Three-dimensional organization of neuronal and glial processes: high voltage electron microscopy. Microsci Res Tech 29, 357–367.

Han ZS, Buhl EH, Lorinczi Z, Somogyi P (1993) A high degree of spatial selectivity in the axonal and dendritic domains of physiologically identified local-circuit neurons in the dentate gyrus of the rat hippocampus. Eur J Neurosci 5, 395–410.

Heinemann U, Beck H, Dreier JP, Ficker E, Stabel J, Zhang CL (1992) The dentate gyrus as a regulated gate for the propagation of epileptiform activity. Epilepsy Res Suppl 7, 273–280.

Howard A, Tamas G, Soltesz I (2005) Lighting the chandelier: new vistas for axo-axonic cells. Trends Neurosci 28, 310–316.

Katona I, Acsady L, Freund TF (1999) Postsynaptic targets of somatostatin-immunoreactive interneurons in the rat hippocampus. Neuroscience 88, 37–55.

Kneisler TB and Dingledine R (1995) Spontaneous and synaptic input from granule cells and the perforant path to dentate basket cells in the rat hippocampus. Hippocampus 5, 151–164.

Li XG, Somogyi P, Tepper JM, Buzsaki G (1992) Axonal and dendritic arborization of an intracellularly labeled chandelier cell in the Ca1 region of rat hippocampus. Exp Brain Res 90, 519–525.

Lothman EW, Stringer JL, Bertram EH (1992) The dentate gyrus as a control point for seizures in the hippocampus and beyond. Epilepsy Res Suppl 7, 301–313.

Lubke J, Frotscher M, Spruston N (1998) Specialized electrophysiological properties of anatomically identified neurons in the hilar region of the rat fascia dentata. J Neurophysiol 79, 1518–1534.

Lytton WW, Hellman KM, Sutula TP (1998) Computer models of hippocampal circuit changes of the kindling model of epilepsy. Artif Intell Med 13, 81–97.

Milo R, Shen-Orr S, Itzkovitz S, Kashtan N, Chklovskii D, Alon U (2002) Network motifs: simple building blocks of complex networks. Science 298, 824–827.

Morgan RJ and Soltesz I (2008) Nonrandom connectivity of the epileptic dentate gyrus predicts a major role for neuronal hubs in seizures. Proc Natl Acad Sci U S A 105, 6179–6184.

Nomura T, Fukuda T, Aika Y, Heizmann CW, Emson PC, Kobayashi T, Kosaka T (1997a) Distribution of nonprincipal neurons in the rat hippocampus, with special reference to their dorsoventral difference. Brain Res 751, 64–80.

Nomura T, Fukuda T, Aika Y, Heizmann CW, Emson PC, Kobayashi T, Kosaka T (1997b) Laminar distribution of non-principal neurons in the rat hippocampus, with special reference to their compositional difference among layers. Brain Res 764, 197–204.

Patton PE and Mcnaughton B (1995) Connection matrix of the hippocampal-formation. 1. the Dentate Gyrus. Hippocampus 5, 245–286.

Prill RJ, Iglesias PA, Levchenko A (2005) Dynamic properties of network motifs contribute to biological network organization. PLoS Biol 3, e343.

Rall W, Burke RE, Holmes WR, Jack JJ, Redman SJ, Segev I (1992) Matching dendritic neuron models to experimental data. Physiol Rev 72, S159–186.

Reigl M, Alon U, Chklovskii DB (2004) Search for computational modules in the *C. elegans* brain. BMC Biol 2, 25.

Ribak CE, Seress L, Amaral DG (1985) The development, ultrastructure and synaptic connections of the mossy cells of the Dentate Gyrus. J Neurocytol 14, 835–857.

Santhakumar V, Aradi I, Soltesz I (2005) Role of mossy fiber sprouting and mossy cell loss in hyperexcitability: a network model of the dentate gyrus incorporating cell types and axonal topography. J Neurophysiol 93, 437–453.

Santhakumar V, Bender R, Frotscher M, Ross ST, Hollrigel GS, Toth Z, Soltesz I (2000) Granule cell hyperexcitability in the early post-traumatic rat dentate gyrus: the 'irritable mossy cell' hypothesis. J Physiol 524 Pt 1, 117–134.

Scharfman HE (1991) Dentate hilar cells with dendrites in the molecular layer have lower thresholds for synaptic activation by perforant path than granule cells. J Neurosci 11, 1660–1673.

Sik A, Penttonen M, Buzsaki G (1997) Interneurons in the hippocampal dentate gyrus: an in vivo intracellular study. Eur J Neurosci 9, 573–588.

Soltesz I and Staley KJ (2008) Computational Neuroscience in Epilepsy. Elsevier, New York.
Song S, Sjostrom PJ, Reigl M, Nelson S, Chklovskii DB (2005) Highly nonrandom features of synaptic connectivity in local cortical circuits. PLoS Biol 3, e68.
Soriano E, Nitsch R, Frotscher M (1990) Axo-axonic chandelier cells in the rat fascia dentata: Golgi-electron microscopy and immunocytochemical studies. J Comp Neurol 293, 1–25.
Sporns O and Kotter R (2004) Motifs in brain networks. PLoS Biol 2, e369.
Staley KJ, Otis TS, Mody I (1992) Membrane properties of dentate gyrus granule cells: comparison of sharp microelectrode and whole-cell recordings. J Neurophysiol 67, 1346–1358.
Walter C, Murphy BL, Pun RY, Spieles-Engemann AL, Danzer SC (2007) Pilocarpine-induced seizures cause selective time-dependent changes to adult-generated hippocampal dentate granule cells. J Neurosci 27, 7541–7552.
Watts DJ and Strogatz SH (1998) Collective dynamics of 'small-world' networks. Nature 393, 440–442.
Wenzel HJ, Buckmaster PS, Anderson NL, Wenzel ME, Schwartzkroin PA (1997) Ultrastructural localization of neurotransmitter immunoreactivity in mossy cell axons and their synaptic targets in the rat dentate gyrus. Hippocampus 7, 559–570.
West MJ (1990) Stereological studies of the hippocampus – a comparison of the hippocampal subdivisions of diverse species including Hedgehogs, Laboratory Rodents, wild mice and men. Progr Brain Res 83, 13–36.
West MJ, Danscher G, Gydesen H (1978) A determination of the volumes of the layers of the rat hippocampal region. Cell Tissue Res 188, 345–359.
Yoshimura Y and Callaway EM (2005) Fine-scale specificity of cortical networks depends on inhibitory cell type and connectivity. Nat Neurosci 8, 1552–1559.

Multi-level Models

Péter Érdi, Tamás Kiss, and Balázs Ujfalussy

Overview

The brain is a prototype of a hierarchical system, as Fig. 1 shows. More precisely, it is hierarchical dynamical system. To specify a dynamical system, characteristic *state variables* and *evolution equations* governing the change of state should be defined. At the molecular level, the dynamic laws can be identified with chemical kinetics, at the channel level with biophysically detailed equations for the membrane potential, and at the synaptic and network levels with learning rules to describe the dynamics of synaptic modifiability (see Table 1).

Neurons are considered the classical building blocks of the brain. *Small-scale* models are focused on from the dynamics of subneuronal structures via single neuron dynamics to small networks. The fundamental method is based on the Hodgkin–Huxley equations. Not a whole neuron, but a part of it, namely the giant axon of the squid, was studied by Hodgkin and Huxley (1952), who quantitatively described the electrogenesis of the action potential. Two channels, the fast sodium channel and the delayed rectifier potassium channel, were included. The total membrane current is the sum of the individual currents transported through individual channels. Channels were assumed to be either in an "open" or "closed" state, and the probability of the transition between them was described by first-order kinetics, with voltage-dependent rate "constants." Three elementary processes namely sodium activation, sodium inactivation, and potassium activation were found, and therefore three ("gating") variables, m, h, and n, respectively, were defined. The experiments were done under the "space clamp" method to eliminate the spatial variation of the membrane potential V. The mathematical consequence is that the partial differential equation is reduced to a four-dimensional system of ordinary differential equations, where the variables are the membrane potential and the three gating variables.

P. Érdi (✉)
Center for Complex Systems Studies, Kalamazoo College, Kalamazoo, Michigan, USA; Department of Biophysics, KFKI Research Institute for Particle and Nuclear Physics of the Hungarian Academy of Sciences, Budapest, Hungary
e-mail: perdi@kzoo.edu

V. Cutsuridis et al. (eds.), *Hippocampal Microcircuits*, Springer Series in Computational Neuroscience 5, DOI 10.1007/978-1-4419-0996-1_18,

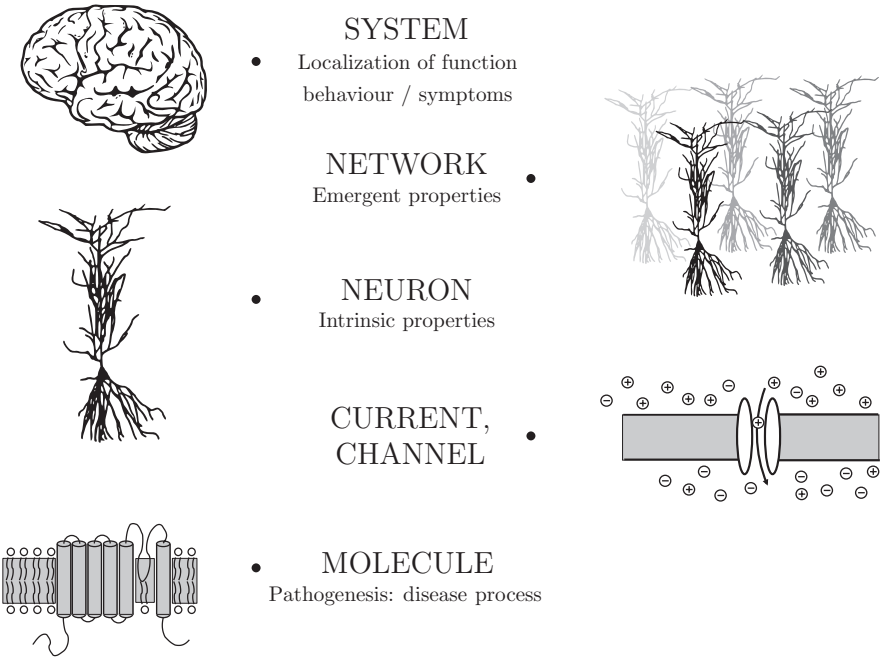

Fig. 1 The brain is a hierarchical dynamic system

Table 1 The brain as a hierarchical dynamical system. The possible state variables and dynamical equations are shown for different levels in the hierarchy

Level	Variables	Equations
Molecule	Chemical composition	Reaction kinetics
Membrane	Membrane potential	Hodgkin–Huxley
Cellular	Cellular activity	McCulloch–Pitts
Synapse	Synaptic efficacy	Elementary learning rules (Hebb)
Network	Synaptic weight matrix	Learning rules

A rather large subset of brain models take the form of networks of intricately connected neurons in which each neuron is modeled as a single-compartment unit whose state is characterized by a single "membrane potential"; anatomical, biophysical, and neurochemical details are neglected. Such neural network models are considered, at a certain level of description, as three-level dynamic systems:

$$\Delta a = f(a(t), \theta(t), W(t), I(t)) \tag{1}$$

$$\Delta \theta = e(a(t)) \tag{2}$$

$$\Delta W = g(a(t), W(t), u, R(t)) \tag{3}$$

Here a is the activity vector, θ is the threshold, W is the matrix of synaptic efficacies, I is the sensory input, R is an additive noise term to simulate environmental noise, u scales the time, and the functions e, f, and g will be discussed soon. One of the main difficulties of establishing a well-founded theory of neurodynamics is to define the functions e, f, and g.

Activity dynamics is often identified with the membrane potential equation, and the potential change (i.e., the form of f) is determined by the rate of presynaptic information transfer and the spontaneous activity decay. The function e describes the time-dependent modification of the threshold due to "adaptation." It is usually neglected; so that θ is supposed to be constant. The function g specifies the learning rule. Current learning theories generally assume that memory traces are somehow stored in the synaptic efficacies. The celebrated Hebb rule (Hebb 1949) has been given as a simple local rule for explaining synaptic strengthening based on the conjunction between pre- and postsynaptic activity.

While it is more or less true, that small-scale models are generally accepted, there are very different *large-scale* models, in terms of their goal and mathematical implementations. A large class of these models, namely mean field theories based on the grand tradition of physics, use some average value of variables characterizing single cells activities. For a review of the transition from small-to large-scale models see (Breakspear and Jirsa 2007).

Conventional neural network models can be interpreted as multi-scale models: they integrate single cell and network dynamics. There are other levels, from channels via networks and macronetworks to behavior, where coupling has a dramatic effect, and lower levels cannot be "averaged out." Multiple-scale or an hierarchical approach to neurodynamics has a tradition, see (Érdi 1983; Freeman 2000; Dayan 2001; Atmanspacher and Rotter 2008).

Here we review some basic models where different levels of neural organization are integrated. The bidirectional coupling of channel kinetics and neural activities leads to multiple time scales. A paradigmatic example for multi-scale modeling is the integration of detailed models of receptor kinetics to conventional network models. The technique seems to be relevant to drug discovery. More macroscopic models take into account neural networks and macronetworks to connect neural architectures and functional dynamics. Dynamical causal models connect brain regions to large-scale neural activities measured by EEG and/or fMRI methods. An integrated hippocampal model is presented to show how hippocampus is involved in spatial representation and navigation. Multi-scale models seem to be indispensable tools to offer new computational approaches to neurological and psychiatric disorders including the search for new therapeutic strategies, and also in designing new devices capable of computation, navigation, etc., based on our knowledge about neural mechanisms.

The Models

Coupling Channel Kinetics to Neuronal Excitation

Channel Kinetics: Markovian, Non-Markovian, Fractal

Coupling between levels, as well the occurrence of multiple time scales can be well demonstrated by integrating channel kinetics to neuronal excitation.

Channels are protein molecules, and functionally they serve as *pores* to let ions flow across the cell membrane. The interaction of specific, mostly voltage-dependent ion channels imply the excitation of a neuron, and the generation of electrical signals, which we call *action potentials*.

There are two issues to be discussed: the state and change of state of the individual channels, and the role of the *large population* of ion channels. Individual ion channels may have a small number of discrete states which correspond to different three-dimensional conformations of a protein molecule. The conformations admit functionally two types of state (*open* and *closed*). Channel proteins show a continuous switch between the open and closed states as Equation (4) shows.

$$\text{Open} \underset{\beta}{\overset{\alpha}{\rightleftharpoons}} \text{Closed} \tag{4}$$

This very fast switch depends on the continuously varying environment due to thermal fluctuations, variations of the voltage difference across the cell membrane, the behavior of neighboring proteins, etc. The patch-clamp technique made possible the measurements of single-channel kinetics (Sakmann and Neher 1983).

According to the predominant paradigm, ion channels exhibit inherent random behavior, i.e., the state of change is described by stochastic models. A basic family of stochastic models, namely the Markovian framework (Sakmann and Neher 1983), is based on the assumptions that the present state determines the transition probability, and the time the channel already has spent in a state is irrelevant. The assumptions of the Markovian models are occasionally debated. There are two alternatives to take into account "memory effects." One is within the stochastic framework when the non-Markovian character of ionic current fluctuations in membrane channels is suggested (Fulinski et al. 1998). The other is the family of deterministic fractal models (Lowen et al. 1999; Liebovitch et al. 2001), where kinetic rate "constants" of the transition between conformations are not constant anymore, but depend on the time the channel already has spent in a given state. Actually the fractal description implies a power-law distribution of state dwell times.

Probably it will be very difficult to decide whether there is a single "most realistic" model. As it was said (Kispersky and White 2008). "Complete resolution of this argument will be very difficult, because any data set of practical length and temporal resolution can in principle be fit by either class of model simply by adding states (in the Markov case) or by designing more elaborate rules of time-dependent

transition rates. It can at least be generally agreed that the correlations in dwell times of many voltage-gated channels are substantially more complex than predicted by the two-state model . . .".

Multiple Time Scales

A direct mutual coupling between channel kinetics and a neuronal excitation (which is a whole cell property) was modeled by (Gilboa et al. 2005). History-dependent characteristic time scales have been reported (Toib et al. 1998), and explained by a model built by a chain of voltage-independent changes between inactive states and an active state. The transition from an active to inactive state is voltage dependent, as it is described by Equation (5):

$$A \underset{\beta}{\overset{\alpha(V)}{\rightleftharpoons}} I_1 \underset{\beta}{\overset{\beta}{\rightleftharpoons}} I_2 \underset{\beta}{\overset{\beta}{\rightleftharpoons}} I_3 \ldots \underset{\beta}{\overset{\beta}{\rightleftharpoons}} I_N \tag{5}$$

where A is the active state, and $I_1 \ldots I_N$ are the inactive states.

A single neuronal excitability variable $X := \mu_A(t)$ was defined (as an approximation) as the fraction of channels in the active state (denoted by A). Channel activation/inactivation depends on the balance of sodium and potassium conductances, and hence neuronal excitability is controlled by the ratio of the available sodium and potassium channels.

A neural response $a_X(s)$ as a continuous firing rate is defined as a sigmoid function of the stimulus s parameterized by the neural excitation X, as Fig. 2 shows.

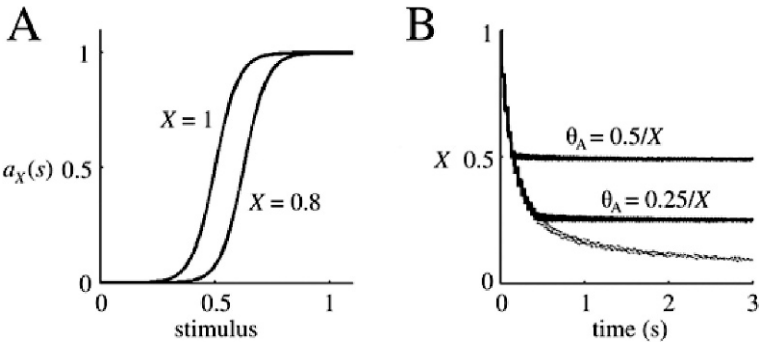

Fig. 2 (**A**) The neural response $a_X(s)$ is a sigmoid function of the stimulus parameterized by the neural excitability variable, X. As excitability increases from 0 toward 1, the activity threshold decreases as $\theta_A = c_A/X$. (**B**) The fraction of available ion channels, X, as a function of time during stimulation in the neuron model (*solid lines*) compared with the model of a membrane patch (*dashed, bottom line*). In the neuron model, this fraction, the neural excitability, fluctuates around a steady-state value, $X \cong c/A$. In the membrane patch, it continuously decreases with time as more and more channels are driven into inactivation. From: Fig. 3 of (Gilboa et al. 2005)

From Stochastic Channels to Deterministic Currents

While single channel fluctuations seem to be important, the dynamics of a whole neuron shows a much reduced fluctuation. Whole cell dynamics relies on the integrated operation of a *large number* of ion channels, and provides a scenario where the deterministic description of the timing of action potentials is appropriate. Neurons are reliable transformers of synaptic inputs to spiking patterns. In an extensively cited paper (Mainen and Sejnowski 1995) it was shown that neuronal noise is low in many cases, so neurons are able to function as deterministic spike encoders.

Integrating Receptor Kinetics and Network Dynamics

A new combined physiological/computational approach to drug discovery was offered (Aradi and Érdi 2006; Érdi P and Tóth 2005; Érdi et al. 2006) by finding optimal temporal patterns of neural activity. Using modeling results, the drug-screening phase of the drug discovery process can be made more effective by narrowing the test set of possible target drugs. Besides this benefit, more selective drugs can be designed if the modeling method is able to identify some specific sites of drug action.

Dynamical systems theory and computational neuroscience integrated with the well established, conventional molecular and electrophysiological methods will offer a broad, innovative prospective in drug discovery and in the search of novel targets and strategies for neurological and psychiatric therapies.

Some work has been done to develop a multi-scale model by integrating *compartmental* neural modeling techniques and *detailed kinetic description* of pharmacological modulation of transmitter – receptor interaction. This is offered as a method to test the electrophysiological and behavioral effects of putative drugs. Even more, an inverse method is suggested as a method for controlling a neural system to realize a prescribed temporal pattern (in EEG). The general plan is illustrated in Fig. 3.

In particular, our proposed working hypothesis is that for given putative anxiolytic drugs we can test their effects on the EEG curve by

- starting from pharmacodynamic data (i.e., from dose–response plots), which of course are different for different recombinant receptors,
- setting the kinetic scheme and a set of rate constants,
- simulating the drug-modulated GABA – receptor interaction,
- calculating the generated postsynaptic current,
- integrating the results into the network model of the EEG generating mechanism,
- simulating the emergent global electrical activity,
- evaluating the result and to decide whether the drug tested has a desirable effect.

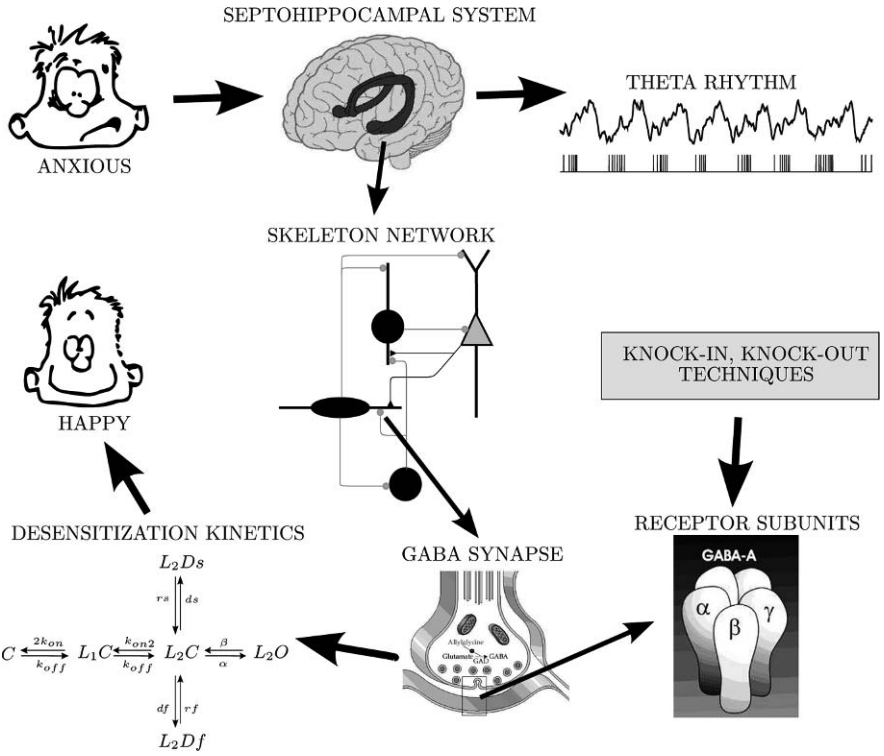

Fig. 3 Integration of detailed model of receptor kinetics and neural network models to test drug effects on system physiology and mood

Setting Up the Model

An illustrative model – integrating the detailed kinetic description of synaptic receptors (Bai et al. 1999) into the biophysical model of a gamma-related theta rhythm generating interneuron network – was given (Orbán et al. 2001; Kiss et al. 2001). This model was used to study the effect of drugs that have a well-identified effect on the chemical reactions taking place in the $GABA_A$ receptor.

Single cell models: The hippocampal CA1 pyramidal cell model was a multicompartmental model modified from (Varona et al. 2000). For the details see the web page http://geza.kzoo.edu/theta/p.html.

The interneurons are modeled by a single compartment containing the Hodgkin – Huxley channels (sodium, potassium, and leak), which were identical for all cells (see 6a–6m). The interneuron model was taken from (Wang and Buzsáki 1996) and obeys the following current balance equation:

$$C_{\mathrm{m}}\frac{\mathrm{d}V}{\mathrm{d}t} = -I_{\mathrm{Na}} - I_{\mathrm{K}} - I_{\mathrm{L}} - I_{\mathrm{syn}} + I_i \tag{6a}$$

$$I_{\mathrm{L}} = g_{\mathrm{L}}\,(V - E_{\mathrm{L}}) \tag{6b}$$

$$I_{\mathrm{Na}} = g_{\mathrm{Na}} m_{\infty} h\,(V - E_{\mathrm{Na}}) \tag{6c}$$

$$m_{\infty} = \frac{\alpha_{\mathrm{m}}}{\alpha_{\mathrm{m}} - \beta_{\mathrm{m}}} \tag{6d}$$

$$\alpha_{\mathrm{m}} = \frac{-0.1\,(V + 35)}{\exp\left(-0.1\,(V + 35)\right) - 1} \tag{6e}$$

$$\beta_{\mathrm{m}} = \frac{1}{\exp\left(-0.1\,(V + 28)\right)} \tag{6f}$$

$$\frac{\mathrm{d}h}{\mathrm{d}t} = \phi\,(\alpha_{\mathrm{h}}\,(1 - h) - \beta_{\mathrm{h}} h) \tag{6g}$$

$$\alpha_{\mathrm{h}} = 0.07 \exp\left(\frac{-(V + 58)}{20}\right) \tag{6h}$$

$$\beta_{\mathrm{h}} = \frac{1}{\exp\left(-0.1\,(V + 28)\right)} \tag{6i}$$

$$I_{\mathrm{K}} = g_{\mathrm{K}} n^4\,(V - E_{\mathrm{K}}) \tag{6j}$$

$$\frac{\mathrm{d}n}{\mathrm{d}t} = \phi\,(\alpha_{\mathrm{n}}\,(1 - n) - \beta_{\mathrm{n}} n) \tag{6k}$$

$$\alpha_{\mathrm{n}} = \frac{-0.1\,(V + 34)}{\exp\left(-0.1\,(V + 34)\right) - 1} \tag{6l}$$

$$\beta_{\mathrm{n}} = 0.125 \exp\left(\frac{-(V + 44)}{80}\right) \tag{6m}$$

with parameters: $g_{\mathrm{L}} = 1\,\mathrm{S/m^2}$, $g_{\mathrm{Na}} = 350\,\mathrm{S/m^2}$, $g_{\mathrm{K}} = 90\,\mathrm{S/m^2}$, $E_{\mathrm{L}} = -65.3\,\mathrm{mV}$, $E_{\mathrm{Na}} = 55\,\mathrm{mV}$, $E_{\mathrm{K}} = -90\,\mathrm{mV}$, $\phi = 5$.

Using this cell model a skeleton network was built. In the next two paragraphs the construction of the network and the used synapse model for connecting neurons by synaptic current $I_{\mathrm{syn}}(t)$ are described.

Skeleton network model: The skeleton network model (Fig. 4) of the hippocampal CA1 region and the septum consisted of five cell populations: pyramidal cells, basket neurons, two types of horizontal neurons, and the septal GABAergic cells.

Connections within and among cell populations were created faithfully following the hippocampal structure. The main excitatory input to horizontal neurons is provided by the pyramidal cells via AMPA (alpha-amino-3-hydroxy-5-methyl-4-isoxazolepropionic acid)-mediated synapses (Lacaille et al. 1987). Synapses of the septally projecting horizontal cells (Jinno and Kosaka 2002) and synapses of the other horizontal cell population, the O-LM cell population, innervating distal apical dendrites of pyramidal cells (Lacaille and Williams 1990) are of the $\mathrm{GABA_A}$ type. O-LM neurons (one of the two horizontal interneurons) also innervate parvalbumin

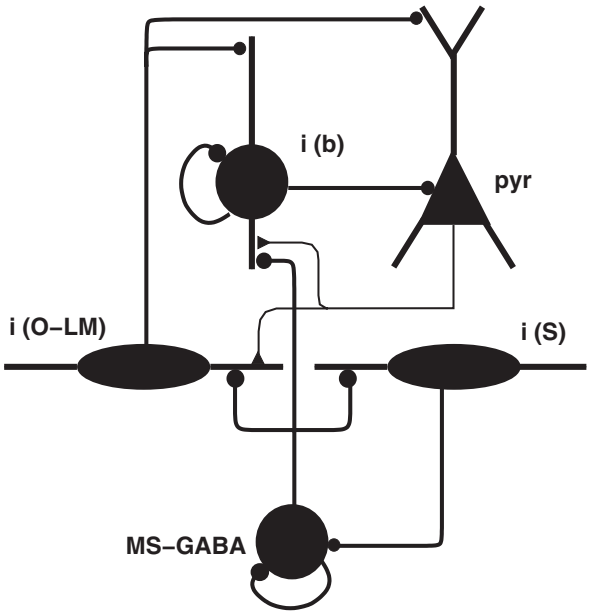

Fig. 4 Computer model of the hippocampal CA1 circuitry. Neuron populations hypothesized to be responsible for the generation of theta oscillation are shown (pyr – pyramidal cells; i(O-LM) – horizontal cells projecting to the distal dendrites of pyramidal cells in the lacunosum molecular layer; i(b) – basket interneurons; i(S) – septally projecting hippocampal horizontal interneurons; MS-GABA – septal GABAergic cells i *triangles* denote excitatory i *dots*, inhibitory synapses). Connections originating and ending at the same population denote recurrent innervation. Neuron population size in network simulations was 50, 50, 50, 100, and 12, respectively, for MS-GABA, i(b), i(s), i(O-LM), and pyramidal neurons

containing basket neurons (Katona et al. 1999). Basket neurons innervate pyramidal cells at their somatic region and other basket neurons (Freund and Buzsáki 1996) as well. Septal GABAergic cells innervate other septal GABAergic cells and hippocampal interneurons (Freund and Antal 1998; Varga et al. 2002) (Fig. 4). For a full description of this model see the online supplementary materials to the paper (Hajós et al. 2004) at: http://geza.kzoo.edu/theta/theta.html.

Interneuron network model: The above-described model captures several elements of the complex structure of the hippocampal CA1 and can be used to account for very precise interactions within this region. However, when the focus of interest is rather on general phenomena taking place during rhythm generation modelers might settle for a simpler architecture. In (Orbán et al. 2001) the authors describe gamma-related theta oscillation generation in the CA3 region of the hippocampus. The architecture of the model is exceedingly simplified: only an interneuron network is simulated in detail. This simplification, however, allowed the authors to introduce an extrahippocampal input and study its effect on rhythm generation. As a result, the model is able to account for basic phenomena necessary for the generation of gamma-related theta oscillation. As an extension of this model, the authors show

(Kiss et al. 2001) that activity of the interneuron network indeed accounts for rhythm generation in pyramidal neurons.

A simple network contained 50 interneurons, modeled with the single-compartment model described above. The interneurons were connected into a random network. Probability of forming a connection between any two neurons was from 60 to 100% in the simulations; autapses were not allowed. The input for each cell was a sinusoid current with the same frequency ($\omega = 37$ Hz) and random phase.

Synapse model: A connection between two interneurons was established through a synaptic mechanism consisting of a phenomenological presynaptic and a chemically realistic postsynaptic part. The presynaptic model describes the transmitter release due to an action potential generated in the presynaptic neuron by a sigmoid transfer function:

$$[L](t) = \frac{0.003}{1 + \exp\left(-\frac{V_{\text{pre}}(t)}{2}\right)} \tag{7}$$

where $[L](t)$ is the released GABA and $V_{\text{pre}}(t)$ is the presynaptic membrane potential.

The value of the released transmitter concentration ($[L]$) is then used in the postsynaptic $GABA_A$ receptor model to calculate the concentration of receptor proteins being in the conducting (two ligand bound open) state ($[L_2O](t)$) (see (8) – (9g)).

Our starting point for the detailed postsynaptic model is the work of Bai et al. (1999), originally developed by Celentano and Wong (1994) to describe the emergence of open channels as the effect of GABA binding to receptors. However, we explicitly show the presence of an essential participant of the model, the ligand L different from Scheme 1 of the cited paper and our previous work (Érdi P and Tóth 2005). Obviously, in the model the ligand L denotes GABA, whereas L_2O denotes the open channels, the notation expressing the fact that two ligand molecules are needed to change the receptor into an open channel:

$$\begin{array}{ccccc} & & & & L_2D_{\text{fast}} \\ & & & & d_f \Vdash r_f \\ L + C & \underset{k_{\text{off}}}{\overset{2k_{\text{on}}}{\rightleftharpoons}} & L_1C & \underset{2k_{\text{off}}}{\overset{k_{\text{on}}}{\rightleftharpoons}} & L_2C \quad \underset{r_s}{\overset{d_s}{\rightleftharpoons}} L_2D_{\text{slow}} \\ & & & & \alpha \Vdash \beta \\ & & & & L_2O \end{array} \tag{8}$$

The induced differential equations are the following:

$$[C]' = -2k_{\text{on}}[L][C] + k_{\text{off}}[L_1C] \tag{9a}$$
$$[L_1C]' = 2k_{\text{on}}[L][C] + 2k_{\text{off}}[L_2C] - (k_{\text{off}} + k_{\text{on}}[L])[L_1C] \tag{9b}$$
$$[L_2C]' = k_{\text{on}}[L][L_1C] + r_f[L_2D_{\text{fast}}] + r_s[L_2D_{\text{slow}}] + \alpha[L_2O] \tag{9c}$$
$$- (2k_{\text{off}} + d_f + d_s + \beta)[L_2C] \tag{9d}$$
$$[L_2D_{\text{fast}}]' = d_f[L_2C] - r_f[L_2D_{\text{fast}}] \tag{9e}$$
$$[L_2D_{\text{slow}}]' = d_s[L_2C] - r_s[L_2D_{\text{slow}}] \tag{9f}$$
$$[L_2O]' = \beta[L_2C] - \alpha[L_2O] \tag{9g}$$

Furthermore, we have the following conservation equation for the total quantity of channels in any form:

$$[C] + [L_1C] + [L_2C] + [L_2D_{\text{fast}}] + [L_2D_{\text{slow}}] + [L_2O] = [C](0) = 1 \tag{10}$$

The synaptic current was thus given by

$$I_{\text{syn}}(t) = \sum_{i=1}^{N} \bar{g}_{\text{syn},i} \cdot [L_2O]_i(t) \cdot (V(t) - V_{\text{syn}}) \tag{11}$$

where N is the number of presynaptic neurons, i indexes these presynaptic neurons, $\bar{g}_{\text{syn}}$ is the maximal synaptic conductance representing the synaptic channel density, $V(t)$ is the postsynaptic membrane potential, and $V_{\text{syn}} = -75\,\text{mV}$ is the reversal potential of the chloride current.

Drug administration: Given the detailed kinetic description of GABA_A receptors the modulation of the synaptic current due to its interaction with the drug can be simulated. Moreover, in the integrated model framework an evaluation of the drug effect on the network level can be performed.

The identification of the effect of a given drug on the kinetic rate parameters of a certain receptor type or subtype is a complicated and tedious undertaking. To present the soundness of our model two known drugs were used in the simulations: propofol and midazolam. However, a considerable effort was made to estimate the change of the rate constants due to the application of the L838,417 compound using the chemical method of parameter estimation. Unfortunately, sufficient kinetic or even pharmacodynamic data could not be found in the public domain to obtain realistic estimation for the rate constants.

Rate constants in the model were set up according to (Baker et al. 2002) to account for the control situation, treatment with propofol and treatment with midazolam (Table 2).

Table 2 Rate constants used to model the effect of Propofol and Midazolam

Parameters	Control	Propofol	Midazolam
k_{on}	1,000/M	1,000/M	1,000/M
k_{off}	0.103	0.056	0.056
d_f	3.0	1.62	3.0
r_f	0.2	0.12	0.2
d_s	0.026	0.014	0.026
r_s	0.0001	0.0001	0.0001
α	0.4	0.4	0.4
β	6.0	6.0	6.0

Simulation Results

Population oscillations reflected by the EEG can be considered as biomarkers for some brain disorders. We used our integrated model to study the effects of two known drugs, the hypnotic propofol and the sedative midazolam on the population theta rhythm. In a previous work (Kiss et al. 2001) it was shown that the population activity of the interneuron network can be used to account for the activity of pyramidal cells, which can be in turn translated into EEG. Thus, to quantify our results, raster plots, a population activity measure, and its Fast Fourier Transform (FFT) were used. Simulation results are summarized in Fig. 5.

Control condition: As shown previously (Orbán et al. 2001; Kiss et al. 2001) in the control situation this model exhibits spike synchronization in the gamma frequency band, which is modulated in the theta band (Fig. 5A). On the raster plot in Fig. 5A each row symbolizes the spike train of a given cell with a black dot representing the firing of an action potential. Note that firing of the cells line up in well-synchronized columns, e.g., from approximately 2.2 to 2.35 s. As a result of heterogeneity in the phase of the driving current and in synaptic contacts, this high synchrony loosens and the columns in the raster plot are less well organized in the 2.35–2.45 s interval. This synchronization – desynchronization of cells is a result of the modulation of the instantaneous frequency of individual cells (Fig. 5A, top – for more details the reader is kindly referred to Orbán et al. (2001)). A qualitative measure of the synchrony is given by the population activity (Fig. 5A, bottom).

As argued in (Kiss et al. 2001) this synchronization – desynchronization of the population activity of interneurons is transposed to principal cells of the hippocampal CA3 region, modulating their firing probability in the theta band. This modulation might be reflected in the EEG or CA3 local field potential. Thus, we propose that there is a mapping between the FFT of the CA3 local field potential or EEG and the FFT of the simulated population activity (Fig. 5A, right), which shows a peak at the theta frequency. Other peaks at higher frequencies are related to the fast firing properties and the resulting synchronization of the interneurons as well as the frequency of the driving current.

Drug treatment: Figure 5B, C shows the effects of propofol and midazolam, respectively, on the network behavior (sub-figures are the same as in Fig. 5A). The purpose of the present chapter is not to give a detailed description and analysis

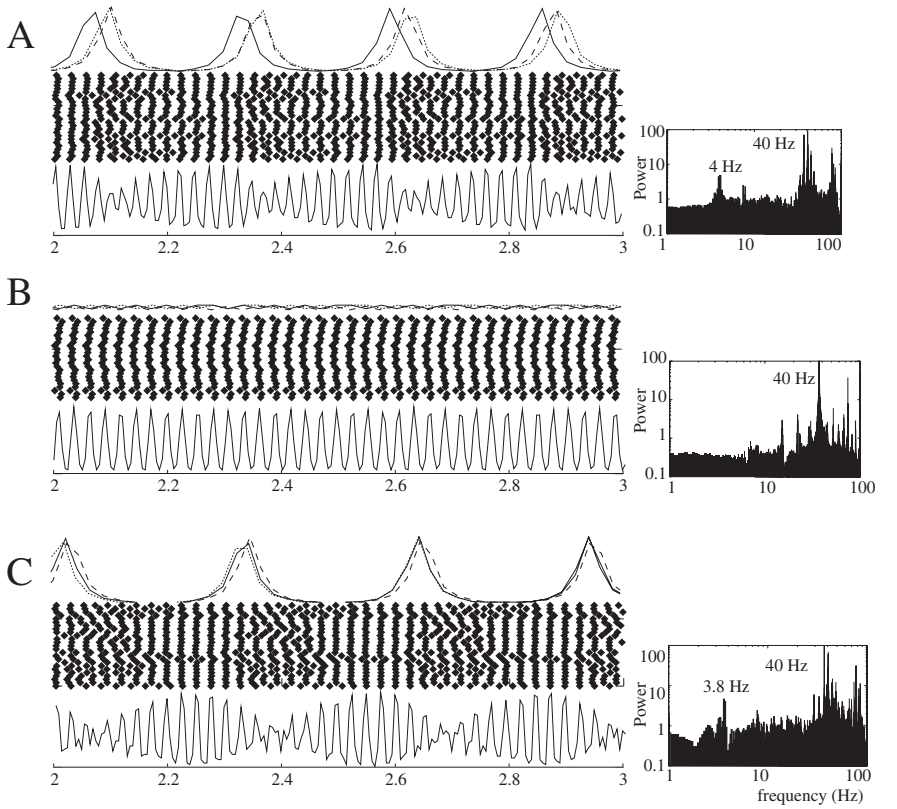

Fig. 5 **A**: Control activity in the model. The raster plot shows the firing of 25 neurons in the network during 1 s (the total population consisted of 50 units). When the neurons are synchronized the *dots* are arranged into *vertical lines* (e.g., at 2.8 s). The network loses its synchrony when neurons increase their firing rate (2.6 s). The instantaneous frequency of three representative cell is shown on the *top* of the rastergram. The population activity (below the rastergram) shows the proportion of neurons that fired in a 5 ms long time bin. The amplitude of the oscillation is modulated by theta. The Fourier spectrum of the population activity shows distinct peaks at 40 Hz (gamma frequency) and at 4 Hz (theta frequency). **B**: The effect of propofol on the activity of the modeled network. The raster plot and the population activity of the network show clear gamma synchrony without any slower modulation. The instantaneous frequency of the neurons is nearly constant. There is a single peak in the power spectrum around 40 Hz. **C**: The midazolam has only a modest effect on the network activity

of the mode of action of these drugs, thus we restrict ourselves to mention that while propofol prolongs deactivation of the receptor and reduces the development of both fast and slow desensitization, midazolam facilitates the accumulation of the receptors into the slow desensitized state, which compensates the current resulting from slower deactivation (Bai et al. 1999). As a result, propofol enhances the tonic synaptic current to a greater extent than midazolam, whereas propofol and mida-

zolam produce similar changes to the time course of single inhibitory postsynaptic currents (IPSCs) (Bai et al. 1998).

On the network level the difference that propofol and midazolam exert on the tonic component of the synaptic current has a grave consequence. While the peak in the FFT at approximately 4 Hz representing the theta modulation of the population activity is still present in the case when synapses were "treated" with midazolam (Fig. 5C, right) it is completely missing for the propofol "treated" case (Fig. 5B, right).

Functional Dynamics: Network – Macronetwork – Behavior

Dynamics of Multi-scale Architectures

Spatial multi-scale: A formal framework for the dynamics of neural systems with multiple spatial structures was given by Breakspear and Stam (2005).

Neurons, microcircuits, cortical modules, macrocolumns, regions, cortical lobes, and hemispheres correspond to different levels of spatial hierarchy, from the more microscopic to the most coarsest scales.

The state of a subsystem is characterized by $\mathbf{V}(x_i, t)$, where $\mathbf{V}$ is an m-dimensional variable at spatial location x_i and at time t. In a deterministic framework, and using a continuous time and discrete space approach, the dynamics is given by

$$\dot{\mathbf{V}} = F(\mathbf{V}(x_i, t)) \tag{12}$$

More precisely, the dynamics of an element depends on the state of the other elements in an ensemble too. The form of the function F depends on a coupling function H:

$$\dot{\mathbf{V}} = F(\mathbf{V}(x_i, t), H(\mathbf{V}(x_i, t))) \tag{13}$$

If H is linear in $\mathbf{V}$, then H_{ii} is the connection strength between the elements i and j. The special case $H_{ij} = 1$ for all ij expresses global coupling. Real data on anatomical or functional connectivities should be incorporated by choosing appropriate H functions.

Breakspear and Stam (2005) introduced also an interscale coupling between coarse-grained (J) and fine-grained (j) scales. Local ensemble at position x_i in the coarse-grained system is governed by $F^{(J)}$, which depends both on within-scale coupling H and interscale coupling G. So, the generalized version of Equation (13) (using somewhat different notation from that in (Breakspear and Stam 2005)) has the form

$$\dot{\mathbf{V}} = F(\mathbf{V}^{\mathbf{J}}(x_i, t), H(\mathbf{V}^{\mathbf{J}}(x_i, t)), G(\mathbf{V}^{J}(x_i, t), \mathbf{V}^{j}(x_i, t))) \tag{14}$$

As it is seen in Fig. 6 for any specific cases, three main steps should be done: (i) at each scale "within module" dynamics is derived by using the governing equations of the given level; (ii) coupling within an ensemble; (iii) coupling between scales. Specific models should prove the power of this framework.

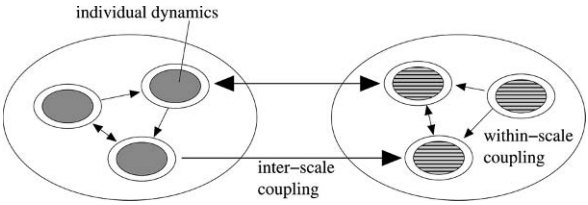

Fig. 6 A skeleton diagram to display the relationship among spatial scales. Individual dynamics, within-scale and inter-scale coupling are demonstrated

A multi-level biomimetic robot model: A multi-level approach to biomimetic robots connecting neural networks and schemas was given by (Weitzenfeld 2000, 2008). As opposed to many bioinspired approaches to robots, not only the phenomenological ("ethological") higher level mechanisms, but the real neural dynamics of learning and adaptations are incorporated. A top–down approach was suggested by using three stages integrating embodiment, behavior, and neural networks. First, an embodied robot is able to interact with its environment by *sensors* and *actuators*. Second, neuroethological data are incorporated to connect "behavioral units" to brain regions. A famous example is the perceptual and motor schemas of the frog for prey acquisition and predator avoidance (small-moving object is food, large-moving object is enemy) and how the naive expectation for the neural implementation is violated by real neural data (Arbib 1899). Third, a schema can be implemented by a network of neurons interconnected by excitatory and inhibitory, often (but not always) plastic synapses. Leaky integrator neuron models have proved to be a good compromise between biological reality and computational efficiency.

Dynamic Causal Modeling

While the electrophysiological results obtained by intracellular recordings have a proper corresponding theory based on compartmental modeling techniques, data derived from brain imaging devices lack coherent theoretical approaches. Though it is clear that the gap between conventional neural modeling techniques and brain imaging data should be narrowed, there is much to be done. A dynamical causal modeling strategy might be called as weakly multi-scale technique. It was offered by Karl Friston and his coworkers as a good first step into this direction (Friston et al. 2003; Stephan et al. 2007). There are two underlying assumptions:

(i) There are n interacting areas, the state of each area is characterized by a scalar variable. The state of the system is modified by these inter-regional interactions and by external input. The latter has two effects, it modulates the connectivity

and has direct effects on regional activities. For the model framework and an illustrative example, see Fig. 7.

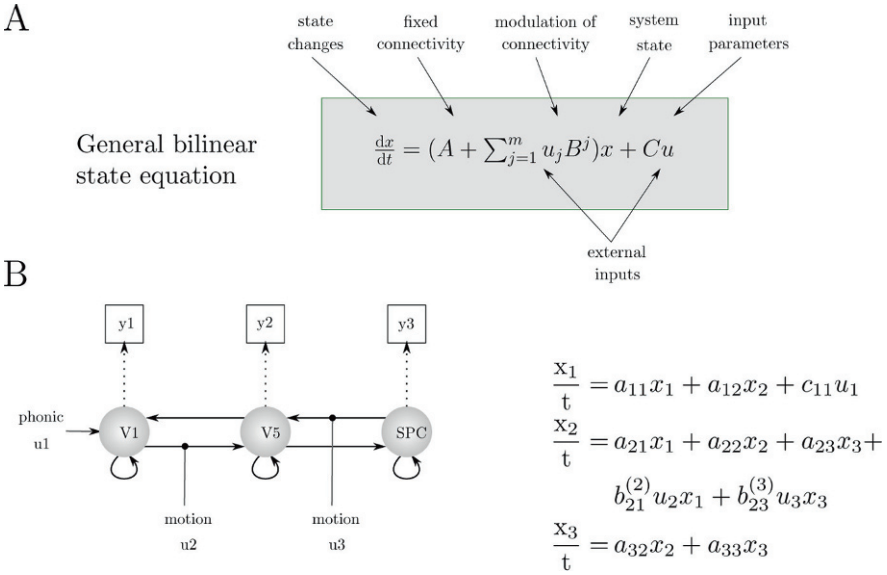

Fig. 7 **A**, The general bilinear state equation of the system. **B**, This particular system consists of three areas V1, V5, and the superior parietal cortex (SPC). Their activity is represented by $(x_1, \ldots, x_3)$. *Black arrows* represent connections, *gray arrows* represent external inputs into the system and *thin dotted arrows* indicate the transformation from neural states into hemodynamic observations (*thin boxes*) for the hemodynamic forward model. Visual stimuli drive activity in V1 which is propagated to V5 and SPC through the connections between the areas. The V1 → V5 connection is allowed to change whenever the visual stimuli are moving, and the SPC → V5 connection is modulated whenever attention is directed to motion. The state equation for this particular example is shown on the *right*. From (Stephan et al. 2007)

(ii) The neuronal state x should be converted into hemodynamic state y to be able to use the model for fMRI. Four auxiliary variables are assumed: the vasodilatory signal, blood flow, volume, and deoxyhemoglobin content.

A Framework of an Integrated Hippocampal Model

A computer model of learning and representing spatial locations was given by (Ujfalussy et al. 2008). There were two goals. The performance of a hippocampus model of the rat (Rolls 1995) – originally created to describe the episodic memory capabilities of the hippocampus – is tested in spatial learning. Second, the algorithm is implemented in a robot simulation software. The structure of the model is illustrated in Fig. 8. We used grid cells (125), view cells (120 cells, panoramic view of a striped wall), and whisker cells (20, also for low-level obstacle detection and

motion control) as input for the model. Two thousand threshold linear units were used to simulate the hippocampus.

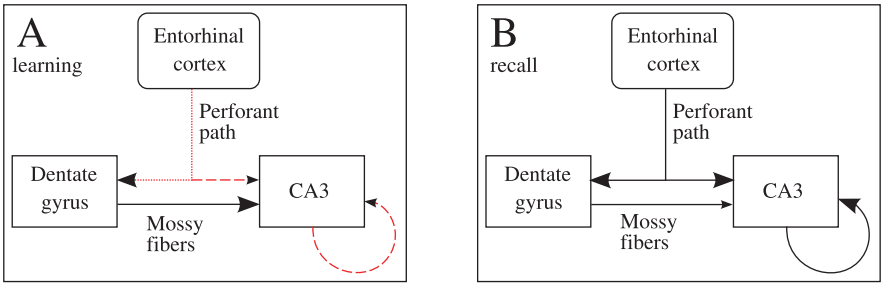

Fig. 8 Modeled areas and the role of the different pathways during learning.(A) and recall (B). *Thick arrows* represent active pathways, i.e., pathways that add to the activation of the target region. *Dashed arrows* represent pathways being modified

The model builds on biological constraints and assumptions drawn from the anatomy and physiology of the hippocampal formation of the rat and demonstrates that (i) using biologically plausible convergence and (ii) mixing different sensory modalities and proprioceptive information (integrated allothetic and idiothetic pathways) result in the formation of place cell activity.

Biological constraints:

1. Representation of memory traces (coding) is sparse in the DG and in the CA3, while denser in the EC.
2. The hippocampus receives pre-processed sensory information from the neocortex via its PP input.
3. The EC innervates both the DG and the CA3, the DG innervates the CA3 and the CA3 innervates itself.
4. The MF synapses are an order of magnitude stronger than the PP or the RC synapses (see assumption 3).
5. Local, Hebbian learning rules are used throughout the model.

Assumptions:

1. The DG translates the dense code of the EC to a sparser code used throughout the hippocampus.
2. The hippocampus operates in two distinct modes: *learning* (also used as encoding) and *recall* (also used as retrieval). During learning, modification of synaptic strengths is allowed. During recall, synaptic strengths are fixed.
3. During encoding activity of CA3 cells is determined by their MF input from the DG cells.

4. Synaptic strengths of the PP – both in the DG and in the CA3 – and of the RC are modifiable, while the strength of MF synapses do not change in time.
5. During retrieval activity of CA3 cells is cued by its PP input. This subsystem operates as a hetero-associative network.
6. Memory recall is refined by the RC synapses of the CA3 region.

The 1,000 dentate granule cells were innervated by the entorhinal units (we used all to all connections). There was no direct connection between granule cells, instead we implemented soft competition between them: the firing threshold was set according to the desired sparseness of the population. The connections are modified by Hebbian plasticity (section "Learning").

CA3 pyramidals were innervated by entorhinal neurons, CA3 pyramidals (recurrent connections) and dentate granule cells (mossy fibers). The connections from entorhinal neurons are all to all and are modified by Hebbian plasticity, while mossy fibers are sparse ($p_{\text{conn}} = 0.02$), and the synapses are not modified. Mossy fibers are active only during learning when they are much stronger than the other two inputs to CA3 (section "Learning"). A soft competition is also implemented in the CA3.

The core of the model are the two algorithms for the hippocampal computation, namely for learning and recall, respectively.

Learning

Treves and Rolls (1994) suggested that any new event to be memorized is represented in the CA3 as a firing rate pattern (vector) of pyramidal cells. To create this pattern, sensory information of the EC is first processed by the DG and its sparse, orthogonalized version is generated. First, the activation of DG cells is calculated

$$h_j^{\text{EC}\to\text{DG}} = \sum_i W_{i,j}^{(\text{EC, DG})} \text{EC}_i \tag{15}$$

using the synaptic weight matrix and the activity of EC cells. Then a threshold linear activation function ($f_j(\cdot)$) is applied on the activation vector to calculate the firing rate of each cell:

$$\text{DG}_j = f_j(\mathbf{h}^{\text{EC}\to\text{DG}}, s^{\text{DG}}) \tag{16}$$

where s^{DG} is the desired sparseness of the code in the DG area, and the threshold depends on the average activity in the layer (so there is a competition between the cells). The sparseness of a given pattern defined by (Rolls and Treves 1990) is based on averaging the r firing rate distributions of cells over the stored patterns p ($a = < r >_p^2 / < r^2 >_p$).

Learning takes place in the associatively modifiable $\mathbf{W}^{(\mathrm{EC,\,DG})}$ synapses based on the following learning rule:

$$\Delta W_{i,j}^{(\mathrm{EC,\,DG})} = \alpha^{(\mathrm{EC,\,DG})} \mathrm{DG}_j \left(\mathrm{EC}_i - W_{i,j}^{(\mathrm{EC,\,DG})} \right) \tag{17}$$

where $\alpha^{(\mathrm{EC,\,DG})}$ is the learning rate. During learning, activation of CA3 cells is determined by the MF (i.e., $\mathbf{W}^{(\mathrm{DG,\,CA3})}$) input ($h_j^{\mathrm{DG}\rightarrow\mathrm{CA3}}$) following the form of Equation (15). Similarly to the case of the DG, activity of CA3 cells is computed by an equation of the form of Equation (16).

Learning takes place in all synaptic pathways of the CA3 region as it is hypothesized that, due to the activation by the DG afferents, the membrane potential of CA3 pyramidal cells is depolarized and enables plastic changes in synapses originating from the PP and the RC:

$$\Delta W_{i,j}^{(\mathrm{EC,\,CA3})} = \alpha^{(\mathrm{EC,\,CA3})} \mathrm{CA3}_j \left(\mathrm{EC}_i - W_{i,j}^{(\mathrm{EC,\,CA3})} \right) \tag{18}$$

$$\Delta W_{i,j}^{(\mathrm{CA3,\,CA3})} = \alpha^{(\mathrm{CA3,\,CA3})} \mathrm{CA3}_j \mathrm{CA3}_i \left(1 - W_{i,j}^{(\mathrm{CA3,\,CA3})} \right) - \beta^{(\mathrm{CA3,\,CA3})} W_{i,j}^{(\mathrm{CA3,\,CA3})} \tag{19}$$

where α is the learning rate and β is the "forgetting" rate, respectively.

Recall

During recall the EC input is used to initiate retrieval of a stored memory pattern. First, the activation of CA3 cells resulting from the PP ($h_j^{\mathrm{EC}\rightarrow\mathrm{CA3}}$) is calculated based on Equation (15), and used to compute the **CA3** activity vector by an equation of the form Equation (16). Second, this initial activity vector is used as the cue to retrieve the memory trace in the autoassociative network. In this process activation vectors $\mathbf{h}^{\mathrm{EC}\rightarrow\mathrm{CA3}}$ and $\mathbf{h}^{\mathrm{CA3}\rightarrow\mathrm{CA3}}$ resulting from the PP and the RC input, respectively, are calculated and normalized to unitary length. Finally, activation of CA3 cells are computed:

$$\mathrm{CA3}_j = f_j(\mathbf{h}^{\mathrm{EC}\rightarrow\mathrm{CA3}} + \chi \mathbf{h}^{\mathrm{CA3}\rightarrow\mathrm{CA3}}, s^{\mathrm{CA3}}) \tag{20}$$

where χ is a scaling factor and s^{CA3} is the sparseness of coding in area CA3. Calculation of $\mathbf{h}^{\mathrm{EC}\rightarrow\mathrm{CA3}}$, $\mathbf{h}^{\mathrm{CA3}\rightarrow\mathrm{CA3}}$, and **CA3** were iterated a number of times (τ_{R}) to allow the network to find a stable attractor corresponding to the memory being recalled.

Simulation Results

Simulation results show that although learning occurs simultaneously in the DG and the CA3, stable place representation evolves in both the DG and the CA3 in under 4

min (2,000 time steps) of exploration (Fig. 9, left panel). We found that in the DG, the majority of the cells exhibit one place field. Out of the 1,000 cells simulated only one had two and one had three place fields. In the CA3, 50% of the cells had one single place field, about 32% had two, 15% had three, and the rest had more than three place fields (Fig. 9, left panel). Place fields were identified as continuous places not smaller than 64 cm^2, where a given cell had high activity (larger than 25% of the maximal firing rate).

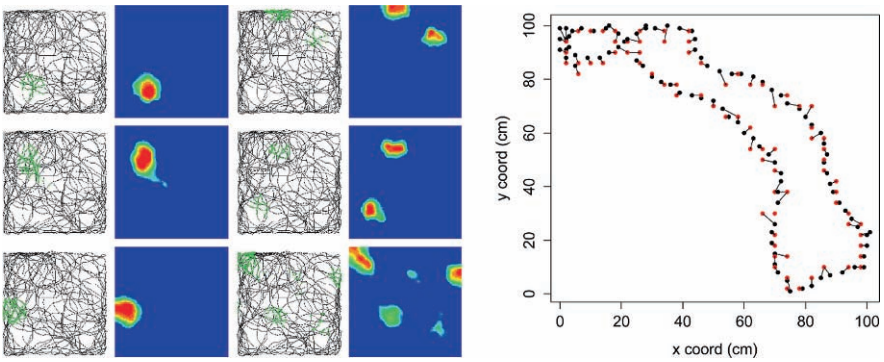

Fig. 9 *Left panel*: Cell activity in the CA3 region. Images in the first and third column show the path of the robot in the 1 × 1 m square arena. *Lines* represent the path of the robot, *green dots* show where a certain cell had non-zero activity. In the second and fourth columns, color-coded images show the firing rate. In the second column, place cells with one single place field, and in the fourth column, place cells with multiple places fields are shown. *Right panel*: Estimation of the robot's position based on the population of place cells. On a short section of the path we predicted the position based on the current activity of place cells. Real position is denoted by *black dots*, estimated position by *red dots* connected to the real positions they estimate. Mean and std of the difference between real and estimated positions was 2.5 ± 1.4 cm

The population of the place cells redundantly covered the space and could reliably be used to predict the location of the robot. For this calculation, first the firing rate map of the CA3 cells was calculated on a 4 × 4 cm lattice (see Fig. 9, left panel, columns 2 and 4). In every step of the recall process, active cells were selected, and their rate maps were multiplied in every spatial point. The maximum value in the resulting matrix was considered to give the most probable location of the robot in Fig. 9, right panel.

Navigation in Real and Memory Spaces or Episodes in Space

In rats trained to run on a one-dimensional track, hippocampal cell assemblies discharge sequentially, with different assemblies on opposite runs: place cells are unidirectional. One-dimensional tasks are formally identical with learning sequentially occurring items in an episode. In contrast, place representations by hippocampal neurons in 2-dimensional environments are omnidirectional, the hallmark of a map. Generation of a map requires exploration, essentially a dead reckoning (path inte-

gration) behavior. The temporal metric of dead reckoning is theta oscillation, and speed can be derived from the firing rate of place cells. Orthogonal and omnidirection navigation through the same places (nodal links) during dead reckoning exploration gives rise to omnidirectional place cells and the generation of a map. Just as dead reckoning is a prerequisite of a cognitive map, Buzsaki suggests (Cycle 11 in (Buzsaki 2006)) that multiple episodes crossing common node(s) of the episodes are necessary to give rise to context-free or semantic memory. Theta oscillation therefore can be conceived as the navigation rhythm through both physical and mnemonic space in all mammals.

Model Justification

Hierachies in the Cortico-hippocampal System

Cortico-hippocampal loops might be considered as the structural basis of a circular causal chain, where information can be stored, circulated, recalled, and even created. More precisely, it was argued (Lavenex and Amaral 2000) that the flow of information within the neocortical–hippocampal loop has a hierarchical structure: perirhinal and parahippocampal circuits, entorhinal cortex, and the hippocampal formation implements the first, second, and third level of integration, respectively. The cortical structures are connected to the medial temporal lobe generally by reciprocal connections. Since the higher level processing has a feedback to the first, neocortical level, we might assume that the anatomical structure implements information processing based on circular causality. Circular causality was analyzed to establish self-organized neural patterns related to intentional behavior (Freeman 1999).

In a paper (Érdi et al. 2005) several phenomena occurring at different structural levels of the *hierarchical organization* have been involved (see Fig. 10).

First, the role of the interplay between the interaction of the somatic and dendritic compartments of a pyramidal cell and the external theta excitation in the (double-) code generation of spatial information is discussed (Lengyel and Érdi 2004; Huhn et al. 2005). While our first study used an integrate-and-fire model framework, the second adopted compartmental modeling techniques.

Second, the interaction among the networks of the hippocampus and the medial septum in generating and controlling the theta rhythm was discussed. The effects of drugs on different binding sites of the $GABA_A$ receptors were studied by the multi-compartmental modeling technique, and results (Hajós et al. 2004) showed that impairment/improvement of the inhibitory mechanisms play a role in mood regulation (see also (Freund 2003)) in connection with population oscillations.

Third, the cortico-hippocampal loop and its role in navigation using a lumped model framework suggested and elaborated by Walter and Freeman (1975) (Freeman 1975) were used by (Kozma et al. 2004). A reinforcement algorithm was incorporated to learn goal-oriented behavior based on global orientation beacons, biased

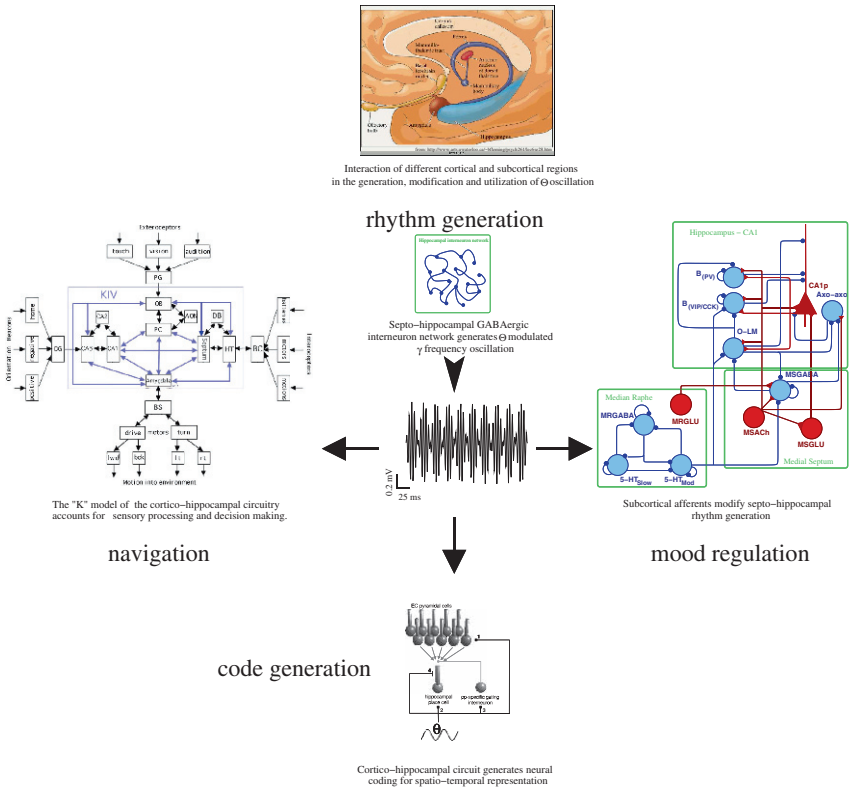

Fig. 10 Generation, control, and some functions of hippocampal theta rhythm. The septum and the hippocampal formation seem to be functionally organized around different oscillatory patterns, one of which is the θ rhythm. The system generates and uses this population activity at the same time. Role of the θ activity is several fold: it takes place in the generation of memory traces and the formation of cognitive maps in the hippocampal formation, it is used as a reference signal for navigation based on previously stored memories, and supposedly reflects or even modulates the mood and alertness of the animal. These functions "interact" with each other, forming a circular causal loop

by local sensory information provided by visual or infra-red sensors. The model, which contains sampling of the environment by theta rhythm, was able to show place field generation and navigation.

Multi-level Neuropharmacology

To get a better understanding about the neural mechanisms of anesthesia, a new perspective was offered by integrating network, cellular, and molecular level modeling (Arhem et al. 2003). At the *macroscopic* level, analysis investigates the brain regions which might be affected by anesthetic drugs. The feedback loops of the

thalamocortical system, which are known to generate and control the brain rhythms related to such mental states as “aroused” or “sleep”states.

At the *mesoscopic* level, a closer analysis is necessary to understand the mechanisms of shifting the system from a conscious state characterized by high-frequency rhythms to an unconscious state (low-frequency activity). Since “both increased and decreased activity as well as increased and decreased coherence characterize anesthetic-induced unconsciousness” much work should be done to understand the probably diverse mechanisms of anesthetic compounds for both the single neuron and network-level rhythms. The authors hint is that one effect of anesthetic drugs is to disrupt coherent oscillatory activity by blocking channels.

At the *microscopic* level, the question is “which anesthetic-induced ion channel modifications are critical in causing anesthesia?” The fundamental candidates are some ligand-gated channels, mostly GABA and NMDA channels, but voltage-gated channels, mostly potassium channels, are subject to modulation and blocking.

The Future

Classical neurodynamics has been dominated by single-level models. Microscopic models have been used to describe the spatiotemporal activity of single cells and of small networks. Macroscopic models adopt the technique to assign a scalar variable to characterize the state of a brain region, and activity propagation among brain regions was governed by simple dynamic equations.

One big goal of neuroscience is to link cellular level physiological mechanism to behavior, i.e., phenomena occurring at millisecond to second or even minutes time scales. A first step in this direction was made by Drew and Abbott (Drew and Abbott 2006), who modeled the coupling between different scales during learning. As it is known, activity-dependent modification of synaptic strengths due to spike-timing-dependent plasticity (STDP) is sensitive to correlations between pre- and postsynaptic firing over time scales of tens of milliseconds, while the temporal associations in behavioral tasks involve times on the order of seconds. They showed “..that the gap between synaptic and behavioral timescales can be bridged if the stimuli being associated generate sustained responses that vary appropriately in time. Synapses between neurons that fire this way can be modified by STDP in a manner that depends on the temporal ordering of events separated by several seconds even though the underlying plasticity has a much smaller temporal window . . .” (Drew and Abbott 2006).

The more systematic investigation of multiple time scales at the level of cortical neuron activity and of synaptic modification started recently (La Camera et al. 2006; Fusi et al. 2007). The functional role of fast and slow components of learning during tasks, such as decision making, might be studied in a more extensive way.

One new field, where a multi-scale modeling technique seems to be a must, is computational neuropsychiatry (Tretter and Albus 2007). It is a new discipline, where the integrated multi-level perspective seems to be the key of further progress.

The connection between levels from molecular to system is implemented by different loops. Specifically, there are anatomical, functional, and neurochemical loops involved in schizophrenia. First, as it was mentioned, cortico-hippocampal–cortex loops might be considered as the structural basis of a circular causal chain, where information can be stored, circulated, recalled, and even created. Second, five interconnected regions (superior parietal cortex, inferio-temporal cortex, prefrontal cortex, primary visual cortex, and the hippocampus) are supposed to form the functional macronetwork of associative memory, an impaired function of schizophrenic patients. Third, neurochemical loops were identified (Carlsson et al. 2000), failures of which may be related to schizophrenia. The dopamine hypothesis, which has been the predominant hypothesis, postulates that symptoms of schizophrenia may result from failure of the dopaminergic control system. Both increases (mostly in striatum) and decreases (mostly in prefrontal regions) in dopaminergic levels have been found. Glutamatergic mechanisms also seem to have a major role. Drugs by blocking neurotransmission at NMDA-type glutamate receptors cause symptoms similar to those of schizophrenia. The relationship among different feedback loops should be clarified. Much work should be done to integrate the two networks shown in Fig. 11.

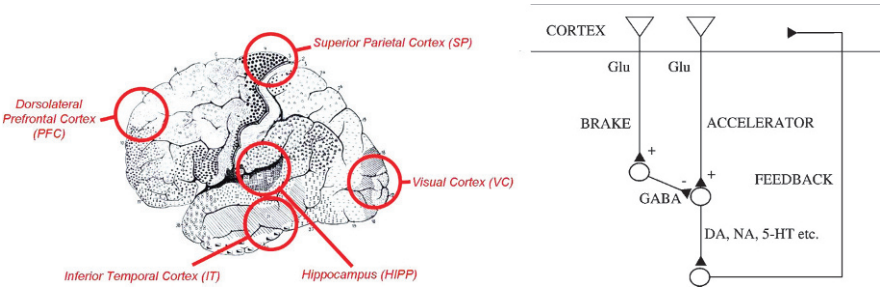

Fig. 11 *Left*: brain regions involved in object-location associative learning. *Right*: Hypothetical scheme showing the cortical regulation of the activity of the monoaminergic brainstem neurons by means of a direct glutamatergic pathway ("accelerator") and an indirect glutamatergic/gabaergic pathway ("brake"). Based on Fig. 1 of (Carlsson et al. 2000). The impairment of the balance between "brake" and "accelerator" may explain both increase and decrease of dopamine level

The dynamical modeling framework for associative learning can be specified within the framework of dynamical causal modeling. Based on available data on the activity of five interconnected regions (superior parietal cortex, inferio-temporal cortex, prefrontal cortex, primary visual cortex, and the hippocampus), a computational model will be established to understand the generation of normal and pathological temporal patterns. A dynamical casual model will be established and used to solve the "inverse problem," i.e., to estimate the effective connectivity parameters. This model framework, illustrated by Fig. 12, would address impaired connections in schizophrenia and the measure of functional reduction of the information flow.

Multi-scale modeling has multiple meanings and goals, including different time and spatial scales, levels of organization, even multi-stage processing. While the

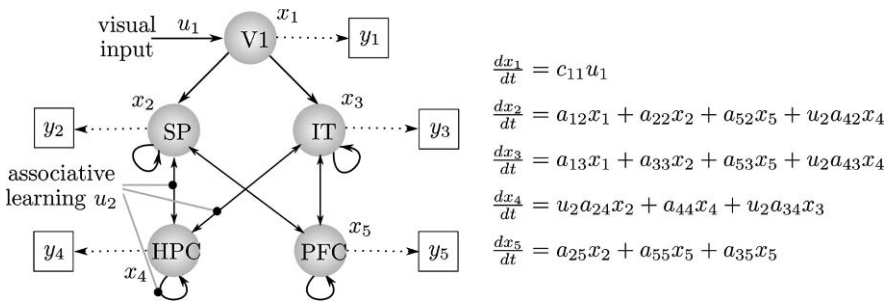

Fig. 12 DCM describing the dynamics in the hierarchical system involved in associative learning. Each area is represented by a single state variable (x). *Black arrows* represent connections, *gray arrows* represent external inputs into the system, and *thin dotted arrows* indicate the transformation from neural states to hemodynamic observations (y). In this example visual stimuli drive the activity in V1 which are propagated through the dorsal and ventral stream to the hippocampus and the PFC. The higher order connections are allowed to change between different blocks (learning, retrieval)

significance and importance of describing neural phenomena at different levels simultaneously are clear in many cases, we certainly do not have a single general mathematical framework. Mostly we have specific examples for coupling two or more levels. The understanding and control of normal and pathological behavior, the transfer of knowledge about the brain function, and dynamics to establish new computational and technological devices need the integration of molecular, cellular, network, regional, and system levels, and now the focus is on elaborating mathematically well founded and biologically significant multi-scale models.

Further Reading

Aradi I and Érdi P (2006) Computational neuropharmacology: dynamical approaches in drug discovery. Trends in Pharmacological Sciences 27, 240–243

Arbib MA (1899) The Metaphorical Brain. 2. John Wiley and Sons, New York

Arhem P, Klement G, and Nilsson J (2003) Mechanisms of anesthesia: towards integrating network, cellular, and molecular level modeling. Neuropsychopharmacology 28, S40–S47

Atmanspacher H and Rotter S (2008) Interpreting neurodynamics: concepts and facts. Cognitive Neurodynamics 2(4), 297–318

Bai D, MacDonald JF, and Orser BA (1998) Midazolam and propofol modulation of tonic GABAergic current and transient IPSCs in cultured hippocampal neurons. Abstracts – Society for Neuroscience 24, 1832

Bai D, Pennefather PS, MacDonald JF, and Orser, B (1999) The general anesthetic propofol slows deactivation and desensitization of $GABA_A$ receptors. The Journal of Neuroscience 19, 10635–10646

Baker PM, Pennefather PS, Orser BA, and Skinner FK (2002) Disruption of coherent oscillations in inhibitory networks with anesthetics: role of $GABA_A$ receptor desensitization. Journal of Neurophysiology 88, 2821–2833

Breakspear M and Jirsa VK (2007) Neuronal dynamics and brain connectivity. In: Handbook of Brain Activity (Jirsa VK and McIntosh AR, eds). Springer, Berlin

Breakspear M and Stam CJ (2005) Dynamics of a neural system with a multiscale architecture. Philosophical Transactions of the Royal Society of London. Series B, Biological Sciences 360, 1051–1074

Buzsaki G (2006) Rhythms of the Brain. Oxford University Press, Oxford

Carlsson A, Waters N, Waters S, and Carlsson ML (2000) Network interactions in schizophrenia – therapeutic implications. Brain Research Reviews 31, 342–349

Celentano JJ and Wong RK (1994) Multiphasic desensitization of the $GABA_A$ receptor in outside-out patches. Biophysical Journal 66, 1039–1050

Dayan P (2001) Levels of analysis in neural modeling. Encyclopedia of Cognitive Science. MacMillan Press, London, England

Drew PJ and Abbott LF (2006) Extending the effects of spike-timing-dependent plasticity to behavioral timescales. Proceedings of National Academic Science USA 103, 8876–8881

Érdi P (1983) Hierarchical thermodynamic approach to the brain. International Journal of Neuroscience 20, 193–216

Érdi P and Tóth J (2005) Towards a dynamic neuropharmacology: integrating network and receptor levels. In: Brain, Vision and Artificial Intelligence (De Gregorio M, Di Maio V, Frucci M and Musio C, eds). Lecture Notes in Computer Science 3704, Springer, Berlin Heidelberg, pp. 1–14

Érdi P, Huhn ZS, and Kiss T (2005) Hippocampal theta rhythms from a computational perspective: code generation, mood regulation and navigation. Neural Networks 18, 1202–1211

Érdi P, Kiss T, Tóth J, Ujfalussy B, and Zalányi L (2006) From systems biology to dynamical neuropharmacology: proposal for a new methodology. IEE Proceedings in Systems Biology 153(4), 299–308

Freeman WJ (1975) Mass Action in the Nervous System: Examination of Neurophysiological Basis of Adoptive Behavior Through the Eeg. Academic Press, Izhikevich

Freeman WJ (1999) Consciousness, intentionality and causality. Journal of Consciousness Studies 6, 143–172

Freeman WJ (2000) Mesoscopic neurodynamics: from neuron to brain. Journal of Physiology-Paris 94, 303–322

Freund T (2003) Interneuron diversity series: rhythm and mood in perisomatic inhibition, Trends in Neurosciences 28, 489–495

Freund TF and Antal M (1998) GABA-containing neurons in the septum control inhibitory interneurons in the hippocampus. Nature 336, 170–173

Freund TF and Buzsáki G (1996) Interneurons of the hippocampus. Hippocampus 6, 347–470

Friston KJ, Harrison L, and Penny W (2003) Dynamic causal modelling. Neuroimage 19, 1273–1302

Fulinski A, Grzywna Z, Mellor I, Siwy Z, and Usherwood PNR (1998) Non-Markovian character of ionic current fluctuations in membrane channels. Review E 58, 919–924

Fusi S, Asaad W, Miller E, and Wang XJ (2007) A neural circuit model of flexible sensorimotor mapping: learning and forgetting on multiple timescales. Neuron 54, 319–333

Gilboa G, Chen R, and Brenner N (2005) History-dependent multiple-time-scale dynamics in a single-neuron model. Journal of Neuroscience 25, 6479–6489

Hajós M, Hoffmann WE, Orbán G, Kiss T, and Érdi P (2004) Modulation of septo-hippocampal θ activity by GABAA receptors: an experimental and computational approach. Neuroscience 126, 599–610

Hebb DO (1949) The Organization of Behavior. John Wiley, New York

Hodgkin A and Huxley A (1952) A quantitative description of membrane current and its application to conduction and excitation in nerve. Journal of Physiology 117, 500–544

Huhn Zs, Orbán G, Lengyel M, and Érdi P (2005) Dendritic spiking accounts for rate and phase coding in a biophysical model of a hippocampal place cell. Neurocomputing 65–66, 331–334

Izhikevich EM (2005) Polychronization: computation with spikes. Neural Computation 18, 245–282

Jinno S and Kosaka T (2002) Immunocytochemical characterization of hippocamposeptal projecting gabaergic nonprincipal neurons in the mouse brain: a retrograde labeling. Brain Research 945, 219–231

Katona I, Acsády L, and Freund TF (1999) Postsynaptic targets of somatostatin immunoreactive interneurons in the rat hippocampus. Neuroscience 88, 37–55

Kispersky T and White JA (2008) Stochastic models of ion channel gating. Scholarpedia 3(1), 1327

Kiss T, Orbán G, and Érdi P (2006) Modelling hippocampal theta oscillation: applications in neuropharmacology and robot navigation. International Journal of Intelligent Systems 21(9), 903–917

Kiss T, Orbán G, Lengyel M, and Érdi P (2001) Intrahippocampal gamma and theta rhythm generation in a network model of inhibitory interneurons. Neuro-computing 38–40, 713–719

Koch C (1999) Biophysics of Computation. Information Processing in Single Neurons. Oxford University Press, Oxford – New York

Kozma R, Freeman, WJ, Wong D, and Érdi P (2004) Learning environmental clues in the KIV model of the cortico-hippocampal formation. Neurocomputing 58–60, 721–728

La Camera G, Rauch A, Thurbon D, Lüscher HR, Senn W, and Fusi S (2006) Multiple time scales of temporal response in pyramidal and fast spiking cortical neurons. Journal of Neurophysiology 96, 3448–3464

Lacaille JC, Mueller AL, Kunkel DD, and Schwartzkroin PA (1987) Local circuit interactions between oriens/alveus interneurons and CA1 pyramidal cells in hippocampal slices: electrophysiology and morphology. Journal of Neuroscience 7, 1979–1993

Lacaille JC and Williams S (1990) Membrane properties of interneurons in stratum oriens-alveus of the CA1 region of rat hippocampus in vitro. Neuroscience 36, 349–359

Lavenex P and Amaral G (2000) Hippocampal–neocortical interaction: a hierarchy of associativity. Hippocampus 10, 420–430

Lengyel M and Érdi P (2004) Theta modulated feed-forward network generates rate and phase coded firing in the entorhino-hippocampal system. IEEE Transactions on Neural Networks 15, 1092–1099

Liebovitch LS, Scheurle D, Rusek M, and Zochowski M (2001) Fractal methods to analyze ion channel kinetics. Methods 24, 359–375

Lowen SB, Liebovitch LS, and White JA (1999) Fractal ion-channel behavior generates fractal firing patterns in neuronal models. Physical Review E 59, 5970

Mainen ZF and Sejnowski TJ (1995) Reliability of spike timing in neocortical neurons. Science 268, 1503–1506

Orbán G, Kiss T, Lengyel M, and Érdi P (2001) Hippocampal rhythm generation: gamma-related theta-frequency resonance in CA3 interneurons. Biological Cybernetics 84, 123–132

Rolls ET (1995) A model of the operation of the hippocampus and entorhinal cortex in memory. International Journal of Neural Systems 6, 51–71

Rolls EY and Treves A (1990) The relative advantages of sparse versus distributed encoding for associative neuronal networks in the brain. Network 1, 407–421

Sakmann B and Neher E (eds) (1983) Single Channel Recordings. Plenum, New York

Stephan KE, Harrison LM, Kiebel SJ, David O, Penny WD, and Friston KJ (2007) Dynamic causal models of neural system dynamics: current state and future extensions. Journal of Biosciences 32, 129–144

Toib A, Lyakhov V, and Marom S (1998) Interaction between duration of activity and time course of recovery from slow inactivation in mammalian brain Na+ channels. Journal of Neuroscience 18, 1893–1903

Tretter F and Albus M (2007) "Computational neuropsychiatry" of working memory disorders in schizophrenia: the network connectivity in prefrontal cortex – data and models. Pharmacopsychiatry 40, S2–S16

Treves A and Rolls ET (1994) Computational analysis of the role of the hippocampus in memory. Hippocampus 4, 374–339

Ujfalussy B, Erős P, Somogyvári Z, and Kiss T (2008) Episodes in Space: A Modelling Study of Hippocampal Place Representation SAB 2008, LNAI 5040, pp. 123–136, Springer-Verlag Berlin Heidelberg

Varga V, Borhegyi Zs, Fabo F, Henter TB, and Freund TF (2002) In vivo recording and reconstruction of gabaergic medial septal neurons with theta related firing. Program No. 870.17. Society for Neuroscience, Washington, DC

Varona P, Ibarz M, López-Aguado L, and Herreras O (2000) Macroscopic and subcellular factors shaping population spikes. Journal of Neurophysiology 83, 2192–2208

Wang XJ and Buzsáki G (1996) Gamma oscillation by synaptic inhibition in a hippocampal interneuron network model. Journal of Neuroscience 16, 6402–6413

Weitzenfeld A (2000) A multi-level approach to biologically inspired robotic systems. Proceedings of NNW 2000 10th International Conference on Artificial Neural Networks and Intelligent Systems

Weitzenfeld A (2008) From schemas to neural networks: a multi-level modeling approach to biologically-inspired autonomous robotic systems. Journal of Robotics and Autonomous Systems 56, 177–197

Biophysics-Based Models of LTP/LTD

Gastone C. Castellani and Isabella Zironi

Introduction

Synaptic plasticity is the process by which neurons change the efficacy (or the strength) of their connections (synapses). In the connectionist paradigm, synaptic plasticity is a central concept because it is widely accepted that memory and learning are biologically encoded by variations of neuronal connections strength. In a more general sense, activity-dependent synaptic plasticity is assumed to be necessary and sufficient to encode and store memory in specific brain areas. Another feature of synaptic plasticity is the bidirectionality, which is the capability to increase or decrease the synaptic weights, thus encompassing the classical Hebbian paradigm.

The biological implementation of synaptic plasticity can take place in different ways with respect to duration in time, protocols, induction and expression. The best known form of synaptic plasticity is LTP and other forms of activity-dependent plasticity that have been found are LTD, the reversal of LTP, EPSP-spike (E-S) potentiation, a changing in the likelihood to have an action potential (AP) following a synaptic stimulus, spike-timing-dependent plasticity (STDP), based on timing of AP in presynaptic and postsynaptic cell, de-potentiation and de-depression, the reversal, respectively, of LTP and LTD but with different properties (Neves et al., 2008).

The phenomenon of LTP, discovered over 30 years ago in the hippocampus (Bliss and Lomo, 1973; Bliss and Collingridge, 1993; Lomo, 2003), has been intensively studied by experimentalist and theoretical researchers: these studies produced a large number of published papers during these years, mainly based on the assumption that LTP is, or potentially would be, an important mechanism for memory formation in the brain. The classical experimental protocol for the induction of LTP is the high-frequency stimulation (HFS) and/or a rapid strong depolarization. A parallel phenomenon to LTP is LTD that is induced by low-frequency stimulation (LFS) and/or milder depolarization. Recent studies show that information can be stored effectively by synaptic long-term potentiation as well as

G.C. Castellani (✉)
Dipartimento di Fisica Università di Bologna and Institute for Brain and Neural Systems, Brown University, Bologna 40127, Italy
e-mail: gastone.castellani@unibo.it

V. Cutsuridis et al. (eds.), *Hippocampal Microcircuits*, Springer Series in Computational Neuroscience 5, DOI 10.1007/978-1-4419-0996-1_19,

depression (Bear, 1996). Behavioural studies testing animal response by inhibitory avoidance learning paradigm demonstrated that the elementary biochemical mechanisms underlying the induction of LTP are activated during this type of learning and memory formation. An one-trial inhibitory avoidance learning caused a spatially restricted increase in the amplitude of the synaptic transmission in hippocampal pyramidal cells (CA1) that prevents the induction of LTP by HFS (Whitlock et al., 2006). Thus, it is possible to conclude that artificial stimuli delivered by a protocol such as HFS, and animal training targeted to induce learning and memory, share a wide array of molecular mechanisms, including phosphorylation state of ionotropic glutammate receptors, establishing a link that will be used as a powerful model to describe this complex process.

Spike-timing-dependent plasticity (STDP) is a type of synaptic functional change based on the timing of action potentials in connected neurons. It has been observed that LTP and LTD could be induced at low-frequency depending on the precise timing relationships between pre- and postsynaptic firing (Abbott and Nelson, 2000). In particular, synaptic modification is maximal for small temporal differences between pre- and postsynaptic spike and vanishes if this difference is greater than a certain value, moreover, the sign of the time difference (that is, whether the presynaptic spike precedes or follows the postsynaptic spike: pre–post or post–pre spiking) determines whether the protocol induces LTP or LTD. At the molecular level STDP is mediated by *N*-methyl-D-aspartate receptors (NMDARs), LTP and LTD components of STDP, are distinct processes and may depend on different populations of NMDARs linked with diverse signalling pathways (Nelson and Turrigiano, 2008).

The activation of NMDARs leads to, at least in the CA3-CA1 synapses, an increasing postsynaptic calcium influx through NMDAR itself with the triggering of a cascade of events such as activation of calcium-calmodulin-dependent protein kinase of type II (CaMKII), and subsequently of a network of calcium (Ca^{2+})-regulated kinases and phosphatases. Regarding the mechanism, it remains unclear whether a single model can explain STDP at different synapses or whether different neurons employ distinct molecular machineries to achieve similar outcomes. Studies are only beginning to examine whether and how STDP depends on several signalling events that have been strongly implicated in conventional LTP and LTD, including secretion of brain-derived neurotrophic factor (BDNF) and nitric oxide (Mu and Poo, 2006), activation of CaMKII (Tzounopoulos et al., 2007) and phosphatases (Froemke et al., 2005) and modification and insertion/removal of α-amino-3-hydroxy-5-methyl-4-isoxazolepropionic acid (AMPA) subtype of glutamate receptors (AMPAr) based on phosphorylation/dephosphorylation.

The AMPAr mediates the majority of fast excitatory synaptic transmission in the mammalian central nervous system. As such, changes in the conductance of individual AMPA receptors (AMPAr) have a significant effect on the efficacy of synaptic transmission. Among the molecular mechanism capable to modify the state of AMPAr, the phosphorylation/dephosphorylation at serine and treonine sites are those widely accepted from a biochemical point of view. The phosphorylation state of AMPAr can impact on two properties of these channels: conductance and trafficking. In particular, the AMPAr phosphorylation state can modulate their insertion

in the postsynaptic membrane as well as their unitary currents. For example, it has been shown that the AMPAr phosphorylation at the serine 831 (Ser^{831}) site significantly increase 30 min after inhibitory avoidance training compared to untrained animals, while no differences has been found at the serine 845 (Ser^{845}) site (Whitlock et al., 2006). This important finding demonstrated that the induction of the inhibitory avoidance form of learning is accompanied by the AMPAr phosphorylation to a specific site and gives further evidence that this molecular mechanisms is associated with memory formation.

AMPAr phosphorylation traditionally has been thought to be mainly involved in the regulation of the channel gating properties or conductance (Barria et al., 1997). A large body of evidence accumulated during recent years strongly suggests that AMPARs are continuously recycled between the cellular membrane and the intracellular compartments via vesicle-mediated plasma membrane insertion and endocytosis. Regulation of either receptor insertion or endocytosis results in a rapid change in the number of these receptors expressed on the plasma membrane surface and in the receptor-mediated responses, thereby playing an important role in mediating synaptic plasticity. The regulation of AMPAr trafficking is a complex phenomenon and its role is strongly dependent from the subunit where the phosphorylation is taking place (Shi et al., 2001). A suggestive hypothesis is that phosphorylation at Ser^{845} and Ser^{831} of GluR1 molecule controls distinct determinants of receptor functions: receptor trafficking and channel conductance (Lee et al., 1998; Derkach et al., 1999; Havekes et al., 2007; Liu et al., 2009; Lee et al., 2000) and that can be related to different tasks at hippocampal level. A key variable controlling the sign and magnitude of synaptic plasticity is the relative concentration of intracellular Ca^{2+}. This concentration might be modulated by ionic fluxes through the postsynaptic glutamate receptor *N*-methyl-D-aspartate (NMDAr). When activated, the NMDAr is permeable to Ca^{2+}, therefore it has been proposed that an increase in postsynaptic Ca^{2+} concentration is a primary signal for the induction of bidirectional synaptic plasticity. For example, a modest NMDAr activation, induced by low-frequency stimulation (LFS), results in LTD, while strong activation induced by HFS produces LTP (Dudek and Bear, 1992; Mulkey and Malenka, 1992; Cummings et al., 1996; Bear et al., 1987; Lisman, 1989; Artola and Singer, 1993).

The transient variation in Ca^{2+} concentration can be transduced into changes, mediated by CAMKII in the phosphorylation state and activity of target proteins such as ion channels, plasma membrane proteins and other kinases. Autophosphorylation of CaMKII reduces the release of bound calcium–calmodulin (k_d, the dissociation constant decreases from 45 to 0.06 nM, respectively, for the unphosphorylated and the phosphorylated CaMKII) with an increase of the release time from less than a second to several hundred seconds. This property enable CaMKII to shift in a new state in which calmodulin is bound to CaM kinase even though the concentration of Ca^{2+} is basal and provides a molecular basis for potentiation of Ca^{2+} transients and may enable detection of their frequency. This property has been proposed more than 20 years ago as a molecular switch for memory capable to store and maintain information by a mechanisms independent from molecular turnover that can be translated in mathematical terms as a bistable dynamical system (Lisman, 1985).

The role of pattern variations in Ca^{2+} concentration such as waves and spikes has been well recognized as central in the control of vesicle cycle by endocytosis and exocytosis processes in presynaptic terminals (Wu and Betz, 1998). During the recent years it has become clear that the variation of Ca^{2+} concentration in the postsynaptic terminal is important for glutamate receptor cycling in hippocampal neurons. The Ca^{2+} concentration in the postsynaptic terminal can vary for several reasons such as release from intracellular store, capacitive Ca^{2+} entry, NMDA and Ca^{2+} channel influx as response to different stimuli (HFS, BDNF) (Nakata and Nakamura, 2007). The Ca^{2+} signalling is essential for the increase of surface expression of AMPAR subunit GluR1 at postsynaptic densities. Moreover, it seems that spatial and temporal properties of Ca^{2+} signalling cascade can play a role in the regulation of AMPAR trafficking in postsynaptic densities of cortical pyramidal neurons.

The regulation of synaptic strength by neuronal activity is bidirectional. Such regulation has been hypothesized to depend on changes in the number and/or composition of the AMPA receptors at the postsynaptic membrane level. Thus, the AMPAr phosphorylation/dephosphorylation cycle has been identified as one of the major molecular mechanisms involved (Lüscher et al., 2000; Scannevin and Huganir, 2000). Furthermore, NMDAr is the critical point of the Ca^{2+} entry into the postsynaptic neuron; their composition and function can also be acutely and bidirectionally modified by cortical activity (Carmignoto and Vicini, 1992; Quinlan et al., 1999; Philpot et al., 2001), dramatically altering the properties of activity-dependent synaptic plasticity.

Molecules Involved in Synaptic Plasticity

Ionotropic Glutamate Receptors

AMPA receptors are tetramers composed of four homologous subunit proteins (GluR1–GluR4) that combine to form different AMPA receptor subtypes. GluR1 is one of the most abundantly expressed subunits in the mammalian hippocampus and neocortex and, in combination with GluR2, is thought to comprise the majority of AMPA receptor complexes in these regions (Lee et al., 2000). AMPAr function is regulated by the composition of individual receptors and/or the phosphorylation/dephosphorylation state of individual subunit proteins (Dudek and Bear, 1992; Mulkey and Malenka, 1992).

NMDA receptors are heteromeric ion channels, composed of NR1 and NR2 subunit proteins (Cummings et al., 1996). Each of the four subtypes of the NR2 subunit confers distinct functional properties to the receptor. As has been demonstrated both in vivo and in heterologous expression systems, NMDAr composed of NR1 and NR2B mediate long-duration currents ($\approx$250 ms), whereas inclusion of the NR2A subunit results in NMDAr with faster kinetics ($\approx$50 ms) (Bear et al., 1987;

Lisman, 1989). NMDArs composed of NR1 and NR2B are observed in the neocortex at birth, and over the course of development, there is an increase in the ratio of NR2A/NR2B (Bear et al., 1987; Lisman, 1989; Artola and Singer, 1993).

Protein Kinases and Phosphatases

Ca^{2+}/Calmodulin-dependent protein kinase II (CaMKII) is abundant in synapses and able to mediate cell signalling in response to Ca^{2+} transients. Both in vitro and in vivo studies revealed that synaptic stimulation causes a rapid translocation of CaMKII to the synapse (Lisman, 1985; Wu and Betz, 1998) and an acute increase of CaMKII activity leads to a potentiation followed by an occlusion of LTP (Wu and Betz, 1998), indicating a key role in synaptic plasticity (Whitlock et al., 2006). The CaMKII property, as multienzymatic systems, to phosphorylate itself, is the molecular basis for a form of switch-like behaviour that is thought to be implicated with memory storing. The CaMKII phosphorylated state, in contraposition to the non-phosphorylated one, is more active even at low calcium concentration and may provide a mechanism for long-lasting memory without gene expression that is under intense investigation from long time (Lisman 85 e nuovo).

The protein kinase A cyclic adenosine monophosphate (cAMP)-dependent (PKA) is thought to be a LTP modulator. Recent studies showed that PKA act as a gating factor for the threshold of LTP induction (Carmignoto and Vicini, 1992), probably through the GluR1 phosphorylation at Ser^{845} site that might increase the AMPAr open-probability (Quinlan et al., 1999).

The protein kinase C (PKC) has attracted great attention in the last 15 years. To date the PKC enzyme family consists of 12 isozymes that can be further categorized into Ca^{2+}-dependent and Ca^{2+}-independent isoforms. Recently PKC has been characterized as responsible for the phosphorylation at the Tir^{840} site of the GluR1 (Philpot et al., 2001).

Protein phosphatase 1 (PP1) complexes are necessary for normal regulation of AMPA- and NMDA-receptors and modulate dendritic spine formation and dynamics (Petralia and Wenthold, 1992). PP1 activity might be antagonistically modulated by cAMP and Ca^{2+} signalling pathways (Walaas and Greengard, 1991), allowing multiple neurotransmitters to fine-tune synaptic plasticity (for review, see Malinow and Malenka, 2002).

PP2B (also known as calcineurin) is the only phosphatase directly modulated by a second messenger (Ca^{2+} acting via calmodulin and the B regulatory subunit). PP2B has a relatively restricted substrate specificity compared with other phosphatases. Because PP2B is activated at lower Ca^{2+}/calmodulin concentrations than CaMKII, weak synaptic stimulation may preferentially activate PP2B, whereas stronger stimulation also recruits CaMKII activation (Tzounopoulos et al., 2007).

AMPA Receptor Cycle

Several serine residues in the intracellular carboxy-terminal tail of GluR1 have been identified as important sites for activity-dependent regulation of AMPAr function by phosphorylation (Table 1). Specifically, PKA phosphorylates S^{845}, while PKC and CaMKII phosphorylate S^{831}. Phosphorylation of S^{831} increases the unitary conductance of the AMPAr, and phosphorylation at S^{845} increases the channel mean open time, in both cases increasing the average channel conductance (McBain and Mayer, 1994; Stocca and Vicini, 1998; Flint et al., 1997; Sheng et al., 1994; Shen and Meyer, 1999). Dephosphorylation at each site is mediated by an activity-dependent protein phosphatase cascade. LTP is associated with an increased phosphorylation at S^{831}, whereas LTD has been associated with a decrease in S^{845} phosphorylation (Sheng et al., 1994; Shen and Meyer, 1999; Lledo et al., 1995). Therefore, the knowledge of GluR1 phosphorylation state may be a strong predictor of the direction of change (increase or decrease) induced by learning and memory tasks (Table 3).

Moreover, the post-synaptic trafficking of AMPAr is tightly regulated at the synapse (Lisman et al., 1997; Blitzer et al., 1998; Roche et al., 1996; Sheng and Lee, 2001; Lee, 2006). Strong synaptic stimuli, as the HFS, lead to a Ca^{2+} influx through NMDAr and a subsequent increase of the intracellular Ca^{2+} concentration able to trigger the insertion of cytosolic AMPAr into the synaptic membrane, while a LFS lead to the removal of AMPAr (Blitzer et al., 1998). Both in LTP and in LTD strong synaptic activity drives sufficient Ca^{2+} entry through NMDA receptors to activate CaMKII that phosphorylate the cytoplasmic tails of GluR1 and GluR4 AMPAr subunits and triggers their incorporation into synapses (Feng et al., 2000). These evidences indicate that different protein kinases play critical roles in the generation of LTP/LTD (Huang et al., 1996), therefore understanding the role of kinases for the delivery of memory formation is pivotal (Table 2).

Table 1 Phosphorylation sites on AMPAr subunits

Phosphorylation site	Kinase	Functions
GluR1 S^{818}	PKC	GluR1 synaptic insertion
GluR1 S^{831}	CaMKII	Increases single channel conductance of homomeric receptors
	PKC	Dephosphorylation after depotentiation
		Homeostatic plasticity
GluR1 T^{840}	PKC	Highly phosphorylated under basal condition
GluR1 S^{845}	PKA	Increases mean open probability of channel
		Persistent dephosphorylation following LTD
		Necessary for LTD expression
		Necessary for synaptic insertion with LTP induction
		Regulates AMPA receptor recycling
		Homeostatic plasticity
GluR2 S^{880}	PKC	Necessary and sufficient for LTD
GluR4 T^{883}	PKC	Increases surface expression in heterologous cells
GluR4 S^{842}	PKC	Necessary for spontaneous activity-driven synaptic insertion

Table 2 Kinases involved in AMPAr cycle

Kinase	Substrate	Functions
CaMKII	CaMKII, GluR1, NR2B	LTP expression, CaMKII-α autophosphorylation, metaplasticity, homeostatic synaptic plasticity
PKA	GluR1, GluR4, NR1, NR2A	LTP expression, LTP induction during early development
PKC	GluR1, GluR2, GluR4, NR1, NR2B	LTP maintenance, LTP induction, PKC-γ necessary for LTP, but not for LTD
Tyrosine kinases	GluR2, NR2A, NR2B	LTP induction and LTP expression, LTD induction

Table 3 Phosphatases involved in synaptic plasticity and AMPAr cycle

Phosphatase	Substrate	Function
PP1	PSD-associated CaMKII-α, GluR1	LTD induction, LTD of NMDAr-mediated synaptic transmission. Negatively regulates LTP induction
PP2A	Soluble CaMKII-α, GluR1	LTD induction
PP2B (Calcineurin)	GluR1, NR2A	LTD induction. Calcineurin-α specifically involved in depotentiation, but not LTD. Negatively regulates LTP induction

The role of CaMKII on AMPAr trafficking is still not completely clear and a working model is that, during LTP, phosphorylation of GluR1 by CaMKII enhances its conductance, while phosphorylation of a protein associated to the AMPA receptor controls its trafficking to the synapse. The signal-transduction cascades controlling synaptic phosphorylation/dephosphorylation are complex, and mathematical descriptions of such networks have been developed in order to obtain a quantitative understanding of their function (Svenningsson et al., 2004; Roche et al., 1996).

Modelling the AMPAr cycle

In many regions of the brain, including the mammalian cortex, magnitude and direction of activity-dependent changes in synaptic strength (synaptic plasticity), as well as their dependence from the history of activity at those synapses (metaplasticity), are implemented by LTP/LTD mechanisms (Svenningsson et al., 2004; Roche et al., 1996). Phosphorylation and dephosphorylation are ubiquitous biochemical processes that can act as regulatory switches in cellular signalling and influence a wide range of cellular functions. The number of different kinases and phosphatases is very high, on the order of 10^3, and their interactions can be described in the framework of dynamical systems on neuronal networks (Bhalla, 2004a, b). The analysis of such dynamical systems has been faced by a number of researchers from long time and produced several theoretical results, such as bistability, multistability,

oscillations and noise amplification among others, that are becoming to be experimentally validated with ad hoc in vitro and in vivo models.

A model has been proposed in which the establishment of LTP and LTD follows a regulated process of phosphorylation and dephosphorylation at the two phosphorylation sites on the GluR1 subunit of the AMPAr: S^{845} and S^{831}. GluR1 can be dephosphorylated at both sites (A), phosphorylated at S^{845} (A^P), phosphorylated at S^{831} (A_P), or phosphorylated at both S^{845} and S^{831} (A_P^P) (Castellani et al., 2001).

We can consider two pairs of enzymes, the enzyme kinase 1/enzyme phosphatase 1, acting on the S^{831} site, and the enzyme kinase 2/enzyme phosphatase 2, acting on the S^{845} site. High-frequency stimulation of the synapses activates protein kinases, resulting in phosphorylation. Low-frequency stimulation of the synapse activates protein phosphatases, resulting in phosphorylation. In the naive synapse, LTD leads to a dephosphorylation at Ser^{845} (PKA site) whereas, in the potentiated synapse, LTD leads to dephosphorylation of Ser^{831} (CaMKII site). The opposite scenario takes place during induction of LTP: the naive synapse becomes phosphorylated at Ser^{831} (CaMKII site) and the depressed synapse becomes phosphorylated at Ser^{845} (PKA site). Combined with the results on the phosphorylation status of GluR4, one can speculate that under basal neuronal activity, the PKA site in GluR1 is phosphorylated. Inducing LTP will lead to an additional CaMKII phosphorylation, whereas the induction of LTD would lead to the dephosphorylation of the PKA site.

All the biochemical information reported can be mapped in a series of biophysical models at various levels of approximation. In Fig. 1, the AMPAr phosphorylation cycle with the involved kinases and phosphatases is represented. These models can be mathematically described by kinetic equations of the following type (Castellani et al., 2005):

$$\begin{aligned}
\dot{A} &= -v_1 + v_2 + v_6 - v_5 \\
\dot{A}_P &= -v_2 + v_1 + v_4 - v_3 \\
\dot{A}^P &= -v_6 + v_5 + v_8 - v_7 \\
\dot{A}_P^P &= -v_4 + v_3 + v_7 - v_8
\end{aligned} \tag{1}$$

where the velocities $v_1, \ldots, v_8$ are referred to the eight enzymatic reactions reported in Fig. 1 and all the reactions are enzymatic reactions of the Michaelis–Menten type

$$E + S \underset{k_{-1}}{\overset{k_1}{\rightleftarrows}} ES \xrightarrow{k_2} E + P \tag{2}$$

This system can be described in a matrix form:

$$\dot{A} = RA \tag{3}$$

where the $\boldsymbol{R}$ matrix is a function of the dynamical variables and A indicates the state of the AMPA receptor $A = (A,\ A_P,\ A^P,\ A_P^P)$.

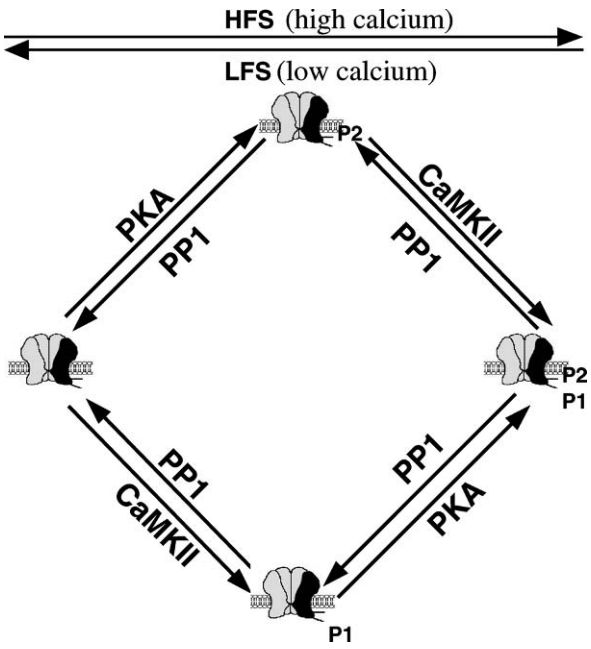

Fig. 1 A possible model for bidirectional synaptic plasticity in CA1. The model is designed to take into account the following four observations regarding NMDA receptor-dependent synaptic plasticity in CA1. First, from a baseline state, synapses can be potentiated in response to HFS and depressed in response to LFS. Second, LTP and LTD can be reversed by LFS and HFS, respectively. Third, expression of LTP from baseline depends on phosphorylation of a postsynaptic CaMKII (but not PKA) substrate. Fourth, expression of LTD from baseline depends on dephosphorylation of a PKA substrate. According to the model, HFS can cause synapses to grow more effective in two distinct ways, depending on the initial state of the synapses. For example, from a depressed state, HFS can cause "de-depression" via phosphorylation of a postsynaptic PKA substrate, while from a baseline state, HFS can cause "potentiation" via phosphorylation of a postsynaptic CaMKII substrate. Similarly, LFS can cause synapses to become weaker in two different ways. For example, from a potentiated state, LFS can cause "depotentiation" via dephosphorylation of a postsynaptic CaMKII substrate, and from a baseline state, LFS can cause "depression" via dephosphorylation of a postsynaptic PKA substrate. The mechanism proposed to implement the model is based on observed changes in phosphorylation of the GluR1 subunit of postsynaptic AMPA receptors following induction of LTD and LTP. The phosphatases involved in depression and depotentiation are not known with certainty

One of the problems of this cycle is the definition of the baseline, the naive state of the synapse, and for this reason the cycle shown in Fig. 2 is preferred. The cycle of Fig. 1 has a metastable behaviour, but a mathematical demonstration of bistability has not been reported. Preliminary data based on reformulation of the equations with the insertion of a multiplicative noise show that this type of noise can bistabilize this cycle, but the deterministic behaviour is still under investigation (unpublished data).

The stability properties, as well as the equivalence with the other model of synaptic plasticity, strongly depend on the type and number of the involved enzymes

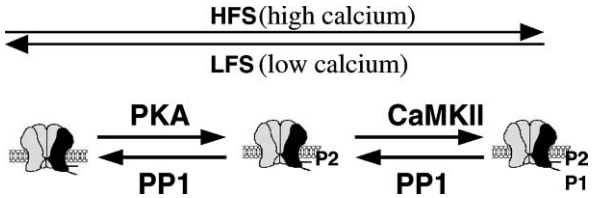

Fig. 2 HFS delivered to naive synapses preferentially activates CaMKII, which increases phosphorylation of GluR1 on Ser ^{831} (CaMKII site; P_{831}) resulting in LTP. In contrast, LFS given in a naive slice activates protein phosphatases (including PP1/2A), which dephosphorylate Ser^{845} (PKA site; P_{845}). However, LFS given to a previously potentiated synapse (LTP) dephosphorylates Ser^{831}. On the other hand, HFS delivered to previously depressed synapses (LTD) phosphorylates Ser^{845}

and ultimately on the structure of the *R* matrix (Roche et al., 1996; Kameyama et al., 1998). In particular, it has been recently demonstrated that the cycle shown in Fig. 2 is bistable for a wide range of parameters and that shows robustness to external perturbation (Kameyama et al., 1998). A more detailed model, where all the enzymes above described are represented, is shown in Fig. 3. The mathematical description of this kinetic schema is obtainable with the same methodology used in the cycle modelled in Figs. 1 and 2.

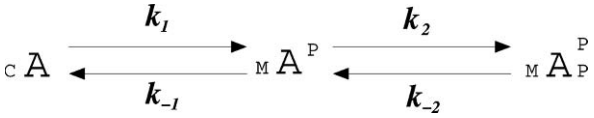

Fig. 3 A simplified three-state scheme for AMPAr phosporylation and membrane insertion. k_1, k_{-1}, k_2 and k_{-2} are the intrinsic constants. The three states indicate, respectively, the cytoplasmatic and non-phosphorylated AMPA, the phosphorylated and membrane-inserted AMPA and the double phosphorylated and membrane inserted AMPAr

The biochemical cycles shown in Figs. 1, 2, and 3 can be described with a formalism based on the concept of transition between states, the evolution of the probability to occupy a discrete state such as bounded or unbounded to a phosphoric group. This kind of approach can unify the description of conductance and expression properties of ion channels, i.e. the state occupancy probability, the expected values of conductance, ionic current, dwell times and the probability to be inserted in the membrane. The evolution of probability among states is a classic topic that has been studied in ion channel and chemical reactions literature and is still under intense investigation to provide quantitative models of gene expression and protein concentration dynamics. These models can be described in the framework of Markov processes by the so-called Chemical Master.

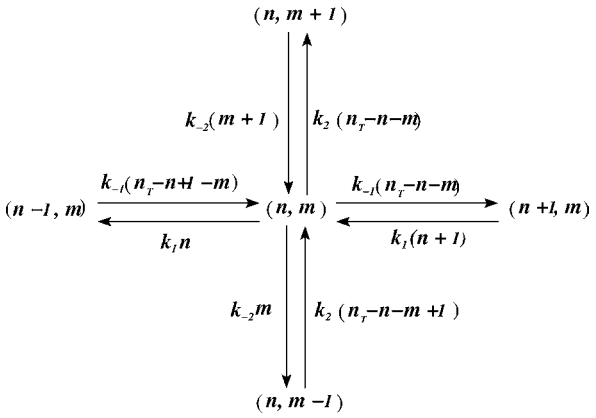

Fig. 4 Diagrammatic procedure to obtain the Chemical Master Equation from a given chemical kinetic scheme. This graph, called *master equation graph*, is the first step to obtain the CME. The kinetic model of Fig. 3 has two independent dynamic species, hence the master equation graph is a two-dimensional grid in which each grid point represents the state of the system by specifying the number of molecules for each dynamic species. The "rate constant" on an arrow in the diagram is determined by the product of the number of molecules of reactants multiplied by the corresponding intrinsic constant. The corresponding CME, Equation (4), is then obtained directly from this diagram

The Chemical Master equation for the cycle shown in Fig. 3 is directly obtainable from the Master Equation Graph shown in Fig. 4:

$$\begin{aligned}\frac{dp(m,n,t)}{dt} &= k_{-2}(m+1)p(n,m+1) + k_{-1}(n_T - n + 1 - m)p(n-1,m)\\ &+ k_2(n_T - n - m + 1)p(n,m-1)\\ &+ k_1(n+1)p(n+1,m) - k_{-2}mp(n,m) - k_2(n_T - n - m)p(n,m)\\ &- k_1np(n,m)\\ &- k_{-1}(n_T - n - m)p(n,m) \qquad (4)\end{aligned}$$

In this equation, n and m are the number of molecules in the state ${}_C A$ and ${}_M A_P^P$, respectively; n_T is the total number of molecules, including those in the state ${}_M A_P^P$; *p(n, m, t)* is the time-dependent probability to have $\boldsymbol{n}$ molecules in the state ${}_C A$ and $\boldsymbol{m}$ molecules in the state ${}_M A_P^P$, *p(n-1, m, t), p(n+1, m, t), p(n, m-1, t)* and *p(n, m+1, t)* are the probabilities to have the other states, where the number of molecules are increased or decreased of one as prescribed by the one-step Poisson process. This modelling is to be used when the number of substrate molecules is low, and the effect of fluctuations may play a relevant role. We note that the number of AMPAr in a synaptic spine is on the order of 10^2, hence the fluctuations effect can be not negligible.

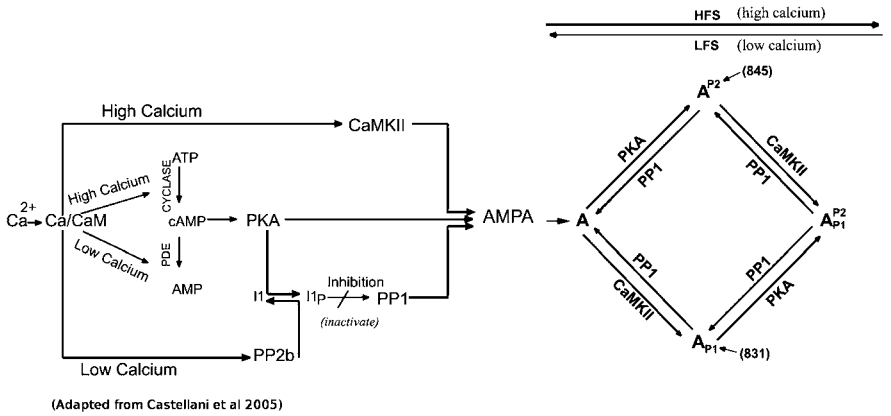

Fig. 5 Calcium-dependent activity of the kinase/phosphatase network. (*Left*) Introduction of specific activity-dependent protein kinases and protein phosphatases into the schematic representation of bidirectional phosphorylation/dephosphorylation of the GluR1 subunit of the AMPAr. A schematic description of the Ca^{2+}-dependent signal transduction cascades that regulate AMPAr phosphorylation. An increase in postsynaptic Ca^{2+} concentration results in an increase in postsynaptic Ca^{2+}–calmodulin (Ca^{2+}–CaM) concentration. Low levels of Ca^{2+}–CaM stimulate PP2B activity directly, while high levels of Ca^{2+}-CaM stimulate CaMKII activity. PKA and PP1 are indirectly regulated by Ca^{2+} (Castellani et al., 2005). PKA is activated by cAMP, which can be generated by Ca^{2+}-dependent adenylyl cyclase (AC) and degraded by phosphodiesterase (PDE). PP1 activity level is inhibited by the protein inhibitor 1. The inhibition is released by dephosphorylation of inhibitor 1 via the activity of PP2B (Modified from Tzounopoulos et al. (2007)). (*Right*) There are two phosphorylation sites on the GluR1 subunit of the AMPAr, S845 and S831. S845 is phosphorylated by PKA and dephosphorylated by PP1; S831 is phosphorylated by CaMKII and dephosphorylated by PP1. HFS of the synapses results in a large increase in postsynaptic Ca^{2+} and a resultant activation of the Ca^{2+}-calmodulin-dependent protein kinases. LFS of the synapse results in a modest increase in postsynaptic Ca^{2+} and a resultant activation of the calcium-calmodulin-dependent protein phosphatases

Conclusions

Changes in synaptic efficacy underlie many fundamental properties of nervous system function, such as developmental refinement of receptive fields, learning and memory. As such, the molecular mechanisms underlying the regulation of synaptic strength have been an area of intense investigation.

AMPAr phosphorylation is a key event in the regulation of receptor trafficking and stabilization at the synapse. CaMKII, PKA and PP1 are the most important molecules involved in this process that have been experimentally validated in several experiments.

The use of experimentally derived properties of intracellular signalling cascades and postsynaptic glutamate receptor phosphorylation to model bidirectional regulation of synaptic strength is of great importance towards the development of realistic plasticity models.

Alternatively, there may be additional unknown phosphorylation sites in GluR1 that are responsible for synaptic plasticity and AMPAr insertion in postsynaptic membrane. Computational predictions based on detection of kinase motifs in GluR1 predict a site phosphorylated by PKC, a kinase that is also important for LTP (Philpot et al., 2001).

From a biophysical point of view, one the most important question to be addressed is the bistability of the cycles shown in Figs. 1 and 2. More precisely, the bistability without the feedback created by the autophosphorylation of the CaMKII molecule (Tzounopoulos et al., 2007). Also the role of noise, both extrinsic and intrinsic, is an important issue that is relevant in this kind of biophysical models due to the low number of molecules involved. We explicitly note that the insertion of an external noise, mainly a multiplicative noise, in the dynamical Michaelis–Menten equation force the interpretation on a more microscopical framework that is the so-called single molecule enzymology

Further Reading

Abbott LF, Nelson SB (2000) Synaptic plasticity: taming the beast. *Nat. Neurosci*. **3**: 1178–1183.

Artola A, Singer W (1993) Long term depression of excitatory synaptic transmission and its relationship to long term potentiation. *Trends Neurosci*. **16**: 480–487.

Barria A, Muller D, Derkach V, Soderling TR (1997) Regulatory phosphorylation of AMPA-type glutamate receptors by CaM-KII during long term potentiation. *Science* **276**: 2042–2045

Bear MF (1996) A synaptic basis for memory storage in the cerebral cortex. *Proc. Natl. Acad. Sci. USA* **93**: 13453–13459.

Bear MF, Cooper LN, Ebner FF (1987) A physiological basis for a theory of synapse modification. *Science* **237**: 42–48.

Bhalla US (2004a) Signaling in small subcellular volumes. I. Stochastic and diffusion effects on individual pathways. *Biophys. J*. **87**: 733–744.

Bhalla US (2004b) Signaling in small subcellular volumes. II. Stochastic and diffusion effects on synaptic network properties. *Biophys. J*. **87**: 745–753.

Bliss TV, Collingridge GL (1993) A synaptic model of memory: long-term potentiation in the hippocampus. *Nature* **361**: 31–39.

Bliss TV, Lomo T (1973) Long-lasting potentiation of synaptic transmission in the dentate area of the anaesthetized rabbit following stimulation of the perforant path. *J. Physiol*. **232**: 331–356

Blitzer RD, Connor JH, Brown GP, Wong T, Shenolikar S, Iyengar R, Landau EM (1998) Gating of CaMKII by cAMP-regulated protein phosphatase activity during LTP. *Science* **280**: 1940–1942.

Carmignoto G, Vicini S (1992) Activity-dependent decrease in NMDA receptor responses during development of the visual cortex. *Science*. **258**: 1007–1011.

Castellani GC, Bazzani A, Cooper LN (2009) Toward a microscopic model of bidirectional synaptic plasticity. *Proc. Natl. Acad. Sci. USA* **106**: 14091–14095

Castellani GC, Quinlan EM, Bersani F, Cooper LN, Shouval HZ (2005) A model of bidirectional synaptic plasticity: from signaling network to channel conductance. *Learn. Mem*. **12**: 423–432

Castellani GC, Quinlan EM, Cooper LN, Shouval HZ (2001) A biophysical model of bidirectional synaptic plasticity: dependence on AMPA and NMDA receptors. *Proc. Natl. Acad. Sci. USA* **98**: 12772–12777

Cummings J, Mulkey R, Nicoll RM, Malenka R (1996) Ca^{2+} signaling requirements for long-term depression in the hippocampus. *Neuron* **16**: 825–833.

Derkach V, Barria A, Soderling T (1999) Ca2+/calmodulin-kinase II enhances channel conductance of -amino-3-hydroxy-5-methyl-4-isoxazolepropionate type glutamate receptors. *Proc. Natl. Acad. Sci. USA* **96**: 3269–3274.

Dudek SM, Bear MF (1992) Homosynaptic long-term depression in area CA1 of hippocampus and effects of N-methyl-D-aspartate receptor blockade. *Proc. Natl. Acad. Sci. USA* **89**: 4363–4367.

Feng J, Yan Z, Ferreira A, Tomizawa K, Liauw JA, Zhuo M, Allen PB, Ouimet CC, Greengard P (2000) Spinophilin regulates the formation and function of dendritic spines. *Proc. Natl. Acad. Sci. USA* **97**: 9287–9292.

Flint AC, Maisch US, Weishaupt JH, Kriegstein AR, Monyer H (1997) NR2A subunit expression shortens NMDA receptor synaptic currents in developing neocortex. *J. Neurosci*. **17**: 2469–2476.

Froemke RC, Poo MM, Dan Y (2005) Spike-timing-dependent synaptic plasticity depends on dendritic location. *Nature* **434**: 221–225.

Havekes R, Timmer M, Van der Zee EA (2007) Regional differences in hippocampal PKA immunoreactivity after training and reversal training in a spatial Y-maze task. *Hippocampus* **17**: 338–348.

Huang YY, Nguyen PV, Abel T, Kandel ER (1996) Long-lasting forms of synaptic potentiation in the mammalian hippocampus. *Learn. Mem*. **3**: 74–85.

Kameyama K, Lee H-K, Bear MF, Huganir RL (1998) Involvement of a postsynaptic protein kinase a substrate in the expression of homosynaptic long-term depression. *Neuron* **21**: 1163–1175.

Lee HK (2006) Synaptic plasticity and phosphorylation. *Pharmacol. Ther.* **112**: 810–832.

Lee H-K, Barbarosie M, Kameyama K, Bear MF, Huganir RL (2000) Regulation of distinct AMPA receptor phosphorylation sites during bidirectional synaptic plasticity. *Nature* **405**: 955–959.

Lee H-K, Kameyama K, Huganir R, Bear MF (1998) NMDA induces long-term synaptic depression and dephosphorylation of the GluR1 subunit of AMPA receptors in hippocampus. *Neuron* **21**: 1151–1162.

Lisman JE (1985) A mechanism for memory storage insensitive to molecular turnover: a bistable autophosphorylating kinase. *Proc. Natl. Acad. Sci. USA* **82**: 3055–3057.

Lisman JA (1989) A mechanism for the Hebb and the anti-Hebb processes underlying learning and memory. *Proc. Natl. Acad. Sci. USA* **86**: 9574–9578.

Lisman J, Malenka RC, Nicoll RA, Malinow R (1997) Learning mechanisms: the case for CaMKII. *Science* **276**: 2001–2002.

Liu Y, Sun QA, Chen Q, Lee TH, Huang Y, Wetsel WC, Michelotti GA, Sullenger BA, Zhang X (2009) Targeting inhibition of GluR1 Ser845 phosphorylation with an RNA aptamer that blocks AMPA receptor trafficking. *J. Neurochem.* **108**: 147–157.

Lledo PM, Hjelmstad GO, Mukherji S, Soderling TR, Malenka RC, Nicoll RA (1995) Calcium/calmodulin-dependent kinase II and long-term potentiation enhance synaptic transmission by the same mechanism. *Proc. Natl. Acad. Sci. USA* **92**: 11175–11179.

Lomo T (2003) The discovery of long-term potentiation. *Philos. Trans. R Soc. Lond. B Biol. Sci*. **358**: 617–620

Lüscher C, Nicoll RA, Malenka RC, Muller D (2000) Synaptic plasticity and dynamic modulation of the postsynaptic membrane. *Nat. Neurosci*. **3**: 545–550.

Malinow R, Malenka RC (2002) AMPA receptor trafficking and synaptic plasticity. *Annu. Rev. Neurosci*. **25**: 103–126

McBain CJ, Mayer ML. (1994) N-methyl-D-aspartic acid receptor structure and function. *Physiol. Rev*. **74**: 723–760.

Mu Y, Poo MM (2006) Spike timing-dependent LTP/LTD mediates visual experience-dependent plasticity in a developing retinotectal system. *Neuron* **50**: 115–125.

Mulkey RM, Malenka RC (1992) Mechanisms underlying induction of homosynaptic long-term depression in area CA1 of the hippocampus. *Neuron* **9**: 967–975.

Nakata H., Nakamura S (2007) Brain-derived ¡?TeX ?¿neurotrophic factor regulates AMPA receptor trafficking to post-synaptic densities via IP3R and TRPC calcium signalling. *FEBS Lett.* **581**: 2047–2054.

Nelson SB, Turrigiano GG (2008) Strength through diversity. *Neuron* **60**: 477–482.

Neves G, Cooke SF, Bliss TV (2008) Synaptic plasticity, memory and the hippocampus: a neural network approach to causality. *Nat. Rev. Neurosci*. **9**: 65–75.

Petralia RS, Wenthold RJ (1992) Light and electron immunocytochemical localization of AMPA-selective glutamate receptors in the rat brain. *J. Comp. Neurol*. **318**: 329–354

Philpot BD, Sekhar AK, Shouval HZ, Bear MF (2001) Visual experience and deprivation bidirectionally modify the composition and function of NMDA receptors in visual cortex. *Neuron* **29**: 157–169.

Quinlan EM, Philpot BD, Huganir RL, Bear MF. (1999) Rapid, experience-dependent expression of synaptic NMDA receptors in visual cortex in vivo. *Nat. Neurosci*. **2**: 352–357.

Roche KW, O'Brien RJ, Mammen AL, Bernhardt J, Huganir RL (1996) Characterization of multiple phosphorylation sites on the AMPA receptor GluR1 subunit. *Neuron* **16**:1179–1188.

Scannevin RH, Huganir RL (2000) Postsynaptic organization and regulation of excitatory synapses. *Nat. Rev. Neurosci*. **1**: 133–141.

Shen K, Meyer T (1999) Dynamic control of CaMKII translocation and localization in hippocampal neurons by NMDA receptor stimulation. *Science* **284**: 162–166.

Sheng M, Cummings J, Roldan LA, Jan YN, Jan LY (1994) Changing subunit composition of heteromeric NMDA receptors during development of rat cortex. *Nature* **368**:144–147.

Sheng M, Lee SH (2001) AMPA receptor trafficking and the control of synaptic transmission. *Cell* **105**: 825–828.

Shi S, Hayashi Y, Esteban JA, Malinow R (2001) Subunit-specific rules governing AMPA receptor trafficking to synapses in hippocampal pyramidal neurons. *Cell* **105**: 331–343.

Stocca G, Vicini S (1998) Increased contribution of NR2A subunit to synaptic NMDA receptors in developing rat cortical neurons. *J. Physiol*. **507**: 13–24.

Svenningsson P, Nishi A, Fisone G, Girault JA, Nairn AC, Greengard P. (2004) DARPP-32: an integrator of neurotransmission. *Annu. Rev. Pharmacol. Toxicol*. **44**: 269–296.

Tzounopoulos T, Rubio ME, Keen JE, Trussell LO (2007) Coactivation of pre- and postsynaptic signaling mechanisms determines cell-specific spike-timing-dependent plasticity. *Neuron*. **54**: 291–301.

Walaas SI, Greengard P (1991) Protein phosphorylation and neuronal function. *Pharmacol. Rev*. **43**: 299–349

Whitlock JR, Heynen AJ, Shuler MG, Bear MF (2006) Learning induces long-term potentiation in the hippocampus. *Science* **313**: 1093–1097

Wu LG, Betz WJ (1998) Kinetics of synaptic depression and vesicle recycling after tetanic stimulation of frog motor nerve terminals. *Biophys. J.* **74**(6): 3003–3009.

A Phenomenological Calcium-Based Model of STDP

Richard C. Gerkin, Guo-Qiang Bi, and Jonathan E. Rubin

Experimental Motivation and Early Models

Activity-dependent synaptic plasticity is believed to underlie functional reconfiguration of neuronal circuits, which in turn serves as the biological substrate of higher brain functions such as learning and memory (Hebb 1949; Milner et al. 1998; Abbott and Nelson 2000). Decades after Donald Hebb's famous neurophysiological postulate (Hebb 1949), various forms of synaptic plasticity including long-term potentiation (LTP) and long-term depression (LTD) have been the subject of intense experimental study (Bliss and Collingridge 1993; Malenka and Nicoll 1999; Lisman et al. 2003; Derkach et al. 2007). Among them, the recently discovered spike timing-dependent plasticity (STDP) – during which the direction and extent of synaptic modification depend critically on the relative timing of pre- and postsynaptic action potentials or spikes (Bell et al. 1997; Magee and Johnston 1997; Markram et al. 1997; Mehta et al. 1997; Bi and Poo 1998; Debanne et al. 1998; Zhang et al. 1998; Feldman 2000) – has gained popularity partly because it is regarded as a physiologically relevant form of Hebbian plasticity (Abbott and Nelson 2000; Bi and Poo 2001; Dan and Poo 2006). Although under certain conditions, synaptic plasticity can be induced without the generation of postsynaptic action potentials (Lisman and Spruston 2005), the importance of the postsynaptic spike should not be overlooked because it is the most common form of neuronal output. In a sense, the significance of STDP is that it is the direct outcome of the interaction between neuronal input and output functions, and thus is uniquely positioned to modify the network to achieve specific I/O relationships, which is the essence of learning.

The temporally asymmetric STDP window first characterized in pairs of excitatory neurons in hippocampal cultures (Fig. 1) and in retinotectal connections in vivo (Bi and Poo 1998; Zhang et al. 1998) is often considered the "canonical" STDP rule because (1) it is perfectly in line with Hebb's postulate that the synapse is strengthened when the presynaptic neuron "takes part in firing" the postsynaptic

R.C. Gerkin (✉)
Department of Neurobiology, University of Pittsburgh School of Medicine, Department of Biological Sciences, Carnegie Mellon University, Pittsburgh, PA 15213, USA
e-mail: rickg@cmu.edu

V. Cutsuridis et al. (eds.), *Hippocampal Microcircuits*, Springer Series in Computational Neuroscience 5, DOI 10.1007/978-1-4419-0996-1_20,

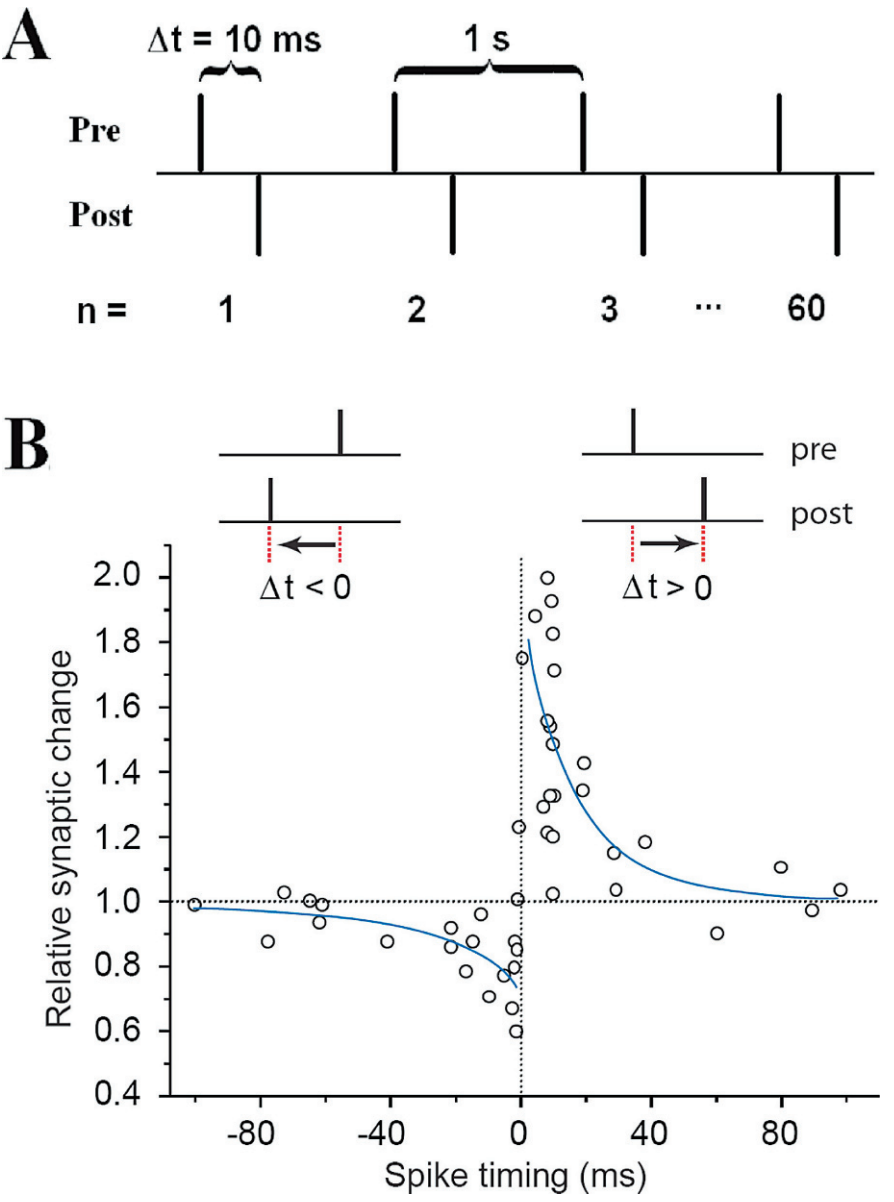

Fig. 1 Synaptic modifications induced by correlated pre- and postsynaptic spiking. **a**, Typical pre-post pairing protocol for STDP, with time Δt between pre- and postsynaptic spikes induced at 1 Hz. **b**, Outcome of experiments illustrated in **a** for a variety of Δt values. Changes were measured 30 min after the delivery of 60 spike pairs. Adapted from (Bi 2002). Used with permission of Springer Berlin/Heidelberg

neuron, and (2) similar windows are commonly observed in many other areas of the brain in different preparations (Caporale and Dan 2008). Since its early discovery, however, STDP found in various preparations has exhibited different quantitative rules, some of which are almost the opposite of others (Abbott and Nelson 2000; Bi and Poo 2001).

The experimental observation of various forms of STDP generated considerable excitement and activity in the theoretical neuroscience community, which continues to this day. Early modeling efforts made the assumption that single pre- and postsynaptic spike pairs would induce STDP, with a mapping from spike timing to plasticity outcome that matched that found experimentally in protocols involving repeated elicitation of spikes with a fixed timing relation. Considered in this way, STDP could act as an online feedback tool through which circuit activity could self-modulate to convert an input stream into some corresponding activity pattern, with significant implications for information storage or sensory processing. Theoretical efforts based on the treatment of STDP as a lookup table based on pairwise spike timing have recently been reviewed elsewhere (Morrison et al. 2008).

The limitations of the pairwise viewpoint became apparent as further experiments proceeded, revealing results from spike triplets, quadruplets, or trains that were incommensurate with predictions coming from summation of pairwise results. For example, in hippocampal cultures, pre-post-pre spike "triplets" result in no change in synaptic strength, whereas post-pre-post spike triplets lead to significant potentiation (Wang et al. 2005). This result is partially consistent with findings in visual cortical slices (Sjostrom et al. 2001). Yet, in a different set of synaptic connections of the visual cortex, pre-post-pre triplets cause potentiation, but post-pre-post triplets cause depression (Froemke and Dan 2002), apparently due to strong short-term depression in both synaptic transmission and backpropagation of spikes (Froemke et al. 2006). Even with simple spike pairs, new experimental evidence shows that the canonical STDP rule can sometimes change with the target and the location of the synapse (Tzounopoulos et al. 2004; Froemke et al. 2005; Letzkus et al. 2006) and can be dynamically regulated by the activity of adjacent synapses (Harvey and Svoboda 2007) or by the action of neuromodulators (Seol et al. 2007; Zhang et al. 2009).

Postsynaptic Calcium as a Signal for STDP

The fact that these results showed different outcomes across different experimental preparations further complicated efforts to develop a universal, purely phenomenological framework for the incorporation of STDP into models. While such efforts continue (Pfister and Gerstner 2006), another approach to circumventing these difficulties is to model a postsynaptic signal generated by pre- and postsynaptic spikes, which could be used as a driver of plasticity outcomes. Variations across different preparations would arise from differences in particular aspects of this signaling pathway, which could be tuned in a unified STDP model. Based in part on the established link between postsynaptic intracellular Ca^{2+} and classical long-term potentiation

(LTP) and long-term depression (LTD), Ca^{2+} was seen as a natural candidate for playing the initial role in such postsynaptic STDP signaling. The feasibility of postsynaptic Ca^{2+} as an STDP initiator was enhanced by the link between postsynaptic depolarization, NMDA receptors and channels, and Ca^{2+}.

NMDAR, with its calcium-permeable pore, is essential for both LTP (Collingridge et al. 1983) and LTD (Dudek and Bear 1992; Mulkey and Malenka 1992). How one type of receptor could mediate both the strong, LTP-inducing calcium signal and the weak, LTD-inducing $[Ca^{2+}]$ signal attracted early attention (Bear and Malenka 1994). The simplest hypothesis stated that differential levels of activation of the NMDAR in response to different stimuli were responsible for $[Ca^{2+}]$ signals unique to LTP or to LTD (Lisman 1989). The NMDAR has a unique property that allows for coincidence detection. Mg^{2+} ions largely block the NMDAR channel pore at resting membrane potentials, precluding calcium influx when glutamate is bound (Mayer et al. 1984; Nowak et al. 1984; McBain and Traynelis 2006). However, at depolarized membrane potentials, such as those associated with postsynaptic spiking, Mg^{2+} block is relieved and the channel exhibits an ohmic current-voltage relationship (Dingledine et al. 1986; Hablitz and Langmoen 1986). Because this change in conductance more than offsets the reduction in driving force for calcium ions experienced at elevated membrane potentials (Jahr and Stevens 1993), NMDAR-mediated calcium currents are enhanced when the presynaptic stimulus is strong enough to evoke postsynaptic spiking. This is consistent with the observation that larger $[Ca^{2+}]$ signals are better at producing LTP, which is often associated with such spiking; likewise, partial blockade of NMDARs during LTP-inducing protocols (Cummings et al. 1996), or during spontaneous activity (Bains et al. 1999), resulting in reduced $[Ca^{2+}]$ signals, can result in LTD. Thus, Ca^{2+} influx through NMDAR channels provides a natural link between pre- and postsynaptic spike timing.

Initial Models Based on Ca^{2+} Signals

This reasoning leads to the questions of what aspects of postsynaptic calcium serve as plasticity signals, how these features are harnessed by other elements within the postsynaptic density, spine, or dendrite, and of course how these components can be modeled in a reasonably concise way. Several groups developed phenomenological computational models of the translation of postsynaptic calcium into plasticity outcomes, based on biophysical underpinnings.

Karmarkar and Buonomano published a model based on the idea that the LTP and LTD components of STDP are modulated by distinct coincidence detectors (Karmarkar and Buonomano 2002). Their LTP detector relied upon the glutamatergic activation of NMDA receptors (NMDARs) and influx of Ca^{2+} through these receptors, while their LTD detector incorporated the flow of Ca^{2+} through voltage-gated calcium channels together with the action of glutamate at metabotropic glutamate receptors (mGluRs), based in part on the finding that mGluR antagonists compromise hippocampal STDP-LTD (Normann et al. 2000).

Mathematically, the front end of the model took the form

$$\mathrm{VCA}' = k_1(v - E_{\mathrm{Ca}})\sigma(v) - \mathrm{VCA}/\tau,$$
$$\mathrm{NCA}' = k_2(v - E_{\mathrm{Ca}})\left(\frac{B(v)R}{k_3}\right)^4$$

where VCA and NCA denote calcium entering the postsynaptic cell via voltage-gated channels and NMDAR channels, respectively, v is the postsynaptic voltage, E_{Ca} denotes the calcium reversal potential, $\sigma(v) = 1/[1 + \exp(0.1 - v)]$, $B(v)$ represents magnesium block of NMDAR channels, R is a glutamate activation term (see (Buonomano 2000)), and $k_1, k_2 < 0$ and $k_3, \tau > 0$ are constants. The quantities $\mathrm{NCA}(t)$ and $m\mathrm{Glu} := \mathrm{VCA}(t) \times g(t)$, for $g(t)$ representing the presence or absence of glutamate, were integrated as LTP and LTD signals, respectively. That is, plasticity outcomes in this model were determined by the total amounts of calcium coming in via two different sources, not the peak calcium level nor the details of the calcium time course.

This model yielded qualitatively appropriate pairwise STDP results and matched data on protocols pairing single presynaptic and multiple postsynaptic spikes. A major flaw in the model, however, was its failure to account for the finding that the NMDAR antagonist APV blocks LTD. The model also did not allow for the possible interactions of the LTP and LTD components and possible contributions of voltage-gated calcium influx to LTP, and it was not applied to other multi-spike experiments. Moreover, no mechanism was provided to connect the abstract signals in the model to molecules present in the postsynaptic density, implicated in synaptic plasticity outcomes.

Shouval and collaborators introduced an alternative model based on what they termed the calcium control hypothesis (Shouval et al. 2002). In their model, synaptic weight changes were driven directly by a nonlinear function of calcium levels, at a rate that itself depended on the calcium level. The corresponding weight equation took the form

$$W' = \eta([\mathrm{Ca}])(\Omega([\mathrm{Ca}]) - W)$$

where $\eta([\mathrm{Ca}])$ was a monotone increasing function and $\Omega([\mathrm{Ca}])$ was a calcium level detector that was near zero for [Ca] near baseline, became negative for larger [Ca], and became positive for still larger [Ca]. The calcium influx was entirely attributed to NMDAR channels and was given by

$$[\mathrm{Ca}]' = I_{\mathrm{NMDA}}(t) - [\mathrm{Ca}]/\tau$$

for a time constant τ. $I_{\mathrm{NMDA}}(t)$ was composed of a linear combination of fast and slow exponential functions, scaled to take into account voltage-dependent magnesium block. Postsynaptic voltage was computed based on the summation of back propagating action potentials and excitatory postsynaptic potentials, each given a

stereotyped time course. This model could largely be characterized as a calcium level detector, although the time-dependent evolution of calcium did factor into the rate of weight change, through η, which in particular avoided excessive cancellation of LTP by LTD during the phase of calcium decline after a spike pairing.

Although this model reproduced a variety of experimentally observed synaptic plasticity outcomes, these results followed under the assumption of a significantly prolonged (e.g., 35 ms) dendritic afterdepolarization. The model also yielded a large region of pre-before-post spike timings for which substantial levels of LTD occurred, in contrast to most experiments (Shouval and Kalantzis 2005). Finally, the model predicted LTP across all $t_{\text{post}} - t_{\text{pre}}$ values for pairings at 5 Hz, at odds with experimental results (Sjostrom et al. 2001).

A third phenomenological, calcium-based model was published by Abarbanel et al. (2003). Simulation of a one-compartment, Hodgkin–Huxley-type model, incorporating AMPA, NMDA, and T-type calcium channels, was used to generate a postsynaptic calcium time course. The resulting calcium signal, Ca(t), was incorporated into a phenomenological representation of kinase and phosphatase interactions assumed to drive changes in synaptic strength $g(t)$ through the equations

$$\begin{aligned}
\mathrm{K}'(t) &= f_{\mathrm{K}}(\mathrm{Ca}(t) - \mathrm{Ca}_0)(1 - \mathrm{K}(t)) - \mathrm{K}(t)/\tau_{\mathrm{K}}, \\
\mathrm{P}'(t) &= f_{\mathrm{P}}(\mathrm{Ca}(t) - \mathrm{Ca}_0)(1 - \mathrm{P}(t)) - \mathrm{P}(t)/\tau_{\mathrm{P}}, \\
g(t)' &= \alpha g_0[\mathrm{P}(t)\mathrm{D}(t)^{\eta} - \mathrm{D}(t)\mathrm{P}(t)^{\eta}]
\end{aligned}$$

where K denotes kinases, P denotes phosphatases, $f_X(c) = c^{n_X}/(\Gamma_X + c^{n_x})$ for $X \in \{\mathrm{K}, \mathrm{P}\}$ with constants $0 < n_{\mathrm{P}} < n_{\mathrm{K}}$ and $\Gamma_{\mathrm{P}}, \Gamma_{\mathrm{K}} > 0$, and where the additional constants satisfy $\tau_{\mathrm{K}} > \tau_{\mathrm{P}} > 0, \alpha > 0$, initial weight strength $g_0 > 0$ and $\eta > 1$.

Although this model generated a full calcium time course, the effective mechanism underlying STDP in the model was essentially based on calcium levels. As a result, the ratio g/g_0 produced by pairwise STDP protocols was nearly symmetric around $\Delta t := t_{\text{post}} - t_{\text{pre}} = 0$, and plasticity outcomes to pre-post-pre and post-pre-post spike triplet paradigms were equivalent, both in contrast to a variety of experimental results. Further, although calcium influx through NMDAR channels was incorporated, the model still produced LTD under NMDA blockage. Finally, the model did not include any representation of BPAPs.

A Hippocampal Culture Model Based on Ca^{2+} Time Course

Based on multi-spike experiments being carried out in the Bi lab (Wang et al. 2005; Gerkin et al. 2007), we also decided to develop a calcium-based plasticity model. It seemed important to us to have a biophysically based representation of the postsynaptic calcium time course, so that we could examine differences in these time courses across simulations that matched various experimental protocols and use these differences to make predictions about what aspects of the calcium signal are really important in driving plasticity.

Indeed, from earlier work on classical LTP and LTD paradigms, we were aware of the idea that high postsynaptic calcium levels, say above θ_P, would elicit LTP, while moderate levels, say in the interval (θ_D, θ_P) for $\theta_D < \theta_P$, would yield LTD. Early on, we realized the flaw in relying on level-based detectors to reproduce pairwise STDP results. Since $\Delta t = 10\,\text{ms}$ produced LTP, the level-based paradigm would imply that the calcium signal produced with that Δt was above θ_P. Similarly, since no weight changes were observed for sufficiently large Δt, say $\Delta t > \Delta\bar{t}$, the level-based model would imply that the calcium signal produced for large Δt was below θ_D. But, assuming calcium influx from known voltage-gated and synaptic sources, the peak calcium is a continuous function of Δt. Thus, by the intermediate value theorem, there would exist a $\Delta t \in (10, \Delta\bar{t})$ sufficiently large that the calcium level would lie below θ_P but sufficiently small that the calcium level would lie above θ_D, and pre-before-post LTD would result for such Δt.

Thus, our goal was to design a calcium time course detector that would yield pre-post LTP and post-pre LTD, without a pre-post LTD window, would reproduce the outcomes observed in multi-spike experiments, would show a loss of LTD under NMDAR antagonist application, and could be easily implemented by known postsynaptic calcium signaling modules.

A Postsynaptic Calcium Detector Constrained by Experimental Data

Neuronal and Synaptic Dynamics

In this section, we review the form and function of a model designed to achieve the goals described above (Rubin et al. 2005). The model combines Hodgkin–Huxley-type membrane dynamics with a phenomenological, yet molecularly inspired, calcium detector system that transforms postsynaptic calcium signals into plasticity outcomes. The voltage components of the model are implemented in two compartments. In each compartment, the membrane potential evolves according to

$$v'(t) = -(I_{\text{L}} + I_{\text{Na}} + I_{\text{Ca}} + I_{\text{K}} + I_{\text{coup}} + I_{\text{in}})/C_{\text{m}} \tag{1}$$

where I_{L} is a leak current; I_{Na} is a sodium current; I_{Ca} is a high-threshold calcium current; I_{K} is the sum of a potassium A-current, a delayed rectifier potassium current, and a calcium-activated potassium afterhyperpolarization current (Table 1), all based on experimental data as modeled by Poirazi et al. (2003).

In Eq. (1), I_{coup} is the electrical coupling between the compartments, and I_{in} corresponds to current injections (in the soma) or to synaptic currents, I_{AMPA} and I_{NMDA} (in the spine). Membrane capacitance C_{m} was normalized to $1\,\mu\text{F/cm}^2$ and all conductances were scaled accordingly to maintain appropriate membrane potential dynamics in our compartmental reduction. Equations governing the evolution of state variables for non-synaptic currents take the form

Table 1 Conductance values for the postsynaptic Ca^{2+} detector model of STDP

Parameter (mS/cm^2)	Value		Conductance description	Source and comments
	Soma	Spine		
g_L	0.1	0.1	Leak	
g_{Na}	30	7	Na^+	
$g_{K(A)}$	7.5	12	A-type K^+	Peak conductances for maximal activation; (Poirazi et al. 2003)
$g_{K(dr)}$	14	0.867	Delayed rectifier K^+	
$g_{K(mAHP)}$	25	0	Afterhyperpolarization	
$g_{Ca(L)}$	7	25	L-type Ca^{2+}	
g_{coup}	1.125	1.125	Inter-compartmental	

$$z' = \alpha_z(v)(1 - z) - \beta_z(v)z$$

For our simulations of this system, we used the fourth-order Runge-Kutta method for numerical integration in XPPAUT (Ermentrout 2002), with a step size of $dt = 0.025$ ms.

We implemented calcium dynamics based on equations due to Traub et al. (1994) in each compartment. These take the form

$$\chi' = \Phi I_{Ca} - \beta_1(\chi - \chi_0) - \beta_2(\chi - \chi_0)^2 - \frac{\Delta\chi}{d}$$

where χ is the calcium concentration in μM, χ_0 denotes the resting calcium concentration, d is a diffusion time constant between compartments, $\Delta\chi$ is the concentration difference between compartments, and $\beta_{1,2}$ control the strength of linear and nonlinear calcium buffering, respectively. The current I_{Ca} denotes calcium influx through voltage-gated channels, with Φ representing the change in calcium concentration per unit of calcium influx. Parameters were selected to match experimental data on dendritic calcium dynamics (Koester and Sakmann 1998; Yuste et al. 1999; Murthy et al. 2000; Sabatini et al. 2001), with resting calcium levels constrained by specific experimental results (Table 2) (Pozzo-Miller et al. 1999; Yuste et al. 1999; Maravall et al. 2000).

Current flowing though NMDARs is composed of a diversity of ions, each with different driving forces and conductance sensitivities to postsynaptic membrane potential. Thus, we distinguished between the calcium current through these channels (used to compute changes in calcium concentration) and the total current (used to compute changes in membrane potential). We computed each of these with equations of the form

$$I = -gsm(v - v_{rev})$$

where g is a constant maximal channel conductance density, s is the time and glutamate-dependent activation level of the channels, m measures the voltage dependence (which for NMDARs is determined by the degree of Mg^{2+} block), and v_{rev} is the reversal potential of the current (Table 3). We chose parameters for NMDARs based on data (Jahr and Stevens 1990a; 1993), using

Table 2 Parameters governing postsynaptic calcium dynamics

Parameter	Value		Description	Source and comments
	Soma	Spine		
Φ	0.01	0.01	Increase in $[Ca^{2+}]$ per unit calcium current	
β_1 (ms^{-1})	0.083	0.083	First-order calcium decay time constant	
β_2 ($ms^{-1}\mu\ M^{-1}$)	0.0138	0.0138	Second-order calcium decay time constant	(Sabatini et al. 2002)
d (ms)	1,000	1,000	$[Ca^{2+}]$ coupling between compartments	
$\chi_0(\mu M)$	0.05	0.07	Baseline $[Ca^{2+}]$	(Yuste et al. 1999; Maravall et al. 2000)

Table 3 Parameters governing postsynaptic glutamate receptors

Parameter	Value			Description	Comments and source
		NMDAR			
	AMPAR	Current	Ca^{2+}		
v_{rev} (mV)	0	0	140	Reversal potential for synaptic current	(Poirazi et al. 2003)
$\gamma(mV^{-1})$	∞	0.062	0.124	V_m-dependence of synaptic currents	(Jahr and Stevens 1990b; 1993)
$g(mS/cm^2)$	0.05	0.3	25	Synaptic conductance	
τ_{rise} (ms)	0.58	2	2	Time constants for the synaptic current	(Perouansky and Yaari 1993; Andrasfalvy and Magee 2001)
τ_{fast} (ms)	7.6	10	10		
τ_{slow} (ms)	25.69	45	45		
a_{fast}	0.903	0.527	0.527	Relative weight given to τ_{fast}	
$k(ms^{-1})$	20	20	20	Used to scale the rising phase to the duration of the simulation time step	

$$m_{\mathrm{NMDA}} = \frac{1}{1 + 0.3[\mathrm{Mg}^{2+}]e^{-\gamma v}}$$

with the extracellular magnesium concentration $[Mg^{2+}] = 2\,mM$, according to the concentration used in STDP experiments in hippocampal culture (Wang et al. 2005). γ reflects the voltage-dependence of this Mg^{2+} block (Jahr and Stevens 1990). For current flowing through AMPARs, which are largely calcium impermeable, we considered only its contribution to membrane potential, and assumed that the channel was non-rectifying ($m = 1$). For both types of synaptic currents, we used activation equations that yield simulated, stimulus-induced time courses that resemble those observed in experiments conducted at room temperature (Perouansky and

Yaari 1993; Andrasfalvy and Magee 2001). These take the form

$$\begin{aligned} s &= s_{\text{rise}} + s_{\text{fast}} + s_{\text{slow}} \\ s'_{\text{rise}} &= -k(1 - s_{\text{fast}} - s_{\text{slow}}) f_{\text{pre}}(t) - s_{\text{rise}}/\tau_{\text{rise}} \\ s'_{\text{fast}} &= k(a_{\text{fast}} - s_{\text{fast}}) f_{\text{pre}}(t) - s_{\text{fast}}/\tau_{\text{fast}} \\ s'_{\text{slow}} &= k(1 - a_{\text{fast}} - s_{\text{slow}}) f_{\text{pre}}(t) - s_{\text{slow}}/\tau_{\text{slow}} \end{aligned}$$

where $f_{\text{pre}}(t)$ represents a step pulse corresponding to the timing of the presynaptic action potential (Table 3).

Calcium Detectors

Plasticity outcomes are computed in this model by a biophysically plausible detection system that responds to $[Ca^{2+}]$ and produces output of the appropriate sign and magnitude. Three detector agents respond to the instantaneous $[Ca^{2+}]$ in a dendritic compartment, which could represent a spine or simply a dendritic segment. Different calcium time courses lead to different time courses of the detectors P, V, and A. An intermediate element B is activated by A, while an additional agent D is activated by B and suppressed, or vetoed, by V. P. and D then compete to influence a plasticity variable W, which is initialized to zero to favor neither potentiation nor depression. W serves as a measure of the sign and magnitude of synaptic strength changes from baseline. D acts as a filter (e.g., extra steps in a signaling pathway) to map $[Ca^{2+}]$ time courses onto the correct final values of W. The detector equations are

$$\begin{aligned} P' &= (f_p(\chi) - c_p A P)/\tau_p \\ V' &= (g_v(\chi) - V)/\tau_v \\ A' &= (f_a(\chi) - A)/\tau_a \\ B' &= (g_b(A) - B - c_d B V)/\tau_b \\ D' &= (g_d(B) - D)/\tau_d \\ W' &= \left[\alpha_w/(1 + e^{(p-P)/k_p}) - \beta_w/(1 + e^{(d-D)/k_d}) - W\right]/\tau_w \end{aligned}$$

where χ in all cases represents $[Ca^{2+}]$ in the non-somatic compartment. We chose the calcium sensitivity for P and A to match the Hill equation:

$$f_\sigma(x) = \frac{c_\sigma}{1 + (\theta_\sigma/x)^{n_\sigma}},\ \sigma \in \{p, a\}$$

with parameters taken from previous modeling work on the activation, autophosphorylation, and dephosphorylation of CaMKII (Holmes 2000; Lisman and Zhabotinsky 2001). The equations for the other detectors (V,B,D) feature functions of the form

$$g_\sigma(x) = \frac{\alpha_\sigma}{1 + e^{(\theta_\sigma - x)/n_\sigma}},\ \sigma \in \{v, b, d\}$$

It is critical that $\theta_p > \theta_a$ and $\theta_v > \theta_a$, ensuring that there is a regime of $[Ca^{2+}]$ in which depression can be activated without being vetoed and without activating potentiation (Table 4).

Table 4 Parameters governing postsynaptic calcium detectors

Parameter	Value	Description	Comments and source
θ_p(μM)	4	$[Ca^{2+}]$ Activation threshold for P (potentiation)	(Zhabotinsky 2000; Lisman and Zhabotinsky 2001)
θ_a(μM)	0.6	$[Ca^{2+}]$ Activation threshold for A(depression)	
θ_v(μM)	2	$[Ca^{2+}]$ Activation threshold for V (veto)	
θ_d(μM)	2.6	B Activation threshold for D (depression)	
θ_b(μM)	0.55	A Activation threshold for B (depression)	
τ_p (ms)	50	Decay time constant for P	
τ_a (ms)	5	Decay time constant for A	
τ_v (ms)	10	Decay time constant for V	
τ_d (ms)	250	Decay time constant for D	
τ_b (ms)	40	Decay time constant for B	
c_p	0.5	Inhibition of P by A	
τ_w (ms)	500	Decay time constant of W	
α_w	0.0016	Relative contribution of potentiation to W	
β_w	0.0012	Relative contribution of depression to W	These are free parameters chosen to recapitulate the experimental results.
n_p	4	Hill exponent for P	
n_a	3	Hill exponent for A	
σ_v(μM)	0.05	Activation width for V	
σ_d	0.01	Activation width (by B) for D	
σ_b	0.02	Activation width (by A) for B	
k_p	0.1	Activation width (by P) for W	
k_d	0.002	Activation width (by D) for W	
α_v	1.0	Growth rate of V	
α_d	1.0	Growth rate of D	
α_b	5.0	Growth rate of B	
c_d	4	Inhibition of B by the veto V	
p	0.3	Activation threshold (by P) for W	
d	0.01	Activation threshold (by D) for W	

Results

The form of the model presented above is based on the claim that it is not simply a postsynaptic $[Ca^{2+}]$ level that determines plasticity outcomes, but the dynamic postsynaptic $[Ca^{2+}]$ time course (Sabatini et al. 2002; Ismailov et al. 2004). The model functions as follows. High $[Ca^{2+}]$ rapidly activates a potentiating process P,

medium [Ca^{2+}] rapidly activates a process V, and low [Ca^{2+}] slowly activates a process A. A in turn activates a depressing process D through an intermediate process B. However, B can be inhibited, or vetoed, by V, allowing V to indirectly inhibit D. The consequence of this arrangement is that only long-lasting, low-level elevations of [Ca^{2+}] can successfully activate D. A schematic representation of the detector system is given in Fig. 2.

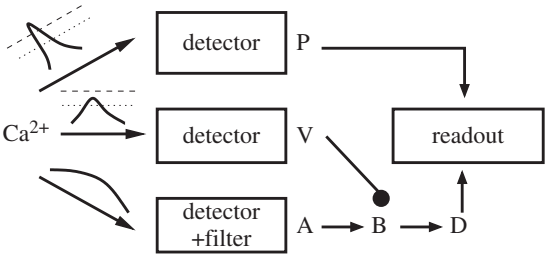

Fig. 2 Schematic illustration of the calcium detector system. The detector uses a set of coupled ODEs to determine the magnitude and sign of the change in synaptic strength, or readout, from the [Ca^{2+}] time course. Adapted from (Rubin et al. 2005). Used with permission of The American Physiological Society

Results for Doublets

To illustrate the function of the model, we show the postsynaptic [Ca^{2+}] time course for four kinds of spike pairings. First, we consider pairings in which presynaptic spikes precede postsynaptic spikes, or so-called AB spike pairings, and second, we consider pairings in which the order of spikes is reversed, or so-called BA spike pairings. For concreteness, we focus on AB pairings with $\Delta t = 10$ and $\Delta t = 40$, as shown in Fig. 3 (left), and on BA pairings with $\Delta t = -10$ and $\Delta t = -60$, as shown in Fig. 3 (right).

A major source of postsynaptic calcium influx is NMDARs, whose conductance depends on a combination of postsynaptic membrane depolarization and glutamate concentration in the synaptic cleft. Thus, large calcium influx will only occur when the postsynaptic spike follows the presynaptic spike at a short latency. Consequently, a large peak [Ca^{2+}] concentration results for spike interval $\Delta t = 10$, activating P, which in turn drives up W. A shorter peak [Ca^{2+}] concentration occurs for $\Delta t = 40$ and fails to activate P, such that W remains at its baseline level.

Why is D not activated by the $\Delta t = 40$ [Ca^{2+}] profile? For both $\Delta t = 10$ and $\Delta t = 40$, there is sufficient [Ca^{2+}] elevation to activate the veto process V (Fig. 4), which inhibits the ability of A to activate B to the threshold level needed to activate D. Combined with the failure of $\Delta t = 40$ to activate P, neither potentiation nor depression results for this spike timing. Thus, the inclusion of the veto V explains the lack of LTD for large, positive Δt. To obtain a complete lack of AB LTD, it is important for parameters to be tuned such that if Δt is sufficiently large that

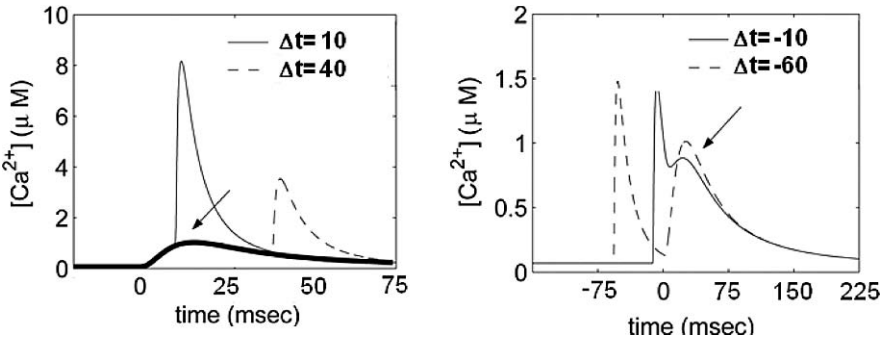

Fig. 3 Postsynaptic calcium time courses for spike doublets. Note the different vertical axis scalings in the two panels. *Left*: Time courses for pre-post or AB pairings and for presynaptic stimulation alone (*thick solid*). *Right*: Time courses for post-pre or BA pairings. The second calcium peak in the $\Delta t = -60$ case has about the same amplitude as the pre-alone peak (*arrows*). Adapted from (Rubin et al. 2005). Used with permission of The American Physiological Society

V is no longer activated, the calcium signal is not sustained above θ_a for a long enough time to activate D (Fig. 4). For negative spike timing, there is no NMDAR conductance during the time of postsynaptic action potential backpropagation. Consequently, the interval $\Delta t = -10$ results in a much shorter peak $[Ca^{2+}]$ that fails to activate P or V. However, the width of the $[Ca^{2+}]$ time course (Fig. 3b) is sufficient to activate A, and then B, which in turn activates D, which drives down W. By contrast, the $[Ca^{2+}]$ profile for $\Delta t = -60$ is not sufficiently wide, due to the large timing gap between pre- and postsynaptic activation, and fails to activate A (or D), such that W remains at baseline.

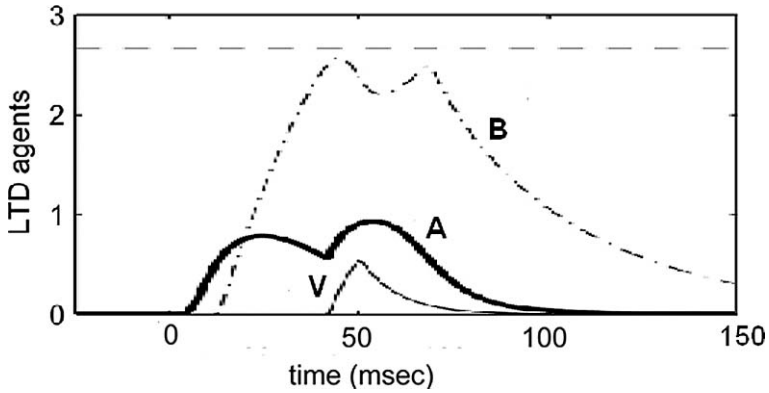

Fig. 4 Veto of depression. Although the calcium time course (not shown) for $\Delta t = 40$ activates A, it also activates the veto V, which prevents B from crossing the threshold (*dashed*) for turning on depression (D). Adapted from (Rubin et al. 2005). Used with permission of The American Physiological Society

Using this detector scheme, the resultant plasticity can be computed for any value of Δt. When spike pairings are repeated at any fixed Δt for which plasticity occurs, $|W|$ rises during the spike pair and decays between spike pairs. After enough spike pairings, these effects equilibrate and W oscillates about some mean. We assume that the sign of the level about which W oscillates determines whether LTP or LTD results, and the magnitude of this level represents the strength of the plasticity outcome. For positive Δt, the amplitude of the rise in P and the duration of time that P spends above θ_p determine the level at which W equilibrates. As Δt grows, the increasing delay between pre- and postsynaptic spikes weakens the calcium signal (Fig. 3a) and the asymptotic W diminishes. As noted above, as Δt grows, V plays an important role in the suppression of D and hence of depression. For negative Δt, the calcium signal is too weak to drive P and hence the asymptotic level of W is determined by the A, B, D system; see Fig. 5 for an example.

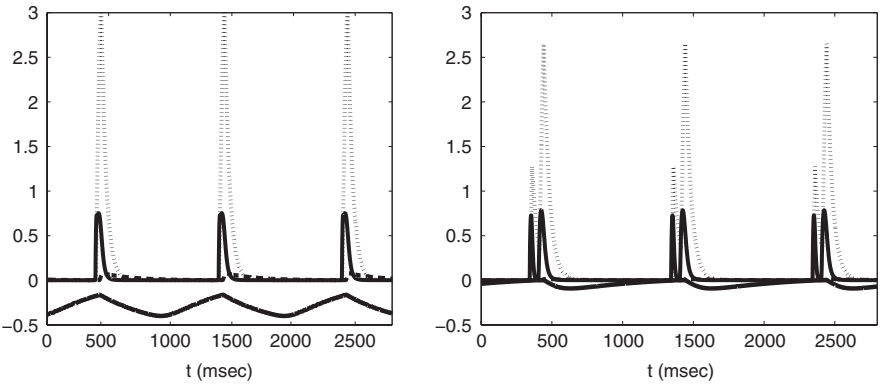

Fig. 5 Asymptotic dynamics of the post-pre depression cascade, including A (*solid*), B (*dotted*), D (*dashed*), and W (*thick solid*). *Left*: For $\Delta t = -10$, with each spike pairing, the sustained calcium signal (not shown) drives up A followed by B, such that D is boosted enough to push down W, corresponding to depression. *Right*: For $\Delta t = -60$, there is a significant decay in calcium during the lag between post- and presynaptic spikes (not shown). Due to the relatively fast time constants of A and B, B does not remain above threshold ($\theta_d = 2.6$) sufficiently to yield a significant rise in D, and only a weak depressive W response results. Adapted from (Rubin et al. 2005). Used with permission of The American Physiological Society

Figure 6 shows the correspondence between the asymptotic levels of W produced by the model and data on percent changes in EPSC sizes obtained from identical pairing protocols in hippocampal cultures (Bi and Poo 1998). Although the units of these two plasticity measures differ, the qualitative agreement in their dependence on Δt is encouraging. This model also reproduces data from non-STDP plasticity protocols; among them are presynaptic stimulation at various frequencies, and the pairing protocol for a range of postsynaptic holding potentials (Rubin et al. 2005).

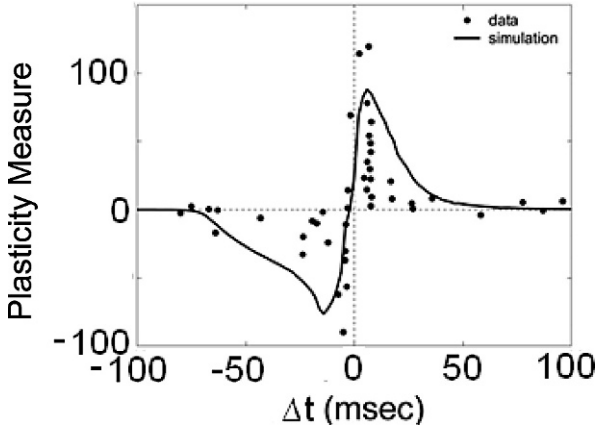

Fig. 6 Plasticity outcomes from hippocampal culture experiments (data, *dotted*) and model simulations (*solid*). Experimental data represent percentage changes in excitatory postsynaptic current amplitudes, while simulation results are asymptotic levels of *W*. Adapted from (Rubin et al. 2005). Used with permission of The American Physiological Society

Results for Triplets

For spike triplets, the same processes described above can explain the plasticity outcomes in the model. Let $\Delta t = \{a, b\}$ denote a triplet stimulus with a time interval a equal to the difference between the first two spikes (where a positive number represents presynaptic activation first, as with doublets), and an interval b between the second and third spike, according to the same sign convention. For the $\Delta t = \{10, -10\}$ stimulus, an example of a pre-post-pre or ABA pairing (Fig. 7a), P and V are both activated due to the large $[Ca^{2+}]$ peak. However, postsynaptic $[Ca^{2+}]$ remains modestly elevated for a greater time compared to the AB (pre-post) stimulus, permitting A to continue its buildup after V has decayed, leading to the activation of D. Because both potentiation and depression are activated, no net plasticity results for the ABA case.

In the case of the $\Delta t = \{-10, 10\}$ stimulus, an example of a post-pre-post or BAB pairing (Fig. 7b), V is activated by calcium influx associated with the second postsynaptic action potential as A is accumulating. It is thus able to veto the effect of A on B and prevent the activation of D, resulting in only potentiation. The results for triplets thus match experimental results from hippocampal cultures (Wang et al. 2005).

Discussion

The calcium time course detection model presented here (Rubin et al. 2005) reproduces the results of spike-timing-dependent plasticity experiments in hippocampal cultured neurons. In contrast to previous models, it does not produce a second "LTD

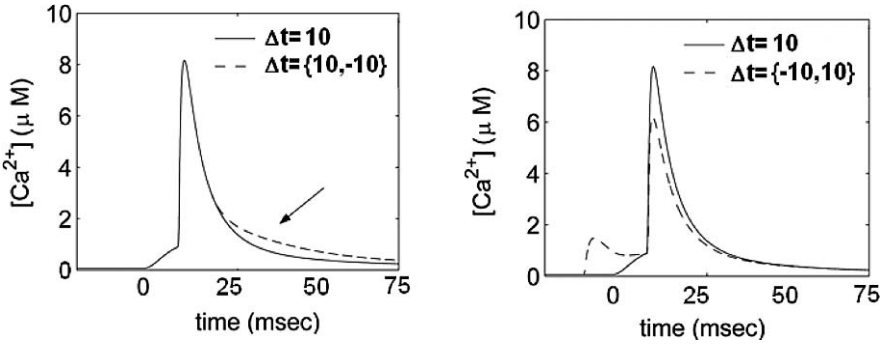

Fig. 7 Calcium time courses for spike triplet protocols, compared to the $\Delta t = 10$ AB doublet protocol. *Left*: pre-post-pre or ABA protocols. The *arrow* highlights that during the decay period, calcium levels are higher in ABA than in AB. *Right*: post-pre-post or BAB protocols. Adapted from (Rubin et al. 2005). Used with permission of The American Physiological Society

window" for $\Delta t > 0$, consistent with several experimental reports (Bi and Poo 1998; Feldman 2000; Froemke et al. 2005), but see (Nishiyama 2000). Because the amplitude of the $[Ca^{2+}]$ transients decays monotonically with increasing $\Delta t > 0$, and the threshold level of $[Ca^{2+}]$ required to produce LTD is believed to be less than that required to produce LTP (Lisman 1989; Artola and Singer 1993), this second LTD window is an inevitable consequence of a detector scheme that only considers peak or average $[Ca^{2+}]$. By using information from the dynamic time course of this $[Ca^{2+}]$ signal, this limitation can be overcome. Thus, it is plausible that neurons actually do use this information to generate their plasticity responses to experimental STDP protocols.

Applicability to Other Experimental Preparations

The same set of detectors yielded plasticity outcomes that matched the results from triplet experiments in which two action potentials occur in one neuron and one occurs in the other. However, the results of triplet experiments are far more system dependent than are doublet experiments. For example, for horizontal connections in layer II/III of the rodent cortex, the efficacy of individual spike pairings is a function of the number and timing of prior presynaptic spikes; earlier presynaptic spikes have a greater effect than later ones (Froemke and Dan 2002). In layer V, LTP always trumps LTD when they are coactivated (Sjostrom et al. 2001). Therefore, the fixed set of parameter values used in our model cannot apply to the STDP signal transduction machinery in all neurons. However, the model can still reproduce these results through a change in parameters, which could correspond to diversity in the activity levels of particular kinases or phosphatases across brain areas or neuronal phenotypes (Bi and Rubin 2005). For example, reducing the decay time constant of V would result in a "veto" of depression in response to any protocol in which P was

activated. In preliminary tests of this parameter regime, potentiation dominates over depression in response to most arbitrary spike trains.

Alternative Models to Explain the Data

There are alternative schemes to avoid the second LTD window and explain the triplet results. Because there are a finite number of postsynaptic NMDARs, and glutamate concentration begins to decay shortly after the presynaptic action potential, the CV of the number of activated NMDARs increases with increasing $\Delta t > 0$. Because of this variability, in some cases, e.g., $\Delta t = 40$, there could either be a large $[Ca^{2+}]$ signal or a negligible $[Ca^{2+}]$ signal. With each spike pairing, the $[Ca^{2+}]$ signal could reach LTP-, LTD-, or no-change-associated levels, even in a classical model that does not take into account the $[Ca^{2+}]$ time course. The mean resultant plasticity over many individual spike pairings could thus be approximately 0, resulting in no second LTD window (Shouval and Kalantzis 2005).

Because neurotransmitter release is stochastic, combinations of pre- and postsynaptic action potentials will result in some pairings in which a presynaptic vesicle is not released, and the postsynaptic compartment only experiences a back-propagating action potential. Thus, at individual synapses, ABA triplets will sometimes manifest as "only" AB or BA pairings. Meanwhile, BAB pairings will often have no presynaptic release at all. In a model where potentiation always trumps depression, not requiring a veto, ABA triplets would yield a linear sum of the resultant plasticity from an effective sequence of potentiating AB pairings and depressing BA pairings, resulting under certain parameter scalings in no net change in synaptic strength. Meanwhile, BAB pairings would only influence synaptic modification in the event of presynaptic release, in which case potentiation would trump depression. Thus, stochastic synaptic transmission could in principle explain the triplet results (Cai et al. 2007). This model would predict that the result of ABA pairings would depend upon the relative probabilties of neurotransmitter release being induced by the first and the second presynaptic action potentials. Experimentally, however, no dependence on paired pulse ratio was found for the plasticity resulting from ABA pairings (Wang et al. 2005).

Correspondence to Biological Signaling Pathways

The schematic shown in Fig. 2 resembles an early calcium-dependent kinase/phosphatase postsynaptic signaling system (Lisman and Zhabotinsky 2001; Bi and Rubin 2005); by analogy, P represents CaMKII, A represents CaN, D PP1, and V could represent PKA. In the biological system, CaMKII is inhibited by PP1, which is in turn activated by CaN and inhibited by PKA. Future experiments are needed to determine if the V module, with its potential to "veto" depression, really exists and functions as hypothesized. If it does exist, we predict that the veto may be based

on the activity of a kinase, such as PKA, associated with inhibiting the effect of postsynaptic protein phosphatases.

Further Reading

H. D. I. Abarbanel, L. Gibb, R. Huerta, and M. I. Rabinovich. Biophysical model of synaptic plasticity dynamics. *Biol Cybern*, 89:214–226, 2003.

L. F. Abbott and S. B. Nelson. Synaptic plasticity: taming the beast. *Nat Neurosci*, 3 Suppl: 1178–83, 2000.

B. K. Andrasfalvy and J. C. Magee. Distance-dependent increase in AMPA receptor number in the dendrites of adult hippocampal CA1 pyramidal neurons. *J Neurosci*, 21(23):9151–9, 2001.

A. Artola and W. Singer. Long-term depression of excitatory synaptic transmission and its relationship to long-term potentiation. *Trends Neurosci*, 16(11):480–7, 1993.

J. S. Bains, J. M. Longacher, and K. J. Staley. Reciprocal interactions between CA3 network activity and strength of recurrent collateral synapses. *Nat Neurosci*, 2(8):720–6, 1999.

M. F. Bear and R. C. Malenka. Synaptic plasticity: LTP and LTD. *Curr Opin Neurobiol*, 4(3): 389–99, 1994.

C. C. Bell, V. Z. Han, Y. Sugawara, and K. Grant. Synaptic plasticity in a cerebellum-like structure depends on temporal order. *Nature*, 387(6630):278–81, 1997.

G. Q. Bi and J. Rubin. Timing in synaptic plasticity: from detection to integration. *Trends in Neurosci*, 28:222–228, 2005.

G. Q. Bi. Spatiotemporal specificity of synaptic plasticity: cellular rules and mechanisms. *Biol Cybern*, 87(5–6):319–32, 2002.

G. Q. Bi and M. M. Poo. Synaptic modification by correlated activity: Hebb's postulate revisited. *Annu Rev Neurosci*, 24:139–66, 2001.

G. Q. Bi and M. M. Poo. Synaptic modifications in cultured hippocampal neurons: dependence on spike timing, synaptic strength, and postsynaptic cell type. *J Neurosci*, 18(24):10464–72, 1998.

T. V. Bliss and G. L. Collingridge. A synaptic model of memory: long-term potentiation in the hippocampus. *Nature*, 361(6407):31–9, 1993.

D. V. Buonomano. Decoding temporal information. *J Neurosci*, 20:1129–41, 2000.

Y. Cai, J. P. Gavornik, L. N. Cooper, L. C. Yeung, and H. Z. Shouval. Effect of stochastic synaptic and dendritic dynamics on synaptic plasticity in visual cortex and hippocampus. *J Neurophysiol*, 97(1):375–86, 2007.

N. Caporale and Y. Dan. Spike timing-dependent plasticity: a hebbian learning rule. *Annu Rev Neurosci*, 31:25–46, 2008. PMID: 18275283.

G. L. Collingridge, S. J. Kehl, and H. McLennan. Excitatory amino acids in synaptic transmission in the schaffer collateral-commissural pathway of the rat hippocampus. *J Physiol*, 334:33–46, 1983.

J. A. Cummings, R. M. Mulkey, R. A. Nicoll, and R. C. Malenka. Ca^{2+} signaling requirements for long-term depression in the hippocampus. *Neuron*, 16(4):825–33, 1996.

Y. Dan and M.-M. Poo. Spike timing-dependent plasticity: from synapse to perception. *Physiol Rev*, 86(3):1033–48, July 2006. PMID: 16816145.

D. Debanne, B. H. Gahwiler, and S. M. Thompson. Long-term synaptic plasticity between pairs of individual CA3 pyramidal cells in rat hippocampal slice cultures. *J Physiol*, 507 (Pt 1):237–47, 1998.

V. A. Derkach, M. C. Oh, E. S. Guire, and T. R. Soderling. Regulatory mechanisms of AMPA receptors in synaptic plasticity. *Nat Rev Neurosci*, 8(2):101–13, February 2007. PMID: 17237803.

R. Dingledine, M. A. Hynes, and G. L. King. Involvement of N-methyl-D-aspartate receptors in epileptiform bursting in the rat hippocampal slice. *J Physiol*, 380:175–89, 1986.

S. M. Dudek and M. F. Bear. Homosynaptic long-term depression in area CA1 of hippocampus and effects of n-methyl-d-aspartate receptor blockade. *Proc Nat Acad Sci USA*, 89(10):4363–7, 1992.

Bard Ermentrout. *Simulating, analyzing, and animating dynamical systems*. SIAM, Philadelphia, PA, 2002.

D. E. Feldman. Timing-based LTP and LTD at vertical inputs to layer ii/iii pyramidal cells in rat barrel cortex. *Neuron*, 27(1):45–56, 2000.

R. C. Froemke and Y. Dan. Spike-timing-dependent synaptic modification induced by natural spike trains. *Nature*, 416(6879):433–8, 2002.

R. C. Froemke, M. M. Poo, and Y. Dan. Spike-timing-dependent synaptic plasticity depends on dendritic location. *Nature*, 434(7030):221–5, 2005.

R. C. Froemke, I. A. Tsay, M. Raad, J. D. Long, and Y. Dan. Contribution of individual spikes in burst-induced long-term synaptic modification. *J Neurophysiol*, 95(3):1620–9, 2006.

R. C. Gerkin, P. M. Lau, D. W. Nauen, Y. T. Wang, and G. Q. Bi. Modular competition driven by NMDA receptor subtypes in spike-timing-dependent plasticity. *J Neurophysiol*, 97(4):2851–62, 2007.

J. J. Hablitz and I. A. Langmoen. n-methyl-d-aspartate receptor antagonists reduce synaptic excitation in the hippocampus. *J Neurosci*, 6(1):102–6, 1986.

C. D. Harvey and K. Svoboda. Locally dynamic synaptic learning rules in pyramidal neuron dendrites. *Nature*, 450(7173):1195–200, 2007.

D. O. Hebb. *The Organization of Behavior*. Wiley, New York, 1949.

W. R. Holmes. Models of calmodulin trapping and CaM Kinase ii activation in a dendritic spine. *J Comput Neurosci*, 8(1):65–85, 2000.

I. Ismailov, D. Kalikulov, T. Inoue, and M. J. Friedlander. The kinetic profile of intracellular calcium predicts long-term potentiation and long-term depression. *J Neurosci*, 24(44):9847–61, 2004.

C. E. Jahr and C. F. Stevens. A quantitative description of NMDA receptor-channel kinetic behavior. *J Neurosci*, 10(6):1830–7, 1990.

C. E. Jahr and C. F. Stevens. Voltage dependence of NMDA-activated macroscopic conductances predicted by single-channel kinetics. *J Neurosci*, 10(9):3178–82, 1990.

C. E. Jahr and C. F. Stevens. Calcium permeability of the n-methyl-d-aspartate receptor channel in hippocampal neurons in culture. *Proc Natl Acad Sci U S A*, 90(24):11573–7, 1993.

U. R. Karmarkar and D. V. Buonomano. A model of spike-timing dependent plasticity: one or two coincidence detectors? *J Neurosci*, 88:507–513, 2002.

H. J. Koester and B. Sakmann. Calcium dynamics in single spines during coincident pre- and postsynaptic activity depend on relative timing of back-propagating action potentials and subthreshold excitatory postsynaptic potentials. *Proc Natl Acad Sci U S A*, 95(16):9596–601, 1998.

J. J. Letzkus, B. M. Kampa, and G. J. Stuart. Learning rules for spike timing-dependent plasticity depend on dendritic synapse location. *J Neurosci*, 26(41):10420–9, 2006.

J. Lisman. A mechanism for the hebb and the anti-hebb processes underlying learning and memory. *Proc Natl Acad Sci U S A*, 86(23):9574–8, 1989.

J. Lisman, J. W. Lichtman, and J. R. Sanes. LTP: perils and progress. *Nat Rev Neurosci*, 4(11): 926–9, 2003.

J. Lisman and N. Spruston. Postsynaptic depolarization requirements for LTP and LTD: a critique of spike timing-dependent plasticity. *Nat Neurosci*, 8(7):839–41, 2005.

J. E. Lisman and A. M. Zhabotinsky. A model of synaptic memory: a camkii/pp1 switch that potentiates transmission by organizing an AMPA receptor anchoring assembly. *Neuron*, 31(2): 191–201, 2001.

J. C. Magee and D. Johnston. A synaptically controlled, associative signal for hebbian plasticity in hippocampal neurons. *Science*, 275(5297):209–13, 1997.

R. C. Malenka and R. A. Nicoll. Long-term potentiation – a decade of progress. *Science*, 285: 1870–1874, 1999.

M. Maravall, Z. F. Mainen, B. L. Sabatini, and K. Svoboda. Estimating intracellular calcium concentrations and buffering without wavelength ratioing. *Biophys J*, 78(5):2655–67, 2000.

H. Markram, J. Lubke, M. Frotscher, and B. Sakmann. Regulation of synaptic efficacy by coincidence of postsynaptic aps and epsps. *Science*, 275(5297):213–5, 1997.

M. L. Mayer, G. L. Westbrook, and P. B. Guthrie. Voltage-dependent block by mg^{2+} of NMDA responses in spinal cord neurones. *Nature*, 309(5965):261–3, 1984.

C. J. McBain and S. F. Traynelis. Malevolent lurkers no more: NMDA receptors come of age. *J Physiol*, 575(Pt 2):317–8, 2006.

M. R. Mehta, C. A. Barnes, and B. L. McNaughton. Experience-dependent, asymmetric expansion of hippocampal place fields. *Proc Natl Acad Sci U S A*, 94(16):8918–21, 1997.

B. Milner, L. R. Squire, and E. R. Kandel. Cognitive neuroscience and the study of memory. *Neuron*, 20(3):445–68, 1998.

A. Morrison, M. Diesmann, and W. Gerstner. Phenomenological models of synaptic plasticity based on spike timing. *Biol Cybern*, 98:459–78, 2008.

R. M. Mulkey and R. C. Malenka. Mechanisms underlying induction of homosynaptic long-term depression in area CA1 of the hippocampus. *Neuron*, 9(5):967–75, 1992.

V. N. Murthy, T. J. Sejnowski, and C. F. Stevens. Dynamics of dendritic calcium transients evoked by quantal release at excitatory hippocampal synapses. *Proc Natl Acad Sci U S A*, 97(2):901–6, 2000.

M. Nishiyama, K. Hong, K. Mikoshiba, M. M. Poo, and K. Kato. Calcium stores regulate the polarity and input specificity of synaptic modification. *Nature*, 408(6812):584–8, 2000.

C. Normann, D. Peckys, C. H. Schulze, J. Walden, P. Jonas, and J. Bischolfberger. Associative long-term depression in the hippocampus is dependent on postsynaptic N-type Ca^{2+} channels. *J Neurosci*, 20:8290–8297, 2000.

L. Nowak, P. Bregestovski, P. Ascher, A. Herbet, and A. Prochiantz. Magnesium gates glutamate-activated channels in mouse central neurones. *Nature*, 307(5950):462–5, 1984.

M. Perouansky and Y. Yaari. Kinetic properties of NMDA receptor-mediated synaptic currents in rat hippocampal pyramidal cells versus interneurones. *J Physiol*, 465:223–44, 1993.

J. P. Pfister and W. Gerstner. Triplets of spikes in a model of spike timing-dependent plasticity. *J Neurosci*, 26:2673–2682, 2006.

P. Poirazi, T. Brannon, and B. W. Mel. Arithmetic of subthreshold synaptic summation in a model CA1 pyramidal cell. *Neuron*, 37(6):977–87, 2003.

L. D. Pozzo-Miller, N. B. Pivovarova, J. A. Connor, T. S. Reese, and S. B. Andrews. Correlated measurements of free and total intracellular calcium concentration in central nervous system neurons. *Microscopy Res Tech*, 46(6):370–9, 1999.

J. E. Rubin, R. C. Gerkin, G. Q. Bi, and C. C. Chow. Calcium time course as a signal for spike-timing-dependent plasticity. *J Neurophysiol*, 93(5):2600–13, 2005.

B. L. Sabatini, M. Maravall, and K. Svoboda. Ca^{2+} signaling in dendritic spines. *Curr Opin Neurobiol*, 11(3):349–56, 2001.

B. L. Sabatini, T. G. Oertner, and K. Svoboda. The life cycle of Ca^{2+} ions in dendritic spines. *Neuron*, 33(3):439–52., 2002.

G. H. Seol, J. Ziburkus, S. Y. Huang, L. Song, I. T. Kim, K. Takamiya, R. L. Huganir, H.-K. Lee, and A. Kirkwood. Neuromodulators control the polarity of spike-timing-dependent synaptic plasticity. *Neuron*, 55(6):919–29, September 2007. PMID: 17880895.

H. Z. Shouval and G. Kalantzis. Stochastic properties of synaptic transmission affect the shape of spike time-dependent plasticity curves. *J Neurophysiol*, 93(2):1069–73, 2005.

H. Z. Shouval, M. F. Bear, and L. N. Cooper. A unified model of NMDA receptor-dependent bidirectional synaptic plasticity. *Proc Natl Acad Sci USA*, 99:10831–10836, 2002.

H. Z. Shouval and G. Kalantzis. Stochastic properties of synaptic transmission affect the shape of spike time-dependent plasticity curves. *J Neurophysiol*, 93:1069–1073, 2005.

P. J. Sjostrom, G. G. Turrigiano, and S. B. Nelson. Rate, timing, and cooperativity jointly determine cortical synaptic plasticity. *Neuron*, 32(6):1149–64, 2001.

P. J. Sjostrom, G. G. Turrigiano, and S. B. Nelson. Rate, timing, and cooperativity jointly determine cortical synaptic plasticity. *Neuron*, 32:1149–1164, 2001.

R. D. Traub, J. G. Jefferys, R. Miles, M. A. Whittington, and K. Toth. A branching dendritic model of a rodent CA3 pyramidal neurone. *J Physiol*, 481 (Pt 1):79–95, 1994.

T. Tzounopoulos, Y. Kim, D. Oertel, and L. O. Trussell. Cell-specific, spike timing-dependent plasticities in the dorsal cochlear nucleus. *Nat Neurosci*, 7(7):719–25, 2004.

H. X. Wang, R. C. Gerkin, D. W. Nauen, and G. Q. Bi. Coactivation and timing-dependent integration of synaptic potentiation and depression. *Nat Neurosci*, 8(2):187–93, 2005.

R. Yuste, A. Majewska, S. S. Cash, and W. Denk. Mechanisms of calcium influx into hippocampal spines: heterogeneity among spines, coincidence detection by NMDA receptors, and optical quantal analysis. *J Neurosci*, 19(6):1976–87, 1999.

A. M. Zhabotinsky. Bistability in the ca(2+)/calmodulin-dependent protein kinase-phosphatase system. *Biophys J*, 79(5):2211–21, 2000.

J. C. Zhang, P. M. Lau, and G. Q. Bi. Gain in sensitivity and loss in temporal contrast of STDP by dopaminergic modulation at hippocampal synapses. *Proc Natl Acad Sci USA*, 106:13028–33, 2009.

L. I. Zhang, H. W. Tao, C. E. Holt, W. A. Harris, and M. Poo. A critical window for cooperation and competition among developing retinotectal synapses. *Nature*, 395(6697):37–44, 1998.

Computer Simulation Environments

Padraig Gleeson, R. Angus Silver, and Volker Steuber

Introduction

This chapter gives a brief overview of simulation tools and resources available to researchers wishing to create computational models of hippocampal function. We outline first a number of software applications which provide a range of functionality for simulating networks of neurons with varying levels of biophysical detail. We then present some ongoing initiatives designed to facilitate the development of models in a transparent and portable way across different environments. Next, we describe some of the publicly accessible databases which can be used as resources by computational modellers. Finally we provide an outlook for the field, highlighting some of the current issues facing biophysically detailed modelling and point out some of the key initiatives and sources of information for future modelling efforts.

Simulation Environments

We discuss several packages which are freely available for researchers interested in modelling hippocampal function (although none of these packages are limited to that brain area). These simulation environments range from those designed for modelling networks of multicompartmental, conductance-based neurons to those for more abstract cells (e.g. integrate-and-fire) in large-scale network simulations, to platforms for simulating any dynamical system which can be modelled by sets of differential equations. A more detailed review of simulators of spiking neurons is presented in (Brette et al., 2007).

P. Gleeson (✉)
Department of Neuroscience, Physiology and Pharmacology, University College London, UK
e-mail: p.gleeson@ucl.ac.uk

V. Cutsuridis et al. (eds.), *Hippocampal Microcircuits*, Springer Series in Computational Neuroscience 5, DOI 10.1007/978-1-4419-0996-1_21,

NEURON

This is a widely used simulation environment specifically designed for creating data-driven models of neurons and neuronal networks (Carnevale and Hines, 2006). It has been used for simulations in many hundreds of publications since the early 1990s. The focus of the platform is on conductance-based neuron models, but its flexibility allows it to be used also for more abstract neural modelling. A large number of cell and network models which have been developed with the platform over the years are available through the ModelDB repository (see Section "ModelDB/NeuronDB").

Several aspects of NEURON make it a good general-purpose platform for modelling biophysically detailed cells and networks. The simulator has a number of inbuilt concepts (such as the section object for cable modelling) designed to make simulation of neuronal systems easy for the user and attempts to separate as much as possible the biophysical aspects of models from the underlying numerical integration details. Great flexibility is conferred by the NMODL language for specifying the behaviour of membrane conductances and synapses, allowing a wide range of voltage- and ligand-gated ion channels and static or plastic synaptic mechanisms to be incorporated. Multiple integration methods are supported for low-level control and optimisation of simulations. The graphical user interface elements are very useful during debugging of simulations and can also facilitate making models more accessible to other researchers (Fig. 1).

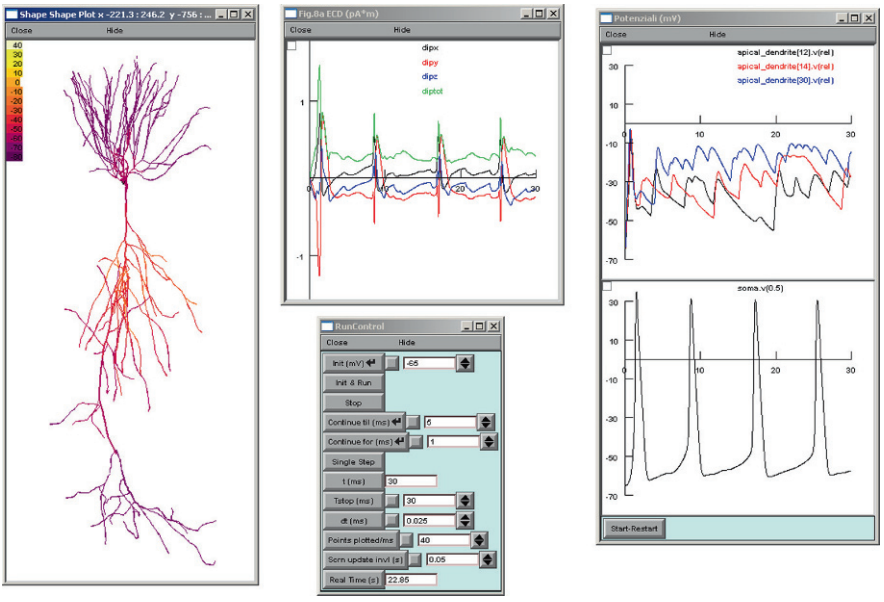

Fig. 1 Screenshot of the NEURON graphical user interface showing a model of a CA1 pyramidal cell (Cassara et al., 2008) which was used to investigate the contribution of neuronal currents to MRI signals (ModelDB reference: 106551)

There have been a number of significant recent additions to NEURON's functionality. These include the option to use Python as an alternative scripting interface. This brings all of the advantages of a modern, well-supported scripting language, as well as giving access to a wide range of libraries which can be used within any Python-based NEURON script (for example, for data analysis, advanced graphing, XML or HDF5 file handling). It also adds the prospect of using the same scripts on multiple simulators (see Section "PyNN"). NEURON also supports import and export of neuronal morphologies (and related information on passive electrical properties and channel conductance densities) in NeuroML format (see Section "NeuroML"). One of the most significant recent developments in NEURON is the ability to run simulations across multiple processors (Hines and Carnevale, 2008; Migliore et al., 2006). This parallel functionality allows near linear speedup of network simulations, i.e. a large network spread across 100 processing cores will run approximately 100 times as fast as the same network on one processor. Recently there has also been the option to split cells with large numbers of sections efficiently across multiple processors, which could help speed up parameter searches for detailed CA1/CA3 cell models, for example.

Main NEURON web site: http://www.neuron.yale.edu/neuron

Strengths: Conceptual separation of neuronal morphology and compartmentalisation aids rapid model development and simulation.

- Ability to add new mechanisms in NMODL provides great flexibility for customised synapses and channel kinetics that do not fit the standard Hodgkin–Huxley formalism.
- Well-designed GUI that allows the construction of simulations with intermediate degrees of complexity without scripting.
- Runs under UNIX/Linux/Mac OS X and MS Windows.
- Event-driven algorithm for the simulation of simple integrate-and-fire networks.
- Active developer community, extensive online documentation and book (Carnevale and Hines, 2006).

When to use this simulation platform: NEURON is most appropriate to use for cell and network models which will incorporate a large amount of morphological and electrophysiological detail. The ongoing development and large user base mean there is a good chance of models developed on this platform being used and built upon by the wider neuroscience community into the future.

GENESIS

Like NEURON, GENESIS is a popular multi-purpose neural simulator that has been developed primarily for simulations of biologically detailed conductance-based neuronal models, although it can also be used for more abstract models (Bower and Beeman, 1997). The name GENESIS (GEneral NEural SImulation System) was chosen to reflect its wide applicability: simulations that have been performed with

GENESIS span a multitude of levels, ranging from biochemical reactions and calcium diffusion to complex multicompartmental neurons and large neuronal networks. Most of these simulations represent a large amount of physiological and anatomical detail and give rise to predictions that can be tested directly in experiments.

One of the key features of GENESIS is its object-oriented design. Simulations are constructed by combining basic building blocks called GENESIS elements. Elements are created from precompiled GENESIS object templates and communicate by passing messages to each other. For example, a simulation of a complex neuron is composed of a number of compartment elements that exchange messages with their neighbouring compartments and with compartment-specific sets of voltage and/or concentration-gated ion channels. Other elements can be created from objects that represent synaptic channels, intracellular ion concentrations and input and output devices such as pulse generators, voltage clamp circuitry, spike frequency measurements and interspike interval histograms. The current GENESIS distribution (version 2.3, March 2006) provides a large number of predefined object types and script language commands, which makes it possible to construct complex simulations with relatively few lines of code. Moreover, the object-oriented character facilitates the exchange and reuse of model components and allows extension of the functionality of GENESIS by adding new user-defined object types, without having to understand or re-write the main simulator code. The simulator also includes graphical objects to facilitate interaction with model components (Fig. 2).

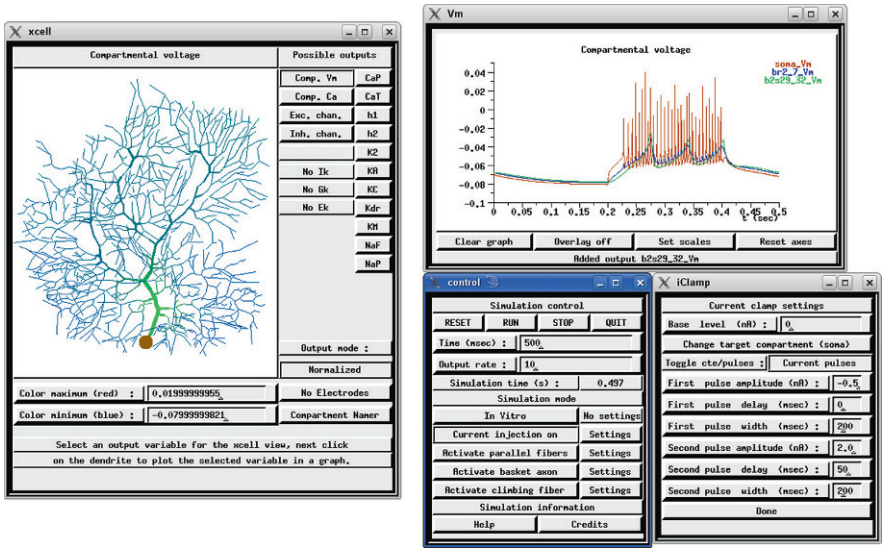

Fig. 2 The GENESIS graphical user interface, illustrating the Purkinje cell model tutorial which is included with the standard distribution

In addition to the GENESIS commands and objects for the simulation of electrophysiological properties of neurons, two specialised libraries allow the simulation of biochemical reactions. GENESIS 2.3 includes version 11 of the Kinetikit utility (Bhalla and Iyengar, 1999), which comprises a kinetics library and a graphical interface for deterministic and four different types of stochastic biochemical simulations. Another set of biochemical objects that also includes objects for diffusion and flux across membranes is provided by the Chemesis library (Blackwell and Hellgren-Kotaleski, 2002) http://www.krasnow.gmu.edu/avrama/chemesis.html).

For simulations of large networks or extensive parameter searches, GENESIS also offers parallel functionality. Parallel GENESIS (PGENESIS, current version 2.3) can be used on any cluster, supercomputer or network of workstations that run UNIX or Linux and support MPI or PVM. PGENESIS was developed at the Pittsburgh Supercomputing Center and additional information can be found on their webpage (http://www.psc.edu/Packages/PGENESIS/).

Work is underway in several projects as part of the GENESIS 3 initiative. The Neurospaces project is developing a number of modular software components which will cover and extend the scope of the original GENESIS simulator. A parser for reading GENESIS 2 scripts is being developed. The MOOSE project is reimplementing from scratch the core of GENESIS and aims to create a more efficient implementation. While it will be backwards compatible with GENESIS 2, in the longer term the aim is to use Python as the main scripting interface.

Main GENESIS web site: http://www.genesis-sim.org/
Neurospaces web site: http://neurospaces.sourceforge.net
MOOSE development site: http://moose.sourceforge.net
Strengths: There is extensive documentation for GENESIS online, a large user community and a book (Bower and Beeman, 1997), which has been the basis for a number of computational neuroscience courses.

- The software is easy to learn, and simulations can be quickly constructed from the 125 precompiled object types.
- The object-oriented design facilitates exchange and reuse of model components.
- It features an intuitive and flexible way of constructing large-scale network simulations.
- Several specialised objects are available for the simulation of biochemical reactions.

When to use this simulation platform: GENESIS is a stable and widely used platform for developing biophysically detailed cell and network models. While GENESIS 2 is no longer under active development, there are a number of published cell models in this format and an online community willing to support the further development of these models. However, someone interested in developing a new cell model, possibly incorporating recent models of channel and synaptic kinetics, should acquaint themselves with the ongoing developments in the GENESIS 3 initiative.

NEST

The NEST (the NEural Simulation Tool) Simulator is an application for simulating networks of neurons of biologically realistic size ($\sim 10^5$ cells) each with a small number of compartments. The emphasis is on efficiency of storage of the network information to allow the investigation of the dynamics of large-scale networks. Neuronal elements in these networks (quite often single compartment integrate-and-fire neurons) can be connected with a range of synaptic models including ones for short-term plasticity (STP) and spike-timing-dependent plasticity (STDP). There are a variety of inbuilt network connectivity schemes to create connections between neurons and groups of neurons.

The NEST Simulator is being developed as part of the NEST Initiative for the development of new neural simulation and analysis tools. The current work on NEST 2 focuses on creating a very efficient implementation for parallel network simulations and incorporation of a Python-based interface (see Section "PyNN"), facilitating sharing and reuse of code between simulation environments.

To date the NEST Simulator has been mainly used for investigations of network activity in generic cortical structures (Kumar et al., 2008), and for studying the technologies needed for large-scale parallel network simulation, and this work has much to offer investigators wishing to create large-scale network simulations of the hippocampus, with simplified neuronal elements.

Main NEST web site: http://www.nest-initiative.org

Strengths: The simulator has been designed from the outset to efficiently handle large-scale network models in a parallel computing environment.

- There have been a number of publications outlining the design philosophy and implementation of the simulator (Diesmann and Gewaltig, 2002; Plesser et al., 2007) and its usage for neuronal network analysis (Morrison et al., 2007; Morrison et al., 2008).
- It is in active development and is endeavouring to ensure compatibility with a number of standardisation initiatives in the computational neuroscience field.

When to use this simulation platform: NEST is very suitable for research into how the basic properties of synaptic and neuronal elements influence the behaviour of large-scale networks. To make the best use most of the platform's features, a user should be willing to look into the technical details of network modelling in a parallel computing environment.

Surf Hippo

This simulation environment has been developed by Lyle J. Graham over the past number of years, mainly for hippocampal and retinal modelling. While it is not as widely used as the NEURON or GENESIS simulation environments, some important modelling work has been done using the simulator, including detailed

investigations of hippocampal ion channel properties (Borg-Graham, 1999), and development of numerical methods targeted for neuronal models such as adaptive time step for Hodgkin–Huxley-type models and ideal voltage clamp of branched structures (Borg-Graham, 2000). Work is ongoing creating biophysically detailed hippocampal pyramidal cell models and networks in this environment, which are highly constrained by experimental data.

The system is based on the LISP high-level language and programming environment, which allows efficient incorporation of user-generated mechanisms, straightforward description of simulation protocols in a near pseudo-code syntax, and immediate access to arbitrary levels of simulation abstraction and details, ranging from full GUI to inspection and, if necessary, manipulation of internal state.

Surf Hippo web site: http://www.neurophys.biomedicale.univ-paris5.fr/~graham/surf-hippo.html

Strengths: The simulation environment has evolved over the years with a specific focus on the efficient modelling of detailed neurons and networks incorporating multiple membrane conductances and synaptic mechanisms.

- The modelling formalism used for the membrane conductances is based on up-to-date understanding of the kinetic properties of the ion channels at varying temperatures.
- The use of LISP code for all aspects of the system, including numerical libraries, allows better cross-validation of models implemented in other simulators which are generally written in C and so will most likely not share any code/underlying libraries.

When to use this simulation platform: Surf Hippo has a similar scope to other biophysical neuronal modelling environments, but the much smaller base of experienced users may be a drawback. Researchers interested in using this environment are encouraged to contact the developers directly.

XPP/XPPAUT

XPPAUT (or XPP, these names are used interchangeably) is a widely used tool for the analysis and simulation of dynamical systems. Typically these comprise sets of ordinary differential equations, but XPPAUT can also solve partial differential equations, discrete finite state models, stochastic systems, delay equations, boundary value problems, and combinations of different types of equations. The current program evolved from the PHASEPLANE tool that was developed by John Rinzel and Bard Ermentrout to demonstrate properties of excitable membranes, and its focus is on understanding the behaviour of equations rather than on providing a pure numerical integrator. XPPAUT provides several graphical tools for analysing dynamical systems, such as space-time plots, 2D and 3D phase-space plots, nullclines, vector fields and Poincaré maps, and it includes some statistical tools for spectral analysis and auto- and cross-correlograms and a Levenberg–Marquardt curve fitter.

Moreover, it incorporates the continuation and bifurcation package AUTO for the tracking of fixed points and limit cycles, which is often used to analyse the dependence of solutions on parameters.

Equations in XPPAUT are written as they would appear on paper, which makes the program very easy to learn. It is commonly used for teaching at workshops and courses such as the Woods Hole Methods in Computational Neuroscience Course and the European Advanced Course in Computational Neuroscience. An extensive tutorial is available online (see below for link), and there is a book that contains complete documentation and many examples (Ermentrout, 2002).

Main XPP web site: http://www.math.pitt.edu/∼ bard/xpp/xpp.html

Strengths: XPPAUT provides a very general and flexible interface for the analysis and simulation of various types of dynamical systems. Online documentation and a book (Ermentrout, 2002) are available.

- The program can be used without having to learn a complex scripting language. Equations can be entered as they appear on paper.
- Different graphical analysis methods are available that help to understand in depth the behaviour of the system and its dependence on parameters.

When to use this simulation platform: Analysis of models of hippocampal function ranging from abstract network representations to those containing biophysical cell models can be performed with this tool, and so it would be suitable for researchers who want complete control over all elements of the dynamics of their models.

Other Simulation Environments

PSICS – Parallel Stochastic Ion Channel Simulator

PSICS is a recently developed simulation environment which differs from other multicompartmental conductance-based simulators in that it focuses on the efficient simulation of cell models containing individually specified stochastic ion channels, modelled using a kinetic scheme-based approach. This allows, for example, the investigation of the effects of stochastic channel opening when low numbers of individual channels are present in regions of the cell.

This approach is complementary to the deterministic, conductance density-based approach normally used in other simulators (although PSICS can also be used for deterministic simulations) and adds a different focus which benefits the investigation of the essential physiological processes underlying cell behaviour.

PSICS web site: http://www.psics.org

MCell – A Monte Carlo Simulator of Cellular Microphysiology

MCell is a tool for simulation of the diffusion and reaction of molecules in realistic 3D geometries inside and between cells. It uses efficient Monte Carlo algorithms

to simulate the paths of individual molecules in these regions and their interactions with one another, ion channels, transporters, etc.

MCell simulates a much finer level of detail than most of the other simulators described here, though much can be learned from such simulations about the behaviour of neurotransmitters and other signalling substances in, for example, synaptic clefts. This type of investigation can be used to create better phenomenological models of synaptic mechanisms, which can be used in larger scale network modelling.

MCell web site: http://www.mcell.cnl.salk.edu

Simulators Created with General Programming Environments

A large number of models in the computational neuroscience field have been developed using the MATLAB environment. The main advantage of using this from a researcher's point of view is that the same language can be used for data analysis as for model construction, and a wide range of researchers are competent in the language. Several MATLAB model implementations are present in ModelDB (Section "ModelDB/NeuronDB"). MATLAB is a commercial product, but most scripts can be executed using the freely available GNU OCTAVE application.

IGOR Pro is also a commercial product for scientific programming and data analysis which can be used for neuronal modelling. The package can also be used for data acquisition, e.g. in electrophysiological experiments, and is often used by experimentalists who have a modelling element to their research.

Quite often neuronal models and simulation environments have been custom made in a single lab and are based on widely used general-purpose programming languages like C++, FORTRAN and Java. While this gives the modellers a very large degree of flexibility, it can often be difficult for those outside the group to reuse the models. The need to produce documentation and support user queries can often be a disincentive to the developers to distribute their software. However, there are a number of models in these languages available on ModelDB, and the developers are often happy to have their work more widely used.

MATLAB: http://www.mathworks.com/products/matlab
GNU Octave: http://www.octave.org
IGOR Pro: http://www.wavemetrics.com

Model Development and Integration

Detailed computational models of neuronal function created in one of the simulation packages described above can take a year or more to create, analyse and document. A number of models have been produced in recent years in various formats and many are available on publicly accessible databases (e.g. ModelDB, see Section "ModelDB/NeuronDB"). These provide a valuable starting point for other researchers who wish to further develop the models for their own investigations. However, the multitude of incompatible programming languages used, the

programmer-specific nature of the scripts and the time commitment needed to learn how best to modify the models are all factors which have discouraged wider use and ongoing development of published models.

The computational neuroscience community is investigating ways to enable greater accessibility of neuronal models and is developing standards to allow greater reuse of model code. A number of reports from international conferences (Cannon et al., 2007; Djurfeldt and Lansner, 2007) have discussed these issues in detail. Some of the ongoing efforts to increase the accessibility and portability of models are described in this section.

NeuroML

NeuroML, the Neural Open Markup Language, is a model description language being developed for specifying the essential physiological elements of biologically detailed neuronal and network models. The motivation for the initiative has been the common set of physiological conceptual models used in simulators such as NEURON and GENESIS, e.g. cable theory and the Hodgkin–Huxley formalism. The main requirements for the language are clarity of the model description, portability of the models between simulators and modularity of model components (Goddard et al., 2001). The specification for the language describes the elements needed in XML (Extensible Markup Language) files for the parameters associated with a particular neuronal model (e.g. cellular morphology, ion channel and network). These NeuroML files can then be mapped to the specific format of supported platforms for simulation.

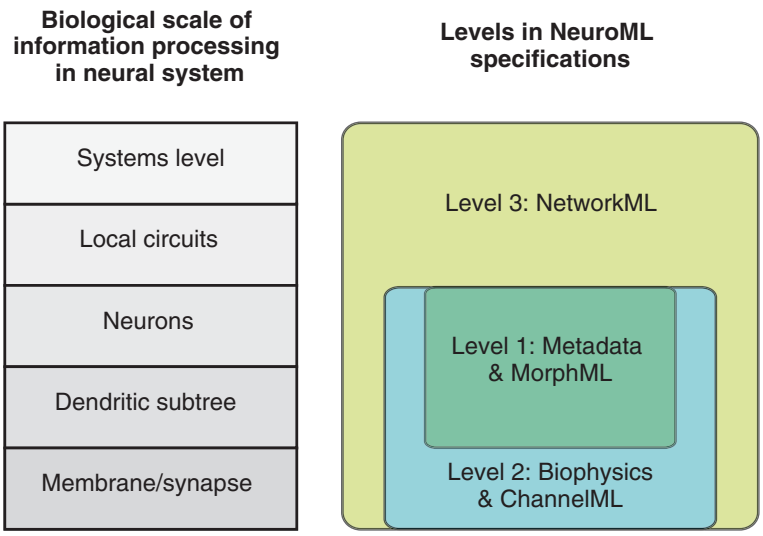

Fig. 3 Levels at which information is processed in neuronal systems and the corresponding Levels in NeuroML

Information is processed in the nervous system at a number of different levels, and various models of neuronal function have been developed across these levels (Fig. 3). The NeuroML specification is split into Levels reflecting this organisation. Level 1 deals with the anatomical properties of single cells. It allows detailed neuronal morphologies to be described in a format which can be mapped on to a number of existing simulator-specific representations (Crook et al., 2007). This level also describes the metadata which can be used to give additional contextual information on any NeuroML file (e.g. authors, publications and links to external databases). Level 2 builds on Level 1 and allows specification of the biophysical properties of cells (passive electrical properties, channel densities on different regions of the cell, etc.) for the creation of conductance-based, spiking neuronal models. It also specifies ChannelML, which can be used to describe the dynamics of voltage and ligand-gated membrane conductances and also synaptic mechanisms. Level 3 deals with network aspects, and the core of this level, NetworkML, is used for detailing the 3D placement of cells, their connectivity and electrical inputs.

While XML is the main technology used in defining the model description language, other open, widely used languages and standards, like Python and HDF5 are being used to enable interoperability of neuronal modelling information, and the NeuroML project is working to ensure compatibility with these initiatives.

NeuroML is an ongoing Open Source project. The main development is taking place via a Sourceforge project, and the associated mailing lists are the main source of the latest information on the ongoing developments. NeuroML will become an important part of the process of model sharing and exchange of ideas in hippocampal modelling as more existing models are converted to the format, but there is still a great deal of collaborative work which can be done with well-written and well-documented models in the native formats of one of the previously mentioned simulators.

Main NeuroML web site: http://www.NeuroML.org
NeuroML Sourceforge project: http://sourceforge.net/projects/neuroml

neuroConstruct

The creation of neuronal models in most current neuronal simulators requires the user to write a number of script files for the model in a format specific to that simulator. This can be a barrier to reuse of the model by experimentalists who have detailed knowledge of the biological system being modelled, but who have no time or experience to investigate in detail the specifics of the modelling language used. neuroConstruct (Gleeson et al., 2007) is a software application which seeks to address this problem. It features a graphical interface for constructing, visualising and analysing the behaviour of networks of conductance-based multicompartmental neuronal models (Fig. 4). The emphasis is on creating 3D network models which have a structure and connectivity with a high degree of biological realism. It automatically generates scripts for either NEURON or GENESIS, allowing the same model to be simulated in both environments. This can be very useful when

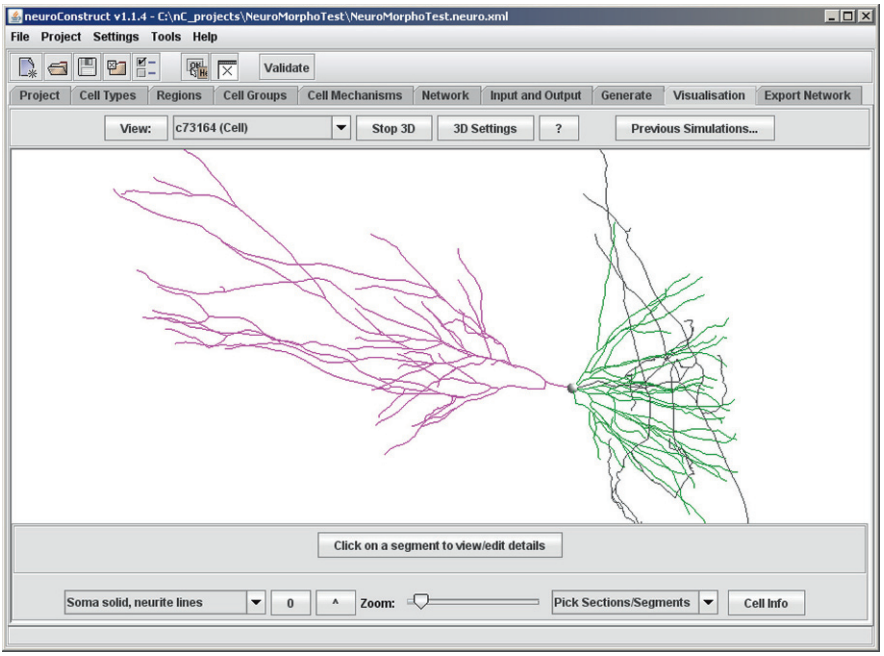

Fig. 4 Main neuroConstruct interface, showing visualisation of a CA3 pyramidal cell imported from NeuroMorpho.org

developing complex network simulations, as it provides a check that the simulation is behaving according to the physiological properties of the model as opposed to a simulator-specific implementation.

The simulator independence of the models created with neuroConstruct is enabled by extensive support for the NeuroML model description language. Cell models are stored in an internal format based on MorphML. Channel mechanisms are preferentially expressed in ChannelML (although channels in legacy simulator script (e.g. NMODL) can be reused too). Generated networks can be imported and exported in NetworkML format allowing networks from multiple sources to be used in the supported simulators.

The application is freely available at the web address below. There are example projects and tutorials included with the code, and documentation on neuroConstruct and related technologies is available on the web site.

neuroConstruct was initially designed for network modelling of the cerebellum, but is also applicable to other brain areas, particularly where 3D structure is important for an understanding of network behaviour, such as in the hippocampus. A network model of the dentate gyrus (Santhakumar et al., 2005) is included with the standard neuroConstruct distribution, and a detailed cell model of a CA1 cell (Migliore et al., 2005) is in development for future releases.

neuroConstruct web site: http://www.neuroConstruct.org

PyNN

PyNN is an initiative which was started in the EU FACETS project to design a common scripting interface based on Python for neuronal network simulators. While recognising that the diversity of network simulators has advantages (a specific simulator can be chosen based on usability, speed, graphical interface, parallel computing support, etc.) there is a large overlap in the scope of the network models they support. A number have recently introduced support for Python and the PyNN initiative seeks to create a specification for a set of common Python commands for setting up network simulations. This will hopefully lead to greater testing of neuronal models across simulators and greater sharing and reuse of code.

PyNN specifies a number of basic functions for setting up neuronal populations and the connections between them. The current focus is on large networks with fairly simple cells (e.g. leaky integrate-and-fire), but which have complex connectivity and possibly incorporate synaptic plasticity mechanisms. Simulators which currently support the language include NEURON, NEST and PCSIM (Parallel neural Circuit SIMulator, http://www.lsm.tugraz.at/pcsim), and there is also work to support the running of such networks on VLSI neuromorphic hardware created by the FACETS project.

PyNN is a specification incorporating procedural descriptions of network structure and is complementary to the declarative model specifications being developed in the NeuroML initiative. Work is under way to use NetworkML (either as XML or HDF5 files) as a storage format for networks generated with PyNN scripts, allowing a network created on a PyNN compliant simulator to be loaded into a NetworkML compliant application, e.g. for visualisation in neuroConstruct. As the scope of PyNN expands to include more detailed cellular models, it will use parts of the MorphML and ChannelML specifications as appropriate.

PyNN in its present form is useful for more abstract network models (e.g. simulating large areas of the hippocampus with simple cells), but it is encouraging that network models created using this language can be more widely tested and shared, and that the associated tools for network and simulation data analysis (also being developed at http://neuralensemble.org) will facilitate investigation of the function of these complex networks.

PyNN development web site: http://neuralensemble.org/PyNN

Resources

Here we discuss some of the online resources which may be of use to modellers of hippocampal function.

ModelDB/NeuronDB

ModelDB and NeuronDB are two integrated neuroscience databases that are part of the SenseLab initiative. The SenseLab resource is a collection of several databases

that were developed to facilitate the sharing of neuronal models and data, with emphasis on, but not limited to, the olfactory system. A prominent feature of the SenseLab databases is that they are based on the EAV/CR (Entity Attribute Values with Classes and Relationships) architecture. The EAV/CR framework, which is also used by the Neuroscience Database Gateway of the Society for Neuroscience (http://ndg.sfn.org), facilitates the addition of new types of information and the integration of data that are distributed over different databases. The supported database interoperability is used by the Entrez LinkOut Broker, which allows recurrent links between the NCBI PubMed web portal (http://www.ncbi.nlm.nih.gov/sites/entrez) and a collection of different databases, including NeuronDB and ModelDB. Another example of database interoperability is the interaction between the NeuronDB and the Cell-Centred Database CCDB, which links the information about neuronal membrane properties that is stored in NeuronDB to microscopic imaging data provided by CCDB.

NeuronDB contains published information about neurotransmitters, neurotransmitter receptors and voltage-gated channels and gives details of the presence of these on various morphological regions for different neuronal types. There is currently (December 2008) detailed information available for 31 neurons from all major vertebrate brain regions, including four types of neurons from the hippocampus. ModelDB is a repository of computational models of neurons, neuronal components and networks that are implemented in a variety of different programming languages and simulators, ranging from C++ and Matlab to NEURON and GENESIS. The database has expanded from four models in 2000 to over 400 models in 2008, and its use is encouraged by journals such as the Journal of Computational Neuroscience, which has recently published an editorial recommending that all models used for articles in this journal should be stored in ModelDB.

ModelDB web site: http://senselab.med.yale.edu/modeldb

NeuronDB web site: http://senselab.med.yale.edu/neurondb

NeuroMorpho.org

NeuroMorpho.org (Ascoli et al., 2007) is an initiative to create a centralised and curated repository of digitally reconstructed neuronal morphologies from multiple labs. It is currently the largest web-searchable collection of 3D reconstructions and associated metadata, with 4,508 morphologies from 33 contributing labs, 10 species, 14 major brain regions and more than 40 cell types in the October 2008 release. One of the main data sets comes from hippocampus; the current collection contains 534 hippocampal neurons from 11 different labs, including the hippocampal reconstructions from the Duke/Southampton archive (Cannon et al., 1998).

For each neuron, the available material includes the digital reconstructions and a large amount of auxiliary information. In addition to the original reconstruction, a standardised morphology file can be downloaded that has been checked for integrity and converted into a uniform SWC/Cvapp text format. The editorial changes and any remaining anomalies are listed in a log file. Other available data include information about histology, microscopy and reconstruction procedures and

several morphometric characteristics such as soma surface, number of bifurcations, total dendritic length, and partition asymmetry. To ensure the quality of the data, only published reconstructions are stored and each neuron has a link to the relevant PubMed reference. There are various options to view the morphologies in 2D and 3D, a conversion tool for the generation of NEURON and GENESIS files and an extensive search engine.

NeuroMorpho web site: http://www.NeuroMorpho.Org

INCF Software Center

The International Neuroinformatics Coordinating Facility (INCF) was set up through the Global Science Forum of the OECD to coordinate global activities related to databasing and modelling efforts in neuroscience. As part of this, the INCF Software Center was created as a central resource where computational neuroscience software developers can register their applications. Researchers can search this site for tools related to their areas of interest: for electrophysiological acquisition, imaging, modelling, data analysis or a number of other areas. The site is being actively updated and will be integrated with the new INCF Portal which will closely link to a number of other online neuroinformatics data resources.

INCF Software Center web site: http://software.incf.net

Neuroscience Information Framework

The Neuroscience Information Framework is an initiative of the US National Institutes of Health designed to create a central resource to facilitate access to information related to neuroscience research. It is a searchable repository of information about the location of experimental data, software tools, databases, portals and educational resources. As the resource is further developed, it is hoped that it will allow greater sharing and reuse of data and can encourage the wider use of tools for analysing and integrating the ever-expanding data sets being produced in brain research.

Neuroscience Information Framework web site: http://nif.nih.gov

Outlook

Computational models of neuronal systems are increasingly being used by experimental neurophysiologists to help explain their experimental findings, and by theoreticians to investigate the general principles of information processing in the brain. These activities are helped enormously by dedicated software packages which allow rapid creation of detailed neuronal models and by online databases of resources for model creation.

The packages which are available to modellers of hippocampal function vary greatly in application area and range from those dedicated to modelling single cells in high levels of biophysical detail (e.g. NEURON, GENESIS) to those which are

more general and flexible and can be used for creating and analysing more abstract models of system function (e.g. XPPAUT, MATLAB). The choice of which package a researcher should use will depend on a number of factors, but will be helped greatly by clearly establishing the research question before choosing a modelling strategy.

A key issue for the future as these models become more complex will be availability of reliable model components across multiple platforms, e.g. not everyone should have to develop their own CA1 cell model from scratch. Developers of simulation environments are increasingly keen on supporting community developed standards with a view to providing such model portability and interoperability (e.g. NeuroML, PyNN). A number of other initiatives not mentioned here are also in development, including MUSIC (MUlti-SImulation Coordinator), a standard interface to allow communication between parallel applications for large-scale network simulations.

The range of tools available for computational modelling is constantly expanding, larger and more usable databases of experimental data are becoming available and funding agencies are increasingly seeing the benefit in supporting the development of such resources. The INCF Software Center (and Portal in the near future) is a good resource for the latest information, as are the mailing lists compneuro@neuroinf.org and connectionists@cs.cmu.edu.

Acknowledgments We thank Marc-Oliver Gewaltig, Reinoud Maex, Koen Vervaeke and Lyle Graham for comments on the chapter. This work was funded in part by grant G0400598 from the Medical Research Council. Padraig Gleeson was supported by an MRC Special Research Training Fellowship in Bioinformatics, Neuroinformatics, Health Informatics and Computational Biology, R. Angus Silver is in receipt of a Wellcome Trust Senior Research Fellowship in Basic Biomedical Science.

Further Reading

Ascoli, G.A., Donohue, D.E., and Halavi, M. (2007). NeuroMorpho.Org: a central resource for neuronal morphologies. *J Neurosci* 27, 9247–9251.

Bhalla, U.S. and Iyengar, R. (1999). Emergent properties of networks of biological signaling pathways. *Science* 283, 381–387.

Blackwell, K. and Hellgren-Kotaleski, J. (2002). Modelling the dynamics of second messenger pathways. In *Neuroscience Databases. A Practical Guide* (Boston: Kluwer Academic Publishers), pp. 63–80.

Borg-Graham, L.J. (1999). Interpretations of data and mechanisms for hippocampal pyramidal cell models. In *Cerebral Cortex, Volume 13: Cortical Model*, P.S. Ulinski, E.G. Jones, and A. Peters, eds. (New York: Plenum Press).

Borg-Graham, L.J. (2000). Additional efficient computation of branched nerve equations: adaptive time step and ideal voltage clamp. *J Comput Neurosci* 8, 209–226.

Bower, J.M. and Beeman, D. (1997). *The Book of GENESIS: Exploring Realistic Neural Models with the GEneral NEural SImulation System* (Springer, New York).

Brette, R., Rudolph, M., Carnevale, T., Hines, M., Beeman, D., Bower, J.M., Diesmann, M., Morrison, A., Goodman, P.H., Harris, F.C., Jr., et al. (2007). Simulation of networks of spiking neurons: a review of tools and strategies. *J Comput Neurosci* 23, 349–398.

Cannon, R., Gewaltig, M.-O., Gleeson, P., Bhalla, U., Cornelis, H., Hines, M., Howell, F., Muller, E., Stiles, J., Wils, S., and De Schutter, E. (2007). Interoperability of neuroscience modelling software: current status and future directions. *Neuroinformatics* 5, 127–138.

Cannon, R.C., Turner, D.A., Pyapali, G.K., and Wheal, H.V. (1998). An on-line archive of reconstructed hippocampal neurons. *J Neurosci Methods* 84, 49–54.

Carnevale, N.T. and Hines, M.L. (2006). *The NEURON Book* (Cambridge: Cambridge University Press).

Cassara, A.M., Hagberg, G.E., Bianciardi, M., Migliore, M., and Maraviglia, B. (2008). Realistic simulations of neuronal activity: a contribution to the debate on direct detection of neuronal currents by MRI. *Neuroimage* 39, 87–106.

Crook, S., Gleeson, P., Howell, F., Svitak, J., and Silver, R.A. (2007). MorphML: level 1 of the NeuroML standards for neuronal morphology data and model specification. *Neuroinformatics* 5, 96–104.

Diesmann, M. and Gewaltig, M.-O. (2002). *NEST: An Environment for Neural Systems Simulations, Vol Forschung und wisschenschaftliches Rechnen, Beitrage zum Heinz-Billing-Preis 2001* (Gottingen: Ges. fur Wiss. Datenverarbeitung).

Djurfeldt, M. and Lansner, A. (2007). Workshop report: 1st INCF workshop on large-scale modeling of the nervous system. *Nat Precedings* (http://dx.doi.org/10.1038/npre.2007.262.1).

Ermentrout, B. (2002). *Simulating, Analyzing, and Animating Dynamical Systems: A Guide to XPPAUT for Researchers and Students* (Philadelphia, PA: SIAM).

Gleeson, P., Steuber, V., and Silver, R.A. (2007). neuroConstruct: A tool for modeling networks of neurons in 3D space. *Neuron* 54, 219–235.

Goddard, N.H., Hucka, M., Howell, F., Cornelis, H., Shankar, K., and Beeman, D. (2001). Towards NeuroML: model description methods for collaborative modelling in neuroscience. *Philos Trans R Soc Lond B Biol Sci* 356, 1209–1228.

Hines, M.L. and Carnevale, N.T. (2008). Translating network models to parallel hardware in NEURON. *J Neurosci Methods* 169, 425–455.

Kumar, A., Rotter, S., and Aertsen, A. (2008). Conditions for propagating synchronous spiking and asynchronous firing rates in a cortical network model. *J Neurosci* 28, 5268–5280.

Migliore, M., Cannia, C., Lytton, W., Markram, H., and Hines, M. (2006). Parallel network simulations with NEURON. *J Comput Neurosci* 21, 119–129.

Migliore, M., Ferrante, M., and Ascoli, G.A. (2005). Signal propagation in oblique dendrites of CA1 pyramidal cells. *J Neurophysiol* 94, 4145–4155.

Morrison, A., Aertsen, A., and Diesmann, M. (2007). Spike-timing-dependent plasticity in balanced random networks. *Neural Comput* 19, 1437–1467.

Morrison, A., Diesmann, M., and Gerstner, W. (2008). Phenomenological models of synaptic plasticity based on spike timing. *Biol Cybern* 98, 459–478.

Plesser, H., Eppler, J., Morrison, A., Diesmann, M., and Gewaltig, M.-O. (2007). Efficient parallel simulation of large-scale neuronal networks on clusters of multiprocessor computers. In *Euro-Par 2007 Parallel Processing*, Volume 4641 of Lecture Notes in Computer Science, Berlin, Springer-Verlag, pp. 672–681.

Santhakumar, V., Aradi, I., and Soltesz, I. (2005). Role of mossy fiber sprouting and mossy cell loss in hyperexcitability: a network model of the dentate gyrus incorporating cell types and axonal topography. *J Neurophysiol* 93, 437–453.

Index

V. Cutsuridis et al. (eds.), *Hippocampal Microcircuits*, Springer Series in Computational Neuroscience 5, DOI 10.1007/978-1-4419-0996-1,

D